Radio

Space Weather Live
https://www.spaceweatherlive.com/en.html

New EOVSA Flare List and Data Products
https://ovsa.njit.edu/flarelist
https://www.ovsa.njit.edu/wiki/index.php/EOVSA_Data_products
https://ovsa.njit.edu//wiki/index.php/EOVSA_Data_Policy
See Bin Chen 2024

The full catalog of /CME_list/radio/type4 1997-2023
https://cdaw.gsfc.nasa.gov/CME_list/radio/type4/
CME-associated type-IV radio bursts: The solar paradigm and the unique case of AD Leo
Atul **Mohan**, Nat Gopalswamy, Surajit Mondal, Anshu Kumari, Sindhuja G
Proceedings of IAUS 388 **2024**
https://arxiv.org/abs/2410.00787

Catalog of the multi-mission **DH type-II events and associated CMEs 2006-2023**
https://cdaw.gsfc.nasa.gov/CME_list/radio/multimission_type2/
A catalog of multi-vantage point observations of type-II bursts: Statistics and correlations
Atul **Mohan**, Nat Gopalswamy, Hemapriya Raju, Sachiko Akiyama
Proceedings of IAUS 388 **2024**
https://arxiv.org/pdf/2410.00814

Kilometric type II radio emissions in Wind/WAVES TNR data and association with interplanetary structures near Earth
Franco **Manini**, Hebe Cremades, Fernando M. López, Teresa Nieves-Chinchilla
Solar Phys. **2023**
https://arxiv.org/pdf/2311.08266.pdf
Table 3.: List of the 134 identified kmTII events, **their associations with shocks and ICMEs**, and main characteristics **between 1 January 2000 and 31 December 2012**

Solar radio bursts and space weather
White, S.M.:,
Asian J. Phys. **16**, 189 – 207, **2007**. **File**
https://arxiv.org/pdf/2405.00959

Level 3 Radio Frequency Spectrometer (RFS) data from Parker Solar Probe is available at the PSP/FIELDS Science Operations Center website (**https://fields.ssl.berkeley.edu/data/**) and CDAWeb (**https://cdaweb.gsfc.nasa.gov/**).

Release notes and code examples in IDL and Python are available at:
https://fields.ssl.berkeley.edu/2023/09/release-notes-for-psp-fields-data-release-16-1/

Chen et al. (**2023**)

Table 1: Current radio facilities that provide radio imaging capabilities relevant to middle corona studies.

Facility	Frequency Range	Elements	Max Baseline	Angular Resolution	Mid-day UT	Solar Dedicated?
MUSER-I[a] (China)	400–2000 MHz	40	~3 km	~1′ at 400 MHz	04 UT	Yes
Nancay[b] (France)	150–450 MHz	47	~3 km	~1′ at 400 MHz	12 UT	Yes
GRAPH[c] (India)	40–150 MHz	32	1.3 km (EW) 0.44 km (NS)	5–8′ at 150 MHz	07 UT	Yes
OVRO-LWA[d] (USA)	20–88 MHz	48	2.6 km	~5′ at 80 MHz	20 UT	Yes
uGMRT[e] (India)	120–1450 MHz	30	25 km	4″ at 650 MHz[j]	07 UT	No
JVLA P Band[f] (USA)	230–470 MHz	27	3.4 km (C config.)	$\lesssim$1′ at 400 MHz	19 UT	No
MWA (Australia)[g]	80–300 MHz	128	~5 km	1.3′ at 150 MHz	04 UT	No
LOFAR (Netherlands)	20–80 MHz (LBA)[h] 120–180 MHz (HBA)[i]	52	>48 km	<16″ at 80 MHz[j]	13 UT	No

a Yan et al. (2021). b Kerdraon & Delouis (1997). c Ramesh et al. (1998). d Chhabra et al. (2021). e Gupta et al. (2017). f See JVLA's 2023A performance. g Beardsley et al. (2019). h Zhang et al. (2022). i Liu et al. (2022). j Note the values quoted here are the theoretical resolution (λ/dmax). The actual resolution is limited by coronal scattering.

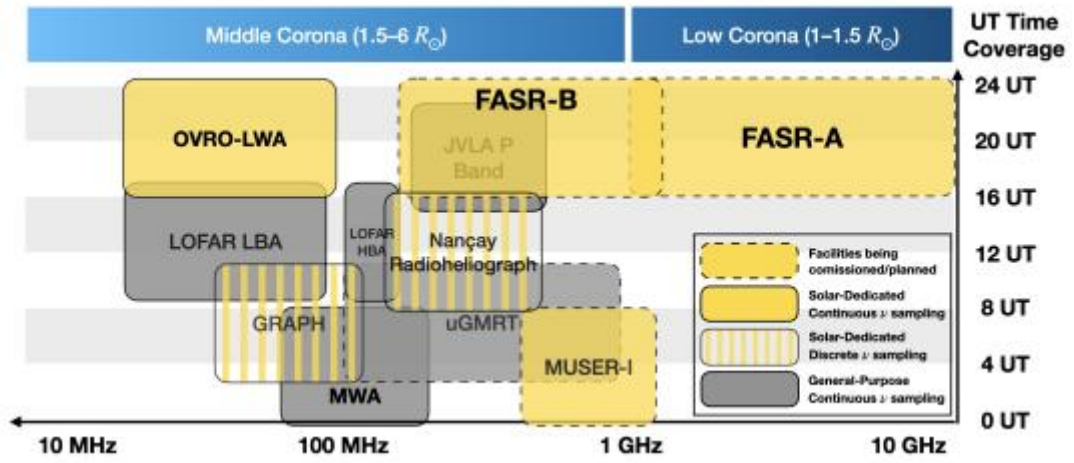

Figure 5: Frequency and UT time coverage of radio imaging facilities listed in Table 1. Filled yellow boxes indicated solar-dedicated instruments with continuous frequency sampling. FASR-B will fill the gap between 0.2–2 GHz in the UT range of ~16–24 UT, by providing radio observations with superior broadband imaging spectropolarimetry.

Wind/WAVES type II bursts and CMEs

https://cdaw.gsfc.nasa.gov/CME_list/radio/waves_type2.html

Nobeyama Radio Polarimeters
https://solar.nro.nao.ac.jp/norp/
ftp://solar-pub.nao.ac.jp/pub/nsro/norp/

The Sun Seen with the Atacama Large mm and sub-mm Array (ALMA) - First Results
https://www.frontiersin.org/research-topics/24755/the-sun-seen-with-the-atacama-large-mm-and-sub-mm-array-alma---first-results#articles

---

THE RESEARCH TOPIC **Solar and Space Weather Radio Physics**
Front. Astron. Space Sci. Vol. 7, **2020**
https://www.frontiersin.org/research-topics/10360/solar-and-space-weather-radio-physics#articles
https://www.frontiersin.org/research-topics/10360/

The **Solar ALMA Science Archive (SALSA)** can now be accessed at **http://sdc.uio.no/salsa**.

See Wind/WAVES type II bursts and CMEs
http://cdaw.gsfc.nasa.gov/CME_list/radio/waves_type2.html

LOFAR Long Term Archive, https://lta.lofar.eu/

The **type II bursts** drift rate (△f△t) in the metric range obtained from the dynamic spectra available
at https://cdaw.gsfc.nasa.gov/meetings/2017_mekelle/00_all_type2.html

Solar Physics with the Square Kilometre Array **Review**
A. **Nindos**, E.P. Kontar, D. Oberoi
Advances in Space Research Volume 63, Issue 4, 15 February 2019, Pages 1404-1424
https://arxiv.org/pdf/1810.04951.pdf

Table 1: Instruments capable of performing solar radio spectroscopic imaging

Instrument	Frequency Range (GHz)	Spectral Resolution (MHz)	Time Resolution (msec)	Angular Resolution (″)	Solar dedicated
EOVSA	1-18	50	20	3-57	Yes
GMRT	0.15-1.50	0.05	100	2-20	No
LOFAR	0.03-0.24	0.1	10	60-540	No
LWA	0.02-0.08	0.008	1	2-8[a]	No
MUSER	0.4-15	25	25-200	1.3-50	Yes
NoRH	17, 34	1700	100	6-12	Yes
NRH	0.15-0.45	23-48	250	18-240	Yes
MWA	0.08-0.30	0.04	500	16-60	No
Siberian RH	4-8	10	560	15-30	Yes
VLA	1-50	1	100	1-35	No

[a] Currently only two LWA stations have been deployed; the angular resolution cited here refers to the originally envisaged array.

The **solar-dedicated instruments** include the upgraded **Expanded Owens Valley Solar Array (EOVSA**; see Gary et al., 2012), the **Mingantu Ultrawide Spectral Radioheliograph (MUSER**; see Yan et al., 2016), the **Nan¸cay Radioheliograph (NRH**; see Kerdraon & Delouis, 1997), the **Nobeyama Radioheliograph (NoRH**; see Nakajima et al., 1994), and the upgraded **Siberian Radioheliograph (Siberian RH**; see Lesovoi et al., 2014) while **the general-purpose instruments** include the expanded **Karl G. Jansky Very Large Array (VLA**; see Perley et al., 2011), the **Low Frequency Array (LOFAR**, e.g. van Haarlem et al., 2013), the **Murchison Widefield Array (MWA**, see Tingay et al., 2013; Bowman et al., 2013), the **Long Wavelength Array (LWA**; see Ellingson et al., 2009), and the **Giant Metre-wave Radio Telescope (GMRT**; see Swarup et al., 1991).

Radio observatories and instrumentation used in space weather science and operations

Eoin P. **Carley**1,2,*, Carla Baldovin3 , Pieter Benthem3 , Mario M. Bisi4 , Richard A. Fallows3 , Peter T. Gallagher2,1, Michael Olberg5 , Hanna Rothkaehl6 , Rene Vermeulen3 , Nicole Vilmer7,8, David Barnes4 , the LOFAR4SW Consortium3

J. Space Weather Space Clim. **2020**, 10, 7 **File** **Review**
https://www.swsc-journal.org/articles/swsc/pdf/2020/01/swsc190064.pdf

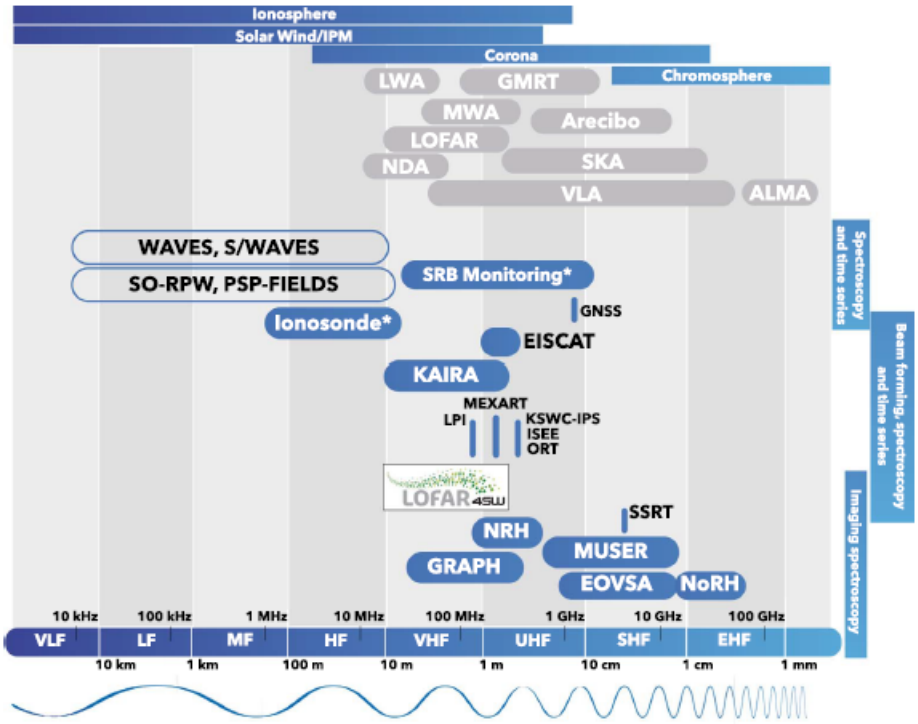

Fig. 4. A comparison of LOFAR4SW to other solar physics or space weather radio instruments. The bottom edge indicates frequency, wavelength, and International Telecommunication Union (ITU) designated name of each frequency band. The top of the graphic indicates the heliospheric domain that such frequencies generally give observational access to. The graphic on the right indicates the observational technique that the instruments use. The bubble for each instrument indicates its frequency range. Instruments in blue are solar/heliosphere/ionosphere dedicated, while those in grey can observe the Sun but are not (will not be) dedicated instruments. Specific details of each instrument are given in Table 1.

Table 1. Radio instruments performing observations for space weather science and/or operations.

Instrument	Frequency (MHz)	Local noon (UTC)[a]	Observable	Angular resolution	Operational phase	SW monitoring[c]
LOFAR	10–240	11	Sun, IPM, Iono	1.4′–30″ (core stations)	>2006	No
LOFAR4SW	10–240	11	Sun, IPM, Iono	1.4′–30″ (core stations)	>2023	Yes
SKA	350–14000	10 (SA), 4 (AUS)	Sun, IPM, Iono	TBD	>2020	No
MUSER	400–15000	4	Sun	1.3′–50″	>2014	Yes
FAST	70–3000	4	Sun	0.8′–30′	>2017	No
EOVSA	1000–18000	20	Sun	0.05′–1′	>2015	Yes
MWA	80–300	4	Sun, IPM, Iono	1′–5′	>2012	No
NRH	150–445	11	Sun	0.9′–2.6′	1997–2014	Yes
GRAPH	50–150	7	Sun	3′–11.2′	1997 – present	Yes
VLA	74–50000	18	Sun	1.2″–13′	>1980	No
OVRO-LWA	10–88	18	Sun, IPM, Iono	2–20°	>2009	Yes[d]
NoRH	17, 34	3	Sun	0.07′–0.1′	>1992	Yes
SSRT	5700	5	Sun	15″	>1996	Yes
EISCAT 3D	218–248	TBD	IPM, Iono	TBD	>2021	TBD
ORT	327	7	IPM	N/A	>1970	Yes
MEXART	140	17	IPM	N/A	>2010	Yes
BSA-LPA	111	7	IPM	N/A	>1970s	Yes
GMRT	150–1500	7	Sun, IPM	2″–1′	>1998	Yes
KSWC-IPS	327	4	IPM	N/A	N/A	Yes
Ionosondes[b]	0.5–20	0–24	Iono	N/A	N/A	Yes
ISEE	327	3	IPM	N/A	>1980s	Yes
KAIRA	10–240	11	Iono	2–20°	>2012	Yes
RSTN	25–85	0–24	Sun	N/A	>1980s	Yes
WIND/WAVES	0.01–14	0–24	Sun, IPM	N/A	>1996	Yes
STEREO/WAVES	0.01–16	0–24	Sun, IPM	N/A	2006–2015	Yes
SO RPW	0.01–20	Intermittent	Sun, IPM	N/A	2019–2022	Yes
PSP FIELDS	0.01–20	Intermittent	Sun, IPM	N/A	2019–2025	Yes
SRB monitoring[b]	10–5000	0–24	Sun	N/A	N/A	Yes

[a] If the observatory performs daytime space weather observations it may do so at any time when the Sun is visible, however nominal operation is likely to be several hours centered on local noon.
[b] There are hundreds of global ionosondes and SRB monitoring observatories. The parameters presented here are a generic representation of their nominal operational ranges.
[c] SW monitoring refers to whether or not the instrument observe the sun, heliosphere or ionopshere constantly throughout its observing window.
[d] OVRO-LWA is currently being upgraded with a solar-dedicated backend for space-weather-capable imaging spectroscopy (completion expected in ~2 years).

2020 Book title: Solar and space weather radio physics

Editors: D. Gary, B. Chen, and N. Vilmer.

See https://www.frontiersin.org/research-topics/10360/solar-and-space-weather-radio-physics
https://www.frontiersin.org/research-topics/10360/solar-and-space-weather-radio-physics

The field of Solar and Space Weather Radio Physics was surveyed in 2004 when the aforementioned instrumentation was only dreamed of. Now that actual instruments exist in the form of non-solar-dedicated instruments such as the **Jansky Very Large Array (VLA), Low-Frequency Array (LOFAR), Atacama Large Millimeter/Submillimeter Array (ALMA), Mileura Wide-Field Array (MWA),** and new solar-dedicated instruments such as the **Expanded Owens Valley Solar Array (EOVSA), Siberian Radio Heliograph (SRH), and Mingantu Ultrawide Spectral Radioheliograph (MUSER),** the time is right for an update to the field that brings together in one place both new results from observations with the above instruments, and the associated multi-wavelength modeling efforts that put the radio observations in context with other data and theories.

Front. Astron. Space Sci., September **2020**
THE RESEARCH TOPIC
Solar and Space Weather Radio Physics

https://www.frontiersin.org/research-topics/10360#articles

Assembled dynamic radio spectra using data from the WAVES experiment onboard the Wind spacecraft (Bougeret et al. 1995). The **Wind/WAVES data** derived from http://lep694.gsfc.nasa.gov/waves/data_products.html consist of one-minute resolution radio recordings from 20 kHz to 13.825 MHz, from the two WAVES receivers known as RAD1 (20 kHz–1.04 MHz) and RAD2 (1.075–13.825 MHz). a. From 2006, onwards, we further used composite radio spectra from STEREO/SWAVES (Bougeret et al. 2008),

Quick-look radio spectrograph plots from http://secchirh.obspm.fr/
and http://www.sws.bom.gov.au/World_Data_Centre/1/9 to identify **type II** radio bursts lower in the corona

---

Compound Astronomical Low-cost Low-frequency Instrument for Spectroscopy in Transportable Observatories (**CALLISTO**)

Radio Astronomy Book Reviews
This link will take you **Books**
to a webpage where many book reviews are listed, all
related to **radio astronomy including space weather and solar radio**
<http://www.reeve.com/RadioScience/Radio%20Astronomy%20Publications/Radio_Astronomy_Book_Reviews.htm>

CESRA 2016: Solar Radio Physics from the Chromosphere to Near Earth
Abstracts http://cesra2016.sciencesconf.org/conference/cesra2016/pages/CESRA2016_prog_abs_book_v1.pdf

---

Topical Issue Solar Phys.

Volume 290, Issue 9, September **2015**

Radio Heliophysics: Science and Forecasting / Guest Editors: Mario M. Bisi, Bernard V. Jackson, and J. Americo Gonzalez-Esparza

---

Long Wavelength Array (LWA)
http://www.ece.vt.edu/swe/lwa/

Solar and Space Weather Radiophysics **Book**
Current Status and Future Developments
Series: Astrophysics and Space Science Library, Vol. 314
Gary, D.E., Keller, C.U. (Eds.)
2004, XXIV, 400 p.

This volume is the outgrowth of several international meetings to discuss a vision for the future of solar radio physics: the development of a new radio instrument. From these discussions, the concept for the Frequency Agile Solar Radiotelescope (FASR) was born.

Radio Astronomy at Long Wavelengths, **Book**
Book Editor(s): Robert G. Stone, Kurt W. Weiler, Melvyn L. Goldstein, Jean-Louis Bougeret
Geophysical Monograph 119, AGU, Washington DC, **2000**.
https://agupubs.onlinelibrary.wiley.com/doi/book/10.1029/GM119

Rapid Fluctuations in Solar Flares
Proceedings of a workshop held at the Ramada Hotel Lanham, Maryland September 30-October 4,1985, NASA Conference Publication 2449, **1987**
Edited by Brian R. Dennis, Larry E.Orwig, AlanL.Kiplinger,
Section 1 - X-rays, Section 2 - Radio and Microwaves
https://www.academia.edu/24803822/Rapid_spectral_and_flux-time_variations_in_a_solar_burst_observed_at_various_dm-mm_wavelengths_and_at_hard_x_rays?auto=download

---

==========

An ALMA Observation of Time Variations in Chromospheric Temperature of a Solar Plage Region
Masashi **Abe,** Toshifumi Shimizu, Masumi Shimojo
Front. Astron. Space Sci. 9:908249. **2022**
doi: 10.3389/fspas.2022.908249
https://www.frontiersin.org/articles/10.3389/fspas.2022.908249/pdf
Nanoflares and the shock formation of magnetohydrodynamic waves in the solar chromosphere have been considered as key physical mechanisms of the heating of the chromosphere and corona. To investigate candidates of their signature in the mm-wavelength, a tiny active region located on the solar disk was observed with the Atacama Large millimeter and sub-millimeter Array (ALMA) at 3 mm, coordinated with observatories on orbit including Hinode SOT spectro-polarimeter in the Cycle 4 solar campaign (19 March 2017). ALMA's spatial resolution was moderate, far from the best performance, but it provided stable conditions that are suitable to investigate temporal variations in the mm-wavelength. We determined that the noise level is less than 20 K (σ) over 1 hour in the 20-s cadence time series of synthesized ALMA images. The time variations with amplitudes above the noise level were observed throughout the field of view, but variations exceeding 200 K, corresponding to energy input to the chromosphere on the order of 1020-22 erg, were localized in two locations. One location was on the polarity inversion line, where tiny concentrated magnetic patches

exist in weak field and a tiny magnetic flux may be emergent. The other location was at the outer edge of a bipolar magnetic region, which was under development with a successive series of magnetic flux emergence. This observation suggests that nanoflare-class energy inputs in the chromosphere can occur associated with emerging flux activities. **19 March 2017**

The Frequency of Occurrence of Pre-Flare Fluctuations in Microwave Radiation of Active Regions.

Abramov-Maximov, V.E., Bakunina, I.A.
Geomagn. Aeron. 63, 916–919 (**2023**).
https://doi.org/10.1134/S0016793223070022
We present a study of the frequency of occurrence of quasi-periodic fluctuations (QPFs) of microwave radiation from solar active regions at the pre-flare stage. We used correlation curves obtained with the Nobeyama Radioheliograph (NoRH). We analyzed 529 flares of classes X, M, and C (according to the GOES classification). In a significant number of considered events (approximately 75% of the powerful flares and 50% of the weaker flares), preflare fluctuations of microwave radiation with a duration of up to ten pulses are observed. The character of preflare fluctuations is different in different cases. In some cases, almost harmonic oscillations are observed. In most cases, the fluctuations are sporadic and look like a sequence of weak flares. It is possible that the nature of the preflare QPFs is different in different cases.

Features of Microwave Radiation and Magnetographic Characteristics of Solar Active Region NOAA 12242 Before the X1.8 Flare on December 20, 2014

V.E.**Abramov-Maximov** (1), V.N.Borovik (1), L.V.Opeikina (2), A.G.Tlatov (1), L.V.Yasnov (3) ((1) Central Astronomical Observatory at Pulkovo, Saint-Petersburg, Russia, (2) Special Astrophysical Observatory, Nizhnii Arkhyz, Russia, (3) St. Petersburg State University, Saint-Petersburg, Russia)
Geomagnetism and Aeronomy, **2017**, Vol. 57, No. 8, p.978
https://arxiv.org/pdf/1711.09134.pdf
This paper continues the cycle of authors' works on the detection of precursors of large flares (M5 and higher classes) in active regions (ARs) of the Sun by their microwave radiation and magnetographic characteristics. Generalization of the detected precursors of strong flares can be used to develop methods for their prediction. This paper presents an analysis of the development of NOAA AR 12242, in which an X1.8 flare occurred on **December 20, 2014**. The analysis is based on regular multiazimuth and multiwavelength observations with the RATAN-600 radio telescope in the range 1.65-10 cm with intensity and circular polarization analysis and data from the Solar Dynamics Observatory (SDO). It was found that a new component appeared in the AR microwave radiation two days before the X-flare. It became dominant in the AR the day before the flare and significantly decreased after the flare. The use of multiazimuth observations from RATAN-600 and observations at 1.76 cm from the Nobeyama Radioheliograph made it possible to identify the radio source that appeared before the X-flare with the site of the closest convergence of opposite polarity fields near the neutral line in the AR. It was established that the X-flare occurred 20 h after the total gradient of the magnetic field of the entire region calculated from SDO/HMI data reached its maximum value. Analysis of the evolution of the microwave source that appeared before the X-flare in AR 12242 and comparison of its parameters with the parameters of other components of the AR microwave radiation showed that the new source can be classified as neutral line associated source (NLS), which were repeatedly detected by the RATAN-600 and other radio telescopes 1-3 days before the large flares.

Dynamics of Microwave Sources Associated with the Neutral Line and the Magnetic-Field Parameters of Sunspots as a Factor in Predicting Large Flares

V. E. **Abramov-Maximov**, V. N. Borovik, L. V. Opeikina, A. G. Tlatov
Solar Phys., **2015**, Volume 290, Issue 1, pp 53-77
We studied the evolution of five active regions (ARs) where strong X-class flares occurred in 2011 – 2012 (NOAA ARs **11158, 11166, 11263, 11283 and 11520**). Our study focuses on the pre-flare phase of these ARs (during a few days before the flare) to reveal features in the microwave radiation and magnetic-field characteristics of the ARs that indicate that a powerful flare is about to take place. One well-developed AR (NOAA AR 11654) that did not produce large flares was also studied. We used daily multiwavelength spectral-polarization solar observations in the range of 1.65 – 6.0 cm made with the RATAN-600 radio telescope and data obtained by the Solar Dynamics Observatory/Helioseismic and Magnetic Imager (SDO/HMI). Whenever X-class flares occurred, we found that a new compact microwave source developed that was associated with the neutral line of the photospheric magnetic field (neutral line associated source – NLS) above the place with highest gradient of magnetic field. In some cases this became predominant in radio emission

of the AR one to two days before a large flare. No such source was detected in AR without a powerful flare. An analysis of magnetic-field characteristics of sunspots (based on SDO/HMI data) showed that the large X-flares we investigated occurred in ARs with high magnetic flux (~ 1022 Mx) and with an increasing magnetic-field gradient. We first identified the positions of the developing microwave source (NLS) with the location of the large flare that was registered in the AR one to two days later. Radio characteristics and dynamics of NLS detected before large flares possibly reflect the place in the corona where the energy for flaring is stored. Thus, an early detection of a rapidly developing microwave source NLS and an increasing magnetic-field gradient can be used as a factor in predicting large flares.

Peculiarities of the development of active regions on the Sun prior to strong X-class flares: Joint analysis of data from the RATAN-600 radio telescope and SDO space observatory

V. E. **Abramov-Maximov**, V. N. Borovik, L. V. Opeikina, A. G. Tlatov

Cosmic Research, January **2014**, Volume 52, Issue 1, pp 1-14

Complex analysis is performed for five active regions on the Sun where strong X-class solar flares occurred in 2011–2012. Radio emissions from the regions were investigated based on daily multi-wave observation of the Sun with the RATAN-600 radio telescope in the 1.6–8.0 cm wavelength range. It is shown that, as in eruptive events that were investigated earlier using the RATAN-600 radio telescope, 1–2 days (in some cases 14–17 h) prior to a strong flare one observes a developing source over the neutral line of photospheric magnetic field, which is projected on the region of the maximum approach of fields of opposite signs. In most cases this source became a dominant component in the microwave emissions of the active region prior to a flare. Simultaneously, analyzing magnetographic measurements of the same active regions, based on the data of the SDO space observatory, it has been shown that development of X-class flares proceeds at sufficiently high levels (F ~1022 Mx) of magnetic flux in groups of sunspots and at sharp growth of flux gradient (G ~ 20 × 1020 Mx/deg), which reflects the geometric approach of sunspots with opposite polarities of the magnetic field. These results can be used to develop methods for forecasting strong flares on the Sun.

Long-Term Oscillations of Sunspots from Simultaneous Observations with the Nobeyama Radioheliograph and Solar Dynamics Observatory

V. E. **Abramov-Maximov**, V. I. Efremov, L. D. Parfinenko, A. A. Solov'ev, and K. Shibasaki

Publ. Astron. Soc. Japan 65, No. SP1, S12 [8 pages] (**2013**)

http://pasj.asj.or.jp/v65/sp1/65S012/65S012.pdf

We present an investigation of oscillatory processes with periods in the range of several tens of minutes for some single sunspots of a new solar cycle, observed in 2010–2011 at the same time intervals in the optical and radio ranges. We used magnetograms from SDO/HMI with a cadence of 45 s, and radio images at a frequency of 17 GHz obtained with the Nobeyama Radioheliograph (NoRH). Radio images in intensity (Stokes parameter Ⅰ) and circular polarization (Stokes parameter Ⅴ) were synthesized with a cadence of ten seconds and ten-second averaging. Time profiles obtained with NoRH and SDO/HMI show a correlation between the radio emission of sunspots and a magnetic field. Wavelet spectra and cross-wavelet transforms give similar oscillation periods: 30–40 min, 60–70 min, 100–110 min, and 150–200 min. The same periods found by fundamentally different methods from ground-based and space observations confirm the solar nature of these oscillations. One of the possible interpretations of our results is that detected oscillations reflect eigen oscillations of a sunspot as a whole predicted by the shallow sunspot model. **Table**

Quasi-periodic Oscillations of Solar Active Regions in Connection with Their Flare Activity – NoRH Observations

V. E. **Abramov-Maximov**, G. B. Gelfreikh and K. Shibasaki

Solar Physics, Volume 273, Number 2, 403-412, **2011**

The sunspot-associated sources at the frequency of 17 GHz give information on plasma parameters in the regions of magnetic field about B=2000 G at the level of the chromosphere-corona transition region. The observations of short period (from one to ten minutes) oscillations in sunspots reflect propagation of magnetohydrodynamic (MHD) waves in the magnetic flux tubes of the sunspots. We investigate the oscillation parameters in active regions in connection with their flare activity. We confirm the existence of a link between the oscillation spectrum and flare activity. We find differences in the oscillations between pre-flare and post-flare phases. In particular, we demonstrate a case of powerful three-minute oscillations that start just before the burst. This event is similar to the cases of the precursors investigated by Sych et al. (Astron. Astrophys. 505, 791, 2009). We also found well-defined eight-minute oscillations of microwave emission from sunspot. We interpret our observations in terms of a relationship between MHD waves propagating from sunspots and flare processes.

11 September 2001, 14 March 2002, 7 October 2002

Multilevel Analysis of Oscillation Motions in Active Regions of the Sun

V. E. **Abramov-Maximov**, G. B. Gelfreikh, N. I. Kobanov, K. Shibasaki and S. A. Chupin
Solar Physics, Volume 270, Number 1, 175-189, **2011**

The nature of the three-minute and five-minute oscillations observed in sunspots is considered to be an effect of propagation of magnetohydrodynamic (MHD) waves from the photosphere to the solar corona. However, the real modes of these waves and the nature of the filters that result in rather narrow frequency bands of these modes are still far from being generally accepted, in spite of a large amount of observational material obtained in a wide range of wave bands. The significance of this field of research is based on the hope that local seismology can be used to find the structure of the solar atmosphere in magnetic tubes of sunspots. We expect that substantial progress can be achieved by simultaneous observations of the sunspot oscillations in different layers of the solar atmosphere in order to gain information on propagating waves. In this study we used a new method that combines the results of an oscillation study made in optical and radio observations. The optical spectral measurements in photospheric and chromospheric lines of the line-of-sight velocity were carried out at the Sayan Solar Observatory. The radio maps of the Sun were obtained with the Nobeyama Radioheliograph at 1.76 cm. Radio sources associated with the sunspots were analyzed to study the oscillation processes in the chromosphere–corona transition region in the layer with magnetic field B=2000 G. A high level of instability of the oscillations in the optical and radio data was found. We used a wavelet analysis for the spectra. The best similarities of the spectra of oscillations obtained by the two methods were detected in the three-minute oscillations inside the sunspot umbra for the dates when the active regions were situated near the center of the solar disk. A comparison of the wavelet spectra for optical and radio observations showed a time delay of about 50 seconds of the radio results with respect to the optical ones. This implies an MHD wave traveling upward inside the umbral magnetic tube of the sunspot. For the five-minute oscillations the similarity in spectral details could be found only for optical oscillations at the chromospheric level in the umbral region or very close to it. The time delays seem to be similar. Besides three-minute and five-minute ones, oscillations with longer periods (8 and 15 minutes) were detected in optical and radio records. Their nature still requires further observational and theoretical study for even a preliminary discussion.

A flare sensitive 3 h solar flux radio index for space weather applications

Acebal, Ariel O.; Sojka, Jan J.
Space Weather, Vol. 9, No. 7, S07004, **2011**
http://dx.doi.org/10.1029/2010SW000585

Many space physics models use the F10.7 as their input for solar activity. The F10.7 is a daily index derived from solar radio measurements taken at 2800 MHz, excluding activity from solar flares. In this paper, we compute a 3 h composite index, similar, in part, to the F10.7, using solar radio observations taken at 2695 MHz (11.1 cm) by the United States Air Force's Radio Solar Telescope Network. This index, called the F11.1 index, is similar to the F10.7. But unlike the F10.7 index, which is measured three times each day, at 1700, 2000, and 23 UT, F11.1 consists of eight measurements each day, uniformly distributed over 24 h. These 3 h intervals are aligned in UT with the planetary geomagnetic index Kp's time intervals. Each interval provides an F11.1 value that minimizes solar flare radio emission data. This composite index also provides two additional pieces of quantitative information that the F10.7 does not provide. The first is a factor, ranging from 0 to 1, indicating how representative the single F11.1 value is of this entire 3 h period (representation accuracy parameter). The second is a measure of how much of the 3 h interval can be classified as solar disturbed or as having a flare in progress (duration parameter). These aspects together have relevance for ionospheric modeling/specification for solar conditions in which significant change can occur over a 24 h period.

Extreme Value Theory Applied to the Daily Solar Radio Flux at 10.7 cm

F. J. **Acero**, J. M. Vaquero, M. C. Gallego, J. A. García
Solar Physics June **2019**, 294:67
https://link.springer.com/content/pdf/10.1007%2Fs11207-019-1457-z.pdf

Extreme Value Theory, a statistical tool widely used to study extreme events in time series corresponding to a broad range of fields, is here used to study the solar radio flux at 10.7 cm at a daily scale for the period 1948 – 2018. The peaks-over-threshold approach is taken to study the parameters of the distribution of the extreme values over a high, predefined threshold. The results led to a negative shape parameter, showing that there is an upper bound for the distribution of the peak values. The return level is also studied, and all of the results are in accordance with those obtained previously for sunspot-number series.

Observation of Solar Radio Bursts Using E-CallistoSystem

J **Adassuriya**, S Gunasekera, KPSC Jayaratne, C Monstein

Proceedings of the Technical Sessions, 30 (**2014**) 43-51
https://arxiv.org/ftp/arxiv/papers/2308/2308.01581.pdf
A CALLISTO system was set up at the Arthur C Clarke Institute and connected to the e-CALLISTO global network which observes the solar radio bursts in 24 hours. CALLISTO is the foremost observation facility to investigate celestial objects in radio region in Sri Lanka. The system consists of the CALLISTO spectrometer and controlling software,logarithmic periodic antenna and pre-amplifier. CALLISTO spectrometer is able to detect solar radio bursts in the frequency range of 45 MHz to 870 MHz with a channel resolution of 62.5 kHz.The log-periodic antenna was designed for 7 dBi gain and achieved the voltage standing wave ratio, less than 1.5 which is acquired by the overall impedance of the antenna, 49.3 ohms. The linear polarized antenna is pointing to zenith and the dipoles directed to north-south direction. The system detects solar radio emissions originated by solar flares and corona mass ejections. The radio bursts occurs as emission stripes in the radio spectra and classify from type I to V mainly on drift rate and band width. The system observed a type III solar radio burst on **5th July 2013** and a type II burst on **25th October 2013** which was originated by X1.7 solar flare. The type II bursts characterize with narrow bandwidth and drift slowly from higher to lower frequencies while the main features of type III bursts are high drift rate and broad bandwidth.

An Investigation of the Role of Propagation Effects in the Formation of Drifting Narrowband Type II Fiber Bursts on the Dynamic Spectrum customarily customarily customarily

A. N. **Afanasiev**
Solar Phys., 261(2), 295-309, **2010**
This paper investigates one of the kinds of fine structure of solar decametric type II radio bursts in the form of drifting narrowband fibers. The appearance of such a structure is customarily explained by the features of the radio emission mechanism in the source, which is formed when the shock wave catches up the previously-generated coronal mass ejection. On the other hand, the characteristics of radio emission in the process of its propagation from the source to the observation point are affected by inhomogeneities in the corona. Hence it is of considerable interest to estimate the role of the propagation effects on the formation of fiber structures in radio bursts. Our calculations show that strong refraction effects (caustics) can give rise to narrowband structures in the dynamic spectrum, resembling in their characteristics the fibers observed.

Fibre structure of decametric type II radio bursts as a manifestation of emission propagation effects in a disturbed near-solar plasma

A. N. **Afanasiev**,
Ann. Geophys., 27, 3933-3940, **2009, File**
This paper addresses the fine structure of solar decametric type II radio bursts in the form of drifting narrowband fibres on the dynamic spectrum. Observations show that this structure appears in those events where there is a coronal mass ejection (CME) traveling in the near-solar space ahead of the shock wave responsible for the radio burst. The diversity in observed morphology of fibres and values of their parameters implies that the fibres may be caused by different formation mechanisms. The burst emission propagates through extremely inhomogeneous plasma of the CME, so one possible mechanism can be related to radio propagation effects. I suggest that the fibres in some events represent traces of radio emission caustics, which are formed due to regular refraction of radio waves on the large-scale inhomogeneous structure of the CME front. To support this hypothesis, I have modeled the propagation of radio waves through inhomogeneous plasma of the CME, taking into consideration the presence of electron density fluctuations in it. The calculations, which are based on the Monte Carlo technique, indicate that, in particular, the emission of the fibres should be harmonic. Moreover, the mechanism under consideration suggests that in solar observations from two different points in space, the observed sets of fibres can be shifted in frequency with respect to one another or can have a different structure. This potentially can be used for identifying fibres caused by the propagation effects.

Mathematical Modeling of the Formation of Type IIId Solar Decameter Radio Bursts with Echo Components,

A. N. **Afanasiev**,
Solar Physics, Volume 238 Number 1, p. 87-104, **2006**.
(See M.V. **Tinin,** Solar Phys (2008) 247: 429–433)

FAILURE OF GPS FUNCTIONING CAUSED BY EXTREME SOLAR RADIO EVENTS

E. L. **Afraimovich**, V. V. Demyanov, D. E. Gary, A. B. Ishin, and G. Ya. Smolkov

BBSO Preprint #1361, 2008
http://solar.njit.edu/preprints/afraimovich1361.pdf
We investigate the performance quality of the Global Positioning System (GPS) during the **2006 December 6 and 2006 December 13** solar flares (soft X-ray class X6.5 and X3.4, respectively), which produced solar radio bursts with unprecedented radio flux density.

Release timescales of solar energetic particles in the low corona

N. **Agueda**1, K.-L. Klein2, N. Vilmer2, R. Rodríguez-Gasén2, O. E. Malandraki3, A. Papaioannou3, M. Subirà1, B. Sanahuja1, E. Valtonen4, W. Dröge5, A. Nindos6, B. Heber7, S. Braune8, I. G. Usoskin9, D. Heynderickx10, E. Talew11 and R. Vainio
A&A 570, A5 (**2014**)
http://www.aanda.org/articles/aa/pdf/2014/10/aa23549-14.pdf
Aims. We present a systematic study of the timing and duration of the release processes of near-relativistic (NR; >50 keV) electrons in the low corona.
Methods. We analyze seven well-observed events using in situ measurements by both the ACE and Wind spacecraft and context electromagnetic observations in soft X-rays, radio, hard X-rays and white light. We make use of velocity dispersion analysis to estimate the release time of the first arriving electrons and compare with the results obtained by using a simulation-based approach, taking interplanetary transport effects into account to unfold the NR electron release time history from in situ measurements.
Results. The NR electrons observed in interplanetary space appear to be released during either short (<30 min) or long (>2 h) periods. The observation of NR electron events showing beamed pitch-angle distributions (PADs) during several hours is the clearest observational signature of sustained release in the corona. On the other hand, the in situ observation of PADs isotropizing in less than a couple of hours is a clear signature of a prompt release of electrons in the low corona. Short release episodes appear to originate in solar flares, in coincidence with the timing of the observed type III radio bursts. Magnetic connectivity plays an important role. Only type III radio bursts reaching the local plasma line measured at 1 AU are found to be related with an associated release episode in the low corona. Other type III bursts may also have a release of NR electrons associated with them, but these electrons do not reach L1. Long release episodes appear associated with signatures of long acceleration processes in the low corona (long decay of the soft X-ray emission, type IV radio bursts, and time-extended microwave emission). Type II radio bursts are reported for most of the events and do not provide a clear discrimination between short and long release timescales. 1999 Jun. 11, 2000 Sep. 12, 2002 Feb. 20, 2002 Jul. 7, 2002 Aug. 14, 2002 Dec. 19, 2004 Nov. 1

On the Emission Region of Type II Radio Bursts in Interplanetary Shock Fronts

E. **Aguilar-Rodriguez** & P. Corona-Romero
Solar Physics volume 295, Article number: 77 (**2020**)
https://link.springer.com/content/pdf/10.1007/s11207-020-01643-x.pdf
We analyze Type II radio emissions observed by the Radio and Plasma Waves instrument onboard Wind to determine the emission region in shock fronts, using the blast wave reconstruction technique. Our results suggest that the processes of emission of a Type II radio burst occur not only in the upstream region of the shock, i.e. the region that precedes the collision, but also that there must be an emission of the material that has been compressed, as well as of the material that is in the compression region within the structure of the shock itself. **2000.06.06, 2000.07.14, 2001.04.26, 2001.09.24, 2001.11.04, 2002.08.16, 2004.12.03, 2005.05.13, 2012.03.07, 2015.06.21**
Table 1 Interplanetary Type II radio bursts selected for this analysis (2010-2015)

Interplanetary Scintiallation (IPS) of the Radio Source 3C48 During Periods of Low and High Solar Activity

E. **Aguilar-Rodriguez**, S. A. Tyul'bashev, I. V. Chashei, E. Romero-Hernandez
Solar Physics September **2015**, Volume 290, Issue 9, pp 2567-2575
We present a comparative study of three techniques used to estimate the scintillation index using interplanetary scintillation (IPS) observations carried out by the Big Scanning Array (BSA), which operates at a frequency of 111 MHz. These techniques are based on: rms analysis on-source and off-source (classic), Fourier, and wavelet transforms. IPS data are analyzed separately for the period of low solar activity (2007 – 2009), and for the year 2013, near the solar-activity maximum. Our results show that, in general, these methods are equivalent. We analyze the radial dependence of the scintillation index at meter wavelengths during these two periods. It is found that the observed radial dependence of the scintillation index during both

periods of U.C. cycle 24 is flatter than the theoretical dependence expected for the case of solar-wind spherical symmetry. This flattening can be explained in terms of the influence of the heliospheric current sheet during the low solar-activity period, and the influence of solar disturbances, such as coronal mass ejections (CMEs), for the high solar-activity period.

Comparison of Solar Wind Speeds Using Wavelet Transform and Fourier Analysis in IPS Data

E. **Aguilar-Rodriguez** , J. C. Mejia-Ambriz, B. V. Jackson, A. Buffington, E. Romero-Hernandez, J. A. Gonzalez-Esparza, M. Rodriguez-Martinez, P. Hick, M. Tokumaru and 1 more
Solar Phys. Volume 290, Issue 9, pp 2507-2518 **2015**
The power spectra of intensity fluctuations in interplanetary scintillation (IPS) observations can be used to estimate solar-wind speeds in the inner heliosphere. We obtain and then compare IPS spectra from both wavelet and Fourier analyses for 12 time series of the radio source 3C48; these observations were carried out at Japan's Solar-Terrestrial Environment Laboratory (STEL) facility, at 327 MHz. We show that wavelet and Fourier analyses yield very similar power spectra. Thus, when fitting a model to spectra to determine solar-wind speeds, both yield comparable results. Although spectra from wavelet and Fourier closely match each other for solar-wind speed purposes, those from the wavelet analysis are slightly cleaner, which is reflected in an apparent level of intensity fluctuations that is enhanced, being ≈ 13 % higher. This is potentially useful for records that show a low signal-to-noise ratio.

A Study of the Drift Rate of Type II Radio Bursts at Different Wavelengths,

Aguilar-Rodriguez, E., Gopalswamy, N., MacDowall, R., Yashiro, S., and Kaiser, M. I.,
in Proceedings of the Solar Wind 11 / SOHO 16, *Connecting Sun and Heliosphere* (ESA SP-592), 12 - 17 June 2005 Whistler, Canada, eds. B. Fleck, T. H. Zurbuchen, and H. Lacoste, p. 393, **2005**
different behavior of metric and IP type II bursts (see Gopalswamy et al., 2001c; 2008a; Aguilar-Rodriguez et al., 2005).

A Study of Coronal Holes Observed by SoHO/EIT and the Nobeyama Radioheliograph

S. **Akiyama**, N. Gopalswamy, S. Yashiro, and P. Mäkelä
Publ. Astron. Soc. Japan 65, No SP1, S15 [10 pages] (**2013**)
http://pasj.asj.or.jp/v65/sp1/65S015/65S015.pdf
Coronal holes (CHs) are areas of reduced emission in EUV and X-ray images that show bright patches of microwave enhancements (MEs) related to magnetic network junctions inside the CHs. A clear correlation between the CH size and the solar wind (SW) speed is well known, but we have less information about the relationship between MEs and other CH and SW properties. We studied the characteristics of 21 equatorial CHs associated with corotating interaction regions (CIRs) during 1996 to 2005. Our CHs were divided into two groups according to the intensity of the associated geomagnetic storms: *Dst* __100 nT (10 events) and 〉 _100 nT (11 events). Using EUV 284 ˚A images obtained by SOHO/EIT and 17 GHz microwave images obtained by the Nobeyama Radioheliograph (NoRH), we found a linear correlation not only between the maximum SW speed and the area of EUV CH (r = 0.62), but also between the maximum SW speed and the area of the ME (r = 0.79). We also compared the EUVCH areas with and without an overlapping ME. The area of the CHs with an ME is better correlated with the SW speed (r = 0.71) than the area of those without an ME (r = 0.36). Therefore, the radio ME may play an important role in understanding the origin of SW.

Exploring the Asymmetry of the Solar Corona Electron Density with Very Long Baseline Interferometry

Dan **Aksim**, Alexey Melnikov, Dmitry Pavlov, Sergey Kurdubov
ApJ **885** 159 **2019**
https://arxiv.org/pdf/1910.10529.pdf
sci-hub.se/10.3847/1538-4357/ab499a
The Sun's corona has interested researchers for multiple reasons, including the search for solution for the famous coronal heating problem and a purely practical consideration of predicting geomagnetic storms on Earth. There exist numerous different theories regarding the solar corona; therefore, it is important to be able to perform comparative analysis and validation of those theories. One way that could help us move towards the answers to those problems is the search for observational methods that could obtain information about the physical properties of the solar corona and provide means for comparing different solar corona models.
In this work we present evidence that VLBI observations are, in certain conditions, sensitive to the electron density of

the solar corona and are able to distinguish between different electron density models, which makes the technique of VLBI valuable for solar corona investigations. Recent works on the subject used a symmetric power-law model of the electron density in solar plasma; in this work, an improvement is proposed based on a 3D numerical model. **2017-05-01, 2018-05-01**

Formation of Radio Type II Bursts During a Multiple Coronal Mass Ejection Event

Firas **Al-Hamadani,** Silja Pohjolainen, Eino Valtonen

Solar Physics December **2017**, 292:183

https://link.springer.com/content/pdf/10.1007%2Fs11207-017-1208-y.pdf

We study the solar event on **27 September 2001** that consisted of three consecutive coronal mass ejections (CMEs) originating from the same active region, which were associated with several periods of radio type II burst emission at decameter–hectometer (DH) wavelengths. Our analysis shows that the first radio burst originated from a low-density environment, formed in the wake of the first, slow CME. The frequency-drift of the burst suggests a low-speed burst driver, or that the shock was not propagating along the large density gradient. There is also evidence of band-splitting within this emission lane. The origin of the first shock remains unclear, as several alternative scenarios exist. The second shock showed separate periods of enhanced radio emission. This shock could have originated from a CME bow shock, caused by the fast and accelerating second or third CME. However, a shock at CME flanks is also possible, as the density depletion caused by the three CMEs would have affected the emission frequencies and hence the radio source heights could have been lower than usual. The last type II burst period showed enhanced emission in a wider bandwidth, which was most probably due to the CME–CME interaction. Only one shock that could reliably be associated with the investigated CMEs was observed to arrive near Earth.

Origin of Radio Enhancements in Type II Bursts in the Outer Corona

Firas **Al-Hamadani,** Silja Pohjolainen, Eino Valtonen

Solar Physics September **2017**, 292:127

https://link.springer.com/content/pdf/10.1007%2Fs11207-017-1148-6.pdf

We study interplanetary (IP) solar radio type II bursts from 2011 – 2014 in order to determine the cause of the intense enhancements in their radio emission. Type II bursts are known to be due to propagating shocks that are often associated with fast halo-type coronal mass ejections (CMEs). We analysed the radio spectral data and the white-light coronagraph data from 16 selected events to obtain directions and heights for the propagating CMEs and the type II bursts. CMEs preceding the selected events were included in the analysis to verify whether CME interaction was possible. As a result, we were able to classify the events into five different groups. 1) Events where the heights of the CMEs and type II bursts are consistent, indicating that the shock is located at the leading front of the CME. The radio enhancements are superposed on the type II lanes, and they are probably formed when the shock meets remnant material from earlier CMEs, but the shock continues to propagate at the same speed. 2) Events where the type II heights agree with the CME leading front and an earlier CME is located at a height that suggests interaction. The radio enhancements and frequency jumps could be due to the merging process of the CMEs. 3) Events where the type II heights are significantly lower than the CME heights almost from the start. Interaction with close-by streamers is probably the cause for the enhanced radio emission, which is located at the CME flank region. 4) Events where the radio enhancements are located within wide-band type II bursts and the causes for the radio enhancements are not clear. 5) Events where the radio enhancements are associated with later-accelerated particles (electron beams, observed as type III bursts) that stop at the type II burst emission lane, and no other obvious reason for the enhancement can be identified.

Most of the events (38%) were due to shock–streamer interaction, while one quarter of the events was due to possible CME–CME interaction. The drift rates, bandwidth characteristics, or cross-correlations of various characteristics did not reveal any clear association with particular category types. The chosen atmospheric density model causes the largest uncertainties in the derived radio heights, although in some cases, the emission bandwidths also lead to relatively large error margins.

Our conclusion is that the enhanced radio emission associated with CMEs and propagating shocks can have different origins, depending on their overall configuration and the associated processes. ***15 February 2011, 7 March 2011, 22 September 2011, 26 November 2011, 19 January 2012, 23 January 2012, 5 March 2012, 10 March 2012, 17 May 2012, 17 July 2012, 31 August 2012, 15 March 2013, 22 May 2013, 29 September 2013, 7 January 2014, 18 April 2014,***

Table 1 Characteristics of the preceding CMEs (CME1, in italics), the primary CMEs (CME2), and their associated flares. 2011-2014

Characteristics of stripes-pattern radio-emission sources

Alielden, Khaled

MNRAS Volume 514, Issue 2, pp.2135-2144 **2022**
https://doi.org/10.1093/mnras/stac1384
https://watermark.silverchair.com/stac1384.pdf

An investigation of the generation mechanism for stripes-pattern radio spectra is important for an understanding of the dynamics of non-thermal electrons in several astronomical objects, including the Sun, Jupiter, and the Crab Pulsar. A new analytical study is carried out to identify the plasma characteristics of fiber- and zebra-pattern emission sources without an underlying density or magnetic model. The analysis demonstrates that the source region of the stripes emission is located underneath the reconnection point, where the ratio s of the instability growth rate to the electron gyrofrequency ωc does not equal unity; that is, $s = k_\perp v_\perp/\omega c \neq 1$. When $|s| < 1$, the plasma condition of the source region becomes $k_\perp v_\perp < \omega p < \omega c$, where ωp is the plasma frequency, and the emission source is likely to produce a fiber radio burst. For $|s| > 1$, the plasma condition of the source region is $\omega c < \omega p < k_\perp v_\perp$, and the emission source is likely to produce zebra-pattern emission. This indicates that the magnetic field in the source region of zebra-pattern radio emission is weak and it is relatively high in the source region of fiber-pattern emission. An approach is applied to estimate the plasma parameters of a zebra-pattern emission source observed on 2011 June 21. The behaviour of the blasted medium, which is produced by magnetic reconnection, is investigated. The results show that the blasted medium propagates isothermally as a sausage-like wave for a short time during the emission. The study discusses the conditions for producing different types of striped radio emission and provides a simple computational approach that could be useful in a number of astronomical contexts. **2011 June 21**

CESRA #3386 **2022** https://www.astro.gla.ac.uk/users/eduard/cesra/?p=3386

Evolution of Coronal and Interplanetary Shock Waves Inferred from a Radio Burst

Khaled **Alielden**

Solar Physics October 2019, 294:159
https://link.springer.com/content/pdf/10.1007%2Fs11207-019-1493-8.pdf

Studying the evolution of the source of a radio burst, which is recognized as a shock wave, is important for understanding its generation mechanism and predicting its hazards. Estimating the kinematics of radio-burst sources using electron-density models is not easy. In this article, the kinematics of the Type-II radio-burst source is estimated without using electron-density models by studying the density variation along the leading surface of the coronal mass ejections (CMEs) (hereafter ejecta) during Type-II radio-burst emission. This technique is valid for analyzing the Type-II radio-burst spectrum in metric and DH ranges, from which we can infer ejecta propagation from the corona into interplanetary space. It is found that the Type-II radio burst can be described by the Sedov–Taylor blast-wave equation by matching the calculated theoretical frequencies with that observed by the RAD1 and RAD2 receivers. The theoretical model showed a good fit with the observed spectra of Type-II radio bursts of different Type-II events. The analysis was consistent with the previous work regarding the conditions of the Sedov–Taylor equation and statistical studies of the density variation on the surface area of an interplanetary CME. The kinematics of a Type-II radio-burst source and the temporal variation of its energy are estimated during the Type-II radio-burst emission. The results of the two cases studied show that the energy of ejecta degraded by ≈14%≈14% of its initial energy at the beginning of metric Type-II radio emission on 16 March 2016, while the energy of ejecta degraded by ≈86%≈86% and ≈20%≈20% for DH Type-II radio burst as recorded by RAD1 and RAD2 on 7 November 2004, respectively. The analysis shows that the radial speed of the blast wave is lower than its transversal speed along the surface of ejecta and extends to a small fraction of $R_\odot$ from its source point on the ejecta. The magnetic-field strength of the ejecta and the ambient medium are estimated during the Type-II radio-burst emission. This study emphasizes that the emission of a blast wave from the reconnection sites within the ejecta is one of the processes that degrades the energy of ejecta during their propagation. **28 October 2003, 7 November 2004, 15 February 2011, 15 March 2015, 16 March 2016**

CESRA #2474 Feb **2020** http://cesra.net/?p=2474

Studying the Characteristics of Shock waves associated with CMEs using solar radio bursts.

Khaled **Alielden**_1 and Ayman Mahrousy2

CESRA **2016**, p.89
http://cesra2016.sciencesconf.org/conference/cesra2016/pages/CESRA2016_prog_abs_book_v3.pdf

Fast CME/shocks propagating in the Corona and the interplanetary medium can generate metric and kilometric Type II radio emissions at the local plasma frequency and/or its harmonic, respectively. So these radio emissions provide a means of remotely tracking CME/shocks. We apply analysis technique, using the frequency drift of metric spectrum

obtained by ground station e-Callisto (Compound Astronomical Low cost Low frequency Instrument for Spectroscopy and Transportable Observatory) in Space Weather Monitoring Center (SWMC) { Helwan University, and estimated by using electron density model the propagation speed of CME/shocks in the corona, and the km-TII spectrum obtained by the WIND/WAVES experiment, to infer, at some adequate intervals, the propagation speed of CME/shocks in the interplanetary medium. We applied this technique on _ve CME/shocks. We combine these results with previously reported speeds from coronagraph white light and interplanetary scintillation observations, and in-situ measurements, to study the temporal speed evolution of the _ve events. The speed values obtained by the metric and km-TII analysis are in a reasonable agreement with the speed measurements obtained by other techniques at di_erent heliocentric distance ranges. The combination of all the speed measurements show a gradual deceleration of the CME/shocks as they propagate to 1 AU. This technique can be useful in studying the evolution and characteristics of fast CME/shocks when adequate intervals of km-TII emissions are available.

Giant post-flare loops in active regions with extremely strong coronal magnetic fields

Costas E. **Alissandrakis**, Gregory D. Fleishman, Viktor V. Fedenev, Stephen M. White, Alexander T. Altyntsev

ApJ **971** 122 **2024**

https://arxiv.org/pdf/2406.14638

https://iopscience.iop.org/article/10.3847/1538-4357/ad5831/pdf

We report for the first time the detection of thermal free-free emission from post-flare loops at 34GHz in images from the Nobeyama Radioheliograph (NoRH). We studied 8 loops, 7 of which were from regions with extremely strong coronal magnetic field reported by Fedenev et al. (2023). Loop emission was observed in a wide range of wavelength bands, up to soft X-rays, confirming their multi-temperature structure and was associated with noise storm emission in metric wavelengths. The comparison of the 17GHz emission with that at 34GHz, after a calibration correction of the latter, showed that the emission was optically thin at both frequencies. We describe the structure and evolution of the loops and we computed their density, obtaining values for the top of the loops between 1 and 6 x 10^10 cm^-3, noticeably varying from one loop to another and in the course of the evolution of the same loop system; these values have only a weak dependence on the assumed temperature, 2 x 10^6 K in our case, as we are in the optically thin regime. Our density values are above those reported from EUV observations, which go up to about 10^10 cm^-3. This difference could be due to the fact that different emitting regions are sampled in the two domains and/or due to the more accurate diagnostics in the radio range, which do not suffer from inherent uncertainties arising from abundances and non-LTE excitation/ionization equilibria. We also estimated the magnetic field in the loop tops to be in the range of 10 to 30G. **6 Nov 1999, 28 Mar 2001, 14 Aug 2004, 13 Jul 2005, 6-10 Sep 2005**

The quiet Sun at mm Wavelengths as Seen by ALMA **Review**

Costas **Alissandrakis**, Timothy Bastian, Roman Brajša

Frontiers in Astronomy and Space Science 9:981320 **2022**

https://arxiv.org/pdf/2209.02569.pdf

https://www.frontiersin.org/articles/10.3389/fspas.2022.981320/pdf

doi: 10.3389/fspas.2022.981320

Solar observations at sub-mm, mm and cm wavelengths offer a straightforward diagnostic of physical conditions in the solar atmosphere because they yield measurement of brightness temperature which, for optically thick features, equals intrinsic temperature - much unlike solar diagnostics in other spectral ranges. The Atacama Large Millimeter and submillimeter Array (ALMA) has therefore opened a new, hitherto underexplored, spectral window for studying the enigmatic solar chromosphere. In this review we discuss initial ALMA studies of the quiet chromosphere that used both single-dish and compact-array interferometric observing modes. We present results on the temperature structure of the chromosphere, comparison with classic empirical models of the chromosphere, and observations of the chromospheric network and spicules. Furthermore, we discuss what may be expected in the future, since the ALMA capabilities continuously expand and improve towards higher angular resolution, wavelength coverage, and polarization measurement for magnetometry. **December 18, 2015, 27 Apr 2017, 12 Apr 2018**

A first look at the submillimeter Sun with ALMA

C. E. **Alissandrakis**, T. S. Bastian, A. Nindos

A&A 661, L4 **2022**

https://arxiv.org/pdf/2205.01008.pdf

https://www.aanda.org/articles/aa/pdf/2022/05/aa43774-22.pdf
https://doi.org/10.1051/0004-6361/202243774
We present the first full-disk solar images obtained with the Atacama Large Millimeter/submillimeter Array (ALMA) in Band 7 (0.86 mm; 347 GHz). In spite of the low spatial resolution (21"), several interesting results were obtained. During our observation, the sun was practically devoid of active regions. Quiet Sun structures on the disk are similar to those in Atmospheric Imaging Assembly (AIA) images at 1600 A and 304 A, after the latter are smoothed to the ALMA resolution, as noted previously for Band 6 (1.26 mm) and Band 3 (3 mm) images; they are also similar to negative Hα images of equivalent resolution. Polar coronal holes, which are clearly seen in the 304 A band and small Hα filaments, are not detectable at 0.86 mm. We computed the center-to-limb variation (CLV) of the brightness temperature, Tb, in Band 7, as well as in Bands 6 and 3, which were obtained during the same campaign, and we combined them to a unique curve of Tb(logμ100), where μ100 is the cosine of the heliocentric angle reduced to 100 GHz. Assuming that the absolute calibration of the Band 3 commissioning observations is accurate, we deduced a brightness temperature at the center of the disk of 6085 K for Band 7, instead of the value of 5500 K, extrapolated from the recommended values for Bands 3 and 6. More importantly, the Tb(logμ100) curve flattens at large values of μ100, and so does the corresponding Te(logτ100) at large τ100. This is probably an indication that we are approaching the temperature minimum. **4 Jan 2020, 8 Jan 2020**

First detection of metric emission from a solar surge

C. E. **Alissandrakis**, S. Patsourakos, A. Nindos, C. Bouratzis, A. Hillaris
A&A 662, A14 **2022**
https://arxiv.org/pdf/2203.01043.pdf
https://www.aanda.org/articles/aa/pdf/2022/06/aa43169-22.pdf
We report the first detection of metric radio emission from a surge, observed with the Nançay Radioheliograph (NRH), STEREO and other instruments. The emission was observed during the late phase of the M9 complex event SOL**2010-02-012**T11:25:00, described in a previous publication and was associated with a secondary energy release, also observed in STEREO 304 Å images: there was no detectable soft X-ray emission. Triangulation of the STEREO images allowed the identification of the surge with NRH sources near the central meridian. The radio emission of the surge occurred in two phases and consisted of two sources, one located near the base of the surge, apparently at or near the site of energy release, and another in the upper part of the surge; these were best visible in the frequency range of 445.0 to about 300MHz, whereas a spectral component of different nature was observed at lower frequencies. Sub-second time variations were detected in both sources during both phases, with 0.2-0.3s a delay of the upper source with respect to the lower, suggesting superluminal velocities. This effect can be explained if the emission of the upper source was due to scattering of radiation from the source at the base of the surge. In addition, the radio emission showed signs of pulsations and spikes. We discuss possible emission mechanisms for the slow time variability component of the lower radio source. Gyrosynchrotron emission reproduced fairly well the characteristics of the observed total intensity spectrum at the start of the second phase of the event, but failed to reproduce the high degree of the observed circular polarization as well the spectra at other instances. On the other hand, type IV-like plasma emission from the fundamental could explain the high polarization and the fine structure in the dynamic spectrum; moreover, it gives projected radio source positions on the plane of the sky, as seen from STEREO-A, near the base of the surge. Taking everything into consideration, we suggest type IV-like plasma emission with a low intensity gyrosynchrotron component as the most plausible mechanism.
CESRA #3363 Jul **2022** https://www.astro.gla.ac.uk/users/eduard/cesra/?p=3363

Multi-wavelength Observations of a Metric Type-II Event

C. E. **Alissandrakis**, A. Nindos, S. Patsourakos, A. Hillaris
A&A 654, A112 **2021**
https://arxiv.org/pdf/2108.02855.pdf
https://www.aanda.org/articles/aa/pdf/2021/10/aa41672-21.pdf
https://doi.org/10.1051/0004-6361/202141672
We have studied a complex metric radio event which originated in a compact flare, observed with the ARTEMIS-JLS radiospectro-graph on **February 12, 2010**. The event was associated with a surge observed at 195 and 304 Å and with a coronal mass ejection observed by instruments on-board STEREO A and B near the East and West limbs respectively. On the disk the event was observed at 10 frequencies by the Nancay Radioheliograph, in Ha by the Catania observatory, in soft x-rays by GOES SXI and Hinode XRT and in hard x-rays by RHESSI. We combined these data, together with MDI longitudinal magnetograms, to get as complete a picture of the event as possible. Our emphasis is on two type-II bursts that occurred near respective maxima in the GOES light curves. The first, associated with the main peak of the event, showed an impressive F-H structure, while the emission of the second consisted of three well-separated bands

with superposed pulsations. Using positional information for the type-IIs from the NRH and triangulation from STEREO A and B, we found that the type IIs were associated neither with the surge nor with the disruption of a nearby streamer, but rather with an EUV wave probably initiated by the surge. The fundamental-harmonic structure of the first type II showed a band split corresponding to a magnetic field strength of 18G, a frequency ratio of 1.95 and a delay of 0.23-0.65s of the fundamental with respect to the harmonic; moreover it became stationary shortly after its start and then drifted again. The pulsations superposed on the second type II were broadband and had started before the burst. In addition, we detected another pulsating source, also before the second type II, polarized in the opposite sense; the pulsations in the two sources were out of phase and hence hardly detectable in the dynamic spectrum. The pulsations had a measurable reverse frequency drift of about 2/s.
CESRA # 3140 **2021** https://www.astro.gla.ac.uk/users/eduard/cesra/?p=3140

Radio Measurements of the Magnetic field in the Solar Chromosphere and the Corona **Review**

C. E. **Alissandrakis**1* and Dale E. Gary2
Front. Astron. Space Sci. Volume 7, id.77 **2020**
https://doi.org/10.3389/fspas.2020.591075
https://www.frontiersin.org/articles/10.3389/fspas.2020.591075/full
The structure of the upper solar atmosphere, on all observable scales, is intimately governed by the magnetic field. The same holds for a variety of solar phenomena that constitute solar activity, from tiny transient brightening to huge Coronal Mass Ejections. Due to inherent difficulties in measuring magnetic field effects on atoms (Zeeman and Hanle effects) in the corona, radio methods sensitive to electrons are of primary importance in obtaining quantitative information about its magnetic field. In this review we explore these methods and point out about its magnetic field. In this review we explore these methods and point out their advantages and limitations. After a brief presentation of the magneto-ionic theory of wave propagation in cold, collisionless plasmas, we discuss how the magnetic field affects the radio emission produced by incoherent emission mechanisms (free-free, gyroresonance and gyrosynchrotron processes) and give examples of measurements of magnetic filed parameters in the quiet sun, active regions and radio CMEs. We proceed by discussing how the inversion of the sense of circular polarization can be used to measure the field above active regions. Subsequently we pass to coherent emission mechanisms and present results of measurements from fiber bursts, zebra patterns and type II burst emission. We close this review with a discussion of the variation of the magnetic field, deduced by radio measurement, from the low corona up to 10 solar radii and with some thoughts about future work. This review is part of the research topic collection "Solar and Space Weather Radio Physics"

Structure of the Solar Atmosphere: A Radio Perspective **Review**

Costas E. **Alissandrakis**
Front. Astron. Space Sci. 7:574460 **2020**
https://sci-hub.st/https://www.frontiersin.org/articles/10.3389/fspas.2020.574460/full
https://doi.org/10.3389/fspas.2020.574460
Solar radio emission has been providing information about the Sun for over half a century. In order to fully exploit this information, one needs to have a broader view of the solar atmosphere, which cannot be provided by radio observations alone. The purpose of this review is to present this background information, which is necessary to understand the physical processes that determine the solar radio emission and to link the radio domain with the rest of the electromagnetic spectrum. Both classic and modern results are presented in a concise manner. After a brief discussion of the solar interior, the basic physics of the solar atmosphere and some elements of radiative transfer are presented. Subsequently the atmospheric structure as a function of height is examined and one-dimensional models of the photosphere, the chromosphere, the transition region and the corona are presented and discussed. An introduction to basicmagnetohydrodynamics precedes the discussion of the rich fine structure of the solar atmosphere as a 3D object. Active regions are briefly discussed in a separate section, and this is followed by a section on the problem of heating of the chromosphere and the corona. I finish with some thoughts on what to expect from the new instruments currently under development.

Modeling the quiet Sun cell and network emission with ALMA

C. E. **Alissandrakis**, A. Nindos, T. S. Bastian, S. Patsourakos
A&A 640, A57 **2020**
https://arxiv.org/pdf/2006.09886.pdf
https://www.aanda.org/articles/aa/pdf/2020/08/aa38461-20.pdf

ALMA observations of the Sun at mm-λ offer a unique opportunity to investigate the temperature structure of the solar chromosphere. In this article we expand our previous work on modeling the chromospheric temperature of the quiet Sun, by including measurements of the brightness temperature in the network and cell interiors, from high resolution ALMA images at 3 mm (Band 3) and 1.26 mm (Band 6). We also examine the absolute calibration of ALMA full-disk images. We suggest that the brightness temperature at the center of the solar disk in Band 6 is ∼440 K above the value recommended by White et al. (2017) and we give improved results for the electron temperature variation of the average quiet Sun with optical depth, as well as the derived spectrum at the center of the disk. We found that the electron temperature in the network is considerably lower than predicted by model F of Fontenla et al. (1993) and that of the cell interior considerably higher than predicted by model A. Depending upon the network/cell segregation scheme, the electron temperature difference between network and cell at τ=1 (100 GHz) is from ∼660 to ∼1550 K, compared to ∼3280 K predicted by the models; similarly, the Te ratio is from ∼1.10, to 1.24, against ∼1.55 of the model prediction. We also found that the network/cell Te(τ) curves diverge as τ decreases, indicating an increase of contrast with height and possibly a steeper temperature rise in the network than in the cell interior. **March 16, 2017**

High-resolution observations with ARTEMIS-JLS and the NRH III. Spectroscopy and imaging of fiber bursts

C.E. **Alissandrakis**, C. Bouratzis, A. Hillaris
A&A 627, A133 **2019**
https://arxiv.org/pdf/1906.03434.pdf
https://www.aanda.org/articles/aa/pdf/2019/07/aa35627-19.pdf
Aims. We study the characteristics of intermediate drift bursts (fibers) embedded in a large type IV event.
Methods. We used high sensitivity, low noise dynamic spectra obtained with the acousto-optic analyzer (SAO) of the ARTEMIS-JLS solar radiospectrograph, in conjunction with high time resolution images from the Nanc¸ay Radioheliograph (NRH) and EUV images from TRACE to study fiber bursts during the **July 14, 2000** large solar event. We computed both 2-dimensional and 1-dimensional images and applied high pass time filtering to the images and the dynamic spectrum in order to enhance the fiber-associated emission. For the study of the background continuum emission we used images averaged over several seconds.
Results. Practically all fibers visible in the SAO dynamic spectra are identifiable in the NRH images. Fibers were first detected after the primary energy release in a moving type IV, probably associated with the rapid eastward expansion of the flare and the post-flare loop arcade. We found that fibers appeared as a modulation of the continuum intensity with a root mean square value of the order of 10%. Both the fibers and the continuum were strongly circularly polarized in the ordinary mode sense, indicating plasma emission at the fundamental. We detected a number of discrete fiber emission sources along two ∼ 300 Mm long parallel stripes, apparently segments of large scale loops encompassing both the EUV loops and the CME-associated flux rope. We found cases of multiple fiber emissions appearing at slightly different positions and times; their consecutive appearance can give the impression of apparent motion with supra-luminal velocities. Images of individual fibers were very similar at 432.0 and 327.0 MHz. From the position shift of the sources and the time delays at low and high frequencies we estimated, for a well observed group of fibers, the exciter speed and the frequency scale length along the loops; we obtained consistent values from imaging and spectral data, supporting the whistler origin of the fiber emission. Finally we found that fibers in absorption and in emission are very similar, thus confirming that they are manifestations of the same wave train.
CESRA nugget #2367 Oct **2019** http://www.astro.gla.ac.uk/users/eduard/cesra/?p=2367

Modeling of the sunspot-associated microwave emission using a new method of DEM inversion

C. E. **Alissandrakis**, V. M. Bogod, T. I. Kaltman, S. Patsourakos, N. G. Peterova
Solar Phys. 294:23 **2018**
https://arxiv.org/pdf/1812.05751.pdf
We developed a method to compute the temperature and density structure along the line of sight by inversion of the differential emission measure (DEM), under the assumptions of stratification and hydrostatic equilibrium. We applied this method to the DEM obtained from AIA observations and used the results, together with potential extrapolations of the photosheric magnetic field, to compute the microwave emission of three sunspots, which we compared with observations from the RATAN-600 radio telescope and the Nobeyama Radioheliograph (NoRH). Our DEM based models reproduced very well the observations of the moderate-size spot on October 2011 and within 25% the data of a similar sized spot on March 2016, but predicted too low values for the big spot of April 14, 2016. The latter was better fitted by a constant conductive flux atmospheric model which, however, could not reproduce the peak brightness temperature of 4.7×106 K and the shape of the source at the NoRH frequency. We propose that these deviations could be due to low intensity non-thermal emission associated to a moving pore and to an opposite polarity light bridge. We also found that the double structure of the big spot at high RATAN-600 frequencies could be interpreted in terms of the

variation of the angle between the magnetic field and the line of sight along the sunspot. **October 10 2011, March 30 2016, April 14, 2016**

Center-to-limb observations of the Sun with ALMA
Implications for solar atmospheric models

C. E. **Alissandrakis** (Κ. Ε. Αλυσσανδράκης)1, S. Patsourakos (Σ. Πατσουράκος)1, A. Nindos (Α. Νίντος)1 and T. S. Bastian2
A&A 605, A78 (**2017**)
https://arxiv.org/pdf/1705.09008.pdf
Aims. We seek to derive information on the temperature structure of the solar chromosphere and compare these results with existing models.
Methods. We measured the center-to-limb variation of the brightness temperature, Tb, from ALMA full-disk images at two frequencies and inverted the solution of the transfer equation to obtain the electron temperature, Te as a function of optical depth, τ.
Results. The ALMA images are very similar to AIA images at 1600 Å. The brightness temperature at the center of the disk is 6180 and 7250 K at 239 and 100 GHz, respectively, with dispersions of 100 and 170 K. Plage regions stand out clearly in the 239/100 GHz intensity ratio, while faculae and filament lanes do not. The solar disk radius, reduced to 1 AU, is 961.1 ± 2.5″ and 964.1 ± 4.5″ at 239 and 100 GHz, respectively. A slight but statistically significant limb brightening is observed at both frequencies.
Conclusions. The inversion of the center-to-limb curves shows that Te varies linearly with the logarithm of optical depth for 0.34 <τ100 GHz< 12, with a slope dTe/ dlnτ = −608 K. Our results are 5% lower than predicted by the average quiet Sun model C of Fontenla et al. (1993, ApJ, 406, 319), but do not confirm previous reports that the mm-λ solar spectrum is better fitted with models of the cell interior. **December 16-20, 2015**,
CESRA highlight #1457 http://cesra.net/?p=1457

Structure and polarization of large spots with RATAN-600 and the NoRH

Costas **Alissandrakis**∗†1 , Vladimir Bogod‡2 , Tatyana Kaltman2 , Natalia Peterova2 , and Tatyana Kaltman
CESRA **2016** p.73
http://cesra2016.sciencesconf.org/conference/cesra2016/pages/CESRA2016_prog_abs_book_v3.pdf
In spite of their moderate spatial resolution, synoptic instruments such as the RATAN- 600 radio telescope and the Nobeyama Radioheliograph can resolve large sunspots. In this report we present some typical cases and we discuss the physical information that can be derived from the structure, in terms of the orientation of the magnetic field and the variation of physical conditions across the spot. We also present results on the structure of the largescale magnetic field of active regions form the analysis of multi-wavelength observations of circular polarization inversion. Finally we will provide information about the height of formation of sunspot-associated emission from observations of rising and setting sunspots.

Analysis of combined ARTEMIS-NRH observations of fine structures in type IV bursts

Costas **Alissandrakis**∗†1 , Alexandros Hillaris‡2 , Costas Bouratzis§2 , Athanasios Kontogeorgos , and Panagiotis Tsitsipis
CESRA Abstract **2016**
http://cesra2016.sciencesconf.org/conference/cesra2016/pages/CESRA2016_prog_abs_book_v1.pdf
We are conducting a systematic study of millisecond fine structures embedded in type IV bursts, based on the high sensitivity, high time resolution (10 ms) observations with the acoustico-optic receiver (SAO) of the ARTEMIS radio spectrograph. For a selected sample of our events we have analysed simultaneous observations with the Nan¸cay Radioheliograph (NRH), which can provide 2D positional information with a smaller time resoluton (125 ms). We computed 1D images using the EW and NS baselines of the NRH, in order to obtain the maximum resolution; this is about a factor of two better than the resolution of the 2D images. Here we will present results on spike and fiber bursts; we compare the position, the size and the brightnes temperature of the fine structure with those of the continuum source and we will discuss the physical implications of our results.

A tiny event producing an interplanetary type III burst

C. E. **Alissandrakis**, A. Nindos, S. Patsourakos, A. Kontogeorgos, P. Tsitsipis
A&A 582, A52 **2015**
http://arxiv.org/pdf/1507.08423v1.pdf

We investigate the conditions under which small scale energy release events in the low corona gave rise to strong interplanetary (IP) type III bursts. We analyze observations of three tiny events, detected by the Nan\c cay Radio Heliograph (NRH), two of which produced IP type IIIs. We took advantage of the NRH positioning information and of the high cadence of AIA/SDO data to identify the associated EUV emissions. We measured positions and time profiles of the metric and EUV sources. We found that the EUV events that produced IP type IIIs were located near a coronal hole boundary, while the one that did not was located in a closed magnetic field region. In all three cases tiny flaring loops were involved, without any associated mass eruption. In the best observed case the radio emission at the highest frequency (435 MHz) was displaced by ~55" with respect to the small flaring loop. The metric type III emission shows a complex structure in space and in time, indicative of multiple electron beams, despite the low intensity of the events. From the combined analysis of dynamic spectra and NRH images we derived the electron beam velocity as well as the height, ambient plasma temperature and density at the level of formation of the 160 MHz emission. From the analysis of the differential emission measure derived from the AIA images we found that the first evidence of energy release was at the footpoints and this was followed by the development of flaring loops and subsequent cooling. We conclude that even small energy release events can accelerate enough electrons to give rise to powerful IP type III bursts. The proximity of the electron acceleration site to open magnetic field lines facilitates the escape of the electrons into the interplanetary space. The offset between the site of energy release and the metric type III location warrants further investigation.
5 July 2011

Microwave and EUV Observations of an Erupting Filament and Associated Flare and CME

Alissandrakis, C. E.; Kochanov, A. A.; Patsourakos, S.; Altyntsev, A. T.; Lesovoi, S. V.; Lesovoya, N. N.
E-print, Sept, **2013**; PASJ
http://arxiv.org/pdf/1309.1703v1.pdf

A filament eruption was observed with the Siberian Solar Radio Telescope (SSRT) on **June 23 2012**, starting around 06:40 UT, beyond the West limb. The filament could be followed in SSRT images to heights above 1 Rs, and coincided with the core of the CME, seen in LASCO C2 images. We discuss briefly the dynamics of the eruption: the top of the filament showed a smooth acceleration up to an apparent velocity of 1100 km/s. Images behind the limb from STEREO-A show a two ribbon flare and the interaction of the main filament, located along the primary neutral line, with an arch-like structure, oriented in the perpendicular direction. The interaction was accompanied by strong emission and twisting motions. The microwave images show a low temperature component, a high temperature component associated with the interaction of the two filaments and another high temperature component apparently associated with the top of flare loops. We computed the differential emission measure from the high temperature AIA bands and from this the expected microwave brightness temperature; for the emission associated with the top of flare loops the computed brightness was 35% lower than the observed.

Microwave and EUV Observations of an Erupting Filament and Associated Flare and Coronal Mass Ejections

C. E. **Alissandrakis**, A. A. Kochanov, S. Patsourakos, A. T. Altyntsev, S. V. Lesovoi, N. N. Lesovoya
Publ. Astron. Soc. Japan 65, No SP1, S8 [10 pages] (**2013**)
http://pasj.asj.or.jp/v65/sp1/65S008/65S008.pdf

A filament eruption was observed with the Siberian Solar Radio Telescope (SSRT) on **2012 June 23**, starting at around 06:40 UT, beyond the west limb. The filament could be followed in SSRT images to heights above 1R˙, and coincided with the core of the CME, seen in LASCO C2 images. We briefly discuss the dynamics of the eruption: the top of the filament showed a smooth acceleration up to an apparent velocity of _1100 km s_1. Images behind the limb from STEREO-A show a two-ribbon flare and the interaction of the main filament, located along the primary neutral line, with an arch-like structure, oriented in the perpendicular direction. The interaction was accompanied by strong emission and twisting motions. The microwave images show a low-temperature component, a high-temperature component associated with the interaction of the two filaments and another high-temperature component apparently associated with the top of flare loops. We computed the differential emission measure from the high-temperature AIA bands and from this the expected microwave brightness temperature; for emission associated with the top of the flare loops, the computed brightness was 35% lower than the observed value.

Observation of Reconstructable Radio Emission Coincident with an X-Class Solar Flare in the Askaryan Radio Array Prototype Station

P. **Allison**, S. Archambault, J. Auffenberg, R. Bard, J. J. Beatty, ...

2018

https://arxiv.org/pdf/1807.03335.pdf

The Askaryan Radio Array (ARA) reports an observation of radio emission coincident with the "Valentine's Day" solar flare on **Feb. 15th, 2011** in the prototype "Testbed" station. We find ∼2000 events that passed our neutrino search criteria during the 70 minute period of the flare, all of which reconstruct to the location of the sun. A signal analysis of the events reveals them to be consistent with that of bright thermal noise correlated across antennas. This is the first natural source of radio emission reported by ARA that is tightly reconstructable on an event-by-event basis. The observation is also the first for ARA to point radio from individual events to an extraterrestrial source on the sky. We comment on how the solar flares, coupled with improved systematic uncertainties in reconstruction algorithms, could aid in a mapping of any above-ice radio emission, such as that from cosmic-ray air showers, to astronomical locations on the sky.

Observations of coronal holes with the Siberian Radioheliograph

Altyntsev, Alexander , Globa, Mariia Meshalkina, Nataliya ; Sych, Robert

Solar-Terrestrial Physics, vol. 10, issue 3, pp. 3-10, **2024**

https://naukaru.ru/en/storage/download/169702

Multi-wavelength observations of a coronal hole (CH) with two-dimensional spatial resolution have been made for the first time in the frequency range from 2.8 to 12 GHz. At frequencies below 6 GHz, the average brightness of the hole is 1.5 times lower than the brightness level of the quiet Sun. The distribution of radio brightness over the hole is inhomogeneous: the ratio of maximum to minimum brightness temperatures falls from several times at low frequencies to tenths of fractions at the upper received frequencies. At frequencies above 6 GHz, the temperature contrast between the CH and regions of the quiet Sun is small. Within the CH, there are compact sources that are bright relative to the quiet Sun. In general, observations of CHs with SRH are promising both for the research into the nature of CHs and for the applied problems of forecasting solar wind characteristics. **April 25, 2023**

CESRA #3879 2024 https://www.astro.gla.ac.uk/users/eduard/cesra/?p=3879

Temporal and spatial association between microwaves and type III bursts in the upper corona

A. T. **Altyntsev**1, H. Reid2, N. S. Meshalkina1, I. I. Myshyakov1 and D. A. Zhdanov1

A&A 671, A30 (**2023**)

https://www.aanda.org/articles/aa/pdf/2023/03/aa44599-22.pdf

One of the most important tasks in solar physics is the study of particles and energy transfer from the lower corona to the outer layers of the solar atmosphere. The most sensitive methods for detecting fluxes of non-thermal electrons in the solar atmosphere is observing their radio emission using modern large radioheliographs. We analyzed joint observations from the **13 April 2019** event observed by LOw-Frequency ARray (LOFAR) at meter wavelengths, and the Siberian Radio Heliograph (SRH) and the Badary Broadband Microwave Spectropolarimeter (BBMS) spectropolarimeter in microwaves performed at the time of the second PSP perihelion. During a period without signatures of non-thermal energy release in X-ray emission, numerous type III and/or type J bursts were observed. During the same two hours we observed soft X-ray brightenings and the appearance of weak microwave emission in an abnormally narrow band around 6 GHz. At these frequencies the increasing flux is well above the noise level, reaching 9 sfu. In the LOFAR dynamic spectrum of 53−80 MHz a region is found that lasts about an hour whose emission is highly correlated with 6 GHz temporal profile. The flux peaks in the meter waves are well correlated with extreme UV (EUV) emission variations caused by repeated surges from the bright X-point. We argue that there is a common source of non-thermal electrons located in the tail of the active region, where two loop systems of very different sizes interacted. The frequencies of type III and/or type J bursts are in accordance with large loop heights around 400 Mm, obtained by the magnetic field reconstruction. The microwave coherent emission was generated in the low loops identified as bright X-ray points seen in soft X-ray and EUV images, produced by electrons with energies several tens of keV at about twice the plasma frequency.

CESRA #3509 **2023** https://www.astro.gla.ac.uk/users/eduard/cesra/?p=3509

Double peak quasi-periodic pulsations in a circular-ribbon flare

A. T. **Altyntsev**, N. S. Meshalkina, R. A. Sych and D. Y. Kolotkov

A&A 663, A149 (**2022**)
https://www.aanda.org/articles/aa/pdf/2022/07/aa43144-22.pdf
We study quasi-periodic pulsations (QPPs) during the impulsive phase of the C8.3 flare SOL**2002-08-06**T01:43. The shape of an extended 5.7 GHz source is similar to a tadpole with the head located above the region of a negative magnetic polarity, surrounded by positive polarity patches and with a remote tail source. The flare configuration includes bright extreme ultraviolet (EUV) ropes with footpoints near the boundary of the negative magnetic field region and it can be identified as a circular ribbon flare. We use simultaneous observations carried out by the Siberian Solar Radio Telescope at 5.7 GHz, the Nobeyama Radio Heliograph (NoRH) at 17 and 34 GHz, the Reuven Ramaty High Energy Solar Spectroscopic Imager (RHESSI)/HXR, and the Transition Region and Coronal Explorer (TRACE) imaging in the extreme ultraviolet. The flare HXR emission is produced by a compact source located at the south periphery of the Negative Magnetic field Region (NMR). The QPPs are observed during a one-minute interval after the start of the impulsive phase, when this HXR source appeared. The remote source is detected on the variation maps of the of the brightness temperature at 17 GHz and is located at the end of tadpole tail about 60 arcsec eastward. More than a dozen cotemporal HXR and microwave pulses with timescales from 1.5 s up to about 8 s were observed in the flare kernel. At 5.7 GHz, the pulses are more prominent near the remote source where they are highly polarized and generated by the electron beams propagating from the flare kernel. The main tone of the QPP periodicity corresponds to the oscillations with a period of 8 s and is accompanied by the variations in the hardness of nonthermal electrons, that is, in the efficiency of the acceleration mechanism. The second intensity harmonic (about a 3-s period) appears due to a double peak structure of the QPP event. Such pulse shapes suggest oscillations of the current sheet during the loop coalescence as a modulation mechanism of the flare energy release. **6 August 2002**

Background Microwave Emission and Microflares in Young Active Region 12635

Alexander T. **Altyntsev**, Nataliia S. Meshalkina, Anastasiya Ya. Fedotova, and Ivan I. Myshyakov
2020 ApJ 905 149
https://doi.org/10.3847/1538-4357/abc54f
The goal of this work is to study the atmospheric heating above isolated AR 12635 during a period in which a quasistationary increase in microwave and soft X-ray emission is combined with a series of B- and C-class microflares. Analysis of photospheric vector magnetograms showed that an increase in the SXR brightness lasting 14 hours was observed during the simplification of the magnetic structure and the growth of vertical currents in the head part of the active region. A long-term increase of SXR and microwave emission occurred when the total unsigned vertical current exceeded the critical value and coincided in time with the increased level of the emission measure calculated from the GOES X-ray data. Against the background of quasistationary emission, microflares lasting 6–10 minutes occurred. In the hard X-ray range, bursts are recorded with RHESSI channels up to 25 keV. In microwave emission, pulsed and smooth components are distinguished during microflares. The first component was recorded in the 4.5–7.5 GHz range at the beginning of microflares and it is generated by a small population of relativistic electrons by the gyrosychrotron mechanism. The smooth component of the bursts dominated at 17 GHz and was emitted by bremsstrahlung. It is shown that the sources of quasistationary emission and microflares coincide with each other and with the bremsstrahlung source calculated from the differential emission measure obtained from the EUV maps. Coronal magnetic field reconstruction shows that the release of energy on both timescales occurs in a stably existing bundle of magnetic field lines. **~10 Feb 2017**

Rapid Variability in the SOL2011-08-04 Flare: Implications for Electron Acceleration

Alexander T. **Altyntsev**, Nataliia S. Meshalkina, Alexandra L. Lysenko, Gregory D. Fleishman
ApJ **883** 38 **2019**
https://arxiv.org/pdf/1909.03593.pdf
https://doi.org/10.3847/1538-4357/ab3808
Particle acceleration in solar flares remains an outstanding problem in solar physics. It is yet unclear which of the acceleration mechanisms dominates and how exactly is the excessive magnetic energy transferred to the nonthermal and other forms of energy. We emphasize, that the ultimate acceleration mechanism must be capable of efficiently working in the most extreme conditions, such as the shortest detected time scales and the highest acceleration efficiency. Here we focus on detailed multiwavelength analysis of a very initial phase of the SOL**2011-08-04** flare, which demonstrated prominent short subpeaks of nonthermal emission during filament eruption associated with the flare. We demonstrate that the three-dimensional configuration of the flare, combined with timing and spectral behavior of the rapidly varying component, put very stringent constraints on the acceleration regime. Specifically, the rapid subpeaks are generated by short injections of nonthermal electrons with a reasonably hard, single power-law spectrum and a relatively narrow spread of pitch-angles along the mean magnetic field. The acceleration site is a compact volume located near the top of

extended coronal loop(s). The electrons are accelerated up to several hundreds of keV promptly, with the characteristic acceleration time shorter than 50 ms. We show, that these properties are difficult to reconcile with widely adopted stochastic acceleration models, while the data inescapably require acceleration by a super-Dreicer electric field, whether regular or random.

Modern instrumentation. Advanced data analysis techniques. Radioheliographs

A. **Altyntsev** **2017**
http://en.iszf.irk.ru/images/e/ef/Alexander_Altyntsev_20170920_keynote.pdf

Flare SOL2012-07-06: On the Origin of the Circular Polarization Reversal Between 17 GHz and 34 GHz

A. **Altyntsev**, N. Meshalkina, I. Myshyakov, V. Pal'shin, G. Fleishman
Solar Physics September **2017**, 292:137
https://arxiv.org/pdf/1709.06252.pdf
The new generation of multiwavelength radioheliographs with high spatial resolution will employ microwave imaging spectropolarimetry to recover flare topology and plasma parameters in the flare sources and along the wave propagation paths. The recorded polarization depends on the emission mechanism and emission regime (optically thick or thin), the emitting particle properties, and propagation effects. Here, we report an unusual flare, SOL2012-07-06T01:37, whose optically thin gyrosynchrotron emission of the main source displays an apparently ordinary mode sense of polarization in contrast to the classical theory that favors the extraordinary mode. This flare produced copious nonthermal emission in hard X-rays and in high-frequency microwaves up to 80 GHz. It is found that the main flare source corresponds to an interaction site of two loops with greatly different sizes. The flare occurred in the central part of the solar disk, which allows reconstructing the magnetic field in the flare region using vector magnetogram data. We have investigated the three possible known reasons of the circular polarization sense reversal – mode coupling, positron contribution, and the effect of beamed angular distribution. We excluded polarization reversal due to contribution of positrons because there was no relevant response in the X-ray emission. We find that a beam-like electron distribution can produce the observed polarization behavior, but the source thermal density must be much higher than the estimate from to the X-ray data. We conclude that the apparent ordinary wave emission in the optically thin mode is due to radio wave propagation across the quasi-transverse (QT) layer. The abnormally high transition frequency (above 35 GHz) can be achieved reasonably low in the corona where the magnetic field value is high and transverse to the line of sight. This places the microwave source below this QT layer, i.e. very low in the corona.
CESRA Highlight #1578 Oct **2017** http://cesra.net/?p=1578

Sources of Quasi-Periodic Pulses in the 18 August 2012 Flare

A. **Altyntsev**, N. Meshalkina, H. Meszarosova, M. Karlicky, V. Palshin, S. Lesovoi
Solar Physics, Volume 291, Issue 2, pp 445-463 **2016**
http://arxiv.org/pdf/1601.02332v1.pdf
We analyzed spatial and spectral characteristics of quasi-periodic pulses (QPP) for the **18 August 2012** limb are, using new data from a complex of spectral and imaging instruments developed by the Siberian Solar Radio Telescope team and the Wind/Konus gamma-ray spectrometer. A sequence of broadband pulses with periods of approximately ten seconds were observed in X-rays at energies between 25 keV and 300 keV, and in microwaves at frequencies from a few GHz up to 34 GHz during an interval of one minute. The QPP X-ray source was located slightly above the limb where the south legs of large and small EUV loop systems were close to each other. Before the QPPs the soft X-ray emission and the Ramaty High Energy Solar Spectroscopic Imager signal from the energy channels below 25 keV were gradually arising for several minutes at the same location. It was found that each X-ray pulse showed the soft-hard-soft behavior. The 17 and 34 GHz microwave source were at footpoints of the small loop system and the source emitting in the 4.2 {7.4 GHz band in the large one. The QPPs were probably generated by modulation of acceleration processes in the energy release site. Analyzing radio spectra we determined the plasma parameters in the radio sources. The microwave pulses could be explained by relatively weak variations of the spectrum hardness of emitting electrons.

THERMAL TO NONTHERMAL ENERGY PARTITION AT THE EARLY RISE PHASE OF SOLAR FLARES

Alexander A. **Altyntsev**1, Gregory D. Fleishman2,3, Sergey V. Lesovoi1, and Nataliia S. Meshalkina
2012 ApJ 758 138
In some flares, the thermal component appears much earlier than the nonthermal component in the X-ray range. Using sensitive microwave observations, we revisit this finding made by Battaglia et al. based on a thorough analysis of

RHESSI data. We have found that nonthermal microwave emission produced by accelerated electrons with energy of at least several hundred keV appears as early as the thermal soft X-ray emission, indicating that the electron acceleration takes place at the very early flare phase. The non-detection of the hard X-rays at that early stage of the flares is thus an artifact of a limited RHESSI sensitivity. In all of the considered events, the microwave emission intensity increases at the early flare phase. We found that either thermal or nonthermal gyrosynchrotron emission can dominate the low-frequency (optically thick) part of the microwave spectrum below the spectral peak occurring at 3-10 GHz. In contrast, the high-frequency optically thin part of the spectrum is always formed by the nonthermal, accelerated electron component, whose power-law energy spectrum can extend up to a few MeV at this early flare stage. This means that even though the total number of accelerated electrons is small at this stage, their nonthermal spectrum is fully developed. This implies that an acceleration process of available seed particles is fully operational. While creation of this seed population (the process commonly called "injection" of the particles from the thermal pool into the acceleration process) has a rather low efficiency at this stage, the plasma heating efficiency is high. This imbalance between the heating and acceleration (in favor of the heating) is difficult to reconcile within most of available flare energization models. Being reminiscent of the trade off between the Joule heating and runaway electron acceleration, it puts additional constraints on the electron injection into the acceleration process. As a byproduct of this study, we demonstrate that for those cases when the optically thick part of the radio spectrum is dominated by the thermal contribution, the microwave spectral data yield reliable estimates of the magnetic field and source area at the early flare phase.

Radioheliograph Observations of Microwave Bursts with Zebra Structures

A. T. **Altyntsev**, S. V. Lesovoi, N. S. Meshalkina, R. A. Sych and Y. Yan

Solar Physics, Volume 273, Number 1, 163-177, **2011**

The so-called zebra structures in radio dynamic spectra, specifically their frequencies and frequency drifts of emission stripes, contain information on the plasma parameters in the coronal part of flare loops. This paper presents observations of zebra structures in a microwave range. Dynamic spectra were recorded by Chinese spectro-polarimeters in the frequency band close to the working frequencies of the Siberian Solar Radio Telescope. The emission sources are localized in the flare regions, and we are able to estimate the plasma parameters in the generation sites using X-ray data. The interpretation of the zebra structures in terms of existing theories is discussed. The conclusion has been arrived at that the preferred generation mechanism of zebra structures in the microwave range is the conversion of plasma waves to electromagnetic emission on the double plasma resonance surfaces distributed across a flare loop.

10 Apr 2001, 21 Aug 2002, 17 September 2002, 5 Jan 2003, 18 Mar 2003, 29 May 2003

Broadband Microwave Burst Produced by Electron Beams

A.T. **Altyntsev**, G.D. Fleishman, G.-L. Huang and V.F. Melnikov
BBSO, #1357, 2008; The Astrophysical Journal, Vol. 677, No. 2: 1367-1377, **2008**.
http://solar.njit.edu/preprints/altyntsev1357.pdf
http://www.journals.uchicago.edu/doi/pdf/10.1086/528841
This paper explores the fact that the electron beams moving oblique to the magnetic field or along the field with some angular scatter around the beam propagation direction can generate microwave continuum bursts via gyrosynchrotron mechanism. The characteristics of the microwave bursts produced by beams differ from those in case of isotropic or loss-cone distributions, which suggests a new tool for quantitative diagnostics of the beams in the solar corona. To demonstrate the potentiality of this tool, we analyze here a radio burst occurred during an impulsive flare 1B / M6.7 on 10 March 2001

Microwave Type III-Like Bursts as Possible Signatures of Magnetic Reconnection

A. T. **Altyntsev**, V. V. Grechnev, N. S. Meshalkina, Y. Yan
Solar Phys., 242(1-2), Page: 111 – 123, **2007**.

Tuning the Exo-Space Weather Radio for Stellar Coronal Mass Ejections

Julián D. **Alvarado-Gómez** (1 and 2), Jeremy J. Drake (2), Federico Fraschetti (2 and 3), Cecilia Garraffo (2 and 4), Ofer Cohen (5), Christian Vocks (1), Katja Poppenhäger (1), Sofia P. Moschou (2), Rakesh K. Yadav (6), Ward B. Manchester IV (7)
ApJ **2020**
https://arxiv.org/pdf/2004.05379.pdf
Coronal mass ejections (CMEs) on stars other than the Sun have proven very difficult to detect. One promising pathway lies in the detection of type II radio bursts. Their appearance and distinctive properties are associated with the development of an outward propagating CME-driven shock. However, dedicated radio searches have not been able to identify these transient features in other stars. Large Alfvén speeds and the magnetic suppression of CMEs in active stars have been proposed to render stellar eruptions "radio-quiet". Employing 3D magnetohydrodynamic simulations, we study here the distribution of the coronal Alfvén speed, focusing on two cases representative of a young Sun-like star and a mid-activity M-dwarf (Proxima Centauri). These results are compared with a standard solar simulation and used to characterize the shock-prone regions in the stellar corona and wind. Furthermore, using a flux-rope eruption model, we drive realistic CME events within our M-dwarf simulation. We consider eruptions with different energies to probe the regimes of weak and partial CME magnetic confinement. While these CMEs are able to generate shocks in the corona, those are pushed much farther out compared to their solar counterparts. This drastically reduces the resulting type II radio burst frequencies down to the ionospheric cutoff, which impedes their detection with ground-based instrumentation**. Feb-March 2011 (CR 2107)**

Properties of High-Energy Solar Particle Events Associated with Solar Radio Emissions

Dheyaa **Ameri**, Eino Valtonen, Silja Pohjolainen
Solar Physics September **2019**, 294:122
sci-hub.se/10.1007/s11207-019-1512-9
We have analysed 58 high-energy proton events and 36 temporally related near-relativistic electron events from the years 1997 – 2015 for which the velocity dispersion analysis of the first-arriving particles gave the apparent path lengths between 1 and 3 AU. We investigated the dependence of the characteristics of the proton events on the associations of type II, III, and IV radio bursts. We also examined the properties of the soft X-ray flares and coronal mass ejections associated with these events. All proton events were associated with decametric type III radio bursts, while type IV emission was observed only in the meter wavelengths in some of the events (32/58). Almost all proton events (56/58) were associated with radio type II bursts: 11 with metric (m) type II only, 11 with decametric–hectometric (DH) only, and 34 with type II radio bursts at both wavelength ranges. By examining several characteristics of the proton events, we discovered that the proton events can be divided into two categories. The characteristics of events belonging to the same category were similar, while they significantly differed between events in different categories. The distinctive factors between the categories were the wavelength range of the associated type II radio emission and the temporal relation of the proton release with respect to the type II onset. In Category 1 are the events which were associated with only metric type II emission or both m and DH type II and the release time of protons was before the DH type II onset (18/56 events). Category 2 consists of the events which were associated with only DH type II emission or both m and

DH type II and the protons were released at or after the DH type II onset (31/56 events). For seven of the 56 events we were not able to determine a definite category due to timing uncertainties. The events in Category 1 had significantly higher intensity rise rates, shorter rise times, lower release heights, and harder energy spectra than Category 2 events. Category 1 events also originated from magnetically well-connected regions and had only small time differences between the proton release times and the type III onsets. The soft X-ray flares for these events had significantly shorter rise times and durations than for Category 2 events. We found 36 electron events temporally related to the proton events, which fulfilled the same path length criterion as the proton events. We compared the release times of protons and electrons at the Sun, and discovered that in 19 of the 36 events protons were released almost simultaneously (within ±7±7 minutes) with the electrons, in 16 events protons were released later than the electrons, and in one event electrons were released after the protons. The simultaneous proton and electron events and the delayed proton events did not unambiguously fall in the two categories of proton events, although most of the events in which the protons were released after the electrons belonged to Category 2. We conclude that acceleration of protons in Category 1 events occurred low in the corona, either by CME-driven shocks or below the CMEs in solar flares or in CME initiation related processes. It seems plausible that protons in Category 2 events were accelerated by CME-driven shocks high in the solar corona. Large delays of protons with respect to type III onsets in the events where protons were released after the electrons suggest late acceleration or release of protons close to the Sun, but the exact mechanism causing the delay remained unclear. **18 June 2000, 11 April 2004**

Table 2 Event list with proton VDA results and onset times of associated solar radio emissions, soft X-ray flares, and CMEs.

Table 3 VDA results for the 36 solar electron events associated with the proton events

Solar radio emissions and ultralight dark matter **Review**

Haipeng **An**, Shuailiang Ge, Jia Liu

An invited review for the special issue "Solar Radio Emissions" in the journal Universe **2023**

https://arxiv.org/pdf/2304.01056.pdf

Ultralight axions and dark photons are well-motivated dark matter candidates. Inside the plasma, once the mass of ultralight dark matter candidates equals the plasma frequency, they can resonantly convert into electromagnetic waves, due to the coupling between the ultralight dark matter particles and the standard model photons. The converted electromagnetic waves are monochromatic. In this article, we review the development of using radio detectors to search for ultralight dark matter conversions in the solar corona and solar wind plasma.

Linear unstable whistler eigenmodes excited by a finite electron beam

Xin **An**, Jacob Bortnik, Bart Van Compernolle

Physics of Plasmas 26, 082114 (**2019**)

https://arxiv.org/pdf/1908.06961.pdf

sci-hub.se/10.1063/1.5097837

Electron beam-generated whistler waves are widely found in the Earth's space plasma environment and are intricately involved in a number of phenomena. Here we study the linear growth of whistler eigenmodes excited by a finite gyrating electron beam, to facilitate the interpretation of relevant experiments on beam-generated whistler waves in the Large Plasma Device at UCLA. A linear instability analysis for an infinite gyrating beam is first performed. It is shown that whistler waves are excited through a combination of cyclotron resonance, Landau resonance and anomalous cyclotron resonance, consistent with our experimental results. By matching the whistler eigenmodes inside and outside the beam at the boundary, a linear growth rate is obtained for each wave mode and the corresponding mode structure is constructed. These eigenmodes peak near the beam boundary, leak out of the beam region and decay to zero far away from the beam.

Record-breaking coronal magnetic field in solar active region 12673

Sergey A. **Anfinogentov**, Alexey G. Stupishin, Ivan I. Mysh'yakov, Gregory D. Fleishman

2019 *ApJL* **880** L29

https://arxiv.org/pdf/1907.06398.pdf

sci-hub.se/10.3847/2041-8213/ab3042

At the Sun, the strongest magnetic fields are routinely detected at dark sunspots. The magnitude of the field is typically about 3000 G, with only a few exceptions that reported the magnetic field in excess of 5000 G. Given that the magnetic field decreases with height in the solar atmosphere, no coronal magnetic field above ~2000 G was ever reported. Here, we present imaging microwave observations of an anomalously strong magnetic field of about 4000 G at the base of the corona in solar active region NOAA 12673 on **06 September 2017**. Combining the photospheric vector measurements

of the magnetic field and the coronal probing, we created and validated a nonlinear force-free field coronal model, with which we quantify the record-breaking coronal magnetic field at various coronal heights.
Erratum **2020** ***ApJL*** 898 **L58** https://iopscience.iop.org/article/10.3847/2041-8213/ab93ce/pdf

Electromagnetic Emission Produced by Three-wave Interactions in a Plasma with Continiously Injected Counterstreaming Electron Beams

V. V. **Annenkov**, E. P. Volchok, I. V. Timofeev
ApJ **904** 88 **2020**
https://arxiv.org/pdf/2010.06565.pdf
https://doi.org/10.3847/1538-4357/abbef2
Three-wave interactions between Langmuir and electromagnetic waves in plasma with unstable electron flows are believed to be the main cause for type II and III solar radio emissions. The narrow band of type II bursts requires to assume that this radiation is generated in some local regions of shock fronts traveling in the solar corona, where the specific conditions for the enhancement of electromagnetic emissions near the plasma frequency harmonics are created. The reason for such enhancement at the second harmonic may be the formation of counter-streaming electron beams. There are different opinions in literature on whether the second harmonic electromagnetic emission in the presence of an additional beam can be efficient enough to markedly dominate emissions produced by a single beam. In the present paper, we carry out particle-in-cell simulations of the collision of two symmetric electron beams in plasma with open boundary conditions and show that the efficiency of beam-to-radiation power conversion can be significantly increased compared to models with periodic boundary conditions and reach the level of a few percent if three-wave interactions with electromagnetic waves near the second harmonic of the plasma frequency becomes available for the most unstable oblique beam driven modes.
CESRA #2778 Jan **2021** http://www.astro.gla.ac.uk/users/eduard/cesra/?p=2778

High-resolution observations with ARTEMIS/JLS and the NRH: IV. Imaging spectroscopy of spike-like structures near the front of type-II bursts

S. **Armatas**, C. Bouratzis, A. Hillaris, C.E. Alissandrakis, P. Preka-Papadema, A. Kontogeorgos, P. Tsitsipis, X. Moussas
A&A 659, A198 **2022**
https://arxiv.org/pdf/2201.07832.pdf
https://www.aanda.org/articles/aa/pdf/2022/03/aa42406-21.pdf
https://doi.org/10.1051/0004-6361/202142406
Narrowband bursts (spikes) appear on dynamic spectra from microwave to decametric frequencies. They are believed to be manifestations of small-scale energy release through magnetic reconnection. We study the position of the spike-like structures relative to the front of type-II bursts and their role in the burst emission. We used high-sensitivity, low-noise dynamic spectra obtained with the acousto-optic analyzer (SAO) of the ARTEMIS-JLS radiospectrograph, in conjunction with images from the Nançay Radioheliograph (NRH) in order to study spike-like bursts near the front of a type-II radio burst during the November 3, 2003 extreme solar event. The spike-like emission in the dynamic spectrum was enhanced by means of high-pass-time filtering. We identified a number of spikes in the NRH images. Due to the lower temporal resolution of the NRH, multiple spikes detected in the dynamic spectrum appeared as single structures in the images. These spikes had an average size of ~200" and their observed brightness temperature was 1.4-5.6x10^9K, providing a significant contribution to the emission of the type-II burst front. At variance with a previous study on the type-IV associated spikes, we found no systematic displacement between the spike emission and the emission between spikes. At 327.0 MHz, the type II emission was located about 0.3 RSUN above the pre-existing continuum emission, which, was located 0.1 RSUN above the western limb. This study indicates that the spike-like chains aligned along the type II burst MHD shock front are not a perturbation of the type II emission, as in the case of type IV spikes, but a manifestation of the type II emission itself. The preponderance of these chains, together with the lack of isolated structures or irregular clusters, points towards some form of small-scale magnetic reconnection, organized along the type-II propagating front**. 3 Nov 2003**

Detection of spike-like structures near the front of type-II bursts

S. **Armatas**, C. Bouratzis, A. Hillaris, C.E. Alissandrakis, P. Preka-Papadema, X. Moussas, E. Mitsakou, P. Tsitsipis, A. Kontogeorgos
A&A 624, A76 **2019**
https://arxiv.org/pdf/1902.10617.pdf
https://doi.org/10.1051/0004-6361/201834982

Aims. We examine high time resolution dynamic spectra for fine structures in type II solar radio bursts
Methods. We used data obtained with the acousto-optic spectrograph (SAO) receiver of the Artemis-JLS (ARTEMIS-IV) solar radio spectrograph in the 450-270 MHz range at 10 ms cadence and identified more than 600 short, narrowband features. Their characteristics, such as instantaneous relative bandwidth and total duration were measured and compared with those of spikes embedded in type IV emissions.
Results. Type II associated spikes occur mostly in chains inside or close to the slowly drifting type II emission. These spikes coexist with herringbone and pulsating structures. Their average duration is 96 ms and their average relative bandwidth 1.7%. These properties are not different from those of type IV embedded spikes. It is therefore possible that they are signatures of small-scale reconnection along the type II shock front. **2003-11-03, 2004-02-04, 2004-07-13, 2011-08-09**
CESRA #2247 July **2019** http://www.astro.gla.ac.uk/users/eduard/cesra/?p=2247

Mid-term Periodicities in Solar Radio Emission Corresponding to Sunspot Number During Solar Cycle 23

Mahender **Aroori**, Panditi Vemareddy, Partha Chowdhury & Ganji Yellaiah
Solar Physics volume 296, Article number: 43 (**2021**)
https://link.springer.com/content/pdf/10.1007/s11207-021-01793-6.pdf
https://doi.org/10.1007/s11207-021-01793-6
We present a systematic time-series analysis of solar radio emission in nine different frequencies to compare with that of daily sunspot number (SSN) during Solar Cycle 23 (1996–2009). Owing to the contribution from quiet-sun emission, the total solar fluxes in microwaves do not decrease as significantly as the sunspot number does during 2006 to 2009. Lomb–Scargle (LS) and wavelet analysis techniques are employed to infer the various periodicities present in the time-series data. False alarm probability (FAP) levels are estimated by the use of background mean power spectrum in the global wavelet spectrum. The LS periodogram contains resolved period peaks, some of which are below FAP levels, for example a well-known rotational period. These peaks are assessed with global significance levels of the wavelet analysis. In all the data sets, the period for solar rotational modulation (26–31 days) is present. The periodogram for the SSN presents Riéger type periods (130–180 days), mid-term periods (300–400 days) and long-term periods (430–850 days). These periods in north and south are not similar, especially long term periods are missing in SSN data of the southern hemisphere. Corresponding to the SSN periodicities, Riéger and near Riéger type of oscillations (130–180 days), quasi-biennial periodicities in the range of 1.2 to 3 years were detected in the time-series data of radio frequencies. Several of these detected periods fall in the range of the periods that are suggested to be connected with magneto-Rossby wave spherical harmonics. Our analysis found reduced power levels in the LS periodograms of low frequencies because of the fact that these low frequency emissions originate higher up in the corona with diminishing contrast to small scale structures.

Order out of randomness: Self-organization processes in astrophysics **Review**

Aschwanden,M.J., Scholkmann,F., Bethune,W., Schmutz,W., Abramenko,W., Cheung,M.C.M., Mueller,D., Benz,A.O., Chernov,G., Kritsuk,A.G., Scargle,J.D., Melatos,A., Wagoner,R.V., Trimble,V., Green,W.
Space Science Reviews 214:55, **2018**
https://link.springer.com/content/pdf/10.1007%2Fs11214-018-0489-2.pdf
Self-organization is a property of dissipative nonlinear processes that are gov- erned by a global driving force and a local positive feedback mechanism, which creates regular geometric and/or temporal patterns, and decreases the entropy locally, in contrast to random processes. Here we investigate for the first time a comprehensive number of (17) self-organization processes that operate in planetary physics, solar physics, stellar physics, galactic physics, and cosmology. Self-organizing systems create spontaneous ?order out of randomness?, during the evolution from an initially disordered system to an ordered quasistationary system, mostly by quasi-periodic limit-cycle dynamics, but also by harmonic (me-chanical or gyromagnetic) resonances. The global driving force can be due to gravity, elec- tromagnetic forces, mechanical forces (e.g., rotation or differential rotation), thermal pres- sure, or acceleration of nonthermal particles, while the positive feedback mechanism is of- ten an instability, such as the magneto-rotational (Balbus-Hawley) instability, the convective (Rayleigh-B?nard) instability, turbulence, vortex attraction, magnetic reconnection, plasma condensation, or a loss-cone instability. Physical models of astrophysical self-organization processes require hydrodynamic, magneto-hydrodynamic (MHD), plasma, or N-body simu- lations. Analytical formulations of self-organizing systems generally involve coupled differ- ential equations with limit-cycle solutions of the Lotka-Volterra or Hopf-bifurcation type.
3 Solar Physics 3.5 Quasi-Periodic Radio Bursts 3.6 Zebra Radio Bursts

The Late Gradual Phase of Large Flares: The Case of November 3, 2003

H. **Aurass**
Solar Phys., **2014**
http://www.aip.de/mitglieder/haurass/paper/the-late-gradual-phase-of-solar-flares/view
The hard X-ray time profiles of most solar eruptive events begin with an impulsive phase which may be followed by a late gradual phase. In a recent article (Aurass et al. 2013, Astron. Astrophys. 555, A40) we analyzed the impulsive phase of the solar eruptive event on November 3, 2003 in radio and X-ray emission. We find evidence of magnetic breakout reconnection using the radio diagnostic of the common effect of the flare current sheet and, at heights of $\pm 0.4\ R_\odot$, of a coronal breakout current sheet (a source site that we call X). In this article we investigate the radio emission during the late gradual phase of the previously analyzed event. The work is based on 40–400 MHz dynamic spectra (Radio Spectrograph Observatorium Tremsdorf, Leibniz Institut f.ur Astrophysik Potsdam, AIP) combined with radio images obtained by the French Nan.cay Multifrequency Radio Heliograph (NRH) of the Observatoire de Paris, Meudon. Additionally we use Ramaty High Energy Solar Spectroscopic Imager (RHESSI) hard X-ray (HXR) flux records, and Solar and Heliospheric Observatory (SOHO) Large Angle and Spectrometric Coronagraph (LASCO) and Extreme ultraviolet Imaging Telescope (EIT) images.
The analysis shows that the late gradual phase is subdivided into two distinct stages. Stage 1 (here lasting five minutes) is restricted to reoccurring radio emission at source site X. We observe plasma emission and an azimuthally moving source (from X toward the NE; speed _1200kms-1) at levels radially ordered against the undisturbed coronal density gradient. These radio sources mark the lower boundary of an overdense region with a huge azimuthal extent. By the end of its motion, the source decays and reappears at point X. This is the onset of stage 2 traced here during its first 13 minutes. By this time, NRH sources observed at frequencies _236.6 MHz radially lift off with a speed of _400kms-1(one third of the front speed of the coronal mass ejection (CME)) as one slowly decaying broadband source. This speed is still observable in SOHO/LASCO C3 difference frames in the wake of the CME four hours later. In stage 2, the radio sources at higher frequencies appear directly above the active region with growing intensity.
We interpret the observations as the transit of the lower boundary of the CME body through the height range of the coronal breakout current sheet. The relaxing global coronal field reconnects with the magnetic surroundings of the current sheets still connecting the CME in its wake with the Sun. The accelerated particles locally excite plasma emission but can escape also toward the active region, the CME, and the large-scale solar magnetic field. The breakout relaxation process may be a source of reconnection- and acceleration rate modulations.
In this view, **the late gradual phase is a certain stage of the coronal breakout relaxation after the release of the CME.** This article is, to our best knowledge, the first observational report of the coronal breakout recovery. Our interpretation of the radio observations agrees with some predictions of magnetic breakout simulations (e.g. Lynch et al. 2008, Astrophys. Journ. 683, 1192). Again, combined spectral and imaging radio observations give a unique access to dynamic coronal
processes which are invisible in other spectral ranges.

Radio evidence for breakout reconnection in solar eruptive events

H. **Aurass**, G. Holman, S. Braune, G. Mann, P. Zlobec
E-print, May **2013, File**; A&A, 555, A40 (**2013**)
Magnetic reconnection is understood to be fundamental to energy release in solar eruptive events (SEEs). In these events reconnection produces a magnetic flux rope above an arcade of hot flare loops. Breakout reconnection, a secondary reconnection high in the corona between this flux rope and the overlying magnetic field, has been hypothesized. Direct observational evidence for breakout reconnection has been elusive, however. The aim of this study is to establish a plausible interpretation of the combined radio and hard X-ray (HXR) emissions observed during the impulsive phase of the near-limb X3.9-class SEE on **2003 November 03**. We study radio spectra (AIP), simultaneous radio images (Nanc{c}ay Multi-frequency Radio Heliograph, NRH), and single-frequency polarimeter data (OAT). The radio emission is nonthermal plasma radiation with a complex structure in frequency and time. Emphasis is on the time interval when the HXR flare loop height was observed by the Ramaty High Energy Solar Spectroscopic Imager (RHESSI) to be at its minimum and an X-ray source was observed above the top of the arcade loops. Two stationary, meter-wavelength sources are observed radially aligned at 0.18 and 0.41Rs above the active region and hard X-ray sources. The lower source is apparently associated with the upper reconnection jet of the flare current sheet (CS), and the upper source is apparently associated with breakout reconnection. Sources observed at lower radio frequencies surround the upper source at the expected locations of the breakout reconnection jets. We believe the upper radio source is the most compelling evidence to date for the onset of breakout reconnection during a SEE. The height stationarity of the breakout sources and their dynamic radio spectrum discriminate them from propagating disturbances. Timing and location arguments reveal for the first time that both the earlier described ``above the flare loop top'' HXR source and the lower radio source are emission from the upper reconnection jet above the vertical flare CS.

RADIO EVIDENCE OF BREAK-OUT RECONNECTION?
H. **Aurass**1, G. Mann1, P. Zlobec2 and M. Karlický3
2011 ApJ 730 57, **File**
We reconsider the **2003 October 28** X17 flare/coronal mass ejection (CME), studying the five minutes immediately before the impulsive flare phase (not discussed in previous work). To this aim we examine complementary dynamic radio spectrograms, single frequency polarimeter records, radio images, space-based longitudinal field magnetograms, and ultraviolet images. We find widely distributed faint and narrowband meter wave radio sources located outside active regions but associated with the boundaries of magnetic flux connectivity cells, inferred from the potential extrapolation of the observed photospheric longitudinal field as a model for coronal magnetic field structures. The meter wave radio sources occur during the initial decimeter wave effects, which are well known to be associated with filament destabilization in the flaring active region (here NOAA 10486). Antiochos et al. predict in their break-out model for CME initiation that "... huge phenomena ... may be controlled by detailed plasma processes that occur in relatively tiny regions." They suggest that the expected faint energy release "... on long field lines far away from any neutral line ... may be detectable in radio/microwave emission from nonthermal particles..." In this paper, we describe meter wave sources whose properties correctly coincide with the quoted predictions of the break-out reconnection model of the CME initiation.

Coronal current sheet signatures during the 17 May 2002 CME-flare

H. **Aurass**1, F. Landini2, G. Poletto
E-print, Aug **2009, File**; A&A
Context. The relation between current sheets (CSs) associated with flares, revealed by characteristic radio signatures, and current sheets associated with coronal mass ejections (CMEs), detected in coronal ultraviolet (UV) and white light data, has not been analyzed, yet.
Aims. We aim at establishing the relationship between CSs associated with a limb flare and CSs associated with the CME that apparently develops after the flare. We use a unique data set, acquired on May 17, 2002, which includes radio and extreme ultraviolet (XUV) observations.
Methods. Spectral radio diagnostics, UV spectroscopic techniques, white light coronograph imaging, and (partly) radio imaging are used to illustrate the relation between the CSs and to infer the physical parameters of the radially aligned features that develop in the aftermath of the CME.
Results. During the flare, several phenomena are interpreted in accordance with earlier work and with reference to the common eruptive flare scenario as evidence of flare CSs in the low corona. These are drifting pulsating structures in dynamic radio spectra, an erupting filament, expanding coronal loops morphologically recalling the later white light CME, and associated with earlier reported hard X-ray source sites. In the aftermath of the CME, UV spectra allowed us to estimate the CS temperature and density, over the 1.5 - 2.1 $R_\odot$ interval of heliocentric altitudes. The UV detected CS, however, appears to be only one of many current sheets that exist underneath the erupting flux rope. A type II burst following the CME radio continuum in time at lower frequencies is considered as the radio signature of a coronal shock excited at the flank of the CME.
Conclusions. *The results show that we can build an overall scenario where the CME is interpreted in terms of an erupting arcade crossing the limb of the Sun and connected to underlying structures via multiple CSs. Eventually, the observed limb flare seems to be a consequence of the ongoing CME.*

Radio burst from converging separatrices

H. **Aurass**, G. Rausche, and G. Mann
A&A 471, L37-L40 (**2007**), DOI: 10.1051/0004-6361:20077544, **File**
Context.In a previous paper on the X17 flare October 28, 2003, we found, among other radio flare sources, one displaced at $\approx$ 0.2 Rs north of the flaring AR 10486, away from the main H α and hard X-ray flare emission. The source came to our attention due to its timing, its spatial displacement from the flaring active region, and due to the behavior of the radio spectral fine structure sources which are embedded in the continuum emission. We speculated that the source is situated at a separator of coronal magnetic flux systems.
Aims.Here we analyze the topology of the potential coronal magnetic field extrapolated from SOHO-MDI data near the source site of this meter-decimeter radio continuum.

Methods.Using the Source Method for magnetic field modeling, and the displacement gradient of the field lines as a connectivity measure, we give a description of the critical field structure. We compare it with the Nançay Radio Heliograph source positions of the continuum which have been classified by the spectral data of Astrophysical Institute Potsdam.
Results.We find that the radio source occurs near the contact of three separatrix surfaces between magnetic flux cells. There are other separatrix surfaces in the field which are not distinguished by a strong radio source during the analyzed flare.
Conclusions.This is the first evidence for the occurence of a strong coronal radio burst continuum source at such coronal magnetic field structures.

Signatures of magnetic reconnection in solar radio observations?

Adv. Space Res. 39(9), *Pages 1407-1414, **2007***
Henry **Aurass**
We summarize the results of some case studies which can be interpreted as radio evidence of magnetic reconnection: under certain conditions, simple spectral structures (pulsation pulses, reverse drift bursts) are formed by simultaneously acting but widely spaced radio sources. Narrowband spikes are emitted as a side-effect during large-scale coronal loop collisions. In dynamic radio spectra, the lower fast mode shock formed in the reconnection outflow appears as type II burst-like but nondrifting emission lane. It has been several times observed at the harmonic mode of the local plasma frequency between 250 and 500 MHz and at heights of ≈200 Mm.

The GLE on Oct. 28, 2003 - radio diagnostics of relativistic electron and proton injection

H. **Aurass**, G. Mann, G. Rausche and A. Warmuth
A&A 457, 681-692 (**2006**); **File**
Timing discrepancies between signatures of accelerated particles at the sun and the arrival times of the particles at near-earth detectors are a matter of fundamental interest for space-weather applications. The solar injection times of various components of energetic particles were derived by Klassen et al. (2005, JGR, 110, A09S04) for the October 28, 2003, X-class/γ-ray flare in NOAA AR 10486. This flare occured in connection with a fast halo coronal mass ejection and a neutron monitor-observed ground level event (GLE).We used radio (Astrophysikalisches Institut Potsdam, *WIND*, Nançay Multifrequency Radio Heliograph), Hα (Observatorium Kanzelhöhe), *RHESSI*, *SOHO* (EIT, LASCO, MDI), and *TRACE* data to study the associated chromospheric and low coronal phenomena. We identify three source sites of accelerated particles in this event. Firstly, there is a source in projection 0.3 *R*_ away from AR 10486, which is the site of the reconnection outflow termination, as revealed by a termination shock signature in the dynamic radio spectrum. Secondly, there is the extended current sheet above a giant coronal postflare loop system in the main flare phase. Thirdly, there is a source situated on a magnetic separatrix surface between several magnetic arcades and neighbouring active regions. This source is 0.2 *R*_ away from AR 10486 and acts during onset and growth of high energy proton injection in space. It is not clear if this source is related to the acceleration of protons, or if it only confirms that energetic particles penetrate a multistructure magnetic loop system after being previously accelerated near the main HXR- and γ-ray sources. **The result is in favour of energetic particle acceleration in the low corona (<0.5 *R*_ above the photosphere) and in contrast to acceleration of the relativistic particles at remotely propagating shock waves.**

Shock-excited radio burst from reconnection outflow jet?

Aurass, H., Vrsnak, B., & Mann, G.
A&A, 384, 273, **2002, File**
Models of dynamic (two-ribbon-, arcade) flares involve the formation of a system of standing slow and possibly also fast mode shock waves associated with the fast reconnection process below the erupting filament. These shocks are anticipated theoretically, but are not unambiguously confirmed by observations. In this paper we identify for the first time the radio signature of a fast mode outflow **termination shock** in a dynamic radio burst spectrogram. The standing fast mode shock is revealed by a **zero-drift type II burst** recorded between 300 and 400 MHz. It started almost 1 hour after the impulsive phase of the **7 April 1997** flare and lasted for more than 30 min. The burst shows a characteristic herringbone fine structure and a band split of (10+/-6)% of the emission frequency. No fundamental-harmonic pattern was observed, and we argue that the feature is fundamental mode emission. Simultaneous imaging observations (Hα , Yohkoh SXT, SOHO EIT) show a relaxed postflare loop arcade with a bright soft X-ray cusp commonly interpreted as a typical reconnection pattern. Conditions for termination shock formation and excitation of radio emision are investigated. Favourable circumstances for the radio detection of a termination shock in the reconnection outflow are a comparatively large height of the diffusion region, a low plasma to magnetic pressure ratio beta upstream of the slow shocks, and a small angle between the reconnecting field lines. Finally, we discuss why similar radio signatures are not

observed more frequently, and why it appeared so late in the event. We stress the implications and point to some inconsistencies which might be a consequence of commonly practiced ad hoc application of idealized model results to realistic conditions.

Coronal Mass Ejections and Type II Radio Bursts

Henry **Aurass**

Coronal Physics from Radio and Space Observations; Proceedings of the CESRA Workshop held in Nouan le Fuzelier, France 3-7 June 1996, edited by Gerard Trottet, Published by Springer, **1997**, p.135-160, **File**

Coronal mass ejections (CMEs) and shock wave induced radio bursts (type II) are reviewed. CMEs are - beneath flare blast waves - invoked to be the drivers of type lI burst emitting super-Alfv~nic disturbances. The paper focuses on the available experimental evidence for this assumption. For instance, the apparent contradiction is discussed between measured speeds of potential shock drivers and their observed type II burst association. Further, several examples are presented for recognizing CMEs by the appearance of other *characteristic* nonthermal radio signatures. Open problems are assembled which should be newly attact by high time and frequency resolution decimeter and meter wave radio spectral and imaging observations from ground combined with visible fight and X-ray imaging data from YOHKOH and SOHO space experiments. The paper shows that radio observations in general, and especially the radiation of shock accelerated electrons, constitute a unique access to the structure and the dynamics of the coronal magnetoplasma. This is important for understanding the timing and the sites of energy release processes in the solar corona and for studying the physics of collisionless shock waves in space plasmas.

Plasma motions in the solar corona and solar wind to 1 au, as inferred from radio wave scattering observations

Francesco **Azzollini**, A. Gordon Emslie, Daniel L. Clarkson, Nicolina Chrysaphi, Eduard P. Kontar

ApJ **968** 72 **2024**

https://arxiv.org/pdf/2403.12680

https://iopscience.iop.org/article/10.3847/1538-4357/ad4154/pdf

Radio signals propagating via the solar corona and solar wind are significantly affected by compressive waves, impacting solar burst properties as well as sources viewed through the turbulent atmosphere. While static fluctuations scatter radio waves elastically, moving, turbulent or oscillating density irregularities act to broaden the frequency of the scattered waves. Using a new anisotropic density fluctuation model based on solar radio bursts, we deduce the plasma velocities required to explain observations of spacecraft signal frequency broadening. The frequency broadening is consistent with motions that are dominated by the solar wind at distances $\gtrsim$10 R$\odot$, but the levels of frequency broadening for $\lesssim$10 R$\odot$ require additional radial speeds $\sim$(100−300) km s−1 and/or transverse speeds $\sim$(20−70) km s−1. The inferred radial velocities appear consistent with the sound or proton thermal speeds, while the speeds perpendicular to the radial direction are consistent with non-thermal motions measured via coronal Doppler-line broadening, interpreted as Alfvénic fluctuations. Landau damping of parallel propagating ion-sound (slow MHD) waves allow an estimate of the proton heating rate. The energy deposition rates due to ion-sound wave damping peak at a heliocentric distance of $\sim$(1−3) R$\odot$ are comparable to the rates available from a turbulent cascade of Alfvénic waves at large scales, suggesting a coherent picture of energy transfer, via the cascade or/and parametric decay of Alfvén waves to the small scales where heating takes place.

CESRA #3783 **2024** https://www.astro.gla.ac.uk/users/eduard/cesra/?p=3783

Fundamental, Harmonic, and Third-harmonic Plasma Emission from Beam-plasma Instabilities: A First-principles Precursor for Astrophysical Radio Bursts

Fabio **Bacchini**, Alexander A. Philippov

MNRAS Volume 529, Issue 1, Pages 169–177, **2024**

https://arxiv.org/pdf/2402.11011.pdf

https://doi.org/10.1093/mnras/stae521

https://academic.oup.com/mnras/article-pdf/529/1/169/56792714/stae521.pdf

Electromagnetic fundamental and harmonic emission is ubiquitously observed throughout the heliosphere, and in particular it is commonly associated with the occurrence of Type II and III solar radio bursts. Classical analytic calculations for the plasma-emission process, though useful, are limited to idealized situations; a conclusive numerical verification of this theory is still lacking, with earlier studies often providing contradicting results on e.g. the precise parameter space in which fundamental and harmonic emission can be produced. To accurately capture the chain of mechanisms underlying plasma emission - from precursor plasma processes to the generation of electromagnetic waves

over long times - we perform large-scale, first-principles simulations of beam-plasma instabilities. By employing a very large number of computational particles we achieve very low numerical noise, and explore (with an array of simulations) a wide parameter space determined by the beam-plasma density ratio and the ion-to-electron temperature ratio. In particular, we observe direct evidence of both fundamental and harmonic plasma emission when the beam-to-background density ratio ≤0.005 (with beam-to-background energy ratio ~0.5), tightly constraining this threshold. We observe that, asymptotically, in this regime ~0.1% of the initial beam energy is converted into harmonic emission, and ~0.001% into fundamental emission. In contrast with previous studies, we also find that this emission is independent of the ion-to-electron temperature ratio. In addition, we report the direct detection of third-harmonic emission in all of our simulations, at power levels compatible with observations. Our findings have important consequences for understanding the viable conditions leading to plasma emission in space systems, and for the interpretation of observed electromagnetic signals throughout the heliosphere.

Tracking a beam of electrons from the low solar corona into interplanetary space with the Low Frequency Array, Parker Solar Probe and 1 au spacecraft

Samuel T. **Badman**, Eoin P. Carley, Luis Alberto Cañizares, Nina Dresing, Lan K. Jian, David Lario, Peter T. Gallagher, Juan C. Martínez-Oliveros, Marc Pulupa, Stuart D. Bale

ApJ **938** 95 **2022**

https://arxiv.org/pdf/2204.08497.pdf

https://iopscience.iop.org/article/10.3847/1538-4357/ac90c2/pdf

Type III radio bursts are the result of plasma emission from mildly relativistic electron beams propagating from the low solar corona into the heliosphere where they can eventually be detected in situ if they align with the location of a heliospheric spacecraft. Here we observe a type III radio burst from 0.1-16 MHz using the Parker Solar Probe (PSP) FIELDS Radio Frequency Spectrometer (RFS), and from 10-80 MHz using the Low Frequency Array (LOFAR). This event was not associated with any detectable flare activity but was part of an ongoing noise storm that occurred during PSP encounter 2. A deprojection of the LOFAR radio sources into 3D space shows that the type III radio burst sources were located on open magnetic field from 1.6-3 R⊙ and originated from a specific active region near the East limb. Combining PSP/RFS observations with WIND/WAVES and Solar Terrestrial Relations Observatory (STEREO)/WAVES, we reconstruct the type III radio source trajectory in the heliosphere interior to PSP's position, assuming ecliptic confinement. An energetic electron enhancement is subsequently detected in situ at the STEREO-A spacecraft at compatible times although the onset and duration suggests the individual burst contributes a subset of the enhancement. This work shows relatively small-scale flux emergence in the corona can cause the injection of electron beams from the low corona into the heliosphere, without needing a strong solar flare. The complementary nature of combined ground and space-based radio observations, especially in the era of PSP, is also clearly highlighted by this study. **2019 April 9**

Radio Imaging of a Type IVM Radio Burst on the 14th of August 2010

H. M. **Bain**1, S. Krucker1,2, P. Saint-Hilaire1, and C. L. Raftery

E-print, Jan **2014; 2014** ApJ 782 43

Propagating coronal mass ejections (CMEs) are often accompanied by burst signatures in radio spectrogram data. We present Nançay Radioheliograph observations of a moving source of broadband radio emission, commonly referred to as a type IV radio burst (type IVM), which occurred in association with a CME on the 14th of August 2010. The event was well observed at extreme ultraviolet (EUV) wavelengths by SDO/AIA and PROBA2/SWAP, and by the STEREO SECCHI and SOHO LASCO white light (WL) coronagraphs. The EUV and WL observations show the type IVM source to be cospatial with the CME core. The observed spectra is well fitted by a power law with a negative slope, which is consistent with optically thin gyrosynchrotron emission. The spectrum shows no turn over at the lowest Nançay frequencies. By comparing simulated gyrosynchrotron spectra with Nançay Radioheliograph observations, and performing a rigorous parameter search we are able to constrain several key parameters of the underlying plasma. Simulated spectra found to fit the data suggest a nonthermal electron distribution with a low energy cutoff of several tens to 100 keV, with a nonthermal electron density in the range 100-102 cm–3, in a magnetic field of a few Gauss. The nonthermal energy content of the source is found to contain 0.001%-0.1% of the sources thermal energy content. Furthermore, the energy loss timescale for this distribution equates to several hours, suggesting that the electrons could be accelerated during the CME initiation or early propagation phase and become trapped in the magnetic structure of the CME core without the need to be replenished.

RADIO IMAGING OF SHOCK-ACCELERATED ELECTRONS ASSOCIATED WITH AN ERUPTING PLASMOID ON 2010 NOVEMBER 3

H. M. **Bain**, Säm Krucker1, L. Glesener, and R. P. Lin

2012 ApJ 750 44

We present observations of a metric type II solar radio burst that occurred on the **3rd of November 2010** in association with an erupting plasmoid. The eruption was well observed by the Atmospheric Imaging Assembly (AIA) on board the Solar Dynamics Observatory and the Reuven Ramaty High Energy Solar Spectroscopic Imager, while the burst occurred in the frequency range of the Nançay Radioheliograph (NRH). Such events, where the type II emission occurs in the NRH frequency range, allowing us to image the burst, are infrequent. Combining these data sets, we find that the type II is located ahead of the hot (~11 MK) core of the plasmoid, which is surrounded by a well-defined envelope of cool (few MK) plasma. Using two methods, we determine the propagation velocity of the shock: (1) fitting the type II emission observed in PHOENIX and HUMAIN radio spectrogram data; (2) direct imaging of the type II source location using NRH observations. We use LASCO C2 polarized brightness images to normalize our coronal density model. However, we find that information from imaging is required in order to fine-tune this normalization. We determine a shock propagation velocity between 1900 km s–1 and 2000 km s–1. This is faster than the plasmoid observed at extreme-ultraviolet wavelengths by AIA (v = 670-1440 km s–1, where the cooler plasma propagates faster than the hot core). The positioning of the type II, ahead of the plasmoid, suggests that the electrons are accelerated in a piston-driven shock.

See RHESSI Science Nugget No. 174, Apr 2012

A Shocking Type II, by Hazel Bain, Sa"m Krucker, and Lindsay Glesener: Global coronal waves getting sorted out. http://sprg.ssl.berkeley.edu/~tohban/wiki/index.php/A_Shocking_Type_II.

Intersunspot Microwave Sources

I. A. **Bakunina**, V. F. Melnikov, A. A. Solov'ev, V. E. Abramov-Maximov

Solar Phys., **2015**, Volume 290, Issue 1, pp 37-52

We studied a number of solar active regions using two-dimensional spatially resolved microwave observations. Data from the Nobeyama Radioheliograph and the Siberian Solar Radio Telescope together with observations by the Michelson Doppler Imager (MDI) onboard the Solar and Heliospheric Observatory (SOHO) have allowed us to identify long-lived intersunspot sources (ISSs) in most of the investigated active regions. Their centers are often located above the line-of-sight magnetic field inversion line that separates the leading and following polarities of a full active region (first type of ISS) or above the inversion line that separates magnetic polarities inside of a complex of sunspots (second type of ISS). ISSs of the first type are extended and, in general, they are sources of bremsstrahlung emission. ISSs of the second type are compact and are, most likely, sources of gyroresonance or gyrosynchrotron emission. We propose a qualitative model involving three types of magnetic connectivity to explain how long-lasting ISSs may be generated.

Long-Period Oscillations of Sunspots by NoRH and SSRT Observations

I. A. **Bakunina**, V. E. Abramov-Maximov, V. M. Nakariakov, S. V. Lesovoy, A. A. Soloviev, Y. V. Tikhomirov, V. F. Melnikov, K. Shibasaki, Y. A. Nagovitsyn, and E. L. Averina

Publ. Astron. Soc. Japan 65, No. SP1, S13 [12 pages] (**2013**)

http://pasj.asj.or.jp/v65/sp1/65S013/65S013.pdf

Long-term oscillations of microwave emission generated in sunspot magnetospheres are detected with the Nobeyama Radioheliograph (NoRH) at a frequency of 17 GHz, and the Siberian Solar Radio Telescope (SSRT) at 5.7 GHz. Significant periodicities in the range of 22–170 min are found in the variation of the emission intensity, polarisation and the degree of circular polarisation. Periods of the oscillations are not stable: they are different in different sunspots and in the same sunspot on different days. A cross-correlation analysis shows the presence of common significant periods in both NoRH and SSRT data. The cross-correlation coefficients are typically lower than 0.5, which can be attributed to the different heights of the emission formation, and different mechanisms for the emission generation (gyroresonance and thermal bremstrahlung at 17 GHz, and pure gyroresonance at 5.7 GHz). The observational results are consistent with the global sunspot oscillation model. **Table**

Solar research with ALMA: ARC as your supporting infrastructure

Miroslav **Barta**
CESRA Abstract **2016** p.52
http://cesra2016.sciencesconf.org/conference/cesra2016/pages/CESRA2016_prog_abs_book_v1.pdf
Regular observations of the Sun will start with coming Cycle 4. This goal has been accomplished by effort of Solar ALMA Development Team. Its European part has been formed by the Czech node of the European ALMA Regional Center (ARC) hosted by the Astronomical Institute in Ondrejov. The main role of the ARC nodes is to provide supporting infrastructure for the ALMA users in all stages of their ALMA-oriented projects. Based on the long-term experience of the Czech ARC node with the ALMA solar observing mode development the node provides a unique opportunity for solar physics community in entire Europe as a primary contact support spot. We will present the results of solar mode development, the SW tools for preparation of solaroriented proposals, services of the ARC node to the user community, ALMA capabilities for upcoming Cycle ˜4 and expectation for the next Cycle 5.

Plasmoid Dynamics in Flare Reconnection and the Frequency Drift of the Drifting Pulsating Structure

M. **Bárta** · M. Karlický · R. Žemli˘cka
Solar Phys (**2008**) 253: 173–189
In the paper by Kliem, Karlický, and Benz (*Astron. Astrophys.* **360**, 715, 2000) it was suggested, that plasmoids formed during the bursty regime of solar flare reconnection can be "visualised" in the radio spectra as drifting pulsating structures via accelerated particles trapped inside the plasmoid. In the present paper we investigate this idea in detail. First, simple statistical analysis supporting this hypothesis is presented. Then, by using the 2.5-D MHD (including gravity) model solar flare reconnection in the inhomogeneous, stratified atmosphere is simulated and the formation and subsequent ejection of the plasmoid is demonstrated. The ejected plasmoid, which is considered to be a trap for accelerated electrons, is traced and its plasma parameters are computed. To estimate the associated plasma radio emission we need to know locations of accelerated electrons and corresponding plasma frequencies. General considerations predict that these electrons should be distributed mainly along the magnetic separatrix surfaces and this was confirmed by using a particle-in-cell simulation. Finally, under some simplifying assumptions the model dynamic radio spectrum is constructed. The relation between the global frequency drift and the plasmoid motion in the inhomogeneous ambient atmosphere is studied. The results are discussed with respect to the observed drifting pulsation structures and their possible utilisation for flare magnetic field diagnostics.

Kodaikanal Solar Observatory Radio Spectrograph

Indrajit V. **Barve**, C. Kathiravan, G. V. S. Gireesh, M. N. Anand, M. Rajesh, M. Rajalingam, E. Ebenezer Chellasamy & R. Ramesh
Solar Physics volume 296, Article number: 132 (**2021**)
https://link.springer.com/content/pdf/10.1007/s11207-021-01879-1.pdf
https://doi.org/10.1007/s11207-021-01879-1
The Indian Institute of Astrophysics (IIA) has commissioned a low frequency (<100 MHz) spectrograph at its Kodaikanal Solar Observatory (KSO) for coordinated observations of transients in the solar atmosphere with other existing optical observing facilities there. The hardware set-up and initial observations are presented. The availability of different instruments in the same observatory helps to quickly plan and jointly observe the energetic phenomena and their signatures in all the three major atmospheric regions of the Sun, i.e. photosphere, chromosphere and corona. **2018 March 30, 2021 May 22**

Solar Observing with the Atacama Large Millimeter-Submillimeter Array **Review**

Timothy **Bastian**, Masumi Shimojo, Miroslav Barta, Stephen White, Kazumasa Iwai
Frontiers in Astronomy and Space Science 9:977368. **2022**
https://arxiv.org/pdf/2209.01659.pdf
https://www.frontiersin.org/articles/10.3389/fspas.2022.977368/pdf
doi: 10.3389/fspas.2022.977368
The Atacama Large Millimeter-submillimeter Array (ALMA), sited on the high desert plains of Chajnantor in Chile, has opened a new window onto solar physics in 2016 by providing continuum observations at millimeter and sub-millimeter wavelengths with an angular resolution comparable to that available at optical (O), ultraviolet (UV), extreme ultraviolet (EUV), and X-ray wavelengths, and with superior time resolution. In the intervening years, progress has been made testing and commissioning new observing modes and capabilities, in developing data calibration strategies, and in data imaging and restoration techniques. Here we review ALMA current solar observing capabilities, the process by which a user may propose to use the instrument, and summarize the observing process and work flow. We then discuss some of the challenges users may encounter in imaging and analyzing their data. We conclude with a discussion of additional

solar observing capabilities and modes under consideration that are intended to further exploit the unique spectral coverage provided by ALMA. **18 Dec 2015**

Radio Observational Constraints on Turbulent Astrophysical Plasmas **Review**

Tim **Bastian**, James Cordes, Justin Kasper, Adam Kobelski, Kelly Korreck, Gregory Howe, Steven Spangler, Chadi Salem, Angelos Vourlidas

White paper submitted to the Astronomy and Astrophysics decadal survey **2019**

https://arxiv.org/pdf/1904.05807.pdf

Remarkable progress has been made in understanding turbulent astrophysical plasmas in past decades including, notably, the solar wind and the interstellar medium. In the case of the solar wind, much of this progress has relied on in situ measurements from space-borne instruments. However, ground-based radio observations also have played a significant role and have the potential to play an even bigger role. In particular, using distant background sources (quasars, pulsars, satellite beacons) to transilluminate the foreground corona and solar wind, a variety of radio propagation phenomena can be used to map plasma properties of the solar corona and heliosphere, as well as the warm interstellar medium. These include angular broadening, interplanetary and interstellar scintillations, and differential Faraday rotation. These observations are highly complementary to in situ observations of the solar wind, and could be a mainstay of investigations into turbulence of the ISM. We point out that the Next Generation Very Large Array (ngVLA) fulfills all the requirements necessary to exploit radio observations of astrophysical turbulence fully.

Diagnostics of Space Weather Drivers Enabled by Radio Observations **Review**

Tim **Bastian**, Hazel Bain, Bin Chen, Dale Gary, Gregory Fleishman, Lindsay Glesener, Pascal Saint-Hilaire, Colin Lonsdale, Stephen White

White paper submitted to the Astronomy and Astrophysics decadal survey **2019**

https://arxiv.org/pdf/1904.05817.pdf

The Sun is an active star that can have a direct impact on the Earth, its magnetosphere, and the technological infrastructure on which modern society depends. Among the phenomena that drive "space weather" are fast solar wind streams and co-rotating interaction regions, solar flares, coronal mass ejections, the shocks they produce, and the energetic particles they accelerate. Radio emission from these and associated phenomena offer unique diagnostic possibilities that complement those available at other wavelengths. Here, the relevant space weather drivers are briefly described, the potential role of radio observations is outlined, and the requirements of an instrument to provide them are provided: specifically, ultrabroadband imaging spectropolarimetry. The insights provided by radio observations of space weather drivers will not only inform the science of space weather, they will pave the way for new tools for forecasting and "nowcasting" space weather. They will also serve as an important touchstone against which local environment of exoplanets and the impact of "exo-space weather" can be evaluated.

Radio, Millimeter, and Sub-millimeter Observations of the Quiet Sun **Review**

Tim **Bastian**, Bin Chen, Dale Gary, Gregory Fleishman, Lindsay Glesener, Colin Lonsdale, Pascal Saint-Hilaire, Stephen White

White paper submitted to the Astronomy and Astrophysics decadal survey **2019**

https://arxiv.org/pdf/1904.05826.pdf

Identification of the mechanisms responsible for heating the solar chromosphere and corona remains an outstanding problem, one of great relevance to late-type stars as well. There has been tremendous progress in the past decade, largely driven by new instruments, new observations, and sophisticated modeling efforts. Despite this progress, gaps remain. We briefly discuss the need for radio coverage of the 3D solar atmosphere and discuss the requirements.

Exploring the Sun with ALMA

Bastian, T. S.; Bárta, M.; Brajša, R.; Chen, B.; Pontieu, B. D.; Gary, D. E.; Fleishman, G. D.; Hales, A. S.; Iwai, K.; Hudson, H.; Kim, S.; Kobelski, A.; Loukitcheva, M.; Shimojo, M.; Skokić, I.; Wedemeyer, S.; White, S. M.; Yan, Y.

The Messenger, vol. 171, p. 25-30, **2018**

https://www.eso.org/sci/publications/messenger/archive/no.171-mar18/messenger-no171-25-30.pdf

The Atacama Large Millimeter/submillimeter Array (ALMA) Observatory opens a new window onto the Universe. The ability to perform continuum imaging and spectroscopy of astrophysical phenomena at millimetre and submillimetre wavelengths with unprecedented sensitivity opens up new avenues for the study of cosmology and the evolution of galaxies, the formation of stars and planets, and astrochemistry. ALMA also allows fundamentally new observations to be made of objects much closer to home, including the Sun. The Sun has long served as a touchstone for our

understanding of astrophysical processes, from the nature of stellar interiors, to magnetic dynamos, non-radiative heating, stellar mass loss, and energetic phenomena such as solar flares. ALMA offers new insights into all of these processes.

A First Comparison of Millimeter Continuum and Mg II Ultraviolet Line Emission from the Solar Chromosphere

T. S. **Bastian**, G. Chintzoglou, B. De Pontieu, M. Shimojo, D. Schmit, J. Leenaarts, M. Loukitcheva
2017
https://arxiv.org/pdf/1706.04532.pdf
We present joint observations of the Sun by the Atacama Large Millimeter/submillimeter Array (ALMA) and the Interface Region Imaging Spectrograph (IRIS). The observations were made of a solar active region on **2015 December 18** as part of the ALMA science verification effort. A map of the Sun's continuum emission of size 2.4′×2.3′ was obtained by ALMA at a wavelength of 1.25 mm (239 GHz) using mosaicing techniques. A contemporaneous map of size 1.9′×2.9′ was obtained in the Mg II h doublet line at 2803.5\AA\ by IRIS. Both mm/submm−λ continuum emission and ultraviolet (UV) line emission are believed to originate from the solar chromosphere and both have the potential to serve as powerful and complementary diagnostics of physical conditions in this poorly understood layer of the solar atmosphere. While a clear correlation between mm-λ brightness temperature TB and the Mg II h line radiation temperature Trad is observed the slope is <1, perhaps as a result of the fact that these diagnostics are sensitive to different parts of the chromosphere and/or the Mg II h line source function includes a scattering component. There is a significant offset between the mean TB(1.25 mm) and mean Trad(Mg II), the former being ≈35% greater than the latter. Partitioning the maps into "sunspot", "quiet regions", and "plage regions" we find that the slope of the scatter plots between the IRIS Mg II h line Trad and the ALMA brightness temperature TB is 0.4 (sunspot), 0.56 (quiet regions), and 0.66 (plage regions). We suggest that this change may be caused by the regional dependence of the formation heights of the IRIS and ALMA diagnostics, and/or the increased degree of coupling between the UV source function and the local gas temperature in the hotter, denser gas in plage regions.

Solar Observations with the Jansky Very Large Array

Timothy **Bastian**
CESRA **2016** p.42
http://cesra2016.sciencesconf.org/conference/cesra2016/pages/CESRA2016_prog_abs_book_v3.pdf
The Jansky Very Large Array (JVLA) represents a significant upgrade in capabilities for solar observing at centimeter wavelengths. With its new suite of receivers and an advanced correlator, the JVLA can now image solar phenomena radio frequencies over significant bandwidths with high spectral and temporal resolution. The JVLA can currently observe at frequencies from 1-8 GHz; progress is being made to extend the range to 1-18 GHz. Some examples of recent work will be presented, including observations of a solar active regions and of radio bursts associated with solar flares. Looking forward to the era of Solar Probe Plus and the Solar Orbiter missions, the JVLA is also doing a pilot study of solar wind tomography using the multitudes of background radio sources that are now accessible thanks to its great sensitivity.

RADIO SPECTRAL EVOLUTION OF AN X-RAYYPOOR IMPULSIVE SOLAR FLARE: IMPLICATIONS FOR PLASMA HEATING AND ELECTRON ACCELERATION

T. S. **Bastian**, G. D. Fleishman, and D. E. Gary
The Astrophysical Journal, 666:1256-1267, **2007**
https://iopscience.iop.org/article/10.1086/520106/pdf
We present radio and X-ray observations of an impulsive solar flare that was moderately intense in microwaves, yet showed very meager EUV and X-ray emission. The flare occurred on **2001 October 24** and was well observed at radio wavelengths by the Nobeyama Radioheliograph (NoRH), the Nobeyama Radio Polarimeters (NoRP), and the Owens Valley Solar Array (OVSA). It was also observed in EUV and X-ray wavelength bands by the TRACE, GOES, and Yohkoh satellites. We find that the impulsive onset of the radio emission is progressively delayed with increasing frequency relative to the onset of hard X-ray emission. In contrast, the time of flux density maximum is progressively delayed with decreasing frequency. The decay phase is independent of radio frequency. The simple source morphology and the excellent spectral coverage at radio wavelengths allowed us to employ a nonlinear $\chi 2$-minimization scheme to fit the time series of radio spectra to a source model that accounts for the observed radio emission in terms of gyrosynchrotron radiation from MeV-energy electrons in a relatively dense thermal plasma. We discuss plasma heating and electron acceleration in view of the parametric trends implied by the model fitting. We suggest that stochastic acceleration likely plays a role in accelerating the radio-emitting electrons.

The Coronal Mass Ejection of 1998 April 20: Direct Imaging at Radio Wavelengths

T. S. **Bastian**1, M. Pick2, A. Kerdraon2, D. Maia2,4, and A. Vourlidas3
2001 ApJ 558 L65
https://iopscience.iop.org/article/10.1086/323421/pdf
Spectroscopic data were obtained between 40 and 800 MHz by the spectrometer at Tremsdorf, Germany, and between 20 kHz and 14 MHz with the WAVES instrument on board the Wind spacecraft. Energetic particle data were obtained from the Wind 3D Plasma and Energetic Particle experiment. The CME was observed in white light by the Large-Angle Spectrometric COronagraph experiment on board the Solar and Heliospheric Observatory spacecraft. For the first time, the expanding CME loops are imaged directly at radio wavelengths. We show that the radio-emitting CME loops are the result of nonthermal synchrotron emission from electrons with energies of ~0.5-5 MeV interacting with magnetic fields of ~0.1 to a few gauss. They appear nearly simultaneously with the onset of an associated type II radio burst, shock-accelerated type III radio bursts, and the initiation of a solar energetic particle event. We suggest possible sources of the energetic electrons responsible for this "radio CME" and point out diagnostic uses for synchrotron emission from CME loops. **20 Apr 1998**

Multiple electron acceleration instances during a series of solar microflares observed simultaneously at X-rays and microwaves

Marina **Battaglia**, Rohit Sharma, Yingjie Luo, Bin Chen, Sijie Yu, Säm Krucker
ApJ **922** 134 **2021**
https://arxiv.org/pdf/2109.12847.pdf
https://doi.org/10.3847/1538-4357/ac2aa6
Even small solar flares can display a surprising level of complexity regarding their morphology and temporal evolution. Many of their properties, such as energy release and electron acceleration can be studied using highly complementary observations at X-ray and radio wavelengths. We present X-ray observations from the Reuven Ramaty High Energy Solar Spectroscopic Imager (RHESSI) and radio observations from the Karl G. Jansky Very Large Array (VLA) of a series of GOES A3.4 to B1.6 class flares observed on **2013 April 23**. The flares, as seen in X-ray and extreme ultraviolet (EUV), originated from multiple locations within active region NOAA 11726. A veritable zoo of different radio emissions between 1 GHz and 2 GHz was observed co-temporally with the X-ray flares. In addition to broad-band continuum emission, broad-band short-lived bursts and narrow-band spikes, indicative of accelerated electrons, were observed. However, these sources were located up to 150 arcsec away from the flaring X-ray sources but only some of these emissions could be explained as signatures of electrons that were accelerated near the main flare site. For other sources, no obvious magnetic connection to the main flare site could be found. These emissions likely originate from secondary acceleration sites triggered by the flare, but may be due to reconnection and acceleration completely unrelated to the co-temporally observed flare. Thanks to the extremely high sensitivity of the VLA, not achieved with current X-ray instrumentation, it is shown that particle acceleration happens frequently and at multiple locations within a flaring active region.
RHESSI Nuggets #417 **2021** https://sprg.ssl.berkeley.edu/~tohban/wiki/index.php/Manifold_Nonthermality

Do solar decimetric spikes originate in coronal X-ray sources?

Marina **Battaglia** and Arnold O. Benz
E-print, April **2009**; A&A L33-L36 (2009)
Context: In the standard solar flare scenario, a large number of particles are accelerated in the corona. Nonthermal electrons emit both X-rays and radio waves. Thus, correlated signatures of the acceleration process are predicted at both wavelengths, coinciding either close to the footpoints of a magnetic loop or near the coronal X-ray source. Aims: We attempt to study the spatial connection between coronal X-ray emission and decimetric radio spikes to determine the site and geometry of the acceleration process.
Methods: The positions of radio-spike sources and coronal X-ray sources are determined and analyzed in a well-observed limb event. Radio spikes are identified in observations from the Phoenix-2 spectrometer. Data from the Nancay radioheliograph are used to determine the position of the radio spikes. RHESSI images in soft and hard X-ray wavelengths are used to determine the X-ray flare geometry. Those observations are complemented by images from GOES/SXI.
Results: We find that the radio emission originates at altitudes much higher than the coronal X-ray source, having an offset from the coronal X-ray source amounting to 90 arcsec and to 113 arcsec and 131 arcsec from the two footpoints, averaged over time and frequency. Conclusions: Decimetric spikes do not originate from coronal X-ray flare sources contrary to previous expectations. However, the observations suggest a causal link between the coronal X-ray source, related to the major energy release site, and simultaneous activity in the higher corona**. 23 Aug 2005**

Auroral Kilometric Radiation -- the Electron Cyclotron Maser Paradigm

W. **Baumjohann**, R. A. Treumann
Front. Astron. Space Sci. 9 (**2022**) 1053303
https://arxiv.org/pdf/2302.02344
Auroral kilometric radiation (AKR) is the paradigm of intense radio emission from planetary magnetospheres. Being close to the electron gyro frequency and/or its lower harmonics, its observation indicates the non-thermal state of the source plasma. Emission is produced when the plasma enters a state of energetic excitation which results in deformation of the electron distribution function. Under certain conditions this leads to "quasi-coherent" emission. It is believed that the weakly-relativistic electron-cyclotron-maser instability is responsible for this kind of radiation. Since energetically radio radiation normally is not of {primary} importance in the large-scale magnetospheric phenomena, AKR as such has, for the purposes of large-scale magnetospheric physics, become considered a marginal problem. Here this notion is questioned. AKR while applying to the auroral region mainly during magnetospherically disturbed times {carries just a fraction of the total substorm energy. It is, however, of diagnostic power in the physics of the upper auroral ionosphere and Space Weather research}. As a fundamental physical problem of generation of radiation in non-thermal plasmas {it remains not resolved yet. Many questions have been left open even when dealing only with the electron-cyclotron-maser. These can advantageously be studied in the magnetosphere proper both by observation and theory, the only continuously accessible place in space. The most important are listet here with hint on how they should be attacked. Its value is to be sought in the role it should play in application to the other magnetized planets, extra-solar planets, and to strongly magnetized astronomical objects} as an important {tool to diagnose the matter state responsible for radiation in the radio frequency range beyond thermal, shock or synchrotron radiation.

An Unsupervised Machine Learning-based Algorithm for Detecting Weak Impulsive Narrowband Quiet Sun Emissions and Characterizing Their Morphology

Shabbir **Bawaji**6,1, Ujjaini Alam1, Surajit Mondal2, Divya Oberoi3, and Ayan Biswas3,4,5
2023 ApJ 954 39
https://iopscience.iop.org/article/10.3847/1538-4357/ace042/pdf
The solar corona is extremely dynamic. Every leap in observational capabilities has been accompanied by unexpected revelations of complex dynamic processes. The ever more sensitive instruments now allow us to probe events with increasingly weaker energetics. A recent leap in the low-frequency radio solar imaging ability has led to the discovery of a new class of emissions, namely weak impulsive narrowband quiet Sun emissions (WINQSEs). They are hypothesized to be the radio signatures of coronal nanoflares and could potentially have a bearing on the long standing coronal heating problem. In view of the significance of this discovery, this work has been followed up by multiple independent studies. These include detecting WINQSEs in multiple data sets, using independent detection techniques and software pipelines, and looking for their counterparts at other wavelengths. This work focuses on investigating morphological properties of WINQSEs and also improves upon the methodology used for detecting WINQSEs in earlier works. We present a machine learning-based algorithm to detect WINQSEs, classify them based on their morphology, and model the isolated ones using 2D Gaussians. We subject multiple data sets to this algorithm to test its veracity. Interestingly, despite the expectations of their arising from intrinsically compact sources, WINQSEs tend to be resolved in our observations. We propose that this angular broadening arises due to coronal scattering. Hence, WINQSEs can provide ubiquitous and ever-present diagnostic of coronal scattering (and, in turn, coronal turbulence) in the quiet Sun regions, which has not been possible until date. **2017 November 27, 2020-06-20**

Exploring Coronal Heating Using Unsupervised Machine-Learning

Shabbir **Bawaji**, Ujjaini Alam, Surajit Mondal, Divya Oberoi
ADASS 2020 proceedings **2021**
https://arxiv.org/pdf/2103.05371.pdf
The perplexing mystery of what maintains the solar coronal temperature at about a million K, while the visible disc of the Sun is only at 5800 K, has been a long standing problem in solar physics. A recent study by Mondal(2020) has provided the first evidence for the presence of numerous ubiquitous impulsive emissions at low radio frequencies from the quiet sun regions, which could hold the key to solving this mystery. These features occur at rates of about five hundred events per minute, and their strength is only a few percent of the background steady emission. One of the next steps for exploring the feasibility of this resolution to the coronal heating problem is to understand the morphology of these emissions. To meet this objective we have developed a technique based on an unsupervised machine learning approach for characterising the morphology of these impulsive emissions. Here we present the results of application of this technique to over 8000 images spanning 70 minutes of data in which about 34,500 features could robustly be characterised as 2D elliptical Gaussians.

Measuring coronal magnetic fields with remote sensing observations of shock waves Review

Alessandro **Bemporad**, Roberto Susino, Federica Frassati, Silvano Fineschi
Frontiers in Astronomy and Space Sciences, Volume 3, id.17 **2016**
https://arxiv.org/ftp/arxiv/papers/1608/1608.05536.pdf
Recent works demonstrated that remote sensing observations of shock waves propagating into the corona and associated with major solar eruptions can be used to derive the strength of coronal magnetic fields met by the shock over a very large interval of heliocentric distances and latitudes. This opinion article will summarize most recent results obtained on this topic and will discuss the weaknesses and strengths of these techniques to open a constructive discussion with the scientific community.

Physical Conditions of Coronal Plasma at the transit of a Shock driven by a Coronal Mass Ejection

A. **Bemporad**, R. Susino, S. Mancuso
ApJ **2015**
http://arxiv.org/pdf/1509.09131v1.pdf
We report here on the determination of plasma physical parameters across a shock driven by a Coronal Mass Ejection using White Light (WL) coronagraphic images and Radio Dynamic Spectra (RDS). The event analyzed here is the spectacular eruption that occurred on **June 7th 2011**, a fast CME followed by the ejection of columns of chromospheric plasma, part of them falling back to the solar surface, associated with a M2.5 flare and a type-II radio burst. Images acquired by the SOHO/LASCO coronagraphs (C2 and C3) were employed to track the CME-driven shock in the corona between 2-12 R⊙ in an angular interval of about 110∘. In these intervals we derived 2-Dimensional (2D) maps of electron density, shock velocity and shock compression ratio, and we measured the shock inclination angle with respect to the radial direction. Under plausible assumptions, these quantities were used to infer 2D maps of shock Mach number MA and strength of coronal magnetic fields at the shock's heights. We found that in the early phases (2-4 R⊙) the whole shock surface is super-Alfv\'enic, while later on (i.e. higher up) it becomes super-Alfvenic only at the nose. This is in agreement with the location for the source of the observed type-II burst, as inferred from RDS combined with the shock kinematic and coronal densities derived from WL. For the first time, a coronal shock is used to derive a 2D map of the coronal magnetic field strength over a 10 R⊙ altitude and ∼110∘ latitude intervals.

Plasma Physical Parameters along Coronal-mass-ejection-driven Shocks. I. Ultraviolet and White-light Observations

A. **Bemporad**1, R. Susino1, and G. Lapenta
2014 ApJ 784 102
http://arxiv.org/pdf/1403.0870v1.pdf
In this work, UV and white-light (WL) coronagraphic data are combined to derive the full set of plasma physical parameters along the front of a shock driven by a coronal mass ejection. Pre-shock plasma density, shock compression ratio, speed, and inclination angle are estimated from WL data, while pre-shock plasma temperature and outflow velocity are derived from UV data. The Rankine-Hugoniot (RH) equations for the general case of an oblique shock are then applied at three points along the front located between 2.2 and 2.6 R ⊙ at the shock nose and at the two flanks. Stronger field deflection (by ~46°), plasma compression (factor ~2.7), and heating (factor ~12) occur at the nose, while heating at the flanks is more moderate (factor 1.5-3.0). Starting from a pre-shock corona where protons and electrons have about the same temperature (Tp ∼ Te ∼ 1.5 × 106 K), temperature increases derived with RH equations could better represent the proton heating (by dissipation across the shock), while the temperature increase implied by adiabatic compression (factor ~2 at the nose, ~1.2-1.5 at the flanks) could be more representative of electron heating: the transit of the shock causes a decoupling between electron and proton temperatures. Derived magnetic field vector rotations imply a draping of field lines around the expanding flux rope. The shock turns out to be super-critical (sub-critical) at the nose (at the flanks), where derived post-shock plasma parameters can be very well approximated with those derived by assuming a parallel (perpendicular) shock.

Super- and sub-critical regions in shocks driven by radio-loud and radio-quiet CMEs.

Bemporad A and Mancuso S
(**2013**) JAdR 4: 287-291

FIRST COMPLETE DETERMINATION OF PLASMA PHYSICAL PARAMETERS ACROSS A CORONAL MASS EJECTION-DRIVEN SHOCK

A. **Bemporad** and S. Mancuso

Astrophysical Journal, 720:130–143, **2010**

We report on the study of a fast coronal mass ejection (CME)-driven shock associated with the solar eruption of **2002 March 22**. This event was observed in the intermediate corona both in white light and the extreme ultraviolet (EUV) by the LASCO and UVCS instruments on board the *Solar and Heliospheric Observatory*, as well as in metric and decametric wavelengths through space- and ground-based radio observatories. Clear signatures of shock transit are (1) strong type II emission lanes observed after the CME initiation, (2) strong Ovi $\lambda\lambda$1032, 1037 line profile broadenings (up to ~2Ч10^7 K) associated with the shock transit across the UVCS slit field of view, and (3) a density enhancement located in LASCO images above the CME front. Since the UVCS slit was centered at 4.1$R_\odot$, in correspondence with the flank of the expanding CME, this observation represents the highest UV detection of a shock obtained so far with the UVCS instrument. White-light and EUV data have been combined in order to estimate not only the shock compression ratio and the plasma temperature, but also the strength of the involved coronal magnetic fields, by applying the Rankine–Hugoniot equations for the general case of oblique shocks. Results show that, for a compression ratio X = 2.06 as derived from LASCO data, the coronal plasma is heated across the shock from an initial temperature of 2.3 Ч 10^5 K up to 1.9 Ч 10^6 K, while at the same time the magnetic field undergoes a compression from a pre-shock value of ~0.02 G up to a post-shock field of ~0.04 G. Magnetic and kinetic energy density increases at the shock are comparable (in agreement with the idea of equipartition of energy), and both are more than two times larger than the thermal energy density increase. This is the first time that a complete characterization of pre- and post-shock plasma physical parameters has been derived in the solar corona.

Zebra Stripes with High Gyro-Harmonic Numbers

Jan **Benáček** & Marian Karlický

Solar Physics volume 297, Article number: 103 (**2022**)

https://link.springer.com/content/pdf/10.1007/s11207-022-02036-y.pdf

Solar radio zebras are used in the determination of the plasma density and magnetic field in solar flare plasmas. Analyzing observed zebra stripes and assuming their generation by the double-plasma resonance (DPR) instability, high values of the gyro-harmonic number are found. In some cases they exceed one hundred, in disagreement with the DPR growth rates computed up to now, which decrease with increasing gyro-harmonic number. We address the question of how zebras with high values of the gyro-harmonic numbers ss are generated. For this purpose, we compute the growth rates of the DPR instability in a very broad range of ss, considering a loss-cone κκ-distribution of superthermal electrons and varying the loss-cone angle, electron energies, and background plasma temperature. We have numerically calculated the dispersion relations and the growth rates of the upper-hybrid waves and found that the growth rates increase with increasing gyro-harmonic numbers if the loss-cone angles are ∼80∘. The highest growth rates for these loss-cone angles are obtained for velocity vκ=0.15cvκ. The growth rates as a function of the gyro-harmonic number still show well distinct peaks, which correspond to zebra-stripe frequencies. The contrast between peak growth rates and surrounding growth rate levels increases as the κκ index increases and the background temperature decreases. Zebras with high values of ss can be generated in regions where loss-cone distributions of superthermal electrons with large loss-cone angles (∼80∘) are present. Furthermore, owing to the high values of ss, the magnetic field is relatively weak and has a small spatial gradient in such regions. **14 February 1999**

CESRA #3425 **2022** https://www.astro.gla.ac.uk/users/eduard/cesra/?p=3425

Expansion of Hot Plasma with Kappa Distribution into Cold Plasma

Jan **Benáček**1 and Marian Karlický2

2020 ApJ 896 9

https://doi.org/10.3847/1538-4357/ab89a5

https://sci-hub.tw/https://iopscience.iop.org/article/10.3847/1538-4357/ab89a5

The X-ray emission of coronal flare sources can be explained by considering the kappa electron distribution. Motivated by this fact, we study the problem of how hot plasma with the kappa distribution of electrons is confined in these sources. For comparison, we analyze the same problem, but with the Maxwellian distribution. We use a 3D particle-in-cell code, which is large in one direction and thus effectively only one-dimensional, but describe all electromagnetic effects. In the case with the Maxwellian distribution, and in agreement with the previous studies, we show a formation of the double layer at the hot–cold transition region that suppresses the flux of hot electrons from hot plasma into the cold

one. In the case with the kappa distribution, contrary to the Maxwellian case, we found that there are several fronts with the double layers in the hot–cold transition region. It is caused by a more extended tail in the kappa case than in the Maxwellian one. The electrons from the extended tail freely escape from the hot plasma into a cold one. They form a beam that generates the return current and also Langmuir turbulence, where Langmuir waves accumulated at some locations. At these locations, owing to the ponderomotive force, Langmuir waves generate density depressions, where the double layers with the thermal fronts that suppress the hot electron flux, are formed. We also show how protons accelerate in these processes. Finally, we compare the Kappa and Maxwellian cases and discuss how these processes could be observed.

Growth Rates of the Electrostatic Waves in Radio Zebra Models

Jan **Benáček**1 and Marian Karlický2
2019 ApJ 881 21
sci-hub.se/10.3847/1538-4357/ab2bfc
Zebras were observed not only in the solar radio emission but also in radio emissions of Jupiter and the Crab Nebula pulsar. In their models, growth rates of the electrostatic waves play an important role. Considering the plasma composed from the thermal background plasma and hot and rare component with the Dory–Guest–Harris distribution, we compute the growth rates γ and dispersion branches of the electrostatic waves in the ω − k ⊥ domain. We show complexity of the electrostatic wave branches in the upper-hybrid band. In order to compare the results, which we obtained using the kinetic theory and particle-in-cell (PIC) simulations, we define and compute the integrated growth rate Γ, where the "characteristic width" of dispersion branches was considered. We found a very good agreement between the integrated growth rates and those from PIC simulations. For maximal and minimal Γ we showed locations of dispersion branches in the ω − k ⊥ domain. We found that Γ has a maximum when the dispersion branches not only cross the region with high growth rates γ, but when the dispersion branches in this region are sufficiently long and wide. We also mentioned the effects of changes in the background plasma and hot component temperatures.

Growth rates of the electrostatic waves in the upper-hybrid band

Jan **Benáček**, Marian Karlický
A&A **2019**
https://arxiv.org/pdf/1904.12601.pdf
The electrostatic waves with the frequencies close to the upper-hybrid frequency (the upper-hybrid band) are important for the generation of solar radio zebras. Considering the plasma composed from the thermal background plasma and hot and rare plasma component in the form of the Dory-Guest-Harris distribution, we study the growth rates of the electrostatic waves in the upper-hybrid band. We use both analytical and numerical methods. Varying the ratio of the electron-plasma and electron-cyclotron frequencies ωpe/ωce in the range of 4.0-5.3 and using analytical expressions we compute the growth rates γ and dispersion branches of the electrostatic waves in the ω−k⊥ domain. In real plasma, the instabilities of waves with different dispersion branches can start simultaneously; therefore we define and compute the integrated growth rate Γ. For maximal and minimal Γ we how locations of the growth rates γ and dispersion branches in the ω−k⊥ domain. We find that Γ has a maximum when the dispersion branches not only cross the region with high growth rates γ but when the dispersion branches in this region are sufficiently long and wide. Around the value of ωpe/ωce = 4.95, we recognize an exciting interchange of dispersion branches, where it is difficult to distinguish types of waves. We also analyze the effects of changes in the background plasma and hot component temperatures. Then in the same range of ωpe/ωce we compute the growth rate of the electrostatic waves (which is naturally the integrated growth rate Γ) using a 3-dimensional Particle-in-Cell model. Finally, we compare both analytical and numerical results.

Double plasma resonance instability as a source of solar zebra emission

Jan **Benáček**, Marian Karlický
A&A 611, A60 **2018**
https://arxiv.org/pdf/1711.04281.pdf
https://www.aanda.org/articles/aa/pdf/2018/03/aa31424-17.pdf
http://sci-hub.tw/https://www.aanda.org/articles/aa/abs/2018/03/aa31424-17/aa31424-17.html
The double plasma resonance (DPR) instability plays a basic role in the generation of solar radio zebras. In the plasma, consisting of the loss-cone type distribution of hot electrons and much denser and colder background plasma, this instability generates the upper-hybrid waves, which are then transformed into the electromagnetic waves and observed as radio zebras. In the present paper we numerically study the double plasma resonance instability from the point of view of the zebra interpretation. We use a 3-dimensional electromagnetic particle-in-cell (3-D PIC) relativistic model. First using the multi-mode model, we study details of the double plasma resonance instability. We show how the distribution function of hot electrons changes during this instability. Then we show that there is a very good agreement

between results obtained by the multi-mode and specific-mode models, which is caused by a dominance of the wave with the maximal growth rate. Therefore, for computations in a broad range of model parameters, we use the specific-mode model. We compute the maximal growth rates of the double plasma resonance instability. The results are compared with the analytical ones. We find a very good agreement between numerical and analytical growth rates. We also compute saturation energies of the upper-hybrid waves in a very broad range of parameters. We find that the saturation energies of the upper-hybrid waves show maxima and minima at almost the same values of ωUH/ωce as the growth rates. Furthermore, we find that the saturation energy of the upper-hybrid waves is proportional to the density of hot electrons. The maximum saturated energy can be up to one percent of the kinetic energy of hot electrons. All these findings can be used in the interpretation of solar radio zebras.

Temperature dependent growth rates of the upper-hybrid waves and solar radio zebra patterns

Jan **Benáček**, Marian Karlický, Leonid V. Yasnov
A&A 598, A106 **2017**
https://arxiv.org/pdf/1701.06520v1.pdf

Context. The zebra patterns observed in solar radio emission are very important for are plasma diagnostics. The most promising model of these patterns is based on double plasma resonance instability, which generates upper-hybrid waves, which can be then transformed into the zebra emission. Aims. We aim to study in detail the double plasma resonance instability of hot electrons, together with a much denser thermal background plasma. In particular, we analyse how the growth rate of the instability depends on the temperature of both the hot plasma and background plasma components. Methods. We numerically integrated the analysed model equations, using Python and Wolfram Mathematica. Results. We found that the growth-rate maxima of the upper-hybrid waves for non-zero temperatures of both the hot and background plasma are shifted towards lower frequencies comparing to the zero temperature case. This shift increases with an increase of the harmonic number s of the electron cyclotron frequency and temperatures of both hot and background plasma components. We show how this shift changes values of the magnetic field strength estimated from observed zebras. We confirmed that for a relatively low hot electron temperature, the dependence of growth rate vs. both the ratio of the electron plasma and electron cyclotron frequencies expresse distinct peaks, and by increasing this temperature these peaks become smoothed. We found that in some cases, the values of wave number vector components for the upper-hybrid wave for the maximal growth rate strongly deviate from their analytical estimations. We confirmed the validity of the assumptions used when deriving model equations.

Observation of an Extraordinary Type V Solar Radio Burst: Nonlinear Evolution of the Electron Two-Stream Instability.

Benz, A.O., Huber, C.R., Timmel, V. *et al.*
Sol Phys **299**, 146 (**2024**).
https://doi.org/10.1007/s11207-024-02395-8
https://link.springer.com/content/pdf/10.1007/s11207-024-02395-8.pdf
https://arxiv.org/pdf/2412.01366

Solar type V radio bursts are associated with type III bursts. Several processes have been proposed to interpret the association, electron distribution, and emission. We present the observation of a unique type V event observed by e-CALLISTO on **7 May 2021**. The type V radio emission follows a group of U bursts. Unlike the unpolarized U bursts, the type V burst is circularly polarized, leaving room for a different emission process. Its starting edge drifts to higher frequency four times slower than the descending branch of the associated U burst. The type V processes seem to be ruled by electrons of lower energy. The observations conform to a coherent scenario where a dense electron beam drives the two-stream instability (causing type III emission) and, in the nonlinear stage, becomes unstable to another instability, previously known as the electron firehose instability (EFI). The secondary instability scatters some beam electrons into velocities perpendicular to the magnetic field and produces, after particle loss, a trapped distribution prone to electron cyclotron masering (ECM). A reduction in beaming and the formation of an isotropic halo are predicted for electron beams continuing to interplanetary space, possibly observable by Parker Solar Probe and Solar Orbiter.

Observations of a Radio-quiet Solar Preflare

A. O. **Benz**, M. Battaglia, M. Guedel
Solar Phys. 292:151 **2017**
https://arxiv.org/pdf/1709.06417.pdf
https://doi.org/10.1007/s11207-017-1175-3

The preflare phase of the flare SOL**2011-08-09**T03:52 is unique in its long duration, its coverage by the {\it Reuven Ramaty High Energy Solar Spectroscopic Imager (RHESSI) and the Nobeyama Radioheliograph}, and the presence of

three well-developed soft X-ray (SXR) peaks. No hard X-rays (HXR) are observed in the preflare phase. Here we report that also no associated radio emission at 17 GHz was found despite the higher sensitivity of the radio instrument. The ratio between the SXR peaks and the upper limit of the radio peaks is larger by more than one order of magnitude compared to regular flares. The result suggests that the ratio between acceleration and heating in the preflare phase was different than in regular flares. Acceleration to relativistic energies, if any, occurred with lower efficiency.
CESRA Highlight #1562 Oct **2017** http://cesra.net/?p=1562
See **Correction** Solar Physics February **2018**, 293:32
https://link.springer.com/content/pdf/10.1007%2Fs11207-018-1256-y.pdf

Location of Decimetric Pulsations in Solar Flares

Arnold O. **Benz**, Marina Battaglia and Nicole Vilmer
Solar Physics, Volume 273, Number 2, 363-375, **2011**
This work investigates the spatial relation between coronal X-ray sources and coherent radio emissions, both generally thought to be signatures of particle acceleration. Two limb events were selected during which the radio emission was well correlated in time with hard X-rays. The radio emissions were of the type of decimetric pulsations as determined from the spectrogram observed by Phoenix-2 of ETH Zurich. The radio positions were measured from observations with the Nançay Radioheliograph between 236 and 432 MHz and compared to the position of the coronal X-ray source imaged with RHESSI. The radio pulsations originated at least 30 – 240 Mm above the coronal hard X-ray source. The altitude of the radio emission increases generally with lower frequency. The average positions at different frequencies are on a line pointing approximately to the coronal hard X-ray source. Thus, the pulsations cannot be caused by electrons trapped in the flare loops, but are consistent with emission from a current sheet above the coronal source.
10 June 2003 14:07 – 14:09 UT and **5 December 2006**

Decimetric pulsations and coronal X-ray sources

A. **Benz**, M. Battaglia, and N. Vilmer
RHESSI Science Nugget, No 150, April **2011**
http://sprg.ssl.berkeley.edu/~tohban/wiki/index.php/Decimetric_pulsations_and_coronal_X-ray_sources
Pulsations are the strongest flare emissions at decimeter radio wavelengths, and they are common. Coherent stellar radio emissions are of a similar type. Sometimes they are regular oscillations with periods of the order of one second, at other times, and especially at high frequencies, they are irregular and faster. The question may come to the mind of the gentle Nugget reader, how such radio emissions may complement our picture of flare physics. Although decimetric pulsations are generally believed to originate from non-thermal electrons, they often do not correlate in time with non-thermal X-rays. We have decided to select cases where the two emissions do correlate within a few seconds and investigate the spatial relations more closely, using flares that occurred near the limb. This simplifies the geometry and the interpretation of the spatial relations. **5 December 2006**

High Spectral Resolution Observation of Decimetric Radio Spikes Emitted by Solar Flares – First Results of the Phoenix-3 Spectrometer

Arnold O. **Benz** · Christian Monstein · Michael Beverland · Hansueli Meyer · Bruno Stuber
Solar Phys (**2009**) 260: 375–388
A new multichannel spectrometer, Phoenix-3, is in operation having capabilities to observe solar flare radio emissions in the 0.1 – 5 GHz range at an unprecedented spectral resolution of 61.0 kHz with high sensitivity. The present setup for routine observations allows measuring circular polarization, but requires a data compression to 4096 frequency channels in the 1 – 5 GHz range and to a temporal resolution of 200 ms. First results are presented by means of a well observed event that included narrowband spikes at 350 – 850 MHz. Spike bandwidths are found to have a power – law distribution, dropping off below a value of 2 MHz for full width at half maximum (FWHM). The narrowest spikes have a FWHM bandwidth less than 0.3 MHz or 0.04% of the central frequency. The smallest half-power increase occurs within 0.104 MHz at 443.5 MHz, which is close to the predicted natural width of maser emission. The spectrum of spikes is found to be asymmetric, having an enhanced low-frequency tail. The distribution of the total spike flux is approximately an exponential.

A World-Wide Net of Solar Radio Spectrometers: e-CALLISTO
A. O. **Benz**, C. Monstein, H. Meyer, P. K. Manoharan, R. Ramesh, A. Altyntsev, A. Lara, J. Paez, K.-S. Cho
Earth Moon Planet (**2009**) 104:277–285, **File** DOI 10.1007/s11038-008-9267-6
Radio spectrometers of the CALLISTO type to observe solar flares have been distributed to nine locations around the globe. The instruments observe automatically, their data is collected every day via internet and stored in a central data base. A public webinterface exists through which data can be browsed and retrieved. The nine instruments form a network called e-CALLISTO. It is still growing in the number of stations, as redundancy is desirable for full 24 h coverage of the solar radio emission in the meter and low decimeter band. The e-CALLISTO system has already proven to be a valuable new tool for monitoring solar activity and for space weather research.

Radio bursts of the non-thermal sun (a review)
A.O. **Benz**
Landolt-Boernstein LB **VI/4B** 4.1.2.8 (**2009), File**

Quiet and slowly varying radio emissions of the sun (**a review**)
A.O. **Benz**
Landolt-Boernstein LB **VI/4B** 4.1.1.6 (**2009), File**

A World-wide Net of Solar Radio Spectrometers ? e-CALLISTO
A.O. **Benz** , C. Monstein, H. Meyer, P. K. Manoharan, R. Ramesh, A. Altyntsev, A. Lara, J. Paez, and K.-S. Cho
E-print, Feb **2008**, **File**; Earth, Moon, and Planets (2008)
Radio spectrometers of the CALLISTO type to observe solar flares have been distributed to 9 locations around the globe. The instruments observe automatically. Their data is collected every day via internet and stored in a central data base. A public web-interface exists through which data can be browsed and retrieved. The 9 instruments form a network called e-CALLISTO. It is still growing in the number of stations, as redundancy is desirable for full 24 hour coverage of the solar radio emission in the meter and low decimeter band. The e-CALLISTO system has already proven to be a valuable new tool for monitoring solar activity and for space weather research.

Are There Radio-quiet Solar Flares?
Arnold O. **Benz,** Roman Braj?a, Jasmina Magdaleni?
Solar Phys., 240 (2), Page: 263 – 270, **2007**

RADIO EMISSION OF SOLAR FLARE PARTICLE ACCELERATION
A. O. **Benz**
A revew, Graz, **2005**, **File**

Callisto – A New Concept for Solar Radio Spectrometers
Arnold O. **Benz**, Christian Monstein, Hansueli Meyer
Solar Physics January **2005**, Volume 226, Issue 1, pp 143–15
A new radio spectrometer, CALLISTO, is presented. It is a dual-channel frequency-agile receiver based on commercially available consumer electronics. Its major characteristic is the low price for hardware and software, and the short assembly time, both two or more orders of magnitude below existing spectrometers. The instrument is sensitive at the physical limit and extremely stable. The total bandwidth is 825 MHz, and the width of individual channel is 300 kHz. A total of 1000 measurements can be made per second. The spectrometer is well suited for solar low-frequency radio observations pertinent to space weather research. Five instruments of the type were constructed until now and put into operation at several sites, including Bleien (Zurich) and NRAO (USA). First results in the 45–870 MHz range are

presented. Some of them were recorded in a preliminary setup during the time of high solar activity in October and November 2003.
See http://files.mail-list.com/m/iswinewsletter/ISWI-Instrument-Data-management-plan-CALLISTO.pdf

Deterministic behaviour in the dynamics of solar metric radio bursts with intermediate drifting patterns

Adolfo L. Mendez **Berhondo** · Ana K. Diaz Rodriguez · P. Zlobec · Lupe Cuendias Perez
Astrophys Space Sci (**2013**) 346:301–306
http://link.springer.com/article/10.1007/s10509-013-1455-9
The dynamic characteristics of solar metric radio bursts with intermediate drifting patterns (fiber bursts) as they evolve at fixed frequency are examined. The data were recorded using the radio polarimeter of the Trieste Astronomical Observatory. The aim is to determine if the underlying process can be described as a deterministic chaos. Correlation dimensions and Hurst exponent are estimated showing deterministic chaotic system of low dimension.

Length scales for September 14, 2005 solar noise storm

Méndez **Berhondo**, Adolfo L.; Rodríguez Taboada, Ramón E.; Zlobec, Paolo; Díaz Rodríguez, Ana K.
Advances in Space Research, Volume 51, Issue 10, p. 1810-1812, **2013**
Source length scales are estimated for the **September 14, 2005** solar noise storm from the spectral and temporal observed characteristics of the background continuum fluctuations and clusters of Type I bursts. The characteristic height of the magnetic structure where the noise storm source is located and the size of the source where Type I bursts clustering takes place were calculated. A lower limit for the height of the magnetic structure supporting the noise storm at 237 MHz was estimated too.

Solar radio pulsating structures during September 9, 2001 at meter wavelength

Adolfo L. Méndez **Berhondo**, Ramón E. Rodríguez Taboada[1] and Paolo Zlobec[2]
Astrophysics and Space Science, Volume 318 Number 1-2, 73 – 78, **2008**
Pulsating structures recorded at 237 MHz that are associated to decimetric continuum enhancement during the September 9, 2001 solar radio burst are described. We analyzed the radiopolarimetric data recorded at the Trieste Solar Radio System (INAF—Trieste Astronomical Observatory—Basovizza Observing Station) with very high time resolution (1 ms) at metric frequencies. Two different types of pulsations that occur in about 4 minutes at the same frequency are described. The possible mechanisms are analyzed and some parameters of the associated magnetic structure are estimated.

Attenuation of decameter wavelength sky noise during x-ray solar flares in 2013–2017 based on the observations of midlatitude HF radars

O.I.**Berngardt**, J.M.RuohoniemibN.NishitanicS.G.ShepherddW.A.BristoweE.S.Millerf
Journal of Atmospheric and Solar-Terrestrial Physics
Volume 173, August **2018**, Pages 1-13
https://reader.elsevier.com/reader/sd/F8CA539213879B508A2352165551EDE6140E0B9E58FA294D2AD5C27F005C51A40AD4F14FDD5537E1C1971E6B4F92310A
Based on a joint analysis of data from 10 midlatitude decameter wavelength radars effects are investigated during 80 x-ray flares that occurred in the period 2013–2017. For the investigation nine mid-latitude SuperDARN radars of the northern hemisphere (Adak Island West and East radars, Blackstone radar, Christmas Valley East and West radars, Fort Hays East and West radars, Hokkaido East radar and Wallops radar) and Ekaterinburg coherent decameter radar of ISTP SB RAS are used. All the radars work in the same 8–20 MHz frequency band and have similar hardware and software. During the analysis the temporal dynamics of noise from each of the radar direction and for each flare is investigated separately. As a result, on the basis of about 13000 daily measurements we found a strong anticorrelation between noise power and x-ray flare intensity, indicating that short-wave sky noise can be used to diagnose the ionospheric effects of x-ray solar flares. It is shown that in 88.3% of cases an attenuation of daytime decameter radio noise is observed during solar flares, and the attenuation correlates with the temporal dynamics of the solar flare. The intensity of decameter noise

anticorrelates well (the Pearson correlation coefficient better than −0.5) with the shape of the X-ray flare in the daytime (for solar elevation angle >0) in 33% of cases, the average Pearson correlation over the daytime is about −0.34. Median regression coefficient between GOES 0.1–0.8 nm x-ray intensity and daytime sky-noise attenuation is about −4.4·104[dB·m2/Wt]. Thus, it is shown that measurements of the sky noise level at midlatitude decameter radars can be used to study the ionospheric absorption of high-frequency waves in the lower ionosphere during x-ray solar flares. This can be explained by the assumption that the larger part of the decameter sky noise detected by the radars is produced by ground sources at distances of the first propagation hop (~3000 km).

Conditions for the Excitation of Type I Solar Bursts.

Bespalov, P.A., Savina, O.N.
Geomagn. Aeron. 63, 910–915 (**2023**).
https://doi.org/10.1134/S0016793223070046
According to modern concepts, Type I noise storms in the meter wavelength range (30–400 MHz), consisting of a large number of narrow-band short bursts, are excited in the rarefied solar corona. These radiations are characterized by a high brightness temperature and circular polarization. Despite many advances in theory and confidence that the mechanism of radiation formation is coherent, there is currently no generally accepted understanding of the nature of Type I noise storms. In this paper, we show that many important properties of radiation can be explained as a result of the BPA (beam-pulse-amplifier) mechanism in a rarefied magnetized plasma with energetic electrons. Short noise electromagnetic pulses with a suitable carrier frequency, with circular polarization and wave normal angle can be amplified in the plasma layer at an extremely high rate, which is characteristic of quasi-hydrodynamic type instability. When this mechanism occurs, high energy and the rate of change in the spectral forms of radiation can take place even in the absence of a noticeable anisotropy of the distribution function of energetic electrons.

Transient Phenomena in the Energetic Behind-the-Limb Solar Flare of September 29, 1989

Bhatnagar, A.; Jain, R. M.; Burkepile, J. T.; Chertok, I. M.; Magun, A.; Urbarz, H.; Zlobec, P.
ASTROPHYSICS AND SPACE SCIENCE I Vol. 243 No. 1 **1996**; edited by S. Ananthakrishnan; A. Pramesh Rao., p.209-213
https://ui.adsabs.harvard.edu/link_gateway/1996Ap%26SS.243..209B/ADS_PDF
The powerful cosmic ray flare of **Sept. 29, 1989** occurred behind the limb and was observed over a wide spectral range. The analysis of optical, radio, and other relevant data suggest two phases of energy release. After an impulsive phase a prolonged post eruption energy release occurred in an extended region of the corona following the eruption of a large coronal mass ejection (CME). This phase is responsible for numerous coronal and interplanetary phenomena including the ground-level increase of cosmic rays.

Properties of Type-II Radio Bursts in Relation to Magnetic Complexity of the Solar Active Regions.

Bhatt, T.N., Jain, R., Gopalswamy, N. et al.
Sol Phys 299, 74 (**2024**).
https://doi.org/10.1007/s11207-024-02318-7
Type-II radio bursts are believed to occur as a result of the shock driven by flares or coronal mass ejections (CMEs). While the shock waves are important for the acceleration of electrons necessary for the generation of the radio emission, the exact nature of the shock and coronal conditions necessary to produce type-II radio emission is still under debate. In this investigation, we probe the relationship of kinematic characteristics of the type-II radio bursts with the magnetic-field complexity (Mj) of the active regions visible on the photosphere. Our investigation of 64 type-II solar radio bursts, which are associated with flares and CMEs, reveals that Mj is linearly correlated in the logarithmic scale with the starting frequency (fs) and drift-rate ($\Delta f/\Delta t$) of type-II radio burst. Further, Mj exhibits a linear correlation with the shock height (r) and electron density (ne) in logarithmic scale. This indicates that high frequency (fs ≥100 MHz) bursts, which occur at the reconnection site near the solar surface, are produced from a strong magnetically complex region. Further, strong and complex magnetic-field regions produce shocks of higher speeds. Based on the derived plasma parameters of the radio bursts and their relationship with fs as well as with Mj, we propose that the high-frequency type-II bursts were generated in a special situation when the shock is produced due to magnetic reconnection occurring in the low-lying coronal loops. We conclude that type-II radio bursts can occur even in the inner corona as well as in the outer corona; however, it depends on the magnetic complexity of the active region in which the event occurs.

Variations in the Solar Coronal Rotation with Altitude - Revisited

Hitaishi **Bhatt**, Rupal Trivedi, Som Kumar Sharma, Hari Om Vats

Solar Phys. 292:55 **2017**
https://arxiv.org/pdf/1702.08297.pdf
http://link.springer.com/content/pdf/10.1007%2Fs11207-017-1071-x.pdf
Here we report in depth reanalysis of a paper by Vats et al. (2001) [Astrophys. J. 548, L87] based on the measurements of differential rotation with altitude as a function of observing frequencies (as lower and higher frequencies indicate higher and lower heights, respectively) in the solar corona. The radial differential rotation of the solar corona is estimated from daily measurements of the disc-integrated solar radio flux at 11 frequencies: (275, 405, 670, 810, 925, 1080, 1215, 1350, 1620, 1755 MHz and 2800 MHz). We use the same data as were used in Vats et al. (2001), but instead of the 12th maxima of autocorrelograms used there, we use the 1st secondary maxima to derive the synodic rotation period. We estimate synodic rotation by Gaussian fit of the 1st secondary maxima. Vats et al. (2001) reported that the sidereal rotation period increases with increasing frequency. The variation found by them was from 23.6 to 24.15 days in this frequency range with a difference of only 0.55 days. The present study finds that sidereal rotation period increases with decreasing frequency. The variation range is from 24.4 to 22.5 days and difference is about three times larger (1.9 days). However, at 925 MHz both studies give similar rotation period. In Vats et al. (2001) the Pearson factor with trend line was 0.86 whereas present analysis obtained a ~ 0.97 Pearson factor with the trend line. Our study shows that the solar corona rotates slower at higher altitudes, which is in contradiction to the findings reported in Vats et al. (2001).

Solar flares associated coronal mass ejections in case of type II radio bursts

Beena **Bhatt** , Lalan Prasad, Harish Chandra, Suman Garia
Astrophysics and Space Science August **2016**, 361:265
We have statistically studied 220 events from 1996 to 2008 (i.e. solar cycle 23). Two set of flare-CME is examined one with Deca-hectometric (DH) type II and other without DH type II radio burst. Out of 220 events 135 (flare-halo CME) are accompanied with DH type II radio burst and 85 are without DH type II radio burst. Statistical analysis is performed to examine the distribution of solar flare-halo CME around the solar disk and to investigate the relationship between solar flare and halo CME parameters in case of with and without DH type II radio burst. In our analysis we have observed that: (i) 10–20° latitudinal belt is more effective than the other belts for DH type II and without DH type II radio burst. In this belt, the southern region is more effective in case of DH type II radio burst, whereas in case of without DH type II radio burst dominance exits in the northern region. (ii) 0–10° longitudinal belt is more effective than the other belts for DH type II radio burst and without DH type II radio burst. In this belt, the western region is more effective in case of DH type II radio burst, while in case of without DH type II radio burst dominance exits in the eastern region. (iii) Mean speed of halo CMEs (1382 km/s) with DH type II radio burst is more than the mean speed of halo CMEs (775 km/s) without DH type II radio burst. (iv) Maximum number of M-class flares is found in both the cases. (v) Average speed of halo CMEs in each class accompanied with DH type II radio burst is higher than the average speed of halo CMEs in each class without DH type II radio burst. (vi) Average speed of halo CMEs, associated with X-class flares, is greater than the other class of solar flares in both the cases.

Imaging-spectroscopy of a band-split type II solar radio burst with the Murchison Widefield Array

Shilpi **Bhunia**, Eoin P. Carley, Divya Oberoi, Peter T. Gallagher
A&A 670, A169 **2023**
https://arxiv.org/pdf/2212.07698.pdf
https://www.aanda.org/articles/aa/pdf/2023/02/aa44456-22.pdf
Type II solar radio bursts are caused by magnetohydrodynamics (MHD) shocks driven by solar eruptive events such as Coronal Mass Ejections (CMEs). Often both fundamental and harmonic bands of type II bursts are split into sub-bands, generally believed to be coming from upstream and downstream regions of the shock; however this explanation remains unconfirmed. Here we present combined results from imaging analysis of type II radio burst band-splitting and other fine structures, observed by the Murchison Widefield Array (MWA) and extreme ultraviolet observations from Solar Dynamics Observatory (SDO)/Atmospheric Imaging Assembly (AIA) on **2014-Sep-28**. The MWA provides imaging-spectroscopy in the range of 80-300 MHz with a time resolution of 0.5 s and frequency resolution of 40 kHz. Our analysis shows that the burst was caused by a piston-driven shock with a driver speed of ∼112 km s−1 and shock speed of ∼580 km s−1. We provide rare evidence that band-splitting is caused by emission from multiple parts of the shock (as opposed to the upstream/downstream hypothesis). We also examine the small-scale motion of type II fine structure radio sources in MWA images. We suggest that this small-scale motion may arise due to radio propagation effects from coronal turbulence, and not because of the physical motion of the shock location. We present a novel technique that uses imaging spectroscopy to directly determine the effective length scale of turbulent density perturbations, which is found

to be 1 - 2 Mm. The study of the systematic and small-scale motion of fine structures may therefore provide a measure of turbulence in different regions of the shock and corona.

A Fokker-Planck Framework for Studying the Diffusion of Radio Burst Waves in the Solar Corona

N. H. **Bian**, A. G. Emslie, E. P. Kontar
2019 ApJ 873 33
https://arxiv.org/pdf/1902.00239.pdf
https://doi.org/10.3847/1538-4357/ab0411
Electromagnetic wave scattering off density inhomogeneities in the solar corona is an important process which determines both the apparent source size and the time profile of radio bursts observed at 1 AU. Here we model the scattering process using a Fokker-Planck equation and apply this formalism to several regimes of interest. In the first regime the density fluctuations are considered quasi-static and diffusion in wavevector space is dominated by angular diffusion on the surface of a constant energy sphere. In the small-angle ("pencil beam") approximation, this diffusion further occurs over a small solid angle in wavevector space. The second regime corresponds to a much later time, by which scattering has rendered the photon distribution near-isotropic resulting in a spatial diffusion of the radiation. The third regime involves time-dependent fluctuations and, therefore, Fermi acceleration of photons. Combined, these results provide a comprehensive theoretical framework within which to understand several important features of propagation of radio burst waves in the solar corona: emitted photons are accelerated in a relatively small inner region and then diffuse outwards to larger distances. En route, angular diffusion results both in source sizes which are substantially larger than the intrinsic source, and in observed intensity-versus-time profiles that are asymmetric, with a sharp rise and an exponential decay. Both of these features are consistent with observations of solar radio bursts.

Resonance broadening due to particle scattering and mode coupling in the quasi-linear relaxation of electron beams

Nicolas H. **Bian**1,*, Eduard P. Kontar1and Heather Ratcliffe
JGR, Volume 119, Issue 6, pages 4239–4255, June **2014**
Of particular interest for radio and hard X-ray diagnostics of accelerated electrons during solar flares is the understanding of the basic nonlinear mechanisms regulating the relaxation of electron beams propagating in turbulent plasmas. In this work, it is shown that in addition to scattering of beam electrons, scattering of the beam-generated Langmuir waves via for instance mode coupling can also result in broadening of the wave-particle resonance. We obtain a resonance-broadened version of weak turbulence theory with mode coupling to ion sound modes. Resonance broadening is presented here as a unified framework which can quantitatively account for the reduction and possible suppression of the beam instability due to background scattering of the beam electrons themselves or due to scattering of the beam-generated Langmuir waves in fluctuating plasmas. Resonance broadening being essentially equivalent to smoothing of the electron phase space distribution is used to construct an intuitive physical picture for the stability of inverted populations of fast electrons that are commonly observed in situ to propagate in the solar wind.

LOFAR For Space Weather (LOFAR4SW): Increasing European Space-Weather Capability with Europe's Largest Radio Telescope

Bisi, Mario M.; Vermeulen, René; Fallows, Richard A. and 11 more
Solar Atmospheric and Interplanetary Environment (SHINE 2019), held 5-9 August, **2019** in Boulder, Colorado. Online at https://shinecon.org/CurrentMeeting.php, id.229
The Low Frequency Array (LOFAR) consists of a dense core of 24 stations within a 4km diameter, 14 stations spread further afield across the northeast area of The Netherlands, and a further 13 stations spread internationally (six across Germany, three in northern Poland, and one each in France, Ireland, Sweden, and the UK). Further international expansion is under way. LOFAR observes over a wide bandwidth in radio frequencies (10-250 MHz) with both a high temporal and spatial resolution. LOFAR is one of the world's most-flexible radio instruments with capabilities that enable studies of several aspects of space weather to be progressed beyond today's state-of-the-art. However, in its present setup, LOFAR can only be used for space-weather purposes on a campaign bases of observations. This is where observing time has to be competed for alongside astronomy and all other types of radio observations requested. The LOFAR For Space Weather (LOFAR4SW) project is a Horizon 2020 (H2020) INFRADEV design study undertaking investigations/design steps into upgrading LOFAR to allow for regular space-weather monitoring observations in parallel with normal radio-astronomy and scientific operations. A fully-implemented LOFAR4SW system would include a wide range of observational capabilities covering the Sun, corona, inner heliosphere, Earth's ionosphere, Jupiter, heliosphere-planetary interactions, and potentially extra-solar space weather on a routine/regular basis adding to our

knowledge, understanding, and prediction capabilities of space weather ─ a global threat. In this presentation, we summarise the LOFAR4SW design study, progress to date post-Preliminary Design Review and pre-Mid-Term Review, and some of the longer-term goals envisaged for LOFAR to become one of Europe's most-comprehensive space-weather observatories, shedding new light on several aspects of the space-weather system, from the Sun to the solar wind to the ionosphere.

Preface: Radio Heliophysics: Science and Forecasting

Mario M. **Bisi** , J. Americo Gonzalez-Esparza , Bernard V. Jackson , Munetoshi Tokumaru, John Leibacher
Solar Physics September **2015**, Volume 290, Issue 9, pp 2393-2396
http://link.springer.com/article/10.1007/s11207-015-0784-y

Decimetric emission 500″ away from a flaring Site: Possible scenarios from GMRT solar radio observations

Susanta Kumar **Bisoi**, H. S. Sawant, P. Janardhan, Y. Yan, L. Chen, Arun Kumar Awasthi, Shweta Srivastava, G. Gao
ApJ **862** 65 **2018**
https://arxiv.org/pdf/1806.05802.pdf
We present a study of decimetric radio activity, using the first high time cadence (0.5 s) images from the Giant Meterwave Radio Telescope (GMRT) at 610 MHz, associated with GOES C1.4 and M1.0 class solar flares, and a coronal mass ejection (CME) onset that occurred on **20 June 2015**. The high spatial resolution images from GMRT show a strong radio source during the C1.4 flare, located ~500″ away from the flaring site with no corresponding bright footpoints or coronal features nearby. In contrast, however, strong radio sources are found near the flaring site during the M1.0 flare and around the CME onset time. Weak radio sources, located near the flaring site, are also found during the maximum of the C1.4 flare activity, which show a temporal association with metric type III bursts identified by the Solar Broadband Radio Spectrometer at Yunnan Astronomical Observatory. Based on a multi-wavelength analysis and magnetic potential field source surface extrapolations, we suggest that the source electrons of GMRT radio sources and metric type III bursts were originated from a common electron acceleration site. We also show that the strong GMRT radio source is generated by a coherent emission process and its apparent location far from the flaring site is possibly due to the wave-ducting effect.
CESRA Highlights #1960 Sept **2018** http://cesra.net/?p=1960

Determination of the Structure of the Coronal Magnetic Field Using Microwave Polarization Measurements

V. M. **Bogod** , L. V. Yasnov
Solar Phys. Volume 291, Issue 11, pp 3317–3328 **2016**
An analysis of the oscillatory motions and wave processes in active regions requires knowledge of the structure of the magnetic fields in the chromosphere and corona. We study the magnetic field structure of active regions at coronal heights, as they are determined by means of multiwave observations of polarized radio emission of active regions in the microwave range. Two methods, a stereoscopic method and the analysis of the radio spectrum are used. The method of stereoscopy rotation allows estimating the height of radio sources in a stable active region relative to the photosphere, based on its apparent motion in the image plane recorded over several days of observation. At various times one-dimensional scans at multiple frequencies spanning the 5.98 – 15.95 GHz frequency range from the RATAN-600 instrument are used. The gyroresonance emission mechanism, which is sensitive to the coronal magnetic field strength, is applied to convert the radio source estimated heights at various frequencies, h(f), to information as regards magnetic field vs. height, B(h). Diagrams of longitude – height of some polarized radio sources revealed multiple reversals, suggestive of a spiral magnetic structure. In all cases, the magnetic field strength maintains high values (800 – 1000 G) at the highest altitudes analysed, which reflects a relatively weak divergence in the field of magnetic flux tubes (in the height range 8 – 14 Mm) responsible for the main part of the radio emission of active regions.

On the recording of an emission with a reduced brightness in the region of a strong sunspot magnetic field

V. M. **Bogod**, N. G. Peterova, B. I. Ryabov, N. A. Topchilo
Cosmic Research, January **2015**, Volume 53, Issue 1, pp 10-20
Observations are reviewed of active regions where radio emission depressions in radio sources above large sunspots is observed. The depression value can be significant and can reach 2000–4000 K relative to the temperature around a quiet

Sun. However, the number of cases of strong depression is small, which is apparently related to the specific features and conditions of sunspot observations and the limited or restrict telescope possibilities of the present day. Usage of the RATAN-600 radio telescope with a high spectral resolution (1%) made it possible to establish that this phenomenon is observed in a limited wavelength range (1.7–3.0) cm. Owing to the special method of RATAN-600 polarization measurements, it has been indicated that the emission depression effect takes place in the ordinary o-mode emission, whereas the emission source above a sunspot is always brighter than the background in the extraordinary e-mode. Two new active regions where the depression phenomenon was registered have been considered, and a comparison with the data from the NoRH radioheliograph, SSRT, and spacecraft has been performed. The values of the magnetic fields above the sunspots at which the region of ordinary and extraordinary wave generation penetrates in the coronal temperature region have been measured. A depression phenomenon modeling, indicating that electron density decreases and the situation is similar to coronal holes, has been performed based on the set of observational data. Possible directions in the study of this phenomenon are discussed.

RATAN-600 Observations of Small Scale Structures with High Spectral Resolution

V. M. **Bogod**, C. E. Alissandrakis, T. I. Kaltman, S. Kh. Tokhchukova
Solar Phys., **2015**, Volume 290, Issue 1, pp 7-20
http://arxiv.org/pdf/1403.7658v1.pdf
We present observations of quiet-sun small-scale structures (SSS) in the microwave range with the {\it Radio Astronomical Telescope of the Academy of Sciences 600} (RATAN-600) spectral-polarization facility in a wide range of frequencies. SSS are regularly recorded in routine observations of the large reflector-type radio telescope and represent manifestations in the radio range of various structures of the quiet-sun: supergranulation network, bright points, plage patches and so on. A comparison with with images from the {\it Solar Dynamics Observatory} (SDO) showed that the microwave emission comes from a region extending from the chromosphere to the low transition region. We measured the properties of the SSS as well as the degree of circular polarization averaged over the beam of the radio telescope and from this we estimated the magnetic field at the formation level of the radiation.

On Magnetic Fields of Active Regions at Coronal Heights

V. M. **Bogod**, A. G. Stupishin und L. V. Yasnov
Solar Physics, Volume 276, Numbers 1-2, 61-73, **2012**
This paper analyzes the magnetic field structure of active regions at coronal heights determined by means of multi-wavelength observations of polarized radio emission in the microwave range, and compares it with the force-free magnetic field extrapolation into the corona from the photospheric magnetograms. Our method of one-dimensional radio stereoscopy indicates higher magnetic field strength compared with the field reconstructed from photospheric magnetograms. It is shown that the sense of inclinations of the field lines we obtained from the radio data matches the shape of the reconstructed magnetic field lines, although the degree of the inclinations is very different.

Polarization of Microwave Radio Emission of Flare-Producing Solar Active Regions

Vladimir M. **Bogod** · Leonid V. Yasnov
Solar Phys (**2009**) 255: 253–271
On the basis of our multiwavelength observations made with the one-dimensional RATAN-600 radio telescope, we study the inversion of the circular polarization in the solar microwave emission at different frequencies. The inversion is detected in the emission of flare-producing active regions (FPARs) at various stages of their development, starting from the pre-flare stage. During the latest 23rd solar cycle maximum, numerous FPARs revealed spectral inhomogeneities in their polarized microwave radiation (Bogod and Tokhchukova, 2003, *Astron. Lett.* **29**, 263). Here, we discuss a particular case of such inhomogeneities, the frequency-dependent double inversion of the sign of circular polarization, which probably reflects some essential processes in FPARs. We consider several mechanisms for the double inversion: linear interaction of waves in the region of a quasitransverse magnetic field, the propagation of waves through a region of zero magnetic field, the scattering of radio waves on waves of high-frequency plasma turbulence, the influence of the current fibrils on the propagation of the radio emission, and the magnetic "dips," in which the direction of magnetic field lines changes the sign relative to the observer. All of them have shortcomings, but the last mechanism explains the observations the best.

LANGMUIR WAVES ASSOCIATED WITH MAGNETIC HOLES IN THE SOLAR WIND

J.J. **Boldú**1,2, D. B. Graham1, M. Morooka1, M. André1 Yu. V. Khotyaintsev1, T. Karlsson3, J. Souček4, D. Píša4, and M. Maksimovic5
Solar Orbiter nugget #3 **2023**

https://www.cosmos.esa.int/web/solar-orbiter/science-nuggets/langmuir-waves-associated-with-magnetic-holes-in-the-solar-wind
2020-06-30

CONSTRUCTION OF AN E-CALLISTO STATION IN KOREA
Su-Chan **Bong**1, Yeon-Han Kim1, HeeSeon Roh2, Kyung-Suk Cho1, Seonghwan Choi1, Ji-Hye Baek1, Christian Monstein3, Arnold O. Benz3, Yong-Jae Moon2, and Sungsoo S. Kim2
Journal of The Korean Astronomical Society **42**: 1 ~ 7, **2009, File**
The e-CALLISTO is a global network of frequency-agile solar radio spectrometers that was constructed in a collaboration between Swiss Federal Institute of Technology Zurich (ETH Zurich) and local host institutes. It is intended to monitor solar radio bursts 24 hours a day in frequency range between 45 MHz and 870 MHz. One of e-CALLISTO spectrometer was installed at Korea Astronomy and Space Science Institute (KASI) in 2007 October. The spectrometer gets signals from a horizontally polarized log-periodic antenna mounted on an automatic Sun-tracking system. Tracking status and data are monitored in Space Weather Monitoring Laboratory (SWML) of KASI in real time, and flare time data are transferred to ETH Zurich data archive daily. Using this spectrometer we obtained a couple of type II solar radio bursts on **2007 December 31**, and found that these bursts are associated with a CME which occurred on the east limb.

The radio and plasma wave investigation on the STEREO mission,
J.L. **Bougeret**, K. Goetz, M.L. Kaiser et al.
Space Science Reviews, Vol 136, issue 1-4, **2008**.
This paper introduces and describes the radio and plasma wave investigation on the STEREO Mission: STEREO/WAVES or S/WAVES. The S/WAVES instrument includes a suite of state-of-the-art experiments that provide comprehensive measurements of the three components of the fluctuating electric field from a fraction of a hertz up to 16 MHz, plus a single frequency channel near 30 MHz. The instrument has a direction finding or goniopolarimetry capability to perform 3D localization and tracking of radio emissions associated with streams of energetic electrons and shock waves associated with Coronal Mass Ejections (CMEs). The scientific objectives include: (i) remote observation and measurement of radio waves excited by energetic particles throughout the 3D heliosphere that are associated with the CMEs and with solar flare phenomena, and (ii) in-situ measurement of the properties of CMEs and interplanetary shocks, such as their electron density and temperature and the associated plasma waves near 1 Astronomical Unit (AU). Two companion papers provide details on specific aspects of the S/WAVES instrument, namely the electric antenna system (Bale et al., Space Sci. Rev., 2007) and the direction finding technique (Cecconi et al., Space Sci. Rev., 2007).

A shock-associated (SA) radio event and related phenomena observed from the base of the solar corona to 1 AU.
Bougeret, J.-L., Zarka, P., Caroubalos, C., Karlick´y, M., Leblanc, Y., Maroulis, D., Hillaris, A., Moussas, X., Alissandrakis, C.E., Dumas, G., Perche, C.:
1998, Geophys. Res. Lett. 25, 2513 – 2516.
We present for the first time an almost complete frequency coverage of a Shock Associated (SA) radio event and related phenomena observed on **May 6, 1996** at 9:27 UT. It is observed from the base of the solar corona up to almost 1 Astronomical Unit (AU) from the Sun by the following radio astronomical instruments: the Ondřejov spectrometer operating between 4.5 GHz and 1 GHz (radiation produced near the chromosphere); the Thermopyles Artemis-IV spectrograph operating between 600 MHz and 110 MHz (distance range about 1.1-1.4 $R_\odot$ from sun center); the Nançay Decameter Array operating between 75 and 25 MHz (distance range about 1.4-2 $R_\odot$) and the RAD2 and RAD1 radio receivers on the WIND spacecraft covering the range from 14 MHz to about 20 kHz (distance range between 3 $R_\odot$ and about 1 AU). Observations at the Nançay Decameter Array clearly show that the SA event starts from a coronal type II radio burst which traces the progression of a shock wave through the corona above 1.8 $R_\odot$-2 $R_\odot$ from the sun center. This SA event has no associated radio emission in the decimetric-metric range, thus there is no evidence for electron injection in the low/middle corona.
Correction: Geophysical Research Letters, Volume 25, Issue 21, p. 4103-4103, **1998**

Waves: The radio and plasma wave investigation on the Wind spacecraft.
Bougeret, J.-L., Kaiser, M.L., Kellogg, P.J., Manning, R., Goetz, K., Monson, S.J., Monge, N., Friel, L., Meetre, C.A., Perche, C., Sitruk, L., Hoang, S.:
1995, Space Sci. Rev. 71, 231 – 263.

http://articles.adsabs.harvard.edu/cgi-bin/nph-iarticle_query?1995SSRv...71..231B&data_type=PDF_HIGH&whole_paper=YES&type=PRINTER&filetype=.pdf
The WAVES investigation on the WIND spacecraft will provide comprehensive measurements of the radio and plasma wave phenomena which occur in Geospace. Analyses of these measurements, in coordination with the other onboard plasma, energetic particles, and field measurements will help us understand the kinetic processes that are important in the solar wind and in key boundary regions of the Geospace. These processes are then to be interpreted in conjunction with results from the other ISTP spacecraft in order to discern the measurements and parameters for mass, momentum, and energy flow throughout geospace. This investigation will also contribute to observations of radio waves emitted in regions where the solar wind is accelerated. The WAVES investigation comprises several innovations in this kind of instrumentation: among which the first use, to our knowledge, of neural networks in real-time on board a scientific spacecraft to analyze data and command observation modes, and the first use of a wavelet transform-like analysis in real time to perform a spectral analysis of a broad band signal.

High resolution observations with Artemis--JLS, (II) Type IV associated intermediate drift bursts

C. **Bouratzis**, A. Hillaris, C.E. Alissandrakis, P. Preka-Papadema, X. Moussas, C. Caroubalos, P. Tsitsipis, A. Kontogeorgos
A&A 625, A58 **2019**
https://arxiv.org/pdf/1904.02262.pdf
sci-hub.se/10.1051/0004-6361/201834792
Aims. We examined the characteristics of isolated intermediate drift bursts (IMDs) and their morphologies on dynamic spectra, in particular the positioning of emission and absorption ridges and the repetition rate of fiber groups. These were compared with a model in order to determine the conditions under which the IMDs appear and exhibit the above characteristics. Methods. We analyzed sixteen metric type IV events with embedded IMDs. The events were recorded with the Artemis-JLS/SAO high resolution (10 ms cadence) receiver in the 270-450MHz range with a frequency resolution of 1.4 MHz. We developed cross- and autocorrelation techniques to measure the duration, spectral width, and frequency drift of fiber bursts in 47 IMD groups. We also developed a semi-automatic algorithm to track fibers on dynamic spectra. Results. We distinguish six morphological groups of fibers, based on the relative position of the emission and absorption ridges. These included fibers with emission or absorption ridges only, fibers with the absorption ridge at lower or higher frequency than the emission, or with two absorption ridges above and below the emission or with two emission ridges were separated by an absorption ridge. Some borderline cases of IMDs with very high drift rate (~0.30 s-1) or very narrow total bandwidth (~8 MHz) were recorded; among them a group of rope-like IMDs with fast repetition rate and relatively narrow total frequency extent. The whistler hypothesis leads to reasonable magnetic field (~4.6 G), but the Alfven-wave hypothesis requires much higher field. We estimated the ratio of the whistler to the cyclotron frequency, x, to be ~ 0.3 to 0.6 and the average frequency scale along the loop of ~220Mm. We present empirical relations between fiber burst parameters and discuss their possible origin. **1999-07-13, 2000-04-15, 2000-07-11, 2003-04-21, 2003-10-28, 2005-01-17, 2005-07-14, 2010-08-01**

Metric Fiber Bursts Observed with the Artemis-IV RadioSpectrograph

Costas **Bouratzis**_1, Alexander Hillaris2, Costas Alissandrakisy3, Panagiota Preka-Papadema2, Xenophon Moussas2, Panagiotis Tsitsipis4, and Athanasios Kontogeorgos5
CESRA **2016**, p.90
http://cesra2016.sciencesconf.org/conference/cesra2016/pages/CESRA2016_prog_abs_book_v3.pdf
We analyzed fifteen metric type-IV events accompanied by intermediate drift bursts, observed by the ARTEMIS-IV radio spectrograph and recorded with the SAO high resolution (100 samples per second) receiver; fourteen events occurred in the 1999-2005 period and one in 2010. Computational tools were developed for the extraction of the _ber emission from the background and other emissions and for the objective measurement of the bulk parameters of fiber burst groups, such as 1-D and 2-D autocorrelation, cross correlation, radial integration of power spectrum and wavelet analysis. We thus measured the drift rate, the instantaneous spectral width, the duration at _xed frequency, the periodicity and the variation of the drift rate and the duration with frequency and time. In addition, particular types of intermediate drift bursts, such as fast drift bursts and ropes, have been studied and compared with the values of typical _bers. Finally, we discuss our results in terms of current theoretical models.

High resolution observations with Artemis-IV and the NRH. I. Type IV associated narrow-band bursts

C. **Bouratzis**, A. Hillaris, C.E. Alissandrakis, P. Preka-Papadema, X. Moussas, C. Caroubalos, P. Tsitsipis, A. Kontogeorgos
A&A 586, A29 **2016**
http://arxiv.org/pdf/1512.02481v1.pdf

Narrow band bursts appear on dynamic spectra from microwave to decametric frequencies as fine structures with very small duration and bandwidth. They are thought to mark small scale magnetic reconnection. We analyzed 27 metric type-IV events with narrow band bursts observed by the ARTEMIS-IV radiospectrograph in 30/6/1999-1/8/2010. We examined the morphological characteristics of isolated narrow-band bursts and groups or chains of spikes. The events were recorded with the SAO (10 ms cadence) receiver of ARTEMIS-IV in the 270-450 MHz range. We measured the duration, spectral width, and frequency drift of ~12000 individual narrow-band bursts, groups, and chains. Spike sources were imaged with the NRH for the event of **21 April 2003**. The mean duration of individual bursts at fixed frequency was ~100 ms, while the instantaneous relative bandwidth was ~2%. Some bursts had measurable frequency drift, positive or negative. Often spikes appeared in chains, which were closely spaced in time (column chains) or in frequency (row chains). Column chains had frequency drifts similar to IIId-bursts; most of the row chains exhibited negative drifts similar to fiber bursts. From the NRH data, we found that spikes were superimposed on a larger, slowly varying, background component. They were polarized in the same sense as the background source, with a slightly higher degree of polarization of ~65%, and their size was ~60% of their size in total intensity. The duration and bandwidth distributions did not show any clear separation in groups. Some chains tended to assume the form of zebra, lace stripes, fibers, or bursts of the type-III family, suggesting that such bursts might be resolved in spikes when viewed with high resolution. The NRH data indicate that the spikes are not fluctuations of the background, but represent additional emission such as what would be expected from small-scale reconnection.
2000−04−15, 2000−07−11, 2000−07−14, 2003−04−21, 2004−01−20, 2004−03−30, 2004−04−06, 2005−01−20, 2005−07−30

Fine Structure of Metric Type-IV Radio Bursts Observed with the ARTEMIS-IV Radio Spectrograph: Association with Flares and Coronal Mass Ejections

C. **Bouratzis**, A. Hillaris, C. E. Alissandrakis, P. Preka-Papadema, X. Moussas, C. Caroubalos, P. Tsitsipis, A. Kontogeorgos
Solar Phys., **2015**, Volume 290, Issue 1, pp 219-286
http://arxiv.org/pdf/1406.1202v1.pdf

Fine structures embedded in type-IV burst continua may be used as diagnostics of the magnetic field restructuring and the corresponding energy release associated with the low corona development of flare/CME events. **A catalog of 36 type-IV bursts observed with the SAO receiver of the ARTEMIS-IV solar radio-spectrograph in the 450--270 MHz range at high cadence (0.01 sec) was compiled;** the fine structures were classified into five basic classes with two or more sub-classes each. The time of fine structure emission was compared with the injection of energetic electrons as evidenced by HXR and microwave emission, the SXR light-curves and the CME onset time. Our results indicate a very good temporal association between energy release episodes and pulsations, spikes, narrow-band bursts of the type-III family and zebra bursts. Of the remaining categories, the featureless broadband continuum starts near the time of the first energy release, between the CME onset and the SXR peak, but extends for several tens of minutes after that, covering almost the full extent of the flare--CME event. The intermediate drift bursts, fibers in their majority, mostly follow the first energy release but have a wider distribution, compared to other fine structures. **21 April 2003, 18-11-2000, 28-10-2003, 6-4-2004, 13-7-1999, 2005−07−14, 2003−04−21; 2004−03−25, 2000−07−11, 2000−07−14,**

Radio Observations of the 20 January 2005 X-class Flare

C. **Bouratzis** · P. Preka-Papadema · A. Hillaris · P. Tsitsipis · A. Kontogeorgos · V.G. Kurt · X. Moussas
Solar Phys, 267, Issue 2, pp.343-359, **2010; File**
http://arxiv.org/pdf/0912.3782v10.pdf

We present a multi-frequency and multi-instrument study of the **20 January 2005** event. We focus mainly on the complex radio signatures and their association with the active phenomena taking place: flares, CMEs, particle acceleration, and magnetic restructuring. As a variety of energetic-particle accelerators and sources of radio bursts are present, in the flare – ejecta combination, we investigate their relative importance in the progress of this event. The

dynamic spectra of ARTEMIS-IV – Wind/Waves – HiRAS, with 2000 MHz – 20 kHz frequency coverage, were used to track the evolution of the event from the low corona to the interplanetary space; these were supplemented with SXR, HXR, and γ-ray recordings. The observations were compared with the expected radio signatures and energetic-particle populations envisaged by the Standard Flare – CME model and the reconnection outflow termination shock model. A proper combination of these mechanisms seems to provide an adequate model for the interpretation of the observational data.

Metric radio bursts and fine structures observed on 17 January, 2005

C. **Bouratzis**[a], P. Preka-Papadema[a], X. Moussas[a], C. Alissandrakis[b] and A. Hillaris
Advances in Space Research, Volume 43, Issue 4, 16 February **2009**, Pages 605-611
http://arxiv.org/pdf/1009.3577v1.pdf
A complex radio event was observed on January 17, 2005 with the radio-spectrograph ARTEMIS-IV, operating at Thermopylae, Greece; it was associated with an X3.8 SXR flare and two fast Halo CMEs in close succession. We present dynamic spectra of this event; the high time resolution (1/100 s) of the data in the 450–270 MHz range, makes possible the detection and analysis of the fine structure which this major radio event exhibits. The fine structure was found to match, almost, the comprehensive Ondrejov Catalogue which it refers to the spectral range 0.8–2 GHz, yet seems to produce similar fine structure with the metric range.

ALMA small-scale features in the quiet Sun and active regions

R. **Brajsa**, I. Skokic, D. Sudar, A. O. Benz, S. Krucker, H.-G. Ludwig, S. H. Saar, C. L. Selhorst
A&A 651, A6 **2021**
https://arxiv.org/pdf/2105.03644.pdf
https://www.aanda.org/articles/aa/pdf/2021/07/aa36231-19.pdf
https://doi.org/10.1051/0004-6361/201936231
Aims. The main aim of the present analysis is to decipher (i) the small-scale bright features in solar images of the quiet Sun and active regions obtained with the Atacama Large Millimeter/submillimeter Array (ALMA) and (ii) the ALMA correspondence of various known chromospheric structures visible in the H-alpha images of the Sun. Methods. Small-scale ALMA bright features in the quiet Sun region were analyzed using single-dish ALMA observations (1.21 mm, 248 GHz) and in an active region using interferometric ALMA measurements (3 mm, 100 GHz). With the single-dish observations, a full-disk solar image is produced, while interferometric measurements enable the high-resolution reconstruction of part of the solar disk, including the active region. The selected quiet Sun and active regions are compared with the H-alpha (core and wing sum), EUV, and soft X-ray images and with the magnetograms. Results. In the quiet Sun region, enhanced emission seen in the ALMA is almost always associated with a strong line-of-sight (LOS) magnetic field. Four coronal bright points were identified, while other small-scale ALMA bright features are most likely associated with magnetic network elements and plages. In the active region, in 14 small-scale ALMA bright features randomly selected and compared with other images, we found five good candidates for coronal bright points, two for plages, and five for fibrils. Two unclear cases remain: a fibril or a jet, and a coronal bright point or a plage. A comparison of the H-alpha core image and the 3 mm ALMA image of the analyzed active region showed that the sunspot appears dark in both images (with a local ALMA radiation enhancement in sunspot umbra), the four plage areas are bright in both images and dark small H-alpha filaments are clearly recognized as dark structures of the same shape also in ALMA. **16 and 18 December 2015**

Observations of the solar chromosphere with ALMA and comparison with theoretical models

R. **Brajša**, D. Sudar, I. Skokic, A. O. Benz, M. Kuhar, A. Kobelski, S. Wedemeyer, S. M. White, H.-G. Ludwig, M. Temmer, S. H. Saar, C. L. Selhorst
The 20th Cambridge Workshop on Cool Stars, Stellar Systems, and the Sun, July 29 - Aug 3 2018, Boston / Cambridge, USA **2018**
https://arxiv.org/pdf/1812.07293.pdf
In this work we use solar observations with the ALMA radio telescope at the wavelength of 1.21 mm. The aim of the analysis is to improve understanding of the solar chromosphere, a dynamic layer in the solar atmosphere between the photosphere and corona. The study has an observational and a modeling part. In the observational part full-disc solar images are analyzed. Based on a modified FAL atmospheric model, radiation models for various observed solar structures are developed. Finally, the observational and modeling results are compared and discussed. **December 18th, 2015**

First analysis of solar structures in 1.21 mm full-disc ALMA image of the Sun

R. **Brajša**1, D. Sudar1, A. O. Benz2, I. Skokić1, M. Bárta3, B. De Pontieu4,10, S. Kim5, A. Kobelski6, M. Kuhar2,7, M. Shimojo8,9, S. Wedemeyer10, S. White11, P. Yagoubov12 and Y. Yan13
A&A 613, A17 (**2018**)
https://www.aanda.org/articles/aa/pdf/2018/05/aa30656-17.pdf
Context. Various solar features can be seen in emission or absorption on maps of the Sun in the millimetre and submillimetre wavelength range. The recently installed Atacama Large Millimetre/submillimetre Array (ALMA) is capable of observing the Sun in that wavelength range with an unprecedented spatial, temporal and spectral resolution. To interpret solar observations with ALMA, the first important step is to compare solar ALMA maps with simultaneous images of the Sun recorded in other spectral ranges.
Aims. The first aim of the present work is to identify different structures in the solar atmosphere seen in the optical, infrared, and EUV parts of the spectrum (quiet Sun, active regions, prominences on the disc, magnetic inversion lines, coronal holes and coronal bright points) in a full-disc solar ALMA image. The second aim is to measure the intensities (brightness temperatures) of those structures and to compare them with the corresponding quiet Sun level.
Methods. A full-disc solar image at 1.21 mm obtained on **December 18, 2015**, during a CSV-EOC campaign with ALMA is calibrated and compared with full-disc solar images from the same day in Hα line, in He I 1083 nm line core, and with various SDO images (AIA at 170 nm, 30.4 nm, 21.1 nm, 19.3 nm, and 17.1 nm and HMI magnetogram). The brightness temperatures of various structures are determined by averaging over corresponding regions of interest in the calibrated ALMA image.
Results. Positions of the quiet Sun, active regions, prominences on the disc, magnetic inversion lines, coronal holes and coronal bright points are identified in the ALMA image. At the wavelength of 1.21 mm, active regions appear as bright areas (but sunspots are dark), while prominences on the disc and coronal holes are not discernible from the quiet Sun background, despite having slightly less intensity than surrounding quiet Sun regions. Magnetic inversion lines appear as large, elongated dark structures and coronal bright points correspond to ALMA bright points.
Conclusions. These observational results are in general agreement with sparse earlier measurements at similar wavelengths. The identification of coronal bright points represents the most important new result. By comparing ALMA and other maps, it was found that the ALMA image was oriented properly and that the procedure of overlaying the ALMA image with other images is accurate at the 5 arcsec level. The potential of ALMA for physics of the solar chromosphere is emphasised.

First analysis of solar structures in 1.21 mm full-disc ALMA image of the Sun

R. **Brajša**, D. Sudar, A. O. Benz, I. Skokić, M. Bárta, B. De Pontieu, S. Kim, A. Kobelski, M. Kuhar, M. Shimojo, S. Wedemeyer, S. White, P. Yagoubov, Y. Yan
A&A **2017**
https://arxiv.org/pdf/1711.06130.pdf
Various solar features can be seen on maps of the Sun in the mm and sub-mm wavelength range. The recently installed Atacama Large Millimeter/submillimeter Array (ALMA) is capable of observing the Sun in that wavelength range with an unprecedented spatial, temporal and spectral resolution. To interpret solar observations with ALMA the first important step is to compare ALMA maps with simultaneous images of the Sun recorded in other spectral ranges. First we identify different structures in the solar atmosphere seen in the optical, IR and EUV parts of the spectrum (quiet Sun (QS), active regions (AR), prominences on the disc, magnetic inversion lines (IL), coronal holes (CH) and coronal bright points (CBPs)) in a full disc solar ALMA image. The second aim is to measure the intensities (brightness temperatures) of those structures and compare them with the corresponding QS level. A full disc solar image at 1.21 mm obtained on **December 18, 2015** during a CSV-EOC campaign with ALMA is calibrated and compared with full disc solar images from the same day in H\alpha, in He I 1083 nm core, and with SDO images (AIA at 170 nm, 30.4 nm, 21.1 nm, 19.3 nm, and 17.1 nm and HMI magnetogram). The brightness temperatures of various structures are determined by averaging over corresponding regions of interest in the ALMA image. Positions of the QS, ARs, prominences on the disc, ILs, CHs and CBPs are identified in the ALMA image. At 1.21 mm ARs appear as bright areas (but sunspots are dark), while prominences on the disc and CHs are not discernible from the QS background, although having slightly less intensity than surrounding QS regions. ILs appear as large, elongated dark structures and CBPs correspond to ALMA bright points. These results are in general agreement with sparse earlier measurements at similar wavelengths. The identification of CBPs represents the most important new result.

Observation and modelling of the solar atmosphere in the mm and sub-mm wavelength ranges

Roman **Brajsa**∗
CESRA Abstract **2016** p.45
http://cesra2016.sciencesconf.org/conference/cesra2016/pages/CESRA2016_prog_abs_book_v1.pdf

Various solar features can be identified in emission or absorption on maps of the Sun in the millimeter and submillimeter wavelength ranges. Several examples of such maps, where active regions, filaments and coronal holes can be seen on solar disk, are presented and compared with images obtained at other wavelength ranges. Additionally, the center-to-limb function is analysed on full-disk solar maps. Thermal bremsstrahlung and gyromagnetic (cyclotron) radiation mechanism are important for explaining the observed phenomena, although the latter process would requier an unusually large megnetic field, especially when going to the shorter wavelengths. A numerical procedure for calculating the brightness temperature for a given wavelength and model atmosphere, which integrates the radiative transfer equation for thermal bremsstrahlung, is used for interpretation of observational findings. The models are developed for different structures in the solar atmosphere in a broad wavelength range (0.3 mm - 10 mm), closely related to that of the Atacama Large Millimeter/submillimeter Array (ALMA) and Mets´'ahovi Radio Observatory (MRO). The results are compared with available test measurements (ALMA) and regular solar measurements with MRO. An important conclusion is that thermal bremsstrahlung is the dominant radiation mechanism in the millimeter and submillimeter wavelength ranges which can explain previous observations. In the very near future it will be possible to compare the numerical results with new observations of the ALMA radio telescope.

An Interpretation of the Coronal Holes' Visibility in the Millimeter Wavelength Range

R. **Brajša** · A.O. Benz · M. Temmer · R. Jurdana-Šepi´c · B. Šaina · H. Wöhl
Solar Phys (**2007**) 245: 167–176

A special solar type II radio burst observed with LOFAR

Frank **Breitling**∗1 , Richard Fallows2 , Gottfried Mann3 , Christian Vocks4 , Mario Bisi5 , Peter Gallagher6 , Alain Kerdraon7 , Jasmina Magdalenic8 , Alec Mackinnon9 , Helmut Rucker10, Alexandr Konovalenko11, Christophe Marque12, Eduard Kontar9 , Bartosz Dabrowski13, Andrzej Krankowski13, Hamish Reid9 , and Bo Thide
CESRA **2016** p.68
http://cesra2016.sciencesconf.org/conference/cesra2016/pages/CESRA2016_prog_abs_book_v3.pdf
On **March 16, 2016**, a special type II radio burst was observed in the frequency range 20- 80 MHz with LOFAR. The type II burst shows the typical fundamental-harmonic structure. Because of the high sensitivity of LOFAR, the 3rd harmonic was measured. Additionally, a lot of herringbones were observed in both the fundamental and harmonic band. A preliminary evaluation of the burst is presented.

The LOFAR Solar Imaging Pipeline and the LOFAR Solar Data Center

Frank **Breitling**, Gottfried Mann, Christian Vocks, Matthias Steinmetz, Klaus G. Strassmeier
Astronomy and Computing, November **2015**, Volume 13, Pages 99-107
http://arxiv.org/pdf/1603.05990v1.pdf
https://reader.elsevier.com/reader/sd/pii/S2213133715000712?token=177356E9EB391F4AC9524722C9D1A45D06239992B812334FF65877DA51B0E65855FFDCF2B975ABA069888FAB2621DB4F
LOFAR is a new and sensitive radio interferometer that can be used for dynamic high-resolution imaging spectroscopy at low radio frequencies from 10 to 90 and 110 to 250 MHz. Here we describe its usage for observations of the Sun and in particular of solar radio bursts. We also describe the processing, archiving and accessing of solar LOFAR data, which is accomplished via the LOFAR Solar Imaging Pipeline and the LOFAR Solar Data Center.

LOFAR Solar Imaging

Frank **Breitling**∗1 , Gottfried Mann1 , and Christian Vocks
CESRA Abstract **2016** p.48
http://cesra2016.sciencesconf.org/conference/cesra2016/pages/CESRA2016_prog_abs_book_v1.pdf
LOFAR is a novel digital radio interferometer for imaging radio sources in the frequency range from 10 to 90 and 110 to 250 MHz with high time and frequency resolution. The LOFAR Key Science Project (KSP) "Solar Physics and Space Weather with LOFAR" uses it for solar observations. I will discuss aspects of solar imaging with LOFAR and present some results.

Propagation of energetic electrons from the corona into interplanetary space and type III radio emission

F. **Breitling**, G. Mann, C. Vocks
Proceedings of the 7th International Workshop on Planetary, Solar and Heliospheric Radio Emissions (PRE VII), held at Graz, Austria, September 15-17, **2010**, p. 373-380
http://arxiv.org/pdf/1511.03123v1.pdf
During solar flares a large amount of electrons with energies greater than 20 keV is generated with a production rate of typically 1036 s−1. A part of them is able to propagate along open magnetic field lines through the corona into interplanetary space. During their travel they emit radio radiation which is observed as type III radio bursts in the frequency range from 100 MHz down to 10 kHz by the WAVES radio spectrometer aboard the spacecraft WIND, for instance. From the drift rates of these bursts in dynamic radio spectra the radial propagation velocity Vr of the type III burst exciting electrons is derived by employing a newly developed density model of the heliosphere. Calculations show that the radio radiation is emitted by electrons with different Vr and therefore by different electrons of the initially produced electron distribution. **2002 Feb 26**
Figure 4: Electron density of the interplanetary space as known from measurements (four data points) and the new model described here.

STEREO database of interplanetary Langmuir electric waveforms†

C. **Briand**, P. Henri, V. Génot, N. Lormant, N. Dufourg, B. Cecconi, Q.N. Nguyen, K. Goetz
JGR Volume 121, Issue 2 Pages 1062–1070 **2016**
This paper describes a database of electric waveforms that is available at the Centre de Données de la Physique des Plasmas (CDPP, http://cdpp.eu/). This database is specifically dedicated to waveforms of Langmuir/Z-mode waves. These waves occur in numerous kinetic processes involving electrons in space plasmas. Statistical analysis from a large data set of such waves is then of interest e.g. to study the relaxation of high velocity electron beams generated at interplanetary shock fronts, in current sheets and magnetic reconnection region, the transfer of energy between high and low frequencies, the generation of electromagnetic waves etc.The Langmuir waveforms were recorded by the Time Domain Sampler (TDS) of the WAVES radio instrument onboard of the STEREO mission. In this paper, we detail the criteria used to identify the Langmuir/Z-mode waves among the whole set of waveforms of the STEREO spacecraft. A database covering the November 2006 - August 2014 period is provided. It includes electric waveforms expressed in the normalized frame with B and Vsw the local magnetic field and solar wind velocity vectors, and the local magnetic field in the variance frame, in an interval of ±1.5min around the time of the Langmuir event. Quicklooks are also provided that display the three components of the electric waveforms together with the spectrum of E∥, together with the magnitude and components of the magnetic field in the 3min interval, in the variance frame. Finally, the distribution of the Langmuir/Z-mode waves peak amplitude is also analyzed.

Inhibition of type III radio emissions due to the interaction between two electron beams: Observations and simulations (pages 2365–2378)

C. **Briand**, P. Henri and S. Hoang
JGR, Volume 119, Issue 4, pages 2365–2378, April **2014**
We report the peculiar interaction of two type III bursts observed in the solar wind. As electron beams propagating on the same magnetic field lines cross, a spectacular depletion of the type III radio emission is observed. We combine observations from the WAVES experiment on board the STEREO mission together with kinetic plasma simulations to study the extinction of type III radio emission resulting from the interaction between two electron beams. The remote observations enable to follow the electron beams in the interplanetary medium and show that the level of radiated radio waves is recovered after the beam crossing. The in situ observations of beam-driven Langmuir waves give evidence for Langmuir decay. The density fluctuations are extracted from in situ observations. The velocity of the beams is independently evaluated from in situ observations of decaying Langmuir waves and remote radio observations. The kinetic simulations show that the level of beam-driven Langmuir waves is reduced as the two beams cross. We show that the slow beam induced a strong reduction of the quasilinear relaxation of the fast beam, limiting the amplitude of the generated Langmuir waves. Moreover, in the case of two electron beams, the lack of Langmuir wave coherence reduces the efficiency of the Langmuir parametric decay. We thus conclude that the observed depletion of the type III radio emission is independent of the radio emission mechanism, as long as it depends on the Langmuir amplitude and coherence.

Faint solar radio structures from decametric observations

C. **Briand**[1], A. Zaslavsky[2], M. Maksimovic[1], P. Zarka[1], A. Lecacheux[1], H. O. Rucker[3], A. A. Konovalenko[4], E. P. Abranin[4], V. V. Dorovsky[4], A. A. Stanislavsky[4], and V. N. Melnik[4]

A&A 490, 339-344 (**2008**), DOI: 10.1051/0004-6361:200809842

Aims. Decameter radio observations of the solar corona reveal the presence of numerous faint frequency drifting emissions, similar to "solar S bursts" which are reported in the literature. We present a statistical analysis of the characteristics of these emissions and propose a mechanism to excite the Langmuir waves thought to be at the origin of these emissions.

Methods. The observations were performed between 1998 and 2002 with the Digital Spectro Polarimeter (DSP) receivers operated at the UTR-2 and Nançay decameter radio telescopes in the frequency range 15–30 MHz. Our theoretical explanation is based on Vlasov-Ampère simulations.

Results. Based on the frequency drift rate, three populations of structures can be identified. The largest population presents an average negative frequency drift of -0.9 MHz s^{-1} and a lifetime up to 11 s (median value of 2.72 s). A second population shows a very small frequency drift of -0.1 MHz s^{-1} and a short lifetime of about 1 s. The third population presents an average positive frequency drift of +0.95 MHz s^{-1} and a lifetime of up to 3 s. Also, the frequency drift as a function of frequency is consistent with the former results, which present results in higher frequency range. No specific relationship was found between the occurrence of these emissions and the solar cycle or presence of flares. Assuming that these emissions are produced by "electron clouds" propagating the solar corona, we deduce electron velocities of about 3–5 times the electron thermal velocity. As previously shown, a localized, time-dependent modulation of the electron distribution function (heating) leads to low velocity electron clouds (consistent with observations), which, in turn, can generate Langmuir waves and electromagnetic signals by nonlinear processes.

A new natural radio emission observed at South Pole Station

M. C. **Broughton**, J. LaBelle and P. H. Yoon

JGR, Volume 119, Issue 1, pages 566–574, January **2014**

Continuous waveform data taken at South Pole Station in 2011–2012 within a few hours of magnetic midnight revealed 12 observations of a new natural radio emission. The waves had frequencies ranging from 1320 to 2160 kHz, bandwidths ranging from 94 to 272 kHz, and durations ranging from 16 to 355 s. Spectral analysis of the waveform data revealed that the emission has a complex combination of at least three kinds of fine structures: broad, banded structures; short-lived, narrowband structures; and striated features that occur predominantly near the lower frequency boundary of the emission. For model auroral electron distributions, positive growth rates for the cyclotron maser instability occurred near the electron cyclotron frequency (fce), which is inconsistent with the observed wave frequencies. On the other hand, Langmuir wave growth could be excited at frequencies consistent with observations. Spatial Langmuir wave growth is more favorable for electron beam energies of hundreds of eV than for those at higher energies.

RHESSI Results Time for a Rethink? **Review**

Brown, J. C.; Kontar, E. P.; Veronig, A. M.

The High Energy Solar Corona: Waves, Eruptions, Particles, Lecture Notes in Physics, Volume 725. ISBN 978-3-540-71569-6. Springer-Verlag Berlin Heidelberg, **2007**, p. 65

https://arxiv.org/pdf/astro-ph/0607440.pdf

Hard X-rays and γ-rays are the most direct signatures of energetic electrons and ions in the sun's atmosphere which is optically thin at these energies and their radiation involves no coherent processes. Being collisional they are complementary to gyro-radiation in probing atmospheric density as opposed to magnetic field and the electrons are primarily 10 100~keV in energy, complementing the (>100 keV) electrons likely responsible for microwave bursts. The pioneering results of the Ramaty High Energy Solar Spectroscopic Imager (RHESSI) are raising the first new major questions concerning solar energetic particles in many years. Some highlights of these results are discussed primarily around RHESSI topics on which the authors have had direct research involvement particularly when they are raising the need for re-thinking of entrenched ideas. Results and issues are broadly divided into discoveries in the spatial, temporal and spectral domains, with the main emphasis on flare hard X-rays/fast electrons but touching also on γ-rays/ions, non-flare emissions, and the relationship to radio bursts. **20 Feb 2002, 14 March 2002, 2002 April 14/15, July 23, 2002**

Comprehensive Characterization of Solar Eruptions With Remote and In-Situ Observations, and Modeling: The Major Solar Events on 4 November 2015

Iver H. **Cairns**, Kamen A. Kozarev, Nariaki V. Nitta, Neus Agueda, Markus Battarbee, Eoin P. Carley, Nina Dresing, Raul Gomez-Herrero, Karl-Ludwig Klein, David Lario, Jens Pomoell, Carolina Salas-Matamoros, Astrid M. Veronig, Bo Li, Patrick McCauley

Solar Phys. **295**, Article number: 32 **2020**
https://arxiv.org/pdf/1910.03319.pdf
https://link.springer.com/content/pdf/10.1007/s11207-020-1591-7.pdf
Solar energetic particles (SEPs) are an important product of solar activity. They are connected to solar active regions and flares, coronal mass ejections (CMEs), EUV waves, shocks, Type II and III radio emissions, and X-ray bursts. These phenomena are major probes of the partition of energy in solar eruptions, as well as for the organization, dynamics, and relaxation of coronal and interplanetary magnetic fields. Many of these phenomena cause terrestrial space weather, posing multiple hazards for humans and their technology from space to the ground. Since particular flares, shocks, CMEs, and EUV waves produce SEP events but others do not, since propagation effects from the low corona to 1 AU appear important for some events but not others, and since Type II and III radio emissions and X-ray bursts are sometimes produced by energetic particles leaving these acceleration sites, it is necessary to study the whole system with a multi-frequency and multi-instrument perspective that combines both in-situ and remote observations with detailed modelling of phenomena. This article demonstrates this comprehensive approach, and shows its necessity, by analysing a trio of unusual and striking solar eruptions, radio and X-ray bursts, and SEP events that occurred on **4 November 2015**. These events show both strong similarities and differences from standard events and each other, despite having very similar interplanetary conditions and only two are sites and CME genesis regions. They are therefore major targets for further in-depth observational studies, and for testing both existing and new theories and models. Based on the very limited modelling available we identify the aspects that are and are not understood, and we discuss ideas that may lead to improved understanding of the SEP, radio, and space-weather events.

Coherent Radio Emissions Associated with Solar System Shocks **A Review**

Iver H. **Cairns**
M.P. Miralles, J. Sánchez Almeida (eds.), *The Sun, the Solar Wind, and the Heliosphere*, IAGA Special Sopron Book Series 4, DOI 10.1007/978-90-481-9787-3_23, c _Springer Science+Business Media B.V. **2011**, pp. 267-338, **File**
Shock waves are associated with multiple powerful coherent radio emissions within the heliosphere and local interstellar medium. The radio emissions definitely driven by shocks include interplanetary type II (solar radio) bursts,"foreshock" emissions from upstream of Earth's bow shock, and rare emissions from corotating interaction regions (CIRs). Emissions likely driven by shocks, but without definitive observational evidence, include coronal type II bursts, the 2–3 kHz emissions from the outer heliosphere, and drifting pulsating structures from the deep corona. Analogous emissions are also predicted, but not yet observed, for mini-magnetospheres and associated bow shocks on the Moon and for moons like Ganymede, the foreshocks of other planets, particularly Mercury and Jupiter, and supernovae. All these emissions are produced near the electron plasma frequency f_{pe} and/or $2f_{pe}$ via the so-called "plasma emission" mechanism or linear mode conversion, two of the four coherent radio emission mechanisms observed to date. In each case the theoretical interpretation requires coupling of multiple physical processes from microscales to macroscales. Microscale physics includes the timevarying magnetic overshoots of reforming shocks, electron reflection and acceleration at shocks, growth of Langmuir waves in the upstream foreshock, and the linear or nonlinear conversion of Langmuir energy into radio emission at f_{pe} and/or $2f_{pe}$. Intermediate scale physics includes the creation of ripples on the shock on scales of order the decorrelation length of the magnetic field, as well as scattering of the radiation by density irregularities. Macroscale physics includes 3D spatiotemporal variations of the plasma and the shock motion, as well as integration of emission from individual shock ripples over the entire shock. This chapter is a comprehensive review of the field, starting with observations of the emissions definitely and probably driven by shocks. Existing theory is then summarized in some detail, followed by detailed reviews of the observation and theory of type II bursts (both coronal and interplanetary) and the 2–3 kHz emissions from the outer heliosphere, including descriptions of the unresolved issues. The discussion focuses on limitations of the theory and existing observations and ways to address them. The overall conclusions are that the basic theory (electron shock acceleration, development of an electron beam, growth of Langmuir waves, and production of f_{pe} and $2f_{pe}$ radiation for a macroscopic, rippled, shock) appears to explain the primary observations semiquantitatively, that many observational details and theoretical limitations remain unresolved, and that the next ten years ought to be an exciting time that sees theory and observations brought together quantitatively.

DIRECT RADIO PROBING AND INTERPRETATION OF THE SUN'S PLASMA DENSITY PROFILE

I. H. **Cairns**1, V. V. Lobzin1, A. Warmuth2, B. Li1, P. A. Robinson1, and G. Mann2
Astrophysical Journal, 706:L265–L269, **2009** December, **File**
The Sun's electron number density profile $n_e(r)$ is vital for solar physics but not well measured or understood within a few solar radii R_S. Here, a new technique extracts $n_e(r)$ directly from coronal type III radio bursts

for 40 _ f _ 180 MHz. Unexpectedly, wind-like regions with $n_e \propto (r - R_S)^{-2}$ are quite common below $2R_S$, and coronal type IIIs often have closely linear $1/f - t$ spectra. The profile $n_e \propto (r - R_S)^{-2}$ is consistent with the radio data and simulations and is interpreted in terms of conical flow from localized sources (e.g., UV funnels) close to the photosphere. It is consistent with solar wind acceleration occurring for 2 _ r/R_S _ 10.

Progress on Coronal, Interplanetary, Foreshock, and Outer Heliospheric Radio Emissions

Iver H. **Cairns** , P. A. Robinson , and G. P. Zank,
PASA, 17 (1), 22, **2000**, **File**. **Review**
http://www.atnf.csiro.au/pasa/17_1/cairns/paper/
http://www.atnf.csiro.au/pasa/17_1/cairns/paper/node5.html
https://www.atnf.csiro.au/pasa/17_1/cairns/paper.pdf
Type II and III solar radio bursts are associated with shock waves and streams of energetic electrons, respectively, which drive plasma waves and radio emission at multiples of the electron plasma frequency as they move out from the corona into the interplanetary medium. Analogous plasma waves and radiation are observed from the foreshock region upstream of Earth's bow shock. In situ spacecraft observations in the solar wind have enabled major progress to be made in developing quantitative theories for these phenomena that are consistent with available data. Similar processes are believed responsible for radio emissions at 2 - 3 kHz that originate in the distant heliosphere, from where the solar wind interacts with the local interstellar medium. The primary goal of this paper is to **review the observations and theories for these four classes of emissions, focusing on recent progress in developing detailed theories for the plasma waves and radiation in the source regions.** The secondary goal is to introduce and review stochastic growth theory, a recent theory which appears quantitatively able to explain the wave observations in type III bursts and Earth's foreshock and is a natural theory to apply to type II bursts, the outer heliospheric emissions, and perhaps astrophysical emissions.

SOLAR TYPE II RADIO BURSTS AND IP TYPE II EVENTS

H. V. **Cane** and W. C. Erickson
Astrophysical Journal, 623:1180–1194, **2005; File**
https://iopscience.iop.org/article/10.1086/428820/pdf
We have examined radio data from the WAVES experiment on the Wind spacecraft in conjunction with groundbased data in order to investigate the relationship between the shocks responsible for metric type II radio bursts and the shocks in front of coronal mass ejections (CMEs). The bow shocks of fast, large CMEs are strong interplanetary (IP) shocks, and the associated radio emissions often consist of single broad bands starting below _4 MHz; such emissions were previously called IP type II events. In contrast, metric type II bursts are usually narrowbanded and display two harmonically related bands. In addition to displaying complete dynamic spectra for a number of events, we also analyze the 135WAVES 1–14MHz slow-drift time periods in 2001–2003.We find that most of the periods contain multiple phenomena, which we divide into three groups: metric type II extensions, IP type II events, and ‘‘blobs and bands.’’About half of theWAVES listings include probable extensions of metric type II radio bursts, but in more than half of these events, there were also other slow-drift features. In the 3 yr study period, there were 31 IP type II events; these were associated with the very fastest CMEs. The most common form of activity in theWAVES events, blobs and bands in the frequency range between 1 and 8 MHz, fall below an envelope consistent with the early signatures of an IP type II event. However, most of this activity lasts only a few tens of minutes, whereas IP type II events last for many hours. In this study we find many examples in the radio data of two shock-like phenomena with different characteristics that occur simultaneously in the metric and decametric/hectometric bands, and no clear example of a metric type II burst that extends continuously down in frequency to become an IP type II event. The simplest interpretation is that metric type II bursts, unlike IP type II events, are not caused by shocks driven in front of CMEs.

Solar flares, type III radio bursts, coronal mass ejections and energetic particles.

Cane, H..V., Erickson, W..C., Prestage, N..P.:
2002, J. Geophys. Res. 107, 1315.
https://agupubs.onlinelibrary.wiley.com/doi/epdf/10.1029/2001JA000320
In this correlative study between >20 MeV solar proton events, coronal mass ejections (CMEs), flares, and radio bursts it is found that essentially all of the proton events are preceded by groups of type III bursts and all are preceded by CMEs. These type III bursts (that are a flare phenomenon) usually are long-lasting, intense bursts seen in the low-frequency observations made from space. They are caused by streams of electrons traveling from close to the solar surface out to 1 AU. In most events the type III emissions extend into, or originate at, the time when type II and type IV bursts are reported (some 5 to 10 minutes after the start of the associated soft X-ray flare) and have starting frequencies

in the 500 to ˜100 MHz range that often get lower as a function of time. These later type III emissions are often not reported by ground-based observers, probably because of undue attention to type II bursts. It is suggested to call them type III-l. Type III-l bursts have previously been called shock accelerated (SA) events, but an examination of radio dynamic spectra over an extended frequency range shows that the type III-l bursts usually start at frequencies above any type II burst that may be present. The bursts sometimes continue beyond the time when type II emission is seen and, furthermore, sometimes occur in the absence of any type II emission. Thus the causative electrons are unlikely to be shock accelerated and probably originate in the reconnection regions below fast CMEs. A search did not find any type III-l bursts that were not associated with CMEs. The existence of low-frequency type III bursts proves that open field lines extend from within 0.5 radius of the Sun into the interplanetary medium (the bursts start above 100 MHz, and such emission originates within 0.5 solar radius of the solar surface). Thus it is not valid to assume that only closed field lines exist in the flaring regions associated with CMEs and some interplanetary particles originating in such flare regions might be expected in all solar particle events. **1997-05-12, 1997-11-04, 1999-12-28, 2000-02-12, 2000-11-08, 2001-04-18, 2000-11-24, 2001-03-10, 2001-04-10, 2001-04-18**
Table 1.Solar Energetic Particle Events, 1997–2001

Tracking solar radio bursts using Bayesian multilateration

L.A. **Cañizares**, S.T. Badman, S.A. Maloney, M.J. Owens, D.M. Weigt, E.P. Carley, P.T. Gallagher
A&A 684, A182 **2024**
https://arxiv.org/pdf/2402.08590.pdf
https://www.aanda.org/articles/aa/pdf/2024/04/aa47747-23.pdf
Solar radio bursts (SRBs), are emitted by electrons propagating through the corona and interplanetary space. Tracking such bursts is key to understanding the properties of accelerated electrons and radio wave propagation as well as the local plasma environment that they propagate through. Here, we present a novel multilateration algorithm called BayEsian LocaLisation Algorithm (BELLA). In addition, apparent SRB positions from BELLA are compared with comparable localisation methods and the predictions of solar wind models. BELLA uses Bayesian inference to create probabilistic distributions of source positions and their uncertainties. This facilitates the estimation of algorithmic, instrumental, and physical uncertainties in a quantitative manner. We validated BELLA using simulations and a Type III SRB observed by STEREO A/B and Wind. BELLA tracked the Type III source from ∼ 10--150 Rsun (2-0.15 MHz) along a spiral trajectory. This allowed for an estimate of an apparent solar wind speed of vsw∼ 400 km s−1 and a source longitude of ϕ0∼ 30deg. We compared these results with well-established methods of positioning: Goniopolarimetric (GP), analytical time-difference-of-arrival (TDOA), and Solar radio burst Electron Motion Tracker (SEMP). We found them to be in agreement with the results obtained by BELLA. Additionally, the results aligned with solar wind properties assimilated by the Heliospheric Upwind Extrapolation with time dependence (HUXt) model. We have validated BELLA and used it to identify apparent source positions as well as velocities and densities of the solar wind. Furthermore, we identified higher than expected electron densities, suggesting that the true emission sources were at lower altitudes than those identified by BELLA, an effect that may be due to appreciable scattering of electromagnetic waves by electrons in interplanetary space.

Observations of shock propagation through turbulent plasma in the solar corona

Dr. Eoin P. **Carley**, Dr. B. Cecconi, Dr. Hamish A. Reid, Carine Briand, Sasikumar Raja, Dr. Sophie Masson, Dr. Vladimir V. Dorovskyy, Caterina Tiburzi, Dr. Nicole Vilmer, Pietro Zucca, Dr. Philippe Zarka, Dr. Michel Tagger, Dr. Jean-Mathias Griessmeier, Prof. Stephane Corbel, Dr. Gilles Theureau, Dr. Alan Loh, Dr. Julien Girard
ApJ **921** 3 **2021**
https://arxiv.org/pdf/2108.05587.pdf
https://iopscience.iop.org/article/10.3847/1538-4357/ac1acd/pdf
https://doi.org/10.3847/1538-4357/ac1acd
In the radio domain the primary signature of such shocks are type II radio bursts, observed in dynamic spectra as bands of emission slowly drifting towards lower frequencies over time. These radio bursts can sometimes have inhomogeneous and fragmented fine structure, but the cause of this fine structure is currently unclear. Here we observe a type II radio burst on **2019-March-20th** using the New Extension in Nançay Upgrading LOFAR (NenuFAR), a radio interferometer observing between 10-85 MHz. We show that the distribution of size-scales of density perturbations associated with the type II fine structure follows a power law with a spectral index in the range of $\alpha = -1.7$ to -2.0, which closely matches the value of $-5/3$ expected of fully developed turbulence. We determine this turbulence to be upstream of the shock, in background coronal plasma at a heliocentric distance of $\sim 2\ R_\odot$. The observed inertial size-scales of the turbulent density inhomogeneities range from ∼62 Mm to ∼209 km. This shows that type II fine structure and fragmentation can

be due to shock propagation through an inhomogeneous and turbulent coronal plasma, and we discuss the implications of this on electron acceleration in the coronal shock.

Radio Observations of Coronal Mass Ejection Initiation and Development in the Low Solar Corona **Review**

Eoin P. **Carley** , Nicole Vilmer and Angelos Vourlidas
Front. Astron. Space Sci. 7:551558. **2020** **File**
https://www.frontiersin.org/articles/10.3389/fspas.2020.551558/full
https://sci-hub.st/https://www.frontiersin.org/articles/10.3389/fspas.2020.551558/full
Coronal mass ejections (CMEs) are large eruptions of plasma and magnetic field from the low solar corona into the heliosphere. These eruptions are often associated with energetic electrons that produce various kinds of radio emission. However, there is ongoing investigation into exactly where, when, and how the electron acceleration occurs during flaring and eruption, and how the associated radio emission can be exploited as a diagnostic of both particle acceleration and CME eruptive physics. Here, we review past and present developments in radio observations of flaring and eruption, from the destabilization of flux ropes to the development of a CME and the eventual driving of shocks in the corona. We concentrate primarily on the progress made in CME radio physics in the past two decades and show how radio imaging spectroscopy provides the ability to diagnose the locations and kinds of electron acceleration during eruption, which provides insight into CME eruptive models in the early stages of their evolution (<<10 R⊙). We finally discuss how new instrumentation in the radio domain will pave the way for a deeper understanding of CME physics in the near future. **20 Apr 1998, 2011-01-27, 2014-03-18, 2014-09-01, 2015 May 9, 2017 September 10**

Radio observatories and instrumentation used in space weather science and operations

Eoin P. **Carley**1,2,*, Carla Baldovin3 , Pieter Benthem3 , Mario M. Bisi4 , Richard A. Fallows3 , Peter T. Gallagher2,1, Michael Olberg5 , Hanna Rothkaehl6 , Rene Vermeulen3 , Nicole Vilmer7,8, David Barnes4 , the LOFAR4SW Consortium3
J. Space Weather Space Clim. **2020**, 10, 7 **File** **Review**
https://www.swsc-journal.org/articles/swsc/pdf/2020/01/swsc190064.pdf
The low frequency array (LOFAR) is a phased array interferometer currently consisting of 13 international stations across Europe and 38 stations surrounding a central hub in the Netherlands. The instrument operates in the frequency range of ~10–240 MHz and is used for a variety of astrophysical science cases. While it is not heliophysics or space weather dedicated, a new project entitled “LOFAR for Space Weather” (LOFAR4SW) aims at designing a system upgrade to allow the entire array to observe the Sun, heliosphere, Earth’s ionosphere, and Jupiter throughout its observing window. This will allow the instrument to operate as a space weather observing platform, facilitating both space weather science and operations. Part of this design study aims to survey the existing space weather infrastructure operating at radio frequencies and show how LOFAR4SW can advance the current state-of-the-art in this field. In this paper, we survey radio instrumentation and facilities that currently operate in space weather science and/or operations, including instruments involved in solar, heliospheric, and ionospheric studies. We furthermore include an overview of the major space weather service providers in operation today and the current state-of-the-art in the radio data they use and provide routinely. The aim is to compare LOFAR4SW to the existing radio research infrastructure in space weather and show how it may advance both space weather science and operations in the radio domain in the near future.
Хороший справочник

Loss-cone instability modulation due to a magnetohydrodynamic sausage mode oscillation in the solar corona

Eoin P. **Carley**, Laura A. Hayes, Sophie A. Murray, Diana E. Morosan, Warren Shelley, Nicole Vilmer & Peter T. Gallagher
Nature Communications volume 10, Article number: 2276 (**2019**)
https://www.nature.com/articles/s41467-019-10204-1.pdf
Solar flares often involve the acceleration of particles to relativistic energies and the generation of high-intensity bursts of radio emission. In some cases, the radio bursts can show periodic or quasiperiodic intensity pulsations. However, precisely how these pulsations are generated is still subject to debate. Prominent theories employ mechanisms such as periodic magnetic reconnection, magnetohydrodynamic (MHD) oscillations, or some combination of both. Here we report on high-cadence (0.25 s) radio imaging of a 228 MHz radio source pulsating with a period of 2.3 s during a solar flare on **2014-April-18**. The pulsating source is due to an MHD sausage mode oscillation periodically triggering electron acceleration in the corona. The periodic electron acceleration results in the modulation of a loss-cone instability,

ultimately resulting in pulsating plasma emission. The results show that a complex combination of MHD oscillations and plasma instability modulation can lead to pulsating radio emission in astrophysical environments.
CESRA #2559 May **2020** http://www.astro.gla.ac.uk/users/eduard/cesra/?p=2559

Estimation of a Coronal Mass Ejection Magnetic Field Strength using Radio Observations of Gyrosynchrotron Radiation

Eoin P. **Carley**, Nicole Vilmer, Paulo J. A. Simões, Brían Ó Fearraigh
A&A 608, A137 **2017**
https://arxiv.org/pdf/1709.05184.pdf
Coronal mass ejections (CMEs) are large eruptions of plasma and magnetic field from the low solar corona into interplanetary space. These eruptions are often associated with the acceleration of energetic electrons which produce various sources of high intensity plasma emission. In relatively rare cases, the energetic electrons may also produce gyrosynchrotron emission from within the CME itself, allowing for a diagnostic of the CME magnetic field strength. Such a magnetic field diagnostic is important for evaluating the total magnetic energy content of the CME, which is ultimately what drives the eruption. Here we report on an unusually large source of gyrosynchrotron radiation in the form of a type IV radio burst associated with a CME occurring on **2014-September-01**, observed using instrumentation from the Nan\c{c}ay Radio Astronomy Facility. A combination of spectral flux density measurements from the Nan\c{c}ay instruments and the Radio Solar Telescope Network (RSTN) from 300MHz to 5 GHz reveals a gyrosynchrotron spectrum with a peak flux density at >1 GHz. Using this radio analysis, a model for gyrosynchrotron radiation, a non-thermal electron density diagnostic using the Fermi Gamma Ray Burst Monitor (GBM) and images of the eruption from the GOES Soft X-ray Imager (SXI), we are able to calculate both the magnetic field strength and the properties of the X-ray and radio emitting energetic electrons within the CME. We find the radio emission is produced by non-thermal electrons of energies >1MeV with a spectral index of $\delta \sim 3$ in a CME magnetic field of 4.4 G at a height of 1.3 $R_\odot$, while the X-ray emission is produced from a similar distribution of electrons but with much lower energies on the order of 10 keV. We conclude by comparing X-ray and radio-emitting electron distributions and how such an analysis can be used to define the plasma properties of a CME.

Radio Diagnostics of electron acceleration sites during the eruption of a flux rope in the solar corona

Eoin **Carley**∗1,2, Nicole Vilmer3 , and Peter Gallagher2
2016 ApJ 833 87
http://arxiv.org/pdf/1609.01463v1.pdf
Electron acceleration in the solar corona is often associated with flares and the eruption of twisted magnetic structures known as flux ropes. However, the locations and mechanisms of such particle acceleration during the flare and eruption are still subject to much investigation. Observing the exact sites of particle acceleration can help confirm how the flare and eruption are initiated are initiated and how they evolve. Here we use the Atmospheric Imaging Assembly to analyse a flare and erupting flux rope on **2014-April-18**, while observations from the Nancay Radio Astronomy Facility allows us to diagnose the sites of electron acceleration during the eruption. Our analysis shows evidence for a pre-formed flux rope which slowly rises and becomes destabilised at the time of a C-class flare, plasma jet and the escape of >75 keV electrons from rope center into the corona. As the eruption proceeds, continued acceleration of electrons with energies of ~5 keV occurs above the flux rope for a period over 5 minutes. At flare peak, one site of electron acceleration is located close to the flare site while another is driven by the erupting flux rope into the corona at speeds of up to 400 km/s. Energetic electrons then fill the erupting volume, eventually allowing the flux rope legs to be clearly imaged from radio sources at 150-445MHz. Following the analysis of Joshi et al. (2015), we conclude that the sites of energetic electrons are consistent with flux rope eruption via a tether-cutting or flux cancellation scenario inside a magnetic fan-spine structure. In total, our radio observations allow us to better understand the evolution of a flux rope eruption and its associated electron acceleration sites, from eruption initiation to propagation into the corona.
See CESRA **2016** p.39
http://cesra2016.sciencesconf.org/conference/cesra2016/pages/CESRA2016_prog_abs_book_v3.pdf
See **CESRA highlight** #1188, March **2017** http://www.astro.gla.ac.uk/users/eduard/cesra/?p=1188

Low frequency radio observations of bi-directional electron beams in the solar corona

Eoin P. **Carley**, Hamish Reid, Nicole Vilmer, Peter T. Gallagher
A&A 581, A100 **2015**
http://arxiv.org/pdf/1508.01065v1.pdf

The radio signature of a shock travelling through the solar corona is known as a type II solar radio burst. In rare cases these bursts can exhibit a fine structure known as `herringbones', which are a direct indicator of particle acceleration occurring at the shock front. However, few studies have been performed on herringbones and the details of the underlying particle acceleration processes are unknown. Here, we use an image processing technique known as the Hough transform to statistically analyse the herringbone fine structure in a radio burst at ∼20-90 MHz observed from the Rosse Solar-Terrestrial Observatory on **2011 September 22**. We identify 188 individual bursts which are signatures of bi-directional electron beams continuously accelerated to speeds of 0.16+0.11−0.10c. This occurs at a shock acceleration site initially at a constant altitude of ∼0.6 R⊙ in the corona, followed by a shift to ∼0.5 R⊙. The anti-sunward beams travel a distance of 170+174−97 Mm (and possibly further) away from the acceleration site, while those travelling toward the sun come to a stop sooner, reaching a smaller distance of 112+84−76 Mm. We show that the stopping distance for the sunward beams may depend on the total number density and the velocity of the beam. Our study concludes that a detailed statistical analysis of herringbone fine structure can provide information on the physical properties of the corona which lead to these relatively rare radio bursts.

Quasiperiodic acceleration of electrons by a plasmoid-driven shock in the solar atmosphere

Eoin P. **Carley**, David M. Long, Jason P. Byrne, Pietro Zucca, D. Shaun Bloomfield, Joseph McCauley, Peter T. Gallagher

(**2013**). Nature Physics, 9, 811-816

http://arxiv.org/pdf/1406.0743v1.pdf ; **File** (**2014**)

Cosmic rays and solar energetic particles may be accelerated to relativistic energies by shock waves in astrophysical plasmas. On the Sun, shocks and particle acceleration are often associated with the eruption of magnetized plasmoids, called coronal mass ejections (CMEs). However, the physical relationship between CMEs and shock particle acceleration is not well understood. Here, we use extreme ultraviolet, radio and white-light imaging of a solar eruptive event on **22 September 2011** to show that a CME-induced shock (Alfv\'en Mach number 2.4+0.7−0.8) was coincident with a coronal wave and an intense metric radio burst generated by intermittent acceleration of electrons to kinetic energies of 2-46 keV (0.1-0.4 c). Our observations show that plasmoid-driven quasi-perpendicular shocks are capable of producing quasi-periodic acceleration of electrons, an effect consistent with a turbulent or rippled plasma shock surface.

Ten Years of the Solar Radiospectrograph ARTEMIS–IV

C. **Caroubalos** et al.

2013

https://olympias.lib.uoi.gr/jspui/bitstream/123456789/16919/1/alissanrakis-2010-Ten%20Years%20of%20the%20Solar%20Radiospectrograph%20ARTEMIS-IV.pdf

The Solar Radiospectrograph of the University of Athens (ARTEMISIV1) is in operation at the Thermopylae Satellite Communication Station since 1996. The observations extend from the base of the Solar Corona (650 MHz) to about 2 Solar Radii (20 MHz) with time resolution 1/10- 1/100 sec. The instruments recordings, being in the form of dynamic spectra, measure radio flux as a function of height in the corona; our observations are combined with spatial data from the Nancay Radioheliograph whenever the need for 3D positional information arises. The ARTEMIS-IV contribution in the study of solar radio bursts is two fold– Firstly, in investigating new spectral characteristics since its high sampling rate facilitates the study of fine structures in radio events. On the other hand it is used in studying the association of solar bursts with interplanetary phenomena because of its extended frequency range which is furthermore, complementary to the range of the WIND/WAVES receivers and the observations may be readily combined. This reports serves as a brief account of this operation. Joint observations with STEREO/WAVES and LOFAR low frequency receivers are envisaged in the future.

Space storm measurements of the July 2005 solar extreme events from the low corona to the Earth

Caroubalos, C.; Preka-Papadema, P.; Mavromichalaki, H.; Moussas, X.; Papaioannou, A.; Mitsakou, E.; Hillaris, A.

Advances in Space Research, Volume 43 , Issue 4, p. 600-604, **2009**.

http://arxiv.org/pdf/1009.3579v1.pdf

The Athens Neutron Monitor Data Processing (ANMODAP) Center recorded an unusual Forbush decrease with a sharp enhancement of cosmic ray intensity right after the main phase of the Forbush decrease on 16 July 2005, followed by a second decrease within less than 12 h. This exceptional event is neither a ground level enhancement nor a geomagnetic effect in cosmic rays. It rather appears as the effect of a special structure of interplanetary disturbances originating from a group of coronal mass ejections (CMEs) in the **13-14 July 2005** period. The initiation of the CMEs was accompanied

by type IV radio bursts and intense solar flares (SFs) on the west solar limb (AR 786); this group of energetic phenomena appears under the label of Solar Extreme Events of July 2005. We study the characteristics of these events using combined data from Earth (the ARTEMIS IV radioheliograph, the Athens Neutron Monitor (ANMODAP)), space (WIND/WAVES) and data archives. We propose an interpretation of the unusual Forbush profile in terms of a magnetic structure and a succession of interplanetary shocks interacting with the magnetosphere.

Solar type II and type IV radio bursts observed during 1998-2000 with the ARTEMIS-IV radiospectrograph

Caroubalos, C., Hillaris, A., Bouratzis *et al.*,
2004, *A&A*, 413, 1125
http://www.aanda.org/articles/aa/pdf/2004/03/aa2532.pdf
The ARTEMIS IV radiospectrograph (Caroubalos *et al.* 2001) observed 40 type II and/or IV radio bursts (1998-2000) which were published in the form of a catalogue (Caroubalos *et al.* 2004).

ARTEMIS IV Radio Observations of the 14 July 2000 Large Solar Event

Caroubalos, C.; Alissandrakis, C. E.; Hillaris, A.; Nindos, A.; Tsitsipis, P.; Moussas, X.; Bougeret, J.-L.; Bouratzis, K.; Dumas, G.; Kanellakis, G.; Kontogeorgos, A.; Maroulis, D.; Patavalis, N.; Perche, C.; Polygiannakis, J.; Preka-Papadema, P.
Solar Physics, v. 204, Issue 1/2, p. 165-177 (**2001**).
http://arxiv.org/pdf/1009.3654v1.pdf
In this report we present a complex metric burst, associated with the 14 July 2000 major solar event, recorded by the ARTEMIS-IV radio spectrograph at Thermopylae. Additional space-borne and Earth-bound observational data are used, in order to identify and analyze the diverse, yet associated, processes during this event. The emission at metric wavelengths consisted of broad-band continua including a moving and a stationary type IV, impulsive bursts and pulsating structures. The principal release of energetic electrons in the corona was 15 20 min after the start of the flare, in a period when the flare emission spread rapidly eastwards and a hard X-ray peak occurred. Backward extrapolation of the CME also puts its origin in the same time interval, however, the uncertainty of the extrapolation does not allow us to associate the CME with any particular radio or X-ray signature. Finally, we present high time and spectral resolution observations of pulsations and fiber bursts, together with a preliminary statistical analysis.

Study of Fine Radio-Burst Structures (FRBS) Observed by the Mexican Array Radio Telescope (MEXART)

G. A. **Casillas-Pérez**, A. Carrillo-Vargas, V. De La Luz & E. Huipe-Domratcheva
Solar Physics volume 297, Article number: 84 (**2022**)
https://doi.org/10.1007/s11207-022-02023-3
Solar events occur in several energy ranges and durations, with emissions involving a wide range of the electromagnetic spectrum. The present work reveals the instrumental capacity of the Mexican Array Radio Telescope (MEXART) to detect solar radio emissions in the VHF band. Particular attention is focused on intense, short-duration solar transient emissions in the form of fine radio-burst structures (FRBS), observed by MEXART at around 140 MHz. A Type-I noise storm event with metric FRBS corresponding to observations on **6 May 2019** is reported. The FRBS exhibited distinct durations within the range of 0.47 – 8.07 s, a mean value of 2.48 s, and intensities between ≈ 1.0 – 8.0 sfu, with the initial FRBS having a longer duration and greater peak intensity levels than the subsequent radio bursts. The time profile of the FRBS has an asymmetric structure consisting of an abrupt rise, a short-term maximum peak, and a slow decay phase with mean values of 1.90 and 2.50 s for the rise and decay times, respectively. Compared with other fast radio transients observed at higher frequencies, the longer duration of the FRBS suggests lack of interaction of an electron beam with its surrounding parcelled low-density plasma environment. The properties of the FRBS structures are discussed.

Study of Solar Radio Spikes and Their Relation to Energetic Solar Events

G. A. **Casillas-Pérez**, S. Jeyakumar, A. Carrillo-Vargas, H. R. Pérez-Enríquez
Solar Physics January **2019**, 294:10
https://link.springer.com/content/pdf/10.1007%2Fs11207-018-1390-6.pdf
We compiled observations of solar radio spikes (RSs) reported in the literature. The compilation spans a wide range in frequency from 0.01 MHz to 8.4 GHz. We also compiled available information of energetic solar events that may be

related to RSs. Using this compilation, though the RS events are associated with other energetic solar events, we show that there is no clear preference to any particular type of solar event. We study the dependence of the duration, bandwidth, emitted flux, polarization and drift rate of the RSs with its observational frequency.

Evolution of electron beam pulses of short duration in the solar corona

G. A. **Casillas-Pérez**, S. Jeyakumar, H. R. Pérez-Enríquez, M. A. Trinidad
AdSpR **2016**
http://arxiv.org/pdf/1606.05751v1.pdf
Narrowband radio bursts with durations of the order of milliseconds, called spikes, are known to be associated with solar flares. In order to understand the particle beams responsible for the radio spike phenomena, evolution of electron beam pulses injected from a solar flare region into the corona is studied. Numerical integration of the Fokker-Planck (FP) equation is used to follow the evolution of the electron beam pulse. The simulations show that the short duration pulses lose most of their energy within a second of propagation into the corona. Electron beam with a small low energy cut off is thermalised faster than that with a high low energy cut off.

Magnetic Diagnostics of the Solar Corona: Synthesizing Optical and Radio Techniques Review

R. **Casini**, S. M. White, P. G. Judge
Space Science Reviews 210(1-4), 145–181 **2017** DOI 10.1007/s11214-017-0400-6
In this contribution we review the current state-of-the-art of coronal magnetometry, in both optical and radio domains. We address the achievable objectives and the challenges of present measurement techniques and interpretation tools. In particular, we focus on the role that these observations can play for constraining and validating numerical models of the global coronal magnetic field. With regard to optical techniques, we mainly focus on the use of M1 diagnostics, further developing the theory of the formation of their polarization signatures in the magnetized corona.

Periodicities in an active region correlated with Type III radio bursts observed by Parker Solar Probe

Cynthia **Cattell**, Lindsay Glesener, Benjamin Leiran, Keith Goetz, Juan Carlos Martínez Oliveros, Samuel T. Badman, Marc Pulupa, Stuart D. Bale
A&A 650, A6 **2021**
https://arxiv.org/pdf/2009.10899.pdf
https://www.aanda.org/articles/aa/pdf/2021/06/aa39510-20.pdf
https://doi.org/10.1051/0004-6361/202039510
Context. Periodicities have frequently been reported across many wavelengths in the solar corona. Correlated periods of ~5 minutes, comparable to solar p-modes, are suggestive of coupling between the photosphere and the corona. Aims. Our study investigates whether there are correlations in the periodic behavior of Type III radio bursts, indicative of non-thermal electron acceleration processes, and coronal EUV emission, assessing heating and cooling, in an active region when there are no large flares. Methods. We use coordinated observations of Type III radio bursts from the FIELDS instrument on Parker Solar Probe (PSP), of extreme ultraviolet emissions by the Solar Dynamics Observatory (SDO)/AIA and white light observations by SDO/HMI, and of solar flare x-rays by Nuclear Spectroscopic Telescope Array (NuSTAR) on **April 12, 2019**. Several methods for assessing periodicities are utilized and compared to validate periods obtained. Results. Periodicities of about 5 minutes in the EUV in several areas of an active region are well correlated with the repetition rate of the Type III radio bursts observed on both PSP and Wind. Detrended 211A and 171A light curves show periodic profiles in multiple locations, with 171A peaks lagging those seen in 211A. This is suggestive of impulsive events that result in heating and then cooling in the lower corona. NuSTAR x-rays provide evidence for at least one microflare during the interval of Type III bursts, but there is not a one-to-one correspondence between the x-rays and the Type-III bursts. Our study provides evidence for periodic acceleration of non-thermal electrons (required to generate Type III radio bursts) when there were no observable flares either in the x-ray data or the EUV. The acceleration process, therefore, must be associated with small impulsive events, perhaps nanoflares.

Radio emission observed in decimetric waves associated with the onset of CMEs

J.R. **Cecatto**, A.C. Soares, F.C.R. Fernandes, F.R.H. Madsen, M.C. Andrade, H.S. Sawant
Journal of Atmospheric and Solar-Terrestrial Physics, Volume 67, Issues 17-18, December **2005**, Pages 1674-1679
Since the first observations by Skylab and SMM satellites coronal mass ejections (CME) have been more and more

investigated. However, until now their origin and trigger mechanism remain an open question no matter if they are associated to flares or not. Recent observations over a broad spectrum suggest that flare energy is released in regions from where the decimetric emission is coming. Then, investigations of decimetric radio emission observed in association with CME phenomena may give clues to solve the previously mentioned questions. Using the Brazilian solar spectroscope (BSS), observations of solar bursts dynamic spectra with high time (100, 50, 20 ms) and frequency (50–100 channels) resolutions have been carried out daily (∼11–19 UT) within the range of 1000–2500 MHz. A sample of 274 CMEs were recorded by the large angle spectroscopic coronagraph (LASCO) instrument, on board the solar and heliospheric observatory (SOHO) satellite, within 11–19 UT, during the period of 1999–2002. From those, 42 CMEs are associated to BSS data and selected for analysis. It is interesting to note that in about half of the cases only one type of burst radio emission was recorded while in the remaining cases either two or more types were observed. There is a dominance of either continuum and/or pulsations. Here, we describe the association of burst radio emission with the starting time of CME phenomena.

Digitizing analogic spectrograms recorded by the Nançay Decameter Array on 35 mm film rolls from 1970 to 1990

Baptiste **Cecconi**, Laurent Lamy, Laurent Denis, Philippe Zarka, Agnès Fave, Marie-Pierre Issartel, Marie-Agnès Dubos, Corentin Louis, Pierre Le Sidaner, Véronique Stoll

Proceeding to the PV2018 conference - Adding value and preserving data, Rutherford Appleton Laboratory, Harwell Space Cluster (UK), 15th-17th May 2018 **2020**

https://arxiv.org/ftp/arxiv/papers/2003/2003.12479.pdf

The Nançay Decameter Array (NDA), which has now passed 40 years old, acquires daily observations of Jovian and Solar low frequency radio emissions over a continuous spectrum ranging from 10 up to 100MHz, forming the largest database of LW radio observations of these two bodies. It also intermittently observed intense radio sources since its opening in 1977. Before that date, decametric observations were conducted on the same site with an interferometer formed of a pair of log-periodic Yagi antennas mounted on mobile booms. These observations have been recorded with a series of analogic recorders (before 1990) and then digital receivers (after 1990), with increasing performances and sensitivities. The NDA scientific team recently retrieved and inventoried the archives of analogic data (35mm film rolls) covering two decades (1970 to 1990). We now plan to digitize those observations, in order to recover their scientific value and to include them into the currently operational database covering a time span starting in 1990 up to now, still adding new files every day. This modern and interoperable database has virtual observatory interfaces. It is a required element to foster scientific data exploitation, including Jovian and Solar data analysis over long timescales. We present the status of this project.

Modulation depth of the gyrosynchrotron emission as identifier of fundamental sausage modes

M. **Cécere**, A. Costa, T. Van Doorsselaere

A&A 676, A8 **2023**

https://arxiv.org/pdf/2306.11095.pdf

https://www.aanda.org/articles/aa/pdf/2023/08/aa46746-23.pdf

We study the intensity, the modulation depth and the mean modulation depth of the gyrosynchrotron (GS) radiation as a function of the frequency and the line of sight (LOS) in fast sausage modes. By solving the 2.5D MHD ideal equations of a straight coronal loop considering the chromosphere and with typical flaring plasma parameters we analyse the wavelet transform of the density and the GS emission for different radio frequencies and different spatial resolutions, given impulsive and general perturbations with energies in the microflare range. A wavelet analysis performed over the GS radiation emission showed that a fast fundamental sausage mode of 7s with a first harmonic mode of 3s developed, for all the initial energy perturbations used. For both the high spatial resolution (central pixel integration) and the low spatial resolution (entire loop integration), the larger the radio frequency, the larger the modulation depth. However, high and low resolution integrations differ in that, the larger the LOS angle with respect to the loop axis, results in a larger and smaller modulation depth, respectively. Fast MHD modes triggered by instantaneous energy depositions of the order of a microflare energy are able to reproduce deep intensity modulation depths in radio emission as observed in solar events. As the trends of the GS emission obtained by Reznikova, Antolin, and Van Doorsselaere (2014), for a linear and forced oscillation, remain present when analysing a more general context, considering the chromosphere and where the sausage mode is triggered by a impulsive, nonlinear perturbation, it seems that the behaviour found can be used as observational identifiers of the presence of sausage modes with respect to other quasi-periodic pulsation features. It can be inferred from this that finite-amplitude sausage modes have the potential to generate the observed deep modulation depths.

Effect of intense December 2006 solar radio bursts on GPS receivers

Cerruti, Alessandro P.; Kintner, Paul M., Jr.; Gary, Dale E.; Mannucci, Anthony J.; Meyer, Robert F.; Doherty, Patricia; Coster, Anthea J.

Space Weather, Vol. 6, No. 10, S10D07 , **2008**

http://dx.doi.org/10.1029/2007SW000375

https://agupubs.onlinelibrary.wiley.com/doi/epdf/10.1029/2007SW000375

Solar radio bursts during December 2006 were sufficiently intense to be measurable with GPS receivers. The strongest event occurred on 6 December 2006 and affected the operation of many GPS receivers. This event exceeded 1,000,000 solar flux unit and was about 10 times larger than any previously reported event. The strength of the event was especially surprising since the solar radio bursts occurred near solar minimum. The strongest periods of solar radio burst activity lasted a few minutes to a few tens of minutes and, in some cases, exhibited large intensity differences between L1 (1575.42 MHz) and L2 (1227.60 MHz). Civilian dual frequency GPS receivers were the most severely affected, and these events suggest that continuous, precise positioning services should account for solar radio bursts in their operational plans. This investigation raises the possibility of even more intense solar radio bursts during the next solar maximum that will significantly impact the operation of GPS receivers.

Observations of radio spectra at 1–2.5 GHz associated with CME start time

José R. **Cecatto**

Proceedings of the International Astronomical Union / Volume 4 / Symposium S257, pp 317 – 321, Published online: 16 Март **2009**

http://journals.cambridge.org/action/displayIssue?iid=4866212

We know Coronal Mass Ejections (CME) and flares are the most energetic phenomena happening on the Sun. Until now the information about origin and trigger mechanism of CMEs remains scarce. Also, there is unconclusive information about the association between them and flares although progress has been made in recent years. Multi-spectral observations suggested that the flare energy release occurs in regions from where the decimetric radio emission originates. In this case, investigations of the solar emission in this wavelength range can give us valuable information about these questions. During last solar maximum the Brazilian Solar Spectroscope (BSS) observed the solar radio spectrum (1–2.5 GHz) with high time (100–20 ms) and frequency (50–100 channels) resolutions on a daily (11–19 UT) basis. A survey during the period 1999–2002, shows that a significant fraction (20% –57 events) of CMEs recorded by LASCO has an association with the spectra of radio bursts recorded by BSS. Analysis of the radio spectrum associated to CME shows there is a dominance of continuum and/or pulsation and that the association becomes stronger when we consider the CME acceleration since its origin on the Sun. A statistics of this association between CME dynamics and the characteristics of decimetric radio bursts recorded by BSS is presented. Emphasis is given to observations of the association with CME start time.

A study of sunspot 3 minute oscillations using ALMA and GST

Yi **Chai**, Dale E. Gary, Kevin P. Reardon, Vasyl Yurchyshyn

ApJ **924** 100 **2021**

https://arxiv.org/pdf/2111.05812.pdf

https://iopscience.iop.org/article/10.3847/1538-4357/ac34f7/pdf

Waves and oscillations are important solar phenomena, not only because they can propagate and dissipate energy in the chromosphere, but also because they carry information about the structure of the atmosphere in which they propagate. The nature of the three-minute oscillations observed in the umbral region of sunspots is considered to be an effect of propagation of magnetohydrodynamic (MHD) waves upward from below the photosphere. We present a study of sunspot oscillations and wave propagation in NOAA AR 12470 using an approximately one-hour long data set acquired on **2015 December 17** by the Atacama Large Millimeter/submillimeter Array (ALMA), the Goode Solar Telescope (GST) operating at the Big Bear Solar Observatory (BBSO), the Atmospheric Imaging Assembly (AIA) on board the Solar Dynamics Observatory (SDO), and the Interface Region Imaging Spectrograph (IRIS). The ALMA data are unique in providing a time-series of direct temperature measurements in the sunspot chromosphere. The two-second cadence of ALMA images allows us to well resolve the three-minute periods typical of sunspot oscillations in the chromosphere. Fourier analysis is applied to ALMA Band 3 (~100 GHz, ~3 mm) and GST Hα data sets to obtain power spectra as well as oscillation phase information. We analysed properties of the wave propagation by combining multiple wavelengths that probe physical parameters of solar atmosphere at different heights. We find that the ALMA temperature fluctuations are consistent with that expected for a propagating acoustic wave, with a slight asymmetry indicating non-linear steepening.

Erratum: 2022 ApJ **933** 247 https://iopscience.iop.org/article/10.3847/1538-4357/ac7c1c/pdf

Solar flares associated coronal mass ejection accompanied with DH type II radio burst in relation with interplanetary magnetic field, geomagnetic storms and cosmic ray intensity

Harish **Chandra**, Beena Bhatt

New Astronomy Volume 60, April **2018**, Pages 22-32

sci-hub.tw/10.1016/j.newast.2017.10.001

In this paper, we have selected 114 flare-CME events accompanied with Deca-hectometric (DH) type II radio burst chosen from 1996 to 2008 (i.e., solar cycle 23). Statistical analyses are performed to examine the relationship of flare-CME events accompanied with DH type II radio burst with Interplanetary Magnetic field (IMF), Geomagnetic storms (GSs) and Cosmic Ray Intensity (CRI). The collected sample events are divided into two groups. In the first group, we considered 43 events which lie under the CME span and the second group consists of 71 events which are outside the CME span. Our analysis indicates that flare-CME accompanied with DH type II radio burst is inconsistent with CSHKP flare-CME model. We apply the Chree analysis by the superposed epoch method to both set of data to find the geo-effectiveness. We observed different fluctuations in IMF for arising and decay phase of solar cycle in both the cases. Maximum decrease in Dst during arising and decay phase of solar cycle is different for both the cases. It is noted that when flare lie outside the CME span CRI shows comparatively more variation than the flare lie under the CME span. Furthermore, we found that flare lying under the CME span is more geo effective than the flare outside of CME span. We noticed that the time leg between IMF Peak value and GSs, IMF and CRI is on average one day for both the cases. Also, the time leg between CRI and GSs is on average 0 to 1 day for both the cases. In case flare lie under the CME span we observed high correlation (0.64) between CRI and Dst whereas when flare lie outside the CME span a weak correlation (0.47) exists. Thus, flare position with respect to CME span play a key role for geo-effectiveness of CME.

Development of a 90–600 MHz Meter-wave Solar Radio Spectrometer

ShuWang **Chang**1,2, Bing Wang1, Guang Lu1, YuPeng Shen, +++

2024 ApJS 272 21

https://iopscience.iop.org/article/10.3847/1538-4365/ad3de7/pdf

Radio observation is important for understanding coronal mass ejections (CMEs), coronal shock waves, and high-energy electron acceleration. Here, we developed a new Chashan broadband solar radio spectrometer at a meter wavelength for observing the (super)fine structure of the solar radio burst spectrum. In the signal-receiving unit, we adopt an antenna system consisting of a 12 m large-aperture parabolic reflector and dual-line polarized logarithmic periodic feed source, as well as a high-precision Sun-tracking turntable system, all of which ensure the high-precision acquisition of solar radiation signals. For the digital receiver, we use a high-speed analog-to-digital converter with a sampling rate of 1.25 GSPS to directly sample the signal amplified and filtered by the analog receiver, simplifying the structure of the analog receiver, and design a 16k-point fast Fourier transform algorithm in the field programmable gate array to perform time–frequency transformation on the sampled signals. The default frequency and temporal resolution of the system are 76.294 kHz and 0.839 ms (up to 0.21 ms), respectively. The noise coefficient of the system is less than 1 dB, the dynamic range is more than 60 dB, and the sensitivity is as high as 1 sfu. We have observed a large number of radio bursts, including type I radio storms, hundreds of type III, ∼20 type II, and ∼15 type IV bursts in the past year. These high-quality data are useful in the further study of CMEs and associated particle acceleration and the origins of solar radio bursts. **2023-02-13, 2023 May 7-8**

Table 1 Comparison of the Main Meter-wave Solar Radio Observation Instruments

CESRA # 3773 **2024** https://www.astro.gla.ac.uk/users/eduard/cesra/?p=3773

Electrostatic Solitary Waves and Electron-beam Instabilities in the Separatrix Region of Magnetic Reconnection

Cong **Chang**1,2, Kai Huang1,2, Quanming Lu1,2, San Lu1,2, Xiancai Yu1,2, Rongsheng Wang1,2, Longlong Sang1,2, and Xinliang Gao1,2

2022 ApJ 933 67

https://iopscience.iop.org/article/10.3847/1538-4357/ac738d/pdf

Using 2D particle-in-cell (PIC) simulations, the generation of electrostatic solitary waves (ESWs) and the associated plasma waves in symmetric magnetic reconnection are studied, and multiple kinds of ESWs with different propagating speeds are identified. Near the current sheet in the outflow region, there are two kinds of ESWs propagating away from the X line: their propagating speeds are about 0.73VTe0 and 1.2VTe0 (where VTe0 is the initial electron thermal velocity), and their generation is associated with the Buneman instability and the electron two-stream instability, respectively. In the separatrix region, there is one kind of ESW propagating toward the X line with a propagating speed of about 1.2 VTe0, which is formed during the nonlinear evolution of the electron two-stream instability. We also run a case with a guide field, and there exist two kinds of ESWs: the ESWs propagating away from the X line can be generated near the separatrices with electron outflow, while the ESWs propagating toward the X line can be generated

near the separatrices with electron inflow. The two kinds of ESWs are associated with the electron two-stream instability and the Buneman instability, respectively.

How Nanoflares Produce Kinetic Waves, Nano-Type III Radio Bursts, and Non-Thermal Electrons in the Solar Wind

H. **Che**

Proceedings of 17th Annual International Astrophysics Conference, Santa Fe, 2018 **2018**

https://arxiv.org/pdf/1807.10942.pdf

Observations of the solar corona and the solar wind discover that the solar wind is unsteady and originates from the impulsive events near the surface of the Sun's atmosphere. How solar coronal activities affect the properties of the solar wind is a fundamental issue in heliophysics. We report a simulation and theoretical investigation of how nanoflare accelerated electron beams affect the kinetic-scale properties of the solar wind and generate coherent radio emission. We show that nanoflare-accelerated electron beams can trigger a nonlinear electron two stream instability, which generates kinetic Alfv\'en and whistler waves, as well as a non-Maxwellian electron velocity distribution function, consistent with observations of the solar wind. The plasma coherent emission produced in our model agrees well with the observations of Type III, J and V solar radio bursts. Open questions in the kinetic solar wind model are also discussed.

How electron two-stream instability drives cyclic Langmuir collapse and continuous coherent emission:

Che, H, Goldstein, M. L., Diamond, P. H., & Sagdeev, R. Z.,

Proceedings of the National Academy of Sciences of the United States of America,1/30/**2017**,Preprint arXiv https://arxiv.org/pdf/1702.00784.pdf

Continuous plasma coherent emission is maintained by repetitive Langmuir collapse driven by the nonlinear evolution of a strong electron two-stream instability. The Langmuir waves are modulated by solitary waves in the linear stage, and by electrostatic whistler waves in the nonlinear stage. Modulational instability leads to Langmuir collapse and electron heating that fills in cavitons. The high pressure is released via excitation of a short wavelength ion acoustic mode that is damped by electrons and that re-excites small-scale Langmuir waves---this process closes a feedback loop that maintains the continuous coherent emission.

See **CESRA Highlights** #1310 April **2017** http://cesra.net/?p=1310

Electron Two-stream Instability and Its Application in Solar and Heliophysics

Haihong **Che**

Modern Physics Letters A Volume 31, Issue 19, id. 1630018-163 (MPLA Homepage) **2016**

http://arxiv.org/pdf/1606.06200v1.pdf

It is well known that electron beams accelerated in solar flares can drive two-stream instability and produce radio bursts in the solar corona as well as in the interplanetary medium. Recent observations show that the solar wind likely originates from nanoflare-like events near the surface of the Sun where locally heated plasma escapes along open field lines into space. Recent numerical simulations and theoretical studies show that electron two-stream instability (ETSI) driven by nanoflare-accelerated electron beams can produce the observed nanoflare-type radio bursts, the non-Maxwellian electron velocity distribution function of the solar wind, and the kinetic scale turbulence in solar wind. This brief review focus on the basic theoretical framework and recent progress in the nonlinear evolution of ETSI, including the formation of electron holes, Langmuir wave generation in warm plasma, and the nonlinear modulation instability and Langmuir collapse. Potential applications in heliophysics and astrophysics are discussed.

Common Origin of Kinetic Scale Turbulence and the Electron Halo in the Solar Wind -- Connection to Nanoflares

Haihong **Che**

Proceedings of the Fourteenth International Solar Wind Conference **2016**

http://arxiv.org/pdf/1603.00549v1.pdf

We summarize our recent studies on the origin of solar wind kinetic scale turbulence and electron halo in the electron velocity distribution function. Increasing observations of nanoflares and microscopic type III radio bursts strongly suggest that nanoflares and accelerated electron beams are common in the corona. Based on particle-in-cell simulations, we show that both the core-halo feature and kinetic scale turbulence observed in the solar wind can be produced by the nonlinear evolution of electron two-stream instability driven by nanoflare accelerated electron beams. The energy

exchange between waves and particles reaches equilibrium in the inner corona and the key features of the turbulence and velocity distribution are preserved as the solar wind escapes into interplanetary space along open magnetic field lines. Observational tests of the model and future theoretical work are discussed.

Spectral Characteristics of Fundamental–Harmonic Pairs of Interplanetary Type III Radio Bursts Observed by PSP

Ling **Chen** (陈玲)1,2, Bing Ma (马兵)1, Dejin Wu (吴德金)1,2, Zongjun Ning (宁宗军)1, Xiaowei Zhou (周晓伟)1, and Stuart D. Bale3,4,5,6

2024 ApJL 975 L37

https://iopscience.iop.org/article/10.3847/2041-8213/ad89c2/pdf

Based on the observations by the Parker Solar Probe (PSP) during its encounter phases of approaching the Sun, I. C. Jebaraj et al. found that fundamental–harmonic (F-H) pairs constitute a majority of interplanetary (IP) type III radio bursts. In the present Letter, spectral characteristics of the IP F-H pairs are identified and analyzed further. The observations were made with the Radio Frequency Spectrometer (RFS) experiment on the PSP spacecraft in its encounter phase from the first to the ninth orbit as it traveled from 0.17 to 0.074 au from the Sun. The result shows that the occurrence rate of F-H pairs rises significantly with the rise in the number of IP type III radio bursts detected by the PSP or the enhancement in the time resolution of the RFS instrument. In particular, we compare the relationship between F and H spectral characteristics, such as the frequency-drift rate, emission intensity, relative bandwidth, duration, and fine structure. The results will be helpful for us to understand the physics underlying the generation and evolution of the IP F-H pairs as well as other IP type III radio bursts. **2019-04-03-09, 2020-09-13, 2021-04-28, 2021-05-03, 2021-08-01**

Data Release of Solar Radio Bursts observed by CBSm at the metric wavelength

Yao **Chen** et al.

CESRA #3773 **2024**

https://www.astro.gla.ac.uk/users/eduard/cesra/?p=3773

Here we release the spectral data of solar radio bursts recorded by the Chashan Broadband Solar radio spectrograph (CBSm), located in the Chashan mountain (E122°.30, N36°.84) that is the southern tip of Shandong Peninsula of China.

Energetic Electrons Accelerated and Trapped in a Magnetic Bottle above a Solar Flare Arcade

Bin **Chen** (1), Xiangliang Kong (2), Sijie Yu (1), Chengcai Shen (3), Xiaocan Li (4), Fan Guo (5), Yixian Zhang (6), Lindsay Glesener (6), Säm Krucker (7, 8)

ApJ **2024** **EOVSA**

https://arxiv.org/pdf/2406.00109 **File**

Where and how flares efficiently accelerate charged particles remains an unresolved question. Recent studies revealed that a "magnetic bottle" structure, which forms near the bottom of a large-scale reconnection current sheet above the flare arcade, is an excellent candidate for confining and accelerating charged particles. However, further understanding its role requires linking the various observational signatures to the underlying coupled plasma and particle processes. Here we present the first study combining multi-wavelength observations with data-informed macroscopic magnetohydrodynamics and particle modeling in a realistic eruptive flare geometry. The presence of an above-the-looptop magnetic bottle structure is strongly supported by the observations, which feature not only a local minimum of magnetic field strength but also abruptly slowing down plasma downflows. It also coincides with a compact hard X-ray source and an extended microwave source that bestrides above the flare arcade. Spatially resolved spectral analysis suggests that nonthermal electrons are highly concentrated in this region. Our model returns synthetic emission signatures that are well-matched to the observations. The results suggest that the energetic electrons are strongly trapped in the magnetic bottle region due to turbulence, with only a small fraction managing to escape. The electrons are primarily accelerated by plasma compression and facilitated by a fast-mode termination shock via the Fermi mechanism. Our results provide concrete support for the magnetic bottle as the primary electron acceleration site in eruptive solar flares. They also offer new insights into understanding the previously reported small population of flare-accelerated electrons entering interplanetary space. **2017 September 10**

Announcing New EOVSA Flare List and Data Products

Bin **Chen**

Solar News 1 Apr **2024**

We are pleased to announce a new flare list compiled from data recorded by the Expanded Owens Valley Solar Array (EOVSA). The novel EOVSA imaging spectroscopy observations also made the processing of the raw visibility data toward science-ready images and spectrograms a rather challenging task. Now, with the development of a semi-automatic flare processing pipeline, which includes applying various instrumental and interferometric calibrations, self-calibrations, deconvolution, and image registration, we have processed over 400 (and counting) flare events. For each of the flare events, we provide full-resolution spectrograms and multi-frequency time-series images in standard FITS format.
The EOVSA flare list can be queried at https://ovsa.njit.edu/flarelist. Similar to the STIX flare list, it also includes interactive flare light curve plots as well as links to view quick-look flare spectrograms/movies and download FITS files. Information on EOVSA data products and instructions for reading and plotting the data can be found at https://www.ovsa.njit.edu/wiki/index.php/EOVSA_Data_products. We also request that users of EOVSA data follow our data policy at https://ovsa.njit.edu//wiki/index.php/EOVSA_Data_Policy.

Weak Solar Radio Bursts from the Solar Wind Acceleration Region Observed by Parker Solar Probe and Its Probable Emission Mechanism

Ling **Chen**, Bing Ma, Dejin Wu, Xiaowei Zhou, Marc Pulupa, PeiJin Zhang, Pietro Zucca, Stuart D. Bale, Justin C. Kasper, SuPing Duan

ApJ **961** 136 **2023**
https://arxiv.org/pdf/2311.17819.pdf
https://iopscience.iop.org/article/10.3847/1538-4357/ad0e65/pdf
The Parker Solar Probe (PSP) provides us the unprecedentedly close approach observation to the Sun, and hence the possibility of directly understanding the "elementary process" which occurs in the kinetic scale of particles collective interactioin in solar coronal plasmas. We reported a kind of weak solar radio bursts (SRBs), which are detected by PSP when it passed a low-density magnetic channel during its second encounter phase. These weak SRBs have low starting frequecny ∼20 MHz and narrow frequency range from a few tens MHz to a few hundres kHz. Their dynamic spectra display a strongly evolving feature of the intermediate relative drift rate decreasing rapidly from above 0.01/s to below 0.01/s. Analyses based on common empirical models of solar coronal plasmas indicate that these weak SRBs originate from the heliocentric distance ∼1.1−6.1 RS (the solar radius), a typical solar wind acceleration region with a low-β plasma, and indicate that their soruces have a typic motion velociy ∼vA (Alfvén velocity) obviously lower than that of fast electrons required by effectively exciting SRBs. We propose that solitary kinetic Alfvén waves with kinetic scales can be responsible for the generation of these small-scalevweak SRBs, called solitary wave radiation (SWR). **April 3-6, 2019**
CESRA #3732 Feb **2024** https://www.astro.gla.ac.uk/users/eduard/cesra/?p=3732

Source positions of an interplanetary type III radio burst and anisotropic radio-wave scattering

Xingyao **Chen**, Eduard P. Kontar, Nicolina Chrysaphi, Peijin Zhang, Vratislav Krupar, Sophie Musset, Milan Maksimovic, Natasha L. S. Jeffrey, Francesco Azzollini, Antonio Vecchio

A&A 680, A1 **2023**
https://arxiv.org/pdf/2306.09160.pdf
https://www.aanda.org/articles/aa/pdf/2023/12/aa47185-23.pdf
https://doi.org/10.1051/0004-6361/202347185
Interplanetary solar radio type III bursts provide the means for remotely studying and tracking energetic electrons propagating in the interplanetary medium. Due to the lack of direct radio source imaging, several methods have been developed to determine the source positions from space-based observations. Moreover, none of the methods consider the propagation effects of anisotropic radio-wave scattering, which would strongly distort the trajectory of radio waves, delay their arrival times, and affect their apparent characteristics. We investigate the source positions and directivity of an interplanetary type III burst simultaneously observed by Parker Solar Probe, Solar Orbiter, STEREO, and Wind and compare the results of applying the intensity fit and timing methods with ray-tracing simulations of radio-wave propagation with anisotropic density fluctuations. The simulation calculates the trajectories of the rays, their time profiles at different viewing sites, and the apparent characteristics for various density fluctuation parameters. The results indicate that the observed source positions are displaced away from the locations where emission is produced, and their deduced radial distances are larger than expected from density models. This suggests that the apparent position is affected by anisotropic radio-wave scattering, which leads to an apparent position at a larger heliocentric distance from the Sun. The methods to determine the source positions may underestimate the apparent positions if they do not consider

the path of radio-wave propagation and incomplete scattering at a viewing site close to the intrinsic source position. **05-June-2020**
CESRA #3707 **2023** https://www.astro.gla.ac.uk/users/eduard/cesra/?p=3707

Radio Studies of the Middle Corona: Current State and New Prospects in the Next Decade

Bin **Chen** (1), Jason E. Kooi (2), David B. Wexler (3), Dale E. Gary (1), Sijie Yu (1), Surajit Mondal (1), Adam R. Kobelski (4), Daniel B. Seaton (5), Matthew J. West (5), Stephen M. White (6), Gregory D. Fleishman (1), Pascal Saint-Hilaire (7), Peijin Zhang (8), Chris R. Gilly (9), James P. Mason (10), Hamish Reid (11

Science **white paper** submitted to the 2024 Solar and Space Physics Decadal Survey. **2023**
All submitted white papers (including this one) are available at this https URL.
https://arxiv.org/pdf/2301.12183.pdf

The "middle corona," defined by West et al. (2022) as the region between ~1.5-6 solar radii, is a critical transition region that connects the highly structured lower corona to the outer corona where the magnetic field becomes predominantly radial. At radio wavelengths, remote-sensing of the middle corona falls in the meter-decameter wavelength range where a critical transition of radio emission mechanisms occurs. In addition, plasma properties of the middle corona can be probed by trans-coronal radio propagation methods including radio scintillation and Faraday rotation techniques. Together they offer a wealth of diagnostic tools for the middle corona, complementing current and planned missions at other wavelengths. These diagnostics include unique means for detecting and measuring the magnetic field and energetic electrons associated with coronal mass ejections, mapping coronal shocks and electron beam trajectories, as well as constraining the plasma density, magnetic field, and turbulence of the "young" solar wind. Following a brief overview of pertinent radio diagnostic methods, this white paper will discuss the current state of radio studies on the middle corona, challenges to obtaining a more comprehensive picture, and recommend an outlook in the next decade. Our specific recommendations for advancing the middle coronal sciences from the radio perspective are: (1) Prioritizing solar-dedicated radio facilities in the ~0.1-1 GHz range with broadband, high-dynamic-range imaging spectropolarimetry capabilities. (2) Developing facilities and techniques to perform multi-perspective, multiple lines-of-sight trans-coronal radio Faraday Rotation measurements.

Radio Imaging Spectropolarimetry of CMEs and CME Progenitors

Bin **Chen** (1), Timothy S. Bastian (2), Sarah Gibson (3), Yuhong Fan (3), Stephen M. White (4), Dale E. Gary (1), Angelos Vourlidas (5), Sijie Yu (1), Surajit Mondal (1), Gregory D. Fleishman (1), Pascal Saint-Hilaire (6)

Science white paper submitted to the 2024 Solar and Space Physics Decadal Survey. **2023**
All submitted white papers (including this one) are available at this https URL
https://arxiv.org/pdf/2301.12188.pdf

Coronal mass ejections (CMEs) are the most important drivers of space weather. Central to most CMEs is thought to be the eruption of a bundle of highly twisted magnetic field lines known as magnetic flux ropes. A comprehensive understanding of CMEs and their impacts hence requires detailed observations of physical parameters that lead to the formation, destabilization, and eventual eruption of the magnetic flux ropes. Recent advances in remote-sensing observations of coronal cavities, filament channels, sigmoids, EUV "hot channels," white light CMEs, and in situ observations of magnetic clouds points to the possibility of significant progress in understanding CMEs. In this white paper, we provide a brief overview of the potential of radio diagnostics for CMEs and CME progenitors, with a particular focus on the unique means for constraining their magnetic field and energetic electron population. Using synthetic observations based on realistic 3D MHD models, we also demonstrate the transformative potential of advancing such diagnostics by using broadband radio imaging spectropolarimetry with a high image dynamic range and high image fidelity. To achieve this goal, a solar-dedicated radio facility with such capabilities is recommended for implementation in the coming decade.

Quantifying Energy Release in Solar Flares and Solar Eruptive Events: New Frontiers with a Next-Generation Solar Radio Facility

Bin **Chen** (1), Dale E. Gary (1), Sijie Yu (1), Surajit Mondal (1), Gregory D. Fleishman (1), Xiaocan Li (2), Chengcai Shen (3), Fan Guo (4), Stephen M. White (5), Timothy S. Bastian (6), Pascal Saint-Hilaire (7), James F. Drake (8), Joel Dahlin (9), Lindsay Glesener (10), Hantao Ji (11), Astrid Veronig (12), Mitsuo Oka (7), Katharine K. Reeves (3), Judith Karpen (9)

Science white paper to the 2024 Solar and Space Physics Decadal Survey **2023**
https://arxiv.org/pdf/2301.12192.pdf

Solar flares and the often associated solar eruptive events serve as an outstanding laboratory to study the magnetic reconnection and the associated energy release and conversion processes under plasma conditions difficult to reproduce in the laboratory, and with considerable spatiotemporal details not possible elsewhere in the universe. In the past decade, thanks to advances in multi-wavelength imaging spectroscopy, as well as developments in theories and numerical modeling, significant progress has been made in improving our understanding of solar flare/eruption energy release. In particular, broadband imaging spectroscopy at microwave wavelengths offered by the Expanded Owens Valley Solar Array (EOVSA) has enabled the revolutionary capability of measuring the time-evolving coronal magnetic fields at or near the flare reconnection region. However, owing to EOVSA's limited dynamic range, imaging fidelity, and angular resolution, such measurements can only be done in a region around the brightest source(s) where the signal-to-noise is sufficiently large. In this white paper, after a brief introduction to the outstanding questions and challenges pertinent to magnetic energy release in solar flares and eruptions, we will demonstrate how a next-generation radio facility with many (~100-200) antenna elements can bring the next revolution by enabling high dynamic range, high fidelity broadband imaging spectropolarimetry along with a sub-second time resolution and arcsecond-level angular resolution. We recommend to prioritize the implementation of such a ground-based instrument within this decade. We also call for facilitating multi-wavelength, multi-messenger observations and advanced numerical modeling in order to achieve a comprehensive understanding of the "system science" of solar flares and eruptions. **2017 Sept. 10**

The frequency ratio and time delay of solar radio emissions with fundamental and harmonic components

Xingyao **Chen**, Eduard P. Kontar, Daniel L. Clarkson, Nicolina Chrysaphi
MNRAS 520, Issue 2, 3117–3126 **2023**
https://arxiv.org/pdf/2301.11299.pdf
https://doi.org/10.1093/mnras/stad325
https://academic.oup.com/mnras/article-pdf/520/2/3117/50319010/stad325.pdf
https://watermark.silverchair.com/stad325.pdf
Solar radio bursts generated through the plasma emission mechanism produce radiation near the local plasma frequency (fundamental emission) and double the plasma frequency (harmonic). While the theoretical ratio of these two frequencies is close to 2, simultaneous observations give ratios ranging from 1.6 to 2, suggesting either a ratio different from 2, a delay of the fundamental emission, or both. To address this long-standing question, we conducted high frequency, high time resolution imaging spectroscopy of type III and type J bursts with fine structures for both the fundamental and harmonic components with LOFAR between 30 and 80 MHz. The short-lived and narrow frequency-band fine structures observed simultaneously at fundamental and harmonic frequencies give a frequency ratio of 1.66 and 1.73, similar to previous observations. However, frequency-time cross-correlations suggest a frequency ratio of 1.99 and 1.95 with a time delay between the F and H emissions of 1.00 and 1.67 s, respectively for each event. Hence, simultaneous frequency ratio measurements different from 2 are caused by the delay of the fundamental emission. Among the processes causing fundamental emission delays, anisotropic radio-wave scattering is dominant. Moreover, the levels of anisotropy and density fluctuations reproducing the delay of fundamental emissions are consistent with those required to simulate the source size and duration of fundamental emissions. Using these simulations we are able to, for the first time, provide quantitative estimates of the delay time of the fundamental emissions caused by radio-wave propagation effects at multiple frequencies, which can be used in future studies. **16 Apr 2015, 7 May 2015**
CESRA #3493 **2023** **https://www.astro.gla.ac.uk/users/eduard/cesra/?p=3493**

Plasma Emission Induced By Electron Beam in Weakly Magnetized Plasmas

Yao **Chen**, Zilong Zhang, Sulan Ni, Chuanyang Li, Hao Ning, Xiangliang Kong
ApJ **2022**
https://arxiv.org/pdf/2201.03937.pdf
Previous studies on the beam-driven plasma emission process were done mainly for unmagnetized plasmas. Here we present fully-kinetic electromagnetic particle-in-cell simulations to investigate such process in weakly-magnetized plasmas of the solar corona conditions. The primary mode excited is the beam-Langmuir (BL) mode via the classical bump-on-tail instability. Other modes include the whistler (W) mode excited by the electron cyclotron resonance instability, the generalized Langmuir (GL) waves that include a superluminal Z-mode component with smaller wave number k and a thermal Langmuir component with larger k, and the fundamental (F) and harmonic (H) branches of plasma emission. Further simulations of different mass and temperature ratios of electrons and protons indicate that the GL mode and the two escaping modes (F and H) correlate positively with the BL mode in intensity, supporting that they are excited through nonlinear wave-wave coupling processes involving the BL mode. We suggest that the dominant

process is the decay of the primary BL mode. This is consistent with the standard theory of plasma emission. Yet, the other possibility of the Z+W→O--F coalescing process for the F emission cannot be ruled out completely.

An Interplanetary Type IIIb Radio Burst Observed by Parker Solar Probe and Its Emission Mechanism

Ling **Chen**1, Bing Ma1,2, Dejin Wu1, Guoqing Zhao3, Jianfei Tang4, and Stuart D. Bale5,6,7,8
2021 ApJL 915 L22
https://doi.org/10.3847/2041-8213/ac0b43
Type IIIb radio bursts were identified as a chain of quasi-periodic striae in dynamic spectra, drifting from high to low frequencies in a manner similar to type III bursts, which fine structures may provide a clue to a better understanding of emission mechanisms. The approaching observation of the Parker Solar Probe (PSP) spacecraft provides a new chance of probing type IIIb bursts in the vicinity of the Sun. In this Letter, combining the in situ measurement of PSP and the empirical model of solar atmospheres in open magnetic field regions, we analyze in detail a typical event of interplanetary (IP) type IIIb bursts observed by PSP, which was first reported by Pulupa et al. Our results show that the electron cyclotron maser (ECM) emission can probably play an important role in the excitation mechanism of the IP type IIIb burst and the formation of the fine striae structure may be attributed to the modulation of Alfvén waves on the growth rate of the ECM instability.

Energetic Electron Distribution of the Coronal Acceleration Region: First results from Joint Microwave and Hard X-ray Imaging Spectroscopy

Bin **Chen** (1), Marina Battaglia (2), Säm Krucker (2), Katharine K. Reeves (3), Lindsay Glesener (4)
ApJL **908** L55 **2021**
https://arxiv.org/pdf/2102.05173.pdf
https://doi.org/10.3847/2041-8213/abe471
Nonthermal sources located above bright flare arcades, referred to as the "above-the-loop-top" sources, have been often suggested as the primary electron acceleration site in major solar flares. The X8.2 limb flare on **2017 September 10** features such an above-the-loop-top source, which was observed in both microwaves and hard X-rays (HXRs) by the Expanded Owens Valley Solar Array (EOVSA) and the Reuven Ramaty High Energy Solar Spectroscopic Imager (RHESSI), respectively. By combining the microwave and HXR imaging spectroscopy observations with multi-filter extreme ultraviolet and soft X-ray imaging data, we derive the energetic electron distribution of this source over a broad energy range from <10 keV up to ~MeV during the early impulsive phase of the flare. The best-fit electron distribution consists of a thermal "core" from ~25 MK plasma. Meanwhile, a nonthermal power-law "tail" joins the thermal core at ~16 keV with a spectral index of ~3.6, which breaks down at above ~160 keV to >6.0. In addition, temporally resolved analysis suggests that the electron distribution above the break energy rapidly hardens with the spectral index decreasing from >20 to ~6.0 within 20 s, or less than ~10 Alfvén crossing times in the source. These results provide strong support for the above-the-loop-top source as the primary site where an on-going bulk acceleration of energetic electrons is taking place very early in the flare energy release.

Sub-second time evolution of Type III solar radio burst sources at fundamental and harmonic frequencies

Xingyao **Chen**, Eduard P. Kontar, Nicolina Chrysaphi, Natasha L.S. Jeffrey, Mykola Gordovskyy, Yihua Yan, Baolin Tan
ApJ **905** 43 **2020**
https://arxiv.org/pdf/2010.08782.pdf
https://iopscience.iop.org/article/10.3847/1538-4357/abc24e/pdf
Recent developments in astronomical radio telescopes opened new opportunities in imaging and spectroscopy of solar radio bursts at sub-second timescales. Imaging in narrow frequency bands has revealed temporal variations in the positions and source sizes that do not fit into the standard picture of type III solar radio bursts, and require a better understanding of radio-wave transport. In this paper, we utilise 3D Monte Carlo ray-tracing simulations that account for the anisotropic density turbulence in the inhomogeneous solar corona to quantitatively explain the image dynamics at the fundamental (near plasma frequency) and harmonic (double) plasma emissions observed at \sim 32~MHz. Comparing the simulations with observations, we find that anisotropic scattering from an instantaneous emission point source can account for the observed time profiles, centroid locations, and source sizes of the fundamental component of type III radio bursts (generated where f_{pe} \approx 32~MHz). The best agreement with observations is achieved when the ratio of the perpendicular to the parallel component of the wave vector of anisotropic density turbulence is around 0.25. Harmonic emission sources observed at the same frequency (\sim 32~MHz, but generated where f_{pe} \approx

16~MHz) have apparent sizes comparable to those produced by the fundamental emission, but demonstrate a much slower temporal evolution. The simulations of radio-wave propagation make it possible to quantitatively explain the variations of apparent source sizes and positions at sub-second time-scales both for the fundamental and harmonic emissions, and can be used as a diagnostic tool for the plasma turbulence in the upper corona.
CESRA #2760 Dec **2020** http://www.astro.gla.ac.uk/users/eduard/cesra/?p=2760

Measurement of magnetic field and relativistic electrons along a solar flare current sheet

Bin **Chen**, Chengcai Shen, Dale E. Gary, Katharine K. Reeves, Gregory D. Fleishman, Sijie Yu, Fan Guo, Säm Krucker, Jun Lin, Gelu Nita, Xiangliang Kong
2020 Nature Astronomy **4**, pages 1140–1147
https://arxiv.org/pdf/2005.12757.pdf **File**
https://www.nature.com/articles/s41550-020-1147-7
https://sci-hub.ru/10.1038/s41550-020-1147-7
In the standard model of solar flares, a large-scale reconnection current sheet is postulated as the central engine for powering the flare energy release and accelerating particles. However, where and how the energy release and particle acceleration occur remain unclear due to the lack of measurements for the magnetic properties of the current sheet. Here we report the measurement of spatially-resolved magnetic field and flare-accelerated relativistic electrons along a current-sheet feature in a solar flare. The measured magnetic field profile shows a local maximum where the reconnecting field lines of opposite polarities closely approach each other, known as the reconnection X point. The measurements also reveal a local minimum near the bottom of the current sheet above the flare loop-top, referred to as a "magnetic bottle". This spatial structure agrees with theoretical predictions and numerical modeling results. A strong reconnection electric field of ~4000 V/m is inferred near the X point. This location, however, shows a local depletion of microwave-emitting relativistic electrons. These electrons concentrate instead at or near the magnetic bottle structure, where more than 99% of them reside at each instant. Our observations suggest that the loop-top magnetic bottle is likely the primary site for accelerating and/or confining the relativistic electrons. **2017 September 10**
Video http://harp.njit.edu/~binchen/download/publications/Chen+2020_RCS/Chen_Supplementary_Video_1.mp4

Microwave Spectral Imaging of an Erupting Magnetic Flux Rope: Implications for the Standard Solar Flare Model in Three Dimensions

Bin **Chen** (1), Sijie Yu (1), Katharine K. Reeves (2), Dale E. Gary (1)
ApJL **895** Issue 2, L50 **2020** **File**
https://arxiv.org/pdf/2005.01900.pdf
https://sci-hub.st/10.3847/2041-8213/ab901a
We report microwave spectral imaging observations of an erupting magnetic flux rope during the early impulsive phase of the X8.2-class limb flare on **2017 September 10**, obtained by the Expanded Owens Valley Solar Array (EOVSA). A few days prior to the eruption, when viewed against the disk, the flux rope appeared as a reverse S-shaped dark filament along the magnetic polarity inversion line. During the eruption, the rope exhibited a "hot channel" structure in extreme ultraviolet and soft X-ray passbands sensitive to ~10 MK plasma. The central portion of the flux rope was nearly aligned with the line of sight, which quickly developed into a teardrop-shaped dark cavity during the early phase of the eruption. A long and thin plasma sheet formed below the cavity, interpreted as the reconnection current sheet viewed edge-on. A nonthermal microwave source was present at the location of the central current sheet, which extended upward encompassing the dark cavity. A pair of nonthermal microwave sources were observed for several minutes at both sides of the main flaring region. They shared a similar temporal behavior and spectral property to the central microwave source below the cavity, interpreted as the conjugate footpoints of the erupting flux rope. These observations are broadly consistent with the magnetic topology and the associated energy release scenario suggested in the three-dimensional standard model for eruptive solar flares. In particular, our detection of nonthermal emission at conjugate flux rope footpoints provides solid evidence of particle transport along an erupting magnetic flux rope.
CESRA #2682 Sep **2020** http://www.astro.gla.ac.uk/users/eduard/cesra/?p=2682

Solar Flare Observations with the Karl G. Jansky Very Large Array **Presentation**

Bin **Chen**
Presentation at the Fleishman's Webinar, April **2020**
http://www.ioffe.ru/LEA/SF_AR/files/Chen_solarwebinar_20200401.pdf

Tracing fast electron beams - Chen et al. 2018, ApJ, 866, 62 - Chen et al. 2013, ApJL, 763, 21 ⊙
Mapping solar flare termination shocks - Luo et al., in prep - Chen et al. 2019, ApJ, 884, 63 - Chen et al. 2015, Science, 350, 1238 ⊙
Imaging waves and oscillations - Yu & Chen, 2019, ApJ, 872, 71 - Wang, Chen & Gary 2017, ApJ, 848, 77 ⊙
Microflares - Battaglia et al., in prep - Sharma et al., in prep

Radio Spectroscopic Imaging of a Solar Flare Termination Shock: Split-Band Feature as Evidence for Shock Compression

Bin **Chen** (1), Chengcai Shen (2), Katharine K. Reeves (2), Fan Guo (3 and 4), Sijie Yu (1)
ApJ **884** 63 **2019**
https://arxiv.org/pdf/1908.09146.pdf
sci-hub.si/10.3847/1538-4357/ab3c58
https://iopscience.iop.org/article/10.3847/1538-4357/ab3c58/pdf
Solar flare termination shocks have been suggested as one of the promising drivers for particle acceleration in solar flares, yet observational evidence remains rare. By utilizing radio dynamic spectroscopic imaging of decimetric stochastic spike bursts in an eruptive flare, Chen et al. found that the bursts form a dynamic surface-like feature located at the ending points of fast plasma downflows above the looptop, interpreted as a flare termination shock. One piece of observational evidence that strongly supports the termination shock interpretation is the occasional split of the emission band into two finer lanes in frequency, similar to the split-band feature seen in fast-coronal-shock-driven type II radio bursts. Here we perform spatially, spectrally, and temporally resolved analysis of the split-band feature of the flare termination shock event. We find that the ensemble of the radio centroids from the two split-band lanes each outlines a nearly co-spatial surface. The high-frequency lane is located slightly below its low frequency counterpart by ~0.8 Mm, which strongly supports the shock upstream-downstream interpretation. Under this scenario, the density compression ratio across the shock front can be inferred from the frequency split, which implies a shock with a Mach number of up to 2.0. Further, the spatiotemporal evolution of the density compression along the shock front agrees favorably with results from magnetohydrodynamics simulations. We conclude that the detailed variations of the shock compression ratio may be due to the impact of dynamic plasma structures in the reconnection outflows, which results in distortion of the shock front.**25 Jan 2002, 2012 March 3**
CESRA # 2412 Nov **2019** http://www.astro.gla.ac.uk/users/eduard/cesra/?p=2412
Rejuvenating Solar Flare Termination Shocks as Particle Accelerators
Bin **CHEN**
RHESSI Science Nuggets #378 **2020**
http://sprg.ssl.berkeley.edu/~tohban/wiki/index.php/Rejuvenating_Solar_Flare_Termination_Shocks_as_Particle_Accelerators

Quasi-periodic Pulsations before and during a Solar Flare in AR 12242

Xingyao **Chen**, Yihua Yan, Baolin Tan, Jing Huang, Wei Wang, Linjie Chen, Yin Zhang, Chengming Tan, Donghao Liu, and Satoshi Masuda
2019 ApJ 878 78
https://iopscience.iop.org/article/10.3847/1538-4357/ab1d64/pdf
Quasi-periodic pulsations (QPPs) are frequently observed in solar flares, which may reveal some essential characteristics of both thermal and nonthermal energy releases. This work presents multi-wavelength imaging observations of an M8.7 flare in active region AR 12242 on **2014 December 17**. We found that there were three different QPPs: UV QPPs with a period of about 4 minutes at 1600 Å images near the center of the active region lasting from the preflare phase to the impulsive phase; EUV QPPs with a period of about 3 minutes along the circular ribbon during the preflare phase; and radio QPPs with a period of about 2 minutes at frequencies of 1.2–2.0 GHz around the flaring source region during the impulsive phase. The observations include the radio images observed by the Mingantu Spectral Radioheliograph in China at frequencies of 1.2–2.0 GHz for the first time, microwave images by the Nobeyama Radioheliograph, UV and EUV images by AIA/SDO, and a magnetogram by HMI/SDO. We suggest that the 4 minute UV QPPs should be modulated by the sunspot oscillations, and the 3 minute EUV QPPs are closely related to the 2 minute radio QPPs for their source regions connected by a group of coronal loops. We propose that the intermittent magnetic reconnecting downward and upward plasmoids may be the possible trigger of both the preflare 3 minute EUV QPPs and the impulsive 2 minute radio QPPs. The other possible mechanism is LRC oscillation, which is associated with the current-carrying

coronal loops. The latter mechanism implies that the existence of preflare QPPs may be a possible precursor to solar flares.

Astro2020 Science White Paper: Probing Magnetic Reconnection in Solar Flares - New Perspectives from Radio Dynamic Imaging Spectroscopy Review

Bin **Chen** (1), Tim Bastian (2), Joel Dahlin (3), James F. Drake (4), Gregory D. Fleishman (1), Dale E. Gary (1), Lindsay Glesener (5), Fan Guo (6), Hantao Ji (7), Pascal Saint-Hilaire (8), Chengcai Shen (9), Stephen M. White

Astro2020: Decadal Survey on Astronomy and Astrophysics, science white papers, no. 507; Bulletin of the American Astronomical Society, Vol. 51, Issue 3, id. 507 **2019**

https://arxiv.org/pdf/1903.11192.pdf

https://113qx216in8z1kdeyi404hgf-wpengine.netdna-ssl.com/wp-content/uploads/2019/05/507_chen.pdf

Magnetic reconnection is a fundamental physical process in many laboratory, space, and astrophysical plasma contexts. Solar flares serve as an outstanding laboratory to study the magnetic reconnection and the associated energy release and conversion processes under plasma conditions difficult to reproduce in the laboratory, and with considerable spatiotemporal details not possible elsewhere in astrophysics. Here we emphasize the unique power of remote-sensing observations of solar flares at radio wavelengths. In particular, we discuss the transformative technique of broadband radio dynamic imaging spectroscopy in making significant contributions to addressing several outstanding challenges in magnetic reconnection, including the capability of pinpointing magnetic reconnection sites, measuring the time-evolving reconnecting magnetic fields, and deriving the spatially and temporally resolved distribution function of flare-accelerated electrons.

Microwave Spectral Imaging of Bi-Directional Magnetic Reconnection Outflow Region of the 2017 Sep 10 X8.2 Flare

Chen, Bin; Gary, Dale E.; Fleishman, Gregory D.; Krucker, Sam; Nita, Gelu M.; Dennis, Brian R.; Yu, Sijie ; Kuroda, Natsuha; Reeves, Katharine K.; Polito, Vanessa; Shih, Albert

Solar Heliospheric and INterplanetary Environment (SHINE **2018**), Proceedings of the conference held 30 July-3 August, **2018** in Cocoa Beach, FL, id.211

The newly commissioned Expanded Owens Valley Solar Array (EOVSA) obtained microwave spectral imaging of the spectacular eruptive solar flare on 2017 September 10 in 2.5–18 GHz. During the early impulsive phase of the flare (15:54 UT), An elongated microwave source appears to connect the top of the flare arcade to the bottom of the erupting magnetic flux rope. Multi-frequency images reveal that the source bifurcates into two parts: One is located at and above the hard X-ray looptop source, and another located behind the flux rope. They appear to follow closely with the bi-directional reconnection downflow and upflow region as inferred from the SDO/AIA EUV images. The spatially resolved spectra of this microwave source show characteristics of gyrosynchrotron radiation, suggesting the presence of high-energy (100s of keV to MeV) electrons throughout the bi-directional reconnection outflow region. We derive physical parameters of the source region, and discuss their implications in magnetic energy release and electron acceleration.

Magnetic Reconnection Null Points as the Origin of Semi-relativistic Electron Beams in a Solar Jet

Bin **Chen**, Sijie Yu, Marina Battaglia, Samaiyah Farid, Antonia Savcheva, Katharine K. Reeves, Säm Krucker, T. S. Bastian, Fan Guo, Svetlin Tassev

ApJ 866(1), 62 **2018**

https://arxiv.org/pdf/1808.05951.pdf

https://iopscience.iop.org/article/10.3847/1538-4357/aadb89/pdf

https://web.njit.edu/~binchen/download/publications/Chen+2018_TP3/Chen_et_al_2018_type3_apj.pdf

Magnetic reconnection, the central engine that powers explosive phenomena throughout the Universe, is also perceived as one of the principal mechanisms for accelerating particles to high energies. Although various signatures of magnetic reconnection have been frequently reported, observational evidence that links particle acceleration directly to the reconnection site has been rare, especially for space plasma environments currently inaccessible to in situ measurements. Here we utilize broadband radio dynamic imaging spectroscopy available from the Karl G. Jansky Very Large Array to observe decimetric type III radio bursts in a solar jet with high angular (~20″), spectral (~1 %), and temporal resolution (50 milliseconds). These observations allow us to derive detailed trajectories of semi-relativistic (tens of keV) electron beams in the low solar corona with unprecedentedly high angular precision (<0″.65). We found that each group of electron beams, which corresponds to a cluster of type III bursts with 1-2-second duration, diverges from an extremely

compact region (~600 km2) in the low solar corona. The beam-diverging sites are located behind the erupting jet spire and above the closed arcades, coinciding with the presumed location of magnetic reconnection in the jet eruption picture supported by extreme ultraviolet/X-ray data and magnetic modeling. We interpret each beam-diverging site as a reconnection null point where multitudes of magnetic flux tubes join and reconnect. Our data suggest that the null points likely consist of a high level of density inhomogeneities possibly down to 10-km scales. These results, at least in the present case, strongly favor a reconnection-driven electron acceleration scenario. **2014 November 1**

Fine Structures of Solar Radio Type III Bursts and their Possible Relationship with Coronal Density Turbulence

Xingyao **Chen**, Eduard P. Kontar, Sijie Yu, Yihua Yan, Jing Huang, Baolin Tan
ApJ **856** 73 **2018**
https://arxiv.org/pdf/1801.07545.pdf
http://sci-hub.tw/http://iopscience.iop.org/0004-637X/856/1/73/
Solar radio type III bursts are believed to be the most sensitive signature of near-relativistic electron beam propagation in the corona. A solar radio type IIIb-III pair burst with fine frequency structures, observed by the Low Frequency Array (LOFAR) with high temporal (~10 ms) and spectral (12.5 kHz) resolutions at 30 - 80 MHz, is presented. The observations show that the type III burst consists of many striae, which have a frequency scale of about 0.1 MHz in both the fundamental (plasma) and the harmonic (double plasma) emission. We investigate the effects of background density fluctuations based on the observation of striae structure to estimate the density perturbation in solar corona. It is found that the spectral index of the density fluctuation spectrum is about −1.7, and the characteristic spatial scale of the density perturbation is around 700 km. This spectral index is very close to a Kolmogorov turbulence spectral index of −5/3, consistent with a turbulent cascade. This fact indicates that the coronal turbulence may play the important role of modulating the time structures of solar radio type III bursts, and the fine structure of radio type III bursts could provide a useful and unique tool to diagnose the turbulence in the solar corona. **16 Apr 2015**
CESRA nugget #1848 May **2018** http://cesra.net/?p=1848

Double Coronal X-ray and Microwave Sources Associated With A Magnetic Breakout Solar Eruption

Yao **Chen**, Zhao Wu, Wei Liu, Richard A. Schwartz, Di Zhao, Bing Wang, Guohui Du
2017 *ApJ* **843** 8
https://arxiv.org/pdf/1705.06074.pdf
http://sci-hub.cc/10.3847/1538-4357/aa7462
Double coronal hard X-ray (HXR) sources are believed to be critical observational evidence of bi-directional energy release through magnetic reconnection in a large-scale current sheet in solar ares. Here we present a study on double coronal sources observed in both HXR and microwave regimes, revealing new characteristics distinct from earlier reports. This event is associated with a footpoint-occulted X1.3-class flare (**25 April 2014**, starting at 00:17 UT) and a coronal mass ejection that are likely triggered by the magnetic breakout process, with the lower source extending upward from the top of the partially-occulted flare loops and the upper source co-incident with rapidly squeezing-in side lobes (at a speed of ~250 km/s on both sides). The upper source can be identified at energies as high as 70-100 keV. The X-ray upper source is characterized by flux curves different from the lower source, a weak energy dependence of projected centroid altitude above 20 keV, a shorter duration and a HXR photon spectrum slightly-harder than those of the lower source. In addition, the microwave emission at 34 GHz also exhibits a similar double source structure and the microwave spectra at both sources are in line with gyro-synchrotron emission given by non- thermal energetic electrons. These observations, especially the co-incidence of the very-fast squeezing-in motion of side lobes and the upper source, indicate that the upper source is associated with (possibly caused by) this fast motion of arcades. This sheds new lights on the origin of the corona double-source structure observed in both HXRs and microwaves.
See RHESSI Science Nuggets #301 May **2017**
http://sprg.ssl.berkeley.edu/~tohban/wiki/index.php/Double_Coronal_X-ray_and_Microwave_Sources_Associated_With_A_Magnetic_Breakout_Solar_Eruption

A self-consistent mechanism for electron-cyclotron maser emission and its application to type III solar radio bursts†

L. **Chen**, D. J. Wu, G. Q. Zhao, J. F. Tang
JGR Volume 122, Issue 1 January **2017** Pages 35–49 DOI: 10.1002/2016JA023312
sci-hub.si/10.1002/2016JA023312

Type III solar radio bursts (SRBs) produced by fast electron beams (FEBs) traveling along solar magnetic fields are the best known and the most important kind of SRBs because of their clearest association with FEBs as well as most frequent observations during solar activities. However, the physics of their emitting mechanism has been a controversial issue. Based on the electron cyclotron maser (ECM) instability driven directly by a magnetized FEB, whose physics is fairly well known from the Earth's auroral kilometric radiation, this paper proposes a self-consistent mechanism for type III SRBs, in which the Alfvén wave (AW) produced by the current instability of the beam-return current system associated with the FEB, called the self-generated AW, plays an important and crucial role. Taking into account of the return-current effect of the FEB, the growth rate and the saturation intensity of the self-generated AW are estimated. Then the effects of the self-generated AW on the ECM emission via the ECM instability driven by the magnetized FEB are further investigated. The results show that the self-generated AW can significantly influence and change the physical properties of the ECM emission. In particular, this novel ECM-emission mechanism can effectively overcome the main difficulties of the conventional ECM-emission mechanism in application to type III SRBs and may potentially provide a self-consistent physics scenario for type III SRBs.

A solar type II radio burst from CME-coronal ray interaction: simultaneous radio and EUV imaging

Yao **Chen**, Guohui Du, Li Feng, Shiwei Feng, Xiangliang Kong, Fan Guo, Bing Wang, Gang Li
2014, ApJ 787 59
http://arxiv.org/pdf/1404.3052v1.pdf
Simultaneous radio and extreme ultraviolet (EUV)/white-light imaging data are examined for a solar type II radio burst occurring on **2010 March 18** to deduce its source location. Using a bow-shock model, we reconstruct the 3-dimensional EUV wave front (presumably the type-II emitting shock) based on the imaging data of the two STEREO spacecraft. It is then combined with the Nan\c{c}ay radio imaging data to infer the 3-dimensional position of the type II source. It is found that the **type II source coincides with the interface between the CME EUV wave front and a nearby coronal ray structure, providing evidence that the type II emission is physically related to the CME-ray interaction.** This result, consistent with those of previous studies, is based on simultaneous radio and EUV imaging data for the first time.

FLARE-ASSOCIATED TYPE III RADIO BURSTS AND DYNAMICS OF THE EUV JET FROM SDO/AIA AND RHESSI OBSERVATIONS

Naihwa **Chen**1, Wing-Huen Ip1,2, and Davina Innes
2013 ApJ 769 96
We present a detailed description of the interrelation between the Type III radio bursts and energetic phenomena associated with the flare activities in active region AR11158 at 07:58 UT on **2011 February 15**. The timing of the Type III radio burst measured by the radio wave experiment on Wind/WAVE and an array of ground-based radio telescopes coincided with an extreme-ultraviolet (EUV) jet and hard X-ray (HXR) emission observed by SDO/AIA and RHESSI, respectively. There is clear evidence that the EUV jet shares the same source region as the HXR emission. The temperature of the jet, as determined by multiwavelength measurements by Atmospheric Imaging Assembly, suggests that Type III emission is associated with hot, 7 MK, plasma at the jet's footpoint.

Passages of Electron Beams

Bin **Chen** and Tim Bastian
RHESSI Science Nugget, No. 193, Feb **2013**
http://sprg.ssl.berkeley.edu/~tohban/wiki/index.php/Passages_of_Electron_Beams
Dynamic imaging spectroscopy at the upgraded VLA - a new capability - reveals some interesting new things about radio type III bursts. **5 Nov 2011**

Tracing Electron Beams in the Sun's Corona with Radio Dynamic Imaging Spectroscopy

Bin **Chen**, Timothy S. Bastian, Stephen M. White, Dale E. Gary, Richard A. Perley, Michael P. Rupen, Brent R. Carlson

E-print, Dec **2012**; ApJL 763 L21, **2013**
https://web.njit.edu/~binchen/download/publications/Chen+2013_TP3/Chen+2013_TP3.pdf
We report observations of type III radio bursts at decimeter wavelengths (type IIIdm bursts) -- signatures of suprathermal electron beams propagating in the low corona -- using the new technique of radio dynamic imaging spectroscopy provided by the recently upgraded Karl G. Jansky Very Large Array (VLA). For the first time, type IIIdm bursts were imaged with high time and frequency resolution over a broad frequency band, allowing electron beam trajectories in the corona to be deduced. Together with simultaneous hard X-ray (HXR) and extreme ultraviolet (EUV) observations, we show these beams emanate from an energy release site located in the low corona at a height below ~15 Mm, and propagate along a bundle of discrete magnetic loops upward into the corona. Our observations enable direct measurements of the plasma density along the magnetic loops, and allow us to constrain the diameter of these loops to be less than 100 km. These over-dense and ultra-thin loops reveal the fundamentally fibrous structure of the Sun's corona. The impulsive nature of the electron beams, their accessibility to different magnetic field lines, and the detailed structure of the magnetic release site revealed by the radio observations indicate that the localized energy release is highly fragmentary in time and space, supporting a bursty reconnection model that involves secondary magnetic structures for magnetic energy release and particle acceleration. **5 Nov 2011**

Spatially and Spectrally Resolved Observations of a Zebra Pattern in Solar Decimetric Radio Burst

Bin **Chen**1,2, T. S. Bastian2, D. E. Gary3, and Ju Jing4
E-print, May **2011, File**; Ap.J. 736 64, **2011**
We present the first interferometric observation of a zebra-pattern radio burst with simultaneous high spectral (¼ 1 MHz) and high time (20 ms) resolution. The Frequency-Agile Solar Radiotelescope (FASR) Subsystem Testbed (FST) and the Owens Valley Solar Array (OVSA) were used in parallel to observe the X1.5 flare on **14 December 2006**. By using OVSA to calibrate the FST the source position of the zebra pattern can be located on the solar disk. With the help of multi-wavelength observations and a nonlinear force-free field (NLFFF) extrapolation, the zebra source is explored in relation to the magnetic field configuration. New constraints are placed on the source size and position as a function of frequency and time. We conclude that the zebra burst is consistent with a double-plasma resonance (DPR) model in which the radio emission occurs in resonance layers where the upper hybrid frequency is harmonically related to the electron cyclotron frequency in a coronal magnetic loop.

Does the F[10.7] index correctly describe solar EUV flux during the deep solar minimum of 2007-2009?

Chen, Yiding; Liu, Libo; Wan, Weixing
J. Geophys. Res., Vol. 116, No. A4, A043046 **2011**
This paper shows that the relationship between solar EUV flux and the F10.7 index during the extended solar minimum (Smin) of 2007–2009 is different from that in the previous Smin. This difference is also seen in the relationship between foF2 and F10.7. We collected SOHO/SEM EUV observations and the F10.7 index, through June 2010, to investigate solar irradiance in the recent Smin. We find that, owing to F10.7 and solar EUV flux decreased from the last Smin to the recent one with different amplitudes (larger in EUV flux), EUV flux is significantly lower in the recent Smin than in the last one for the same F10.7. Namely, F10.7 does not describe solar EUV irradiance in the recent Smin as it did in the last Smin. That caused remarkable responses in ionospheric foF2. For the same F10.7, foF2 in the recent Smin is lower than that in the last one; further, it is also lower than that in other previous Smins. Therefore, F10.7 is not an ideal indicator of foF2 during the recent Smin, which implies that F10.7 is not an ideal proxy for solar EUV irradiance during this period, although it has been adequate during previous Smins. Solar irradiance models and ionospheric models will need to take this into account for solar cycle investigations.

SHORT-LIVED ABSORPTIVE TYPE IIIY-LIKE MICROWAVE BURSTS AS A SIGNATURE OF FRAGMENTED ELECTRON INJECTIONS

Bin **Chen** and Yihua Yan
Astrophysical Journal, 689:1412Y1420, **2008**
In this paper, we devote ourselves to interpreting the short-lived absorptive type IIIYlike microwave bursts in the **2006 December 13** flare event observed with high temporal and spectral resolutions (8 ms and 10 MHz) by the Chinese Solar Broadband Radio Spectrometer (SBRS/Huairou) at 2.6-3.8 GHz. In the decimeter-centimeter wavelength range, we first present the observations of short-lived bursts represented as a number of absorptive ‘‘spikes’’ superposed on the type IV continuum that can be connected by fast-drifting lines. The mean drift rate, the instantaneous bandwidth,

and the absorption depth of these absorptive spikes are about _12 GHz s_1, 70MHz, and 40%, respectively. The duration at a single frequency band can be less than the instrument resolution of 8 ms. On the basis of numerical investigations of the loss-cone instability, we suggest that fragmented electron injections with durations of as short as several milliseconds into the loss cone could be the most appropriate mechanism with which to explain the bursts. The length of an electron beam is estimated to be about 400 km, on the basis of the observational results. These injections may be related to the fragmented energy release processes during the flare. We also observe some absorptive type III-like bursts accompanying ordinary type III bursts with reverse drifts. They start at the same frequency, and the starting frequency slowly drifts to the low-frequency region. This could be a signature of propagating bidirectional electron beams originating near the reconnection region.

On the Origin of Zebra-Pattern with Pulsating Superfine Structures on April 21, 2002

Bin **Chen** ¢ Yi-hua Yan

E-print, Oct 2007; Solar Phys. (**2007**) 246: 431–443

http://www.springerlink.com/content/h48k347355666105/fulltext.pdf

Through the data around 3 GHz from the Radio Spectrometer in Huairou, Beijing, zebra-pattern structures from the 21 April 2002 event have been studied. Zebra stripes consist of periodically pulsating superfine structures in this event. An analysis of temporal profiles of intensities at multiple frequency channels shows that the Gaussian temporal profiles of pulse groups on zebra stripes are caused by drifting zebra stripes with Gaussian spectral profiles. The observed quasiperiodic pulsations with about 30 ms period have a peculiar feature of oscillation near a steady state, probably resulting from relaxation oscillations, which modulate the electron cyclotron maser emission that forms the zebra stripes during the process of wave – particle interactions. All the main properties of the zebra stripes with pulsating superfine structures indicate that the double plasma resonance model might be the most suitable one, with the relaxation oscillations, to form the superfine structures. The model of LaBelle *et al.* (*Astrophys. J.* **593**, 1195, 2003) could not account for the observed properties of zebra-pattern structures in this event nor for most zebra-pattern structures occupying a wide frequency range, mainly because the allowable frequency range of the zebra-pattern structures in their model is too narrow to reproduce the observed zebras.

Mitigation of Radio Frequency Interference in the Solar Radio Spectrum Based on Deep Learning

Jun **Cheng**, Yanzuo Li, Yanjun Zhang, Yihua Yan, Chengming Tan, Linjie Chen & Wei Wang

Solar Physics volume 297, Article number: 46 (**2022**)

https://link.springer.com/content/pdf/10.1007/s11207-022-01975-w.pdf

Radio frequency interference (RFI) may contaminate the signal received by solar radio telescopes. The existence of RFI in the solar radio spectrum affects the accuracy and efficiency of the extraction of burst parameters, which is related to the quality of scientific results and even the authenticity of conclusions. Therefore, it is necessary to carry out research on RFI recognition algorithms for solar radio data. This article aims to compare the recognition performance of six different deep-learning networks (FCN, Deconvnet, Segnet, Unet, Dual-Resunet, and DSC Based Dual-Resunet) on the RFI in solar radio spectra observed by the Chinese Solar Broadband Radio Spectrometer (SBRS). The accuracy and convergence speed in the training process, as well as various performance metrics in the test, indicate that the proposed DSC Based Dual-Resunet is the most suitable neural-network for this task and can achieve both performance and light weight. The RFI recognition accuracy of the DSC Based Dual-Resunet is close to Unet when there is no burst in the spectrum, but in the case of a burst DSC Based Dual-Resunet is obviously better than Unet in terms of RFI recognition. Moreover the model size and number of parameters are approximately 12.5% of those of Unet, and the amount of computation is 38% of that of Unet, which greatly improves the computation efficiency and is of great significance for the realization of the network on mobile hardware. It is promising for the large-scale application of RFI recognition for solar radio telescopes.

SCALE SEQUENTIALLY CLEAN FOR MINGANTU SPECTRAL RADIOHELIOGRAPH

Jun **Cheng**, Yihua Yan, Dong Zhao, Long Xu

Solar-Terrestrial Physics. **2019**. Vol. 5. Iss. 2. P. 50–57.

Solnechno-zemnaya fizika. 2019. Vol. 5. Iss. 2. P. 55–62.

https://naukaru.ru/en/storage/view/36900

MingantU SpEctral Radioheliograph (MUSER) is a solar-dedicated radio heliograph, adopting aperture synthesis technique to image the Sun in the frequency range of 0.4 GHz to 15 GHz. MUSER has extremely high spatial resolution, temporal resolution, and frequency resolution beyond those of contemporary devices of the same category. For aperture synthesis, the number of antennas is limited, so sparse sampling of Fourier components is actually obtained for solar observation, which corresponds to the situation that a clean image is convolved by a dirty beam with strong sidelobe in a spatial domain. Thus, the deconvolution, such as CLEAN, is generally required for imaging the aperture synthesis to

remove artifacts caused by the convolving dirty beam. The traditional Högbom CLEAN is based on the assumption that an observed object is only composed of point sources. This assumption does not hold for solar observation, where the solar disk is an extended source containing complex structures and diffuse features. In this paper, we make the first attempt to employ scale sequentially CLEAN for MUSER imaging, including Multi-Resolution CLEAN and Wavelet CLEAN. The experimental results demonstrate that the scale sequentially CLEAN, especially wavelet CLEAN, is superior to the traditional CLEAN algorithm in smaller number of iterations and improved image quality. We provide optimized wavelet parameters to further improve the performance of wavelet CLEAN.

A Type II Radio Burst without a Coronal Mass Ejection

Su, W., **Cheng**, X., Ding, M. D., Chen, P. F., and Sun, J. Q.
ApJ **2015**
http://arxiv.org/pdf/1503.00861v1.pdf
Type II radio bursts are thought to be a signature of coronal shocks. In this paper, we analyze a short-lived type II burst that started at 07:40 UT on **2011 February 28**. By carefully checking white-light images, we find that the type II radio burst is not accompanied by a coronal mass ejection, only with a C2.4 class flare and narrow jet. However, in the extreme-ultraviolet (EUV) images provided by the Atmospheric Imaging Assembly (AIA) on board the Solar Dynamics Observatory (SDO), we find a wave-like structure that propagated at a speed of ~600 km/s during the burst. The relationship between the type II radio burst and the wave-like structure is in particular explored. For this purpose, we first derive the density distribution under the wave by the differential emission measure (DEM) method, which is used to restrict the empirical density model. We then use the restricted density model to invert the speed of the shock that produces the observed frequency drift rate in the dynamic spectrum. The inverted shock speed is similar to the speed of the wave-like structure. This implies that the wave-like structure is most likely a coronal shock that produces the type II radio burst. We also examine the evolution of the magnetic field in the flare-associated active region and find continuous flux emergence and cancellation taking place near the flare site. Based on these facts, we propose a new mechanism for the formation of the type II radio burst, i.e., the expansion of the strongly-inclined magnetic loops after reconnected with nearby emerging flux acts as a piston to generate the shock wave.

Slowly drifting radio fibres

G P **Chernov**, V V Fomichev
MNRAS, Volume 522, Issue 2, June **2023**, Pages 1930–1938,
https://doi.org/10.1093/mnras/stad929
The fine structure in the continuum radiation of type IV solar radio bursts is very rich in various structures (zebra structure, fibres, pulsations, spikes, etc.). So far, however, no attention has been paid to the isolated fibres that occasionally appear in the metre and decimetre ranges. Here we give and discuss examples of the dynamic spectra of such bursts obtained many years ago (in the metre waveband from 1969) as well in recent years (in the decimetre and microwave wavebands from 2003–2013). Isolated fibres are observed mostly in the decimetre range (although there are examples in both the metre and microwave ranges), and they reveal a number of features of classical fibre bursts. As a generation mechanism for such fibres, the process of interaction of whistlers with Langmuir plasmons was suggested. An analysis of conditions for the realization of this process in solar magnetic arch structures and its efficiency was carried out. Estimates of the intensity of low-frequency turbulence (whistlers) and magnetic field strength in the solar corona were obtained using the data of radio fibres.

On the Issue of the Origin of Type II Solar Radio Bursts

Gennady **Chernov**1 and Valery Fomichev1
2021 ApJ 922 82
https://iopscience.iop.org/article/10.3847/1538-4357/ac1f32/pdf
https://doi.org/10.3847/1538-4357/ac1f32
Type II solar radio bursts are among the most powerful events in the solar radio emission in the meter wavelength range. It is generally accepted that the agents generating type II radio bursts are magnetohydrodynamic shock waves. But the relationship between the shock waves and the other manifestations of the large-scale disturbances in the solar atmosphere (coronal mass ejections, Morton waves, EUW waves) remains unclear. To clarify a problem, it is important to determine the conditions of generation of type II radio bursts. Here, the model of the radio source is based on the generation of radio emission within the front of the collisionless shock wave where the Buneman instability of plasma waves is developed. In the frame of this model, the Alfvén magnetic Mach number must exceed the critical value, and there is a strict restriction on the perpendicularity of the front. The model allows us to obtain the information about the parameters of the shock waves and the parameters of the medium by the parameters of type II bursts. The estimates, obtained in this paper for several events with the band splitting of the fundamental and harmonic emission bands of the

type II bursts, confirm the necessary conditions of the model. In this case the registration of type II radio bursts is an indication of the propagation of shock waves in the solar atmosphere, and the absence of type II radio bursts is not an indication of the absence of shock waves. Such a situation should be taken into account when investigating the relationship between type II radio bursts and other manifestations of solar activity. **2003 November 3**

Recent Results on the Fine Structure in Cosmic Radio Emission **Book**

Zebra Pattern in Solar and Pulsar Radio Emission

G.P. **Chernov**, V. Fomichev, S. Fainshtein

LAP LAMBERT Academic Publishing **2021** **File**

Latest Data on the fine Structure in Solar radio Emission **Book**

G.P. **Chernov**

LAP LAMBERT Academic Publishing **2019** 292 pp.

The study of the fine structure of the solar radio emission is a key to understanding of plasma processes in the solar corona. Over the past 10 years or so, new solar instruments have been built (radio spectrographs and radio heliographs). In addition, radio data began to be studied comprehensively with new data in other wavelength ranges, in X-ray (GOES, RHESSI) and ultraviolet (SDO), which made it possible to obtain information on the position of radio sources. Such a textbook cover wide field of the Solar Radio Physics and it will be suitable for graduate students and researchers.

Alternative zebra-structure models in solar radio emission

G.P. **Chernov**

Chapter IV in book Research advances in astronomy, Ed. N.Mehler, Nova Sience Publishers, New York, **2018**, pp. 119_146

https://arxiv.org/ftp/arxiv/papers/1807/1807.08818.pdf

In the literature, discussion continues about the nature of the zebra structure (ZS) in type IV radio bursts, and understanding even the most extended mechanism associated with double plasma resonance has been improved in series of works. Moreover, in the recent work (Ben\'a\v{c}hek, Karlick\'y, Yasnov, 2017) its ineffectiveness was shown under the usually adopted conditions in the radio source. In this case in a number of works we demonstrated the possibility of modeling with whistlers to explain many thin components of ZS stripes, taking into account the effects of scattering whistlers on fast particles. This situation stimulates the search for new mechanisms. For example, earlier we showed the importance of explosive instability, at least for large flares with the ejections of protons. In the system a weakly relativistic beam of protons, nonisothermic plasma, the slow beam mode of the space charge possesses negative energy, and in the triplet slow and fast beam modes and ion acoustic wave an explosive cascade of harmonics from ionic sound is excited. Electromagnetic waves in the form of ZS stripes appear as a result of the fast protons scattering on these harmonics. Such a mechanism can also be promising for a ZS in radio emission from the pulsar in the Crab nebula.

18 July 2000, May 29, 2003, August 1, 2010

CESRA #1980 **2018** http://cesra.net/?p=1980

A Model of Zebra Patterns in Solar Radio Emission

G. P. **Chernov**, V. V. Fomichev, R. A. Sych

Geomagnetism and Aeronomy, **2017**, Vol. 57, No. 6, pp. 738_751 **2018**

https://arxiv.org/ftp/arxiv/papers/1806/1806.08532.pdf

We analyze complex zebra patterns and fiber bursts during type-IV solar radio bursts on **August 1, 2010**. It was shown that all of the main details of sporadic zebra patterns can be explained within the model of zebra patterns and fiber bursts during the interaction of plasma waves with whistlers. In addition, it was shown that the major variations in the stripes of the zebra patterns are caused by the scattering mechanism of fast particles on whistlers, which leads to the transition of whistler instability from the normal Doppler effect to an anomalous one.

Development of Solar Flares and Features of the Fine Structure of Solar Radio Emission

G.P. **Chernov**, V.V. Fomichev, Y. Yan, B. Tan, Ch. Tan, Q.Fu

Geomagnetism and Aeronomy **2017**

https://arxiv.org/ftp/arxiv/papers/1711/1711.07531.pdf

The reason for the occurrence of different elements of the fine structure of solar radio bursts in the decimeter and centimeter wavelength ranges has been determined based on all available data from terrestrial and satellite observations. In some phenomena, fast pulsations, a zebra structure, fiber bursts, and spikes have been observed almost simultaneously. Two phenomena have been selected to show that the pulsations of radio emission are caused by particles

accelerated in the magnetic reconnection region and that the zebra structure is excited in a source, such as a magnetic trap for fast particles. The complex combination of unusual fiber bursts, zebra structure, and spikes in the phenomenon on **December 1, 2004**, is associated with a single source, a magnetic island formed after a coronal mass ejection. **2013-06-21**

Comparison of alternative zebra-structure models in solar radio emission

G.P. **Chernov**, V.V. Fomichev, R.A. Sych

Oral report at the conference: XII Solar System Plasma Conference, February 6, **2017**, Space Research Institute of RAS, Moscow, Russia **2017**

https://arxiv.org/ftp/arxiv/papers/1704/1704.02528.pdf

Discussion about the nature of zebra-structure (ZS) in the type IV radio bursts continues, despite the ten proposed models. First of all, this is due to the wide variety of stripes in each new phenomenon, when the explanation of all the fine details by any one mechanism becomes impossible. The most widespread explanation is the emission at different levels of double plasma resonance (DPR), sequential on the height surfaces in the magnetic trap, where the upper hybrid frequency (ωUH) becomes equal to the integer of electronic cyclotron harmonics sωBe:ωUH=(ω2Pe+ω2Be)1/2=sωBe (Zheleznyakov, Zlotnik, 1975, Winglee, Dulk, 1986, Kuznetsov & Tsap (2007)). An important alternative mechanism is the interaction of plasma waves with the whistlers: l+w⇒t(Chernov, 1976, 2006). Here, we will show the possibility of explaining the main features of the zebra stripes in the model with whistlers, using the example of the phenomenon on **August 1, 2010**.

See CESRA highlights #1341 May 2017 http://cesra.net/?p=1341

Last news on zebra pattern

Gennady **Chernov**

See a new monograph " **SOLAR FLARES: Investigations and selected Research**" , Chapter 5 P. 101-149 **2016**

http://www.nova-authors.com/ Encrypted/WEB_Links_Storage/e-Books/978-1-53610-221-5_eBook.pdf **File**

http://arxiv.org/ftp/arxiv/papers/1512/1512.06311.pdf

The publications of the last three years concerning to studying of the most intriguing fine structure in type IV solar radio bursts - zebra pattern (ZP), are surveyed. The main attention is paid to new observations, irrespective of whether a paper does include detailed interpretation of an event or simply reports about the beginning of operation of a new tool. The radiation mechanism of the ZP on a double plasma resonance (DPR) remains the most widespread and standard, though ten alternative mechanisms were offered. However, in a number of works difficulties with the explanation of a complex zebra are noted, especially in a combination with fiber bursts and spikes. Therefore, several papers in which the radiation mechanism of a zebra on the DPR is improved, are considered in more detail. Without positional observations we have a great opportunity to follow the dynamics of flare processes using SDO / AIA images in several EUV lines. In the discussion, the debatable questions with the comparison of mechanism on DPR with the model of interaction of plasma waves with whistlers are illuminated. **17 September 2002, 29.05.2003, 22 July 2004, 2004-12-01, 2006 December 13-14, 12-02-2010, 2010-08-01, 2011-02-15, 19 April 2012 , 11 Apr 2013,**

Flare processes evolution and polarization changes of fine structures of solar radio emission in the April 11, 2013 event

Gennady **Chernov**, Robert Sych, Baolin Tan, Yihua Yan, Chengming Tan, Qijun Fu, Marian Karlicky, Valery Fomichev

Research in Astronomy and Astrophysics (RAA), **2015**

http://arxiv.org/pdf/1509.06487v1.pdf

The measurement of positions and sizes of radio sources in the observations of solar radio spectral fine structures in an M6.5 flare on April 11, 2013 were observed simultaneously by several radio instruments at four different observatories: Chinese Solar Broadband Radio Spectrometers at Huairou (SBRS/Huairou), Ondrejov Radio spectrograph in the Czech Republic (ORSC/Ondrejov), Badary Broadband Microwave spectropolarimeter (BMS/Irkutsk), and spectrograph/IZMIRAN (Moscow, Troit 29.05.2003sk). The fine structures include microwave zebra patterns (ZP), fast pulsations, and fibers. They were observed during the flare brightening located at the tops of a loop arcade. The dynamics of the polarization was associated with the motion of the flare exciter, which was observed in EUV images at 171A and 131A (SDO/AIA). Combining magnetograms observed by the SDO Helioseismic and Magnetic Imager (HMI) with the homologous assumption of EUV flare brightening and ZP bursts, we deduced that the observed ZPs correspond to the ordinary radio emission mode. However, future analysis needs to verify the assumption that zebra

radio sources are really related to a closed magnetic loop, and are located at lower heights in the solar atmosphere than the source of pulsations.

Dynamics of flare processes and variety of the fine structure of solar radio emission over a wide frequency range of 30 - 7000 MHz

Gennady **Chernov** , Valery Fomichev, Baolin Tan, Yihua Yan, Chengming Tan, Qijun Fu
Solar Phys., **2015**, Volume 290, Issue 1, pp 95-114
http://arxiv.org/pdf/1409.0660v1.pdf

Radiobursts exibiting fine structure observe d over two years during the rising phase of Cycle 24 by the Chinese Solar Broadband Radio Spectrometer (SBRS/Huairou) in the range 1?7.6 GHz and the spectrograph IZMIRAN in the meter range (25 - 270 MHz) are analyzed. In five events zebra structure, various fiber bursts and fast pulsations were observed. These observations have great importance for testing different theoreti cal models of fine structure formation, as, for example, only for explaining the zebra-structure more than ten mechanisms have been proposed. Events on **15 and 24 February 2011** are of the greatest interest. In the course of the flare on 15 February (which occurred close to the center of disk) zebra structure was observed during three sequential flare brightenings. The polarization changed sign in the third. This behavior of polarization combined with images of the corresponding flare brightenings, obtained in extreme ultraviolet radiation by the Solar Dynamics Observatory (SDO/AIA, 171 ?) provides important clues. The polarization of radio emission in all three cases is related to the ordinary wave mode of radio emission. The zebra structure was present at frequencies 190-220 MHz in the Culgoora spectrum. The event on 24 February 2011 is remarkable , as the zebra structure at frequencies of 2.6- 3.8 GHz was not polarized and it appeared duri ng the magnetic reconnection observed by SDO/AIA 171 ? in this limb flare. In the event on **9 August 2011**, for the first time, a superfine millisecond structure was registered simultaneously in the fast pulsations and the stripes of zebra structure. In the event on **1 August 2010** after the zebra structure two families of fibers bursts with an opposite frequency drift were observed. On **19 April 2012** the fibers against the background of type III bursts were observed by IZMIRAN and Nan?ay spectrographs. In the band of 42 ? 52 MHz a group of nine slowly drifting narrow-band

Fine structural features of radio-frequency radiation of the solar flare of February 12, 2010

Chernov, G. P. ; Fomichev, V. V. ; Gorgutsa, R. V. ; Markeev, A. K. ; Sobolev, D. E. ; Hillaris, A. ; Alissandrakis, K.
Geomagnetism and Aeronomy, Volume 54, Issue 4, pp.406-415, **2014**
DOI: 10.1134/S0016793214040021

Solar radio emission records received at the IZMIRAN spectrograph (25-270 MHz) during the solar flare event of **February 12, 2010** are analyzed. Different fine structures were observed in three large groups of type III bursts against a low continuum. According to data from the Nancay radioheliograph, sources of all three groups of bursts were located in one active region, 11046, and their emissions were accompanied by soft X-ray bursts (GOES satellite): C7.9 at 0721 UT, B9.6 at 0940 UT, and M8.3 at 1125 UT. After the first group of bursts, classical fiber bursts were observed in combination with reverse-drift fiber bursts with unusual arc drift. After the third (the most powerful) group, stable second-length pulsations and slow-drift fiber bursts were observed, the instantaneous frequency bands of which were an order of magnitude larger than the frequency band of classical fiber bursts, and the frequency drift was several times lower. More complex fiber bursts were observed in the weakest group in the time range 0940:39-0942:00 UT. They were narrow-band (~0.5 MHz) fiber bursts, periodically recurring in a narrow frequency band (5-6 MHz) during several seconds. The presence of many chaotically drifting ensembles of fibers, crossing and superimposing on one another, is a feature of this event. It is assumed that occurrence of these structures can be connected with the existence of many small shock fronts behind the leading edge of a coronal mass ejection.

The importance of source positions during radio fine structure observations

Guennadi P. **Chernov**1,2, Yi-Hua Yan1 and Qi-Jun Fu
Research in Astronomy and Astrophysics, Volume 14, Number 7, 831-842, **2014**

The measurement of positions and sizes of radio sources in the observations of the fine structure of solar radio bursts is a determining factor for the selection of the radio emission mechanism. The identical parameters describing the radio sources for zebra structures (ZSs) and fiber bursts confirm there is a common mechanism for both structures. It is very important to measure the size of the source in the corona to determine if it is distributed along the height or if it is point-like. In both models of ZSs (the double plasma resonance (DPR) and the whistler model) the source must be distributed along the height, but by contrast to the stationary source in the DPR model, in the whistler model the source should be moving. Moreover, the direction of the space drift of the radio source must correlate with the frequency drift of stripes in the dynamic spectrum. Some models of ZSs require a local source, for example, the models based on the Bernstein

modes, or on explosive instability. The selection of the radio emission mechanism for fast broadband pulsations with millisecond duration also depends on the parameters of their radio sources.

CONCERNING SPIKES IN EMISSION AND ABSORPTION IN MICROWAVE RANGE
G.P.**Chernov**, R.A.Sych, G.L.Huang, H.S. Ji, Y.H.Yan, and C.M.Tan
E-print, July **2012**, Research in Astron. Astrophys.
In some events weak fast solar bursts (near the quiet Sun level) were observed at the background of numerous spikes in emission and absorption. In such a case the background contains the noise signals of the receiver. In the events **16 September 2005 and 14 April 2002** the solar origin of fast busts was confirmed by simultaneous registration of the bursts in several remote observatories. The background noisy pixels in emission and absorption can be excluded by more high subtracted level of continuum during construction of spectra. The wavelet spectrum, noisy profiles in different polarization channels and the spectrum with greater subtracting zero level of the continuum prove a noisy character of shortest pixels in emission and absorption. Thus, in each case, in order to judge the solar origin of all spikes, it is necessary to determine the level of continuum against the background of which the solar bursts are observed. Several models of microwave spikes are discussed. The ECM emission mechanism runs into serious problems with the interpretation the microwave millisecond spikes: the main obstacles are too high values of the magnetic field strength in the source (w_Pe < w_Be). The probable mechanism is the interaction of plasma Langmuir waves with ion-sound waves (l+s -->t) in a source related with shock fronts in the reconnection region.

COMPLEX RADIO ZEBRA PATTERNS ESCAPING FROM THE SOLAR CORONA AND NEW GENERATION MECHANISMS
G. P. **Chernov**
E-print, June **2012**, NovaPublishers.com
Sources of solar radio bursts in meter/decimeter/microwave ranges are located in the solar corona. The study of the radio fine structure is a key to understanding of plasma processes in the solar corona. The most intriguing fine structure is the zebra pattern (ZP) in continuous type-IV radio bursts (the regular harmonics in emission and absorption). A disputable discussion about nature of the ZP in the type IV radio bursts continues more than 40 years. Only in the last 5 years about 10 works devoted to an improvement of the mechanism based on the double plasma resonance (DPR, when upper hybrid frequency is equal to an integer of the cyclotron frequency) were published, and 5 new models were proposed. The explanation to this is connected with the new observations of the uncommon forms of ZP, which it is difficult to interpret as the regular harmonics within the framework of known models. According to all works, which analyze mechanism based on the DPR, we must observe ZP in all continuous bursts. But observations suggest otherwise: ZP appears in the pulsation regime, and in not all bursts. Nevertheless, it is sometimes asserted that mechanism on DPR explains all basic properties of ZP, and it is indicated on the error of many authors in the calculations of the growth rates of plasma waves at the upper hybrid frequency: it is not possible to enlarge calculations for the regions adjacent with the hybrid band, since the dispersion relation - is correct only inside the hybrid band. However, the calculations, which show the significance of this erroneous approach should be conducted for the loss-cone distribution of fast particles in the relativistic approximation. Moreover, in a whole series of works it is noted that the contribution of the term, connected with the harmonic in the hybrid band, considerably exceeds contribution from those harmonics adjacent from above, especially for the slightly non-perpendicular propagation in the relativistic examination. New observations and incompleteness of many known mechanisms stimulate for the new developments. We show some properties of the ZP which cannot explained in the framework of the DPR model: the frequency drift of ZP stripes which changes synchronously with the space drift of the radio sources, the frequency splitting of the ZP stripes, the superfine structure of the stripes in the form of millisecond spike-bursts etc. It is shown that simultaneous excitation of waves at ~30 DPR-levels in the corona is impossible for any realistic profile of the plasma density and magnetic field. All new properties of ZP are considered in the light of both old and new theoretical models. The main properties of the emission and absorption stripes can be explained in a model involving interactions between electrostatic plasma waves and whistlers, taking into account the quasi-linear diffusion of fast particles with the loss-cone distribution on whistlers. We also propose a new advanced model of the ZP. It is shown that in the system the weakly-relativistic mono-velocity beam of protons - the strongly nonisothermic plasma the slow beam mode can possess negative energy and the explosive instability with interaction of slow and rapid beam modes and ionic sound is developed. As a result of the weak spatial dispersion the generation of ionic sound is accompanied by the cascade process of coalescence, and the stabilization of explosive instability occurs. ZP is formed by scattering of fast protons on the ion-acoustic harmonics. The effectiveness of new mechanism in comparison with the previously discussed hypotheses is explained.

Spectral and spatial observations of microwave spikes and zebra structure in the short radio burst of May 29, 2003
G. P. **Chernov**1,2, R. A. Sych1,3, N. S. Meshalkina1,3, Y. Yan1 and C. Tan

A&A 538, A53 (**2012**)
Context. The unusual radio burst of **May 29, 2003** connected with the M1.5 flare in AR 10368 has been analyzed. It was observed by the Solar Broadband Radio Spectrometer (SBRS/Huairou station, Beijing) in the 5.2–7.6 GHz range. It proved to be only the third case of a neat zebra structure appearing among all observations at such high frequencies. Despite the short duration of the burst (25 s), it provided a wealth of data for studying the superfine structure with millisecond resolution (5 ms).
Aims. We localize the site of emission sources in the flare region, estimate plasma parameters in the generation sites, and suggest applicable mechanisms for interpretating spikes and zebra-structure generation.
Methods. We analyze of flare area structures and spectral parameters of millisecond spikes and their radio sources. We then interpret the superfine structure in the framework of known models.
Results. Positions of radio bursts were obtained by the Siberian Solar Radio Telescope (SSRT) (5.7 GHz) and Nobeyama radioheliograph (NoRH) (17 GHz). The flare configuration includes two systems of loops with the common base near the N-spot. The loop bases coincide with polarized emission sources at 17 GHz. The sources in intensity gravitated to tops of short loops at 17 GHz, and to long loops at 5.7 GHz. Short pulses at 17 GHz (with a temporal resolution of 100 ms) are registered in the R-polarized source over the N-magnetic polarity (extraordinary mode). The positions of the subsecond pulse sources at 5.7 GHz change from pulse to pulse and are level with the tops of some loops over the magnetic field's neutral line. Dynamic spectra show that all the emission comprised millisecond pulses (spikes) of 5–10 ms duration in the instantaneous band of 70 to 100 MHz, forming the superfine structure of different bursts, essentially in the form of fast or slow-drift fibers and various zebra-structure stripes. Five scales of zebra structures have been singled out. The occurrence of the spikes is associated with the formation of two new radio sources with different polarities, which appeared simultaneously on SSRT and NoRH maps. This took place after new magnetic fluxes of opposite polarity had emerged in the leading spot and a new magnetic "delta" configuration had been formed.
Conclusions. As the main mechanism for generating spikes (as the initial emission) we suggest the coalescence of plasma waves with whistlers in the pulse regime of interaction between whistlers and ion-sound waves. In this case one can explain the appearance of fibers and sporadic zebra-structure stripes exhibiting the frequency splitting.

Fine Structure of Solar Radio Bursts **Book**

G. P. **Chernov**
Astrophysics and Space Science Library
DOI 10.1007/978-3-642-20015-1 Springer Heidelberg Dordrecht London New York
2011 File

Spiky Fine Structure of Type III-like Radio Bursts in Absorption

G. P. **Chernov**, Y. H. Yan1, C. M. Tan1, B. Chen1 and Q. J. Fu1
Solar Phys. **Volume 262, Number 1 / March, 2010**, p. 149-170
An uncommon fine structure in the radio spectrum consisting of bursts in absorption was observed with the Chinese Solar Broadband Radiospectrometer (SBRS) in the frequency range of 2.6 – 3.8 GHz during an X3.4/4B flare on **13 December 2006** in active region NOAA 10930 (S05W33). Usual fine structures in emission such as spikes, zebra stripes, and drifting fibers were observed at the peak of every new flare brightening. Within an hour at the decay phase of the event we observed bursts consisting of spikes in absorption, which pulsated periodically in frequency. Their instantaneous frequency bandwidths were found to be in the 75 MHz range. Moreover, in the strongest Type III-like bursts in absorption, the spikes showed stripes of the zebra-pattern (ZP) that drifted to higher frequencies. All spikes had the duration as short as down to the limit of the instrument resolution of ≈8 ms. The TRACE 195 Å images indicate that the magnetic reconnection at this moment occurred in the western edge of the flare loop arcade. Taking into account the presence of the reverse-drifting bursts in emission, in the course of the restoration of the magnetic structures in the corona, the acceleration of the beams of fast particles must have occurred both upward and downward at different heights. The upward beams will be captured by the magnetic trap, where the loss-cone distribution of fast particles (responsible for the emission of continuum and ZP) were formed. An additional injection of fast particles will fill the loss-cone later, breaking the loss-cone distribution. Therefore, the generation of continuum will be quenched at these moments, which was evidenced by the formation of bursts in absorption.

Unusual Zebra Patterns in the Decimeter Wave Band

G.P. **Chernov** · Yihua Yan · Qijun Fu · Chengming Tan · Shujuan Wang
Solar Phys (**2008**) 250: 115–131
http://www.springerlink.com/content/f64763541p052895/fulltext.pdf
An analysis of new observations showing fine structures consisting of narrowband fiber bursts as substructures of large-scale zebra-pattern stripes is carried out.We study

four events using spectral observations taken with a newly built spectrometer located at the Huairou station, China, in the frequency range of 1.1 – 2.0 GHz with extremely high frequency and time resolutions (5 MHz and 1.25 ms).

Solar Radio Bursts with Drifting Stripes in Emission and Absorption
G. P. **Chernov**
Space Science Reviews, Volume 127 Number 1-4, 195-326, **2006**
http://www.springerlink.com/content/2n15325745673706/

Fine Structure of Solar Radio Bursts Observed at Decametric and Hectometric Waves
G. P. **Chernov**, M. L. Kaiser, J.-L. Bougeret, V. V. Fomichev, R. V. Gorgutsa
Solar Phys. , 241 (1), Page: 145 – 169, **2007**.

Violent solar events of October–November 2003 as recorded by IZMIRAN radio observations
I. M. **CHERTOK***, V. V. FOMICHEV, A. A. GNEZDILOV, R. V. GORGUTSA, A. K. MARKEEV and D. E. SOBOLEV
Astronomical and Astrophysical Transaction, Vol. 24, No. 1, February **2005**, 45–52
The extreme solar activity of October–November 2003 was recorded at IZMIRAN with digital radiospectrographs at 25–270MHz and fixed-frequency radiometers at 169, 204 and 3000 MHz. An outstanding metre-wavelength noise storm took place during the fist passage of the grandiose evolving active complex across the disc which testifies to permanent electron acceleration over the complex with energy of up to tens of kiloelectronvolts. Against this background, intense metric and microwave radio bursts were recorded in association with several outstanding flare and huge coronal mass ejection (CME) events. The dynamic spectra of these events display multiband and sometimes fine-structure type II bursts, initiated by coronal shocks, and various continuum emissions. In some cases, a corresponding microwave burst at 3000MHz includes not only an impulsive component coinciding with a flare maximum but also a predominating delayed long-duration component with a smooth time profile. The latter component is thought to be linked with a post-eruptive energy release and particle acceleration when the magnetic field, strongly disturbed by a CME, relaxes to a new quasi-equilibrium configuration via reconnection in high coronal levels.

MULTI-SCALE TEMPORAL FEATURES OF THE 14 JULY 2000 METERWAVELENGTH DYNAMIC RADIO SPECTRUM COMPARED WITH TRACE DATA
I. M. **CHERTOK**1, V. V. FOMICHEV1, A. A. GNEZDILOV1, R. V. GORGUTSA1, V. V. GRECHNEV2, A. K. MARKEEV1, R. W. NIGHTINGALE3 and D. E. SOBOLEV1
Solar Physics **204:** 141–154, **2001**.
The 14 July 2000 (‘Bastille Day’) eruptive and geoeffective flare event was observed by the digital IZMIRAN radio spectrograph in the frequency range of 25–270 MHz. This instrument allowed the analysis of various features of the dynamic radio spectrum and their comparison with other observational data, in particular with development of a spectacular EUV post-eruption arcade recorded aboard the Transition Region and Coronal Explorer (TRACE). (1) A compressed multihour radio spectrum shows that the event caused a conspicuous weakening of the pre-existing noise storm. This phenomenon was perhaps caused by interaction of a large halo coronal mass ejection (CME), recorded by the the Large Angle and Spectroscopic Coronagraph (LASCO) aboard the Solar and Heliospheric Observatory (SOHO), with emitting coronal structures. (2) Several type II bands are present at the initial and maximum phases of the flare event. The frequency drifts of the clearest bands correspond to the estimated shock wave speed of 1100–2300 km s−1 that is comparable with the CME speed observed in the sky plane. (3) Significant broadband enhancements of the metric radio emission took place around of 10:24–10:27 UT coinciding with sharp development of the EUV arcade in the northeast direction. It appears to correspond to the intensification of the electron acceleration in a process of post-eruption loop formation. (4) The high-resolution radio spectrum revealed a superposition of numerous type III-like bursts and/or pulsations with a time scale ranging from a few seconds to several tens of seconds. These features can be attributed particularly to successive formation of new loops of the arcade and corresponding temporal fragmentation of the electron acceleration in the course of the post-eruption reconnection. In summary, the analysis demonstrates

the correspondence between the multi-scale temporal features of the metric radio emission and such phenomena as the CME and post-eruption EUV arcade. Some spectra, images, and movies illustrating the event are presented also on the accompanying CD-ROM.

Sharp Decreases of Solar Metric Radio Storm Emission

Chertok, I. M.; Kahler, S.; Aurass, H.; Gnezdilov, A. A.
Solar Physics, v. 202, Issue 2, p. 337-354 (**2001**).
We discuss a little-known variety of sharp decreases of long-duration meter-wavelength noise storms and type IV bursts. A survey of the IZMIRAN and AIP radio observations shows that a decrease or nearly complete disappearance of the continuum and bursts developing over tens of minutes without a subsequent recovery of the radio flux occasionally occurs. The decrease is usually preceded by a short-duration (several tens of minutes) enhancement of the radio emission. In these events, the onset of the flux decrease drifts from high to low frequencies with a rate of -(0.05-0.35) MHz s^-1, comparable to the drift rates of noise-storm onsets and of chains of type I bursts. White-light coronagraph observations, as well as the characteristics of the accompanying microwave and soft X-ray emissions, provide evidence that such radio decreases appear to be associated with coronal mass ejections (CMEs) and post-CME phenomena. Yohkoh/SXT images show radio flux decrease events which are accompanied by significant rearrangements of coronal structures. We suggest that the radio flux variations are caused by CME interactions with pre-existing coronal arcade structures which are sources of noise storms and energetic electron acceleration. The fact that the noise-storm decreases develop with delays of several tens of minutes relative to the associated microwave burst peak, when the corresponding CME front is located at heights of several R_solar, however, is not explained.

On the relationship between solar flares, coronal mass ejections, and post-eruption energy release

Chertok, I. M.
Radiophysics and Quantum Electronics, Volume 39, Issue 11-12, pp. 940-943, **1996**
We present and illustrate a concept that involves two basic statements: (a) solar pulse flares and coronal mass ejections (CME) are physically similar, but, generally speaking, independent phenomena, which can occur both individually and jointly, initiating each other in different cause and- effect combinations; (b) in the analysis of the relationship between the flares and CMEs one must take into account that the latter result in significant post-eruption flare-like energy release in the corona, which can be accompanied by many important phenomena including the prolonged acceleration of particles.

Sharp attenuation of solar noise radio storms under action of coronal mass ejecta.

Chertok, I. M.; Gnezdilov, A. A.; Aurass, G.
Bull. Russ. Acad. Sci., Phys., Vol. 60, No. 8, p. 1290 – 1297, **1996**
According to data on solar meter radio emission acquired in Troitsk (Russia) and Tremsdorf (Germany), the phenomena with a sharp (during few tens of minutes) attenuation or complete ceasing of noise storms are analyzed as well as type IV bursts. Comparison to direct observations by coronagraphs in white light and characteristics of accompanying microwave and X-ray bursts give grounds to suppose that such large-scale variations of durable meter radio emission are conditioned by significant variations in structure and/or parameters of coronal magnetic traps, as well as in sources of energetic electrons acceleration under action of coronal mass ejecta.

Signatures of Type III Solar Radio Bursts from Nanoflares: Modeling

Sherry **Chhabra**, James A. Klimchuk, Dale E. Gary
ApJ **922** 128 **2021**
https://arxiv.org/pdf/2109.03355.pdf
https://doi.org/10.3847/1538-4357/ac2364
There is a wide consensus that the ubiquitous presence of magnetic reconnection events and the associated impulsive heating (nanoflares) is a strong candidate for solving the solar coronal heating problem. Whether nanoflares accelerate particles to high energies like full-sized flares is unknown. We investigate this question by studying the type III radio bursts that the nanoflares may produce on closed loops. The characteristic frequency-drifts that type III bursts exhibit can be detected using a novel application of the time-lag technique developed by Viall & Klimchuk (2012) even when there are multiple overlapping bursts. We present a simple numerical model that simulates the expected radio emission from nanoflares in an active region (AR), which we use to test and calibrate the technique. We find that in the case of closed loops the frequency spectrum of type III bursts is expected to be extremely steep such that significant emission is

produced at a given frequency only for a rather narrow range of loop lengths. We also find that the signature of bursts in the time-lag signal diminishes as: (1)the variety of participating loops within that range increases; (2)the occurrence rate of bursts increases; (3) the duration of bursts increases; and (4) the brightness of the bursts decreases relative to noise. In addition, our model suggests a possible origin of type I bursts as a natural consequence of type III emission in a closed-loop geometry. **28 Jan 2014**

CESRA # 3203 2022 https://www.astro.gla.ac.uk/users/eduard/cesra/?p=3203

Imaging Spectroscopy of CME-Associated Solar Radio Bursts

Sherry **Chhabra**, Dale E. Gary, Gregg Hallinan, Marin M. Anderso, Bin Chen, Lincoln J. Greenhill, Danny C. Price

2021 *ApJ* **906** 132

https://arxiv.org/pdf/2011.06073.pdf

https://doi.org/10.3847/1538-4357/abc94b

We present first results of a solar radio event observed with the Owens Valley Radio Observatory Long Wavelength Array (OVRO-LWA) at metric wavelengths. We examine a complex event consisting of multiple radio sources/bursts associated with a fast coronal mass ejection (CME) and an M2.1 GOES soft X-ray flare from **2015 September 20**. Images of 9--s cadence are used to analyze the event over a 120-minute period, and solar emission is observed out to a distance of ≈3.5R⊙, with an instantaneous bandwidth covering 22~MHz within the frequency range of 40--70~MHz. We present our results from the investigation of the radio event, focusing particularly on one burst source that exhibits outward motion, which we classify as a moving type IV burst. We image the event at multiple frequencies and use the source centroids to obtain the velocity for the outward motion. Spatial and temporal comparison with observations of the CME in white light from the LASCO(C2) coronagraph, indicates an association of the outward motion with the core of the CME. By performing graduated-cylindrical-shell (GCS) reconstruction of the CME, we constrain the density in the volume. The electron plasma frequency obtained from the density estimates do not allow us to completely dismiss plasma emission as the underlying mechanism. However, based on source height and smoothness of the emission in frequency and time, we argue that gyrosynchrotron is the more plausible mechanism. We use gyrosynchrotron spectral fitting techniques to estimate the evolving physical conditions during the outward motion of this burst source.

Observation of the Solar Corona Using Radio Scintillation with the Akatsuki Spacecraft: Difference Between Fast and Slow Wind

Shota **Chiba**, Takeshi Imamura, Munetoshi Tokumaru, Daikou Shiota, Takuma Matsumoto, Hiroki Ando, Hiroshi Takeuchi, Yasuhiro Murata, Atsushi Yamazaki, Bernd Häusler & Martin Pätzold

Solar Physics volume 297, Article number: 34 (**2022**)

https://link.springer.com/content/pdf/10.1007/s11207-022-01968-9.pdf

The properties of the coronal plasma at heliocentric distances of 1.5 – 8.9 R⊙ (solar radii) were studied with radio-occultation observations using JAXA's Akatsuki spacecraft in 2016. Physical parameters that characterize the solar wind were retrieved from the intensity-scintillation time series by fitting a theoretical spectrum to the observed power spectra. The derived solar-wind velocity clearly shows a difference between the fast wind and the slow wind, which was identified based on IPS observations. The inner scale, at which fluid motions dissipate and kinetic energy is converted to heat, increases with the heliocentric distance, and the fast wind has larger inner scales than the slow wind. By applying wavelet analysis to the frequency time series, we detected quasi-periodic fluctuations in the electron density. The density oscillations are considered to be manifestations of acoustic waves, which were generated from Alfvén waves originating from the photosphere, and the energy fluxes of those acoustic waves were estimated. The relative density-amplitude peaks around 4 – 6 R⊙ and the wave-energy flux decreases beyond ≈ 6 R⊙, implying that the acoustic waves dissipate to heat the corona. The phase-scintillation spectrum that we obtained cannot be expressed by a single power law. A break is seen around the frequency of 0.5 – 2 Hz beyond ≈ 6 R⊙, suggesting an excess power other than turbulence at lower frequencies. The enhancement of the relative density amplitude around 6 R⊙ found by the wavelet analysis might explain this excess power. The acoustic wave-energy flux in the fast solar wind tends to exceed that in the slow wind, suggesting that the fast wind is powered by a larger injection of Alfvén-wave energy than the slow wind.

Correction: ***Solar Physics*** volume 298**, Article number: 38 (2023)**

IRIS and ALMA Observations Uncovering a Type-II Spicule and the Dynamic Nature of a Chromospheric Plage Region

Georgios **Chintzoglou**, Bart De Pontieu, Juan Martínez-Sykora, Viggo Hansteen, Jaime de la Cruz Rodríguez, Mikolaj Szydlarski, Shahin Jafarzadeh, Sven Wedemeyer, Timothy S. Bastian, Alberto Saínz Dalda
ApJ **2020**
https://arxiv.org/pdf/2005.12717.pdf
We present observations of the solar chromosphere obtained simultaneously with the Atacama Large Millimeter/submillimeter Array (\emph{ALMA}) and the Interface Region Imaging Spectrograph (\emph{IRIS}). The observatories targeted a chromospheric plage region of which the spatial distribution (split between strongly and weakly magnetized regions) allowed the study of linear-like structures in isolation, free of contamination from background emission. Using these observations in conjunction with a radiative magnetohydrodynamic 2.5D model covering the upper convection zone all the way to the corona that considers non-equilibrium ionization effects, we report the detection of an on-disk chromospheric spicule with \emph{ALMA} and confirm its multithermal nature. In addition, we discuss the strikingly high degree of similarity between chromospheric plage features observed in \emph{ALMA}/Band6 and \emph{IRIS}/\ion{Si}{4} (also reproduced in our model) suggesting that \emph{ALMA}/Band6 does not observe in the low chromosphere as previously thought but rather observes the upper chromospheric parts of structures such as spicules and other bright structures above plage at geometric heights near transition region temperatures. We also show that \emph{IRIS}/\ion{Mg}{2} is not as well correlated with \emph{ALMA}/Band6 as was previously thought. For these comparisons, we propose and employ a novel empirical method for the determination of plage regions, which seems to better isolate plage from its surrounding regions as compared to other methods commonly used. We caution that isolating plage from its immediate surroundings must be done with care to mitigate stastistical bias in quantitative comparisons between different chromospheric observables. Lastly, we report indications for chromospheric heating due to traveling shocks supported by the \emph{ALMA}/Band6 observations. **22-Apr-2017**

A HIGH-FREQUENCY TYPE II SOLAR RADIO BURST ASSOCIATED WITH THE 2011 FEBRUARY 13 CORONAL MASS EJECTION

K.-S. **Cho**1,2,3, N. Gopalswamy2, R.-Y. Kwon2,3, R.-S. Kim1,2,3, and S. Yashiro
2013 ApJ 765 148
https://iopscience.iop.org/article/10.1088/0004-637X/765/2/148/pdf
We examine the relationship between the high-frequency (425 MHz) type II radio burst and the associated white-light coronal mass ejection (CME) that occurred on **2011 February 13**. The radio burst had a drift rate of 2.5 MHz s–1, indicating a relatively high shock speed. From SDO/AIA observations we find that a loop-like erupting front sweeps across high-density coronal loops near the start time of the burst (17:34:17 UT). The deduced distance of shock formation (0.06 Rs) from the flare center and speed of the shock (1100 km s–1) using the measured density from SDO/AIA observations are comparable to the height (0.05 Rs, from the solar surface) and speed (700 km s–1) of the CME leading edge observed by STEREO/EUVI. We conclude that the type II burst originates even in the low corona (<59 Mm or 0.08 Rs, above the solar surface) due to the fast CME shock passing through high-density loops.

Relationship between multiple type II solar radio bursts and CME observed by STEREO/SECCHI A16

K.-S. **Cho**, S.-C. Bong, Y.-J. Moon, A. Shanmugaraju, R.-Y. Kwon and Y. D. Park
A&A 530, A16 (**2011**); **File**
Aims. Two or more type II bursts are occasionally observed in close time sequence during solar eruptions, which are known as multiple type II bursts. The origin of the successive burst has been interpreted in terms of coronal mass ejections (CMEs) and/or flares. Detailed investigations of the relationship between CMEs and the bursts enable us to understand the nature of the multiple type II bursts. In this study, we examine multiple type II bursts and compare their kinematics with those of a CME occurring near the time of the bursts.
Methods. To do this, we selected multiple type II bursts observed by the Culgoora radiospectrographs and a limb CME detected in the low corona field of view (1.4−4 Rs) of a STEREO/SECCHI instrument **on December 31, 2007**. To determine the 3D kinematics of the CME, we applied the stereoscopic technique to the STEREO/SECCHI data.
Results. Our main results are as follows: (1) the multiple type II bursts occurred successively at ten minute intervals and displayed various emission structures and frequency drifting rates; (2) near the time of the bursts, the CME was observed by STEREO and SOHO simultaneously, but no evidence of other CMEs was detected; (3) inspection of the 3D kinematics of the CME using the stereoscopic observation by STEREO/SECCHI revealed that the CME propagated along the eastward radial direction as viewed from the Earth; (4) very close time and height associations were found between the CME nose and the first type II burst, and between CME-streamer interaction and the second type II burst.

Conclusions. On the basis of these results, we suggest that a single shock in the leading edge of the CME could be the source of the multiple type II bursts and support the notion that the CME nose and the CME-streamer interaction are the two main mechanisms able to generate the bursts.

Low coronal observations of metric type II associated CMEs by MLSO coronameters:

K.-S. **Cho**, S.-C. Bong, Y.-H. Kim, Y.-J. Moon, M. Dryer, A. Shanmugaraju, J. Lee and Y. D. Park
A&A 491 (**2008**) 873-882, **File**
http://www.aanda.org/10.1051/0004-6361:20079013

Aims. We have investigated the relationship between coronal mass ejections (CMEs) and coronal type II radio bursts by using type II associated CMEs whose low coronal observations by MLSO MK coronameters (1.08-2.85 solar radii for MK4) were available.
Methods. For this we considered all type II burst data at 17:00 UT to 22:00 UT from 1996 to 2003, and then compared them with CME images that were obtained during the same MLSO (Mauna Loa Solar Observatory) observing periods. As a result, we selected 19 type II associated CMEs whose kinematics are well identified. A relationship between CMEs and type IIs has been examined in terms of spatial and temporal closeness without any extrapolation of CME kinematics as well as in terms of CME-streamer interaction.
Results. We found that: (1) except one event, all the metric type II events occur simultaneously or after the CME appearance in MK field of view within 30 min, mostly within 10 min after; (2) the distribution of height difference between the CME front and type II formation shows that there are double peaks, one at the CME fronts and the other at about 1 solar radius behind the front; (3) about half of the events (9/19) are identified to have CME-streamer interaction (seven streamer deflection and two overlapping), and the interaction heights are very similar to those of type II formation as well as their interaction times are nearly coincident with those of type II starting; (4) for the other events (10/19), the CME front heights at the starting time of type IIs are comparable to the heights of type II formation.
Conclusions. Our low coronal observations of type II associated CMEs suggest that CME front and/or CME-streamer interaction at CME flank are two main mechanisms to generate type II bursts.

A Study of CME and Type II Shock Kinematics Based on Coronal Density Measurement

K.-S. **Cho**, J. Lee, Y.-J. Moon, M. Dryer, S.-C. Bong, Y.-H. Kim and Y.D. Park
A&A 461 (**2007**) 1121-1125, **File**

We therefore conclude that the type II burst was generated at the interface of the CME flank and the streamer, as favorable for the shock formation.

Link: http://solar.njit.edu/preprints/lee1316.pdf

Aims.The aim of this paper is to determine location and speed of a coronal shock from a type II burst spectrum without relying on any coronal density model, and to use the result to discuss the relationship between the type II burst and Coronal Mass Ejection (CME).
Methods. This study is made for the 2004 August 18 solar eruption observed by Green Bank Solar Radio Burst Spectrometer (GBSRBS) and a limb CME/streamer simultaneously detected by Mauna Loa Solar Observatory (MLSO) MK4 coronameter. We determine the background density distribution over the area of interest by inverting the MLSO MK4 polarization map taken just before the CME onset. Using the twodimensional
density distribution and the type II emission frequencies, we calculate the type II shock heights along several radial directions selected to encompass the entire position angles of the CME. We then compare these emission heights with those of the CME to determine at which position angle the type II burst propagated. Along the most plausible position angle, we finally determine the height and speed of the shock as functions of time.
Results. It turns out that the type II emission height calculated along a southern streamer best agrees to the observed height of the CME flank. Along this region, both the shock and CME moved at a speed ranging from 800 to 600 km s_1. We also found that the streamer boundary already had enhanced density compared to other parts before the CME and formed an appropriately-low Alfv´enic region.
Conclusions.We therefore conclude that the type II burst was generated at the interface of the CME flank and the streamer, as was favorable for the shock formation.

MAGNETIC FIELD STRENGTH IN THE SOLAR CORONA FROM TYPE II BAND SPLITTING

K.-S. **Cho**,[1,2] J. Lee,[2] D. E. Gary,[2] Y.-J. Moon,[1] and Y. D. Park[1]
E-print, June **2007, File,** Astrophysical Journal, 665:

The phenomenon of band splitting in type II bursts can be a unique diagnostic for the magnetic field in the corona, which is, however, inevitably sensitive to the ambient density. We apply this diagnostic to the CME-flare event on 2004 August 18, for which we are able to locate the propagation of the type II burst and determine the ambient coronal electron density by other means.

Examination of type II origin with SOHO/LASCO observations.
Cho, K.S., Moon, Y.J., Dryer, M., Shanmugaraju, A., *et al.*:
2005, *J. Geophys. Res. (Space Phys.)* **110**, A12101. doi:10.1029/2004JA010744.

Period persistence of long period oscillations in sunspots
N. **Chorley**1, C. Foullon1, B. Hnat1, V. M. Nakariakov1,2 and K. Shibasaki3
A&A 529, A123 (**2011**)
Long period oscillations in the microwave radiation intensity generated over the sunspot of NOAA AR 10330 are studied with the Nobeyama Radioheliograph as the sunspot passes over the solar disk, over the course of 9 days (06−15 April 2003). Periodogram, Fourier and global wavelet analyses reveal the presence of a significant oscillatory component in the range P ≈ 50−120 min over the course of the observations. The spectral amplitudes of five significant Fourier components in the range P = 50−150 min are also seen to be stable over the observations, when the data are not affected by changes in magnetic configuration in the region. The ground-based nature of the instrument naturally introduces long data gaps in such long duration observations and the presence of the gaps does not allow any conclusion as to the stability of the phases of the oscillations. As a model to explain the persistence of the dominant long periods, a simple oscillator with a nonlinear driving term is proposed. The spectral difference between distinct peaks within, e.g. the 3 min spectral band, is expected to be able to resonate with the long period one hour oscillations.

First determination of the angular dependence of rise and decay times of solar radio bursts using multi-spacecraft observations
Nicolina **Chrysaphi**, Milan Maksimovic, Eduard P. Kontar, Antonio Vecchio, Xingyao Chen, Aikaterini Pesini
A&A 687, L12 **2024**
https://arxiv.org/pdf/2404.01497.pdf
https://www.aanda.org/articles/aa/pdf/2024/07/aa48175-23.pdf
Radio photons interact with anisotropic density fluctuations in the heliosphere, which can alter their trajectory and influence properties deduced from observations. This is particularly evident in solar radio observations, where anisotropic scattering leads to highly-directional radio emissions. Consequently, observers at varying locations will measure different properties, including different source sizes, source positions, and intensities. However, it is not known if measurements of the decay time of solar radio bursts are also affected by the observer's position. Decay times are dominated by scattering effects, and so are frequently used as proxies of the level of density fluctuations in the heliosphere, making the identification of any location-related dependence crucial. We combine multi-vantage observations of interplanetary Type III bursts from four non-collinear, angularly-separated spacecraft with simulations, to investigate the dependence of both the decay- and rise-time measurements on the separation of the observer from the source. We propose a function to characterise the entire time profile of radio signals, allowing for the simultaneous estimation of the peak flux, decay time, and rise time, while demonstrating that the rise phase of radio bursts has a non-constant, non-exponential growth rate. We determine that the decay and rise times are independent of the observer's position, identifying them as the only properties to remain unaffected, thus not requiring corrections for the observer's location. Moreover, we examine the ratio between the rise and decay times, finding that it does not depend on the frequency. Therefore, we provide the first evidence that the rise phase is also significantly impacted by scattering effects, adding to our understanding of the plasma emission process. **18-Nov-2020, 16-Jul-2021, 22-Aug-2021**
CESRA naggets #3852 Aug **2024** **https://www.astro.gla.ac.uk/users/eduard/cesra/?p=3852**

Fine structures of solar radio bursts: origins and radio-wave propagation effects
Nicolina **Chrysaphi**
PhD **Thesis**, University of Glasgow, **2021**.
https://arxiv.org/pdf/2103.13745.pdf
Solar eruptive events are associated with radio emissions that appear as impulsive increases in intensity, known as solar radio bursts. Turbulence in the solar corona impacts the propagation of radio waves, obscuring the intrinsic emission properties. Here, anisotropic scattering on small-scale density fluctuations is investigated using novel 3D radio-wave

propagation simulations. Several observed radio properties are simultaneously reproduced for the first time, verifying the necessity to consider anisotropic scattering. The sub-second evolution of fine radio burst properties at a single frequency is also investigated, enabled by conducting observations that utilise the unprecedented imaging capabilities of the LOw-Frequency ARray (LOFAR). The fundamental and harmonic sources of a Type IIIb burst are quantitatively compared, demonstrating that harmonic emissions arise from an intrinsic source with a finite size and finite emission duration. Drift-pair burst observations are successfully described by the radio echo hypothesis. It is shown that the radio echo, which produces the second Drift-pair component, is detected only when the anisotropy is strong. A dependence of the observed properties on the source's intrinsic location and on the assumed emission-to-plasma frequency ratio is inferred. Moreover, the subbands of a split-band Type II burst are simultaneously imaged for the first time. Despite the large separations observed between subband sources, it is shown that once scattering is quantitatively accounted for, the sources become co-spatial. Corrections on the observed source locations also allude to lower coronal densities. Additionally, the first observation of a Type II burst that transitions between a stationary and drifting state—termed as a transitioning Type II burst—is reported. The radio emissions are related to a jet eruption that drives a streamer-puff CME. Overall, state-of-the-art simulations and radio observations are combined and compared. The importance of accounting for radio-wave propagation effects—primarily anisotropic scattering—and the consequence of neglecting to do so on any subsequent interpretations is illustrated. **24 Aug 2004, 16 April 2015, 25 Jun 2015, 12 July 2017, 15 July 2017**

1.3.1 LOFAR: the LOw-Frequency ARray

First Observation of a Type II Solar Radio Burst Transitioning Between a Stationary and Drifting State

Nicolina **Chrysaphi**, Hamish A. S. Reid, Eduard P. Kontar
ApJ **893** 115 **2020**
https://arxiv.org/pdf/2003.11101.pdf
https://iopscience.iop.org/article/10.3847/1538-4357/ab80c1/pdf
Standing shocks are believed to be responsible for stationary Type II solar radio bursts, whereas drifting Type II bursts are excited by moving shocks often related to coronal mass ejections (CMEs). Observations of either stationary or drifting Type II bursts are common, but a transition between the two states has not yet been reported. Here, we present a Type II burst which shows a clear, continuous transition from a stationary to a drifting state, the first observation of its kind. Moreover, band splitting is observed in the stationary parts of the burst, as well as intriguing negative and positive frequency-drift fine structures within the stationary emissions. The relation of the radio emissions to an observed jet and a narrow CME were investigated across multiple wavelengths, and the mechanisms leading to the transitioning Type II burst were determined. We find that a jet eruption generates a **streamer-puff CME** and that the interplay between the CME-driven shock and the streamer is likely to be responsible for the observed radio emissions. **LOFAR spike 2017 July 15**
CESRA #2579 May **2020** http://www.astro.gla.ac.uk/users/eduard/cesra/?p=2579

CME-driven shock and Type II solar radio burst band-splitting

Nicolina **Chrysaphi**, Eduard P. Kontar, Gordon D. Holman, Manuela Temmer
ApJ **868** 79 **2018**
https://arxiv.org/pdf/1810.08026.pdf
sci-hub.tw/10.3847/1538-4357/aae9e5
https://iopscience.iop.org/article/10.3847/1538-4357/aae9e5/pdf
Coronal Mass Ejections (CMEs) are believed to be effective in producing shocks in the solar corona and the interplanetary space. One of the important signatures of shocks and shock acceleration are Type II solar radio bursts that drift with the shock speed and produce bands of plasma fundamental and higher harmonic radio emission. An intriguing aspect of Type II radio bursts is the occasional split of a harmonic band into thinner lanes, known as band-splitting. Here, we report a detailed imaging and spectroscopic observation of a CME-driven shock producing band-splitting in a Type II burst. Using the Low Frequency Array (LOFAR), we examine the spatial and temporal relation of the Type II burst to the associated CME event, use source imaging to calculate the apparent coronal density, and demonstrate how source imaging can be used to estimate projection effects. We consider two widely accepted band-splitting models that make opposing predictions regarding the locations of the true emission sources with respect to the shock front. Our observations suggest that the locations of the upper and lower sub-band sources are spatially separated by $\sim 0.2 \pm 0.05 R_\odot$. However, we quantitatively show, for the first time, that such separation is consistent with radio-wave scattering of plasma radio emission from a single region, implying that the split-band Type II sources could originate from nearly co-spatial locations. Considering the effects of scattering, the observations provide supporting

evidence for the model that interprets the band-splitting as emission originating in the upstream and downstream regions of the shock front, two virtually co-spatial areas. **2015 June 25**

CESRA nugget #2109 Jan **2019** http://www.astro.gla.ac.uk/users/eduard/cesra/?p=2109

Rejuvenating Solar Flare Termination Shocks as Particle Accelerators

Bin **CHEN**

RHESSI Science Nuggets #378 **2020**

http://sprg.ssl.berkeley.edu/~tohban/wiki/index.php/Rejuvenating_Solar_Flare_Termination_Shocks_as_Particle_Accelerators

Properties and magnetic origins of solar S-bursts

Brendan P. **Clarke**, Diana E. Morosan, Peter T. Gallagher, Vladimir V. Dorovskyy, Alexander A. Konovalenko, Eoin P. Carley

A&A 622, A204 **2019**

https://arxiv.org/pdf/1901.07424.pdf

sci-hub.se/10.1051/0004-6361/201833939

Context. Solar activity is often accompanied by solar radio emission, consisting of numerous types of solar radio bursts. At low frequencies (<100 MHz) radio bursts with short durations of milliseconds, such as solar S-bursts, have been identified. To date, their origin and many of their characteristics remain unclear.

Aims. We report observations from the Ukrainian T-shaped Radio telescope, (UTR-2), and the LOw Frequency ARray (LOFAR) which give us new insight into their nature.

Methods. Over 3000 S-bursts were observed on **9 July 2013** at frequencies of 17.4-83.1 MHz during a period of low solar activity. Leading models of S-burst generation were tested by analysing the spectral properties of S-bursts and estimating coronal magnetic field strengths.

Results. S-bursts were found to have short durations of 0.5-0.9 s. Multiple instruments were used to measure the dependence of drift rate on frequency which is represented by a power law with an index of 1.57. For the first time, we show a linear relation between instantaneous bandwidth and frequency over a wide frequency band. The flux calibration and high sensitivity of UTR-2 enabled measurements of their fluxes, which yielded 11+3 SFU. The source particle velocities of S-bursts were found to be ~0.07 c. S-burst source heights were found to range from 1.3 R_Sun to 2 R_Sun. Furthermore, a contemporary theoretical model of S-burst generation was used to conduct remote sensing of the coronal magnetic field at these heights which yielded values of 0.9-5.8 G. Within error, these values are comparable to those predicted by various relations between magnetic field strength and height in the corona.

CESRA #2177 Apr **2019** http://www.astro.gla.ac.uk/users/eduard/cesra/?p=2177

Magnetic Field Geometry and Anisotropic Scattering Effects on Solar Radio Burst Observations

Daniel L. **Clarkson**, Eduard P. Kontar

2025 *ApJ* **978** 73

https://arxiv.org/pdf/2411.19630

https://iopscience.iop.org/article/10.3847/1538-4357/ad969c/pdf

The fine structures of solar radio bursts reveal complex dynamics in the corona, yet the observed characteristics of these sub-second bursts are additionally complicated by radio wave scattering in the turbulent solar corona. We examine the impact of anisotropic turbulence in radio-wave propagation simulations with non-radial magnetic field structures in shaping the morphology, time-characteristics, and source position of fine structures. The apparent sources are found to move along the direction of the magnetic-field lines and not along the density gradient, whereas the major axis of the scattered source is perpendicular to the local magnetic field (the scattering anisotropy axis). Using a dipolar magnetic field structure of an active region, we reproduce observed radio fine structure source motion parallel to the solar limb associated with a coronal loop and provide a natural explanation for puzzling observations of solar radio burst position motions with LOFAR. Furthermore, the anisotropy aligned with a dipolar magnetic field causes the apparent source images to bifurcate into two distinct components, with characteristic sizes smaller than in unmagnetized media. The temporal broadening induced by scattering reduces the observed frequency drift rate of fine structures, depending on the contribution of scattering to the time profile. The findings underscore the role of magnetic field geometry and anisotropic scattering for the interpretation of solar radio bursts and highlight that anisotropic scattering produces more than a single source.

Solar Radio Spikes and Type IIIb Striae Manifestations of Sub-second Electron Acceleration Triggered by a Coronal Mass Ejection

Daniel L. **Clarkson**, Eduard P. Kontar, Nicole Vilmer, Mykola Gordovskyy, Xingyao Chen, Nicolina Chrysaphi

ApJ **946** 33 **2023**

https://arxiv.org/pdf/2302.11265.pdf

https://iopscience.iop.org/article/10.3847/1538-4357/acbd3f/pdf

Understanding electron acceleration associated with magnetic energy release at sub-second scales presents a major challenges in solar physics. Solar radio spikes observed as sub-second, narrow bandwidth bursts with $\Delta f/f \sim 10^{-3}-10^{-2}$ are indicative of sub-second evolution of the electron distribution. We present a statistical analysis of frequency, and time-resolved imaging of individual spikes and Type IIIb striae associated with a coronal mass ejection (CME). LOFAR imaging reveals that co-temporal (<2 s) spike and striae intensity contours almost completely overlap. On average, both burst types have similar source size with fast expansion at millisecond scales. The radio source centroid velocities are often superluminal, and independent of frequency over 30-45 MHz. The CME perturbs the field geometry, leading to increased spike emission likely due to frequent magnetic reconnection. As the field restores towards the prior configuration, the observed sky-plane emission locations drift to increased heights over tens of minutes. Combined with previous observations above 1 GHz, average decay time and source size estimates follow $\sim 1/f$ dependency over three decades in frequency, similar to radio-wave scattering predictions. Both time and spatial characteristics of the bursts between 30-70 MHz are consistent with radio-wave scattering with strong anisotropy of the density fluctuation spectrum. Consequently, the site of radio-wave emission does not correspond to the observed burst locations and implies acceleration and emission near the CME flank. The bandwidths suggest intrinsic emission source sizes <1 arcsec at 30 MHz, and magnetic field strengths a factor of two larger than average in events that produce decameter spikes. **2017-July-15**

CESRA #3521 **2023** https://www.astro.gla.ac.uk/users/eduard/cesra/?p=3521

First Frequency-Time-Resolved Imaging Spectroscopy Observations of Solar Radio Spikes

Daniel L. **Clarkson**, Eduard P. Kontar, Mykola Gordovskyy, Nicolina Chrysaphi, Nicole Vilmer

ApJLett **917** L32 **2021**

https://arxiv.org/pdf/2108.06191.pdf

https://iopscience.iop.org/article/10.3847/2041-8213/ac1a7d/pdf

https://doi.org/10.3847/2041-8213/ac1a7d

Solar radio spikes are short duration and narrow bandwidth fine structures in dynamic spectra observed from GHz to tens of MHz range. Their very short duration and narrow frequency bandwidth are indicative of sub-second small-scale energy release in the solar corona, yet their origin is not understood. Using the LOw Frequency ARray (LOFAR), we present spatially, frequency and time resolved observations of individual radio spikes associated with a coronal mass ejection (CME). Individual radio spike imaging demonstrates that the observed area is increasing in time and the centroid positions of the individual spikes move superluminally parallel to the solar limb. Comparison of spike characteristics with that of individual Type IIIb striae observed in the same event show similarities in duration, bandwidth, drift rate, polarization and observed area, as well the spike and striae motion in the image plane suggesting fundamental plasma emission with the spike emission region on the order of ~ 108 cm, with brightness temperature as high as 10^{13} K. The observed spatial, spectral, and temporal properties of the individual spike bursts are also suggesting the radiation responsible for spikes escapes through anisotropic density turbulence in closed loop structures with scattering preferentially along the guiding magnetic field oriented parallel to the limb in the scattering region. The dominance of scattering on the observed time profile suggests the energy release time is likely to be shorter than what is often assumed. The observations also imply that the density turbulence anisotropy along closed magnetic field lines is higher than along open field lines. **15 Jul 2017**

CESRA # 3080 **2021** https://www.astro.gla.ac.uk/users/eduard/cesra/?p=3080

On the association between type II radio bursts and CMEs

H. T. **Classen** and H. Aurass

A&A 384, 1098{1106 (**2002**); **File**

Ground-based observations of metric (coronal) type II radio bursts are compared with observations of coronal mass ejections (CMEs) obtained by the LASCO coronagraph aboard SOHO and with decametric (interplanetary) type II bursts recorded by the WAVES instrument aboard Wind. The basic data sample comprises 63 metric type II radio bursts observed during di_erent phases of the solar cycle, i.e., 20 events in 1997 and 43 events in 1999/2000. Our analysis is based on temporal coincidence and velocity data derived from heighttime

plots of CMEs and frequency drift rates of type II radio bursts, respectively. The results suggest that there are three scenarios leading to metric type II burst excitation: The radio emission is generated either at flarerelated blast wave shocks (class 1), at shocks driven by the leading edge of the CME (class 2), or at shocks driven by internal parts or the flanks of the CME (class 3). This classi_cation is supported by an analysis of the association with H_ flare sites. The _rst class of events comprises 19 events (30%), the second 19 events (30%), and the third 18 events (29%). 7 events (11%) were not classi_ed. Furthermore, we notice a possible solar cycle dependence of the relative occurrence of the di_erent scenarios.

Is the F10.7cm – Sunspot Number relation linear and stable?

Frédéric **Clette***

J. Space Weather Space Clim. **2021**, 11, 2

https://doi.org/10.1051/swsc/2020071

Is the F10.7cm – Sunspot Number relation linear and stable? (swsc-journal.org)

The F10.7cm radio flux and the Sunspot Number are the most widely used long-term indices of solar activity. They are strongly correlated, which led to the publication of many proxy relations allowing to convert one index onto the other. However, those existing proxies show significant disagreements, in particular at low solar activity. Moreover, a temporal drift was recently found in the relative scale of those two solar indices. Our aim is to bring a global clarification of those many issues. We compute new polynomial regressions up to degree 4, in order to obtain a more accurate proxy over the whole range of solar activity. We also study the role of temporal averaging on the regression, and we investigate the issue of the all-quiet F10.7 background flux. Finally, we check for any change in the F10.7–Sunspot Number relation over the entire period 1947–2015. We find that, with a 4th-degree polynomial, we obtain a more accurate proxy relation than all previous published ones, and we derive a formula giving standard errors. The relation is different for daily, monthly and yearly mean values, and it proves to be fully linear for raw non-averaged daily data. By a simple two-component model for daily values, we show how temporal averaging leads to non-linear proxy relations. We also show that the quiet-Sun F10.7 background is not absolute and actually depends on the duration of the spotless periods. Finally, we find that the F10.7cm time series is inhomogeneous, with an abrupt 10.5% upward jump occurring between 1980 and 1981, and splitting the series in two stable intervals. Our new proxy relations bring a strong improvement and show the importance of temporal scale for choosing the appropriate proxy and the F10.7 quiet-Sun background level. From historical evidence, we conclude that the 1981 jump is most likely due to a unique change in the F10.7 scientific team and the data processing, and that the newly re-calibrated sunspot number (version 2) will probably provide the only possible reference to correct this inhomogeneity.

Extreme solar events **Review**

Edward W. **Cliver**, Carolus J. Schrijver, Kazunari Shibata & Ilya G. Usoskin

Living Reviews in Solar Physics volume 19, Article number: 2 (**2022**)

https://link.springer.com/content/pdf/10.1007/s41116-022-00033-8.pdf

We trace the evolution of research on extreme solar and solar-terrestrial events from the 1859 Carrington event to the rapid development of the last twenty years. Our focus is on the largest observed/inferred/theoretical cases of sunspot groups, flares on the Sun and Sun-like stars, coronal mass ejections, solar proton events, and geomagnetic storms. The reviewed studies are based on modern observations, historical or long-term data including the auroral and cosmogenic radionuclide record, and Kepler observations of Sun-like stars. We compile a table of 100- and 1000-year events based on occurrence frequency distributions for the space weather phenomena listed above. Questions considered include the Sun-like nature of superflare stars and the existence of impactful but unpredictable solar "black swans" and extreme "dragon king" solar phenomena that can involve different physics from that operating in events which are merely large.

774 AD, 17 Sep 1770, 1 September 1859, 4 Feb 1872, 14-15 May 1921, 28 Feb 1942, 5 April 1947, 23 May 1967, 2–11 August 1972 , 29 Apr 1973, 21 Apr 2002, 28 October 2003; 6, 13, 14 Dec 2006, 9 Nov 2011, 28 Oct 2013, 4 Nov 2015

Table 5 Historical fast transit ICME events

Minimal Magnetic States of the Sun and the Solar Wind: Implications for the Origin of the Slow Solar Wind **Review**

E. W. **Cliver** , R. von Steiger

Space Science Reviews **2016**

During the last decade it has been proposed that both the Sun and the solar wind have minimum magnetic states, lowest order levels of magnetism that underlie the 11-yr cycle as well as longer-term variability. Here we review the literature on basal magnetic states at the Sun and in the heliosphere and draw a connection between the two based on the recent

deep 2008–2009 minimum between cycles 23 and 24. In particular, we consider the implications of the low solar activity during the recent minimum for the origin of the slow solar wind.

THE SOLAR DECIMETRIC SPIKE BURST OF 2006 DECEMBER 6: POSSIBLE EVIDENCE FOR FIELD-ALIGNED POTENTIAL DROPS IN POST-ERUPTION LOOPS

E. W. **Cliver**1,2, S. M. White1,3 and K. S. Balasubramaniam

2011 ApJ 743 145, **File**

A 1.4 GHz solar radio burst associated with a 3B/X6 eruptive flare on **2006 December 6** had the highest peak flux density (~106 sfu) of any event yet recorded at this frequency. The decimetric event characteristics during the brightest emission phase (numerous intense, short-lived, narrow-band bursts that overlapped to form a continuous spectrum) suggest electron cyclotron maser (ECM) emission. The peak 1.4 GHz emission did not occur during the flare impulsive phase but rather ~45 minutes later, in association with post-eruption loop activity seen in Hα and by the Hinode EUV Imaging Spectrometer. During the Waves/LASCO era, **three other delayed bursts with peak intensities >105** sfu in the 1.0-1.6 GHz (L-band) frequency range have been reported that appear to have characteristics similar to the December 6 burst. In each of these three cases, high-frequency type IV bursts were reported in a range from ~150 to ~1500 MHz. Assuming a common ECM emission mechanism across this frequency range implies a broad span of source heights in the associated post-eruption loop systems. Difficulties with an ECM interpretation for these events include the generation of the lower frequency component of the type IVs and the long-standing problem of escape of the ECM emission from the loops. Magnetic-field-aligned potential drops, analogous to those observed for Earth's auroral kilometric radiation, could plausibly remove both of these objections to ECM emission.

Coronal shocks of November 1997 revisited: The CME type II timing problem

Cliver, E.W., Nitta, N.V., Thompson, B.J., Zhang, J.: 2004,.

Solar Phys. **225**, 105 – 139. doi:10.1007/s11207-004-3258-1, **2004**.

ON THE ORIGIN OF SOLAR METRIC TYPE II BURSTS_

EDWARD W. **CLIVER**1, DAVIDF.WEBB2 and RUSSELL A. HOWARD

Solar Physics **187:** 89–114, **1999; File**.

The vast majority of solar flares are not associated with metric Type II radio bursts. For example, for the period February 1980–July 1982, corresponding to the first two and one-half years of the Solar Maximum Mission, 95% of the _2500 flares with peak > 25 keV count rates > 100 c s_1 lacked associated Type II emission. Even the _360 largest flares, i.e., those having > 25 keV peak count rates > 1000 c s_1, had a Type II association rate of only 24%. The lack of a close correlation between flare size and Type II occurrence implies the need for a 'special condition' that distinguishes flares that are accompanied by metric Type II radio bursts from those of comparable size that are not. The leading candidates for this special condition are: (1) an unusually low Alfvén speed in the flaring region; and (2) fast material motion. We present evidence based on SMM and GOES X-ray data and *Solwind* coronagraph data that argues against the first of these hypotheses and supports the second. Type II bursts linked to flares within 30_ of the solar limb are well associated (64%; 49/76) with fast (> 400 km s_1) coronal mass ejections (CMEs); for Type II flares within 15_ of the limb, the association rate is 79% (30/38). An examination of the characteristics of 'non-CME' flares associated with Type IIs does not support the flare-initiated blast wave picture that has been proposed for these events and suggests instead that CMEs may have escaped detection. While the degree of Type II–CME association increases with flare size, there are notable cases of small Type II flares whose outstanding attribute is a fast CME. Thus we argue that metric Type II bursts (as well as the Moreton waves and kilometric Type II bursts that may accompany them) have their root cause in fast coronal mass ejections.

Solar Gradual Hard X-Ray Bursts and Associated Phenomena

Cliver, E. W.; Dennis, B. R.; Kiplinger, A. L.; Kane, S. R.; Neidig, D. F.; Sheeley, N. R., Jr.; Koomen, M. J.

1986 ApJ...305..920-935

http://articles.adsabs.harvard.edu/full/1986ApJ...305..920C

DOI: 10.1086/164306
White-light coronagraph, H-alpha and radio data are presented as well as hard X-ray data for a sample of 10 gradual hard X-ray bursts (GHBs) in an attempt to better understand the nature of these events. It is found that: (1) the hard X-ray photon energy spectrum began to harden near the onset of the GHBs and continued in this fashion during the decay phase; (2) a coronal mass ejection (CME) occurred in association with at least nine of the GHBs; (3) the GHBs occurred in the late phase of major flares; (4) the centimeter wavelength bursts associated with the GHBs had relatively low frequency spectral maxima, and in relation to the observed hard X-ray emission, they were microwave-rich; (5) the associated decimetric bursts showed significant intensity variations on time scales ranging from 0.1 to approximately greater than 1 minute; and (6) the GHBs were most strongly associated with type IV events. It is concluded that the acceleration and trapping of radiating electrons occurs in the postflare loop systems following CMEs. **6 Apr 1980, 1 May 1980, 24 Apr 1981, 26 Apr 1981, 13 May 1981, 14 Nov 1981, 7 Mar 1982, 6 Jun 1982, 10 Jun 1982, 17 Dec 1982**
Table

Secondary Peaks in Solar Microwave Outbursts

Cliver, E. W.
Solar Physics, Volume 84, Issue 1-2, pp. 347-359, **1983**
http://articles.adsabs.harvard.edu/pdf/1983SoPh...84..347C
https://link.springer.com/content/pdf/10.1007%2FBF00157467.pdf
Observations are presented for several large solar flares in which a timing association is observed between late ($\gtrsim$ 30 min after the flash phase) microwave peaks and late stationary decametric continua. **It is suggested that the late microwave peaks are a phenomenon of the post flare loop (relaxation) stage of large flares and are caused by field line reconnections occurring above the Hα and soft X-ray emitting loops.** A simple model to account for the association between the secondary radio peaks observed at discrete frequencies and the late decametric continua is proposed.

Localising pulsations in the hard X-ray and microwave emission of an X-class flare

Hannah **Collier**, Laura A. Hayes, Sijie Yu, Andrea F. Battaglia, William Ashfield, Vanessa Polito, Louise K. Harra, Säm Krucker
A&A 684, A215 **2024**
https://arxiv.org/pdf/2402.10546.pdf
https://www.aanda.org/articles/aa/pdf/2024/04/aa48652-23.pdf
Aims: This work aims to identify the mechanism driving pulsations in hard X-ray (HXR) and microwave emission during solar flares. Here, by using combined HXR and microwave observations from Solar Orbiter/STIX and EOVSA we investigate an X1.3 GOES class flare, **2022-03-30**T17:21:00, which displays pulsations on timescales evolving from ~ 7 s in the impulsive phase to ~ 35 s later in the flare.
Methods: The temporal, spatial and spectral evolution of the HXR and microwave pulsations during the impulsive phase of the flare are analysed. Images are reconstructed for individual peaks in the impulsive phase and spectral fitting is performed at high cadence throughout the first phase of pulsations.
Results: Imaging analysis demonstrates that the HXR and microwave emission originates from multiple sites along the flare ribbons. The brightest sources and the location of the emission changes in time. Through HXR spectral analysis, the electron spectral index is found to be anti-correlated with the HXR flux showing a "soft-hard-soft" spectral index evolution for each pulsation. The timing of the associated filament eruption coincides with the early impulsive phase.
Conclusions: Our results indicate that periodic acceleration and/or injection of electrons from multiple sites along the flare arcade is responsible for the pulsations observed in HXR and microwave. The evolution of pulsation timescales is likely a result of changes in the 3D magnetic field configuration in time related to the associated filament eruption.

Kinematics of ICMEs/shocks: blast wave reconstruction using type II emissions

P. **Corona-Romero**, J.A. Gonzalez-Esparza, E. Aguilar-Rodriguez, V. de-la-Luz, J.C. Mejia-Ambriz
Solar Phys. Volume 290, Issue 9, pp 2439-2454 **2015**
http://arxiv.org/pdf/1501.05551v1.pdf
We present a physical methodology to reconstruct the trajectory of interplanetary shocks using type II radio emission data. This technique calculates the shock trajectory assuming that the disturbance propagates as a blast wave in the interplanetary medium. We applied this Blast Wave Reconstruction (BWR) technique to analyze eight fast Earth-directed ICMEs/shocks associated with type II emissions. The technique deduces a shock trajectory that reproduces the type II frequency drifts, and calculates shock onset speed, shock transit time and shock speed at 1~AU. There were good agreements comparing the BWR results with the type II spectra, with data from coronagraph images, {\it in situ}

measurements, and interplanetary scintillation (IPS) observations. Perturbations on the type II data affect the accuracy of the BWR technique. This methodology could be applied to track interplanetary shocks causing TII emissions in real-time, to predict the shock arrival time and shock speed at 1~AU. **6 Jun 2000, 14 July 2000, 26 Apr 2001, 24 Sept 2001, 20011104, 20011122, 20040725, 20050513**

Propagation of Fast Coronal Mass Ejections and Shock Waves Associated with Type II Radio-Burst Emission: An Analytic Study

P. **Corona-Romero**, J. A. Gonzalez-Esparza and E. Aguilar-Rodriguez
Solar Physics, July **2013**, Volume 285, Issue 1-2, pp 391-410 Coronal mass ejections (CMEs) are large-scale eruptive events in the solar corona. Once they are expelled into the interplanetary (IP) medium, they propagate outwards and "evolve" interacting with the solar wind. Fast CMEs associated with IP shocks are a critical subject for space weather investigations. We present an analytic model to study the heliocentric evolution of fast CME/shock events and their association with type II radio-burst emissions. The propagation model assumes an early stage where the CME acts as a piston driving a shock wave; beyond this point the CME decelerates, tending to match the ambient solar wind speed and its shock decays. We use the shock speed evolution to reproduce type II radio-burst emissions. We analyse four fast CME halo events that were associated with kilometric type II radio bursts, and in-situ measurements of IP shock and CME signatures. The results show good agreement with the dynamic spectra of the type II frequency drifts and the in-situ measurements. This suggests that, in general, IP shocks associated with fast CMEs evolve as blast waves approaching 1 AU, implying that the CMEs do not drive their shocks any further at this heliocentric range.

Solar Burst Analysis with 3D Loop Models

J. E. R. **Costa**, P. J. A. Simões, T. S. N. Pinto, and V. F. Melnikov
Publ. Astron. Soc. Japan 65, No. SP1, S5 [10 pages] (**2013**)
http://pasj.asj.or.jp/v65/sp1/65S005/65S005.pdf
A sample of Nobeyama flares was selected and analyzed using a loop model for important flare parameters. The model for the flaring region consists of a three-dimensional dipolar magnetic field, and spatial distributions of nonthermal electrons. We constructed a database by calculating the flare microwave emission for a wide range of these parameters. Out of this database with more than 5000 cases, we extracted general flare properties by comparing the observed and calculated microwave spectra. The analysis of the Nobeyama Radio Polarimeter data was mostly based on the center-to-limb variation of the flare properties with looptop and footpoint electron distributions, and for the Nobeyama Radioheliograph maps on the resultant distribution of emission. One important aspect of this work is a comparison of the analysis of a flare using an inhomogeneous source model and a simplistic homogeneous source model. Our results clearly show that the homogeneous source hypothesis is not appropriate to describe the possible flare geometry, and its use can easily produce misleading results in terms of non-thermal electron density and magnetic field strength. A center darkening of flares was also obtained as a geometrical property of the loop-like sources.

Low-frequency type II radio detections and coronagraph data to describe and forecast the propagation of 71 CMEs/shocks

H. **Cremades** , F. A. Iglesias, O. C. St. Cyr, H. Xie, M. L. Kaiser, N. Gopalswamy
Solar Phys. Volume 290, Issue 9, pp 2455-2478 **2015**
http://arxiv.org/pdf/1505.01730v1.pdf
The vulnerability of technology on which present society relies demands that a solar event, its time of arrival at Earth, and its degree of geoeffectiveness be promptly forecasted. Motivated by improving predictions of arrival times at Earth of shocks driven by coronal mass ejections (CMEs), we have analyzed 71 Earth-directed events in different stages of their propagation. The study is primarily based on approximated locations of interplanetary (IP) shocks derived from type II radio emissions detected by the Wind/WAVES experiment during 1997-2007. Distance-time diagrams resulting from the combination of white-light corona, IP type II radio, and in situ data lead to the formulation of descriptive profiles of each CME's journey toward Earth. Furthermore, two different methods to track and predict the location of CME-driven IP shocks are presented. The linear method, solely based on Wind/WAVES data, arises after key modifications to a pre-existing technique that linearly projects the drifting low-frequency type II emissions to 1 AU. This upgraded method improves forecasts of shock arrival time by almost 50%. The second predictive method is proposed on the basis of information derived from the descriptive profiles, and relies on a single CME height-time point and on low-frequency type II radio emissions to obtain an approximate value of the shock arrival time at Earth. In

addition, we discuss results on CME-radio emission associations, characteristics of IP propagation, and the relative success of the forecasting methods.
Table 1.: CME-kmTII-shock associations and main characteristics of the 71 analyzed events.

A tool to improve space weather forecasts: Kilometric radio emissions from Wind/WAVES

To improve predictions of the arrival time of magnetohydrodynamic shock, which can occur as coronal mass ejections propagate through interplanetary space, scientists study low frequency radio emissions detected by the WIND/WAVES satellite.

Cremades, H.; St. Cyr, O. C.; Kaiser, M. L.
Space Weather, Vol. 5, No. 8, S08001, **2007, File**
http://dx.doi.org/10.1029/2007SW000314

For decades, space environment forecasters have used the appearance of metric Type II radio emission as a proxy for eruptions in the solar corona. The drift rate of these near-Sun emissions is often turned into a speed, commonly assumed to be that of an MHD shock. However, their utility to forecast shock arrival times has not proved to be conclusive. Metric emissions can be detected by ground-based antennae, while lower-frequency components of these slowly drifting emissions can also be tracked by spacecraft in interplanetary space, as far down in frequency as that of the local plasma frequency. For a spacecraft at L1, this corresponds to about 25 kHz, or an electron density of about 7 cm−3 in the ambient solar wind. Here we report a recent study that aims to improve the predictions of shock arrival time at L1 by means of the low-frequency emissions detected by WIND/WAVES. This technique, implemented on an extensive sample of hectometric and kilometric type II radio bursts, has yielded promising results.
Table

Asymmetric precipitation in a coronal loop as explanation of a singular observed spectrum

G. **Cristiania**, C.G. Giménez de Castrob, C.H. Mandrinia, 1, M.E. Machadoc and M.G. Roviraa
Advances in Space Research, Volume 44, Issue 11, 1 December **2009**, Pages 1314-1320

Almost 10 years of solar submillimeter observations have shown new aspects of solar activity, such as the presence of rapid solar spikes associated with the launch of coronal mass ejections and an increasing submillimeter spectral component in flares. We analyse the singular microwave–submillimeter spectrum of an M class solar flare on 20 December, 2002. Flux density observations measured by Sun patrol telescopes and the Solar Submillimeter Telescope are used to build the radio spectrum, which is fitted using Ramaty's code. At submillimeter frequencies the spectrum shows a component different from the microwave classical burst. The fitting is achieved proposing two homogeneous sources of emission. This theoretical fitting is in agreement with differential precipitation through a magnetically asymmetric loop or set of loops. From a coronal magnetic field model we infer an asymmetric magnetic structure at the flare location. The model proposed to quantify the differential precipitation rates due to the asymmetry results in a total precipitation ratio Q2/Q1≈104–105, where Q1(Q2) represents the total precipitation in the loop foot with the high (low) magnetic field intensity. This ratio agrees with the electron total number ratio of the two sources proposed to fit the radio spectrum.

A solar burst with a spectral component observed only above 100═GHz during an M class flare:

G. **Cristiani**, C. G. GimИnez de Castro, C. H. Mandrini, M. E. Machado, I. de Benedetto e Silva, P. Kaufmann and M. G. Rovira
A&A 492 (**2008**) 215-222

Context. Since the installation of submillimeter solar radio telescopes, a new spectral burst component was discovered at frequencies above 100 GHz, creating the THz burst category. In all the reported cases, the events were X-class flares and the THz component was increasing.
Aims. We report for the first time an M class flare that shows a different submillimeter radio spectral component from the microwave classical burst. Two successive bursts of 2 min duration and separated by 2 min occurred in active region NOAA 10226, starting around 13:15 UT and having an M 6.8 maximum intensity in soft X-rays.
Methods. Submillimeter flux density measured by the Solar Submillimeter Telescope (SST) is used, in addition to microwave total Sun patrol telescope observations. Images with H α filters, from the H α Solar Telescope for Argentina

(HASTA), and extreme UV observations, from the Extreme-ultraviolet Imaging Telescope (EIT) aboard the Solar and Heliospheric Observatory (SoHO), are used to characterize the flaring region. An extensive analysis of the magnetic topology evolution is derived from the Michelson Doppler Imager (SoHO, MDI) magnetograms and used to constrain the solution space of the possible emission mechanisms.
Results. The submillimeter component is only observed at 212 GHz. We have upper limits for the emission at 89.4 and 405 GHz, which are less than the observed flux density at 212 GHz. The analysis of the magnetic topology reveals a very compact and complex system of arches that reconnects at low heights, while from the soft X-ray observations we deduce that the flaring area is dense ($n \sim 10^{12}$ cm-3). The reconnected arches are anchored in regions with magnetic field intensity differing by an order of magnitude. Accordingly, we conclude that the microwave emission comes from mildly relativistic electrons spiraling down along the reconnected loops. A very small portion of the accelerated electrons can reach the footpoint with the stronger magnetic field (2000 G) and produce synchrotron emission, which is observed at submillimeter frequencies.
Conclusions. The finding of a submillimeter burst component in a medium-size flare indicates that the phenomenon is more universal than shown until now. The multiwavelength analysis reveals that neither positron synchrotron nor free-free emission could produce the submillimeter component, which is explained here by synchrotron of accelerated electrons in a rather complex and compact magnetic configuration.
20 Dec 2002

Spatial Characterization of a Flare Using Radio Observations and Magnetic Field Topology

G. **Cristiani**, G. Martinez, C. H. Mandrini, C. G. Giménez De Castro, C. W. Da Silva, M. G. Rovira, P. Kaufmann
Solar Phys., 240 (2), Page: 271 – 281, **2007**
November 28, 2001
The analysis of the magnetic field connectivity allows us to conclude that magnetic field reconnection between two different coronal/chromospheric sets of arches was at the origin of the flare and surge, respectively.

Observed flux density enhancement at submillimeter wavelengths during an X-class flare

Adv. Space Res. 39(9), Pages 1447-1452, **2007**
G. **Cristiani**, C.G. Giménez de Castro, M.L. Luoni, C.H. Mandrini, M.G. Rovira, P. Kaufmann and M. Machado
We analyse the 30 October, 2004, X1.2/SF solar event that occurred in AR 10691 (N13 W18) at around 11:44 UT. Observations at 212 and 405 GHz of the Solar Submillimeter Telescope (SST), with high time resolution (5 ms), show an intense impulsive burst followed by a long-lasting thermal phase.

Transient Mass Loss Analysis of Solar Observations using Stellar Methods

M. K. **Crosley**, R. A. Osten, C. Norman
2017
https://arxiv.org/pdf/1707.01928.pdf
Low frequency dynamic spectra of radio bursts from nearby stars offer the best chance to directly detect the stellar signature of transient mass loss on low mass stars. Crosley et al. (2016) proposes a multi-wavelength methodology to determine coronal mass ejection parameters, such as Coronal Mass Ejection (CME) speed, mass, and kinetic energy. We test the validity and accuracy of the results derived from the methodology by using Geostationary Operational Environmental Satellite X-ray observations and Bruny Island Radio Spectrometer radio observations. These are analogous observations to those which would be found in the stellar studies. Derived results from these observations are compared to direct white light measurements of the Large Angle and Spectrometric Coronagraph.
We find that, when a pre-event temperature can be determined, that the accuracy of CME speeds are within a few hundred km/s, and are reliable when specific criteria has been met. CME mass and kinetic energies are only useful in determining approximate order of magnitude measurements when considering the large errors associated to them. These results will be directly applicable to interpretation of any detected stellar events and derivation of stellar CME properties. **2011-01-28, 2011-02-13, 2012-03-17, 2012-06-03 , 2012-07-06, 2013-05-02, 2013-10-24, 2013-11-08, 2014-01-08 , 2014-02-20, 2014-03-20, 2014-04-25, 2014-11-03, 2014-12-17,**
Table 2. SOHO/LASCO Measurements
Table 4. Parameters from GOES Measurements

Chapter 23 - Extreme Ionospheric Storms and Their Effects on GPS Systems **Review**

Geoff **Crowley**, IrfanAzeem

In: Extreme Events in Geospace Origins, Predictability, and Consequences **2018**, Pages 555-586

http://sci-hub.tw/10.1016/B978-0-12-812700-1.00023-6

Given the central importance of Global Positioning System (GPS) to modern society, it is important to consider the effects of extreme ionospheric storms on GPS signals. We describe the ionosphere and ionospheric storms, and the main ionospheric effects on GPS caused by gradients in TEC, by scintillation and by Traveling Ionospheric Disturbances. We summarize the GPS impacts of the three largest ionospheric storms of the last 15 years. Finally, we discuss the implications for extreme ionospheric storms and their effects on operational systems, with a focus on GPS-reliant systems. We note that GPS outages can affect not only the surveyor (positioning) or farmer (precision agriculture), but also the critical infrastructure, including financial institutions, transportation, communications, and the internet, and perhaps most importantly, the power grid, which relies on timing signals provided by the GPS system. While mitigation efforts are important, it is also vital to continue fundamental research to better understand ionospheric variability.

Flare parameters inferred from a 3D loop model data base

Valente A **Cuambe** J E R Costa P J A Simões

Monthly Notices of the Royal Astronomical Society, Volume 477, Issue 2, 21 June **2018**, Pages 1508–1519

https://sci-hub.tw/10.1093/mnras/sty867

We developed a data base of pre-calculated flare images and spectra exploring a set of parameters which describe the physical characteristics of coronal loops and accelerated electron distribution. Due to the large number of parameters involved in describing the geometry and the flaring atmosphere in the model used, we built a large data base of models (∼250 000) to facilitate the flare analysis. The geometry and characteristics of non-thermal electrons are defined on a discrete grid with spatial resolution greater than 4 arcsec. The data base was constructed based on general properties of known solar flares and convolved with instrumental resolution to replicate the observations from the Nobeyama radio polarimeter spectra and Nobeyama radioheliograph (NoRH) brightness maps. Observed spectra and brightness distribution maps are easily compared with the modelled spectra and images in the data base, indicating a possible range of solutions. The parameter search efficiency in this finite data base is discussed. 8 out of 10 parameters analysed for 1000 simulated flare searches were recovered with a relative error of less than 20 per cent on average. In addition, from the analysis of the observed correlation between NoRH flare sizes and intensities at 17 GHz, some statistical properties were derived. From these statistics, the energy spectral index was found to be $\delta \sim 3$, with non-thermal electron densities showing a peak distribution $\gtrapprox 107$ cm−3, and Bphotosphere $\gtrsim 2000$ G. Some bias for larger loops with heights as great as ∼2.6 × 109 cm, and looptop events were noted. An excellent match of the spectrum and the brightness distribution at 17 and 34 GHz of the **2002 May 31** flare is presented as well.

Shock wave driven by CME evidenced by metric type II burst and EUV wave

R.D. **Cunha-Silva**, , F.C.R. Fernandes, C.L. Selhorst

Advances in Space Research Volume 56, Issue 12, 15 December **2015**, Pages 2804–2810

http://www.sciencedirect.com/science/article/pii/S0273117715005311

Solar type II radio bursts are produced by plasma oscillations in the solar corona as a result of shock waves. The relationship between type II bursts and coronal shocks is well evidenced by observations since the 1960s. However, the drivers of the shocks associated with type II events at metric wavelengths remain as a controversial issue among solar physicists. The flares and the coronal mass ejections (CMEs) are considered as potential drivers of these shocks. In this article, we present an analysis of a metric type II burst observed on **May 17, 2013**, using data provided by spectrometers from e-CALLISTO (extended-Compound Astronomical Low-cost Low-frequency Instrument for Spectroscopy and Transportable Observatories) and EUV images from the Extreme Ultraviolet Imager (EUVI), aboard the Solar Terrestrial Relations Observatory (STEREO). The event was associated with an M3.2 SXR flare and a halo CME. The EUV wave produced by the expansion of the CME was clear from the EUV images. The heights of the EUV wave fronts proved to be consistent with the heights of the radio source obtained with the 2–4 × Newkirk density model, which provided a clue to an oblique propagation of the type-II-emitting shock segment. The results for the magnetic field in the regions of the shock also revealed to be consistent with the heights of the radio source obtained using the 2–4 × Newkirk density model. Exponential fit on the intensity maxima of the harmonic emission provided a shock speed of ∼580–990 km s−1, consistent with the average speed of the associated EUV wave front of 626 km s−1.

Solar type II radio bursts associated with CME expansions as shown by EUV waves

R. D. **Cunha-Silva**, F. C. R. Fernandes, C. L. Selhorst

A&A 578, A38 **2015**
http://arxiv.org/pdf/1504.04323v1.pdf
We investigate the physical conditions of the sources of two metric Type-II bursts associated with CME expansions with the aim of verifying the relationship between the shocks and the CMEs, comparing the heights of the radio sources and the heights of the EUV waves associated with the CMEs. The heights of the EUV waves associated with the events were determined in relation to the wave fronts. The heights of the shocks were estimated by applying two different density models to the frequencies of the Type-II emissions and compared with the heights of the EUV waves. For the 13 June 2010 event, with band-splitting, the shock speed was estimated from the frequency drifts of the upper and lower branches of the harmonic lane, taking into account the H/F frequency ratio fH/fF = 2. Exponential fits on the intensity maxima of the branches revealed to be more consistent with the morphology of the spectrum of this event. For the 6 June 2012 event, with no band-splitting and with a clear fundamental lane on the spectrum, the shock speed was estimated directly from the frequency drift of the fundamental emission, determined by linear fit on the intensity maxima of the lane. For each event, the most appropriate density model was adopted to estimate the physical parameters of the radio source. The **13 June 2010** event presented a shock speed of 664-719 km/s, consistent with the average speed of the EUV wave fronts of 609 km/s. The **6 June 2012** event was related to a shock of speed of 211-461 km/s, also consistent with the average speed of the EUV wave fronts of 418 km/s. For both events, the heights of the EUV wave revealed to be compatible with the heights of the radio source, assuming a radial propagation of the shock.

Solar Type II Radio Bursts Recorded by the Compound Astronomical Low-Frequency Low-Cost Instrument for Spectroscopy in Transportable Observatories in Brazil

R. D. **Cunha-Silva**, F. C. R. Fernandes, C. L. Selhorst
Solar Phys. **2014**
It is well established that solar Type-II radio bursts are signatures of magnetohydrodynamical (MHD) shock waves propagating outward through the solar corona. Nevertheless, there are long-standing controversies about how these shocks are formed; solar flares and the coronal mass ejections (CMEs) are considered to be the most likely drivers. We present the results of the analysis of four solar Type-II bursts recorded between **20 January 2010 and 17 November 2011** by the Compound Astronomical Low-frequency Low-cost Instrument for Spectroscopy in Transportable Observatories (CALLISTO-BR) (in Brazil), which operates in the frequency range of 45 – 870 MHz. For all four solar Type-II radio bursts, which consisted of one event without band splitting and three split-band variants, the outcomes are consistent with those reported in the literature. All four Type-II radio bursts were accompanied by both solar flares and CMEs, which are associated with the impulsive phase of the flares and, very likely, with the acceleration phase of the CMEs.

Interferometric imaging of the type IIIb and U radio bursts observed with LOFAR on 22 August 2017

Bartosz **Dabrowski**, Katarzyna Mikula, Pawel Flisek, Christian Vocks, PeiJin Zhang, et al.
A&A 669, A52 **2022**
https://arxiv.org/pdf/2211.12756.pdf
https://www.aanda.org/articles/aa/pdf/2023/01/aa42905-21.pdf
The Sun is the source of different types of radio bursts that are associated with solar flares, for example. Among the most frequently observed phenomena are type III solar bursts. Their radio images at low frequencies (below 100 MHz) are relatively poorly studied due to the limitations of legacy radio telescopes. We study the general characteristics of types IIIb and U with stria structure solar radio bursts in the frequency range of 20 - 80 MHz, in particular the source size and evolution in different altitudes, as well as the velocity and energy of electron beams responsible for their generation. In this work types IIIb and U with stria structure radio bursts are analyzed using data from the LOFAR telescope including dynamic spectra and imaging observations, as well as data taken in the X-ray range (GOES and RHESSI satellites) and in the extreme ultraviolet (SDO satellite). In this study we determined the source size limited by the actual shape of the contour at particular frequencies of type IIIb and U solar bursts in a relatively wide frequency band from 20 to 80 MHz. Two of the bursts seem to appear at roughly the same place in the studied active region and their source sizes are similar. It is different in the case of another burst, which seems to be related to another part of the magnetic field structure in this active region. The velocities of the electron beams responsible for the generation of the three bursts studied here were also found to be different. **22 August 2017**

Observations of the Sun using LOFAR Bałdy station

B.P.**Dąbrowski**, D.E.MorosanbgR.A.FallowscL.BłaszkiewiczadA.KrankowskiaJ.MagdalenićeC.Vocksf G.MannfP.ZuccacT. SidorowiczaM.HajdukaK.KotulakaA.FrońaK.Śniadkowskaa
Advances in Space Research Volume 62, Issue 7, 1 October **2018**, Pages 1895-1903
http://sci-hub.tw/https://linkinghub.elsevier.com/retrieve/pii/S0273117718305210
We report first results of solar spectroscopic observations carried out with the Bałdy LOFAR (LOw-Frequency ARray) station, Poland from October 2016 to July 2017. During this time, we observed different types of radio emission: type I and type III radio bursts. Our observations show that the station is fully operational and it is capable to work efficiently in the single station mode for solar observations. Furthermore, in this paper we will briefly describe the observational technique and instrument capabilities and show some examples of first observations. **22 January 2017, 14 July 2017, 16 July 2017, 21 July 2017**

Fourier Analysis of Radio Bursts Observed with Very High Time Resolution

B. P. **Dąbrowski**, M. Karlický, P. Rudawy
Solar Phys. **2014**
Numerous solar radio bursts were observed in 2000 – 2001 using the Toruń radio spectrograph with its unique time resolution of 80 microseconds. This high time resolution enables an in-depth analysis of the time evolution of the power spectra and Fourier spectral indices of selected short radio bursts. We analyze the power-spectrum parameters and variability for two millisecond radio dm-spike events and one drifting pulsation structure (DPS) event, for which the structures of the recorded signals were analyzed with an effective time resolution of 0.0008 s in five adjacent frequency bands of their radio spectra.
We found that Fourier spectral indices varied rapidly when radio fine structures were recorded. Otherwise they remained close to zero, indicating the presence of noise. For the 10 – 40 Hz frequency interval of the power spectra the mean values of the Fourier spectral indices varied up to −1.51 for the dm-spikes and up to −1.53 for the DPS event. Cross-correlation coefficients of radio fluxes in adjacent frequency bands varied between 0.12 and 0.60 for dm-spikes and between 0.77 and 0.94 for the DPS event. The shortest fine structure found in the studied events lasted 0.001 s.
These results are entirely new for dm-radio spikes and confirm a single previous result found for the DPS events. On the basis of our results, we propose that dm-spikes and DPS events are physically similar and that both are signatures of cascades of interacting plasmoids of different sizes.

Millisecond Radio Spikes in the Decimetric Band

B. P. **Dabrowski**, P. Rudawy and M. Karlický
Solar Physics, Volume 273, Number 2, 377-392, **2011**
We present the results of the analysis of thirteen events consisting of dm-spikes observed in Toruń between 15 March 2000 and 30 October 2001. The events were obtained with a very high time resolution (80 microseconds) radio spectrograph in the 1352 – 1490 MHz range. These data were complemented with observations from the radio spectrograph at Ondřejov in the 0.8 – 2.0 GHz band. We evaluated the basic characteristics of the individual spikes (duration, spectral width, and frequency drifts), as well as their groups and chains, the location of their emission sources, and the temporal correlations of the emissions with various phases of the associated solar flares. We found that the mean duration and spectral width of the radio spikes are equal to 0.036 s and 9.96 MHz, respectively. Distributions of the duration and spectral widths of the spikes have positive skewness for all investigated events. Each spike shows positive or negative frequency drift. The mean negative and positive drifts of the investigated spikes are equal to −776 MHz s−1 and 1608 MHz s−1, respectively. The emission sources of the dm-spikes are located mainly at disk center. We have noticed two kinds of chains, with and without frequency drifts. The mean durations of the chains vary between 0.067 s and 0.509 s, while their spectral widths vary between 7.2 MHz and 17.25 MHz. The mean duration of an individual spike observed in a chain was equal to 0.03 s. While we found some agreement between the global characteristics of the groups of spikes recorded with the two instruments located in Toruń and Ondřejov, we did not find any one-to-one relation between individual spikes.
26 March 2000, 26 April 2000, *11 July 2000*

Correlation between decimetric radio emission and hard X-rays in solar flares

Bartosz P. **Dabrowski** and Arnold O. Benz

A&A, 504, 565-573; **2009, File**

*Aims.*The emission of decimetric flare radiation, in particular narrowband spikes and pulsations, is generally considered to originate in accelerated, non-thermal particles. On the other hand, non-thermal hard X-rays are also understood to be products of this acceleration. Do radio emission and hard X-ray signatures originate from the same acceleration process? A strong correlation between the light curves in the radio and HXR ranges may help answer this question.

Methods. The delay between the radio and hard X-ray emission was determined by cross-correlation. The time profiles of X-ray and radio emission include a wide range of energies and frequencies. Thus, correlation is not simply a yes/no question, but must be systematically searched for in various ranges. The high spectral resolution of RHESSI ensured that it was possible to carefully choose the energy range, excluding thermal emission. The broad bandwidth of *Phoenix-2* allowed the selection of any emission in the full decimetre range. The energy range and duration in hard X-rays, and the frequency range in radio spectrograms were chosen to optimize the correlation. The cross-correlation coefficient was then analyzed by a Gaussian fitting method.

Results.The measured delays have a distribution of FWHM4.9 s and 4.7 s for pulsations and spikes, respectively, evaluated from such a Gaussian fitting method. The mean delay for pulsations was found to be −1.4±0.9 seconds (minus indicates that hard X-ray emission comes first), and for narrowband spikes to −2.5±2.5 seconds. There are broad wings in the distribution, which we interpret as chance coincidences. The delays do not depend on centre frequency, cross-correlation coefficient, duration of the correlating sequence, and position on the disk. However, we find an increase in the delay for the spikes with GOES magnitude (peak soft X-ray emission) of the flare and with peak hard X-ray flux. This was not the case for pulsations.

Conclusions. In contrast to previous reports, the average delays for all pulsations and all spike groups are consistent with zero. Thus, correlated decimetric pulsations and spikes are, on average, concomitant with non-thermal X-rays.

The shock driving capability of a CME inferred from multiwavelength observations

Fithanegest Kassa **Dagnew**, Nat Gopalswamy, Solomon Belay Tessema, Ange Cynthia Umuhire, Seiji Yashiro, Pertti Mäkelä, Hong Xie

Sun and Geosphere, **Vol.14, No. 2, 2019** p. 105-110

https://arxiv.org/ftp/arxiv/papers/2002/2002.04056.pdf

http://newserver.stil.bas.bg/SUNGEO//00SGArhiv/SG_v14_No2_2019-pp105-110.pdf

The radial speed of a coronal mass ejection (CME) determines the shock-driving capability of a CME as indicated by the presence of a type II radio burst. Here we report on the **April 18, 2014** CME that was associated with a type II radio burst in the metric and interplanetary domains. We used the radio-burst data provided by the San Vito Solar Observatory of the Radio Solar Telescope Network and data from the Wind spacecraft. The CME is a full halo in the field of view of the coronagraphs on board the Solar and Heliospheric Observatory (SOHO). The CME was also observed by the coronagraphs on board the Solar Terrestrial Relations Observatory (STEREO). We computed the CME shock and flux rope speeds based on the multi-view observations by the different coronagraphs and by EUV instruments. We determined the shock speed from metric and interplanetary radio observations and found them to be consistent with white-light observations, provided the metric type II burst and its continuation into the decameter-hectometric domain are produced at the shock flanks, where the speed is still high enough to accelerate electrons that produce the type II bursts. Interestingly, there was an interplanetary type II burst segment consistent with an origin at the shock nose suggesting that the curved shock was crossing plasma levels separated by a few solar radii. We conclude that the CME speed is high enough to produce the interplanetary Type II burst and a solar energetic particle (SEP) event. However, the speed is not high enough to produce a ground level enhancement (GLE) event, which requires the shock to form at a height of ~1.5 Rs.

Observations of a soft X-ray rising loop associated with a type II burst and a coronal mass ejection in the 03 November 2003 X-ray flare --

C. **Dauphin**, N. Vilmer, S. Krucker (E-print, May **2006**)
Astronomy and Astrophysics, Volume 455, Issue 1, pp.339-348, **2006**.
We report observations of a type II burst - the signature of a shock wave - starting at the unusual high frequency of 650 MHz during the 03 November 2003 flare. This flare is associated with the propagation of a soft X-ray coronal loop and with a coronal mass ejection (CME).

The Submillimeter Active Region Excess Brightness Temperature during Solar Cycles 23 and 24

C. Guillermo Giménez **de Castro** (1 and 2), André L. G. Pereira (1), J. Fernando Valle Silva (1), Caius L. Selhorst (3), Cristina H. Mandrini (2), Germán D. Cristiani (2), Jean-Pierre Raulin (1), Adriana Valio (1)
ApJ **902** 136 **2020**
https://arxiv.org/pdf/2009.03445.pdf
https://doi.org/10.3847/1538-4357/abb59e
We report the temporal evolution of the excess brightness temperature above solar active regions (ARs) observed with the Solar Submillimeter Telescope (SST) at 212 ({\lambda} = 1.4 mm) and 405 GHz ({\lambda} = 0.7 mm) during Cycles 23 and 24. Comparison with the sunspot number (SSN) yields a Pearson's correlation coefficient R = 0.88 and 0.74 for 212 and 405 GHz, respectively. Moreover, when only Cycle 24 is taken into account the correlation coefficients go to 0.93 and 0.81 for each frequency. We derive the spectral index {\alpha} between SST frequencies and found a slight anti-correlation with the SSN (R = -0.25); however, since the amplitude of the variation is lower than the standard deviation we cannot draw a definite conclusion. Indeed, {\alpha} remains almost constant within the uncertainties with a median value approximate to 0 characteristic of an optically thick thermal source. Since the origin of the AR submillimeter radiation is thermal continuum produced at chromospheric heights, the strong correlation between the excess brightness temperature and the magnetic cycle evolution could be related to the available free magnetic energy to be released in reconnection events. **2011-03-26**

HATS: A Ground-Based Telescope to Explore the THz Domain

C.G. Giménez **de Castro**, J.-P. Raulin, A. Valio, G. Alaia, V. Alvarenga, E.C. Bortolucci, S.H. Fernandes, C. Francile, T. Giorgetti, A.S. Kudaka, F.M. López, R. Marcon, A. Marún, M. Zaquela
Solar Phys. **2020**
https://arxiv.org/pdf/2003.12907.pdf
The almost unexplored frequency window from submillimeter to mid-infrared (mid-IR) may bring new clues about the particle acceleration and transport processes and the atmospheric thermal response during solar flares. Because of its technical complexity and the special atmospheric environment needed, observations at these frequencies are very sparse. The High Altitude THz Solar Photometer (HATS) is a full-Sun ground-based telescope designed to observe the continuum from the submillimeter to the mid-IR. It has a 457-mm spherical mirror with the sensor in its primary focus. The sensor is a Golay cell with high sensitivity in a very wide frequency range. The telescope has a polar mount, and a custom-built data acquisition system based on a 32 ksamples per second, 24 bits (72 dB dynamic range), 8 channels analog-to-digital board. Changing only the composition of the low- and band-pass filters in front of the Golay cell, the telescope can be setup to detect very different frequency bands; making the instrument very versatile. In this article we describe the telescope characteristics and its development status. Moreover, we give estimates of the expected fluxes during flares.
RHESSI Science Nuggets #404 March **2021**
https://sprg.ssl.berkeley.edu/~tohban/wiki/index.php/The_Superflare_SOL2017-09-06:_from_submm_to_mid-IR

The 6 September 2017 X9 Super Flare Observed From Submillimeter to Mid-IR

C. G. Giménez **de Castro**, J.-P. Raulin, J. F. Valle Silva, P. J. A. Simões, A. S. Kudaka, A. Valio
Space Weather Volume16, Issue9 Pages 1261-1268 **2018**
http://sci-hub.tw/10.1029/2018SW001969
Active Region 12673 is the most productive active region of solar cycle 24: in a few days of early September 2017, four X-class and 27 M-class flares occurred. SOL2017-09-06T12:00, an X9.3 flare also produced a two-ribbon white light emission across the sunspot detected by Solar Dynamics Orbiter/Helioseismic and Magnetic Imager. The flare was observed at 212 and 405 GHz with the arcminute-sized beams of the Solar Submillimeter Telescope focal array while making a solar map and at 10 μm, with a 17 arcsec diffraction-limited infrared camera. Images at 10 μm revealed that

the sunspot gradually increased in brightness while the event proceeded, reaching a temperature similar to quiet Sun values. From the images we derive a lower bound limit of 180-K flare peak excess brightness temperature or 7,000 sfu if we consider a similar size as the white light source. The rising phase of mid-IR and white light is similar, although the latter decays faster, and the maximum of the mid-IR and white light emission is ~200 s delayed from the 15.4-GHz peak occurrence. The submillimeter spectrum has a different origin than that of microwaves from 1 to 15 GHz, although it is not possible to draw a definitive conclusion about its emitting mechanism.

High frequency physics and sub-THz emission

Guillermo Giménez **de Castro**
CESRA Abstract **2016**
http://cesra2016.sciencesconf.org/conference/cesra2016/pages/CESRA2016_prog_abs_book_v1.pdf
If we consider high frequency as the frequency frontier of astronomical detectors imposed by the current technology, a broad band above 100 GHz and below the IR can be included. The interest in this particular spectral range can be measured in the number of new facilities that are being constructed or already installed in the last 15 years. The expectation for solar physics is to unveil the dynamics of very high energy particles during flares, and / or to diagnose low atmospheric layers. But in essence is the curiosity to see where nobody has seen before. In this talk we review the last 15 years of continuous high frequency observations, their interpretations and the perspectives for the years to come. The most impressive results were obtained during flares: it is now accepted the existence of a different spectral component at high frequencies that is visible only during some flares. Different speculations have been made to explain this second spectral component, but the lack of a more detailed description in frequency, in polarization and in spatial distribution have precluded a definite conclusion. The episodic characteristic draws more relevance to the new spectral component for it must be due to a very peculiar origin. Although our focus are flares; we also present relevant and previously unknown characteristics of quiescent structures at these high frequencies. In the next years we hope to address some of the present observing mentioned deficiencies, since the ALMA interferometer with its receivers from 100 to 1000 GHz, is starting to offer solar observations and the LLAMA single dish antenna, to start working in a couple of years and with a similar receiver setup as ALMA, is preparing a solar observing program. Moreover, THz telescopes are being built and may start sooner rather than later to give new insights in this spectral realm

Analysis of intermittency in submillimeter radio and Hard X-Rays during the impulsive phase of a solar flare

C. Guillermo Giménez **de Castro**, Paulo J. A. Simões, Jean-Pierre Raulin, Odilon M. Guimarães Jr
Solar Phys. Volume 291, Issue 7, pp 2003–2016 **2016**
http://arxiv.org/pdf/1605.07677v1.pdf
We present an analysis of intermittent processes occurred during the impulsive phase of the flare SOL**2012-03-13**, using hard X-rays and submillimeter radio data. Intermittency is a key characteristic in turbulent plasmas and have been a analyzed recently for Hard X-rays data only. Since in a typical flare the same accelerated electron population is believed to produce both Hard X-rays and gyrosynchrotron, we compare both time profiles searching for intermittency signatures. For that we define a cross-wavelet power spectrum, that is used to obtain the Local Intermittency Measure or LIM. When greater than 3, the square LIM coefficients indicate a local intermittent process. The LIM 2 coefficient distribution in time and scale helps to identify avalanche or cascade energy release processes. We find two different and well separated intermittent behaviors in the submillimeter data: for scales greater than 20 s, a broad distribution during the rising and maximum phases of the emission seems to favor a cascade process; for scales below 1 s, short pulses centered on the peak time, are representative of avalanches. When applying the same analysis to Hard X-rays, we find only the scales above 10 s producing a distribution related to a cascade energy fragmentation. Our results suggest that different acceleration mechanisms are responsible for tens of keV and MeV energy ranges of electrons.
See CESRA highlight #1013, Nov **2016** http://www.astro.gla.ac.uk/users/eduard/cesra/?p=1013

A Burst with Double Radio Spectrum Observed up to 212 GHz

C. G. Giménez **de Castro**, G. D. Cristiani, P. J. A. Simões, C. H. Mandrini, E. Correia, P. Kaufmann
Solar Physics, June **2013**, Volume 284, Issue 2, pp 541-558
We study a solar flare that occurred on **10 September 2002**, in active region NOAA 10105, starting around 14:52 UT and lasting approximately 5 minutes in the radio range. The event was classified as M2.9 in X-rays and 1N in Hα. Solar Submillimeter Telescope observations, in addition to microwave data, give a good spectral coverage between 1.415 and

212 GHz. We combine these data with ultraviolet images, hard and soft X-ray observations, and full-disk magnetograms. Images obtained from Ramaty High Energy Solar Spectroscopic Imager data are used to identify the locations of X-ray sources at different energies, and to determine the X-ray spectrum, while ultraviolet images allow us to characterize the coronal flaring region. The magnetic field evolution of the active region is analyzed using Michelson Doppler Imager magnetograms. The burst is detected at all available radio frequencies. X-ray images (between 12 keV and 300 keV) reveal two compact sources. In the 212 GHz data, which are used to estimate the radio-source position, a single compact source is seen, displaced by 25″ from one of the hard X-ray footpoints. We model the radio spectra using two homogeneous sources, and we combine this analysis with that of hard X-rays to understand the dynamics of the accelerated particles. Relativistic particles, observed at radio wavelengths above 50 GHz, have an electron index evolving with the typical soft–hard–soft behavior.

Submillimeter and X-ray observations of an X Class flare

Gimenez **de Castro**, C.G., Trottet, G., Silva-Valio, A., Krucker, S., Costa, J.E.R., Kaufmann, P., Correia, E., Levato, H

E-print, Aug **2009**; A&A

The GOES X1.5 class flare that occurred on **August 30,2002** at 1327:30 UT is one of the few events detected so far at submillimeter wavelengths. We present a detailed analysis of this flare combining radio observations from 1.5 to 212 GHz (an upper limit of the flux is also provided at 405 GHz) and X-ray. Although the observations of radio emission up to 212 GHz indicates that relativistic electrons with energies of a few MeV were accelerated, no significant hard X-ray emission was detected by RHESSI above ~250 keV. Images at 12-20 and 50-100 keV reveal a very compact, but resolved, source of about ~10"x10". EUV TRACE images show a multi-kernel structure suggesting a complex (multipolar) magnetic topology. During the peak time the radio spectrum shows an extended flatness from ~7 to 35 GHz. Modeling the optically thin part of the radio spectrum as gyrosynchrotron emission we obtained the electron spectrum (spectral index delta, instantaneous number of emitting electrons). It is shown that in order to keep the expected X-ray emission from the same emitting electrons below the RHESSI background at 250 keV, a magnetic field above 500 G is necessary. On the other hand, the electron spectrum deduced from radio observations >=50 GHz is harder than that deduced from ~70-250 keV X-ray data, meaning that there must exist a breaking energy around a few hundred keV. During the decay of the impulsive phase, a hardening of the X-ray spectrum is observed which is interpreted as a hardening of the electron distribution spectrum produced by the diffusion due to Coulomb collisions of the trapped electrons in a medium with an electron density of n_e ~ 3E10 - 5E10 cm-3.

The Chromospheric Solar Limb Brightening at Radio, Millimeter, Sub-millimeter, and Infrared Wavelengths

Victor **De la Luz**

ApJ **825** 138 **2016**

http://arxiv.org/pdf/1605.01355v1.pdf

Observations of the emission at radio, millimeter, sub-millimeter, and infrared wavelengths in the center of the solar disk validate the auto-consistence of semi-empirical models of the chromosphere. Theoretically, these models must reproduce the emission at the solar limb. In this work, we tested both the VALC and the C7 semi-empirical models by computing their emission spectrum in the frequency range from 2 GHz to 10 THz, at solar limb altitudes. We calculate the Sun's theoretical radii as well as their limb brightening. Non-Local Thermodynamic Equilibrium (NLTE) was computed for hydrogen, electron density, and H-. In order to solve the radiative transfer equation a 3D geometry was employed to determine the ray paths and Bremsstrahlung, H-, and inverse Bremsstrahlung opacity sources were integrated in the optical depth. We compared the computed solar radii with high resolution observations at the limb obtained by Clark (1994). We found that there are differences between observed and computed solar radii of 12000 km at 20 GHz, 5000 km at 100 GHz, and 1000 km at 3 THz for both semi-empirical models. A difference of 8000 km in the solar radii was found comparing our results against heights obtained from H{\alpha} observations of spicules-off at the solar limb. We conclude that the solar radii can not be reproduced by VALC and C7 semi-empirical models at radio - infrared wavelengths. Therefore, the structures in the high chromosphere provides a better measurement of the solar radii and their limb brightening as shown in previous investigations.

Solar Limb Theoretical Tomography at Millimeter, Sub-millimeter, and Infrared Wavelengths

Victor **De la Luz**, J. A. Gonzalez-Esparza, P. Corona-Romero, J. Mejia-Ambriz
Advances in Space Research **2016**
http://arxiv.org/pdf/1604.07719v1.pdf
Semi-empirical models of the solar Chromosphere show in their emission spectrum, tomography property at millimeter, sub-millimeter, and infrared wavelengths for the center of the solar disk. In this work, we studied this property in the solar limb using our numerical code PakalMPI, focusing in the region where the solar atmosphere becomes optically thick. Individual contribution of Bremsstrahlung and H- opacities was take into account in the radiative transfer process. We found that the tomography property remains in all the spectrum region under study at limb altitudes. For frequencies be- tween 2 GHz and 5 THz the contribution of Bremsstrahlung is the dominant process above the solar limb.

The Chromospheric Solar Millimeter-wave Cavity; a Common Property in the Semi-empirical Models

De la Luz Victor, Chavez Miguel, Bertone Emanuele
Geofisica Internacional, **2014**
http://arxiv.org/pdf/1407.4404v1.pdf
The semi-empirical models of the solar chromosphere are useful in the study of the solar radio emission at millimeter - infrared wavelengths. However, current models do not reproduce the observations of the quiet sun. In this work we present a theoretical study of the radiative transfer equation for four semi- empirical models at these wavelengths. We found that the Chromospheric Solar Milimeter-wave Cavity (CSMC), a region where the atmosphere becomes locally optically thin at millimeter wavelengths, is present in the semi-empirical models under study. We conclude that the CSMC is a general property of the solar chromosphere where the semi-empirical models shows temperature minimum.

The Relation Between the Radial Temperature Profile in the Chromosphere and the Solar Spectrum at Centimeter, Millimeter, Submillimeter, and Infrared Wavelengths

V. **De la Luz**, M. Chavez, E. Bertone, G. Gimenez de Castro
Solar Physics , Volume 289, Issue 8, pp 2879-2889 **2014**
Solar observations from millimeter to ultraviolet wavelengths show that there is a temperature minimum between photosphere and chromosphere. Analyses based on semi-empirical models locate this point at about 500 km above the photosphere. The consistency of these models has been tested by means of millimeter to infrared observations. We show that variations of the theoretical radial temperature profile near the temperature minimum impact the brightness temperature at centimeter, submillimeter, and infrared wavelengths, but the millimeter wavelength emission remains unchanged. We found a region between 500 and 1000 km above the photosphere that remains hidden to observations at the frequencies that we studied here.

THE CHROMOSPHERIC SOLAR MILLIMETER-WAVE CAVITY ORIGINATES IN THE TEMPERATURE MINIMUM REGION

Victor **De la Luz1**,2, Jean-Pierre Raulin3, and Alejandro Lara
2013 ApJ 762 84
We present a detailed theoretical analysis of the local radio emission at the lower part of the solar atmosphere. To accomplish this, we have used a numerical code to simulate the emission and transport of high-frequency electromagnetic waves from 2 GHz up to 10 THz. As initial conditions, we used VALC, SEL05, and C7 solar chromospheric models. In this way, the generated synthetic spectra allow us to study the local emission and absorption processes with high resolution in both altitude and frequency. Associated with the temperature minimum predicted by these models, we found that the local optical depth at millimeter wavelengths remains constant, producing an optically thin layer that is surrounded by two layers of high local emission. We call this structure the Chromospheric Solar Millimeter-wave Cavity (CSMC). The temperature profile, which features temperature minimum layers and a subsequent temperature rise, produces the CSMC phenomenon. The CSMC shows the complexity of the relation between the theoretical temperature profile and the observed brightness temperature and may help us to understand the dispersion of the observed brightness temperature in the millimeter wavelength range.
Erratum: 2015 ApJ 802 142

SYNTHETIC SPECTRA OF RADIO, MILLIMETER, SUB-MILLIMETER, AND INFRARED REGIMES WITH NON-LOCAL THERMODYNAMIC EQUILIBRIUM APPROXIMATION

Victor **De la Luz**1,2, Alejandro Lara1 and Jean-Pierre Raulin

2011 ApJ 737 1

We use a numerical code called PAKALMPI to compute synthetic spectra of the solar emission in quiet conditions at millimeter, sub-millimeter, and infrared wavelengths. PAKALMPI solves the radiative transfer equation, with non-local thermodynamic equilibrium (NLTE), in a three-dimensional geometry using a multiprocessor environment. The code is able to use three opacity functions: classical bremsstrahlung, H–, and inverse bremsstrahlung. In this work, we have computed and compared two synthetic spectra, one in the common way: using bremsstrahlung opacity function and considering a fully ionized atmosphere; and a new one considering bremsstrahlung, inverse bremsstrahlung, and H– opacity functions in NLTE. We analyzed in detail the local behavior of the low atmospheric emission at 17, 212, and 405 GHz (frequencies used by the Nobeyama Radio Heliograph and the Solar Submillimeter Telescope). We found that the H– is the major emission mechanism at low altitudes (below 500 km) and that at higher altitudes the classical bremsstrahlung becomes the major mechanism of emission. However, the brightness temperature remains unalterable. Finally, we found that the inverse bremsstrahlung process is not important for radio emission at these heights.

Synoptic observations at centimetric wavelengths are needed for a better description of solar forcing on the upper atmosphere

Thierry Dudok **De Wit**_y1, Sean Bruinsma2, Louis Hecker , Cl_emence Le F_evre , Pascal Perrachon , and Philippe Yaya

CESRA **2016**, p.80

Dudok de Wit, T., & Bruinsma, S. (2017). The 30 cm radio flux as a solar proxy for thermosphere density modelling *Journal of Space Weather and Space Climate, 7* DOI: **10.1051/swsc/2017008**

http://www.swsc-journal.org.sci-hub.cc/articles/swsc/abs/2017/01/swsc160042/swsc160042.html

http://cesra2016.sciencesconf.org/conference/cesra2016/pages/CESRA2016_prog_abs_book_v3.pdf

While the F10.7 index (ux at 10.7 cm) is probably the most widely used proxy for solar activity, radio emissions at other centimetric wavelengths are also good tracers. In particu- lar, the radio ux at 30 cm has an important contribution from thermal emissions, making it more sensitive to solar features such as plages an faculae. In contrast, the F10.7 index has a strong contribution from gyroemissions, and is a better proxy for the energetic part of the UV spectrum.

By replacing the F10.7 index by the 30 cm ux, we recently found that the performance of the DTM2013 model for satellite drag improves. By using blind source separation, we showed how the solar rotational variability in these centimetric wavelengths is made out of three contributions, one of which is thermal.

These properties of the 30 cm ux have motivated us to set up a prototype service that col- lects daily values at several wavelengths from the Nobeyama radio observatory, pre-processes them, and _nally delivers them in near real-time (with a forecast) for upper atmospheric mod- elling.

Here we discuss the di_erences between the F10.7 index and other centimetric wavelengths, and show why it is essential to consider multi-wavelength observations for achieving a better description of solar forcing on the upper atmosphere.

CESRA highlight #1423 June 2017 http://www.astro.gla.ac.uk/users/eduard/cesra/?p=1423

Synoptic radio observations as proxies for upper atmosphere modelling

Dudok **de Wit**, T., Bruinsma, S., and Shibasaki, K.

(**2014**), Space Weather Space Climate, 4(26):A06

https://www.swsc-journal.org/articles/swsc/pdf/2014/01/swsc130037.pdf

The specification of the upper atmosphere strongly relies on solar proxies that can properly reproduce the solar energetic input in the UV. Whilst the microwave flux at 10.7 cm (also called F10.7 index) has been routinely used as a solar proxy, we show that the radio flux at other wavelengths provides valuable complementary information that enhances their value for upper atmospheric modelling. We merged daily observations from various observatories into a single homogeneous data set of fluxes at wavelengths of 30, 15, 10.7, 8 and 3.2 cm, spanning from 1957 to today. Using blind source separation (BSS), we show that their rotational modulation contains three contributions, which can be interpreted in terms of thermal bremsstrahlung and gyro-resonance emissions. The latter account for 90% of the rotational variability in the F10.7 index. Most solar proxies, such as the MgII index, are remarkably well reconstructed by simple linear combination of radio fluxes at various wavelengths. The flux at 30 cm stands out as an excellent proxy and is

better suited than the F10.7 index for the modelling the thermosphere-ionosphere system, most probably because it receives a stronger contribution from thermal bremsstrahlung. This better performance is illustrated here through comparison between the observed thermospheric density, and reconstructions by the Drag Temperature Model.

A single picture for solar coronal outflows and radio noise storms

G. **Del Zanna**1, G. Aulanier2, K.-L. Klein2, and T. T¨or¨ok2

E-print, Sept **2010, File**; A&A 526, A137 (**2011**)

We propose a unified interpretation for persistent coronal outflows and metric radio noise storms, two phenomena typically observed in association with quiescent solar active regions. Our interpretation is based on multi-wavelength observations of two such regions as they crossed the meridian in **May and July 2007**. For both regions, we observe a persistent pattern of blue-shifted coronal emission in high-temperature lines with Hinode/EIS, and a radio noise storm with the Nanc?ay Radioheliograph. The observations are supplemented by potential and linear force-free extrapolations of the photospheric magnetic field over large computational boxes, and by a detailed analysis of the coronal magnetic field topology. We find true separatrices in the coronal field and null points high in the corona, which are preferential locations for magnetic reconnection and electron acceleration. We suggest that the continuous growth of active regions maintains a steady reconnection across the separatrices at the null point. This interchange reconnection occurs between closed, high-density loops in the core of the active region and neighbouring open, low-density flux tubes. Thus, the reconnection creates strong pressure imbalances which are the main drivers of plasma upflows. Furthermore, the acceleration of low-energy electrons in the interchange reconnection region sustains the radio noise storm in the closed loop areas, as well as weak type III emission along the open field lines. For both active regions studied, we find a remarkable agreement between the observed places of persistent coronal outflows and radio noise storms with their locations as predicted by our interpretation.

Initiation and Development of the white-light and radio CME on 15 April 2001

P. **Demoulin**, A. Vourlidas, M. Pick, A. Bouteille

E-print, 9 March **2012, File**; **2012** ApJ 750 147

The 2001 April 15 event was one of the largest of the last solar cycle. A former study (Maia et al., 2007) established that this event was associated with a coronal mass ejection (CME) observed both at white light and radio frequencies. This radio CME is illuminated by synchrotron emission from relativistic electrons. In this paper, we investigate the relation of the radio CME to its extreme ultraviolet (EUV) and white light counterpart and reach four main conclusions. i) The radio CME corresponds to the white light flux rope cavity. ii) The presence of a reconnecting current sheet behind the erupting flux rope is framed, both from below and above, by bursty radio sources. This reconnection is the source of relativistic radiating electrons which are injected down along the reconnected coronal arches and up along the flux rope border forming the radio CME. iii) Radio imaging reveals an important lateral over expansion in the low corona; this over expansion is at the origin of compression regions where type II and III bursts are imaged. iv) Already in the initiation phase, radio images reveal large scale interactions of the source active region with its surroundings, including another active region and open magnetic fields. Thus, these complementary radio, EUV, white light data validate the flux rope eruption model of CMEs.

ERRATUM: 2012 ApJ 754 156

Decametric N burst: a consequence of the interaction of two coronal mass ejections

Demoulin, P., Klein, K.L., Goff, C.P., van Driel-Gesztelyi, L., Culhane, J.L., Mandrini, C.H., Matthews, S.A., Harra, L.K.

Solar Phys., 240 (2), Page: 301 – 313, **2007, File**

E-print, Oct 2006

Reconnection of the expanding ejecta with the magnetic structure of a previous CME, launched about 8 hours earlier, injects electrons in the same manner as with type III bursts but into open field lines having a local dip and apex.

See **CESRA highlight** https://www.astro.gla.ac.uk/users/eduard/cesra/?p=298

The Korean Solar Radio Burst Locator (KSRBL)

http://kswrc.kasi.re.kr/en/about/facilities/ksrbl

Korean Solar Radio Burst Locator (KSRBL) is a single dish radio spectrograph, which has been developed in collaboration with New Jersey Institute of Technology and installed at KASI in August 2009. KSRBL records the spectra of solar microwave bursts with high time and frequency resolution, and locates their positions on the solar disk. Solar radio burst needs to be continuously monitored as it could disturb many kinds of high-tech radio instruments such

as cellular phone, GPS, and radar. The data of KSRBL are used in solar flare research and space weather forecast in the future. **7 June 2013**

Comparative analysis of solar radio bursts before and during CME propagation

G.**Dididze**, B.M. Shergelashvili, V.N. Melnik, V.V. Dorovskyy, A.I. Brazhenko, S. Poedts, T.V. Zaqarashvili, M. Khodachenko
A&A 625, A63 **2019**
https://arxiv.org/pdf/1903.12279.pdf
sci-hub.se/10.1051/0004-6361/201629489
Context. As is well known, CME propagation often results in the fragmentation of the solar atmosphere on smaller regions of density (magnetic field) enhancement (depletion). It is expected that this type of fragmentation may have radio signatures.
Aims. The general aim of the present paper is to perform a comparative analysis of type III solar and narrow-band type-III-like radio burst properties before and during CME events, respectively. The main goal is to analyze radio observational signatures of the dynamical processes in solar corona. In particular, we aim to perform a comparison of local plasma parameters without and with CME propagation, based on the analysis of decameter radio emission data.
Methods. In order to examine this intuitive expectation, we performed a comparison of usual type III bursts before the CME with narrow-band type-III-like bursts, which are observationally detectable on top of the background type IV radio bursts associated with CME propagation. We focused on the analysis of in total 429 type III and 129 narrow-band type-III-like bursts. We studied their main characteristic parameters such as frequency drift rate, duration, and instantaneous frequency bandwidth using standard statistical methods. Furthermore, we inferred local plasma parameters (e.g., density scale height, emission source radial sizes) using known definitions of frequency drift, duration, and instantaneous frequency bandwidth.
Results. The analysis reveals that the physical parameters of coronal plasma before CMEs considerably differ from those during the propagation of CMEs (the observational periods 2 and 4 with type IV radio bursts associated with CMEs). Local density radial profiles and the characteristic spatial scales of radio emission sources vary with radial distance more drastically during the CME propagation compared to the cases of quasistatic solar atmosphere without CME(s) (observational periods 1 and 3).
Conclusions. The results of the work enable us to distinguish different regimes of plasma state in the solar corona. Our results create a solid perspective from which to develop novel tools for coronal plasma studies using radio dynamic spectra. **2014-06-13**

Correlated oscillations due to similar multi-path effects seen in two widely separated radio telescopes

P.N. **Diep**, N.T. Phuong, P. Darriulat, P.T. Nhung, P.T. Anh, P.N. Dong, D.T. Hoai, N.T. Thao
Publ. Astron. Soc. Aust.31, e029, **2014**
http://arxiv.org/pdf/1405.1525v1.pdf
A multipath mechanism similar to that used in Australia sixty years ago by the Sea-cliff Interferometer is shown to generate correlations between the periods of oscillations observed by two distant radio telescopes pointed to the Sun. The oscillations are the result of interferences between the direct wave detected in the main antenna lobe and its reflection on ground detected in a side lobe. A model is made of such oscillations in the case of two observatories located at equal longitudes and opposite tropical latitudes, respectively in Ha Noi (Viet Nam) and Learmonth (Australia), where similar radio telescopes are operated at 1.4 GHz. Simple specular reflection from ground is found to give a good description of the observed oscillations and to explain correlations that had been previously observed and for which no satisfactory interpretation, instrumental or other, had been found.

Is the enhancement of type II radio bursts during CME interactions related to the associated solar energetic particle event?

Liu-Guan **Ding**, Zhi-Wei Wang, Li Feng, Gang Li, Yong Jiang
Research in Astronomy and Astrophysics **2018**
https://arxiv.org/pdf/1808.04720.pdf
We investigated 64 pairs of interacting-CME events identified by the simultaneous observations of SOHO and STEREO spacecraft from 2010 January to 2014 August, to examine the relationship between the large SEP events in the energy of 25-60MeV and the properties of the interacting CMEs. We found that during CME interactions the large SEP events in this study were all generated by CMEs with the presence of enhanced type II radio bursts, which also have wider

longitudinal distributions comparing to events with the absence of type II radio burst or its enhancement (almost associated with small SEP events). It seems that the signature of type II radio bursts enhancement is a good discriminator between large SEP and small or none SEP event producers during CME interactions. The type II radio burst enhancement is more likely to be generated by CME interactions, with the main CME having larger speed (v), angular width (WD), mass (m) and kinetic energy (E_k), that taking over the preceding CMEs which also have higher v, WD, m and E_k, than those preceding CMEs in CME pairs missing the type II radio bursts or enhancements. Our analysis also revealed that the intensities of associated SEP events correlate negatively with the intersection height of the two CMEs. Most of type-II-enhanced events and SEP events are coincidentally and almost always made by the fast and wide main CMEs that sweeping fully over a relatively slower and narrower preceding CMEs. We suggest that a fast CME with enough energy completely overtaking a relatively narrower preceding CME, especially in low height, can drive more energetic shock signified by the enhanced type II radio bursts. The shock may accelerate ambient particles and lead to large SEP event more easily.

2014.08.25, 2014.08.28

Table 1 The properties of two interacting CMEs (2010-2014)

Interaction between Two Coronal Mass Ejections in the 2013 May 22 Large Solar Energetic Particle Event

Liu-Guan **Ding**1,2, Gang Li2, Yong Jiang3, Gui-Ming Le4, Cheng-Long Shen5, Yu-Ming Wang5, Yao Chen6, Fei Xu1, Bin Gu1, and Ya-Nan Zhang

2014 ApJ 793 L35.

We investigate the eruption and interaction of two coronal mass ejections (CMEs) during the large **2013 May 22** solar energetic particle event using multiple spacecraft observations. Two CMEs, having similar propagation directions, were found to erupt from two nearby active regions (ARs), AR11748 and AR11745, at ~08:48 UT and ~13:25 UT, respectively. The second CME was faster than the first CME. Using the graduated cylindrical shell model, we reconstructed the propagation of these two CMEs and found that the leading edge of the second CME caught up with the trailing edge of the first CME at a height of ~6 solar radii. After about two hours, the leading edges of the two CMEs merged at a height of ~20 solar radii. **Type II solar radio bursts showed strong enhancement during this two hour period.** Using the velocity dispersion method, we obtained the solar particle release (SPR) time and the path length for energetic electrons. Further assuming that energetic protons propagated along the same interplanetary magnetic field, we also obtained the SPR time for energetic protons, which were close to that of electrons. These release times agreed with the time when the second CME caught up with the trailing edge of the first CME, indicating that the CME-CME interaction (and shock-CME interaction) plays an important role in the process of particle acceleration in this event.

Forward Modeling of EUV and Gyrosynchrotron Emission from Coronal Plasmas with FoMo

Tom Van **Doorsselaere**, Patrick Antolin, Ding Yuan, Veronika Reznikova, and Norbert Magyar

Front. Astron. Space Sci., 3:4. **2016** |

https://www.frontiersin.org/articles/10.3389/fspas.2016.00004/full

https://doi.org/10.3389/fspas.2016.00004

The FOMO code was developed to calculate the EUV and UV emission from optically thin coronal plasmas. The input data for FOMO consists of the plasma density, temperature and velocity on a 3D grid. This is translated to emissivity on the 3D grid, using CHIANTI data. Then, the emissivity is integrated along the line-of-sight (LOS) to calculate the emergent spectral line for synthetic spectrometer observations. The code also generates the emission channels for synthetic AIA imaging observations. Moreover, the code has been extended to model also the gyrosynchrotron emission from plasmas with a population of non-thermal particles. In this case, also optically thick plasmas may be modeled. The radio spectrum is calculated over a large wavelength range, allowing for the comparison with data from a wide range of radio telescopes.

Properties of individual S-bursts observed in the frequency band of 10-32 MHz during the rising phase of 25-th solar cycle

Vladimir **Dorovskyy**, Valentin Melnik, Anatolii Brazhenko, and Anatolii Frantsuzenko

Front. Astron. Space Sci., Volume 11 : 1403135 **2024**

https://doi.org/10.3389/fspas.2024.1403135

https://www.frontiersin.org/journals/astronomy-and-space-sciences/articles/10.3389/fspas.2024.1403135/full

The properties of the S-bursts observed during the storm on **20–21 June 2022** in frequency band 10–32 MHz by the radio telescope URAN-2 are discussed in this paper. The storm was highly populated with other solar bursts, such as Type III bursts and drift pairs. The occurrence rate of S-bursts was very high reaching 60 bursts per minute. All

observed S-bursts were characterized by low fluxes with respect to the background radio emission. Thus special processing methods are used to retrieve spectral properties of the bursts. Some individual “long” S-bursts covered the whole frequency band of the URAN-2 radio telescope from 10 to 32 MHz. Such extended in frequency S-bursts were recorded for the first time. 50 extended S-bursts were selected for the further analysis.

Ground Based Support of the Space Mission Parker Performed with Ukrainian Low Frequency Radio Telescopes

Vladimir **Dorovskyy**, Valentin Melnik, Anatolii Brazhenko
Radio Physics and Radio Astronomy. Vol. 28, No. 2, **2023**
https://arxiv.org/ftp/arxiv/papers/2307/2307.03016.pdf
The purpose of this work is to demonstrate the effectiveness of ground-based support for space missions, primarily PSP, using large Ukrainian decameter radio telescopes. Another goal of the work is to carry out cross calibration of the radiometers onboard spacecraft using the calibrated data of the ground-based radio telescopes. One of the most common methods of remote diagnostics of the solar corona is the study of radio emission, the sources of which are located in the solar corona at different heliocentric altitudes. The technique of joint space terrestrial observations consists in the simultaneous observation of individual events and their analysis in the widest possible frequency band during the maximum approach of the PSP vehicle to the Sun. At the same time, observation in the common frequency band is proposed to be used for calibration of the onboard radio receivers. The methods of planning joint space terrestrial observations are substantiated. Using the data of the UTR 2, URAN 2 radio telescopes and the PSP probe, the dynamic and polarization spectra of the simultaneously observed bursts on **June 9, 2020** were obtained. The identification and comparison of individual bursts was carried out. A common dynamic spectrum of the bursts in the frequency band 0.5 ... 32 MHz was obtained. Cross calibration of the HFR receiver of the FIELDS PSP module in the frequency band 10...18 MHz was made using the calibrated data of terrestrial radio telescopes. The effectiveness of ground-based support of the PSP mission by the large Ukrainian radio telescopes is shown. Examples of joint observations are given, and the method of cross calibration of the FIELD PSP module receivers is demonstrated. Prospects for further ground based support for solar space missions are presented

Solar Type U Burst Associated with a High Coronal Loop

V. V. **Dorovskyy**, V. N. Melnik, A. A. Konovalenko, S. N. Yerin, I. N. Bubnov
296, Article number: 1 (**2021**)
https://arxiv.org/ftp/arxiv/papers/2012/2012.08991.pdf
https://link.springer.com/content/pdf/10.1007/s11207-020-01741-w.pdf
An inverted U burst with equally developed ascending and descending branches observed by Giant Ukrainian Radio Telescope (GURT) on **18 April 2017** in meter wavelengths band is discussed. This U burst was attributed to the high coronal loop above the limb active region NOAA 12651. Under the assumption that, associated with the burst, the coronal loop confines isothermal plasma stratified according to a Boltzmann density relation, the geometrical and physical parameters of the loop were estimated. According to our model coronal loops may contain plasma which is up to 20 times denser than the surrounding coronal plasma. In general the proposed model gives the relation between the plasma temperature and the height of the loop in such a way that under the given parameters of the associated U burst, higher loops contain cooler plasma and vice versa. An alternative method of coronal loop height determination was suggested. Assuming that the observed U burst and the preceding type III burst were generated by the same exciter we define the height of the loop from the delay of the former with respect to the latter at certain frequency. We show that defining of coronal loops heights by another independent method, e.g. interferometric or tied-array imaging may solve the uncertainty of the inside-the-loop plasma temperature determination.

Spatial properties of the complex decameter type II burst observed on 31 May 2013

V.V. **Dorovskyy**, V.N. Melnik, A.A. Konovalenko, A.I. Brazhenko, H.O. Rucker
Sun and Geosphere, vol.13, no.1, p.25-30, (**2018**)
https://arxiv.org/pdf/2308.00552
http://newserver.stil.bas.bg/SUNGEO//00SGArhiv/SG_v13_No1_2018-pp-25-30.pdf
We present the results of observations of complex powerful type II burst associated with narrow Earth-directed CME, which was ejected at around 11 UT on **31 May 2013**. The observations were performed by radio telescope UTR-2, which operated as local interferometer, providing the possibility of detection of the spatial parameters of the radio emission source. There are also polarization data from URAN-2 radio telescope. The CME was detected by two space-born coronagraphs SOHO/LASCO/C2 and STEREO/COR1-BEHIND, and was absolutely invisible for STEREO-AHEAD spacecraft. The associated type II burst consisted of two successive parts of quite different appearance on the dynamic spectrum. The first burst was narrow in frequency, had cloudy structure and was completely unpolarized while

the second one represented rich herring-bone structure and exposed high degree of circular polarization. Both parts of the whole event reveal band splitting and well distinguished harmonic structure. The positions and sizes of the sources of the type II burst were found using cross-correlation functions of interferometer bases. The sources of the type II bursts elements were found to be of about 15 arcmin in size in average, with the smallest ones reaching as low as 10 arcmin. Corresponding brightness temperatures were estimated. In most cases these temperatures were between 1011 and 1012 K with maximum value as high as 1014 K. The spatial displacement of the source was measured and model independent velocities of the type II burst sources were determined.

Decameter U-burst Harmonic Pair from a High Loop

Dorovskyy, Melnik, Konovalenko, Bubnov , Gridin, Shevchuk, Rucker, Poedts and Panchenko
CESRA highlight **2016** p.692
http://www.astro.gla.ac.uk/users/eduard/cesra/?p=692
We discuss the results of recent observations of a solar U-burst harmonic pair in the frequency range 10-70 MHz, performed by the radio telescope UTR-2 and the recently built first section of the new Giant Ukrainian Radio Telescope (GURT) (see Dorovskyy et al. 2015). A considerably extended frequency range of the new telescope makes the detection of harmonically connected pairs much more probable. In particular, we focus on interpreting the time delay between the harmonic (H) and fundamental (F) components of the burst, which appeared to be as large as 7 s. It's rather difficult to estimate the F-to-H mutual delay using type III harmonic pairs since they have smooth spectra lacking any specific "reference markers". U-bursts [see also previous CESRA nugget on N and U bursts] do have such reference markers – the U-bursts turnover points. The explanation of the delay is based on the difference of group velocities of H and F waves during their travel inside a high, hot and dense coronal loop**. 8 August 2012**

Decameter U-burst Harmonic Pair from a High Loop

V. V. **Dorovskyy**, V. N. Melnik, A. A. Konovalenko, I. N. Bubnov, A. A. Gridin, N. V. Shevchuk, H. O. Rucker, S. Poedts, M. Panchenko
Solar Physics, January **2015**, Volume 290, Issue 1, pp 181-192
The results of the first observations of solar sporadic radio emission within 10 – 70 MHz by theGiant Ukrainian Radio Telescope (GURT) are presented and discussed. Observations in such a wide range of frequencies considerably facilitate the registration of harmonic pairs. The solar U-burst harmonic pair observed on **8 August 2012** is analyzed. The burst key features were determined. Among them, the time delay between the fundamental and harmonic emissions was of special interest. The fundamental emission was delayed for 7 s with respect to the harmonic emission. A model for explaining the occurrence of such a delay is proposed, in which the emission source is located inside a magnetic loop containing plasma of increased density. In this case, the delay appears due to the difference in group velocities of electromagnetic waves at the fundamental and the harmonic frequencies.
See CESRA Highlight, 2016 http://www.astro.gla.ac.uk/users/eduard/cesra/?p=692

Fine and Superfine Structure of the Decameter–Hectometer Type II Burst on 7 June 2011

V. V. **Dorovskyy**, V. N. Melnik, A. A. Konovalenko, A. I. Brazhenko, M. Panchenko, S. Poedts, V. A. Mykhaylov
Solar Phys., Volume 290, Issue 7, pp 2031-2042 **2015**
http://arxiv.org/pdf/1508.06801v1.pdf
The characteristics of a type II burst with a herringbone structure observed both with ground-based radio telescopes (UTR-2 and URAN-2) and space-borne spectrometers (STEREO-A and B) are discussed. The burst was recorded on **7 June 2011** in the frequency band 3 – 33 MHz. It was characterized by extremely rich fine structure. Statistical analysis of more than 300 herringbone sub-bursts constituting the burst was performed separately for the positively (reverse) and negatively (forward) drifting sub-bursts. The sense and the degree of circular polarization of the herringbone sub-bursts were measured in a wide frequency band (16 – 32 MHz). A second-order fine frequency structure of the herringbone sub-bursts was observed and studied for the first time. Using STEREO/COR1 and SOHO/LASCO-C2 images, we determined the direction and radial speed of the coronal mass ejection responsible for the studied type II burst. The possible location of the type II burst source on the flank of the shock was found.

Dou, Y., Gary, D. E., Liu, Z., Nita, G. M., Bong, S.-C., Cho, K.-S., Park, Y.-D., & Moon, Y. J.
2009, PASP, 121, 512

This paper describes the design and operation of the Korean Solar Radio Burst Locator (KSRBL). The KSRBL is a radio spectrometer designed to observe solar decimeter and microwave bursts over a wide band (0.245-18 GHz) as well as to detect the burst locations without interferometry or mechanical sweeping. As a prototype, it is temporarily observing at the Owens Valley Radio Observatory (OVRO), California, USA, and after commissioning will be operated at the Korea Astronomy and Space Science Institute (KASI), Daejeon, Republic of Korea. The control system can agilely choose four 500 MHz intermediate frequency (IF) bands (2 GHz instantaneous bandwidth) from the entire 0.245-18 GHz band, with a standard time resolution of 100 ms, although higher time resolution is possible subject to data-rate constraints. To cover the entire band requires 10 tunings, which are therefore completed in 1 s. Each 500 MHz band is sampled at a 1 GS s (gigasample per second) rate, and 4096 time samples are Fast Fourier transformed (FFT) to 2048 subchannels for a frequency resolution of 0.24 MHz. To cover the entire range also requires two different feeds, a dual-frequency Yagi centered at 245 and 410 MHz, and a broadband spiral feed covering 0.5-18 GHz. The dynamic range is 35 dB over the 0.5-18 GHz band, and 55 dB in the 245 and 410 MHz bands, set by using switchable attenuators in steps of 5 dB. Each 500 MHz IF has a further 63 dB of settable analog attenuation. The characteristics of the spiral feed provide the ability to locate flaring sources on the Sun to typically 2'. The KSRBL will provide a broadband view of solar bursts for the purposes of studying solar activity for basic research, and for monitoring solar activity as the source of Space Weather and solar-terrestrial effects.

Injection of solar energetic particles into both loop legs of a magnetic cloud

Nina **Dresing**, Ra?l Gómez-Herrero, Bernd Heber, Miguel Angel Hidalgo, Andreas Klassen, Manuela Temmer, Astrid Veronig

A&A **2016**

http://arxiv.org/pdf/1601.00491v1.pdf

Context. Each of the two Solar TErrestrial RElations Observatory (STEREO) spacecraft carries a Solar Electron and Proton Telescope (SEPT) which measures electrons and protons. Anisotropy observations are provided in four viewing directions: along the nominal magnetic field Parker spiral in the ecliptic towards the Sun (SUN) and away from the Sun (Anti-Sun / ASUN), and towards the north (NORTH) and south (SOUTH). The solar energetic particle (SEP) event on **7 November 2013** was observed by both STEREO spacecraft, which were longitudinally separated by 68? at that time. While STEREO A observed the expected characteristics of an SEP event at a well-connected position, STEREO B detected a very anisotropic bi-directional distribution of near-relativistic electrons and was situated inside a magnetic-cloud-like structure during the early phase of the event.
Aims. We examine the source of the bi-directional SEP distribution at STEREO B. On the one hand this distribution could be caused by a double injection into both loop legs of the magnetic cloud (MC). On the other hand, a mirroring scenario where the incident beam is reflected in the opposite loop leg could be the reason. Furthermore, the energetic electron observations are used to probe the magnetic structure inside the magnetic cloud.
Methods. We investigate in situ plasma and magnetic field observations and show that STEREO B was embedded in an MC-like structure ejected three days earlier on **4 November** from the same active region. We apply a Graduated Cylindrical Shell (GCS) model to the coronagraph observations from three viewpoints as well as the Global Magnetic Cloud (GMC) model to the in situ measurements at STEREO B to determine the orientation and topology of the MC close to the Sun and at 1 AU. We also estimate the path lengths of the electrons propagating through the MC to estimate the amount of magnetic field line winding inside the structure.
Results. The relative intensity and timing of the energetic electron increases in the different SEPT telescopes at STEREO B strongly suggest that the bi-directional electron distribution is formed by SEP injections in both loop legs of the MC separately instead of by mirroring farther away beyond the STEREO orbit. Observations by the Nancay Hadioheliograph (NRH) of two distinct radio sources during the SEP injection further support the above scenario. The determined electron path lengths are around 50% longer than the estimated lengths of the loop legs of the MC itself (based on the GCS model) suggesting that the amount of field line winding is moderate.

A Solar Radio Dynamic Spectrograph with Flexible Temporal-spectral Resolution

Qing-Fu **Du**, Lei Chen, Yue-Chang Zhao, Xin Li, Yan Zhou, Jun-Rui Zhang, Fa-Bao Yan, Shi-Wei Feng, Chuan-Yang Li, Yao Chen

Research in Astronomy and Astrophysics **17** 098 **2018**

https://arxiv.org/pdf/1706.07915.pdf

https://iopscience.iop.org/article/10.1088/1674-4527/17/9/98/pdf

The observation and research of the solar radio emission have unique scientific values in solar and space physics and related space weather forecasting applications, since the observed spectral structures may carry important information about energetic electrons and underlying physical mechanisms. In this study, we present the design of a novel dynamic

spectrograph that is installed at the Chashan solar radio station operated by Laboratory for Radio Technologies, Institute of Space Sciences at Shandong University. The spectrograph is characterized by the real-time storage of digitized radio intensity data in the time domain and its capability to perform off-line spectral analysis of the radio spectra. The analog signals received via antennas and amplified with a low-noise amplifier are converted into digital data at a speed reaching up to 32 k data points per millisecond. The digital data are then saved into a high-speed electronic disk for further off-line spectral analysis. Using different word length (1 k - 32 k) and time cadence (5 ms - 10 s) for the off-line fast Fourier transform analysis, we can obtain the dynamic spectrum of a radio burst with different (user-defined) temporal (5 ms - 10 s) and spectral (3 kHz ~ 320 kHz) resolution. This brings a great flexibility and convenience to data analysis of solar radio bursts, especially when some specific fine spectral structures are under study. **2016-07-18/19**

Table 1 Parameters of solar radio observing system in the world

AN OBSERVATIONAL REVISIT OF BAND-SPLIT SOLAR TYPE-II RADIO BURSTS

Guohui **Du**1, Xiangliang Kong1, Yao Chen1, Shiwei Feng1, Bing Wang1, and Gang Li
2015 ApJ 812 52
http://arxiv.org/pdf/1509.03832v1.pdf

The band split of solar type II radio bursts, discovered several decades ago, is a fascinating phenomenon, with the type II lanes exhibiting two almost parallel sub-bands with similar morphology. The underlying split mechanism remains elusive. One popular interpretation is that the splitting bands are emitted from the shock upstream and downstream, respectively, with their frequency ratio (γ) determined by the shock compression ratio. This interpretation has been taken as the physical basis of many published references. Here we report on an observational analysis of type II events with a nice split selected from ground-based RSTN data from 2001 to 2014, in the metric–decametric wavelength. We investigate the temporal variation and distribution of γ, and conduct correlation analyses on the deduced spectral values. It is found that γ varies in a very narrow range with >80% of γ (one-minute averaged data) being between 1.15 and 1.25. For some well-observed and long-lasting events, γ does not show a systematic variation trend within observational uncertainties, from the onset to the termination of the splits. In addition, the parameters representing the propagation speed of the radio source (presumably the coronal shock) show a very weak or basically no correlation with γ. We suggest that these results do not favor the upstream–downstream scenario of band splits.

Table 1: Some basic parameters of the type-II events.

Temporal Spectral Shift and Polarization of a Band-splitting Solar Type II Radio Burst

Guohui **Du**1, Yao Chen1, Maoshui Lv1, Xiangliang Kong1, Shiwei Feng1, Fan Guo2, and Gang Li
2014 ApJ 793 L39

In many type II solar radio bursts, the fundamental and/or the harmonic branches of the bursts can split into two almost parallel bands with similar spectral shapes and frequency drifts. However, the mechanisms accounting for this intriguing phenomenon remain elusive. In this study, we report a special band-splitting type II event in which spectral features appear systematically earlier on the upper band (with higher frequencies) than on the lower band (with lower frequencies) by several seconds. Furthermore, the emissions carried by the splitting band are moderately polarized with the left-hand polarized signals stronger than the right-hand ones. The polarization degree varies in a range of –0.3 to –0.6. These novel observational findings provide important constraints on the underlying physical mechanisms of band-splitting of type II radio bursts.

Homologous Accelerated Electron Beams, Quasi-periodic fast-propagating Wave and CME Observed in one Fan-spine Jet

Yadan **Duan**, Yuandeng Shen, Xinping Zhou, Zehao Tang, Chengrui Zhou, Song Tan
ApJ **2022**
https://arxiv.org/pdf/2201.08982.pdf

Using imaging and radio multi-wavelength observations, we studied the origin of two homologous accelerated electron beams and a quasi-periodic fast-propagating (QFP) wave train associated with a solar jet on **2012 July 14**. The jet occurred in a small-scale fan-spine magnetic system embedding in a large-scale pseudostreamer, which associated with a GOES C1.4 flare, a jet-like coronal mass ejection (CME), a type II radio burst, and a type III radio burst. During the initial stage, a QFP wave train and a fast moving on-disk radio source were detected in succession ahead of the jet along the outer spine of the fan-spine system. When the jet reached a height of about 1.3 solar radii, it underwent a bifurcation into two branches. Based on our analysis results, all the observed phenomena in association with the jet can be explained

by using a fan-spine magnetic system. We propose that both the type III radio burst and the on-disk fast moving radio source were caused by the same physical process, i.e., the energetic electrons accelerated by the magnetic reconnection at the null point, and they were along the open field lines of the pseudostreamer and the closed outer spine of the fan-spine structure, respectively. Due to the bifurcation of the jet body, the lower branch along the closed outer spine of the fan-spine structure fell back to the solar surface, while the upper branch along the open field lines of the pseudostreamer caused the jet-like CME in the outer corona.

*The **Korean Solar Radio Burst Locator** (KSRBL|described in detail in Dou et al. 2009) is the first spectrometer to employ the technique of Spectral Kurtosis (SK|Nita et al. 2007) to identify and remove radio frequency interference (RFI) signals in the radio spectrum*.

Slipping magnetic reconnection during an X-class solar flare observed by SDO/AIA

J. **Dudik**, M. Janvier, G. Aulanier, G. Del Zanna, M. Karlicky, H. Mason, B. Schmieder
E-print, Jan **2014, File**; ApJ
http://arxiv.org/pdf/1401.7529v1.pdf

We present SDO/AIA observations of an eruptive X-class flare of **July 12, 2012**, and compare its evolution with the predictions of a 3D numerical simulation. We focus on the dynamics of flare loops that are seen to undergo slipping reconnection during the flare. In the AIA 131A observations, lower parts of 10 MK flare loops exhibit an apparent motion with velocities of several tens of km/s along the developing flare ribbons. In the early stages of the flare, flare ribbons consist of compact, localized bright transition-region emission from the footpoints of the flare loops. A DEM analysis shows that the flare loops have temperatures up to the formation of Fe XXIV. A series of very long, S-shaped loops erupt, leading to a CME observed by STEREO. The observed dynamics are compared with the evolution of magnetic structures in the ``standard solar flare model in 3D". This model matches the observations well, reproducing both the apparently slipping flare loops, S-shaped erupting loops, and the evolution of flare ribbons. All of these processes are explained via 3D reconnection mechanisms resulting from the expansion of a torus-unstable flux rope. The AIA observations and the numerical model are complemented by radio observations showing a noise storm in the metric range. Dm-drifting pulsation structures occurring during the eruption indicate plasmoid ejection and enhancement of reconnection rate. The bursty nature of radio emission shows that the slipping reconnection is still intermittent, although it is observed to persist for more than an hour.

Хорошее Введение.

The non-Maxwellian continuum in the X-ray, UV, and radio range⋆

J. **Dudík**1,2, J. Kašparová2, E. Dzifčáková2, M. Karlický2 and Š. Mackovjak
A&A 539, A107 (**2012**), **E-print** 7 March 2012

Aims. We investigate the X-ray, UV, and also the radio continuum arising from plasmas with a non-Maxwellian distribution of electron energies. The two investigated types of distributions are the κ- and n-distributions.
Methods. We derived analytical expressions for the non-Maxwellian bremsstrahlung and free-bound continuum spectra. The spectra were calculated using available cross-sections. Then we compared the bremsstrahlung spectra arising from the different bremsstrahlung cross-sections that are routinely used in solar physics.
Results. The behavior of the bremsstrahlung spectra for the non-Maxwellian distributions is highly dependent on the assumed type of the distribution. At flare temperatures and hard X-ray energies, the bremsstrahlung is greatly increased for κ-distributions and exhibits a strong high-energy tail. With decreasing κ, the maximum of the bremsstrahlung spectrum decreases and moves to higher wavelengths. In contrast, the maximum of the spectra for n-distributions increases with increasing n, and the spectrum then falls off very steeply with decreasing wavelength. In the millimeter radio range, the non-Maxwellian bremsstrahlung spectra are almost parallel to the thermal bremsstrahlung. Therefore, the non-Maxwellian distributions cannot be detected by off-limb observations made by the ALMA instrument. The free-bound continua are also highly dependent on the assumed type of the distribution. For n-distributions, the ionization edges disappear and a smooth continuum spectrum is formed for $n \geqq 5$. Opposite behavior occurs for κ-distributions where the ionization edges are in general significantly enhanced, with details depending on κ and T through the ionization equilibrium. We investigated how the non-Maxwellian κ-distributions can be determined from the observations of the continuum and conclude that one can sample the low-energy part of the distribution from the continuum.

The Class of Type III-L Solar Radio Bursts and Their Associations with Solar Energetic Proton Events

Duffin R.T.

Thesis, **2011**

The source protons of Solar Energetic particle Proton events (defined as "SEP" events for this research) not associated with the Coronal Mass Ejection (CME) shock front are thought to come from either the flare site or the reconnection region beneath the CME. The Type III-L, a new class of solar radio burst has been defined by Cane et al. (2002) and MacDowall et al. (2003) as a sub-set of the Type III burst, beginning after the onset of the soft X-ray (SXR) flare, is long lasting and extends down to at least 1 MHz. The emission source region of Type III-Ls is believed to be at the reconnection region beneath the CME or on the flanks of the CME. Past association studies between SEP events and Type III-Ls began with a biased SEP-selected sample set to see if there can be found support for the emission source region of Type III-Ls and SEPs to come from the same accelerator site at the reconnection region beneath the CME. Unlike previous studies using an SEP-selected sample, I find that when using a radio-selected sample for well-connected SEP events with a solar source in the western hemisphere, the majority of the Type III-L events are associated with SEP events, but not all, and that Type III-L events associated with M- and X- class SXR flares, do not appear to be better predictors of SEP events than do Type II bursts which are associated with the CME shock. Also, I find that the occurrence of Type II events in the radio spectra of SEPs is just as common as the occurrence of Type III-Ls. This indicates that Type III-Ls should not be used as a predictor for SEP events, that the emission source region of Type III-Ls might not be at the reconnection region beneath the CME and reduces the strength of the support found by previous SEP-Type III-L association studies, that the source protons for SEP events necessarily come from the reconnection region beneath the CME. I found that Type III-L events have no strong longitude preference, but SEP events do have a 60% preference between W30 and W90 solar longitude. New data from new long wavelength arrays will help with position mapping the emission source regions of Type III-L bursts. An investigation was done on the internal structure of Type III-Ls. An implication of the result that the separation between components of the Type III-L burst was found to be longer than the separation between the components of Impulsive-Phase Type IIIs (defined as "Imp-Type IIIs"), is that the duration of the Type III-L components appears to be longer than those of Imp-Type IIIs. The result that the components of the Imp-Type IIIs have a faster frequency-time drift-rate than those of the Type III-Ls, shows that the source electrons for the Imp-Type IIIs appear to have a faster source emission velocity than do Type III-Ls. This is understandable as the source electrons for the Imp-Type IIIs are thought to come directly from the active region flare site, whereas the source electrons for Type III-Ls have a longer path along the neutral current sheet to either the reconnection region beneath the CME or up to the flanks of the CME. This gives us a reason as to why the Type III-L emission is delayed in respect to the Imp-Type IIIs. With their energy decreased, these Type III-L source electrons would form emission with a source velocity and frequency-time drift-rate slower than that of the Imp-Type IIIs. Data with better time and frequency resolution should help determine if there are additional weaker Type III-L components. Timing studies between SXR flares, the expansion of CMEs and the evolution of Type III-L components, should determine if electron accelerator sites for the Type III-L components are at a reconnection region beneath the CME or on the flanks of the CME.

A multiwavelength study of an M-class flare and the origin of an associated eruption from NOAA AR 11045

Dwivedi, B. N.; Srivastava, Abhishek K.; Kumar, Mukul; Kumar, Pankaj

E-print, March **2012**, New Astr.

In this paper, we study multiwavelength observations of an M6.4 flare in Active Region NOAA 11045 on **7 February 2010**. The space- and ground-based observations from STEREO, SoHO/MDI, EIT, and Nobeyama Radioheliograph were used for the study. This active region rapidly appeared at the north-eastern limb with an unusual emergence of a magnetic field. We find a unique observational signature of the magnetic field configuration at the flare site. Our observations show a change from dipolar to quadrapolar topology. This change in the magnetic field configuration results in its complexity and a build-up of the flare energy. We did not find any signature of magnetic flux cancellation during this process. We interpret the change in the magnetic field configuration as a consequence of the flux emergence and photospheric flows that have opposite vortices around the pair of opposite polarity spots. The negative-polarity spot rotating counterclockwise breaks the positive-polarity spot into two parts. The STEREO-A 195 ? and STEREO-B 171 ? coronal images during the flare reveal that a twisted flux tube expands and erupts resulting in a coronal mass ejection (CME). The formation of co-spatial bipolar radio contours at the same location also reveals the ongoing reconnection

process above the flare site and thus the acceleration of non-thermal particles. The reconnection may also be responsible for the detachment of a ring-shaped twisted flux tube that further causes a CME eruption with a maximum speed of 446 km/s in the outer corona.

Quasiperiodic oscillations in the active solar regionsfrom the data of nobeyama radioheliograph

L. N. **Dzhimbeeva**
Solar System Research, Vol. 45, Issue 1, **2011**

Quasiperiodic oscillations of the sub-mHz band in near-sun plasma according to the coherent radio occultation data

A. I. **Efimov**, L. A. Lukanina, I. V. Chashei, S. F. Kolomiets, M. K. Bird, M. Pätzold
Cosmic Research January **2018**, Volume 56, Issue 1, pp 1–10
Kosmicheskie Issledovaniya, **2018**, Vol. 56, No. 1, pp. 6–15.
In 2013 and 2015, investigations of the internal solar wind were carried out using the method of two-frequency radio sounding by signals from the Mars Express European spacecraft. The values of the S- and X-bands' frequency and the differential frequency were registered with a sampling rate of 1s at the American and European networks of ground-based tracking stations. The spatial distribution of the frequency fluctuation's level has been studied. It has been shown that the intensity of frequency fluctuation considerably decreases at high heliolatitudes. In some radio sounding sessions, quasiperiodic oscillations of sub-mHz band have been observed in the temporal spectra of frequency fluctuations; they are supposed to be associated with the density inhomogeneities, the sizes of which are close to the turbulence outer scale.

Coronal Radio Occultation Experiments with the Helios Solar Probes: Correlation/Spectral Analysis of Faraday Rotation Fluctuations

A. I. **Efimov**, L. A. Lukanina, A. I. Rogashkova, L. N. Samoznaev, I. V. Chashei, M. K. Bird, M. Pätzold
Solar Physics September **2015**, Volume 290, Issue 9, pp 2397-2408
The coronal Faraday rotation (FR) experiments using the linearly polarized signals of the Helios-1and Helios-2 interplanetary probes remain a unique investigation of the magnetic field of the solar corona and its aperiodic and quasi-periodic variations. The unexpectedly long lifetime of these spacecraft (1974 – 1986) enabled studies from very deep solar-activity minimum (1975 – 1976) into the strong activity maximum (1979). Important experimental data were also obtained for the rising (1977 – 1978) and declining (1980 – 1984) branches of the solar-activity cycle. Previous publications have presented results of the initial experimental data only for coronal-sounding experiments performed during individual solar-conjunction opportunities. This report is a more detailed analysis of the Helios FR measurements for the entire period 1975 – 1984. Radial profiles of the FR fluctuation (FRF) intensity recorded during the deepest solar-activity minimum in 1975 – 1976 are shown to differ distinctly from those during the strong solar-activity maximum in 1979. In particular, the decrease of the FRF intensity with solar-offset distance is substantially steeper in 1979 than in 1975/1976. In all cases, however, the FR data reveal quasi-periodic wave-like fluctuations in addition to the random background with a power-law spectrum. The dominant period of these fluctuations, recorded during 35 % of the total measurement time, is found to be close to five minutes. Large-scale FR variations at considerably longer periods (1.1 – 2.7 hours) were observed during 20 % of the measurement time. Knowing the intrinsic motion of the radio ray path from spacecraft to Earth and making a reasonable assumption about the solar-wind velocity, FRF observations at widely spaced ground stations have been used to estimate the velocity of coronal Alfvén waves. The velocity values range between 290 and 550 km s−1 at heliocentric distances between 3.5 and 4.5 R⊙ and are marginally lower (150 – 450 km s−1) at distances between 5.5 and 6.5 R⊙. Occasional FR variations with a period near 160 minutes and harmonics with periods 60, 30, and 20 minutes were also observed.

Finding Spots in a CME-Related Shock Where Physical Conditions Can Emerge Favoring Type II Radio Burst Generation on 2010 June 13

Y. I. **Egorov**, V. G. Fainshtein & D. V. Prosovetskiy
Solar Physics volume 296, Article number: 58 (**2021**)

https://doi.org/10.1007/s11207-021-01788-3
https://link.springer.com/content/pdf/10.1007/s11207-021-01788-3.pdf
The 13 June 2010 event was chosen as an example to find spots on a CMErelated shock where type II radio bursts were generated. We used the Atmospheric Imaging Assembly (AIA) aboard the Solar Dynamics Observatory (SDO) data to find the shock and calculate the emission measure distribution over the solar limb in order to obtain various plasma characteristics ahead of and behind the shock front. A region was found in the shock where the electron density jump X on the shock front, the Alfvén Mach number Ma and the shock velocity Vsh reach a maximum simultaneously. Moreover, the calculated value of X in this region was found to be closest to the value of Xrb based on type II radio burst data, (Xrb) = N2/N1 = (fu/fl)2, where N2 and N1 are the electron densities at the upstream and downstream shock regions, fu and fl are the radio emission frequencies at the upper and lower band of the dynamic spectrum, in the second harmonic region. Based on these findings, we hypothesized that it is this shock region that is the source of type II radio bursts (type II RB). This region moves at an angle of +20◦ from the center of the circle approximating the shock, relative to the direction through the shock middle. The type II radio burst source velocity is shown to be close to the CME-related shock velocity. This can be regarded as indirect evidence of the shocks being the source of type II radio bursts. A dependence, N1(Rsh), has been obtained in the +20◦ direction, where Rsh is the shock front location. This dependence is shown to differ noticeably from the coronal background electron densities obtained by Newkirk (Astrophys. J. 133, 983, 1961) and Saito et al. (Ann. Tokyo Astron. Obs. 12, 53, 1970) density models. **13 June 2010**

Deep solar ALMA neural network estimator for image refinement and estimates of small-scale dynamics

Henrik **Eklund**1,2,3
A&A 669, A106 (**2023**)
https://www.aanda.org/articles/aa/pdf/2023/01/aa44484-22.pdf
Context. The solar atmosphere is highly dynamic, and observing the small-scale features is valuable for interpretations of the underlying physical processes. The contrasts and magnitude of the observable signatures of small-scale features degrade as angular resolution decreases.
Aims. The estimates of the degradation associated with the observational angular resolution allows a more accurate analysis of the data.
Methods. High-cadence time-series of synthetic observable maps at $\lambda = 1.25$ mm were produced from three-dimensional magnetohydrodynamic Bifrost simulations of the solar atmosphere and degraded to the angular resolution corresponding to observational data with the Atacama Large Millimeter/sub-millimeter Array (ALMA). The deep solar ALMA neural network estimator (Deep-SANNE) is an artificial neural network trained to improve the resolution and contrast of solar observations. This is done by recognizing dynamic patterns in both the spatial and temporal domains of small-scale features at an angular resolution corresponding to observational data and correlated them to highly resolved nondegraded data from the magnetohydrodynamic simulations. A second simulation, previously never seen by Deep-SANNE, was used to validate the performance.
Results. Deep-SANNE provides maps of the estimated degradation of the brightness temperature across the field of view, which can be used to filter for locations that most probably show a high accuracy and as correction factors in order to construct refined images that show higher contrast and more accurate brightness temperatures than at the observational resolution. Deep-SANNE reveals more small-scale features in the data and achieves a good performance in estimating the excess temperature of brightening events with an average of 94.0% relative to the highly resolved data, compared to 43.7% at the observational resolution. By using the additional information of the temporal domain, Deep-SANNE can restore high contrasts better than a standard two-dimensional deconvolver technique. In addition, Deep-SANNE is applied on observational solar ALMA data, for which it also reveals eventual artifacts that were introduced during the image reconstruction process, in addition to improving the contrast. It is important to account for eventual artifacts in the analysis.
Conclusions. The Deep-SANNE estimates and refined images are useful for an analysis of small-scale and dynamic features. They can identify locations in the data with high accuracy for an in-depth analysis and allow a more meaningful interpretation of solar observations.

Utilizing the slope of the brightness temperature continuum as a diagnostic tool of solar ALMA observations

Henrik **Eklund**, Mikolaj Szydlarski, Sven Wedemeyer
A&A 669, A105 **2022**
https://arxiv.org/pdf/2211.05586.pdf
https://www.aanda.org/articles/aa/pdf/2023/01/aa44400-22.pdf

The intensity of radiation at millimeter wavelengths from the solar atmosphere is closely related to the plasma temperature and the height of formation of the radiation is wavelength dependent. From that follows that the slope of the brightness temperature (Tb) continuum, samples the local gradient of the gas temperature of the sampled layers in the solar atmosphere. We use solar observations from the Atacama Large Millimeter/sub-millimeter Array (ALMA) and perform estimations and prediction of the slope of the Tb continuum based on differences between synthetic observables at different ALMA receiver sub-bands (2.8-3.2 mm; band 3) and (1.20-1.31 mm; band 6) from a state-of-the-art 3D rMHD simulation. The slope of the continuum is coupled to the small-scale dynamics and a positive sign indicates an increase in temperature with height while a negative sign implies a decrease. Network patches are dominated by large positive slopes while quiet Sun region show a mixture of positive and negative slopes, much in connection to propagating shock waves and the temporal evolution of the slopes can therefore be used to identify shocks. The observability of the slope of brightness temperatures is estimated for angular resolutions corresponding to ALMA observations. The simulations also show that the radiation of both bands 3 and 6 can origin from several components at different heights simultaneously and that the delay of shock signatures between two wavelengths does not necessarily reflect the propagation speed, but could be caused by different rate of change of opacity of above-lying layers. The slope of the Tb continuum sampled at different ALMA receiver sub-bands serves as indicator of the slope of the local plasma temperature at the sampled heights in the atmosphere, which offers new diagnostic possibilities to measure the underlying physical properties. **April 12, 2018**

The Sun at millimeter wavelengths. III. Impact of the spatial resolution on solar ALMA observations

Henrik **Eklund**, Sven Wedemeyer, Mikołaj Szydlarski, Shahin Jafarzadeh
A&A 656, A68 **2021**
https://arxiv.org/pdf/2109.13826.pdf
https://www.aanda.org/articles/aa/pdf/2021/12/aa40972-21.pdf
https://doi.org/10.1051/0004-6361/202140972
Context. Interferometric observations of the Sun with the Atacama Large Millimeter/sub-millimeter Array (ALMA) provide valuable diagnostic tools for studying the small-scale dynamics of the solar atmosphere.
Aims. The aims are to perform estimations of the observability of the small-scale dynamics as a function of spatial resolution for regions with different characteristic magnetic field topology facilitate a more robust analysis of ALMA observations of the Sun.
Methods. A three-dimensional model of the solar atmosphere from the radiation-magnetohydrodynamic code Bifrost was used to produce high-cadence observables at millimeter and submillimeter wavelengths. The synthetic observables for receiver bands 3–10 were degraded to the angular resolution corresponding to ALMA observations with different configurations of the interferometric array from the most compact, C1, to the more extended, C7. The observability of the small-scale dynamics was analyzed in each case. The analysis was thus also performed for receiver bands and resolutions that are not commissioned so far for solar observations as a means for predicting the potential of future capabilities.
Results. The minimum resolution required to study the typical small spatial scales in the solar chromosphere depends on the characteristic properties of the target region. Here, a range from quiet Sun to enhanced network loops is considered. Limited spatial resolution affects the observable signatures of dynamic small-scale brightening events in the form of reduced brightness temperature amplitudes, potentially leaving them undetectable, and even shifts in the times at which the peaks occur of up to tens of seconds. Conversion factors between the observable brightness amplitude and the original amplitude in the fully resolved simulation are provided that can be applied to observational data in principle, but are subject to wavelength-dependent uncertainties. Predictions of the typical appearance at the different combinations of receiver band, array configuration, and properties of the target region are conducted.
Conclusions. The simulation results demonstrate the high scientific potential that ALMA already has with the currently offered capabilities for solar observations. For the study of small-scale dynamic events, however, the spatial resolution is still crucial, and wide array configurations are preferable. In any case, it is essential to take the effects due to limited spatial resolution into account in the analysis of observational data. Finally, the further development of observing capabilities including wider array configurations and advanced imaging procedures yields a high potential for future ALMA observations of the Sun.

The Sun at millimeter wavelengths -- II. Small-scale dynamic events in ALMA Band 3

Henrik **Eklund**, Sven Wedemeyer, Mikolaj Szydlarski, Shahin Jafarzadeh, Juan Camilo Guevara Gómez
A&A 644, A152 **2020**
https://arxiv.org/pdf/2010.06400.pdf
https://www.aanda.org/articles/aa/pdf/2020/12/aa38250-20.pdf

Solar observations with the Atacama Large Millimeter/sub-millimeter Array (ALMA) facilitate studying the atmosphere of the Sun at chromospheric heights at high spatial and temporal resolution at millimeter wavelengths. ALMA intensity data at mm-wavelengths are used for a first detailed systematic assessment of the occurrence and properties of small-scale dynamical features in the quiet Sun. ALMA Band 3 data (~ 3 mm / 100 GHz) with spatial resolution ~ 1.4 - 2.1 arcsec and a duration of ~ 40 min are analysed together with SDO/HMI magnetograms. The temporal evolution of the mm-maps is studied to detect pronounced dynamical features which are connected to dynamical events via a k-means clustering algorithm. The physical properties of the resulting events are studied and it is explored if they show properties consistent with propagating shock waves. For this purpose, observable shock wave signatures at mm wavelengths are calculated from one- and three-dimensional model atmospheres. There are 552 dynamical events detected with an excess in brightness temperature (ΔTb) of at least $\geq$400 K. The events show a large variety in size up to ~ 9 arcsec, amplitude ΔTb up to ~ 1200 K with typical values between ~ 450 - 750 K and lifetime at FWHM of ΔTb between ~ 43 - 360 s, with typical values between ~ 55 - 125 s. Furthermore, many of the events show signature properties that suggest that they are likely produced by propagating shock waves. There are a lot of small-scale dynamic structures detected in the Band 3 data, even though the spatial resolution sets limitations of the size of events that can be detected. The amount of dynamic signatures in the ALMA mm data is very low in areas with photospheric footpoints with stronger magnetic fields, which is consistent with the expectation for propagating shock waves. **December 22nd, 2016**

Characterisation of shock wave signatures at millimetre wavelengths from Bifrost simulations

Henrik **Eklund**, Sven Wedemeyer, Ben Snow, David B. Jess, Shahin Jafarzadeh, Samuel D.T. Grant, Mats Carlsson, Mikolaj Szydlarski

Philosophical Transactions A of the Royal Society **2020**

https://arxiv.org/pdf/2008.05324.pdf

Observations at millimetre wavelengths provide a valuable tool to study the small scale dynamics in the solar chromosphere. We evaluate the physical conditions of the atmosphere in the presence of a propagating shock wave and link that to the observable signatures in mm-wavelength radiation, providing valuable insights into the underlying physics of mm-wavelength observations. A realistic numerical simulation from the 3D radiative Magnetohydrodynamic (MHD) code Bifrost is used to interpret changes in the atmosphere caused by shock wave propagation. High-cadence (1 s) time series of brightness temperature (Tb) maps are calculated with the Advanced Radiative Transfer (ART) code at the wavelengths 1.309 mm and 1.204 mm, which represents opposite sides of spectral band~6 of the Atacama Large Millimeter/submillimeter Array (ALMA). An example of shock wave propagation is presented. The brightness temperatures show a strong shock wave signature with large variation in formation height between ~0.7 to 1.4 Mm. The results demonstrate that millimetre brightness temperatures efficiently track upwardly propagating shock waves in the middle chromosphere. In addition, we show that the gradient of the brightness temperature between wavelengths within ALMA band 6 can potentially be utilised as a diagnostics tool in understanding the small-scale dynamics at the sampled layers.

What to Do When the F10.7 Goes Out?

Sean **Elvidge**, David R. Themens, Matthew K. Brown, Elizabeth Donegan-Lawley

Space Weather Volume21, Issue4 e2022SW003392 **2023**

https://doi.org/10.1029/2022SW003392

https://agupubs.onlinelibrary.wiley.com/doi/epdf/10.1029/2022SW003392

The solar radio flux at 10.7 cm, known as F10.7, is a critical operational space weather index. However, without a clear backup, any interruption to the service can result in substantial errors in model outputs. In this paper we show the impact of one such outage in March 2022 on the models TIE-GCM and NeQuick, and present a number of alternative solutions that could be used for future outages. The analysis is extended to the F10.7 time series since 1951 and the approach resulting in the smallest reconstruction error of F10.7 uses the solar radio flux observations at alternative wavelengths (the best giving a percentage error of 3.1%). Alternatively, use of Sunspot Number, a regular, robust alternative observation, results in a mean percentage error of 8.2% and is also a reliable fallback solution. Additionally, analysis of the error on the use of the conversion between the 12-month rolling sunspot number (R12) and its conversion to F10.7 is included. **18 Mar-10 Apr 2022**

Observations of a Flare-Generated Blast Wave in a Pseudo Coronal Mass Ejection Event

V. G. **Eselevich**, M. V. Eselevich, I. V. Zimovets,

Solar Physics June **2019**, 294:73

sci-hub.se/10.1007/s11207-019-1467-x

We present an analysis of the event near the east limb, **SOL2014-03-06T09**:23, in which a pseudo coronal mass ejection (CME) was detected by the Large Angle and Spectrometric Coronagraph (LASCO) C2 instrument and indicated as "Poor Event; Only C2" in the Solar and Heliospheric Observatory (SOHO) LASCO CME Catalog. The analysis was performed based on two main methods: 1) investigation of the difference brightness profiles along specific directions in the solar corona using the EUV observations by the Atmospheric Imaging Assembly (AIA) instrument onboard the Solar Dynamics Observatory (SDO); 2) investigation of the spatially-resolved observations of the type II radio bursts made with the Nançay Radioheliograph. Based on the analysis performed we argue that the observed pseudo-CME could be a blast wave caused by impulsive flare energy release in the low corona. We also argue that, in the limited height range of ≈0.2R⊙--0.5R⊙, the front of this blast wave could steepen into a shock front.

Evidence for shock generation in the solar corona in the absence of coronal mass ejections.

Eselevich, V.G., Eselevich, M.V., Zimovets, I.V., Sharykin, I.N.:
2017, Astron. Rep. 61, 805. DOI. ADS.
sci-hub.se/10.1134/S1063772917080030
The solar event **SOL2012-10-23T03:13**, which was associated with a X1.8 flare without an accompanying coronal mass ejection (CME) and with a Type II radio burst, is analyzed. A method for constructing the spatial and temporal profiles of the difference brightness detected in the AIA/SDOUVand EUV channels is used together with the analysis of the Type II radio burst. The formation and propagation of a region of compression preceded by a collisional shock detected at distances R < 1.3 R ⊙ from the center of the Sun is observed in this event (R ⊙ is the solar radius). Comparison with a similar event studied earlier, SOL2011-02-28T07:34 [1], suggests that the region of compression and shock could be due to a transient (impulsive) action exerted on the surrounding plasma by an eruptive, high-temperature magnetic rope. The initial instability and eruption of this rope could be initiated by emerging magnetic flux, and its heating from magnetic reconnection. The cessation of the eruption of the rope could result from its interaction with surrounding magnetic structures (coronal loops).

Evidence of a blast shock wave formation in a "CME–streamer" interaction

V.G. **Eselevich**a, , M.V. Eselevicha, , V.M. Sadykovb, c, , I.V. Zimovets
Advances in Space Research Volume 56, Issue 12, 15 December **2015**, Pages 2793–2803
http://www.sciencedirect.com/science/article/pii/S0273117715002434
Analysis of the solar event on **16 February 2011** (SOL2011-02-16T14:19) allows to classify it as an "impulsive" coronal mass ejection (CME) event. It is argued that the observed deviation of a streamer ray from its pre-event state and generation of a metric type II radio burst in this event was a result of a "CME–streamer" interaction in the lower corona (r≲1.5R⊙). Most probably, it was a consequence of an impulsive action of a compressed magnetic field to the streamer. This compression of the coronal magnetic field was due to a moving and expanding magnetic flux rope, which was a core of the CME. The estimated radial speed of the type II burst sources was significantly (≈2–8 times) larger than the radial speed of the erupting flux rope, and it decreased rapidly with time. This indicates that during the "CME–streamer" interaction a blast shock wave could be excited and propagated along the streamer.

ALFVE´N PROFILE IN THE LOWER CORONA: IMPLICATIONS FOR SHOCK FORMATION

R. M. **Evans** and M. Opher, W. B. Manchester IV and T. I. Gombosi
Astrophysical Journal, 687:1355-1362, **2008**
http://www.journals.uchicago.edu/doi/pdf/10.1086/592016
Observations of type II radio bursts and energetic electron events indicate that shocks can form at 1Y3 solar radii and are responsible for the GeV nucleon_1 energies observed in ground level solar energetic particle (SEP) events. Here we provide the first study of the lower corona produced from 10 state-of-the-art models. In particular, we look to the Alfve´n speed profiles as the criterion for shock formation, independent of exciting agent (e.g., flares and CMEs). Global magnetohydrodynamic models produce Alfve´n speed profiles that are in conflict with observations: (1) multiple SEP events are observed with a single exciting agent, but most profiles are missing the ''hump'' required to form multiple shocks; and (2) few slow CMEs cause large SEP events, but most profiles drop very quickly, allowing all slow CMEs to drive strong shocks to form between 1 and 3 R_. Simplified Alfve´n wave-driven wind models have steeper profiles, but are still in disagreement with multiple shock formation. Only studies that include Alfve´n waves with physically based damping are in agreement with observations. This implies the results of these one-dimensional local studies must be included in global models before we can study shock formation in the lower corona.

Spectroscopy of Electric-Field Oscillations in the Solar Wind During the Passage of a Type III Radio Burst Using Observations Compared with Self-Similar Theory

Joseph **Fainberg** & Vladimir Osherovich

Solar Physics volume 297, Article number: 50 (**2022**)

We present a spectrum of electric-field oscillations observed in situ in the solar wind by the WAVES experiment on the Wind spacecraft during the passage of a type III solar radio burst. 19 frequencies of this spectrum are compared with recent predictions of a self-similar nonlinear theory of two-dimensional electron oscillations (Osherovich and Fainberg, 2018).

The scintillating tail of comet C/2020 F3 (Neowise)⋆

R. A. **Fallows**1,3, B. Forte2, M. Mevius1, M. A. Brentjens1, C. G. Bassa1, M. M. Bisi3, A. Offringa1, G. Shaifullah4,5,6, C. Tiburzi6, H. Vedantham1 and P. Zucca1

A&A 667, A57 (**2022**)

https://www.aanda.org/articles/aa/pdf/2022/11/aa44377-22.pdf

Context. The occultation of a radio source by the plasma tail of a comet can be used to probe structure and dynamics in the tail. Such occultations are rare, and the occurrence of scintillation, due to small-scale density variations in the tail, remains somewhat controversial.

Aims. A detailed observation taken with the Low-Frequency Array (LOFAR) of a serendipitous occultation of the compact radio source 3C196 by the plasma tail of comet C/2020 F3 (Neowise) is presented. 3C196 tracked almost perpendicularly behind the tail, providing a unique profile cut only a short distance downstream from the cometary nucleus itself.

Methods. Interplanetary scintillation (IPS) is observed as the rapid variation of the intensity received of a compact radio source due to density variations in the solar wind. IPS in the signal received from 3C196 was observed for five hours, covering the full transit behind the plasma tail of comet C/2020 F3 (Neowise) on **16 July 2020**, and allowing an assessment of the solar wind in which the comet and its tail are embedded.

Results. The results reveal a sudden and strong enhancement in scintillation which is unequivocally attributable to the plasma tail. The strongest scintillation is associated with the tail boundaries, weaker scintillation is seen within the tail, and previously-unreported periodic variations in scintillation are noted, possibly associated with individual filaments of plasma. Furthermore, contributions from the solar wind and comet tail are separated to measure a sharp decrease in the velocity of material within the tail, suggesting a steep velocity shear resulting in strong turbulence along the tail boundary.

Brazilian Decimetric Array (BDA) project - Phase II

C. **Faria**1, S. Stephany2, H. S. Sawant2, J. R. Cecatto2
and F. C. R. Fernandes3

Solar and Stellar Variability: Impact on Earth and Planets
Proceedings IAU Symposium No. 264, **2009**
A.G. Kosovichev, A.H. Andrei & J.-P. Rozelot, eds.

Y:\obridko\otchet09

The configuration of the second phase of the Brazilian Decimetric Array (BDA), installed at Cachoeira Paulista, Brazil (Longitude 45 0' 20" W and Latitude 22 41' 19" S), is a T-shaped array where 21 antennas are being added to existing 5 antennas of the first phase. In the third phase, in each arm of the T array, four more antennas will be added and baselines will be increased to 2.5 x 1.25 km in east-west and south directions, respectively. The antennas will be equally spaced at the distances of 250 meters from the central antenna of the T-array. Also, the frequency range will be increased to 1.2-1.7, 2.8 and 5.6 GHz. The Second phase of the BDA should be operational by the middle of 2010 and will operate in the frequency range of (1.2-1.7) GHz for solar and non solar observations. Here, we present the characteristics of the second phase of the BDA project, details of the array configuration, the u-v coverage, the synthesized beam obtained for the proposed configuration.

Spatial Structure and Spectra of X-Ray Sources During the 0.8 – 4.5 GHz Reverse Drift Bursts Observations

F. Fárník · M. Karlický

Solar Phys (2007) 240: 121–134

Strongest coronal magnetic fields in solar cycles 23-24: probing, statistics, and implications

V. V. **Fedenev**, S. A. Anfinogentov, G. D. Fleishman

ApJ **943** 160 **2023**

https://arxiv.org/pdf/2301.08922.pdf

https://iopscience.iop.org/article/10.3847/1538-4357/acac33/pdf

Strong coronal magnetic field, when present, manifests itself as bright microwave sources at high frequencies produced by gyroresonant (GR) emission mechanism in thermal coronal plasma. The highest frequency at which this emission is observed is proportional to the absolute value of the strongest coronal magnetic field on the line of sight. Although no coronal magnetic field larger than roughly 2,000 G was expected, recently the field at least twice larger has been reported. Here, we report a search for and statistical study of such strong coronal magnetic fields using high-frequency GR emission. A historic record of spatially resolved microwave observations at high frequencies, 17 and 34 GHz, is available from Nobeyama RadioHeliograph for more than 20 years (1995-2018). Here we employ this data set to identify sources of bright GR emission at 34 GHz and perform a statistical analysis of the identified GR cases to quantify the strongest coronal magnetic fields during two solar cycles. We found that although active regions with the strong magnetic field are relatively rare (less than 1% of all active regions), they appear regularly on the Sun. These active regions are associated with prominent manifestations of solar activity. **16 Feb 2011, 5 Sep 2011, 2 Feb 2014, 17 Nov 2014, 2017-Sep-06, 2017-Sep-07,**

Table 1. Final GR-34 event list with properties and associations 1999-2017

Solar Type J Radio Bursts and the Associated Coronal Loop

S. W. **Feng**1,2, H. X. Xie3, and H. Misawa4

2024 ApJ 964 108

https://iopscience.iop.org/article/10.3847/1538-4357/ad267f/pdf

The solar type J radio burst is a variant of type III bursts, which are a probe for understanding solar energetic electrons and local electron density. This study investigates a type J burst event on **2017 September 9**. We have combined the data from the extreme-ultraviolet (EUV) imaging and the EUV Imaging Spectrometer (EIS) to analyze the event. Within 4 minutes several type J bursts with similar morphology occur. Two of them, with clear fundamental and second harmonic bands, are studied in detail. We find a delay of 2 ± 0.5 s between their different harmonic bands. During type J bursts, only one coronal loop brightens significantly at its northern footpoint, in correlation with the continuous injection of erupting jets into the loop. The EUV intensity of the brightening footpoint is correlated with the radio flux at 245 and 410 MHz, with correlation coefficients of 0.2 and 0.4, respectively. These observations suggest that the type J bursts should originate from this coronal loop. By analyzing the electron number density distribution along the coronal loop diagnosed from the EIS data and the time evolution of the plasma frequency calculated from the type J burst, we determine that the velocities of the energetic electrons exciting the two type Js are $0.10 \pm 0.02c$ and $0.12 \pm 0.02c$. Our results confirm previous studies on type J bursts.

Harmonics of Solar Radio Spikes at Metric Wavelengths

Shiwei **Feng**, Yao Chen, Chuanyang Li, Bing Wang, Zhao Wu, Xiangliang Kong, Qingfu Du, Junrui Zhang, Guoqing Zhao

Solar Phys. 293:39 **2018**

https://arxiv.org/pdf/1802.03541.pdf

https://link.springer.com/content/pdf/10.1007%2Fs11207-018-1263-z.pdf

This paper presents the latest observations from the newly-built solar radio spectrograph at the \emph{Chashan Solar Observatory}. On **July 18 2016**, the spectrograph records a solar spike burst event, which has several episodes showing harmonic structures, with the second, third, and fourth harmonics. The lower harmonic radio spike emissions are observed later than the higher harmonic bands, and the temporal delay of the second (third) harmonic relative to the fourth harmonic is about 30\ --\ 40 (10) ms. Based on the electron cyclotron maser emission mechanism, we analyze possible causes of the temporal delay and further infer relevant coronal parameters, such as the magnetic field strength and the electron density at the radio source.

An imaging study of a complex solar coronal radio eruption

S. W. **Feng**, Y. Chen, H. Q. Song, B. Wang, X. L. Kong

2016 *ApJ* **827** L9

http://arxiv.org/pdf/1608.00073v1.pdf

Solar coronal radio bursts are enhanced radio emission excited by energetic electrons accelerated during solar eruptions, studies on which are important for investigating the origin and physical mechanism of energetic particles and further diagnosing coronal parameters. Earlier studies suffered from a lack of simultaneous high-quality imaging data of the radio burst and the eruptive structure in the inner corona. Here we present a study on a complex solar radio eruption consisting of a type II and three reversely-drifting type III bursts, using simultaneous EUV and radio imaging data. It is found that the type II burst is closely associated with a propagating and evolving CME-driven EUV shock structure, originated initially at the northern shock flank and later transferred to the top part of the shock. This source transfer is co-incident with the presence of shock decay and enhancing signatures observed at the corresponding side of the EUV front. The electron energy accelerated by the shock at the flank is estimated to be ~ 0.3 c by examining the imaging data of the fast-drifting herringbone structure of the type II burst. The reversely-drifting type III sources are found to be within the ejecta and correlated with a likely reconnection event therein. Implications on further observational studies and relevant space-weather forecasting techniques are discussed. **24 August 2014**

Simultaneous Radio and EUV Imaging of a Multi-lane Coronal Type II Radio Burst

S. W. **Feng**, G. H. Du, Y. Chen, X. L. Kong, G. Li, F. Guo

Solar Phys. Volume 290, Issue 4, pp 1195-1205 **2015**

A multi-lane solar type II radio burst was observed by several solar spectrographs on **16 February 2011**. The event was also recorded by the Nançay Radioheliograph (NRH) at several metric wavelengths, by the Atmospheric Imaging Assembly (AIA) onboard the Solar Dynamics Observatory (SDO), and by the Extreme Ultraviolet Imager (EUVI) onboard the Solar TErrestrial Relations Observatory (STEREO) in a number of EUV passbands. These multi-wavelength data provide a rare opportunity to reveal the emission source of the multiple type II lanes. Our study shows that all lanes are associated with a single EUV wave, presumably the radio-emitting shock. The EUV wave was driven by a coronal mass ejection (CME) associated with an M1.6 flare and a filament eruption. With the NRH data and the three-dimensional (3D) bow-shock reconstruction that we built using the multi-viewpoint data of the EUV wave, we are able to deduce the 3D coordinates of the radio sources. We conclude that all the three type II lanes originated from the western flank of the shock, with two of them from closely adjacent locations on the southern part, the other one from a distinct location on the northern part. This case study demonstrates how the type II origin can be pinpointed by combining analyses of different data sets.

DIAGNOSTICS ON THE SOURCE PROPERTIES OF A TYPE II RADIO BURST WITH SPECTRAL BUMPS

S. W. **Feng**, Y. Chen, X. L. Kong, G. Li, H. Q. Song, X. S. Feng, and Fan Guo

2013 ApJ 767 29; **File**

In recent studies, we proposed that source properties of type II radio bursts can be inferred through a causal relationship between the special shape of the type II dynamic spectrum (e.g., bump or break) and simultaneous extreme ultraviolet (EUV)/white light imaging observations (e.g., CME-shock crossing streamer structures). As a further extension of these studies, in this paper we examine the coronal mass ejection (CME) event on **2007 December 31** associated with a multiple type II radio burst. We identify the presence of two spectral bump features on the observed dynamic spectrum. By combining observational analyses of the radio spectral observations and the EUV-white light imaging data, we conclude that the two spectral bumps result from a CME-shock propagating across dense streamers on the southern and northern sides of the CME. It is inferred that the corresponding two type II emissions originate separately from the two CME-shock flanks where the shock geometries are likely quasi-perpendicular or oblique. Since the emission lanes are bumped as a whole within a relatively short time, it suggests that the type II radio bursts with bumps of this study are emitted from spatially confined sources (with a projected lateral dimension smaller than 0.05-0.1 R ⊙ at a fundamental frequency level of 20-30 MHz).

RADIO SIGNATURES OF CORONAL-MASS-EJECTION–STREAMER INTERACTION AND SOURCE DIAGNOSTICS OF TYPE II RADIO BURST

S. W. **Feng**, Y. Chen, X. L. Kong, G. Li, H. Q. Song, X. S. Feng, and Ying Liu

2012 ApJ 753 21, **File**

http://sprg.ssl.berkeley.edu/~liuxying/pubs/2012_apj_feng.pdf

It has been suggested that type II radio bursts are due to energetic electrons accelerated at coronal shocks. Radio observations, however, have poor or no spatial resolutions to pinpoint the exact acceleration locations of these electrons.

In this paper, we discuss a promising approach to infer the electron acceleration location by combining radio and white light observations. The key assumption is to relate specific morphological features (e.g., spectral bumps) of the dynamic spectra of type II radio bursts to imaging features (e.g., coronal mass ejection (CME) going into a streamer) along the CME (and its driven shock) propagation. In this study, we examine the CME-streamer interaction for the solar eruption dated on **2003 November 1**. The presence of spectral bump in the relevant type II radio burst is identified, which is interpreted as a natural result of the shock-radio-emitting region entering the dense streamer structure. The study is useful for further determinations of the location of type II radio burst and the associated electron acceleration by CME-driven shock**.**

Spectral Trends of Solar Bursts at Sub-THz Frequencies

L. O. T. **Fernandes,** P. Kaufmann, E. Correia, C. G. Giménez de Castro, A. S. Kudaka, A. Marun, P. Pereyra, J.-P. Raulin, A. B. M. Valio

Solar Physics January **2017**, 292:21

http://sci-hub.cc/10.1007/s11207-016-1043-6

Previous sub-THz studies were derived from single-event observations. We here analyze for the first time spectral trends for a larger collection of sub-THz bursts. The collection consists of a set of 16 moderate to small impulsive solar radio bursts observed at 0.2 and 0.4 THz by the Solar Submillimeter-wave Telescope (SST) in 2012 – 2014 at El Leoncito, in the Argentinean Andes. The peak burst spectra included data from new solar patrol radio telescopes (45 and 90 GHz), and were completed with microwave data obtained by the Radio Solar Telescope Network, when available. We critically evaluate errors and uncertainties in sub-THz flux estimates caused by calibration techniques and the corrections for atmospheric transmission, and introduce a new method to obtain a uniform flux scale criterion for all events. The sub-THz bursts were searched during reported GOES soft X-ray events of class C or larger, for periods common to SST observations. Seven out of 16 events exhibit spectral maxima in the range 5 – 40 GHz with fluxes decaying at sub-THz frequencies (three of them associated to GOES class X, and four to class M). Nine out of 16 events exhibited the sub-THz spectral component. In five of these events, the sub-THz emission fluxes increased with a separate frequency from that of the microwave spectral component (two classified as X and three as M), and four events have only been detected at sub-THz frequencies (three classified as M and one as C). The results suggest that the THz component might be present throughout, with the minimum turnover frequency increasing as a function of the energy of the emitting electrons. The peculiar nature of many sub-THz burst events requires further investigations of bursts that are examined from SST observations alone to better understand these phenomena. **27 Jan 2012, 6 March 2012, March 13, 2012, 9 May 2012, 22 Oct 2012,February 17, 2013, April 12, 2013, 13 May 2013, 5 Nov 2013, 7 Nov 2013, 28 Jan 2014, 22 Oct 2014, 27 Oct 2014, 5 Nov 2014, 7 Nov 2014**

Table 1 List of well identified impulsive sub-THz solar bursts

Comparative Study of Solar Bursts at Sub-THz Frequencies

Fernandes, L. O. T.; Kaufmann, P.; Correia, E.; Marun, A.; Pereyra, P.; Raulin, J.-P.; Valio, A. B. M.

Ground-based Solar Observations in the Space Instrumentation Era

ASP Conference Series, Vol. 504, p. 87, **2016**

http://aspbooks.org/publications/504/087.pdf

We analyze a large set of 17 solar radio bursts observed at sub-THz (0.2 and 0.4 THz) in 2012-2014 together with the new solar patrol radio telescopes (45 and 90 GHz), operated at El Leoncito, in the Argentinean Andes, allowing the derivation of complete burst spectra in this unexplored range of frequencies. We discuss the uncertainties in sub-THz flux estimates caused by calibration techniques and the corrections for atmospheric transmission. The burst spectra were completed with microwave bursts data obtained by the Radio Solar Telescope Network – RSTN. The events selection was based on GOES soft X-rays burst reported for classes stronger then C. Nearly 50 percent of the bursts exhibited a frequency increasing sub-THz spectral component. The results suggest that the THz component might be always present, with the minimum turn-over frequencies shifting to higher frequencies for larger energies of the electrons producing the emissions.

Flaring loop parameters estimated from solar decimeter type U-like and type J-like fine structures

Francisco C.R. **Fernandes**a, , , José Augusto S.S. Dutraa, Rafael D. Cunha da Silvaa, Hanumant S. Sawant

Advances in Space Research, Volume 49, Issue 11, 1 June **2012**, Pages 1607–1614

This work presents the analysis of five fine structures in the solar radio emission, observed between June 2000 and October 2001 by the Brazilian Solar Spectroscope (BSS), in the decimeter frequency band of 950–2500 MHz. Based on

their morphological characteristics identified in the dynamic spectra, the fine structures had been classified as type U-like or type J-like bursts. Such emissions are variants of the type III bursts. They support the hypothesis of generation by plasma emission mechanism, from interaction of electron beams accelerated during solar flares, propagating along closed magnetic structures, within the trapped plasma of the solar corona. The spectral and temporal characteristics of the five fine structures had been obtained from the dynamic spectra and the parameters of the agent and the emitting source have been determined, assuming both fundamental and harmonic emissions. The analysis revealed the flux density of the structures is less than 20–80 s.f.u. For assumption of harmonic emission, the interval of values for the source parameters estimated are: the loop size is (0.3–5.1) × 1010 cm; the electron beam velocity is in the range of 0.16–0.53 c; the temperature of coronal loop top is of the order of (0.25–1.55) × 107 K; and the low limit for the magnetic field is of 7–26 G. These results are in agreement with previous determinations reported in the literature.

(Stellar) Coronal mass ejections and type II radio emission variability during a magnetic cycle on the solar-type star ε Eridani

Dúalta Ó **Fionnagáin**, Robert D. Kavanagh, Aline A. Vidotto, Sandra V. Jeffers, Pascal Petit, Stephen Marsden, Julien Morin, Aaron A Golden

ApJ **2021**

https://arxiv.org/pdf/2111.02284.pdf

We simulate possible stellar coronal mass ejection (CME) scenarios over the magnetic cycle of ϵ Eridani (18 Eridani; HD 22049). We use three separate epochs from 2008, 2011, and 2013, and estimate the radio emission frequencies associated with these events. These stellar eruptions have proven to be elusive, although a promising approach to detect and characterise these phenomena are low-frequency radio observations of potential type II bursts as CME induced shocks propagate through the stellar corona. **Stellar type II radio bursts** are expected to emit below 450 MHz, similarly to their solar counterparts. We show that the length of time these events remain above the ionospheric cutoff is not necessarily dependent on the stellar magnetic cycle, but more on the eruption location relative to the stellar magnetic field. We find that these type II bursts would remain within the frequency range of LOFAR for a maximum of 20-30 minutes post-eruption for the polar CMEs, (50 minutes for 2nd harmonics). We find evidence of slower equatorial CMEs, which result in slightly longer observable windows for the 2008 and 2013 simulations. Stellar magnetic geometry and strength has a significant effect on the detectability of these events. We place the CMEs in the context of the stellar mass-loss rate (27-48 × solar mass-loss rate), showing that they can amount to 3-50% of the stellar wind mass-loss rate for ϵ Eridani. Continuous monitoring of likely stellar CME candidates with low-frequency radio telescopes will be required to detect these transient events.

An Interpretation of a Possible Mechanism for the First Ground-Level Enhancement of Solar Cycle 24

K. A. **Firoz**, W. Q. Gan, Y. P. Li, J. Rodríguez-Pacheco

Solar Phys. **201**4

It is well known that solar flares and shocks driven by coronal mass ejections (CMEs) are high-energy particle acceleration processes that might cause a high-energy particle event known as a ground-level enhancement (GLE). In this context, we have attempted to understand the processes responsible for the first GLE event (GLE71 **17 May 2012** 01:50 UT) of Solar Cycle 24. We studied the spatial and spectral data from the Solar Dynamics Observatory (SDO) the Culgoora radio-heliograph, and Wind/WAVES instrument, and analyzed the temporal data of the solar-flare components, the solar radio-flux density, and the electron fluxes from the Reuven Ramaty High Energy Solar Spectroscopic Imager (RHESSI), the Geostationary Operational Environmental Satellite (GOES), the Radio Solar Telescope Network (RSTN), and Wind spacecraft. The flare had two ribbons separated by the neutral line between negative and positive magnetic polarity. Their structure was also almost consistent with the contours of some flare components, which were almost saturated during the flare-peak time. As indicated by the metric–kilometric Type-II burst, and because it extended over a wide heliolongitude ($>\approx 41^{\circ}$) range, the CME-driven shock was fast enough to cause high-energy particle acceleration at a high altitude in the solar corona. Moreover, the CME and flare-flash phases were aligned along the same direction, which implies that if the CME-driven shock played the leading role in causing the GLE, preceding flare components may have contributed to the shock.

An Interpretation of GLE71 Concurrent CME-driven Shock Wave

Firoz, Kazi A.; Zhang, Q. M.; Gan, W. Q.; Li, Y. P.; Rodríguez-Pacheco, J.; Moon, Y.-J.; Kudela, K.; Park, Y.-D.; Dorman, Lev I.

Astrophysical Journal Supplement, Volume 213, Issue 2, article id. 24, 14 pp. (**2014**)

Particle accelerations in solar flares and CME-driven shocks can sometimes result in very high-energy particle events (>=1 GeV) that are known as ground level enhancements (GLEs). Recent studies on the first GLE event (GLE71 **2012 May 17** 01:50 UT) of solar cycle 24 suggested that CME-driven shock played a leading role in causing the event. To verify this claim, we have made an effort to interpret the GLE71 concurrent shock wave. For this, we have deduced the possible speed and height of the shock wave in terms of the frequency (MHz) of the solar radio type II burst and its drift rate (MHz min-1), and studied the temporal evolution of the particle intensity profiles at different heights of the solar corona. For a better perception of the particle acceleration in the shock, we have studied the solar radio type II burst with concurrent solar radio and electron fluxes. When the particle intensity profiles are necessarily shifted in time at ~1 AU, it is found that the growth phases of the electron and cosmic ray intensity fluxes are strongly correlated (>0.91 >=0.87) with the frequency drift rate of the type II burst, which is also consistent with the intensive particle accelerations at upper coronal heights (~>=0.80 R S < 1.10 R S). Thus, we conclude that the CME-driven shock was possibly capable of producing the high-energy particle event. However, since the peaks of some flare components are found to be strongly associated with the fundamental phase of the type II burst, the preceding flare is supposed to contribute to the shock acceleration process.

On the possible mechanism of the first ground level enhancement in cosmic ray intensity of solar cycle 24

Firoz, Kazi A.; Gan, W. Q.; Li, Y. P.; Rodriguez-Pacheco, J.
Astrophysics and Space Science, Volume 350, Issue 1, pp.21-32, **2014**
We have carried out this work to comprehend the possible mechanisms of the first ground level enhancement (GLE71 **17 May 2012** 01:50 UT) in cosmic ray intensity of the solar cycle 24. For this, the cosmic ray intensities registered by neutron monitors at several sites have been analyzed and studied with concurrent solar flares of different energy channels. To assess empirically whether the GLE might have been caused by the energy released from solar flare or CME-driven shock, we identify the possible time line in terms of the lowest spectral index determined from proton fluxes. If the GLE is caused by the energy released from particle acceleration in solar flare, the intensive phase of the flare representing the extreme emission should exist within/around the possible time line. In this respect, it is observed that the possible time line lies within the prominent phase of CME-driven shock. For better understanding, we have checked the possible relativistic energy with respect to solar flare as well as CME-driven shock. As witnessed, if the extreme emission phase of the flare is considered as the reason for the causation of GLE peak, the flare components procured insufficient amount of energy (≤˜0.085 GeV) to produce a GLE. If the extreme emission phase of the flare is also considered as the dominator along GLE onset, the possible energy procurement (≤˜0.414 GeV) is still not adequate to produce a GLE. In contrast, the CME-driven shock is capable of procuring enough possible relativistic energy (≥˜1.21 GeV) that is sufficient amount of the energy for a GLE production. Any amount of the energy (<0.414 GeV) released from preceding flare components is supposed to have been contributed to the shock process. Thus, it is assumed that the GLE71 was possibly caused by the energy released from the shock acceleration, which might have been boosted by the energy emanated from preceding flare.

What aspects of solar flares can be clarified with mm/submm observations? Review

Gregory D. **Fleishman**, Juan Carlos, Martinez Oliveros, Enrico Landi, Lindsay Glesener
Front. Astron. Space Sci. 9:966444. **2022**
doi: 10.3389/fspas.2022.966444
https://www.frontiersin.org/articles/10.3389/fspas.2022.966444/pdf
This paper identifies several unsolved questions about solar flares, which can potentially be answered or at least clarified with mm/submm observations with ALMA. We focus on such questions as preflare phases and the initiation of solar flares and the efficiency of particle acceleration during flares. To investigate the preflare phase we propose to use the extraordinary sensitivity and high spatial resolution of ALMA, which promises to identify very early enhancements of preflare emission with high spatial resolution and link them to the underlying photospheric magnetic structure and chromospheric flare ribbons. In addition to revealing the flare onsets, these preflare measurements will aid in the investigation of particle acceleration in multiple ways. High-frequency imaging spectroscopy data in combination with the microwave data will permit the quantification of the high-energy cutoff in the nonthermal electron spectra, thus helping to constrain the acceleration efficiency. Detection and quantification of secondary relativistic positron (produced due to nonthermal accelerated ions) contribution using the imaging polarimetry data will help constrain acceleration efficiency of nonthermal nuclei in flares. Detection of a “mysterious” rising spectral component with high spatial resolution will help determine the emission mechanism responsible for this component, and will then help in quantifying this either nonthermal or thermal component of the flaring plasma. We discuss what ALMA observing mode(s) would be the most suitable for addressing these objectives. **2001-08-25**, **24 Aug 2007**

Solar flare accelerates nearly all electrons in a large coronal volume

Gregory D. **Fleishman**, Gelu M. Nita, Bin Chen, Sijie Yu & Dale E. Gary

Nature (**2022**)

https://www.nature.com/articles/s41586-022-04728-8.pdf **File**

https://doi.org/10.1038/s41586-022-04728-8

Solar flares, driven by prompt release of free magnetic energy in the solar corona1,2, are known to accelerate a substantial portion (ten per cent or more)3,4 of available electrons to high energies. Hard X-rays, produced by high-energy electrons accelerated in the flare5, require a high ambient density for their detection. This restricts the observed volume to denser regions that do not necessarily sample the entire volume of accelerated electrons6. Here we report evolving spatially resolved distributions of thermal and non-thermal electrons in a solar flare derived from microwave observations that show the true extent of the acceleration region. These distributions show a volume filled with only (or almost only) non-thermal electrons while being depleted of the thermal plasma, implying that all electrons have experienced a prominent acceleration there. This volume is isolated from a surrounding, more typical flare plasma of mainly thermal particles with a smaller proportion of non-thermal electrons. This highly efficient acceleration happens in the same volume in which the free magnetic energy is being released2. **10 Sep 2017**

Gyroresonance and free-free radio emissions from multi-thermal multi-component plasma

Gregory D. **Fleishman**, Alexey A. Kuznetsov, Enrico Landi

ApJ **914** 52 **2021**

https://arxiv.org/pdf/2104.07655.pdf

https://doi.org/10.3847/1538-4357/abf92c

https://iopscience.iop.org/article/10.3847/1538-4357/abf92c/pdf

Thermal plasma of solar atmosphere includes a wide range of temperatures. This plasma is often quantified, both in observations and models, by a differential emission measure (DEM). DEM is a distribution of the thermal electron density square over temperature. In observations, the DEM is computed along a line of sight, while in the modeling -- over an elementary volume element (voxel). This description of the multi-thermal plasma is convenient and widely used in the analysis and modeling of extreme ultraviolet emission (EUV), which has an optically thin character. However, there is no corresponding treatment in the radio domain, where optical depth of emission can be large, more than one emission mechanism are involved, and plasma effects are important. Here, we extend the theory of the thermal gyroresonance and free-free radio emissions in the classical mono-temperature Maxwellian plasma to the case of a multi-temperature plasma. The free-free component is computed using the DEM and temperature-dependent ionization states of coronal ions, contributions from collisions of electrons with neutral atoms, exact Gaunt factor, and the magnetic field effect. For the gyroresonant component, another measure of the multi-temperature plasma is used which describes the distribution of the thermal electron density over temperature. We give representative examples demonstrating important changes in the emission intensity and polarization due to considered effects. The theory is implemented in available computer code. **11 Jul 2012**

CESRA Highlights #2993 **2021** http://www.astro.gla.ac.uk/users/eduard/cesra/?p=2993

Coronal Heating Law Constrained by Microwave Gyroresonant Emission

Gregory D. **Fleishman**, Sergey A. Anfinogentov, Alexey G. Stupishin, Alexey A. Kuznetsov, Gelu M. Nita

ApJ **909** 89 **2021**

https://arxiv.org/pdf/2101.03651.pdf

https://doi.org/10.3847/1538-4357/abdab1

https://iopscience.iop.org/article/10.3847/1538-4357/abf92c/pdf

The question why the solar corona is much hotter than the visible solar surface still puzzles solar researchers. Most theories of the coronal heating involve a tight coupling between the coronal magnetic field and the associated thermal structure. This coupling is based on two facts: (i) the magnetic field is the main source of the energy in the corona and (ii) the heat transfer preferentially happens along the magnetic field, while is suppressed across it. However, most of the information about the coronal heating is derived from analysis of EUV or soft X-ray emissions, which are not explicitly sensitive to the magnetic field. This paper employs another electromagnetic channel -- the sunspot-associated microwave gyroresonant emission, which is explicitly sensitive to both the magnetic field and thermal plasma. We use nonlinear force-free field reconstructions of the magnetic skeleton dressed with a thermal structure as prescribed by a field-aligned hydrodynamics to constrain the coronal heating model. We demonstrate that the microwave gyroresonant emission is extraordinarily sensitive to details of the coronal heating. We infer heating model parameters consistent with observations. **2012 Jul 12**

Characterization of turbulent magnetic reconnection in solar flares with microwave imaging spectroscopy

Gregory **Fleishman**, Dale Gary, Bin Chen, Sijie Yu, Natsuha Kuroda, and Gelu Nita
EGU2020-2099 May **2020**
https://meetingorganizer.copernicus.org/EGU2020/displays/36057

Magnetic reconnection plays a central role in highly magnetized plasma, for example, in solar corona. Release of magnetic energy due to reconnection is believed to drive such transient phenomena as solar flares, eruptions, and jets. This energy release should be associated with a decrease of the coronal magnetic field. Quantitative measurements of the evolving magnetic field strength in the corona are required to find out where exactly and with what rate this decrease takes place. The only available methodology capable of providing such measurements employs microwave imaging spectroscopy of gyrosynchrotron emission from nonthermal electrons accelerated in flares. Here, we report microwave observations of a solar flare, showing spatial and temporal changes in the coronal magnetic field at the cusp region; well below the nominal reconnection X point. The field decays at a rate of ~5 Gauss per second for 2 minutes. This fast rate of decay implies a highly enhanced, turbulent magnetic diffusivity and sufficiently strong electric field to account for the particle acceleration that produces the microwave emission. Moreover, spatially resolved maps of the nonthermal and thermal electron densities derived from the same microwave spectroscopy data set allow us to detect the very acceleration site located within the cusp region. The nonthermal number density is extremely high, while the thermal one is undetectably low in this region indicative of a bulk acceleration process exactly where the magnetic field displays the fast decay. The decrease in stored magnetic energy is sufficient to power the solar flare, including the associated eruption, particle acceleration, and plasma heating. We discuss implications of these findings for understanding particle acceleration in solar flares and in a broader space plasma context.

Decay of the coronal magnetic field can release sufficient energy to power a solar flare

Gregory D. **Fleishman**[1,*], Dale E. Gary[1], Bin Chen[1], Natsuha Kuroda[2,3], Sijie Yu[1], Gelu M. Nita[1]
Science 17 Jan **2020**: Vol. 367, Issue 6475, pp. 278-280 **File**
sci-hub.si/10.1126/science.aax6874

Solar flares are powered by a rapid release of energy in the solar corona, thought to be produced by the decay of the coronal magnetic field strength. Direct quantitative measurements of the evolving magnetic field strength are required to test this. We report microwave observations of a solar flare, showing spatial and temporal changes in the coronal magnetic field. The field decays at a rate of ~5 Gauss per second for 2 minutes, as measured within a flare subvolume of ~1028 cubic centimeters. This fast rate of decay implies a sufficiently strong electric field to account for the particle acceleration that produces the microwave emission. The decrease in stored magnetic energy is enough to power the solar flare, including the associated eruption, particle acceleration, and plasma heating. **10 Sept 2017**

The coronal volume of energetic particles in solar flares as revealed by microwave imaging

Gregory D. **Fleishman**, Maria A. Loukitcheva, Varvara Yu. Kopnina, Gelu M. Nita, Dale E. Gary
ApJ 867:81 **2018**
https://arxiv.org/pdf/1809.04753.pdf
sci-hub.ru/10.3847/1538-4357/aae0f6
https://iopscience.iop.org/article/10.3847/1538-4357/aae0f6/pdf

The spectrum of gyrosynchrotron emission from solar flares generally peaks in the microwave range. Its optically-thin, high-frequency component, above the spectral peak, is often used for diagnostics of the nonthermal electrons and the magnetic field in the radio source. Under favorable conditions, its low-frequency counterpart brings additional, complementary information about these parameters as well as thermal plasma diagnostics, either through gyrosynchrotron self-absorption, free-free absorption by the thermal plasma, or the suppression of emission through the so-called Razin effect. However, their effects on the low-frequency spectrum are often masked by spatial nonuniformity. To disentangle the various contributions to low-frequency gyrosynchrotron emission, a combination of spectral and imaging data is needed. To this end, we have investigated Owens Valley Solar Array (OVSA) multi-frequency images for 26 solar bursts observed jointly with Reuven Ramaty High Energy Solar Spectroscopic Imager (RHESSI) during the first half of 2002. For each, we examined dynamic spectra, time- and frequency-synthesis maps, RHESSI images with overlaid OVSA contours, and a few representative single-frequency snapshot OVSA images. We focus on the frequency dependence of microwave source sizes derived from the OVSA images and their effect on the low-frequency microwave spectral slope. We succeed in categorizing 18 analyzed events into several groups. Four events demonstrate clear evidence of being dominated by gyrosynchrotron self-absorption, with an inferred brightness temperature of ≥ 108~K. The low-frequency spectra in the remaining events are affected to varying degree by Razin suppression. We find that

many radio sources are rather large at low frequencies, which can have important implications for solar energetic particle production and escape. **2 Apr 2002, 19 Apr 2002**
Table: Events (March-May 2002)

Revealing evolution of nonthermal electrons in solar flares using 3D modeling

Gregory D. **Fleishman**, Gelu M. Nita, Natsuha Kuroda, Sabina Jia, Kevin Tong, Richard R. Wen, Zhou Zhizhuo
ApJ **2018**
https://arxiv.org/pdf/1803.09847.pdf
Understanding nonthermal particle generation, transport, and escape in solar flares requires detailed quantification of the particle evolution in the realistic 3D domain where the flare takes place. Rather surprisingly, apart of standard flare scenario and integral characteristics of the nonthermal electrons, not much is known about actual evolution of nonthermal electrons in the 3D spatial domain. This paper attempts to begin to remedy this situation by creating sets of evolving 3D models, the synthesized emission from which matches the evolving observed emission. Here we investigate two contrasting flares: a dense, "coronal-thick-target" flare SOL**2002-04-12**T17:42, that contained a single flare loop observed in both microwave and X-ray, and a more complex flare, SOL**2015-06-22**T17:50, that contained at least four distinct flaring loops needed to consistently reproduce the microwave and X-ray emission. Our analysis reveals differing evolution pattern of the nonthermal electrons in the dense and tenuous loops; however, both of which imply the central role of resonant wave-particle interaction with turbulence. These results offer new constraints for theory and models of the particle acceleration and transport in solar flares.

A Large-scale Plume in an X-Class Solar Flare

Gregory D. **Fleishman**, Gelu M. Nita, Dale E. Gary
ApJ **2017**
https://arxiv.org/pdf/1707.06636.pdf
Ever-increasing multi-frequency imaging of solar observations suggests that solar flares often involve more than one magnetic fluxtube. Some of the fluxtubes are closed, while others can contain open field. The relative proportion of nonthermal electrons among those distinct loops is highly important for understanding the energy release, particle acceleration, and transport. The access of nonthermal electrons to the open field is further important as the open field facilitates the solar energetic particle (SEP) escape from the flaring site, and thus controls the SEP fluxes in the solar system, both directly and as seed particles for further acceleration. The large-scale fluxtubes are often filled with a tenuous plasma, which is difficult to detect in either EUV or X-ray wavelengths; however, they can dominate at low radio frequencies, where a modest component of nonthermal electrons can render the source optically thick and, thus, bright enough to be observed. Here we report detection of a large-scale `plume' at the impulsive phase of an X-class solar flare, **SOL2001-08-25T16**:23, using multi-frequency radio data from Owens Valley Solar Array. To quantify the flare spatial structure, we employ 3D modeling utilizing force-free-field extrapolations from the line-of-sight SOHO/MDI magnetograms with our modeling tool GX Simulator. We found that a significant fraction of the nonthermal electrons accelerated at the flare site low in the corona escapes to the plume, which contains both closed and open field. We propose that the proportion between the closed and open field at the plume is what determines the SEP population escaping into interplanetary space.
CESRA highlights #1499, Sept **2017 EUV-invisible reservoir of solar energetic particles**
http://cesra.net/?p=1499

Narrowband Gyrosynchrotron Bursts: Probing Electron Acceleration in Solar Flares

Gregory D. **Fleishman**, Gelu M. Nita, Eduard P. Kontar, Dale E. Gary
ApJ **826** 38 **2016 File**
http://arxiv.org/pdf/1605.00948v1.pdf
Recently, in a few case studies we demonstrated that gyrosynchrotron microwave emission can be detected directly from the acceleration region when the trapped electron component is insignificant. For the statistical study reported here, we have identified events with steep (narrowband) microwave spectra that do not show a significant trapped component and at the same time show evidence of source uniformity, which simplifies the data analysis greatly. Initially, we identified a subset of more than 20 radio bursts with such narrow spectra, having low- and high-frequency spectral indices larger than 3 in absolute value. A steep low-frequency spectrum implies that the emission is nonthermal (for optically-thick thermal emission, the spectral index cannot be steeper than 2), and the source is reasonably dense and uniform. A steep high-frequency spectrum implies that no significant electron trapping occurs; otherwise a progressive spectral flattening would be observed. Roughly half of these radio bursts have RHESSI data, which allows for detailed, joint diagnostics of the source parameters and evolution. Based on an analysis of radio-to-X-ray spatial relationships, timing, and spectral

fits, we conclude that the microwave emission in these narrowband bursts originates directly from the acceleration regions, which have relatively strong magnetic field, high density, and low temperature. In contrast, the thermal X-ray emission comes from a distinct loop with smaller magnetic field, lower density, but higher temperature. Therefore, these flares occurred likely due to interaction between two (or more) magnetic loops.

A Cold Flare With Delayed Heating

Gregory D. **Fleishman**, Valentin D. Pal'shin, Natalia Meshalkina, Alexandra L. Lysenko, Larisa K. Kashapova, Alexander T. Altyntsev

ApJ **2016**

http://arxiv.org/pdf/1603.07273v1.pdf **File**

Recently, a number of peculiar flares have been reported, which demonstrate significant non-thermal particle signatures with a low, if any, thermal emission, that implies close association of the observed emission with the primary energy release/electron acceleration region. This paper presents a flare that appears a "cold" one at the impulsive phase, while displaying a delayed heating later on. Using HXR data from \kw, microwave observations by SSRT, RSTN, NoRH and NoRP, context observations, and 3D modeling, we study the energy release, particle acceleration and transport, and the relationships between the nonthermal and thermal signatures. The flaring process is found to involve interaction between a small and a big loop and the accelerated particles divided in roughly equal numbers between them. Precipitation of the electrons from the small loop produced only weak thermal response because the loop volume was small, while the electrons trapped in the big loop lost most of their energy in the coronal part of the loop, which resulted in the coronal plasma heating but no or only weak chromospheric evaporation, and thus unusually weak soft X-ray emission. Energy losses of fast electrons in the big tenuous loop were slow resulting in the observed delay of the plasma heating. We determined that the impulsively accelerated electron population had a beamed angular distribution in the direction of electric force along the magnetic field of the small loop. The accelerated particle transport in big loop was primarily mediated by turbulent waves like in the other reported cold flares. **March 10, 2002**

Validation Of The Coronal Thick Target Source Model

Gregory D. **Fleishman**, Yan Xu, Gelu N. Nita, Dale E. Gary

ApJ **816** 62 **2016**

http://arxiv.org/pdf/1511.06947v1.pdf

We present detailed 3D modeling of a dense, coronal thick target X-ray flare using the GX Simulator tool, photospheric magnetic measurements, and microwave imaging and spectroscopy data. The developed model offers a remarkable agreement between the synthesized and observed spectra and images in both X-ray and microwave domains, which validates the entire model. The flaring loop parameters are chosen to reproduce the emission measure, temperature, and the nonthermal electron distribution at low energies derived from the X-ray spectral fit, while the remaining parameters, unconstrained by the X-ray data, are selected such as to match the microwave images and total power spectra. The modeling suggests that the accelerated electrons are trapped in the coronal part of the flaring loop, but away from where the magnetic field is minimal, and, thus, demonstrates that the data are clearly inconsistent with electron magnetic trapping in the weak diffusion regime mediated by the Coulomb collisions. Thus, the modeling supports the interpretation of the coronal thick-target sources as sites of electron acceleration in flares and supplies us with a realistic 3D model with physical parameters of the acceleration region and flaring loop. **April 12, 2002**

Solar ALMA: Observation-Based Simulations of the mm and sub-mm Emissions from Active Regions

Gregory **Fleishman**, Maria Loukitcheva, Gelu Nita

presentation at the Tokyo ALMA meeting at Dec., 2014, **2015**

http://arxiv.org/pdf/1506.08395v1.pdf

We developed an efficient algorithm integrated in our 3D modeling tool, GX Simulator (Nita et al. 2015), allowing quick computation of the synthetic intensity and polarization maps of solar active regions (AR) in the ALMA spectral range. The algorithm analyzes the photospheric input (white light and magnetogram) to classify a given photospheric pixel to belong to a given photospheric structure. Then, a 1D chromospheric model (Fontenla et al. 2009) is added on top of each pixel, which forms a chromospheric model of the AR. Next step is computation of the mm and sub-mm emission produced from this chromosphere model. A huge advantage of this approach is that emission from any given AR can be synthesized very fast, on the order of a few minutes after the AR selection. Using the GX Simulator tool it is also possible to produce synthetic maps of the microwave (gyroresonance) and EUV emission from the same AR model and compare them with the ALMA synthetic maps and with the corresponding observed microwave and/or EUV data.

10 Sep 2014

Energy Partitions and Evolution in a Purely Thermal Solar Flare

Gregory D. **Fleishman**, Gelu M. Nita, Dale E. Gary

ApJ **802** 122 **2015**

This paper presents a solely thermal flare, which we detected in the microwave range from the thermal gyro- and free-free emission it produced. An advantage of analyzing thermal gyro emission is its unique ability to precisely yield the magnetic field in the radiating volume. When combined with observationally-deduced plasma density and temperature, these magnetic field measurements offer a straightforward way of tracking evolution of the magnetic and thermal energies in the flare. For the event described here, the magnetic energy density in the radio-emitting volume declines over the flare rise phase, then stays roughly constant during the extended peak phase, but recovers to the original level over the decay phase. At the stage where the magnetic energy density decreases, the thermal energy density increases; however, this increase is insufficient, by roughly an order of magnitude, to compensate for the magnetic energy decrease. When the magnetic energy release is over, the source parameters come back to nearly their original values. We discuss possible scenarios to explain this behavior. **2001 Apr 15**

Theory of Gyroresonance and Free-Free Emissions from Non-Maxwellian Quasi-steady-state Electron Distributions

Gregory D. **Fleishman**1,2,3 and Alexey A. Kuznetsov

2014 ApJ 781 77

Currently there is a concern about the ability of the classical thermal (Maxwellian) distribution to describe quasi-steady-state plasma in the solar atmosphere, including active regions. In particular, other distributions have been proposed to better fit observations, for example, kappa- and n-distributions. If present, these distributions will generate radio emissions with different observable properties compared with the classical gyroresonance (GR) or free-free emission, which implies a way of remotely detecting these non-Maxwellian distributions in the radio observations. Here we present analytically derived GR and free-free emissivities and absorption coefficients for the kappa- and n-distributions, and discuss their properties, which are in fact remarkably different from each other and from the classical Maxwellian plasma. In particular, the radio brightness temperature from a gyrolayer increases with the optical depth τ for kappa-distribution, but decreases with τ for n-distribution. This property has a remarkable consequence allowing a straightforward observational test: the GR radio emission from the non-Maxwellian distributions is supposed to be noticeably polarized even in the optically thick case, where the emission would have strictly zero polarization in the case of Maxwellian plasma. This offers a way of remote probing the plasma distribution in astrophysical sources, including solar active regions as a vivid example. See http://plasma2014.cosmos.ru/presentations

Microwave Signature of Relativistic Positrons in Solar Flares

G. D. **Fleishman**, A. T. Altyntsev, and N. S. Meshalkina

Publ. Astron. Soc. Japan 65, No. SP1, S7 [5 pages] (**2013**)

http://pasj.asj.or.jp/v65/sp1/65S007/65S007.pdf

Relativistic antiparticles can be created in high-energy nuclear interactions; thus, the detection of antiparticles in an astrophysical source can tell us something remarkable about the underlying high-energy processes and nuclear interactions. However, once created, the antiparticles remain a minor fraction of their conjugant normal particles, so the detection of the antiparticles represents a big science challenge. To address this challenge we employ the imaging and polarimetry of microwave radiation produced as the positrons gyrate in the ambient magnetic field. The key property of the radiation used in this method is that the oppositely charged particles, electrons and positrons, produce radiation with opposite helicity, easily distinguishable by currently operating radio facilities. Analysis of available spatially resolved microwave data augmented by independent magnetic field measurements allows us to remotely detect the relativistic positron component in several solar flares. **2000 Mar 13**

PROBING DYNAMICS OF ELECTRON ACCELERATION WITH RADIO AND X-RAY SPECTROSCOPY, IMAGING, AND TIMING IN THE 2002 APRIL 11 SOLAR FLARE

Gregory D. **Fleishman**1,2, Eduard P. Kontar3, Gelu M. Nita1, and Dale E. Gary

2013 ApJ 768 190
Based on detailed analysis of radio and X-ray observations of a flare on **2002 April 11** augmented by realistic three-dimensional modeling, we have identified a radio emission component produced directly at the flare acceleration region. This acceleration region radio component has distinctly different (1) spectrum, (2) light curves, (3) spatial location, and, thus, (4) physical parameters from those of the separately identified trapped or precipitating electron components. To derive evolution of physical parameters of the radio sources we apply forward fitting of the radio spectrum time sequence with the gyrosynchrotron source function with five to six free parameters. At the stage when the contribution from the acceleration region dominates the radio spectrum, the X-ray- and radio-derived electron energy spectral indices agree well with each other. During this time the maximum energy of the accelerated electron spectrum displays a monotonic increase with time from ~300 keV to ~2 MeV over roughly one minute duration indicative of an acceleration process in the form of growth of the power-law tail; the fast electron residence time in the acceleration region is about 2-4 s, which is much longer than the time of flight and so requires a strong diffusion mode there to inhibit free-streaming propagation. The acceleration region has a relatively strong magnetic field, B ~ 120 G, and a low thermal density, ne 2 × 109 cm–3. These acceleration region properties are consistent with a stochastic acceleration mechanism.

New Interactive Solar Flare Modeling and Advanced Radio Diagnostics Tools

Gregory D. **Fleishman**1,2, Gelu M. Nita1 and Dale E. Gary1
BBSO Preprint # 1478, **2011**
Advances in Plasma Astrophysics, Proceedings IAU Symposium No. 274, 2010
A. Bonanno, E. de Gouveia Dal Pino & A. Kosovichev, eds.
The coming years will see routine use of solar data of unprecedented spatial and spectral resolution, time cadence, and completeness in the wavelength domain. To capitalize on the soon to be available radio facilities such as the expanded OVSA, SSRT and FASR, and the challenges they present in the visualization and synthesis of the multi-frequency datasets, we propose that realistic, sophisticated 3D active region and flare modeling is timely now and will be a forefront of coronal studies over the coming years. Here we summarize our 3D modeling efforts, aimed at forward fitting of imaging spectroscopy data, and describe currently available 3D modeling tools. We also discuss plans for future generalization of our modeling tools.

A COLD, TENUOUS SOLAR FLARE: ACCELERATION WITHOUT HEATING

Gregory D. **Fleishman**1,2, Eduard P. Kontar3, Gelu M. Nita1 and Dale E. Gary
2011 ApJ 731 L19**; File**
We report the observation of an unusual cold, tenuous solar flare, which reveals itself via numerous and prominent non-thermal manifestations, while lacking any noticeable thermal emission signature. RHESSI hard X-rays and 0.1-18 GHz radio data from OVSA and Phoenix-2 show copious electron acceleration (1035 electrons s-1 above 10 keV) typical for GOES M-class flares with electrons energies up to 100 keV, but GOES temperatures not exceeding 6.1 MK. The imaging, temporal, and spectral characteristics of the flare have led us to a firm conclusion that the bulk of the microwave continuum emission from this flare was produced directly in the acceleration region. The implications of this finding for the flaring energy release and particle acceleration are discussed.

Fast Gyrosynchrotron Codes

Gregory D. **Fleishman** & Alexey A. Kuznetsov
BBSO preprint # 1420, **2010** ApJ 721 1127, **File**
Radiation produced by charged particles gyrating in a magnetic field is highly significant in the astrophysics context. Persistently increasing resolution of astrophysical observations calls for corresponding 3D modeling of the radiation. However, available exact equations are prohibitively slow to compute comprehensive table of high-resolution models

required for many practical applications. To remedy this situation, we develop approximate gyrosynchrotron (GS) codes capable of fast calculating the GS emission (in non-quantum regime) from both isotropic and anisotropic electron distributions in non-relativistic, mildly relativistic, and ultrarelativistic energy domains applicable throughout a broad range of source parameters including dense or tenuous plasmas and weak or strong magnetic field. The computation time is reduced by several orders of magnitude compared with the exact GS algorithm. The new algorithm performance can gradually be adjusted to the user needs depending of what — precision or computation speed — is to be optimized for the given modeling. The codes are made available for the users as a supplement to this paper.

SUB-THZ RADIATION MECHANISMS IN SOLAR FLARES
Gregory D. **Fleishman**1,2 and Eduard P. Kontar3
BBSO preprint # 1408, **2009**
Observations in the sub-THz range of large solar flares have revealed a mysterious spectral component increasing with frequency and hence distinct from the microwave component commonly accepted to be produced by gyrosynchrotron (GS) emission from accelerated electrons. Evidently, having a distinct sub-THz component requires either a distinct emission mechanism (compared to the GS one), or different properties of electrons and location, or both. We find, however, that the list of possible emission mechanisms is incomplete. This Letter proposes a more complete list of emission mechanisms, capable of producing a sub-THz component, both well-known and new in this context and calculates a representative set of their spectra produced by a) free-free emission, b) gyrosynchrotron emission, c) synchrotron emission from relativistic positrons/electrons, d) diffusive radiation, and e) Cherenkov emission. We discuss the possible role of the mechanisms in forming the sub-THz emission and emphasize their diagnostics potential for flares.

DYNAMIC MAGNETOGRAPHY OF SOLAR FLARING LOOPS
Gregory D. **Fleishman**1,2, Gelu M. Nita1, and Dale E. Gary1
Astrophysical Journal, 698:L183–L187, **2009**

http://www.iop.org:80/EJ/toc/-alert=43191/1538-4357/698/2

We develop a practical forward fitting method based on the SIMPLEX algorithm with shaking, which allows the derivation of the magnetic field and other parameters along a solar flaring loop using microwave imaging spectroscopy of gyrosynchrotron emission.We illustrate the method using a model loop with spatially varying magnetic field, filled with uniform ambient density and an evenly distributed fast electron population with an isotropic, power-law energy distribution.

Broadband Quasi-periodic Radio and X-Ray Pulsations in a Solar Flare
Gregory D. **Fleishman**1,2, T. S. Bastian3, and Dale E. Gary1
2008 ApJ 684 1433
https://iopscience.iop.org/article/10.1086/589821/pdf
We describe microwave and hard X-ray observations of strong quasi-periodic pulsations from the GOES X1.3 solar flare on **2003 June 15**. The radio observations were made jointly by the Owens Valley Solar Array (OVSA), the Nobeyama Polarimeter (NoRP), and the Nobeyama Radioheliograph (NoRH). Hard X-ray observations were made by RHESSI. Using Fourier analysis, we study the frequency- and energy-dependent oscillation periods, differential phase, and

modulation amplitudes of the radio and X-ray pulsations. Focusing on the more complete radio observations, we also examine the modulation of the degree of circular polarization and of the radio spectral index. The observed properties of the oscillations are compared with those derived from two simple models for the radio emission. In particular, we explicitly fit the observed modulation amplitude data to the two competing models. The first model considers the effects of MHD oscillations on the radio emission. The second model considers the quasi-periodic injection of fast electrons. We demonstrate that quasi-periodic acceleration and injection of fast electrons is the more likely cause of the quasi-periodic oscillations observed in the radio and hard X-ray emission, which has important implications for particle acceleration and transport in the flaring sources.

Data-driven solar wind model and prediction of type II bursts

M. S. L. **Florens**, Iver H. Cairns, S. A. Knock, P. A. Robinson
GEOPHYSICAL RESEARCH LETTERS, VOL. 34, L04104, doi:10.1029/2006GL028522, **2007**
Type II solar radio bursts are produced by shock waves moving through the corona and solar wind. An existing theory predicts Type II dynamic spectra by considering electron acceleration at the shock, growth of Langmuir waves, and their conversion into radiation. Two contributions are presented, both relevant to space weather research and missions like STEREO. First, a more realistic 2-dimensional model for the solar wind is developed, based on spacecraft data at 1 AU, and illustrated for a specific period. It relates time to longitude and extrapolates to different heliocentric distances using MHD style equations and power-law temperature models. Second, the type II theory is combined with the data-driven solar wind model to predict the dynamic spectrum of a specific Type II burst. The results show reasonable semiquantitative agreement with observations. Issues and possible improvements are outlined.

Solar radio bursts impact on the International GNSS Service Network during Solar Cycle 24

Manuel **Flores-Soriano***
J. Space Weather Space Clim. **2024**, 14, 32
https://www.swsc-journal.org/articles/swsc/pdf/2024/01/swsc240021.pdf
Solar radio bursts (SRB) are a known source of noise for Global Navigation Satellite Systems (GNSS) such as GPS or Galileo. They can degrade the carrier-to-noise ratio of satellite signals, thereby diminishing system performance and, in severe cases, causing total service outages. Although a small amount of particularly intense events have already been studied in detail, the commonness and intensity of SRBs that could potentially impair GNSS performance remain uncertain. This study broadens the scope beyond merely extreme SRBs, studying the impact of SRBs on GNSS throughout Solar Cycle 24. Solar 1.4 GHz observations from the Radio Solar Telescope Network are used to find the 20 most intense SRBs at that frequency. The impact of each SRB is then evaluated in terms of GNSS signal strength decrease, reduction in the number of available satellites, and precision degradation. The results show that at the GPS L1 frequency only one event presented extended service degradation, while at the L2 frequency, minimum operational requirements were not met by at least one station during seven of the SRBs. Only a modest correlation between performance degradation and SRB intensity is found. In particular, it is reported how some mild SRBs affected satellite signals while others almost ten times more intense went unnoticed. The fundamental role that the SRB circular polarization plays in these discrepancies is shown with new 1.4 GHz circular polarization observations from the SMOS satellite. The different responses of GNSS receivers to SRBs depending on the receiver manufacturer are also explored.
24 September 2011, 11 April 2013, 25 June 2015
Table 1. List of the 20 most intense 1.4 GHz SRBs from Solar Cycle 24 observed by the RSTN. 2011-2017

Validation of the SMOS mission for Space Weather operations: The potential of near real-time solar observation at 1.4 GHz

M. **Flores-Soriano** , C. Cid , R. Crapolicchio
Space Weather e2020SW002649 **Volume19, Issue3** **2021**
https://agupubs.onlinelibrary.wiley.com/doi/epdf/10.1029/2020SW002649
https://doi.org/10.1029/2020SW002649
Soil Moisture and Ocean Salinity (SMOS) is an ESA mission observing Earth at 1.4 GHz with full polarimetry. SMOS images are affected by a noise of solar origin produced by the Sun appearing in the antenna's field of view. In this paper

we study whether this solar signal is of any use for scientific and space weather observations. We analyze the response of the SMOS Sun brightness temperature (BT) to thermal and non-thermal solar emissions, and compare them with observations from ground radio telescopes, GOES X-ray flares and CMEs from SOHO/LASCO. We find that the SMOS Sun BT can detect weak variations in the solar emission such as the progress of the 11-year activity cycle, the solar rotation and the thermal emission from flares. Solar radio bursts detected by the SMOS Sun BT are generally observed during flares from the visible hemisphere of the Sun that are associated with a CME. We also find a correlation between the amount of solar flux released at 1.4 GHz and the speed, angular width and kinetic energy of the CMEs. We conclude that the unique capability of the SMOS mission to perform 24h near real-time observation of the Sun with full polarimetry makes it a promising instrument for monitoring solar interferences affecting GNSS, radar and L-band wireless communications, as well as for early assessment of flares geoeffectiveness. Nevertheless, the current limitations of the solar data as byproduct of the SMOS data reduction pipeline, make it necessary to create a dedicated product for solar observations. **2006-12-06, 2011-09-24, 2014-02-25 , 2014 Oct 25, 2015-06-25 , 2016-07-23 , 2016-12-22**

Termination shock as a source of unusual solar radio bursts

Valery **Fomichev**, Gennady Chernov
2020 *ApJ* **901** 65
https://arxiv.org/ftp/arxiv/papers/2008/2008.06105.pdf
https://doi.org/10.3847/1538-4357/abad9f
https://iopscience.iop.org/article/10.3847/1538-4357/abad9f/pdf
Using centimeter wave and decimeter wave solar radio spectral observations of the flares of **November 18, 2003 and September 12, 2004,** we have discussed two type II like bursts at the meter waves. The radio bursts show that the ordinary frequency drift from high to low frequencies slows down and stops, and a frequency drift from low to high frequencies appears. An analysis of all data on the corresponding flares provides evidence of formation of quasi standing fast mode shocks (termination shocks, TS). TS are able to generate energetic electrons, responsible for the appearance of new sources of hard X ray radiation and generation of fast radio bursts (spikes), fibers and zebra structures. The sources of the radio emission bands with the unusual frequency drift are situated above the top of the post flare loops (lower TS) or are connected with the erupting prominence or coronal mass ejection (CME, upper TS). Estimations of the critical Mach numbers for the ordinary plasma parameters in the solar flares give the values 1.3 easily realized in the flare events. The conditions necessary for generation of unusual radio bursts are likely to occur in the helmet shaped magnetic structures in the solar corona.

On the Possibility of Generating Harmonics of the Electron Plasma Frequency in the Solar Atmosphere due to Explosive Instability in a System of Interpenetrating Electron and Ion Flows

V. V. **Fomichev**, S. M. Fainshtein, G. P. Chernov
Plasma Physics Reports, **2018**, Vol. 44, No. 11, pp. 1048..1052
An alternative mechanism is proposed for the generation of harmonics of the electron plasma frequency due to the development of explosive instability in a system of interpenetrating electron and proton flows in the solar atmosphere. The efficiency of the new mechanism in comparison with the earlier discussed mechanisms involving multistage processes of nonlinear interaction of waves in plasma is determined. It is shown that the development of explosive instability can lead to the excitation of the second and third harmonics of the plasma frequency with comparable amplitudes.

Excitation of electron Langmuir frequency harmonics in the solar atmosphere

V. V. **Fomichev**, S. M. Fainshtein, and G. P. Chernov
Plasma Physics Reports, Volume 39, Issue 5, pp.387-393, **2013**
An alternative mechanism for the excitation of electron Langmuir frequency harmonics as a result of the development of explosive instability in a weakly relativistic beam-plasma system in the solar atmosphere is proposed. The efficiency of the new mechanism as compared to the previously discussed ones is analyzed.

A Possible Interpretation of the Zebra Pattern in Solar Radiation

V. V. **Fomichev**, S. M. Fainshtein, and G. P. Chernov
Plasma Physics Reports, 2009, Vol. 35, No. 12, pp. 1032–1035. ***2009, File.***
Original Russian Text © V.V. Fomichev, S.M. Fainshtein, G.P. Chernov, 2009, published in Fizika Plazmy, ***2009****, Vol. 35, No. 12, pp. 1114–1117.*

The nature of the zebra pattern in continual type_IV solar radio bursts is discussed. It is shown that, when a weakly relativistic monoenergetic proton beam propagates in a highly nonisothermal plasma, the energy of the slow beam mode can be negative and explosive instability can develop due to the interaction of the slow and fast beam modes with ion sound. Due to weak spatial dispersion, ion sound generation is accompanied by cascade merging, which leads to stabilization of explosive instability. The zebra pattern forms due to the scattering of fast protons by ion sound harmonics. The efficiency of the new mechanism is compared with that of previously discussed mechanisms.

Interpretation of Radio Wave Scintillation Observed through LOFAR Radio Telescopes

Biagio **Forte**1, Richard A. Fallows2,3, Mario M. Bisi3, Jinge Zhang4, Andrzej Krankowski5, Bartosz Dabrowski5, Hanna Rothkaehl6, and Christian Vocks7
2022 ApJS 263 36
https://iopscience.iop.org/article/10.3847/1538-4365/ac6deb/pdf
Radio waves propagating through a medium containing irregularities in the spatial distribution of the electron density develop fluctuations in their intensities and phases. In the case of radio waves emitted from astronomical objects, they propagate through electron density irregularities in the interstellar medium, the interplanetary medium, and Earth's ionosphere. The LOFAR radio telescope, with stations across Europe, can measure intensity across the VHF radio band and thus intensity scintillation on the signals received from compact astronomical objects. Modeling intensity scintillation allows the estimate of various parameters of the propagation medium, for example, its drift velocity and its turbulent power spectrum. However, these estimates are based on the assumptions of ergodicity of the observed intensity fluctuations and, typically, of weak scattering. A case study of single-station LOFAR observations of the strong astronomical source Cassiopeia A in the VHF range is utilized to illustrate deviations from ergodicity, as well as the presence of both weak and strong scattering. Here it is demonstrated how these aspects can lead to misleading estimates of the propagation medium properties, for example, in the solar wind. This analysis provides a method to model errors in these estimates, which can be used in the characterization of both the interplanetary medium and Earth's ionosphere. Although the discussion is limited to the case of the interplanetary medium and Earth's ionosphere, its ideas are also applicable to the case of the interstellar medium. **2018 September 23**

FROM LARGE-SCALE LOOPS TO THE SITES OF DENSE FLARING LOOPS: PREFERENTIAL CONDITIONS FOR LONG-PERIOD PULSATIONS IN SOLAR FLARES

C. **Foullon** 1, L. Fletcher 2, I. G. Hannah 2, E. Verwichte 1, B. Cecconi 3, V. M. Nakariakov 1, K. J. H. Phillips 4 and B. L. Tan
2010 ApJ 719 151
Long-period quasi-periodic pulsations (QPPs) of solar flares are a class apart from shorter period events. By involving an external resonator, the mechanism they call upon differs from traditional QPP models, but has wider applications. We present a multi-wavelength analysis of spatially resolved QPPs, with periods around 10 minutes, observed in the X-ray spectrum primarily at energies between 3 and 25 keV. Complementary observations obtained in Hα and radio emission in the kHz to GHz frequency range, together with an analysis of the X-ray plasma properties provide a comprehensive picture that is consistent with a dense flaring loop subject to periodic energization and thermalization. The QPPs obtained in Hα and type III radio bursts, with similar periods as the QPPs in soft X-rays, have the longest periods ever reported for those types of data sets. We also report 1-2 GHz radio emission, concurrent with but unrestricted to the QPP time intervals, which is multi-structured at regularly separated narrowband frequencies and modulated with ~18 minute periods. This radio emission can be attributed to the presence of multiple "quiet" large-scale loops in the background corona. Large scale but shorter inner loops below may act as preferential resonators for the QPPs. The observations support interpretations consistent with both inner and outer loops subject to fast kink magnetohydrodynamic waves. Finally, X-ray imaging indicates the presence of double coronal sources in the flaring sites, which could be the particular signatures of the magnetically linked inner loops. We discuss the preferential conditions and the driving mechanisms causing the repeated flaring.

Estimate of Plasma Temperatures Across a CME-Driven Shock from a Comparison Between EUV and Radio Data

Federica **Frassati**, Salvatore Mancuso & Alessandro Bemporad
Solar Physics volume 295, Article number: 124 (**2020**)
https://link.springer.com/content/pdf/10.1007/s11207-020-01686-0.pdf

In this work, we analyze the evolution of an EUV wave front associated with a solar eruption that occurred on **30 October 2014**, with the aim of investigating, through differential emission measure (DEM) analysis, the physical properties of the plasma compressed and heated by the accompanying shock wave. The EUV wave was observed by the Atmospheric Imaging Assembly (AIA) onboard the Solar Dynamics Observatory (SDO) and was accompanied by the detection of a metric Type II burst observed by ground-based radio spectrographs. The EUV signature of the shock wave was also detected in two of the AIA channels centered at 193 Å and 211 Å as an EUV intensity enhancement propagating ahead of the associated CME. The density compression ratio XX of the shock as inferred from the analysis of the EUV data is X≈1.23X≈1.23, in agreement with independent estimates obtained from the analysis of the Type II band-splitting of the radio data and inferred by adopting the upstream–downstream interpretation. By applying the Rankine–Hugoniot jump conditions under the hypothesis of a perpendicular shock, we also estimate the temperature ratio as TD/TU≈1.55TD/TU≈1.55 and the post-shock temperature as TD≈2.75TD≈2.75 MK. The modest compression ratio and temperature jump derived from the EUV analysis at the shock passage are typical of weak coronal shocks.
CESRA #2735 Dec **2020** http://www.astro.gla.ac.uk/users/eduard/cesra/?p=2735

Comprehensive Analysis of the Formation of a Shock Wave Associated with a Coronal Mass Ejection

Federica **Frassati**1,2, Roberto Susino1, Salvatore Mancuso1, and Alessandro Bemporad
2019 ApJ 871 212
http://sci-hub.tw/10.3847/1538-4357/aaf9af
On **2014 November 1**, a solar prominence eruption associated with a C2.7 class flare and a type II radio burst resulted in a fast partial halo coronal mass ejection (CME). Images acquired in the extreme ultraviolet (EUV) by the Solar Dynamics Observatory/Atmospheric Imaging Assembly (AIA) and PROBA2/SWAP and in white light (WL) by Solar and Heliospheric Observatory/Large Angle and Spectrometric Coronagraph show the expansion of a bright compression front ahead of the CME. In this work, we present a detailed investigation of the CME-driven shock associated with this event following the early evolution of the compression front observed near the Sun up to the extended corona. Our aim is to shed light on the long-debated issue concerning the location and timing of shock formation in the corona. Through differential emission measure analysis, we derived, for the first time, the compression ratio across the expanding EUV front observed by AIA at different temperature ranges: higher compression ratios corresponded to higher plasma temperature ranges, as expected. Moreover, comparison between up- and downstream temperatures and those expected via adiabatic compression shows that no additional heating mechanisms occurred in the early front expansion phase, implying that the shock formed beyond the AIA field of view. Finally, the analysis of the associated type II radio burst, in combination with the inferred coronal density distribution, allowed us to identify a well-defined region located northward of the CME source region as the site for shock formation and to outline its kinematics in accordance with the evolution of the expanding front as obtained from the EUV and WL data.

Comparative Study of Microwave Polar Brightening, Coronal Holes, and Solar Wind Over the Solar Poles

Ken'ichi **Fujiki**, Kiyoto Shibasaki, Seiji Yashiro, Munetoshi Tokumaru, Kazumasa Iwai, Satoshi Masuda
Solar Phys. 294:30 **2019**
https://arxiv.org/pdf/1902.10951.pdf
http://sci-hub.tw/https://link.springer.com/article/10.1007/s11207-019-1418-6
We comparatively studied the long-term variation (1992-2017) in polar brightening observed with the Nobeyama Radioheliograph, the polar solar wind velocity with interplanetary scintillation observations at the Institute for Space-Earth Environmental Research, and the coronal hole distribution computed by potential field calculations of the solar corona using synoptic magnetogram data obtained at Kitt Peak National Solar Observatory. First, by comparing the solar wind velocity (V) and the brightness temperature (T_b) in the polar region, we found good correlation coefficients (CCs) between V and T_b in the polar regions, CC = 0.91 (0.83) for the northern (southern) polar region, and we obtained the V-T_b relationship as V =12.6 (T_b-10,667)^{1/2}+432. We also confirmed that the CC of V-T_b is higher than those of V-B and V-B/f, where B and f are the polar magnetic field strength and magnetic flux expansion rate, respectively. These results indicate that T_b is a more direct parameter than B or B/f for expressing solar wind velocity. Next, we analyzed the long-term variation of the polar brightening and its relation to the area of the polar coronal hole (A). As a result, we found that the polar brightening matches the probability distribution of the predicted coronal hole and that the CC between T_b and A is remarkably high, CC = 0.97. This result indicates that the polar brightening is strongly coupled to the size of the polar coronal hole. Therefore, the reasonable correlation of V-T_b is explained by V-A. In

addition, by considering the anti-correlation between A and f found in a previous study, we suggest that the V-T_b relationship is another expression of the Wang-Sheeley relationship (V-1/f) in the polar regions.

Relationship Between Solar Wind Speed and Coronal Magnetic Field Properties

Ken'ichi **Fujiki**, Munetoshi Tokumaru, Tomoya Iju, Kazuyuki Hakamada, Masayoshi Kojima
Solar Phys. Volume 290, Issue 9, pp 2491-2505 **2015**
http://arxiv.org/pdf/1507.03301v2.pdf
We have studied the relationship between the solar-wind speed [V] and the coronal magnetic-field properties (a flux expansion factor [f] and photospheric magnetic-field strength [Bs]) at all latitudes using data of interplanetary scintillation and solar magnetic field obtained for 24 years from 1986 to 2009. Using a cross-correlation analyses, we verified that V is inversely proportional to f and found that V tends to increase with Bs if f is the same. As a consequence, we find that V has extremely good linear correlation with Bs/f. However, this linear relation of V and Bs/f cannot be used for predicting the solar-wind velocity without information on the solar-wind mass flux. We discuss why the inverse relation between V and f has been successfully used for solar-wind velocity prediction, even though it does not explicitly include the mass flux and magnetic-field strength, which are important physical parameters for solar-wind acceleration.

Global Nature of Solar Coronal Shock Waves shown by Inconsistency between EUV Waves and Type II Radio Bursts

Aarti **Fulara**, Ryun-Young Kwon
ApJLetters **2021**
https://arxiv.org/pdf/2109.01509.pdf
We re-examine the physical relationship between Extreme-UltraViolet (EUV) waves and type II radio bursts. It has been often thought that they are two observational aspects of a single coronal shock wave. However, a lack of their speed correlation hampers the understanding of their respective (or common) natures in a single phenomenon. Knowing the uncertainties in identifying true wave components from observations and measuring their speeds, we re-examine the speeds of EUV waves reported in previous literature and compare these with type II radio bursts and Coronal Mass Ejections (CMEs). This confirms the inconsistency between the speeds of EUV waves and their associated type II radio bursts. Second, CME speeds are found to have a better correlation with type II radio bursts than EUV waves. Finally, there exists a tendency for type II speeds and their range to be much greater than those of EUV waves. We demonstrate that the speed inconsistency is in fact an intrinsic tendency and elucidate the nature of a coronal shock wave consisting of both driven and non-driven parts. This suggests that the speed inconsistency would remain even if all other uncertainties were removed. **2013 April 11**

Tracking CME effects from “the Sun to the mud”

Peter **Gallagher**, Pietro Zucca, Eoin Carley and Joe McCauley
UKSP nugget, May **2011**
http://www.uksolphys.org/?p=2633
In order to study Type II radio bursts and their relationship with CMEs, in September 2010 we set up an autonomous solar radio observing station, the Rosse Solar-Terrestrial Observatory (Figure 2).

Fundamental and harmonic plasma emission in different plasma environments

Urs **Ganse**, Patrick Kilian, Felix Spanier, Rami Vainio
A&A 564, A15 **2014**
http://arxiv.org/pdf/1403.2240v1.pdf
Aims: Emission of radio waves from plasmas through plasma emission with fundamental and harmonic frequencies is a familiar process known from solar type II radio bursts. Current models assume the existence of counterstreaming electron beam populations excited at shocks as sources for these emission features, which limits the plasma parameters to reasonable heliospheric shock conditions. However, situations in which counterstreaming electron beams are present can also occur with different plasma parameters, such as higher magnetisation, including but not limited to our Sun. Similar radio emissions might also occur from these situations.
Methods: We used particle-in-cell simulations, to compare plasma microphysics of radio emission processes from counterstreaming beams in different plasma environments that differed in density and magnetization.
Results: Although large differences in wave populations are evident, the emission process of type II bursts appears to be qualitatively unaffected and shows the same behaviour in all environments.

Emission of Type II Radio Bursts – Single-Beam Versus Two-Beam Scenario

U. **Ganse**, P. Kilian, R. Vainio and F. Spanier

Solar Physics, October **2012**, Volume 280, Issue 2, pp 551-560

The foreshock region of a CME shock front, where shock accelerated electrons form a beam population in the otherwise quiescent plasma is generally assumed to be the source region of type II radio bursts. Nonlinear wave interaction of electrostatic waves excited by the beamed electrons are the prime candidates for the radio waves' emission.
To address the question whether a single, or two counterpropagating beam populations are a requirement for this process, we have conducted 2.5D particle-in-cell simulations using the fully relativistic ACRONYM code.
Results show indications of three-wave interaction leading to electromagnetic emission at the fundamental and harmonic frequency for the two-beam case. For the single-beam case, no such signatures were detectable.

NONLINEAR WAVE INTERACTIONS AS EMISSION PROCESS OF TYPE II RADIO BURSTS

Urs **Ganse**1, Patrick Kilian1, Felix Spanier1, and Rami Vainio

2012 ApJ 751 145

The emission of fundamental and harmonic frequency radio waves of type II radio bursts are assumed to be products of three-wave interaction processes of beam-excited Langmuir waves. Using a particle-in-cell code, we have performed simulations of the assumed emission region, a coronal mass ejection foreshock with two counterstreaming electron beams. Analysis of wavemodes within the simulation shows self-consistent excitation of beam-driven modes, which yield interaction products at both fundamental and harmonic emission frequencies. Through variation of the beam strength, we have investigated the dependence of energy transfer into electrostatic and electromagnetic modes, confirming the quadratic dependence of electromagnetic emission on electron beam strength**.**

The Broken Lane of a Type II Radio Burst Caused by Collision of a Coronal Shock with a Flare Current Sheet

Guannan **Gao**, Min Wang, Ning Wu, Jun Lin, E. Ebenezer, Baolin Tan

Solar Phys. Volume 291, Issue 11, pp 3369–3384 **2016**

http://link.springer.com/article/10.1007/s11207-016-1007-x
https://arxiv.org/pdf/1612.01784v1.pdf

We investigated a peculiar metric type II solar radio burst with a broken lane structure that was observed on **November 13, 2012**. In addition to the radio data, we also studied the data in other wavelengths. The bursts were associated with two coronal mass ejections (CMEs) and two flares that originated from Active Region AR 11613. A long current sheet developed in the first CME, and the second CME collided with the current sheet first and then merged with the first CME. Combined information revealed by the multi-wavelength data indicated that a coronal shock was accountable for the type II radio burst and that the collision of this shock with the current sheet resulted in the broken lane of the type II radio burst. The type II burst lane re-formed after the shock passed through the current sheet. Furthermore, we estimated the thickness of the current sheet from a gap in the lane of the type II burst, and found that the result is consistent with previous ones obtained for various events observed in different wavelengths by different instruments. In addition, the regular type II burst associated with the first CME/flare was also studied, and the magnetic field in each source region of the two type II bursts was deduced in different ways.

Decimetric type U solar radio bursts and associated EUV phenomena on 2011 February 9

Guannan **Gao** (corr-auth), Qiangwei Cai, Shaojie Guo, Min Wang

ApJ **923** 268 **2021**

https://arxiv.org/pdf/2110.10012.pdf
https://iopscience.iop.org/article/10.3847/1538-4357/ac3135/pdf
https://doi.org/10.3847/1538-4357/ac3135

A GOES M1.9 flare took place in active region AR 11153 on **February 9,2011**. With the resolution of 200 kHz and a time cadence of 80 ms, the reverse-drifting (RS) type III bursts, intermittent sequence of type U bursts, drifting pulsation structure (DPS), and fine structures were observed by the Yunnan Observatories Solar Radio Spectrometer(YNSRS). Combined information revealed by the multi-wavelength data indicated that after the DPS which observed by YNSRS, the generation rate of type U bursts suddenly increased 5 times than before. In this event, the generation rate of type U bursts may depend on the magnetic reconnection rate. Our observations are consistent with previous numerical simulations results. After the first plasmoid produced (plasma instability occurred), the magnetic reconnection rate

increased suddenly 5-8 times than before. Furthermore, after the DPS, the frequency range of turnover frequency of type U bursts is obviously broadened 3 times than before, which indicates the fluctuation amplitude of the density in the loop-top. Our observations also support the numerical simulations during the flare impulsive phase. The turbulence occurs at the top of the flare loop, the plasmoids can trap the non-thermal particles and cause the density fluctuation at the loop-top. The observations are generally consistent with the results of numerical simulations, helping us to better understand the characteristics of the whole physical process of eruption.

Decimetric and metric digital solar radio spectrometers of the Yunnan Astronomical Observatories and the first-light results

G. **Gao**, M. Wanga, L. Donga, N. Wu, J. Lin
New Astron. Volume 30, July **2014**, Pages 68–78
http://www.sciencedirect.com/science/article/pii/S1384107614000153
Based on an old decimetric solar radio spectrometer working in the frequency range of 625–1500 MHz of the Yunnan Astronomical Observatories (YNAO) during the last solar cycle, we designed a fully digital Fast Fourier Transform (FFT) spectrometer to upgrade the old one. The new digital spectrometer has the spectral resolution of 200 kHz, much higher than the old one (about 1.3 MHz). In addition, we also established a new metric solar radio telescope working in the frequency range of 70–700 MHz located at the Fuxian Solar Observatory of YNAO, deploying the same type of the digital FFT spectrometer. The two instruments have begun to operate in a daily survey mode since September 2009 and March 2012, respectively, and many solar radio bursts have been observed. In these events, various types of decimetric and metric fine structures with fairly meticulous spectral features were recognized. These features were never resolved in previous observation and studies. We have introduced these two instruments with their detailed technological components, as well as a set of observational data obtained during the first-light of the instruments. The information revealed by these data can improve our knowledge and understanding of the physics of the energy conversion, particle acceleration and transportation during the solar eruption. **2010-08-01, 2011-02-09, 2011-02-15, 2012-03-05, 2012-03-09, 2012-07-27, 2012-11-13, 2013-03-15, 2013-05-17**

Radio observations of the fine structure inside a post-CME current sheet

Guan-Nan **Gao**1,2,3, Min Wang1,3,4, Jun Lin1, Ning Wu5, Cheng-Ming Tan4, Berhard Kliem1,6 and Yang Su7
Research in Astronomy and Astrophysics, Volume 14, Number 7, 843-854, **2014**
A solar radio burst was observed in a coronal mass ejection/flare event by the Solar Broadband Radio Spectrometer at the Huairou Solar Observing Station on **2004 December 1**. The data exhibited various patterns of plasma motions, suggestive of the interaction between sunward moving plasmoids and the flare loop system during the impulsive phase of the event. In addition to the radio data, the associated white-light, Hα, extreme ultraviolet light, and soft and hard X-rays were also studied.

Frequency Agile Solar Radiotelescope: A Next-Generation Radio Telescope for Solar Physics and Space Weather

Dale E. **Gary**, Bin Chen, James F. Drake, Gregory D. Fleishman, Lindsay Glesener, Pascal Saint-Hilaire, Stephen M. White
White Paper submitted to the Solar and Space Physics 2024 Decadal Survey **2022**
https://arxiv.org/pdf/2210.10827.pdf
The Frequency Agile Solar Radiotelescope (FASR) has been strongly endorsed as a top community priority by both Astronomy & Astrophysics Decadal Surveys and Solar & Space Physics Decadal Surveys in the past two decades. Although it was developed to a high state of readiness in previous years (it went through a CATE analysis and was declared ``doable now''), the NSF has not had the funding mechanisms in place to fund this mid-scale program. Now it does, and the community must seize this opportunity to modernize the FASR design and build the instrument in this decade. The concept and its science potential have been abundantly proven by the pathfinding Expanded Owens Valley Solar Array (EOVSA), which has demonstrated a small subset of FASR's key capabilities such as dynamically measuring the evolving magnetic field in eruptive flares, the temporal and spatial evolution of the electron energy distribution in flares, and the extensive coupling among dynamic components (flare, flux rope, current sheet). The FASR concept, which is orders of magnitude more powerful than EOVSA, is low-risk and extremely high reward, exploiting a fundamentally new research domain in solar and space weather physics. Utilizing dynamic broadband imaging spectropolarimetry at radio wavelengths, with its unique sensitivity to coronal magnetic fields and to both thermal plasma and nonthermal electrons from large flares to extremely weak transients, the ground-based FASR will make synoptic measurements of the coronal magnetic field and map emissions from the chromosphere to the middle corona in

3D. With its high spatial, spectral, and temporal resolution, as well as its superior imaging fidelity and dynamic range, FASR will be a highly complementary and synergistic component of solar and heliospheric capabilities needed for the next generation of solar science.

A Solar FRB

D. **Gary**, H. Hudson
RHESSI Nuggets #400 February **2021**
https://sprg.ssl.berkeley.edu/~tohban/wiki/index.php/A_Solar_FRB
2019-05-06

Microwave and Hard X-Ray Observations of the 2017 September 10 Solar Limb Flare

Dale E. **Gary**, Bin Chen, Brian R. Dennis, Gregory D. Fleishman, Gordon J. Hurford, Sa"m Krucker, James M. McTiernan, Gelu M. Nita, Albert Y. Shih,Stephen M. White, Sijie Yu
ApJ **863** 83 **2018**
https://arxiv.org/pdf/1807.02498.pdf
http://sci-hub.tw/http://iopscience.iop.org/article/10.3847/1538-4357/aad0ef/meta
We report the first science results from the newly completed Expanded Owens Valley Solar Array (EOVSA), which obtained excellent microwave imaging spectroscopy observations of SOL2017-09-10, a classic partially-occulted solar limb flare associated with an erupting flux rope. This event is also well-covered by the Reuven Ramaty High Energy Solar Spectroscopic Imager (RHESSI) in hard X-rays (HXRs). We present an overview of this event focusing on microwave and HXR data, both associated with high-energy nonthermal electrons, and discuss them within the context of the flare geometry and evolution revealed by extreme ultraviolet (EUV) observations from the Atmospheric Imaging Assembly aboard the Solar Dynamics Observatory (SDO/AIA). The EOVSA and RHESSI data reveal the evolving spatial and energy distribution of high-energy electrons throughout the entire flaring region. The results suggest that the microwave and HXR sources largely arise from a common nonthermal electron population, although the microwave imaging spectroscopy provides information over a much larger volume of the corona.
RHESSI Science Nuggets #327 **2018**
http://sprg.ssl.berkeley.edu/~tohban/wiki/index.php/Microwave_Imaging_Spectroscopy_of_Flares_is_Here

Role of solar radio observations in space weather. **Review**

Gary DE.
2016. In: 2016 URSI Asia-Pacific Radio Science Conference (URSI AP-RASC), 21–25 August, Seoul, South Korea, pp. 1–4.
https://doi.org/10.1109/URSIAP-RASC.2016.7883552.

Early Observations with the Expanded Owens Valley Solar Array

Dale **Gary**∗
CESRA Abstract **2016** p.43
http://cesra2016.sciencesconf.org/conference/cesra2016/pages/CESRA2016_prog_abs_book_v1.pdf
The Expanded Owens Valley Solar Array (EOVSA) is a newly expanded and upgraded, solar-dedicated radio array consisting of 13 antennas of 2.1 m diameter equipped with receivers designed to cover the 1-18 GHz frequency range. Two large (27-m diameter) dishes are being outfitted with He-cooled receivers for use in calibration of the small dishes. During 2015, the array obtained observations from dozens of flares in total power mode on 8 antennas. Since February 2016, it has begun taking solar data on all 13 small antennas with full interferometric correlations, as well as calibration observations with the first of the two large antennas equipped with its He-cooled receiver. The second He-cooled receiver is nearly complete, and will be available around the time of the meeting. We briefly review the commissioning activities leading up to full operations, including polarization and gain measurements and calibration methods, and resulting measures of array performance. We then present some early imaging observations with the array, emphasizing the remarkable temporal and spectral resolution of the instrument, together with joint RHESSI hard X-ray and SDO EUV observations.

Space Weather Effects of Solar Radio Bursts

Dale **Gary**∗1 and Gelu Nita

CESRA Abstract **2016**

http://cesra2016.sciencesconf.org/conference/cesra2016/pages/CESRA2016_prog_abs_book_v1.pdf

The effects of solar radio noise on wireless navigation and communications systems have been clearly demonstrated in a few cases, with the most serious being outages of the Global Positioning System (GPS) over the entire sunlit hemisphere of the Earth in December 2006. We review what is known about both the actual observed effects and assessments of the prevalence of such effects in the future, and point out the need for better monitoring of solar bursts. We also discuss strategies for reducing or mitigating the threat of solar radio noise on wireless technological systems.

EOVSA Coverage of a Recent Gamma-ray Flare

Dale **Gary** and Gregory Fleishman.

RHESSI Science Nugget No. 252, May **2015**

http://sprg.ssl.berkeley.edu/~tohban/wiki/index.php/EOVSA_Coverage_of_a_Recent_Gamma-Ray_Flare

Expanded Owens Valley Solar Array (EOVSA) Imaging spectroscopy in the microwave range from the new Owens Valley instrument. **2015-05-05**

SOL2015-05-05 flare was quite remarkable due to the fact that its X-ray emission extends well into the gamma-ray range. This nugget gives an overview of the flare and shows the correspondence between the microwave and hard X-ray emissions.

The recent X2.7 flare of SOL2015-05-05 was unusually energetic in its non-thermal properties, and merits further study. The unique microwave data provided EOVSA give the opportunity to study the time behavior of the pulsations more closely, and to relate them to the magnetic field in the source region due to the microwave spectral dependence of peak frequency on magnetic field strength.

Magnetography of Solar Flaring Loops with Microwave Imaging Spectropolarimetry

D. E. **Gary**, G. D. Fleishman, G. M. Nita

Solar Physics, December **2013**, Volume 288, Issue 2, pp 549-565

We have developed a general framework for modeling gyrosynchrotron and free–free emission from solar flaring loops and used it to test the premise that 2D maps of source parameters, particularly the magnetic field, can be deduced from spatially resolved microwave spectropolarimetry data. We show quantitative results for a flaring loop with a realistic magnetic geometry, derived from a magnetic-field extrapolation, and containing an electron distribution with typical thermal and nonthermal parameters, after folding through the instrumental profile of a realistic interferometric array. We compare the parameters generated from forward-fitting a homogeneous source model to each line of sight through the folded image data cube both with the original parameters used in the model and with parameters generated from forward-fitting a homogeneous source model to the original (unfolded) image data cube. We find excellent agreement in general, but with systematic effects that can be understood as due to the finite resolution in the folded images and the variation of parameters along the line of sight, which are ignored in the homogeneous source model. We discuss the use of such 2D parameter maps within a larger framework of 3D modeling, and the prospects for applying these methods to data from a new generation of multifrequency radio arrays now or soon to be available.

A Wideband Spectrometer with RFI Detection

Dale E. **Gary**, Zhiwei Liu and Gelu Nita

BBSO #1411, **2010**

We report on the design and construction of a wideband spectrometer of 500 MHz instantaneous bandwidth that includes automatic Radio Frequency Interference (RFI) detection. The implementation is based on hardware developed at the Center for Astronomical Signal Processing and Electronics Research (CASPER). The unique aspect of the spectrometer is that it accumulates both power and power-squared, which are then used to develop a "spectral kurtosis" (SK) estimator. The SK estimator statistics are used for real-time detection and excision of certain types of RFI embedded in the received signal. We report on the use of this spectrometer in the Korean Solar Radio Burst Locator (KSRBL). This instrument utilizes four of these 500 MHz bandwidth SK spectrometers in parallel, to achieve a 2 GHz instantaneous bandwidth that is time multiplexed over the entire 0.24-18 GHz radio frequency range, to study solar bursts. The performance of the spectrometers for excising RFI over this range is presented. It is found that the algorithm is especially useful for excising highly intermittent RFI, but is less successful for RFI due to digital signals. A method we call multiscale SK is presented that addresses the known blindness of Kurtosis-based estimators to 50% duty-cycle

RFI. The SK algorithm can also be applied to pre-correlation spectral channels of an FX correlator to remove unwanted RFI from interferometer data.

CAUSE AND EXTENT OF THE EXTREME RADIO FLUX DENSITY REACHED BY THE SOLAR FLARE OF 2006 DECEMBER 06
Dale E. **Gary**
BBSO Preprint #1360, **2008**
http://solar.njit.edu/preprints/gary1360.pdf
Goodman, J.M. (Editor-in-Chief), **2008** Ionospheric Effects Symposium (Proceedings); (JMG Associates Ltd: Sheridan Books), accession No. PB2008-112709
https://arxiv.org/ftp/arxiv/papers/1901/1901.09262.pdf
The solar burst of **2006 December 06** reached a radio flux density of more than 1 million solar flux units (1 sfu = 10^{-22} W/m^2/Hz), as much as 10 times the previous record, and caused widespread loss of satellite tracking by GPS receivers. The event was well observed by NJIT's Owens Valley Solar Array (OVSA). This study concentrates on an accurate determination of the flux density (made difficult due to the receiver systems being driving into non-linearity), and discusses the physical conditions on the Sun that gave rise to this unusual event. At least two other radio outbursts occurred in the same region (on **2006 December 13 and 14**) that had significant, but smaller effects on GPS. We discuss the differences among these three events, and consider the implications of these events for the upcoming solar cycle.

Dale E. **Gary**
In: Proceedings of Nobeyama Symposium 2004, 121, **2006**.
The next step toward developing radio diagnostics of coronal explosive phenomena is timeresolved broadband imaging spectroscopy. This requirement will materialize with the development of the **Frequency-agile Solar Radio Telescope** (FASR; see *e.g.*, Gary, 2006), whose frequency range will cover the solar atmosphere from the chromosphere to the corona out to about 1*Rs* above the photosphere.

Type II bursts, shock waves, and coronal transients – The event of 29 June 1980, 0233 UT.
Gary, D.E., Dulk, G.A., House, L., Illing, R., *et al.*:
1984, *Astron. Astrophys.* **134**, 222 – 233.

Radio impulsive events in quiet solar corona and Axion Quark Nugget Dark Matter
Shuailiang **Ge**, Md Shahriar Rahim Siddiqui, Ludovic Van Waerbeke, Ariel Zhitnitsky
2020
https://arxiv.org/pdf/2009.00004.pdf
The Murchison Widefield Array (MWA) has recorded \cite{Mondal-2020} impulsive radio events in the quiet solar corona at frequencies 98, 120, 132, and 160 MHz. We propose that these radio events represent the direct manifestation of the dark matter annihilation events within the so-called axion quark nugget (AQN) framework. It has been previously argued that the AQN annihilation events in the quiet solar corona \cite{Zhitnitsky:2017rop,Raza:2018gpb} can be identified with nanoflares originally conjectured by Parker long ago \cite{Parker-1983}. In the present work we further support this claim by demonstrating that the radio observations \cite{Mondal-2020}, including the frequency of appearance, temporal and spatial distributions, energetics, and other related observables are nicely matching the generic consequences of the AQN annihilation events in the quiet corona. We propose to test these ideas by analyzing the correlated clustering radio impulsive events in the different frequency bands. We also make generic predictions for low (80 and 89) MHz and high (179, 196, 217 and 240) MHz frequency bands which had been already recorded but not published by \cite{Mondal-2020} yet. We also suggest to test this proposal by studying possible cross-correlation between MWA radio signals and Solar Orbiter recording of the extreme ultraviolet photons (coined as the "campfires") to support or refute this proposal.

Observation of solar radio burst events from Mars orbit with the Shallow Radar instrument

Christopher **Gerekos**, Gregor Steinbrügge, Immanuel Jebaraj, Andreas Casillas, Elena Donini, Beatriz Sánchez-Cano, Mark Lester, Jasmina Magdalenić, Sean Peters, Andrew Romero-Wolf, Donald Blankenship
A&A 683, A56 (**2024**)
https://arxiv.org/pdf/2307.01747.pdf
https://www.aanda.org/articles/aa/pdf/2024/03/aa47900-23.pdf

Context. Multispacecraft and multiwavelength observations of solar eruptions, such as flares and coronal mass ejections, are essential to understanding the complex processes behind these events. The study of solar burst events in the radio frequency spectrum has relied almost exclusively on data from ground-based observations and a few dedicated heliophysics missions such as STEREO or Wind.
Aims. By reanalysing existing data from the Mars Reconnaissance Orbiter (MRO) Shallow Radar (SHARAD) instrument, a Martian planetary radar sounder, we discovered the instrument was also capable of detecting solar radio bursts and that it was able to do so with unprecedented resolution for a space-based solar instrument. In this study, we aim to demonstrate the reliability and value of SHARAD as a new solar radio observatory.
Methods. We characterised the sensitivity of the instrument to type III solar radio bursts through a statistical analysis of correlated observations using STEREO and Wind as references. Using 38 correlated detections, we established the conditions under which SHARAD can observe solar bursts in terms of acquisition geometry. As an example of scientific application, we also present the first analysis of type III characteristic times at high resolution beyond 1 AU.
Results. A simple logistic model based purely on geometrical acquisition parameters can predict burst show versus no-show in SHARAD data with an accuracy of 79.2%, demonstrating the reliability of the instrument in detecting solar bursts and laying the foundation for using SHARAD as a solar radio observatory. The extremely high resolution of the instrument, both in temporal and frequency directions; its bandwidth; and its position in the Solar System enable SHARAD to make significant contributions to heliophysics. Notably, it could provide data on plasma processes on the site of the burst generation and along the propagation path of associated fast electron beams.. **22 Dec 2011, 1 Jan 2012, 30 Dec 2020**

On the Signature of Chaotic Dynamics in 10.7 cm Daily Solar Radio Flux

Oindrilla **Ghosh** , T. N. Chatterjee
Solar Phys. Volume 290, Issue 11, pp 3319-3330 **201**5

We examine the properties of the time-series of daily values of the 10.7-cm solar radio flux and sunspot-number activity indices, and their relative behavior. The analysis and the comparisons are based upon the estimation of the embedded dimension and the use of recurrence plots. The result shows higher-order chaos in 10.7-cm radio flux, and a similar but not identical chaotic nature in the sunspot number indicative of a change in the phase space of the Sun. Both data series show a stochastic behavior only during the rising and peak phase of Solar Cycle 23.

Multi-technique Analysis of the Solar 10.7 cm Radio Flux Time-Series in Relation to Predictability

Oindrilla **Ghosh**, Tanushree Ghosh, T. N. Chatterjee
Solar Physics, June **2014**, Volume 289, Issue 6, pp 2297-2315

We studied the predictability of the 10.7 cm solar radio flux by using stationary and non-stationary time-series analysis techniques of fractal theory to find the correlation exponent, the spectral exponent, the Hurst exponent, and the fluctuation exponent of the time series. The Hurst exponent was determined, from which the fractal dimension and consequently the predictability was evaluated. The results suggest that stationary methods of analysis yield inconsistent result, that is, amongst the four techniques used, the values of the exponents show great disparity. While two of the techniques, namely the auto-correlation function analysis and the spectral analysis, indicate long-term positive correlation, the other two methods, specifically the Hurst rescaled range-analysis and the fluctuation analysis, clearly exhibit the anti-correlated nature of the time series. The two non-stationary methods, that is, the discrete wavelet transform and the centered moving-average analysis, yielded values of the Hurst exponent that are indicative of positive correlation, of persistent behavior, and also showed that the time series is predictable to a certain extent.

Analysis of the Radio Solar Telescope Network's Noon Flux Observations Over Three Solar Cycles (1988–2020)

O. **Giersch**, J. Kennewell
Radio Science Volume57, Issue8 August **2022** e2022RS007456

https://doi.org/10.1029/2022RS007456
https://agupubs.onlinelibrary.wiley.com/doi/epdf/10.1029/2022RS007456
The Sun is a readily accessible source of wideband noise that can be used for the calibration of a wide variety of radio systems. Since 1979 the United States Air Force Radio Solar Telescope Network (RSTN) has performed solar flux observations around noon on eight frequencies between 245 and 15,400 MHz. These fluxes are disseminated by the National Ocean and Atmospheric Administration (NOAA) and are used by many radio and radar system operators to perform system calibration. Little analysis has been performed on the RSTN noon flux values. Here we review the calibration procedures of RSTN and perform statistical tests between the four sites comprising RSTN. For system operators who require precise system calibration the noted variations may be large enough to cast doubt on RSTN flux values for such calibration. However, for many communication systems a calibration within one or two dB is adequate. We discuss the reported variation both in linear and logarithmic terms. When it is possible to used smoothed data the inter-site variation becomes less of a problem, although the correlation between sites at Ku band (15,400 MHz) still appears excessively large. We update some simple empirical models for wideband solar flux based purely on the 10 cm flux at any time, as these have also been used in solar radio calibration procedures. We give practical advice on the use of solar flux for radio system calibration and make some recommendations that we believe could improve the accuracy and utility of solar radio flux reports.
2 The Solar Radio Burst Contribution to Space Weather

Radio Interferometric Observations of the Sun Using Commercial Dish TV Antennas

G. V. S. **Gireesh**, C. Kathiravan, Indrajit V. Barve & R. Ramesh
Solar Physics volume 296, Article number: 121 (**2021**)
https://arxiv.org/pdf/2109.07422
https://link.springer.com/content/pdf/10.1007/s11207-021-01871-9.pdf
https://doi.org/10.1007/s11207-021-01871-9
The radio astronomy group in the Indian Institute of Astrophysics (IIA) has been carrying out routine observations of radio emission from the solar corona at low frequencies (≈40 – 440 MHz) at the Gauribidanur observatory, about 100 km north of Bangalore. Since IIA has been performing regular observations of the solar photosphere and chromosphere using different optical telescopes in its Kodaikanal Solar Observatory (KSO) also
(see https://www.iiap.res.in/kodai.htm), the possibilities of obtaining two-dimensional radio images of the solar chromosphere using low-cost instrumentation to supplement the optical observations are being explored. As a part of the exercise, recently the group had developed prototype instrumentation for interferometric observations of radio emission from the solar chromosphere at high frequencies (≈11.2 GHz) using two commercial dish TV antennas. The hardware set-up and initial observations are presented. **21 June 2020**
CESRA #3100 **2021** https://www.astro.gla.ac.uk/users/eduard/cesra/?p=3100

Solar Radio Burst Statistics and Implications for Space Weather Effects
O. D. **Giersch**, J. Kennewell, M. Lynch
Space Weather 16 November **2017** Vol: 15, Pages: 1511–1522
https://sci-hub.ru/10.1002/2017SW001658

Solar Radio Burst Statistics and Implications for Space Weather Effects

O. D. **Giersch**, J. Kennewell, M. Lynch
Space Weather 16 November **2017** Vol: 15, Pages: 1511–1522
https://sci-hub.ru/10.1002/2017SW001658
Solar radio bursts have the potential to affect space and terrestrial navigation, communication, and other technical systems that are sometimes overlooked. However, over the last decade a series of extreme L band solar radio bursts in December 2006 have renewed interest in these effects. In this paper we point out significant deficiencies in the solar radio data archives of the National Centers for Environmental Information (NCEI) that are used by most researchers in analyzing and producing statistics on solar radio burst phenomena. In particular, we examine the records submitted by the United States Air Force (USAF) Radio Solar Telescope Network (RSTN) and its predecessors from the period 1966 to 2010. Besides identifying substantial missing burst records we show that different observatories can have statistically different burst distributions, particularly at 245 MHz. We also point out that different solar cycles may show statistically different distributions and that it is a mistake to assume that the Sun shows similar behavior in different sunspot cycles. Large solar radio bursts are not confined to the period around sunspot maximum, and prediction of such events that utilize historical data will invariably be an underestimate due to archive data deficiencies. It is important that researchers and forecasters use historical occurrence frequency with caution in attempting to predict future cycles.

Electron Acceleration and Jet-Facilitated Escape in an M Class Solar Flare on 2002 August 19

Lindsay **Glesener**, Gregory D. Fleishman

ApJ **867** 84 **2018**

https://arxiv.org/pdf/1806.00858.pdf

sci-hub.tw/10.3847/1538-4357/aacefe

Sudden jets of collimated plasma arise from many locations on the Sun, including active regions. The magnetic field along which a jet emerges is often open to interplanetary space, offering a clear "escape route" for any flare-accelerated electrons and making jets lucrative targets for studying particle acceleration and the solar sources of transient heliospheric events. Bremsstrahlung hard X-rays (HXRs) could, in principle, trace the accelerated electrons that escape along the paths of the jets, but measurements of the escaping electron beams are customarily difficult due to the low densities of the corona. In this work, we augment HXR observations with gyrosynchrotron emission observed in microwaves, as well as extreme ultraviolet (EUV) emission and modeling to investigate flare-accelerated electrons in a coronal jet. HXR and microwave data from RHESSI and OVSA, respectively, give complementary insight into electron spectra and locations, including the presence of accelerated electrons in the jet itself. High-time-resolution HXR data from the Konus-Wind instrument suggest electron acceleration timescales on the order of 1 second or shorter. We model the energetic electron distributions in the GX Simulator framework using SoHO/MDI, RHESSI, TRACE, and OVSA data as constraints. The result is a modeled distribution, informed and constrained by measurements, of accelerated electrons as they escape the Sun. Combining the detection of microwave gyrosynchrotron emission from an open, rather than closed, magnetic configuration, with realistic 3D modeling constrained by magnetograms, EUV, and X-ray emission, we obtain the most stringent constraints to date on the accelerated electrons within a solar jet.

The first results of the 2D solar observations obtained by Irkutsk incoherent scatter radar

Mariia **Globa**_1, Hamish Reidy2, Larisa Kashapova1, Roman Vasilyev1, Valentin Lebedev1, Dmitriy Kushnarev1, and Andrey Medvedev1

CESRA **2016**, p.92

http://cesra2016.sciencesconf.org/conference/cesra2016/pages/CESRA2016_prog_abs_book_v3.pdf

The Irkutsk Incoherent Scatter Radar (IISR) is used for a variety of di_erent purposes such as the study of the ionosphere, monitoring of space debris and radioastronomy. The IISR detects emission in the 150 { 162 MHz frequency range. The operation of the directivity pattern (DP) is performed by the frequency scanning technique. We have developed the method of IISR data processing that allows reconstructing radio brightness distributions of the Sun and we present the _rst results obtained with this method. The question of the possible instrumental origin of the obtained distribution was studied by the comparison of the results with observations from the Nan_cay Radioheliograph. We show that comparison with quiet Sun observations and radio noise storms display a good agreement from both instruments.

Observation of quasi-periodic solar radio bursts associated with propagating fast-mode waves

C. R. **Goddard**, G. Nisticò, V. M. Nakariakov, I. V. Zimovets, S. M. White

A&A 594, A96 **2016**

http://arxiv.org/pdf/1608.04232v1.pdf

Radio emission observations from the Learmonth and Bruny Island radio spectrographs are analysed to determine the nature of a train of discrete, periodic radio \lq sparks\rq (finite-bandwidth, short-duration isolated radio features) which precede a type II burst. We analyse extreme ultraviolet (EUV) imaging from SDO/AIA at multiple wavelengths and identify a series of quasi-periodic rapidly-propagating enhancements, which we interpret as a fast wave train, and link these to the detected radio features. The speeds and positions of the periodic rapidly propagating fast waves and the coronal mass ejection (CME) were recorded using running-difference images and time-distance analysis. From the frequency of the radio sparks the local electron density at the emission location was estimated for each. Using an empirical model for the scaling of density in the corona, the calculated electron density was used to obtain the height above the surface at which the emission occurs, and the propagation velocity of the emission location. The period of the radio sparks, $\delta tr=1.78\pm0.04$ min, matches the period of the fast wave train observed at 171 $\AA$, $\delta tEUV=1.7 \pm 0.2$ min. The inferred speed of the emission location of the radio sparks, 630 km s^{-1}, is comparable to the measured speed of the CME leading edge, 500 km s^{-1}, and the speeds derived from the drifting of the type II lanes. The calculated height of the radio emission (obtained from the density) matches the observed location of the CME leading edge. From

the above evidence we propose that the radio sparks are caused by the quasi-periodic fast waves, and the emission is generated as they catch up and interact with the leading edge of the CME. **2014-11-03**
CESRA highlight #1159 Jan **2017** http://www.astro.gla.ac.uk/users/eduard/cesra/?p=1159

The Sun at millimeter wavelengths IV. Magnetohydrodynamic waves in small-scale bright features

Juan Camilo Guevara **Gómez**, Shahin Jafarzadeh, Sven Wedemeyer, Samuel D. T. Grant, Henrik Eklund, Mikolaj Szydlarski
A&A 671, A69 **2022**
https://arxiv.org/pdf/2212.11096.pdf
https://doi.org/10.1051/0004-6361/202244228
https://www.aanda.org/articles/aa/pdf/2023/03/aa44228-22.pdf
We used solar observations of a plage/enhanced network with the Atacama Large Millimeter/sub-millimeter Array (ALMA) in Band 3 and Band 6 together with synthetic continuum maps from numerical simulations with Bifrost at the same bands to carry out a detailed study of bright small-scale magnetic features. To this end, we have used an algorithm to automatically identify and trace the features within the field of view (FoV) of the observations and the simulation. We found 193 and 293 features in the Bands 3 and 6 observations, respectively. In the degraded simulation, the total number of features were 24 for Band 3 and 204 for Band 6. In the original simulation, the total number of features were 36 for Band 3 and 392 for Band 6. Based on the simulation, we confirm the magnetic nature of the features which exhibit an oscillatory behaviour in temperature, size and horizontal velocity. The average oscillation periods were of 30-99\,s for temperature, 37-92\,s for size and 37-78\,s for horizontal velocity. There are indications for the possible presence of transverse (kink) waves with average amplitude velocities of 2.1-5.0\,km\,s−1. An anti-phase behaviour between temperature and size oscillations suggest the presence of compressible fast-sausage Magnetohydrodynamics (MHD) modes. Finally, we have estimated the flux of energy of the fast-sausage waves at the chromospheric heights sampled by ALMA as 453-1838\,W\,m−2 for Band 3 and 3640-5485\,W\,m−2 for Band 6. The decrease of wave energy-flux with height (from Band 6 to Band 3) could possibly suggest energy dissipation at chromospheric heights, thus wave heating, with the assumptions that the identified small-scale waves are typical at each band and they propagate upward through the chromosphere.

Propagation of transverse waves in the solar chromosphere probed at different heights with ALMA sub-bands

Juan Camilo Guevara **Gómez**, Shahin Jafarzadeh, Sven Wedemeyer, Mikolaj Szydlarski
A&A Let 665, L2 **2022**
https://arxiv.org/pdf/2208.12070.pdf
https://www.aanda.org/articles/aa/pdf/2022/09/aa44387-22.pdf
The Atacama Large Millimeter/sub-millimeter Array (ALMA) has provided us with an excellent diagnostic tool for studies of the dynamics of the Solar chromosphere, albeit through a single receiver band at one time presently. Each ALMA band consists of four sub-bands that are comprised of several spectral channels. To date, however, the spectral domain has been neglected in favour of ensuring optimal imaging, so that time-series observations have been mostly limited to full-band data products, thereby limiting studies to a single chromospheric layer. Here, we report the first observations of a dynamical event (i.e. wave propagation) for which the ALMA Band 3 data (centred at 3\,mm; 100\,GHz) is split into a lower and an upper sideband. In principle, this approach is aimed at mapping slightly different layers in the Solar atmosphere. The side-band data were reduced together with the Solar ALMA Pipeline (SoAP), resulting in time series of brightness-temperature maps for each side-band. Through a phase analysis of a magnetically quiet region, where purely acoustic waves are expected to dominate, the average height difference between the two side-bands is estimated as 73±16~km. Furthermore, we examined the propagation of transverse waves in small-scale bright structures by means of wavelet phase analysis between oscillations at the two atmospheric heights. We find 6\% of the waves to be standing, while 54\% and 46\% of the remaining waves are propagating upwards and downwards, respectively, with absolute propagating speeds on the order of ≈96~km/s, resulting in a mean energy flux of 3800\,W/m2. **22 April 2017**

High-frequency oscillations in small chromospheric bright features observed with ALMA

Juan Camilo Guevara **Gómez**, Shahin Jafarzadeh, Sven Wedemeyer, Mikolaj Szydlarski, Marco Stangalini, Bernhard Fleck, Peter Keys
Philosophical Transactions of the Royal Society A **2020**
https://arxiv.org/pdf/2008.04179.pdf

We report detection of oscillations in brightness temperature, size, and horizontal velocity of three small bright features in the chromosphere of a plage/enhanced-network region. The observations, which were taken with high temporal resolution (i.e., 2-sec cadence) with the Atacama Large Millimeter/submillimeter Array (ALMA) in Band 3 (centred at 3 mm; 100 GHz), exhibit three small-scale features with oscillatory behaviour with different, but overlapping, distributions of period on the order of, on average, 90±22 s, 110±12 s and 66±23 s, respectively. We find anti-correlations between perturbations in brightness temperature and size of the three features, which suggest the presence of fast sausage-mode waves in these small structures. In addition, the detection of transverse oscillations (although with a larger uncertainty) may suggest as well the presence of Alfvénic oscillations which are likely representative of kink waves. This work demonstrates the diagnostic potential of high-cadence observations with ALMA for detecting high-frequency magnetohydrodynamic waves in the solar chromosphere. Such waves can potentially channel a vast amount of energy into the outer atmosphere of the Sun. **2017 April 22**

Sunward-propagating Solar Energetic Electrons inside Multiple Interplanetary Flux Ropes

Raúl **Gómez-Herrero**1, Nina Dresing2, Andreas Klassen2, Bernd Heber2, Manuela Temmer3, Astrid Veronig3, Radoslav Bučík4,5, Miguel A. Hidalgo1, Fernando Carcaboso1, Juan J. Blanco
2017 ApJ 840 85
http://sci-hub.cc/10.3847/1538-4357/aa6c5c
On **2013 December 2 and 3**, the SEPT and STE instruments on board STEREO-A observed two solar energetic electron events with unusual sunward-directed fluxes. Both events occurred during a time interval showing typical signatures of interplanetary coronal mass ejections (ICMEs). The electron timing and anisotropies, combined with extreme-ultraviolet solar imaging and radio wave spectral observations, are used to confirm the solar origin and the injection times of the energetic electrons. The solar source of the ICME is investigated using remote-sensing observations and a three-dimensional reconstruction technique. In situ plasma and magnetic field data combined with energetic electron observations and a flux-rope model are used to determine the ICME magnetic topology and the interplanetary electron propagation path from the Sun to 1 au. Two consecutive flux ropes crossed the STEREO-A location and each electron event occurred inside a different flux rope. In both cases, the electrons traveled from the solar source to 1 au along the longest legs of the flux ropes still connected to the Sun. During the December 2 event, energetic electrons propagated along the magnetic field, while during the December 3 event they were propagating against the field. As found by previous studies, the energetic electron propagation times are consistent with a low number of field line rotations $N < 5$ of the flux rope between the Sun and 1 au. The flux rope model used in this work suggests an even lower number of rotations. **2013 November 29**

Speed Evolution of Fast CME/Shocks: Analysis of Kilometric Type II Emissions

J. A. **Gonzalez-Esparza** and E. Aguilar-Rodriguez
Ann. Geophys., 27, 3957-3966, **2009, File**
Fast CME/shocks propagating in the interplanetary medium can generate kilometric Type II (km-TII) radio emissions at the local plasma frequency and/or its harmonic, so these radio emissions provide a means of remotely tracking CME/shocks. We apply a new analysis technique, using the frequency drift of km-TII spectrum obtained by the Thermal Noise Receiver (TNR) of the WIND/WAVES experiment, to infer, at some adequate intervals, the propagation speed of six CME/shocks. We combine these results with previously reported speeds from coronagraph white light and interplanetary scintillation observations, and in-situ measurements, to study the temporal speed evolution of the six events. The speed values obtained by the km-TII analysis are in a reasonable agreement with the speed measurements obtained by other techniques at different heliocentric distance ranges. The combination of all the speed measurements show a gradual deceleration of the CME/shocks as they propagate to 1 AU. This new technique can be useful in studying the evolution of fast CME/shocks when adequate intervals of km-TII emissions are available.

Solar Energetic Particle Events and Radio Bursts **Review**

Nat **Gopalswamy**
Proc. UN/Germany workshop on the International Space Weather Initiative: Preparing for the Solar Maximum, 10-14 June, 2024 **2024**
https://arxiv.org/pdf/2410.08690 **File**
Solar Energetic Particles (SEPs) and radio bursts are indicators of particle acceleration on the Sun and in the heliosphere. The accelerated particles have energies significantly higher than thermal particles up to several orders of magnitude. SEPs are detected directly by particle detectors on Earth and in space. Understanding SEPs is important from both science and application points of view because they are poorly understood and present space weather hazard to humans and their technology in space. SEPs accompany energetic flares, coronal mass ejections (CMEs), and intense

radio bursts, which help us understand particle properties such as intensity, spectra, and time evolution. This paper summarizes how SEP properties are closely related to solar eruptions and the associated solar radio bursts. **2000.09.12, 2001.04.15, 2002.04.21, 2006.12.14, 2011.03.09**

Type III Radio Bursts from Solar Eruptions and their Connection to GLE and SGRE Events

Nat **Gopalswamy**, Anshu Kumari, Pertti A. Mäkelä
Proceedings of the URSI GASS 2023, Sapporo, Japan, 19 to 26 August 2023 **2023**
https://arxiv.org/ftp/arxiv/papers/2308/2308.11779.pdf **File**
We report on the close similarity of coronal mass ejection (CME) properties in ground level enhancement (GLE) in solar energetic particle (SEP) events and sustained gamma ray emission (SGRE) from the Sun as indicated by low frequency type III radio bursts observed in the interplanetary medium. The complex type III bursts have an average 1 MHz duration of 36 and 34 min in the SGRE and GLE events, respectively. Similarly, the CMEs underlying SGRE and GLE have average space speeds of 1866 and 2084 km/s, respectively. These are larger than the corresponding values (32 min, 1407 km/s) for a control sample of type III bursts associated with frontside halo CMEs with sky plane speed exceeding 800 km/s. These results are consistent with the idea that energetic CME driven shocks accelerate particles to very high energies that are responsible for GLE and SGRE events. **2014 February 24-25**

Can Type III Radio Storms be a Source of Seed Particles to Shock Acceleration?

Nat **Gopalswamy**, Sachiko Akiyama, Pertti Mäkelä, Seiji Yashiro, Hong Xie
Proc. 3rd URSI AT-AP-RASC, Gran Canaria, 29 May to 3 June 2022, **2022**
https://arxiv.org/ftp/arxiv/papers/2205/2205.15233.pdf
An intense type III radio storm has been disrupted by a fast halo coronal mass ejection (CME) on **2000 April 4**. The CME is also associated with a large solar energetic particle (SEP) event. The storm recovers after about10 hrs. We identified another CME that occurs on **2003 November 11** with similar CME properties but there is no type III storm in progress. The 2003 November 11 CME is also not associated with an SEP event above the background (less than 2 pfu), whereas the one with type III storm has an intense SEP event (about 56 pfu). One of the factors affecting the intensity of SEP events is the presence of seed particles that are accelerated by CME-driven shocks. We suggest that the type III storm source, which accelerates electrons to produce the storm, also accelerates ions that serve as seed particles to the CME shock. **15 Jan 2005**

A Weak Fermi Gamma-ray Event Associated with a Halo CME and a Type II Radio Burst

N. Gopalswamy, P. Mäkelä, S. Yashiro
Proceedings URSI GASS 2020 **2021**
https://arxiv.org/ftp/arxiv/papers/2105/2105.01212.pdf
We report on the **2015 June 25** sustained gamma-ray emission (SGRE) event associated with a halo coronal mass ejection and a type II radio burst in the decameter-hectometric (DH) wavelengths. The duration and ending frequency of the type II burst are linearly related to the SGRE duration as found in previous works involving intense gamma-ray events. This study confirms that the SGRE event is due to protons accelerated in the shock that produced the DH type II burst.
Table 1. The five halo CMEs from AR 12371 (18 Jun- 01 Jul)

Diffuse Interplanetary Radio Emission from a Polar Coronal Mass Ejection

N. **Gopalswamy**, P. Makela, S. Yashiro, S. Akiyama
URSI 2020 Proceedings **2021**
https://arxiv.org/ftp/arxiv/papers/2105/2105.01216.pdf
We report on the first detection of nonthermal radio emission associated with a polar coronal mass ejection. We call the radio emission as diffuse interplanetary radio emission (DIRE), which occurs in the decameter-hectometric wavelengths. The radio emission originates from the shock flanks that interact with nearby streamers. **18 Apr 2000**

Diffuse Interplanetary Radio Emission: Shock Emission or a Type III storm?

Nat **Gopalswamy**, Sachiko Akiyama, Pertti Mäkelä, Seiji Yashiro
Radio Science Letters **2020**
https://arxiv.org/ftp/arxiv/papers/2011/2011.12763.pdf
We present a clear case of a Diffuse Interplanetary Radio Emission (DIRE) event observed during **2002 March 11-12** in association with a fast coronal mass ejection (CME). In the previous event reported [1], there were two CMEs, and a detailed analysis was required to pin down the underlying CME. In the event presented here, the CME association is unambiguous, and the DIRE is found to originate from the flanks of the CME-driven shock. We also provide

quantitative explanation for not observing radio emission from the shock nose. We also clarify that DIRE is not a type III storm because the latter occurs outside of solar eruptions.

Interplanetary Radio Emission: A Summary of Recent Results Review

Nat **Gopalswamy**

Journal of Computational and Interdisciplinary Science **2020**

https://arxiv.org/ftp/arxiv/papers/2008/2008.09222.pdf **File**

This paper summarizes some recent results in the low-frequency radio physics of the Sun. The spatial domain covers the space from the outer corona to the orbit of Earth. The results obtained make use of radio dynamic spectra and white-light coronagraph images and involve radio bursts associated with solar eruptions and those occurring outside solar eruptions. ***In particular, the connection between type II radio bursts and the sustained gamma-ray emission from the Sun is highlighted.*** The directivity of interplanetary type IV bursts found recently is discussed to understand the physical reason behind it. A new event showing the diffuse interplanetary radio emission (DIRE) is introduced and its properties are compared with those of regular type II bursts. The DIRE is from the flanks of a CME-driven shock propagating through nearby streamer. Finally, a new noise storm observed by two spacecraft is briefly discussed to highlight its evolution over two solar rotations including the disruption and recovery by solar eruptions. **24 Nov 2000, 10 Mar 2002, 5 Mar 2012, 7 July 2012, 25 Feb 2014, 1 Sep 2014, 27 Aug 2017, 1 Sep 2017, 4 Sep 2017, 6 Sep 2017**

A Catalog of Type II Radio Bursts Observed by Wind/WAVES and their Statistical Properties

Nat **Gopalswamy**, Pertti Mäkelä, Seiji Yashiro

Sun and Geosphere **Vol.14, No. 2, 2019 p. 111-122 2019**

https://arxiv.org/ftp/arxiv/papers/1912/1912.07370.pdf **File**

Solar type II radio bursts are the signature of particle acceleration by shock waves in the solar corona and interplanetary medium. The shocks originate in solar eruptions involving coronal mass ejections (CMEs) moving at super-Alfvenic speeds. Type II bursts occur at frequencies ranging from hundreds of MHz to tens of kHz, which correspond to plasma frequencies prevailing in the inner heliosphere from the base of the solar corona to the vicinity of Earth. Type II radio bursts occurring at frequencies below the ionospheric cutoff are of particular importance, because they are due to very energetic CMEs that can disturb a large volume of the heliosphere. The underlying shocks accelerate not only electrons that produce the type II bursts, but also protons and heavy ions that have serious implications for space weather. The type II radio burst catalog (this https URL) presented here provides detailed information on the bursts observed by the Radio and Plasma Wave Experiment (WAVES) on board the Wind Spacecraft. The catalog is enhanced by compiling the associated flares, **CMEs**, solar energetic particle (**SEP**) events including their basic properties. We also present the statistical properties of the radio bursts and the associated phenomena, including solar-cycle variation of the occurrence rate of the type II bursts. **2000.11.09, 2005.01.15-16. 2012.07.04**

See https://cdaw.gsfc.nasa.gov/CME_list/radio/waves_type2.html

Interplanetary Type II Radio Bursts from Wind/WAVES and Sustained Gamma-Ray Emission from Fermi/LAT: Evidence for Shock Source

Nat **Gopalswamy**1, Pertti Mäkelä1,2, Seiji Yashiro1,2, Alejandro Lara1,2, Hong Xie1,2, Sachiko Akiyama1,2, and Robert J. MacDowall1

2018 ApJL 868 L19

http://iopscience.iop.org/article/10.3847/2041-8213/aaef36/pdf **File**

We present quantitative evidence that interplanetary type II radio bursts and sustained gamma-ray emission (SGRE) events from the Sun are closely related. Out of about 30 SGRE events reported in Share et al. we consider 13 events that had a duration exceeding ~5 hr to exclude any flare-impulsive phase gamma-rays. The SGRE duration also has a linear relation with the ending frequency of the bursts. The synchronism between the ending times of SGRE and the type II emission strongly supports the idea that the same shock accelerates electrons to produce type II bursts and protons (>300 MeV) that propagate from the shock to the solar surface to produce SGRE via pion decay. The acceleration of high-energy particles is confirmed by the associated solar energetic particle (SEP) events detected at Earth and/or at the Solar Terrestrial Relations Observatory spacecraft. Furthermore, the presence of >300 MeV protons is corroborated by the fact that the underlying coronal mass ejections (CMEs) had properties identical to those associated with ground-level enhancement events: they had speeds of >2000 km s−1 and all were full-halo CMEs. Many SEP events did not have detectable flux at Earth in the >300 MeV energy channels, presumably because of poor magnetic connectivity. **1991 June 11 , 2011 Mar 7, 2012 Jan 23 , 2012 Mar 5, 2012 Mar 7, 2012 Mar 9, 2012 Mar 10, 2013 May 13, 2013 May 14, 2013 May 15, 2014 Feb 25, 2015 Jun 21, September 6 2017, 2017 Sep 10**

Table 1 Properties of SGREs and the Associated CMEs, Type II Bursts, and SEP Events

Properties of DH Type II Radio Bursts and Their Space Weather Implications

N. **Gopalswamy**, P. Mäkelä

submitted to the URSI AP-RASC 2019 **2018**

https://arxiv.org/ftp/arxiv/papers/1810/1810.11173.pdf

We report on the properties of type II radio bursts observed by the Radio and Plasma Wave Experiment (WAVES) on board the Wind spacecraft over the past two solar cycles. We confirm that the associated coronal mass ejections (CMEs) are fast and wide, more than half the CMEs being halos. About half of the type II bursts extend down to 0.5 MHz, corresponding to a heliocentric distance of tens of solar radii. The DH type II bursts are mostly confined to the active region belt and their occurrence rate follows the solar activity cycle. Type II burst occurring on the western hemisphere of the Sun and extending to lower frequencies are good indicators of a solar energetic particle event.

2001/12/28 , 2002/07/20 , 2005/07/27, 2005 September 7, 2011 September 22, 2013/06/21 , 2014 February 25

Table 1. Large SEP events from the east limb

Fermi, Wind, and SOHO Observations of Sustained Gamma-Ray Emission from the Sun

N. **Gopalswamy**, P. Makela, S. Yashiro, A. Lara, H. Xie, S. Akiyama, R. J. MacDowall

Submitted to 2019 URSI Asia Pacific Radio Science Conference **2018**

https://arxiv.org/ftp/arxiv/papers/1810/1810.08958.pdf

We report on the linear relationship between the durations of two types of electromagnetic emissions associated with shocks driven by coronal mass ejections: sustained gamma-ray emission (SGRE) and interplanetary type II radio bursts. The relationship implies that shocks accelerate about 10 keV electrons (for type II bursts) and greater than 300 MeV protons (for SGRE) roughly over the same duration. The SGRE events are from the Large Area Telescope (LAT) on board the Fermi satellite, while the type II bursts are from the Radio and Plasma Wave Experiment (WAVES) on board the Wind spacecraft. Here we consider five SGRE events that were not included in a previous study of events with longer duration (greater than 5 hours). The five events are selected by relaxing the minimum duration to 3 hours. We found that some SGRE events had a tail that seems to last until the end of the associated type II burst. We pay special attention to the 2011 June 2 SGRE event that did not have a large solar energetic particle event at Earth or at the STEREO spacecraft that was well connected to the eruption. We suggest that the preceding CME acted as a magnetic barrier that mirrored protons back to Sun. **2-3 June 2011, 2011 June 7, 27-28 Jan 2012, 2012 May 17, 13 May 2013**

Sun-to-Earth Propagation of the 2015 June 21 Coronal Mass Ejection Revealed by Optical, EUV, and Radio Observations

N. **Gopalswamy**, P. Makela, S. Akiyama, S. Yashiro, H. Xie, N. Thakur

JASTP **2018**

https://arxiv.org/ftp/arxiv/papers/1807/1807.10979.pdf

We investigate the propagation of the **2015 June 21** CME-driven shock as revealed by the type II bursts at metric and longer wavelengths and coronagraph observations. The CME was associated with the second largest geomagnetic storm of solar cycle 24 and a large solar energetic particle (SEP) event. The eruption consisted of two M-class flares, with the first one being confined, with no metric or interplanetary radio bursts. However, there was intense microwave burst, indicating accelerated particles injected toward the Sun. The second flare was eruptive that resulted in a halo CME. The CME was deflected primarily by an equatorial coronal hole that resulted in the modification of the intensity profile of the associated SEP event and the duration of the CME at Earth. The interplanetary type II burst was particularly intense and was visible from the corona all the way to the vicinity of the Wind spacecraft with fundamental-harmonic structure. We computed the shock speed using the type II drift rates at various heliocentric distances and obtained information on the evolution of the shock that matched coronagraph observations near the Sun and in-situ observations near Earth. The depth of the geomagnetic storm is consistent with the 1-AU speed of the CME and the magnitude of the southward component.

Long-term Solar Activity Studies using Microwave Imaging Observations and Prediction for Cycle 25

N. **Gopalswamy**, P. Makela, S. Yashiro, S. Akiyama

Journal of Atmospheric and Solar-Terrestrial Physics **2018**

https://arxiv.org/ftp/arxiv/papers/1804/1804.02544.pdf

We use microwave imaging observations from the Nobeyama Radioheliograph at 17 GHz for long-term studies of solar activity. In particular, we use the polar and low-latitude brightness temperatures as proxies to the polar magnetic field

and the active-regions, respectively. We also use the location of prominence eruptions as a proxy to the filament locations as a function of time. We show that the polar microwave brightness temperature is highly correlated with the polar magnetic field strength and the fast solar wind speed. We also show that the polar microwave brightness at one cycle is correlated with the low latitude brightness with a lag of about half a solar cycle. We use this correlation to predict the strength of the solar cycle: the smoothed sunspot numbers in the southern and northern hemispheres can be predicted as 89 and 59, respectively. These values indicate that cycle 25 will not be too different from cycle 24 in its strength. We also combined the rush to the pole data from Nobeyama prominences with historical data going back to 1860 to study the north-south asymmetry of sign reversal at solar poles. We find that the reversal asymmetry has a quasi-periodicity of 3-5 cycles.

A Hierarchical Relationship between the Fluence Spectra and CME Kinematics in Large Solar Energetic Particle Events: A Radio Perspective

N **Gopalswamy**, P Mäkelä, S Yashiro, N Thakur, S Akiyama, H Xie

Journal of Physics: Conference Series (JPCS), Proceedings of the 16th Annual International Astrophysics Conference held in Santa Fe, NM, **2017**

https://arxiv.org/ftp/arxiv/papers/1707/1707.00209.pdf

We report on further evidence that solar energetic particles are organized by the kinematic properties of coronal mass ejections (CMEs)[1]. In particular, we focus on the starting frequency of type II bursts, which is related to the distance from the Sun where the radio emission starts. We find that the three groups of solar energetic particle (SEP) events known to have distinct values of CME initial acceleration, also have distinct average starting frequencies of the associated type II bursts. SEP events with ground level enhancement (GLE) have the highest starting frequency (107 MHz), while those associated with filament eruption (FE) in quiescent regions have the lowest starting frequency (22 MHz); regular SEP events have intermediate starting frequency (81 MHz). Taking the onset time of type II bursts as the time of shock formation, we determine the shock formation heights measured from the Sun center. We find that the shocks form on average closest to the Sun (1.51 Rs) in GLE events, farthest from the Sun in FE SEP events (5.38 Rs), and at intermediate distances in regular SEP events (1.72 Rs). Finally, we present the results of a case study of a CME with high initial acceleration (~3 km s^-2) and a type II radio burst with high starting frequency (~200 MHz) but associated with a minor SEP event. We find that the relation between the fluence spectral index and CME initial acceleration continues to hold even for this minor SEP event. **2010 June 12, 2011 November 26, 2012 May 17**

Low-Frequency Radio Bursts and Space Weather **Review**

Nat **Gopalswamy**

URSI Asia-Pacific Radio Science Conference in Seoul, August 21-25, 2016 **2016**

http://arxiv.org/pdf/1605.02218v1.pdf **File**

Low-frequency radio phenomena are due to the presence of nonthermal electrons in the interplanetary (IP) medium. Understanding these phenomena is important in characterizing the space environment near Earth and other destinations in the solar system. Substantial progress has been made in the past two decades, because of the continuous and uniform data sets available from space-based radio and white-light instrumentation. This paper highlights some recent results obtained on IP radio phenomena. In particular, the source of type IV radio bursts, the behavior of type III storms, shock propagation in the IP medium, and the solar-cycle variation of type II radio bursts are considered. All these phenomena are closely related to solar eruptions and active region evolution. The results presented were obtained by combining data from the Wind and SOHO missions.

Solar Activity Studies using Microwave Imaging Observations

Nat **Gopalswamy**

URSI Asia-Pacific Radio Science Conference in Seoul, August 21-25, 2016 **2016**

http://arxiv.org/pdf/1605.02221v1.pdf

We report on the status of solar cycle 24 based on polar prominence eruptions (PEs) and microwave brightness enhancement (MBE) information obtained by the Nobeyama radioheliograph. The north polar region of the Sun had near-zero field strength for more than three years (2012 to 2015) and ended only in September 2015 as indicated by the presence of polar PEs and the lack of MBE. The zero-polar-field condition in the south started only around 2013, but it ended by June 2014. Thus the asymmetry in the times of polarity reversal switched between cycle 23 and 24. The polar MBE is a good proxy for the polar magnetic field strength as indicated by the high degree of correlation between the two. The cross-correlation between the high- and low-latitude MBEs is significant for a lag of ~5.5 to 7.3 years, suggesting that the polar field of one cycle indicates the sunspot number of the next cycle in agreement with the Babcock-Leighton mechanism of solar cycles. The extended period of near-zero field in the north-polar region should result in a weak and delayed sunspot activity in the northern hemisphere in cycle 25. **11 Dec 2014, 30 Aug 2015**

On the Directivity of Low-Frequency Type IV Radio Bursts

Nat **Gopalswamy**, Sachiko Akiyama, Pertti Mäkelä, Seiji Yashiro, Iver H. Cairns
URSI Asia-Pacific Radio Science Conference in Seoul, August 21-25, 2016 **2016**
http://arxiv.org/pdf/1605.02223v1.pdf

An intense type IV radio burst was observed by the STEREO Behind (STB) spacecraft located about 144 degres behind Earth. The burst was associated with a large solar eruption that occurred on the backside of the Sun (N05E151) close to the disk center in the STB view. The eruption was also observed by the STEREO Ahead (STA) spacecraft (located at 149 degrees ahead of Earth) as an eruption close to the west limb (N05W60) in that view. The type IV burst was complete in STB observations in that the envelope reached the lowest frequency and then receded to higher frequencies. The burst was partial viewed from STA, revealing only the edge coming down to the lowest frequency. The type IV burst was not observed at all near Earth because the source was 61 degrees behind the east limb. The eruption was associated with a low-frequency type II burst observed in all three views, although it was not very intense. Solar energetic particles were also observed at both STEREOs and at SOHO, suggesting that the shock was much extended, consistent with the very high speed of the CME (about 2048 km/s). These observations suggest that the type IV emission is directed along a narrow cone above the flare site. We confirm this result statistically using the type IV bursts of solar cycle 23. 2005 January 15, 2005 Sept 9 **2013 November 7**

CMEs during the Two Activity Peaks in Cycle 24 and their Space Weather Consequences

N. **Gopalswamy**, P. Mäkelä, S. Akiyama, S. Yashiro, N. Thakur
Sun and Geosphere, **2015**
http://arxiv.org/pdf/1509.04216v1.pdf **File**

We report on a comparison between space weather events that occurred around the two peaks in the sunspot number (SSN) during solar cycle 24. The two SSN peaks occurred in the years 2012 and 2014. Even though SSN was larger during the second peak, we find that there were more space weather events during the first peak. The space weather events we considered are large solar energetic particle (SEP) events and major geomagnetic storms associated with coronal mass ejections (CMEs). We also considered interplanetary type II radio bursts, which are indicative of energetic CMEs driving shocks. When we compared the CME properties between the two SSN peaks, we find that more energetic CMEs occurred during the 2012 peak. In particular, we find that CMEs accompanying IP type II bursts had an average speed of 1543 km/s during the 2012 peak compared to 1201 km/s during the 2014 peak. This result is consistent with the reduction in the average speed of the general population of CMEs during the second peak. All SEP events were associated with the interplanetary type II bursts, which are better than halo CMEs as indicators of space weather. The comparison between the two peaks also revealed the discordant behavior CME rate and SSN is more pronounced during the second peak. None of the 14 disk-center halo CMEs was associated with a major storm in 2014. The lone major storm in 2014 was due to the intensification of the (southward) magnetic field in the associated magnetic cloud by a shock that caught up and propagated into the magnetic cloud. **23-24 Apr 2012; 18-19 Feb 2014**
Table 2. List of DH-km type II bursts in 2012, the associated CMEs and SEP events
Table 3. List of DH-km type II bursts in 2014, the associated CMEs and SEP events

Large Solar Energetic Particle Events Associated with Filament Eruptions Outside of Active Regions

N. **Gopalswamy**, P. Makela, S. Akiyama, S. Yashiro, H. Xie, N. Thakur, S. W. Kahler
ApJ **2015**
http://arxiv.org/ftp/arxiv/papers/1504/1504.00709.pdf

We report on four large filament eruptions (FEs) from solar cycles 23 and 24 that were associated with large solar energetic particle (SEP) events and interplanetary type II radio bursts. The post-eruption arcades corresponded to *mostly C-class soft X-ray enhancements, but an M1.0 flare was associated with one event. However, the associated* coronal mass ejections (CMEs) were fast (speeds about 1000 km/s) and appeared as halo CMEs in the coronagraph field of view. The interplanetary type II radio bursts occurred over a wide wavelength range indicating the existence of strong shocks throughout the inner heliosphere. No metric type II bursts were present in three events, indicating that the shocks formed beyond 2 to 3 Rs. In one case, there was a metric type II burst with low starting frequency indicating a shock formation height of about 2 Rs. The FE-associated SEP events did have softer spectra (spectral index greater than 4) in the 10 to 100 MeV range, but there were other low-intensity SEP events with spectral indices >/=4. Some of these events are likely FE-SEP events, but were not classified so in the literature because they occurred close to active regions. Some were definitely associated with large active region flares, but the shock formation height was large. We definitely find a

diminished role for flares and complex type III burst durations in these large SEP events. Fast CMEs and shock formation at larger distances from the Sun seem to be the primary characteristics of the FE-associated SEP events. **2000/04/04, 2000/07/22, 2000/09/12, 2000/10/25, 2001/09/15, 2001/10/19, 2002/03/16, 2002/04/17, 2002/05/22, 2002/08/14, 2003/05/31, 2004/04/11, 2010/08/14, 2011/08/09, 2011/11/26, 2012/09/28, 2013/09/29, 2014/02/20**

Obscuration of Flare Emission by an Eruptive Prominence

Nat **Gopalswamy** ans Seiji Yashiro
E-print, Sept **2013, File**, Publ. Astron. Soc. Japan 65, SP1, S11 [8 pages] (**2013**)
http://pasj.asj.or.jp/v65/sp1/65S011/65S011.pdf
We report on the eclipsing of microwave flare emission by an eruptive prominence from a neighboring region as observed by the Nobeyama Radioheliograph at 17 GHz. The obscuration of the flare emission appears as a dimming feature in the microwave flare light curve. We use the dimming feature to derive the temperature of the prominence and the distribution of heating along the length of the filament. We find that the prominence is heated to a temperature above the quiet Sun temperature at 17 GHz. The duration of the dimming is the time taken by the eruptive prominence in passing over the flaring region. We also find evidence for the obscuration in EUV images obtained by the Solar and Heliospheric Observatory (SOHO) mission. **2002/05/21-22**

Height of Shock Formation in the Solar Corona Inferred from Observations of Type II Radio Bursts and Coronal Mass Ejections

N. **Gopalswamy**, H. Xie, P. Makela, S. Yashiro, S. Akiyama, W. Uddin., A. K. Srivastava, N. C. Joshi, R. Chandra, P. K. Manoharan, K. Mahalakshmi, V. C. Dwivedi, R. Jain and A. K. Awasthi, N. V. Nitta, M. J. Aschwanden, D. P. Choudhary
E-print, Jan **2013**; Adv. Space Res., v. 51, No. 11, p. 1981-1989, **File**
Employing coronagraphic and EUV observations close to the solar surface made by the Solar Terrestrial Relations Observatory (STEREO) mission, we determined the heliocentric distance of coronal mass ejections (CMEs) at the starting time of associated metric type II bursts. We used the wave diameter and leading edge methods and measured the CME heights for a set of 32 metric type II bursts from solar cycle 24. We minimized the projection effects by making the measurements from a view that is roughly orthogonal to the direction of the ejection. We also chose image frames close to the onset times of the type II bursts, so no extrapolation was necessary. We found that the CMEs were located in the heliocentric distance range from 1.20 to 1.93 solar radii (Rs), with mean and median values of 1.43 and 1.38 Rs, respectively. We conclusively find that the shock formation can occur at heights substantially below 1.5 Rs. In a few cases, the CME height at type II onset was close to 2 Rs. In these cases, the starting frequency of the type II bursts was very low, in the range 25 ? 40 MHz, which confirms that the shock can also form at larger heights. The starting frequencies of metric type II bursts have a weak correlation with the measured CME/shock heights and are consistent with the rapid decline of density with height in the inner corona.
Table 2010-2012; 20100612, 20100613; 20100807; 20101016; 20101103; 20101103; 20101112; 20101215; 20101231; 20110127; 20110128; 20110211; 20110213; 20110214; 20110215; 20110216; 20110307; 20110308; 20110325; 20110511; 20110530; 20110802; 20110810; 20110828; 20110906; 20110930; 20111119; 20120105; 20120118; 20120120; 20120324; 20120424

Solar Radio Bursts and Space Weather

N. **Gopalswamy**
ISWI Workshop, Oct **2012**, Presentation, **File**

Radio-loud CMEs from the disk center lacking shocks at 1 AU

N. **Gopalswamy**, P. Makela, S. Akiyama, S. Yashiro, H. Xie, R. J. MacDowall, M. L. Kaiser
E-print, June **2012**, JGR, 117, A08106, **2012**
A coronal mass ejection (CME) associated with a type II burst and originating close to the center of the solar disk typically results in a shock at Earth in 2-3 days and hence can be used to predict shock arrival at Earth. However, a significant fraction (about 28%) of such CMEs producing type II bursts were not associated with shocks at Earth. We examined a set of 21 type II bursts observed by the Wind/WAVES experiment at decameter-hectometric (DH) wavelengths that had CME sources very close to the disk center (within a central meridian distance of 30 degrees), but did not have a shock at Earth. We find that the near-Sun speeds of these CMEs average to ~644 km/s, only slightly

higher than the average speed of CMEs associated with radio-quiet shocks. However, the fraction of halo CMEs is only ~30%, compared to 54% for the radio-quiet shocks and 91% for all radio-loud shocks. We conclude that the disk-center radio-loud CMEs with no shocks at 1 AU are generally of lower energy and they drive shocks only close to the Sun and dissipate before arriving at Earth. There is also evidence for other possible processes that lead to the lack of shock at 1 AU: (i) overtaking CME shocks merge and one observes a single shock at Earth, and (ii) deflection by nearby coronal holes can push the shocks away from the Sun-Earth line, such that Earth misses these shocks. The probability of observing a shock at 1 AU increases rapidly above 60% when the CME speed exceeds 1000 km/s and when the type II bursts propagate to frequencies below 1 MHz.

BEHAVIOR OF SOLAR CYCLES 23 AND 24 REVEALED BY MICROWAVE OBSERVATIONS

N. **Gopalswamy**1, S. Yashiro1,2, P. Mäkelä1,2, G. Michalek3, K. Shibasaki4, and D. H. Hathaway
2012 ApJ 750 L42

Using magnetic and microwave butterfly diagrams, we compare the behavior of solar polar regions to show that (1) the polar magnetic field and the microwave brightness temperature during solar minimum substantially diminished during the cycle 23/24 minimum compared to the 22/23 minimum. (2) The polar microwave brightness temperature (Tb) seems to be a good proxy for the underlying magnetic field strength (B). The analysis indicates a relationship, B = 0.0067Tb - 70, where B is in G and Tb in K. (3) Both the brightness temperature and the magnetic field strength show north-south asymmetry most of the time except for a short period during the maximum phase. (4) The rush-to-the-pole phenomenon observed in the prominence eruption (PE) activity seems to be complete in the northern hemisphere as of 2012 March. (5) The decline of the microwave brightness temperature in the north polar region to the quiet-Sun levels and the sustained PE activity poleward of 60oN suggest that solar maximum conditions have arrived at the northern hemisphere. The southern hemisphere continues to exhibit conditions corresponding to the rise phase of solar cycle 24.
ERRATUM: 2013 ApJ 763 L24

CORONAL MAGNETIC FIELD MEASUREMENT FROM EUV IMAGES MADE BY THE SOLAR DYNAMICS OBSERVATORY

Nat **Gopalswamy**1, Nariaki Nitta2, Sachiko Akiyama1,3, Pertti Mäkelä1,3 and Seiji Yashiro
2012 ApJ 744 72, **File**

By measuring the geometrical properties of the coronal mass ejection (CME) flux rope and the leading shock observed on **2010 June 13** by the Solar Dynamics Observatory (SDO) mission's Atmospheric Imaging Assembly we determine the Alfvén speed and the magnetic field strength in the inner corona at a heliocentric distance of ~1.4 Rs. The basic measurements are the shock standoff distance (ΔR) ahead of the CME flux rope, the radius of curvature of the flux rope (R c), and the shock speed. We first derive the Alfvénic Mach number (M) using the relationship, $\Delta R/R\ c = 0.81[(\gamma-1)M^2 + 2]/[(\gamma+1)(M^2 - 1)]$, where γ is the only parameter that needed to be assumed. For $\gamma = 4/3$, the Mach number declined from 3.7 to 1.5 indicating shock weakening within the field of view of the imager. The shock formation coincided with the appearance of a type II radio burst at a frequency of ~300 MHz (harmonic component), providing an independent confirmation of the shock. The shock compression ratio derived from the radio dynamic spectrum was found to be consistent with that derived from the theory of fast-mode MHD shocks. From the measured shock speed and the derived Mach number, we found the Alfvén speed to increase from ~140 km s^{-1} to 460 km s^{-1} over the distance range 1.2-1.5 Rs. By deriving the upstream plasma density from the emission frequency of the associated type II radio burst, we determined the coronal magnetic field to be in the range 1.3-1.5 G. The derived magnetic field values are consistent with other estimates in a similar distance range. This work demonstrates that the EUV imagers, in the presence of radio dynamic spectra, can be used as coronal magnetometers.

Coronal Mass Ejections and Solar Radio Emissions **Review**

N. **Gopalswamy**

Accepted for Publication in the book **Planetary Radio Emissions VII**, Eds. Rucker, H. O., W. S. Kurth, P. Louarn, G. Fischer, Austrian Academy of Sciences Press, Vienna, in press (**2011**), **File**

In Proceedings of the 7th International Workshop on Planetary, Solar and Heliospheric Radio Emissions (PRE VII) p. 325-342

Three types of low-frequency nonthermal radio bursts are associated with coronal mass ejections (CMEs): Type III bursts due to accelerated electrons propagating along open magnetic field lines, type II bursts due to electrons accelerated in shocks, and type IV bursts due to electrons trapped in post-eruption arcades behind CMEs. This paper presents a summary of results obtained during solar cycle 23 primarily using the white-light coronagraphic observations from the Solar Heliospheric Observatory (SOHO) and the WAVES experiment on board Wind.

LOW-FREQUENCY TYPE III RADIO BURSTS AND SOLAR ERGEIC PATCLE EVENTS.

Gopalswamy1 andP.Mäkelä2

Cent. Eur. Astrophys. Bul. Vol. 1 (**2011), File**

Complex type III bursts at low-frequencies (>14 MHz) are thought to indicate large solar energetic particle (SEP) events. We analyzed six complex type III bursts from the same active region, one of which was not accompanied by a SEP event. This event was accompanied by a fast and wide coronal mass ejection (CME), but lacked a type II burst and an interplanetary shock. When we examined the evolution and the magnetic configuration of the active region, we did not find anything peculiar. The lowest frequency of type III emission occurred at the local plasma frequency in the vicinity of the Wind spacecraft that observed the type III, which confirms that the magnetic connectivity of the source region was good. We conclude that the lack of SEPs is due to the lack of production rather than due to poor magnetic connectivity. We also show that neither the type III burst duration nor the burst intensity was able to distinguish between SEP and non-SEP events. The lack of SEP event can be readily explained under the shock-acceleration paradigm, but not under the flare-acceleration paradigm.

2004 April

LONG-DURATION LOW-FREQUENCY TYPE III BURSTS AND SOLAR ENERGETIC PARTICLE EVENTS

Nat **Gopalswamy**1 and Pertti M¨akel¨a

Astrophysical Journal Letters, 721:L62–L66, **2010**: **File**

We analyzed the coronal mass ejections (CMEs), flares, and type II radio bursts associated with a set of three complex, long-duration, low-frequency (<14 MHz) type III bursts from active region 10588 in **2004 April**. The durations were measured at 1 and 14 MHz using data from *Wind*/WAVES and were well above the threshold value (>15 minutes) normally used to define these bursts. One of the three type III bursts was not associated with a type II burst, which also lacked a solar energetic particle (SEP) event at energies >25 MeV. The 1 MHz duration of the type III burst (28 minutes) for this event was near the median value of type III durations found for gradual SEP events and ground level enhancement events. Yet, there was no sign of an SEP event. On the other hand, the other two type III bursts from the same active region had similar duration but were accompanied by WAVES type II bursts; these bursts were also accompanied by SEP events detected by *SOHO*/ERNE. The CMEs for the three events had similar speeds, and the flares also had similar size and duration. This study suggests that the occurrence of a complex, long-duration, low-frequency type III burst is not a good indicator of an SEP event.

INTERPLANETARY SHOCKS LACKING TYPE II RADIO BURSTS

N. **Gopalswamy**1, H. Xie2, P. M¨akel¨a2, S. Akiyama2, S. Yashiro3, M. L. Kaiser1, R. A. Howard4, and J.-L. Bougeret5

Astrophysical Journal, 710:1111–1126, **2010** February, **File**

We report on the radio-emission characteristics of 222 interplanetary (IP) shocks detected by spacecraft at Sun–Earth L1 during solar cycle 23 (1996 to 2006, inclusive). A surprisingly large fraction of the IP shocks (~34%) was radio quiet (RQ; i.e., the shocks lacked type II radio bursts).We examined the properties of coronal mass ejections (CMEs) and soft X-ray flares associated with such RQ shocks and compared them with those of the radio-loud (RL) shocks. The CMEs associated with the RQ shocks were generally slow (average speed ~535 km s−1) and only ~40% of the CMEs were halos. The corresponding numbers for CMEs associated with RL shocks were 1237 km s−1 and 72%, respectively. Thus, the CME kinetic energy seems to be the deciding factor in the radio-emission properties of shocks. The lower kinetic energy of CMEs associated with RQ shocks is also suggested by the lower peak soft X-ray flux of the associated flares (C3.4 versus M4.7 for RL shocks). CMEs associated with RQ CMEs were generally accelerating within the coronagraph field of view (average acceleration ~+6.8 m s−2), while those associated with RL shocks were decelerating (average acceleration ~ –3.5 m s−2). This suggests that many of the RQ shocks formed at large distances from the Sun, typically beyond 10 Rs, consistent with the absence of metric and decameter—hectometric (DH) type II radio bursts. A small fraction of RL shocks had type II radio emission solely in the kilometric (km) wavelength domain. Interestingly, the kinematics of the CMEs associated with the km type II bursts is similar to those of RQ shocks, except that the former are slightly more energetic. Comparison of the shock Mach numbers at 1 AU shows that the RQ shocks are mostly subcritical, suggesting that they were not efficient in accelerating electrons. The Mach number values also indicate that most of these are quasi-perpendicular shocks. The radio-quietness is predominant in the rise phase and decreases through the maximum and declining phases of solar cycle 23. About 18% of the IP shocks do not have discernible ejecta behind them. These shocks are due to CMEs moving at large angles from the Sun–Earth line and hence are not blast waves. The solar sources of the shock-driving CMEs follow the sunspot butterfly diagram, consistent with the higher-energy requirement for driving shocks.

Relation Between Type II Bursts and CMEs Inferred from STEREO Observations

Gopalswamy, N.; Thompson, W. T.; Davila, J. M.; Kaiser, M. L.; Yashiro, S.; M?kel?, P.; Michalek, G.; Bougeret, J.-L.; Howard, R. A.

E-print, July 2009; Solar Phys. (**2009**) 259: 227–254; **File**

The inner coronagraph (COR1) of the Solar Terrestrial Relations Observatory (STEREO) mission has made it possible to observe CMEs in the spatial domain overlapping with that of the metric type II radio bursts. The type II bursts were associated with generally weak flares (mostly B and C class soft X-ray flares), but the CMEs were quite energetic. Using CME data for a set of type II bursts during the declining phase of solar cycle 23, we determine the CME height when the type II bursts start, thus giving an estimate of the heliocentric distance at which CME-driven shocks form. This distance has been determined to be ?1.5Rs (solar radii), which coincides with the distance at which the Alfv?n speed profile has a minimum value. We also use type II radio observations from STEREO/WAVES and Wind/WAVES observations to show that CMEs with moderate speed drive either weak shocks or no shock at all when they attain a height where the Alfv?n speed peaks (?3Rs ? 4Rs). Thus the shocks seem to be most efficient in accelerating electrons in the heliocentric distance range of 1.5Rs to 4Rs. By combining the radial variation of the CME speed in the inner corona (CME speed increase) and interplanetary medium (speed decrease) we were able to correctly account for the deviations from the universal drift-rate spectrum of type II bursts, thus confirming the close physical connection between type II bursts and CMEs. The average height (?1.5Rs) of STEREO CMEs at the time of type II bursts is smaller than that (2.2Rs) obtained for SOHO (Solar and Heliospheric Observatory) CMEs. We suggest that this may indicate, at least partly, the density reduction in the corona between the maximum and declining phases, so a given plasma level occurs closer to the Sun in the latter phase. In two cases, there was a diffuse shock-like feature ahead of the main body of the CME, indicating a standoff distance of 1Rs ? 2Rs by the time the CME left the LASCO field of view.

Erratum to: Relation Between Type II Bursts and CMEs Inferred from STEREO Observations, Solar Physics, Volume 277, Number 2, 459, 2012

Type II Radio Emission and Solar Energetic Particle Events

Nat **Gopalswamy**

Proc. of 7th IGPP Astrophysics Conference, Kauai, HI, March 7-13, **2008**.

A preprint of this paper can be downloaded as a pdf file.

Type II radio bursts, solar energetic particle (SEP) events, and interplanetary (IP) shocks all have a common cause, viz., fast and wide (speed > 900 km/s and width > 60 deg) coronal mass ejections (CMEs). Deviations from this general picture are observed as (i) lack of type II bursts during many fast and wide CMEs and IP shocks, (ii) slow CMEs associated with type II bursts and SEP events, and (iii) lack of SEP events during many type II bursts. I examine the reasons for these deviations. I also show that ground level enhancement (GLE) events areconsistent with shock acceleration because a type II burst is present in every event well beforethe release of GLE particles and SEPs at the Sun.

Coronal Mass Ejections, Type II Radio Bursts, and Solar Energetic Particle Events in the SOHO Era

N. **Gopalswamy**1, S. Yashiro2, S. Akiyama2, P. Makela2, H. Xie2, M. L. Kaiser1, R. A. Howard3 and J. L. Bougeret4

E-print, Feb **2008**, **File**; Annales Geophysicae

A preprint of this paper can be downloaded as a pdf file.

Using the extensive and uniform data on coronal mass ejections (CMEs), solar energetic particle (SEP) events, and type II radio bursts during the SOHO era, we discuss how the CME properties such as speed, width and solar-source longitude decide whether CMEs are associated with type II radio bursts and SEP events. We discuss why some radio-quiet CMEs are associated with small SEP events while some radio-loud CMEs are not associated with SEP events. We conclude that either some fast and wide CMEs do not drive shocks or they drive weak shocks that do not produce significant levels of particle acceleration. We also infer that the Alfv?n speed in the corona and near-Sun interplanetary medium ranges from <200 km/s to ~1600 km/s. Radio-quiet fast and wide CMEs are also poor SEP producers and the association rate of type II bursts and SEP events steadily increases with CME speed and width (i.e., energy). If we consider western hemispheric CMEs, the SEP association rate increases linearly from ~30% for 800 km/s CMEs to 100% for ≥1800 km/s. Essentially all type II bursts in the decametre-hectometric (DH) wavelength range are associated with SEP events once the source location on the Sun is taken into account. This is a significant result for space weather applications, because if a CME originating from the western hemisphere is accompanied by a DH type II burst, there is a high probability that it will produce an SEP event.

Radio Quiet Fast and Wide Coronal Mass Ejections

N. **Gopalswamy**1, S. Yashiro2, H. Xie2, S. Akiyama2, E. Aguilar-Rodriguez2, M. L. Kaiser1, R. A., Howard3 and J.-L. Bougeret4

E-print, Nov. 2007; Ap. J., Vol. 674, p. 560, **2008**

A preprint of this paper can be downloaded as a pdf file.

We report on the properties of radio-quiet (RQ) and radio-loud (RL) coronal mass ejections (CMEs) that are fast and wide (FW). RQ CMEs lack of type II radio bursts in the metric and decameterhectometric (DH) wavelengths. RL CMEs are associated with metric or DH type II bursts.

The RQ FW CMEs suggest that the Alfven speed in the low-latitude outer corona can often exceed 1000 km/s and can vary over a factor of ≥3. None of the RQ CMEs was associated with large solar energetic particles, which is useful information for space weather applications.

Coronal Mass Ejections and Type II Radio Bursts

Nat **Gopalswamy**

Geophysical Monograph Series - Volume 165: Solar Eruptions and Energetic Particles (American Geophysical Union, Washington DC), p 207, **2006, File**
The simultaneous availability of white light data on CMEs from the Solar and Heliospheric Observatory (SOHO) and radio data on shock waves from the Radio and Plasma Wave experiment on board the Wind spacecraft over the past decade have helped in making rapid pro-gress in understanding the CME-driven shocks. I review some recent de-velopments in the type II - CME relationship, focusing on the properties of CMEs as shock drivers and those of the medium supporting shock propagation. I also discuss the solar cycle variation of the type II bursts in comparison with other eruptive phenomena such as CMEs, flares, large solar energetic particle events, and shocks detected in situ. The hierarchi-cal relationship found between the CME kinetic energy and wavelength range of type II radio bursts, non-existence of CMEless type II bursts, and the explanation of type II burst properties in terms of shock propagation with a realistic profile of the fast mode speed suggest that the underlying shocks are driven by CMEs, irrespective of the wavelength domain. Such a unified approach provides an elegant understanding of the entire type II phenomenon (coronal and interplanetary). The blast wave scenario re-mains an alternative hypothesis for type II bursts only over a small spatial domain (within one solar radius above the solar surface) that is not acces-sible to in situ observation. Therefore the existence of blast waves cannot be directly confirmed. CMEs, on the other hand, can be remote sensed from this domain.

Type II radio bursts and energetic solar eruptions.
Gopalswamy N, Aguilar-Rodriguez E, Yashiro S, Nunes S, Kaiser ML, Howard RA
(**2005a**) JGRA 110:A12S07

Recent Advances in the Long-Wavelength Radio Physics of the Sun

N. **Gopalswamy**
Planetary and Space Science, Vol 52 (15), p. 1399, 2004 , **2004, File**
Solar radio bursts at long wavelengths provide information on the solar disturbances such as coronal mass ejections and shocks at the moment of their departure from the Sun. The radio bursts also provide information on the physical properties (density, temperature and magnetic field) of the medium that supports the propagation of the disturbances with a valuable cross-check from direct imaging of the quiet outer corona. The primary objective of this paper is to review some of the past results and highlight recent recent results obtained from long-wavelength observations. In particular, the discussion will focus on radio phenomena occurring in the outer corona and beyond in relation to those observed in white light. Radio emission from nonthermal electrons confined to closed and open magnetic structures and in large-scale shock fronts will be discussed with particular emphasis on its relevance to solar eruptions. Solar cycle variation of the occurrence rate of shock-related radio bursts will be discussed in comparison with those of interplanetary shocks and solar proton events. Finally, case studies describing the newly-discovered radio signatures of interacting CMEs will be presented.

Near-Sun and near-Earth manifestations of solar eruptions

N. **Gopalswamy**, A. Lara, M. L. Kaiser, and J.-L. Bougeret
Journal of Geophysical Research, Vol. 106 , No. A11 , p. 25,261 (**2001**), **File**
We compare the near-Sun and near-Earth manifestations of solar eruptions that occurred during November 1994 to June 1998. We compared white-light coronal mass ejections, metric type II radio bursts, and extreme ultraviolet wave transients (near the Sun) with interplanetary (IP) signatures such as decameter-hectometric type II bursts, kilometric type II bursts, IP ejecta, and IP shocks. We did a two-way correlation study to (1) look for counterparts of metric type II bursts that occurred close to the central meridian and (2) look for solar counterparts of IP shocks and IP ejecta. We used data from Wind and Solar and Heliospheric Observatory missions along with metric radio burst data from ground-based solar observatories. Analysis shows that (1) most (93%) of the metric type II bursts did not have IP signatures, (2) most (80%) of the IP events (IP ejecta and shocks) did not have metric counterparts, and (3) a significant fraction (26%) of IP shocks were detected in situ without drivers. In all these cases the drivers (the coronal mass ejections) were ejected transverse to the Sun-Earth line, suggesting that the shocks have a much larger extent than the drivers. Shocks originating from both limbs of the Sun arrived at Earth, contradicting earlier claims that shocks from the west limb do not reach Earth. These shocks also had go/d type II radio burst association. We provide an explanation for the observed relation between metric, decameter-hectometric, and kilometric type II bursts based on the fast mode magnetosonic speed profile in the solar atmosphere.

Radio Signatures of Coronal Mass Ejection Interaction: Coronal Mass Ejection Cannibalism?
Gopalswamy N, Yashiro S, Kaiser ML, Howard RA, Bougeret, J-L
(**2001a**) ApJ 548:L91-L94

Type II Solar Radio Bursts. **Review**
Gopalswamy, N.,
Radio Astronomy at Long Wavelengths, Geophysical Monograph 119, AGU, Washington DC, 123-135, **2000**. Book Editor(s): Robert G. Stone, Kurt W. Weiler, Melvyn L. Goldstein, Jean-Louis Bougeret

Microwave Enhancement in Coronal Holes: Statistical Properties.
Gopalswamy N, Shibasaki K, Salem M
(**2000**) JApA 21:413

Automatic Burst Detection in Solar Radio Spectrograms Using Deep Learning: deARCE Method

Javier Bussons **Gordo**, Mario Fernández Ruiz, +++
Solar Physics volume 298, Article number: 82 (**2023**)
https://link.springer.com/content/pdf/10.1007/s11207-023-02171-0.pdf
We present in detail an automatic radio-burst detection system, based on the AlexNet convolutional neural network, for use with any kind of solar spectrogram. A full methodology for model training, performance evaluation, and feedback

to the model generator has been developed with special emphasis on i) robustness tests against stochastic and overfitting effects, ii) specific metrics adapted to the unbalanced nature of the solar-burst scenario, iii) tunable parameters for probability-threshold optimization, and iv) burst-coincidence cross match among e-Callisto stations and with external observatories (NOAA-SWPC). The resulting neural network configuration has been designed to accept data from observatories other than e-Callisto, either ground- or spacecraft-based. Typical False Negative and False Positive Scores in single-observatory mode are, respectively, in the 10 – 16% and 6 – 8% ranges, which improve further in cross-match mode. This mode includes new services (deARCE, Xmatch) allowing the end-user to check at a glance if a solar radio burst has taken place with a high level of confidence.

Sizes and shapes of sources in solar metric radio bursts

M. **Gordovskyy**, E.P. Kontar, D.L. Clarkson, N. Chrysaphi, P.K. Browning

ApJ **925** 140 **2022**

https://arxiv.org/pdf/2111.07777.pdf

https://iopscience.iop.org/article/10.3847/1538-4357/ac3bb7/pdf

Metric and decametric radio-emissions from the Sun are the only direct source of information about the dynamics of non-thermal electrons in the upper corona. In addition, the combination of spectral and imaging (sizes, shapes, and positions) observations of low-frequency radio sources can be used as a unique diagnostic tool to probe plasma turbulence in the solar corona and inner heliosphere. The geometry of the low-frequency sources and its variation with frequency are still not understood, primarily due to the relatively low spatial resolution available for solar observations. Here we report the first detailed multi-frequency analysis of the sizes of solar radio sources observed by the Low-Frequency Array (LOFAR). Furthermore, we investigate the source shapes by approximating the derived intensity distributions using 2D Gaussian profiles with elliptical half-maximum contours. These measurements have been made possible by a novel empirical method for evaluating the instrumental and ionospheric effects on radio maps based on known source observations. The obtained deconvolved sizes of the sources are found to be smaller than previous estimations, and often show higher ellipticity. The sizes and ellipticities of the sources inferred using 2D Gaussian approximation, and their variation with frequency are consistent with models of anisotropic radio-wave scattering in the solar corona. **16 Apr 2015, 27 Apr 2015, 6 May 2015, 20 Jun 2015, 25 Jun 2015, 12-13 July 2017, 15 July 2017, 9 Sep 2017**

CESRA #3260 Apr **2022** https://www.astro.gla.ac.uk/users/eduard/cesra/?p=3260

Frequency–Distance Structure of Solar Radio Sources Observed by LOFAR

Mykola **Gordovskyy**1, Eduard Kontar2, Philippa Browning1, and Alexey Kuznetsov

2019 ApJ 873 48

https://iopscience.iop.org/article/10.3847/1538-4357/ab03d8/pdf

Low-frequency radio observations make it possible to study the solar corona at distances up to 2–3 R⊙. Frequency of plasma emission is a proxy for electron density of the emitting plasma and, therefore, observations of solar radio bursts can be used to probe the density structure of the outer corona. In this study, positions of solar radio sources are investigated using the Low-Frequency Array (LOFAR) spectral imaging in the frequency range 30–50 MHz. We show that there are events where apparent positions of the radio sources cannot be explained using the standard coronal density models. Namely, the apparent heliocentric positions of the sources are 0.1–0.7 R ⊙ further from the Sun compared with the positions predicted by the Newkirk model, and these shifts are frequency-dependent. We discuss several possible explanations for this effect, including enhanced plasma density in the flaring corona, as well as scattering and refraction of the radio waves. **2015 June 20, 2015 June 25, 6 Jul 2017, 9 Jul 2017, 2017 July 12, 2017 July 15, 2017 August 12, 9 Sep 2017**

Table 1 Characteristics of the Considered LOFAR Sources (2015-2017)

CESRA nuggets #2206 May **2019** http://www.astro.gla.ac.uk/users/eduard/cesra/?p=2206

Microwave Emission from Twisted Magnetic Fields

Mykola **Gordovskyy**, Philippa Browning

RHESSI Science Nugget No. 286, Nov **2016**

http://sprg.ssl.berkeley.edu/~tohban/wiki/index.php/Microwave_Emission_from_Twisted_Magnetic_Fields

Based on our synthetic microwave maps, we can conclude that the cross-loop polarisation gradient can be used to detect twisted loops, provided that the loop width can be resolved; the patterns can be observed for the first half of the fast energy release phase (an impulsive phase in a flare), which is about 30-40 s long in a 80 Mm loop with typical coronal parameters. The best visibiliity is in the optically thin emission above the peak frequency. Depending on the model parameters, this frequency in our models is between 2 and 20 GHz.

Polarisation of microwave emission from reconnecting twisted coronal loops

Mykola **Gordovskyy**, Philippa Browning, Eduard Kontar

A&A 604, A116 **2016**
https://arxiv.org/pdf/1611.02237v1.pdf
Magnetic reconnection and particle acceleration due to the kink instability in twisted coronal loops can be a viable scenario for confined solar flares. Detailed investigation of this phenomenon requires reliable methods for observational detection of magnetic twist in solar flares, which may not be possible solely through extreme UV and soft X-ray thermal emission. The gradient of microwave polarisation across flaring loops can serve as one of the detection criteria. The aim of this study is to investigate the effect of magnetic twist in flaring coronal loops on the polarisation of gyro-synchrotron microwave emission, and determine whether microwave emission polarisation could provide a means for observational detection. We use time-dependent magnetohydrodynamic and test-particle models, developed using LARE3D and GCA codes to investigate twisted coronal loops relaxing following the kink-instability, and calculate synthetic microwave emission maps (I and V Stokes components) using GX simulator. It is found that flaring twisted coronal loops would yield some characteristic observational patterns, such as a gradient of Stokes V parameter across the loop. However, these patterns may be visible only for a relatively short period of time due to fast magnetic reconfiguration after the instability. We find that normally they will be visible for only a minute after onset of magnetic reconnection (or after the beginning of the impulsive phase). The visibility will also depend on the orientation and position of the loop on solar disk. Typically, it would be difficult to see the characteristic polarisation pattern if the twisted loop is seen from the top (close to the centre of the solar disk), but easier if the twisted loop is seen from the side (i.e. observed very close to the limb).

Microwave polarisation as a detection tool for magnetic twist in solar flares
Mykola **Gordovskyy**∗1 , Philippa Browning1 , Eduard Kontar2 , Rui Pinto3 , and Nicole Vilmer4
CESRA **2016** p.59
http://cesra2016.sciencesconf.org/conference/cesra2016/pages/CESRA2016_prog_abs_book_v3.pdf
Reconnecting twisted coronal loops are a good alternative to the standard model for explaining some types of solar flares. Particularly, they can be a good candidate for interpreting smaller flares observed in isolated coronal loops. Furthermore, twisted flux ropes often form an essential element of the standard model for larger, eruptive flares. Therefore, it is important to be able to identify twisted magnetic fields in the flaring corona. We explore various observational features obtained using coupled MHD and test-particle models of thermal and non-thermal plasmas in reconnecting twisted coronal loops, developed using the Lare3D and GCA codes, and GX simulator. It is shown, that both thermal (EUV and SXR) and non-thermal (HXR and microwave) emission can be used for observational detection of twisted loops. In particular, I will discuss the microwave emission from twisted loops, and use of the cross-loop circular polarisation gradient of gyrosynchrotron emission (Sharykin & Kuznetsov 2016; Gordovskyy et al. 2016) as a potential detection tool, and its limitations for different field configurations and loop orientations.

The Langmuir waves associated with the 1 December 2013 type II burst
D. B. **Graham**, Iver H. Cairns
JGR Volume 120, Issue 6 June **2015** Pages 4126–4141
The Langmuir waves associated with an interplanetary type II source region are presented. The type II burst was first observed on **29 November 2013** by STEREO A and B, with the shock crossing STEREO A on 1 December 2013. In the foreshock region upstream of the shock, 11 Langmuir-like waveforms were recorded by STEREO A's Time Domain Sampler on three orthogonal antennas. The observed Langmuir wave electric fields are of large amplitude and aligned with the background magnetic field. Some of the waveforms show evidence of electrostatic decay, and several are consistent with Langmuir eigenmodes of density wells. Harmonic electric fields are observed simultaneously with the Langmuir waveforms and are consistent with fields produced by nonlinear currents. The beam speeds vb exciting the Langmuir waves are estimated from the waveform data, yielding speeds vb≈ (0.01–0.04)c. These are consistent with previous observations. The beam speeds are slower than those associated with type III solar radio bursts, consistent with the Langmuir wave electric fields being field aligned. The evidence found for electrostatic decay and against strong perpendicular fields, and so low-wave number Langmuir/z-mode waves, suggests that the dominant emission mechanisms for this type II foreshock involve electrostatic decay and nonlinear wave processes, rather than linear-mode conversion. Harmonic radio emission via antenna mechanisms involving Langmuir waves remains possible.

Dynamical evidence for nonlinear Langmuir wave processes in type III solar radio bursts
D. B. **Graham** and Iver H. Cairns
JGR, Volume 119, Issue 4, pages 2430–2457, April **2014**
The nonlinear processes and evolution of Langmuir waves in the source regions of type III solar radio bursts are explored in detail. Langmuir waves recorded by the Time Domain Sampler of the STEREO/WAVES instrument can be roughly classified into six groups based on the waveform, power spectra, and field strength perpendicular to the local magnetic field. It is argued that these groups correspond to either different stages of the evolution of Langmuir waves generated by electron beams or differ due to the direction of the magnetic field relative to the solar wind velocity. Approximately half of the observed Langmuir waves have strong perpendicular fields, meaning that understanding how

these fields are produced is crucial for understanding type III sources. Most events recorded are either localized waveforms consistent with Langmuir eigenmodes or have two or more spectral peaks consistent with electrostatic (ES) decay of Langmuir/z mode waves. The remaining events appear to correspond to either earlier or later stages of Langmuir wave evolution or are decay events for which the Doppler shift is insufficient to distinguish the beam-driven and product Langmuir waves. This is supported by the fact that most events exceed the threshold for ES decay even though their spectra show no evidence for decay and some of the events are observed when the solar wind flow is approximately perpendicular to the magnetic field, minimizing Doppler shifting. Low-frequency fields produced by intense Langmuir waves are quantitatively consistent with density perturbations produced by the ponderomotive force, ion-acoustic waves produced by ES decay, or sheath rectification. Above the observed nonlinear threshold, quantitative analysis suggests that the observed low-frequency signals are consistent with perturbations produced by ponderomotive effects and ion-acoustic waves produced by ES decay, but effects of sheath rectification may also contribute.

Harmonic waves and sheath rectification in type III solar radio bursts

D. B. **Graham**1,*, Iver H. Cairns2 andD. M. Malaspina

JGR, Volume 119, Issue 2, pages 723–741, February **2014**

In type III solar radio bursts and planetary foreshocks, Langmuir waves are produced by electron beams and converted partially to radio waves by linear and nonlinear processes. Lower amplitude second harmonic electric fields are observed simultaneously during the most intense Langmuir wave events in type III source regions. The electric fields at the harmonic frequencies can arise from various mechanisms, such as radio wave emission by either coalescence or antenna mechanisms, nonlinear currents, harmonics of Langmuir waves, electron trapping in Langmuir wave potentials, and Langmuir wave rectification at the sheath surrounding the spacecraft, or they can result from instrumental harmonics. In this paper the relative powers and electric field vectors of Langmuir waves and the harmonic fields are compared for multiple events. The structure of the harmonic field is shown to be determined by the Langmuir waveform, but the harmonic field direction is typically closely aligned with the solar wind flow. The magnitude, structure, and orientation of the harmonic fields is used to determine which processes are responsible. It is shown that the dominant process generating the observed harmonic fields is Langmuir wave rectification at the sheath surrounding the spacecraft.

Electrostatic decay of Langmuir/z-mode waves in type III solar radio bursts†

D. B. **Graham**1,2,*, Iver H. Cairns

JGR, **2013**, Volume 118, Issue 7, pages 3968–3984

About 40% of the waveforms observed by STEREO during type III solar radio bursts exhibits Langmuir beating and have split spectral peaks, suggestive of decay into product Langmuir and ion-acoustic waves. For lower electron beam speeds $v_b/c \lesssim 0.1$ the spectra of Langmuir events with split spectral peaks are shown to be consistent with electrostatic (ES) decay into Langmuir-like waves with frequencies above the electron plasma frequency. For faster beam speeds $v_b/c \lesssim 0.1$ the spectra are consistent with one or more successive generations of ES decay and an end-state of low wave number Langmuir/z-mode waves with strong electric fields perpendicular to the magnetic field. For many of the split spectral peak events an intense low frequency response occurs that is consistent with ion-acoustic waves produced by ES decay, providing further evidence that these events are ES decay. An observed event is shown to be consistent with three successive backscatter decays but such events are very rare in type III bursts. About 90% of the split spectral peak events occur when $T_i/T_e \lesssim 0.6$. Similarly, over 80% of the split peak events have energy densities above the theoretical nonlinear threshold for electrostatic decay (for reasonable Langmuir damping rates $\lesssim 10^{-3}\omega_p$). All events have beam speeds and energy densities below the maxima appropriate for ES decay of beam-driven Langmuir waves.

Do Langmuir wave packets in the solar wind collapse?

Graham, D. B., I. H. Cairns, D. R. Prabhakar, R. E. Ergun, D. M. Malaspina, S. D. Bale, K. Goetz, and P. J. Kellogg

J. Geophys. Res., 117, A09107, doi:10.1029/2012JA018033, **2012**

Intense localized Langmuir waves in the solar wind are often associated with type III solar radio bursts. Wave packets with a Gaussian fall-off of electric field with distance are shown to be consistent with strong turbulence simulations. The collapse threshold for these Gaussian wave packets is calculated analytically and shown to be consistent with previous estimates and simulations. We then assess whether intense Langmuir events detected by the SWAVES instrument on the twin STEREO spacecraft during type III bursts are consistent with known conditions for wave packet collapse. Eight different type III events are selected and a total of 167 wave packets analyzed. An approximate analysis of the observed spatial scales and electric fields shows that none of the wave packets are consistent with collapse. The electric field structures predicted for collapsing wave packets, based on the nucleation mechanism and extensive three-dimensional electrostatic and electromagnetic Zakharov simulations, are also fitted to the observed data: about a third of the packets are well fitted by a potential with a Gaussian radial function. Where good fits can be found, the wave packets do not meet the requirements for collapse. Good eigenmode fits are found for wave packets with waveforms

well fitted by the structural form of collapsing wave packets. This is because the electric field envelopes of collapsing wave packets and trapped Langmuir eigenmodes are both Hermite-Gauss functions. This rules out the possibility of wave packet collapse and strong turbulence being important processes in type III source regions.

EVIDENCE AGAINST THE OSCILLATING TWO-STREAM INSTABILITY AND SPATIAL COLLAPSE OF LANGMUIR WAVES IN SOLAR TYPE III RADIO BURSTS

D. B. **Graham**1, Iver H. Cairns1, D. M. Malaspina2, and R. E. Ergun

2012 ApJ 753 L18

Recently Thejappa et al. studied a specific Langmuir wave packet observed by STEREO A and argued based on the electric field from one of the three antennas that this packet satisfied the conditions for the oscillating two-stream instability (OTSI) and was undergoing wave collapse. We analyze the same event using all three electric components and show that, while the wave packet has structure consistent with collapse simulations and theory, the field strength is well below that required for collapse to proceed. Analyzing the three electric field components shows that the power spectrum and dominance of wave power perpendicular to the local magnetic field are inconsistent with OTSI. We show that this packet and other more intense packets are inconsistent with collapse and show no evidence of OTSI, but are likely trapped eigenmodes in density wells. Therefore, OTSI and collapse are unlikely explanations for intense Langmuir events observed in the solar wind.

Reconciliation of Observational Challenges to the Impulsive-Piston Shock-Excitation Scenario.
II. Shock Waves Produced in CME-less Events with a Null-Point Topology.

Grechnev, V.V., Kiselev, V.I., Uralov, A.M., Myshyakov, I.I.:

Solar Phys., **297**, Article number: 123 **2022, File See movies of 16 Apr 2014**

Continuing Article I, we revisit challenging events previously identified by different authors, whose analysis led to conclusions about various mechanisms of the shock-wave excitation. Here, we reconsider four events that involved fan-spine coronal configurations with a null-point topology (NPT). The presence of Type-II radio bursts in all events as well as extreme-ultraviolet disturbances (EUV waves) observed in three events evidence the presence of shock waves, whereas no coronal mass ejections (CMEs) were detected in most events. One idea proposed to explain the observations was the shock-wave excitation by the straightening of a postreconnection kinked loop. The Type-II burst in another event appeared in association with a compact flare with a high thermal pressure that looked to be in favor of a flare-generated blast wave. One event was associated with a possible pseudo-CME. All of these challenging events have been reconciled in terms of an impulsively excited piston shock. CME-less filament eruptions in NPT configurations appear to represent a distinct category of events responsible for some of the observed shock waves. **14 November 2005 , 28 February 2011 , 6 March 2014 , 16 April 2014**

Reconciliation of Observational Challenges to the Impulsive-Piston Shock-Excitation Scenario.
I. Kinematic Challenges

V.V. **Grechnev** · V.I. Kiselev · A.M. Uralov

Solar Phys. **297**, Article number: 106 **2022 File See movies of 8 December 2007**

Until now, there is no consensus on the origin of coronal shock waves.
Questions also remain about the patterns that govern the propagation of the pre-
sumably related disturbances observed in the extreme ultraviolet (EUV waves).
We present arguments in favor of the initial excitation of the waves by the
impulsive acceleration of erupting structures. We consider two puzzling events
that have been known thanks to the efforts of different research teams. Using
recent findings and our methods, we aim to figure out what might actually have
happened in these challenging events. In the first event, the expansion of the
coronal mass ejection (CME) was determined by gravity starting from the low
corona. The previous analysis led the authors to a conclusion about the flare-
related origin of the associated shock wave. We also consider another event, in
which an EUV wave had a strange kinematics. This was one of the weakest
flares accompanied by EUV waves. Both of these challenging events have been
reconciled in terms of an impulsively-excited piston shock. **24 December 1996, 8 December 2007**

Twin Null-Point-Associated Major Eruptive Three-Ribbon Flares with Unusual Microwave Spectra

V.V. **Grechnev**, N.S. Meshalkina, A.M. Uralov, A.A. Kochanov, S.V. Lesovoi, I.I. Myshyakov, V.I. Kiselev, D.A. Zhdanov, A.T. Altyntsev, M.V. Globa

Solar Phys. **295**, Article number: 128 **2020**
https://arxiv.org/pdf/2009.10350.pdf
https://link.springer.com/content/pdf/10.1007/s11207-020-01702-3.pdf
On **23 July 2016** after 05:00\,UTC, the first 48-antenna stage of the Siberian Radioheliograph detected two flares of M7.6 and M5.5 GOES importance that occurred within half an hour in the same active region. Their multi-instrument analysis reveals the following. The microwave spectra were flattened at low frequencies and the spectrum of the stronger burst had a lower turnover frequency. Each flare was eruptive, emitted hard X-rays and gamma-rays exceeding 800\,keV, and had a rare three-ribbon configuration. An extended hard X-ray source associated with a longest middle ribbon was observed in the second flare. The unusual properties of the microwave spectra are accounted for by a distributed multi-loop system in an asymmetric magnetic configuration that our modeling confirms. Microwave images did not to resolve compact configurations in these flares that may also be revealed incompletely in hard X-ray images because of their limited dynamic range. Being apparently simple and compact, non-thermal sources corresponded to the structures observed in the extreme ultraviolet. In the scenario proposed for two successive three-ribbon eruptive flares in a configuration with a coronal-null region, the first eruption causes a flare and facilitates the second eruption that also results in a flare.

Radio, Hard X-Ray, and Gamma-Ray Emissions Associated with a Far-Side Solar Event

V.V. **Grechnev** (1), V.I. Kiselev (1), L.K. Kashapova (1, 2), A.A. Kochanov (1, 2), I.V. Zimovets (3, 4, 5), A.M. Uralov (1), B.A. Nizamov (6, 7), I.Yu. Grigorieva(8), D.V. Golovin (3), M.L. Litvak (3), I.G. Mitrofanov (3), A.B. Sanin
Solar Phys. **2018**
https://arxiv.org/pdf/1808.10103.pdf **File**
The SOL**2014-09-01** far-side solar eruptive event produced hard electromagnetic and radio emissions observed with detectors at near-Earth vantage points. Especially challenging was a long-duration >100 MeV γ-ray burst probably produced by accelerated protons exceeding 300 MeV. This observation raised a question of how high-energy protons could reach the Earth-facing solar surface. Some preceding studies discussed a scenario in which protons accelerated by a CME-driven shock high in the corona return to the solar surface. We continue with the analysis of this challenging event, involving radio images from the Nan\c{c}ay Radioheliograph and hard X-ray data from the High Energy Neutron Detector (HEND) of the Gamma-Ray Spectrometer onboard the Mars Odyssey space observatory located near Mars. HEND recorded unocculted flare emission. The results indicate that the emissions observed from the Earth's direction were generated by flare-accelerated electrons and protons trapped in static long coronal loops. Their reacceleration is possible in these loops by a shock wave, which was excited by the eruption, being initially not CME-driven. The results highlight the ways to address remaining questions.

Multi-instrument view on solar eruptive events observed with the Siberian Radioheliograph: From detection of small jets up to development of a shock wave and CME

V. V. **Grechnev**, S. V. Lesovoi, A. A. Kochanov, A. M. Uralov, A. T. Altyntsev, A. V. Gubin, D. A. Zhdanov, E. F. Ivanov, G. Ya. Smolkov, L. K. Kashapova (Institute of Solar-Terrestrial Physics, Irkutsk, Russia)
Journal of Atmospheric and Solar-Terrestrial Physics Volume 174, September **2018**, Pages 46-65
https://arxiv.org/pdf/1805.02564.pdf **File**
https://www.sciencedirect.com/journal/journal-of-atmospheric-and-solar-terrestrial-physics/vol/174/suppl/C
The first 48-antenna stage of the Siberian Radioheliograph (SRH) started single-frequency test observations early in 2016, and since August 2016 it routinely observes the Sun at several frequencies in the 4-8 GHz range with an angular resolution of 1-2 arc minutes and an imaging interval of about 12 seconds. With limited opportunities of the incomplete antenna configuration, a high sensitivity of about 100 Jy allows the SRH to contribute to the studies of eruptive phenomena along three lines. First, some eruptions are directly visible in SRH images. Second, some small eruptions are detectable even without a detailed imaging information from microwave depressions caused by screening the background emission by cool erupted plasma. Third, SRH observations reveal new aspects of some events to be studied with different instruments. We focus on an eruptive C2.2 flare on **16 March 2016** around 06:40, one of the first flares observed by the SRH. Proceeding from SRH observations, we analyze this event using extreme-ultraviolet, hard X-ray, white-light, and metric radio data. An eruptive prominence expanded, brightened, and twisted, which indicates a time-extended process of the flux-rope formation together with the development of a large coronal mass ejection (CME). The observations rule out a passive role of the prominence in the CME formation. The abrupt prominence eruption impulsively excited a blast-wave-like shock, which appeared during the microwave burst and was manifested in an "EUV wave" and Type II radio burst. The shock wave decayed and did not transform into a bow shock because of the low speed of the CME. Nevertheless, this event produced a clear proton enhancement near Earth. Comparison with our previous studies of several events confirms that the impulsive-piston shock-excitation scenario is typical of various events. **16 March 2016, 1 May 2017, 3 August 2017, 9 September 2017,**
Table 1: Summary of shock waves studied

The 26 December 2001 Solar Eruptive Event Responsible for GLE63.
II. Multi-Loop Structure of Microwave Sources in a Major Long-Duration Flare
V.V. **Grechnev** . A. M. Uralov, V. I. Kiselev, A.A. Kochanov
Solar Phys. January **2017**, 292:3 **File**
https://arxiv.org/pdf/1611.08349v1.pdf
Our analysis of the observations of the SOL**2001-12-26** event, which was related to ground-level enhancement of cosmic-ray intensity GLE63, including microwave spectra and images from the *Nobeyama Radioheliograph* at 17 and 34 GHz, from the *Siberian Solar Radio Telescope* at 5.7 GHz, and from the *Transition Region and Coronal Explorer* in 1600 A, has led to the following results: A flare ribbon overlapped with the sunspot umbra, which is typical of large particle events. Atypical were i) the long duration of the flare, which lasted more than one hour; ii) the moderate intensity of the microwave burst, which was about 104 sfu; iii) the low peak frequency of the gyrosynchrotron spectrum, which was about 6 GHz; and its insensitivity to the flux increase by more than one order of magnitude. This was accompanied by a nearly constant ratio of the flux emitted by the volume in the high-frequency part of the spectrum to its elevated low-frequency part determined by the area of the source. With the self-similarity of the spectrum, a similarity was observed between the moving microwave sources and the brightest parts of the flare ribbons in 1600 A images. We compared the 17 GHz and 1600 A images and confirm that the microwave sources were associated with multiple flare loops, whose footpoints appeared in the ultraviolet as intermittent bright kernels. To understand the properties of the event, we simulated its microwave emission using a system of several homogeneous gyrosynchrotron sources above the ribbons. The scatter between the spectra and the sizes of the individual sources is determined by the inhomogeneity of the magnetic field within the ribbons. The microwave flux is mainly governed by the magnetic flux passing through the ribbons and the sources. The apparent simplicity of the microwave structures is caused by a poorer spatial resolution and dynamic range of the microwave imaging. The results indicate that microwave manifestations of accelerated electrons correspond to the structures observed in thermal emissions, as well-known models predict.
See CESRA Highlight # 1375, May 2017 http://www.astro.gla.ac.uk/users/eduard/cesra/?p=1375

The 26 December 2001 Solar Event Responsible for GLE63.
I. Observations of a Major Long-Duration Flare with the Siberian Solar Radio Telescope
V.V. **Grechnev** . A.A. Kochanov
Solar Phys. Volume 291, Issue 12, pp 3705–3723 **2016 File**
http://arxiv.org/pdf/1609.02256v1.pdf
Ground Level Enhancements (GLEs) of cosmic-ray intensity occur, on average, once a year. Due to their rareness, studying the solar sources of GLEs is especially important to approach understanding their origin. The SOL2001-12-26 eruptive-flare event responsible for GLE63 seems to be challenging in some aspects. Deficient observations limited its perception. Analysis of extra observations found for this event provided new results presented in three companion papers. This paper, Paper I, addresses the observations of this flare with the Siberian Solar Radio Telescope (SSRT). Taking advantage of its instrumental particularities, we analyze the detailed SSRT observations of a major long-duration flare at 5.7 GHz without cleaning the images. The analysis confirms that the source of GLE63 was associated with an event in active region 9742 that was manifested in the first flare and the main flare. The first flare (04:30-05:03 UT) reached a GOES level of about M1.6. Two microwave sources have been revealed, whose brightness temperatures at 5.7 GHz exceeded 10 MK. The main flare, up to the M7.1 level, started at 05:04 UT, and occurred in strong magnetic .elds. The observed microwave sources reached about 250 MK. They appeared on the weaker-fi.eld periphery of the active region, approached each other nearly along the magnetic neutral line, coming closer to a stronger-field core of the active region, and then moved away from the neutral line like expanding ribbons. These motions rule out an association of the non-thermal microwave sources with a single flaring loop. These issues and the possible causes of the high proton productivity of this event are addressed in Paper II and Paper III.

Relations Between Microwave Bursts and Near-Earth High-Energy Proton Enhancements and Their Origin
V. V. **Grechnev** , V. I. Kiselev, N. S. Meshalkina, I. M. Chertok
Solar Phys. Volume 290, Issue 10, pp. 2827-2855 **2015**
http://arxiv.org/pdf/1511.05839v1.pdf
We further study the relations between parameters of bursts at 35 GHz recorded with the Nobeyama Radio Polarimeters during 25 years and solar proton events (Grechnev et al. in Publ. Astron. Soc. Japan 65, S4, 2013a). Here we address the relations between the microwave fluences at 35 GHz and near-Earth proton fluences above 100 MeV to find information on their sources and evaluate their diagnostic potential. The correlation between the microwave and proton fluences is pronouncedly higher than between their peak fluxes. This probably reflects a dependence of the total number

of protons on the duration of the acceleration process. In events with strong flares, the correlation coefficients of high-energy proton fluences with microwave and soft X-ray fluences are higher than those with the speeds of coronal mass ejections. The results indicate a statistically larger contribution of flare processes to high-energy proton fluxes. Acceleration by shock waves seems to be less important at high energies in events associated with strong flares, although its contribution is probable and possibly prevails in weaker events. The probability of a detectable proton enhancement was found to directly depend on the peak flux, duration, and fluence of the 35 GHz burst, while the role of the Big Flare Syndrome might have been overestimated previously. Empirical diagnostic relations are proposed. **Table 1.** Analyzed events 6, **7 January 2014**

Responsibility of a Filament Eruption for the Initiation of a Flare, CME, and Blast Wave, and its Possible Transformation into a Bow Shock

V. V. **Grechnev** (1), A. M. Uralov (1), I. V. Kuzmenko (2), A. A. Kochanov (1), I. M. Chertok (3), S. S. Kalashnikov

Solar Phys., **2014**

http://arxiv.org/pdf/1410.8696v1.pdf

Multi-instrument observations of two filament eruptions on **24 February and 11 May 2011** suggest the following updated scenario for eruptive flare, CME and shock wave evolution. An initial destabilization of a filament results in stretching out of magnetic threads belonging to its body and rooted in the photosphere along the inversion line. Their reconnection leads to i) heating of parts of the filament or its environment, ii) initial development of the flare arcade cusp and ribbons, and iii) increasing similarity of the filament to a curved flux rope and its acceleration. Then the pre-eruption arcade enveloping the filament gets involved in reconnection according to the standard model and continues to form the flare arcade and ribbons. The poloidal magnetic flux in the curved rope developing from the filament progressively increases and forces its toroidal expansion. This flux rope impulsively expands and produces an MHD disturbance, which rapidly steepens into a shock. The shock passes through the arcade expanding above the filament and then freely propagates ahead of the CME like a decelerating blast wave for some time. If the CME is slow, then the shock eventually decays. Otherwise, the frontal part of the shock changes into the bow-shock regime. This was observed for the first time in the 24 February 2011 event. When reconnection ceases, the flux rope relaxes and constitutes the CME core-cavity system. The expanding arcade develops into the CME frontal structure. We also found that reconnection in the current sheet of a remote streamer forced by the shock's passage results in a running flare-like process within the streamer responsible for a type II burst. The development of dimming and various associated phenomena are discussed.

A Challenging Solar Eruptive Event of 18 November 2003 and the Causes of the 20 November Geomagnetic Superstorm.
II. CMEs, Shock Waves, and Drifting Radio Bursts

V.V. **Grechnev**, A.M. Uralov, I.M. Chertok, V.A. Slemzin, B.P. Filippov, Ya.I. Egorov, V.G. Fainshtein, A.N. Afanasyev, N.P. Prestage, M. Temmer

E-print, Aug **2013**; Solar Phys.

We continue our study (Grechnev et al. (2013), doi:10.1007/s11207-013-0316-6; Paper I) on the 18 November 2003 geoffective event. To understand possible impact on geospace of coronal transients observed on that day, we investigated their properties from solar near-surface manifestations in extreme ultraviolet, LASCO white-light images, and dynamic radio spectra. We reconcile near-surface activity with the expansion of coronal mass ejections (CMEs) and determine their orientation relative to the earthward direction. The kinematic measurements, dynamic radio spectra, and microwave and X-ray light curves all contribute to the overall picture of the complex event and confirm an additional eruption at 08:07-08:20 UT close to the solar disk center presumed in Paper I. Unusual characteristics of the ejection appear to match those expected for a source of the 20 November superstorm but make its detection in LASCO images hopeless. On the other hand, none of the CMEs observed by LASCO seem to be a promising candidate for a source of the superstorm being able to produce, at most, a glancing blow on the Earth's magnetosphere. Our analysis confirms free propagation of shock waves revealed in the event and reconciles their kinematics with "EUV waves" and dynamic radio spectra up to decameters.

An Updated View of Solar Eruptive Flares and Development of Shocks and CMEs: History of the 2006 December 13 GLE-Productive Extreme Event

V. **Grechnev**, V. Kiselev, A. Uralov, N. Meshalkina, A. Kochanov

E-print, Aug **2013**; Publ. Astron. Soc. Japan 65, No SP1, S9 [18 pages] (2013)), **File**

An extreme **2006 December 13** event marked the onset of the Hinode era being the last major flare in the solar cycle 23 observed with NoRH and NoRP. The event produced a fast CME, strong shock, and big particle event responsible for GLE70. We endeavor to clarify relations between eruptions, shock wave, and the flare, and to shed light on a debate over the origin of energetic protons. One concept relates it with flare processes. Another one associates acceleration of

ions with a bow shock driven by a CME at (2-4)R_sun. The latter scenario is favored by a delayed particle release time after the flare. However, our previous studies have established that a shock wave is typically excited by an impulsively erupting magnetic rope (future CME core) during the flare rise, while the outer CME surface evolves from an arcade whose expansion is driven from inside. Observations of the 2006 December 13 event reveal two shocks following each other, whose excitation scenario contradicts the delayed CME-driven bow-shock hypothesis. Actually, the shocks developed much earlier, and could accelerate protons still before the flare peak. Then, the two shocks merged into a single stronger one and only decelerated and dampened long afterwards.

Negative Microwave Bursts

Victor **Grechnev** and Hugh Hudson
RHESSI Science Nugget, No. 206, Aug **2013**.
http://sprg.ssl.berkeley.edu/~tohban/wiki/index.php/Negative_Microwave_Bursts
Negative microwave bursts happen, in association with flares and with "Hyder flares," and modern instrumentation makes them very interesting again

Microwave Negative Bursts as Indications of Reconnection between Eruptive Filaments and Large-Scale Coronal Magnetic Environment

V. **Grechnev**, I. Kuzmenko, A. Uralov, I. Chertok, A. Kochanov
E-print, Aug **2013**, Publ. Astron. Soc. Japan 65, No. SP1, S10 [9 pages] (**2013)**
Low-temperature plasma ejected in solar eruptions can screen active regions as well as quiet solar areas. Absorption phenomena can be observed in microwaves as 'negative bursts' and in different spectral domains. We analyze two very different recent events with such phenomena and present an updated systematic view of solar events associated with negative bursts. Related filament eruptions can be normal, without essential changes of shape and magnetic configuration, and 'anomalous'. The latter are characterized by disintegration of an eruptive filament and dispersal of its remnants as a cloud over a large part of solar disk. Such phenomena can be observed as giant depressions in the He II 304 A line. One of possible scenarios for an anomalous eruption is proposed in terms of reconnection of filament's internal magnetic fields with external large-scale coronal surrounding. **2004 July 13.,** ***2011 June 7, 2011 December 13.***

Relations between strong high-frequency microwave bursts and proton events

V. **Grechnev**, N. Meshalkina, I. Chertok, V. Kiselev
E-print, Aug **2013**; Publ. Astron. Soc. Japan 65, No. SP1, S4, **2013**
http://pasj.asj.or.jp/v65/sp1/65S004/65S004.pdf
Proceeding from close association between solar eruptions, flares, shock waves, and CMEs, we analyze relations between bursts at 35 GHz recorded with the Nobeyama Radio Polarimeters during 1990-2012, on the one hand, and solar energetic particle (SEP) events, on the other hand. Most west to moderately east solar events with strong bursts at 35 GHz produced near-Earth proton enhancements of J(E > 100 MeV) > 1 pfu. The strongest and hardest those caused ground level enhancements. There is a general, although scattered, correspondence between proton enhancements and peak fluxes at 35 GHz, especially pronounced if the 35 GHz flux exceeds 10^4 sfu and the microwave peak frequency is high. These properties indicate emission from numerous high-energy electrons in very strong magnetic fields suggesting a high rate of energy release in the flare-CME formation process. Flaring above the sunspot umbra appears to be typical of such events. Irrespective of the origin of SEPs, these circumstances demonstrate significant diagnostic potential of high-frequency microwave bursts and sunspot-associated flares for space weather forecasting. Strong prolonged bursts at 35 GHz promptly alert to hazardous SEP events with hard spectra. A few exceptional events with moderate bursts at 35 GHz and strong proton fluxes look challenging and should be investigated. **Table. 2000 November 8, 2001 August 25, 2001 December 26, 2002 April 21, 2005 January 20, 2006 December 13, 2012 March 07, 2012 May 17**

Coronal Shock Waves, EUV Waves, and Their Relation to CMEs. III. Shock-Associated CME/EUV Wave in an Event with a Two-Component EUV Transient

V. V. **Grechnev**, A. N. Afanasyev, A. M. Uralov, I. M. Chertok, M. V. Eselevich, V. G. Eselevich, G. V. Rudenko and Y. Kubo
Solar Physics, Volume 273, Number 2, 461-477, **2011, File in Chertok's papers**
On **17 January 2010**, STEREO-B observed in extreme ultraviolet (EUV) and white light a large-scale dome-shaped expanding coronal transient with perfectly connected off-limb and on-disk signatures. Veronig et al. (Astrophys. J. Lett. 716, L57, 2010) concluded that the dome was formed by a weak shock wave. We have revealed two EUV components, one of which corresponded to this transient. All of its properties found from EUV, white light, and a metric type II burst match expectations for a freely expanding coronal shock wave, including correspondence with the fast-mode speed distribution, while the transient sweeping over the solar surface had a speed typical of EUV waves. The shock wave was

presumably excited by an abrupt filament eruption. Both a weak shock approximation and a power-law fit match kinematics of the transient near the Sun. Moreover, the power-law fit matches the expansion of the CME leading edge up to 24 solar radii. The second, quasi-stationary EUV component near the dimming was presumably associated with a stretched CME structure; no indications of opening magnetic fields have been detected far from the eruption region.

Coronal Shock Waves, EUV Waves, and Their Relation to CMEs. I. Reconciliation of "EIT Waves", Type II Radio Bursts, and Leading Edges of CMEs

V. V. **Grechnev**, A. M. Uralov, I. M. Chertok, I. V. Kuzmenko, A. N. Afanasyev, N. S. Meshalkina, S. S. Kalashnikov and Y. Kubo

Solar Physics, Volume 273, Number 2, 433-460, **2011, File in Chertok's papers**

We show examples of the excitation of coronal waves by flare-related abrupt eruptions of magnetic rope structures. The waves presumably rapidly steepened into shocks and freely propagated afterwards like decelerating blast waves that showed up as Moreton waves and EUV waves. We propose a simple quantitative description for such shock waves to reconcile their observed propagation with drift rates of metric type II bursts and kinematics of leading edges of coronal mass ejections (CMEs). Taking account of different plasma density falloffs for propagation of a wave up and along the solar surface, we demonstrate a close correspondence between drift rates of type II bursts and speeds of EUV waves, Moreton waves, and CMEs observed in a few previously studied events.

24 September 1997, 1 June 2002, 13 July 2004, 19 May 2007

Absorption Phenomena and a Probable Blast Wave in the 13 July 2004 Eruptive Event

V.V. **Grechnev** · A.M. Uralov · V.A. Slemzin · I.M. Chertok · I.V. Kuzmenko · K. Shibasaki

Solar Phys (**2008**) 253: 263–290. **File in Chertok's papers**

We present a case study of the **13 July 2004** solar event, in which disturbances caused by eruption of a filament from an active region embraced a quarter of the visible solar surface. Remarkable are the absorption phenomena observed in the SOHO/EIT 304 Å channel, which were also visible in the EIT 195 Å channel, in the H〈 line, and even in total radio flux records. Coronal and Moreton waves were also observed. Multispectral data allowed reconstructing an overall picture of the event. An explosive filament eruption and related impulsive flare produced a CME and blast shock, both of which decelerated and propagated independently. Coronal and Moreton waves were kinematically close and both decelerated in accordance with an expected motion of a coronal blast shock. The CME did not resemble a classical three-component structure, probably because some part of the ejected mass fell back onto the Sun. Quantitative evaluations from different observations provide close estimates of the falling mass,~ 3×1015 g, which is close to the estimated mass of the CME. The falling material was responsible for the observed large-scale absorption phenomena, in particular, shallow widespread moving dimmings observed at 195 Å. By contrast, deep quasi-stationary dimmings observed in this band near the eruption center were due to plasma density decrease in coronal structures.

Plasma Parameters in a Post-Eruptive Arcade Observed with CORONAS-F/SPIRIT, Yohkoh/SXT, SOHO/EIT, and in Microwaves

Grechnev, Victor V.; Uralov, Arkadiy M.; Zandanov, Vasily G.; Rudenko, George V.; Borovik, Valery N. Grigorieva, Irina Y.; Slemzin, Vladimir A.Bogachev, Sergey A.; Kuzin, Sergei V.; Zhitnik, Igor'a.; Pertsov, Andrey A.;Shibasaki, Kiyoto; Livshits, Moisey A.

Publications of the Astronomical Society of Japan, Vol.58, No.1, pp. 55-68, **2006**

https://ui.adsabs.harvard.edu/link_gateway/2006PASJ...58...55G/PUB_PDF

The SPectroheliographIc X-Ray Imaging Telescope (SPIRIT) aboard the CORONAS-F spacecraft sometimes observes in the Mg XII 8.42Å line (Tmax ~ 9 MK) large, bright features existing for many hours high in the corona. This fact suggests that plasma beta there might not be small. We identify such a feature observed on 2001 October 22 at a height of 100Mm with a hot part of a post-eruptive arcade. Using multi-spectral data and radio astronomy methods, we estimate the plasma parameters in the arcade and reveal the coronal magnetic configuration. Several hours after the eruption, the temperature in the arcade was 6-8MK, and the plasma density was (5-10) \cdot 109 cm-3. We confirm the results by the accord of the quantities obtained from different observations using different methods and by the extrapolation of the photospheric magnetograms into the corona, from which we have obtained a magnetic field strength of about 7G at that height. Hence, indeed $\beta \geq 1$ in the post-eruptive arcade. The high-beta possibility had previously

been stated, e.g., by Ichimoto et al. (1994), but still not investigated. We address this issue in terms of the ``standard flare model" elaborated by Shibata and Yokoyama. During this event, Yohkoh/SXT observed McKenzie-Hudson dark moving features. Those features are filled with cold material, if they are not empty, and may affect the arcade.

Observations of CME-related phenomena in a wide spectral range

Grechnev, V. V.; Zandanov, V. G.; Uralov, A. M.; Maksimov, V. P.; Rudenko, V. G.; Borovik, V. N.; Gelfreikh, G. B.; Grigorieva, I. Y.; Medar, V. G.; Korzhavin, A. N.
Solar Physics, Volume 225, Issue 2, pp.379-401, **2004**
https://ui.adsabs.harvard.edu/link_gateway/2004SoPh..225..379G/PUB_HTML
We study pre-eruptive, eruptive, and post-eruptive phenomena related to a CME that occurred on November 23, 2000 by means of joint analyses of data from various spectral ranges. Almost all known CME-associated phenomena were observed during this event, i.e., a filament eruption, solar flare, dimmings, and a post-eruptive arcade formation. Following a chain of events observed in various spectral ranges, we find that the event occurred in an activity complex consisting of active regions 9231 and 9238, and that it was triggered by a magnetic flux emergence, which caused a flare in AR 9231. In turn, the flare triggered activation and eruption of the filament followed by the CME and the flare in AR 9238 in which the post-eruptive arcade was observed. We discuss some characteristics of the flare and CME and also estimate the magnetic field strength in the coronal arcade to be about 200 G from spatially resolved polarization measurements in microwaves with radio telescopes. In this particular case, the only significant emission mechanism is optically thin free-free emission, and the possible contribution of nonthermal emissions cannot change our estimate of the magnetic field strength in the corona. However, generally one should make sure that the nonthermal contribution cannot be important in similar cases; otherwise, the magnetic field can be well overestimated. Here, we specifically address the identification technique of the radio emission mechanism.

The Siberian Solar Radio Telescope: the current state of the instrument, observations, and data

Grechnev V. V., Lesovoi S. V., Smolkov G. Ya. et al.
Sol. Phys. **2003**. Vol. 216, no. 1. P. 239–272.
https://link.springer.com/article/10.1023%2FA%3A1026153410061
The Siberian Solar Radio Telescope (SSRT) is one of the world's largest solar radio heliographs. It commenced operation in 1983, and since then has undergone several upgrades. The operating frequency of the SSRT is 5.7 GHz. Since 1992 the instrument has had the capability to make one-dimensional scans with a high time resolution of 56 ms and an angular resolution of 15 arc sec. Making one of these scans now takes 14 ms. In 1996 the capability was added to make full, two-dimensional images of the solar disk. The SSRT is now capable of obtaining images with an angular resolution of 21 arc sec every 2 min. In this paper we describe the main features and operation of the instrument, particularly emphasizing issues pertaining to the imaging process and factors limiting data quality. Some of the data processing and analysis techniques are discussed. We present examples of full-disk solar images of the quiet Sun, recorded near solar activity minimum, and images of specific structures: plages, coronal bright points, filaments and prominences, and coronal holes. We also present some observations of dynamic phenomena, such as eruptive prominences and solar flares, which illustrate the high-time-resolution observations that can be done with this instrument. We compare SSRT observations at 5.7 GHz, including computed `light curves', both morphologically and quantatively, with observations made in other spectral domains, such as 17 GHz radio images, Hα filtergrams and magnetograms, extreme-ultraviolet and X-ray observations, and dynamic radio spectra.

The Post-Eruptive Arcade Formation in The Limb Event on July 31, 2004 From Microwave Solar Observations with the RATAN-600 Radio Telescope.

Irina Yu. **Grigoryeva**1, Larisa K. Kashapova2, Valery N. Borovik1, Moisey A. Livshits3
Sun and Geosphere, **2010**; 5(2): 58-60
http://www.shao.az/SG/v5n2/SG_v5_No2_2010-pp-58-60.pdf
A CME/flare event occurred at the western limb on 31 July 2004. Five successive multi-wavelength scans in centimeter range were obtained with the RATAN-600 radio telescope starting at the early stage of post-eruptive arcade formation (24 min after a C8.3 flare peak) and lasting for 4 hours. Microwave radio emission of the arcade was rather intense at initial stage indicating a predominant contribution of thermal emission and then considerably decreased during the decay phase. Its maximum was co-spatial with the 195 E Fe XII loop tops. At the end of microwave observations the contribution of the emission from accelerated particles became significant. The similarity of microwave characteristics of two eruptive events (on **31 July 2004** at the western limb and on **25 January 2007** at the eastern limb) is shown.

Post-Eruptive Arcade Formation in the 25 January 2007 CME/Flare Limb Event: Microwave Observations with the RATAN-600 Radio Telescope

I.Y. **Grigoryeva** · V.N. Borovik · M.A. Livshits · V.E. Abramov-Maximov · L.V. Opeikina · V.M. Bogod · A.N. Korzhavin
Solar Phys (**2009**) 260: 157–175; **File**
A CME/flare event occurred at the eastern limb on **25 January, 2007**. Seven successive multi-wavelength scans in the range 1.8 cm– 5.0 cm were obtained with the RATAN-600 radio telescope starting just at the beginning of the post-eruptive arcade formation (30 min after a C6.3 flare peak) and lasting for 3.5 hours. The conditions were favorable to study the off-limb microwave radio source associated with the post-eruptive arcade in different phases of its formation. Microwave radio emission of the arcade was rather intense initially and then considerably decreased; its maximum was co-spatial with the 195 Å Fe XII loop tops. The RATAN-600 total flux spectra of the off-limb radio source were practically flat during the first two hours indicating a predominant contribution of thermal emission. The X-ray spectrum was thermal (according to RHESSI data) at that time. Data available in the meter wavelength range during this phase were indicative of weak non-thermal processes likely due to accelerated particles. However, free – free emission of an isothermal source dominated in microwaves. This is indicative of the presence of a large amount of plasma in the region of arcade formation at the initial stage of the event. The weak microwave emission during the decay phase might be interpreted as the thermal cyclotron emission of the loops in the arcade.

The Air Force RSTN System //
Guidice D. A., Cliver E. W., Barron W. R., Kahler S.
Bull. Am. Astron. Soc. Vol. 13. **1981**. Mar. P. 553.
http://articles.adsabs.harvard.edu/pdf/1981BAAS...13Q.553G

Sagamore Hill Radio Observatory, Air Force Geophysics Laboratory, Hanscom Air Force Base, Massachusetts 01731. Report.
Guidice, D. A.; Eadon, E. J.
Bulletin of the Astronomical Society, Vol. 13, p. 400 – 401, **1981**
http://articles.adsabs.harvard.edu/pdf/1981BAAS...13..400G

Quiescent Prominences in the Era of ALMA. II. Kinetic Temperature Diagnostics
Stanislav **Gunár**1, Petr Heinzel1, Ulrich Anzer2, and Duncan H. Mackay
2018 ApJ 853 21
http://sci-hub.tw/http://iopscience.iop.org/0004-637X/853/1/21/
We provide the theoretical background for diagnostics of the thermal properties of solar prominences observed by the Atacama Large Millimeter/submillimeter Array (ALMA). To do this, we employ the 3D Whole-Prominence Fine Structure (WPFS) model that produces synthetic ALMA-like observations of a complex simulated prominence. We use synthetic observations derived at two different submillimeter/millimeter (SMM) wavelengths—one at a wavelength at which the simulated prominence is completely optically thin and another at a wavelength at which a significant portion of the simulated prominence is optically thick—as if these were the actual ALMA observations. This allows us to develop a technique for an analysis of the prominence plasma thermal properties from such a pair of simultaneous high-resolution ALMA observations. The 3D WPFS model also provides detailed information about the distribution of the kinetic temperature and the optical thickness along any line of sight. We can thus assess whether the measure of the kinetic temperature derived from observations accurately represents the actual kinetic temperature properties of the observed plasma. We demonstrate here that in a given pixel the optical thickness at the wavelength at which the prominence plasma is optically thick needs to be above unity or even larger to achieve a sufficient accuracy of the derived information about the kinetic temperature of the analyzed plasma. Information about the optical thickness cannot be directly discerned from observations at the SMM wavelengths alone. However, we show that a criterion that can identify those pixels in which the derived kinetic temperature values correspond well to the actual thermal properties in which the observed prominence can be established.

QUIESCENT PROMINENCES IN THE ERA OF ALMA: SIMULATED OBSERVATIONS USING THE 3D WHOLE-PROMINENCE FINE STRUCTURE MODEL
Stanislav **Gunár**1, Petr Heinzel1, Duncan H. Mackay2, and Ulrich Anzer
2016 ApJ 833 141
We use the detailed 3D whole-prominence fine structure model to produce the first simulated high-resolution ALMA observations of a modeled quiescent solar prominence. The maps of synthetic brightness temperature and optical

thickness shown in the present paper are produced using a visualization method for synthesis of the submillimeter/millimeter radio continua. We have obtained the simulated observations of both the prominence at the limb and the filament on the disk at wavelengths covering a broad range that encompasses the full potential of ALMA. We demonstrate here extent to which the small-scale and large-scale prominence and filament structures will be visible in the ALMA observations spanning both the optically thin and thick regimes. We analyze the relationship between the brightness and kinetic temperature of the prominence plasma. We also illustrate the opportunities ALMA will provide for studying the thermal structure of the prominence plasma from the cores of the cool prominence fine structure to the prominence–corona transition region. In addition, we show that detailed 3D modeling of entire prominences with their numerous fine structures will be important for the correct interpretation of future ALMA observations of prominences.

Non-thermal Electron Acceleration in Low Mach Number Collisionless Shocks. I. Particle Energy Spectra and Acceleration Mechanism

Xinyi **Guo**, Lorenzo Sironi1, and Ramesh Narayan
2014 ApJ 794 153
http://arxiv.org/pdf/1409.7393v1.pdf
Electron acceleration to non-thermal energies in low Mach number (Ms 5) shocks is revealed by radio and X-ray observations of galaxy clusters and solar flares, but the electron acceleration mechanism remains poorly understood. Diffusive shock acceleration, also known as first-order Fermi acceleration, cannot be directly invoked to explain the acceleration of electrons. Rather, an additional mechanism is required to pre-accelerate the electrons from thermal to supra-thermal energies, so they can then participate in the Fermi process. In this work, we use two- and three-dimensional particle-in-cell plasma simulations to study electron acceleration in low Mach number shocks. We focus on the particle energy spectra and the acceleration mechanism in a reference run with Ms = 3 and a quasi-perpendicular pre-shock magnetic field. We find that about 15% of the electrons can be efficiently accelerated, forming a non-thermal power-law tail in the energy spectrum with a slope of p 2.4. Initially, thermal electrons are energized at the shock front via shock drift acceleration (SDA). The accelerated electrons are then reflected back upstream where their interaction with the incoming flow generates magnetic waves. In turn, the waves scatter the electrons propagating upstream back toward the shock for further energization via SDA. In summary, the self-generated waves allow for repeated cycles of SDA, similarly to a sustained Fermi-like process. This mechanism offers a natural solution to the conflict between the bright radio synchrotron emission observed from the outskirts of galaxy clusters and the low electron acceleration efficiency usually expected in low Mach number shocks.

THE EFFECT OF LARGE-SCALE MAGNETIC TURBULENCE ON THE ACCELERATION OF ELECTRONS BY PERPENDICULAR COLLISIONLESS SHOCKS

Fan **Guo** and Joe Giacalone
Astrophysical Journal, 715:406–411, **2010** May
We study the physics of electron acceleration at collisionless shocks that move through a plasma containing largescale magnetic fluctuations. We numerically integrate the trajectories of a large number of electrons, which are treated as test particlesmoving in the time-dependent electric and magnetic fields determined from two-dimensional hybrid simulations (kinetic ions and fluid electron). The large-scale magnetic fluctuations effect the electrons in a number of ways and lead to efficient and rapid energization at the shock front. Since the electrons mainly follow along magnetic lines of force, the large-scale braiding of field lines in space allows the fast-moving electrons to cross the shock front several times, leading to efficient acceleration. Ripples in the shock front occurring at various scales will also contribute to the acceleration bymirroring the electrons.Our calculation shows that this process favors electron acceleration at perpendicular shocks. The current study is also helpful in understanding the injection problem for electron acceleration by collisionless shocks. It is also shown that the spatial distribution of energetic electrons is similar to in situ observations. *The process may be important to our understanding of energetic electrons in planetary bow shocks and interplanetary shocks, and explaining herringbone structures seen in some* ***type II solar radio*** *bursts.*

A Simple Method for Modeling Collision Processes in Plasmas with a Kappa Energy Distribution

M. **Hahn** and D. W. Savin
2015 ApJ 809 178
We demonstrate that a nonthermal distribution of particles described by a kappa distribution can be accurately approximated by a weighted sum of Maxwell–Boltzmann distributions. We apply this method to modeling collision processes in kappa-distribution plasmas, with a particular focus on atomic processes important for solar physics. The relevant collision process rate coefficients are generated by summing appropriately weighted Maxwellian rate coefficients. This method reproduces the rate coefficients for a kappa distribution to an estimated accuracy of better

than 3%. This is equal to or better than the accuracy of rate coefficients generated using "reverse-engineering" methods, which attempt to extract the needed cross sections from the published Maxwellian rate coefficient data and then reconvolve the extracted cross sections with the desired kappa distribution. Our approach of summing Maxwellian rate coefficients is easy to implement using existing spectral analysis software. Moreover, the weights in the sum of the Maxwell–Boltzmann distribution rate coefficients can be found for any value of the parameter κ, thereby enabling one to model plasmas with a time-varying κ. Tabulated Maxwellian fitting parameters are given for specific values of κ from 1.7 to 100. We also provide polynomial fits to these parameters over this entire range. Several applications of our technique are presented, including the plasma equilibrium charge state distribution (CSD), predicting line ratios, modeling the influence of electron impact multiple ionization on the equilibrium CSD of kappa-distribution plasmas, and calculating the time-varying CSD of plasmas during a solar flare.

Observations of Different Type of Bursts Associatedwith M 6.3 Solar Flares

Z. S. **Hamidi**1,*, N. N. M. Shariff

International Letters of Chemistry, Physics and Astronomy 4, 29-36, **2014**

https://www.academia.edu/5352283/Observations_of_Different_Type_of_Bursts_Associated_with_M_6.3_Solar_Flares?email_work_card=view-paper

Variation of solar bursts due to solar flares such as type an isolated type III , a complex type III, U is being highlighted. These bursts occurred on **9th March 2012** at the National Space Centre, Sg. Lang, Selangor, Malaysia Here, we study a unique case with a combination of two types burst associated with solar flare and CMEs. Our observation is focused on the low frequency region starting from 150 MHz till 400 MHz. We found that a solar flare type solar flare type M 6.3 which occurred in active region AR 1429 starting from 3:32 UT and ending at 05:00 UT. The flare has been confirmed to be the largest flare since 2005. Some physical parameters will be measured. We then compared our results with X-ray data from NOAA Space Weather Prediction Centre (SWPC)

Probability of Solar Flares Turn Out to Form a Coronal Mass Ejections Events Due to the Characterization of Solar Radio Burst Type II and III **Book**

Zety Sharizat **Hamidi**

International Letters of Chemistry, Physics and Astronomy 16 (**2014**) 1-85

https://ui.adsabs.harvard.edu/search/filter_database_fq_database=OR&filter_database_fq_database=database%3A"astronomy"&filter_database_fq_database=database%3A"physics"&fq=%7B!type%3Daqp%20v%3D%24fq_database%7D&fq_database=(database%3A"astronomy"%20OR%20database%3A"physics")&q=author%3A("Hamidi")%20AND%20pubdate%3A%5B2014-01%20TO%202014-12%5D&sort=date%20desc%2C%20bibcode%20desc&p_=0

https://www.academia.edu/10330915/Probability_of_Solar_Flares_Turn_Out_to_Form_a_Coronal_Mass_Ejections_Events_Due_to_the_Characterization_of_Solar_Radio_Burst_Type_II_and_III?email_work_card=view-paper

The solar flare and Coronal Mass Ejections (CMEs) are well known as one of the most massiveeruptions which potentially create major disturbances in the interplanetary medium and initiate severe magnetic storms when they collide with the Earth‟s magnetosphere. However, how far the solar flarecan contribute to the formation of the CMEs is still not easy to be understood. These phenomena areassociated with II and III burst it also divided by sub-type of burst depending on the physicalcharacteristics and different mechanisms. In this work, we used a Compound Astronomical Low-costLow-frequency Instrument for Spectroscopy in Transportable Observatories (CALLISTO) system.The aim of the present study is to reveal dynamical properties of solar burst type II and III due toseveral mechanisms. Most of the cases of both solar radio bursts can be found in the range less that400 MHz. Based on solar flare monitoring within 24 hours, the CMEs that has the potential to explodewill dominantly be a class of M1 solar flare. Overall, the tendencies of SRBT III burst form the solarradio burst type III at 187 MHz to 449 MHz. Based on solar observations, it is evident that theexplosive, short time-scale energy release during flares and the long term, gradual energy releaseexpressed by CMEs can be reasonably understood only if both processes are taken as common
and probably not independent signatures of a destabilization of pre-existing coronal magnetic fieldstructures. The configurations of several active regions can be sourced regions of CMEs formation.The study of the formation, acceleration and propagation of CMEs requires advanced and powerful observational tools in different spectral ranges as many „stages‟ as possible between the photosphere of the Sun and magnetosphere of the Sun and magnetosphere of the Earth. In conclusion, this range isa current regime of solar radio bursts during CMEs events. **9th March 2012, 13th November 2012, 23rd October 2012, 30th March 2013,**

Observations of coronal mass ejections (CMEs) at low frequency radio region on 15th April 2012.

Hamidi, Z. S., Abidin, Z. Z., Ibrahim, Z. A., Shariff, N. N. M., & Monstein, C.

AIP Conf. Proc. 1528, 55 (**2013**)

sci-hub.se/10.1063/1.4803568

ORFEES – a radio spectrograph for the study of solar radio bursts and space weather applications

Abdallah **Hamini**1,2, Gabriel Auxepaules2, Lionel Birée3, Guy Kenfack2, Alain Kerdraon1, Karl-Ludwig Klein1,2*, Patrice Lespagnol2, Sophie Masson1,2, Lucile Coutouly2, Christian Fabrice2 and Renaud Romagnan1
J. Space Weather Space Clim. **2021**, 11, 57
https://www.swsc-journal.org/articles/swsc/pdf/2021/01/swsc210035.pdf
https://doi.org/10.1051/swsc/2021039
Radio bursts are sensitive tracers of non-thermal electron populations in the solar corona. They are produced by electron beams and shock waves propagating through the corona and the heliosphere, and by trapped electron populations in coronal mass ejections (CMEs) and in quiescent active regions. Combining space-borne and ground-based radio spectrographs allows one to track disturbances between the low corona, near or at the sites of particle acceleration, and the spacecraft. Radio observations are, therefore, a significant tool in probing the solar origin of heliospheric disturbances, which is a central research topic as witnessed by the Parker Solar Probe and Solar Orbiter missions. The full scientific return of these projects needs vigorous ground-based support, which at radio wavelengths covers altitudes up to about a solar radius above the photosphere. Besides research in solar and heliospheric physics, monitoring solar radio bursts also supports space weather services. On occasion, radio bursts can themselves be a space weather hazard. The Nançay radio astronomy station in central France has a long tradition of monitoring radio emission at decimetre-to-meter wavelengths. This article describes the radio spectrograph ORFEES (Observations Radiospectrographiques pour FEDOME et l'Etude des Eruptions Solaires). It observes the whole-Sun flux density between 144 and 1004 MHz, pertaining to regions between the low corona and about half a solar radius above the photosphere. ORFEES results from a partnership between Observatoire de Paris and the French Air Force, which operates the experimental space weather service FEDOME. The primary use of the instrument at the Paris Observatory is astrophysical observation. Low-resolution data with rapid availability are presently produced for the French Air Force. Similar information can be made available to a broader range of space weather service providers. This article gives an overview of the instrument design and access to the data and shows a few illustrative observations. **2015 Nov 04, 2016 Jul 18, 2017 September 06, 2019 May 05**

Double-Loop Configuration of Solar Flares

Hanaoka, Yoichiro
1997 Sol. Ph..173..319-346
https://link.springer.com/content/pdf/10.1023/A:1004953003558.pdf
We analyzed several flares, which are presumed to be caused by interactions between an emerging loop and an overlying loop. We call such a basic combination of loops a 'double-loop configuration', and we reveal its topology on the basis of the microwave and soft X-ray observations of the flares and the magnetograms. In many cases, the magnetic field of the flare loops shows a 'bipolar + remote unipolar' structure, rather than a quadrapole structure. The footpoints of two loops are distributed in three magnetic patches, and two of the footpoints of the loops, one from the emerging loop and the other from the overlying loop, are included in a single magnetic polarity patch. Therefore, the two loops form a 'three-legged' structure, and the two loops are not anti-parallel as assumed in the traditional reconnection models. Typically, the emergence of a parasitic polarity near the major preceding-polarity region or the following one in an active region creates this configuration, but, in one of the analyzed flares, two active regions are involved in the configuration. Not only the flares, but various other active phenomena – microflares, thermal plasma flows like jets, and surges – occur in the same magnetic configuration. Hence, the interaction between two loops, which forms the three-legged structure, is an important source of the various types of activity. **1992 AUGUST 21 , 1992 OCTOBER 23 , 1992 December 15 , 1993 FEBRUARY 6 , 1993 April 10, 1993 April 11 , 1993 June 7, 1993 SEPTEMBER 30, 1994 December 14**

Flares and Plasma Flow Caused by Interacting Coronal Loops

Hanaoka, Yoichiro
1996 Sol. Ph..165..275-301
http://articles.adsabs.harvard.edu/pdf/1996SoPh..165..275H
Active region NOAA 7360 was observed in 1992 December with various instruments including the Yohkoh satellite. In this region, a small loop emerged near one of the footpoints of a pre-existing large coronal loop. These loops show evidence that interactions between coronal loops cause flares, microflares, and plasma flow. All of the four flares observed in this region show that brightenings in the small loop occurred first, and then the large loop flared up. The brightenings in the large loop can not occur by themselves, but must be triggered by the brightenings in the small loop. There must be interactions between the loops to cause these flares. As well as the flares, many microflares occurred in the small loop. More than half of them are accompanied by plasma ejection phenomena from the small loop into the large loop. The large loop is filled with ejected plasma with velocities of about 1000 km s-1. These ejection phenomena are considered as X-ray jets. The associated occurrences of the microflares and the jets suggest that they are also caused by interactions between the loops. The recurrent occurrences of the homologous flares and microflares mean that the

magnetic field structure in this region inevitably causes the activity due to loop-loop interactions; the flares and jets occur under a common magnetic field structure. **14-17 Dec 1992**

F10.7 Daily Forecast Using LSTM Combined With VMD Method

Yuhang **Hao**, Jianyong Lu, Guangshuai Peng, Ming Wang, Jingyuan Li, Guanchun Wei
Space Weather Volume22, Issue1 e2023SW003552 **2024**
https://doi.org/10.1029/2023SW003552
https://agupubs.onlinelibrary.wiley.com/doi/epdf/10.1029/2023SW003552
The F10.7 solar radiation flux is a well-known parameter that is closely linked to solar activity, serving as a key index for measuring the level of solar activity. In this study, the Variational Mode Decomposition (VMD) and Long Short-term Memory (LSTM) network are combined to construct a VMD-LSTM model for predicting F10.7 values. The F10.7 sequence is decomposed into several intrinsic mode functions (IMF) by VMD, then the LSTM neural network is utilized to forecast each IMF. All IMF prediction results are aggregated to obtain the final F10.7 value. The data sets from 1957 to 2008 are used for training and the data sets from 2009 to 2019 are used for testing. The results show that the VMD-LSTM model achieves an annual average root mean square error of only 4.47 sfu and an annual average correlation coefficient (R) of 0.99 during solar cycle 24, which is significantly better than the accuracy of the LSTM model (W. Zhang et al., 2022, https://doi.org/10.3390/universe8010030), the AR model (Du, 2020, https://doi.org/10.1007/s11207-020-01689-x), and the BP model (Xiao et al., 2017, https://doi.org/10.11728/cjss2017.01.001). The VMD-LSTM model exhibits strong predictive capability for the F10.7 index during solar cycle 24.

Offset Power-law Dependence of the Sun's Radial Electron Density Profile: Evidence and Implications

J. C. **Harding**, Iver H. Cairns, and V. V. Lobzin
2019 ApJ 877 25
sci-hub.se/10.3847/1538-4357/ab19a0
The radial electron density profile n e (r) of the Sun's corona and solar wind contains information on the sources, heating, and acceleration of the coronal and solar wind plasma. Currently, several empirically derived density models are used to describe the corona, with varying degrees of success and little physical justification or predictive power. The offset power-law (OPL) profile $n_e(r) = A(r - r_0)^{-\alpha}$, with radial offset r 0 and power-law index α, models radial outflow from r 0 that conserves total electron number and may be accelerated and heated (affecting α), thus having physical significance and predictive power. We fit the OPL model to multiple sets of published radial density profiles obtained from spectroscopic, white light, and radio data from different regions on the Sun and during different periods of solar activity. The spectroscopic and white light data yield r0 = (1.02 ± 0.06) R S , where the uncertainties are standard errors of the mean, and $\langle\alpha\rangle = -2.4 \pm 0.2$, consistent with plasma originating near the chromosphere and acceleration similar to the nominal Parker solar wind model. Comparisons with time-lapse coronagraph and spectroscopic observations are favorable and show evidence for significant variations with position and time. These are expected given the corona's well-known asymmetries, three-dimensional structures, and time variability. Radio burst data yield flatter profiles α < 2, suggesting that pre-flare activity alters the density profile by increasing the coronal density at large heights. We discuss the possible interpretations and implications for coronal physics and solar radio bursts.

Simultaneous Near-Sun Observations of a Moving Type IV Radio Burst and the Associated White-Light Coronal Mass Ejection

K. **Hariharan** , R. Ramesh, C. Kathiravan, T. J. Wang
Solar Phys. Volume 291, Issue 5, pp 1405-1416 **2016** DOI: 10.1007/s11207-016-0918-x
http://sci-hub.cc/10.1007/s11207-016-0918-x
We present rare contemporaneous low-frequency (\(< 100~\mbox{MHz}\)) imaging, spectral, and polarimetric observations of a moving type IV radio burst that had close spatio-temporal association with a white-light coronal mass ejection (CME) near the Sun. We estimate the electron density near the burst region from white-light coronagraph polarized brightness (pB) images of the CME as well as the two-dimensional radio imaging observations of the thermal free-free emission at a typical radio frequency such as 80 MHz. We analyze the burst properties such as the degree of circular polarization, the spectral index, and fine structures using the radio polarimeter and the radio spectral observations. The obtained results suggest that second harmonic plasma emission from the enhanced electron density in the leading edge of the CME is the cause of the radio burst. We determine the strength of the coronal magnetic field (\(B\)) for the first time based on this interpretation. The estimated value (\(B \approx 1\) gauss) in the CME leading edge at a heliocentric distance of \(\approx 2.2~R_{\odot }\) agrees well with the similar \(B\) values reported earlier based on other types of observations. **31 March 2014**
See CESRA science highlight #1169, Jan 2017 http://www.astro.gla.ac.uk/users/eduard/cesra/?p=1169

High Dynamic Range Observations of Solar Coronal Transients at Low Radio Frequencies with a Spectro-correlator

Hariharan, K.; Ramesh, R.; Kathiravan, C.; Abhilash, H. N.; Rajalingam, M.
Astrophysical Journal Supplement Series, Volume 222, Issue 2, article id. 21, 7 pp. (**2016**)
A new antenna system with a digital spectro-correlator that provides high temporal, spectral, and amplitude resolutions has been commissioned at the Gauribidanur Observatory near Bangalore in India. Presently, it is used for observations of the solar coronal transients in the scarcely explored frequency range ≈30-15 MHz. The details of the antenna system, the associated receiver setup, and the initial observational results are reported. Some of the observed transients exhibited quasi-periodicity in their time profiles at discrete frequencies. Estimates of the associated magnetic field strength (B) indicate that B ≈ 0.06-1 G at a typical frequency such as 19.5 MHz.

Observations of Near-Simultaneous Split-Band Solar Type-II Radio Bursts at Low Frequencies

K. **Hariharan**, R. Ramesh, C. Kathiravan
Solar Physics September **2015**, Volume 290, Issue 9, pp 2479-2489
We report ground-based radio spectral and polarimeter observations of two successive split-band Type-II bursts that occurred on **20 February 2014** at low frequencies (<100 MHz) in association with a solar coronal mass ejection (CME). The temporal interval between the onset of the two bursts was very small, ≈ one minute. Both of the bursts exhibited fundamental–harmonic structure. The coronal magnetic-field strength [B] in the upstream region of the associated magnetohydrodynamic (MHD) shock, estimated from the split-band observations, is in the range B≈1.3--1.1 G over the radial distance [r] interval r≈1.49--1.58 R⊙ for the first Type-II burst, and B≈1.3--1.0 G overr≈1.49--1.64 R⊙ for the second Type-II burst. Based on the results obtained, we show that the first and the second Type-II bursts in the present case were likely due to MHD shocks generated by the near-simultaneous interaction of two different regions of the aforementioned CME with a preceding CME and a pre-existing coronal streamer.

An Estimate of the Coronal Magnetic Field near a Solar Coronal Mass Ejection from Low-frequency Radio Observations

K. **Hariharan**1, R. Ramesh1, P. Kishore1, C. Kathiravan1, and N. Gopalswamy
2014 ApJ 795 14
We report ground-based, low-frequency (<100 MHz) radio imaging, spectral, and polarimeter observations of the type II radio burst associated with the solar coronal mass ejection (CME) that occurred on 2013 May 2. The spectral observations indicate that the burst has fundamental (F) and harmonic (H) emission components with split-band and herringbone structures. The imaging observations at 80 MHz indicate that the H component of the burst was located close to leading edge of the CME at a radial distance of r 2 R ⊙ in the solar atmosphere. The polarimeter observations of the type II burst, also at 80 MHz, indicate that the peak degree of circular polarization (dcp) corresponding to the emission generated in the corona ahead of and behind the associated MHD shock front are 0.05 ± 0.02 and 0.1 ± 0.01, respectively. We calculated the magnetic field B in the above two coronal regions by adopting the empirical relationship between the dcp and B for the harmonic plasma emission and the values are (0.7-1.4) ± 0.2 G and (1.4-2.8) ± 0.1 G, respectively.

The active region source of a type III radio storm observed by Parker Solar Probe during Encounter 2

L. **Harra**, D. H. Brooks, S. D. Bale, C. H. Mandrini, K. Barczynski, R. Sharma, S. T. Badman, S. Vargas Dominguez, M. Pulupa
A&A 650, A7 **2021**
https://arxiv.org/pdf/2102.04964.pdf
https://www.aanda.org/articles/aa/pdf/2021/06/aa39514-20.pdf
https://doi.org/10.1051/0004-6361/202039514
Context. To investigate the source of a type III radio burst storm during encounter 2 of NASA's Parker Solar Probe (PSP) mission.
Aims. It was observed that in encounter 2 of NASA's Parker Solar Probe mission there was a large amount of radio activity, and in particular a noise storm of frequent, small type III bursts from **31st March to 6th April 2019**. Our aim is to investigate the source of these small and frequent bursts.
Methods. In order to do this, we analysed data from the Hinode EUV Imaging Spectrometer (EIS), PSP FIELDS, and the Solar Dynamics Observatory (SDO) Atmospheric Imaging Assembly (AIA). We studied the behaviour of active region 12737, whose emergence and evolution coincides with the timing of the radio noise storm and determined the possible origins of the electron beams within the active region. To do this, we probe the dynamics, Doppler velocity, non-thermal velocity, FIP bias, densities, and carry out magnetic modelling.
Results. We demonstrate that although the active region on the disk produces no significant flares, its evolution indicates it is a source of the electron beams causing the radio storm. They most likely originate from the area at the

edge of the active region that shows strong blue-shifted plasma. We demonstrate that as the active region grows and expands, the area of the blue-shifted region at the edge increases, which is also consistent with the increasing area where large-scale or expanding magnetic field lines from our modelling are anchored. This expansion is most significant between 1 and 4 April 2019, coinciding with the onset of the type III storm and the decrease of the individual burst's peak frequency, indicating the height at which the peak radiation is emitted increases as the active region evolves. **31st March - 6th April 2019**
CESRA #3058 **2021** https://www.astro.gla.ac.uk/users/eduard/cesra/?p=3058

Solar Radio Burst Detection Based on the MobileViT-SSDLite Lightweight Model

Hailan **He**1, Guowu Yuan1,2, Hao Zhou1,2, Chengming Tan3,4, and Shaojie Guo5
2023 ApJS 269 51
https://iopscience.iop.org/article/10.3847/1538-4365/ad036c/pdf
Real-time detection of solar radio bursts is crucial in solar physics research and space weather forecasting. However, current research on the automatic detection of solar radio bursts is limited to identifying the presence or absence of solar radio bursts or recognizing only a single type of burst, such as type II or III. Furthermore, existing methods cannot learn spectral and temporal features and often suffer from the drawbacks of large network models, resulting in slow speeds. This paper proposes an automatic recognition and localization method based on a lightweight object detection model for solar radio burst events. We collected observation data from e-CALLISTO and established a data set containing type II, III, IV, and V solar radio bursts. To address the real-time requirements of practical applications and consider the temporal and frequency domain information of spectrogram images, we improved a vision transformer with a self-attention mechanism and adopted a lightweight model for detection. The experimental results demonstrate that our proposed method achieves an average precision at a 50% intersection-over-union threshold of 78.2% and a recall rate of 92% on the established solar radio burst data set. Additionally, the model operates at a detection speed of 54.8 frames s–1, where a frame refers to a spectral image with a duration of 15 minutes, enabling efficient automated detection and localization of type II, III, IV, and V solar radio bursts.

Tracking the Source of Solar Type II Bursts through Comparisons of Simulations and Radio Data

Alexander M. **Hegedus** (1), Ward B. Manchester IV (1), Justin C. Kasper (1)
ApJ **922** 203 **2021**
https://arxiv.org/pdf/2102.07875.pdf
https://iopscience.iop.org/article/10.3847/1538-4357/ac2361/pdf
https://doi.org/10.3847/1538-4357/ac2361
The most intense solar energetic particle events are produced by coronal mass ejections (CMEs) accompanied by intense type II radio bursts below 15 MHz. Understanding where these type II bursts are generated relative to an erupting CME would reveal important details of particle acceleration near the Sun, but the emission cannot be imaged on Earth due to distortion from its ionosphere. Here, a technique is introduced to identify the likely source location of the emission by comparing the observed dynamic spectrum observed from a single spacecraft against synthetic spectra made from hypothesized emitting regions within a magnetohydrodynamic (MHD) numerical simulation of the recreated CME. The radio-loud **2005 May 13** CME was chosen as a test case, with Wind/WAVES radio data used to frame the inverse problem of finding the most likely progression of burst locations. An MHD recreation is used to create synthetic spectra for various hypothesized burst locations. A framework is developed to score these synthetic spectra by their similarity to the type II frequency profile derived from Wind/WAVES data. Simulated areas with 4x enhanced entropy and elevated de Hoffmann Teller velocities are found to produce synthetic spectra similar to spacecraft observations. A geometrical analysis suggests that the eastern edge of the entropy derived shock around (-30, 0) degrees in heliocentric coordinates was emitting in the first hour of the event before ceasing emission, and that the western/southwestern edge of the shock centered around (6, -12) degrees was a dominant area of radio emission for the 2 hours of simulation data out to 20 solar radii. **2012-01-19**

Prominence Observations with ALMA **Review**
Petr **Heinzel**, Miroslav Bárta, Stanislav Gunár, Nicolas Labrosse, Jean-Claude Vial
Front. Astron. Space Sci. 9: 983707. **2022**
doi 10.3389/fspas.2022.983707
https://www.frontiersin.org/articles/10.3389/fspas.2022.983707/pdf
We review past prominence observations in the mm/sub-mm radio domain and summarize the basic physics behind the formation of such continua under the prominence conditions. Prior to ALMA observations, simulations of the prominence/filament visibility in mm/sub-mm bands were performed using specific models and assumptions and we review this effort here. A core part of the review is the description and analysis of the first ALMA observations of a quiescent prominence, focusing on various physical as well as geometrical (like the importance of the PoS filling factor) aspects. It is first time when the prominence was observed in the mm domain with a spatial resolution as high as 1-2

arcsec, comparable to ground-based coronagraphic observations in thehydrogen Hα line, and we demonstrate why the fine structuresin both ALMA Band 3 and Hα images are quite similar. Finally, we briefly discuss future prospects of ALMA prominence observations,to be coordinated with optical and UV spectra and images.

ALMA as a prominence thermometer: First observations

Petr **Heinzel**, Arkadiusz Berlicki, Miroslav Bárta, Paweł Rudawy, Stanislav Gunár, Nicolas Labrosse, Krzysztof Radziszewski

ApJL **2022**

https://arxiv.org/pdf/2202.12761.pdf

We present first prominence observations obtained with ALMA in Band 3 at the wavelength of 3 mm. High-resolution observations have been coaligned with the MSDP Hα data from Wroclaw-Bialków large coronagraph at similar spatial resolution. We analyze one particular co-temporal snapshot, first calibrating both ALMA and MSDP data and then demonstrating a reasonable correlation between both. In particular we can see quite similar fine-structure patterns in both ALMA brightness temperature maps and MSDP maps of Hα intensities. Using ALMA we intend to derive the prominence kinetic temperatures. However, having current observations only in one band, we use an independent diagnostic constraint which is the Hα line integrated intensity. We develop an inversion code and show that it can provide realistic temperatures for brighter parts of the prominence where one gets a unique solution, while within faint structures such inversion is ill conditioned. In brighter parts ALMA serves as a prominence thermometer, provided that the optical thickness in Band 3 is large enough. In order to find a relation between brightness and kinetic temperatures for a given observed Hα intensity, we constructed an extended grid of non-LTE prominence models covering a broad range of prominence parameters. We also show the effect of the plane-of-sky filling factor on our results. **April 19, 2018,**

On the Visibility of Prominence Fine Structures at Radio Millimeter Wavelengths

P. **Heinzel**, A. Berlicki, M. Bárta, M. Karlický, P. Rudawy

Solar Physics Volume 290, Issue 7, pp 1981-2000 **2015**

Prominence temperatures have so far mainly been determined by analyzing spectral line shapes, which is difficult when the spectral lines are optically thick. The radio spectra in the millimeter range offer a unique possibility to measure the kinetic temperature. However, studies in the past used data with insufficient spatial resolution to resolve the prominence fine structures. The aim of this article is to predict the visibility of prominence fine structures in the submillimeter/millimeter (SMM) domain, to estimate their brightness temperatures at various wavelengths, and to demonstrate the feasibility and usefulness of future high-resolution radio observations of solar prominences with ALMA (Atacama Large Millimeter-submillimeter Array). Our novel approach is the conversion of Hα coronagraphic images into microwave spectral images. We show that the spatial variations of the prominence brightness both in the Hα line and in the SMM domain predominantly depend on the line-of-sight emission measure of the cool plasma, which we derive from the integrated intensities of the observed Hα line. This relation also offers a new possibility to determine the SMM optical thickness from simultaneous Hα observations with high resolution. We also describe how we determine the prominence kinetic temperature from SMM spectral images. Finally, we apply the ALMA image-processing software Common Astronomy Software Applications (CASA) to our simulated images to assess what ALMA would detect at a resolution level that is similar to the coronagraphic Hα images used in this study. Our results can thus help in preparations of first ALMA prominence observations in the frame of science and technical verification tests.

Optical-to-Radio Continua in Solar Flares

P. **Heinzel** and E. H. Avrett

Solar Physics, Volume 277, Number 1, 31-44, **2012**

Spectral continua observed during solar flares may contain information about both thermal and non-thermal heating mechanisms. Using two semi-empirical flare models F2 and FLA, we synthesize the thermal continua from optical to mm–radio domains and compare their intensities with quiet-Sun values computed from a recent model C7. In this way, the far-infrared and sub-mm/mm continua are studied for the first time, and we present our results as a benchmark for further modeling and for planning new observations, especially with the ALMA instrument. Finally, we demonstrate how these continua are formed and show a close correspondence between their brightness temperature and the kinetic-temperature structure of the flaring atmosphere.

Electromagnetic Simulations of Solar Radio Emissions

P. **Henri** , A. Sgattoni , C. Briand, F. Amiranoff, C. Riconda

JGR Volume124, Issue3 March **2019** Pages 1475-1490

sci-hub.se/10.1029/2018JA025707

Solar radio emissions are electromagnetic waves emitted in the solar wind as a consequence of electron beams accelerated during solar flares or interplanetary shocks such as interplanetary coronal mass ejections. Different physical mechanisms have been suggested to describe their origin. A good understanding of the emission process would enable to infer the kinetic energy transferred from accelerated electrons to radio waves. Even if the electrostatic case has been extensively studied, full electromagnetic simulations were attempted only recently. In this work, we report large-scale 2D3V electromagnetic particle-in-cell simulations that enable to identify the generation of both electrostatic and electromagnetic waves originated by a succession of plasma instabilities. They confirm that an efficient mechanism to generate solar radio emissions close to T2f, the harmonic of the plasma frequency, is a multistage model based on a succession of nonlinear three-wave interaction processes. Through a parametric study of the electron beam parameters, we show that (i) the global efficiency of the multistep conversion mechanism from the electron beam kinetic energy to the T2f radio wave is independent of the beam parameters, approximately 10−5 in all tested configurations, while (ii) the directivity of the electromagnetic radio wave strongly depends on the origin electron beam. Those results represent a step forward toward the use of solar wind radio emissions, observed remotely, as a diagnostic for the properties of the electron beam located at the source of the radio emission, and therefore to eventually better characterize remotely electron acceleration mechanisms in space regions not directly accessible to in situ measurements.

Vlasov-Poisson simulations of electrostatic parametric instability for localized Langmuir wave packets in the solar wind

Henri, P.; Califano, F.; Briand, C.; Mangeney, A.
J. Geophys. Res., Vol. 115, No. A6, A06106, **2010**
http://dx.doi.org/10.1029/2009JA014969
Recent observation of large-amplitude Langmuir waveforms during a type III event in the solar wind has been interpreted as the signature of the electrostatic decay of beam-driven Langmuir waves. This mechanism is thought to be a first step to explain the generation of type III radio emission. The threshold for this parametric instability in the typical solar wind condition has been investigated through 1D-1V Vlasov-Poisson simulations. We show that the amplitude of the observed Langmuir beatlike waveforms is of the order of the effective threshold computed from the simulations. The expected levels of associated ion acoustic density fluctuations have also been computed for comparison with observations.

Evidence for wave coupling in type III emissions

Henri, P., C. Briand, A. Mangeney, S. D. Bale, F. Califano, K. Goetz, and M. Kaiser
J. Geophys. Res., 114, A03103, **2009**
http://dx.doi.org/10.1029/2008JA013738
Using new capabilities of waveform analyses provided by the S/WAVES instruments onboard the two **STEREO** spacecraft, we present for the first time a complete set of direct evidence for three-wave coupling occurring during a type III emission and involving two Langmuir waves and an ion acoustic wave. Information on the Doppler-shifted frequencies and especially the phases of the waves are used in order to check first the conservation of momentum and energy, through Fourier analyses, and second the phase locking between the waves, through bicoherence analyses. Wavelet analyses allow us to resolve for the first time the coupling regions, in which spatial length is estimated to be 18 ± 5 km. The wave packets travel at comparable speed, and the characteristic available interaction time is about 1 s. Interpretations of the phase coupling and evaluation of the growth rate of the waves tend to favor the parametric decay, at least in the observational events considered in this work.

The Solar ALMA Science Archive (SALSA)

Vasco M. J. **Henriques**, Shahin Jafarzadeh, Juan Camilo Guevara Gómez, Henrik Eklund, Sven Wedemeyer, Mikołaj Szydlarski, Stein Vidar H. Haugan1, Atul Mohan
A&A **2021**
https://arxiv.org/pdf/2109.02374.pdf
In December 2016, the Atacama Large Millimeter/submillimeter Array (ALMA) carried out the first regular observations of the Sun. These early observations and the reduction of the respective data posed a challenge due to the novelty and complexity of observing the Sun with ALMA.
The difficulties with producing science-ready time-resolved imaging products in a format familiar and usable by solar physicists based on the measurement sets delivered by ALMA had so far limited the availability of such data. With the development of the Solar ALMA Pipeline (SoAP), it has now become possible to routinely reduce such data sets.
As a result, a growing number of science-ready solar ALMA datasets is now offered in the form of Solar ALMA Science Archive (SALSA).
So far, SALSA contains primarily time series of single-pointing interferometric images at cadences of one or two seconds. The data arrays are provided in FITS format.
We also present the first version of a standardised header format that accommodates future expansions and fits within the scope of other standards including the ALMA Science Archive itself and SOLARNET. The headers also include information designed to aid the reproduction of the imaging products from the raw data. Links to co-observations, if

available, with a focus on those of the Interface Region Imaging Spectrograph (IRIS), are also provided. SALSA is accompanied by the Solar ALMA Library of Auxiliary Tools (SALAT) that contains IDL and Python routines for convenient loading and quick-look analysis of SALSA data. **2016-12-22, 2017-04-22**

Size and amplitude of Langmuir waves in the solar wind

Hess, S. L. G.; Malaspina, D. M.; Ergun, R. E.
J. Geophys. Res., Vol. 116, No. A7, A07104, **2011**
Langmuir waves in the solar wind are known to be the origin of many types of solar radio emissions. In situ observations have shown that the most intense Langmuir waves often appear as wave packets. Several models have been proposed to explain this localization, such as kinetic localization and eigenmode formation. In the present paper we investigate the role of background turbulence on the size of the Langmuir wave packets through modeling of both quasi-planar growth in constant density regions and eigenmode growth in density wells. We compute both numerically and analytically the growth of the waves, the size of the wave packets, and the amplitude of these packets. Our theoretical results are compared to the in situ measurements of Ulysses and STEREO and appear to be consistent with the measured amplitude distributions.

The analysis of type II and type III solar radio bursts: GUI for the e-CALLISTO data

Yashan
Hettiarachchi a, Janaka Adassuriya b, Chandana Jayaratne b, Sasani Jayawardhana a, Christian Monstein c
New Astronomy Volume 109, July **2024**, 102194
https://doi.org/10.1016/j.newast.2024.102194
Solar radio bursts are sudden peaks in the low-frequency radio emissions originating from the sun. These emissions, while revealing important insights into underlying physical mechanisms in solar physics, can also help predict space weather events that could have adverse effects on satellite communications and the global energy grid. A thorough understanding of this phenomena demands the collection and analysis of solar emission data over vast geographical and time scales. In this regard, the e-CALLISTO network plays a major role through having already archived more than 20 years worth of solar radio burst data. Leveraging on the advances in data analysis techniques, this data can be used to review the statistical significance of burst properties of type II and type III solar radio bursts and hence more importantly the magnetic field measurements of the active regions. In order to process the e-CALLISTO data, a software containing several data reduction processes is introduced to optimize the data analysis via a graphical user interface (GUI). The program is capable of reading out data from any CALLISTO receiving station, while offering visualization capabilities such as the color-corrected spectrum view, the plot of frequencies of the highest intensity, the individual frequency spectrum, the solar burst isolation portal, the fitting model for the radio burst, and the drift rate curve of the burst. These are achieved through using the raw “fits” files of spectra to perform background RFI reduction, identify and isolate solar radio burst regions, model the peak frequency variation using curve fitting, and thereby determine the frequency drift rates. The method can be directly applied to Type II and III solar bursts while providing space for tailoring and modification. In this work, the slow drift type II radio bursts were fitted by exponential decay and the fast drift type III radio bursts were approximated as linear decay. Hence, the frequency drift rates were computed for type II and type III radio bursts. The application is used to analyze several Type II and Type III solar radio bursts and depending on the bust type shock speed and electron velocity were determined. The GUI interface eliminates the time-consuming subjective manual analysis of e-CALLISTO data thereby making the analysis of solar radio bursts a routine and rapid process. **13 Jun 2010, 18 Feb 2021**
CESRA #3809 **2024** https://www.astro.gla.ac.uk/users/eduard/cesra/?p=3809

Radio Observation of Solar-Activity-Related mHz Oscillations

N. V. **Hiep**, P. T. Nhung, P. Darriulat, P. N. Diep, P. T. Anh, P. N. Dong, D. T. Hoai, N. T. Thao
Solar Physics, March **2014**, Volume 289, Issue 3, pp 939-950
The VATLY radio telescope, operating at 1.415 GHz in Ha Noi, has been used to track the Sun in the summer – autumn months in 2012. Evidence has been obtained for solar activity, including occasional flares and variable oscillations with amplitudes at the percent level and periods of about 6 min. Comparison with data collected at the same frequency by the Learmonth Observatory in Australia suggests that the observed oscillations were associated with solar activity. A joint analysis of both data sets is presented, evaluating the correlations between them. We describe the common and different main features.
See: Publ. Astron. Soc. Aust.31, e029, **2014**, **Diep**, P.N., Phuong, N.T., Darriulat, P., Nhung, P.T., Anh, P.T., Dong, P.N., Hoai, D.T., Thao, N.T., **Correlated Oscillations Due to Similar Multipath Effects Seen in Two Widely Separated Radio Telescopes.** http://arxiv.org/pdf/1405.1525v1.pdf

SOLAR MICROWAVE BURSTS FROM ELECTRON POPULATIONS WITH A 'BROKEN' ENERGY SPECTRUM

J. **HILDEBRANDT**1, A. KRÜGER1, I.M. CHERTOK2, V.V. FOMICHEV2 and R.V. GORGUTSA2

Solar Physics **181:** 337–349, **1998**.

Usually the gyrosynchrotron emission of microwave bursts from electron populations with a power-law (PL) energy distribution has been considered under the assumption that the spectral index of the distribution is constant over a wide range of energies. Meanwhile, there is strong evidence, in particular from hard X-ray and -ray, but also from cm/mm wavelength radio observations, that in many solar flare events the spectrum of the emitting electrons is characterized by a significant hardening at energies above 100–500 keV.We present some examples of calculated microwave burst spectra at cm/mm wavelengths taking into account the above evidence. It is shown that a break in the energy spectrum of the PL electrons can indeed result in a spectral hardening sometimes observed in microwave bursts at frequencies above 10–30 GHz.

Type II Solar Radio Bursts : 2. Detailed comparison of theory with observations

Hillan, D. S.; Cairns, I. H.; Robinson, P. A.

J. Geophys. Res., Vol. 117, No. A6, A06105, 2012**, File**

In this paper, the second in a two paper series, we quantitatively compare a detailed theory for type II solar radio bursts with observations and extract the parameters of the associated shocks. We use the techniques and assessment parameters developed and demonstrated in the companion paper for artificial data sets and solar wind models. Here we investigate three relatively well-observed type II events with estimates of shock parameters from LASCO/SOHO observations of coronal mass ejections (CMEs) or other data. Using these parameters we obtain reasonable qualitative and semiquantitative agreement (25-40% correlations) between the theory and observed dynamic spectra. Then, using an iterative downhilll simplex method with two assessment parameters, we extract model shock parameters that increase the agreement between theory and observation in terms of relative flux levels, spectral intensifications and drift rates. The extracted parameters agree qualitatively and semiquantitatively with the parameters (speed, size and expansion index) estimated from CME observations for one of the studied events. The extracted parameters agree qualitatively with the remaining two events and yield new initial shock speeds. The agreement between this multi-process theory and observations is promising for these first quantitative comparisons performed here. Quantitatively, the bulk of the radio emission agrees to within 5 to 10 dB with observations, with the theory typically overpredicting the intensity of bright spots in the dynamic spectra. The methods and analyses presented here show potential for the remote inference of CME-driven shock parameters and the prediction of radio and space weather events.

Type II solar radio bursts: Modeling and extraction of shock parameters

Hillan, D. S.; Cairns, I. H.; Robinson, P. A.

J. Geophys. Res., Vol. 117, No. A3, A03104, **2012, File**

http://dx.doi.org/10.1029/2011JA016754

This first paper in a two part series summarizes the current theory and the data-driven solar wind model for simulating dynamic spectra of type II radio bursts. It also introduces performance metrics and techniques for extraction of model shock parameters from these dynamic spectra. We use an iterative downhill simplex method which compares two dynamic spectra and quantitatively assesses and improves the agreement using two figures of merit: the first is based on the correlation function and the second is based on a normalized differences over the data set. By maximizing the agreement we are able to extract the input model shock parameters to within 30% or better when using model solar winds of increasing complexity. The effects on the spectra predicted and on the figures of merit from changing the model shock parameters and solar wind model are also investigated. The iterative downhill extraction method is then applied to the type II dynamic spectrum predicted using a realistic model solar wind and a shock model estimated for an observed type II event. The shock parameters are recovered to within 10% of the correct solution.

Interplanetary Type IV Bursts

Alexander **Hillaris**, Constantine Bouratzis, Alexander Nindos

Solar Physics Volume 291, Issue 7, pp 2049–2069 **2016**

http://arxiv.org/pdf/1604.07677v1.pdf **File**

In this work we study the characteristics of moving type IV radio bursts which extend to the hectometric wavelengths (interplanetary type IV or type IV IP bursts) and their relationship with energetic phenomena on the Sun. Our dataset comprised 48 Interplanetary type IV bursts observed by the Wind/WAVES in the 13.825 MHz-20 KHz frequency range. The dynamic spec tra of the RSTN, DAM, ARTEMIS-IV, CULGOORA, Hiraiso and IZMIRAN Radio-spectrographs were used to track the evolution of the events in the low corona; these were supplemented with SXR flux recordings from GOES and CME data from LASCO. Positional information for the coronal bursts were obtained by the

Nan\c{c}ay radioheliograph (NRH). We examined the relationship of the type IV events with coronal radio bursts, CMEs and SXR ?ares. The majority of the events (45) were characterized as compact; their duration was on average 106 min. This type of events were, mostly, associated with M and X class flares (40 out of 45) and fast CMEs; 32 of these events had CMEs faster than 1000 Km/s. Furthermore, in 43 compact events the CME was, possibly, subject to reduced aerodynamic drag as it was propagating in the wake of a previous CME. A minority (3) of long lived type IV IP bursts was detected, with durations from 960 min to 115 hours. These events are referred to as extended or long duration events and appeared to replenish their energetic electron content, possibly from electrons escaping from the corresponding coronal type IV bursts. The latter were found to persist on the disk, for tens of hours to days. Prominent among them was the unusual Interplanetary Type IV Burst of **2002 May 18-23** which is the longest event in the Wind/WAVES catalog. The 3 extended events were, usually, accompanied by a number of flares, of GOES class C in their majority, and of CMEs, many of which were slow and narrow. **1998 May 02, 1999 May 27–28, 2003 October 28, 2003 October 29, 2005 January 15, 2005 January 15, 2005, January 17, 2005 January 19, 2005 May 11 , 2005 August 22, 2005 September 09 , 2005 September 13, /2006 December 13 , 2006 December 14 , 22 September 2011 ,24 September 2011 , 2012 January 27, 2012 March 04 , 2012 March 05**

Table A1.: Type IVIP Radio Bursts and Associated Activity (1998-2012, 48 events)

See CESRA **2016**, p.93

http://cesra2016.sciencesconf.org/conference/cesra2016/pages/CESRA2016_prog_abs_book_v3.pdf

The 17 January 2005 Complex Solar Radio Event Associated with Interacting Fast Coronal Mass Ejections

A. **Hillaris**, O. Malandraki, K.-L. Klein, P. Preka-Papadema, X. Moussas, C. Bouratzis, E. Mitsakou, P. Tsitsipis and A. Kontogeorgos

Solar Physics, Volume 273, Number 2, 493-509, **2011**

http://arxiv.org/pdf/1101.5759v7.pdf

On **17 January 2005** two fast coronal mass ejections were recorded in close succession during two distinct episodes of a 3B/X3.8 flare. Both were accompanied by metre-to-kilometre type-III groups tracing energetic electrons that escape into the interplanetary space and by decametre-to-hectometre type-II bursts attributed to CME-driven shock waves. A peculiar type-III burst group was observed below 600 kHz 1.5 hours after the second type-III group. It occurred without any simultaneous activity at higher frequencies, around the time when the two CMEs were expected to interact. We associate this emission with the interaction of the CMEs at heliocentric distances of about 25 $R_\odot$. Near-relativistic electrons observed by the EPAM experiment onboard ACE near 1 AU revealed successive particle releases that can be associated with the two flare/CME events and the low-frequency type-III burst at the time of CME interaction. We compare the pros and cons of shock acceleration and acceleration in the course of magnetic reconnection for the escaping electron beams revealed by the type-III bursts and for the electrons measured in situ.

Solar flares with and without SOHO/LASCO coronal mass ejections and type II shocks

Hillaris, A.; Petousis, V.; Mitsakou, E.; Vassiliou, C.; Moussas, X.; Polygiannakis, J.; Preka-Papadema, P.; Caroubalos, C.; Alissandrakis, C.; Tsitsipis, P.; Kontogeorgos, A.; Bougeret, J.-L.; Dumas, G.

Advances in Space Research, Volume 38, Issue 5, p. 1007-1010, **2006**.

http://arxiv.org/pdf/1009.3636v1.pdf

We analyse of a set of radio rich (accompanied by type IV or II bursts) solar flares and their association with SOHO/LASCO Coronal Mass Ejections in the period 1998 2000. The intensity, impulsiveness and energetics of these events are investigated. We find that, on the average, flares associated both with type IIs and CMEs are more impulsive and more energetic than flares associated with type IIs only (without CME reported), as well as flares accompanied by type IV continua but not type II shocks. From the last two classes, flares with type II bursts (without CMEs reported) are the shortest in duration and the most impulsive.

Radio tracking of the interplanetary coronal mass ejection driven shock crossed by Ulysses on 10 May 2001

Hoang, S.; Lacombe, C.; MacDowall, R. J.; Thejappa, G.

J. Geophys. Res., Vol. 112, No. A9, A09102

We report on the detection of type II radio emission which was observed for more than a day prior to the arrival of an interplanetary shock at Ulysses. We use local spectral emission peaks, computerized from time-averaged intensity spectra of the type II burst, to track the associated emitting shock.

The measured brightness temperature of the type II harmonic emission is found to peak at a value of $\simeq 3 \times 10^{13}$ K just after the shock crossing; just before, the harmonic brightness temperature is $\simeq 10^{12}$ K and the fundamental brightness temperature $\simeq 8 \times 10^{11}$ K.

Favourable Magnetic Field Configurations for Generation of Flare-Associated Meter-Wave Type III Radio Bursts
A. Hofmann · V. Ruždjak
Solar Phys (2007) 240: 107–119
the location of the H-alpha flare in the bipolar pattern turned out to be crucial for the association rate. **It is almost one order of magnitude larger for flares occurring at the border of the active regions**, compared to flares located inside the general bipolar pattern.

Multi-Wavelength Observations of Quasi-Periodic Pulsations in a Solar Flare
Zhenxiang **Hong**, Dong Li, Minghui Zhang, Chengming Tan, Suli Ma & Haisheng Ji
Solar Physics volume 296, Article number: 171 (**2021**)
https://link.springer.com/content/pdf/10.1007/s11207-021-01922-1.pdf
https://doi.org/10.1007/s11207-021-01922-1
We report our analysis of multi-wavelength observations of quasi-periodic pulsations (QPPs) during the impulsive phase of the C6.7 flare on **9 May 2019**. The flare was simultaneously observed by Fermi, the New Vacuum Solar Telescope, the Mingantu Spectral Radioheliograph, the Nobeyama Radio Polarimeters, and the Atmospheric Imaging Assembly (AIA) of the Solar Dynamics Observatory. Three well-pronounced pulsations are detected in full-disk hard X-ray and microwave fluxes, as well as the local light curves at wavelengths of the Hαα line core, AIA 304 Å, 171 Å, 211 Å, and 335 Å between ≈05:43:30 UT and ≈05:48:15 UT. The quasi-periods of about 90 – 110 seconds are determined from their Morlet wavelet power spectra. Meanwhile, a sequence of three groups of Type-III radio bursts is seen in the radio dynamic spectrum during the same time interval. Our observations suggest that the flare QPPs are possibly related to nonthermal electrons accelerated by the intermittent magnetic reconnection during the flare's impulsive phase.

MINIFILAMENT ERUPTION AS THE SOURCE OF A BLOWOUT JET, C-CLASS FLARE, AND TYPE-III RADIO BURST
Junchao **Hong**, Yunchun Jiang, Jiayan Yang, Haidong Li1, and Zhe Xu1
2017 ApJ 835 35
http://sci-hub.cc/doi/10.3847/1538-4357/835/1/35
We report a strong minifilament eruption associated with Geostationary Operational Environmental Satellite C1.6 flare and WIND type-III radio burst. The minifilament, which lies at the periphery of active region 12259, is detected by Hα images from the New Vacuum Solar Telescope. The minifilament undergoes a partial and then a full eruption. Simultaneously, two co-spatial jets are successively observed in extreme ultraviolet images from the Solar Dynamic Observatory. The first jet exhibits a typical fan-spine geometry, suggesting that the co-spatial minifilament is possibly embedded in magnetic fields with a fan-spine structure. However, the second jet displays blowout morphology when the entire minifilament erupts upward, leaving behind a hard X-ray emission source in the base. Differential emission measure analyses show that the eruptive region is heated up to about 4 MK during the fan-spine jet, while up to about 7 MK during the blowout jet. In particular, the blowout jet is accompanied by an interplanetary type-III radio burst observed by WIND/WAVES in the frequency range from above 10 to 0.1 MHz. Hence, the minifilament eruption is correlated with the interplanetary type-III radio burst for the first time. These results not only suggest that coronal jets can result from magnetic reconnection initiated by erupting minifilaments with open fields, but also shed light on the potential influence of minifilament eruption on interplanetary space. **2015 January 14,**

A Type II Radio Burst Driven by a Blowout Jet on the Sun
Zhenyong **Hou**, Hui Tian, Wei Su, Maria S. Madjarska, Hechao Chen, Ruisheng Zheng, Xianyong Bai, Yuanyong Deng
ApJ **953** 171 **2023**
https://arxiv.org/pdf/2306.16725.pdf
https://iopscience.iop.org/article/10.3847/1538-4357/ace31b/pdf
Type II radio bursts are often associated with coronal shocks that are typically driven by coronal mass ejections (CMEs) from the Sun. Here, we conduct a case study of a type II radio burst that is associated with a C4.5 class flare and a blowout jet, but without the presence of a CME. The blowout jet is observed near the solar disk center in the extreme-ultraviolet (EUV) passbands with different characteristic temperatures. Its evolution involves an initial phase and an

ejection phase with a velocity of 560 km/s. Ahead of the jet front, an EUV wave propagates at a projected velocity of 403 km/s in the initial stage. The moving velocity of the source region of the type II radio burst is estimated to be 641 km/s, which corresponds to the shock velocity against the coronal density gradient. The EUV wave and the type II radio burst are closely related to the ejection of the blowout jet, suggesting that both are likely the manifestation of a coronal shock driven by the ejection of the blowout jet. The type II radio burst likely starts lower than those associated with CMEs. The combination of the velocities of the radio burst and the EUV wave yields a modified shock velocity at 757 km/s. The Alfven Mach number is in the range of 1.09-1.18, implying that the shock velocity is 10%-20% larger than the local Alfven velocity. **12 Nov 2022**

Identification and Extraction of Solar Radio Spikes Based on Deep Learning

Y. C. **Hou**, Q. M. Zhang, S. W. Feng, Q. F. Du, C. L. Gao, Y. L. Zhao & Q. Miao
Solar Physics volume 295, Article number: 146 (**2020**)
https://link.springer.com/content/pdf/10.1007/s11207-020-01718-9.pdf
Solar radio spikes are short-duration, narrow-band burst signals, which are a fine structure of solar radio bursts. The processing and analysis of their observed data are of great significance in the study of electron acceleration in the process of solar flares and electron acceleration during the explosion and diagnosis of corona parameters. Deep learning interprets data by mimicking the mechanism of the human brain. Faster Region-based Convolutional Neural Network (Faster R-CNN) is a branch of deep learning based on region nomination, and its classification results have considerable advantages in accuracy. In this paper, Faster R-CNN will be used to identify and extract solar radio spikes. In order to improve the detection ability of small events, a multi-scale detection frame and a multi-layer feature fusion training method are used. The analysis results show that the Average Precision (AP) value of the improved network is close to 91%, which is nearly 10% higher than the original network. So the improved Faster R-CNN method can also be used for the identification and extraction of small-scale fine structures in other fields. **2016 July 18**

Measuring the magnetic field of coronal mass ejections near the Sun using pulsars,
Howard, T.A., K. Stovall, Dowell, J., G. Taylor, and S. White,
Astrophys. J., 831 208, **2016.**
http://sci-hub.cc/10.3847/0004-637X/831/2/208
The utility of Faraday rotation to measure the magnetic field of the solar corona and large-scale transients within is a small, yet growing field in solar physics. This is largely because it has been recognized as a potentially valuable frontier in space weather studies, because the ability to measure the intrinsic magnetic field within coronal mass ejections (CMEs) when they are close to the Sun is of great interest for understanding a key element of space weather. Such measurements have been attempted over the last few decades using radio signals from artificial sources (i.e., spacecraft on the far side of the Sun), but studies involving natural radio sources are scarce in the literature. We report on a preliminary study involving an attempt to detect the Faraday rotation of a CME that passed in front of a pulsar (PSR B0950+08) in 2015 August. We combine radio measurements with those from a broadband visible light coronagraph, to estimate the upper limit of the magnetic field of the CME when it was in the corona. We find agreement between different approaches for obtaining its density, and values that are consistent with those predicted from prior studies of CME density close to the Sun. **2015-08-21**

Sun-to-Earth Characteristics of the 2012 July 12 Coronal Mass Ejection and Associated Geo-effectiveness

Huidong **Hu**, Ying D. Liu, Rui Wang, Christian Möstl, Zhongwei Yang
ApJ **2016**
http://arxiv.org/pdf/1607.06287v1.pdf **File**
We analyze multi-spacecraft observations associated with the 2012 July 12 Coronal Mass Ejection (CME), covering the source region on the Sun from SDO, stereoscopic imaging observations from STEREO, magnetic field characteristics at MESSENGER, and type II radio burst and in situ measurements from Wind. A triangulation method based on STEREO stereoscopic observations is employed to determine the kinematics of the CME, and the outcome is compared with the result derived from the type II radio burst with a solar wind electron density model. A Grad-Shafranov technique is applied to Wind in situ data to reconstruct the flux-rope structure and compare it with the observation of the solar source region, which helps understand the geo-effectiveness associated with the CME structure. Conclusions are as follows: (1) the CME undergoes an impulsive acceleration, a rapid deceleration before reaching MESSENGER, and then a gradual deceleration out to 1 AU, which should be noticed in CME kinematics models; (2) the type II radio burst was probably produced from a high-density interaction region between the CME-driven shock and a nearby streamer or from the shock flank with lower heights, which implies uncertainties in the determination of CME kinematics using solely type II radio bursts; (3) the flux-rope orientation and chirality deduced from in situ reconstruction at Wind agree with those obtained from solar source observations; (4) the prolonged southward magnetic field near the Earth is mainly

from the axial component of the largely southward inclined flux rope, which indicates the importance of predicting both the flux-rope orientation and magnetic field components in geomagnetic activity forecasting.

Clusters of Solar Radio Spikes Modulated by Quasi-Periodic Pulsations in a Confined Flare

Huang, Jing ; Tan, Chengming ; Chen, Xingyao ; Tan, Baolin ; Yan, Yihua ; Zhang, Yin ; Ma, Suli ; Zhou, Zhichao ; Zhang, Minghui ; Wang, Wei ; Chen, Linjie
Universe, vol. 8, issue 7, p. 348, **2022**
https://www.mdpi.com/2218-1997/8/7/348/pdf?version=1656060155
Spikes are typical radio bursts in solar flares, which are proposed to be the signal of energy release in the solar corona. The whole group of spikes always shows different spectral patterns in the dynamic spectrum. Here, we present a special new feature at 0.6–2 GHz in a confined flare. Each group of spikes is composed of many quasi-periodic sub-clusters, which are superposed on the broadband quasi-periodic pulsations (QPPs). The quasi-periodic cluster of spikes (QPSs) have very intense emissions, and each cluster includes tens of individual spikes. When the intensity of background pulsation is increased, the intensity, duration and bandwidth of the spike cluster are also enlarged. There are 21 groups of QPSs throughout the confined flare. The central frequency of the whole group shifts from 1.9 to 1.2 GHz, and the duration of each cluster shows a negative exponential decay pattern. We propose that nonthermal electron beams play a crucial role in emitting both pulsations and spikes. The tearing-mode oscillations of a confined flux rope produce periodic accelerated electron beams. These electron beams travel inside the closed magnetic structure to produce frequency drifting pulsations via plasma emission and scattered narrowband spikes by electron-cyclotron maser emission (ECME). The slow rise of flux rope makes the source region move upward, and thus, QPSs shift towards low frequency. We propose that the confined flux rope may provide the essential conditions for the formation of QPSs. **21 June 2015**

Localized Microwave and EUV Bright Structures in an Eruptive Prominence

Jing **Huang**1, Baolin Tan1, Satoshi Masuda2, Xin Cheng3, Susanta Kumar Bisoi1, and Victor Melnikov1
2019 ApJ 874 176
sci-hub.se/10.3847/1538-4357/ab0e80
We study a solar eruptive prominence with flare/coronal mass ejection (CME) event by microwave and extreme ultraviolet (EUV) observations. Its evolution can be divided into three phases: slow rise, fast expansion, and ejection. In the slow-rise phase, the prominence continuously twists for more than one hour with a patch of bright emission appearing around the top. When the north leg interacts with the local small-size loops, the fast expansion is initiated and the flare takes place there. The prominence grows rapidly, and a series of localized brightenings appear in the whole prominence structure. Then the ejection occurs, followed by a CME. In microwave images, the brightness temperature (T b) at 17 and 34 GHz can be divided into three components. The strongest emission with T b at 25,000–300,000 K is related to the bright flare region near the north foot. The medium T b (10,000–20,000 K) outlines a series of small-scale bright enhancements scattering in the prominence, which are superposed on a weak background with T b at 5000–10,000 K. These localized bright structures, first appearing at the top and then scattering in the entire prominence structure, are cospatial with EUV bright threads, fibers, or spots in both high- and low-temperature passbands. They display significant temporal variations on the scale of 3–5 s in the microwave observations. Thus, the plasma inside the prominence is spatially structured and changes with time in both density and temperature. This behavior could be interpreted in the frame of the small-scale and short-term process of energy releases in the twisted magnetic structure. **2015 May 9**
RHESSI Nuggets #353 June **2019**
http://sprg.ssl.berkeley.edu/~tohban/wiki/index.php/Localized_Microwave_and_EUV_Bright_Structures_in_an_Eruptive_Prominence
CESRA #2291 July **2019** http://www.astro.gla.ac.uk/users/eduard/cesra/?p=2291

QUASI-PERIODIC ACCELERATION OF ELECTRONS IN THE FLARE ON 2012 JULY 19

Jing **Huang**1,2, Eduard P. Kontar3, Valery M. Nakariakov4, and Guannan Gao
2016 ApJ 831 119
Quasi-periodic pulsations (QPPs) of nonthermal emission in an M7.7 class flare on **2012 July 19** are investigated with spatially resolved observations at microwave and HXR bands and with spectral observations at decimetric, metric waves. Microwave emission at 17 GHz of two footpoints, HXR emission at 20–50 keV of the north footpoint and loop top, and type III bursts at 0.7–3 GHz show prominent in-phase oscillations at 270 s. The microwave emission of the loop leg has less pulsation but stronger emission. Through the estimation of plasma density around the loop top from EUV observations, we find that the local plasma frequency would be 1.5 GHz or even higher. Thus, type III bursts at 700 MHz originate above the loop top. Quasi-periodic acceleration or injection of energetic electrons is proposed to dominate these in-phase QPPs of nonthermal emission from footpoints, loop top, and above. In the overlying region, drifting pulsations (DPS) at 200–600 MHz oscillate at a distinct period (200 s). Its global structure drifts toward lower frequency, which is closely related to upward plasmoids observed simultaneously from EUV emission. Hence, nonthermal emission from overlying plasmoids and underlying flaring loops show different oscillating periods. Two

individual systems of quasi-periodic acceleration of electrons are proposed to coincide in the bi-direction outflows from the reconnection region.
See CESRA highlight #1214 Feb **2017** http://www.astro.gla.ac.uk/users/eduard/cesra/?p=1214

Quasi-Periodic Pulsations with Varying Period in Multi-Wavelength Observations of an X-class Flare

Jing **Huang**1, Baolin Tan1, Yin Zhang1, Marian Karlický2, and Hana Mészárosová
2014 ApJ 791 44
This work presents an interesting phenomenon of the period variation in quasi-periodic pulsations (QPPs) observed during the impulsive phase of a coronal mass ejection-related X1.1 class flare on **2012 July 6**. The period of QPPs was changed from 21 s at soft X-rays (SXR) to 22-23 s at microwaves, to ~24 s at extreme ultraviolet emissions (EUV), and to 27-32 s at metric-decimetric waves. The microwave, EUV, and SXR QPPs, emitted from flare loops of different heights, were oscillating in phase. Fast kink mode oscillations were proposed to be the modulation mechanism, which may exist in a wide region in the solar atmosphere from the chromosphere to the upper corona or even to the interplanetary space. Changed parameters of flare loops through the solar atmosphere could result in the varying period of QPPs at different wavelengths. The first appearing microwave QPPs and quasi-periodic metric-decimetric type III bursts were generated by energetic electrons. This may imply that particle acceleration or magnetic reconnection were located between these two non-thermal emission sources. Thermal QPPs (in SXR and EUV emissions) occurred later than the nonthermal ones, which would suggest a some time for plasma heating or energy dissipation in flare loops during burst processes. At the beginning of flare, a sudden collapse and expansion of two separated flare loop structures occurred simultaneously with the multi-wavelength QPPs. An implosion in the corona, including both collapse and expansion of flare loops, could be a trigger of loop oscillations in a very large region in the solar atmosphere.

Energetic Electron Propagation in the Decay Phase of Non-thermal Flare Emission

Jing **Huang**1, Yihua Yan1, and Yuri T. Tsap
2014 ApJ 787 123
On the basis of the trap-plus-precipitation model, the peculiarities of non-thermal emission in the decay phase of solar flares have been considered. The calculation formulas for the escape rate of trapped electrons into the loss cone in terms of time profiles of hard X-ray (HXR) and microwave (MW) emission have been obtained. It has been found that the evolution of the spectral indices of non-thermal emission depend on the regimes of the pitch angle diffusion of trapped particles into the loss cone. The properties of non-thermal electrons related to the HXR and MW emission of the solar flare on **2004 November 3** are studied with Nobeyama Radioheliograph, Nobeyama Radio Polarimeters, RHESSI, and Geostationary Operational Environmental Satellite observations. The spectral indices of non-thermal electrons related to MW and HXR emission remained constant or decreased, while the MW escape rate as distinguished from that of the HXRs increased. This may be associated with different diffusion regimes of trapped electrons into the loss cone. New arguments in favor of an important role of the superstrong diffusion for high-energy electrons in flare coronal loops have been obtained.

Microwave Bursts with Fine Structures in the Decay Phase of a Solar Flare

Huang, J. and Tan, B.L.
E-print, Nov 2011**, 2012 ApJ 745 186**
This paper presents the microwave bursts with fine structures (FSs) at 1.10-1.34 GHz in the decay phase of a solar flare observed by the Chinese Solar Broadband Radio Spectrometer in Huairou, which show a peak-to-peak correlation with 25-50 keV hard X-ray (HXR) bursts observed by RHESSI. In the microwave spectra, we have identified stripe-like bursts such as lace bursts, fiber structures, zebra patterns (ZPs), and quasi-periodic pulsations. We also have detected short narrowband bursts such as dots, type III, and spikes. The lace bursts had rarely been reported, but in this event they are observed to occur frequently in the decay phase of the flare. The similarity between 25 and 50 keV HXR light curve and microwave time profiles at 1.10-1.34 GHz suggests that these microwave FSs are related to the properties of electron acceleration. The electron velocity inferred from the frequency drift rates in short narrowband bursts is in the range of 0.13c-0.53c and the corresponding energy is about 10-85 keV, which is close to the energy of HXR-emitting electrons. From the Alfvén soliton model of fiber structures, the double plasma resonance model of ZPs, and the Bernstein model of the lace bursts, we derived a similar magnetic field strength in the range of 60-70 G. Additionally, the physical conditions of the source regions such as height, width, and velocity are estimated.

CO-ANALYSIS OF SOLAR MICROWAVE AND HARD X-RAY SPECTRAL EVOLUTIONS. II. IN THREE SOURCES OF A FLARING LOOP

Guangli **Huang** and Jianping Li

2011 ApJ 740 46

Based on the spatially resolvable data of the Reuven Ramaty High Energy Solar Spectroscopic Imager (RHESSI) and Nobeyama Radio Heliograph (NoRH), co-analysis of solar hard X-ray and microwave spectral evolution is performed in three separate sources located in one looptop (LT) and two footpoints (FPs) of a huge flaring loop in the **2003 October 24** flare. The RHESSI image spectral evolution in 10-100 keV is always fitted by the well-known soft-hard-soft (SHS) pattern in the three sources. When the total energy is divided into four intervals similar to the Yohkoh/Hard X-ray Telescope, i.e., 12.5-32.5 keV, 32.5-52.5 keV, 52.5-72.5 keV, and 72.5-97.5 keV, the SHS pattern in lower energies is converted gradually to the hard-soft-hard (HSH) pattern in higher energies in all three sources. However, the break energy in the LT and the northeast FP (~32.5 keV) is evidently smaller than that in the southwest FP (~72.5 keV). Regarding microwave spectral evolution of the NoRH data, the well-known soft-hard-harder pattern appeared in the southwest FP, while the HSH pattern coexisted in the LT and the northeast FP. The different features of the hard X-ray and microwave spectral evolutions in the three sources may be explained by the loop-loop interaction with another huge loop in the LT and with a compact loop in the northeast FP, where the trapping effect is much stronger than that in the southwest FP. The comparison between the LT and FP spectral indices suggests that the radiation mechanism of X-rays may be quite different in different energy intervals and sources. The calculated electron spectral indices from the predicted mechanisms of X-rays gradually become closer to those from the microwave data with increasing X-ray energies.

INITIATION AND EARLY DEVELOPMENT OF THE 2008 APRIL 26 CORONAL MASS EJECTION

J. **Huang**1,2, P. D´emoulin2, M. Pick2, F. Auch`ere3, Y. H. Yan1, and A. Bouteille2

Astrophysical Journal, 729:107 (10pp), **2011, File**

We present a detailed study of a coronal mass ejection (CME) with high temporal cadence observations in radio and extreme-ultraviolet (EUV). The radio observations combine imaging of the low corona with radio spectra in the outer corona and interplanetary space. The EUV observations combine the three points of view of the *STEREO* and *SOHO* spacecraft. The beginning of the CME initiation phase is characterized by emissions that are signatures of the reconnection of the outer part of the erupting configuration with surrounding magnetic fields. Later on, a main source of emission is located in the core of the active region. It is an indirect signature of the magnetic reconnection occurring behind the erupting flux rope. Energetic particles are also injected in the flux rope and the corresponding radio sources are detected. Other radio sources, located in front of the EUV bright front, trace the interaction of the flux rope with the surrounding fields. Hence, the observed radio sources enable us to detect the main physical steps of the CME launch. We find that imaging radio emissions in the metric range permits us to trace the extent and orientation of the flux rope which is later detected in interplanetary space. Moreover, combining the radio images at various frequencies with fast EUV imaging permits us to characterize in space and time the processes involved in the CME launch.

Statistics of Flaring Loops Observed by the Nobeyama Radioheliograph. III. Asymmetry of Two Footpoint Emissions

Guangli **Huang**, Qiwu Song and Yu Huang

2010 ApJ 723 1806-1816

Two footpoint (FP) emissions are compared in a total of 24 events with loop-like structures imaged by the Nobeyama Radioheliograph (NoRH), which are divided into two groups: when the optically thin radio spectrum in the looptop is harder than those in the two FPs (group 1) and when it is softer than those in at least one FP (group 2). There are always correlative variations of the brightness temperatures and polarization degrees, the spectral indices, the column densities of nonthermal electrons, and magnetic field strengths in the two FPs. The maximum differences of these parameters in the two FPs may reach one or two orders of magnitude (except the polarization degree). The logarithm of the ratio of the magnetic field strengths in the two FPs is always anti-correlated with the logarithms of the ratios of the brightness temperatures in the two FPs, but correlated with the differences of the spectral indices in the two FPs. Only two anti-correlations exist in group 1, between the difference of the absolute polarization degrees in the two FPs and the logarithm of the ratio of the brightness temperatures in the two FPs and between the difference of the spectral indices in the two FPs and the logarithm of the ratio of the column densities of nonthermal electrons in the two FPs. Only two positive correlations appear in group 1, between the difference of the absolute polarization degrees in the two FPs and the relative ratio of magnetic field strengths in the two FPs and between the logarithm of the ratio of the column densities of nonthermal electrons in the two FPs and the logarithm of the ratio of the brightness temperatures in the two

FPs. These four statistics in group 2 are just opposite to those in group 1, which may be directly explained by gyrosynchrotron theory. Moreover, the asymmetry of the two FP emissions in group 2 is more evident than that in group 1, which may be explained by two kinds of flare models, respectively, in the two groups of events, i.e., the energy release above a single loop (group 1) and in the coalescence of two flaring loops (group 2). The asymmetry of the two FP emissions cannot simply be explained by the mirroring effect, but it may strongly depend on the asymmetry of the initial pitch angles of nonthermal electrons in the two FPs. The normal or abnormal events are defined as whether a stronger emission corresponds to a stronger or weaker polarization in the two FPs, with a comparable proportion of the normal and abnormal events in the two groups.

The statistical features of radio bursts with fine structure at 1.1–7.6 GHz

Jing **Huang**, a, , Yihua Yana, and Yuying Liu

Advances in Space Research, Volume 46, Issue 11, 1 December **2010**, Pages 1388-1393

This work presents the spectral and temporal features of radio bursts with fine structures (FSs) at broad band from 1.1 to 7.6 GHz. Fifteen burst events are studied with high frequency and temporal cadence observation from the Solar Broadband Radio Spectrometer at three frequency bands. It is found that the amount and species of radio FS decrease with increasing frequency band; the pulsation, type III burst and continuum are most frequently recorded; almost in all the burst events, more radio FSs occur before the soft X-ray (SXR) maximum than after; at 1.1–2.06 GHz, all types of radio FSs have more before the SXR peak except fiber; at 2.6–3.8 GHz, pulsation, fiber and spike prefer to appear after the peak; the separation between neighboring emission lines of zebra pattern increases with increasing frequency and the magnetic field deduced from the whistler model is 29–86 G at 1.1–2.06 GHz and 89–268 G at 2.6–3.8 GHz.

Frequency Dependence of the Relation Between Repetition Rate and Burst Flux in Solar Radio Pulsations

G.L. **Huang** ·Q.W. Song

Solar Phys (**2010**) 264: 345–351

The frequency dependence of the quasi-quantized energy release is reported for the first time in 14 bursts with pulsations of seconds at 1.0, 2.0, 3.75, 9.4, 17, and 35 GHz, observed by the Nobeyama Radio Polarimeters (NoRP). There is a linear correlation between the repetition rate of pulsations and the radio flux during the burst, the so-called $R - S$ relation, at each burst frequency. The slope in the linear fitting, which is equivalent to the energy release in an individual pulse, becomes maximum at a particular frequency around 10 GHz, which can be explained by electrons accelerated in solar flares with maximum energy density around this frequency or coronal height.

ANALYSIS OF KINETIC PROCESS OF ENERGETIC ELECTRON DURING A FLARE ON 2004 DECEMBER 1

Jing Huang1,2 and Yihua Yan1

ApJ 705 1063-1072, **2009**

We analyze the M1.1 flare event peaked at 07:20:00 UT on 2004 December 1 mainly from radio and hard X-ray (HXR) observations. By eliminating the thermal component from the observed total radio emission flux, the non-thermal part of the radio and HXR burst process is investigated in a self-consistent way. The spectral index of energetic electrons deduced from the radio burst evolves as a Soft-Hard-Hard pattern and that from HXR as a Soft-Hard-Soft pattern corresponding to an initial-main-decay phase. The trap-plus-precipitation model is applied in the kinetic process of energetic electrons for this flare event. The radio fluxes at six frequencies selected from the 2.6-7.6 GHz range are fitted with a gyrosynchrotron radiation mechanism. It is found that a linearly increasing electron escape rate can best fit to the observed radio fluxes from 07:00:00 UT to 07:40:00 UT and the slope of the electron escape rate for the six selected frequencies decreases with increasing frequency. During the decay phase from 07:15:00 UT to 07:20:00 UT, the hardened spectrum of the radio burst may be due to the increasing amount of trapped electrons with higher energy by a lower escape rate. Meanwhile, the increasing amount of precipitating electrons with a lower energy band may soften the HXR spectrum. In the decay phase after 07:20:00 UT, thermal emission is the dominating component for the radio burst.

Study of backward propagating and second harmonic Langmuir waves by 2D particle-in-cell simulation

Y. **Huang**1, 2 and G. L. Huang1
A&A 503, 207-211 (**2009**)
Context. Backward propagating and second harmonic Langmuir waves (LWs) play an important role in the second harmonic emission of solar radio type III bursts and they are numerically studied in detail with a new method.
Aims. We paid particular attention to the excitation mechanism of the backward propagating LWs, as well as the second harmonic LWs with two-dimensional (2D) particle-in-cell (PIC) simulations.
Methods. We performed simulations with two different types of initial conditions, i.e., the beam-exited and the wave-excited cases. In the second case, the beam-excited LWs were considered to represent the free energy instead of the beam itself.
Results. It is firstly found that the backward propagating LWs are suppressed by about 20% by the beam electrons. Hence, the beam electrons just have a negative contribution to the backward LWs, which can be explained in a preliminary way by the Landau damping of the beam electrons. On the other hand, the second harmonic LWs are contributed mainly (about 80%) by the beam electrons, only 20% originating from beam-excited forward LWs, which is quite different from earlier results.
Conclusions. Therefore, we found that the backward propagating LWs can't be amplified directly by the electron beam, and we must assume that they are generated by the beam-excited forward LWs scattered by ion sound waves. The direct amplification of beam-plasma instability may play an important role in producing the second harmonic LWs.

Diagnostics of the Low-Cutoff Energy of Nonthermal Electrons in Solar Microwave and Hard X-Ray Bursts

Guangli **Huang**
Solar Phys. 257(2), Page: 323 – 334, **2009**
The low-cutoff energy has a strong effect on the relationship between the radiation and electron spectral indices in both nonthermal gyrosynchrotron and bremsstrahlung theories. Hence, we have to calculate or fit the low-cutoff energy together with the electron spectral index as two independent parameters. Theoretical calculations of nonthermal gyrosynchrotron and bremsstrahlung radiations suggest a new method to obtain the exact solutions of the low-cutoff energy and the electron spectral index from the observable photon spectral indices at two adjacent energy or frequency bands (double power law). One flare on **10 June 2000** was studied as an example of the hard X-ray and microwave diagnostics for the low-cutoff energy and the electron spectral index. The results showed some differences between hard X-ray and microwave diagnostics.

STATISTICS OF FLARING LOOPS OBSERVED BY NOBEYAMA RADIOHELIOGRAPH. II. SPECTRAL EVOLUTION

Guangli **Huang**1 and Hiroshi Nakajima2
ApJ 702 19-26, **2009** doi: 10.1088/0004-637X/702/1/19
The spectral evolution of solar microwave bursts is studied in 10 impulsive events with loop-like structures, which are selected in the flare list of Nobeyama Radioheliograph. Most events have a brighter and harder looptop (LT) with maximum time later than at least one of its two footpoints (FPs), and have a common feature of the spectral evolution in the LT and the two FPs. There are five simple impulsive bursts with a well known pattern of soft-hard-soft or soft-hard-harder (SHH). It is first found that the other five events have multiple subpeaks in their impulsive phase, and mostly have a new feature of hard-soft-hard (HSH) in each subpeak, but, the well known tendency of SHH is still maintained in the total spectral evolution of these events. All of these features in the spectral evolution of the 10 selected events are consistent with the full Sun observations of Nobeyama Radio Polarimeters in these events. The new feature of HSH may be explained by the thermal free-free emission before, during, and after these bursts, together with multiple injections of nonthermal electrons, while the SHH pattern in the total duration may be directly caused by the trapping effect.

STATISTICAL ANALYSIS OF FLARING LOOPS OBSERVED BY NOBEYAMA RADIOHELIOGRAPH. I. COMPARISON OF LOOPTOP AND FOOTPOINTS

Guangli **Huang**1 and Hiroshi Nakajima2
Astrophysical Journal, 696:136–142, **2009**
http://www.iop.org/EJ/toc/-alert=43190/0004-637X/696/1
Twenty-four events with looplike structures at 17 and 34 GHz are selected from the flare list of Nobeyama Radioheliograph. We obtained the brightness temperatures at 17 and 34 GHz, the polarization degrees at 17 GHz, and the power-law spectral indices at the radio peak time for one looptop (LT) and two footpoints (FPs) of each event. We also calculated the magnetic field strengths and the column depths of nonthermal electrons in the LT and FPs of each event, using the equations modified from the gyrosynchrotron equations by Dulk. The main statistical results from those data are summarized as follows. (1) The spectral indices, the brightness temperatures at 17 and 34 GHz, the polarization degrees at 17 GHz, the calculated magnetic field strengths, and

the calculated column densities of nonthermal electrons are always positively correlated between the LT and the two FPs of the selected events. (2) About one-half of the events have the brightest LT at 17 and 34 GHz. (3) The spectral indices in the two FPs are larger (softer) than those in the corresponding LT in most events. (4) The calculated magnetic field strengths in the two FPs are always larger than those in the corresponding LT. (5) Most of the events have the same positive or negative polarization sense in the LT and the two FPs. (6) The brightness temperatures at 17 and 34 GHz in each of the LT and the two FPs statistically decrease with their spectral indices and the calculated magnetic field strengths, but increase with their calculated column densities of nonthermal electrons. Moreover, we try to discuss the possible causes of the present statistical results.

A Study of Solar Radio Bursts with Fine Structures during Flare/CME Events

J. **Huan**g · Y.H. Yan · Y.Y. Liu
Solar Phys (**2008**) 253: 143–160
We have selected 27 solar microwave burst events recorded by the Solar Broadband Radio Spectrometer (SBRS) of China, which were accompanied by M/X class flares and fast CMEs. A total of 70.4% of radio burst events peak at 2.84 GHz before the peaks of the related flares' soft X-ray flux with an average time difference of about 6.7 minutes. Almost all of the CMEs start before or around the radio burst peaks. At 2.6 – 3.8 GHz bandwidth, 234 radio fine structures (FSs) were classified. More often, some FSs appear in groups, which can contain several individual bursts. It is found that many more radio FSs occur before the soft X-ray maxima and even before the peaks of radio bursts at 2.84 GHz. The events with high peak flux at 2.84 GHz have many more radio FSs and the durations of the radio bursts are independent of the number of radio FSs. Parameters are given for zebra patterns, type III bursts, and fiber structures, and the other types of FSs are described briefly. These radio FSs include some special types of FSs such as double type U bursts andW-type bursts.

Study of backward propagating Langmuir waves with PIC simulation

Huang Yu and Huang Guangli
Advances in Space Research , Volume 41, Issue 8, **2008**, Pages 1202-1205
The conversion of Langmuir waves into electromagnetic radiations is an important mechanism of solar type *III* bursts. Langmuir waves can be easily excited by electron beam instability, and they can be converted into backward propagating Langmuir waves by wave–wave interaction. Generally, the backward propagating Langmuir waves are very important for the second harmonic emission of solar type *III* bursts. In this work, we pay particular attention to the mechanism of the backward propagating Langmuir waves by particle in cell (PIC) simulations. It is confirmed that the ions play a key role in exiting the backward propagating Langmuir waves. Moreover, the electron beam can hardly generated the backward propagating Langmuir waves directly, but may directly amplify the second harmonic Langmuir waves.

Diagnosis of coronal magnetic field and nonthermal electrons from Nobeyama observations of a simple flare

G.L. **Huang**
Advances in Space Research , Volume 41, Issue 8, Pages *1191-1194* (2008)
Coronal magnetic field and nonthermal electrons are very important parameters for understanding of the global heliophysical processes. A flare on **November 1, 2004** is selected for self-consistent calculations of coronal magnetic field parallel and perpendicular to the line-of-sight, and density of nonthermal electrons from Nobeyama observations. Both of the diagnosis methods and results are discussed in this paper.

The Radio Signature of Magnetic Reconnection for the M-Class Flare of 2004 November 1

Guangli **Huang**, Haisheng Ji, and Guiping Wu
The Astrophysical Journal Letters, Vol. 672, No. 2: L131-L134.
http://www.journals.uchicago.edu/doi/abs/10.1086/527294
The main finding is that the magnitude of the transverse magnetic field summed around the magnetic neutral line of the *SOHO* MDI magnetogram has a short-term impulsive increase during the rising phase of the flare. We propose that the increase of the transverse magnetic field may be considered evidence of the magnetic reconnection process in this flare. The computed mean angle between the magnetic field and line of sight decreases steadily during the flare, clearly

indicating the reconfiguration of the magnetic field, presumably the relaxation of the sheared magnetic field. Moreover, the calculated density of nonthermal electrons increases from footpoints to looptop, while the spectral index calculated by the Nobeyama Radio Heliograph at 17 and 34 GHz decreases from footpoints (soft) to looptop (hard), which may confirm that the reconnection site is close to the looptop source.

Simultaneous observations of second and sub-second time structures in H α , radio and hard X-ray data due to the periodical particle acceleration and MHD waves in the November 1, 2004 flare

Huang Guangli and Ji Haisheng
Astrophysics and Space Science, Volume 312, Numbers 1-2, 127-138, 2007.
http://www.springerlink.com/content/u512lw1tp0160813/fulltext.pdf

Search for a Flare Anticipation Index (FAI)

Hugh **HUDSON**, Jim McTIERNAN
RHESSI Science Nuggets #460 **2023**
https://sprg.ssl.berkeley.edu/~tohban/wiki/index.php/Search_for_a_Flare_Anticipation_Index_(FAI)
To quantify the microwave and soft X-ray signatures of flare precursor activity, we have devised "flare anticipation indices" for soft X-ray and microwave data with some success. This clearly establishes the possibility of a joint FAI development, using both of these but also others of the signatures listed above, to establish a robust (and infallible?) few-minute FAI capability. Now some hard work is necessary to refine and improve on these findings. Also, it should go without saying, we need to figure out how these various precursors relate physically to their flares... it is certainly not simply "preheating," as we perhaps used to think. **4 Sep 2017**

A slow HOPE with microwave context

H. **Hudson**
RHESSI Science Nuggets #441 Feb **2023**
https://sprg.ssl.berkeley.edu/~tohban/wiki/index.php/A_slow_HOPE_with_microwave_context
A new microwave facility at Chashan Observatory, and a prototypical Hot Onset Precursor Event.
2022-04-20

The Post-Burst Increase

Hugh **Hudson**
RHESSI Nugget, No. 208, Sept **2013**
http://sprg.ssl.berkeley.edu/~tohban/wiki/index.php/The_Post-Burst_Increase
Here we discuss the microwave bursts classified as "Post-Burst Increase" (PBI) and "Gradual Rise and Fall". This relationship between microwave thermal signatures and those at other wavelengths has not been tested quantitatively for decades, but the hard X-ray, EUV, UV, optical, and radio data have vastly improved now. This Nugget re-introduces this topic, following in the footsteps of Negative Microwave Bursts. There is a great deal to be learned about several aspects of flare physics from such comparisons.

"Impulse Response Flares" and Gamma Rays

Hugh **Hudson** and Stephen White
RHESSI Nugget, No. 188, Nov **2012**
We've speculated in this Nugget that we can identify two distinct radiation signatures with the same process: the prompt acceleration of primary protons to energies above 100 MeV in regions of intense magnetic fields. The impulse-response time profile of this process may reveal a somewhat different paradigm for flare energetics, one that has a characteristic temporal signature on a time scale of about 20 s. If this is so, we may expect to see more such events with Fermi and at even shorter radio wavelengths with the new ALMA facility. RHESSI may also have signatures of this process that have not yet been disentangled from other features it detects at its highest energies.
mm-wave radio observations recorded at 86 GHz at the Hat Creek Observatory SOL2010-06-12

First Solar Radio Burst Observations by the Mexican Array Radio Telescope (MEXART) at 140 MHz

E. **Huipe-Domratcheva**, V. De la Luz, G. A. Casillas-Perez, J. C. Mejia-Ambriz, E. Perez-Leon, J. A. Gonzalez-Esparza, C. Monstein & W. Reeve
Solar Physics volume 297, Article number: 9 (**2022**)
https://link.springer.com/content/pdf/10.1007/s11207-021-01916-z.pdf
The National Laboratory of Space Weather in Mexico (Laboratorio Nacional de Clima Espacial: LANCE) coordinates instrumentation for monitoring the space-weather impact over Mexico. Two of these instruments are the Mexican Array

Radio Telescope (MEXART) and Compound Astronomical Low frequency Low cost Instrument for Spectroscopy and Transportable Observatory (CALLISTO) station of the e-CALLISTO network (CALLMEX). Both instruments are located at the same facility (Coeneo Michoacan, Mexico) and share a spectral band centered at 140 MHz. In this work, we show the capabilities of the e-CALLISTO network as support to identify a solar radio burst in the signal of the MEXART radiotelescope. We identified 75 solar radio bursts in the MEXART signal: five events of Type II and 70 of Type III between September 2015 and May 2019. The analysis of solar radio bursts in the MEXART signal provides us valuable information about the development of the radio event due to their high sensitivity, time resolution, and isotropic response. In the case of Type-III solar radio events, we identify four characteristic phases in the dynamical evolution of the signal at 140 MHz: a pre-phase, a main peak, a decay phase, and a post-event phase. A Morlet wave transform was done of MEXART signals in the Type-III solar radio busts; in their spectra, a pine tree structure was identified preceding the main event in the time series. These characteristics are not observable in the data from the e-CALLISTO network. **2015-09-29, 2016-05-04, 2016-05-26, 2016-07-10, 2017-08-18, 2017-09-04, 06, 07; 2019-05-06**

Burst locating capability of the Korean Solar Radio Burst Locator (KSRBL)

J-E **Hwangbo**, Su-Chan Bong, Show all 7 authors, Young-Deuk Park
Journal of Astronomy and Space Science 32(1):91-99, **2015**
https://www.researchgate.net/publication/275227108_Burst_locating_capability_of_the_Korean_Solar_Radio_Burst_Locator_KSRBL
The Korean Solar Radio Burst Locator (KSRBL) is a solar radio spectrograph observing the broad frequency range from 0.245 to 18 GHz with the capability of locating wideband gyrosynchrotron bursts. Due to the characteristics of a spiral feed, the beam center varies in a spiral pattern with frequency, making a modulation pattern over the wideband spectrum. After a calibration process, we obtained dynamic spectra consistent with the Nobeyama Radio Polarimeter (NoRP). We compared and analyzed the locations of bursts observed by KSRBL with results from the Nobeyama Radioheliograph (NoRH) and Atmospheric Imaging Assembly (AIA). As a result, we found that the KSRBL provides the ability to locate flaring sources on the Sun within around 2′. **15-Feb-2011, 24-Feb-2011, 7 June 2011, 04-Aug-2011, 09-Aug-2011**

Magnetic Structure and Nonthermal Electrons in the X6.9 Flare on 2011 August 9

Jung-Eun **Hwangbo**, Jeongwoo Lee, Sung-Hong Park, Sujin Kim, Dae-Young Lee, Su-Chan Bong, Yeon-Han Kim, Kyung-Suk Cho, and Young-Deuk Park
ApJ, 796 80, **2014**
The **2011 August 9** flare is one of the largest X-ray flares of sunspot cycle 24, but spatial information is rather limited due to its position close to the western limb. This paper presents information about the location of high-energy electrons derived from hard X-ray and microwave spectra obtained with the Reuven Ramaty High-Energy Solar Spectroscopic Imager (RHESSI) and the **Korean Solar Radio Burst Locator (KSRBL),** respectively. The KSRBL microwave spectrum shows significant fluxes at low frequencies, implying that the high-energy electrons reside in a coronal volume highly concentrated at strong magnetic fields, and rapidly expanding with decreasing magnetic fields. After a simple modeling of the microwave spectrum, we found that the microwave source should be located above the inner pair of magnetic poles in a large quadrupolar configuration. The time-dependent evolution of the magnetic field distribution and total nonthermal energy derived from the microwave spectra is also consistent with the standard picture of multiple magnetic reconnections recurring at a magnetic null point that forms above the magnetic quadrupoles and moves up with time.

Comparison Between Radio Loud and Radio Quiet Fast CMEs: A Reason for Radio Quietness

M. Syed **Ibrahim**, E. Ebenezer & A. Shanmugaraju
Solar Physics volume 298, Article number: 59 (**2023**)
https://doi.org/10.1007/s11207-023-02151-4
It is well known that fast CMEs are mostly associated with magnetohydrodynamic (MHD) shocks in the solar corona, forming type-II radio bursts. However, the absence of type-II radio bursts is not uncommon. Herein, we aim to analyze the differences between the radio loud (RL) and radio quiet (RQ) fast Coronal Mass Ejections (CMEs) (speed ≥ 900 km s−1) during Solar Cycle 24 (2008 – 2021). From the 309 fast CMEs, we could identify 143 events with a known source origin on the visible disk (Earth view). We identified the associated flares/CMEs for 143 events using running-difference images from (i) Solar Dynamic Observatory/Atmospheric Imaging Assembly (SDO/AIA) and (ii) Large Angle Spectrometric Coronagraph (LASCO) observations. Among these 143 events, RQ and RL groups have 70 and 73 events, respectively. CALLISTO and Wind/WAVES observations are used to identify these RL and RQ sets. We analyzed the possibilities of streamer-CME and CME-CME interaction. In this study, we report the important differences between RL and RQ CMEs and the underlying reasons for the radio quietness of fast CMEs. In the LASCO

field of view, the majority of RL CMEs (almost 90%) interacted with streamers and/or pre-CMEs, whereas only 25% of RQ CMEs did the same, and there was no pre-CME interaction. The observational evidence led to the conclusion that substantial density perturbation/interaction increases the probability of production of type-II radio emissions by the shock of RL CMEs.

Constraining the amplitude of turbulence in solar corona using observations of angular broadening of radio sources

Madhusudan **Ingale**, Prasad Subramanian, Iver H. Cairns
2014, Bull. Astr. Soc. India (**2013**)
http://arxiv.org/pdf/1406.5326v1.pdf
The angular broadening of compact radio sources observed through a medium having turbulent density irregularities is usually estimated using the phase structure function. We employ an exact formulation for the phase structure function that helps in obtaining an accurate estimate of angular broadening when the baseline lengths are comparable to the inner scale of the turbulent spectrum.

Quasi-periodic pulsations in solar and stellar flares: re-evaluating their nature in the context of power-law flare Fourier spectra

A. R. **Inglis**, J. Ireland, M. Dominique
ApJ, **2014**
http://arxiv.org/pdf/1410.8162v1.pdf
The nature of quasi-periodic pulsations in solar and stellar flares remains debated. Recent work has shown that power-law-like Fourier power spectra, also referred to as 'red' noise processes, are an intrinsic property of solar and stellar flare signals, a property that many previous studies of this phenomenon have not accounted for. Hence a re-evaluation of the existing interpretations and assumptions regarding QPP is needed. Here we adopt a Bayesian method for investigating this phenomenon, fully considering the Fourier power law properties of flare signals. Using data from the PROBA2/LYRA, Fermi/GBM, Nobeyama Radioheliograph and Yohkoh/HXT instruments, we study a selection of flares from the literature identified as QPP events. Additionally we examine optical data from a recent stellar flare that appears to exhibit oscillatory properties. We find that, for all but one event tested, an explicit oscillation is not required in order to explain the observations. Instead, the flare signals are adequately described as a manifestation of a power law in the Fourier power spectrum, rather than a direct signature of oscillating components or structures. However, for the flare of **1998 May 8**, strong evidence for the existence of an explicit oscillation with P ~ 14-16 s is found in the 17 GHz radio data and the 13-23 keV Yohkoh HXT data. We conclude that, most likely, many previously analysed events in the literature may be similarly described in terms of power laws in the flare Fourier power spectrum, without the need to invoke a narrowband, oscillatory component. As a result the prevalence of oscillatory signatures in solar and stellar flares may be less than previously believed. The physical mechanism behind the appearance of the observed power laws is discussed.

Multi-wavelength spatially resolved analysis of quasi-periodic pulsations in a solar flare:

A. R. **Inglis**, V. M. Nakariakov and V. F. Melnikov
A&A 487 (**2008**) 1147-1153
http://www.aanda.org/10.1051/0004-6361:20079323
Aims. We aim to perform a spatially resolved analysis of a quasi-periodic pulsation event from 8th May 1998 using microwave data from the Nobeyama Radioheliograph and Radiopolarimeter, and X-ray data from the Yohkoh satellite.
Methods. Time spectra of the signals integrated over the emission source are constructed with the use of the Lomb-Scargle periodogram method, revealing the presence of a pronounced 16 s periodicity. The Pixon image reconstruction algorithm and Hanaoka algorithm are used to reconstruct images from the hard X-ray data from Yohkoh/HXT and Nobeyama Radioheliograph respectively. The phase relationship of the microwave emission was analysed with the use of cross-correlation techniques.
Results. The flaring loop was resolved in the microwave band. The hard X-ray sources are found to be located near the footpoint and at the loop apex determined by the soft X-ray image. The apex source is much fainter than footpoint one. In microwave, all parts of the loop are seen to oscillate with the same period and almost in phase. It was not possible to determine the spatial structure of the oscillation in the hard X-ray band. The period and the coherent spatial structure of the oscillation are indicative of the presence of either an MHD sausage mode or a periodic regime of magnetic reconnection.

Observations of solar X-ray and EUV jets and their related phenomena **Review**

Davina **Innes**, Radoslav Bucik, Li-Jia Guo, Nariaka Nitte
Astronomische Nachrichten **2016**

http://arxiv.org/pdf/1603.03258v1.pdf
Solar jets are fast-moving, elongated brightenings related to ejections seen in both images and spectra on all scales from barely visible chromospheric jets to coronal jets extending up to a few solar radii. The largest, most powerful jets are the source of type III radio bursts, energetic electrons and ions with greatly enhanced 3He and heavy element abundances. The frequent coronal jets from polar and equatorial coronal holes may contribute to the solar wind. The primary acceleration mechanism for all jets is believed to be release of magnetic stress via reconnection; however the energy buildup depends on the jets' source environment. In this review, we discuss how certain features of X-ray and EUV jets, such as their repetition rate and association with radio emission, depends on their underlying photospheric field configurations (active regions, polar and equatorial coronal holes, and quiet Sun). **3 Aug 2010, 2012 July 02, 2014 May 16**

EUV jets, type III radio bursts and sunspot waves investigated using SDO/AIA observations

D.E. **Innes**, R.H. Cameron, S.K. Solanki
E-print, June **2011, File**; A&A Letters
Images from the Solar Dynamics Observatory (SDO) at 211A are used to identify the solar source of the type III radio bursts seen in WIND/WAVES dynamic spectra. We analyse a 2.5 hour period during which six strong bursts are seen. The radio bursts correlate very well with the EUV jets coming from the western side of a sunspot in AR11092. The EUV jet emission also correlates well with brightening at what looks like their footpoint at the edge of the umbra. For 10-15 min after strong EUV jets are ejected, the footpoint brightens at roughly 3 min intervals. In both the EUV images and the extracted light curves, it looks as though the brightening is related to the 3-min sunspot oscillations, although the correlation coefficient is rather low. The only open field near the jets is rooted in the sunspot. We conclude that active region EUV/X-ray jets and interplanetary electron streams originate on the edge of the sunspot umbra. They form along a current sheet between the sunspot open field and closed field connecting to underlying satellite flux. Sunspot running penumbral waves cause roughly 3-min jet footpoint brightening. The relationship between the waves and jets is less clear.

EUV jets, type III radio bursts and sunspot waves investigated using SDO/AIA observations

D. E. **Innes**, R. H. Cameron and S. K. Solanki
E-print, June **2011**; A&A 531, L13 (**2011**) **, File**
Context. Quasi-periodic plasma jets are often ejected from the Sun into interplanetary space. The commonly observed signatures are day-long sequences of type III radio bursts.
Aims. The aim is to identify the source of quasi-periodic jets observed on **3 Aug. 2010** in the Sun's corona and in interplanetary space.
Methods. Images from the Solar Dynamics Observatory (SDO) at 211 Å are used to identify the solar source of the type III radio bursts seen in WIND/WAVES dynamic spectra. We analyse a 2.5 h period during which six strong bursts are seen. The radio signals are cross-correlated with emission from extreme ultraviolet (EUV) jets coming from the western side of a sunspot in AR 11092. The jets are further cross-correlated with brightening at a small site on the edge of the sunspot umbra, and the brightening with 3-min sunspot intensity oscillations.
Results. The radio bursts correlate very well with the EUV jets. The EUV jet emission also correlates well with brightening at what looks like their footpoint at the edge of the umbra. The jet emission lags the radio signals and the footpoint brightening by about 30 s because the EUV jets take time to develop. For 10–15 min after strong EUV jets are ejected, the footpoint brightens at roughly 3 min intervals. In both the EUV images and the extracted light curves, it looks as though the brightening is related to the 3-min sunspot oscillations, although the correlation coefficient is rather low. The only open field near the jets is rooted in the sunspot.
Conclusions. Active region EUV/X-ray jets and interplanetary electron streams originate on the edge of the sunspot umbra. They form along a current sheet between the sunspot open field and closed field connecting to underlying satellite flux. Sunspot running penumbral waves cause roughly 3-min jet footpoint brightening. The relationship between the waves and jets is less clear.

Observation of the Solar Eclipse on October 25, 2022 on Radio Telescopes of the Institute of Applied Astronomy, Russian Academy of Sciences (First Results).

Ivanov, D.V., Rakhimov, I.A., D'akov, A.A. et al.
Geomagn. Aeron. 63, 1015–1023 (**2023**).
https://doi.org/10.1134/S0016793223070125
The solar eclipse on **October 25, 2022**, is the ninth case of observations of solar eclipses using the fully rotatable RT-32 and RT-13 radio telescopes of the Institute of Applied Astronomy, Russian Academy of Sciences located at the Svetloye observatory in the Leningrad Region and Zelenchukskaya observatory in the North Caucasus. This eclipse is also the second case of observation using the WVR-4 water vapor radiometer as a full-fledged research tool for observing the Sun. Unlike the previous two eclipses in 2020 and 2021, when the Sun was at a deep minimum, the activity of the Sun in 2022 increased significantly, which made it possible to return to the traditional task of eclipse

observations, i.e., the study of the fine spatial structure of various active solar formations, which should include the distribution of radio brightness near the solar limb. Observations on RT-13 and RT-32 have been performed at 1.0 cm, 3.5, 6.2, and 13 cm wavelengths with circular polarization analysis, and on WVR-4 at wavelengths of 0.96 cm and 1.45 cm in intensity. Individual details of the structure of microwave radiation sources have been identified by comparison with observations of the Sun in other frequency ranges. We have studied two morphologically different active regions (the region with a large NOAA 13 131 spot and an extensive spotless bipolar region) and the regions of contacts I and IV. The pre-processing of observations allowed us to obtain a quasi-two-dimensional distribution of the radio brightness of the NOAA 13 131 active region located close to the limb. The nature of the distribution changes significantly with the wavelength. A small-scale image structure associated with radiogranulation has been identified within the spotless active region (plage). The observations of contacts confirmed the previously found small value of the radio radius corresponding to a quasi-quiet atmosphere. We measured the brightness temperature of the Sun averaged over the disk in the range of the water vapor line (1.35 cm), which coincides within the error with observations of the eclipse of 2021.

Magnetohydrodynamic simulation of coronal mass ejections using interplanetary scintillation data observed from radio sites ISEE and LOFAR

Kazumasa **Iwai**, Richard A. Fallows, Mario M. Bisi, Daikou Shiota, Bernard V. Jackson, Munetoshi Tokumaru, Ken'ichi Fujiki

Advances in Space Research **2022**

https://arxiv.org/ftp/arxiv/papers/2209/2209.12486.pdf

Interplanetary scintillation (IPS) is a useful tool for detecting coronal mass ejections (CMEs) throughout interplanetary space. Global magnetohydrodynamic (MHD) simulations of the heliosphere, which are usually used to predict the arrival and geo-effectiveness of CMEs, can be improved using IPS data. In this study, we demonstrate an MHD simulation that includes IPS data from multiple stations to improve CME modelling. The CMEs, which occurred on 09-10 September 2017, were observed over the period 10-12 September 2017 using the Low-Frequency Array (LOFAR) and IPS array of the Institute for Space-Earth Environmental Research (ISEE), Nagoya University, as they tracked through the inner heliosphere. We simulated CME propagation using a global MHD simulation, SUSANOO-CME, in which CMEs were modeled as spheromaks, and the IPS data were synthesised from the simulation results. The MHD simulation suggests that the CMEs merged in interplanetary space, forming complicated IPS g-level distributions in the sky map. We found that the MHD simulation that best fits both LOFAR and ISEE data provided a better reconstruction of the CMEs and a better forecast of their arrival at Earth than from measurements when these simulations were fit from the ISEE site alone. More IPS data observed from multiple stations at different local times in this study can help reconstruct the global structure of the CME, thus improving and evaluating the CME modelling. **9-12 Sep 2017**

Spectral Structures of Type II Solar Radio Bursts and Solar Energetic Particles

Kazumasa **Iwai,** Seiji Yashiro, Nariaki V. Nitta, Yuki Kubo

ApJ **888** 50 **2020**

https://arxiv.org/ftp/arxiv/papers/1911/1911.05897.pdf

sci-hub.si/10.3847/1538-4357/ab57ff **File**

We investigated the relationship between the spectral structures of type II solar radio bursts in the hectometric and kilometric wavelength ranges and solar energetic particles (SEPs). To examine the statistical relationship between type II bursts and SEPs, we selected 26 coronal mass ejection (CME) events with similar characteristics (e.g., initial speed, angular width, and location) observed by the Large Angle and Spectrometric Coronagraph (LASCO), regardless of the characteristics of the corresponding type II bursts and the SEP flux. Then, we compared associated type II bursts observed by the Radio and Plasma Wave Experiment (WAVES) onboard the Wind spacecraft and the SEP flux observed by the Geostationary Operational Environmental Satellite (GOES) orbiting around the Earth. We found that the bandwidth of the hectometric type II bursts and the peak flux of the SEPs has a positive correlation (with a correlation coefficient of 0.64). This result supports the idea that the nonthermal electrons of type II bursts and the nonthermal ions of SEPs are generated by the same shock and suggests that more SEPs may be generated for a wider or stronger CME shock with a longer duration. Our result also suggests that considering the spectral structures of type II bursts can improve the forecasting accuracy for the peak flux of gradual SEPs. **2006-12-13, 2013-08-18, 2013 October 28, 2017 September 4**

Table 1. CME events and X-ray flares, SEPs, and type II bursts used in the statistical analysis in this study (2006-2019).

CESRA nugget #2514 Mar **2020** http://www.astro.gla.ac.uk/users/eduard/cesra/?p=2514

ALMA Discovery of Solar Umbral Brightness Enhancement at λ=3 mm

Kazumasa **Iwai**, Maria Loukitcheva, Masumi Shimojo, Sami K. Solanki, Stephen M. White

ApJL 841 L20 **2017**

https://arxiv.org/pdf/1705.03147.pdf

We report the discovery of a brightness enhancement in the center of a large sunspot umbra at a wavelength of 3 mm using the Atacama Large Millimeter/sub-millimeter Array (ALMA). Sunspots are amongst the most prominent features on the solar surface, but many of their aspects are surprisingly poorly understood. We analyzed a {\lambda}=3 mm (100 GHz) mosaic image obtained by ALMA, which includes a large sunspot within the active region AR12470 on **December 16, 2015**. The 3 mm map has a field-of-view and spatial resolution, which is the highest spatial-resolution map of an entire sunspot in this frequency range. We find a gradient of 3 mm brightness from a high value in the outer penumbra to a low value in the inner penumbra/outer umbra. Within the inner umbra, there is a marked increase in 3mm brightness temperature, which we call an umbral brightness enhancement. This enhanced emission corresponds to a temperature excess of 800 K relative to the surrounding inner penumbral region and coincides with excess brightness in the 1330 and 1400 {\AA} slitjaw images of the Interface Region Imaging Spectrograph (IRIS), adjacent to a partial lightbridge. This {\lambda}=3 mm brightness enhancement may be an intrinsic feature of the sunspot umbra at chromospheric heights, such as a manifestation of umbral flashes, or it could be related to a coronal plume since the brightness enhancement was coincident with the footpoint of a coronal loop observed at 171 {\AA}.

The Brightness Temperature of the Quiet Solar Chromosphere at 2.6 mm

Kazumasa **Iwai**, Masumi Shimojo, Shinichiro Asayama, Tetsuhiro Minamidani, Stephen White, Timothy Bastian, Masao Saito

Solar Phys. 292:22 **2017**

https://arxiv.org/pdf/1612.08241v1.pdf

The absolute brightness temperature of the Sun at millimeter wavelengths is an important diagnostic of the solar chromosphere. Because the Sun is so bright, measurement of this property usually involves the operation of telescopes under extreme conditions and requires a rigorous performance assessment of the telescope. In this study, we establish solar observation and calibration techniques at 2.6-mm wavelength for the Nobeyama 45-m telescope and derive the absolute solar brightness temperature accurately. We tune the superconductor-insulator-superconductor (SIS) receiver by inducing different bias voltages onto the SIS mixer to prevent saturation. Then, we examine the linearity of the receiver system by comparing outputs derived from different tuning conditions. Further, we measure the lunar filled beam efficiency of the telescope using the New Moon, and then derive the absolute brightness temperature of the Sun. The derived solar brightness temperature is 7700+-310 K at 115 GHz. The telescope beam pattern is modeled as a summation of three Gaussian functions and derived using the solar limb. The real shape of the Sun is determined via deconvolution of the beam pattern from the observed map. Such well-calibrated single-dish observations are important for high-resolution chromospheric studies because they provide the absolute temperature scale missing from interferometer observations. **20 Jan 2015**

See [CESRA] highlight #1325 Apr **2017**

http://www.astro.gla.ac.uk/users/eduard/cesra/?p=1325

OCTAD-S: digital fast Fourier transform spectrometers by FPGA

OCTAD: Optically Connected Transmission system for Analog to Digital Conversion

Iwai, Kazumasa ; Kubo, Yûki ; Ishibashi, Hiromitsu ; Naoi, Takahiro ; Harada, Kenichi ; Ema, Kenji ; Hayashi, Yoshinori ; Chikahiro, Yuichi

Earth, Planets and Space, Volume 69, Issue 1, article id.95, 8 pp. **2017**

https://arxiv.org/ftp/arxiv/papers/1706/1706.08863.pdf

https://earth-planets-space.springeropen.com/counter/pdf/10.1186/s40623-017-0681-8.pdf

We have developed a digital fast Fourier transform spectrometer made of an analog-to-digital converter (ADC) and a field-programmable gate array (FPGA). The base instrument has independent ADC and FPGA modules, which allow us to implement different spectrometers in a relatively easy manner. Two types of spectrometers have been instrumented: one with 4.096 GS/s sampling speed and 2048 frequency channels and the other with 2.048 GS/s sampling speed and 32,768 frequency channels. The signal processing in these spectrometers has no dead time, and the accumulated spectra are recorded in external media every 8 ms. A direct sampling spectroscopy up to 8 GHz is achieved by a microwave track-and-hold circuit, which can reduce the analog receiver in front of the spectrometer. Highly stable spectroscopy with a wide dynamic range was demonstrated in a series of laboratory experiments and test observations of solar radio bursts.

the Yamagawa radio spectrograph (9 GHz - 70 MHz)

Observation of the Solar Chromosphere at 2.6 mm

Kazumasa **Iwai**_1, Masumi Shimojo2, Shinichiro Asayama2, Tetsuhiro Minamidani2, Stephen White3, Timothy Bastian4, and Masao Saito2

CESRA **2016**, p.94

http://cesra2016.sciencesconf.org/conference/cesra2016/pages/CESRA2016_prog_abs_book_v3.pdf

The main emission mechanism of the Sun at millimeter wavelengths is thermal free-free emission from the chromosphere. The opacity of thermal free-free emission depends on the density and temperature pro_les in the atmosphere. In addition, the Rayleigh-Jeans law

is applicable for these wavelength ranges. Hence, the observation of the radio brightness temperature at millimetric range can be a good diagnostics of the solar chromosphere. In this paper, we report on the single-dish observation of the Sun at 115 GHz (2.6 mm) using the Nobeyama 45 m telescope, whose typical spatial resolution is 15" at 115 GHz. We enabled the solar observation by detuning the SIS mixer to prevent the saturation of the receiver system. We observed a solar sunspot which is usually surrounded by bright plage regions. We removed the plage e_ect using the deconvolution of the telescope's side lobes. The observed result suggests that the sunspot umbra is darker than the quiet region by a minimum of 100 K at 115 GHz. This result is inconsistent with current sunspot models, which predict a higher brightness temperature of the sunspot umbra at this wavelength. This inconsistency suggests that the temperature of the region at which the 115 GHz radio emission becomes optically thick should be lower than that predicted by the models. ALMA has better beam shapes and more accurate calibration system than those of our observation. Therefore, ALMA will facilitate important progress in not only interferometry, but also single-dish observations of the Sun.

Fine Spectral Structures of Solar Radio Type-I Bursts observed by AMATERAS

Kazumasa **Iwai**

CESRA Abstract **2016**

http://cesra2016.sciencesconf.org/conference/cesra2016/pages/CESRA2016_prog_abs_book_v1.pdf

Fine spectral structures of solar radio bursts contain information of radio wave generations and propagations. We investigated the fine spectral structures of solar radio type-I bursts using the radio telescope AMATERAS. AMATERAS is a ground-based solar radio telescope for spectropolarimetry in the metric range. The observation band of this telescope is 150–500 MHz with a 10 ms accumulation time and a 61 kHz bandwidth. The spectral characteristics, such as the peak flux, duration, and bandwidth, of the individual burst elements were satisfactorily detected by the highly resolved spectral data of AMATERAS. The peak flux of the type-I bursts followed a power-law distribution with a spectral index of 2.9- 3.3, whereas their duration and bandwidth were distributed more exponentially. There were almost no correlations between the peak flux, duration, and bandwidth. That means there was no similarity in the shapes of the burst spectral structures. We defined the growth rate of a burst as the ratio between its peak flux and duration. There was a strong correlation between the growth rate and peak flux. These results suggest that the free energy of type-I bursts that is originally generated by nonthermal electrons is modulated in the subsequent stages of the generation of nonthermal electrons, such as plasma wave generation, radio wave emissions, and propagation. The variation of the timescale of the growth rate is significantly larger than that of the coronal environments. These results can be explained by the situation wherein the source region may have the inhomogeneity of an ambient plasma environment, such as the boundary of open and closed field lines, and the superposition of entire emitted bursts was observed by the spectrometer.

Chromospheric sunspots in millimeter range as observed by Nobeyama Radioheliograph

Kazumasa **Iwai**, Hideki Koshiishi, Kiyoto Shibasaki, Satoshi Nozawa, Shun Miyawaki, Takuro Yoneya

ApJ 816 91 **2016**

http://arxiv.org/pdf/1511.08991v1.pdf

We investigate the upper chromosphere and the transition region of the sunspot umbra using the radio brightness temperature at 34 GHz (corresponding to 8.8-mm observations) as observed by the Nobeyama Radioheliograph (NoRH). Radio free-free emission in the longer millimeter range is generated around the transition region, and its brightness temperature yields the region's temperature and density distribution. We use the NoRH data at 34 GHz by applying the Steer-CLEAN image synthesis. These data and the analysis method enable us to investigate the chromospheric structures in the longer millimeter range with high spatial resolution and sufficient visibilities. We also perform simultaneous observations of one sunspot using the NoRH and the Nobeyama 45-m telescope operating at 115 GHz. We determine that 115-GHz emission mainly originates from the lower chromosphere while 34-GHz emission mainly originates from the upper chromosphere and transition region. These observational results are consistent with the radio emission characteristics estimated from the current atmospheric models of the chromosphere. On the other hand, the observed brightness temperature of the umbral region is almost the same as that of the quiet region. This result is inconsistent with the current sunspot models, which predict a considerably higher brightness temperature of the sunspot umbra at 34 GHz. This inconsistency suggests that the temperature of the region at which the 34 GHz radio emission becomes optically thick should be lower than that predicted by the models. **2014 January 8, 2014 February 12, 2014 October 24**

Observation of Chromospheric Sunspot at Millimeter Range with the Nobeyama 45 m Telescope

Kazumasa **Iwai**, Masumi Shimojo

ApJ **804** 48 **2015**

http://arxiv.org/ftp/arxiv/papers/1503/1503.00096.pdf

The brightness temperature of the radio free-free emission at millimeter range is an effective tool for characterizing the vertical structure of the solar chromosphere. In this paper, we report on the first single-dish observation of a sunspot at 85 and 115 GHz with sufficient spatial resolution for resolving the sunspot umbra using the Nobeyama 45 m telescope. We used radio attenuation material, i.e. a solar filter, to prevent the saturation of the receivers. Considering the contamination from the plage by the side-lobes, we found that the brightness temperature of the umbra should be lower than that of the quiet region. This result is inconsistent with the preexisting atmospheric models. We also found that the brightness temperature distribution at millimeter range strongly corresponds to the ultraviolet (UV) continuum emission at 1700 {\AA}, especially at the quiet region. **2014 February 12**

Coronal magnetic field and the plasma beta determined from radio and multiple satellite observations

Kazumasa **Iwai**, Kiyoto Shibasaki, Satoshi Nozawa, Takuya Takahashi, Shinpei Sawada, Jun Kitagawa, Shun Miyawaki, Hirotaka Kashiwagi

Earth planets and Space (EPS), CAWSES-II special issue, **2014**

http://arxiv.org/pdf/1411.1913v1.pdf

We derived the coronal magnetic field, plasma density, and temperature from the observation of polarization and intensity of radio thermal free-free emission using the Nobeyama Radioheliograph (NoRH) and extreme ultraviolet (EUV) observations. We observed a post-flare loop on the west limb **11 April 2013**. The line-of-sight magnetic field was derived from the circularly polarized free-free emission observed by NoRH. The emission measure and temperature were derived from the Atmospheric Imaging Assembly (AIA) onboard Solar Dynamics Observatory (SDO). The derived temperature was used to estimate the emission measure from the NoRH radio free-free emission observations. The derived density from NoRH was larger than that determined using AIA, which can be explained by the fact that the low temperature plasma is not within the temperature coverage of the AIA filters used in this study. We also discuss the other observation of the post-flare loops by the EUV Imager onboard the Solar Terrestrial Relations Observatory (STEREO), which can be used in future studies to reconstruct the coronal magnetic field strength. The derived plasma parameters and magnetic field were used to derive the plasma beta, which is a ratio between the magnetic pressure and the plasma pressure. The derived plasma beta is about 5.7*10^(-4) to 7.6*10^(-4) at the loop top region.

Spectral Structures and Their Generation Mechanisms for Solar Radio Type-I Bursts

Kazumasa **Iwai**, Yoshizumi Miyoshi, Satoshi Masuda, Fuminori Tsuchiya, Akira Morioka, Hiroaki Misawa

ApJ, 789 4, **2014**

http://arxiv.org/pdf/1405.0708v1.pdf

The fine spectral structures of solar radio type-I bursts were observed by the solar radio telescope AMATERAS. The spectral characteristics, such as the peak flux, duration, and bandwidth, of the individual burst elements were satisfactorily detected by the highly resolved spectral data of AMATEAS with the burst detection algorithm that is improved in this study. The peak flux of the type-I bursts followed a power-law distribution with a spectral index of 2.9-3.3, whereas their duration and bandwidth were distributed more exponentially. There were almost no correlations between the peak flux, duration, and bandwidth. That means there were no similarity shapes in the burst spectral structures. We defined the growth rate of a burst as the ratio between its peak flux and duration. There was a strong correlation between the growth rate and peak flux. These results suggest that the free energy of type-I bursts that is originally generated by non-thermal electrons is modulated in the subsequent stages of the generation of non-thermal electrons, such as plasma wave generation, radio wave emissions, and propagation. The variation of the time scale of the growth rate is significantly larger than that of the coronal environments. These results can be explained by the situation that the source region may have the inhomogeneity of an ambient plasma environment, such as the boundary of open and closed field lines, and the superposition of entire emitted bursts was observed by the spectrometer. **January 16, 23, and 26, 2011**

Measurements of Coronal and Chromospheric Magnetic Fields using Polarization Observations by the Nobeyama Radioheliograph

K. **Iwai** and K. Shibasaki

Publ. Astron. Soc. Japan 65, No SP1, S14 [7 pages] (**2013**)

http://pasj.asj.or.jp/v65/sp1/65S014/65S014.pdf

Coronal and chromospheric magnetic fields are derived from polarization and spectral observations of the thermal

free–free emission using the Nobeyama Radioheliograph (NoRH). In magnetized plasma, the ordinary and extraordinary modes of free–free emission have different optical depths. This creates a circularly polarized component in an atmosphere with a temperature gradient. We observed an active region on **2012 April 13** to derive its coronal and chromospheric magnetic fields. The observed degree of circular polarization was between 0.5% and 1.7%. The radio circular polarization images were compared with ultraviolet images observed by the Atmospheric Imaging Assembly and the photospheric magnetic field observed by the Helioseismic and Magnetic Imager, both on board the Solar Dynamic Observatory. At the edge of the active region, the radio circular polarization was emitted mainly from coronal loops, and the coronal magnetic field was derived to be about 70 G. At the center of the active region, the chromospheric and coronal components cannot be separated. The derived magnetic field is about 20% to 50% of the corresponding photospheric magnetic field, which is an emission-measure-weighted average of the coronal and chromospheric magnetic fields.

PEAK FLUX DISTRIBUTIONS OF SOLAR RADIO TYPE-I BURSTS FROM HIGHLY RESOLVED SPECTRAL OBSERVATIONS

K. **Iwai**1, S. Masuda2, Y. Miyoshi2, F. Tsuchiya3, A. Morioka3, and H. Misawa
2013 ApJ 768 L2
http://iopscience.iop.org/2041-8205/768/1/L2/pdf/2041-8205_768_1_L2.pdf
Solar radio type-I bursts were observed on **2011 January 26** by high resolution observations with the radio telescope AMATERAS in order to derive their peak flux distributions. We have developed a two-dimensional auto burst detection algorithm that can distinguish each type-I burst element from complex noise storm spectra that include numerous instances of radio frequency interference (RFI). This algorithm removes RFI from the observed radio spectra by applying a moving median filter along the frequency axis. Burst and continuum components are distinguished by a two-dimensional maximum and minimum search of the radio dynamic spectra. The analysis result shows that each type-I burst element has one peak flux without double counts or missed counts. The peak flux distribution of type-I bursts derived using this algorithm follows a power law with a spectral index between 4 and 5.

IPRT/AMATERAS: A New Metric Spectrum Observation System for Solar Radio Bursts

K. **Iwai** · F. Tsuchiya · A. Morioka · H. Misawa
Solar Phys. Volume 277, Number 2, 447-457, **2012, File**
A new radio spectropolarimeter for solar radio observation has been developed at Tohoku University and installed on the *Iitate Planetary Radio Telescope* (IPRT) at the Iitate observatory in Fukushima prefecture, Japan. This system, named AMATERAS (*the Assembly of Metric-band Aperture TElescope and Real-time Analysis System*), enables us to observe solar radio bursts in the frequency range between 150 and 500 MHz. The minimum detectable flux in the observation frequency range is less than 0.7 SFU with an integration time of 10 ms and a bandwidth of 61 kHz. Both left and right polarization components are simultaneously observed in this system. These specifications are accomplished by combining the large aperture of IPRT with a high-speed digital receiver. Observational data are calibrated and archived soon after the daily observation. The database is available online. The high-sensitivity observational data with the high time and frequency resolutions from AMATERAS will be used to analyze spectral fine structures of solar radio bursts.

SOLAR RADIO TYPE-I NOISE STORM MODULATED BY CORONAL MASS EJECTIONS

K. **Iwai**1, Y. Miyoshi2, S. Masuda2, M. Shimojo3, D. Shiota4, S. Inoue5, F. Tsuchiya1, A. Morioka1 and H. Misawa
2012 ApJ 744 167, **File**
http://dx.doi.org.sci-hub.cc/10.1088/0004-637X/744/2/167
The first coordinated observations of an active region using ground-based radio telescopes and the Solar Terrestrial Relations Observatory (STEREO) satellites from different heliocentric longitudes were performed to study solar radio type-I noise storms. A type-I noise storm was observed between 100 and 300 MHz during a period from **2010 February 6 to 7**. During this period the two STEREO satellites were located approximately 65fl (ahead) and –70fl (behind) from the Sun-Earth line, which is well suited to observe the earthward propagating coronal mass ejections (CMEs). The radio flux of the type-I noise storm was enhanced after the preceding CME and began to decrease before the subsequent CME. This time variation of the type-I noise storm was directly related to the change of the particle acceleration processes around its source region. Potential-field source-surface extrapolation from the Solar and Heliospheric Observatory/Michelson Doppler Imager (SOHO/MDI) magnetograms suggested that there was a multipolar magnetic system around the active region from which the CMEs occurred around the magnetic neutral line of the system. From our observational results, we suggest that the type-I noise storm was activated at a side-lobe

reconnection region that was formed after eruption of the preceding CME. This magnetic structure was deformed by a loop expansion that led to the subsequent CME, which then suppressed the radio burst emission.

Iterative Tomography: A Key to Providing Time- dependent 3-D Reconstructions of the Inner Heliosphere and the Unification of Space Weather Forecasting Techniques

Bernard **Jackson**1*, Andrew Buffington1, Lucas Cota1, Dusan Odstrcil2, Mario M. Bisi3, Richard Fallows4 and Munetoshi Tokumaru
Front. Astron. Space Sci. **2020**|
doi: 10.3389/fspas.2020.568429
https://www.frontiersin.org/articles/10.3389/fspas.2020.568429/full
Over several decades UCSD has developed and continually updated a time dependent iterative three-dimensional (3-D) reconstruction technique to provide global heliospheric parameters – density, velocity, and component magnetic fields. For expediency, this has used a kinematic model as a kernel to provide a fit to either interplanetary scintillation (IPS) or Thomson-scattering observations. This technique has been used in near real time over this period, employing Institute for Space-Earth Environmental Research (ISEE), Japan IPS data to predict the propagation of these parameters throughout the inner heliosphere.
We have extended the 3-D reconstruction analysis to include other IPS Stations around the Globe in a Worldwide Interplanetary Scintillation Stations (WIPSS) Network. In addition, we also plan to resurrect the Solar Mass Ejection Imager (SMEI) Thomson-scattering analysis as a basis for 3-D analysis to be used by the latest NASA Small Explorer heliospheric imagers of the Polarimeter to Unify the Corona and Heliosphere (PUNCH) mission, the All Sky Heliospheric Imager (ASHI), and other modern wide-field imagers. Better data require improved Heliospheric modeling that incorporates non-radial transport of heliospheric flows, and shock processes. Looking ahead to this, we have constructed an interface between the 3-D reconstruction tomography and 3-D MHD models, and currently include the ENLIL model as a kernel in the reconstructions to provide this fit. In short, we are now poised to provide all of these innovations in a next step: to include them for planned ground-based and spacecraft instruments, all to be combined into a truly global 3-D heliospheric system which utilizes these aspects in their data and modeling.

The solar chromosphere at millimetre and ultraviolet wavelengths. I. Radiation temperatures and a detailed comparison

Shahin **Jafarzadeh**, Sven Wedemeyer, Mikolaj Szydlarski, Bart De Pontieu, Reza Rezaei, Mats Carlsson
A&A 622, A150 **2019**
https://arxiv.org/pdf/1901.05763.pdf
Solar observations with the Atacama Large Millimeter/submillimeter Array (ALMA) provide us with direct measurements of the brightness temperature in the solar chromosphere. We study the temperature distributions obtained with ALMA Band 6 (in four sub-bands at 1.21, 1.22, 1.29, and 1.3 mm) for various areas at, and in the vicinity of, a sunspot, comprising quasi-quiet and active regions with different amounts of underlying magnetic fields. We compare these temperatures with those obtained at near- and far-ultraviolet (UV) wavelengths (and with the line-core intensities of the optically-thin far-UV spectra), co-observed with the Interface Region Imaging Spectrograph (IRIS) explorer. These include the emission peaks and cores of the Mg II k 279.6 nm and Mg II h 280.4 nm lines as well as the line cores of C II 133.4 nm, O I 135.6 nm, and Si IV 139.4 nm, sampling the mid-to-high chromosphere and the low transition region. Splitting the ALMA sub-bands resulted in an slight increase of spatial resolution in individual temperature maps, thus, resolving smaller-scale structures compared to those produced with the standard averaging routines. We find that the radiation temperatures have different, though somewhat overlapping, distributions in different wavelengths and in the various magnetic regions. Comparison of the ALMA temperatures with those of the UV diagnostics should, however, be interpreted with great caution, the former is formed under the local thermodynamic equilibrium (LTE) conditions, the latter under non-LTE. The mean radiation temperature of the ALMA Band 6 is similar to that extracted from the IRIS C II line in all areas with exception of the sunspot and pores where the C II poses higher radiation temperatures. In all magnetic regions, the Mg II lines associate with the lowest mean radiation temperatures in our sample. These will provide constraints for future numerical models. **18 December 2015**

Turbulence dynamics and flow speeds in the inner solar corona: results from radio-sounding experiments by the Akatsuki spacecraft

Richa N **Jain**, R K Choudhary, Anil Bhardwaj, T Imamura, Anshuman Sharma, Umang M Parikh
Monthly Notices of the Royal Astronomical Society, Volume 525, Issue 3, **2023**, Pages 3730–3739,
https://doi.org/10.1093/mnras/stad2491
The solar inner corona is a region that plays a critical role in energizing the solar wind and propelling it to supersonic and supra-Alfvénic velocities. Despite its importance, this region remains poorly understood because of being least explored due to observational limitations. The coronal radio-sounding technique in this context becomes useful as it helps in providing information in parts of this least explored region. To shed light on the dynamics of the solar wind in the inner corona, we conducted a study using data obtained from coronal radio-sounding experiments carried out by the Akatsuki spacecraft during the 2021 Venus-solar conjunction event. By analysing X-band radio signals recorded at two

ground stations (Indian Deep Space Network in Bangalore and Usuda Deep Space Center in Japan), we investigated plasma turbulence characteristics and estimated flow speed measurements based on isotropic quasi-static turbulence models. Our analysis revealed that the speed of the solar wind in the inner corona (at heliocentric distances from 5 to 13 solar radii), ranging from 220 to 550 km s−1, was higher than the expected average flow speeds in this region. By integrating our radio-sounding results with extreme ultraviolet (EUV) images of the solar disc, we gained a unique perspective on the properties and energization of high-velocity plasma streams originating from coronal holes. We tracked the evolution of fast solar wind streams emanating from an extended coronal hole as they propagated to increasing heliocentric distances. Our study provides unique insights into the least-explored inner coronal region by corroborating radio-sounding results with EUV observations of the corona.

Estimating the total energy content in escaping accelerated solar electron beams

Alexander W. **James**, Hamish A. S. Reid

ApJ **976** 128 **2024**

https://arxiv.org/pdf/2409.15091

https://iopscience.iop.org/article/10.3847/1538-4357/ad7b38/pdf

Quantifying the energy content of accelerated electron beams during solar eruptive events is a key outstanding objective that must be constrained to refine particle acceleration models and understand the electron component of space weather. Previous estimations have used in situ measurements near the Earth, and consequently suffer from electron beam propagation effects. In this study, we deduce properties of a rapid sequence of escaping electron beams that were accelerated during a solar flare on **22 May 2013** and produced type III radio bursts, including the first estimate of energy density from remote sensing observations. We use extreme-ultraviolet observations to infer the magnetic structure of the source active region NOAA 11745, and Nançay Radioheliograph imaging spectroscopy to estimate the speed and origin of the escaping electron beams. Using the observationally deduced electron beam properties from the type III bursts and co-temporal hard X-rays, we simulate electron beam properties to estimate the electron number density and energy in the acceleration region. We find an electron density (above 30 keV) in the acceleration region of 102.5 cm−3 and an energy density of 2×10−5 erg cm−3. Radio observations suggest the particles travelled a very short distance before they began to produce radio emission, implying a radially narrow acceleration region. A short but plausibly wide slab-like acceleration volume of 1026−1028 cm3 atop the flaring loop arcade could contain a total energy of 1023−1025 erg (∼100 beams), which is comparable to energy estimates from previous studies.

Statistical study of type III bursts and associated HXR emissions

James, Tomin ; Vilmer, Nicole

Astronomy & Astrophysics, Volume 673, id.A57, 13 pp. **2023**

https://www.aanda.org/articles/aa/pdf/2023/05/aa45825-22.pdf

Context. Flare-accelerated electrons may produce closely temporarily related hard X-ray (HXR) emission while interacting with the dense solar atmosphere and radio type III bursts when propagating from the low corona to the interplanetary medium. The link between these emissions has been studied in previous studies. We present here new results on the correlation between the number and spectrum of HXR-producing electrons and the type III characteristics (flux, starting frequency).

Aims: The aim of this study is to extend the results from previous statistical studies of radio type III bursts and associated HXR emissions: in particular, to determine what kind of correlation, if any, exists between the HXR-emitting electron numbers and the radio flux, as well as whether any correlations between the electron numbers or energy spectra are deduced from associated HXR emissions and type III starting (stopping) frequencies.

Methods: This study is based on thirteen years of data between 2002 and 2014. We shortlisted ≃200 events with a close temporal association between HXR emissions and radio type III bursts in the 450-150 MHz range. We used X-ray flare observations from RHESSI and Fermi/GBM to calculate the number of electrons giving rise to the observed X-ray flux and observations from the Nançay Radioheliograph to calculate the peak radio flux at different frequencies in the 450-150 MHz range. Under the assumption of thick-target emissions, the number of HXR-producing electrons and their energy spectra were computed. The correlation between electron numbers, power-law indices, and the peak radio fluxes at different frequencies were analysed as well as potential correlations between the electron numbers and starting frequency of the radio burst. Bootstrap analysis for the correlation coefficients was performed to quantify the statistical significance of the fit.

Results: The correlation between the number of HXR electrons and the peak flux of the type III emission decreases with increasing frequency. This correlation is larger when considering the electron number above 20 keV rather than the electron number above 10 keV. A weak anti-correlation is also found between the absolute value of the electron spectral index and the peak radio flux at 228 MHz. A rough correlation is found between the HXR-producing electron number above 20 keV and the type III starting frequency. This correlation is smaller if the electron number above 10 keV is considered. All the results are discussed in the framework of results from previous studies and in the context of numerical simulations of bump-in-tail instabilities and subsequent radio emissions. **10-03-2003, 26-08-2011, 22-04-2013, 20-10-2013**

RHESSI Nuggets, #451 **2023**
https://sprg.ssl.berkeley.edu/~tohban/wiki/index.php/Statistical_study_of_Type_III_bursts_and_associated_HXR_emissions

Energetics of small electron acceleration episodes in the solar corona from radio noise storm observations

Tomin **James**, Prasad Subramanian
MNRAS 479, Issue 2, 11 September **2018**, Pages 1603–1611
https://arxiv.org/pdf/1805.07559.pdf
http://sci-hub.tw/10.1093/mnras/sty1216
Observations of radio noise storms can act as sensitive probes of nonthermal electrons produced in small acceleration events in the solar corona. We use data from noise storm episodes observed jointly by the Giant Metrewave Radio Telescope (GMRT) and the Nancay Radioheliograph (NRH) to study characteristics of the nonthermal electrons involved in the emission. We find that the electrons carry 1021 to 1024 erg/s, and that the energy contained in the electrons producing a representative noise storm burst ranges from 1020 to 1023 ergs. These results are a direct probe of the energetics involved in ubiquitous, small-scale electron acceleration episodes in the corona, and could be relevant to a nanoflare-like scenario for coronal heating. **27 Aug 2002**

Small electron acceleration episodes in the solar corona

Tomin **James**, Prasad Subramanian, Eduard P Kontar
MNRAS 471, 89 **2017**
https://arxiv.org/pdf/1706.04031.pdf
We study the energetics of nonthermal electrons produced in small acceleration episodes in the solar corona. We carried out an extensive survey spanning 2004--2015 and shortlisted 6 impulsive electron events detected at 1 AU that was not associated with large solar flares(GOES soft X-ray class > C1) or with coronal mass ejections. Each of these events had weak, but detectable hard Xray (HXR) emission near the west limb, and were associated with interplanetary type III bursts. In some respects, these events seem like weak counterparts of "cold/tenuous" flares. The energy carried by the HXR producing electron population was ≈1023 -- 1025 erg, while that in the corresponding population detected at 1 AU was ≈1024--1025 erg. The number of electrons that escape the coronal acceleration site and reach 1 AU constitute 6 % to 148 % of those that precipitate downwards to produce thick target HXR emission. **28-02-2004, 16-03-2004, 26-06-2004, 27-06-2004, 25-12-2004**
Table 1. Impulsive electron events detected in-situ at 1 AU: first shortlist
Table 2. Final shortlist and spectral parameters
CESRA Highlight # 1635 Nov **2017** http://cesra.net/?p=1635

Direct Measurements of Synchrotron-emitting Electrons at Near-Sun Shocks

I. C. **Jebaraj**1, O. V. Agapitov2,3, M. Gedalin4, L. Vuorinen1,5, M. Miceli6, C. M. S. Cohen7, A. Voshchepynets2,8, A. Kouloumvakos9, N. Dresing1, A. Marmyleva10Show full author list
2024 ApJL 976 L7
https://iopscience.iop.org/article/10.3847/2041-8213/ad8eb8/pdf
In this study, we present the first-ever direct measurements of synchrotron-emitting heliospheric traveling shocks, intercepted by the Parker Solar Probe (PSP) during its close encounters. Given that much of our understanding of powerful astrophysical shocks is derived from synchrotron radiation, these observations by PSP provide an unprecedented opportunity to explore how shocks accelerate relativistic electrons and the conditions under which they emit radiation. The probe's unparalleled capabilities to measure both electromagnetic fields and energetic particles with high precision in the near-Sun environment has allowed us to directly correlate the distribution of relativistic electrons with the resulting photon emissions. Our findings reveal that strong quasi-parallel shocks emit radiation at significantly higher intensities than quasi-perpendicular shocks due to the efficient acceleration of ultrarelativistic electrons. These experimental results are consistent with theory and recent observations of supernova remnant shocks and advance our understanding of shock physics across diverse space environments. **2022 September 5, 2023 March 13**

Fundamental-harmonic pairs of interplanetary type III radio bursts

Immanuel Christopher **Jebaraj**, Vladimir Krasnoselskikh, Marc Pulupa, Jasmina Magdalenic, Stuart Bale
ApJL **955** L20 **2023**
https://arxiv.org/pdf/2309.05763.pdf
https://iopscience.iop.org/article/10.3847/2041-8213/acf857/pdf
Type III radio bursts are not only the most intense but also the most frequently observed solar radio bursts. However, a number of their defining features remain poorly understood. Observational limitations, such as a lack of sufficient spectral and temporal resolution, have hindered a full comprehension of the emission process, especially in the hecto-kilometric wavelengths. Of particular difficulty is the ability to detect the harmonics of type III radio bursts. Hereafter

we report for the first detailed observations of type III fundamental-harmonic pairs in the hecto-kilometric wavelengths, observed by the Parker Solar Probe. We present the statistical analysis of spectral characteristics and the polarization measurements of the fundamental-harmonic pairs. Additionally, we quantify various characteristic of the fundamental-harmonic pairs, such as the time-delay and time-profile asymmetry. Our report and preliminary analysis conclude that fundamental-harmonic pairs constitute a majority of all type III radio bursts observed during close encounters 6 -- 10 when the probe is in close proximity to the source region and propagation effects are less pronounced. **21-22 Nov 2021**
Table 1. The list of 31 F-H pairs of type III bursts analysed in this study. 2020-2021

Multiple injections of energetic electrons associated with the flare/CME event on 9 October 2021

Immanuel Christopher **Jebaraj**, Athanasios Kouloumvakos, Nina Dresing, Alexander Warmuth, Nicolas Wijsen, Christian Palmroos, Jan Gieseler, Rami Vainio, Vratislav Krupar, Jasmina Magdalenic, Thomas Wiegelmann, Frederic Schuller, Andrea Battaglia, Annamaria Fedeli
A&A **2023**
https://arxiv.org/pdf/2301.03650.pdf File
We study the solar energetic particle (SEP) event observed on **9 October 2021**, by multiple spacecraft including Solar Orbiter (SolO). The event was associated with an M1.6 flare, a coronal mass ejection (CME) and a shock wave. During the event, high-energy protons and electrons were recorded by multiple instruments located within a narrow longitudinal cone. An interesting aspect of the event was the multi-stage particle energization during the flare impulsive phase and also what appears to be a separate phase of electron acceleration detected at SolO after the flare maximum. We aim to investigate and identify the multiple sources of energetic electron acceleration. We utilize SEP electron observations from the Energetic Particle Detector (EPD) and hard X-ray (HXR) observations from the Spectrometer/Telescope for Imaging X-rays (STIX) on-board SolO, in combination with radio observations at a broad frequency range. We focus on establishing an association between the energetic electrons and the different HXR and radio emissions associated with the multiple acceleration episodes. We have found that the flare was able to accelerate electrons for at least 20 minutes during the nonthermal phase observed in the form of five discrete HXR pulses. We also show evidence that the shock wave has contributed to the electron acceleration during and after the impulsive flare phase. The detailed analysis of EPD electron data shows that there was a time difference in the release of low- and high-energy electrons, with the high-energy release delayed. Also, the observed electron anisotropy characteristics suggest different connectivity during the two phases of acceleration.
See Introduction

Structured type III radio bursts observed in interplanetary space

Immanuel C. **Jebaraj**, Jasmina Magdalenić, Vladimir Krasnoselskikh, Vratislav Krupar, Stefaan Poedts
A&A 670, A20 **2023**
https://arxiv.org/pdf/2209.12333.pdf
https://www.aanda.org/articles/aa/pdf/2023/02/aa43494-22.pdf
Context: The last few decades has seen numerous studies dedicated to fine structures of type III radio bursts observed in the metric to decametric wavelengths. Majority of explanations of the structured radio emission involve the propagation of electron beam through the strongly inhomogeneous plasma in the low corona. Until now only few studies of single type III bursts with fine structures, observed in the hecto-kilometric wavelengths, were reported. Aims: Herein we report about existence of numerous structured type III radio bursts observed during the STEREO era by all three WAVES instruments on board STEREO A, B, and Wind. The aim of the study is to report, classify structured type III bursts, and present the characteristics of their fine structures. The final goal is to try to understand the physical mechanism responsible for the generation of structured radio emission. Methods: In this study we used data from all available spacecraft, specifically the STEREO and the Wind spacecraft. We employ 1D density models to obtain the speed of the source of type III radio emission, the electron beam. We also perform spectral analysis of the fine structures in order to compare their characteristics with the metric-decametric fine structures. Results: The presented similarities of the type III fine structures in the metric to decametric and interplanetary wavelengths indicate that the physical processes responsible for the generation of structured type III radio bursts could be the same, at the heights, all the way from the low corona to the interplanetary range. We show that the observed structuring and intermittent nature of the type III bursts can be explained by the variation in the level of density fluctuations, at different distances from the Sun. **12 Nov 2010, 19 Sep 2011, 21 Nov 2011, 30 Nov 2011, 27-28 Sep 2012**

Generation of interplanetary type II radio emission

I. C. **Jebaraj**1,2, A. Kouloumvakos3, J. Magdalenic1,2, A. P. Rouillard3, G. Mann4, V. Krupar5,6 and S. Poedts2,7
A&A 654, A64 (**2021**)
https://www.aanda.org/articles/aa/pdf/2021/10/aa41695-21.pdf
https://doi.org/10.1051/0004-6361/202141695

Context. Coronal mass ejections (CMEs) are eruptive phenomena that can accelerate energetic particles and drive shock waves. The CME-driven shocks propagate from the low corona to interplanetary space. The radio emission that results from fast electrons energised by shock waves are called type II bursts. This radio emission can provide information on the physical properties of the shock and its evolution as it travels through the corona and interplanetary space.
Aims. We present a comprehensive analysis of the shock wave associated with two type II radio bursts observed on **27 September 2012.** The aim of the study is to isolate and understand the shock wave properties necessary for accelerating electrons, leading to the production of the radio emission.
Methods. First, we modelled the 3D expansion of the shock wave by exploiting multi-viewpoint reconstruction techniques based on extreme ultraviolet imaging. The physical properties of the shock front were then deduced by comparing the triangulated 3D expansion with properties of the background corona provided by a 3D magnetohydrodynamic model. The radio triangulation technique provided the location of radio source on the surface of the modelled wave in order to compare radio sources with the shock properties.
Results. This study is focused on the temporal evolution of the shock wave parameters and their role in the generation of radio emission. Results show a close relationship between the shock wave strength and its geometry. We deduce from this analysis that there may be several mechanisms at play that generally contribute to the generation of radio emission.
Conclusions. The comparison between the reconstructed sources of radio emission and the ambient shock wave characteristics reveals the complex relationship between shock parameters and show how they can influence the morphology of the observed type II radio emission.

Using radio triangulation to understand the origin of two subsequent type II radio bursts

Immanuel Christopher **Jebaraj**, Jasmina Magdalenic, Tatiana Podladchikova, Camilla Scolini, Jens Pomoell, Astrid Veronig, Karin Dissauer, Vratislav Krupar, Emilia Kilpua, Stefaan Poedts
A&A 639, A56 **2020**
https://arxiv.org/pdf/2006.04586.pdf
https://www.aanda.org/articles/aa/pdf/2020/07/aa37273-19.pdf
Context: Eruptive events such as coronal mass ejections (CMEs) and flares accelerate particles and generate shock waves which can arrive at Earth and can disturb the magnetosphere. Understanding the association between CMEs and CME-driven shocks is therefore highly important for space weather studies.
Aims: We present a study of the CME/flare event associated with two type II bursts observed on **September 27, 2012**. The aim of the study is to understand the relationship between the observed CME and the two distinct shock wave signatures.
Methods: The multi-wavelength study of the eruptive event (CME/flare) was complemented with radio triangulation of the associated radio emission and modelling of the CME and the shock wave employing MHD simulations.
Results: We found that, although temporal association between the type II bursts and the CME is good, the low-frequency type II(LF-type II) burst occurs significantly higher in the corona than the CME and its relationship to the CME is not straightforward. The analysis of the EIT wave (coronal bright front) shows the fastest wave component to be in the southeast quadrant of the Sun. This is also the quadrant in which the source positions of the LF-type II were found to be located, probably resulting from the interaction between the shock wave and a streamer.
Conclusions: The relationship between the CME/flare event and the shock wave signatures is discussed using the temporal association,as well as the spatial information of the radio emission. Further, we discuss the importance and possible effects of the frequently non-radial propagation of the shock wave.

Impulsively Generated Wave Trains in a Solar Coronal Loop

Petr **Jelinek** and Marian Karlicky
E-print, Sept 2010; IEEE Trans. Plasma Sci., 38(9), 2243, **2010**
Impulsively generated fast magnetoacoustic wave trains in a solar coronal loop are numerically studied. The problem is considered as 2-D in space, and for the description, the full set of magnetohydrodynamic (MHD) equations is used. The numerical solution of the MHD equations is performed by means of the LaxflWendroff algorithm on a uniformly structured mesh. The wavelet analysis of the obtained wave trains shows out the typical tadpole shapes, i.e., a narrow tail followed by a broadband head. In this paper, we discuss the propagation speed and periods of the wave trains as well as the shapes of the tadpoles in dependence on the plasma beta parameter. These studies are very important in connection with the observations because the **tadpole signatures**, firstly discovered during the solar eclipse in 1999 by the SECIS instrument, have been recently recognized also **in decimetric type IV** radio events by the Ondrejov radiospectrograph.

Modeling FETCH Observations of 2005 May 13 CME

Elizabeth A. **Jensen**, Ward B. Manchester IV, David B. Wexler, Jason E. Kooi, Teresa Nieves-Chinchilla, Lan K. Jian, Alexei Pevtsov, Shing Fung
ApJ **2022**
https://arxiv.org/pdf/2209.03350.pdf

This paper evaluates the quality of CME analysis that has been undertaken with the rare Faraday rotation observation of an eruption. Exploring the capability of the FETCH instrument hosted on the MOST mission, a four-satellite Faraday rotation radio sounding instrument deployed between the Earth and the Sun, we discuss the opportunities and challenges to improving the current analysis approaches.

The Comparison of Total Electron Content Between Radio and Thompson Scattering

E. A. **Jensen**, R. Frazin, C. Heiles, P. Lamy, A. Llebaria, J. D. Anderson, M. M. Bisi,R. A. Fallows
Solar Phys. **2016**

The total electron content (TEC) of the solar corona in June 2002 is calculated by three observational techniques and the results are compared. The first technique is solar rotational tomography (SRT) applied to a 14-day time series of LASCO-C2 polarized brightness images, and the other two techniques use the Cassini spacecraft radio beacon for Doppler tracking (phase delay) and ranging (group delay). While the Doppler-tracking technique has an arbitrary zero-point, it is otherwise found that the three methods produce consistent estimates of the TEC to within established uncertainties, providing an independent check on the calibrations. The verification of the accuracy of the Doppler-tracking technique enables a significant improvement to the use of spacecraft data sets in studying the heliosphere: the density component to Faraday rotation can be separated from the magnetic-field component as variable structures cross, such as coronal mass ejections and magnetohydrodynamic waves. Furthermore, we show that the unique frequency-time variable characteristics of the hydrodynamic components of waves can be studied. Based on this work, future Faraday rotation studies of variable solar phenomena will isolate the electron density changes from the magnetic-field contribution. This capability will enable advanced research into variable heliospheric magnetic fields.

Electromagnetic Waves near the Proton Cyclotron Frequency: STEREO Observations

L. K. **Jian**1,2, H. Y. Wei3, C. T. Russell3, J. G. Luhmann4, B. Klecker5, N. Omidi6, P. A. Isenberg7, M. L. Goldstein2, A. Figueroa-Viñas2, and X. Blanco-Cano
2014 ApJ 786 123

Transverse, near-circularly polarized, parallel-propagating electromagnetic waves around the proton cyclotron frequency were found sporadically in the solar wind throughout the inner heliosphere. They could play an important role in heating and accelerating the solar wind. These low-frequency waves (LFWs) are intermittent but often occur in prolonged bursts lasting over 10 minutes, named "LFW storms." Through a comprehensive survey of them from Solar Terrestrial Relations Observatory A using dynamic spectral wave analysis, we have identified 241 LFW storms in 2008, present 0.9% of the time. They are left-hand (LH) or right-hand (RH) polarized in the spacecraft frame with similar characteristics, probably due to Doppler shift of the same type of waves or waves of intrinsically different polarities. In rare cases, the opposite polarities are observed closely in time or even simultaneously. Having ruled out interplanetary coronal mass ejections, shocks, energetic particles, comets, planets, and interstellar ions as LFW sources, we discuss the remaining generation scenarios: LH ion cyclotron instability driven by greater perpendicular temperature than parallel temperature or by ring-beam distribution, and RH ion fire hose instability driven by inverse temperature anisotropy or by cool ion beams. The investigation of solar wind conditions is compromised by the bias of the one-dimensional Maxwellian fit used for plasma data calibration. However, the LFW storms are preferentially detected in rarefaction regions following fast winds and when the magnetic field is radial. This preference may be related to the ion cyclotron anisotropy instability in fast wind and the minimum in damping along the radial field.

Narrowband Pulsating Decimeter Structure Observed by the New Ondˇrejov Solar Radio Spectrograph

K. **Jiˇriˇcka** · M. Karlický
Solar Phys (**2008**) 253: 95–101, DOI 10.1007/s11207-008-9118-7

The new 0.8 – 2.0 GHz Ondˇrejov radio spectrograph with high time resolution (10 ms) is presented. As an example of first observations the 0.95 – 1.3 GHz narrowband pulsating structure with a characteristic quasi-period of about 150 ms, observed during the impulsive phase of the 9 June 2007 M1.0 flare, is shown. Some of the pulses show very fast but measurable frequency drift of about −17 GHz s^{-1}. The model of this pulsating structure, based on the tearing and coalescence processes in the current sheet, is briefly discussed.

DH type II radio bursts during solar cycles 23-25: Origin and association with solar eruptive events

Bhuwan **Joshi** (USO-PRL, India), Binal D. Patel (USO-PRL, India), Kyung-Suk Cho (KASI, South Korea), Rok-Soon Kim (KASI, South Korea)
Proceedings IAU Symposium No. 388 **2024**
https://arxiv.org/pdf/2409.02554

We analyses occurrence of DH type II solar radio bursts spanning over solar cycles 23-25 during which a total of 590 DH type II bursts are reported with confirmed 568 and 462 cases of associated CME and flares, respectively. We find short-term yet important differences in DH type II activity when the data is examined in terms of event counts and their durations, e.g., temporal shift in the peak activity during cycle 24 and variation in the growth rate of the activity level during cycle 25. For an in-depth exploration, DH type II bursts are classified in 3 categories based on their end-frequencies: Low-, Medium-, and High- Frequency Groups (LFG, MFG, and HFG, respectively). The HFG category is the most populous (~47 %) while the LFG category occupy about a quarter of the events (~24 %). The LFG events show a clear inclination toward fastest CMEs and X-class flares with a quarter of events exhibiting end frequency below 50 MHz.

Two-stage evolution of an extended C-class eruptive flaring activity from sigmoid active region NOAA 12734: SDO and Udaipur-CALLISTO observations

Bhuwan **Joshi** , Prabir K. Mitra , R. Bhattacharyya , Kushagra Upadhyay , Divya Oberoi , K. Sasikumar Raja , Christian Monstein

Solar Phys. **2021**

https://arxiv.org/pdf/2104.10947.pdf

We present a multi-wavelength investigation of a C-class flaring activity that occurred in the active region NOAA 12734 on **8 March 2019**. The investigation utilises data from AIA and HMI on board the SDO and the Udaipur-CALLISTO solar radio spectrograph of the Physical Research Laboratory. This low intensity C1.3 event is characterised by typical features of a long duration event (LDE), viz. extended flare arcade, large-scale two-ribbon structures and twin coronal dimmings. The eruptive event occurred in a coronal sigmoid and displayed two distinct stages of energy release, manifested in terms of temporal and spatial evolution. The formation of twin dimming regions are consistent with the eruption of a large flux rope with footpoints lying in the western and eastern edges of the coronal sigmoid. The metric radio observations obtained from Udaipur-CALLISTO reveals a broad-band (≈50-180 MHz), stationary plasma emission for ≈7 min during the second stage of the flaring activity that resemble a type IV radio burst. A type III decametre-hectometre radio bursts with starting frequency of ≈2.5 MHz precedes the stationary type IV burst observed by Udaipur-CALLISTO by ≈5 min. The synthesis of multi-wavelength observations and Non-Linear Force Free Field (NLFFF) coronal modelling together with magnetic decay index analysis suggests that the sigmoid flux rope underwent a zipping-like uprooting from its western to eastern footpoints in response to the overlying asymmetric magnetic field confinement. The asymmetrical eruption of the flux rope also accounts for the observed large-scale structures viz. apparent eastward shift of flare ribbons and post flare loops along the polarity inversion line (PIL), and provides an evidence for lateral progression of magnetic reconnection site as the eruption proceeds.

A Major Geoeffective CME from NOAA 12371: Initiation, CME–CME Interactions, and Interplanetary Consequences

Bhuwan **Joshi**, M. Syed Ibrahim, A. Shanmugaraju, D. Chakrabarty

Solar Physics July **2018**, 293:107

http://sci-hub.tw/http://link.springer.com/10.1007/s11207-018-1325-2

In this article, we present a multi-wavelength and multi-instrument investigation of a halo coronal mass ejection (CME) from active region NOAA 12371 on **21 June 2015** that led to a major geomagnetic storm of minimum Dst=−204Dst=−204 nT. The observations from the Atmospheric Imaging Assembly onboard the Solar Dynamics Observatory in the hot EUV channel of 94 Å confirm the CME to be associated with a coronal sigmoid that displayed an intense emission (T∼6T∼6 MK) from its core before the onset of the eruption. Multi-wavelength observations of the source active region suggest tether-cutting reconnection to be the primary triggering mechanism of the flux rope eruption. Interestingly, the flux rope eruption exhibited a two-phase evolution during which the “standard” large-scale flare reconnection process originated two composite M-class flares. The eruption of the flux rope is followed by the coronagraphic observation of a fast, halo CME with linear projected speed of 1366 km s−1. *The dynamic radio spectrum in the decameter-hectometer frequency range reveals multiple continuum-like enhancements in type II radio emission which imply the interaction of the CME with other preceding slow speed CMEs in the corona within ≈10≈10 – 90 R⊙90 R⊙.* The scenario of CME–CME interaction in the corona and interplanetary medium is further confirmed by the height–time plots of the CMEs occurring during 19 – 21 June. In situ measurements of solar wind magnetic field and plasma parameters at 1 AU exhibit two distinct magnetic clouds, separated by a magnetic hole. Synthesis of near-Sun observations, interplanetary radio emissions, and in situ measurements at 1 AU reveal complex processes of CME–CME interactions right from the source active region to the corona and interplanetary medium that have played a crucial role towards the large enhancement of the geoeffectiveness of the halo CME on 21 June 2015.

A Collection of German Science Interests in the Next Generation Very Large Array

M. **Kadler** (1), D. A. Riechers (2), A. K. Baczko (3,20), H. Beuther (4) +++

2023

https://arxiv.org/pdf/2311.10056.pdf

The Next Generation Very Large Array (ngVLA) is a planned radio interferometer providing unprecedented sensitivity at wavelengths between 21 cm and 3 mm. Its 263 antenna element array will be spatially distributed across North America to enable both superb low surface brightness recovery and sub-milliarcsecond angular resolution imaging. The project was developed by the international astronomy community under the lead of the National Radio Astronomy Observatory (NRAO), and is anticipated to be built between 2027 and 2037. Two workshops have been held in 2022 and 2023 with the goal to discuss and consolidate the scientific interests in the ngVLA within the German astronomical community. This community paper constitutes a collection of 41 science ideas which the German community aims to pursue with the ngVLA in the 2030s. This is not a complete list and the ideas are not developed at the level of a "Science Book", such that the present document is mainly to be considered a "living document", to provide a basis for further discussion within the community. As such, additional contributions are welcome, and will be considered for inclusion in future revisions.

Are Solar Energetic Particle Events and Type II Bursts Associated with Fast and Narrow Coronal Mass Ejections?

S. W. **Kahler**, A. G. Ling, N. Gopalswamy
Solar Physics September **2019**, 294:134 **File**
https://doi.org/10.1007/s11207-019-1518-3
sci-hub.se/10.1007/s11207-019-1518-3
Gradual solar energetic (E>10 MeV) particle (SEP) events and metric through kilometric wavelength type II radio bursts are usually associated with shocks driven by fast (V≥900 kms−1) and wide (W≥60∘) coronal mass ejections (FW CMEs). This criterion was established empirically by several studies from solar cycle 23. The characteristic Alfvén speed in the corona, which ranges over 500 – 1500 km s−1 at heights ≥2 Ro, provides the minimum V requirement for a CME to drive a shock, but the general absence of SEP events or type II bursts with fast and narrow (W<60∘) CMEs has not been explained. We review and confirm the earlier studies with a more comprehensive comparison of SEP events and type II bursts with fast and narrow (FN) CMEs. We offer an explanation for the lack of SEP event and type II burst associations with FN CMEs in terms of recent heuristic arguments and modeling that show that the response of a magnetized plasma to the propagation of a CME depends on the CME geometry as well as on its speed. A clear distinction is made between a projectile that propagates through the medium to produce a bow shock, and a 3D piston that everywhere accumulates material to produce a broad shock and sheath. The bow shock is unfavorable for producing SEP events and type II bursts, but the 60∘ cut-off is not explained.

SOLAR RADIO BURST AND SOLAR WIND ASSOCIATIONS WITH INFERRED NEAR-RELATIVISTIC ELECTRON INJECTIONS

S. W. **Kahler**, H. Aurass, G. Mann, A. Klassen
The Astrophysical Journal, 656:567Y576, **2007**, File
The solar injections of near-relativistic (NR) electron events observed at 1 AU appear to be systematically delayed by ~10 minutes from the associated flare impulsive phases.
Electron events with long (_2 hr) beaming times at 1 AU are preferentially associated with type II bursts, which supports the possibility of a class of shock-accelerated NR electron events.

Kinematic study of radio-loud CMEs associated with solar flares and DH type II radio emissions during solar cycles 23 and 24

P. Pappa **Kalaivani**, O. Prakash, A. Shanmugaraju, G. Michalek, G. Selvarani
Solar Phys. **297**, Article number: 57 **2022**
https://arxiv.org/pdf/2204.07968.pdf
https://doi.org/10.1007/s11207-022-01985-8
We have statistically analyzed 379 radio-loud (RL) CMEs and their associated flares during the period 1996 - 2019 covering both solar cycles (SC) 23 and 24. We classified them into two sets of populations based on the observation period: i) 235 events belong to SC 23 (August 1996 - December 2008) and ii) 144 events belong to SC 24 (January 2009 - December 2019). The average residual acceleration of RL CMEs in SC 24 (--17.39 ± 43.51 m s−2) is two times lower than that of the RL CMEs in SC 23 (--8.29 ± 36.23 m s−2), which means that deceleration of RL CMEs in SC 24 is twice as fast as in SC 23. RL CMEs of SC 23 (1443 ± 504 km s−1; 13.82 ± 7.40 \emph{R}⊙) reach their peak speed at higher altitudes than RL CMEs of SC 24 (1920 ± 649 km s−1; 12.51 ± 7.41 \emph{R}⊙).We also observed that the mean apparent widths of RL CMEs in SC 23 are less than in SC 24which is statistically significant. SC 23 has a lower average CME nose height (3.85 \emph{R}⊙) at the start time of DH type II bursts than that of SC 24 (3.46 \emph{R}⊙). The starting frequencies of DH type II bursts associated with RL CMEs for SC 24 are significantly larger (formed at lower heights) than that of SC 23. We found that there is a good correlation between the drift rates and the mid-frequencies of DH type II radio bursts for both the solar cycles (\emph{R} = 0.80, ϵ = 1.53). Most of the RL CMEs kinematics and their associated solar flare properties are found similar for SC 23 and SC 24. We concluded that the reduced total pressure in the heliosphere for SC 24 enables RL CMEs to expand wider and decelerate faster, resulting in DH type II radio emissions at lower heights than SC 23.

Analysis of type II and type III radio bursts associated with SEPs from non-interacting/interacting radio-loud CMEs

P Pappa **Kalaivani**, O Prakash, A Shanmugaraju, Li Feng, Lei Lu, Weiqun Gan, G Michalek
Astrophysics **2021**
https://arxiv.org/pdf/2107.09955.pdf
We analyze radio bursts observed in events with interacting/non-interacting CMEs that produced major SEPs (Ip > 10 MeV) fromApril 1997 to December 2014.We compare properties of meter (m), deca-hectometer (DH) type II as well as DH type III bursts, and time lags for interacting-CME-associated (IC) events and non-interacting-CME-associated (NIC) events. About 70\% of radio emissions were observed in events of both types from meters to kilometers. We found high correlations between the drift rates and mid-frequencies of type II radio bursts calculated as the mean geometric between their starting and ending frequencies for both NIC and IC-associated events (Correlation coefficient \textit{R}2 = 0.98, power-law index ε = 1.68 ± 0.16 and \textit{R}2 = 0.93, ε = 1.64 ± 0.19 respectively).We also found a correlation between the frequency drift rates of DH type II bursts and space speeds of CMEs in NIC-associated events. The absence of such correlation for IC-associated events confirms that the shock speeds changed in CME--CME interactions. For the events with western source locations, the mean peak intensity of SEPs in IC-associated events is four times larger than that in NIC-associated SEP events. From the mean time lags between the start times of SEP events and the start of m, DH type II, and DH type III radio bursts, we inferred that particle enhancements in NIC-associated SEP events occurred earlier than in IC-associated SEP events. The difference between NIC events and IC events in the mean values of parameters of type II and type III bursts is statistically insignificant. **18 Apr 2014**

First Type III Solar Radio Bursts of Solar Cycle 25

Juha **Kallunki**, Derek McKay & Merja Tornikoski
Solar Physics volume 296, Article number: 57 (**2021**)
https://doi.org/10.1007/s11207-021-01790-9
https://link.springer.com/content/pdf/10.1007/s11207-021-01790-9.pdf
The minimum of the previous solar cycle, Solar Cycle 24, occurred in December 2019, which also marked the start of the new Solar Cycle 25. The first radio bursts of the new solar cycle were observed in the spring season 2020. In this work we will present three type III solar bursts which were observed in May and June 2020 at radio frequencies between 18 – 90 MHz. There are two radio observatories in Finland that are capable of doing low-frequency solar radio observations: Aalto University Metsähovi Radio Observatory (MRO) and Kilpisjärvi Atmospheric Imaging Receiver Array (KAIRA) of the Sodankylä Geophysical Observatory, University of Oulu. The instruments of the two institutes have different design and characteristics, and they operate in rather different radio interference environments. We will compare simultaneous observations from these two instruments and we will also discuss the properties of these type III solar bursts. **2020-05-28-29, 2020-06-05**

Identifying 8 mm Radio Brightenings During the Solar Activity Minimum

Juha **Kallunki**, Merja Tornikoski & Irene Björklund
Solar Physics volume 295, Article number: 105 (**2020**)
https://link.springer.com/content/pdf/10.1007/s11207-020-01673-5.pdf
Strong solar radio brightenings have been extensively studied in the past, and their correlation to the sunspots and active regions are already well known. But even when the Sun is ostensibly quiet, there is practically always some activity that can be detected in the radio domain. In this article we investigate these semi-active features at 8 mm using the radio telescope at Aalto University Metsähovi Radio Observatory. The observations were made between May and September 2019 when the solar activity was very low, and for our detailed study we chose dates when no active regions were identified on the solar surface by the National Oceanic and Atmospheric Administration. The brightness temperature of these radio regions during this quiescent period of solar activity is at maximum approximately 250 K above the quiet-Sun level. We compared our millimeter data with data taken in extreme ultraviolet, and we found that these weak radio brightenings are mostly related to coronal hole features and magnetic bright points. We also found that there are two different categories of bright points: those with and without flux tube structure. The formation of the weak radio brightenings is comparable to the stronger radio brightenings: the rising fluxes from the weak photospheric features can be detected as a radio source. **30 May 2019, 2 June 2019, 16 June 2019**
Table 2 A summary of detected radio brightenings at 8 mm that correlate with coronal holes (2019).

Solar polarization observations at 3 and 13 mm

Kallunki, Juha; Tornikoski, Merja; Kirves, Petri; Oinaskallio, Erkki; Aatrokoski, Juha; Mujunen, Ari; Tammi, Joni
Astronomische Nachrichten, Volume 341, Issue 1, pp. 118-124, **2020**
https://onlinelibrary.wiley.com/doi/pdf/10.1002/asna.202013684
The first solar radio polarization observations at 3 mm (86 GHz) and 13 mm (22 GHz) were made at Aalto University Metsähovi Radio Observatory in Finland in spring 2019. This was the first time that 3 mm (86 GHz) and 13 mm (1.3

cm) solar polarization observations were made with the same radio telescope. In this paper, we describe the observing system and data analysis, and present the first results. We also compare our data with polarization observations made with the Nobeyama Radioheliograph and find that the results are consistent. Additionally, we determine the quiet Sun level brightness temperature at 3 mm (86 GHz) using the New Moon for reference, and obtain a mean value of 6,310 K.
April 4, 2019, May 9, 2019
CESRA #2549 Apr 2020 http://www.astro.gla.ac.uk/users/eduard/cesra/?p=2549

Measurements of the Quiet-Sun Level Brightness Temperature at 8 mm

J. **Kallunki**, M. Tornikoski
Solar Physics November **2018**, 293:156
https://link.springer.com/content/pdf/10.1007%2Fs11207-018-1380-8.pdf
Defining the solar brightness temperature accurately at millimeter wavelengths has always been challenging. One of the main reasons has been the lack of a proper calibration source. New Moon was used earlier as a calibration source. We carried out a new extensive set of observations at 8 mm using the New Moon for calibration. The solar and Moon observations were made using the 14-meter radiotelescope operated by the Aalto University Metsähovi Radio Observatory in Finland. In this article, we present our method for defining the brightness temperature of the quiet-Sun level (QSL). Based on these observations, we found 8100 K±300 K8100 K±300 K to be the mean value for the QSL temperature. This value is between the values that were reported in earlier studies. **17 March 2018, 2018-05-14**

Eruptive Solar Prominence at 37 GHz

J. **Kallunki**, M. Tornikoski
Solar Physics July **2017**, 292:84
On **27 June 2012**, an eruptive solar prominence was observed in the extreme ultraviolet (EUV) and radio wavebands. At the Aalto University Metsähovi Radio Observatory (MRO) it was observed at 37 GHz. It was the first time that the MRO followed a radio prominence with dense sampling in the millimetre wavelengths. This prompted us to study the connection of the 37 GHz event with other wavelength domains. At 37 GHz, the prominence was tracked to a height of around 1.6 R⊙1.6 R⊙, at which the loop structure collapsed. The average velocity of the radio prominence was 55±6 kms−155±6 kms−1. The brightness temperature of the prominence varied between 800±100800±100 K and 3200±1003200±100 K. We compared our data with the Solar Dynamic Observatory (SDO)/Atmospheric Imaging Assembly (AIA) instrument's 304 Å EUV data, and found that the prominence behaves very similarly in both wavelengths. The EUV data also reveal flaring activity nearby the prominence. We present a scenario in which this flare works as a trigger that causes the prominence to move from a stable stage to an acceleration stage.

Daily solar mm-observations at Aalto University Metsahovi Radio Observatory

Juha **Kallunki** and Minttu Uunila:
RHESSI Nugget No. 248, March **2015**
http://sprg.ssl.berkeley.edu/~tohban/wiki/index.php/Daily_solar_mm-observations_at_Aalto_University_Metsähovi_Radio_Observatory
The Aalto University Metsähovi Radio Observatory has been actively doing solar observations since 1978 at 37 GHz, and we note that high radio frequencies are particularly interesting in the RHESSI context. Currently we do continuous solar observations at 11.2 GHz and 50-845 MHz, and produce daily solar maps at 37 GHz. Due to MRO's far-Northern location 14-hour long solar observations are possible during summers..

Radio pulsating structures with coronal loop contraction

J. **Kallunki**1 · S. Pohjolainen
E-print, April **2012**; Solar Phys., October **2012**, Volume 280, Issue 2, pp 491-507
We present a multi-wavelength study of a solar eruption event on **20 July 2004**, comprising observations in Ha, EUV, soft X-rays, and in radio waves with a wide frequency range. The analysed data show both oscillatory patterns and shock wave signatures during the impulsive phase of the flare. At the same time, large-scale EUV loops located above the active region were observed to contract. Quasi-periodic pulsations with 10 and 15 s oscillation periods were detected both in microwave–millimeter waves and in decimeter–meter waves. Our calculations show that MHD oscillations in the large EUV loops – but not likely in the largest contracting loops – could have produced the observed periodicity in radio emission, by triggering periodic magnetic reconnection and accelerating particles. As the plasma emission in decimeter–meter waves traces the accelerated particle beams and the microwave emission shows a typical gyrosynchrotron flux spectrum (emission created by trapped electrons within the flare loop), we find that the particles responsible for the two different types of emission could have been accelerated in the same process. Radio imaging of the pulsed decimetric–metric emission and the shock-generated radio type II burst in the same wavelength range suggest a rather complex scenario for the emission processes and locations. The observed locations cannot be explained

by the standard model of flare loops with an erupting plasmoid located above them, driving a shock wave at the CME front.

Microwave response to kink oscillations of a plasma slab

T. I. **Kaltman**, E. G. Kupriyanova
MNRAS Volume 520, Issue 3, Pages 4147–4153, **2023**
https://arxiv.org/pdf/2302.00451.pdf
https://doi.org/10.1093/mnras/stad421
The modulation of the intensity of microwave emission from a plasma slab caused by a standing linear kink fast magnetoacoustic wave is considered. The slab is stretched along a straight magnetic field, and can represent, for example, a current sheet in a flaring active region in corona of the Sun, or a streamer or pseudostreamer stalk. The plasma density is non-uniform in the perpendicular direction and described by a symmetric Epstein profile. The plasma parameter β is taken to be zero, which is a good approximation for solar coronal active regions. The microwave emission is caused by mildly relativistic electrons which occupy a layer within the oscillating slab and radiate via the gyrosynchrotron (GS) mechanism. Light curves of the microwave emission were simulated in the optically thin part of the GS spectrum, and their typical Fourier spectra were analysed. It is shown that the microwave response to a linear kink magnetohydrodynamic wave is non-linear. It is found that, while the microwave light curves at the node oscillate with the same frequency as the frequency of the perturbing kink mode, the frequency of the microwave oscillations at the anti-node is two times higher than the kink oscillation frequency. Gradual transformation the one type of the light curves to another occurs when sliding from the node to the anti-node. This result does not depend on the width of the GS-emitting layer inside the oscillating slab. This finding should be considered in the interpretation of microwave quasi-periodic pulsations in solar and stellar flares.

Solar plasma diagnostics: magnetosphere of active regions with RATAN-600 microwave observations

Tatyana **Kaltman**_1, Vladimir Bogod1, Leonid Yasnov2, Alexei Stupishin2, Anatoly Korzhavin1, and Natalia Peterova1
CESRA **2016**, p.95
http://cesra2016.sciencesconf.org/conference/cesra2016/pages/CESRA2016_prog_abs_book_v3.pdf
The active regions on the Sun are the complex 3-D formations, including the totality of magnetic phenomena: the con_guration of the spots on the photosphere and the magnetic structure extending through the chromosphere into the corona with di_erent substructures of closed and open magnetic _elds. The spectral-polarization microwave measurements with RATAN-600 test the physical conditions in the various structures of the active regions mag-netosphere measuring their emission spectra, degree of polarization, brightness temperature and size. We present the possibilities to analyse thermal cyclotron radiation of the spots, the bremsstrahlung emission of the plages and coronal loops, and long lasting nonthermal processes of energy release in stable active regions. We demonstrate this by examples of recent observations of several active regions.

The Self-Inversion of the Sign of Circular Polarization in flHalofl Microwave Sources

T. I. **Kaltman,** A. N. Korzhavin, N. G. Peterova
Solar Phys. 242(1-2), Page: 125 – 142, **2007.**

Detection of Propagating Fast Sausage Waves through Detailed Analysis of a Zebra-pattern Fine Structure in a Solar Radio Burst

K. **Kaneda**1, H. Misawa1, K. Iwai2, S. Masuda2, F. Tsuchiya1, Y. Katoh3, and T. Obara
2018 ApJL 855 L29
http://sci-hub.tw/http://iopscience.iop.org/2041-8205/855/2/L29/
Various magnetohydrodynamic (MHD) waves have recently been detected in the solar corona and investigated intensively in the context of coronal heating and coronal seismology. In this Letter, we report the first detection of short-period propagating fast sausage mode waves in a metric radio spectral fine structure observed with the Assembly of Metric-band Aperture Telescope and Real-time Analysis System. Analysis of Zebra patterns (ZPs) in a type-IV burst revealed a quasi-periodic modulation in the frequency separation between the adjacent stripes of the ZPs (Δf). The observed quasi-periodic modulation had a period of 1–2 s and exhibited a characteristic negative frequency drift with a rate of 3–8 MHz s−1. Based on the double plasma resonance model, the most accepted generation model of ZPs, the observed quasi-periodic modulation of the ZP can be interpreted in terms of fast sausage mode waves propagating

upward at phase speeds of 3000–8000 km s−1. These results provide us with new insights for probing the fine structure of coronal loops. **2011 June 21**

Polarization Characteristics of Zebra Patterns in Type IV Solar Radio Bursts

K. **Kaneda**1, H. Misawa1, K. Iwai2, F. Tsuchiya1, T. Obara1, Y. Katoh3, and S. Masuda4
2017 ApJ 842 45
http://sci-hub.cc/10.3847/1538-4357/aa74c1
https://arxiv.org/ftp/arxiv/papers/1508/1508.02604.pdf
https://arxiv.org/ftp/arxiv/papers/1707/1707.00414.pdf
The polarization characteristics of zebra patterns (ZPs) in type IV solar bursts were studied. We analyzed 21 ZP events observed by the Assembly of Metric-band Aperture Telescope and Real-time Analysis System between 2010 and 2015 and identified the following characteristics: a degree of circular polarization (DCP) in the range of 0%–70%, a temporal delay of 0–70 ms between the two circularly polarized components (i.e., the right- and left-handed components), and dominant ordinary-mode emission in about 81% of the events. For most events, the relation between the dominant and delayed components could be interpreted in the framework of fundamental plasma emission and depolarization during propagation, though the values of DCP and delay were distributed across wide ranges. Furthermore, it was found that the DCP and delay were positively correlated (rank correlation coefficient R = 0.62). As a possible interpretation of this relationship, we considered a model based on depolarization due to reflections at sharp density boundaries assuming fundamental plasma emission. The model calculations of depolarization including multiple reflections and group delay during propagation in the inhomogeneous corona showed that the DCP and delay decreased as the number of reflections increased, which is consistent with the observational results. The dispersive polarization characteristics could be explained by the different numbers of reflections causing depolarization. **21 June 2011, 2011 September 6**
Table 1 ZP Events and Their General Characteristics (2011-2015)

Frequency Dependence of Polarization of Zebra Pattern in Type-IV Solar Radio Bursts

Kazutaka **Kaneda**1, H. Misawa1, K. Iwai2, F. Tsuchiya1, and T. Obara
2015 ApJ 808 L45
http://arxiv.org/ftp/arxiv/papers/1508/1508.02604.pdf
https://arxiv.org/ftp/arxiv/papers/1508/1508.02604.pdf
We investigated the polarization characteristics of a zebra pattern (ZP) in a type-IV solar radio burst observed with AMATERAS on **2011 June 21** for the purpose of evaluating the generation processes of ZPs. Analyzing highly resolved spectral and polarization data revealed the frequency dependence of the degree of circular polarization and the delay between two polarized components for the first time. The degree of circular polarization was 50%–70% right-handed and it varied little as a function of frequency. Cross-correlation analysis determined that the left-handed circularly polarized component was delayed by 50–70 ms relative to the right-handed component over the entire frequency range of the ZP and this delay increased with the frequency. We examined the obtained polarization characteristics by using pre-existing ZP models and ***concluded that the ZP was generated by the double-plasma-resonance process.*** Our results suggest that the ZP emission was originally generated in a completely polarized state in the O-mode and was partly converted into the X-mode near the source. Subsequently, the difference between the group velocities of the O-mode and X-mode caused the temporal delay.

Spectropolarimetric Radio Imaging of Faint Gyrosynchrotron Emission from a CME : A Possible Indication of the Insufficiency of Homogeneous Models

Devojyoti **Kansabanik**, Surajit Mondal, Divya Oberoi
ApJ **968** 55 **2024**
https://arxiv.org/pdf/2404.14714.pdf
https://iopscience.iop.org/article/10.3847/1538-4357/ad43e9/pdf
The geo-effectiveness of coronal mass ejections (CMEs) is determined primarily by their magnetic fields. Modeling of Gyrosynchrotron (GS) emission is a promising remote sensing technique to measure the CME magnetic field at coronal heights. However, faint GS emission from CME flux ropes is hard to detect in the presence of bright solar emission from the solar corona. With high dynamic-range spectropolarimetric meter wavelength solar images provided by the Murchison Widefield Array, we have detected faint GS emission from a CME out to ∼8.3 R⊙, the largest heliocentric distance reported to date. High-fidelity polarimetric calibration also allowed us to robustly detect circularly polarized emission from GS emission. For the first time in literature, Stokes V detection has jointly been used with Stokes I spectra to constrain GS models. One expects that the inclusion of polarimetric measurement will provide tighter constraints on GS model parameters. Instead, we found that homogeneous GS models, which have been used in all prior works, are unable to model both the total intensity and circular polarized emission simultaneously. This strongly suggests the need for using inhomogeneous GS models to robustly estimate the CME magnetic field and plasma parameters. **3-4 May 2014**
CESRA #3871 2024 **https://www.astro.gla.ac.uk/users/eduard/cesra/?p=3871**

Spectroscopic Imaging of the Sun with MeerKAT: Opening a New Frontier in Solar Physics

Devojyoti **Kansabanik**1, Surajit Mondal2, Divya Oberoi1, James O. Chibueze3,4,5, N. E. Engelbrecht4, R. D. Strauss4, E. P. Kontar6, G. J. J. Botha7, P. J. Steyn4, and Amoré E. Nel8

2024 ApJ 961 96

https://iopscience.iop.org/article/10.3847/1538-4357/ad0b7f/pdf

Solar radio emissions provide several unique diagnostics to estimate different physical parameters of the solar corona, which are otherwise simply inaccessible. However, imaging the highly dynamic solar coronal emissions spanning a large range of angular scales at radio wavelengths is extremely challenging. At gigahertz frequencies, MeerKAT radio telescope is possibly globally the best-suited instrument at present for providing high-fidelity spectroscopic snapshot solar images. Here, we present the first published spectroscopic images of the Sun made using the observations with MeerKAT in the 880–1670 MHz band. This work demonstrates the high fidelity of spectroscopic snapshot MeerKAT solar images through a comparison with simulated radio images at MeerKAT frequencies. The observed images show extremely good morphological similarities with the simulated images. Our analysis shows that below ∼900 MHz MeerKAT images can recover essentially the entire flux density from the large angular-scale solar disk. Not surprisingly, at higher frequencies, the missing flux density can be as large as ∼50%. However, it can potentially be estimated and corrected for. We believe once solar observation with MeerKAT is commissioned, it will enable a host of novel studies, open the door to a large unexplored phase space with significant discovery potential, and also pave the way for solar science with the upcoming Square Kilometre Array-Mid telescope, of which MeerKAT is a precursor.

2020 September 26-27

CESRA Nugget #3746 Apr 2024 https://www.astro.gla.ac.uk/users/eduard/cesra/?p=3746

Deciphering Radio Emission from Solar Coronal Mass Ejections using High-fidelity Spectropolarimetric Radio Imaging

Devojyoti **Kansabanik**

Submitted at Tata Institute of Fundamental Research, Mumbai, India, Ph.D Thesis **2023**

https://arxiv.org/pdf/2310.16072.pdf

Coronal mass ejections (CMEs) are large-scale expulsions of plasma and magnetic fields from the Sun into the heliosphere and are the most important driver of space weather. The geo-effectiveness of a CME is primarily determined by its magnetic field strength and topology. Measurement of CME magnetic fields, both in the corona and heliosphere, is essential for improving space weather forecasting. Observations at radio wavelengths can provide several remote measurement tools for estimating both strength and topology of the CME magnetic fields. Among them, gyrosynchrotron (GS) emission produced by mildly-relativistic electrons trapped in CME magnetic fields is one of the promising methods to estimate magnetic field strength of CMEs at lower and middle coronal heights. However, GS emissions from some parts of the CME are much fainter than the quiet Sun emission and require high dynamic range (DR) imaging for their detection. This thesis presents a state-of-the-art calibration and imaging algorithm capable of routinely producing high DR spectropolarimetric snapshot solar radio images using data from a new technology radio telescope, the Murchison Widefield Array. This allows us to detect much fainter GS emissions from CME plasma at much higher coronal heights. For the first time, robust circular polarization measurements have been jointly used with total intensity measurements to constrain the GS model parameters, which has significantly improved the robustness of the estimated GS model parameters. A piece of observational evidence is also found that routinely used homogeneous and isotropic GS models may not always be sufficient to model the observations. In the future, with upcoming sensitive telescopes and physics-based forward models, it should be possible to relax some of these assumptions and make this method more robust for estimating CME plasma parameters at coronal heights.

Spectroscopic Imaging of the Sun with MeerKAT: Opening a New Frontier in Solar Physics

Devojyoti **Kansabanik**, Surajit Mondal, Divya Oberoi, James O. Chibueze, N. E. Engelbrecht, R. D. Strauss, Eduard P. Kontar, Gert J. J. Botha, Ruhann Steyn

ApJ **961** 96 **2024**

https://arxiv.org/pdf/2307.01895.pdf

https://iopscience.iop.org/article/10.3847/1538-4357/ad0b7f/pdf

Solar radio emissions provide several unique diagnostics to estimate different physical parameters of the solar corona, which are otherwise simply inaccessible. However, imaging the highly dynamic solar coronal emissions spanning a large range of angular scales at radio wavelengths is extremely challenging. At GHz frequencies, the MeerKAT radio telescope is possibly globally the best-suited instrument at the present time and can provide high-fidelity spectroscopic snapshot solar images. Here, we present the first images of the Sun made using the observations with the MeerKAT at L-band (856 -- 1711 MHz). This work demonstrates the high fidelity of the MeerKAT solar images through a comparison with simulated radio images at the MeerKAT frequencies. The observed images show extremely good

mophological similarities with the simulated images. A detailed comparison between the simulated radio map and observed MeerKAT radio images demonstrates that there is significant missing flux density in MeerKAT images at the higher frequencies of the observing band, though it can potentially be estimated and corrected for. We believe once solar observations with the MeerKAT are commissioned, they will not only enable a host of novel studies but also open the door to a large unexplored phase space with significant discovery potential. **24-30 Sep 2020**

Space Weather Research using Spectropolarimetric Radio Imaging Combined With Aditya-L1 and PUNCH Missions

Devojyoti **Kansabanik**, Surajit Mondal, Divya Oberoi, Puja Majee

Conference proceedings, The 21st Cambridge Workshop on Cool Stars, Stellar Systems, and the Sun, Edited by A. S. Brun, J. Bouvier, P. Petit **2023**

https://arxiv.org/pdf/2301.13673.pdf

Low-frequency radio observations have been expected to serve as a powerful tool for Space Weather (SW) observations for decades. Radio observations are sensitive to a wide range of SW-related observations ranging from emissions from coronal mass ejections (CMEs) to the solar wind. Ground-based radio observatories allow one gathering of high-sensitivity data at high time and spectral resolution for an extended period, which remains a challenge for most space-based observatories. While radio techniques like Interplanetary Scintillation (IPS) are well established, radio imaging studies have remained technically challenging. This is now changing with the confluence of data from instruments, like the Murchison Widefield Array (MWA), and robust unsupervised analysis pipelines. This pipeline delivers full Stokes radio images with unprecedented fidelity and dynamic range. This will serve as a powerful tool for coronal and heliospheric studies. We present the recent developments and achievements to measure the magnetic fields of the CME plasma and shock front at coronal heights and also share the current status of the objective to measure the heliospheric Faraday rotation towards numerous background linearly polarised radio sources with the Sun in the field of view. We envision that in the coming years, the availability of new-generation radio instruments combined with the Aditya-L1 and PUNCH mission will mark the start of a new era in Space Weather modeling and prediction. **4 May 2014, 28 Sep 2014**

Deciphering Faint Gyrosynchrotron Emission from Coronal Mass Ejection using Spectro-polarimetric Radio Imaging

Devojyoti **Kansabanik**, Surajit Mondal, Divya Oberoi

ApJ **950** 164 **2023**

https://arxiv.org/pdf/2301.06522.pdf

https://iopscience.iop.org/article/10.3847/1538-4357/acc385/pdf

Measurements of the plasma parameters of coronal mass ejections (CMEs), particularly the magnetic field and non-thermal electron population entrained in the CME plasma, are crucial to understand their propagation, evolution, and geo-effectiveness. Spectral modeling of gyrosynchrotron (GS) emission from CME plasma has been regarded as one of the most promising remote sensing technique for estimating spatially resolved CME plasma parameters. Imaging the very low flux density CME GS emission in close proximity to the Sun with orders of magnitude higher flux density, however, has proven to be rather challenging. This challenge has only recently been met using the high dynamic range imaging capability of the Murchison Widefield Array (MWA). Although routine detection of GS is now within reach, the challenge has shifted to constraining the large number of free parameters in GS models, a few of which are degenerate, using the limited number of spectral points at which the observations are typically available. These degeneracies can be broken using polarimetric imaging. For the first time, we demonstrate this using our recently developed capability of high fidelity polarimetric imaging on the data from the MWA. We show that, in addition to breaking the degeneracies, spectro-polarimetric spectroscopic imaging also yields tighter constraints on the plasma parameters of key interest than possible with total intensity spectroscopic imaging alone. **4 May 2014**

CESRA #3666 **2023** https://www.astro.gla.ac.uk/users/eduard/cesra/?p=3666

Tackling the Unique Challenges of Low-frequency Solar Polarimetry with the Square Kilometre Array Low Precursor: Pipeline Implementation

Devojyoti **Kansabanik**, Apurba Bera, Divya Oberoi, Surajit Mondal

ApJ **264** 47 **2023**

https://arxiv.org/pdf/2209.06666.pdf

https://iopscience.iop.org/article/10.3847/1538-4365/acac79/pdf

The dynamics and the structure of the solar corona are determined by its magnetic field. Measuring coronal magnetic fields is, however, extremely hard. The polarization of the low-frequency radio emissions is one of the few observational probes of magnetic fields in the mid and high corona. Polarimetric calibration and imaging of the Sun at these frequencies is challenging. The brightness temperature and degree of polarization of the low-frequency solar radio emissions can vary by several orders of magnitude. These emissions also show dramatic spectral and temporal variations. Hence, to study these radio emissions, one needs high dynamic range spectro-polarimetric snapshot imaging.

The Murchison Widefield Array (MWA), a Square Kilometre Array (SKA) precursor, is exceptionally well-suited for this purpose. Calibration and imaging of solar data to extract this information are, however, significant challenges in themselves - requiring a deep understanding of the instrument, capable sophisticated algorithms, and their reliable implementation. To meet these challenges we have developed an unsupervised and robust polarization calibration and imaging software pipeline. Here we present the architecture and some implementation details of this pipeline. It delivers high-fidelity and high-dynamic-range full polarimetric solar radio images at high spectro-temporal resolutions. We expect this pipeline to enable exciting new science with instruments like the MWA. We also hope that by not requiring a significant prior background in radio interferometric imaging, this pipeline will encourage wider use of radio imaging data in the larger solar physics community. The algorithm implemented here can easily be adapted for future arrays like the SKA.

Working Principle of the Calibration Algorithm for High Dynamic Range Solar Imaging with *Square Kilometre Array Precursor*

Devojyoti **Kansabanik**

Solar Phys. **297**, Article number: 122 **2022**

https://arxiv.org/pdf/2207.11665.pdf

Imaging the low-frequency radio Sun is an intrinsically challenging problem. Meter wavelength solar emission span angular scales from a few arcminutes to a few degrees. These emissions show temporal and spectral variability in sub-second and sub-MHz scales. The brightness temperature of these emissions also varies by many orders of magnitude, which requires high-dynamic-range spectroscopic snapshot imaging. With the unique array configuration of the Murchison Widefield Array (MWA), and the robust calibration and imaging pipeline, AIRCARS produces the best spectroscopic snapshot solar images available to date. The working principle and the strength of this algorithm are demonstrated using statistical analysis and simulation. AIRCARS uses the partial phase stability of the MWA, which has a compact core with a large number of antenna elements distributed over a small array footprint. The strength of this algorithm makes it a state of the art calibration and imaging pipeline for low-frequency solar imaging, which is expected to be highly suitable for the upcoming Square Kilometre Array (SKA) and other future radio interferometers for producing high-dynamic-range and high-fidelity images of the Sun. **2014 May 05, 2015 November 11**

A novel algorithm for high fidelity spectro-polarimetric snapshot imaging of the low-frequency radio Sun using SKA-low precursor

Devojyoti **Kansabanik**, Divya Oberoi, Surajit Mondal

2022 3rd URSI Atlantic and Asia Pacific Radio Science Meeting (AT-AP-RASC)

https://arxiv.org/pdf/2207.11924.pdf

Magnetic field couples the solar interior to the solar atmosphere, known as the corona. The coronal magnetic field is one of the crucial parameters which determines the coronal structures and regulates the space weather phenomena like flares, coronal mass ejections, energetic particle events, and solar winds. Measuring the magnetic field at middle and higher coronal heights are extremely difficult problem and to date there is no single measurement technique available to measure the higher coronal magnetic fields routinely. polarization measurements of the low-frequency radio emissions are an ideal tool to probe the coronal magnetic fields at higher coronal heights (>1R⊙). To date, most of the low-frequency polarization observations of the Sun were limited to bright solar radio bursts. Here we developed a novel algorithm for performing precise polarization calibration of the solar observations done with the Murchison Widefield Array, a future Square Kilometer Array (SKA) precursor. We have brought down the instrumental polarization <1%. We anticipate this method will allow us to detect very low-level polarised emissions from coronal thermal emissions, which will become a tool for routine measurements of the global coronal magnetic fields at higher coronal heights. This method can be easily adapted for future SKA and open a window of new discoveries using high fidelity spectro-polarimetric snapshot imaging of the Sun at low radio frequencies. **28 Sep, 24 Oct, 3 Nov 2014**

Tackling the Unique Challenges of Low-Frequency Solar-Polarimetry with SKA-Low Precursor : The Algorithm

Devojyoti **Kansabanik**, Divya Oberoi, Surajit Mondal

ApJ **932** 110 **2022**

https://arxiv.org/pdf/2204.04578.pdf

https://iopscience.iop.org/article/10.3847/1538-4357/ac6758/pdf

Coronal magnetic fields are well known to be one of the crucial parameters defining coronal physics and space weather. However, measuring the global coronal magnetic fields remains challenging. The polarization properties of coronal radio emissions are sensitive to coronal magnetic fields. While they can prove to be useful probes of coronal and heliospheric magnetic fields, their usage has been limited by technical and algorithmic challenges. We present a robust algorithm for precise polarization calibration and imaging of low-radio frequency solar observations and demonstrate it on data from the Murchison Widefield Array, a Square Kilometer Array (SKA) precursor. This algorithm is based on the {\it Measurement Equation} framework, which forms the basis of all modern radio interferometric calibration and imaging. It delivers high dynamic range and fidelity full Stokes solar radio images with instrumental polarization

leakages <1%, on par with general astronomical radio imaging, and represents the state-of-the-art. Opening up this rewarding, yet unexplored, phase space will enable multiple novel science investigations and offer considerable discovery potential. Examples include detection of low-level of circularly polarization from thermal coronal emission to estimate large-scale quiescent coronal fields; polarization of faint gyrosynchrotron emissions from coronal mass ejections for robust estimation of plasma parameters; and detection of the first-ever linear polarization at these frequencies. This method has been developed with the SKA in mind and will enable a new era of high fidelity spectro-polarimetric snapshot solar imaging at low-radio frequencies. **4 May 2014, 28 Sep 2014, 14 oct 2014, 24 Oct 2014, 3 Nov 2014**

CESRA #3375 Aug **2022** https://www.astro.gla.ac.uk/users/eduard/cesra/?p=3375

Robust absolute solar flux density calibration for the Murchison Widefield Array

Devojyoti **Kansabanik**, Surajit Mondal, Divya Oberoi, Ayan Biswas, Shilpi Bhunia

ApJ **927** 17 **2022**

https://arxiv.org/pdf/2201.01267.pdf

https://iopscience.iop.org/article/10.3847/1538-4357/ac4bba/pdf

Sensitive radio instruments are optimized for observing faint astronomical sources, and usually need to attenuate the received signal when observing the Sun. There are only a handful of flux density calibrators which can comfortably be observed with the same attenuation set up as the Sun. Additionally, for wide field-of-view (FoV) instruments like the Murchison Widefield Array (MWA) calibrator observations are generally done when the Sun is below the horizon to avoid the contamination from solar emissions. These considerations imply that the usual radio interferometric approach to flux density calibration is not applicable for solar imaging. A novel technique, relying on a good sky model and detailed characterization of the MWA hardware, was developed for solar flux density calibration for MWA (Oberoi et al. 2017). Though successful, this technique is not general enough to be extended to the data from the extended configuration of the MWA Phase II. Here we present a robust flux density calibration method for solar observations with MWA independent of the array configuration. We use different approaches -- the serendipitous presence of strong sources; detection of numerous background sources using high dynamic range images in the FoV along with the Sun and observations of strong flux density calibrators with and without the additional attenuation used for solar observations; to obtain the flux scaling parameters required for the flux density calibration. Using the present method we have achieved an absolute flux density uncertainty ∼10% for solar observations even in absence of dedicated calibrator observations.

Periods and Frequency Drifts of Groups of the Decimetric Spikes in Two Solar Flares.

Karlický, M., Dudík, J. & Rybák, J.

Sol Phys 299, 113 (**2024**).

https://doi.org/10.1007/s11207-024-02359-y

https://link.springer.com/content/pdf/10.1007/s11207-024-02359-y.pdf

We studied the radio emission occurring as narrowband decimetric spikes observed during the **10 May 2022 and 26 August 2022** flares. In the radio spectra, these spikes were distributed in groups that occurred quasi-periodically with the periods 5.1 s in the 10 May 2022 flare and 9.1 s in the 26 August 2022 flare. In some parts of these groups, even subgroups of spikes distributed with the quasi-periods of 0.19 s (10 May 2022 flare), and 0.17 s and 0.21 s (26 August 2022 flare) were found. Some of these subgroups even drifted to higher or lower frequencies, which was observed for the first time. At the time of the dm-spikes observation, a pair of reconnecting loops are identified in the SDO/AIA EUV observations of the 10 May 2022 flare, one of which is interpreted as belonging to a small erupting filament. We propose that these loops reconnect in the dynamic quasi-periodic regime (the period 0.19 s) and this reconnection is modulated by an oscillation of one of the interacting loops (the period 5.1 s). Accelerated electrons from this process are trapped in reconnecting plasma outflows, and thus the drifting groups of spikes are generated. The 26 August 2022 flare is a complex event with several systems of bright loops; nevertheless, it also shows a disintegrating erupting filament similar to the 10 May 2022 flare, meaning that the dm-spikes are likely generated by similar reconnection processes.

CESRA https://www.astro.gla.ac.uk/users/eduard/cesra/?p=3860

Turbulence in Sources of Decimetric Flare Continua

Marian **Karlický**

Solar Physics volume 298, Article number: 95 (**2023**)

https://link.springer.com/content/pdf/10.1007/s11207-023-02188-5.pdf

Decimetric continua are commonly observed during long-lasting solar flares. Their frequency boundaries vary with time. We studied frequency boundary variations using the power spectrum analysis. Analyzing five decimetric continua, we found that their power spectra have a power-law form with the power-law index close to the Kolmogorov turbulence index −5/3. The same power index was also found in the power spectra of radio flux variations at frequencies in the range of the frequency boundary variations. Moreover, these frequency boundary variations were highly correlated with the radio flux ones. We interpret these results to be due to turbulent density variations in the reconnection plasma outflow to the termination shock formed above flare loops. In three cases of decimetric continua, we estimated the level

of the plasma density turbulence to be 7.6 – 11.2% of the mean plasma density. We think that the analysis of variations of decimetric continua can be used in studies of the plasma turbulence in solar flares. **30 December 2004, 1 August 2010, 24 Feb 2011, 26 Oct 2013, 25 June 2015**

Radio bursts observed during solar eruptive flares and their schematic summary **Review**

Marian **Karlický**

2023

https://arxiv.org/pdf/2307.07144.pdf

In this review we summarize results of our analysis of the observations of solar eruptive flares made by the Ondřejov radiospectrograph for more than twenty years. We also present some Potsdam-Tremsdorf radio spectra from our common studies. Considering a 3-dimensional model of eruptive flares together with the results of our magnetohydrodynamic and particle-in-cell simulations we show an importance of decimetric radio bursts for understanding of plasma processes in eruptive flares. We present drifting pulsation structures as signatures of plasmoids, an unusual zebra pattern in the very early flare stage, narrowband dm-spikes as the bursts generated in the reconnection plasma outflows, radio bursts indicating a merging of plasmoids, pair of decimetric type III bursts indicating the electron beams propagating upwards and downwards in the solar atmosphere from the acceleration site, and a special decimetric type III burst formed probably around the plasmoid. We present unusual radio bursts connected with the rising magnetic rope at the very beginning of eruptive flares. Furthermore, based on the analysis of decimetric continua we estimated the level of the plasma turbulence in a vicinity of the flare termination shock. Interpretations of all these bursts are based on models and time coincidences with observations in X-ray, UV and optical ranges; in most cases an information about positions of these radio sources is missing. To show an importance of positional information, we present a rare example of observations, where the drifting pulsation structure was observed simultaneously with the observations made by the EOVSA radiointerferometer. All the presented bursts are then summarized in a new scheme of bursts and compared with the schema commonly used. **18 August 1998, 28 March 2001, 12 April 2001, 24 September 2001, 28 September 2001, 26 September 2011, 25 June 2015, 6 September 2017, 10 September 2017, 2 April 2022**

Simulations of solar radio zebras

M. **Karlický**

A&A 661, A56 (**2022**)

https://doi.org/10.1051/0004-6361/202142497

https://www.aanda.org/articles/aa/pdf/2022/05/aa42497-21.pdf

Context. Solar radio zebras are used in diagnostics of solar flare plasmas and it is of great importance to construct accurate models to correctly characterize them.

Aims. We simulated two zebras to verify their double-plasma resonance (DPR) model.

Methods. In our zebra simulations, we used the DPR model in an expanding and compressing part of the loop as well as with the wave propagating along the loop.

Results. Using the DPR model in such a loop, we successfully simulated zebras from the **1 August 2010 and 21 June 2011** flares. We found that increasing the density or decreasing the magnetic field in the part of the loop, where zebra-stripe sources are located, the zebra stripes are shifted to higher frequencies and vice versa. In the case of the 21 June 2011 flare, we confirm that small deviations of zebra-stripe frequencies from their mean values can be explained by waves propagating along the loop. We also confirm high values for the gyro-harmonic number of zebra stripes. We explain an inconsistency in the wave velocities derived from the plasma parameters and from the frequency drift in combination with the density model of the solar atmosphere. Finally, we discuss the high values of the gyro-harmonic number found in the studied zebras.

Narrowband spikes observed during the 13 June 2012 flare in the 800-2000 MHz range

M. **Karlicky**, J. Rybak, J. Benacek, J. Kasparova

Solar Phys. **297**, Article number: 54 **2022**

https://arxiv.org/pdf/2204.09327.pdf

https://doi.org/10.1007/s11207-022-01989-4

Narrowband (~5 MHz) and short-lived (~0.01 s) spikes with three different distributions on the 800-2000 MHz radio spectrum of the **13 June 2012** flare are detected and analyzed. We designate them as SB (spikes distributed in broad band or bands), SZ (spikes distributed in zebra-like bands) and SBN (spikes distributed in broad and narrow bands). Analyzing AIA/SDO images of the active region NOAA 11504, a rough correspondence between groups of the spikes observed on 1000 MHz and peaks in the time profiles of AIA channels taken from the flare sub-area close to the leading sunspot is found. Among types of spikes the SZ type is the most interesting because it resembles to zebras. Therefore, using auto-correlation and cross-correlation methods we compare SZ and SBN spikes with the typical zebra observed in the same frequency range. While the ratio of SZ band frequencies with their frequency separation (220 MHz) is about 4, 5 and 6, in the zebra the frequency stripe separation is about 24 MHz and the ratio is around 50. Moreover, the bandwidth of SZ bands, which consists of clouds of narrowband spikes, is much broader than that of zebra stripes. This

comparison indicates that SZ spikes are generated different way than the zebra, but similar way as SBN spikes. We successfully fit the SZ band frequencies by the Bernstein modes. Based on this fitting we interpret SZ and SBN spikes as those generated in the model with Bernstein modes. Thus, the magnetic field and plasma density in the SZ spike source is estimated as about 79 G and 8.4x10^9 cm-3, respectively.
CESRA #3378 Sep **2022** https://www.astro.gla.ac.uk/users/eduard/cesra/?p=3378

Narrowband Spikes Observed during the 2013 November 7 Flare

Marian **Karlický**1, Jan Benáček2, and Ján Rybák3
2021 ApJ 910 108
https://arxiv.org/pdf/2104.01345.pdf
https://doi.org/10.3847/1538-4357/abe62b
Narrowband spikes have been observed in solar flares for several decades. However, their exact origin is still discussed. To contribute to understanding of these spikes, we analyze the narrowband spikes observed in the 800–2000 MHz range during the impulsive phase of the 2013 November 7 flare. In the radio spectrum, the spikes started with typical broadband clouds of spikes, and then their distribution in frequencies changed into unique, very narrow bands having noninteger frequency ratios. We successfully fitted frequencies of these narrow spike bands by those, calculating dispersion branches and growth rates of the Bernstein modes. For comparison, we also analyzed the model where the narrow bands of spikes are generated at the upper-hybrid frequencies. Using both models, we estimated the plasma density and magnetic field in spike sources. Then, the models are discussed, and arguments in favor of the model with the Bernstein modes are presented. Analyzing frequency profiles of this spike event by the Fourier method, we found the power-law spectra with the power-law indices varying in the −0.8 to −2.75 interval. Because at some times this power-law index was close to the Kolmogorov spectral index (−5/3), we propose that the spikes are generated through the Bernstein modes in turbulent plasma reconnection outflows or directly in the turbulent magnetic reconnection of solar flares. **14 September 1992, 10 June 2003, 7 November 2013**
CESRA #2972 Jun **2021** http://www.astro.gla.ac.uk/users/eduard/cesra/?p=2972

Spatial quasi-periodic variations of the plasma density and magnetic field in zebra radio sources

M. **Karlický**1 and L. V. Yasnov2,3
A&A 646, A179 (**2021**)
https://doi.org/10.1051/0004-6361/202039850
https://www.aanda.org/articles/aa/pdf/2021/02/aa39850-20.pdf
Context. Radio bursts and their fine structures are an integral part of solar flares. Fine structures in particular are used for diagnostics of solar flare processes. The so-called zebras belong to the most important of such fine structures.
Aims. We analyze seven zebra events in order to search for spatial variations in the plasma density and magnetic field in zebra-stripe sources.
Methods. We used an improved method for estimating the gyroharmonic numbers of zebra-stripe frequencies. We compared observed zebra-stripe frequencies with those calculated in the zebra model. The differences in these frequencies vary and thus show spatial variations in the plasma density and magnetic field.
Results. In six out of seven analyzed zebras, we found a rather high correlation coefficient (about 0.7 and higher) between spatial variations in the density and magnetic field and a strictly periodic function. These density and magnetic field variations are explained by the torsional or sausage magnetoacoustic waves in the loop in which zebra-stripe sources are located. We present the wavelengths of these waves in dependence on the zebra frequency and estimate their periods.

The 2017 September 6 Flare: Radio Bursts and Pulsations in the 22–5000 MHz Range and Associated Phenomena

M. **Karlicky**, J. Rybak
ApJS **250** 31 **2020**
https://arxiv.org/pdf/2009.05756.pdf **File**
https://doi.org/10.3847/1538-4365/abb19f
For the 2017 September 6 flare (**SOL2017-Sep-06T11**:53) we present not only unusual radio bursts but also their interesting time association with the other flare phenomena observed in extreme ultraviolet (EUV), white-light, X-ray, and γ-ray emissions. Using our new method based on wavelets we found quasi-periodic pulsations (QPPs) in several locations of the whole time–frequency domain of the analyzed radio spectrum (11:55–12:07 UT and 22–5000 MHz). Among them the drifting QPPs are new and the most interesting, especially a bidirectional QPP at the time of the hard X-ray and γ-ray peaks and a sunquake start. In the pre-impulsive phase we show an unusual drifting pulsation structure (DPS) in association with the EUV brightenings caused by the interaction of magnetic ropes. In the flare impulsive phase we found an exceptional radio burst drifting from 5000 to 800 MHz. In connection with this drifting burst, we show a U burst at about the onset time of an EUV writhed structure and a drifting radio burst as a signature of a shock

wave at high frequencies (1050–1350 MHz). In the peak flare phase we found an indication of an additional energy-release process located at higher altitudes in the solar atmosphere. These phenomena are interpreted considering a rising magnetic rope, magnetosonic waves, and particle beams. Using a density model we estimated the density, wave velocities, and source heights for the bidirectionally drifting QPPs, the density for the pre-impulsive DPS and U burst, and the density and magnetic field strength for the drifting radio burst.
CESRA #2725 Nov **2020** http://www.astro.gla.ac.uk/users/eduard/cesra/?p=2725

Estimating density and magnetic field turbulence in solar flares using radio zebra observations A22

M. **Karlický** and L. Yasnov
A&A 638, A22 (**2020**)
DOI: https://doi.org/10.1051/0004-6361/202037936
https://www.aanda.org/articles/aa/pdf/2020/06/aa37936-20.pdf
Context. In solar flares the presence of magnetohydrodynamic turbulence is highly probable. However, information about this turbulence, especially the magnetic field turbulence, is still very limited.
Aims. In this paper we present a new method for estimating levels of the density and magnetic field turbulence in time and space during solar flares at positions of radio zebra sources.
Methods. First, considering the double-plasma resonance model of zebras, we describe a new method for determining the gyro-harmonic numbers of zebra stripes based on the assumption that the ratio R = Lb/Ln (Ln and Lb are the density and magnetic field scales) is constant in the whole zebra source.
Results. Applying both the method proposed in this work and one from a previous paper for comparison, in the **14 February 1999** zebra event we determined the gyro-harmonic numbers of zebra stripes. Then, using the zebra-stripe frequencies with these gyro-harmonic numbers, we estimated the density and magnetic field in the zebra-stripe sources as n = (2.95−4.35) × 1010 cm−3 and B = 17.2−31.9 G, respectively. Subsequently, assuming that the time variation of the zebra-stripe frequencies is caused by the plasma turbulence, we determined the level of the time varying density and magnetic field turbulence in zebra-stripe sources as $|\Delta n/n|_t$ = 0.0112–0.0149 and $|\Delta B/B|_t$ = 0.0056–0.0074, respectively. The new method also shows deviations in the observed zebra-stripe frequencies from those in the model. We interpret these deviations as being caused by the spatially varying turbulence among zebra-stripe sources; i.e., they depend on their gyro-harmonic numbers. Comparing the observed and model zebra-stripe frequencies at a given time, we estimated the level of this turbulence in the density and magnetic field as $|\Delta n/n|_s$ = 0.0047 and $|\Delta B/B|_s$ = 0.0024. We found that the turbulence levels depending on time and space in the **14 February 1999** zebra event are different. This indicates some anisotropy of the turbulence, probably caused by the magnetic field structure in the zebra source.
CESRA #2621 July **2020** http://www.astro.gla.ac.uk/users/eduard/cesra/?p=2621

Drifting Pulsation Structure at the Very Beginning of the 2017 September 10 Limb Flare

M. **Karlicky**, B. Chen, D. E. Gary, J. Kasparova, J. Rybak
ApJ **889** 72 **2020**
https://arxiv.org/pdf/1912.12518.pdf
https://doi.org/10.3847/1538-4357/ab63d0
Drifting pulsation structures (DPSs) are important radio fine structures usually observed at the beginning of eruptive solar flares. It has been suggested that DPSs carry important information on the energy release processes in solar flares. We study DPS observed in an X8.2-class flare on 2017 September 10 in the context of spatial and spectral diagnostics provided by microwave, EUV, and X-ray observations. We describe DPS and its sub-structures that were observed for the first time. We use a new wavelet technique to reveal characteristic periods in DPS and their frequency bands. Comparing the periods of pulsations found in this DPS with those in previous DPSs we found new very short periods in the 0.09-0.15 s range. We present EOVSA images and spectra of microwave sources observed during the DPS. This DPS at its very beginning has pulsations in two frequency bands (1000-1300 MHz and 1600--1800 MHz) which are interconnected by fast drifting bursts. We show that these double-band pulsations started just at the moment when the ejected filament splits apart in a tearing motion at the location where a signature of the flare current sheetlater appeared. Using the standard flare model and previous observations of DPSs, we interpret these double-band pulsations as a radio signature of superthermal electrons trapped in the rising magnetic rope and flare arcade at the moment when the flare magnetic reconnection starts. The results are discussed in a scenario with the plasmoid in the rising magnetic rope.

Radio, EUV, and X-Ray Observations during a Filament Rise in the 2011 June 7 Solar Flare

Marian **Karlický**1, Jana Kašparová1, and Robert Sych2
2020 ApJ 888 18
https://doi.org/10.3847/1538-4357/ab5801
https://arxiv.org/pdf/2004.00122.pdf
The most energetic flares start with a filament rise followed by magnetic reconnection below this filament. The start of the reconnection corresponds to the beginning of the flare impulsive phase. In this paper we study processes before this phase. During the filament rise we recognize an unusual radio continuum with a starting boundary drifting toward lower

frequencies. The estimated velocity of the agent generating this continuum boundary is about 400 km s−1, similar to that of the rising filament. In association with this filament rise, transient X-ray sources and extreme ultraviolet (EUV) brightenings are found near the filament footpoint and outside the locations where later two parallel flare ribbons appear. Moreover, oscillations with a ~30 s period are found simultaneously in radio, EUV, and X-ray observations. Around the end of these oscillations the flare impulsive phase starts as seen in observations of the drifting pulsation structure and X-ray source located at the upper part of the rising filament. We interpret the unusual radio continuum and transient X-ray sources, which are located outside the two parallel flare ribbons, as those generated during an interaction of the rising filament with the above-lying magnetic loops. The EUV brightening at the filament footpoint could be a signature of the magnetic reconnection inside the magnetic rope carrying the filament. Possible scenarios of the ~30 s period oscillations in radio, X-ray, and EUV are discussed.

Zebra-stripe sources in the double-plasma resonance model of solar radio zebras

M. **Karlický**1 and L. Yasnov2,3
A&A 624, A119 (**2019**)
sci-hub.se/10.1051/0004-6361/201935281
Context. Radio bursts with fine structures are used in diagnostics of solar flare plasmas, of which zebra structures are the most important. However, there is still a debate about their origin.
Aims. The most probable model of zebras is that based on double-plasma resonance (DPR) instability. The paper wants to contribute to a verification of this model.
Methods. We used analytical methods.
Results. We studied the DPR model in two scenarios: a model with the zebra-stripe sources in a single loop and a model with the zebra-stripe sources moving through a fan of magnetic field lines. In the first case, we found several new relations among the parameters of zebra stripes and their sources, which can be used to analyze observed zebras and thus to verify if the zebra is generated according to the DPR model. These relations were derived for the zebra-stripe sources distributed along the loop and also for those having some extent in the loop radius. In the scenario with the moving zebra-stripe sources, we determined the parameters of the **14 December 2006** zebra and estimated a change of the ratio of magnetic field and density scales causing the change of zebra-stripe frequencies. In this case we found that this zebra can be also explained in the model with the zebra-stripe sources in a single loop. Both the interpretations are discussed.

Determination of Plasma Parameters in Radio Sources of Solar Zebra-patterns Based on Relations between the Zebra-stripe Frequencies and Gyro-harmonic Numbers

Marian **Karlický**1 and Leonid V. Yasnov2,3
2018 ApJ 867 28
sci-hub.tw/10.3847/1538-4357/aae1f8
Solar radio zebras belong to the most important radio fine structures used in diagnostics of solar flare plasmas. In the present paper, assuming the double plasma-resonance model of zebras, we study the relation between zebra-stripe frequencies and gyro-harmonic numbers. We artificially generated two possible types of zebras: the zebra with Sequence A and Sequence B, where an increase of the zebra-stripe frequency corresponds to decrease or increase of the gyro-harmonic number. Analyzing these ideal zebras, we found that the frequency ratios of the neighboring zebra stripes increase in zebras with Sequence A and decrease in zebras with Sequence B. This criterion and corresponding diagrams were applied for nine observed zebras. All these zebras were found to be with Sequence A. Then we checked and confirmed these results by using the new numerical method, where the gyro-harmonic numbers of the zebra stripes with the lowest frequency s 1 were also determined. We found that in all these zebras, the spatial scale of the magnetic field in the zebra-stripe sources was always shorter than that of the plasma density. Knowing the gyro-harmonic numbers and corresponding zebra-stripe frequencies, we determined the magnetic field and plasma density in zebra sources to be 0.84–37.31 G and 0.026 × 1010–16.03 × 1010 cm−3, respectively. Finally, we found that with increasing the gyro-harmonic number s 1, the ratio of perpendicular and parallel scales of the magnetic field and plasma density in the zebra-stripe sources also increases. **1998 May 2, 2006 Dec 14, 2010 Aug 01**
Table 2 List of the Analyzed Zebras and Their Parameters

Fourier Power Spectra of Solar Noise Storms

Marian **Karlický**, Ján Rybák, Christian Monstein
Solar Physics October **2018**, 293:143
sci-hub.tw/10.1007/s11207-018-1367-5
We analyzed three noise storms recorded on 200 – 400 MHz Trieste Callisto radio spectra on **2 July 2012, 8 July 2012, and 16 July 2012** by the Fourier method. We divided intervals of the noise storms into five-minute intervals, and in these intervals we computed the mean Fourier spectra as a function of the wave numbers in the frequency and height-scale spaces. We found that these Fourier spectra, where the spectrum from the quiet-activity interval was subtracted, are power-law spectra. The mean power-law index of these spectra in the

range ln(kz)=[1.8,2.9]ln⁡(kz)=[1.8,2.9] (where kzkz is the wave number in the height-scale space) is −1.7±0.14−1.7±0.14, −1.6±0.14−1.6±0.14, and −1.5±0.12−1.5±0.12 for the 2 July 2012, the 8 July 2012, and the 16 July 2012 noise storms, respectively. It appears that as the number of Type-I bursts in the studied interval increases, the power-law index becomes closer to −5/3−5/3; this is known as the Kolmogorov spectral index. The power-law index of the noise storms is very similar to that of the narrowband dm-spikes found in our previous studies. Furthermore, we found a break in the power spectra at ln(kz)≈2.9ln⁡(kz)≈2.9, and the mean power-law index values above this break are −2.9±0.46−2.9±0.46, −3.1±0.65−3.1±0.65, and −3.4±0.98−3.4±0.98, respectively.

Double plasma-resonance surfaces in flare loops and radio zebra emission

M. **Karlický**1 and L. Yasnov2,3
A&A 618, A60 (**2018**)
sci-hub.tw/10.1051/0004-6361/201833516
Aims. The zebra structures observed in radio waves during solar flares are some of the most important structures used as diagnostics of solar flare plasmas. We here not only analyze the so-called double plasma-resonance (DPR) surfaces, but also estimate the effects of their form on the size of the zebra sources and brightness temperature.
Methods. To compute the DPR surfaces, we used numerical and analytical methods.
Results. We found that except for the case of a constant magnetic field across the loop, the DPR surfaces deviate from the constant plasma density surfaces. We found that the regime with a finite height scale has three forms of resonance surfaces depending on the magnetic field variation across the loop. This magnetic field variation also determines if in the generated zebra structure, an increase in gyro-harmonic number leads to an increase or decrease of the zebra stripe frequency. In the case with an infinite height scale, the resonance surfaces are parallel to the loop axis. Furthermore, we found that for highly polarized zebra structures that are generated at DPR surfaces close to the plasma frequency, the zebra emission is limited to the narrow escaping cone and the emitting source area increases with increasing viewing angle compared to the loop axis. Moreover, with increasing deviation of the DPR surfaces from those of constant density surfaces, the frequency bandwidth of the DPR emission increases and can cause the zebra stripes to overlap, which limits the zebra generation. For the zebra structures observed on **14 February 1999, 6 June 2000, and 1 August 2010** and the observed view perpendicular to the loop axis, we estimated that the brightness temperature is 3.67 × 1014 K, 6.58 × 1013 K, and 7.35 × 1015 K, respectively. These brightness temperatures are much lower than those derived for the view along the loop axis (up to 1017 K), and thus are more realistic. The area of the emitting source for coronal loops in the view perpendicular to the loop axis can be larger by several orders of magnitude than that in the view along the loop axis.

Solar radio burst associated with the falling bright EUV blob

Marian **Karlicky**, Alena Zemanova, Jaroslav Dudik, Krzysztof Radiszewski
Astrophysical Journal Letters, Volume 854, Issue 2, article id. L29, 6 pp. (**2018**)
https://arxiv.org/pdf/1804.06206.pdf
At the beginning of the **4 November 2015** flare, in the 1300 -- 2000 MHz frequency range, we observed a very rare slowly positively drifting burst. We searched for associated phenomena in simultaneous EUV observations made by IRIS, SDO/AIA, Hinode/XRT and in H alpha observations. We found that this radio burst was accompanied with the bright blob, visible at transition region, coronal, and flare temperatures, falling down to the chromosphere along the dark loop with the velocity of about 280 km/s. The dark loop was visible in H alpha but disappeared afterwards. Furthermore, we found that the falling blob interacted with the chromosphere as expressed by a sudden change of the H alpha spectra at the location of this interaction. Considering different possibilities we propose that the observed slowly positively drifting burst is generated by the thermal conduction front formed in front of the falling hot EUV blob.

Oscillations and Waves in Radio Source of Drifting Pulsation Structures

M. **Karlicky**, J. Rybak, M. Barta
Solar Phys. 293:62 **2018**
https://arxiv.org/pdf/1803.06148.pdf
https://link.springer.com/content/pdf/10.1007%2Fs11207-018-1282-9.pdf
Drifting pulsation structures (DPSs) are considered to be radio signatures of the plasmoids formed during magnetic reconnection in the impulsive phase of solar flares. In the present paper we analyze oscillations and waves in seven examples of drifting pulsation structures, observed by the 800-2000 MHz Ondrejov radiospectrograph. For their analysis we use a new type of oscillation maps which give us a much more information about processes in DPSs than that in previous analyzes. Based on these oscillation maps, made from radio spectra by the wavelet technique, we recognized quasi-periodic oscillations with periods ranging from about 1 to 108 s in all studied DPSs. This strongly supports the idea that DPSs are generated during a fragmented magnetic reconnection. Phases of most the oscillations in DPSs, especially for the period around 1 s, are synchronized ("infinite" frequency drift) in the whole frequency range of DPSs. For longer periods in some DPSs we found that the phases of the oscillations drift with the frequency drift in the interval from -17 to +287 MHz\s. We propose that these drifting phases can be caused (a) by the fast or slow

magnetosonic waves generated during the magnetic reconnection and propagating through the plasmoid, (b) by a quasi-periodic structure in the plasma inflowing to the reconnection forming a plasmoid, and (c) by a quasi-periodically varying reconnection rate in the X-point of the reconnection close to the plasmoid. **1992 Oct. 5, 1998 Aug. 18, 2002 May 20, 2002 Aug. 30, 2003 May 27, 2014 Apr. 18**

Solar Radio Burst Associated with the Falling Bright EUV Blob

Marian **Karlický**1, Alena Zemanová1, Jaroslav Dudík1, and Krzysztof Radziszewski2
2018 ApJL 854 L29
http://sci-hub.tw/http://iopscience.iop.org/2041-8205/854/2/L29/
At the beginning of the **2015 November 4** flare, in the 1300–2000 MHz frequency range, we observed a very rare slow positively drifting burst. We searched for associated phenomena in simultaneous EUV observations made by IRIS, SDO/AIA, and Hinode/XRT, as well as in H αobservations. We found that this radio burst was accompanied with the bright blob, visible at transition region, coronal, and flare temperatures, falling down to the chromosphere along the dark loop with a velocity of about 280 km s−1. The dark loop was visible in H α but disappeared afterward. Furthermore, we found that the falling blob interacted with the chromosphere as expressed by a sudden change of the H α spectra at the location of this interaction. Considering different possibilities, we propose that the observed slow positively drifting burst is generated by the thermal conduction front formed in front of the falling hot EUV blob.
CESRA nugget #1870 June **2018** http://cesra.net/?p=1870

Oscillations in the 45-5000 MHz Radio Spectrum of the 18 April 2014 Flare

M. **Karlicky**, J. Rybak, C. Monstein
Solar Phys. 292:94 **2017**
https://arxiv.org/pdf/1706.02836.pdf
Using a new type of oscillation map, made from the radio spectra by the wavelet technique, we study the **18 April 2014** M7.3 flare (SOL**2014-04-18**T13:03:00L245C017). We find a quasi-periodic character of this flare with periods in the range 65-115 seconds. At the very beginning of this flare, in connection with the drifting pulsation structure (plasmoid ejection) we find the 65-115 s oscillation phase drifting slowly towards lower frequencies, which indicates an upward propagating wave initiated at the start of the magnetic reconnection. In the drifting pulsation structure many periods (1-200 seconds) are found documenting multi-scale and multi-periodic processes. On this drifting structure fiber bursts with a characteristic period of about one second are superimposed, whose frequency drift is similar to that of the drifting 65-115 s oscillation phase. We also check periods found in this flare by EUV Imaging Spectrometer (EIS)/Hinode and Interface Region Imaging Spectrograph (IRIS) observations. We recognize the type III bursts (electron beams) as proposed, but their time coincidence with the EIS and IRIS peaks is not very good. This is probably due to the radio spectrum beeing a whole-disk record consisting of all bursts from any location while the EIS and IRIS peaks are emitted only from locations of slits in the EIS and IRIS observations.
CESRA highlight #1494, Sept 2017 http://www.astro.gla.ac.uk/users/eduard/cesra/?p=1494

Chains of type-I radio bursts and drifting pulsation structures

Marian **Karlicky**
A&A 602, A122 **2017**
https://arxiv.org/pdf/1704.08532.pdf
Aims. Owing to similarities of chains of type-I radio bursts and drifting pulsation structures the question arises as to whether both these radio bursts are generated by similar processes.
Methods. Characteristics and parameters of both these radio bursts are compared.
Results. We present examples of both types of bursts and show their similarities and differences. Then, for chains of type-I bursts, a similar model as for drifting pulsation structures (DPSs) is proposed. We show that, similar to the DPS model, the chains of type-I bursts can be generated by the fragmented magnetic reconnection associated with plasmoid interactions. To support this new model of chains of type-I bursts, we present an effect of merging two plasmoids to form one larger plasmoid on the radio spectrum of DPS. This process can also explain the 'wavy' appearance of some chains of type-I bursts. Further, we show that the chains of type-I bursts with the wavy appearance can be used for estimation of the magnetic field strength in their sources. We think that differences of chains of type-I bursts and DPSs are mainly owing to different regimes of the magnetic field reconnection. While in the case of chains of type-I bursts, the magnetic reconnection and plasmoid interactions are in the quasi-separatrix layer of the active region in more or less quasi-saturated regime, in the case of DPSs, observed in the impulsive phase of eruptive flares, the magnetic reconnection and plasmoid interactions are in the current sheet formed under the flare magnetic rope, which moves upwards and forces this magnetic reconnection.
4 Apr 2002, 30 June 2002, 14 Feb 2003, 11 May 2005, 1,2,17,29 July 2012

Oscillation Maps in the Broadband Radio Spectrum of the 1 August 2010 Event

M. **Karlicky**, J. Rybak

Solar Phys. **2017**, 292:1
https://arxiv.org/pdf/1611.02074v1.pdf
We search for indications of waves in the 25-2000 MHz radio spectrum of the 1 August 2010 event (SOL2010-08-01T08:57:00L075C013), where fast propagating waves in the solar corona with the periods of 181, 69, and 40 seconds were detected in UV observations. Using the wavelet technique we construct a new type of map of oscillations for selected periods in the whole domain of the radio spectrum. While the oscillation with the period of 181 seconds was recognized in the whole 25-2000 MHz radio spectrum, oscillations with periods of 69 and 40 seconds were confirmed only in the 250-870 MHz frequency range. In the 800-2000 MHz range we found periods of 50 and 80 seconds. Moreover, in the 250-870 MHz frequency range, the oscillation with the period of about 420 seconds was detected. We also made maps of phases of the 181-second oscillations in order to analyze their frequency drift. At the beginning of the radio event, in the 2000-500 MHz frequency range the phase of the 181-second oscillation drifts towards lower frequencies. On the other hand, at frequencies 25-500 MHz we found that the phase is nearly synchronous. While the phase drift at higher frequencies can be interpreted as being caused by the UV wave, the synchronization of the phase on lower frequencies is explained by the fast-electron beams, whose acceleration is modulated by the UV wave. Owing to this modulation, the electron beams are accelerated with the period of the UV wave (181 seconds). These beams propagate upwards through the solar corona and generate the 25-500 MHz radio emission with the 181-second period. Due to high beam velocity (~c/3, where c is the light speed) the 25-500 MHz radio emission, corresponding to a large interval of heights in the solar corona, is nearly synchronous.

Determination of plasma parameters in solar zebra radio sources

M. **Karlický**1 and L. V. Yasnov
A&A 581, A115 (**2015**)
http://www.aanda.org/articles/aa/pdf/2015/09/aa26785-15.pdf
Aims. We present a new method for determining the magnetic field strength and plasma density in the solar zebra radio sources.
Methods. Using the double plasma resonance (DPR) model of the zebra emission, we analytically derived the equations for computing the gyroharmonic number s of selected zebra lines and then solved these equations numerically.
Results. The method was successfully tested on artificially generated zebras and then applied to observed ones. The magnetic field strength and plasma density in the radio sources were determined. Simultaneously, we evaluated the parameter Lnb = 2Lb/ (2Ln − Lb), where Ln and Lb are the characteristic scale-heights of the plasma density and magnetic field strength in the zebra source, respectively. Computations show that the maximum frequency of the low-polarized zebras is about 8 GHz, in very good agreement with observations. For the high-polarized zebras, this limit is about four times lower. Microwave zebras are preferentially generated in the regions with steep gradients of the plasma density, such as in the transition region. In models with smaller density gradients, such as those with a barometric density profile, the microwave zebras cannot be produced owing to the strong bremsstrahlung and cyclotron absorptions. We also show that our DPR model is able to explain the zebras with frequency-equidistant zebra lines.
14 February 1999, 6 June 2000

Solar flares: radio and X-ray signatures of magnetic reconnection processes **Review**

Marian **Karlický**
Research in Astronomy and Astrophysics, Volume 14, Number 7, 753-772, **2014**
DOI: 10.1088/1674-4527/14/7/002 ?
This review summarizes new trends in studies of magnetic reconnection in solar flares. It is shown that plasmoids play a very important role in this primary flare process. Using the results of magnetohydrodynamic and particle-in-cell simulations, we describe how the plasmoids are formed, how they move and interact, and how a flare current sheet is fragmented into a cascade of plasmoids. Furthermore, it is shown that during the interactions of these plasmoids electrons are not only very efficiently accelerated and heated, but electromagnetic (radio) emission is also produced. We also describe possible mechanisms for the triggering of magnetic reconnection. The relevant X-ray and radio signatures of these processes (such as radio drifting pulsation structures, narrowband dm-spikes, and the loop-top and above-the-loop-top X-ray sources) are then described. It is shown that plasmoids can also be formed in kinked magnetic ropes. A mapping of X-points of the magnetic reconnection on the chromosphere (as e.g. a splitting of flare ribbons) is mentioned. Supporting EUV and white-light observations of plasmoids are added. The significance of all these processes for the fast magnetic reconnection and electron acceleration is outlined. Their role in fusion experiments is briefly mentioned

Frequency variations of solar radio zebras and their power-law spectra

M. **Karlický**
A&A 561, A34 **(2014)**

Context. During solar flares several types of radio bursts are observed. The fine striped structures of the type IV solar radio bursts are called zebras. Analyzing them provides important information about the plasma parameters of their radio sources. We present a new analysis of zebras.
Aims. Power spectra of the frequency variations of zebras are computed to estimate the spectra of the plasma density variations in radio zebra sources.
Methods. Frequency variations of zebra lines and the high-frequency boundary of the whole radio burst were determined with and without the frequency fitting. The computed time dependencies of these variations were analyzed with the Fourier method.
Results. First, we computed the variation spectrum of the high-frequency boundary of the whole radio burst, which is composed of several zebra patterns. This power spectrum has a power-law form with a power-law index –1.65. Then, we selected three well-defined zebra-lines in three different zebra patterns and computed the spectra of their frequency variations. The power-law indices in these cases are found to be in the interval between –1.61 and –1.75. Finally, assuming that the zebra-line frequency is generated on the upper-hybrid frequency and that the plasma frequency ωpe is much higher than the electron-cyclotron frequency ωce, the Fourier power spectra are interpreted to be those of the electron plasma density in zebra radio sources. **1 August 2010**

Radio continua modulated by waves: Zebra patterns in solar and pulsar radio spectrafl

M. **Karlický**
E-print, April **2013**; A&A 552, A90 (**2013**)
Aims. We aim to answer the question how waves with plasma density variations affect the radio continua generated by the plasma emission mechanism.
Methods. We built a simple semi-empirical model of the radio continuum modulation. Assuming that the waves with density variations are in the source of this radio continuum, we modeled the artificial radio spectrum, which we compared with observed spectra.
Results. We show that the waves with density variations modulate the radio continua generated by the plasma emission mechanism. Considering a single slow magnetoacoustic wave, we model the radio spectra, which resemble solar zebra patterns. We show that this modulation generates zebra effects even when the radio continuum is composed of many spiky bursts. Generalizing from one single wave to a wave turbulence we find that the computed radio spectrum is similar to so-called lace bursts. Finally, using the same procedure, but for fast magnetoacoustic waves, we modeled the radio spectrum similar to that observed during the interpulse phase of the radio emission of the Crab Nebula pulsar.
18 March 2003

Radio fiber bursts and fast magnetoacoustic wave trains

M. **Karlický**1, H. Mészárosová1 and P. Jelínek
E-print, March **2013**; A&A 550, A1 (**2013**)
Aims. We present a model for dm-fiber bursts that is based on assuming fast sausage magnetoacoustic wave trains that propagate along a dense vertical filament or current sheet.
Methods. Eight groups of dm-fiber bursts that were observed during solar flares were selected and analyzed by the wavelet analysis method. To model these fiber bursts we built a semi-empirical model. We also did magnetohydrodynamic simulations of a propagation of the magnetoacoustic wave train in a vertical and gravitationally stratified current sheet.
Results. In the wavelet spectra of the fiber bursts computed at different radio frequencies we found the wavelet tadpoles, whose head maxima have the same frequency drift as the drift of fiber bursts. It indicates that the drift of these fiber bursts can be explained by the propagating fast sausage magnetoacoustic wave train. Using new semi-empirical and magnetohydrodynamic models with a simple radio emission model we generated the artificial radio spectra of the fiber bursts, which are similar to the observed ones.

SUCCESSIVE MERGING OF PLASMOIDS AND FRAGMENTATION IN A FLARE CURRENT SHEET AND THEIR X-RAY AND RADIO SIGNATURES

Marian **Karlický**1 and Miroslav Bárta
2011 ApJ 733 107
Based on our recent MHD simulations, a conception of the successive merging of plasmoids and fragmentation in the current sheet in the standard flare model is presented. Then, using a 2.5-dimensional electromagnetic particle-in-cell model with free boundary conditions, these processes are modeled on the kinetic level of plasma description. We recognize the plasmoids that mutually interacted and finally merged into one large plasmoid. Between interacting plasmoids, additional plasmoids and current sheets on smaller spatial scales were formed, congruent with the fragmentation found in MHD simulations. During interactions (merging-coalescences) between the plasmoids, the electrons were very efficiently accelerated and heated. We find that after a series of such merging processes, the electrons in some regions reached the energies necessary for emission in the hard X-ray range. Considering these

energetic electrons and assuming a plasma density of 109-1010 cm–3 and a source volume equal to the **2007 December 31** flare, we compute the X-ray spectra as produced by the bremsstrahlung emission process. Comparing these spectra with observations, we think that these processes can explain the observed above-the-loop-top hard X-ray sources. Furthermore, we show that the process of fragmentation between two merging plasmoids can generate narrow-band dm-spikes. Formulae for schematic fractal reconnection structures are derived.

Magnetoacoustic waves in the narrowband dm-spikes sources

M. **Karlický**1, P. Jelínek2 and H. Mészárosová

A&A 529, A96 (**2011**)

Aims. A new type of analysis of the narrowband dm-spikes in solar radio radiation is introduced to look for magnetoacoustic waves in their sources.

Methods. The Fourier and wavelet methods were used. For the first time, the tadpole structures in the wavelet spectra of this radio emission were searched for.

Results. Fifteen groups of the narrowband dm-spikes, observed during solar flares, were selected and analyzed by the Fourier and wavelet analysis methods. We found that the mean Fourier spectra of these spikes in frequency space are the powerlaws with a power-law index in the range −1.2 –−1.8. Furthermore, their wavelet spectra based on time series reveal tadpoles at some frequencies, which indicates the presence of magnetoacoustic waves. These waves are interpreted as propagating through a source of the narrowband dm-spikes. It is proposed that the spikes are generated by driven coalescence and fragmentation processes in turbulent reconnection outflow. This interpretation is supported by a simultaneous observation of drifting pulsating structures (DPSs) and spikes. Finally, modeling of the magnetoacoustic waves and tadpoles in the Harris current sheet supports this interpretation.

Solar Research with ALMA

M. **Karlický** · M. Bárta · B.P. D¸abrowski · P. Heinzel

Solar Phys (**2011**) 268: 165–173

The *Atacama Large Millimeter/sub-millimeter Array* (ALMA) is a large interferometer that will consist up to 64 high-precision antennas operating in the **31.3 – 950 GHz** frequency range. In this frequency range, which is largely unexplored, unique observations with a broad range of scientific objectives (cosmology, cold universe, galaxies, stars and their formation, planets and so on) are expected. Among these tasks there is a unique possibility to observe the Sun and to address several outstanding issues of solar physics. First, the ALMA is briefly described and then the new ESO-ALMA European node (ARC), built at Ond˘rejov Observatory, is presented. In Europe, this ARC is the only one oriented to solar physics. Consequently, the requirements and limitations for ALMA solar observations, as well as some examples of possible solar-oriented ALMA projects, are shown. A procedure of the preparation and submission of proposals for ALMA observations is mentioned.

Reconnection of a Kinking Flux Rope Triggering the Ejection of a Microwave and Hard X-ray Source I. Observations and Interpretation

M. **Karlický** · B. Kliem

Solar Phys (**2010**) 266: 71–89, DOI 10.1007/s11207-010-9606-4

Imaging microwave observations of an eruptive, partially occulted solar flare on **18 April 2001** suggest that the global structure of the event can be described by the helical kink instability of a twisted magnetic flux rope. This model is suggested by the inverse gamma shape of the source exhibiting crossing legs of a rising flux loop and by evidence that the legs interact at or near the crossing point. The interaction is reflected by the location of peak brightness near the crossing point and by the formation of superimposed compact nonthermal sources most likely at or near the crossing point. These sources propagate upward along both legs, merge into a single, bright source at the top of the structure, and continue to rise at a velocity >1000 km s−1. The compact sources trap accelerated electrons which radiate in the radio and hard X-ray ranges. This suggests that they are plasmoids, although their internal structure is not revealed by the data. They exhibit variations of the radio brightness temperature at a characteristic time scale of ~40 s, anti-correlated to their area, which also support their interpretation as plasmoids. Their propagation path differs from the standard scenario of plasmoid formation and propagation in the flare current sheet, suggesting the helical current sheet formed by the instability instead.

Tearing, coalescence and fragmentation processes in solar flare current sheet and drifting pulsating structures

M. **Karlický**

Advances in Space Research

Volume 46, Issue 4, 16 August **2010**, Pages 377-381

The paper presents a summary of results from two different simulations which study the tearing, coalescence and fragmentation of current sheets, the associated production of energetic electrons and of plasma waves from these electrons which could explain drifting pulsation structures observed at radio wavelengths. Using a 2.5-D particle-in-cell (PIC) model of the current sheet it is shown that due to the tearing mode instability the current sheet tears into plasmoids and these plasmoids later on coalesce into larger ones. During these processes electrons are accelerated and they produce observable electromagnetic waves. Furthermore, the 3-D PIC model with two current sheets extended in the electric current direction shows their fast fragmentation associated with the exponential dissipation of the free magnetic field energy. An example of the drifting pulsating structure which is considered to be a radio signature of the above mentioned processes in solar flares is shown.

Radio spectra generated during coalescence processes of plasmoids in a flare current sheet

M. **Karlický**1, M. Bárta1,2 and J. Rybák3

A&A 514, A28 (**2010**)

Aims. Motivated by observations of the drifting pulsating structures (DPSs) in solar radio spectra, we study the electromagnetic (radio) emission generated during tearing and coalescence processes in a flare current sheet.
Methods. For numerical simulations, we used a 2.5-D particle-in-cell electromagnetic relativistic code. Numerical data were analyzed by the wavelet methods.
Results. It is found that the electromagnetic emission is generated during a coalescence of plasmoids, and it has a quasi-periodic character. Detailed analysis reveals that the electromagnetic emission is produced around the interacting plasmoids just before their coalescence into a larger one. The period in variations of electromagnetic emission corresponds to that of magnetic field at the same region. Reflections of the electromagnetic waves between interacting plasmoids are recognized. The computed and observed periodicities are discussed. The similarity of the DPSs with some radio bursts observed during star flares indicates a broader applicability for this model.

Subsecond (0.1 s) Pulsations in the 11 April 2001 Radio Event

M. **Karlický**, P. Zlobec & H. Mészárosová

Solar Phys., 261(2), 281-294, **2010**

Radio pulsations observed during the **11 April 2001** event at six single frequencies (237, 327, 408, 610, 1420, and 2695 MHz) by the Trieste radio-polarimeter with a time resolution 10 ms are analyzed. A wavelet analysis method as well as time delay and polarization measurements are used. Both methods reveal pulsations with a period of about 0.1 s at all observed frequencies. Furthermore, the 0.1 s pulsations drift toward higher and lower frequencies, starting at about 1420 MHz. The polarization of pulsations increases with frequency and time. The remarkable fact that the detected 0.1 s period of pulsations does not depend on frequency in a very broad frequency range is discussed in terms of existing models of pulsations.

Drifting pulsating structures generated during tearing and=coalescence processes in a flare current sheet:

M. **Karlicky** and M. BArta

A&A 464 (**2007**) 735-740 (Section 'The Sun')

http://www.aanda.org/10.1051/0004-6361:20065983

*Aims.*Based on particle-in-cell simulations, drifting pulsating structures are interpreted as the radio emission generated during tearing and coalescence processes in the current sheet of a flare.
*Methods.*A 2.5D particle-in-cell electromagnetic relativistic code was used considering two versions of the model: a) the model with one current sheet with free boundary conditions and b) the model with two current sheets and periodic boundary conditions. The dispersion diagrams of electromagnetic waves we then constructed using the 2D Fourier transform.
*Results.*It is found that electrons are accelerated most efficiently in the region near the x-point of the magnetic field structure in the phase at the end of tearing process and at the beginning of plasmoid coalescence. The most energetic electrons are distributed mainly along the *x*-lines of the magnetic field structure. During these processes, Langmuir waves are generated, along with the electromagnetic (radio) ones. It looks as these electromagnetic waves can be

observed mainly on the second harmonics of the plasma frequencies corresponding to the plasma densities in the external parts of the plasmoids.

Magnetic reconnection in solar flares and corresponding radio bursts

Adv. Space Res. 39(9), *Pages 1415-1420*, ***2007***

M. **Karlický** and M. Bárta

While shocks can contribute to the type II radio burst, the superthermal electrons trapped in plasmoids can generate so called drifting pulsating structures. Furthermore, regions with the MHD turbulence may manifest themselves as the lace or dm-spike bursts.

Common origin of quasi-periodic pulsations in microwave and decimetric solar radio bursts

Larisa **Kashapova**, Dmitrii Kolotkov, Elena Kupriyanova, Anastasiia Kudriavtseva, Chengming Tan, Hamish Reid

Solar Phys. **296**, Article number: 185 **2021**

https://arxiv.org/pdf/2110.07880.pdf

https://link.springer.com/content/pdf/10.1007/s11207-021-01934-x.pdf

https://doi.org/10.1007/s11207-021-01934-x

We analyse quasi-periodic pulsations (QPP) detected in the microwave and decimeter radio emission of the **SOL2017-09-05**T07:04 solar flare, using simultaneous observations by the Siberian Radioheliograph 48 (SRH-48, 4-8 GHz) and Mingantu Spectral Radioheliograph (MUSER-I, 0.4-2 GHz). The microwave emission was broadband with a typical gyrosynchrotron spectrum, while a quasi-periodic enhancement of the decimetric emission appeared in a narrow spectral band (500-700 MHz), consistent with the coherent plasma emission mechanism. The periodicity that we found in microwaves is about 30 s, coming from a compact loop-like source with a typical height of about 31 Mm. The decimetric emission demonstrated a periodicity about 6 s. We suggested a qualitative scenario linking the QPPs observed in both incoherent and coherent spectral bands and their generation mechanisms. The properties of the QPPs found in the microwave signal are typical for perturbations of the flare loop by the standing sausage mode of a fast magnetohydrodynamic (MHD) wave. Our analysis indicated that this sausage-oscillating flare loop was the primary source of oscillations in the discussed event. The suggested scenario is that a fundamental sausage harmonic is the dominant cause for the observed QPPs in the microwave emission. The initiation of oscillations in the decimetric emission is caused by the third sausage harmonic via periodic and nonlinear triggering of the acceleration processes in the current sheets, formed at the interface between the sausage-oscillating flare loop and the external coronal loop that extended to higher altitudes. Our results demonstrate the possible role of MHD wave processes in the release and transport of energy during solar flares, linking coherent and incoherent radio emission mechanisms. **2017-09-05**

Correction: Solar Physics volume 297, Article number: 152 (**2022**)

https://link.springer.com/content/pdf/10.1007/s11207-022-02088-0.pdf **5 September 2017**

The origin of quasi-periodicities during circular ribbon flares

L. K. **Kashapova**, E. G. Kupriyanova, Z. Xu, H. A. S. Reid, D. Y. Kolotkov

A&A **2020**

https://warwick.ac.uk/fac/sci/physics/research/cfsa/people/kolotkov/eprints/kashapova_et_al_arxiv.pdf

Context. Solar flares with a fan-spine magnetic topology can form circular ribbons. The previous study based on Hα line observations of the solar flares during **March 05, 2014** by Xu et al. (2017) revealed uniform and continuous rotation of the magnetic fan-spine. Preliminary analysis of the flare time profiles revealed quasi-periodic pulsations (QPPs) with similar properties in hard X-rays, Hα, and microwaves.

Aims. In this work, we address which process the observed periodicities are related to: periodic acceleration of electrons or plasma heating?

Methods. QPPs are analysed in the Hα emission from the centre of the fan (inner ribbon R1), a circular ribbon (R2), a remote source (R3), and an elongated ribbon (R4) located between R2 and R3. The methods of correlation, Fourier, wavelet, and empirical mode decomposition are used. QPPs in Hα emission are compared with those in microwave and X-ray emission.

Results. We found multi-wavelength QPPs with periods around 150 s, 125 s, and 190 s. The 150-s period is seen to co-exist in Hα, hard X-rays, and microwave emissions, that allowed us to connect it with flare kernels R1 and R2. These kernels spatially coincide with the site of the primary flare energy release. The 125-s period is found in the Hα emission of the elongated ribbon R4 and the microwave emission at 5.7 GHz during the decay phase. The 190-s period is present in the emission during all flare phases in the Hα emission of both the remote source R3 and the elongated ribbon R4, in soft X-rays, and microwaves at 4–8 GHz.

Conclusions. We connected the dominant 150-s QPPs with the slipping reconnection mechanism occurring in the fan. We suggested that the period of 125 s in the elongated ribbon can be caused by a kink oscillation of the outer spine

connecting the primary reconnection site with the remote footpoint. The period of 190 s is associated with the 3-min sunspot oscillations.

Detection of Acceleration Processes During the Initial Phase of the 12 June 2010 Flare

L. K. **Kashapova**, N. S. Meshalkina, M. S. Kisil
Solar Physics, October **2012**, Volume 280, Issue 2, pp 525-535
We present an analysis of the plasma parameters during the initial phase of the 12 June 2010 flare (**SOL2010-06-12T00:57**). A peculiarity of the flare was the detection of γ-ray emission that is unusual for such weak and short event. The analysis revealed the presence of a flare precursor detected about five minutes before the flare onset in 94 Å images which spatially coincided with the non-polarized microwave (MW) source at 17 GHz (the Nobeyama Radio Heliograph) that is the Neutral Line associated Source (NLS). A comparison of the results obtained from MW data by the Nobeyama Radio Polarimeters and the multi-frequency Siberian Radioheliograph (the new 10-antenna radio heliograph prototype at 4.6 and 6.4 GHz) and hard X-ray (HXR) observations by the Fermi Gamma-ray Space Telescope reveal the presence of accelerated electrons during the flare's initial phase. The analysis of MW and HXR spectra also confirms the presence of accelerated particles. Moreover, a good temporal correlation between several light curves in different HXR energy bands and at MW frequencies indicates the generation of both HXR and MW emission by a common population of accelerated electrons. Detection of accelerated particles during the initial phase of the flare and soft-hard-harder (SHH) behavior of the spectra indicate several episodes of particle acceleration and confirm the non-impulsive type of the flare evolution.

RADIO OBSERVATIONS OF THE SOLAR CORONA DURING AN ECLIPSE

C. **Kathiravan**, R. Ramesh, Indrajit V. Barve, and M. Rajalingam
Astrophysical Journal, 730:91 (4pp), **2011**
We carried out radio observations of the solar corona at 170 MHz during the eclipse of **2008 August 1**, from the Gauribidanur observatory located about 100 km north of Bangalore in India. The results indicate the presence of a discrete radio source of very small angular dimension (≈15_) in the corona from where the observed radiation originated.

The Post-Coronal Mass Ejection Solar Atmosphere and Radio Noise Storm Activity

C. **Kathiravan,** R. Ramesh, and H. S. Nataraj
The Astrophysical Journal, 656: L37–L40, **2007, File**

Generation Mechanism of the Slowly Drifting Narrowband Structure in the Type IV Solar Radio Bursts Observed by Amateras

Y. **Katoh**1, K. Iwai2, Y. Nishimura1, A. Kumamoto1, H. Misawa3, F. Tsuchiya3, and T. Ono
2014 ApJ 787 45
We investigate the type IV burst event observed by AMATERAS on **2011 June 7**, and reveal that the main component of the burst was emitted from the plasmoid eruption identified in the EUV images of the Solar Dynamics Observatory (SDO)/AIA. We show that a slowly drifting narrowband structure (SDNS) appeared in the burst's spectra. Using statistical analysis, we reveal that the SDNS appeared for a duration of tens to hundreds of milliseconds and had a typical bandwidth of 3 MHz. To explain the mechanism generating the SDNS, we propose wave-wave coupling between Langmuir waves and whistler-mode chorus emissions generated in a post-flare loop, which were inferred from the similarities in the plasma environments of a post-flare loop and the equatorial region of Earth's inner magnetosphere. We assume that a chorus element with a rising tone is generated at the top of a post-flare loop. Using the magnetic field and plasma density models, we quantitatively estimate the expected duration of radio emissions generated from coupling between Langmuir waves and chorus emissions during their propagation in the post-flare loop, and we find that the observed duration and bandwidth properties of the SDNS are consistently explained by the proposed generation mechanism. While observations in the terrestrial magnetosphere show that the chorus emissions are a group of large-amplitude wave elements generated naturally and intermittently, the mechanism proposed in the present study can explain both the intermittency and the frequency drift in the observed spectra.

Bright 30 THz impulsive solar bursts†

P. **Kaufmann**, S.M. White, R. Marcon, A.S. Kudaka, D. P. Cabezas, M.M. Cassiano, C. Francile, L.O.T. Fernandes, R.F. Hidalgo Ramirez, M. Luoni, A. Marun, P. Pereyra and R. V. de Souza
JGR Volume 120, Issue 6 Pages 4155–4163 **2015**
http://arxiv.org/ftp/arxiv/papers/1505/1505.06177.pdf

Impulsive 30 THz continuum bursts have been recently observed in solar flares, utilizing small telescopes with a unique and relatively simple optical setup concept. The most intense burst was observed together with a GOES X2 class event on **October 27, 2014**, also detected at two sub-THz frequencies, RHESSI X-rays and SDO/HMI and EUV. It exhibits strikingly good correlation in time and in space with white light flare emission. It is likely that this association may prove to be very common. All three 30 THz events recently observed exhibited intense fluxes in the range of 104 solar flux units, considerably larger than those measured for the same events at microwave and sub-mm wavelengths. The 30 THz burst emission might be part of the same spectral burst component found at sub-THz frequencies. The 30 THz solar bursts open a promising new window for the study of flares at their origin.
See CESRA highlight, **2016** http://www.astro.gla.ac.uk/users/eduard/cesra/?p=743

A BRIGHT IMPULSIVE SOLAR BURST DETECTED AT 30 THz
P. **Kaufmann**1,2,8, S. M. White3, S. L. Freeland4, R. Marcon5,6, L. O. T. Fernandes1, A. S. Kudaka1, R. V. de Souza1, J. L. Aballay7, G. Fernandez7, R. Godoy7, A. Marun7, A. Valio1, J.-P. Raulin1, and C. G. Giménez de Castro
2013 ApJ 768 134; preprint **File**
Ground- and space-based observations of solar flares from radio wavelengths to gamma-rays have produced considerable insights but raised several unsolved controversies. The last unexplored wavelength frontier for solar flares is in the range of submillimeter and infrared wavelengths. Here we report the detection of an intense impulsive burst at 30 THz using a new imaging system. The 30 THz emission exhibited remarkable time coincidence with peaks observed at microwave, mm/submm, visible, EUV, and hard X-ray wavelengths. The emission location coincides with a very weak white-light feature, and is consistent with heating below the temperature minimum in the atmosphere. However, there are problems in attributing the heating to accelerated electrons. The peak 30 THz flux is several times larger than the usual microwave peak near 9 GHz, attributed to non-thermal electrons in the corona. The 30 THz emission could be consistent with an optically thick spectrum increasing from low to high frequencies. It might be part of the same spectral component found at sub-THz frequencies whose nature remains mysterious. Further observations at these wavelengths will provide a new window for flare studies. **March 13, 2012**

Unusual Emissions at Various Energies Prior to the Impulsive Phase of the Large Solar Flare and Coronal Mass Ejection of 4 November 2003
Pierre **Kaufmann**, Gordon D. Holman, Yang Su, C. Guillermo Gimenez de Castro, Emilia Correia, Luis O. T. Fernandes, Rodney V. de Souza, Adolfo Marun and Pablo Pereyra
Solar Physics, Volume 279, Number 2 (**2012**), 465-475
The GOES X28 flare of **4 November 2003** was the largest ever recorded in its class. It produced the first evidence for two spectrally separated emission components, one at microwaves and the other in the THz range of frequencies. We analyzed the pre-flare phase of this large flare, twenty minutes before the onset of the major impulsive burst. This period is characterized by unusual activity in X-rays, sub-THz frequencies, Hα, and microwaves. The CME onset occurred before the onset of the large burst by about 6 min. It was preceded by pulsations of 3 – 5 s periods at sub-THz frequencies together with X-ray and microwave enhancements. The sub-THz pulsations faded out as impulsive bursts were detected at 100 – 300 keV and 7 GHz, close to the time of the first Hα brightening and the CME onset. The activities detected prior to and at the CME onset were located nearly 2 arcmin south of the following large flare, suggesting they were separate events. This unusual activity brings new clues to understanding the complex energy buildup mechanisms prior to the CME onset, occurring at a distinct location and well before the major flare that exploded afterwards.

SUB-THz AND Hα ACTIVITY DURING THE PREFLARE AND MAIN PHASES OF A GOES CLASS M2 EVENT
Pierre **Kaufmann**1,2, Rogério Marcon3,4, C. Guillermo Giménez de Castro1, Stephen M. White5, Jean-Pierre Raulin1, Emilia Correia1,6, Luis Olavo Fernandes1, Rodney V. de Souza1, Rodolfo Godoy7, Adolfo Marun7 and Pablo Pereyra7
2011 ApJ 742 106
Radio and optical observations of the evolution of flare-associated phenomena have shown an initial and rapid burst at 0.4 THz only followed subsequently by a localized chromospheric heating producing an Hα brightening with later heating of the whole active region. A major instability occurred several minutes later producing one impulsive burst at microwaves only, associated with an M2.0 GOES X-ray flare that exhibited the main Hα brightening at the same site as the first flash.The possible association between long-enduring time profiles at soft X-rays, microwaves, Hα, and sub-THz wavelengths is discussed. In the decay phase, the Hα movie shows a disrupting magnetic arch structure ejecting

dark, presumably chromospheric, material upward. The time sequence of events suggests genuine interdependent and possibly non-thermal instabilities triggering phenomena, with concurrent active region plasma heating and material ejection.

RAPID PULSATIONS IN SUB-THz SOLAR BURSTS
Pierre **Kaufmann**1,2, C. Guillermo Gim.enez de Castro1, Emilia Correia1,3, Joaquim E. R. Costa3, Jean-Pierre Raulin1,
and Adriana Silva V.alio1
Astrophysical Journal, 697:420–427, **2009**
A new solar burst emission spectral component has been found showing sub-THz fluxes increasing with frequency, spectrally separated from the well known microwave component. Rapid pulsations are found present in all events observed at the two frequencies of the solar submillimeter-wave telescope: 212 and 405 GHz. They were studied in greater detail for three solar bursts exhibiting the new THz spectral component. The pulse amplitudes are of about 5%–8% of the mean flux throughout the bursts durations, being comparable for both frequencies. Pulsations range from one pulse every few seconds to 8–10 per second. The pulse repetition rates (R) are linearly proportional to the mean burst fluxes (S), following the simple relationship $S = kR$, suggesting that the pulsations might be the response to discrete flare particle accelerator injections quantized in energy. Although this result is consistent with qualitative trends previously found in the GHz range, the pulse amplitude relative to the mean fluxes at the sub-THz frequencies appear to be nearly ten times smaller than expected from the extrapolation of the trends found in the GHz range. However there are difficulties to reconcile the nearly simultaneous GHz and THz burst emission spectrally separated components, exhibiting rapid pulsations with considerably larger relative intensities in the GHz range.
2003 November 4 and 2 and 2006 December 6

Sub-terahertz, Microwaves and High Energy Emissions During the 6 December 2006 Flare, at 18:40 UT
Pierre **Kaufmann** · Gérard Trottet · C. Guillermo Giménez de Castro · Jean-Pierre Raulin · Säm Krucker · Albert Y. Shih · Hugo Levato
Solar Phys (**2009**) 255: 131–142, DOI 10.1007/s11207-008-9312-7
The presence of a solar burst spectral component with flux density increasing with frequency in the sub-terahertz range, spectrally separated from the well-known microwave spectral component, bring new possibilities to explore the flaring physical processes, both observational and theoretical. The solar event of **6 December 2006**, starting at about 18:30 UT, exhibited a particularly well-defined double spectral structure, with the sub-THz spectral component detected at 212 and 405 GHz by the Solar Submilimeter Telescope (SST) and microwaves (1 – 18 GHz) observed by the Owens Valley Solar Array (OVSA). Emissions obtained by instruments onboard satellites are discussed with emphasis to ultraviolet (UV) obtained by the Transition Region And Coronal Explorer (TRACE), soft X-rays from the Geostationary Operational Environmental Satellites (GOES) and X- and γ –rays from the Ramaty High Energy Solar Spectroscopic Imager (RHESSI). The sub-THz impulsive component had its closer temporal counterparts only in the higher energy X- and γ –rays ranges. The spatial positions of the centers of emission at 212 GHz for the first flux enhancement were clearly displaced by more than one arc-minute from positions at the following phases. The observed sub-THz fluxes and burst source plasma parameters were difficult to be reconciled with a purely thermal emission component. We discuss possible mechanisms to explain the double spectral components at microwaves and in the THz ranges.

THE RELATIONSHIP BETWEEN EXTREME ULTRAVIOLET NON-THERMAL LINE BROADENING AND HIGH-ENERGY PARTICLES DURING SOLAR FLARES
T. **Kawate**1,2 and S. Imada
2013 ApJ 775 122
http://arxiv.org/pdf/1308.3415v1.pdf
We have studied the relationship between the location of EUV non-thermal broadening and high-energy particles during large flares using the EUV Imaging Spectrometer on board Hinode, the Nobeyama Radio Polarimeter, the Nobeyama Radioheliograph, and the Atmospheric Imaging Assembly on board the Solar Dynamic Observatory. We have analyzed five large flare events that contain thermal-rich, intermediate, and thermal-poor flares classified by the definition discussed in the paper. We found that, in the case of thermal-rich flares, the non-thermal broadening of Fe XXIV occurred at the top of the flaring loop at the beginning of the flares. The source of 17 GHz microwaves is located at the footpoint of the flare loop. On the other hand, in the case of intermediate/thermal-poor flares, the non-thermal broadening of Fe XXIV occurred at the footpoint of the flare loop at the beginning of the flares. The source of 17 GHz microwaves is located at the top of the flaring loop. We discussed the difference between thermal-rich and intermediate/thermal-poor flares based on the spatial information of non-thermal broadening, which may provide clues that the presence of turbulence plays an important role in the pitch angle scattering of high-energy electrons.

HARD X-RAY AND MICROWAVE EMISSIONS FROM SOLAR FLARES WITH HARD SPECTRAL INDICES

T. **Kawate**1, N. Nishizuka2, A. Oi3, M. Ohyama4 and H. Nakajima

2012 ApJ 747 131

We analyze 10 flare events that radiate intense hard X-ray (HXR) emission with significant photons over 300 keV to verify that the electrons that have a common origin of acceleration mechanism and energy power-law distribution with solar flares emit HXRs and microwaves. Most of these events have the following characteristics. HXRs emanate from the footpoints of flare loops, while microwaves emanate from the tops of flare loops. The time profiles of the microwave emission show delays of peak with respect to those of the corresponding HXR emission. The spectral indices of microwave emissions show gradual hardening in all events, while the spectral indices of the corresponding HXR emissions are roughly constant in most of the events, though rather rapid hardening is simultaneously observed in some for both indices during the onset time and the peak time. These characteristics suggest that the microwave emission emanates from the trapped electrons. Then, taking into account the role of the trapping of electrons for the microwave emission, we compare the observed microwave spectra with the model spectra calculated by a gyrosynchrotron code. As a result, we successfully reproduce the eight microwave spectra. From this result, we conclude that the electrons that have a common acceleration and a common energy distribution with solar flares emit both HXR and microwave emissions in the eight events, though microwave emission is contributed to by electrons with much higher energy than HXR emission.

Observations of transverse Z mode and parametric decay in the solar wind

P. J. **Kellogg**1,*, K. Goetz1, S. J. Monson1, A. Opitz

JGR, Volume 118, Issue 8, pages 4766–4775, August **2013**

1] The frequency resolution of the Time Domain Samplers of the S/WAVES experiments on the STEREO spacecraft has allowed clear observations of the nature of the Langmuir-Z-mode waves observed in the solar Wind in conjunction with Type III radio bursts. These include observations of transverse polarization of what are usually identified as Langmuir waves, observations of three-wave decay, indications of the cause of the broadening of the spectrum of the observed waves, new understanding of the threshold for the three-wave-decay instability, and contributions to the understanding of conversion of these waves to electromagnetic waves. Analysis, using the decay relations, shows that decay often occurs to the Z mode, or near it. Z-mode waves cannot be produced directly by the electrons of Type III bursts. The damping of Z mode and near Z mode is very small, accounting for the common occurrence of this nonlinear process. In particular, three-wave parametric decay of a Langmuir wave to another Langmuir wave has become recognized as the dominant nonlinear process for Langmuir waves from Type III bursts. It is found, however, that decay usually leaves much of the wave energy in the daughter wave and that this wave often falls in a region where modulational instability must be considered in addition to three-wave decay. On rare occasions, further decays follow the first. In these cases, the path length of the stimulating electron beam can sometimes be determined.

Plasma wave measurements with STEREO S/WAVES: Calibration, potential model, and preliminary results,

Kellogg, P. J., K. Goetz, S. J. Monson, S. D. Bale, M. J. Reiner, and M. Maksimovic (2009),

J. Geophys. Res., 114, A02107, http://dx.doi.org/10.1029/2008JA013566, **2009**

The S/WAVES experiments on the two STEREO spacecraft measure waves, both in situ plasma waves and remotely generated waves such as Type II and Type III solar bursts. A part of the experiment is aimed at understanding the generation of electromagnetic waves from electrostatic Langmuir waves. For this, rapid measurements of plasma density, sufficiently rapid to be on the time scale of Langmuir wave fluctuations, are deemed necessary. Measurements of the potential of the antennas relative to the spacecraft can supply these rapid measurements. The antennas were not provided with a bias current, and so this unbiased technique has not been used previously. However, the cylindrical antennas of S/WAVES respond to temperature as well as the density of the ambient plasma, giving five quantities, n_e, T_e, and 3 components of E, to be determined from the three measurements of antenna potential. The work presented here discusses the analysis and interpretation of these measurements from the early part of the mission, when there were frequent observations of foreshock Langmuir waves to use for calibration. A model of the photoemission-plasma equilibrium has been constructed, using these and other measurements. It is shown that the response to one or a few of the five quantities may be negligible, depending on the phenomenon observed, so that useful measurements are obtained of the others. Application to observation and analysis of various plasma wave phenomena will be discussed.

THE CORONAL AND HELIOSPHERIC 2007 MAY 19 EVENT: CORONAL MASS EJECTION, EXTREME ULTRAVIOLET IMAGER WAVE, RADIO BURSTS, AND ENERGETIC ELECTRONS

A. **Kerdraon**1, M. Pick1, S. Hoang1, Y.-M.Wang2, and D. Haggerty3

Astrophysical Journal, 715:468–476, **2010** May, **File**

We study the global development of the **2007 May 19** event and investigate the origin and the escape of the energetic electrons responsible for the interplanetary bursts and for the solar energetic particle event. The data analysis combines radio spectral and imaging observations with *STEREO* EUV observations. We also use the direction-finding capabilities on the *Wind*/Waves radio instrument. Electron acceleration and injections into the interplanetary medium occur with some delay after the flare. It is shown that they are related to the expansion of the coronal mass ejection and of the extreme ultraviolet imager wave. There are two accelerations at two different locations in the corona which correspond to two different electron trajectories in the interplanetary medium.

Quasilinear relaxation of a beam with power law injected electrons propagating through solar corona

H. **Khalilpour**

Astrophysics and Space Science May **2015**, 357:108

It is assumed that the electron beam propagating thorough the Maxwellian solar corona plasma has a power law spectra. Using numerical simulations of the quasilinear equations, the effects of power law injected electrons on the generation of Langmuir waves are compared with a Maxwellian beam. It is found that the level of Langmuir waves increases in the presence of power law injected electrons. The average velocity of the beam propagation is constant for both Maxwellian and power law injected electrons but its value increases in the second case. The influence of the power law injected electrons on the evolution of gas-dynamical parameters such as the height of the plateau in the beam distribution function in velocity space, its upper and lower velocities boundary, and the local velocity of the beam and its spread is investigated. It is shown that the these parameters are dependent on the characteristics of the power law injected electrons, p (spectral index), and v 0 (the break speed). The upper boundary of plateau decreases (increases) with the p(v 0) but the lower boundary has inverse behavior. The height of plateau p(x,t) is a decreasing function of p and for a fixed value of p it has a maximum in a certain value of v 0 at a given time and position.

Observations of the coronal dynamics associated with solar radio spike burst emission

J. I. **Khan**1 and H. Aurass2

A&A 457, 319-328 (**2006**) , DOI: 10.1051/0004-6361:20054034

Association of solar flares with coronal mass ejections accompanied by Deca-Hectometric type II radio burst for two solar cycles 23 and 24

Hema **Kharayat**, Lalan Prasad & Sumit Pant

Astrophysics and Space Science May **2018**, 363:87

http://sci-hub.tw/10.1007/s10509-018-3309-y

The aim of present study is to find the association of solar flares with coronal mass ejections (CMEs) accompanied by Deca-Hectometric (DH) type II radio burst for the period 1997–2014 (solar cycle 23 and ascending phase of solar cycle 24). We have used a statistical analysis and found that 10–20◦ latitudinal belt of northern region and 80–90◦ longitudinal belts of western region of the sun are more effective for flare-CME accompanied by DH type II radio burst events. M-class flares (52%) are in good association with the CMEs accompanied by DH type II radio burst. Further, we have calculated the flare position and found that most frequent flare site is at the center of the CME span. However, the occurrence probability of all flares is maximum outside the CME span. X-class flare associated CMEs have maximum speed than that of M, C, and B-class flare associated CMEs. We have also found a good correlation between flare position and central position angle of CMEs accompanied by DH type II radio burst.

Possible manifestation of large-scale transverse oscillations of coronal loops in solar microwave emission

M. L. **Khodachenko**1, K. G. Kislyakova2, T. V. Zaqarashvili1,3, A. G. Kislyakov2, M. Panchenko1, V. V. Zaitsev4, O. V. Arkhypov5 and H. O. Rucker1

A&A 525, A105 (**2011**)

Aims. We interpret long-periodic (minutes) modulations detected in solar microwave emission during flaring events as signatures of large-scale transverse oscillations of coronal loops.

Methods. Our data analysis method is based methodologically on a sliding-window Fourier transform combined with the Vigner-Wille technique. We analyze three different events where TRACE detected post-flare oscillating loops (on **Mar. 23, 2000; Sep. 15, 2001; Sep. 07, 2001**)

Results. For the transverse large-scale oscillatory motion of a loop, a properly located observer, in addition to the modulation caused by the emission diagram pattern motion at the main frequency of the loop oscillation, may detect a modulation at twice the frequency, produced by the varying magnetic field during each inclination of the loop. Our main result consists in identification of these “modulation pairs” in the dynamic spectra of solar microwave emission and their association with the observed oscillating coronal loops.

Longitudinal wave instability due to rotating beam-plasma interaction in weakly turbulent astrophysical plasmas

S. M. **Khorashadizade**h, 1? Sh. Abbasi Rostami,1 A. R. Niknam,2 † S. Vasheghani Farahani,3 and R. Fallah

MNRAS Volume 489, Issue 3, November **2019**, Pages 3059–3065

sci-hub.se/10.1093/mnras/stz2281

The aim of the present study is to highlight the temporal evolution of the longitudinal wave instability due to the interaction between a rotating electron beam and the magnetoactive plasma region in space plasma structures. The plasma structure which could be either in the solar atmosphere or any active plasma region in space is considered weakly turbulent, where the quasilinear theory is implemented to enable analytic insight on the wave-particle interaction in the course of the event. It is found that in a weakly turbulent plasma, quasilinear saturation of the longitudinal wave is accompanied by a significant alteration in the distribution function in the resonant region. In case of a pure electrostatic wave, the wave amplitude experiences elevation due to the energy transfer from the plasma particles. This causes flattening of the bump on tail(BOT) in the electron distribution function. If the gradient of the distribution function is positive, the chance that the beam would excite the wave is probable. In such a situation a plateau on the distribution function ($\partial f / \partial v \approx 0$) is formed that will stop the diffusion of beam particles in the velocity space. Evolution of the electron distribution function experiences a decreases of the instability of the longitudinal wave. It is deduced that the growth rate of the wave instability is inversely proportional to the wave energy. Regarding the Sun, in addition to creating micro-turbulence due to wave-particle interaction, as the wave elevates to higher altitudes it enters a saturated energy state before releasing energy that may be a candidate for the generation of radio bursts.

Triggering Mechanism for Eruption of Two Filaments Observed by the Solar Dynamics Observatory, Nobeyama Radioheliograph, and RHESSI

Sujin **Kim**1 and Vasyl Yurchyshyn2

2022 ApJL 932 L18

https://iopscience.iop.org/article/10.3847/2041-8213/ac7236/pdf

We investigate the eruptive process of two filaments, which is associated with an M-class flare that occurred in **2011 August 4.** The filaments are partly overlapped, one in the active region and the other just beside it, and erupt together as a halo coronal mass ejection. For this study, we used the Atmospheric Imaging Assembly and the Heliospheric Magnetic Imager on board the Solar Dynamics Observatory, the Nobeyama Radioheliograph 17 GHz, and the RHESSI Hard X-ray satellite. We found three distinct phases in the microwave flux profile and in the rising pattern of the filaments during the event. In the first phase, there was weak nonthermal emission at 17 GHz and hard X-rays. Those nonthermal sources appeared on one edge of the western filament (F2) in the active region. The F2 began to be bright and rose upward rapidly, while the eastern filament (F1), which was extended to the quiet region, started to brighten from the peak time of the 17 GHz flux. In the second phase, the nonthermal emission weakened and the F2 rose up slowly, while the F1 began to rise up. In the third phase, two filaments erupted together. Since the F1 was stable for a long time in the quiet region, breaking the equilibrium state of the F1 would be decisive for the successful eruption of two filaments and it seems clear that the evolution of the F2 provoked the unstable F1. We suggest that tether-cutting reconnection between two overlapped filaments triggers the eruption of the two filaments as a tangled identity.

Plasma Upflows and Microwave Emission in Hot Supra-arcade Structure Associated with an M1.6 Limb Flare

S. **Kim**, K. Shibasaki, H.-M. Bain, and K.-S. Cho

2014 ApJ 785 106

We have investigated a supra-arcade structure associated with an M1.6 flare, which occurred on the south-east limb on **2010 November 4**. It is observed in EUV with the Atmospheric Imaging Assembly (AIA) on board the Solar Dynamics Observatory, microwaves at 17 and 34 GHz with the Nobeyama Radioheliograph (NoRH), and soft X-rays of 8-20 keV with RHESSI. Interestingly, we found exceptional properties of the supra-arcade thermal plasma from the AIA 131 Å and the NoRH: (1) plasma upflows along large coronal loops and (2) enhancing microwave emission. RHESSI detected two soft X-ray sources, a broad one in the middle of the supra-arcade structure and a bright one just above the flare-arcade. We estimated the number density and thermal energy for these two source regions during the decay phase of the flare. In the supra-arcade source, we found that there were increases of the thermal energy and the density at the early and last stages, respectively. On the contrary, the density and thermal energy of the source on the top of the flare-arcade decreases throughout. The observed upflows imply that there is continuous energy supply into the supra-arcade structure from below during the decay phase of the flare. It is hard to explain by the standard flare model in which the energy release site is located high in the corona. Thus, we suggest that a potential candidate of the energy source for the hot supra-arcade structure is the flare-arcade, which has exhibited a predominant emission throughout.

Systematic Microwave Source Motions along a Flare-Arcade Observed by Nobeyama Radioheliograph and AIA/SDO

S. **Kim**, S. Masuda, K. Shibasaki, and S.-C. Bong
Publ. Astron. Soc. Japan 65, 2 [7 pages] (**2013**)
http://pasj.asj.or.jp/v65/sp1/65S002/65S002.pdf
We found systematic microwave source motions along a flare-arcade using Nobeyama Radioheliograph (NoRH) 17 GHz images. The motions were associated with an X-class disk flare that occurred on **2011 February 15**. For this study, we also used EUV images from Atmospheric Imaging Assembly (AIA) and magnetograms from Helioseismic and Magnetic Imager (HMI) onboard Solar Dynamics Observatory, and multi-channel microwave data from Nobeyama Radio Polarimeters (NoRP) and Korean Solar Radio Burst Locator (KSRBL). We traced centroids of the microwave source observed by NoRH 17 GHz during the flare, and found two episodes of the motion based on several facts: (1) The microwave source moved systematically along the flare-arcade, which was observed by the AIA 94 ˚A channel, in a direction parallel to the neutral line. (2) The period of each episode was 5 min and 14 min, respectively. (3) Estimated parallel speed was 34 kms_1 for the first episode and 22 km s_1 for the second episode. The spectral slope of the microwave flux above 10 GHz obtained by NoRP and KSRBL was negative for both episodes, and for the last phase of the second episodes it was flat with a flux of 150 sfu. The negative spectrum and the flat with high flux indicate that the gyrosynchrotron emission from accelerated electrons was dominant during the source motions. The sequential images from the AIA 304 ˚A and 94 ˚A channels revealed that there were successive plasma eruptions, and each eruption was initiated just before the start time of the microwave sources motion. Based on the results, we suggest that the microwave source motion manifests the displacement of the particle acceleration site caused by plasma eruptions.

SLOW MAGNETOACOUSTIC OSCILLATIONS IN THE MICROWAVE EMISSION OF SOLAR FLARES

S. **Kim**1, V. M. Nakariakov2,3, and K. Shibasaki
2012 ApJ 756 L36
Analysis of the microwave data, obtained in the 17 GHz channel of the Nobeyama Radioheliograph during the M1.6 flare on **2010 November 4**, revealed the presence of 12.6 minute oscillations of the emitting plasma density. The oscillations decayed with the characteristic time of about 15 minutes. Similar oscillations with the period of about 13.8 minutes and the decay time of 25 minutes are also detected in the variation of EUV emission intensity measured in the 335 Å channel of the Solar Dynamics Observatory/Atmospheric Imaging Assembly. The observed properties of the oscillations are consistent with the oscillations of hot loops observed by the Solar and Heliospheric Observatory/Solar Ultraviolet Measurement of Emitted Radiation (SUMER) in the EUV spectra in the form of periodic Doppler shift. Our analysis presents the first direct observations of the slow magnetoacoustic oscillations in the microwave emission of a solar flare, complementing accepted interpretations of SUMER hot loop oscillations as standing slow magnetoacoustic waves.

Global Positioning System and solar radio burst forensics

Kintner, P. M.; O'Hanlon, B.; Gary, D. E.; Kintner, P. M. S.
Radio Science, Volume 44, Issue 2, CiteID RS0A08, **2009**
On 6 December 2006, a solar radio burst associated with a class X6 solar flare demonstrated that GPS receiver operation is vulnerable to solar radio burst noise at 1.2 GHz and 1.6 GHz. Within 8 days, two more solar radio bursts confirmed the initial results. These solar radio bursts occurred at solar minimum when they were least expected. Given that measurements of solar radio bursts extend back to at least 1960, why did 40 years pass before anyone realized that solar radio bursts could be so intense or pose a potential threat to the continuous availability of GPS operationsfl An investigation has been conducted to see if archived solar radio burst data or GPS data could be used to detect intense solar radio bursts. With the exception of the intense solar radio bursts of December 2006, we find that when both GPS data and Radio Solar Telescope Network (RSTN) data are available, they agree within the limits presented by differing reception frequencies and unknown polarization. However, inconsistencies and lapses within the RSTN data set were also discovered, making it unlikely that we will ever know the true number of intense (>150,000 solar flux unit) solar radio bursts that may have occurred during the last 40 years.

CONSTRAINING THE SOLAR CORONAL MAGNETIC FIELD STRENGTH USING SPLIT-BAND TYPE II RADIO BURST OBSERVATIONS

P. **Kishore**1, R. Ramesh1, K. Hariharan1, C. Kathiravan1, and N. Gopalswamy
2016 ApJ 832 59
http://sci-hub.cc/10.3847/0004-637X/832/1/59
We report on low-frequency radio (85–35 MHz) spectral observations of four different type II radio bursts, which exhibited fundamental-harmonic emission and split-band structure. Each of the bursts was found to be closely associated with a whitelight coronal mass ejection (CME) close to the Sun. We estimated the coronal magnetic field strength from the split-band characteristics of the bursts, by assuming a model for the coronal electron density distribution. The choice of the model was constrained, based on the following criteria: (1) when the radio burst is observed simultaneously in the upper and lower bands of the fundamental component, the location of the plasma level

corresponding to the frequency of the burst in the lower band should be consistent with the deprojected location of the leading edge (LE) of the associated CME; (2) the drift speed of the type II bursts derived from such a model should agree closely with the deprojected speed of the LE of the corresponding CMEs. With the above conditions, we find that: (1) the estimated field strengths are unique to each type II burst, and (2) the radial variation of the field strength in the different events indicate a pattern. It is steepest for the case where the heliocentric distance range over which the associated burst is observed is closest to the Sun, and vice versa. **2013Oct 08, 2013 November 8, 2013Nov 19, 2014 Feb 10**

A Low-Frequency Radio Spectropolarimeter for Observations of the Solar Corona

P. **Kishore**, R. Ramesh, C. Kathiravan, M. Rajalingam
Solar Physics Volume 290, Issue 9, pp 2409-2422 **2015**
A new spectropolarimeter for dedicated ground-based observations of radio emission from the solar corona at low frequencies (<100 MHz) has recently been commissioned at the Gauribidanur Radio Observatory near Bengaluru, India. We report the observational setup, the calibration scheme, and first results

Gauribidanur Low-Frequency Solar Spectrograph

P. **Kishore**, C. Kathiravan, R. Ramesh, M. Rajalingam, Indrajit V. Barve
Solar Physics, Volume 289, Issue 10, pp 3995-4005, **2014**, **File**
A new radio spectrograph, dedicated to observe the Sun, has been recently commissioned by the Indian Institute of Astrophysics (IIA) at the Gauribidanur Radio Observatory, about 100 km North of Bangalore. The instrument, called the Gauribidanur Low-frequency Solar Spectrograph (GLOSS), operates in the frequency range≈40 – 440 MHz. Radio emission in this frequency range originates close to the Sun, typically in the radial distance range r≈1.1 – 2.0 R⊙. This article describes the characteristics of the GLOSS and the first results.

Long-period oscillations of the solar microwave emission<<<

K. G. **Kislyakova,** V. V. Zaitsev, S. Urpo & A. Riehokainen
Astronomy Reports, Volume 55, Number 3, 275-283, **2011**
Modulations of the microwave emission of the Sun at 11.7 GHz have been studied using more than 40 events observed in 2001 at the Metsähovi Radio Observatory. In nearly all the observed events, low-frequency modulations with periods of 3–90 min were detected. As a rule, simultaneous modulation of the emission at several frequencies was observed. One possible origin of such modulations with periods 5–10 min is parametric resonance arising in coronal magnetic loops as a result of interactions with the 5-min photospheric oscillations, while the long-period modulations could be a manifestation of sunspot oscillations. Torsional (ϑ-mode) and radial (r-mode) oscillations have such periods. The frequency of occurrence of oscillations with the determined periods is considered, and a lower limit for the brightness temperature of the oscillations is estimated.

Almost fifty years of Metsähovi solar observations on 37 GHz with recovered digitised historical maps

Sami **Kivistö** (1,2), Frederick Gent (2,3,5,6,7), Merja Tornikoski (1), Joni Tammi (1), Maarit Korpi-Lagg
A&A **2024**
https://arxiv.org/pdf/2402.12849.pdf
Context. Aalto University Metsähovi Radio Observatory has collected solar intensity maps for over 45 years. Most data coverage is on the 37 GHz frequency band, tracking emissions primarily at the chromosphere and coronal transition region. The data spans four sunspot cycles or two solar magnetic cycles. Aims. We present solar maps, including recently restored data prior to 1989, spanning 1978 to 2020 after correcting for observational and temporal bias. Methods. The solar maps consist of radio intensity sampled along scanlines of the antenna sweep. We fit a circular disk to the set of intensity samples, neglecting any exceptional features in the fitting process to improve accuracy. Applying a simple astronomical model of Sun and Earth, we assign each radio specimen its heliographic coordinates at the time of observation. We bin the sample data by time and heliographic latitude to construct a diagram analoguous to the classic butterfly diagram of sunspot activity. Results. Radio butterfly diagram at 37 GHz, spanning solar cycles 21 to 24 and extending near to the poles. Conclusions. We have developed a method for compensating for seasonal and atmospheric bias in the radio data, as well as correcting for the effects of limb brightening and beamwidth convolution to isolate physical features. Our observations are consistent with observations in nearby bandwidths and indicate the possibility of polar cyclic behaviour with a period exceeding the solar 11 year cycle.

Solar origin of in-situ near-relativistic electron spikes observed with SEPT/STEREO

A. **Klassen**, R. Gflmez-Herrero, B. Heber, Y. Kartavykh, W. Drflge, K.-L. Klein
E-print, April **2012**; A&A
During 2010 - 2011 the Solar Electron Proton Telescope (SEPT) onboard the twin STEREO spacecraft detected a number of typical impulsive electron events showing a prompt intensity onset followed by a long decay, as well as several near-relativistic so-called electron spike events. These spikes are characterized by a very short duration of below 10 - 20 min at FWHM, almost symmetric time profiles, velocity dispersion and strong anisotropy, revealing a very weak scattering during particle propagation from the Sun to STEREO. Spikes are detected at energies below 300 keV and appear simulateneously with type III radio bursts detected by SWAVES/STEREO and narrow EUV jets in active regions. Using particle, EUV and radio imaging observations we found that nearrelativistic electrons were accelerated simultaneously and at the same location as the electrons emitting the accompanying type III radio bursts and together with coronal EUV jets. Furthermore, the sources of type III radio bursts match very well the locations and the trajectories of the associated EUV jet. Applying a particle propagation model we demonstrate that the spike characteristics reflect both, properties of the accelerator and effects of interplanetary propagation.
26 February 2011, 19 March 2011

Electron Spikes, Type III Radio Bursts and EUV Jets on 22 February 2010

A. **Klassen**, R. Gómez-Herrero and B. Heber
Solar Physics, Volume 273, Number 2, 413-419, **2011**
The Solar Electron Proton Telescope on board the twin STEREO spacecraft measures electrons and ions in the energy range from 30 to above 400 keV with an energy resolution better than 10%. On **22 February 2010** during a short interval of 100 minutes, a sequence of impulsive energetic electron events in the range below 120 keV was observed with the STEREO-A/SEPT instrument. Each of the four events was associated with a type III radio burst and a narrow EUV jet. All the events show nearly symmetric “spike”-like time profiles with very short durations $\simeq 5$ min. The estimated electron injection time for each individual event shows a small time delay between the electron spike and the corresponding type III radio emission and a close coincidence with an EUV jet. These observations reveal the existence of spike-like electron events showing nearly “scatter-free” propagation from the Sun to STEREO-A. From the time coincidence we infer that the mildly relativistic electrons are accelerated at the same time and at the same location as the accompanying type III emitting electrons and coronal EUV jets. The characteristics of the spikes reflect the injection and acceleration profiles in the corona rather than interplanetary propagation effects.

Catalogue of the 1997 SOHO-EIT coronal transient waves and associated type II radio burst spectra.

Klassen, A., Aurass, H., Mann, G., Thompson, B.J.,
2000. Astron. Astrophys. Suppl. 141, 357–369.

Radio evidence on shock wave formation in the solar corona.

Klassen, A., Aurass, H., Klein, K.L., Hofmann, A., Mann, G.:
1999, *Astron. Astrophys.* **343**, 287 – 296.

Non-thermal electrons in an eruptive solar event: Magnetic structure, confinement, and escape into the heliosphere

Karl-Ludwig **Klein**1,2,⋆, Carolina Salas Matamoros3,⋆, Abdallah Hamini1,2 and Alexander Kollhoff4,⋆
A&A, 690, A382 (**2024**)
https://doi.org/10.1051/0004-6361/202450456
https://www.aanda.org/articles/aa/pdf/2024/10/aa50456-24.pdf
Context. Filament eruptions and coronal mass ejections (CMEs) reveal large-scale instabilities of magnetic structures in the solar corona. Some of them are accompanied by radio emission, which at decimetric and longer wavelengths is a signature of electron acceleration that may be different from the acceleration in impulsive flares. The radio emission is part of the broadband continua at decimetre and metre wavelengths called type IV bursts.
Aims. In this article we investigate a particularly well-observed combination of a filament eruption seen in Hα and at extreme ultraviolet (EUV) wavelengths and a moving type IV burst on **2021 August 24**. The aim is to shed light on the relationship between the large-scale erupting magnetic structure and the acceleration and transport of non-thermal electrons.
Methods. We used imaging observations of a moving radio source and associated burst groups with the refurbished Nançay Radioheliograph and whole-Sun radio spectrography from different ground-based and space-borne instruments, in combination with X-ray, radio, and in situ electron observations at tens of keV from Solar Orbiter and EUV imaging by SDO/AIA. The radio sources are located with respect to the erupting magnetic structure traced by the filament (EUV 30.4 nm), and the timing of the electrons detected in situ is compared with the timing of the different radio emissions.

Results. We find that the moving radio source is located at the top of the erupting magnetic structure outlined by the filament, which we interpret as a magnetic flux rope. The flux rope erupts in a strongly non-radial direction, guided by the overlying magnetic field of a coronal hole. The electrons detected at Solar Orbiter are found to be released mainly in two episodes, 10–40 minutes after the impulsive phase. The releases coincide with two groups of radio bursts, which originate respectively on the flank and near the top of the erupting flux rope.
Conclusions. The observation allows an unusually clear association between a moving type IV radio burst, an erupting magnetic flux rope as core structure of a CME, and particle releases into the heliosphere. Non-thermal electrons are confined in the flux rope. Electrons escape to the heliosphere mainly in two distinct episodes, which we relate to magnetic reconnection between the flux rope and ambient open field lines.

Radio astronomical tools for the study of solar energetic particles II.Time-extended acceleration at subrelativistic and relativistic energies **Review**

Karl-Ludwig **Klein1***
Front. Astron. Space Sci. Volume 7, id.93 (**2020**)
https://doi.org/10.3389/fspas.2020.580445
https://www.frontiersin.org/articles/10.3389/fspas.2020.580445/full
Solar energetic particle (SEP) events are commonly separated in two categories: numerous 'impulsive' events of relatively short duration, and a few 'gradual' events, where SEP-intensities may stay enhanced over several days at energies up to several tens of MeV. In some gradual events the SEP spectrum extends to relativistic energies (> 1 GeV), over shorter durations. The two categories are strongly related to an idea developed in the 1960s based on radio observations: Type III bursts, which were addressed in a companion chapter, outline impulsive acceleration of electrons to subrelativistic energies, while the large and the relativistic SEP events were ascribed to a second acceleration process. At radio wavelengths, typical counterparts were bursts emitted by electrons accelerated at coronal shock waves (type II bursts) and by electron populations in large-scale closed coronal structures (type IV bursts). Both burst types are related to coronal mass ejections (CMEs). Type II bursts from metric to kilometric wavelengths tend to accompany large SEP events, which is widely considered as a confirmation that CME-driven shocks accelerate the SEPs. But type II bursts, especially those related to SEP events, are most often accompanied by type IV bursts, where the electrons are rather accelerated in the wake of the CME. Individual event studies suggest that although the CME shock is the most plausible accelerator of SEPs up to some yet unknown limiting energy, the relativistic SEP events show time structure that rather points to coronal acceleration related to type IV bursts. This chapter addresses the question what type II bursts tell us about coronal shock waves and how type II and type IV radio bursts are related with relativistic proton signatures as seen by particle detectors on the Earth and by their gamma-ray emission in the solar atmosphere, focusing on two relativistic SEP events, on **2005 Jan 20** and **2017 Sep 10**. The importance of radio emissions as a complement to the upcoming SEP observations from close to the Sun is underlined.

Radio astronomical tools for the study of solar energetic particles I. Correlations and diagnostics of impulsive acceleration and particle propagation **Review**

Karl-Ludwig **Klein**
Front. Astron. Space Sci. Volume 7, id.105 **2020**
https://doi.org/10.3389/fspas.2020.580436
https://www.frontiersin.org/articles/10.3389/fspas.2020.580436/full **File**
Solar energetic particles (SEPs) are sporadically ejected from the Sun during flares and coronal mass ejections. They are of major astrophysical interest, because the proximity of the Sun allows for detailed multi-messenger studies. They affect space weather due to interactions with electronics, with the Earth's atmosphere, and with humans if they leave the protective shield of the magnetosphere of the Earth. Since early studies in the 1950s, starting with particle detectors on the ground, SEP events have been related to radio bursts.Two subjects are addressed in this chapter: attempts to establish quantitative correlations between SEPs and microwave bursts produced by gyro synchrotron radiation of mildly relativistic electrons, and the information derived from type III radio bursts on impulsive processes of particle acceleration and the coronal and interplanetary propagation. Type III radio bursts produced by electron beams on open magnetic field lines have a wide range of applications, including the identification of acceleration regions, the identification of confined particle acceleration with coronal signatures, but no SEPs, and the paths that the electrons, and energetic charged particles in general, take to travel from the low corona to the Heliosphere in case they escape. Simple scenarios of coronal particle acceleration are confirmed in relatively simple and short events. But the comparison with particle transport models shows that longer and delayed acceleration episodes exist especially in large SEP events. They will be discussed in a companion chapter. **2 Apr 1995, 7 Apr 1997, 6 Nov 1997, 1 May 2000, 26 Dec 2001, 5 Nov 2011**

Solar radio bursts as a tool for space weather forecasting

Klein, Karl-Ludwig; Matamoros, Carolina Salas; Zucca, Pietro
Comptes rendus - Physique, Volume 19, Issue 1-2, p. 36-42, **2018**.

https://reader.elsevier.com/reader/sd/pii/S1631070518300148?token=D537F952710CF6363FBFFAA0FCDAD2C023FF41B2CE662268302A75A4269C47C6EF93BD3474EEE4AA2545C31B0BFDD8D1
https://www.sciencedirect.com/science/article/pii/S1631070518300148?via%3Dihub
The solar corona and its activity induce disturbances that may affect the space environment of the Earth. Noticeable disturbances come from coronal mass ejections (CMEs), which are large-scale ejections of plasma and magnetic fields from the solar corona, and solar energetic particles (SEPs). These particles are accelerated during the explosive variation of the coronal magnetic field or at the shock wave driven by a fast CME. In this contribution, it is illustrated how full Sun microwave observations can lead to (1) an estimate of CME speeds and of the arrival time of the CME at the Earth, (2) the prediction of SEP events attaining the Earth. **4 Nov 2015**

X-Ray, Radio and SEP Observations of Relativistic Gamma-Ray Events **Review**

Karl-Ludwig **Klein**, Kostas Tziotziou, Pietro Zucca, Eino Valtonen, Nicole Vilmer, Olga E. Malandraki, Clarisse Hamadache, Bernd Heber, and Jürgen Kiener
In: O.E. Malandraki, N.B. Crosby (eds.), Solar Particle Radiation Storms Forecasting and Analysis Chapter 8, **2018**
https://link.springer.com/content/pdf/10.1007%2F978-3-319-60051-2.pdf
File Malandraki_Crosby_SEPs_Forecasting and Analysis_Book.pdf
The rather frequent occurrence, and sometimes long duration, of - ray events at photon energies above 100 MeV challenges our understanding of particle acceleration processes at the Sun. The emission is ascribed to pion-decay photons due to protons with energies above 300 MeV. We study the X-ray and radio emissions and the solar energetic particles (SEPs) in space for a set of 25 Fermi -ray events. They are accompanied by strong SEP events, including, in most cases where the parent activity is well-connected, protons above 300 MeV. Signatures of energetic electron acceleration in the corona accompany the impulsive and early post-impulsive -ray emission. -ray emission lasting several hours accompanies in general the decay phase of long-lasting soft X-ray bursts and decametric-tokilometric type II bursts. We discuss the impact of these results on the origin of the -ray events. **1982 Jun 3, 11 June 1991, 7 March 2011, 23 Jan 2012, 7 March 2012, 16-17 May 2012, 3 June 2012, 11 Apr 2013, 25 Feb 2014, 1 Sept 2014**

Solar radio monitoring at Nan¸cay: status and future perspectives

Karl-Ludwig **Klein**∗1,2, Abdallah Hamini3 , Christian Fabrice2 , Gabriel Auxepaules2 , Sophie Masson3 , Dominique Benoist2 , Guy Kenfack2 , and Christophe Taffoureau
CESRA Abstract **2016** p.50
http://cesra2016.sciencesconf.org/conference/cesra2016/pages/CESRA2016_prog_abs_book_v1.pdf
The Nan¸cay radio observatory has been carrying out dedicated radio observation at the Sun for many years. The three presently available instruments conduct spectrography (1000- 140 MHz: ORFEES spectrograph; 80-10 MHz: Decametre Array NDA) and imaging at selected frequencies in the 150-45 ˜MHz band (Radioheliograph NRH). This set of instruments observes the Sun during about 7 hours per day centred around noon. An assessment of the present status, recent work and perspectives for the coming years will be given:
1) The NRH is in a phase of major upgrading, comprising the data acquisition system, the replacement of the correlator, which will provide all correlations between the available antennae, and the maintenance of the focal systems. This work has led to an interruption of the observing service since more than a year. It is ongoing. Observational tests of the new systems are to start in May.
2) The ORFEES spectrograph is a new instrument, built with support by the French Air Force. It was put into operation in 2012.
3) The NDA shares observing time between the Sun and Jupiter. Its capacity of spectrography with high sensitivity has been extended to lower frequencies by a new data acquisition system that identifies and reduces terrestrial interference, and allows observations down to 10 ˜MHz, depending on the state of the ionosphere. This allows ideally a seamless connection with spectrography from space. Overview plots and to some extent data can be accessed via the dedicated web site radiomonitoring.obspm.fr, which also shows observations of other radio observatories. A dedicated database for the distribution of all solar data taken in Nan¸cay is under construction. The programmatic workshop of the Astronomy and Astrophysics branch of the French research organisation CNRS concluded in 2014 to the importance of solar monitoring at radio frequencies in Nan¸cay as a ground-based support for the coming Solar Orbiter mission.

Open magnetic flux tubes in the corona and the transport of solar energetic particles

Karl-Ludwig **Klein**1, S¨am Krucker2, Guillaume Lointier1,3, and Alain Kerdraon1
File 2008, A&A, 486, 589-596 (**2008**)
We investigate how magnetic fields guide energetic particles through the corona into interplanetary space and eventually to a spacecraft near the Earth. A set of seven simple particle events is studied, where energetic electrons (30-500 keV; *Wind* spacecraft) or protons (5-55 MeV; SoHO) were released together with low-energy electron beams producing metric-to-kilometric type III emission. Imaging of the coronal (metre-wave) part of this emission with the Nanc¸ay Radioheliograph is used to identify the open flux tubes that guide these electrons - and by inference all

particles detected at 1 AU. Open coronal field lines are also computed using potential magnetic field extrapolations, constrained by a source surface and by SoHO/MDI measurements in the photosphere (code by Schrijver and DeRosa). We find that in all events the type III radio sources lie in open flux tubes in the potential magnetic field extrapolations. The open flux tubes are rooted in small parts of the parent active region, covering a heliocentric angle of a few degrees in the photosphere. *But they expand rapidly above the neighbouring closed magnetic structures and cover several tens of degrees in longitude on the source surface. Some of these open field lines are found to connect the parent active region to the footpoint of the nominal Parker spiral on the source surface, within the uncertainty of about ±10◦ inherent to the evaluation of its connection longitude.* This is so even when the parent active region is as far as 50◦ away. In two cases where the coronal flux tubes point to high heliolatitudes, the detection of Langmuir waves at the *Wind* spacecraft in the ecliptic plane suggests that the interplanetary field lines curve down to the ecliptic before reaching 1 AU. *We conclude that non-radial open flux tubes in the corona can transport particles over several tens of degrees in longitude even in simple impulsive particle events. In all events we studied, potential magnetic field models give an adequate description of these structures.*

Suprathermal Electrons in Non-flaring Active Regions (Invited review) Noise storm Review

Klein, Karl-Ludwig
Second Advances in Solar Physics Euroconference: Three-Dimensional Structure of Solar Active Regions, ASP Conf. Series Vol. 155, Ed. by Costas E. Alissandrakis & Brigitte Schmieder. (**1998**), p.182; **File**

X-ray and radio evidence on the origin of a coronal shock wave.

Klein, K.L., Khan, J.I., Vilmer, N., Delouis, J.M., Aurass, H.:
1999,*Astron. Astrophys.* **346**, L53 – L56.

Reconnection of a Kinking Flux Rope Triggering the Ejection of a Microwave and Hard X-Ray Source II. Numerical Modeling

B. **Kliem** · M.G. Linton · T. Török · M. Karlický
Solar Phys (**2010**) 266: 91–107, DOI 10.1007/s11207-010-9609-1

Numerical simulations of the helical (m=1) kink instability of an arched, linetied flux rope demonstrate that the helical deformation enforces reconnection between the legs of the rope if modes with two helical turns are dominant as a result of high initial twist in the range _ _ 6π. Such a reconnection is complex, involving also the ambient field. In addition to breaking up the original rope, it can form a new, low-lying, less twisted flux rope. The new flux rope is pushed downward by the reconnection outflow, which typically forces it to break as well by reconnecting with the ambient field. The top part of the original rope, largely rooted in the sources of the ambient flux after the break-up, can fully erupt or be halted at low heights, producing a “failed eruption.” The helical current sheet associated with the instability is squeezed between the approaching legs, temporarily forming a double current sheet. The leg – leg reconnection proceeds at a high rate, producing sufficiently strong electric fields that it would be able to accelerate particles. It may also form plasmoids, or plasmoid-like structures, which trap energetic particles and propagate out of the reconnection region up to the top of the erupting flux rope along the helical current sheet. The kinking of a highly twisted flux rope involving leg – leg reconnection can explain key features of an eruptive but partially occulted solar flare on 18 April 2001, which ejected a relatively compact hard X-ray and microwave source and was associated with a fast coronal mass ejection.

The contribution of microbunching instability to solar flare emission in the GHz to THz range of frequencies

J. Michael **Klopf**, Pierre Kaufmann, Jean-Pierre Raulin, Sérgio Szpigel
ApJ, 791 31, **2014**
http://arxiv.org/pdf/1406.5499v1.pdf
Recent solar flare observations in the sub-THz range have provided evidence of a new spectral component with fluxes increasing for larger frequencies, separated from the well-known microwave emission that maximizes in the GHz range. Suggested interpretations explain the THz spectral component, but do not account for the simultaneous microwave component. We present a mechanism for producing the observed double-spectra. Based on coherent enhancement of synchrotron emission at long wavelengths in laboratory accelerators, we consider how similar processes may occur within a solar flare. The instability known as microbunching arises from perturbations that produce electron beam density modulations, giving rise to broadband coherent synchrotron emission at wavelengths comparable to the

characteristic size of the microbunch structure. The spectral intensity of this coherent synchrotron radiation (CSR) can far exceed that of the incoherent synchrotron radiation (ISR), which peaks at higher frequency, thus producing a double-peaked spectrum. Successful CSR simulations are shown to fit actual burst spectral observations, using typical flaring physical parameters and power-law energy distributions for the accelerated electrons. The simulations consider an energy threshold below which microbunching is not possible because of Coulomb repulsion. Only a small fraction of the radiating charges accelerated to energies above the threshold is required to produce the microwave component observed for several events. The ISR-CSR mechanism can occur together with other emission processes producing the microwave component. It may bring an important contribution at microwaves at least for certain events where physical conditions for the occurrence of the ISR-CSR microbunching mechanism are possible. **November 4, 2003**

The May 1967 Great Storm and Radio Disruption Event: Extreme Space Weather and Extraordinary Responses

D. J. **Knipp**1,2, A. C. Ramsay3, E. D. Beard3, A. L. Boright3, W. B. Cade4, I. M. Hewins5, R. McFadden5, W. F. Denig6, L. M. Kilcommons1, M. A. Shea7 and D. F. Smart7
Space Weather **2016** doi: 10.1002/2016SW001423 **File**
Although listed as one of the most significant events of the last 80 years, the space weather storm of late May 1967 has been of mostly fading academic interest. The storm made its initial mark with a colossal solar radio burst causing radio interference at frequen-cies between 0.01-9.0 GHz and near-simultaneous disruptions of dayside radio communica-tion by intense fluxes of ionizing solar X-rays. Aspects of military control and communica-tion were immediately challenged. Within hours a solar energetic particle event disrupted high frequency communication in the polar cap. Subsequently record-setting geomagnetic and ionospheric storms compounded the disruptions. We explain how the May 1967 storm was nearly one with ultimate societal impact, were it not for the nascent efforts of the United States Air Force in expanding its terrestrial weather monitoring-analysis-warning-prediction efforts into the realm of space weather forecasting. An important and long-lasting outcome of this storm was more formal Department of Defense support for current-day space weather forecasting. This story develops during the rapid rise of solar cycle 20 and the intense Cold War in the latter half of the 20th Century. We detail the events of late May 1967 in the inter-secting categories of solar-terrestrial interactions and the political-military backdrop of the Cold War. This was one of the ―Great Storms‖ of the 20th century, despite the lack of large geomagnetically-induced currents. Radio disruptions like those discussed here warrant the attention of today‘s radio-reliant, cellular-phone and satellite-navigation enabled world. **May 23 1967**

RatanSunPy: A robust preprocessing pipeline for RATAN-600 solar radio observations data

I. **Knyazeva**, I. Lysov, E. Kurochkin, A. Shendrik, D. Derkach, N. Makarenko
Astronomy and Computing **2024**
https://arxiv.org/pdf/2412.08230
The advancement of observational technologies and software for processing and visualizing spectro-polarimetric microwave data obtained with the RATAN-600 radio telescope opens new opportunities for studying the physical characteristics of solar plasma at the levels of the chromosphere and corona. These levels remain some difficult to detect in the ultraviolet and X-ray ranges. The development of such methods allows for more precise investigation of the fine structure and dynamics of the solar atmosphere, thereby deepening our understanding of the processes occurring in these layers. The obtained data also can be utilized for diagnosing solar plasma and forecasting solar activity. However, using RATAN-600 data requires extensive data processing and familiarity with the RATAN-600. This paper introduces RatanSunPy, an open-source Python package developed for accessing, visualizing, and analyzing multi-band radio observations of the Sun from the RATAN-600 solar complex. The package offers comprehensive data processing functionalities, including direct access to raw data, essential processing steps such as calibration and quiet Sun normalization, and tools for analyzing solar activity. This includes automatic detection of local sources, identifying them with NOAA (National Oceanic and Atmospheric Administration) active regions, and further determining parameters for local sources and active regions. By streamlining data processing workflows, RatanSunPy enables researchers to investigate the fine structure and dynamics of the solar atmosphere more efficiently, contributing to advancements in solar physics and space weather forecasting.

Solar Observations with the Atacama Large Millimeter/submillimeter Array (ALMA)

Kobelski, A.; ALMA Solar Development Team
Ground-based Solar Observations in the Space Instrumentation Era
ASP Conference Series, Vol. 504, p. 67, **2016**
http://aspbooks.org/publications/504/327.pdf
The Atacama Large Millimeter/Submillimeter Array (ALMA) is a joint North American, European, and East Asian project that opens the mm-sub mm wavelength part of the electromagnetic spectrum for general astrophysical exploration, providing high-resolution imaging in frequency bands currently ranging from 84 GHz to 950 GHz (300 microns to 3 mm). It is located in the Atacama desert in northern Chile at an elevation of 5000 m. Despite being a general purpose instrument, provisions have been made to enable solar observations with ALMA. Radiation emitted at

ALMA wavelengths originates mostly from the chromosphere, which plays an important role in the transport of matter and energy, and the in heating the outer layers of the solar atmosphere. Despite decades of research, the solar chromosphere remains a significant challenge: both to observe, owing to the complicated formation mechanisms of currently available diagnostics; and to understand, as a result of the complex nature of the structure and dynamics of the chromosphere. ALMA has the potential to change the scene substantially as it serves as a nearly linear thermometer at high spatial and temporal resolution, enabling us to study the complex interaction of magnetic fields and shock waves and yet-to-be-discovered dynamical processes. Moreover, ALMA will play an important role in the study of energetic emissions associated with solar flares at sub-THz frequencies.

Imaging of the solar atmosphere by the Siberian Solar Radio Telescope at 5.7 GHz with an enhanced dynamic range

Alexey **Kochanov**, Sergey Anfinogentov, Dmitry Prosovetsky, George Rudenko, Victor Grechnev
E-print, Oct **2013**, http://arxiv.org/pdf/1310.4250v1.pdf; Publ. Astron. Soc. Japan **65**, S19, **2013**
http://pasj.asj.or.jp/v65/sp1/65S019/65S019.pdf

The Siberian Solar Radio Telescope (SSRT) is a solar-dedicated directly-imaging interferometer observing the Sun at 5.7 GHz. The SSRT operates in the two-dimensional mode since 1996. The imaging principle of the SSRT restricts its opportunities in observations of very bright flare sources, while it is possible to use `dirty' images in studies of low-brightness features, which do not overlap with side lobes from bright sources. The interactive CLEAN technique routinely used for the SSRT data provides imaging of active regions but consumes much time and efforts and does not reveal low-brightness features below the CLEAN threshold. The newly developed technique combines the CLEAN routine with the directly-imaging capability of the SSRT and provides clean images with an enhanced dynamic range automatically. These elaborations considerably extend the range of tasks, which can be solved with the SSRT. We show some examples of the present opportunities of the SSRT and compare its data with the images produced by the Nobeyama Radioheliograph at 17 GHz as well as observations in different spectral ranges.

Measuring the Solar Magnetic Field with STEREO A Radio Transmissions: Faraday Rotation Observations using the 100m Green Bank Telescope

Kobelski, A.; Jensen, E.; Wexler, D.; Heiles, C.; Kepley, A.; Kuiper, T.; Bisi, M.
Ground-based Solar Observations in the Space Instrumentation Era
ASP Conference Series, Vol. 504, p. 99, **2016**
http://aspbooks.org/publications/504/099.pdf

The STEREO mission spacecraft recently passed through superior conjunction, providing an opportunity to probe the solar corona using radio transmissions. Strong magnetic field and dense plasma environment induce Faraday rotation of the linearly polarized fraction of the spacecraft radio carrier signal. Variations in the Faraday rotation signify changes in magnetic field components and plasma parameters, and thus can be used to gain understanding processes of the quiescent sun as well as active outbursts including coronal mass ejections. Our 2015 observing campaign resulted in a series of measurements over several months with the 100m Green Bank Telescope (GBT) to investigate the coronal Faraday rotation at various radial distances. These observations reveal notable fluctuations in the Faraday rotation of the signal in the deep corona, and should yield unique insights into coronal magnetohydrodynamics down to a 1.5 solar radius line-of-sight solar elongation.

OBSERVED CORE OF A GRADUAL SOLAR ENERGETIC PARTICLE EVENT

L. **Kocharov**1, M. J. Reiner2, A. Klassen3, B. J. Thompson2, and E. Valtonen1
Astrophysical Journal, 725:2262–2269, **2010, File**

Using space-borne particle and EUV detection and radio spectrograms from both ground-based and space-borne instruments, we study the first phase of the major solar energetic particle (SEP) event associated with the western solar flare and fast and wide coronal mass ejection (CME) on **2000 April 4.** The SEP event being observed at the magnetic connection to the eruption's center starts with deka–MeV nucl-1 helium- and relativistic electron-rich production from coronal sources identified with the electromagnetic diagnostics and the SEP event modeling. The broadband observations and modeling of the initial phase of the "well-connected" major SEP event support the idea that acceleration of SEPs starts in the helium-rich plasma of the eruption's core in association with coronal shocks and magnetic reconnections caused by the CME liftoff, and that the coronal component dominates during the first hour of the SEP event considered, not yet being shielded by the CME bow shock in the solar wind. The first phase of the SEP event is followed by a second phase of SEP production associated with a decelerating CME-driven shock wave in the solar wind, which accelerates ions from a distinct, helium-poor seed particle population that may originate from the CME interaction with a coronal streamer.

The interaction of a plasmoid with a loop-top kernel

S. **Kolomanski**1, 2 and M. Karlický1

A&A 475, 685-693 (**2007**)

We study the interaction between a downward moving plasmoid and a loop-top kernel recognized in the **30 November 2000** flare. Such an interaction is predicted by some numerical models of solar flares.
Many details of this interaction are found, e.g., an increase of the X-ray and decimetric radio fluxes and an increase of the plasma temperature at the interaction site. Just after the coalescence of the plasmoid with the loop-top kernel, the 1-2 GHz pulsating radio structure and hard X-ray source above the coalescence site were observed.

Flare-associated X-ray plasma ejections and radio drifting structures.

Koloma´nski, S., Tomczak, M., Ronowicz, P., Karlický, M., Aurass, H.:

2007, *Cent. Eur. Astrophys. Bull.* **31**, 125 – 134.

Fast magnetoacoustic wave trains: from tadpoles to boomerangs

Dmitrii Y. **Kolotkov**, Valery M. Nakariakov, Guy Moss, Paul Shellard

MNRAS **2021**

https://arxiv.org/pdf/2105.13696.pdf

Rapidly propagating fast magnetoacoustic wave trains guided by field-aligned plasma non-uniformities are confidently observed in the Sun's corona. Observations at large heights suggest that fast wave trains can travel long distances from the excitation locations. We study characteristic time signatures of fully developed, dispersive fast magnetoacoustic wave trains in field-aligned zero-β plasma slabs in the linear regime. Fast wave trains are excited by a spatially localised impulsive driver and propagate along the waveguide as prescribed by the waveguide-caused dispersion. In slabs with steeper transverse density profiles, developed wave trains are shown to consist of three distinct phases: a long-period quasi-periodic phase with the oscillation period shortening with time, a multi-periodic (peloton) phase in which distinctly different periods co-exist, and a short-lived periodic Airy phase. The appearance of these phases is attributed to a non-monotonic dependence of the fast wave group speed on the parallel wavenumber due to the waveguide dispersion, and is shown to be different for axisymmetric (sausage) and non-axisymmetric (kink) modes. In wavelet analysis, this corresponds to the transition from the previously known tadpole shape to a new boomerang shape of the wave train spectrum, with two well-pronounced arms at shorter and longer periods. We describe a specific previously published radio observation of a coronal fast wave train, highly suggestive of a change of the wavelet spectrum from a tadpole to a boomerang, broadly consistent with our modelling. The applicability of these boomerang-shaped fast wave trains for probing the transverse structuring of the waveguiding coronal plasma is discussed.

The origin of the modulation of the radio emission from the solar corona by a fast magnetoacoustic wave

Dmitrii Y. **Kolotkov**,1 Valery M. Nakariakov,1, 2 and Eduard P. Kontar3

2018 *ApJ* **861** 33

https://warwick.ac.uk/fac/sci/physics/research/cfsa/people/kolotkov/eprints/lofar_fast_r1.pdf

https://arxiv.org/pdf/1805.08282.pdf

Observational detection of quasi-periodic drifting fine structures in a type III radio burst associated with a solar flare SOL**2015-04-16**T11:22, with Low Frequency Array, is presented. Although similar modulations of the type III emission have been observed before and were associated with the plasma density fluctuations, the origin of those fluctuations was unknown. Analysis of the striae of the intensity variation in the dynamic spectrum allowed us to reveal two quasi-oscillatory components. The shorter component has the apparent wavelength of ∼ 2 Mm, phase speed of ∼ 657 km s−1 , which gives the oscillation period of ∼ 3 s, and the relative amplitude of ∼ 0.35%. The longer component has the wavelength of ∼ 12 Mm, and relative amplitude of ∼ 5.1%. The short frequency range of the detection does not allow us to estimate its phase speed. However, the properties of the shorter oscillatory component allowed us to interpret it as a fast magnetoacoustic wave guided by a plasma non-uniformity along the magnetic field outwards from the Sun. The assumption that the intensity of the radio emission is proportional to the amount of plasma in the emitting volume allowed us to show that the superposition of the plasma density modulation by a fast wave and a longer-wavelength oscillation of an unspecified nature could readily reproduce the fine structure of the observed dynamic spectrum. The observed parameters of the fast wave give the absolute value of the magnetic field model.

Modulation of radio emission, fast magnetoacoustic waves and magnetic field measurements in the solar corona with LOFAR

Dmitrii Y. **Kolotkov**, Valery M. Nakariakov, and Eduard P. Kontar

CESRA nuggets #1954, Aug **2018** http://cesra.net/?p=1954

2015 April 16

Multi-mode quasi-periodic pulsations in a solar flare

D. Y. **Kolotkov**1, V. M. Nakariakov1,2,3, E. G. Kupriyanova3, H. Ratcliffe1 and K. Shibasaki
A&A 574, A53 (**2015**)

Context. Quasi-periodic pulsations (QPP) of the electromagnetic radiation emitted in solar and stellar flares are often detected in microwave, white light, X-ray, and gamma-ray bands. Mechanisms for QPP are intensively debated in the literature. Previous studies revealed that QPP may manifest non-linear, non-stationary and, perhaps, multi-modal processes operating in flares.
Aims. We study QPP of the microwave emission generated in an X3.2-class solar flare on **14 May, 2013**, observed with the Nobeyama Radioheliograph (NoRH), aiming to reveal signatures of the non-linear, non-stationary, and multi-modal processes in the signal.
Methods. The NoRH correlation signal obtained at the 17 GHz intensity has a clear QPP pattern. The signal was analysed with the Hilbert-Huang transform (HHT) that allows one to determine its instant amplitude and frequency, and their time variation.
Results. It was established that the QPP consists of at least three well-defined intrinsic modes, with the mean periods of 15, 45, and 100 s. All the modes have quasi-harmonic behaviour with different modulation patterns. The 100 s intrinsic mode is a decaying oscillation, with the decay time of 250 s. The 15 s intrinsic mode shows a similar behaviour, with the decay time of 90 s. The 45 s mode has a wave-train behaviour.
Conclusions. Dynamical properties of detected intrinsic modes indicate that the 100 s and 15 s modes are likely to be associated with fundamental kink and sausage modes of the flaring loop, respectively. The 100 s oscillation could also be caused by the fundamental longitudinal mode, while this interpretation requires the plasma temperature of about 30 million K and hence is not likely. The 45 s mode could be the second standing harmonics of the kink mode.

Observation of a Metric Type N Solar Radio Burst

Xiangliang **Kong**, Yao Chen, Shiwei Feng, Guohui Du, Chuanyang Li, Artem Koval, V. Vasanth, Bing Wang, Fan Guo, Gang Li
ApJ 830 37 **2016**
http://arxiv.org/pdf/1608.00093v1.pdf

. Type III and type-III-like radio bursts are produced by energetic electron beams guided along coronal magnetic fields. As a variant of type III bursts, Type N bursts appear as the letter "N" in the radio dynamic spectrum and reveal a magnetic mirror effect in coronal loops. Here, we report a well-observed N-shaped burst consisting of three successive branches at metric wavelength with both fundamental and harmonic components and a high brightness temperature (>109 K). We verify the burst as a true type N burst generated by the same electron beam from three aspects of the data. First, durations of the three branches at a given frequency increase gradually, may due to the dispersion of the beam along its path. Second, the flare site, as the only possible source of non-thermal electrons, is near the western feet of large-scale closed loops. Third, the first branch and the following two branches are localized at different legs of the loops with opposite sense of polarization. We also find that the sense of polarization of the radio burst is in contradiction to the O-mode and there exists a fairly large time delay (~3-5 s) between the fundamental and harmonic components. Possible explanations accounting for these observations are presented. Assuming the classical plasma emission mechanism, we can infer coronal parameters such as electron density and magnetic field near the radio source and make diagnostics on the magnetic mirror process. **2014 May 6**

Electron Acceleration at a Coronal Shock Propagating Through a Large-scale Streamer-like Magnetic Field

Xiangliang **Kong**, Yao Chen, Fan Guo, Shiwei Feng, Guohui Du, Gang Li
ApJ **821** 32 **2016**
http://arxiv.org/pdf/1602.08170v1.pdf

With a test-particle simulation, we investigate the effect of large-scale coronal magnetic fields on electron acceleration at an outward-propagating coronal shock with a circular front. The coronal field is approximated by an analytical solution with a streamer-like magnetic field featured by partially open magnetic field and a current sheet at the equator atop the closed region. We show that the large-scale shock-field configuration, especially the relative curvature of the shock and the magnetic field line across which the shock is sweeping, plays an important role in the efficiency of electron acceleration. At low shock altitudes, when the shock curvature is larger than that of magnetic field lines, the electrons are mainly accelerated at the shock flanks; at higher altitudes, when the shock curvature is smaller, the electrons are mainly accelerated at the shock nose around the top of closed field lines. The above process reveals the shift of efficient electron acceleration region along the shock front during its propagation. It is also found that in general the electron acceleration at the shock flank is not so efficient as that at the top of closed field since at the top a collapsing magnetic trap can be formed. In addition, we find that the energy spectra of electrons is power-law like, first hardening then softening with the spectral index varying in a range of -3 to -6. Physical interpretations of the results and implications on the study of solar radio bursts are discussed**.**

Possible role of coronal streamer as magnetically-closed structure in shock-induced energetic electrons and metric type II radio bursts

Xiangliang **Kong**, Yao Chen, Fan Guo, Shiwei Feng, Bing Wang, Guohui Du, Gang Li
2015 *ApJ* **798** 81
http://arxiv.org/pdf/1410.7994v1.pdf
Two solar type II radio bursts, separated by ~24 hours in time, are examined together. Both events are associated with coronal mass ejections (CMEs) erupting from the same active region (NOAA 11176) beneath a well-observed helmet streamer. We find that the type II emissions in both events ended once the CME/shock fronts passed the white-light streamer tip, which is presumably the magnetic cusp of the streamer. This leads us to conjecture that the closed magnetic arcades of the streamer may play a role in electron acceleration and type II excitation at coronal shocks. To examine such a conjecture, we conduct a test-particle simulation for electron dynamics within a large-scale partially-closed streamer magnetic configuration swept by a coronal shock. We find that the closed field lines play the role of an electron trap, via which the electrons are sent back to the shock front for multiple times, and therefore accelerated to high energies by the shock. Electrons with an initial energy of 300eV can be accelerated to tens of keV concentrating at the loop apex close to the shock front with a counter-streaming distribution at most locations. These electrons are energetic enough to excite Langmuir waves and radio bursts. Considering the fact that most solar eruptions originate from closed field regions, we suggest that the scenario may be important to the generation of more metric type IIs. This study also provides an explanation to the general ending frequencies of metric type IIs at or above 20-30 MHz and the disconnection issue between metric and interplanetary type IIs. **2011 March 25**

A BROKEN SOLAR TYPE II RADIO BURST INDUCED BY A CORONAL SHOCK PROPAGATING ACROSS THE STREAMER BOUNDARY

X. L. **Kong**, Y. Chen, G. Li, S. W. Feng, H. Q. Song, F. Guo, and F. R. Jiao
2012 ApJ 750 158, **File**
We discuss an intriguing type II radio burst that occurred on **2011 March 27**. The dynamic spectrum was featured by a sudden break at about 43 MHz on the well-observed harmonic branch. Before the break, the spectrum drifted gradually with a mean rate of about –0.05 MHz s–1. Following the break, the spectrum jumped to lower frequencies. The post-break emission lasted for about 3 minutes. It consisted of an overall slow drift which appeared to have a few fast-drift sub-bands. Simultaneous observations from the Solar TErrestrial RElations Observatory and the Solar Dynamics Observatory were also available and are examined for this event. We suggest that the slow-drift period before the break was generated inside a streamer by a coronal eruption driven shock, and the spectral break as well as the relatively wide spectrum after the break is a consequence of the shock crossing the streamer boundary where density drops abruptly. It is suggested that this type of radio bursts can be taken as a unique diagnostic tool for inferring the coronal density structure, as well as the radio-emitting source region.

Absorption in Burst Emission

A.A. **Konovalenko** · A.A. Stanislavsky · E.P. Abranin · V.V. Dorovsky · V.N. Mel'nik · M.L. Kaiser · A. Lecacheux · H.O. Rucker
Solar Phys (2007) 245: 345–354
http://www.springerlink.com/content/68l46247578pm622/fulltext.pdf
Here we report a radio burst in absorption at 9 – 30 MHz observed with the UTR-2 telescope. This event occurred on **19 August 2003** about 11:16 – 11:26 UT, against solar type IV/II emission background. It is the first event where absorption was observed below 30 MHz. The absorption region, comparable with the solar radius size, traveled a long distance into the upper corona from the Sun. We show that the burst minimum corresponds to the almost full absorption of the solar radio emission up to a background level of the quiescent Sun. This supports the interpretation of the phenomenon as an absorption. The result is examined independently with the Nançay Decameter Array measurements and the *Wind*
WAVES instrument records.

Advection-nonlinear-diffusion model of flare accelerated electron transport in Type III solar radio bursts

Eduard P. **Kontar**, Francesco Azzollini, Olena Lyubchyk
ApJ **976** 233 **2024**
https://arxiv.org/pdf/2410.11409
https://iopscience.iop.org/article/10.3847/1538-4357/ad8560/pdf
Electrons accelerated by solar flares and observed as type III solar radio bursts are not only a crucial diagnostic tool for understanding electron transport in the inner heliosphere but also a possible early indication of potentially hazardous space weather events. The electron beams travelling in the solar corona and heliosphere along magnetic field lines generate Langmuir waves and quasilinearly relax towards a plateau in velocity space. The relaxation of the electron

beam over the short distance in contrast to large beam-travel distances observed is often referred to as Sturrok's dilemma. Here, we develop a new electron transport model with quasilinear distance/time self-consistently changing in space and time. The model results in a nonlinear advection-diffusion equation for the electron beam density with nonlinear diffusion term that inversely proportional to the beam density. The solution predicts slow super-diffusive (ballistic) spatial expansion of a fast propagating electron beam. The model also provides the evolution of the spectral energy density of Langmuir waves, which determines brightness temperature of plasma radiation in solar bursts. The model solution is consistent with the results of numerical simulation using kinetic equations and can explain some characteristics of type III solar radio bursts.

RHESSI Science Nugget, No. **481**, Dec **2024**

https://heliowiki.smce.nasa.gov/wiki/index.php/Advection_and_super-diffusive_expansion_as_the_model_of_flare_accelerated_electron_transport_in_type_III_solar_radio_bursts

An Anisotropic Density Turbulence Model from the Sun to 1 au Derived From Radio Observations

Eduard P. **Kontar**, A. Gordon Emslie, Daniel L. Clarkson, Xingyao Chen, Nicolina Chrysaphi, Francesco Azzollini, Natasha L. S. Jeffrey, Mykola Gordovskyy

ApJ **956** 112 **2023**

https://arxiv.org/pdf/2308.05839.pdf

https://iopscience.iop.org/article/10.3847/1538-4357/acf6c1/pdf

Solar radio bursts are strongly affected by radio-wave scattering on density inhomogeneities, changing their observed time characteristics, sizes, and positions. The same turbulence causes angular broadening and scintillation of galactic and extra-galactic compact radio sources observed through the solar atmosphere. Using large-scale simulations of radio-wave transport, the characteristics of anisotropic density turbulence from 0.1R⊙ to 1 au are explored. For the first time, a profile of heliospheric density fluctuations is deduced that accounts for the properties of extra-solar radio sources, solar radio bursts, and in-situ density fluctuation measurements in the solar wind at 1 au. The radial profile of the spectrum-weighted mean wavenumber of density fluctuations (a quantity proportional to the scattering rate of radio-waves) is found to have a broad maximum at around (4−7)R⊙, where the slow solar wind becomes supersonic. The level of density fluctuations at the inner scale (which is consistent with the proton resonance scale) decreases with heliocentric distance as ⟨δni2⟩(r)≃2×107(r/R⊙−1)−3.7 cm−6. Due to scattering, the apparent positions of solar burst sources observed at frequencies between 0.1 and 300 MHz are computed to be essentially cospatial and to have comparable sizes, for both fundamental and harmonic emission. Anisotropic scattering is found to account for the shortest solar radio burst decay times observed, and the required wavenumber anisotropy is q∥/q⊥=0.25−0.4, depending on whether fundamental or harmonic emission is involved. The deduced radio-wave scattering rate paves the way to quantify intrinsic solar radio burst characteristics.

CESRA #3691 **2023** https://www.astro.gla.ac.uk/users/eduard/cesra/?p=3691

CESRA #3723 **2024** https://www.astro.gla.ac.uk/users/eduard/cesra/?p=3723

The efficiency of electron acceleration during the impulsive phase of a solar flare

Eduard P. **Kontar**, A. Gordon Emslie, Galina G. Motorina, Brian R. Dennis

ApJ **947** L13 **2023**

https://arxiv.org/pdf/2304.01088.pdf

https://iopscience.iop.org/article/10.3847/2041-8213/acc9b7/pdf

Solar flares are known to be prolific electron accelerators, yet identifying the mechanism(s) for such efficient electron acceleration in solar flare (and similar astrophysical settings) presents a major challenge. This is due in part to a lack of observational constraints related to conditions in the primary acceleration region itself. Accelerated electrons with energies above ~20~keV are revealed by hard X-ray (HXR) bremsstrahlung emission, while accelerated electrons with even higher energies manifest themselves through radio gyrosynchrotron emission. Here we show, for a well-observed flare on **2017~September~10**, that a combination of \emph{RHESSI} hard X-ray and and SDO/AIA EUV observations provides a robust estimate of the fraction of the ambient electron population that is accelerated at a given time, with an upper limit of $\lapprox 10^{-2}$ on the number density of nonthermal (≥20~keV) electrons, expressed as a fraction of the number density of ambient protons in the same volume. This upper limit is about two orders of magnitude lower than previously inferred from microwave observations of the same event. Our results strongly indicate that the fraction of accelerated electrons in the coronal region at any given time is relatively small, but also that the overall duration of the HXR emission requires a steady resupply of electrons to the acceleration site. Simultaneous measurements of the instantaneous accelerated electron number density and the associated specific electron acceleration rate provide key constraints for a quantitative study of the mechanisms leading to electron acceleration in magnetic reconnection events.

RHESSI Nugget #449 2023

https://sprg.ssl.berkeley.edu/~tohban/wiki/index.php/Did_a_Solar_Flare_Accelerate_all_the_Ambient_Electrons_in_the_Coronal_Acceleration_Region%3F...

CESRA #3538 **2023** https://www.astro.gla.ac.uk/users/eduard/cesra/?p=3538

Anisotropic Radio-Wave Scattering and the Interpretation of Solar Radio Emission Observations

Eduard P. **Kontar**, Xingyao Chen, Nicolina Chrysaphi, Natasha L.S. Jeffrey, A. Gordon Emslie, Vratislav Krupar, Milan Maksimovic, Mykola Gordovskyy, Philippa K. Browning

ApJ **884** 122 **2019**

https://arxiv.org/pdf/1909.00340.pdf

https://doi.org/10.3847/1538-4357/ab40bb

The observed properties (i.e., source size, source position, time duration, decay time) of solar radio emission produced through plasma processes near the local plasma frequency, and hence the interpretation of solar radio bursts, are strongly influenced by propagation effects in the inhomogeneous turbulent solar corona. In this work, a 3D stochastic description of the propagation process is presented, based on the Fokker-Planck and Langevin equations of radio-wave transport in a medium containing anisotropic electron density fluctuations. Using a numerical treatment based on this model, we investigate the characteristic source sizes and burst decay times for Type III solar radio bursts. Comparison of the simulations with the observations of solar radio bursts shows that predominantly perpendicular density fluctuations in the solar corona are required, with an anisotropy factor ~0.3 for sources observed at around 30~MHz. The simulations also demonstrate that the photons are isotropized near the region of primary emission, but the waves are then focused by large-scale refraction, leading to plasma radio emission directivity that is characterized by a half-width-half-maximum of about 40~degrees near 30~MHz. The results are applicable to various solar radio bursts produced via plasma emission.

CESRA highlights #2399 **2019** http://www.astro.gla.ac.uk/users/eduard/cesra/?p=2399

Dynamics of electron beams in the solar corona plasma with density fluctuations

Eduard P. **Kontar**

A&A **2019**

https://arxiv.org/pdf/1904.05650.pdf

The problem of beam propagation in a plasma with small scale and low intensity inhomogeneities is investigated. It is shown that the electron beam propagates in a plasma as a beam-plasma structure and is a source of Langmuir waves. The plasma inhomogeneity changes the spatial distribution of the waves. The spatial distribution of the waves is fully determined by the distribution of plasma inhomogeneities. The possible applications to the theory of radio emission associated with electron beams are discussed.

Nonlinear development of electron-beam-driven weak turbulence in an inhomogeneous plasma

E. P. **Kontar**, H. L. Pecseli

2019

https://arxiv.org/pdf/1903.08368.pdf

The self-consistent description of Langmuir wave and ion-sound wave turbulence in the presence of an electron beam is presented for inhomogeneous non-isothermal plasmas. Full numerical solutions of the complete set of kinetic equations for electrons, Langmuir waves, and ion-sound waves are obtained for a inhomogeneous unmagnetized plasma. The result show that the presence of inhomogeneity significantly changes the overall evolution of the system. The inhomogeneity is effective in shifting the wavenumbers of the Langmuir waves, and can thus switch between different process governing the weakly turbulent state. The results can be applied to a variety of plasma conditions, where we choose solar coronal parameters as an illustration, when performing the numerical analysis.

Frequency rising sub-THz emission from solar flare ribbons

E.P. **Kontar**, G.G. Motorina, N.L.S. Jeffrey, Y.T. Tsap, G.D. Fleishman, A.V. Stepanov

A&A 620, A95 **2018**

https://arxiv.org/pdf/1810.03922.pdf

http://sci-hub.tw/https://www.aanda.org/articles/aa/abs/2018/12/aa34124-18/aa34124-18.html

Observations of solar flares at sub-THz frequencies (mm and sub-mm wavelengths) over the last two decades often show a spectral component rising with frequency. Unlike a typical gyrosynchrotron spectrum decreasing with frequency, or a weak thermal component from hot coronal plasma, the observations can demonstrate a high flux level (up to ~10^4 s.f.u. at 0.4 THz) and fast variability on sub-second time scales. Although, many models has been put forward to explain the puzzling observations, none of them have clear observational support. Here we propose a scenario to explain the intriguing sub-THz observations. We show that the model, based on free-free emission from the plasma of flare ribbons at temperatures 10^4-10^6 K, is consistent with all existing observations of frequency-rising sub-THz flare emission. The model provides a temperature diagnostic of the flaring chromosphere and suggests fast

heating and cooling of the dense transition region plasma. **2000-03-22, 2001-04-12, 2003-10-27, 2003-10-28, 2003-11-02, 2003-11-04, 2006-12-06, 2012-01-27, 2012-03-13, 2012-10-22, 2012-07-04, 2012-07-05, 2013-02-17, 2014-10-22, 2014-10-27, 2014-11-05, 2014-11-07**
Table 1. A list of flares with a rising spectrum of sub-THz emission (2000-2014)
Table 2. A list of flares with a decreasing spectrum of sub-THz emission. (2012-2014)
CESRA #2157 March **2019** **http://www.astro.gla.ac.uk/users/eduard/cesra/?p=2157**

Combined Radio and Space-based Solar Observations: From Techniques to New Results **Review**

E.P. **Kontar**, A. Nindos
Solar Phys. 293:90 **2018**
https://arxiv.org/pdf/1806.05919.pdf
https://link.springer.com/content/pdf/10.1007%2Fs11207-018-1309-2.pdf
The phenomena observed at the Sun have a variety of unique radio signatures that can be used to diagnose the processes in the solar atmosphere. The insights provided by radio obervations are further enhanced when they are combined with observations from space-based telescopes. This special issue demonstrates the power of combination methodology at work and provides new results on i) type I solar radio bursts and thermal emission to study active regions; ii) type II and IV bursts to better understand the structure of coronal mass ejections; iii)~non-thermal gyro-synchrotron and/or type III bursts to improve characterization of particle acceleration in solar flares. The ongoing improvements in time, frequency, and spatial resolutions of ground-based telescopes reveal new levels of solar phenomena complexity and pose new questions. 2003-10-28

Imaging Spectroscopy of Solar Radio Burst Fine Structures

E. P. **Kontar**, S. Yu, A. A. Kuznetsov, A. G. Emslie, B. Alcock, N. L. S. Jeffrey, V. N. Melnik, N. H. Bian, P. Subramanian
Nature Communications **8**, Article number: 1515 (**2017**) DOI: **10.1038/s41467-017-01307-8**
https://arxiv.org/pdf/1708.06505.pdf
sci-hub.se/10.1038/s41467-017-01307-8
https://doi.org/10.1038/s41467-017-01307-8
Solar radio observations provide a unique diagnostic of the outer solar atmosphere. However, the inhomogeneous turbulent corona strongly affects the propagation of the emitted radio waves, so decoupling the intrinsic properties of the emitting source from the effects of radio-wave propagation has long been a major challenge in solar physics. Here we report quantitative spatial and frequency characterization of solar radio burst fine structures observed with the LOw Frequency Array (LOFAR), an instrument with high time resolution that also permits imaging at scales much shorter than those corresponding to radio-wave propagation in the corona. The observations demonstrate that radio-wave propagation effects, and not the properties of the intrinsic emission source, dominate the observed spatial characteristics of radio burst images. These results permit more accurate estimates of source brightness temperatures, and open opportunities for quantitative study of the mechanisms that create the turbulent coronal medium through which the emitted radiation propagates. **2015 April 16**,
CESRA highlight #1675 Nov **2017** http://cesra.net/?p=1675

Imaging spectroscopy of fine structures with LOFAR: implication for radio wave propgation

Eduard **Kontar**∗1 , Sijie Yu , Alexey Kuznetsov , Xingyao Chen , Yihua Yan , and Valentin Melnik
CESRA **2016 p.36**
http://cesra2016.sciencesconf.org/conference/cesra2016/pages/CESRA2016_prog_abs_book_v3.pdf
The solar radio bursts observed at frequencies below 300 MHz sometimes demonstrate fine structures, so that the dynamic spectrum of the burst looks like a collection of multiple stria, so called type IIIb bursts. Recent observations with LOFAR allow us to determine the location of individual stria and determine how they evolve in space at the time scales less than 0.5 sec. In this work, we present the first imaging observations of stria evolution for a well observed type IIIb-type III event and show how the spatial characteristics of the burst emitted at fundamental and harmonic are related to the spectral features in the range 30-80 MHz. The implication for poorly understood escape and propagation of radio waves will be presented.

Onsets and spectra of impulsive solar energetic electron events

observed near the Earth
Eduard P. **Kontar** and Hamish A. S. Reid
E-print, March **2009**; ApJL, **695,** L140-L144 doi: 10.1088/0004-637X/695/2/L140
Impulsive solar energetic electrons are often observed in the interplanetary space near the Earth and have an attractive diagnostic potential for poorly understood solar flare acceleration processes. We investigate the transport of solar flare energetic electrons in the heliospheric plasma to understand the role of transport to the observed onset and spectral

properties of the impulsive solar electron events. The propagation of energetic electrons in solar wind plasma is simulated from the acceleration region at the Sun to the Earth, taking into account self-consistent generation and absorption of electrostatic electron plasma (Langmuir) waves, effects of non-uniform plasma, collisions and Landau damping. The simulations suggest that the beam-driven plasma turbulence and the effects of solar wind density inhomogeneity play a crucial role and lead to the appearance of a) spectral break for a single power-law injected electron spectrum, with the spectrum flatter below the break, b) apparent early onset of low-energy electron injection, c) the apparent late maximum of low-energy electron injection. We show that the observed onsets, spectral flattening at low energies, and formation of a break energy at tens of keV is the direct manifestation of wave-particle interactions in non-uniform plasma of a single accelerated electron population with
an initial power-law spectrum.

Dynamics of electron beams in the inhomogeneous solar corona plasma

Eduard P. **Kontar**

Solar Physics August **2001**, Volume 202, Issue 1, pp 131–149

https://arxiv.org/pdf/1903.08867.pdf

Dynamics of an spatially limited electron beam in the inhomogeneous solar corona plasma is considered in the framework of weak turbulence theory when the temperature of the beam significantly exceeds that of surrounding plasma. The numerical solution of kinetic equations manifests that generally the beam accompanied by Langmuir waves propagates as a beam-plasma structure with a decreasing velocity. Unlike the uniform plasma case the structure propagates with the energy losses in the form of Langmuir waves. The results obtained are compared with the results of observations of type III bursts. It is shown that the deceleration of type III sources can be explained by the corona inhomogeneity. The frequency drift rates of the type III sources are found in a good agreement with the numerical results of beam dynamics.

Numerical consideration of quasilinear electron cloud dynamics in plasma

Eduard P. **Kontar**

Computer Physics Communications Volume 138, Issue 3, 15 August **2001**, Pages 222-233

https://arxiv.org/pdf/1903.08651.pdf

The dynamics of a hot electron cloud in the solar corona-like plasma based on the numerical solution of kinetic equations of weak turbulence theory is considered. Different finite difference schemes are examined to fit the exact analytical solutions of quasilinear equations in hydrodynamic limit (gas-dynamic solution). It is shown that the scheme suggested demonstrates correct asymptotic behavior and can be employed to solve initial value problems for an arbitrary initial electron distribution function.

Measuring solar radio bursts in 20–650 MHz

A. **Kontogeorgos** a,b,*, P. Tsitsipis a,b, C. Caroubalos a , X. Moussas a , P. Preka-Papadema a , A. Hilaris a , V. Petoussis a,b, J.-L. Bougeret c , C.E. Alissandrakis d , G. Dumas c

Measurement 41 (**2008**) 251–258

http://artemis-iv.phys.uoa.gr/pubs/2008_Kontogeorgos&al.pdf

The solar radiospectrograph of the University of Athens is installed at the Thermopylae Satellite Telecommunication Station. The observations cover the frequency range from 20 to 650 MHz. The spectrograph has a 7-m moving parabola feeding by a log-period antenna for 100–650 MHz and a stationary inverted V fat dipole antenna for 20–100 MHz. Two receivers are operating in parallel: a sweep frequency for the whole range (10 spectra/s, 630 channels/spectrum) and an acousto-optical receiver for the range 270–450 MHz (10 spectra/s, 128 channels/spectrum). The data acquisition system consists of two PCs (equipped with 12 bit, 225 ksamples/s DAC, one for every receiver). The daily operation is fully automated: receiving universal time from a GPS, pointing the antenna to the Sun, initiating system calibration, starting and stopping the observations at preset times, data acquisition, and archiving on DVD. We can also control the whole system through modem or Internet. The instrument can be used either by itself to study the onset and evolution of solar radio bursts and associated interplanetary phenomena or in conjunction with other instruments

The improved ARTEMIS IV multichannel solar radio spectrograph of the University of Athens

Kontogeorgos, A.; Tsitsipis, P.; Caroubalos, C.; Moussas, X.; Preka-Papadema, P.; Hilaris, A.; Petoussis, V.; Bouratzis, C.; Bougeret, J.-L.; Alissandrakis, C. E.; Dumas, G.

Experimental Astronomy, Volume 21, Issue 1, pp.41-55, **2006**

http://arxiv.org/pdf/1009.3628v1.pdf

http://users.uoa.gr/~ahilaris/2006B_Kontogeorgos&al.pdf

We present the improved solar radio spectrograph of the University of Athens operating at the Thermopylae Satellite Telecommunication Station. Observations now cover the frequency range from 20 to 650 MHz. The spectrograph has a 7-meter moving parabola fed by a log-periodic antenna for 100 650 MHz and a stationary inverted V fat dipole antenna

for the 20 100 MHz range. Two receivers are operating in parallel, one swept frequency for the whole range (10 spectrums/sec, 630 channels/spectrum) and one acousto-optical receiver for the range 270 to 450 MHz (100 spectrums/sec, 128 channels/spectrum). The data acquisition system consists of two PCs (equipped with 12 bit, 225 ksamples/sec ADC, one for each receiver). Sensitivity is about 3 SFU and 30 SFU in the 20 100 MHz and 100 650 MHz range respectively. The daily operation is fully automated: receiving universal time from a GPS, pointing the antenna to the sun, system calibration, starting and stopping the observations at preset times, data acquisition, and archiving on DVD. We can also control the whole system through modem or Internet. The instrument can be used either by itself or in conjunction with other instruments to study the onset and evolution of solar radio bursts and associated interplanetary phenomena. ***26 April 2003***

Multipoint Radio Probe of the Solar Corona: the Trans-Coronal Radio Array Fleet (T-CRAF)

Jason **Kooi**, David Wexler, Elizabeth Jensen, and Brian Wood
Front. Astron. Space Sci. 9: 1026422 **2022**
https://doi.org/10.3389/fspas.2022.1026422
https://www.frontiersin.org/articles/10.3389/fspas.2022.1026422/pdf
The Trans-Coronal Radio Array Fleet (T-CRAF) is a mission concept designed to continuously probe the magnetic field and plasma density structure of the corona at heliocentric distances of ≈ 2 − 10 R⊙ (solar radius, R⊙ = 695, 700 km). T-CRAF consists of thirty small satellites orbiting the Sun-Earth Lagrange Point L3 in order to provide thirty lines of sight (LOS) for ground- or space-based radio propagation studies. T-CRAF is divided into three sets of orbits, each with ten satellites: the first group provides LOS at a solar offset, SO (i.e. closest solar approach) of heliocentric distances 2–4 R⊙ to provide continuous coverage in the middle corona, including initial slow solar wind acceleration; the second group of spacecraft probes the corona at SO = 4–7 R⊙ to cover the region including transition to a supersonic slow solar wind; the outer T-CRAF group is positioned to afford coverage for SO > 7 R⊙ as the winds continue to accelerate towards the Alfvén speed threshold. Each satellite is equipped with a multi-frequency (S-band, C-band, and X-band) linearly polarized transmitter. T-CRAF provides the capability to simultaneously measure the mean values and fluctuations of the magnetic field and plasma density within the solar wind, stream interaction regions, and coronal mass ejections (CMEs). Multiple downlink frequencies provide opportunities to use radio ranging (measurement of group time delay) and apparent-Doppler tracking (measurement of frequency shifts) to infer the plasma density and density gradient along each LOS. Linearly polarized signals provide the ability to detect Faraday rotation (FR) and FR fluctuations, used to infer the magnetic field and field fluctuations along each LOS. **2000 February 27**

Modern Faraday Rotation Studies to Probe the Solar Wind

Jason **Kooi**, David Wexler, Elizabeth Jensen, Megan Kenny, Teresa Nieves-Chinchilla, Lynn Wilson III, Brian Wood, Lan Jian, Shing Fung, Alexei Pevtsov, Nat Gopalswamy, and Ward Manchester
Front. Astron. Space Sci., 9:841866. **2022** |
https://doi.org/10.3389/fspas.2022.841866
https://www.frontiersin.org/articles/10.3389/fspas.2022.841866/full
https://www.frontiersin.org/articles/10.3389/fspas.2022.841866/pdf
For decades, observations of Faraday rotation have provided unique insights into the plasma density and magnetic field structure of the solar wind. Faraday rotation (FR) is the rotation of the plane of polarization when linearly polarized radiation propagates through a magnetized plasma, such as the solar corona, coronal mass ejection (CME), or stream interaction region. FR measurements are very versatile: they provide a deeper understanding of the large-scale coronal magnetic field over a range of heliocentric distances (especially ≈1.5≈1.5 to 20 R⊙) not typically accessible to in situ spacecraft observations; detection of small-timescale variations in FR can provide information on magnetic field fluctuations and magnetohydrodynamic wave activity; and measurement of differential FR can be used to detect electric currents. FR depends on the integrated product of the plasma density and the magnetic field component along the line of sight to the observer; historically, models have been used to distinguish between their contributions to FR. In the last two decades, though, new methods have been developed to complement FR observations with independent measurements of the plasma density based on the choice of background radio source: calculation of the dispersion measure (pulsars), measurement of Thomson scattering brightness (radio galaxies), and application of radio ranging and apparent-Doppler tracking (spacecraft). New methods and new technology now make it possible for FR observations of solar wind structures to return not only the magnitude of the magnetic field, but also the full vector orientation. In the case of a CME, discerning the internal magnetic flux rope structure is critical for space weather applications. **2003 October 28 , 2011 August 17 , 2012 August 2, 2013 May 10, 2015 July 31, 2015 August 21,**

VLA Measurements of Faraday Rotation Through a Coronal Mass Ejection Using Multiple Lines of Sight

Jason E. **Kooi**, Madison L. Ascione, Lianis V. Reyes-Rosa, Sophia K. Rier & Mohammad Ashas
Solar Physics volume 296, Article number: 11 (**2021**)

https://link.springer.com/content/pdf/10.1007/s11207-020-01755-4.pdf
Coronal mass ejections (CMEs) are large eruptions of magnetized plasma from the Sun that play an important role in space weather. The key to understanding the fundamental physics of a CME is measurement of the plasma properties within heliocentric distances of <20 R⊙. Faraday rotation, a radioastronomical propagation measurement, is an extremely valuable diagnostic for studying CMEs. Faraday rotation measurements [RM] contain information on the magnetic field in the medium causing the Faraday rotation. Recent observations of CME-induced Faraday rotation (e.g., Howard et al. in Astrophys. J. 831, 208, 2016; Kooi et al. in Solar Phys. 292, 56, 2017; Bisi et al. in EGU General Assembly Conference Abstracts, 13243, 2017) have all been restricted to a single line of sight (LOS) and, therefore, limited to providing estimates of the magnetic field strength. Modeling by Liu et al. (Astrophys. J. 665, 1439, 2007) and Jensen and Russell (Geophys. Res. Lett. 35, L02103, 2008) demonstrated that multiple LOS are necessary to recover the magnetic field strength and structure of the observed CME. We report the first successful observations of Faraday rotation through a CME using multiple lines of sight: 13 LOS across seven target radio fields. We made these radio observations using the Karl G. Jansky Very Large Array (VLA) at 1−2 GHz frequencies in the triggered operation mode on **31 July 2015**, using a constellation of cosmic radio sources through the solar corona at heliocentric distances of 8.2−19.5 R⊙. For LOS within 10 R⊙, the CME's contribution to the measured RM was ≈0 to −20 rad m−2, a significant enhancement over the coronal contribution. We assumed a force-free flux-rope structure for the CME's magnetic field and explored three separate models for the CME's plasma density: constant density, thin shell, and thick shell. The plasma densities and axial magnetic field strengths for the three models ranged over 5.4−6.4×103 cm−3 and 26−35 mG, respectively. Further, using all 13 LOS, we successfully determined the CME's orientation and helicity.
CESRA #2793 Feb **2021** http://www.astro.gla.ac.uk/users/eduard/cesra/?p=2793

Modeling Differential Faraday Rotation in the Solar Corona

Jason E. **Kooi** & Molly E. Kaplan
Solar Physics volume 295, Article number: 114 (**2020**)
https://link.springer.com/content/pdf/10.1007/s11207-020-01684-2.pdf
For decades, radio remote-sensing techniques have been used to probe the plasma structure of the solar corona at distances of 2 – 20 R⊙. Measurement of Faraday rotation, the change in the polarization position angle of linearly polarized radiation as it propagates through a magnetized plasma, has proven to be one of the best methods for determining the coronal magnetic-field strength and structure. Faraday-rotation observations of spatially extended radio sources provide the unique opportunity to measure differential Faraday rotation [ΔRM] the difference in the Faraday-rotation measure between two closely spaced lines of sight (LOS) through the corona. ΔRM is proportional to the electric current within an Ampèrian loop formed, in part, by the two closely spaced LOS. We report the expected ΔΔRM for two sets of models for the corona: one set of models for the corona employs a spherically symmetric plasma density, while the other breaks this symmetry by assuming that the heliospheric current sheet (HCS) is a finite-width streamer-belt region containing a high-density plasma. For each plasma-density model, we evaluate the ΔRM for three model coronal magnetic fields: a radial dipole and interplanetary magnetic field (DIMF), a dipole + current sheet (DCS), and a dipole + quadrupole + current sheet (DQCS). These models predict values of 0.01≲ΔRM≲120 radm−20.01≲ΔRM≲120 radm−2 over the range of parameter space accessible by modern instruments such as the Karl G. Jansky Very Large Array. We conclude that the HCS contribution to ΔΔRM is not negligible at moderate heliocentric distances (<8 R⊙) and may account for ≲20% of previous observations of ΔΔRM (e.g. made by Spangler, Astrophys. J. 670, 841, 2007). **16-18 Aug 2003, 17 Aug 2011**

VLA Measurements of Faraday Rotation through Coronal Mass Ejections

Jason E. **Kooi**, Patrick D. Fischer, Jacob J. Buffo, Steven R. Spangler
Solar Physics April **2017**, 292:56
http://link.springer.com/content/pdf/10.1007%2Fs11207-017-1074-7.pdf
Coronal mass ejections (CMEs) are large-scale eruptions of plasma from the Sun, which play an important role in space weather. Faraday rotation is the rotation of the plane of polarization that results when a linearly polarized signal passes through a magnetized plasma such as a CME. Faraday rotation is proportional to the path integral through the plasma of the electron density and the line-of-sight component of the magnetic field. Faraday-rotation observations of a source near the Sun can provide information on the plasma structure of a CME shortly after launch. We report on simultaneous white-light and radio observations made of three CMEs in August 2012. We made sensitive Very Large Array (VLA) full-polarization observations using 1 – 2 GHz frequencies of a constellation of radio sources through the solar corona at heliocentric distances that ranged from 6 – \(15~\mathrm{R}_{\odot}\). Two sources (0842+1835 and 0900+1832) were occulted by a single CME, and one source (0843+1547) was occulted by two CMEs. In addition to our radioastronomical observations, which represent one of the first active hunts for CME Faraday rotation since Bird et al. (Solar Phys., 98, 341, 1985) and the first active hunt using the VLA, we obtained white-light coronagraph images from the Large Angle and Spectrometric Coronagraph (LASCO) C3 instrument to determine the Thomson-scattering brightness [\(\mathrm{B}_{\mathrm{T}}\)], providing a means to independently estimate the plasma density and determine its contribution to the observed Faraday rotation. A constant-density force-free flux rope embedded in the background corona was used to model the effects of the CMEs on \(\mathrm{B}_{\mathrm{T}}\) and Faraday rotation.

The plasma densities (\(6\,\mbox{--}\,22\times10^{3}~\mbox{cm}^{-3}\)) and axial magnetic-field strengths (2 – 12 mG) inferred from our models are consistent with the modeling work of Liu et al. (Astrophys. J., 665, 1439, 2007) and Jensen and Russell (Geophys. Res. Lett., 35, L02103, 2008), as well as previous CME Faraday-rotation observations by Bird et al. (1985). **2 August 2012, 30 August 2012**
CESRA highlight: Nov 2017 http://cesra.net/?p=1671

Microwave Imaging of Quasi-periodic Pulsations at Flare Current Sheet

Yuankun **Kou**, Xin Cheng, Yulei Wang, Sijie Yu, Bin Chen, Eduard P. Kontar, Mingde Ding
Nature Communications (**2022**) 13:7680
https://arxiv.org/pdf/2212.08318.pdf
Quasi-periodic pulsations (QPPs) are frequently detected in solar and stellar flares, but the underlying physical mechanisms are still to be ascertained. Here, we show microwave QPPs during a solar flare originating from quasi-periodic magnetic reconnection at the flare current sheet. They appear as two vertically detached but closely related sources with the brighter ones located at flare loops and the weaker ones along the stretched current sheet. Although the brightness temperatures of the two microwave sources differ greatly, they vary in phase with periods of about 10--20 s and 30--60 s. The gyrosynchrotron-dominated microwave spectra also present a quasi-periodic soft-hard-soft evolution. These results suggest that relevant high-energy electrons are accelerated by quasi-periodic reconnection, likely arising from the modulation of magnetic islands within the current sheet as validated by a 2.5-dimensional magnetohydrodynamic simulation. **2017 July 13**
CESRA # 3435 Jan 2023 https://www.astro.gla.ac.uk/users/eduard/cesra/?p=3435

Radio Imaging of Quasi-periodic Magnetic Reconnection and Electron Acceleration during a Solar Flare

Y. K. **Kou**, X. Cheng, S. J. Yu, B. Chen, and M. D. Ding
Presentation at ESP Meeting **2021**
https://indico.ict.inaf.it/event/794/contributions/9868/attachments/4946/10132/yuankun_espm.pdf
13 Jul 2017

What determine Solar Flares Producing Interplanetary Type III Radio Bursts?

Y. K. **Kou**, Z. C. Jing, X. Cheng, W. Q. Pan, Y. Liu, C. Li, M. D. Ding
ApJL **898** L24 **2020**
https://arxiv.org/pdf/2007.03852.pdf
https://doi.org/10.3847/2041-8213/aba362
Energetic electrons accelerated by solar flares often give rise to type III radio bursts at a broad waveband and even interplanetary type III bursts (IT3) if the wavelength extends to decameter-kilometer. In this Letter, we investigate the probability of the flares that produce IT3, based on the sample of 2272 flares above M-class observed from 1996 to 2016. It is found that only 49.6% of the flares are detected to be accompanied with IT3. The duration, peak flux, and fluence of the flares with and without IT3 both present power-law distributions in the frequency domain, but the corresponding spectral indices for the former (2.06±0.17, 2.04±0.18, and 1.55±0.09) are obviously smaller than that for the latter (2.82±0.22, 2.51±0.19, and 2.40±0.09), showing that the flares with IT3 have longer durations and higher peak fluxes. We further examine the relevance of coronal mass ejections (CMEs) to the two groups of flares. It is found that 58% (655 of 1127) of the flares with IT3 but only 19% (200 of 1078) of the flares without IT3 are associated with CMEs, and that the associated CMEs for the flares with IT3 are inclined to be wider and faster. ***This indicates that CMEs may also play a role in producing IT3, speculatively facilitating the escape of accelerated electrons from the low corona to the interplanetary space.*** **2011 March 7, 2012 October 20**

Analyzing the propagation of EUV waves and their connection with type II radio bursts by combining numerical simulations and multi-instrument observations⋆

A. **Koukras**1,2, C. Marqué2, C. Downs3 and L. Dolla
A&A 644, A90 (**2020**)
https://doi.org/10.1051/0004-6361/202038699
https://www.aanda.org/articles/aa/pdf/2020/12/aa38699-20.pdf
Context. EUV (EIT) waves are wavelike disturbances of enhanced extreme ultraviolet (EUV) emission that propagate away from an eruptive active region across the solar disk. Recent years have seen much debate over their nature, with three main interpretations: the fast-mode magneto-hydrodynamic (MHD) wave, the apparent wave (reconfiguration of the magnetic field), and the hybrid wave (combination of the previous two).
Aims. By studying the kinematics of EUV waves and their connection with type II radio bursts, we aim to examine the capability of the fast-mode interpretation to explain the observations, and to constrain the source locations of the type II radio burst emission.

Methods. We propagate a fast-mode MHD wave numerically using a ray-tracing method and the WKB (Wentzel-Kramers-Brillouin) approximation. The wave is propagated in a static corona output by a global 3D MHD Coronal Model, which provides density, temperature, and Alfvén speed in the undisturbed coronal medium (before the eruption). We then compare the propagation of the computed wave front with the observed wave in EUV images (PROBA2/SWAP, SDO/AIA). Lastly, we use the frequency drift of the type II radio bursts to track the propagating shock wave, compare it with the simulated wave front at the same instant, and identify the wave vectors that best match the plasma density deduced from the radio emission. We apply this methodology for two EUV waves observed during SOL**2017-04-03**T14:20:00 and SOL**2017-09-12**T07:25:00.
Results. The simulated wave front displays a good qualitative match with the observations for both events. Type II radio burst emission sources are tracked on the wave front all along its propagation. The wave vectors at the ray-path points that are characterized as sources of the type II radio burst emission are quasi-perpendicular to the magnetic field.
Conclusions. We show that a simple ray-tracing model of the EUV wave is able to reproduce the observations and to provide insight into the physics of such waves. We provide supporting evidence that they are likely fast-mode MHD waves. We also narrow down the source region of the radio burst emission and show that different parts of the wave front are responsible for the type II radio burst emission at different times of the eruptive event.
CESRA nugget # 2817 March **2021** http://www.astro.gla.ac.uk/users/eduard/cesra/?p=2817

Coronal Conditions for the Occurrence of Type II Radio Bursts

Athanasios **Kouloumvakos**1, Alexis Rouillard1, Alexander Warmuth2, Jasmina Magdalenic3,4, Immanuel. C. Jebaraj3,4, Gottfried Mann2, Rami Vainio5, and Christian Monstein6
2021 ApJ 913 99
https://iopscience.iop.org/article/10.3847/1538-4357/abf435/pdf
https://doi.org/10.3847/1538-4357/abf435
Type II radio bursts are generally observed in association with flare-generated or coronal-mass-ejection-driven shock waves. The exact shock and coronal conditions necessary for the production of type II radio emission are still under debate. Shock waves are important for the acceleration of electrons necessary for the generation of the radio emission. Additionally, the shock geometry and closed field line topology, e.g., quasi-perpendicular shock regions or shocks interacting with streamers, play an important role for the production of the emission. In this study we perform a 3D reconstruction and modeling of a shock wave observed during the **2014 November 5** solar event. We determine the spatial and temporal evolution of the shock properties and examine the conditions responsible for the generation and evolution of type II radio emission. Our results suggest that the formation and evolution of a strong, supercritical, quasi-perpendicular shock wave interacting with a coronal streamer were responsible for producing type II radio emission. We find that the shock wave is subcritical before and supercritical after the start of the type II emission. The shock geometry is mostly quasi-perpendicular throughout the event. Our analysis shows that the radio emission is produced in regions where the supercritical shock develops with an oblique to quasi-perpendicular geometry.

Properties of solar energetic particle events inferred from their associated radio emission

A. **Kouloumvakos**, A. Nindos, E. Valtonen, C.E. Alissandrakis, O. Malandraki, P. Tsitsipis, A. Kontogeorgos, X. Moussas, A. Hillaris
A&A 580, A80 **2015**
http://arxiv.org/pdf/1507.03776v1.pdf
We study selected properties of Solar Energetic Particle (SEP) events as inferred from their associated radio emissions. We used a catalogue of 115 SEP events that consists of entries of proton intensity enhancements at one AU, with complete coverage over solar cycle 23, based on high-energy (~68 MeV) protons from SOHO/ERNE and we calculated the proton release time at the Sun using velocity dispersion analysis (VDA). After an initial rejection of cases with unrealistic VDA path lengths, we assembled composite radio spectra for the remaining events using data from ground-based and space-borne radio-spectrographs. For every event we registered the associated radio emissions and we divided the events in groups according to their associated radio emissions. The proton release was found to be most often accompanied by both type III and II radio bursts, but a good association percentage was also registered in cases accompanied by type IIIs only. The worst association was found for the cases with type II only association. *These radio association percentages support the idea that both flare- and shock-resident particle release processes are observed in high-energy proton events.* In cases of type III-associated events we extended our study to the timings between the type III radio emission, the proton release, and the electron release as inferred from VDA based on Wind/3DP 20-646 keV data. Typically, the protons are released after the start of the associated type III bursts and simultaneously or before the release of energetic electrons. For the cases with type II radio association we found that the distribution of the proton release heights had a maximum at ~2.5 Rs. Most (69%) of the flares associated to our SEP events were located at the western hemisphere, with a peak within the well-connected region of 50-60 deg western longitude.

CME Expansion as the Driver of Metric Type II Shock Emission as Revealed by Self-Consistent Analysis of High Cadence EUV Images and Radio Spectrograms

Kouloumvakos, A.; Patsourakos, S.; Hillaris, A.; Vourlidas, A.; Preka-Papadema, P.; Moussas, X.; Caroubalos, C.; Tsitsipis, P.; Kontogeorgos, A.
E-print, Dec **2013**, **File**; Solar Phys. June **2014**, Volume 289, Issue 6, pp 2123-2139
http://arxiv.org/pdf/1311.5159v2.pdf
On **13 June 2010**, an eruptive event occurred near the solar limb. It included a small filament eruption and the onset of a relatively narrow coronal mass ejection (CME) surrounded by an extreme ultraviolet wave front recorded by the Solar Dynamics Observatory's (SDO) Atmospheric Imaging Assembly (AIA) at high cadence. The ejection was accompanied by a GOES M1.0 soft X-ray flare and a Type-II radio burst; high-resolution dynamic spectra of the latter were obtained by the ARTEMIS IV radio spectrograph. The combined observations enabled a study of the evolution of the ejecta and the EUV wavefront and its relationship with the coronal shock manifesting itself as metric Type-II burst. By introducing a novel technique, which deduces a proxy of the EUV compression ratio from AIA imaging data and compares it with the compression ratio deduced from the band-split of the Type-II metric radio burst, we are able to infer the potential source locations of the radio emission of the shock on that AIA images. Our results indicate that the expansion of the CME ejecta is the source for both EUV and radio shock emissions. Early in the CME expansion phase, the Type-II burst seems to originate in the sheath region between the EUV bubble and the EUV shock front in both radial and lateral directions. This suggests that both the nose and the flanks of the expanding bubble could have driven the shock.

Spectral cleaving in solar type II radio bursts: Observations and interpretation

Artem **Koval**1,⋆, Marian Karlický1, Anatolii Brazhenko2, Aleksander Stanislavsky3, Anatolii Frantsuzenko2, Marek Vandas1, Aleksander Konovalenko3, Miroslav Bárta1, Ihor Bubnov3, Rositsa Miteva4 and Serge Yerin3
A&A, 689, A345 (**2024**)
https://www.aanda.org/articles/aa/pdf/2024/09/aa51010-24.pdf
https://doi.org/10.1051/0004-6361/202451010
Context. Shock waves in the solar corona are associated with solar flares and coronal mass ejections (CMEs). Type II solar bursts are radio signatures of shock waves in the solar corona. They are driven by solar flares or CMEs. Despite extensive studies, the intricate spectral patterns observed in type II solar bursts occasionally pose new challenges for the theory of electron acceleration in shocks.
Aims. We study a newly identified feature in type II solar bursts called spectral cleaving. This feature is characterized by the actual branching of a type II radio emission lane in radio spectral data.
Methods. We analyzed the type II burst exhibiting spectral cleaving in high-fidelity dynamic spectra obtained using the URAN-2 radio telescope (8.25–33 MHz; Poltava region, Ukraine) on 2011 February 14. The high-resolution spectrograms were examined to ascertain its spectral morphology.
Results. Our research represents the first recognition of spectral cleaving as a peculiarity of type II bursts that is yet to be classified. This effect occurs due to the shift (or migration) of radio source(s) along a shock front, which in turn is caused by changes in the magnetic field orientation ahead of the propagating shock front.
Conclusions. The spectral cleaving observed in solar type II bursts reveals a distinct phenomenon that indicates complex interactions between shock waves and magnetic fields in the solar corona. This discovery enhances our understanding of the mechanisms behind solar radio emissions and emphasizes the need for further observational studies to verify these findings. **2011-02-14**
CESRA # 3902 **2024** https://www.astro.gla.ac.uk/users/eduard/cesra/?p=3902

Morphology of Solar Type II Bursts Caused by Shock Propagation through Turbulent and Inhomogeneous Coronal Plasma

Artem **Koval**1, Aleksander Stanislavsky2,3, Marian Karlický1, Bing Wang4, Serge Yerin2, Aleksander Konovalenko2, and Miroslav Bárta1
2023 ApJ 952 51
https://iopscience.iop.org/article/10.3847/1538-4357/acdbcc/pdf
Type II solar bursts are radio signatures of shock waves in the solar corona driven by solar flares or coronal mass ejections (CMEs). Therefore, these bursts present complex spectral morphologies in solar dynamic spectra. Here, we report meter–decameter radio observations of a type II burst on **2014 July 25** made with the Ukrainian radio telescopes UTR-2 (8.25–33 MHz) and GURT (8.25–78 MHz). The burst demonstrates fundamental and harmonic components, band splitting, a herringbone structure, and a spectral break. These specific spectral features, observed jointly in a single type II burst, are rarely detected. To contribute to our understanding of such puzzling type II events, we carried out a detailed analysis of the recorded type II dynamic spectrum. In particular, the herringbone pattern has been exploited to study electron density turbulence in the solar corona. We calculated the power spectral densities of the flux variations in selected herringbones. The spectral index is in the range of $\alpha = -1.69$ to -2.00 with an average value of -1.897, which is slightly higher than the Kolmogorov spectral index of $-5/3$ for fully developed turbulence. We also recognized that the second type II burst consists of three drifting lanes. The lane onset times coincide with the spectral break in the first

type II burst. We regard that the CME/shock passage through a streamer caused the spectral break and triggered the multilane type II radio emission. Thus, we support one of the proposed scenarios for type II burst occurrence as being the result of CME/shock–streamer interaction.
CESRA #3638 **2023** https://www.astro.gla.ac.uk/users/eduard/cesra/?p=3638

Shock-wave radio probing of solar wind sources in coronal magnetic fields

A. **Koval**, M. Karlicky, A. Stanislavsky, B. Wang, M. Barta, R. **Gorgutsa**
ApJ **923** 255 **2021**
https://arxiv.org/pdf/2110.15863.pdf
https://iopscience.iop.org/article/10.3847/1538-4357/ac2f3f/pdf
https://doi.org/10.3847/1538-4357/ac2f3f
The Space Weather effects in the near-Earth environment as well as in atmospheres of other terrestrial planets arise by corpuscular radiation from the Sun, known as the solar wind. The solar magnetic fields govern the solar corona structure. Magnetic-field strength values in the solar wind sources - key information for modeling and forecasting the Space Weather climate - are derived from various solar space- and ground-based observations, but, so far not accounting for specific types of radio bursts. These are "fractured" type II radio bursts attributed to collisions of shock waves with coronal structures emitting the solar wind. Here, we report about radio observations of two "fractured" type II bursts to demonstrate a novel tool for probing of magnetic field variations in the solar wind sources. These results have direct impact on interpretations of this class of bursts and contribute to the current studies of the solar wind emitters. **17 Mar 2004**
CESRA #3192 Jan **2022** https://www.astro.gla.ac.uk/users/eduard/cesra/?p=3192

Direct Observations of Traveling Ionospheric Disturbances as Focusers of Solar Radiation: Spectral Caustics

Artem **Koval**, Yao Chen, Takuya Tsugawa, Yuichi Otsuka, Atsuki Shinbori, Michi Nishioka, Anatoliy Brazhenko, Aleksander Stanislavsky, Aleksander Konovalenko, Qing-He Zhang, Christian Monstein, Roman Gorgutsa
ApJ **2019**
https://arxiv.org/pdf/1904.09577.pdf
https://doi.org/10.3847/1538-4357/ab1b52
The solar radiation focusing effect is related to the specific phenomenon of propagation of the Sun-emitted HF and VHF waves through terrestrial ionosphere. This natural effect is observed with ground-based radio instruments running within 10-200 MHz range, as distinctive patterns - the Spectral Caustics (SCs) - on the solar dynamic spectra. It has been suggested that SCs are associated with medium-scale traveling ionospheric disturbances (MSTIDs). In this paper, we present the first direct observations of SCs induced by MSTIDs, using solar dynamic spectra with SCs obtained by different European radio telescopes on **January 8, 2014** and simultaneous two-dimensional detrended total electron content (dTEC) maps over Europe. Spatial examination of dTEC maps as well as precise timing analysis of the maps and the dynamic spectra have been performed. First, we found several pairs of one-to-one (TID-SC) correspondences. The study provides strong observational evidence supporting the suggestion that MSTIDs are the cause of SCs.
CESRA #2323 **2019** http://cesra.net/?p=2323

Simulation of Focusing Effect of Traveling Ionospheric Disturbances on Meter-Decameter Solar Dynamic Spectra

Artem **Koval**, Yao Chen, Aleksander Stanislavsky, Anton Kashcheyev, Qing-He Zhang
JGR **2018**
https://arxiv.org/pdf/1811.00263.pdf
For the first time we present simulation results of the focusing effect of the ionospheric plasma density irregularities, namely, Medium Scale Traveling Ionospheric Disturbances (MSTIDs), on solar radio emission by applying a ray-tracing method to the Earth's ionosphere with MSTIDs. With this technique we investigate the focusing effect which manifests itself in the form of peculiar spectral disturbances in intensity with specific morphology, so-called Spectral Caustics (SCs), occasionally appearing in dynamic spectra of different solar radio instruments operating in the meter-decameter wavelength range. We show that the simulated spectral shapes of SCs are in good agreement with the ones detected in real solar radio spectrograms. In particular, SCs that are classified as inverted V-like, V-like, X-like, and fiber-like types have been reproduced. It is also found that the seasonal dependence in the occurrence of SCs, which has been discovered recently, can be understood through a strong relation between the focusing frequency - the most important characteristic point in most SCs patterns - and the elevation angle of the Sun. We find that under typical parameters of MSTIDs with spatial and temporal periods set to be 300 km and 40 min, respectively, the focusing frequency decreases with the growth of the elevation angle. Physical interpretations of the results and implications on the analysis of solar radio data with SCs are discussed.
CESRA highlights #2090 **2019** http://www.astro.gla.ac.uk/users/eduard/cesra/?p=2090

Traveling ionospheric disturbances as huge natural lenses: Solar radio emission focusing effect,
Koval, A., Y. Chen, A. Stanislavsky, and Q.-H. Zhang
(**2017**). J. Geophys. Res. Space Physics, 122 Issue 9 Pages 9092–9101
http://sci-hub.cc/10.1002/2017JA024080
We present an in-depth study into spectral perturbations appearing in solar dynamic spectra and being manifestations of the focusing effect of low-frequency solar emission by the Earth's ionosphere. Such perturbations are considered to be the result of radio waves focusing by medium scale traveling ionospheric disturbances (MSTIDs). Using the Nançay Decametric Array (NDA) data set, we have conducted a statistical analysis of the spectral structures in solar dynamic spectra within 10-80 MHz. We have detected the spectral structures in the NDA spectral data for 129 observation days from 1999 till 2015. On spectrograms they appear as intensity variations different from well-known solar radio bursts. The sharp edges with enhanced intensity are distinctive characteristics of the structures for most events. Due to this spectral feature they are termed as Spectral Caustics (SCs). We have classified the SCs observed by the NDA as several types, based on their spectral morphology, namely: inverted V-like, V-like, X-like, fiber-like, and fringe-like. We have found that the rate of occurrence of SCs in dynamic spectra depends on the phase of the solar cycle. About 81% of all days with detected SCs fall on active phases of solar cycles 23 and 24 (48% and 33%, respectively). We have also established the seasonal dependence in occurrence of the SCs. It was found that about 95% of days with SCs belong to autumn-winter months, whereas only near 5% of days with SCs belong to spring-summer months. This is well-correlated with the reported dependence in MSTID occurrence rate. **1999 Feb 15, 1999 Nov 29, 2001 Jan 06, 2001 Mar 30, 2001 Dec 26, 2002 Nov 15, 2005 Feb 17, 2005 Jan 15, 2006 Dec 06, 2012 Jan 12, 2012 Dec 18, 2013 Jan 14, 2013 Dec 12, 2014 Jan 08, 2014 Jan 07, 2014 Dec 09,**
CESRA highlights #1480 Aug 2017 http://www.astro.gla.ac.uk/users/eduard/cesra/?p=1473

Decameter Stationary Type IV Burst in Imaging Observations on the 6th of September 2014
Artem **Koval**, Aleksander Stanislavsky, Yao Chen, Shiwei Feng, Aleksander Konovalenko, Yaroslav Volvach
ApJ **826** 125 **2016**
http://arxiv.org/pdf/1606.00990v1.pdf
First-of-its-kind radio imaging of decameter solar stationary type IV radio burst has been presented in this paper. On 6 September 2014 the observations of type IV burst radio emission have been carried out with the two-dimensional heliograph based on the Ukrainian T-shaped radio telescope (UTR-2) together with other telescope arrays. Starting at 09:55 UT and throughout 3 hours, the radio emission was kept within the observational session of UTR-2. The interesting observation covered the full evolution of this burst, "from birth to death". During the event lifetime, two C-class solar X-ray flares with peak times 11:29 UT and 12:24 UT took place. The time profile of this burst in radio has a double-humped shape that can be explained by injection of energetic electrons, accelerated by the two flares, into the burst source. According to the heliographic observations we suggest the burst source was confined within a high coronal loop, which was a part of a relatively slow coronal mass ejection. The latter has been developed for several hours before the onset of the event. Through analyzing about 1.5 million of heliograms (3700 temporal frames with 4096 images in each frame that correspond to the number of frequency channels) the radio burst source imaging shows a fascinating dynamical evolution. Both space-based (GOES, SDO, SOHO, STEREO) data and various ground-based instrumentation (ORFEES, NDA, RSTO, NRH) records have been used for this study.

OFF-LIMB SOLAR CORONAL WAVEFRONTS FROM SDO/AIA EXTREME-ULTRAVIOLET OBSERVATIONS—IMPLICATIONS FOR PARTICLE PRODUCTION
K. A. **Kozarev**1,5, K. E. Korreck2, V. V. Lobzin3, M. A. Weber2 and N. A. Schwadron
2011 ApJ 733 L25, **File**
http://arxiv.org/pdf/1406.2372v1.pdf
We derive kinematic properties for two recent solar coronal transient waves observed off the western solar limb with the Atmospheric Imaging Assembly (AIA) on board the Solar Dynamics Observatory (SDO) mission. The two waves occurred over ~10 minute intervals on consecutive days—**2010 June 12 and 13**. For the first time, off-limb waves are imaged with a high 12 s cadence, making possible detailed analysis of these transients in the low corona between ~1.1 and 2.0 solar radii (RS). We use observations in the 193 and 211 Å AIA channels to constrain the kinematics of both waves. We obtain initial velocities for the two fronts of ~1287 and ~736 km s–1, and accelerations of –1170 and –800 m s–2, respectively. Additionally, differential emission measure analysis shows the June 13 wave is consistent with a weak shock. Extreme-ultraviolet (EUV) wave positions are correlated with positions from simultaneous type II radio burst observations. We find good temporal and height association between the two, suggesting that the waves may be the EUV signatures of coronal shocks. Furthermore, the events are associated with significant increases in proton fluxes

at 1 AU, possibly related to how waves propagate through the coronal magnetic field. Characterizing these coronal transients will be key to connecting their properties with energetic particle production close to the Sun.

Second Harmonic Electromagnetic Wave Emissions from a Turbulent Plasma with Random Density Fluctuations

C. **Krafft**1,2 and A. S. Volokitin3,4
2024 ApJ 964 65
https://iopscience.iop.org/article/10.3847/1538-4357/ad20ee/pdf
In the solar wind, electromagnetic waves at the harmonic plasma frequency 2ωp can be generated as a result of coalescence between forward- and backward-propagating Langmuir waves. A new approach to calculate their radiation efficiency in plasmas with external background density fluctuations is developed. The evolution of Langmuir wave turbulence is studied by solving numerically the Zakharov equations in a two-dimensional randomly inhomogeneous plasma. Then, the dynamics of the nonlinear electric currents modulated at frequencies close to 2ωp are calculated, as well as their radiation into harmonic electromagnetic waves. In the frame of this non-self-consistent approach where all transformations of Langmuir waves on density inhomogeneities are taken into account, the electromagnetic wave radiation rate (emissivity) is determined numerically as well as analytically, providing in both cases similar results. Moreover, scaling laws of the harmonic wave emissivity as a function of the ratio of the light velocity to the electron plasma thermal velocity are found. It is also shown how the emissivity depends on the average level of density fluctuations and on the isotropic/anisotropic character of the Langmuir waves' and density fluctuations' spectra.

Dynamics of Two-dimensional Type III Electron Beams in Randomly Inhomogeneous Solar Wind Plasmas

C. **Krafft**1 and P. Savoini1
2023 ApJ 949 24
https://iopscience.iop.org/article/10.3847/1538-4357/acc1e4/pdf
The dynamics of a type III electron beam generating Langmuir wave turbulence and subsequent electromagnetic emissions is studied owing to two-dimensional Particle-In-Cell simulations performed in both homogeneous and randomly inhomogeneous solar wind plasmas. Important differences in the beam dynamics are highlighted between both cases, due to Langmuir waves' transformations on the density fluctuations. This paper studies the dynamics of a weak beam interacting with Langmuir wave turbulence scattered by initially applied plasma density fluctuations, in terms of particle acceleration, non-Gaussian suprathermal electron tails, broadening and relaxation of velocity distributions, beam density localization, and electron diffusion or trapping in a turbulent plasma. Density fluctuations are the cause of beam acceleration during its relaxation stage; after Langmuir wave saturation, it gains up to half the energy lost during deceleration while wave turbulence is damping, exhibiting asymptotically a suprathermal tail of electrons carrying around 30% of its initial kinetic energy. Some important features observed for one-dimensional beams exciting Langmuir wave turbulence in randomly inhomogeneous plasmas can be recovered.

Third and Fourth Harmonics of Electromagnetic Emissions by a Weak Beam in a Solar Wind Plasma with Random Density Fluctuations

C**. Krafft**1 and P. Savoini1
2022 ApJL 934 L28
https://iopscience.iop.org/article/10.3847/2041-8213/ac7f28/pdf
Electromagnetic emissions $\mathcal{H}_3$ and $\mathcal{H}_4$ at the third and fourth harmonics of the plasma frequency ωp were observed during the occurrence of type II and type III solar radio bursts. Two-dimensional particle-in-cell simulations are performed using a weak beam, high space and time resolutions, and a plasma with density fluctuations of a few percent, for parameters relevant to regions of type III bursts. For the first time, a detailed study of the different wave coalescence processes involved in the generation of $\mathcal{H}_3$ and $\mathcal{H}_4$ waves is presented and the impact of density fluctuations on the wave interaction mechanisms is demonstrated. Energy ratios between the second, third, and fourth harmonics $\mathcal{H}_2$, $\mathcal{H}_3$, and $\mathcal{H}_4$ are consistent with space observations. It is shown that, in both homogeneous and inhomogeneous plasmas, the dominant processes generating $\mathcal{H}_3$ ($\mathcal{H}_4$) are the coalescence of $\mathcal{H}_2$ ($\mathcal{H}_3$) with a Langmuir wave, in spite of the random density fluctuations modifying the waves' resonance conditions by energy transport in the wavevector space and of the damping of Langmuir waves. The role of the backscattered (forward-propagating) Langmuir waves coming from the first (second) cascade of the electrostatic decay of beam-driven Langmuir waves is determinant in these processes. Understanding such wave coalescence mechanisms can provide indirect information on Langmuir and ion acoustic wave turbulence, the average level of density inhomogeneities, and suprathermal electron fluxes generated in solar wind regions where the harmonics manifest. Causes for the rarity of their observations are discussed.
CESRA #3403 **2022** https://www.astro.gla.ac.uk/users/eduard/cesra/?p=3403

Fundamental Electromagnetic Emissions by a Weak Electron Beam in Solar Wind Plasmas with Density Fluctuations

C. **Krafft**1 and P. Savoini1
2022 ApJL 924 L24
https://iopscience.iop.org/article/10.3847/2041-8213/ac46a7/pdf
The generation of Langmuir wave turbulence by a weak electron beam in a randomly inhomogeneous plasma and its subsequent electromagnetic radiation are studied owing to two-dimensional particle-in-cell simulations in conditions relevant to type III solar radio bursts. The essential impact of random density fluctuations of average levels of a few percents of the background plasma on the characteristics of the electromagnetic radiation at the fundamental plasma frequency ωp is shown. Not only wave nonlinear interactions but also processes of Langmuir waves' transformations on the density fluctuations contribute to the generation of such emissions. During the beam relaxation, the amount of electromagnetic energy radiated at ωp in a plasma with density fluctuations strongly exceeds that observed when the plasma is homogeneous. The fraction of Langmuir wave energy involved in the generation of electromagnetic emissions at ωp saturates around 10−4, i.e., one order of magnitude above that reached when the plasma is uniform. Moreover, whereas harmonic emission at 2ωp dominates over fundamental emission during the time evolution in a homogeneous plasma, fundamental emission is strongly dominant when the plasma contains density fluctuations, at least during several thousands of plasma periods before being overcome by harmonic emission when the total electromagnetic energy begins to saturate.
CESRA #3239 Apr **2022** https://www.astro.gla.ac.uk/users/eduard/cesra/?p=3239

Dynamics of Langmuir Wave Spectra in Randomly Inhomogeneous Solar Wind Plasmas

C. **Krafft**1 and A. S. Volokitin2,3
2021 ApJ 923 103
https://doi.org/10.3847/1538-4357/ac2153
Solar coronal and wind plasmas often contain density fluctuations of various scales and amplitudes. The scattering of Langmuir wave turbulence on these inhomogeneities modifies the properties of the radiated electromagnetic emissions traveling from the Sun to the Earth. This paper shows the similarities between the physical results obtained by (i) a model based on the Zakharov equations, describing the self-consistent dynamics of Langmuir wave turbulence spectra in a plasma with external density fluctuations, and (ii) a modeling, within the framework of geometric optics approximation, of quasi-particles (representing plasmon quanta) moving in a fluctuating potential. It is shown that the dynamics of the Langmuir spectra is governed by anomalous diffusion processes, as a result of multiple scattering of waves on the density fluctuations; the same dynamics are observed in the momenta distributions of quasi-particles moving in potential structures with random inhomogeneities. These spectra and distributions are both characterized by a fast broadening during which energy is transported to larger wavevectors and momenta, exhibiting nonlinear time dependence of the average squares of wavevectors and quasi-particle momenta as well as non-Gaussian tails in the asymptotic stage. The corresponding diffusion coefficients depend on the time and are proportional to the square of the average level of density (or potential) fluctuations. It appears that anomalous transport and superdiffusion phenomena are responsible for the spectral broadening.

Second Harmonic Electromagnetic Emissions by an Electron Beam in Solar Wind Plasmas with Density Fluctuations

C. **Krafft**1 and P. Savoini1
2021 ApJL 917 L23
https://doi.org/10.3847/2041-8213/ac1795
Two-dimensional particle-in-cell simulations are performed to study the electromagnetic radiation emitted at the second harmonic 2ωp of the plasma frequency by a weak electron beam propagating in a background plasma with random density fluctuations, in solar wind conditions relevant to Type III solar radio bursts. The dynamics of the waves, the beam, and the plasma are calculated over several thousands of plasma periods. For relevant comparisons, simulations with and without applied density fluctuations are performed for the same parameters. This Letter evidences for the first time the impact of density fluctuations on the physical mechanisms driving the generation of electromagnetic waves emitted at 2ωp. Results obtained show that (i) the beam radiates electromagnetic waves at 2ωp as a result of nonlinear processes of Langmuir waves' coalescence, despite wave scattering on the density fluctuations that strongly affect the Langmuir spectra; (ii) the fraction of initial beam energy transferred asymptotically to the electromagnetic waves at 2ωp is by one order of magnitude smaller when the plasma involves density fluctuations of average level around 5%; (iii) compared to the homogeneous case, the ratio of electromagnetic energy radiated at 2ωp to the energy carried by the Langmuir wave turbulence is significantly larger during all the nonlinear stage; (iv) asymptotically, when the plasma is inhomogeneous, electromagnetic emissions at 2ωp present isotropized spectra whereas quadrupolar radiation occurs for the homogeneous plasma case.

Electromagnetic radiation from upper-hybrid wave turbulence in inhomogeneous solar plasmas.

Krafft, C & Volokitin, A S
2020 Plasma Phys. Control. Fusion 62 (2), 024007

ELECTRON ACCELERATION BY LANGMUIR WAVES PRODUCED BY A DECAY CASCADE
C. **Krafft**1,1 and A. S. Volokitin
2016 ApJ 821 99
It was recently reported that a significant part of the Langmuir waveforms observed by theSTEREO satellite during type III solar radio bursts are likely consistent with the occurrence of electrostatic decay instabilities, when a Langmuir wave $\mathcal{L}$ resonantly interacts with another Langmuir wave $\mathcal{L}'$ and an ion sound wave $\mathcal{S}'$ through the decay channel $\mathcal{L} \rightarrow \mathcal{L}' + \mathcal{S}'$. Usually such wave–wave interactions occur in regions of the solar wind where the presence of electron beams can drive Langmuir turbulence to levels allowing waves $\mathcal{L}$ to decay. Moreover, such solar wind plasmas can present long-wavelength, randomly fluctuating density inhomogeneities or monotonic density gradients which can significantly modify the development of such resonant instabilities. If some conditions are met, the waves can encounter a second decay cascade (SDC) according to $\mathcal{L}' \rightarrow \mathcal{L}'' + \mathcal{S}''$. Analytical estimates and observations based on numerical simulations show that the Langmuir waves $\mathcal{L}''$ produced by this SDC can accelerate beam particles up to velocities and kinetic energies exceeding two times the beam drift velocity vb and half the initial beam energy, respectively. Moreover, this process can be particularly efficient if the scattering effects of waves on the background plasma inhomogeneities have already accelerated a sufficient amount of beam electrons up to the velocity range where the phase velocities of the $\mathcal{L}''$ waves are lying. The paper shows that the conditions necessary for such process to occur can be easily met in solar wind plasmas if the beam velocities do not exceed around 35 times the plasma thermal velocity.
See CESRA Highlight #1072 Dec **2016** http://www.astro.gla.ac.uk/users/eduard/cesra/?p=1072

Langmuir Wave Decay in Inhomogeneous Solar Wind Plasmas: Simulation Results
C. **Krafft**1,2, A. S. Volokitin3,4, and V. V. Krasnoselskikh
2015 ApJ 809 176
Langmuir turbulence excited by electron flows in solar wind plasmas is studied on the basis of numerical simulations. In particular, nonlinear wave decay processes involving ion-sound (IS) waves are considered in order to understand their dependence on external long-wavelength plasma density fluctuations. In the presence of inhomogeneities, it is shown that the decay processes are localized in space and, due to the differences between the group velocities of Langmuir and IS waves, their duration is limited so that a full nonlinear saturation cannot be achieved. The reflection and the scattering of Langmuir wave packets on the ambient and randomly varying density fluctuations lead to crucial effects impacting the development of the IS wave spectrum. Notably, beatings between forward propagating Langmuir waves and reflected ones result in the parametric generation of waves of noticeable amplitudes and in the amplification of IS waves. These processes, repeated at different space locations, form a series of cascades of wave energy transfer, similar to those studied in the frame of weak turbulence theory. The dynamics of such a cascading mechanism and its influence on the acceleration of the most energetic part of the electron beam are studied. Finally, the role of the decay processes in the shaping of the profiles of the Langmuir wave packets is discussed, and the waveforms calculated are compared with those observed recently on board the spacecraft Solar TErrestrial RElations Observatory and WIND.

Waveforms of Langmuir turbulence in inhomogeneous solar wind plasmas†
C. **Krafft**1,2,*, A.S. Volokitin3,4, V.V. Krasnoselskikh5 and T. Dudok de Wit
JGR, Volume 119, Issue 12, pages 9369–9382, December **2014**
http://onlinelibrary.wiley.com/doi/10.1002/2014JA020329/pdf
Modulated Langmuir waveforms have been observed by several spacecraft in various regions of the heliopshere, such as the solar wind, the electron foreshock, the magnetotail or the auroral ionosphere. Many observations revealed the bursty nature of these waves, which appear to be highly modulated, localized and clumped into spikes with peak amplitudes typically three orders of magnitude above the mean. The paper presents Langmuir waveforms calculated using a Hamiltonian model describing self-consistently the resonant interaction of an electron beam with Langmuir wave packets in a plasma with random density fluctuations. These waveforms, obtained for different profiles of density fluctuations and ranges of parameters relevant to solar type III electron beams and plasmas measured at 1 AU, are presented in the form they would appear if recorded by a satellite moving in the solar wind. Comparison with recent measurements by the STEREO and WIND satellites shows that their characteristic features are very similar to the observations

Interaction of Energetic Particles with Waves in Strongly Inhomogeneous Solar Wind Plasmas
C. **Krafft**1,2, A. S. Volokitin3,4, and V. V. Krasnoselskikh
2013 ApJ 778 111

Observations performed in the solar wind by different satellites show that electron beams accelerated in the low corona during solar flares can propagate up to distances around 1 AU, that Langmuir waves' packets can be clumped into spikes with peak amplitudes three orders of magnitude above the mean, and that the average level of density fluctuations can reach several percents. A Hamiltonian model is built describing the properties of Langmuir waves propagating in a plasma with random density fluctuations by the Zakharov's equations and the beam by means of particles moving self-consistently in the fields of the waves. Numerical simulations, performed using parameters relevant to solar type III conditions at 1 AU, show that when the average level of density fluctuations is sufficiently low, the beam relaxation and the wave excitation processes are very similar to those in a homogeneous plasma and can be described by the quasilinear equations of the weak turbulence theory. On the contrary, when the average level of density fluctuations overcomes some threshold depending on the ratio of the thermal velocity to the beam velocity, the plasma inhomogeneities crucially influence the characteristics of the Langmuir turbulence and the beam-plasma interaction.

On the Efficiency of the Linear-mode Conversion for Generation of Solar Type III Radio Bursts

Vladimir **Krasnoselskikh**, Andrii Voshchepynets, Milan Maksimovic
2019 ApJ 879 51
Type III solar radio bursts are generated by streams of energetic electrons accelerated at the Sun during periods of solar activity. The generation occurs in two steps. Initially, electron beams generate electrostatic Langmuir waves and then these waves are transformed into electromagnetic emissions. Recent studies showed that the level of density fluctuations in the solar wind and in the solar corona is so high that it may significantly affect beam–plasma interaction. Here, we show that the presence of intense density fluctuations not only crucially influences the process of beam–plasma interaction, but also changes the mechanism of energy transfer from electrostatic waves into electromagnetic. Reflection of the Langmuir waves from the density inhomogeneities may result in partial transformation of the energy of electrostatic waves into electromagnetic around plasma frequency. We show that the linear wave energy transformation for the level of fluctuations of the order of 1% or higher is efficient enough to produce radio bursts with a brightness temperature of 1014–1015 K.

On the mechanism of radio emission in type III Solar Radiobursts

Vladimir **Krasnoselskikh**, Andrii Voshchepynets, Milan Maksimovic
ApJ **2018**
https://arxiv.org/pdf/1812.10440.pdf
sci-hub.se/10.3847/1538-4357/ab22bf
Type III solar radio bursts are generated by streams of energetic electrons accelerated at the Sun during periods of the solar activity. The generation occurs in two steps. Initially, electron beams generate electrostatic Langmuir waves and then these waves are transformed in electromagnetic emissions. It is widely accepted that the mechanism of generation of emission on fundamental frequency close to plasma frequency is due to induced scattering of Langmuir waves into electromagnetic. However this process imposes quite restrictive limit of the ratios of effective brightness temperatures of electromagnetic and Langmuir waves in the source region. Recent studies showed that the level of density fluctuations in the solar wind and in the solar corona is so high that it may significantly affect beam-plasma interaction. Here we show that the presence of intense density fluctuations not only crucially influence the process of beam plasma interaction but also changes the mechanism of energy transfer from electrostatic waves into electromagnetic. Reflection of the Langmuir waves from the density inhomogeneities may result in partial transformation of the energy of electrostatic wave into electromagnetic. We show that the linear wave energy transformation for the level of fluctuations of the order of 1\% or higher may be significantly more efficient for generation of type III solar radio bursts than conventionally considered process of nonlinear conversion due to induced scattering on ions.

Electron beam-plasma instability in the randomly inhomogeneous solar wind

Vladimir **Krasnoselskikh**∗1 , Andrii Voshchepynets† , Catherine Krafft , and Alexandre Volokitin
CESRA Abstract **2016**
http://cesra2016.sciencesconf.org/conference/cesra2016/pages/CESRA2016_prog_abs_book_v1.pdf
We propose a new model that describes effects of plasma density fluctuations in the solar wind on the relaxation of the electron beams ejected from the Sun during the solar flares. The density fluctuations are supposed to be responsible for the changes in the local phase velocity of the Langmuir waves generated by the beam instability. We use the property that for the wave with a given frequency the probability distribution of density fluctuations uniquely determines the probability distribution of phase velocity of wave. We replace the continuous spatial interval by a discrete one, consisting of small equal spatial subintervals with linear density profile. This approach allows us to describe the changes in the wave phase velocity during the wave propagation in terms of probability distribution function. Using this probability distribution, we describe resonant wave particle interactions by a system of equations, similar to a well-known quasi-linear approximation, where the conventional velocity diffusion coefficient and the wave growth rate are replaced by the averaged in the velocity space. The averaged diffusion coefficient and wave growth rate depend on a

form of the probability distribution function for the density fluctuations. This last distribution is obtained from the spectrum of the density fluctuations measured aboard ISEE satellites when they were in the solar wind. It was shown that the process of relaxation of electron beam is accompanied by transformation of significant part of the beam kinetic energy to energy of the accelerated particles via generation and absorption of the Langmuir waves. We discovered that for the very rapid beams with beam velocity vb> 15vt, where vt is a thermal velocity of background plasma, the relaxation process consists of two well-separated steps. On first step the major relaxation process occurs and the wave growth rate almost everywhere in the velocity space becomes close to zero or negative. At the second stage the system remains close to the state of marginal stability long enough to explain how the beam may be preserved traveling distances over 1 AU while still being able to generate the Langmuir waves.

Observations of Near-Simultaneous Split-Band Solar type-II Radio Bursts at Low Frequencies

Hariharan **Krishnan**_y1, Ramesh Rz , and Kathiravan C
CESRA **2016**, p.97
http://cesra2016.sciencesconf.org/conference/cesra2016/pages/CESRA2016_prog_abs_book_v3.pdf
We report ground-based radio spectral and polarimeter observations of two successive split-band Type-II bursts that occurred on **20 February 2014** at low frequencies (less than 100 MHz) in association with a solar coronal mass ejection (CME). The temporal interval between the onset of the two bursts was very small, _ one minute. Both of the bursts exhibited fundamental{harmonic structure. The coronal magnetic-_eld strength [B] in the upstream region of the associated magnetohydrodynamic (MHD) shock, estimated from the split-band observations, is in the range B _ 1.3{1.1 G over the radial distance [r] interval r _ 1.49 { 1.58 R for the _rst Type-II burst, and B _ 1.3{1.0 G over r _ 1.49 { 1.64 R for the second Type-II burst. Based on the results obtained, we show that the _rst and the second Type-II bursts in the present case were likely due to MHD shocks generated by the near-simultaneous interaction of two di_erent regions of the aforementioned CME with a preceding CME and a pre-existing coronal streamer.

High Dynamic Range Observations of Solar Coronal Transients at Low Radio Frequencies With a Spectro-Correlator

Hariharan **Krishnan**∗1 , Ramesh R , Kathiravan C , Abhilash H N , and Rajalingam M
CESRA **2016** p.53
http://cesra2016.sciencesconf.org/conference/cesra2016/pages/CESRA2016_prog_abs_book_v3.pdf
A new antenna system with a digital spectro-correlator that provides high temporal, spectral, and amplitude resolutions has been commissioned at the Gauribidanur Observatory near Bangalore in India. Presently, it is used for observations of the solar coronal transients in the scarcely explored frequency range ≈30–15 MHz. The details of the antenna system, the associated receiver setup, and the initial observational results are reported. Some of the observed transients exhibited quasi-periodicity in their time profiles at discrete frequencies. Estimates of the associated magnetic field strength (B) indicate that B ≈ 0.06–1 G at a typical frequency such as 19.5 MHz.

Microwave and Hard X-Ray Flare Observations by NoRH/NoRP and RHESSI: Peak-flux Correlations

Säm **Krucker**1,2,3, Satoshi Masuda1, and Stephen M. White4
2020 ApJ 894 158
https://doi.org/10.3847/1538-4357/ab8644
sci-hub.tw/10.3847/1538-4357/ab8644
This paper presents initial results from a statistical study of solar microwave and hard X-ray flares jointly observed over the past two solar cycles by the Nobeyama Radio Polarimeters, the Nobeyama Radio Heliograph, and the Reuven Ramaty High Energy Solar Spectroscopic Imager. As has been previously demonstrated, the microwave (17 GHz and 34 GHz) peak flux shows a linear correlation with the nonthermal hard X-ray bremsstrahlung peak emission seen above 50 keV. The correlation holds for the entire rise phase of each individual burst, while the decay phases tend to show more extended emission at microwaves than is generally attributed to particle trapping. While the correlation is highly significant (coefficient of 0.92) and holds over more than four orders of magnitude, individual flares can be above or below the fitted line by an average factor of about 2. By restricting the flare selection to source morphologies with the radio emission from the top of the flare loop, the correlation tightens significantly, with a correlation coefficient increasing to 0.99 and the scatter reduced to a factor of 1.3. These findings corroborate the assumption that gyrosynchrotron microwave and hard X-ray bremsstrahlung emissions are produced by the same flare-accelerated electron population. The extent of the linear correlation over four orders of magnitude suggests that magnetic field strengths within nonthermal 17 GHz sources are surprisingly similar over a wide range of flare sizes.

Table 1 Nobeyama/RHESSI Event List, 2002-2016, 40 >M7flares, **Flare profiles**

Solar flares at submillimeter wavelengths **A review**

Sam **Krucker** · C.G. Gimenez de Castro · H.S. Hudson · G. Trottet · T.S. Bastian · A.S. Hales · J. Kašparova · K.-L. Klein · M. Kretzschmar · T. Luthi · A. Mackinnon · S. Pohjolainen · S.M. White
Astronomy and Astrophysics Review, Volume 21, Issue 1, (**2013**) 21:58; **File**

We discuss the implications of the first systematic observations of solar flares at submillimeter wavelengths, defined here as observing wavelengths shorter than 3~mm (frequencies higher than 0.1 THz). The events observed thus far show that this wave band requires a new understanding of high-energy processes in solar flares. Several events, including observations from two different observatories, show during the impulsive phase of the flare a spectral component with a positive (increasing) slope at the highest observable frequencies (up to 405~GHz). To emphasize the increasing spectra and the possibility that these events could be even more prominent in the THz range, we term this spectral feature a ``THz component". Here we review the data and methods, and critically assess the observational evidence for such distinct component(s). This evidence is convincing. We also review the several proposed explanations for these feature(s), which have been reported in three distinct flare phases. These data contain important clues to flare development and particle acceleration as a whole, but many of the theoretical issues remain open. We generally have lacked systematic observations in the millimeter-wave to far-infrared range that are needed to complete our picture of these events, and encourage observations with new facilities. **2000-03-22T18:44; 2001-04-06T19:19, 2001-04-12T10:28, 2001-08-25T16:32; 2001-11-28T16:34; 2002-08-30T13:28; 2002-09-10T14:53; 2002-12-20T13:18; 2003-10-27T12:31; 2003-10-28T11:10; 2003-11-02T17:17; 2003-11-04T19:44; 2004-10-30T11:44; 2006-12-06T18:44**

CORONAL HARD X-RAY EMISSION ASSOCIATED WITH RADIO TYPE III BURSTS

Sa¨m **Krucker**,1 P. Saint-Hilaire,1 S. Christe,1,2 S. M. White,3
A. D. Chavier,4 S. D. Bale,1,2 and R. P. Lin1,2
The Astrophysical Journal, 681:644–649, **2008**
http://www.journals.uchicago.edu/doi/pdf/10.1086/588549

We report on a purely coronal hard X-ray source detected in a partially disk-occulted solar flare by the Reuven Ramaty High Energy Solar Spectroscopic Imager (RHESSI) that is associated with radio type III bursts and a suprathermal electron event detected near 1 AU by the WIND 3-D Plasma and Energetic Particle (3DP) instrument. Several observational characteristics suggest that the coronal hard X-ray source is thin target bremsstrahlung emission from the escaping electrons that produce the radio type III bursts. The hard X-ray emission correlates in time with the radio type III bursts and originates from a radially elongated source in the corona with a length (_65 Mm) similar to typical coronal density scale heights. Furthermore, the difference between the hardX-ray photon spectral index (_ j 4:1 _ 0:4) and the electron spectral index of the in situ observed event (_in situ j 2:9 _ 0:3) is around 1, consistent with the thin target interpretation. A further test for the thin target scenario is to compare the number of electrons needed to produce the observed hard X-ray emission with the number of in situ observed electrons. However, the number of escaping electrons derived from the single-spacecraft WIND measurement is in the best case an order of magnitude estimate and could easily underestimate the actual number of escaping electrons. Using the WIND observations, the estimated number of escaping electrons is about an order of magnitude too low. Thus, the thin target interpretation only holds if the WIND measurements are significantly underestimating the actual number of escaping electrons. Future multispacecraft observations with STEREO, Solar Orbiter, and Sentinels will resolve this uncertainty.

Radial Variations in Solar Type III Radio Bursts

Vratislav **Krupar**1,2, Oksana Kruparova1,2, Adam Szabo2, Lynn B. Wilson III2, Frantisek Nemec3, Ondrej Santolik3,4, Marc Pulupa5, Karine Issautier6, Stuart D. Bale5,7, and Milan Maksimovic6
2024 ApJL 967 L32
https://iopscience.iop.org/article/10.3847/2041-8213/ad4be7/pdf

Type III radio bursts are generated by electron beams accelerated at reconnection sites in the corona. This study, utilizing data from the Parker Solar Probe's first 17 encounters, closely examines these bursts down to 13 solar radii. A focal point of our analysis is the near-radial alignment (within 5°) of the Parker Solar Probe, STEREO-A, and Wind spacecraft relative to the Sun. This alignment, facilitating simultaneous observations of 52 and 27 bursts by STEREO-A and Wind respectively, allows for a detailed differentiation of radial and longitudinal burst variations. Our observations reveal no significant radial variations in electron beam speeds, radio fluxes, or exponential decay times for events below 50 solar radii. In contrast, closer to the Sun we noted a decrease in beam speeds and radio fluxes. This suggests potential effects of radio beaming or alterations in radio source sizes in this region. Importantly, our results underscore the necessity of considering spacecraft distance in multispacecraft observations for accurate radio burst analysis. A critical threshold of 50 solar radii emerges, beyond which beaming effects and changes in beam speeds and radio fluxes become significant. Furthermore, the consistent decay times across varying radial distances point toward a stable trend extending from 13 solar radii into the inner heliosphere. Our statistical results provide valuable insights into the

propagation mechanisms of type III radio bursts, particularly highlighting the role of scattering near the radio source when the frequency aligns with the local electron plasma frequency. **2023 March 18, 2022 June 3**
Table 1 Intervals of Radial Alignment for Parker Solar Probe with STEREO-A and Wind (Separation Angle <5°)

Comparative Analysis of Type III Radio Bursts and Solar Flares: Spatial Localization and Correlation with Solar Flare Intensity

Vratislav **Krupar**1,2, Oksana Kruparova1,2, Adam Szabo2, Frantisek Nemec3 +++
2024 ApJ 961 88
https://iopscience.iop.org/article/10.3847/1538-4357/ad12ba/pdf
We present a comprehensive study of type III radio bursts and their association with solar flares of magnitude M1.0 and larger, as observed by four widely separated spacecraft (Parker Solar Probe, Solar Orbiter, STEREO-A, and Wind). Our main focus is the introduction and validation of two methods for localizing radio bursts using the available multispacecraft data. The first method utilizes intensity fitting with a circular Gaussian distribution, while the second method is based on the time arrival of radio bursts. We demonstrate the effectiveness of these methods through the analysis of a single type III burst event and compare their results with the traditional radio triangulation technique. Furthermore, we conduct a statistical study of 17 type III bursts associated with M- and X-class solar flares in years 2020–2022. Our findings suggest a possible correlation between solar flare intensities and longitudes, with east limb flares tending to be weaker than west limb flares. We also observe a systematic drift of radio burst longitudes toward the east, potentially explained by a poleward component of the local density gradient. Our results suggest a strong correlation between solar flare intensities and radio burst properties, enhancing our understanding of the relationship between solar flares and type III radio bursts. **2022 March 28**
Table 1 Solar Flares and Type III Bursts 2020-2022

Enhancing Triangulation of Interplanetary Type III Bursts through Wavevector Correction

Vratislav **Krupar**1,2, Oksana Kruparova1,2, Adam Szabo2, Rui F. Pinto3,4, Milan Maksimovic5, and Juan Carlos Martinez Oliveros6
2024 ApJ 960 101
https://iopscience.iop.org/article/10.3847/1538-4357/ad150e/pdf
Interplanetary Type III bursts, generated by relativistic electron beams at solar flare reconnection sites, are explored through an investigation of 152 instances observed by the Solar Terrestrial Relations Observatory mission. This study reveals that the absolute values of the wavevector deviations from the Sun–spacecraft line are statistically 3.72 and 2.10 larger than predicted by the density model, assuming fundamental and harmonic emission, respectively. Through Monte Carlo simulations, we examine the impact of scattering by density inhomogeneities on the apparent locations of radio emissions in the interplanetary medium. The findings indicate that relative density fluctuations of 0.40 can account for the observed angular shift, a conclusion supported by the multiple flux-tube solar wind model, which confirms the presence of such magnitude of relative perpendicular density fluctuations in the solar wind. We propose a wavevector correction that incorporates this effect to enhance the triangulation of interplanetary Type III bursts, demonstrating that radio triangulation, with this correction, can reliably track electron beams in the interplanetary medium. **2010 January 10**

Density Fluctuations in the Solar Wind Based on Type III Radio Bursts Observed by Parker Solar Probe

Vratislav **Krupar**, Adam Szabo, Milan Maksimovic, Oksana Kruparova, Eduard P. Kontar, Laura A. Balmaceda, Xavier Bonnin, Stuart D. Bale, Marc Pulupa, David M. Malaspina, John W. Bonnell, Peter R. Harvey, Keith Goetz, Thierry Dudok de Wit, Robert J. MacDowall, Justin C. Kasper, Anthony W. Case, Kelly E. Korreck, Davin E. Larson, Roberto Livi, Michael L. Stevens, Phyllis L. Whittlesey, Alexander M. Hegedus
ApJS **246** 57 **2020**
https://arxiv.org/pdf/2001.03476.pdf
https://iopscience.iop.org/article/10.3847/1538-4365/ab65bd/pdf
Radio waves are strongly scattered in the solar wind, so that their apparent sources seem to be considerably larger and shifted than the actual ones. Since the scattering depends on the spectrum of density turbulence, better understanding of the radio wave propagation provides indirect information on the relative density fluctuations $\epsilon=\langle\delta n\rangle/\langle n\rangle$ at the effective turbulence scale length. Here, we have analyzed 30 type III bursts detected by Parker Solar Probe (PSP). For the first time, we have retrieved type III burst decay times τd between 1 MHz and 10 MHz thanks to an unparalleled temporal resolution of PSP. We observed a significant deviation in a power-law slope for frequencies above 1 MHz when compared to previous measurements below 1 MHz by the twin-spacecraft Solar TErrestrial RElations Observatory (STEREO) mission. We note that altitudes of radio bursts generated at 1 MHz roughly coincide with an expected location of the Alfvén point, where the solar wind becomes super-Alfvénic. By comparing PSP observations and Monte Carlo simulations, we predict relative density fluctuations ϵ at the effective turbulence scale length at radial distances between 2.5R$\odot$ and 14R$\odot$ to range from 0.22 and 0.09. Finally, we calculated relative density fluctuations ϵ measured

in situ by PSP at a radial distance from the Sun of 35.7~R⊙ during the perihelion \#1, and the perihelion \#2 to be 0.07 and 0.06, respectively. It is in a very good agreement with previous STEREO predictions (ϵ=0.06−0.07) obtained by remote measurements of radio sources generated at this radial distance. **2019 April 1–10; 2019-04-03**
Table 1. The list of type III burst time-frequency intervals
CESRA #2535 March **2020** http://www.astro.gla.ac.uk/users/eduard/cesra/?p=2535

Statistical Survey of Coronal Mass Ejections and Interplanetary Type II Bursts

V. **Krupar**1,2,3, J. Magdalenić4, J. P. Eastwood5, N. Gopalswamy2, O. Kruparova3, A. Szabo2, and F. Němec
2019 ApJ 882 92
https://iopscience.iop.org/article/10.3847/1538-4357/ab3345/pdf
Coronal mass ejections (CMEs) are responsible for most severe space weather events, such as solar energetic particle events and geomagnetic storms at Earth. Type II radio bursts are slow drifting emissions produced by beams of suprathermal electrons accelerated at CME-driven shock waves propagating through the corona and interplanetary medium. Here, we report a statistical study of 153 interplanetary type II radio bursts observed by the two STEREO spacecraft between 2008 March and 2014 August. The shock associated radio emission was compared with CME parameters included in the Heliospheric Cataloguing, Analysis and Techniques Service catalog. We found that faster CMEs are statistically more likely to be associated with the interplanetary type II radio bursts. We correlate frequency drifts of interplanetary type II bursts with white-light observations to localize radio sources with respect to CMEs. Our results suggest that interplanetary type II bursts are more likely to have a source region situated closer to CME flanks than CME leading edge regions**. 2012 October 22**

Interplanetary Type III Bursts and Electron Density Fluctuations in the Solar Wind

V. **Krupar**, M. Maksimovic, E. P. Kontar, A. Zaslavsky, O. Santolik, J. Soucek, O. Kruparova, J. P. Eastwood, and A. Szabo
2018 ApJ 857 82
http://sci-hub.tw/http://iopscience.iop.org/0004-637X/857/2/82/
Type III bursts are generated by fast electron beams originated from magnetic reconnection sites of solar flares. As propagation of radio waves in the interplanetary medium is strongly affected by random electron density fluctuations, type III bursts provide us with a unique diagnostic tool for solar wind remote plasma measurements. Here, we performed a statistical survey of 152 simple and isolated type III bursts observed by the twin-spacecraft Solar TErrestrial RElations Observatory mission. We investigated their time–frequency profiles in order to retrieve decay times as a function of frequency. Next, we performed Monte Carlo simulations to study the role of scattering due to random electron density fluctuations on time–frequency profiles of radio emissions generated in the interplanetary medium. For simplification, we assumed the presence of isotropic electron density fluctuations described by a power law with the Kolmogorov spectral index. Decay times obtained from observations and simulations were compared. We found that the characteristic exponential decay profile of type III bursts can be explained by the scattering of the fundamental component between the source and the observer despite restrictive assumptions included in the Monte Carlo simulation algorithm. Our results suggest that relative electron density fluctuations $\langle \delta n_e \rangle / n_e$ in the solar wind are 0.06–0.07 over wide range of heliospheric distances. **2010-11-13**

An analysis of interplanetary solar radio emissions associated with a coronal mass ejection

Vratislav **Krupar**, Jonathan Eastwood, Oksana Kruparova, Ondrej Santolik, Jan Soucek, Jasmina Magdalenic, Angelos Vourlidas, Milan Maksimovic, Volker Bothmer, Niclas Mrotzek, Adam Pluta, David Barnes, Jackie Davies, Juan Carlos Martinez Oliveros, Stuart Bale
ApJ 823 L5 **2016**
http://arxiv.org/pdf/1606.04301v1.pdf
Coronal mass ejections (CMEs) are large-scale eruptions of magnetized plasma that may cause severe geomagnetic storms if Earth-directed. Here we report a rare instance with comprehensive in situ and remote sensing observa- tions of a CME combining white-light, radio, and plasma measurements from four different vantage points. For the first time, we have successfully applied a radio direction-finding technique to an interplanetary type II burst detected by two identical widely separated radio receivers. The derived locations of the type II and type III bursts are in general agreement with the white light CME recon- struction. We find that the radio emission arises from the flanks of the CME, and are most likely associated with the CME-driven shock. Our work demon- strates the complementarity between radio triangulation and 3D reconstruction techniques for space weather applications. **2013 November 29**
See CESRA Highlights #**817**, Sept 2016 https://www.astro.gla.ac.uk/users/eduard/cesra/?p=817

Radio triangulation of solar radio emissions: STEREO/Waves measurements

Vratislav **Krupar**∗1,2, Eastwood Jonathan1 , Oksana Kruparova2 , Ondrej Santolik2,3, Jan Soucek2 , Jasmina Magdalenic4 , Vourlidas Angelos5 , Milan Maksimovic6 , Xavier Bonnin6 , Volker Bothmer7 , Niclas Mrotzek7 , Adam Pluta7 , David Barnes8 , Jackie Davies8 , Juan Carlos Martinez Oliveros9 , and Stuart Bale
CESRA Abstract **2016**
http://cesra2016.sciencesconf.org/conference/cesra2016/pages/CESRA2016_prog_abs_book_v1.pdf
We present an analysis of radio signatures associated with a CME-driven shock on **29 November 2013**. We benefit from comprehensive in situ and remote sensing observations of the CME, combining white-light, radio, and plasma measurements from four different vantage points. We have successfully applied a radio direction-finding technique to type II and type III bursts detected by two identical widely separated radio receivers onboard the STEREO spacecraft. We performed the radio triangulation to localise radio sources in the interplanetary medium. The derived locations of the type II and type III bursts are in general agreement with the white light CME reconstruction. We find that the radio emissions arise from the flanks of the CME, and are most likely associated with the CME-driven shock.

AN ANALYSIS OF INTERPLANETARY SOLAR RADIO EMISSIONS ASSOCIATED WITH A CORONAL MASS EJECTION

V. **Krupar**1,2, J. P. Eastwood1, O. Kruparova2, O. Santolik2,3, J. Soucek2, J. Magdalenić4, A. Vourlidas5, M. Maksimovic6, X. Bonnin6, V. Bothmer7, N. Mrotzek7, A. Pluta7, D. Barnes8, J. A. Davies8, J. C. Martínez Oliveros9, and S. D. Bale9,10
2016 ApJ 823 L5
http://arxiv.org/pdf/1606.04301v1.pdf
Coronal mass ejections (CMEs) are large-scale eruptions of magnetized plasma that may cause severe geomagnetic storms if Earth directed. Here, we report a rare instance with comprehensive in situ and remote sensing observations of a CME combining white-light, radio, and plasma measurements from four different vantage points. For the first time, we have successfully applied a radio direction-finding technique to an interplanetary type II burst detected by two identical widely separated radio receivers. The derived locations of the type II and type III bursts are in general agreement with the white-light CME reconstruction. We find that the radio emission arises from the flanks of the CME and are most likely associated with the CME-driven shock. Our work demonstrates the complementarity between radio triangulation and 3D reconstruction techniques for space weather applications.
See CESRA Highlight#817 http://www.astro.gla.ac.uk/users/eduard/cesra/?p=817
November 29, 2013

On the speed and acceleration of electron beams triggering interplanetary type III radio bursts

Vratislav **Krupar** (1), Eduard P. Kontar (2), Jan Soucek (1), Ondrej Santolik (1 and 3), Milan Maksimovic (4),Oksana Kruparova
2015 A&A 580, A137
http://arxiv.org/pdf/1507.06874v1.pdf
Type III radio bursts are intense radio emissions triggered by beams of energetic electrons often associated with solar flares. These exciter beams propagate outwards from the Sun along an open magnetic field line in the corona and in the interplanetary (IP) medium. We performed a statistical survey of 29 simple and isolated IP type III bursts observed by STEREO/Waves instruments between January 2013 and September 2014. We investigated their time-frequency profiles in order to derive the speed and acceleration of exciter electron beams. We show these beams noticeably decelerate in the IP medium. Obtained speeds range from ~ 0.02c up to ~0.35c depending on initial assumptions. It corresponds to electron energies between tens of eV and hundreds of keV, and in order to explain the characteristic energies or speeds of type III electrons (~0.1c) observed simultaneously with Langmuir waves at 1 au, the emission of type III bursts near the peak should be predominately at double plasma frequency. Derived properties of electron beams can be used as input parameters for computer simulations of interactions between the beam and the plasma in the IP medium.
September 27, 2013

Statistical Survey of Type III Radio Bursts at Long Wavelengths Observed by the Solar TErrestrial RElations Observatory (STEREO)/Waves Instruments: Goniopolarimetric Properties and Radio Source Locations

Vratislav **Krupar**, Milan Maksimovic, Ondrej Santolik, Baptiste Cecconi, Oksana Kruparova
Solar Phys. **2014**
http://arxiv.org/pdf/1410.6135v1.pdf

We have performed statistical analysis of a large number of Type III radio bursts observed by STEREO between May 2007 and February 2013. Only intense, simple, and isolated cases have been included in our data set. We have focused on the goniopolarimetric (GP, also referred to as direction-finding) properties at frequencies between 125 kHz and 2 MHz. The apparent source size γ is very extended (≈60∘) for the lowest analyzed frequencies. Observed apparent source sizes γ expand linearly with a radial distance from the Sun at frequencies below 1 MHz. We have shown that Type III radio bursts statistically propagate in the ecliptic plane. Calculated positions of radio sources suggest that scattering of the primary beam pattern plays an important role in the propagation of Type III radio bursts in the IP medium. **28 January 2008:** 2 May 2009:

Statistical Survey of Type III Radio Bursts at Long Wavelengths Observed by the Solar TErrestrial RElations Observatory (STEREO)/Waves Instruments: Radio Flux Density Variations with Frequency

V. **Krupar**, M. Maksimovic, O. Santolik, E. P. Kontar, B. Cecconi, S. Hoang, O. Kruparova, J. Soucek, H. Reid, A. Zaslavsky

Solar Phys., Volume 289, Issue 8, pp 3121-3135 **2014**

http://arxiv.org/pdf/1410.2053v1.pdf

We have performed a statistical study of 152 Type III radio bursts observed by Solar TErrestrial RElations Observatory (STEREO)/Waves between May 2007 and February 2013. We investigated the flux density between 125 kHz and 16 MHz. Both high- and low-frequency cutoffs were observed in 60 % of events, suggesting an important role of propagation. As already reported by previous authors, we observed that the highest flux density occurs at 1 MHz on both spacecraft. We developed a simplified analytical model of the flux density as a function of radial distance and compared it with the STEREO/Waves data.

Unveiling the Interplanetary Solar Radio Bursts of the 2024 Mother's Day Solar Storm

Oksana **Kruparova**1,2, Vratislav Krupar1,2, Adam Szabo2, David Lario2, Teresa Nieves-Chinchilla2, and Juan Carlos Martinez Oliveros3

2024 ApJL 970 L13

https://iopscience.iop.org/article/10.3847/2041-8213/ad5da6/pdf

We report on a comprehensive study of interplanetary type III radio bursts linked to X-class solar flares from NOAA active region 13664, which instigated the intense 2024 Mother's Day solar storm, marked by a geomagnetic storm of −412 nT, the strongest in over two decades. Utilizing novel localization techniques with direction-finding data from STEREO-A, we identify an average eastward drift of 13.°42 ± 11.°63 in radio source locations relative to GOES observations. Our analysis reveals a significant correlation between solar flare intensity and longitude (Kendall's tau = 0.535) and a strong correlation between radio flux at 1 MHz and GOES 1–8 Å soft X-ray flux (Kendall's tau = 0.648). The timing analysis shows that peak soft X-ray fluxes typically follow electron beam liftoff by 3.24 ± 4.42 minutes. These insights into solar radio burst propagation and localization enhance our understanding of solar–terrestrial interactions and improve space weather forecasting capabilities. **8-15, 8, 9, 10, 11, 14 May 2024**

Table 1 Solar Flares, Type III Bursts, and CMEs

Oblique Bernstein Mode Generation Near the Upper-hybrid Frequency in Solar Pre-flare Plasmas

A. **Kryshtal**, V. Fedun , S. Gerasimenko, A. Voitsekhovska

Solar Phys. 2015, Volume 290, Issue 11, pp 3331-3341 **2015** Open Access

http://link.springer.com/article/10.1007/s11207-015-0793-x

We study analytically the generation process of the first harmonics of the pure electron weakly oblique Bernstein modes. This mode can appear as a result of the rise and development of a corresponding instability in a solar active region. We assume that this wave mode is modified by the influence of pair Coulomb collisions and a weak large-scale sub-Dreicer electric field in the pre-flare chromosphere near the footpoints of a flare loop. To describe the pre-flare plasma we used the model of the solar atmosphere developed by Fontenla, Avrett, and Loeser (Astrophys. J. 406, 319,1993). We show that the generated first harmonic is close to the upper-hybrid frequency. This generation process begins at the very low threshold values of the sub-Dreicer electric field and well before the beginning of the preheating phase of a flare. We investigate the necessary conditions for the existence of non-damped first harmonics of oblique Bernstein waves with small amplitudes in the flare area.

Japanese new solar radio spectrograph: from Hiraiso to Yamagawa

Yuki **Kubo**∗1 , Kazumasa Iwai∗1 , Hiromitsu Ishibashi1 , and Shinichi Watari1

CESRA **2016** p.54

http://cesra2016.sciencesconf.org/conference/cesra2016/pages/CESRA2016_prog_abs_book_v3.pdf

Solar radio burst is one of the most important events for not only space weather forecasting but also investigating high-energy phenomena in solar corona. The MHz range radio observations are useful to detect the shock wave formation in

the solar corona and to estimate shock strength and speed, which is essential parameter in space weather forecasting. On the other hand, the GHz range radio observations are useful for studying high energy phenomena such as particle acceleration in solar flares. While the MHz solar radio bursts, especially type II and III bursts, are radiated via mode conversion of Langmuir waves excited by high energy electrons, the GHz solar radio bursts are synchrotron radiation emitted by high energy electrons at lower corona. These high energy electrons are accelerated at reconnection regions in solar flare and shock waves in solar corona. Therefore, MHz and GHz solar radio waves are closely related each other through the accelerated high energy electrons. So, wide frequency range (MHz to GHz) radio wave observations with high time resolution are required to comprehensively understand high energy phenomena in solar corona. We have been operating solar radio spectrograph called HiRAS for over twenty years in Hiraiso Solar Observatory, National Institute of Information and Communications Technology (NICT), but the system has been decrepit and radio wave environment in Hiraiso is getting worse. So, we have developed wide band (70MHz-9GHz) and high resolution (8msec) solar radio spectrograph in Yamagawa radio observation facility, NICT for space weather forecasting and for obtaining science data. In this presentation, we introduce current status of development of Japanese new solar radio spectrograph in NICT.

The New 30 THz Solar Telescope in São Paulo, Brazil

A. S. **Kudaka**, M. M. Cassiano, R. Marcon, D. P. Cabezas, L. O. T. Fernandes, R. F. Hidalgo Ramirez, P. Kaufmann, R. V. de Souza

Solar Phys. Volume 290, Issue 8, pp 2373-2379 **2015**

It has been found that solar bursts exhibit one unexpected spectral component with fluxes increasing with frequency in the sub-THz range, which is distinct from the well-known microwave emission that peaks at a few to some tens of GHz. This component has been found to extend into the THz range of frequencies by recent 30 THz solar flare observations of impulsive bursts with flux intensities considerably higher than fluxes at sub-THz and microwaves frequencies. High-cadence solar observations at 30 THz (continuum) are therefore an important tool for the study of active regions and flaring events. We report the recent installation of a new 30 THz solar telescope in São Paulo, located at the top of one of the University's buildings. The instrument uses a Hale-type coelostat with two 20 cm diameter flat mirrors sending light to a 15 cm mirror Newtonian telescope. Radiation is directed to a microbolometer array camera that is kept at room temperature. Observations are usually obtained with 5 frames−1 cadence. One 60 mm refractor has been added to observe Hα images simultaneously. We describe our new telescopes and the new observatory examples of the first results obtained.

On the influence of Langmuir wave spectra on the spectra of electromagnetic waves generated in solar plasma with double plasma frequency

Igor V **Kudryavtsev**, T I Kaltman

Monthly Notices of the Royal Astronomical Society, Volume 503, Issue 4, June **2021**, Pages 5740–5745

https://academic.oup.com/mnras/article/503/4/5740/6225352

https://doi.org/10.1093/mnras/stab377

In this paper, we consider the spectral dependences of transverse electromagnetic waves generated in solar plasma at the coalescence of Langmuir waves. It is shown that different spectra of Langmuir waves lead to characteristic types of transversal electromagnetic wave spectra, what makes it possible to diagnose the features of the spectra of Langmuir waves generated in solar plasma. **2004 DECEMBER 1**

X-ray/Radio Quasi-periodic Pulsations Associated with Plasmoids in Solar Flare Current Sheets

Pankaj **Kumar**, Judith T. Karpen, Joel T. Dahlin

ApJ **2024**

https://arxiv.org/pdf/2412.05193

Plasmoids (or magnetic islands) are believed to play an important role in the onset of fast magnetic reconnection and particle acceleration during solar flares and eruptions. Direct imaging of flare current sheets and formation/ejection of multiple plasmoids in extreme ultraviolet (EUV) images, along with simultaneous X-ray and radio observations, offers significant insights into the mechanisms driving particle acceleration in solar flares. Here we present direct imaging of the formation and ejection of multiple plasmoids in flare plasma/current sheets and associated quasi-periodic pulsations (QPPs) observed in X-ray and radio wavelengths, using observations from SDO/AIA, RHESSI, and Fermi GBM. These plasmoids propagate bidirectionally upward and downward along the flare current sheet beneath the erupting flux rope during two successive flares associated with confined/failed eruptions. The flux rope exhibits evidence of helical kink instability with formation and ejection of multiple plasmoids in the flare current sheet, as predicted in an MHD simulation of a kink-unstable flux rope. RHESSI X-ray images show double coronal sources (``loop-top" and higher coronal sources) located at both ends of the flare current/plasma sheet. Moreover, we detected an additional transient faint X-ray source (6-12 keV) located between the double coronal sources, which was co-spatial with multiple plasmoids in the flare current sheet. X-ray (soft and hard) and radio (decimetric) observations unveil QPPs (periods≈10-

s and 100-s) associated with the ejection and coalescence of plasmoids. These observations suggest that energetic electrons are accelerated during the ejection and coalescence of multiple plasmoids in the flare current sheet. **22 April 2015**

Characteristics of Radio-Loud CMEs

Pankaj **Kumar**, P.K. Manoharan, K.S. Cho

2017

https://www.researchgate.net/publication/315637846_Characteristics_of_radio-loud_CMEs

In this paper, we study the characteristics of 46 radio-loud (RL) Coronal Mass Ejections (CMEs), which occurred during 1997-2006. All these RL CMEs were associated with M-and X-class flares. We selected 46 RL CMEs, out of which 26 events (57%) were associated with Solar Energetic Particle (SEP) events detected at 1 AU. Furthermore, we study the link between the flare accelerated electrons in the low corona and protons at 1 AU and found a positive correlation (30%). It suggests the link between the injection sites for electrons and protons, which are most likely accelerated at the flare current sheet. We also study the relation between the CME speed and peak proton flux (>10 MeV) at 1 AU and found a good correlation (~60%), which suggests the proton acceleration by CME driven shocks. In addition, we found two branches (lower and upper) of SEP events with different characteristics. The lower branch SEP events are associated with impulsive rise along with more proton flux whereas the upper branch SEP events exhibit gradual rise and less proton flux. We suggest that flares (current sheet) and CMEs (shocks) both are involved in the particle acceleration for the lower branch, whereas in the upper branch mostly CME driven shocks play an important role in the particle acceleration. **2 May 1998, 29 March, 2001**

Quasi-Periodic Radio Bursts Associated with Fast-mode Waves near a Magnetic Null Point

Pankaj **Kumar**, Valery M. Nakariakov, Kyung-Suk Cho

ApJ **844** 149 **2017**

https://arxiv.org/pdf/1706.09988.pdf

http://sci-hub.cc/10.3847/1538-4357/aa7d53

This paper presents an observation of quasi-periodic rapidly-propagating waves observed in the AIA 171/193 \AA~ channels during the impulsive phase of an M1.9 flare occurred on **7 May 2012**. The instant period was found to decrease from 240~s to 120~s, the speed of the wave fronts was in the range of ~664-1416 km/s. Almost simultaneously, quasi-periodic bursts with similar instant periods, ~70~s and ~140~s, occur in the microwave emission and in decimetric type IV, and type III radio bursts, and in the soft X-ray emission. The magnetic field configuration of the flare site was consistent with a breakout topology, i.e., a quadrupolar field along with a magnetic null point. The quasi-periodic rapidly-propagating wavefronts of the EUV emission are interpreted as a fast magnetoacoustic wave train. The observations suggest that the fast-mode waves are generated during the quasi-periodic magnetic reconnection in the cusp-region above the flare arcade loops. For the first time, we provide the evidence of a tadpole wavelet signature at about 70--140~s in decimetric (245/610~MHz) radio bursts, along with the direct observation of a coronal fast-mode wave train in EUV. In addition, at AIA 131/193 \AA\ we observed quasi-periodic EUV disturbances with the periods of 95~s and 240~s propagating downward at the apparent speed of 172-273 km/s. The nature of these downward propagating disturbances is not revealed, but they could be connected with magnetoacoustic waves or periodically shrinking loops.

Observation of a Short Period Quasi-Periodic Pulsation in Solar X-ray, Microwave and EUV Emissions

Pankaj **Kumar**, Valery M. Nakariakov, Kyung-Suk Cho

ApJ **2017**

https://arxiv.org/pdf/1701.02159v1.pdf

This paper presents the multi-wavelength analysis of a 13 s quasi-periodic pulsation (QPP) observed in hard X-ray (12-300 keV) and microwave (4.9-34 GHz) emissions during a C-class flare occurred on **21 September 2015**. AIA 304 and 171 \AA~ images show an emerging loop/flux tube (L1) moving radially outward, which interacts with preexisting structures within the active region. The QPP was observed during the expansion and rising motion of L1. The Nobeyama Radioheliograph (NoRH) microwave images in 17/34 GHz channels reveal a single radio source, which was co-spatial with a neighboring loop (L2). In addition, using AIA 304 \AA~ images, we detected intensity oscillations in the legs of loop L2 with a period of about 26 s. A similar oscillation period was observed in the GOES soft X-ray flux derivative. This oscillation period seems to increase with time. We suggest that the observed QPP is most likely generated by the interaction between loops L2 and L3 observed in the AIA hot channels (131 and 94 \AA). The merging speed of loops L2 and L3 was ~35 km/s. Loop L1 destroyed possibly by its interaction with preexisting structures in the active region and produced a cool jet with the speed ~106-118 km/s associated with a narrow CME (~770 km/s). Another mechanism of the QPP in terms of a sausage oscillation of the loop (L2) is also possible.

Initiation of a type II radio burst without a CME

Pankaj **Kumar**, Davina Innes, and Kyung-Suk Cho
RHESSI Science Nuggets #278 July **2016**
http://sprg.ssl.berkeley.edu/~tohban/wiki/index.php/Initiation_of_a_type_II_radio_burst_without_a_CME
We present a well-observed type II burst associated with a flare-generated shock wave on **24 April 2016** (SOL2014-04-16 (M1.0)) [1]. This event did not show any evidence of an associated CME. However, a mini-filament was seen to erupt in the opposite direction of the fast **EUV wave**. Such events are of great interest, because they challenge a common assumption that CMEs are always required to generate coronal shocks.
We have reported direct observation of a fast EUV (shock) wave propagating through solar coronal arcade loops, which was associated with CME-less type II radio burst. The wave was observed in the AIA 335, 193, and 171 channels, with a speed of 800-1490 km/s. The wave was most likely triggered by a magnetic reconnection process. A small filament eruption (~340 km/s) was observed shortly after the formation of a quasi-circular ribbon, which moved in the opposite direction of the shock wave and failed to erupt. We did not see any EUV wavefront ahead of filament and speed of the filament was 3-4 times less than the EUV wave speed. The EUV wave was highly directional [3] and excited kink oscillations of the arcade loops during its passage through them.

Flare Generated Shock Wave Propagation Through Solar Coronal Arcade Loops and Associated Type II Radio Burst

Pankaj **Kumar**, D.E. Innes, K.S. Cho
ApJ **828** 28 **2016**
http://arxiv.org/pdf/1606.05056v1.pdf
This paper presents multiwavelength observations of a flare-generated type II radio burst. The kinematics of the shock derived from the type II closely match a fast EUV wave seen propagating through coronal arcade loops. The EUV wave was closely associated with an impulsive M1.0 flare without a related coronal mass ejection, and was triggered at one of the footpoints of the arcade loops in active region NOAA 12035. It was initially observed in the AIA 335 \AA\ images with a speed of ~800 km/s and accelerated to ~1490 km/s after passing through the arcade loops. A fan-spine magnetic topology was revealed at the flare site. A small, confined filament eruption (~340 km/s) was also observed moving in the opposite direction to the EUV wave. We suggest that breakout reconnection in the fan-spine topology triggered the flare and associated EUV wave that propagated as a fast shock through the arcade loops. **16 April 2014**.

Observation of a Quasi-periodic Pulsation in Hard X-ray, Radio and Extreme-ultraviolet Wavelengths

Pankaj **Kumar**, Valery M. Nakariakov, Kyung-Suk Cho
ApJ **822** 7 **2016**
http://arxiv.org/pdf/1603.03121v1.pdf
We present multi-wavelength analysis of a quasi-periodic pulsation (QPP) observed in the hard X-ray, radio, and extreme-ultraviolet (EUV) channels during an M1.9 flare occurred on **23-24 September 2011**. The non-thermal hard X-ray emission in 25-50 keV observed by RHESSI shows five distinct impulsive peaks of decaying amplitude with a period of about three minutes. Similar QPP was observed in the microwave emission recorded by the Nobeyama Radioheliograph and Polarimeter in the 8.8, 15, 17 GHz channels. Interestingly, the 3-min QPP was also observed in the metric and decimetric radio frequencies (25-180, 245, 610 MHz) as repetitive type III bursts. Multi-wavelength observations from the SDO/AIA, Hinode/SOT, and STEREO/SECCHI suggest a fan-spine topology at the eruption site, associated with the formation of a quasi-circular ribbon during the flare. A small filament was observed below the fan-loops before the flare onset. The filament rose slowly and interacted with the ambient field. This behaviour was followed by an untwisting motion of the filament. Two different structures of the filament showed ~3-min periodic alternate rotation in the clockwise and counterclockwise directions. The 3-min QPP was found to highly correlate with 3-min oscillations in a nearby sunspot. We suggest that the periodic reconnection (modulated either by sunspot slow-mode wave or by untwisting filament) at a magnetic null-point most likely causes the repetitive particle acceleration, generating the QPP observed in hard X-ray, microwave and type III radio bursts.
See http://www.astro.gla.ac.uk/users/eduard/cesra/?p=646

Multiwavelength Observations of an Eruptive Flare: Evidence for Blast Waves and Break-Out

Pankaj **Kumar**, D. E. Innes
E-print, April **2013; File,** Solar Physics, November 2013, Volume 288, Issue 1, pp 255-268
Images of an east-limb flare on **3 November 2010** taken in the 131 Å channel of the Atmospheric Imaging Assembly onboard the Solar Dynamics Observatory provide a convincing example of a long current sheet below an erupting plasmoid, as predicted by the standard magnetic reconnection model of eruptive flares. However, the 171 Å and 193 Å

channel images hint at an alternative scenario. These images reveal that large-scale waves with velocity greater than 1000 km s−1 propagated alongside and ahead of the erupting plasmoid. Just south of the plasmoid, the waves coincided with type-II radio emission, and to the north, where the waves propagated along plume-like structures, there was increased decimetric emission. Initially, the cavity around the hot plasmoid expanded. Later, when the erupting plasmoid reached the height of an overlying arcade system, the plasmoid structure changed, and the lower parts of the cavity collapsed inwards. Hot loops appeared alongside and below the erupting plasmoid. We consider a scenario in which the fast waves and the type-II emission were a consequence of a flare blast wave, and the cavity collapse and the hot loops resulted from the break-out of the flux rope through an overlying coronal arcade.

Simultaneous EUV and radio observations of bidirectional plasmoids ejection during magnetic reconnection⋆

Pankaj **Kumar** and Kyung-Suk Cho
A&A 557, A115 (**2013**)
We present a multiwavelength study of the X-class flare, which occurred in active region (AR) NOAA 11339 on **3 November 2011**. The extreme ultraviolet (EUV) images recorded by SDO/AIA show the activation of a remote filament (located north of the AR) with footpoint brightenings about 50 min prior to the flare's occurrence. The kinked filament rises up slowly, and after reaching a projected height of ~49 Mm, it bends and falls freely near the AR, where the X-class flare was triggered. Dynamic radio spectrum from the Green Bank Solar Radio Burst Spectrometer (GBSRBS) shows simultaneous detection of both positive and negative drifting pulsating structures (DPSs) in the decimetric radio frequencies (500–1200 MHz) during the impulsive phase of the flare. The global negative DPSs in solar flares are generally interpreted as a signature of electron acceleration related to the upward-moving plasmoids in the solar corona. The EUV images from AIA 94 Å reveal the ejection of multiple plasmoids, which move simultaneously upward and downward in the corona during the magnetic reconnection. The estimated speeds of the upward- and downward-moving plasmoids are ~152−362 and ~83–254 km s-1, respectively. These observations strongly support the recent numerical simulations of the formation and interaction of multiple plasmoids due to tearing of the current-sheet structure. On the basis of our analysis, we suggest that the simultaneous detection of both the negative and positive DPSs is most likely generated by the interaction or coalescence of the multiple plasmoids moving upward and downward along the current-sheet structure during the magnetic reconnection process. Moreover, the differential emission measure (DEM) analysis of the active region reveals a hot flux-rope structure (visible in AIA 131 and 94 Å) prior to the flare initiation and ejection of the multitemperature plasmoids during the flare impulsive phase.

Multiwavelength Study of a Solar Eruption from AR NOAA 11112: II. Large-Scale Coronal Wave and Loop Oscillation

Pankaj **Kumar**1 , K.-S. Cho1, 2, 3, P. F. Chen4, S.-C. Bong1 and Sung-Hong Park
Solar Physics, **2012**, doi 10.1007/s11207-012-0158-7, **File**
We analyze multiwavelength observations of an M2.9/1N flare that occurred in AR NOAA 11112 on **16 October 2010**. AIA 211 Å EUV images reveal the presence of a faster coronal wave (decelerating from ≈ 1390 to ≈ 830 km s−1) propagating ahead of a slower wave (decelerating from ≈ 416 to ≈ 166 km s−1) towards the western limb. The dynamic radio spectrum from Sagamore Hill radio telescope shows the presence of a metric type II radio burst, which reveals the presence of a coronal shock wave (speed ≈ 800 km s−1). The speed of the faster coronal wave, derived from AIA 211 Å images, is found to be comparable to the coronal shock speed. AIA 171 Å high-cadence observations showed that a coronal loop, which was located at a distance of ≈ 0.32R ⊙ to the west of the flaring region, started to oscillate by the end of the impulsive phase of the flare. The results indicate that the faster coronal wave may be the first driver of the transversal oscillations of coronal loop. As the slower wave passed through the coronal loop, the oscillations became even stronger. There was a plasmoid eruption observed in EUV and a white-light CME was recorded, having velocity of ≈ 340 – 350 km s−1. STEREO 195 Å images show an EIT wave, propagating in the same direction as the lower-speed coronal wave observed in AIA, but decelerating from ≈ 320 to ≈ 254 km s−1. These observations reveal the co-existence of both waves (i.e. coronal Moreton and EIT waves), and the type II radio burst seems to be associated with the coronal Moreton wave.

Evidence of Solar Flare Triggering due to Loop-Loop Interaction Caused by Footpoint Shear-Motion

Kumar, Pankaj; Srivastava, A. K.; Somov, B. V.; Manoharan, P. K.; Erdelyi, R.; Uddin, Wahab
E-print, Sept **2010**, ApJ, ApJ 723 1651-1664, **2010**
We analyze multi-wavelength data of a M7.9/1N class solar flare which occurred on **27 April, 2006** from AR NOAA 10875. GOES soft X-ray images provide the most likely signature of two interacting loops and their reconnection, which triggers the solar flare. TRACE 195 A images also reveal the loop-loop interaction and the formation of `X' points with converging motion (~30 km/s) at the reconnection site in-between this interacting loop system. This

provides the evidence of progressive reconnection and flare maximization at the interaction site in the active region. The absence of type III radio burst during this time period indicates no opening of magnetic field lines during the flare energy release, which implies only the change of field lines connectivity/orientation during the loop-loop interaction and reconnection process. The Ondrejov dynamic radio spectrum shows an intense decimetric (DCIM) radio burst (2.5--4.5 GHz, duration ~3 min) during flare initiation, which reveals the signature of particle acceleration from the reconnection site during loop-loop interaction. The double peak structures at 4.9 and 8.8 GHz provide the most likely confirmatory signature of the loop-loop interaction at the flare site in the active region. RHESSI hard X-ray images also show the loop-top and footpoint sources of the corresponding two loop system and their coalescence during the flare maximum, which act like the current carrying flux-tubes with resultant opposite magnetic fields and the net force of attraction. We also suggest that the shear motion/rotation of the footpoint of the smaller loop, which is anchored in the opposite polarity spot, may be responsible for the flare energy buildup and then its release due to the loop-loop interaction.

Type II radio bursts and their association with coronal mass ejections in solar cycles 23 and 24

Anshu **Kumari**, Diana E. Morosan, E. K. J. Kilpua, F. Daei

A&A 675, A102 **2023**

https://arxiv.org/pdf/2305.18992.pdf

https://www.aanda.org/articles/aa/pdf/2023/07/aa44015-22.pdf

Metre wavelength type II solar radio bursts are believed to be the signatures of shock-accelerated electrons in the corona. Studying these bursts can give information about the initial kinematics, dynamics and energetics of CMEs in the absence of white-light observations. In this study, we investigate the occurrence of type II bursts in solar cycles 23 and 24 and their association with coronal mass ejections (CMEs). We also explore the possibility of occurrence of type II bursts in the absence of a CME. We performed statistical analysis of type II bursts that occurred between 200 - 25 MHz in solar cycle 23 and 24 and found the temporal association of these radio bursts with CMEs. We categorised the CMEs based on their linear speed and angular width, and studied the distribution of type II bursts with `fast' (speed ≥500km/s), `slow' (speed <500km/s), `wide' (width ≥60o) and `narrow' (width <60o) CMEs. We explored the type II bursts occurrence dependency with solar cycle phases. Our results suggest that type II bursts dominate at heights ≈1.7−2.3±0.3 R⊙ with a clear majority having an onset height around 1.7 ±0.3 R⊙ assuming the four-fold Newkirk model. The results indicate that most of the type II bursts had a white-light CME counterpart, however there were a few type II which did not have a clear CME association. There were more CMEs in cycle 24 than cycle 24. However, the number of type II radio bursts were less in cycle 24 compared to cycle 23. The onset heights of type IIs and their association with wide CMEs reported in this study indicate that the early CME lateral expansion may play a key role in the generation of these radio bursts. **November 04, 2015**

Type IV Radio Bursts and Associated Active Regions in the Sunspot Cycle 24

Anshu **Kumari**

Solar Phys. **297**, Article number: 98 **2022**

https://arxiv.org/pdf/2205.02482.pdf

https://link.springer.com/content/pdf/10.1007/s11207-022-02032-2.pdf

In this article, the association of solar radio type IV bursts with active region location on the Sun is studied for the solar cycle 24. The active regions associated with moving and stationary type IV bursts are categorised as close to disk center and far from disk center regions based on their location on the solar surface (i.e, ≤45∘ or ≥45∘, respectively). The location of the active regions associated with type IV bursts accompanied with coronal mass ejections (CMEs) are also studied. We found that ≈30−40% of the active regions are located far from disk center for all the bursts. It is found that most of the active regions associated with stationary type IV bursts are close to disk center (≈60−70%). The active regions associated with moving type IV bursts are more evenly distributed across the surface, i.e ≈56% and ≈44%, close to disk center and far from disk center regions, respectively. Most of the burst having active region close to disk center indicate that these bursts can be used to obtain physical properties such as electron density and magnetic fields of the coronal mass ejections responsible for geomagnetic storms. **September 24, 2011**

Solar Radio Spectro-polarimetry (50-500 MHz) : Design and Development of Cross-Polarized Log-Periodic Dipole antenna and configuration of receiver system

Anshu **Kumari**, G. V. S. Gireesh, C. Kathiravan, V. Mugundhan, Indrajit V. Barve

IEEE Transactions on Antennas and Propagation **2021**

https://arxiv.org/pdf/2101.05088.pdf

A radio spectro-polarimeter was developed at the Gauribidanur radio observatory to study the characteristics of the polarized radio waves that are emitted by the impetuous solar corona in the 50 - 500 MHz frequency range. The instrument has three major components : a Cross-polarized Log-Periodic Dipole Antenna (CLPDA), an analog receiver, and a digital receiver (spectrum analyzer). This article elaborates the design and developmental aspects of the CLPDA, its characteristics and briefs about the configurations of the analog and digital receivers, setting up of the spectro-

polarimeter, stage-wise tests performed to characterize it, etc. To demonstrate the instrumental capability, the estimation of the solar coronal magnetic field strength (B {\it Vs} heliocentric height), using the spectral data obtained with it, is exemplified. Throughout the above band, the CLPDA has a gain, return loss and polarization cross-talk of ≈ 6.6 dBi, ≲ -10 dB, and ≲ -27 dB, respectively. The design constraints, the procedure to tune its impedance and to minimize its dimension, etc. are elaborated. The analog receiver has a noise figure of ≈3 dB and a receiver-noise-temperature (Trcvr) of about 290 K. The receiver-flux-density (Srcvr) is ≈5.3×103, and ≈5.3×105 Jy at 50 and 500 MHz, respectively. The observed spectral data shows a Signal-to-Noise Ratio and Dynamic range of about 30 dB and 40 dB, respectively, at 50 MHz. The average polarization isolation / cross-talk of the CLPD varies from -30 dB to -24 dB over an azimuthal angle of ±45∘ with respect to the reference position angle (0∘). The average degree of circular polarization (DCP) is ≈100% at the reference position and found to decrease gradually and reaches ≈80% at an azimuthal angle of ±45∘. **May 02, 2016, March 30, 2018**

On the occurrence of type IV solar radio bursts in the solar cycle 24 and their association with coronal mass ejections

Anshu **Kumari**, D. E. Morosan, E. K. J. Kilpua

2021 *ApJ* **906** 79

https://arxiv.org/pdf/2011.03509.pdf

https://doi.org/10.3847/1538-4357/abc878

Solar activity, in particular coronal mass ejections (CMEs), are often accompanied by bursts of radiation at metre wavelengths. Some of these bursts have a long duration and extend over a wide frequency band, namely, type IV radio bursts. However, the association of type IV bursts with coronal mass ejections is still not well understood. In this article, we perform the first statistical study of type IV solar radio bursts in the solar cycle 24. Our study includes a total of 446 type IV radio bursts that occurred during this cycle. Our results show that a clear majority, ∼81% of type IV bursts, were accompanied by CMEs, based on a temporal association with white-light CME observations. However, we found that only ∼2.2% of the CMEs are accompanied by type IV radio bursts. We categorised the type IV bursts as moving or stationary based on their spectral characteristics and found that only ∼18% of the total type IV bursts in this study were moving type IV bursts. Our study suggests that type IV bursts can occur with both `Fast' (≥500 km/s) and `Slow' (<500 km/s), and also both `Wide' (≥60∘) and `Narrow' (<60∘) CMEs. However, the moving type IV bursts in our study were mostly associated with `Fast' and `Wide' CMEs (∼52%), similar to type II radio bursts. Contrary to type II bursts, stationary type IV bursts have a more uniform association with all CME types. **October 03, 2011, October 18, 2017**
CESRA # 2807 March **2021** http://www.astro.gla.ac.uk/users/eduard/cesra/?p=2807

Direct Estimates of the Solar Coronal Magnetic Field Using Contemporaneous Extreme-ultraviolet, Radio, and White-light Observations

Anshu **Kumari**, R. Ramesh, C. Kathiravan, T. J. Wang, N. Gopalswamy

ApJ **881** 24 **2019**

https://arxiv.org/pdf/1907.09721.pdf

sci-hub.se/10.3847/1538-4357/ab2adf

We report a solar coronal split-band type II radio burst that was observed on **2016 March 16** with the Gauribidanur Radio Spectro-Polarimeter (GRASP) in the frequency range ≈\,90\,-\,50 MHz, and the Gauribidanur RadioheliograPH (GRAPH) at two discrete frequencies, viz. 80 MHz and 53.3 MHz. Observations around the same epoch in extreme-ultraviolet (EUV) and white-light show that the above burst was associated with a flux rope structure and a coronal mass ejection (CME), respectively. The combined height-time plot generated using EUV, radio, and whitelight data suggest that the different observed features (i.e. the flux rope, type II burst and the CME) are all closely associated. We constructed an empirical model for the coronal electron density distribution (Ne(r), where r is the heliocentric distance) from the above set of observations themselves and used it to estimate the coronal magnetic field strength (B) over the range of r values in which the respective events were observed. The B values are consistent with each other. They vary as B(r)=2.61×r−2.21 \textrm{G} in the range r≈\,1.1\,-\,2.2R⊙. As far as we know, similar `direct' estimates of B in the near-Sun corona without assuming a model for Ne(r), and by combining co-temporal set of observations in two different regions (radio and whitelight) of the electromagnetic spectrum, have rarely been reported. Further, the present work is a novel attempt where the characteristics of a propagating EUV flux rope structure, considered to be the signature of a CME close the Sun, have been used to estimate B(r) in the corresponding distance range.

Addendum to: Strength of the Solar Coronal Magnetic Field – A Comparison of Independent Estimates Using Contemporaneous Radio and White-Light Observations

Anshu **Kumari**, R. Ramesh, C. Kathiravan, T. J. Wang

Solar Physics December **2017**, 292:177

https://link.springer.com/content/pdf/10.1007%2Fs11207-017-1203-3.pdf

Strength of the Solar Coronal Magnetic Field – A Comparison of Independent Estimates Using Contemporaneous Radio and White-Light Observations

Anshu **Kumari**, R. Ramesh, C. Kathiravan, T. J. Wang
Solar Physics November **2017**, 292:161
https://arxiv.org/pdf/1711.02307.pdf
We estimated the coronal magnetic field strength (BB) during the **23 July 2016** coronal mass ejection (CME) event using i) the flux rope structure of the CME in the white-light coronagraph images and ii) the band-splitting in the associated type II burst. No models were assumed for the coronal electron density (N(r)N(r)) we used in the estimation. The results obtained with these two independent methods correspond to different heliocentric distances (rr) in the range ≈2.5--4.5 R⊙≈2.5--4.5 R⊙, but they show excellent consistency and could be fit with a single power-law distribution of the type B(r)=5.7r−2.6 GB(r)=5.7r−2.6 G, which is applicable in that distance range. The power-law index (i.e. −2.6) is in good agreement with the results obtained in previous studies by different methods.

New Evidence for a Coronal Mass Ejection-driven High Frequency Type II Burst near the Sun

Anshu **Kumari**1, R. Ramesh1, C. Kathiravan1, and N. Gopalswamy
2017 ApJ 843 10
http://sci-hub.cc/10.3847/1538-4357/aa72e7
We report observations of the high frequency type II radio burst (≈430–30 MHz) that occurred in the solar corona on **2015 November 4**. The drift rate of the burst, estimated close to the start frequency of its fundamental component (≈215 MHz), is unusually high (≈2 MHz s−1). Our analysis shows that the estimated speed of the magnetohydrodynamic shock driver of the burst varies with time. The peak speed and acceleration are very large, $\approx 2450\ \mathrm{km\ s^{-1}}$ and $\approx 17\ \mathrm{km\ s^{-2}}$, respectively. There is spatio-temporal correlation between the type II burst and the associated coronal mass ejection (CME) in the whitelight and extreme-ultraviolet images. The time profile of the shock speed and the light curve of the associated soft X-ray flare correlate well. These results indicate that in the present case, (i) the magnetohydrodynamic shock responsible for the high frequency coronal type II burst is driven by the CME and (ii) the time profile of the type II burst shock speed represents the near-Sun kinematics of the CME.
CESRA highlight #1818, April **2018** http://cesra.net/?p=1818

Sunspots at Centimeter Wavelengths

Mukul R. **Kundu** and Jeongwoo Lee
Preprint BBSO#1457, **2010;** *Physics of Sun and Star Spots Proceedings IAU Symposium No. 273, 2010*
The early solar observations of Covington (1947) established a good relation between 10.7 cm solar flux and the presence of sunspots on solar disk. The first spatially resolved observation with a two-element interferometer at arc min resolution by Kundu (1959) found that the radio source at 3 cm has a core-halo structure; the core is highly polarized and corresponds to the umbra of a sunspot with magnetic fields of several hundred gauss, and the halo corresponds to the diffuse penumbra or plage region. The coronal temperature of the core was interpreted as due to gyroresonance opacity produced by acceleration of electrons gyrating in a magnetic field. Since the opacity is produced at resonant layers where the frequency matches harmonics of the gyrofrequency, the radio observation could be utilized to measure the coronal magnetic field. Since this simple interferometric observation, the next step for solar astronomers was to use arc second resolution offered by large arrays at cm wavelengths such as Westerbrock Synthesis Radio Telescope and the Very Large Array, which were primarily built for cosmic radio research. Currently, the Owens Valley Solar Array operating in the range 1-18 GHz and the Nobeyama Radio Heliograph at 17 and 34 GHz are the only solar dedicated radio telescopes. Using these telescopes at multiple wavelengths it is now possible to explore three dimensional structure of sunspot associated radio sources and therefore of coronal magnetic fields. We shall present these measurements at wavelengths ranging from 1.7 cm to 90 cm and associated theoretical developments.

High-Energy Emission from a Solar Flare in Hard X-rays and Microwaves

M.R. **Kundu**, V.V. Grechnev, S.M. White, E.J. Schmahl, N.S. Meshalkina, L.K. Kashapova
E-print, Aug **2009**; Solar Phys. (**2009**) 260: 135–156; **File**
We investigate accelerated electron energy spectra for different sources in a large flare using simultaneous observations obtained with two instruments, the Nobeyama Radio Heliograph (NoRH) at 17 and 34 GHz, and the Reuven Ramaty High Energy Solar Spectroscopic Imager (RHESSI) at hard X-rays. This flare is one of the few in which emission up to energies exceeding 200 keV can be imaged in hard X-rays. Furthermore, we can investigate the spectra of individual sources up to this energy. We discuss and compare the HXR and microwave spectra and morphology. Although the event overall appears to correspond to the standard scenario with magnetic reconnection under an eruptive filament, several of its features do not seem to be consistent with popular flare models. In particular we find that (1) microwave emissions might be optically thick at high frequencies despite a low peak frequency in the total flux radio spectrum, presumably due to the inhomogeneity of the emitting source; (2) magnetic fields in high-frequency radio sources might

be stronger than sometimes assumed; (3) sources spread over a very large volume can show matching evolution in their hard X-ray spectra that may provide a challenge to acceleration models. Our results emphasize the importance of studies of sunspot-associated flares and total flux measurements of radio bursts in the millimeter range. **17 June 2003**

Modulation of the solar microwave emission by sausage oscillations

Elena G. **Kupriyanova**, Tatyana I. Kaltman, Alexey A. Kuznetsov
MNRAS Volume 516, Issue 2, Pages 2292–2299, **2022**
https://arxiv.org/pdf/2208.11345.pdf
https://doi.org/10.1093/mnras/stac2386
The modulation of the microwave emission intensity from a flaring loop by a standing linear sausage fast magnetoacoustic wave is considered in terms of a straight plasma slab with the perpendicular Epstein profile of the plasma density, penetrated by a magnetic field. The emission is of the gyrosynchrotron (GS) nature, and is caused by mildly relativistic electrons which occupy a layer in the oscillating slab, i.e., the emitting and oscillating volumes do not coincide. It is shown that the microwave response to the linear sausage wave is highly non-linear. The degree of the non-linearity, defined as a ratio of the Fourier power of the second harmonic to the Fourier power of the principal harmonic, is found to depend on the combination of the width of the GS source and the viewing angle, and is different in the optically thick and optically thin parts of the microwave spectrum. This effect could be considered as a potential tool for diagnostics of the transverse scales of the regions filled in by the accelerated electrons.

Relationship of type III radio bursts with quasi-periodic pulsations in a solar flare

E. G. **Kupriyanova**, L. K. Kashapova, H. A. S. Reid, I. N. Myagkova
Solar Phys. Volume 291, Issue 11, pp 3427–3438 **2016**
http://arxiv.org/pdf/1608.00129v1.pdf
We studied a solar flare with pronounced quasi-periodic pulsations detected in the microwave, X-ray, and radio bands. We used the methods of correlation, Fourier, and wavelet analyses to examine the temporal fine structures and relationships between the time profiles in each wave band. We found that the time profiles of the microwaves, hard X-rays and type III radio bursts vary quasi-periodically with the common period of 40-50 s. The average amplitude of the variations is high, above 30% of the background flux level and reaching 80% after the flare maximum. We did not find the periodicity in either the thermal X-ray flux component or source size dynamics. *Our findings indicate that the detected periodicity is likely to be associated with periodic dynamics in the injection of non-thermal electrons, that can be produced by periodic modulation of magnetic reconnection.* **May 6, 2005**
See CESRA highlight #846, Sept **2016** http://www.astro.gla.ac.uk/users/eduard/cesra/?p=846

Long-period pulsations of the thermal microwave emission of the solar flare of June 2, 2007 from data with high spatial resolution

E. G. **Kupriyanova**, V. F. Melnikov, V. M. Puzynya, K. Shibasaki, H. S. Ji
Astronomy Reports, August **2014**, Volume 58, Issue 8, pp 573-577
*Astronomicheskii Zhurnal, **2014**, Vol. 91, No. 8, pp. 652–661.*
Data from the Nobeyama Radioheliograph at 17 GHz with high spatial and temporal resolution are used to detect quasi-periodic pulsations with periods from 55 to 250 s in the thermal component of the microwave emission of a solar flare loop observed on **June 2, 2007**. Observed pulsations with periods of about 110–120 s are co-phased along the entire loop axis. The observed periodicity is most likely due to modulation of the radio emission by slow magnetoacoustic waves trapped in the filamentary flare loop.

Evolution of the Source of Quasi-Periodic Microwave Pulsations in a Single Flaring Loop

E. G. **Kupriyanova**, V. F. Melnikov, and K. Shibasaki
Publ. Astron. Soc. Japan 65, 3 [4 pages] (**2013**)
http://pasj.asj.or.jp/v65/sp1/65S003/65S003.pdf
Quasi-periodic pulsations (QPP) of the microwave emission of a solar flare on **2002 July 3**, observed with the Nobeyama Radioheliograph (Japan), were investigated with emphasise on the spatial structure of the emission source. It was shown that the time profiles of the variation of the distance between two main sources of the emission and the microwave flux are similar, with a common quasi-periodicity. The most significant QPP is found to be at 30 s. The increase in the microwave emission flux from the Northern source, as well as the increase in the spatiallyintegrated signal, is accompanied by a decrease in the distance between the sources. In contrast, the decrease in the flux corresponds to the decrease in the source separation. This behaviour, together with the observed spatial localisation of the QPP, is very consistent with the vertically polarised global kink mode of the flaring loop.

Spatially Resolved Microwave Observations of Multiple Periodicities in a Flaring Loop

E. G. **Kupriyanova**, V. F. Melnikov, K. Shibasaki

Solar Physics, June **2013**, Volume 284, Issue 2, pp 559-578
Quasi-periodic pulsations (QPPs) with at least three simultaneously existing spectral components with periods P≥30 s, P≈20 s, and about P≈10 s were detected during the decay phase of a solar flare on **3 July 2002**, observed with the Nobeyama Radioheliograph (NoRH). A detailed study of the spatial structure of the Fourier amplitudes of QPPs along a flaring loop has revealed different spatial distributions of the three components. It is shown that the source of the QPPs with period P≥30 s has its maximum amplitude in the inner region of the loop, between the footpoints. QPPs with period P≈20 s are localized at the periphery of the loop, mainly in the outer parts of the footpoints. The spatial distribution of oscillations with period about P≈10 s contains three regions of high QPP amplitudes: two near the footpoints and one in the middle of the flaring region. It is shown that the observed properties of the spectral components are most accurately described by the fundamental, second, and third harmonics of the kink mode standing waves. This is the first identification of the kink mode in flare loops which is based on strict limitations derived from data on the spatial structure of a pulsating flare region.

Types of Microwave Quasi-Periodic Pulsations in Single Flaring Loops

E.G. **Kupriyanova** · V.F. Melnikov · V.M. Nakariakov · K. Shibasaki

Solar Phys (**2010**) 267: 329–342
Quasi-periodic pulsations (QPP) of microwave emission generated in single flaring loops observed with the *Nobeyama Radioheliograph* (NoRH) and *Nobeyama Radio Polarimeters* (NoRP) are studied. Specific features of the time profiles, *i.e.* the visible presence or absence of QPPs, are not accounted for in the selection. The time evolution of the periods of the QPPs is examined using wavelet and correlation analyses. In ten out of twelve considered events, at least one or more significant spectral components with periods from 5 – 60 s have been found. The quality of the oscillations is rather low: $Q = \pi N$, where N is the number of cycles, mostly varies in the range 12 to 40, with an average of 25.We suggest that the detected QPPs can be classified into four types: *i*) those with stable mean periods (*e.g.* of 15 – 20 s or 8 – 9 s, the prevailing type); *ii*) those with spectral drift to shorter periods (mostly in the rise phase of the microwave emission); *iii*) those with drift to longer periods (mostly in the decay phase); *iv*) those with multiple periods showing an X-shaped drift (*e.g.* in the range from 20 – 40 s in the rise phase).

Evolution of Flare-accelerated Electrons in the Solar Corona and Chromosphere Revealed by Spatially Resolved Microwave and Hard X-Ray Analysis

Natsuha **Kuroda**, Gregory Fleishman, Dale Gary, Gelu Nita, Bin Chen, and Sijie Yu
EGU2020-3145 May **2020**
https://meetingorganizer.copernicus.org/EGU2020/displays/36057
Hard X-ray (HXR) and microwave (MW) observations are highly complementary for studying electron acceleration and transport processes in solar flares. In recent years, a new effort has been made in the MW domain using new high-resolution, multifrequency data from The Expanded Owens Valley Solar Array (EOVSA) and a breakthrough numerical modeling infrastructure that enables us to study properties of high-energy electrons in unprecedented cadence and quantitative detail. This study introduces the observation of an M1.2 flare that occurred on **2017 September 9** and analyzes the evolution of the nonthermal electrons in the corona based on EOVSA MW spectral imaging data. We find a significant spectral hardening of the MWemitting nonthermal electron population in the corona, using EOVSA lower-frequency (<7 GHz) observations over a selected 4-minute window of the flare's impulsive phase. We compare this spectral evolution with the evolution of the spectral index of nonthermal electrons emitting in the chromosphere, derived from HXR observations from the Reuven Ramaty High Energy Solar Spectroscopic Imager. We discuss the general picture of the evolution of the nonthermal electron population in this flare by incorporating observations at the two complementary wavelengths. We also make an estimate of the total energy of the nonthermal electrons contained in the observed coronal low-frequency MW source and discuss its temporal evolution.
Presentation #3145 https://presentations.copernicus.org/EGU2020/presentations-ST1.7.zip

Evolution of Flare-accelerated Electrons Quantified by Spatially Resolved Analysis

Natsuha **Kuroda**, Gregory D. Fleishman, Dale E. Gary, Gelu M. Nita, Bin Chen, Sijie Yu
Front. Astron. Space Sci. **7**:22 **2020**
https://www.frontiersin.org/articles/10.3389/fspas.2020.00022/full
https://arxiv.org/pdf/2004.13155.pdf
Nonthermal electrons accelerated in solar flares produce electromagnetic emission in two distinct, highly complementary domains - hard X-rays (HXRs) and microwaves (MWs). This paper reports MW imaging spectroscopy

observations from the Expanded Owens Valley Solar Array of an M1.2 flare that occurred on **2017 September 9**, from which we deduce evolving coronal parameter maps. We analyze these data jointly with the complementary Reuven Ramaty High-Energy Solar Spectroscopic Imager HXR data to reveal the spatially-resolved evolution of the nonthermal electrons in the flaring volume. We find that the high-energy portion of the nonthermal electron distribution, responsible for the MW emission, displays a much more prominent evolution (in the form of strong spectral hardening) than the low-energy portion, responsible for the HXR emission. We show that the revealed trends are consistent with a single electron population evolving according to a simplified trap-plus-precipitation model with sustained injection/acceleration of nonthermal electrons, which produces a double-powerlaw with steadily increasing break energy.

Three-dimensional Forward-fit Modeling of the Hard X-Ray and the Microwave Emissions of the 2015 June 22 M6.5 Flare

Natsuha **Kuroda**, Dale E. Gary, Haimin Wang, Gregory Fleishman, Gelu M. Nita, Ju Jing
2018 ApJ 852 32
https://arxiv.org/pdf/1712.07253.pdf
The well-established notion of a "common population" of the accelerated electrons simultaneously producing the hard X-ray (HXR) and the microwave (MW) emission during the flare impulsive phase has been challenged by some studies reporting the discrepancies between the HXR-inferred and the MW-inferred electron energy spectra. The traditional methods of their spectral inversion have some problems that can be mainly attributed to the unrealistic and the oversimplified treatment of the flare emission. To properly address this problem, we use a Non-linear Force Free Field (NLFFF) model extrapolated from an observed photospheric magnetogram as input to the three-dimensional, multi-wavelength modeling platform GX Simulator, and create a unified electron population model that can simultaneously reproduce the observed HXR and MW observations. We model the end of the impulsive phase of the **2015-06-22** M6.5 flare, and constrain the modeled electron spatial and energy parameters using observations made by the highest-resolving instruments currently available in two wavelengths, the Reuven Ramaty High Energy Solar Spectroscopic Imager (RHESSI) for HXR and the Expanded Owens Valley Solar Array (EOVSA) for MW. Our results suggest that the HXR-emitting electron population model fits the standard flare model with a broken power-law spectrum (E_break ~ 200 keV) that simultaneously produces the HXR footpoint emission and the MW high frequency emission. The model also includes an "HXR invisible" population of nonthermal electrons that are trapped in a large volume of magnetic field above the HXR-emitting loops, which is observable by its gyrosynchrotron (GS) radiation emitting mainly in MW low frequency range.

Observation of 2011-02-15 X2.2 flare in Hard X-ray and Microwave

Natsuha **Kuroda**, Haimin Wang, Dale E. Gary
ApJ **807** 124 **2015**
http://arxiv.org/pdf/1506.01424v1.pdf
Previous studies have shown that the energy release mechanism of some solar flares follow the Standard magnetic-reconnection model, but the detailed properties of high-energy electrons produced in the flare are still not well understood. We conducted a unique, multi-wavelength study that discloses the spatial, temporal and energy distributions of the accelerated electrons in the X2.2 solar flare on 2011, Feb. 15. We studied the source locations of seven distinct temporal peaks observed in hard X-ray (HXR) and microwave (MW) lightcurves using the Reuven Ramaty High Energy Solar Spectroscopic Imager (RHESSI) in 50 to 75 keV channels and Nobeyama Radioheliograph (NoRH) in 34 GHz, respectively. We found that the seven emission peaks did not come from seven spatially distinct sites in HXR and MW, but rather in HXR we observed a sudden change in location only between the second and the third peak, with the same pattern occurring, but evolving more slowly in MW. Comparison between the HXR lightcurve and the temporal variations in intensity in the two MW source kernels also confirmed that the seven peaks came predominantly from two sources, each with multiple temporal peaks. In addition, we studied the polarization properties of MW sources, and time delay between HXR and MW. We discuss our results in the context of the tether-cutting model.

Large-scale contraction and subsequent disruption of coronal loops during various phases of the M6.2 flare associated with the confined flux rope eruption

Upendra **Kushwaha**, Bhuwan Joshi, Astrid M. Veronig, Yong-Jae Moon
ApJ **2015**
http://arxiv.org/pdf/1504.01888v1.pdf
We present a detailed multi-wavelength study of the M6.2 flare which was associated with a confined eruption of a prominence using TRACE, RHESSI, and NoRH observations. The pre-flare phase of this event is characterized by spectacular large-scale contraction of overlying extreme ultraviolet (EUV) coronal loops during which the loop system

was subjected to an altitude decrease of ~20 Mm for an extended span of ~30 min. This contraction phase is accompanied by sequential EUV brightenings associated with hard X-ray (HXR) (up to 25 keV) and microwave (MW) sources from low-lying loops in the core of the flaring region which together with X-ray spectra indicate strong localized heating in the source region before the filament activation and associated M-class flare. With the onset of the impulsive phase of the M6.2 flare, we detect HXR and MW sources that exhibit intricate temporal and spatial evolution in relation with the fast rise of the prominence. Following the flare maximum, the filament eruption slowed down and subsequently confined within the large overlying active region loops; the event did not lead to a coronal mass ejection (CME). During the confinement process of the erupting prominence, we detect MW emission from the extended coronal region with multiple emission centroids which likely represent emission from hot blobs of plasma formed after the collapse of the expanding flux rope and entailing prominence material. RHESSI observations reveal high plasma temperature (~30 MK) and substantial non-thermal characteristics with electron spectral index (~5) during the impulsive phase of the flare. The time-evolution of thermal energy exhibits a good correspondence with the variations in cumulative non-thermal energy which suggest that the energy of accelerated particles efficiently converted to hot flare plasma implying an effective validation of the Neupert effect. **2004-07-14**

Impulsive Energy Release and Non-thermal Emission in a Confined M4.0 Flare Triggered by Rapidly Evolving Magnetic Structures

Upendra **Kushwaha**1, Bhuwan Joshi1, Kyung-Suk Cho2, Astrid Veronig3, Sanjiv Kumar Tiwari4, and S. K. Mathew

2014 ApJ 791 23

We present observations of a confined M4.0 flare from NOAA 11302 on **2011 September 26**. Observations at high temporal, spatial, and spectral resolution from the Solar Dynamics Observatory, Reuven Ramaty High Energy Solar Spectroscopic Imager, and Nobeyama Radioheliograph observations enabled us to explore the possible triggering and energy release processes of this flare despite its very impulsive behavior and compact morphology. The flare light curves exhibit an abrupt rise of non-thermal emission with co-temporal hard X-ray (HXR) and microwave (MW) bursts that peaked instantly without any precursor emission. This stage was associated with HXR emission up to 200 keV that followed a power law with photon spectral index (γ) ~ 3. Another non-thermal peak, observed 32 s later, was more pronounced in the MW flux than the HXR profiles. Dual peaked structures in the MW and HXR light curves suggest a two-step magnetic reconnection process. Extreme ultraviolet (EUV) images exhibit a sequential evolution of the inner and outer core regions of magnetic loop systems while the overlying loop configuration remained unaltered. Combined observations in HXR, (E)UV, and Hα provide support for flare models involving the interaction of coronal loops. The magnetograms obtained by the Helioseismic and Magnetic Imager reveal emergence of magnetic flux that began ~five hr before the flare. However, the more crucial changes in the photospheric magnetic flux occurred about one minute prior to the flare onset with opposite polarity magnetic transients appearing at the early flare location within the inner core region. The spectral, temporal, and spatial properties of magnetic transients suggest that the sudden changes in the small-scale magnetic field have likely triggered the flare by destabilizing the highly sheared pre-flare magnetic configuration.

A Depression of Microwave Emission as a Response to the Appearance of a Jet

Kuzmenko, I. V.

Geomagnetism and Aeronomy, Volume 63, Issue 7, p.1047-1053, **2023**

DOI: 10.1134/S0016793223070150

Numerous jets were observed in the extreme ultraviolet images of the SDO/AIA space observatory in **early March 2015** in the developing active region of a complex magnetic configuration located near the eastern limb of the Sun. The analysis of the observations of several jets showed that the place of their origin and the direction of motion of the material was such that it absorbed the radiation of the regions of the quiet Sun with an area of less than 1% of the area of the solar disk. There was also a partial screening of the flare radio source located to the north of the stationary one. Only in one case, the appearance of jet led to a response in the microwave range in the form of a small depression of radio emissions (negative burst), registered on the records of the Nobeyama radio polarimeters and the Ussuriysk radiometer. Distinguishing features of this event from other jets are revealed. Simultaneously with the studied jet, whose material moved to the east of the active region, small jets were observed to the northwest of it. This led to an increase in the total screening area of the quiet Sun regions, which exceeded 1% of the area of the solar disk. Another jet arose immediately before the jet, as a result of which the material returned to the solar surface probably had a large mass compared to other jets, which manifested itself in the maximum absorption value compared to other cases. The radio burst before the depression of radio emissions was impulsive and there was no activity in other regions of the Sun. The combination of these factors was the cause of the negative burst of small depth. In other cases, the possible depression of radio emissions could be compensated by an increased level of radio emissions due to additional activity, or the mass of the jet material was insufficient for the occurrence of negative bursts.

Development and Parameters of a Non-Self-Similar CME Caused by Eruption of a Quiescent Prominence

I.V. **Kuzmenko** (1), V.V. Grechnev
Solar Phys. **2017**
https://arxiv.org/pdf/1709.01226.pdf **File**

The eruption of a large quiescent prominence on **17 August 2013** and associated coronal mass ejection (CME) were observed from different vantage points by Solar Dynamics Observatory (SDO), Solar-Terrestrial Relations Observatory (STEREO), and Solar and Heliospheric Observatory (SOHO). Screening of the quiet Sun by the prominence produced an isolated negative microwave burst. We estimated parameters of the erupting prominence from a model of radio absorption and measured from 304 \AA\ images. Their variations obtained by both methods are similar and agree within a factor of two. The CME development was studied from the kinematics of the front and different components of the core and their structural changes. The results are verified using movies in which the CME expansion was compensated according to the measured kinematics. We found that the CME mass (3.6×1015 g) was mainly supplied by the prominence (≈6×1015 g), while a considerable part drained back. The mass of the coronal-temperature component did not exceed 1015 g. The CME was initiated by the erupting prominence, which constituted its core and remained active. The structural and kinematical changes started in the core and propagated outward. The CME structures continued to form during expansion, which did not become self-similar up to 25R⊙. The aerodynamic drag was insignificant. The core formed until 4R⊙. Some of its components were observed to straighten and stretch forward, indicating the transformation of tangled structures of the core into a simpler flux rope, which grew and filled the cavity as the CME expanded.

Electron acceleration and transport in the 2023-03-06 solar flare

Alexey **Kuznetsov**, Zhao Wu, Sergey Anfinogentov, Yang Su, Yao Chen
Frontiers in Astronomy and Space Sciences 11: 1407955. **2024**
doi: 10.3389/fspas.2024.1407955
https://arxiv.org/pdf/2405.18850
https://www.frontiersin.org/journals/astronomy-and-space-sciences/articles/10.3389/fspas.2024.1407955/full

We investigated in detail the M5.8 class solar flare that occurred on **2023-03-06**. This flare was one of the first strong flares observed by the Siberian Radioheliograph in the microwave range and the Advanced Space-based Solar Observatory in the X-ray range. The flare consisted of two separate flaring events (a “thermal” and a “cooler” ones), and was associated with (and probably triggered by) a filament eruption. During the first part of the flare, the microwave emission was produced in an arcade of relatively short and low flaring loops. During the second part of the flare, the microwave emission was produced by energetic electrons trapped near the top of a large-scale flaring loop; the evolution of the trapped electrons was mostly affected by the Coulomb collisions. Using the available observations and the GX Simulator tool, we created a 3D model of the flare, and estimated the parameters of the energetic electrons in it.

Ultimate Fast Gyrosynchrotron Codes

Alexey A. **Kuznetsov**, Gregory D. Fleishman
ApJ Volume 922, Issue 2, id.103 **2021**
https://arxiv.org/pdf/2109.10954.pdf
https://iopscience.iop.org/article/10.3847/1538-4357/ac29c0/pdf

The past decade has seen a dramatic increase of practical applications of the microwave gyrosynchrotron emission for plasma diagnostics and three-dimensional modeling of solar flares and other astrophysical objects. This break-through turned out to become possible due to apparently minor, technical development of Fast Gyrosynchrotron Codes, which enormously reduced the computation time needed to calculate a single spectrum, while preserving accuracy of the computation. However, the available fast codes are limited in that they could only be used for a factorized distribution over the energy and pitch-angle, while the distributions of electrons over energy or pitch-angle are limited to a number of predefined analytical functions. In realistic simulations, these assumptions do not hold; thus, the codes free from the mentioned limitations are called for. To remedy this situation, we extended our fast codes to work with an arbitrary input distribution function of radiating electrons. We accomplished this by implementing fast codes for a distribution function described by an arbitrary numerically-defined array. In addition, we removed several other limitations of the available fast codes and improved treatment of the free-free component. The Ultimate Fast Codes presented here allow for an arbitrary combination of the analytically and numerically defined distributions, which offers the most flexible use of the fast codes. We illustrate the code with a few simple examples.

Radio Echo in the Turbulent Corona and Simulations of Solar Drift-pair Radio Bursts

Alexey A. **Kuznetsov**1,2, Nicolina Chrysaphi1, Eduard P. Kontar1, and Galina Motorina3,4
2020 ApJ 898 94
https://arxiv.org/pdf/2007.14648.pdf
https://iopscience.iop.org/article/10.3847/1538-4357/aba04a/pdf

Drift-pair bursts are an unusual type of solar low-frequency radio emission, which appear in the dynamic spectra as two parallel drifting bright stripes separated in time. Recent imaging spectroscopy observations allowed for the quantitative characterization of the drifting pairs in terms of source size, position, and evolution. Here, the drift-pair parameters are qualitatively analyzed and compared with the newly developed Monte Carlo ray-tracing technique simulating radio-wave propagation in the inhomogeneous anisotropic turbulent solar corona. The results suggest that drift-pair bursts can be formed due to a combination of refraction and scattering processes, with the trailing component being the result of turbulent reflection (turbulent radio echo). The formation of drift-pair bursts requires an anisotropic scattering with the level of plasma density fluctuations comparable to that in type III bursts, but with a stronger anisotropy at the inner turbulence scale. The anisotropic radio-wave scattering model can quantitatively reproduce the key properties of drift-pair bursts: the apparent source size and its increase with time at a given frequency, the parallel motion of the source centroid positions, and the delay between the burst components. The trailing component is found to be virtually cospatial and following the main component. The simulations suggest that drift-pair bursts are likely to be observed closer to the disk center and below 100 MHz due to the effects of free–free absorption and scattering. The exciter of drift pairs is consistent with propagating packets of whistlers, allowing for a fascinating way to diagnose the plasma turbulence and the radio emission mechanism. **2017 July 12**
CESRA #2666 Aug **2020** http://www.astro.gla.ac.uk/users/eduard/cesra/?p=2666

First imaging spectroscopy observations of solar drift pair bursts

Alexey **Kuznetsov**, Eduard Kontar
Astronomy & Astrophysics Letters 631, L7 **2019**
https://arxiv.org/pdf/1910.09864.pdf
sci-hub.se/10.1051/0004-6361/201936447
Drift pairs are an unusual type of fine structure sometimes observed in dynamic spectra of solar radio emission. They appear as two identical short narrowband drifting stripes separated in time; both positive and negative frequency drifts are observed. Using the Low Frequency Array (LOFAR), we report unique observations of a cluster of drift pair bursts in the frequency range of 30-70 MHz made on **12 July 2017**. Spectral imaging capabilities of the instrument have allowed us for the first time to resolve the temporal and frequency evolution of the source locations and sizes at a fixed frequency and along the drifting pair components. Sources of two components of a drift pair have been imaged and found to propagate in the same direction along nearly the same trajectories. Motion of the second component source is delayed in time with respect to that of the first one. The source trajectories can be complicated and non-radial; positive and negative frequency drifts correspond to opposite propagation directions. The drift pair bursts with positive and negative frequency drifts, as well as the associated broadband type-III-like bursts, are produced in the same regions. The visible source velocities are variable from zero to a few 104 (up to ∼105) km/s, which often exceeds the velocities inferred from the drift rate (∼104 km/s). The visible source sizes are of about 10′−18′; they are more compact than typical type III sources at the same frequencies. The existing models of drift pair bursts cannot adequately explain the observed features. We discuss the key issues that need to be addressed, and in particular the anisotropic scattering of the radio waves. The broadband bursts observed simultaneously with the drift pairs differ in some aspects from common type III bursts and may represent a separate type of emission.
CESRA nugget #2432 Dec **2019** http://www.astro.gla.ac.uk/users/eduard/cesra/?p=2432

Observations of a CME-related type IV burst with LOFAR

Alexey **Kuznetsov**∗† and Eduard Kontar1
CESRA Abstract **2016**
http://cesra2016.sciencesconf.org/conference/cesra2016/pages/CESRA2016_prog_abs_book_v1.pdf
We present the first observations of a moving type IV solar radio burst with the LOw Frequency ARray (LOFAR). The burst was observed for about 2 hours on **20 June 2015** in the frequency range of 30-80 MHz with high spectral, temporal and spatial resolution. The dynamic spectrum consisted of multiple aperiodic short (˜5 s) broadband pulses; the emission demonstrated an overall negative frequency drift of about 10 kHz/s. Radio imaging revealed a loop-like structure over the limb, with three dominant emission sources: two footpoints and the loop top. The loop size was of about two solar radii; it slowly ascended with the speed of up to 100 km/s. The radio brightness distributions both along and across the loop were frequency-dependent: high- and low-frequency emissions originated predominantly from different footpoints, and higher-frequency emission originated from slightly lower heights. We conclude that gyrosynchrotron radiation of weakly-relativistic electrons (with the energy of ˜50 keV) in a magnetic field of a few Gauss can be responsible for almost all observed emission features. However, some short and very bright narrowband spikes require a coherent (e.g., maser) emission mechanism. All observed emission characteristics seem to be affected strongly by the propagation effects. The most likely origin of the accelerated electrons is a shock formed at a boundary of an expanding magnetic arch.

Synthetic radio views on simulated solar flux ropes

Alexey **Kuznetsov**, Rony Keppens, Chun Xia

Solar Phys. Volume 291, Issue 3, pp 823-845 **2016**
http://arxiv.org/pdf/1601.02370v1.pdf
In this paper, we produce synthetic radio views on simulated flux ropes in the solar corona, where finite-beta magnetohydrodynamic (MHD) simulations serve to mimic the flux rope formation stages, as well as their stable endstates. These endstates represent twisted flux ropes where balancing Lorentz forces, gravity and pressure gradients determine the full thermodynamic variation throughout the flux rope. The obtained models are needed to quantify radiative transfer in radio bands, and allow us to contrast weak to strong magnetic field conditions. Field strengths of up to 100 G in the flux rope yield the radio views dominated by optically thin free-free emission. The forming flux rope shows clear morphological changes in its emission structure as it deforms from an arcade to a flux rope, both on disk and at the limb. For an active region filament channel with a field strength of up to 680 G in the flux rope, gyroresonance emission (from the third-fourth gyrolayers) can be detected and even dominates over free-free emission at the frequencies of up to 7 GHz. Finally, we also show synthetic views on a simulated filament embedded within a (weak-field) flux rope, resulting from an energetically consistent MHD simulation. For this filament, synthetic views at the limb show clear similarities with actual observations, and the transition from optically thick (below 10 GHz) to optically thin emission can be reproduced. On the disk, its dimension and temperature conditions are as yet not realistic enough to yield the observed radio brightness depressions.

Simulations of Gyrosynchrotron Microwave Emission from an Oscillating 3D Magnetic Loop

Alexey **Kuznetsov**, Tom Van Doorsselaere, Veronika Reznikova
Solar Phys. Volume 290, Issue 4, pp 1173-1194 **2015**
Radio observations of solar flares often reveal various periodic or quasi-periodic oscillations. Most likely, these oscillations are caused by magnetohydrodynamic (MHD) oscillations of flaring loops which modulate the emission. Interpretation of the observations requires comparing them with simulations. We simulate the gyrosynchrotron radio emission from a semi-circular (toroidal-shaped) magnetic loop containing sausage-mode MHD oscillations. The aim is to detect the observable signatures specific to the considered MHD mode and to study their dependence on the various source parameters. The MHD waves are simulated using a linear three-dimensional model of a magnetized plasma cylinder; both standing and propagating waves are considered. The curved loop is formed by replicating the MHD solutions along the plasma cylinder and bending the cylinder; this model allows us to study the effect of varying the viewing angle along the loop. The radio emission is simulated using a three-dimensional model and its spatial and temporal variations are analyzed. We consider several loop orientations and different parameters of the magnetic field, plasma, and energetic electrons in the loop. In the model with low plasma density, the intensity oscillations at all frequencies are synchronous (with the exception of a narrow spectral region below the spectral peak). In the model with high plasma density, the emission at low frequencies (where the Razin effect is important) oscillates in anti-phase with the emissions at higher frequencies. The oscillations at high and low frequencies are more pronounced in different parts of the loop (depending on the loop orientation). The layers where the line-of-sight component of the magnetic field changes sign can produce additional peculiarities in the oscillation patterns.

Microwave Images of a Single-Loop Flare: Observations and Simulations

Alexey **Kuznetsov** and Eduard Kontar
RHESSI Science Nuggets, No. 225, **2014**
http://sprg.ssl.berkeley.edu/~tohban/wiki/index.php/Microwave_Images_of_a_Single-Loop_Flare:_Observations_and_Simulations
a flare analysis making use of the new GX Simulator modeling software.
The accelerated electrons in this event were strongly concentrated near the loop top (see Fig. 3) – probably, as a result of trapping in the inhomogeneous magnetic field. This feature explains the non-detection of hard X-rays at high energies (>100 keV), because such X-rays are produced mainly in the dense plasma in the loop footpoints, whereas in the considered event the concentration of the high-energy electrons in the loop footpoints was very low.
Spatially-resolved microwave observations together with 3D simulations can be an effective tool for diagnosing the energetic electrons in solar flares. However, this diagnosing method currently requires some additional data – namely, the extrapolated magnetic field. We anticipate that the multiwavelength imaging radio/microwave observations with new instruments might allow us to put observational constraints on the magnetic field as well.

Spatially-resolved Energetic Electron Properties for the 21 May 2004 Flare from Radio Observations and 3D Simulations

Alexey **Kuznetsov**, Eduard Kontar
Solar Phys, **2015**, Volume 290, Issue 1, pp 79-93
http://arxiv.org/pdf/1403.5751v1.pdf
We investigate in detail the **21 May 2004** flare using simultaneous observations of the Nobeyama Radioheliograph, Nobeyama Radiopolarimeters, Reuven Ramaty High Energy Solar Spectroscopic Imager (RHESSI) and Solar and Heliospheric Observatory (SOHO). The flare images in different spectral ranges reveal the presence of a well-defined single flaring loop in this event. We have simulated the gyrosynchrotron microwave emission using the recently developed interactive IDL tool GX Simulator. By comparing the simulation results with the observations, we have

deduced the spatial and spectral properties of the non-thermal electron distribution. The microwave emission has been found to be produced by the high-energy electrons (>100 keV) with a relatively hard spectrum (δ≃2); the electrons were strongly concentrated near the loop top. At the same time, the number of high-energy electrons near the footpoints was too low to be detected in the RHESSI images and spatially unresolved data. The SOHO Extreme-ultraviolet Imaging Telescope images and the low-frequency microwave spectra suggest the presence of an extended "envelope" of the loop with lower magnetic field. Most likely, the energetic electron distribution in the considered flare reflects the localized (near the loop top) particle acceleration (injection) process accompanied by trapping and scattering.

THREE-DIMENSIONAL SIMULATIONS OF GYROSYNCHROTRON EMISSION FROM MILDLY ANISOTROPIC NONUNIFORM ELECTRON DISTRIBUTIONS IN SYMMETRIC MAGNETIC LOOPS

Alexey A. **Kuznetsov**1,2, Gelu M. Nita3 and Gregory D. Fleishman
2011 ApJ 742 87

Microwave emission of solar flares is formed primarily by incoherent gyrosynchrotron radiation generated by accelerated electrons in coronal magnetic loops. The resulting emission depends on many factors, including pitch-angle distribution of the emitting electrons and the source geometry. In this work, we perform systematic simulations of solar microwave emission using recently developed tools (GS Simulator and fast gyrosynchrotron codes) capable of simulating maps of radio brightness and polarization as well as spatially resolved emission spectra. A three-dimensional model of a symmetric dipole magnetic loop is used. We compare the emission from isotropic and anisotropic (of loss-cone type) electron distributions. We also investigate effects caused by inhomogeneous distribution of the emitting particles along the loop. It is found that the effect of the adopted moderate electron anisotropy is the most pronounced near the footpoints and it also depends strongly on the loop orientation. Concentration of the emitting particles at the looptop results in a corresponding spatial shift of the radio brightness peak, thus reducing effects of the anisotropy. The high-frequency (50 GHz) emission spectral index is specified mainly by the energy spectrum of the emitting electrons; however, at intermediate frequencies (around 10-20 GHz), the spectrum shape is strongly dependent on the electron anisotropy, spatial distribution, and magnetic field nonuniformity. The implications of the obtained results for the diagnostics of the energetic electrons in solar flares are discussed.

Optimized gyrosynchrotron algorithms and fast codes

Alexey A. **Kuznetsov**1,2 and Gregory D. Fleishman3
BBSO Preprint # 1479, **2011**
http://solar.njit.edu/preprints/kuznetsov1479.pdf
Advances in Plasma Astrophysics, Proceedings IAU Symposium No. 274, 2010
A. Bonanno, E. de Gouveia Dal Pino, & A. Kosovichev, eds.

Gyrosynchrotron (GS) emission of charged particles spiraling in magnetic fields plays an exceptionally important role in astrophysics. In particular, this mechanism makes a dominant contribution to the continuum solar and stellar radio emissions. However, the available exact equations describing the emission process are extremely slow computationally, thus limiting the diagnostic capabilities of radio observations. In this work, we present approximate GS codes capable of fast calculating the emission from anisotropic electron distributions. The computation time is reduced by several orders of magnitude compared with the exact formulae, while the computation error remains within a few percent. The codes are implemented as the executable modules callable from IDL; they are made available for users via web sites.

MANIFESTATIONS OF ENERGETIC ELECTRONS WITH ANISOTROPIC DISTRIBUTIONS IN SOLAR FLARES. II. GYROSYNCHROTRON MICROWAVE EMISSION

Alexey A. **Kuznetsov**1,2 and Valentina V. Zharkova3
Astrophysical Journal, 722:1577–1588, **2010**

We investigate the spectra and polarization of the gyrosynchrotron microwave (MW) emission generated by anisotropic electron beams in the solar corona. The electron distributions are selected from the steady propagation/precipitation model of beam electrons obtained from the time-dependent solutions of the Fokker–Planck equation taking into account particle anisotropic precipitation into a converging magnetic tube while losing energy in collisions and Ohmic losses induced by a self-induced electric field.We separate the effects of converging magnetic field from those of self-induced electric field for beams with different initial energy fluxes and spectral indices. The effect of returning electrons of the beam is negligible for the beams with relatively weak energy fluxes (F _ 10^{10} erg cm^{-2} s^{-1}), while it becomes very important for the electron beams with F _ 10^{12} erg cm^{-2} s^{-1}. Electric field-induced losses lead to the increase of MW emission intensity, especially at larger viewing angles (θ _ 140°, looking at the loop from a side). The polarization remains typical for the beam-like distributions. The combined effect of the self-induced electric field and converging magnetic field reveals a noticeable (up to a factor

of 10) increase of the emission intensity (for the viewing angles θ _ 140◦–150◦) in comparison with the models considering only collision factor, especially in the deeper precipitation layers (near the loop footpoints). Thus, considering the self-induced electric field is especially important for the resulting MW emission intensity, spectra shape, and polarization that can provide much closer correlation of simulations with observations in solar flares. **2002 July 23**

Superfine Temporal Structure of the Microwave Burst on 21 April 2002: What Can We Learn about the Emission Mechanismfl

A.A. **Kuznetsov**

Solar Phys (**2008**) 253: 103–116

Zebra pattern is observed as a number of almost parallel bright and dark stripes in the dynamic spectrum of solar radio emission. Recent observations show that zebra patterns in the microwave range often have superfine temporal structure, when the zebra stripes consist of individual short pulses similar to millisecond spikes. In this article, the burst on **21 April 2002** is investigated. The burst with a distinct superfine structure was detected at the Huairou Station (China) in 2.6 – 3.8 GHz frequency range. It is found that the emission pulses are quasi-periodic, the pulse period is about 25 – 40 ms and decreases with an increase of the emission frequency. The degree of circular polarization of zebra pattern increases with an increase of the emission frequency, it varies from moderate (about 20%) to relatively high (> 60%) values. The temporal delay between the signals with left- and righthanded polarization is not found. The conclusion is made that the emission is generated by plasma mechanism at the fundamental plasma frequency in a relatively weak magnetic field. The observed polarization of the emission is formed during its propagation due to depolarization effects. A model is proposed in which the superfine temporal structure is formed due to modulation of the emission mechanism by downward propagating MHD oscillations; this model allows us to explain the observed variation of the pulse period with the emission frequency.

Double plasma resonance and fine spectral structure of solar radio bursts

*Adv. Space Res. 39(9), Pages 1434-1440, **2007***

Alexey A. **Kuznetsov** and Yury T. Tsap

28 October 2003 flare: High Energy Gamma Emission, Type II Radio Emission and Solar Particle Observations

Kuznetsov, S. N.; Kurt, V. G.; Yushkov, B. Yu.; Myagkova, I. N.; Kudela, K.; Belov, A. V.; Caroubalos, C.; Hilaris, A.; Mavromichalaki, H.; Moussas, X.; Preka-Papadema, P.

International Journal of Modern Physics A, Volume 20, Issue 29, pp. 6705-6707 (**2005**).

http://arxiv.org/pdf/1009.3646v1.pdf

The **28 October 2003** flare gave us the unique opportunity to compare the acceleration time of high-energy protons with the escaping time of those particles which have been measured onboard spacecraft and by neutron monitors network as GLE event. High-energy emission time scale and shock wave height and velocity time dependencies were also studied.

First High Resolution Interferometric Observation of a Solar Prominence With ALMA

Nicolas **Labrosse**, Andrew S. Rodger, Krzysztof Radziszewski, Paweł Rudawy, Patrick Antolin, Lyndsay Fletcher, Peter J. Levens, Aaron W. Peat, Brigitte Schmieder, Paulo J. A. Simões

MNRAS **2022**

https://arxiv.org/pdf/2202.12434.pdf

We present the first observation of a solar prominence at 84−116 GHz using the high resolution interferometric imaging of ALMA. Simultaneous observations in Hα from Białkaw Observatory and with SDO/AIA reveal similar prominence morphology to the ALMA observation. The contribution functions of 3 mm and Hα emission are shown to have significant overlap across a range of gas pressures. We estimate the maximum millimetre-continuum optical thickness to be τ3mm≈2, and the brightness temperature from the observed Hα intensity. The brightness temperature measured by ALMA is ∼6000−7000 K in the prominence spine, which correlates well with the estimated brightness temperature for a gas temperature of 8000 K. **19th April 2018**

Critical Mach Numbers for Magnetohydrodynamic Shocks with Accelerated Particles and Waves

J. Martin **Laming**

ApJ **940** 98 **2022**

https://arxiv.org/pdf/2210.09365.pdf

https://iopscience.iop.org/article/10.3847/1538-4357/ac98bb/pdf
The first critical fast Mach number is defined for a magnetohydrodynamic shock as the Mach number where the shock transitions from subcritical, laminar, behavior to supercritical behavior, characterized by incident ion reflection from the shock front. The ensuing upstream waves and turbulence are convected downstream leading to a turbulent shock structure. Formally this is the Mach number where plasma resistivity can no longer provide sufficient dissipation to establish a stable shock, and is characterized by the downstream flow speed becoming subsonic. We revisit these calculations, including in the MHD jump conditions terms modeling the plasma energy loss to accelerated particles and the presence of waves associated with these particles. The accelerated particle contributions make an insignificant change, but the associated waves have a more important effect. Upstream waves can be strongly amplified in intensity on passing through the shock, and represent another means of shock dissipation. The presence of such waves therefore increases the first critical fast Mach number, especially at quasi-parallel shock where wave excitation is strongest. These effects may have significance for the solar regions where shock waves accelerate particles and cause Type II and Type III radio bursts, and also contribute to the event-to-event variability of SEP acceleration.

Possible Estimation of the Solar Cycle Characteristic Parameters by the 10.7 cm Solar Radio Flux

George **Lampropoulos**, Helen Mavromichalaki, Vasilis Tritakis
Solar Phys. Volume 291, Issue 3, pp 989-1002 **2016**
Two independent methods for estimating basic parameters of the solar cycle are presented. The first of them, the ascending-descending triangle method, is based on a previous work by Tritakis (Astrophys. Space Sci. 82, 463, 1982), which described how the fundamental parameters of a certain solar cycle could be predicted from the shape of the previous one. The relation between the two cycles before and after a specific 11-year solar cycle is tighter than between the two cycles belonging to the same 22-year solar cycle (even-odd cycle). The second is the MinimaxX method, which uses a significant relation in the international sunspot number between the maximum value of a solar cycle and its value 2.5 or 3 years (depending on the enumeration of the even or odd cycle) before the preceding minimum. The tests applied to Cycles 12 to 24 indicate that both methods can estimate the peak of the 11-year solar radio flux at a high confidence level. The data used in this study are the 10.7 cm solar radio flux since 1947, which have been extrapolated back to 1848 from the strong correlation between the monthly international sunspot numbers and the adjusted values of the 10.7 cm radio flux.

1977-2017: 40 years of decametric observations of Jupiter and the Sun with the Nançay Decameter Array

L. **Lamy**, P. Zarka, B. Cecconi, L.-K. Klein, S. Masson, L. Denis, A. Coffre, C. Viou
Proceedings of the 8th International Workshop on Planetary, Solar and Heliospheric Radio Emissions (PRE VIII), Seggauberg, Austria, Oct. 25-27, 2016 **2017**
https://arxiv.org/pdf/1709.03821.pdf
The Nan\c{c}ay Decameter Array (NDA) routinely observes low frequency (10-100 MHz) radio emissions of Jupiter and the Sun since 4 decades. The NDA observations, acquired with a variety of receivers with increasing performances, were the basis for numerous studies of jovian and solar radio emissions and now form a unique long-term database spanning >3 solar cycles and jovian revolutions. In addition, the NDA historically brought a fruitful support to space-based radio observatories of the heliosphere, to multi-wavelength analyses of solar activity and contributes to the development of space weather services. After having summarized the NDA characteristics, this article presents latest instrumental and database developments, some recent scientific results and perspectives for the next decade. **27 January 2011**

The Quiet-Sun Differential Emission Measure from Radio and UV Measurements

E. **Landi** and F. Chiuderi Drago
The Astrophysical Journal, Vol. 675, No. 2: 1629-1636, **2008**.
http://www.journals.uchicago.edu/doi/pdf/10.1086/527285
In the present work we combine UVand radio observations of the quiet Sun to determine the differential emission measure (DEM) of the average quiet solar atmosphere from the photosphere (5600 K) to the corona. UV line intensities have been used to constrain the DEM above 30,000 K, and the radio spectrum from 1.5 to 345 GHz has been used to extend the DEM determination down to 5600 K. Radio observations are shown to provide a much more reliable diagnostic tool for DEM determination than UVand EUV lines at T < 30;000 K. The resulting average quiet-Sun DEMthat we found is in excellent agreement with curves from the literature for temperatures larger than 60,000 K, but is lower than previous determinations bymore than 1 order ofmagnitude in the 10,000Y30,000Ktemperature range. The present work determines the DEM below 10,000 K for the first time, in a temperature region where UVand EUV lines cannot be used.

Langmuir-Slow Extraordinary Mode Magnetic Signature Observations with Parker Solar Probe

A. **Larosa**1, T. Dudok de Wit1, V. **Krasnoselskikh**1,2, S. D. Bale2,3, O. Agapitov +++
2022 ApJ 927 95
https://iopscience.iop.org/article/10.3847/1538-4357/ac4e85/pdf
Radio emission from interplanetary shocks, planetary foreshocks, and some solar flares occurs in the so-called "plasma emission" framework. The generally accepted scenario begins with electrostatic Langmuir waves that are driven by a suprathermal electron beam on the Landau resonance. These Langmuir waves then mode-convert to freely propagating electromagnetic emissions at the local plasma frequency fpe and/or its harmonic 2fpe. However, the details of the physics of mode conversion are unclear, and so far the magnetic component of the plasma waves has not been definitively measured. Several spacecraft have measured quasi-monochromatic Langmuir or slow extraordinary modes (sometimes called z-modes) in the solar wind. These coherent waves are expected to have a weak magnetic component, which has never been observed in an unambiguous way. Here we report on the direct measurement of the magnetic signature of these waves using the Search Coil Magnetometer sensor of the Parker Solar Probe/FIELDS instrument. Using simulations of wave propagation in an inhomogeneous plasma, we show that the appearance of the magnetic component of the slow extraordinary mode is highly influenced by the presence of density inhomogeneities that occasionally cause the refractive index to drop to low values where the wave has strong electromagnetic properties.
2020 May 27
CESRA # 3267 May 2022 **https://www.astro.gla.ac.uk/users/eduard/cesra/?p=3267**

A Catalog of Metric Type II Radio Bursts Detected by RSTN During Solar Cycle 24.

Lawrance, B., Devi, P., Chandra, R. et al.
Sol Phys 299, 75 (**2024**).
https://doi.org/10.1007/s11207-024-02317-8
In this study, we compile a catalog of metric type II radio bursts using the Radio Solar Telescope Network (RSTN) to study the occurrence, associations, and properties of the emission and their parent solar activity phenomena. According to the intensity and clarity of the radio emission features, we have divided the m-type II radio bursts into two qualitative categories, namely certain and uncertain. We analyzed RSTN data in Solar Cycle 24 (**2009 – 2019**), which is freely available from four worldwide stations: Learmonth, Sanvito, Sagamore Hills, and Palehua. Through careful visual inspection, we have collected all metric type II bursts detected in the range of **25 – 180 MHz**. The relationships between these bursts and solar eruptive events, such as solar flares and coronal mass ejections (CMEs), are studied, and the results are presented and discussed. The outcomes could be used to reveal the occurrence of solar and space-weather activities based on the ground-based radio perspective. The newly assembled catalog of metric type II and associated solar events will be made freely available to the solar scientific community.
CESRA #3826 2024 **https://www.astro.gla.ac.uk/users/eduard/cesra/?p=3826**

Coronal Mass Ejections with and without DH Type II Radio Bursts

M. Bendict **Lawrance** , A. Shanmugaraju, Bojan Vršnak
Solar Phys. Volume 290, Issue 11, pp 3365-3377 **201**5
A statistical analysis of 135 out of 141 X-class flares observed during 1997 – 2012 with and without deca-hectometric (DH) type II radio bursts has been performed. It was found that 79 events (X-class flares and coronal mass ejections – Group I) were associated with DH type II radio bursts and 62 X-class flare events were not. Out of these 62 events without DH type IIs, 56 events (Group II) have location information, and they were selected for this study. Of these 56 events, only 32 were associated with CMEs. Most of the DH-associated X-class events (~79 %) were halo CMEs, in contrast to 14 % in Group II. The average CME speed of the X-class flares associated with DH type IIs is 1555 km s−1, which is nearly twice that of the X-class flare-associated CMEs without DH event (744 km s−1). The X-class flares associated with DH radio bursts have a mean flare intensity (3.63×10−4 Wm−2) that is 38 % greater than that of X-class flares without DH radio bursts (2.23×10−4 Wm−2). In addition to the greater intensity, it is also found that the the duration and rise time of flares associated with DH radio emission (DH flares) is more than twice than that of the flares without DH radio emission. When the events were further divided into two categories with respect to their source locations in eastern and western regions, 65 % of the events in the radio-loud category (with DH radio bursts) are from the western hemisphere and the remaining 35 % are from the eastern hemisphere. On the other hand, in the radio-quiet category (without DH radio bursts), nearly 60 % of the events are from the eastern hemisphere in contrast to those of the radio-loud category. It is found that 81 % of the events from eastern regions have flare durations > 30 min in the DH-flare category, in contrast to a nearly equal number from the western side for flare durations longer/shorter than 30 min. Similarly, the eastern events in the DH-flare category have a longer average rise-time of 34 min, while the western events have an average flare rise-time of 26 min. On the other hand, the CME speed and flare strength are found to be nearly equal among east and west side events, except that both these parameters are greater for events with DH type IIs.

Kappa-Distributed Electrons in Solar Outflows: Beam-Plasma Instabilities and Radio Emissions

M. **Lazar**, R. A. López, S. Poedts & S. M. Shaaban

Solar Physics volume 298, Article number: 72 (**2023**)
https://doi.org/10.1007/s11207-023-02159-w

Electrostatic (ES) wave instabilities are assumed to be at the origin of radio emissions from interplanetary shocks, and solar coronal sources are most likely induced by electron beams, more energetic but less dense than electron strahls in the solar wind. In this paper, we present the results of a new dispersion and stability analysis for electron populations with Kappa velocity distributions, as often indicated by in situ observations. We investigate, both theoretically and numerically, three electron plasma beam configurations with different implications in the generation of radio emissions. The same three cases, but for Maxwellian distributed electrons, were considered in numerical simulations by Thurgood and Tsiklauri (Astronomy and Astrophysics 584:A83, 2015). Our kinetic plasma approach clarifies the nature of the unstable mode as being an electron beam ES instability (and not a Langmuir instability) in all cases, and for both Kappa and Maxwellian approaches. Electron beam waves are Landau resonant and with frequencies of the fastest growing modes close to but below the plasma frequency (i.e., $\omega \lesssim \omega pe$). Suprathermal Kappa tails tend to inhibit the instability by reducing the growth rates, but these effects become minor if the drift speed of the beam is sufficiently high compared to the thermal speed of the electrons. The frequency downshift, also revealed by the observations, clearly tends to increase in the presence of a Kappa-distributed beam. Particle-in-cell (PIC) simulations confirm the inhibiting effects of (initially) Kappa-distributed electrons, but these minor effects in the linear and quasi-linear phases unexpectedly lead to significant decreases in the wave energy levels of the (primary) ES fluctuations near the plasma frequency and higher harmonics. As a result, EM radio (secondary) emissions generated nonlinearly after saturation are even more drastically reduced and can even be completely suppressed. However, the EM emissions around the second harmonic ($\omega \lesssim 2\omega pe$) are markedly powered by two symmetric countermoving beams, even in the presence of Kappa electrons. These results offer real promise for a realistic interpretation and modeling of radio emissions observed in heliosphere, arguing in favor of a rigorous spectral analysis of the wave instabilities at their origin.

The Radio Observatory on the Lunar Surface for Solar studies

T. Joseph W. **Lazio**a, b, , , R.J. MacDowallc, b, Jack O. Burnsd, b, D.L. Jonese, b, K.W. Weilera, b, L. Demaioc, A. Cohenf, N. Paravastu Dalalg, E. Polisenskya, K. Stewarta, S. Baleh, N. Gopalswamyc, M. Kaiserc, J. Kasperi

Advances in Space Research, Volume 48, Issue 12, 15 December **2011**, Pages 1942-1957

The Radio Observatory on the Lunar Surface for Solar studies (ROLSS) is a concept for a near-side low radio frequency imaging interferometric array designed to study particle acceleration at the Sun and in the inner heliosphere. The prime science mission is to image the radio emission generated by Type II and III solar radio burst processes with the aim of determining the sites at and mechanisms by which the radiating particles are accelerated. Specific questions to be addressed include the following: (1) Isolating the sites of electron acceleration responsible for Type II and III solar radio bursts during coronal mass ejections (CMEs); and (2) Determining if and the mechanism(s) by which multiple, successive CMEs produce unusually efficient particle acceleration and intense radio emission. Secondary science goals include constraining the density of the lunar ionosphere by searching for a low radio frequency cutoff to solar radio emission and constraining the low energy electron population in astrophysical sources. Key design requirements on ROLSS include the operational frequency and angular resolution. The electron densities in the solar corona and inner heliosphere are such that the relevant emission occurs at frequencies below 10 MHz. Second, resolving the potential sites of particle acceleration requires an instrument with an angular resolution of at least 2fl, equivalent to a linear array size of approximately 1000 m. Operations would consist of data acquisition during the lunar day, with regular data downlinks. No operations would occur during lunar night.

ROLSS is envisioned as an interferometric array, because a single aperture would be impractically large. The major components of the ROLSS array are 3 antenna arms arranged in a Y shape, with a central electronics package (CEP) located at the center. The Y configuration for the antenna arms both allows for the formation of reasonably high dynamic range images on short time scales as well as relatively easy deployment. Each antenna arm is a linear strip of polyimide film (e.g., Kapton™) on which 16 science antennas are located by depositing a conductor (e.g., silver). The antenna arms can be rolled for transport, with deployment consisting of unrolling the rolls. Each science antenna is a single polarization dipole. The arms also contain transmission lines for carrying the radio signals from the science antennas to the CEP. The CEP itself houses the receivers for the science antennas, the command and data handling hardware, and, mounted externally, the downlink antenna.

Tracing shock waves from the corona to 1 AU: Type II radio emission and relationship with CMEs.

Leblanc, Y., Dulk, G.A., Vourlidas, A., Bougeret, J.L.:

2001, *J. Geophys. Res.* **106**, 25301 – 25312. doi:10.1029/2000JA000260.

Generation of Type U Bursts in Solar Radio Emission

V.G. **Ledenev**

Solar Phys (**2008**) 253: 191–198

If plasma waves propagate in the direction of the plasma density decrease, their spectrum shifts to large wave numbers (to small phase velocities). This means that the spectrum of plasma waves excited by an electron beam concentrates near the distribution function ("plateau") border, which shifts in the region of low velocities in the process of quasilinear relaxation. As the spectrum of excited plasma waves shifts in the region of large wave numbers, their frequency grows in accordance with the dispersion equation, which describes these waves. When the growth of the plasma wave frequency exceeds the decrease of the frequency owing to the regular inhomogeneity in the corona, the branch with positive frequency drift appears on the dynamic spectrum of the radio emission. Our computations allow us to estimate the density and energy of electron beams generating type U bursts.

Characteristics of plasma turbulence and radio emission from an interplanetary shock wave:

V. G. **Ledenev**, E. Aguilar-Rodriguez, V. V. Tirsky and V. M. Tomozov

A&A 477 (**2008**) 293-298

http://www.aanda.org/10.1051/0004-6361:20078208

https://sci-hub.st/https://www.aanda.org/articles/aa/abs/2008/49/aa8208-07/aa8208-07.html

*Aims.*We investigate the characteristics of energetic electron beams, plasma turbulence and radio emission from interplanetary shock waves.

*Methods.*Numerical calculations of spectra and Landau damping of hot plasma eigen oscillations in the magnetic field are used.

*Results.*It is shown that the longitudinal wave spectrum, excited in the solar wind plasma, extends with the increase of the refractive index *n* over range of values *n*>10. This result allows us to explain the broad band of emission, the constant value of the average ratio of frequency-band to radio emission frequency from interplanetary shock wave fronts, and to estimate the electron beam density and amplitude of Langmuir waves at the shock. It is shown that a spectrum of radio emission is determined by the spectrum of Langmuir waves excited upstream of the interplanetary shock wave by heated electrons escaping from the shock wave front.

Microwave Perspective on Magnetic Breakout Eruption

Jeongwoo **Lee**

Front. Astron. Space Sci., 9:855737. **2022**

https://www.frontiersin.org/articles/10.3389/fspas.2022.855737/full

https://www.frontiersin.org/articles/10.3389/fspas.2022.855737/pdf

https://doi.org/10.3389/fspas.2022.855737

Microwave maps may provide critical information on the flux rope interaction and the breakout eruption if their polarization is measured with high precision. We demonstrate this diagnostic capability using the 17 GHz maps from the Nobeyama Radioheliograph (NoRH) of a circular ribbon flare SOL**2014-12-17**T04:51. The EUV images from SDO/AIA and the coronal magnetic field extrapolated from the HMI magnetogram are also used to support the interpretation of the microwave data. The most obvious evidence for the breakout eruption comes from the sign change of the microwave polarization over the AR at heliographic coordinates S20E09, indicating change of the overlying fields from a closed fan structure to a spine-like structure. Another important piece of evidence comes from the spatial and temporal variations of quasi-periodic pulsations (QPP) detected at the 17 GHz. The QPP was more obvious in one loop leg before the eruption and later moved to the spine field region on and after the flare. This indicates that the oscillatory power is transferred from an interacting flux rope to the outer spine, along which the reconnection launches torsional Alfvén waves, in good agreement with MHD model predictions for breakout eruption. In the practical viewpoint, these two diagnostics work because microwave observations are free of saturation even in strong flaring regions.

Simulation of plasma emission in magnetized plasmas

Sang-Yun **Lee**, Peter H. Yoon, Ensang Lee, Weichao Tu

ApJ **924** 36 **2022**

https://arxiv.org/pdf/2109.11663.pdf

https://iopscience.iop.org/article/10.3847/1538-4357/ac32bb/pdf

The recent Parker Solar Probe (PSP) observations of type III radio bursts show that the effects of finite background magnetic field can be an important factor in the interpretation of data. In the present paper, the effects of background magnetic field on the plasma emission process, which is believed to be the main emission mechanism for solar coronal and interplanetary type III radio bursts, are investigated by means of the particle-in-cell simulation method. The effects

of ambient magnetic field are systematically surveyed by varying the ratio of plasma frequency to electron gyro-frequency. The present study shows that for a sufficiently strong ambient magnetic field, the wave-particle interaction processes lead to a highly field-aligned longitudinal mode excitation and anisotropic electron velocity distribution function, accompanied by a significantly enhanced plasma emission at the second harmonic plasma frequency. For such a case, the polarization of the harmonic emission is almost entirely in the sense of extraordinary mode. On the other hand, for moderate strengths of the ambient magnetic field, the interpretation of the simulation result is less than clear. The underlying nonlinear mode coupling processes indicate that to properly understand and interpret the simulation results require sophisticated analyses involving interactions among magnetized plasma normal modes including the two transverse modes of the magneto-active plasma, namely, extraordinary and ordinary modes, as well as electron-cyclotron-whistler, plasma oscillation, and upper-hybrid modes. At present, a nonlinear theory suitable for quantitatively analyzing such complex mode-coupling processes in magnetized plasmas is incomplete, which calls for further theoretical research, but the present simulation results could provide a guide for future theoretical efforts.

Microwave Study of a Solar Circular Ribbon Flare

Jeongwoo **Lee**1, Stephen M. White2, Xingyao Chen3, Yao Chen4, Hao Ning4, Bo Li4, and Satoshi Masuda5
2020 ApJL 901 L10
https://doi.org/10.3847/2041-8213/abb4dd
https://arxiv.org/pdf/2009.11926.pdf
A circular ribbon flare (CRF) SOL**2014-12-17**T04:51 is studied using the 17/34 GHz maps from the Nobeyama Radioheliograph along with (E)UV and magnetic data from the Solar Dynamics Observatory. We report the following three findings as important features of the microwave CRF. (1) The first preflare activation comes in the form of a gradual increase of the 17 GHz flux without a counterpart at 34 GHz, which indicates thermal preheating. The first sign of nonthermal activity occurs in the form of stepwise flux increases at both 17 and 34 GHz about 4 minutes before the impulsive phase. (2) Until the impulsive phase, the microwave emission over the entire active region is in a single polarization state matching the magnetic polarity of the surrounding fields. During and after the impulsive phase, the sign of the 17 GHz polarization state reverses in the core region, which implies a magnetic breakout–type eruption in a fan–spine magnetic structure. (3) The 17 GHz flux around the time of the eruption shows quasi-periodic variations with periods of 1–2 minutes. The pre-eruption oscillation is more obvious in total intensity at one end of the flare loop, and the post-eruption oscillation, more obvious in the polarized intensity at a region near the inner spine. We interpret this transition as transfer of oscillatory power from kink mode oscillation to torsional Alfvén waves propagating along the spine field after the eruption. We argue that these three processes are interrelated and indicate a breakout process in a fan–spine structure.
RHESSI Science Nuggets #387 Oct **2020**
https://sprg.ssl.berkeley.edu/~tohban/wiki/index.php/Circular_Ribbon_Flare_at_Microwaves

Particle-in-cell and weak turbulence simulations of plasma emission

Sang-Yun **Lee**, L. F. Ziebell, P. H. Yoon, R. Gaelzer, E. S. Lee
2019 *ApJ* **871** 74
https://arxiv.org/pdf/1811.02392.pdf
sci-hub.tw/10.3847/1538-4357/aaf476
The plasma emission process, which is the mechanism for solar type II and type III radio bursts phenomena, is studied by means of particle-in-cell and weak turbulence simulation methods. By plasma emission, it is meant as a loose description of a series of processes, starting from the solar flare associated electron beam exciting Langmuir and ion-acoustic turbulence, and subsequent partial conversion of beam energy into the radiation energy by nonlinear processes. Particle-in-cell (PIC) simulation is rigorous but the method is computationally intense, and it is difficult to diagnose the results. Numerical solution of equations of weak turbulence (WT) theory, termed WT simulation, on the other hand, is efficient and naturally lends itself to diagnostics since various terms in the equation can be turned on or off. Nevertheless, WT theory is based upon a number of assumptions. It is, therefore, desirable to compare the two methods, which is carried out for the first time in the present paper with numerical solutions of the complete set of equations of the WT theory and with two-dimensional electromagnetic PIC simulation. Upon making quantitative comparisons it is found that WT theory is largely valid, although some discrepancies are also found. The present study also indicates that it requires large computational resources in order to accurately simulate the radiation emission processes, especially for low electron beam speeds. Findings from the present paper thus imply that both methods may be useful for the study of solar radio emissions as they are complementary.

Magnetic Structure of a Composite Solar Microwave Burst

Jeongwoo **Lee**1,2, Stephen M. White3, Chang Liu1, Bernhard Kliem2,4, and Satoshi Masuda
2018 ApJ 856 70
http://sci-hub.tw/http://iopscience.iop.org/0004-637X/856/1/70/
A composite flare consisting of an impulsive flare SOL2015-06-21T01:42 (GOES class M2.0) and a more gradual, long-duration flare SOL2015-06-21T02:36 (M2.6) from NOAA Active Region 12371, is studied using observations

with the Nobeyama Radioheliograph (NoRH) and the Solar Dynamics Observatory (SDO). While composite flares are defined by their characteristic time profiles, in this paper we present imaging observations that demonstrate the spatial relationship of the two flares and allow us to address the nature of the evolution of a composite event. The NoRH maps show that the first flare is confined not only in time, but also in space, as evidenced by the stagnation of ribbon separation and the stationarity of the microwave source. The NoRH also detected another microwave source during the second flare, emerging from a different location where thermal plasma is so depleted that accelerated electrons could survive longer against Coulomb collisional loss. The AIA 131 Å images show that a sigmoidal EUV hot channel developed after the first flare and erupted before the second flare. We suggest that this eruption removed the high-lying flux to let the separatrix dome underneath reconnect with neighboring flux and the second microwave burst follow. This scenario explains how the first microwave burst is related to the much-delayed second microwave burst in this composite event. **2015-06-21**

Thermal and Nonthermal Emissions of a Composite Flare Derived from NoRH and SDO Observations

Jeongwoo **Lee**1,2, Stephen M. White3, Ju Jing4, Chang Liu4, Satoshi Masuda2, andJongchul Chae1
2017 ApJ 850 124

Differential emission measure (DEM) derived from the extreme ultraviolet (EUV) lines of theAtmospheric Imaging Assembly (AIA) on board the Solar Dynamic Observatory is used in the analysis of a solar flare observed by the Nobeyama Radioheliograph (NoRH). The target was a composite event consisting of an impulsive flare, SOL**2015-06-21**T01:42 (GOES class M2.0), and a gradual flare, SOL2015-06-21T02:36 (M2.6), for which separation of thermal plasma heating from nonthermal particle acceleration was of major interest. We have calculated the thermal free–free intensity maps with the AIA-derived DEM and compared them against the observed NoRH maps to attribute the difference to the nonthermal component. In this way, we were able to locate three distinct sources: the major source with thermal and nonthermal components mixed, a nonthermal source devoid of thermal particles, and a thermal source lacking microwave emission. Both the first and the second nonthermal sources produced impulsively rising 17 GHz intensities and moved away from the local magnetic polarization inversion lines in correlation with the flare radiation. In contrast, the thermal sources stay in fixed locations and show temporal variations of the temperature and emission measure uncorrelated with the flare radiation. We interpret these distinct properties as indicating that nonthermal sources are powered by magnetic reconnection and thermal sources passively receive energy from the nonthermal donor. The finding of these distinct properties between thermal and nonthermal sources demonstrates the microwave and EUV emission measure combined diagnostics.

Coronal electron density distributions estimated from CMEs, DH type II radio bursts, and polarized brightness measurements

Jae-Ok **Lee**, Yong-Jae Moon, Jin-Yi Lee, Kyoung-Sun Lee, Rok-Soon Kim
JGR 25 April 2016 Vol: 121, Pages: 2853–2865 **2016**,
http://sci-hub.cc/doi/10.1002/2015JA022321

We determine coronal electron density distributions (CEDDs) by analyzing deca-hectometric (DH) type II observations under two assumptions: DH type II bursts are generated by either (1) shocks at the leading edges of coronal mass ejections (CMEs) or (2) CME shock-streamer interactions. Among 399 Wind/WAVES type II bursts (from 1997 to 2012) associated with SOHO/LASCO CMEs, we select 11 limb events whose fundamental and second harmonic emission lanes are well identified. We determine the lowest frequencies of fundamental emission lanes and the heights of leading edges of their associated CMEs. We also determine the heights of CME shock-streamer interaction regions. The CEDDs are estimated by minimizing the root mean square error between the heights from the CME leading edges (or CME shock-streamer interaction regions) and DH type II bursts. We also estimate CEDDs of 7 events using polarized brightness (pB) measurements. We find the following results. Under the first assumption, the average of estimated CEDDs from 3 to 20 Rs is about 5-fold Saito's model (NSaito(r)). Under the second assumption, the average of estimated CEDDs from 3 to 10 Rs is 1.5-fold NSaito(r). While the CEDDs obtained from pB measurements are significantly smaller than those based on the first assumption and CME flank regions without streamers, they are well consistent with those on the second assumption. Our results show that not only about 1-fold NSaito(r) is a proper CEDD for analyzing DH type II bursts, but also CME shock-streamer interactions could be a plausible origin for generating DH type II bursts. **22 March 2002**

Table 1. Information of 11 DH Type II Radio Bursts and Their Related Limb CMEs and Streamersa

Are the Faint Structures Ahead of Solar Coronal Mass Ejections Real Signatures of Driven Shocksfl

Jae-Ok **Lee**1, Y.-J. Moon1,2, Jin-Yi Lee2, Kyoung-Sun Lee3, Sujin Kim4, and Kangjin Lee
2014 ApJ 796 L16

Recently, several studies have assumed that the faint structures ahead of coronal mass ejections (CMEs) are caused by CME-driven shocks. In this study, we have conducted a statistical investigation to determine whether or not the appearance of such faint structures depends on CME speeds. For this purpose, we use 127 Solar and Heliospheric Observatory/Large Angle Spectroscopic COronagraph (LASCO) front-side halo (partial and full) CMEs near the limb from 1997 to 2011. We classify these CMEs into two groups by visual inspection of CMEs in the LASCO-C2 field of view: Group 1 has the faint structure ahead of a CME and Group 2 does not have such a structure. We find the following results. (1) Eighty-seven CMEs belong to Group 1 and 40 CMEs belong to Group 2. (2) Group 1 events have much higher speeds (average = 1230 km s–1 and median = 1199 km s–1) than Group 2 events (average = 598 km s–1 and median = 518 km s–1). (3) The fraction of CMEs with faint structures strongly depends on CME speeds (V): 0.93 (50/54) for fast CMEs with V ≥ 1000 km s–1, 0.65 (34/52) for intermediate CMEs with 500 km s–1 ≤ V < 1000 km s–1, and 0.14 (3/21) for slow CMEs with V < 500 km s–1. We also find that the fraction of CMEs with deca-hecto metric type II radio bursts is consistent with the above tendency. Our results indicate that the observed faint structures ahead of fast CMEs are most likely an enhanced density manifestation of CME-driven shocks.

CORONAL THICK TARGET HARD X-RAY EMISSIONS AND RADIO EMISSIONS

Jeongwoo **Lee**1,2, Daye Lim2, G. S. Choe2, Kap-Sung Kim2, and Minhwan Jang
2013 ApJ 769 L11
A distinctive class of hard X-ray (HXR) sources located in the corona was recently found, which implies that the collisionally thick target model (CTTM) applies even to the corona. We investigated whether this idea can be independently verified by microwave radiations which have been known as the best companion to HXRs. This study is conducted on the GOES M2.3 class flare which occurred on **2002 September 9** and was observed by the Reuven Ramaty High-Energy Solar Spectroscopic Imager and the Owens Valley Solar Array. Interpreting the observed energy-dependent variation of HXR source size under the CTTM, the coronal density should be as high as 5 × 1011 cm–3 over a distance of up to 12". To explain the cutoff feature of the microwave spectrum at 3 GHz, however, we require a density no higher than 1 × 1011 cm–3. Additional constraints must be placed on the temperature and magnetic field of the coronal source in order to reproduce the microwave spectrum as a whole. First, a spectral feature called the Razin suppression requires a magnetic field in a range of 250-350 G along with high viewing angles around 75fl. Second, to avoid excess fluxes at high frequencies due to the free-free emission that was not observed, we need a high temperature ≥2 × 107 K. These two microwave spectral features, Razin suppression and free-free emissions, become more significant at regions of high thermal plasma density and are essential for validating and determining additional parameters of the coronal HXR sources.

Microwave Depolarization above Sunspots

Jeongwoo **Lee**1 and Stephen M. White
Preprint BBSO#1458, 2010; *Physics of Sun and Star Spots Proceedings IAU Symposium No. 273, **2010***
Microwave emissions from sunspots are circularly polarized in the sense of rotation (right or left) determined by the polarity (north or south) of coronal magnetic fields. However, they may convert into unpolarized emissions under certain conditions of magnetic field and electron density in the corona, and this phenomenon of depolarization could be used to derive those parameters. We propose another diagnostic use of microwave depolarization based on the fact that an observed depolarization strip actually represents the coronal magnetic polarity inversion line (PIL) at the heights of effective mode coupling, and its location itself carries information on the distribution of magnetic polarity in the corona. To demonstrate this diagnostic utility we generate a set of magnetic field models for a complex active region with the observed line-of-sight magnetic fields but varying current density distribution and compare them with the 4.9 GHz polarization map obtained with the Very Large Array (VLA). The field extrapolation predicts very different locations of the depolarization strip in the corona depending on the amount of electric currents assumed to exist in the photosphere. Such high sensitivity of microwave depolarization to the coronal magnetic field can therefore be useful for validating electric current density maps inferred from vector magnetic fields observed in the photosphere.

ELECTRON ENERGY AND MAGNETIC FIELD DERIVED FROM SOLAR MICROWAVE BURST SPECTRA

JEONGWOO **LEE**1 , GELU M. NITA1 , AND DALE E. GARY1
Astrophysical Journal, 696:274–279, **2009** May
http://www.iop.org/EJ/toc/-alert=43190/0004-637X/696/1
BBSO, Number: 1383, 2008
http://solar.njit.edu/preprints/lee1383.pdf
Microwave bursts during solar flares are known to be sensitive to high energy electrons and magnetic field, both of which are important ingredients of solar flare physics. This paper presents such information derived from the microwave bursts of the 412 flares that were measured with the Owens Valley Solar Array (OVSA). We assumed that these bursts are predominantly due to gyrosynchrotron radiation by nonthermal electrons in a single power-law energy distribution to use the simplified formulae for gyrosynchrotron radiation in the data

analysis. A second major assumption was that statistical properties of flare electrons derived from this microwave database should agree with an earlier result based on the Hard X-Ray Burst Spectrometer (HXRBS) on SMM. Magnetic field information was obtained in the form of a scaling law between average magnetic field and total source area, which turns out to a narrow distribution around »400 gauss. The derived nonthermal electron energy is related to the peak flux, peak frequency, and spectral index, through a multi-step regression fit, which can be used for a quick estimate for the nonthermal electron energy from spatially-integrated microwave spectral observations.

Radio Emissions from Solar Active Regions

Jeongwoo **Lee**
BBSO, Number: 1337, **2007**
Space Science Reviews, Volume 133, Numbers 1-4, 2007
DOI 10.1007/s11214-007-9206-2
This article reviews the efforts for understanding these radiative processes, and utilizing them as diagnostic tools in addressing a number of critical issues involved with active regions.

Flat Microwave Spectra Seen at X-Class Flares

Lee, Jeongwoo W.; Gary, Dale E.; Zirin, H.
Solar Physics, Volume 152, Issue 2, pp.409-428, **1994**
https://link.springer.com/content/pdf/10.1007%2FBF00680447.pdf
We report peculiar spectral activity of four large microwave bursts as obtained from the Solar Arrays at the Owens Valley Radio Observatory during observations of X-class flares on 1990 May 24 and 1991 March 7, 8, and 22. Main observational points that we newly uncovered are: (1) flat flux spectra over 1 18 GHz in large amounts of flux ranging from 102 to 104 s.f.u. at the maximum phase, (2) a common evolutionary pattern in which the spectral region of dominant flux shifts from high frequencies at the initial rise to low frequencies at the decaying phase, and (3) unusual time profiles that are impulsive at high frequencies but more extended at lower frequencies. In an attempt to elucidate these new properties, we carry out the model calculations of microwave spectra under assumptions of gyrosynchrotron mechanism and a dipole field configuration to reproduce the observational characteristics. Our results are summarized as follows. First, a flat microwave spectrum reaching up to 102 104 s.f.u. may occur in a case where a magnetic loop is extended to an angular size of ~(0.7 7.0) × 10-7 sterad and contains a huge number (N(E > 10 keV) ~ 1036 1038) of nonthermal electrons with power-law indexδ ~ 3 3.5 over the entire volume. Second, the observed spectral activity could adequately be accounted for by the shrinking of the region of nonthermal electrons to the loop top and by the softening of the power-law spectrum of electrons in a time scale ranging 3 45 min depending on the event. Third, the extended microwave activity at lower frequencies is probably due to electrons trapped in the loop top where magnetic fields are low. Finally, we clarify the physical distinction between these large, extended microwave bursts and the gradual/post-microwave bursts often seen in weak events, both of which are characterized by long-period activity and broadband spectra. **24 May 1990, 7 Mar 1990, 8 Mar 1990, 22 Mar 1990**

Sources of SEP Acceleration during a Flare–CME Event

N.J. **Lehtinen** · S. Pohjolainen, K. Huttunen-Heikinmaa · R. Vainio, E. Valtonen · A.E. Hillaris
E-print, Nov 2007, Solar Phys., File
Solar Phys (**2008**) 247: 151–169, **File**
http://www.springerlink.com/content/q8262j85pj35p663/fulltext.pdf
A high-speed halo-type coronal mass ejection (CME), associated with a GOES M4.6 soft X-ray flare in NOAA AR 0180 at S12W29 and an EIT wave and dimming, occurred on **9 November 2002**. A complex radio event was observed during the same period. It included narrow-band fluctuations and frequency drifting features in the metric wavelength range, type III burst groups at metric–hectometric wavelengths, and an interplanetary type II radio burst, which was visible in the dynamic radio spectrum below 14 MHz. To study the association of the recorded solar energetic particle (SEP) populations with the propagating CME and flaring, we perform a multi-wavelength analysis using radio spectral and imaging observations combined with white-light, EUV, hard X-ray, and magnetogram data. Velocity dispersion analysis of the particle distributions (SOHO and Wind in situ observations) provides estimates for the release times of electrons and protons. Our analysis indicates that proton acceleration was delayed compared to the electrons. The dynamics of the interplanetary type II burst identify the burst source as a bow shock created by the fast CME. The type III burst groups, with start times close to the estimated electron release times, trace electron beams travelling along open field lines into the interplanetary space. The type III bursts seem to encounter a steep density gradient as they overtake the type II shock front, resulting in an abrupt change in the frequency drift rate of the type III burst emission. *Our study presents evidence in support of a scenario in which electrons are accelerated low in the corona behind the CME shock front, while protons are accelerated later, possibly at the CME bow shock high in the corona.*

The challenges of low-frequency radio polarimetry: lessons from the Murchison Widefield Array

Emil **Lenc**, C. S. Anderson, N. Barry, J. D. Bowman, I. H. Cairns, J. S. Farnes, B. M. Gaensler, G. Heald, M. Johnston-Hollitt, D. L. Kaplan, C. R. Lynch, P. I. McCauley, D. A. Mitchell, J. Morgan, M. F. Morales, T. Murphy, A. R. Offringa, S. M. Ord, B. Pindor, C. Riseley, E. M. Sadler, C. Sobey, M. Sokolowski, I. S. Sullivan, S. P. O'Sullivan, X. H. Sun, S. E. Tremblay, C. M. Trott, R. B. Wayth

Publications of the Astronomical Society of Australia (PASA) **2017**

https://arxiv.org/pdf/1708.05799.pdf

We present techniques developed to calibrate and correct Murchison Widefield Array (MWA) low frequency (72-300 MHz) radio observations for polarimetry. The extremely wide field-of-view, excellent instantaneous (u, v)-coverage and sensitivity to degree-scale structure that the MWA provides enable instrumental calibration, removal of instrumental artefacts, and correction for ionospheric Faraday rotation through imaging techniques. With the demonstrated polarimetric capabilities of the MWA, we discuss future directions for polarimetric science at low frequencies to answer outstanding questions relating to polarised source counts, source depolarisation, pulsar science, low-mass stars, exoplanets, the nature of the interstellar and intergalactic media, and the solar environment.

First observations with the Siberian Radioheliograph

Sergey **Lesovoi**1 , Alexander Altyntsev1 , Eugene Ivanov1 , Victor Grechnev1 , Alexey Gubin1 , Larisa Kashapova1 , Alexey Kochanov1 , Alexey Kuznetsov∗†1 , Natalia Meshalkina1 , and Dmitry Zhdanov1

CESRA Abstract **2016** p.49

http://cesra2016.sciencesconf.org/conference/cesra2016/pages/CESRA2016_prog_abs_book_v1.pdf

The Siberian Radioheliograph (SRH) is a new multiwavelength instrument developed as a successor of the Siberian Solar Radio Telescope. The instrument is located in the Badary Valley, 220 km from Irkutsk, Russia. SRH is a T-shaped antenna array designed for imaging observations of the Sun at many frequencies simultaneously. At the first stage, it will contain 96 antennae operating in the frequency range of 4-8 GHz, with the angular resolution up to 13” at 8 GHz and the time resolution of 1 s. In 2016, we have started daily singlefrequency observations with the 48-antenna core of the array. This configuration provides the angular resolution of about 40-50” at 8 GHz and the sensitivity of about 100 K; the working frequency is software-controlled. We have obtained the calibrated images of the quiet Sun, active regions and flares, as well as the light curves of flaring microwave sources with high time resolution. In this report, we present the results of the first observations with the SRH and discuss the plans and perspectives of its future development.

CESRA highlight #1426 July **2017** http://www.astro.gla.ac.uk/users/eduard/cesra/?p=1426

A 96-antenna radioheliograph

Sergey V. **Lesovoi**, Alexander T. Altyntsev, Eugene F. Ivanov and Alexey V. Gubin

Research in Astronomy and Astrophysics, Volume 14, Number 7, 864-868, **2014**

http://sci-hub.cc/10.1088/1674-4527/14/7/008

Here we briefly present some design approaches for a multifrequency 96-antenna radioheliograph. The configuration of the array antenna, transmission lines and digital receivers is the main focus of this work. The radioheliograph is a T-shaped centrally condensed radiointerferometer operating in the frequency range 4–8 GHz. The justification for the choice of such a configuration is discussed. The signals from antennas are transmitted to a workroom by analog optical links. The dynamic range and phase errors of the microwave-over-optical signal are considered. The signals after downconverting are processed by digital receivers for delay tracking and fringe stopping. The required step of delay tracking and data rates are considered. Two 3-bit data streams (I and Q) are transmitted to a correlator with the transceivers embedded in Field Programmed Gate Array chips and with PCI Express cables.

The Multifrequency Siberian Radioheliograph

S. V. **Lesovoi**, A. T. Altyntsev, E. F. Ivanov, A. V. Gubin

Solar Physics, October **2012**, Volume 280, Issue 2, pp 651-661

The ten-antenna prototype of the multifrequency Siberian radioheliograph is described. The prototype consists of four parts: antennas with broadband front-ends, analog back-ends, digital receivers and a correlator. The prototype antennas are mounted on the outermost stations of the Siberian Solar Radio Telescope (SSRT) array. A signal from each antenna is transmitted to a workroom by an analog fiber optical link, laid in an underground tunnel. After mixing, all signals are digitized and processed by digital receivers before the data are transmitted to the correlator. The digital receivers and the correlator are accessible by the Local Area Network (LAN). The frequency range of the prototype is from 4 to 8

GHz. Currently the frequency switching observing mode is used. The prototype data include both circular polarizations at a number of frequencies given by a list. This prototype is the first stage of the multifrequency Siberian radioheliograph development. It is assumed that the radioheliograph will consist of 96 antennas and will occupy stations of the West–East–South subarray of the SSRT. The radioheliograph will be fully constructed in the autumn of 2012. We plan to reach the brightness temperature sensitivity of about 100 K for the snapshot image, a spatial resolution up to 13 arcseconds at 8 GHz and a polarization measurement accuracy about a few percent.
First results with the ten-antenna prototype are presented of observations of solar microwave bursts. The prototype's abilities to estimate source size and locations at different frequencies are discussed.

Automatic detection of solar flares observed at 45 GHz by the POEMAS telescope

Vanessa **Lessa**, Adriana Valio
Astronomy and Computing, **2023**, Volume 44, 100738
https://arxiv.org/pdf/2309.06536.pdf
Every 11 years, the Sun goes through periods of activity, with the occurrence of many solar flares and mass ejections, both energetic phenomena of magnetic origin. Due to its effects on Earth, the study of solar activity is of paramount importance. POEMAS (Polarization of Millimeter Emission of Solar Activity) is a system of two telescopes, installed at CASLEO (El Leoncito Astronomical Complex) in Argentina, which monitors the Sun at two millimeter wavelengths (corresponding frequencies of 45 and 90 GHz). The objective of this work is to automatically detect solar flares observed by the polarimeter. First it is necessary to eliminate the background noise, caused mainly by instrumental problems, from the light curves of millimeter solar emission. The methodology used to exclude the noise proposed in this work is to use the tendency of time series. The subtraction of this model from the light curves provides the input to automate the detection of solar flares using artificial intelligence techniques. A Neural Network was trained to recognize patterns and analyze a dataset in order to identify solar flares. Previously, a total of 30 flares had been visually identified and analyzed in the POEMAS database between 2011/11/22 and 2013/12/10. The methodology presented here confirmed 87% of these events, moreover the neural network was able to identify at least 9 new events. As the neural network was trained to detect impulsive events (lasting less than 5 min), long duration bursts were not automatically detected, nor were they detected visually due to the background noise of the telescope. Visual inspection of the POEMAS data, when comparing with microwave data from the RSTN, allowed the identification of an additional 10 long-duration solar flares at 45 GHz. We discuss some problems encountered and possible solutions for future work.
2012/01/27, 2012/05/07, 2012/07/12, 2012 July 28, 2013/05/13

Prevalence of non-standard collapsing of strong Langmuir turbulence in solar corona plasmas

Yaokun **Li**, Haomin Sun, Hao Ning, Sulan Ni, Xiangliang Kong, Jiansen He, Yao Chen
2024
https://arxiv.org/pdf/2406.05467
We present a fully-kinetic simulation of the full life cycle of strong Langmuir turbulence (SLT) excited by electron beams that are accelerated under the solar corona conditions. We find that (1) most packets (∼80%) are affected by their neighbors during their collapse, as a result, their spatial scale variations present non-standard evolutionary features, i.e., deviating away from what was predicted by the Zakharov model; (2) the collapsing cavity is too shallow to trap the wave packet due to the growth of the Coulomb force, as a result a majority (∼70%) of the packet energy runs away and a secondary localization may occur. The study indicates that the non-standard Langmuir collapse may play an important role in coronal plasmas interacting with an intense electron beam, that may be eventually confirmed by humanity's first mission to fly through the corona.

Annual and Seasonal Occurrence Pattern of Auroral Kilometric Radiation Associated with the Interplanetary Magnetic Field*

Ping **Li**1, Sai Zhang1,2, Fuliang Xiao1,2, Hongming Yang3, Shengyi Ye4, Si Liu1,2, Yihua He1, Qiwu Yang1, Jiawen Tang1, and Archie James Johnston3
2024 ApJL 966 L26
https://iopscience.iop.org/article/10.3847/2041-8213/ad40a7/pdf
Auroral kilometric radiation (AKR) is a widely existing strong radio emission from the Earth's magnetosphere and is generated by suprathermal (1–10 keV) electrons in the polar cavity. Previous works have demonstrated that AKR can contribute to the coupling of the magnetosphere–ionosphere–atmosphere, but its relation to the interplanetary magnetic field (IMF) has not been studied so far. Here, we examine the data of Van Allen Probes and identify a total of 5000 AKR events from 2012 October to 2019 July. Most AKR events (4282) correspond to the dominant parallel component ⫽(=(⬜⬜)2+(⬜⬜)2) of IMF. There are the most (1391) events in 2018 (the solar minimum year) and the least (258) events in 2014 (the solar maximum year), corresponding to more (less) occurrences for the longer duration (> 30 minutes) of southward IMF (Bz < 0) in 2018 (2014). In the Earth's Northern Hemisphere, there are the most (865) events in the autumn (August–October), corresponding to dominant Bx < 0. In the Earth's Southern Hemisphere, there are the most (830) events in the autumn (February–April), corresponding to dominant Bx > 0. The probable reason for the above results is that the longer duration of Bz < 0 can yield the longer magnetic reconnection, and the

dominant Bx < 0 (Bx > 0) is favorable for the single-lobe magnetic reconnection in the northern (southern) hemisphere, allowing more suprathermal electrons into the polar source cavity and generating more AKRs. These current results suggest that IMF is very important for the occurrence of AKR and can be widely applied to similar auroral radio emissions in other magnetized planets of the solar system.

Predicting the Arrival Time of an Interplanetary Shock Based on DSRT Spectrum Observations for the Corresponding Type II Radio Burst and a Blast Wave Theory

Ran **Li** 1,2, Xinhua Zhao 1,3, Jingye Yan 1,3, Lin Wu 1,3, Yang Yang 1,3, +++

2024 ApJ 962 178

https://iopscience.iop.org/article/10.3847/1538-4357/ad150f/pdf

Since fast head-on coronal mass ejections and their associated shocks represent potential hazards to the space environment of the Earth and even other planets, forecasting the arrival time of the corresponding interplanetary shock is a priority in space weather research and prediction. Based on the radio spectrum observations of the 16-element array of the Daocheng Solar Radio Telescope (DSRT), the flagship instrument of the Meridian Project of China, during its construction, this study determines the initial shock speed of a type II solar radio burst on 2022 April 17 from its drifting speed in the spectrum. Assuming that the shock travels at a steady speed during the piston-driven phase (determined from the X-ray flux of the associated flare) and then propagates through interplanetary space as a blast wave, we estimate the propagation and arrival time of the corresponding shock at the orbit of the Solar Terrestrial Relations Observatory-A (STEREO-A). The prediction shows that the shock will reach STEREO-A at 14:31:57 UT on 2022 April 19. The STEREO-A satellite detected an interplanetary shock at 13:52:12 UT on the same day. The discrepancy between the predicted and observed arrival time of the shock is only 0.66 hr. The purpose of this paper is to establish a general method for predicting the shock's propagation and arrival time from this example, which will be utilized to predict more events in the future based on the observations of ground-based solar radio spectrometers or telescopes like DSRT. **2022-04-17-19**

High-harmonic Plasma Emission Induced by Electron Beams in Weakly Magnetized Plasmas

Chuanyang **Li**, Yao Chen, Zilong Zhang, Hao Ning, TangMu Li

ApJ **960** 111 **2024**

https://arxiv.org/pdf/2312.13617.pdf

https://iopscience.iop.org/article/10.3847/1538-4357/ad10a8/pdf

Electromagnetic radiation at higher harmonics of the plasma frequency ($\omega \sim n\omega_{pe}, n>2$) has been occasionally observed in type II and type III solar radio bursts, yet the underlying mechanism remains undetermined. Here we present two-dimensional fully kinetic electromagnetic particle-in-cell simulations with high spectral resolution to investigate the beam-driven plasma emission process in weakly magnetized plasmas of typical coronal conditions. We focused on the generation mechanisms of high-harmonic emission. We found that a larger beam velocity (ud) favors the generation of the higher-harmonic emission. The emissions grow later for higher harmonics and decrease in intensity by ∼2 orders of magnitude for each jump of the harmonic number. The second and third harmonic (H2 and H3) emissions get closer in intensity with larger ud. We also show that (1) the H3 emission is mainly generated via the coalescence of the H2 emission with the Langmuir waves, i.e., H2+L→H3, wherein the coalescence with the forward-propagating beam-Langmuir wave leads to the forward-propagating H3, and coalescence with the backward-propagating Langmuir wave leads to the backward-propagating H3; and (2) the H4 emission mainly arises from the coalescence of the H3 emission with the forward- (backward-) propagating Langmuir wave, in terms of H3+L→H4.

Quasi-periodic Accelerations of Energetic Particles during a Solar Flare

Dong **Li**, Wei Chen

ApJL **931** L28 **2022**

https://arxiv.org/abs/2205.07423

https://iopscience.iop.org/article/10.3847/2041-8213/ac6fd2/pdf

We report the observation of non-stationary Quasi-Periodic Pulsations (QPPs) in high-energy particles during the impulsive phase of an X4.8 flare on 2002 July 23 (SOL2002-07-23T00:35). The X4.8 flare was simultaneously measured by the Reuven Ramaty High Energy Solar Spectroscopic Imager, Nobeyama Radio Polarimeters, and Nobeyama Radioheliograph. The quasi-period of about 50 s, determined by the wavelet transform, is detected in the Gamma-ray line emission. Using the same method, a quasi-period of about 90 s is found in Gamma-ray continuum, hard X-ray (HXR) and radio emissions during almost the same time. Our observations suggest that the flare QPPs should be associated with energetic ions and nonthermal electrons that quasi-periodically accelerated by the repetitive magnetic reconnection. The different quasi-periods between Gamma-ray line and continuum/HXR/radio emissions indicate an apparent difference in acceleration or propagation between energetic ions and nonthermal electrons of this solar flare. **2002 July 23**

Modeling Electron Acceleration and Transport in the Early Impulsive Phase of the 2017 September 10 Solar Flare

Xiaocan **Li**, Fan Guo, Bin Chen, Chengcai Shen, Lindsay Glesener
ApJ **932** 92 **2022**
https://arxiv.org/pdf/2205.04946.pdf
https://iopscience.iop.org/article/10.3847/1538-4357/ac6efe/pdf
The X8.2-class limb flare on **September 10, 2017** is among the best studied solar flare events owing to its great similarity to the standard flare model and the broad coverage by multiple spacecraft and ground-based observations. These multiwavelength observations indicate that electron acceleration and transport are efficient in the reconnection and flare looptop regions. However, there lacks a comprehensive model for explaining and interpreting the multi-faceted observations. In this work, we model the electron acceleration and transport in the early impulsive phase of this flare. We solve the Parker transport equation that includes the primary acceleration mechanism during magnetic reconnection in the large-scale flare region modeled by MHD simulations. We find that electrons are accelerated up to several MeV and fill a large volume of the reconnection region, similar to the observations shown in microwaves. The electron spatial distribution and spectral shape in the looptop region agree well with those derived from the microwave and hard X-ray emissions before magnetic islands grow large and dominate the acceleration. Future emission modelings using the electron maps will enable direct comparison with microwave and hard X-ray observations. These results shed new light on the electron acceleration and transport in a broad region of solar flares within a data-constrained realistic flare geometry.

Particle-in-cell simulation of plasma emission in solar radio bursts

T. M. **Li**2,1, C. Li1,2, P. F. Chen1,2 and W. J. Ding1,2
A&A 653, A169 (**2021**)
https://www.aanda.org/articles/aa/pdf/2021/09/aa40973-21.pdf
https://doi.org/10.1051/0004-6361/202140973
Aims. The present study aims to shed light on our understanding of the radiation processes of solar radio bursts associated with nonthermal electron propagation in the corona and interplanetary space.
Methods. We performed 2.5-dimensional particle-in-cell (PIC) simulations to investigate the plasma emission excited by a relativistic electron beam using different pitch angles in the magnetized plasma.
Results. Langmuir waves at the fundamental and harmonic frequencies were excited via the energy dissipation of the electron beam. For the first time, the backward Langmuir waves up to the third harmonic frequencies were reproduced in the cases of large pitch angles, likely arising from the relecting and scattering of density fluctuations to the Langmuir waves during electrom beam-plasma interaction. Electromagnetic (EM) waves were generated via the mode conversion of electrostatic (ES) waves and the nonlinear wave coupling. Specifically, the harmonic EM emission comes from the coupling of forward and backward Langmuir waves, namely, $L + L' \rightarrow 2H$, while the higher harmonic EM emissions generally come from the coupling of the Langmuir wave and lower-order harmonic EM wave, namely, $L + (n - 1)H \rightarrow nH$. When the electron beam exhibits a large pitch angle, another possible mechanism for the third harmonic EM emission might be the coalescence of three ES waves, namely, $L + L' + L'' \rightarrow 3H$.
CESRA #3151 Dec **2021** https://www.astro.gla.ac.uk/users/eduard/cesra/?p=3151

PIC Simulation of Double Plasma Resonance and Zebra Pattern of Solar Radio Bursts

Chuanyang **Li**, Yao Chen, Sulan Ni, Baolin Tan, Hao Ning, Zilong Zhang
ApJ **909** L5 **2021**
https://arxiv.org/pdf/2102.09172.pdf
https://doi.org/10.3847/2041-8213/abe708
Latest study reports that plasma emission can be generated by energetic electrons of DGH distribution via the electron cyclotron maser instability (ECMI) in plasmas characterized by a large ratio of plasma oscillation frequency to electron gyro-frequency ($\omega pe/\Omega ce$). In this study, on the basis of the ECMI-plasma emission mechanism, we examine the double plasma resonance (DPR) effect and the corresponding plasma emission at both harmonic (H) and fundamental (F) bands using PIC simulations with various $\omega pe/\Omega ce$. This allows us to directly simulate the feature of zebra pattern (ZP) observed in solar radio bursts for the first time. We find that (1) the simulations reproduce the DPR effect nicely for the upper hybrid (UH) and Z modes, as seen from their variation of intensity and linear growth rate with $\omega pe/\Omega ce$, (2) the intensity of the H emission is stronger than that of the F emission by ~ 2 orders of magnitude and vary periodically with increasing $\omega pe/\Omega ce$, while the F emission is too weak to be significant, therefore we suggest that it is the H emission accounting for solar ZPs, (3) the peak-valley contrast of the total intensity of H is ~ 4, and the peak lies around integer values of $\omega pe/\Omega ce$ (= 10 and 11) for the present parameter setup. We also evaluate the effect of energy of energetic electrons on the characteristics of ECMI-excited waves and plasma radiation. The study provides novel insight on the physical origin of ZPs of solar radio bursts.
CESRA #2937 May **2021** http://www.astro.gla.ac.uk/users/eduard/cesra/?p=2937

Observations of a quasi-periodic pulsation in the coronal loop and microwave flux during a solar preflare phase

Dong **Li**, Ying Li, Lei Lu, Qingmin Zhang, Zongjun Ning, Sergey Anfinogentov
ApJL 893:L17 **2020**
https://arxiv.org/pdf/2003.09567.pdf
https://iopscience.iop.org/article/10.3847/2041-8213/ab830c/pdf
We report a quasi-periodic pulsation (QPP) event simultaneously detected from the spatial displacements of coronal loop at both EUV images and microwave emission during the preflare phase of a C1.1 flare on **2016 March 23**. Using the motion magnification technique, a low-amplitude transverse oscillation with the growing period is discovered in a diffuse coronal loop in Atmospheric Imaging Assembly (AIA) image sequences at wavelength of 171 A, and the initial oscillation period is estimated to be ~397 s with a slow growth rate of 0.045. At the same time, a QPP with growing periods from roughly 300 s to nearly 500 s is discovered in the microwave flux in the same active region. Based on the imaging observations measured at EUV wavelengths by the AIA and at microwave 17 GHz by Nobeyama Radioheliograph, the diffuse coronal loop and the microwave radiation source are found to be connected through a hot loop seen in AIA images at wavelength of 94 A. The growing period of the QPP should be related to the modulation of LRC-circuit oscillating process in a current-carrying plasma loop. The existence of electric currents may imply the non-potentialities in the source region during the preflare phase.

Quasi-periodic pulsations of gamma-ray emissions from a solar flare on 2017 September 06

D. **Li**, D. Y. Kolotkov, V. M. Nakariakov, L. Lu, Z. J. Ning
ApJ **888** 53 **2019**
https://arxiv.org/pdf/1912.01145.pdf
https://doi.org/10.3847/1538-4357/ab5e86
We investigate quasi-periodic pulsations (QPPs) of high-energy nonthermal emissions from an X9.3 flare (SOL2017-Sep-06T11:53), the most powerful flare since the beginning of solar cycle 24. The QPPs are identified as a series of regular and repeating peaks in the light curves in the gamma- and hard X-ray (HXR) channels recorded by the Konus-Wind, as well as the radio and microwave fluxes measured by the CALLISTO radio spectrograph during the impulsive phase. The periods are determined from the global wavelet and Fourier power spectra, as 24-30 s in the HXR and microwave channels which are associated with nonthermal electrons, and ~20 s in the gamma-ray band related to nonthermal ions. Both nonthermal electrons and ions may be accelerated by repetitive magnetic reconnection during the impulsive phase. However, we could not rule out other mechanisms such as the MHD oscillation in a sausage mode. The QPP detected in this study is useful for understanding the particle acceleration and dynamic process in solar flares and also bridging the gap between stellar and solar flares since the energy realm of the X9.3 solar flare is almost compared with a typical stellar flare.

Synthesising Solar Radio Images From Atmospheric Imaging Assembly Extreme-Ultraviolet Data

Z. F. **Li**, S. H. Hua, X. Cheng, M. D. Ding
Research in Astronomy and Astrophysics **2019**
https://arxiv.org/pdf/1909.11923.pdf
During non-flaring times, the radio flux of the Sun at the wavelength of a few centimeters to several tens of centimeters mostly originates from the thermal bremsstrahlung emission, very similar to the EUV radiation. Owing to such a proximity, it is feasible to investigate the relationship between the EUV emission and radio emission in a quantitative way. In this paper, we reconstruct the radio images of the Sun through the differential emission measure obtained from the multi-wavelength EUV images of the Atmospheric Imaging Assembly on board Solar Dynamic Observatory. Through comparing the synthetic radio images at 6 GHz with those observed by Siberian Radioheliograph, we find that the predicted radio flux is qualitatively consistent with the observed value, confirming thermal origin of the coronal radio emission during non-flaring times. The results further show that the predicted radio flux is closer to the observations in the case of including the contribution of the plasma with temperatures above 3 MK than in the case of only involving the low temperature plasma as was usually done in the era of pre-SDO. We also discuss the applications of the method and uncertainties of the results. **2016 March 16**

Effect of the Temperature of Background Plasma and the Energy of Energetic Electrons on Z-mode Excitation

Chuanyang **Li**1, Yao Chen1, Xiangliang Kong1, M. Hosseinpour1,2, and Bing Wang1
2019 ApJ 880 31
sci-hub.se/10.3847/1538-4357/ab270f
It has been suggested that the Z-mode instability driven by energetic electrons with a loss-cone type velocity distribution is one candidate process behind the continuum and zebra pattern of solar type-IV radio bursts. Both the temperature of background plasma (T0) and the energy of energetic electrons (ve) are considered to be important to the variation of the maximum growth rate (γmax). Here we present a detailed parameter study on the effect of T0 and ve, within a regime of the frequency ratio (w pe□ □W 10 30 ce). In addition to γmax, we also analyze the effect on the

corresponding wave frequency (wr max) and propagation angle (θmax). We find that (1) γmax generally decreases with increasing ve, while its variation with T0 is more complex depending on the exact value of ve. (2) With increasing T0 and ve, wr max presents stepwise profiles with jumps separated by gradual or very weak variations, and due to the warm plasma effect on the wave dispersion relation wr max can vary within the hybrid band (the harmonic band containing the upper hybrid frequency) and the higher band. (3) The propagation is either perpendicular or quasi-perpendicular, and θmax presents variations in line with those of wr max , as constrained by the resonance condition. We also examine the profiles of γmax with w W pe ce for different combinations of T0 and ve to clarify some earlier calculations which show inconsistent results.

COMPARING SIMULATED RESULTS OF FOLDED AND UNFOLDED LOG-PERIODIC ANTENNA USED FOR OBSERVING THE SUN

Sha **Li**, Yihua Yan, Zhijun Chen, Wei Wang.
Solar-Terrestrial Physics. **2019**. Vol. 5. Iss. 2. P. 45–49.
Solnechno-zemnaya fizika. 2019. Vol. 5. Iss. 2. P. 49–54.
https://naukaru.ru/en/storage/view/36899
There figureare two antenna arrays located in Mingantu Spectral Radio Heliograph (MUSER). MUSER-I and MUSER-II cover the frequency band ranging from 0.4 to 2 GHz and from 2 to 15 GHz respectively. A third antenna array covering 30–240 MHz will be established in the coming years. A log-periodic antenna is one of the choices for MUSER low frequency band; it radiates structures capable of maintaining consistent impedance characteristics over a wide bandwidth. Due to the ability of achieving high gain, it is widely used in many broadband applications. In this program, folded and unfolded log-periodic antennas are simulated for the Meridian project. In order to improve its return loss, this antenna is optimized with the width of each pole and the height of the substrate. This optimized process has been implemented in the simulated software HFSS.

Effect of the Temperature of Background Plasma and the Energy of Energetic Electrons on Z-Mode Excitation

Chuanyang **Li**, Yao Chen, Xiangliang Kong, M. Hosseinpour, Bing Wang
2019
https://arxiv.org/pdf/1906.01218.pdf
It has been suggested that the Z-mode instability driven by energetic electrons with a loss-cone type velocity distribution is one candidate process behind the continuum and zebra pattern of solar type-IV radio bursts. Both the temperature of background plasma (T0) and the energy of energetic electrons (ve) are considered to be important to the variation of the maximum growth rate (γmax). Here we present a detailed parameter study on the effect of T0 and ve, within a regime of the frequency ratio ($10 \le \omega_{pe}/\Omega_{ce} \le 30$). In addition to γmax, we also analyze the effect on the corresponding wave frequency (ωrmax) and propagation angle (θmax). We find that (1) γmax in-general decreases with increasing ve, while its variation with T0 is more complex depending on the exact value of ve; (2) with increasing T0 and ve, ωrmax presents step-wise profiles with jumps separated by gradual or very-weak variations, and due to the warm-plasma effect on the wave dispersion relation ωrmax can vary within the hybrid band (the harmonic band containing the upper hybrid frequency) and the band higher; (3) the propagation is either perpendicular or quasi-perpendicular, and θmax presents variations in line with those of ωrmax, as constrained by the resonance condition. We also examine the profiles of γmax with ω_{pe}/Ω_{ce} for different combinations of T0 and ve to clarify some earlier calculations which show inconsistent results.

Observations of Electron-driven Evaporation during a Flare Precursor

Dong **Li**, Ying Li, Wei Su, Yu Huang, Zongjun Ning
ApJ **2018**
https://arxiv.org/pdf/1801.06755.pdf
We investigate the relationship between the blue shifts of a hot emission line and the nonthermal emissions in microwave and hard X-ray (HXR) wavelengths during the precursor of a solar flare on **2014 October 27**. The flare precursor is identified as a small but well-developed peak in soft X-ray and extreme-ultraviolet passbands before the GOES flare onset, which is accompanied by a pronounced burst in microwave 17 & 34 GHz and HXR 25-50 keV. The slit of Interface Region Imaging Spectrograph (IRIS) stays at one ribbon-like transient during the flare precursor, where shows visible nonthermal emissions in NoRH and RHESSI images. The IRIS spectroscopic observations show that the hot line of Fe XXI 1354.09 A (logT ~ 7.05) displays blue shifts, while the cool line of Si IV 1402.77 A (logT ~ 4.8) exhibits red shifts. The blue shifts and red shifts are well correlated to each other, indicative of an explosive chromospheric evaporation during the flare precursor particularly combining with a high nonthermal energy flux and a short characteristic timescale. In addition, the blue shifts of Fe XXI 1354.09 A are well correlated with the microwave and HXR emissions, implying that the explosive chromospheric evaporation during the flare precursor is driven by nonthermal electrons.

EUV and Magnetic Activities Associated with Type-I Solar Radio Bursts

Chuanyang **Li**, Yao Chen, Bing Wang, Guiping Ruan, Shiwei Feng, Guohui Du, Xiangliang Kong
Solar Phys. 292:82 **2017**
https://arxiv.org/pdf/1705.01666.pdf

Type-I bursts (i.e. noise storms) are the earliest-known type of solar radio emission at the metre wavelength. They are believed to be excited by non-thermal energetic electrons accelerated in the corona. The underlying dynamic process and exact emission mechanism still remain unresolved. Here, with a combined analysis of extreme ultraviolet (EUV), radio and photospheric magnetic field data of unprecedented quality recorded during a type-I storm on **30 July 2011**, we identify a good correlation between the radio bursts and the co-spatial EUV and magnetic activities. The EUV activities manifest themselves as three major brightening stripes above a region adjacent to a compact sunspot, while the magnetic field there presents multiple moving magnetic features (MMFs) with persistent coalescence or cancelation and a morphologically similar three-part distribution. We find that the type-I intensities are correlated with those of the EUV emissions at various wavelengths with a correlation coefficient of 0.7-0.8. In addition, in the region between the brightening EUV stripes and the radio sources there appear consistent dynamic motions with a series of bi-directional flows, suggesting ongoing small-scale reconnection there. Mainly based on the induced connection between the magnetic motion at the photosphere and the EUV and radio activities in the corona, we suggest that the observed type-I noise storms and the EUV brightening activities are the consequence of small-scale magnetic reconnection driven by MMFs. This is in support of the original proposal made by Bentely et al. (Solar Phys. 193, 227, 2000).

Explosive chromospheric evaporation driven by nonthermal electrons around one footpoint of a solar flare loop

Dong **Li**, Zongjun Ning, Yu Huang, Qingmin Zhang
ApJL 841 L9 **2017**
https://arxiv.org/pdf/1705.02448.pdf
http://sci-hub.cc/10.3847/2041-8213/aa71b0

We explore the temporal relationship between microwave/HXR emission and Doppler velocity during the impulsive phase of a solar flare on **2014 October 27** (SOL2014-10-27), which displays a pulse on the light curves in microwave (34 GHz) and hard X-ray (HXR, 25-50 keV) bands before the flare maximum. Imaging observation shows that this pulse mainly comes from one footpoint of a solar flare loop. The slit of Interface Region Imaging Spectrograph (IRIS) stays at this footpoint during this solar flare. The Doppler velocities of Fe XXI 1354.09 A and Si IV 1402.77 A are extracted from the Gaussian fitting method. We find that the hot line of Fe XXI 1354.09 A (logT~7.05) in corona exhibits blue shift, while the cool line of Si IV 1402.77 A (logT~4.8) in transition region exhibits red shift, indicating explosive chromospheric evaporation. The evaporative upflows along the flare loop are also observed in the AIA 131 A image. To our knowledge, this is the first report of chromospheric evaporation evidence from both spectral and imaging observations in the same flare. Both microwave and HXR pulses are well correlated with the Doppler velocities, suggesting that the chromospheric evaporation is driven by nonthermal electrons around this footpoint of a solar flare loop.

Comparisons of Mapped Magnetic Field Lines with the Source Path of the 7 April 1995 Type III Solar Radio Burst†

B. **Li**, Iver H. Cairns, J.T. Gosling, D.M. Malaspina, D. Neudegg, G. Steward, V.V. Lobzin
JGR Volume 121, Issue 7 Pages 6141–6156 **2016**

Ideally, the sources of type III solar radio bursts, which are produced mainly by flare-accelerated electron beams, trace the magnetic field lines along which the beams propagate from the Sun to interplanetary space. A recently developed 2-D approach for large-scale mapping of magnetic field lines between the Sun and Earth in the solar equatorial plane is applied to the sources of the **7 April 1995** type III radio burst imaged by Ulysses and Wind. The approach uses near-Earth solar wind data and a solar wind model with intrinsic non-radial magnetic field at the source surface of the solar wind. Quantitative agreement is found between the mapped field lines, the observed path of the radio source centroids, and the field configurations inferred from solar wind suprathermal electrons observed by Wind. Moreover, the mapped field lines are consistent with Wind not observing the in situ type III electron beam, Langmuir waves, and local radio emission for this type III event.

Study of Temporal Evolution of Emission Spectrum in a Steeply Rising Submillimeter Burst

J. P. **Li**, A. H. Zhou, X. D. Wang
A&A **2015**
http://arxiv.org/pdf/1506.05363v1.pdf

In the paper the spectral temporal evolution of a steeply rising submillimeter (THz) burst occurred on **2003 November 2** was investigated in detail for the first time. Observations show that the flux density of the THz spectrum increased steeply with frequency above 200 GHz. Their average rising rates reached a value of 235 sfu/GHz (corresponding spectral index α of 4.8) during the burst. The flux densities reached about 4,000 and 70,000 sfu at 212 and 405 GHz at

maximum phase, respectively. The emissions at 405 GHz maintained continuous high level that they exceed largely the peak values of the microwave (MW) spectra during the main phase. Our studies suggest that only energetic electrons with a low-energy cutoff of ∼1 MeV and number density of ∼106--108 cm−3 can produce such strong and steeply rising THz component via gyrosynchrotron (GS) radiation based on numerical simulations of burst spectra in the nonuniform magnetic field case. The electron number density N, derived from our numerical fits to the THz temporal evolution spectra, increased substantially from 8×106 to 4×108 cm−3, i.e., N value increased 50 times during the rise phase. During the decay phase it decreased to 7×107 cm−3, i.e., decreased about five times from the maximum phase. The total electron number decreased an order of magnitude from the maximum phase to the decay phase. Nevertheless the variation amplitude of N is only about one time in the MW emission source during this burst, and the total electron number did not decrease but increased by about 20% during the decay phase. Interestingly, we find that the THz source radius decreased by about 24% while the MW source one, on the contrary, increased by 28% during the decay phase.

Fundamental Emission of Type III Bursts Produced in Non-Maxwellian Coronal Plasmas with Kappa-Distributed Background Particles

B. **Li**, Iver H. Cairns

Solar Physics, March **2014**, Volume 289, Issue 3, pp 951-976

Detailed simulations based on quasi-linear theory are presented for fundamental (fp) emission of type III bursts produced in non-Maxwellian, suprathermal, background coronal plasma by injection of energetic electrons during flares with a power-law or Maxwellian velocity distribution, where fp is the electron plasma frequency. The background plasma is assumed to have a kappa (κ) distribution, as inferred from solar wind data and proposed by theories for the corona and solar wind. The predicted type III beam speeds, Langmuir wave levels, and the drift rate and flux of fp emission are strongly sensitive to the presence of suprathermal background electrons in the corona. The simulations show the following results. i) Fast beams with speeds vb>0.5c are produced for coronal background electrons with small κ (κ≲5) by injected electrons with power-law spectra. ii) Moderately fast beams with vb≈0.3--0.5c are generated in coronal plasma with κ≲8 by injections of power-law or Maxwellian electrons. iii) Slow beams with vb<0.3c are produced for coronal background electrons with large κ (κ>8), including the asymptotic limit κ→∞ where the electrons are Maxwellian, for both power-law and Maxwellian injections. The observation of fast type III beams (with vb>0.5c) thus suggests that these beams are produced in coronal regions where the background electron distribution has small κ by injected electrons with power-law spectra, at least when such beams are observed. The simulations, from the viewpoint of type III bursts, thus support: i) the presence, at least sometimes, of suprathermal background electrons in the corona and the associated mechanisms for coronal heating and solar wind acceleration; ii) power-law spectra for injected energetic electrons, consistent with observations of such electrons in situ and of X-ray emission.

Type III bursts produced by power-law injected lectrons in maxwellian background coronal plasmas†

Bo **Li**, Iver H. Cairns

JGR, Volume 118, Issue 8, pages 4748–4759, **2013**

Simulations are presented for coronal type III bursts produced by injection of energetic electrons with power-law speed spectra onto open magnetic field lines embedded in an otherwise unmagnetized Maxwellian background coronal plasma, including quasilinear wave-particle interactions and nonlinear wave-wave processes. The simulations show that although fast electrons with speeds > 0.3*c* are injected they are important only to the onset and not to the peak of *fp* emission, where *fp* is the local electron plasma frequency. Instead, slower beam electrons are the major drivers of the peak *fp* emission. Therefore, the type III beam speeds derived from the drift rates of peak *fp* emission are less than the typical speeds of *c*/3 observed for coronal type III bursts. This occurs mainly because the number of fast beam electrons with speeds > 0.3*c* is much less than the slower ones, causing weaker *fp* emission from these fast beam electrons. Comparisons are made with injected electrons having Maxwellian spectra. We find that type III beams are faster when the injection has power-law spectra, since there are more fast electrons injected than for Maxwellian spectra. These results suggest that type III beams produced in the corona with Maxwellian background particle distributions and either power-law or Maxwellain spectra can account only for the lower half of the observed range 0.1 − 0.6*c* of type III beam speeds, but not for the upper half.

TYPE III RADIO BURSTS IN CORONAL PLASMAS WITH KAPPA PARTICLE DISTRIBUTIONS

B. **Li** and Iver H. Cairns

2013 ApJ 763 L34

We present the first simulations of type III bursts produced in the corona with suprathermal non-Maxwellian background particles, as inferred from solar wind data and proposed by theories for the corona and solar wind. The coronal background particles are assumed to follow kappa (κ) distributions. The predicted fp emission of type III bursts is sensitive via the κ index to the presence of suprathermal background particles, where fp is the local plasma

frequency. The simulations show that (1) the speeds vb of type III beams are much larger (e.g., vb 0.58c for κ = 5) and so type III bursts drift much faster for low κ (≤5) background plasmas than for Maxwellian backgrounds (producing vb < 0.3c), and (2) fp emission generated in a κ-distributed background corona has a larger total bandwidth than in a Maxwellian background, for similar onset frequencies. Type III beams are thus more persistent, i.e., extending over larger distances, in κ-distributed corona. Consequently, observations of fast-drifting coronal type III bursts and associated fast electron beams suggest that the ambient electrons in the corona are κ-distributed, at least when such bursts are observed. These results support, from the new viewpoint of nonthermal radio emission, the occasional presence of suprathermal background electrons in the corona and the associated mechanisms (e.g., "velocity filtration") for coronal heating and solar wind acceleration. The new results also help resolve longstanding issues regarding the speeds and persistence of type III beams, and the production of remotely observable levels of fp emission despite severe losses during propagation.

TYPE III RADIO BURSTS PERTURBED BY WEAK CORONAL SHOCKS
B. **Li** and Iver H. Cairns
2012 ApJ 753 124
Some type III bursts are observed to undergo sudden flux modifications, e.g., reductions and intensifications, when type III beams cross shocks in the upper corona or solar wind. First simulations are presented for type III bursts perturbed by weak coronal shocks, which type III beams traverse. The simulations incorporate spatially localized jumps in plasma density and electron and ion temperatures downstream of a shock. A shock is predicted to produce significant modulations to a type III burst: (1) a broadband flux reduction or frequency gap caused by the shock's density jump, (2) a narrowband flux intensification originating from where the downstream plasma density locally has a small gradient, (3) a possible intensification from the shock front or just upstream, and (4) changes in the frequency drift rate profile and the temporal evolution of radiation flux at frequencies corresponding to the shocked plasma. The modulations are caused primarily by fundamental modifications to the radiation processes in response to the shocked density and temperatures. The predicted intensifications and reductions appear qualitatively consistent with the available small number of reported observations, although it is unclear how representative these observations are. It is demonstrated that a weak shock can cause an otherwise radio-quiet type III beam to produce observable levels of narrowband radio emission. The simulations suggest that type III bursts with frequency-time fine structures may provide a tool to probe shocks in the corona and solar wind, especially for weak shocks that do not radiate by themselves.

Frequency Fine Structures of Type III Bursts Due to Localized Medium-Scale Density Structures Along Paths of Type III Beams

B. **Li**, Iver H. Cairns and P. A. Robinson
Solar Physics, Volume 279, Number 1 (**2012**), 173-196
Predictions from large-scale kinetic simulations are presented for the effects on coronal type III bursts of localized, medium-scale, enhanced density structures superposed on the coronal background along the paths of type III beams. The simulations show that these density structures can produce pronounced frequency fine structures in type III spectra. Flux intensifications and reductions of f p and 2f p emission relative to those for the unperturbed background corona occur at frequencies corresponding to the density structures, where f p is the local electron plasma frequency. Frequency fine structures that are intense, slowly drifting, and narrowband, and thus resemble the characteristics of stria bursts, are predicted for the 2f p emission. The 2f p results are consistent with the qualitative proposal of Takakura and Yousef (Solar Phys. 40, 421, 1975) for the interpretation of stria/type IIIb bursts. However, the predicted f p emission is much weaker than the 2f p emission and generally below observable levels, and the predicted frequency fine structures do not always show stria characteristics. The predictions are thus inconsistent with the qualitative suggestion of Takakura and Yousef and the interpretations of many observers that stria bursts occur more often in f p than in 2f p emission. The significant discrepancies for f p emission between our numerical calculations and the qualitative proposition of Takakura and Yousef (1975) are mainly caused by: i) differences in the detailed emission processes, ii) neglect of scattering of f p emission off small-scale density fluctuations by Takakura and Yousef (1975), and iii) other simplifications made in both works. Possible improvements to the simulations are discussed, including improvements to the emission processes and the coronal and beam conditions (e.g., beam speed), in order to produce realistic stria/type IIIb bursts in f p emission.

Decimetric Type III Bursts: Generation and Propagation

B. **Li**, Iver H. Cairns, Y.H. Yan, P.A. Robinson
ApJ Letts, vol 738, L9, **2011**
Simulations are presented for decimetric type III radio bursts at 2fp, where fp is the local electron plasma frequency. The simulations show that 2fp radiation can be observed at Earth in two scenarios for the radiation's generation and propagation. In Scenario A, radiation is produced and propagates in warm plasmas in the lower corona that are caused by previous magnetic reconnection outflows and/or chromospheric evaporation. In Scenario B radiation is generated in normal plasmas, then due to its natural directivity pattern and refraction radiation partly propagates into nearby regions,

which are hot because of previous reconnection/evaporation. The profiles of plasma density ne(r) and electron temperature Te(r) in the lower corona (r-Rs < 100 Mm) are found to be crucial to whether radiation can be produced and escape at observable levels against the effects of free-free absorption, where r is the heliocentric distance. Significantly, the observed wide ranges of radiation properties (e.g., drift rates) require ne(r) with a large range of scale heights hs, consistent nonetheless for Scenario B with short observed EUV loops. This is relevant to problems with large hs inferred from tall EUV loops. The simulations suggest: (1) ne(r) with small hs, such as ne(r) ~ (r-Rs)^{-2.38} for flaring regions, are unexpectedly common deep in the corona. This result is consistent with recent work on ne(r) for r ~ (1.05-2) Rs extracted from observed metric type IIIs. (2) The dominance of reverse-slope bursts over normal bursts sometimes observed may originate from asymmetric reconnection/acceleration, which favors downgoing beams.

EFFECTS OF SPATIAL VARIATIONS IN CORONAL ELECTRON AND ION TEMPERATURES ON TYPE III BURSTS. II. VARIATIONS IN ION TEMPERATURE

B. **Li**, Iver H. Cairns and P. A. Robinson

2011 ApJ 730 21

Quasilinear-based simulations are presented for the effects on coronal type III bursts of spatially varying ion temperature Ti in the corona. The simulations use a newly developed method for integrating spatial variations of coronal temperatures into our previous simulations for constant temperatures. The effects are simulated for monotonic Ti variations and/or for spatially localized enhancements in Ti . Generally, a localized enhancement in Ti has stronger effects on type III bursts than a corresponding monotonic variation in Ti . A localized Ti enhancement causes modulations to the dynamic spectra of fp and 2fp emission at frequencies corresponding to the disturbance: a narrowband slowly drifting intensification for both fp and 2fp emission and a narrowband suppression for 2fp emission. The fp emission may become observable due to the disturbance, although still much weaker than the 2fp emission. Signatures of the Ti enhancement are found in the 2fp spectral characteristics, e.g., the maximum flux and frequency drift rate. Importantly, these signatures are distinct from those of localized disturbances in electron temperature Te . The results indicate that coronal type III bursts provide a new tool to probe and distinguish localized disturbances in Ti or Te in the corona. Additionally, the presence of multiple spatially confined Ti enhancements at different heights may produce some observed fine structures in type III bursts; e.g., stria bursts and associated flux modulations in type IIIb bursts, and flux modulations in type IIIs whose beams traverse coronal shocks.

RADIO EMISSION FROM ACCELERATION SITES OF SOLAR FLARES

Yixuan **Li**1 and Gregory D. Fleishman1,2

Astrophysical Journal, 701:L52–L58, **2009** August

This Letter takes up the question of what radio emission is produced by electrons at the very acceleration site of a solar flare. Specifically, we calculate incoherent radio emission produced within two competing acceleration models—stochastic acceleration by cascading MHD turbulence and regular acceleration in collapsing magnetic traps. Our analysis clearly demonstrates that radio emission from acceleration sites (1) has sufficiently strong intensity to be observed by currently available radio instruments, and (2) has spectra and light curves that are distinctly different in these two competing models, which makes them observationally distinguishable. In particular, we suggest that some of the narrowband microwave and decimeter continuum bursts may be a signature of the stochastic acceleration in solar flares.

Simulations of coronal type III solar radio bursts: 3. Effects of beam and coronal parameters

Bo **Li**, Iver H. Cairns, Peter A. Robinson

J. Geophys. Res., 114, A02104, doi:10.1029/2008JA013687, **2009**.

http://dx.doi.org/10.1029/2008JA013687

A recently developed simulation model is used to investigate the effects of varying the coronal and electron heating conditions on the dynamic spectra of coronal type III bursts (70–370 MHz) observed at Earth. The flux of $2f_p$ emission is significantly higher than that of f_p emission, which is unlikely to be observable except under very favorable propagation conditions. Moreover, the $2f_p$ emission is unlikely to continue into the solar wind, although some bursts are very strong and will extend into the upper corona with lower frequencies than simulated, consistent qualitatively with observations. The flux and brightness temperature of $2f_p$ emission are affected significantly by variations in the parameters, while the frequency drift rate and half-power duration are affected only weakly. Further, the simulations confirm the standard interpretation of the drift rate of $2f_p$ emission in terms of the plasma density profile and a characteristic beam speed that agrees quantitatively with the simulated beam dynamics for wide ranges of coronal and heating conditions. For weak heating events or events with high coronal electron temperature, the remote radiation shows characteristics that agree quantitatively with microbursts. When the heating is even weaker and/or the electron temperature is even higher, the heating events are radio quiet, consistent qualitatively with hard X-ray observations. For similar heating originating in similar frequency ranges, different density models yield quantitatively similar results except for the drift rate. Variations of the levels of a given density profile, corresponding to background corona or coronal streamers, can also cause significant changes in spectral characteristics.

Quasilinear-based simulations of bidirectional type III bursts,

Li, B., P. A. Robinson, and I. H. Cairns

J. Geophys. Res., 113, A10101, (**2008**),

http://dx.doi.org/10.1029/2008JA013255

Quasilinear-based simulations are presented of bidirectional type III bursts that originate in the corona and are observed at Earth, assuming plasma emission. By extending a recent simulation model to more realistic three-dimensional source structures and including Langmuir collisional damping, dynamic spectra of both the normal-drifting (normal) and the reverse-slope-drifting (RS) bursts are simulated and studied in detail for realistic electron-release and coronal parameters. The radio flux, brightness temperature, frequency drift rate, and time duration of the bursts agree semiquantitatively with typical observations. The flux of $2f_p$ emission is significantly higher than that of f_p emission, which is below the noise thresholds of typical radio instruments. This is mainly because the f_p emission is strongly free-free absorbed and further damped by scattering off density fluctuations. The $2f_p$ emission is asymmetric between the normal and RS bursts, with the normal burst stronger and lasting longer than the RS burst, consistent with observations. This occurs primarily because of the downgoing beam being weaker, not faster, and narrower in velocity space than the upgoing beam, and because of stronger free-free absorption for the RS burst than for the normal burst, consistent with a semiquantitative theory. Furthermore, the RS burst terminates at frequencies lower than the maximum simulated, and the normal burst extends to lower frequencies not simulated because of computational limitations. Collisional damping reduces the Langmuir wave levels and consequently suppresses the flux levels and washes out the dynamic spectral structures associated with successive wave-wave interactions when the damping is switched off.

Simulations of coronal type III solar radio bursts: 1. Simulation model,

Li, B., I. H. Cairns, and P. A. Robinson

J. Geophys. Res., 113, A06104, **2008**

http://dx.doi.org/10.1029/2007JA012957

A simulation model is developed for type III bursts that originate in the solar corona and are observed at Earth. The model incorporates the three-dimensional structure of the source region, dynamics in the source of electron beam, Langmuir waves, ion-sound waves, electromagnetic emissions at the fundamental (f_p) and second harmonic ($2f_p$) of the plasma frequency, and propagation of electromagnetic radiation from the corona to interplanetary space, and it predicts the radiation dynamic spectrum measured by a remote observer. During the propagation of the radiation, the effects of refraction and reflection on large-scale density variations, scattering off small-scale density fluctuations, and free-free absorption are taken into account. The scattering of f_p emission is modeled numerically on the basis of an analytic approach developed previously. The numerical results confirm approximations made in the approach and generalize it to more realistic solar plasma conditions.

Simulations of coronal type III solar radio bursts: 2. Dynamic spectrum for typical parameters

Li, B., I. H. Cairns, and P. A. Robinson

J. Geophys. Res., 113, A06105, **2008**
http://dx.doi.org/10.1029/2007JA012958
Predictions are presented for the dynamic spectrum of a coronal type III burst observed at Earth, using a newly developed simulation model and employing realistic electron release and coronal parameters. The spectrum is studied in detail in association with the dynamics of beam and waves in the source. The frequency drift rate, radio flux, brightness temperature, and temporal profile of the type III burst agree semiquantitatively with typical observations. The simulation model is thus viable. Because of strong free-free absorption and scattering-induced damping, the flux of f_p emission is significantly lower than that of $2f_p$ emission and is below the lower thresholds of typical radio instruments. Moreover, the f_p emission terminates at frequencies higher than the minimum simulated, and the $2f_p$ emission appears to terminate at higher coronal altitudes that are not simulated because of computational limitations. Further simulations indicate that F-H pairs may exist under favorable conditions (e.g., generally, lower levels and larger length scales of the density fluctuations).

Li, Y. P., Gan, W. Q. **The shrinkage of flare radio loops**. ApJ 629, L137-L139, 2005.

Theoretical Investigation of the Onsets of Type II Radio Bursts during Solar Eruptions

Jun **Lin,** Salvatore Mancuso, and Angelos Vourlidas
The Astrophysical Journal, 649:1110-1123, **2006; File**
On the basis of previous works, we investigated coronal mass ejection (CME) propagations and the consequent type II radio bursts invoked by the CME-driven shocks. The results indicate that the onset of type II bursts depends on the local Alfve´n speed (or the magnetoacoustic wave speed in the nonYforce-free environment), which is governed by both the magnetic field and the plasma density. This determines that the type II burst cannot appear at any altitude. Instead, its onset positions can never be lower than a critical height for the given coronal environment, which consequently determines the start frequencies of the emission: for an eruption taking place in the magnetic configuration with a background field of 100 G, the onset of type II bursts should occur at around 0.5 R_ from the solar surface, and the corresponding start frequency of the fundamental component is about 150 MHz. This result is consistent with similar estimates based on observations that bring the corresponding frequency to a few hundred MHz. Our results further indicate that the onset of type II bursts depends on the rate of magnetic reconnection as well. When magnetic reconnection during the eruption is not fast enough, a type II burst may not occur at all even if the associated CME is fast (say, faster than 800 km s_1). This may account for the fast and radio-quiet CMEs. Related to these results, properties of the associated solar flares and type III radio bursts, especially those used as the precursors of the type II radio bursts, are also discussed.

Parallel-propagating Waves and Instabilities in Plasmas with Streaming Proton and Alpha Particles

Zhifeng **Liu**1,2, Jinsong Zhao2, Heyu Sun2,3, Liang Xiang2,3, Wen Liu2,3, Jianyong Lu1, and Weican Zhou1
2019 ApJ 874 128
sci-hub.se/10.3847/1538-4357/ab0896
Streaming proton and alpha particles are permeating in the solar wind and solar atmosphere. These particles considerably affect the normal waves in electron–proton–alpha plasmas, especially inducing electrostatic and electromagnetic ion/ion beam instabilities. This paper gives a comprehensive investigation on stable and unstable parallel-propagating wave modes in plasmas with streaming proton and alpha particles. It illustrates that at a large beam velocity condition, the backward-propagating fast-magnetosonic/whistler wave (Alfvén/proton-beam or Alfvén/alpha beam mode wave) turns to forward propagation in the core proton rest frame, and couples with forward-propagating Alfvén/alpha-cyclotron and alpha-cyclotron/proton-cyclotron waves (fast-magnetosonic/whistler wave), triggering Alfvén/proton-cyclotron and fast-magnetosonic/whistler instabilities. Furthermore, as perpendicular thermal pressures of proton and alpha beams are larger than their parallel thermal pressures, several new electromagnetic instabilities arise in the case of the low ion streaming velocity, where both Alfvén/proton-cyclotron and fast-magnetosonic/whistler instabilities are stable. This paper also predicts the possible ion/ion electromagnetic instabilities in solar coronal holes, which can give a constraint on the ion differential drift velocity therein.

Propagation and Interaction Properties of Successive Coronal Mass Ejections in Relation to a Complex Type II Radio Burst

Ying D. **Liu**1,2, Xiaowei Zhao1,2, and Bei Zhu
2017 ApJ 849 112

http://sci-hub.cc/10.3847/1538-4357/aa9075
We examine the propagation and interaction properties of three successive coronal mass ejections (CMEs) from **2001 November 21–22**, with a focus on their connection with the behaviors of the associated long-duration complex type II radio burst. In combination with coronagraph and multi-point in situ observations, the long-duration type II burst provides key features for resolving the propagation and interaction complexities of the three CMEs. The two CMEs from November 22 interacted first and then overtook the November 21 CME at a distance of about 0.85 au from the Sun. The timescale for the shock originally driven by the last CME to propagate through the preceding two CMEs is estimated to be about 14 and 6 hr, respectively. We present a simple analytical model without any free parameters to characterize the whole Sun-to-Earth propagation of the shock, which shows a remarkable consistency with all the available data and MHD simulations even out to the distance of Ulysses (2.34 au). The coordination of in situ measurements at the Earth and Ulysses, which were separated by about 71°.4 in latitude, gives important clues for the understanding of shock structure and the interpretation of in situ signatures. The results also indicate a means by which to increase geo-effectiveness with multiple CMEs, which can be considered as another manifestation of the "perfect storm" scenario proposed by Liu et al., although the current case is not "super" in the same sense as the 2012 July 23 event.

Statistical origin and properties of kappa distributions

George **Livadiotis**
Journal of Physics: Conference Series, Volume 900, Number 1 012014 **2017**
http://iopscience.iop.org/article/10.1088/1742-6596/900/1/012014/pdf
Classical particle systems reside at thermal equilibrium with their velocity distribution function stabilized into a Maxwell distribution. On the contrary, collisionless and correlated particle systems, such as space and astrophysical plasmas, are characterized by a non-Maxwellian behavior, typically described by kappa distributions, or combinations thereof. Empirical kappa distributions have become increasingly widespread across space and plasma physics. A breakthrough in the field came with the connection of kappa distributions to non-extensive statistical mechanics. Understanding the statistical origin of kappa distributions was the cornerstone of further theoretical developments and applications, namely, (i) the concept of temperature; (ii) the physical meaning of the kappa index; (iii) the N-particle description of kappa distributions; and the (iv) the generalization to phase-space kappa distribution of a Hamiltonian with non-zero potential.

Statistical background and properties of kappa distributions in space plasmas†

George **Livadiotis**
JGR **2015**
Empirical kappa distributions provide a straightforward replacement of the Maxwell distribution for systems out of thermal equilibrium such as space plasmas. Kappa distributions have become increasingly widespread across space physics with the number of relevant publications following, remarkably, an exponential growth rate. However, a breakthrough in the field came with the connection of kappa distributions with the framework of non-extensive statistical mechanics. This introductory paper clarifies fundamental physical concepts and provides mathematical formulations of the theory of kappa distributions, which are a consequence of the connection of kappa distributions with a solid statistical background. Among others, the paper presents the existence of a consistent definition of temperature in systems out of thermal equilibrium described by kappa distributions, the physical meaning of the kappa index, and the formulation of the kappa distribution of a Hamiltonian. In addition, the paper examines the most frequent values of kappa indices in space plasmas. Statistical analysis reveals trends between the characteristic values of density, temperature, and kappa index of space plasmas. Finally, understanding the kinetic interpretation of the temperature as the mean kinetic energy, and of the kappa index as the correlation of kinetic energies, helps to develop all the possible formulations of isotropic/anisotropic kappa distributions.

DECREASING SUNSPOT MAGNETIC FIELDS EXPLAIN UNIQUE 10.7 cm RADIO FLUX

W. **Livingston**1, M. J. Penn1, and L. Svalgaard
2012 ApJ 757 L8
Infrared spectral observations of sunspots from 1998 to 2011 have shown that on average sunspots changed, the magnetic fields weakened, and the temperatures rose. The data also show that sunspots or dark pores can only form at the solar surface if the magnetic field strength exceeds about 1500 G. Sunspots appear at the solar surface with a variety of field strengths, and during the period from 1998 to 2002 a histogram of the sunspot magnetic fields shows a normal distribution with a mean of 2436 ± 26 G and a width of 323 ± 20 G. During this observing period the mean of the magnetic field distribution decreased by 46 ± 6 G per year, and we assume that as the 1500 G threshold was approached, magnetic fields appeared at the solar surface which could not form dark sunspots or pores. With this assumption we propose a quantity called the sunspot formation fraction and give an analytical form derived from the magnetic field distribution. We show that this fraction can quantitatively explain the changing relationship between sunspot number and solar radio flux measured at 10.7 cm wavelengths.

Interferometric imaging, and beam-formed study of a moving Type IV Radio burst with LOFAR

Hongyu **Liu**, Pietro Zucca, Kyung-Suk Cho, Anshu Kumari, Peijin Zhang, Jasmina Magdalenic, Rok-Soon Kim, Sujin Kim, Juhyung Kang

Solar Phys. **297**, Article number: 115 **2022**

https://arxiv.org/pdf/2208.13670.pdf

https://link.springer.com/content/pdf/10.1007/s11207-022-02042-0.pdf

Type IV radio burst has been studied for over 50 years. However, the specifics of the radio emission mechanisms is still an open question. In order to provide more information about the emission mechanisms, we studied a moving type IV radio burst with fine structures (spike group) by using the high resolution capability of Low-Frequency Array (LOFAR) on **Aug 25, 2014**\textbf{ (SOLA-D-21-00188)}. We present a comparison of Nançay RadioHeliograph (NRH) and the first LOFAR imaging data of type IV radio burst. The degree of circular polarization (DCP) is calculated at frequencies in the range 20∼180 MHz using LOFAR data, and it was found that the value of DCP gradually increased during the event, with values of 10\%∼20\%. LOFAR interferometric data were combined with white light observations in order to track the propagation of this type IV. The kinematics shows a westward motion of the radio sources, slower than the CME leading edge. The dynamic spectrum of LOFAR shows a large number of fine structures with duration of less than 1s and high brightness temperature (TB), i.e. 1012∼1013 K. The gradual increase of DCP supports gyrosynchrotron emission as the most plausible mechanism for the type IV. However, coherent emissions such as Electron Cyclotron Maser (ECM) instability can be responsible for small scale fine structures. Countless fine structures altogether were responsible for such high TB.

A Solar Stationary Type IV Radio Burst and Its Radiation Mechanism

Hongyu **Liu**, Yao Chen, Kyungsuk Cho, Shiwei Feng, Veluchamy Vasanth…

Solar Physics April **2018**, 293:58

https://link.springer.com/content/pdf/10.1007%2Fs11207-018-1280-y.pdf

A stationary Type IV (IVs) radio burst was observed on **September 24, 2011**. Observations from the Nançay RadioHeliograph (NRH) show that the brightness temperature (TBTB) of this burst is extremely high, over 1011 K at 150 MHz and over 108 K in general. The degree of circular polarization (qq) is between −60%∼−100%−60%∼−100%, which means that it is highly left-handed circularly polarized. The flux–frequency spectrum follows a power-law distribution, and the spectral index is considered to be roughly −3∼−4−3∼−4 throughout the IVs. Radio sources of this event are located in the wake of the coronal mass ejection and are spatially dispersed. They line up to present a formation in which lower-frequency sources are higher. Based on these observations, it is suggested that the IVs was generated through electron cyclotron maser emission.

Quasi-periodic Fast-mode Magnetosonic Wave Trains Within Coronal Waveguides Associated with Flares and CMEs

Wei **Liu**, Leon Ofman, Brittany Broder, Marian Karlicky, and Cooper Downs

Proceedings of the 14th International Solar Wind Conference, **201**5

http://sun.stanford.edu/~weiliu/research/publications/2016/2016AIP_WeiLiu_QFPs_SolWind14.pdf

Quasi-periodic, fast-mode, propagating wave trains (QFPs) are a new observational phenomenon recently discovered in the solar corona by the Solar Dynamics Observatory with extreme ultraviolet (EUV) imaging observations. They originate from flares and propagate at speeds up to ~2000 km s-1 within funnel-shaped waveguides in the wakes of coronal mass ejections (CMEs). QFPs can carry sufficient energy fluxes required for coronal heating during their occurrences. They can provide new diagnostics for the solar corona and their associated flares. We present recent observations of QFPs focusing on their spatio-temporal properties, temperature dependence, and statistical correlation with flares and CMEs. Of particular interest is the **2010-Aug-01** C3.2 flare with correlated QFPs and **drifting zebra and fiber radio bursts**, which might be different manifestations of the same fast-mode wave trains. We also discuss the potential roles of QFPs in accelerating and/or modulating the solar wind.

A Reconnecting Current Sheet Imaged in A Solar Flare

Rui **Liu**, Jeongwoo Lee, Tongjiang Wang, Guillermo Stenborg, Chang Liu, Haimin Wang

E-print, Sept 2010, **File** ; ApJL, 723, L28, **2010**

Magnetic reconnection changes the magnetic field topology and powers explosive events in astrophysical, space and laboratory plasmas. For flares and coronal mass ejections (CMEs) in the solar atmosphere, the standard model predicts the presence of a reconnecting current sheet, which has been the subject of considerable theoretical and numerical modeling over the last fifty years, yet direct, unambiguous observational verification has been absent. In this Letter we show a bright sheet structure of global length (>0.25 Rsun) and macroscopic width ((5 - 10)x10^3 km) distinctly above

the cusp-shaped flaring loop, imaged during the flare rising phase in EUV. The sheet formed due to the stretch of a transequatorial loop system, and was accompanied by various reconnection signatures that have been dispersed in the literature. This unique event provides a comprehensive view of the reconnection geometry and dynamics in the solar corona. **2004 July 29, slow drifting radio continuum: свидетельства связи с процессами в РЕ токовом слое.**

RELATIONSHIP BETWEEN A CORONAL MASS EJECTION-DRIVEN SHOCK AND A CORONAL METRIC TYPE II BURST

Y. **Liu**, J. G. Luhmann, S. D. Bale, and R. P. Lin
ApJL 691 L151-L155 **2009; File**
http://www.iop.org/EJ/abstract/1538-4357/691/2/L151
It has been an intense matter of debate whether coronal metric type II bursts are generated by coronal mass ejection (CME)-driven shocks or flare blast waves. Using unprecedented high-cadence observations from STEREO/SECCHI, we investigate the relationship between a metric type II event and a shock driven by the **2007 December 31** CME. The existence of the CME-driven shock is indicated by the remote deflection of coronal structures, which is in good timing with the metric type II burst. The CME speed is about 600 km s–1 when the metric type II burst occurs, much larger than the Alfvén speed of 419-489 km s–1 determined from band splitting of the type II burst. A causal relationship is well established between the metric and decametric-hectometric type II bursts. The shock height-time curve determined from the type II bands is also consistent with the shock propagation obtained from the streamer deflection. These results provide unambiguous evidence that the metric type II burst is caused by the CME-driven shock.

Introduction to special section on Origins and Properties of Kappa Distributions: Statistical Background and Properties of Kappa Distributions in Space Plasmas

George **Livadiotis**
JGR Volume 120, Issue 3 March **2015** Pages 1607–1619
Empirical kappa distributions provide a straightforward replacement of the Maxwell distribution for systems out of thermal equilibrium such as space plasmas. Kappa distributions have become increasingly widespread across space physics with the number of relevant publications following, remarkably, an exponential growth rate. However, a breakthrough in the field came with the connection of kappa distributions with the framework of nonextensive statistical mechanics. This introductory paper clarifies fundamental physical concepts and provides mathematical formulations of the theory of kappa distributions, which are a consequence of the connection of kappa distributions with a solid statistical background. Among others, the paper presents the existence of a consistent definition of temperature in systems out of thermal equilibrium described by kappa distributions, the physical meaning of the kappa index, and the formulation of the kappa distribution of a Hamiltonian. In addition, the paper examines the most frequent values of kappa indices in space plasmas. Statistical analysis reveals trends between the characteristic values of density, temperature, and kappa index of space plasmas. Finally, understanding the kinetic interpretation of the temperature as the mean kinetic energy, and of the kappa index as the correlation of kinetic energies, helps to develop all the possible formulations of isotropic/anisotropic kappa distributions.

Automatic recognition of type III solar radio bursts in STEREO/WAVES data for onboard real-time and archived data processing

V. V. **Lobzin**, Iver H. Cairns and A. Zaslavsky
JGR, Volume 119, Issue 2, pages 742–750, February **2014**
Type III radio bursts are produced near the local electron plasma frequency and/or near its harmonic by fast electrons ejected from the solar active regions and moving through the corona and solar wind. These bursts have dynamic spectra with frequency rapidly falling with time. This paper presents two new methods developed to detect type III bursts automatically in the data from High Frequency Receiver (HFR) of the STEREO/WAVES radio instrument onboard the STEREO spacecraft. The first technique is applicable to the low-frequency band (HFR-1: 125 kHz to 1.975 MHz) only. This technique can possibly be implemented in onboard satellite software aimed at preliminary detection of bursts and identification of time intervals with relatively high solar activity. In the second technique the bursts are detected in both the low-frequency band and the high-frequency band (HFR-2: 2.025 MHz to 16.025 MHz), with the computational burden being higher by 1 order of magnitude as compared with that for the first technique. Preliminary tests of the method show that the performance of the first technique is quite high, PdL=72%±3%. The performance of the second technique is considerably higher, PdL+H=81%±1%, while the number of false alarms does not exceed 10% for one daily spectrum.

RIEGER-TYPE PERIODICITY IN THE OCCURRENCE OF SOLAR TYPE III RADIO BURSTS

V. V. **Lobzin**, Iver H. Cairns, and P. A. Robinson
2012 ApJ 754 L28

This Letter presents the first observations of a Rieger-type periodicity with the period of days in the occurrence rate of solar coronal type III radio bursts. The periodicity was detected during the time interval from 2000 June 22 to 2003 December 31. This interval partially contains the maximum and the declining phase of solar cycle 23. The radio spectra were provided by the Learmonth Solar Radio Observatory in Western Australia, part of the USAF Radio Solar Telescope Network.

EVIDENCE FOR GENTLY SLOPING PLASMA DENSITY PROFILES IN THE DEEP CORONA: TYPE III OBSERVATIONS

V. V. **Lobzin**1, I. H. Cairns1, P. A. Robinson1, A. Warmuth2, G. Mann2, R. V. Gorgutsa3, and V. V. Fomichev3

Astrophysical Journal, 724:1099–1107, **2010, File**

Type III radio bursts are produced near the local electron plasma frequency f_p and near its harmonic $2f_p$ by fast electrons ejected from the solar active regions and moving through the corona and solar wind. The coronal bursts have dynamic spectra with frequency rapidly falling with time, the typical duration being about 1–3 s. In the present paper, 37 well-defined coronal type III radio bursts (25–450 MHz) are analyzed. The results obtained substantiate an earlier statement that the dependence of the central frequency of the emission on time can be fitted to a power-law model, $f(t) \propto (t - t_0)^{-\alpha}$, where α can be as low as 1. In the case of negligible plasma acceleration and conical flow, it means that the electron number density within about 1 solar radius above the photosphere will decrease as r^{-2}, like in the solar wind. For the data set chosen, the index α varies in the range from 0.2 to 7 or bigger, with mean and median values of 1.2 and 0.5, respectively. A surprisingly large fraction of events, 84%, have α _ 1.2. These results provide strong evidence that in the type III source regions the electron number density scales as $n(r) \propto (r - r_0)^{-\beta}$, with minimum, mean, and median $\beta = 2\alpha$ of 0.4, 2.4, and 1.0, respectively. Hence, the typical density profiles are more gently sloping than those given by existing empirical coronal models. Several events are found with a wind-like dependence of burst frequency on time. Smaller power-law indices could result from the effects of non-conical geometry of the plasma flow tubes, deceleration of coronal plasma, and/or the curvature of the magnetic field lines. The last effect is shown to be too weak to explain such low power-law indices. A strong tendency is found for bursts from the same group to have similar power-law indices, thereby favoring the hypothesis that they are usually produced by the same source region.

AUTOMATIC RECOGNITION OF CORONAL TYPE II RADIO BURSTS: THE AUTOMATED RADIO BURST IDENTIFICATION SYSTEM METHOD AND FIRST OBSERVATIONS

Vasili V. **Lobzin**1, Iver H. Cairns1, Peter A. Robinson1, Graham Steward2, and Garth Patterson2

Astrophysical Journal Letters, 710:L58–L62, **2010** February, **File**

Major space weather events such as solar flares and coronal mass ejections are usually accompanied by solar radio bursts, which can potentially be used for real-time space weather forecasts. Type II radio bursts are produced near the local plasma frequency and its harmonic by fast electrons accelerated by a shock wave moving through the corona and solar wind with a typical speed of ~1000 km s−1. The coronal bursts have dynamic spectra with frequency gradually falling with time and durations of several minutes. This Letter presents a new method developed to detect type II coronal radio bursts automatically and describes its implementation in an extended Automated Radio Burst Identification System (ARBIS 2). Preliminary tests of the method with spectra obtained in 2002 show that the performance of the current implementation is quite high, ~80%, while the probability of false positives is reasonably low, with one false positive per 100–200 hr for high solar activity and less than one false event per 10000 hr for low solar activity periods. The first automatically detected coronal type II radio burst is also presented.

EVIDENCE FOR WIND-LIKE REGIONS, ACCELERATION OF SHOCKS IN THE DEEP CORONA, AND RELEVANCE OF 1/*f* DYNAMIC SPECTRA TO CORONAL TYPE II BURSTS

V. V. **Lobzin**, Iver H. Cairns, and P. A. Robinson

The Astrophysical Journal, 677:L129–L132, **2008, File**

http://www.journals.uchicago.edu/doi/pdf/10.1086/587980

Type II radio bursts are produced near the local plasma frequency and near by shocks moving through *f* 2*f p p* the corona and solar wind. In the present Letter eight well-defined coronal type II radio bursts (30–300 MHz) are analyzed. Three results are presented. First, it is found that the dependence of the central frequency on time can be fitted to a power-law model, , with . Assuming a constant shock velocity, these _a $f \propto (t$ _ $t)$ $0.6 \leq a \leq 1.3$ 0 results provide evidence that the density profile in the type II source regions closely resembles the solar n (r) e wind, with . One possible interpretation is that the solar wind starts within a few solar radii of the _2 n $(r) \propto r$ e

photosphere, most probably within 1 solar radius. Another relies on a gasdynamic Whitham analysis and demonstrates a possibility for blast shocks to accelerate, thereby reducing apparent power-law indices to solar wind–like values. Second, for the events considered it is found that radio burst emission in the form of versus t $1/f$ dynamic spectra closely follows straight lines. In future this will allow much more objective identification of type II bursts in solar radio data and plausibly real-time correlation with coronagraph and other solar radar. Third, it is demonstrated that versus t dynamic spectra can provide direct evidence for acceleration of the shock $1/f$ deep in the corona, thus complementing coronagraph studies.

Production of Fine Structures in Type III Solar Radio Bursts Due to Turbulent Density Profiles

Shyeh Tjing **Loi**, Iver H. Cairns, and Bo Li
2014 ApJ 790 67
Magnetic reconnection events in the corona release energetic electron beams along open field lines, and the beams generate radio emission at multiples of the electron plasma frequency fp to produce type III solar radio bursts. Type III bursts often exhibit irregularities in the form of flux modulations with frequency and/or local temporal advances and delays, and a type IIIb burst represents the extreme case where a type III burst is fragmented into a chain of narrowband features called striae. Remote and in situ spacecraft measurements have shown that density turbulence is ubiquitous in the corona and solar wind, and often exhibits a Kolmogorov power spectrum. In this work, we numerically investigate the effects of one-dimensional macroscopic density turbulence (along the beam direction) on the behavior of type III bursts, and find that this turbulence produces stria-like fine structures in the dynamic spectra of both fp and 2 fp radiation. Spectral and temporal fine structures in the predicted type III emission are produced by variations in the scattering path lengths and group speeds of radio emission, and in the locations and sizes of emitting volumes. Moderate turbulence levels yield flux enhancements with much broader half-power bandwidths in fp than 2 fp emission, possibly explaining the often observed type IIIb-III harmonic pairs as being where intensifications in 2 fp radiation are not resolved observationally. Larger turbulence levels producing trough-peak regions in the plasma density profile may lead to broader, resolvable intensifications in 2 fp radiation, which may account for the type IIIb-IIIb pairs that are sometimes observed.

Localised acceleration of energetic particles by a weak shock in the solar corona

David M. **Long**, Hamish A. S. Reid, Gherardo Valori, Jennifer O'Kane
ApJ **921** 61 **2021**
https://arxiv.org/pdf/2108.05068.pdf
https://doi.org/10.3847/1538-4357/ac1cdf
Globally-propagating shocks in the solar corona have long been studied to quantify their involvement in the acceleration of energetic particles. However, this work has tended to focus on large events associated with strong solar flares and fast coronal mass ejections (CMEs), where the waves are sufficiently fast to easily accelerate particles to high energies. Here we present observations of particle acceleration associated with a global wave event which occurred on **1 October 2011**. Using differential emission measure analysis, the global shock wave was found to be incredibly weak, with an Alfvén Mach number of ~1.008-1.013. Despite this, spatially-resolved type III radio emission was observed by the Nançay RadioHeliograph at distinct locations near the shock front, suggesting localised acceleration of energetic electrons. Further investigation using a magnetic field extrapolation identified a fan structure beneath a magnetic null located above the source active region, with the erupting CME contained within this topological feature. We propose that a reconfiguration of the coronal magnetic field driven by the erupting CME enabled the weak shock to accelerate particles along field lines initially contained within the fan and subsequently opened into the heliosphere, producing the observed type III emission. These results suggest that even weak global shocks in the solar corona can accelerate energetic particles via reconfiguration of the surrounding magnetic field.

A Statistical Analysis of the Solar Phenomena Associated with Global EUV Waves (Review)

David M. **Long**, Pearse Murphy, Georgina Graham, Eoin P. Carley, David Pérez-Suárez
Solar Phys. **2017**
https://arxiv.org/pdf/1711.02530.pdf
Solar eruptions are the most spectacular events in our solar system and are associated with many different signatures of energy release including solar flares, coronal mass ejections, global waves, radio emission and accelerated particles. Here, we apply the Coronal Pulse Identification and Tracking Algorithm (CorPITA) to the high cadence synoptic data provided by the Solar Dynamic Observatory (SDO) to identify and track global waves observed by SDO. 164 of the 362 solar flare events studied (45%) are found to have associated global waves with no waves found for the remaining 198 (55%). A clear linear relationship was found between the median initial velocity and the acceleration of the waves, with faster waves exhibiting a stronger deceleration (consistent with previous results). No clear relationship was found between global waves and type II radio bursts, electrons or protons detected in-situ near Earth. While no relationship was found between the wave properties and the associated flare size (with waves produced by flares from B to X-class), more than a quarter of the active regions studied were found to produce more than one wave event. These results

suggest that the presence of a global wave in a solar eruption is most likely determined by the structure and connectivity of the erupting active region and the surrounding quiet solar corona rather than by the amount of free energy available within the active region. **2010 August 14, 2011 January 27, 2011 June 7**
Table CorPITA analysis. 2010-2016

The Murchison Widefield Array: Design Overview

Lonsdale, C.J.; Cappallo, R.J.; Morales, M.F.; Briggs, F.H.; Benkevitch, L.; Bowman, J.D.; et al.
2009, Proc. IEEE, 97, 1497-1506
The Murchison Widefield Array is a dipole-based aperture array synthesis telescope designed to operate in the 80-300 MHz frequency range. It is capable of a wide range of science investigations but is initially focused on three key science projects: detection and characterization of three-dimensional brightness temperature fluctuations in the 21 cm line of neutral hydrogen during the epoch of reionization (EoR) at redshifts from six to ten; solar imaging and remote sensing of the inner heliosphere via propagation effects on signals from distant background sources; and high-sensitivity exploration of the variable radio sky. The array design features 8192 dual-polarization broadband active dipoles, arranged into 512 ldquotilesrdquo comprising 16 dipoles each. The tiles are quasi-randomly distributed over an aperture 1.5 km in diameter, with a small number of outliers extending to 3 km. All tile-tile baselines are correlated in custom field-programmable gate array based hardware, yielding a Nyquist-sampled instantaneous monochromatic uv coverage and unprecedented point spread function quality. The correlated data are calibrated in real time using novel position-dependent self-calibration algorithms. The array is located in the Murchison region of outback Western Australia. This region is characterized by extremely low population density and a superbly radio-quiet environment, allowing full exploitation of the instrumental capabilities.

A solar flare driven by thermal conduction observed in mid-infrared

Fernando M. **López**, C. Guillermo Giménez de Castro, Cristina H. Mandrini, Paulo J. A. Simões, Germán D. Cristiani, Dale E. Gary, Carlos Francile, Pascal Démoulin
A&A 657, id.A51 **2022**
https://arxiv.org/pdf/2110.15751.pdf
https://www.aanda.org/articles/aa/pdf/2022/01/aa41967-21.pdf
https://doi.org/10.1051/0004-6361/202141967
The mid-infrared (mid-IR) range has been mostly unexplored for the investigation of solar flares. It is only recently that new mid-IR flare observations have begun opening a new window into the response and evolution of the solar chromosphere. These new observations have been mostly performed by the AR30T and BR30T telescopes that are operating in Argentina and Brazil, respectively. We present the analysis of SOL**2019-05-15**T19:24, a GOES class C2.0 solar flare observed at 30~THz (10 μm) by the ground-based telescope AR30T. Our aim is to characterize the evolution of the flaring atmosphere and the energy transport mechanism in the context of mid-IR emission. We performed a multi-wavelength analysis of the event by complementing the mid-IR data with diverse ground- and space-based data from the Solar Dynamics Observatory (SDO), the H--α Solar Telescope for Argentina (HASTA), and the Expanded Owens Valley Solar Array (EOVSA). Our study includes the analysis of the magnetic field evolution of the flaring region and of the development of the flare. The mid-IR images from AR30T show two bright and compact flare sources that are spatially associated with the flare kernels observed in ultraviolet (UV) by SDO. We confirm that the temporal association between mid-IR and UV fluxes previously reported for strong flares is also observed for this small flare. The EOVSA microwave data revealed flare spectra consistent with thermal free-free emission, which lead us to dismiss the existence of a significant number of non-thermal electrons. We thus consider thermal conduction as the primary mechanism responsible for energy transport. Our estimates for the thermal conduction energy and total radiated energy fall within the same order of magnitude, reinforcing our conclusions.
RHESSI Nuggets #425 Jan **2022**
https://sprg.ssl.berkeley.edu/~tohban/wiki/index.php/A_solar_flare_driven_by_thermal_conduction_observed_in_mid-infrared

Solar Electron Beam—Langmuir Wave Interactions and How They Modify Solar Electron Beam Spectra: Solar Orbiter Observations of a Match Made in the Heliosphere

Camille Y. **Lorfing**1, Hamish A. S. Reid1, Raúl Gómez-Herrero2, Milan Maksimovic3, Georgios Nicolaou1, Christopher J. Owen1, Javier Rodriguez-Pacheco2, Daniel F. Ryan4, Domenico Trotta5, and Daniel Verscharen1
2023 ApJ 959 128
https://iopscience.iop.org/article/10.3847/1538-4357/ad0be3/pdf
https://arxiv.org/pdf/2311.14444.pdf
Solar Orbiter's four in situ instruments have recorded numerous energetic electron events at heliocentric distances between 0.5 and 1 au. We analyze energetic electron fluxes, spectra, pitch-angle distributions, associated Langmuir

waves, and type III solar radio bursts for three events to understand what causes modifications in the electron flux and identify the origin and characteristics of features observed in the electron spectrum. We investigate what electron beam properties and solar wind conditions are associated with Langmuir wave growth and spectral breaks in the electron peak flux as a function of energy. We observe velocity dispersion and quasilinear relaxation in the electron flux caused by the resonant wave–particle interactions in the deca-keV range, at the energies at which we observe breaks in the electron spectrum, cotemporal with the local generation of Langmuir waves. We show, via the evolution of the electron flux at the time of the event, that these interactions are responsible for the spectral signatures observed around 10 and 50 keV, confirming the results of simulations by Kontar and Reid. These signatures are independent of pitch-angle scattering. Our findings highlight the importance of using overlapping FOVs when working with data from different sensors. In this work, we exploit observations from all in situ instruments to address, for the first time, how the energetic electron flux is modified by the beam–plasma interactions and results in specific feature appearing in the local spectrum. Our results, corroborated with numerical simulations, can be extended to a wider range of heliocentric distances. **2020-11-24, 2021 October 9, 2022 April 15**

Solar Orbiter Science Nuggets #31 2024 **https://www.cosmos.esa.int/web/solar-orbiter/-/science-nugget-electron-beam-langmuir-wave-interactions**

Solar Electron Beam Velocities That Grow Langmuir Waves in the Inner Heliosphere

Camille Y. **Lorfing** & Hamish A. S. Reid
Solar Physics volume 298, Article number: 52 (**2023**)
https://link.springer.com/content/pdf/10.1007/s11207-023-02145-2.pdf
Solar accelerated electron beams, a component of space weather, are emitted by eruptive events at the Sun. They interact with the ambient plasma to grow Langmuir waves, which subsequently produce radio emission, changing the electrons' motion through space. Solar electron beam–plasma interactions are simulated using a quasilinear approach to kinetic theory to probe the variations in the maximum electron velocity [ΞΞ] responsible for Langmuir wave growth between the Sun's surface and 50 R⊙ above the surface. We find that it peaks at 5 R⊙ at 0.38 c and decreases as r−0.5 to 0.16 c at 50 R⊙. The role of the initial beam density [nbeam] and velocity spectral index [α] on the energy density of the beam and ΞΞ is extensively studied. We show that a high spectral index yields a lower ΞΞ, while a high nbeam yields a higher ΞΞ, and vice versa. We observe at different energy channels that below 60 keV, electrons arrive up to 0.75 minutes earlier than expected at 13 R⊙ while higher energy electrons propagate scatter free in the plasma. A special focus on the associated Type III radio burst shows that the energy range [ΔE] of electrons producing Langmuir waves evolves from 7 keV to 1 keV between 0 and 28 R⊙. Understanding the transport effect on the electron beam kinetics and arrival time at Earth has space weather implications. The results of this simulation can be tested against readily available in-situ data from Solar Orbiter and Parker Solar Probe.
CESRA #3590 **2023** https://www.astro.gla.ac.uk/users/eduard/cesra/?p=3590

First looks at solar active regions with ALMA

Maria **Loukitcheva**, and Kevin Reardon
Front. Astron. Space Sci. 9:1025368. **2022**
doi: 10.3389/fspas.2022.1025368
https://www.frontiersin.org/articles/10.3389/fspas.2022.1025368/pdf
During the first few years of observing the Sun with the Atacama Large Millimeter/submillimeter Array (ALMA), the scientific community has acquired a number of observational datasets targeting various structures in active regions, including sunspot umbra and penumbra, active region pores, and plages. In this paper we review the results obtained from the extensive analysis of these interferometric millimeter data, together with the coordinated observations from IRIS, SDO, IBIS, and Hinode, that reveal information on the chromospheric thermal structure above active regions and properties of small-scale heating events near magnetic field concentrations. We discuss the properties of waves (especially the three-minute oscillations) in sunspots, plage, and network. We speculate how high-resolution millimeter data can supplement spectral line observations in the visible and UV and can improve chromospheric spectroscopic inversions. We identify challenges in the interpretation of the millimeter continuum emission due to the complex, non-local and time-dependent processes that determine the electron density through the chromosphere. Finally we overview the prospects for future active regions observations with ALMA during the ascending phase of the solar cycle.

Measuring magnetic field with Atacama Large Millimeter/Submillimeter Array **Review**

Maria **Loukitcheva**
Front. Astron. Space Sci. **7**:45 **2020**
https://www.frontiersin.org/articles/10.3389/fspas.2020.00045/full
https://doi.org/10.3389/fspas.2020.00045
This article reviews the use of magnetic bremsstrahlung at short radio wavelengths to measure solar magnetic fields. The vertical component of the chromospheric magnetic field can be deduced from the observed polarization and

brightness temperature spectrum at millimeter wavelengths. State-of-the-art 3D radiative magnetohydrodynamic (R-MHD) simulations of the quiet solar atmosphere were used to synthesize observational deliverables at the wavelengths of the Atacama Large Millimeter/Submillimeter Array (ALMA) and to test the applicability of the method. The article provides selected observational examples of the successful application of the method and presents an overview of the recent developments and potential of the magnetic field measurements with ALMA. **February 2, 2011, April 13, 2012, May 23, 2012**

ALMA detection of dark chromospheric holes in the quiet Sun

Maria A. **Loukitcheva**, Stephen M. White, Sami K. Solanki
ApJL **877** L26 **2019**
https://arxiv.org/pdf/1905.06763.pdf
sci-hub.se/10.3847/2041-8213/ab2191
We present Atacama Large Millimeter/submillimeter Array (ALMA) observations of a quiet-Sun region at a wavelength of 3 mm, obtained during the first solar ALMA cycle on **April 27, 2017**, and compare them with available chromospheric observations in the UV and visible as well as with photospheric magnetograms. ALMA images clearly reveal the presence of distinct particularly dark/cool areas in the millimeter maps having temperatures as low as 60% of the normal quiet Sun at 3 mm, which are not seen in the other data. We speculate that ALMA is sensing cool chromospheric gas, whose presence had earlier been inferred from infrared CO spectra.

First solar observations with ALMA

Maria **Loukitcheva**
Advances in Space Research Volume 63, Issue 4, 15 February **2019**, Pages 1396-1403
https://arxiv.org/pdf/1809.00430.pdf
The Atacama Large Millimeter-Submillimeter Array (ALMA) has opened a new window for studying the Sun via high-resolution high-sensitivity imaging at millimeter wavelengths. In this contribution I review the capabilities of the instrument for solar observing and describe the extensive effort taken to bring the possibility of solar observing with ALMA to the scientific community. The first solar ALMA observations were carried out during 2014 and 2015 in two ALMA bands, Band 3 (3 mm) and Band 6 (1.3 mm), in single-dish and interferometric modes, using single pointing and mosaicing observing techniques, with spatial resolution up to 2arcsec and 1arcsec in the two bands, respectively. I overview several recently published studies which made use of the first solar ALMA observations, describe current status of solar observing with ALMA and briefly discuss the future capabilities of the instrument. **16 Dec 2015, 17 December 2015**

Solar ALMA observations: constraining the chromosphere above sunspots

Maria **Loukitcheva**, Kazumasa Iwai, Sami K. Solanki, Stephen M. White, Masumi Shimojo
ApJ **850** 35 **2017**
https://arxiv.org/pdf/1710.03812.pdf
We present the first high-resolution Atacama Large Millimeter/Submillimeter Array (ALMA) observations of a sunspot at wavelengths of 1.3 mm and 3 mm, obtained during the solar ALMA Science Verification campaign in 2015, and compare them with the predictions of semi-empirical sunspot umbral/penumbral atmosphere models. For the first time millimeter observations of sunspots have resolved umbral/penumbral brightness structure at the chromospheric heights, where the emission at these wavelengths is formed. We find that the sunspot umbra exhibits a radically different appearance at 1.3 mm and 3 mm, whereas the penumbral brightness structure is similar at the two wavelengths. The inner part of the umbra is ~600 K brighter than the surrounding quiet Sun (QS) at 3 mm and is ~700 K cooler than the QS at 1.3 mm, being the coolest part of sunspot at this wavelength. On average, the brightness of the penumbra at 3 mm is comparable to the QS brightness, while at 1.3 mm it is ~1000 K brighter than the QS. Penumbral brightness increases towards the outer boundary in both ALMA bands. Among the tested umbral models, that of Severino et al. (1994) provides the best fit to the observational data, including both the ALMA data analyzed in this study and data from earlier works. No penumbral model amongst those considered here gives a satisfactory fit to the currently available measurements. ALMA observations at multiple mm wavelengths can be used for testing existing sunspot models, and serve as an important input to constrain new empirical models.
2015 December 16, 2015-12-18
CESRA Highlight #1777, Feb **2018** http://cesra.net/?p=1777

Millimeter radiation from a 3D model of the solar atmosphere II. Chromospheric magnetic field

Maria **Loukitcheva**, Stephen M. White, Sami K. Solanki, Gregory D. Fleishman, Mats Carlsson
A&A 601, A43 **2017**
https://arxiv.org/pdf/1702.06018.pdf
We use state-of-the-art, three-dimensional non-local thermodynamic equilibrium (non-LTE) radiative magnetohydrodynamic simulations of the quiet solar atmosphere to carry out detailed tests of chromospheric magnetic

field diagnostics from free-free radiation at millimeter and submillimeter wavelengths (mm/submm). The vertical component of the magnetic field was deduced from the mm/submm brightness spectra and the degree of circular polarization synthesized at millimeter frequencies. We used the frequency bands observed by the Atacama Large Millimeter/Submillimeter Array (ALMA) as a convenient reference. The magnetic field maps obtained describe the longitudinal magnetic field at the effective formation heights of the relevant wavelengths in the solar chromosphere. The comparison of the deduced and model chromospheric magnetic fields at the spatial resolution of both the model and current observations demonstrates a good correlation, but has a tendency to underestimate the model field. The systematic discrepancy of about 10 percent is probably due to averaging of the restored field over the heights contributing to the radiation, weighted by the strength of the contribution. On the whole, the method of probing the longitudinal component of the magnetic field with free-free emission at mm/submm wavelengths is found to be applicable to measurements of the weak quiet-Sun magnetic fields. However, successful exploitation of this technique requires very accurate measurements of the polarization properties (primary beam and receiver polarization response) of the antennas, which will be the principal factor that determines the level to which chromospheric magnetic fields can be measured. Consequently, high-resolution and high-precision observations of circularly polarized radiation at millimeter wavelengths can be a powerful tool for producing chromospheric longitudinal magnetograms.

Probing the Sun with ALMA: observations and simulations brief **Review**

Maria **Loukitcheva**, Sami K. Solanki, Stephen M. White, Mats Carlsson
Proceedings of the International conference "Revolution in Astronomy with ALMA - The 3rd Year", December 8 - 11, 2014 Tokyo, Japan **2015**
http://arxiv.org/pdf/1508.05686v1.pdf
ALMA will open a new chapter in the study of the Sun by providing a leap in spatial resolution and sensitivity compared to currently available mm wave- length observations. In preparation of ALMA, we have carried out a large number of observational tests and state-of-the-art radiation MHD simulations. Here we review the best available observations of the Sun at millimeter wavelengths.Using state of the art radiation MHD simulations of the solar atmosphere we demonstrate the huge potential of ALMA observations for uncovering the nature of the solar chromosphere. We show that ALMA will not only provide a reliable probe of the thermal structure and dynamics of the chromosphere, it will also open up a powerful new diagnostic of magnetic field at chromospheric heights, a fundamentally important, but so far poorly known parameter.

Millimeter radiation from a 3D model of the solar atmosphere I. Diagnosing chromospheric thermal structure

Maria **Loukitcheva**, Sami Solanki, Mats Carlsson, Stephen White
A&A 575, A15 **2015**
http://arxiv.org/pdf/1501.02898v1.pdf
Aims. We use advanced 3D NLTE radiative magnetohydrodynamic simulations of the solar atmosphere to carry out detailed tests of chromospheric diagnostics at millimeter and submillimeter wavelengths. Methods. We focused on the diagnostics of the thermal structure of the chromosphere in the wavelength bands from 0.4 mm up to 9.6 mm that can be accessed with the Atacama Large Millimeter/Submillimeter Array (ALMA) and investigated how these diagnostics are affected by the instrumental resolution. Results. We find that the formation height range of the millimeter radiation depends on the location in the simulation domain and is related to the underlying magnetic structure. Nonetheless, the brightness temperature is a reasonable measure of the gas temperature at the effective formation height at a given location on the solar surface. There is considerable scatter in this relationship, but this is significantly reduced when very weak magnetic fields are avoided. Our results indicate that although instrumental smearing reduces the correlation between brightness and temperature, millimeter brightness can still be used to reliably diagnose electron temperature up to a resolution of 1". If the resolution is more degraded, then the value of the diagnostic diminishes rapidly. Conclusions. We conclude that millimeter brightness can image the chromospheric thermal structure at the height at which the radiation is formed. Thus multiwavelength observations with ALMA with a narrow step in wavelength should provide sufficient information for a tomographic imaging of the chromosphere.

The chromosphere above sunspots at millimeter wavelengths

M. **Loukitcheva**1,2, S. K. Solanki1,3 and S. M. White4
A&A 561, A133 (**2014**)
http://arxiv.org/pdf/1403.3436v1.pdf
Aims. The aim of this paper is to demonstrate that millimeter wave data can be used to distinguish between various atmospheric models of sunspots, whose temperature structure in the upper photosphere and chromosphere has been the source of some controversy.

Methods. We use observations of the temperature contrast (relative to the quiet Sun) above a sunspot umbra at 3.5 mm obtained with the Berkeley-Illinois-Maryland Array (BIMA), complemented by submm observations from Lindsey & Kopp (1995) and 2 cm observations with the Very Large Array. These are compared with the umbral contrast calculated from various atmospheric models of sunspots.
Results. Current mm and submm observational data suggest that the brightness observed at these wavelengths is low compared to the most widely used sunspot models. These data impose strong constraints on the temperature and density stratifications of the sunspot umbral atmosphere, in particular on the location and depth of the temperature minimum and the location of the transition region.
Conclusions. A successful model that is in agreement with millimeter umbral brightness should have an extended and deep temperature minimum (below 3000 K). Better spatial resolution as well as better wavelength coverage are needed for a more complete determination of the chromospheric temperature stratification above sunspot umbrae.

ALMA as the ideal probe of the solar chromosphere

Maria A. **Loukitcheva** · Sami K. Solanki · Stephen White
Astrophys Space Sci (**2008**) 313: 197–200
http://www.springerlink.com/content/4h73t442561552k2/fulltext.pdf
The very nature of the solar chromosphere, its structuring and dynamics, remains far from being properly understood, in spite of intensive research. Here we point out the potential of chromospheric observations at millimeter wavelengths to resolve this long-standing problem. Computations carried out with a sophisticated dynamic model of the solar chromosphere due to Carlsson and Stein demonstrate that millimeter emission is extremely sensitive to dynamic processes in the chromosphere and the appropriate wavelengths to look for dynamic signatures are in the range 0.8–5.0 mm. The model also suggests that high resolution observations at mm wavelengths, as will be provided by the Atacama Large Millimeter Array (ALMA), will have the unique property of reacting to both the hot and the cool gas, and thus will have the potential of distinguishing between rival models of the solar atmosphere. Thus, initial results obtained from the observations of the quiet Sun at 3.5 mm with the BIMA array (resolution of 12″) reveal significant oscillations with amplitudes of 50–150 K and frequencies of 1.5–8 mHz with a tendency toward short-period oscillations in internetwork and longer periods in network regions. However higher spatial resolution, such as that provided by ALMA, is required for a clean separation between the features within the solar atmosphere and for an adequate comparison with the output of the comprehensive dynamic simulations.

Spatially Resolved Moving Radio Burst in Association with an EUV Wave

Lei **Lu**, Li Feng, Weiqun Gan
ApJL **931** L8 **2022**
https://arxiv.org/pdf/2205.03047.pdf
https://iopscience.iop.org/article/10.3847/2041-8213/ac6ced/pdf
Coronal mass ejections (CMEs) are large clouds of magnetized plasma ejected from the Sun, and are often associated with acceleration of electrons that can result in radio emission via various mechanisms. However, the underlying mechanism relating the CMEs and particle acceleration still remains a subject of heated debate. Here, we report multi-instrument radio and extreme ultraviolet (EUV) imaging of a solar eruption event on **24 September 2011**. We determine the emission mechanism of a moving radio burst, identify its three-dimensional (3D) location with respect to a rapidly expanding EUV wave, and find evidence for CME shocks that produce quasiperiodic acceleration of electron beams.

Observational Signatures of Tearing Instability in the Current Sheet of a Solar Flare

Lei **Lu**, Li Feng, Alexander Warmuth, Astrid M. Veronig, Jing Huang, Siming Liu, Weiqun Gan, Zongjun Ning, Beili Ying, Guannan Gao
ApJ **2021**
https://arxiv.org/pdf/2112.07857.pdf
Magnetic reconnection is a fundamental physical process converting magnetic energy into not only plasma energy but also particle energy in various astrophysical phenomena. In this letter, we show a unique dataset of a solar flare where various plasmoids were formed by a continually stretched current sheet. EUV images captured reconnection inflows, outflows, and particularly the recurring plasma blobs (plasmoids). X-ray images reveal nonthermal emission sources at the lower end of the current sheet, presumably as large plasmoids with a sufficiently amount of energetic electrons trapped in. In the radio domain, an upward slowly drifting pulsation structure, followed by a rare pair of oppositely drifting structures, was observed. These structures are supposed to map the evolution of the primary and the secondary plasmoids formed in the current sheet. Our results on plasmoids at different locations and scales shed important light on the dynamics, plasma heating, particle acceleration, and transport processes in the turbulent current sheet and provide observational evidence for the cascading magnetic reconnection process. **July 19, 2012**

Two-dimensional Particle-in-cell Simulation of Magnetic Reconnection in the Downstream of a Quasi-perpendicular Shock

Quanming **Lu**1,2, Zhongwei Yang3, Huanyu Wang1,2, Rongsheng Wang1,2, Kai Huang1,2, San Lu1,2, and Shui Wang1,2

2021 ApJ 919 28

https://doi.org/10.3847/1538-4357/ac18c0

In this paper, by performing a two-dimensional particle-in-cell simulation, we investigate magnetic reconnection in the downstream of a quasi-perpendicular shock. The shock is nonstationary, and experiences cyclic reformation. At the beginning of the reformation process, the shock front is relatively flat, and part of the upstream ions are reflected by the shock front. The reflected ions move upward in the action of the Lorentz force, which leads to the upward bending of the magnetic field lines at the foot of the shock front, and then a current sheet is formed due to the squeezing of the bending magnetic field lines. The formed current sheet is brought toward the shock front by the solar wind, and the shock front becomes irregular after interacting with the current sheet. Both the current sheet carried by the solar wind and the current sheet associated with the shock front are then fragmented into many small filamentary current sheets. Electron-scale magnetic reconnection may occur in several of these filamentary current sheets when they are convected into the downstream, and magnetic islands are generated. A strong reconnection electric field and energy dissipation are also generated around the X line, and a high-speed electron outflow is also formed.

Quasi-Periodic Pulsations Detected in Lyα and Nonthermal Emissions During Solar Flares

Lei **Lu**, Dong Li, Zongjun Ning, Li Feng, Weiqun Gan

Solar Phys. **2021**

https://arxiv.org/pdf/2108.03820.pdf

We report quasi-periodic pulsations (QPPs) with double periods during three solar flares (viz. SOL**2011-Feb-15**T01:44, SOL**2011-Sep-25**T04:31, SOL**2012-May-17**T01:25). The flare QPPs were observed from light curves in Lyα, hard X-ray (HXR) and microwave emissions, with the Lyα emission recorded by the Geostationary Operational Environmental Satellite, the HXR emission recorded by the Reuven Ramaty High-Energy Solar Spectroscopic Imager and the Fermi Gamma-ray Burst Monitor, and the microwave emission recorded by the Nobeyama Radio Polarimeters and Radioheliograph. By using the Markov chain Monte Carlo (MCMC) method, QPPs with double periods of about two minutes and one minute were first found in the Lyα emission. Then using the same method, a QPP with nearly the same period of about two minutes was also found in HXR and microwave emissions. Considering the possible common origin (nonthermal electrons) between Lyα and HXR/microwave emission, we suggest that the two-minute QPP results from the periodic acceleration of nonthermal electrons during magnetic reconnections. The ratio between the double periods in the Lyα emission was found to be close to two, which is consistent with the theoretical expectation between the fundamental and harmonic modes. However, we cannot rule out other possible driving mechanisms for the one-minute QPPs in HXR/microwave emissions due to their relatively large deviations.

Statistical properties of radio flux densities of solar flares

Wang **Lu**, Liu Si-ming, Ning Zong-jun

Research in Astronomy and Astrophysics **2020**

https://arxiv.org/pdf/2006.02121.pdf

Short timescale flux variations are closely related to the energy release process of magnetic reconnection during solar flares. Radio light curves at 1, 2, 3.75, 9.4, and 17 GHz of 209 flares observed by the Nobeyama Radio Polarimeter from 2000 to 2010 are analyzed with a running smooth technique. We find that the impulsive component (with a variation timescale shorter than 1 second) of 1 GHz emission of most flares peaks at a few tens of solar flux unit and lasts for about 1 minute and the impulsive component of 2 GHz emission lasts a shorter period and peaks at a lower flux level, while at the three high frequency channels the occurrence frequency of flares increases with the decrease of the flux density up to the noise level of the corresponding background. The gradual components of these emissions, however, have similar duration and peak flux density distributions. We also derive the power spectrum on different timescales and a normalized wavelet analysis is used to confirm features on short timescales. At a time resolution of 0.1 second, more than ~ 60% of these radio light curves show significant flux variation on 1 second or shorter time scales. This fraction increases with the decrease of frequency and reaches ~ 100% at 1 GHz, implying that short timescale processes are universal in solar flares. We also study the correlation between the impulsive radio flux densities and soft X-ray fluxes obtained with the GOES satellites and find that more than 65% of the flares with an impulsive component have their impulsive radio emission reach a peak value ahead of the soft X-ray fluxes and this fraction increases with the radio frequency. **2000.07.25, 2001.03.25, 2001.05.20, 2001.11.30, 2002.04.09, 2003.10.24, 2004.01.07, 2004.07.24, 2004.11.10, 13 Dec 2006**

Measure the Propagation of a halo CME and Its Driven Shock with the Observations from a Single Perspective at Earth

Lei **Lu**, Bernd Inhester, Li Feng, Siming Liu, Xinhua Zhao

ApJ **2017**
https://arxiv.org/pdf/1612.09360v1.pdf
We present a detailed study of an earth-directed coronal mass ejection (Full halo CME) event happened on **2011 February 15** making use of white light observations by three coronagraphs and radio observations by Wind/WAVES. We applied three different methods to reconstruct the propagation direction and traveling distance of the CME and its driven shock. We measured the kinematics of the CME leading edge from white light images observed by STEREO A and B, tracked the CME-driven shock using the frequency drift observed by Wind/WAVES together with an interplanetary density model, and obtained the equivalent scattering centers of the CME by Polarization Ratio(PR) method. For the first time, we applied PR method to different features distinguished from LASCO/C2 polarimetric observations and calculated their projections onto white light images observed by STEREO A and B. By combining the graduated cylindrical shell (GCS) forward modeling with the PR method, we proposed a new GCS-PR method to derive 3D parameters of a CME observed from a single perspective at Earth. Comparisons between different methods show a good degree of consistence in the derived 3D results.

The Interaction of Successive Coronal Mass Ejections: A Review

Noé **Lugaz** Manuela Temmer Yuming Wang Charles J. Farrugia
Sol Phys (**2017**) 292: 64. **File**
http://sci-hub.cc/10.1007/s11207-017-1091-6
We present a review of the different aspects associated with the interaction of successive coronal mass ejections (CMEs) in the corona and inner heliosphere, focusing on the initiation of series of CMEs, their interaction in the heliosphere, the particle acceleration associated with successive CMEs, and the effect of compound events on Earth's magnetosphere. The two main mechanisms resulting in the eruption of series of CMEs are sympathetic eruptions, when one eruption triggers another, and homologous eruptions, when a series of similar eruptions originates from one active region. CME – CME interaction may also be associated with two unrelated eruptions. The interaction of successive CMEs has been observed remotely in coronagraphs (with the Large Angle and Spectrometric Coronagraph Experiment – LASCO – since the early 2000s) and heliospheric imagers (since the late 2000s), and inferred from in situ measurements, starting with early measurements in the 1970s. The interaction of two or more CMEs is associated with complex phenomena, including magnetic reconnection, momentum exchange, the propagation of a fast magnetosonic shock through a magnetic ejecta, and changes in the CME expansion. The presence of a preceding CME a few hours before a fast eruption has been found to be connected with higher fluxes of solar energetic particles (SEPs), while CME – CME interaction occurring in the corona is often associated with unusual radio bursts, indicating electron acceleration. Higher suprathermal population, enhanced turbulence and wave activity, stronger shocks, and shock – shock or shock – CME interaction have been proposed as potential physical mechanisms to explain the observed associated SEP events. When measured in situ, CME – CME interaction may be associated with relatively well organized multiple-magnetic cloud events, instances of shocks propagating through a previous magnetic ejecta or more complex ejecta, when the characteristics of the individual eruptions cannot be easily distinguished. CME – CME interaction is associated with some of the most intense recorded geomagnetic storms. The compression of a CME by another and the propagation of a shock inside a magnetic ejecta can lead to extreme values of the southward magnetic field component, sometimes associated with high values of the dynamic pressure. This can result in intense geomagnetic storms, but can also trigger substorms and large earthward motions of the magnetopause, potentially associated with changes in the outer radiation belts. Future in situ measurements in the inner heliosphere by Solar Probe+ and Solar Orbiter may shed light on the evolution of CMEs as they interact, by providing opportunities for conjunction and evolutionary studies. **2000-06-10, 25-26 Nov 2000, 19-20 March 2001, 26 Mar-26 Apr 2001, 1 Apr 2001, 31March – 1 April 2001, 1 August 2010, 25 May 2010, e August 2010 events f, 2011-08-01, 10 November 2012, 2013-05-22, 2011-02-15, 19 Feb2014**
3. Effects of Successive CMEs on Particle Acceleration
3.2. Radio Signatures of CME – CME Interaction

Multiple Regions of Nonthermal Quasi-Periodic Pulsations during the Impulsive Phase of a Solar Flare

Yingjie **Luo**, Bin Chen, Sijie Yu, Marina Battaglia, Rohit Sharma
ApJ **940** 137 **2022**
https://arxiv.org/pdf/2210.06219.pdf
https://iopscience.iop.org/article/10.3847/1538-4357/ac997a/pdf
Flare-associated quasi-periodic pulsations (QPPs) in radio and X-ray wavelengths, particularly those related to nonthermal electrons, contain important information about the energy release and transport processes during flares. However, the paucity of spatially resolved observations of such QPPs with a fast time cadence has been an obstacle for us to further understand their physical nature. Here, we report observations of such a QPP event occurred during the impulsive phase of a C1.8-class eruptive solar flare using radio imaging spectroscopy data from the Karl G. Jansky Very Large Array (VLA) and complementary X-ray imaging and spectroscopy data. The radio QPPs, observed by the VLA in the 1--2 GHz with a sub-second cadence, are shown as three spatially distinct sources with different physical

characteristics. Two radio sources are located near the conjugate footpoints of the erupting magnetic flux rope with opposite senses of polarization. One of the sources displays a QPP behavior with a ~5-s period. The third radio source, located at the top of the post-flare arcade, coincides with the location of an X-ray source and shares a similar period of ~25--45 s. We show that the two oppositely polarized radio sources are likely due to coherent electron cyclotron maser (ECM) emission. On the other hand, the looptop QPP source, observed in both radio and X-rays, is consistent with incoherent gyrosynchrotron and bremsstrahlung emission, respectively. We conclude that the concurrent, but spatially distinct QPP sources must involve multiple mechanisms which operate in different magnetic loop systems and at different periods. **February 18, 2016**.

Radio Spectral Imaging of an M8.4 Eruptive Solar Flare: Possible Evidence of a Termination Shock

Yingjie **Luo** (1), Bin Chen (1), Sijie Yu (1), Timothy S. Bastian (2), Samuel Krucker (3)
ApJ **911** 4 **2021**
https://arxiv.org/pdf/2102.06259.pdf
https://doi.org/10.3847/1538-4357/abe5a4
Solar flare termination shocks have been suggested as one of the viable mechanisms for accelerating electrons and ions to high energies. Observational evidence of such shocks, however, remains rare. Using radio dynamic spectroscopic imaging of a long-duration C1.9 flare obtained by the Karl G. Jansky Very Large Array (VLA), Chen et al. (2015) suggested that a type of coherent radio bursts, referred to as "stochastic spike bursts", were radio signature of nonthermal electrons interacting with myriad density fluctuations at the front of a flare termination shock. Here we report another stochastic spike burst event recorded during the extended energy release phase of a long-duration M8.4-class eruptive flare on **2012 March 10**. VLA radio spectroscopic imaging of the spikes in 1.0--1.6 GHz shows that, similar to the case of Chen et al. (2015), the burst centroids form an extended, ~10"-long structure in the corona. By combining extreme ultraviolet imaging observations of the flare from two vantage points with hard X-ray and ultraviolet observations of the flare ribbon brightenings, we reconstruct the flare arcade in three dimensions. The results show that the spike source is located at ~60 Mm above the flare arcade where a diffuse supra-arcade fan and multitudes of plasma downflows are present. Although the flare arcade and ribbons seen during the impulsive phase do not allow us to clearly understand how the observed spike source location is connected to the flare geometry, cooling flare arcade observed two hours later suggest that the spikes are located in the above-the-loop-top region, where a termination shock presumably forms.

Automated detection and statistical study of solar radio spikes

P. R. **Lv**, Y. C. Hou, S. W. Feng, Q. F. Du & C. M. Tan
Astrophysics and Space Science volume **368**, Article number: 14 (**2023**)
https://link.springer.com/content/pdf/10.1007/s10509-023-04172-8.pdf
The most typical observational features of solar radio spikes are their short duration and narrow bandwidth. We have improved the YOLOv5s network model for these characteristics by adding inclined bounding frames and attention and feature fusion mechanism modules. The decimeter- and meter-wavelength spikes observed by the Solar Broad-band Radio Spectrometer in Huairou and the Chashan Solar Radio Observatory spectrograph are used to carry out experiments, respectively. The results demonstrate that the AP value obtained by the improved network is 74%, which is almost 14% higher than the original network. The improved network detects 9709 (1379) decimeter- (meter-) wavelength spikes in two events with durations, bandwidths, relative bandwidths, and frequency-drift rates. The spikes at decimeter and meter wavelengths are again categorized based on their frequency-drift rates, such as positive, negative, and no measurable frequency-drift rates. We have carried out a statistical study on these categorized spikes. These statistical results and findings constrain solar radio spikes' formation.
CESRA #3531 **2023** https://www.astro.gla.ac.uk/users/eduard/cesra/?p=3531

Imaging Preflare Broadband Pulsations in the Decimetric-metric Wavelengths

Maoshui **Lv**, Baolin Tan, Ruisheng Zheng, Zhao Wu, Bing Wang, Xiangliang Kong, Yao Chen
ApJ **950** 2 **2023**
https://arxiv.org/pdf/2304.11785.pdf
https://iopscience.iop.org/article/10.3847/1538-4357/accf92/pdf
Preflare activities contain critical information about the pre-cursors and causes of solar eruptions. Here we investigate the characteristics and origin of a group of broadband pulsations (BBPs) in the decimetric-metric wavelengths, taking place during the preflare stage of the M7.1 flare dated on **2011 September 24**. The event was recorded by multiple solar instruments including the Nançay Radioheliograh that measure the properties of the radio source. The BBPs start ~24 min before the flare onset, extending from < 360 to above 800 MHz with no discernible spectral drift. The BBPs consist of two stages, during the first stage the main source remains stationary, during the second stage it moves outward along with a steepening extreme-ultraviolet (EUV) wave driven by the eruption of a high-temperature structure. In both stages, we observe frequent EUV brightenings and jets originating from the flare region. During the

second stage, the BBPs become denser in number and stronger in general, with the level of the polarization increasing gradually from < 20% to > 60% in the right-handed sense. These observations indicate the steepening EUV wave is important to the BBPs during the second stage, while the preflare reconnections causing the jets and EUV brightenings are important in both stages. This is the first time such a strong association of an EUV wave with BBPs is reported. We suggest a reconnection plus shock-sweeping-across-loop scenario for the cause of the BBPs.
CESRA #3562 **2023** https://www.astro.gla.ac.uk/users/eduard/cesra/?p=3562

An Observational Revisit of Stationary Type IV Solar Radio Bursts

Maoshui **Lv**, Yao Chen, V. Vasanth, Mohd Shazwan Radzi, Zamri Zainal Abidin & Christian Monstein
Solar Physics volume 296, Article number: 38 (**2021**)
https://link.springer.com/content/pdf/10.1007/s11207-021-01769-6.pdf
Stationary type IV solar radio bursts (IVSs) are broadband continuum emission observed at decimetric–decametric wavelength without apparent source motions. They are closely associated with solar flares and/or coronal mass ejections. Earlier studies on IVSs suffered from limited number of events, frequency coverage and available channels, and spatial resolution. Here we present an analysis on 34 IVSs using two-dimensional imaging data provided by Nançay Radioheliograh (NRH) at 10 frequencies from 150 to 445 MHz. The events are recorded from **2010 to 2014**. We focus on general properties including the spatial dispersion of sources with frequency, brightness temperature (TBTB) and corresponding spectra, and polarization. Main findings are: (i) In the majority of events (23/34) regular and systematic source dispersion with frequency can be clearly recognized. (ii) In most (31/34) events the maximum brightness temperature (TEBMTBME) exceeds 108 K108 K, and exceeds 109 K109 K in 23 events. The histogram distribution of TfBMTBMf, i.e. the maximum brightness temperature of a source at certain frequency (ff) of a specific event (referred to as event-ff source, there are 247 such sources in total) exhibits a clear declining trend with increasing frequencies. The dominant type of TBTB spectra is power-law like with a negative index. (iii) In most events (30/34) the sense of polarization remains unchanged and the number of events with right and left-handed polarization are comparable. In 57% of all 247 event-ff sources the level of polarization does not change considerably, in about 39% sources the level of polarization exhibits significant variation yet with a fixed sense, and in only 4% the sense of polarization changes. These results provide strong constraints on radiation mechanism of IVSs. **2010-08-14, 2011-03-07, 2011-08-09, 2011-09-24, 2011-10-05, 2012-03-04, 2012-03-05, 2012-06-14, 2012-07-08, 2012-07-10, 2013-10-26, 2013-12-23, 2014-02-11, 2014-08-21**
Table 1 List of IVSs and the characteristics of their spatial dispersion,

Sources of the Multi-Lane Type II Solar Radio Burst on 5 November 2014

M. S. **Lv**, Y. Chen, C. Y. Li, I. Zimovets, G. H. Du, B. Wang, S. W. Feng, S. L. Ma
Solar Physics December **2017**, 292:194
https://link.springer.com/content/pdf/10.1007%2Fs11207-017-1218-9.pdf
We report the well-observed event of a multi-lane type II solar radio burst with a combined analysis of radio dynamic spectra and radio and extreme-ultraviolet (EUV) imaging data. The burst is associated with an EUV wave driven by a coronal mass ejection (CME) that is accompanied by a GOES X-ray M7.9 flare on 5 November 2014. This type of event is rarely observed with such a complete data set. The type II burst presents three episodes (referred to as A, B, and C), characterized by a sudden change in spectral drift, and contains more than ten branches, including both harmonic-fundamental (H–F) pairs and split bands. The sources of the three episodes present a general outward propagating trend. There exists a significant morphology change from single source (Episode A) to double source (Episode B). Episode C maintains the double-source morphology at 150 MHz (no imaging data are available at a lower frequency). The double-source centroids are separated by ∼300″ to 500″. The southeastern (SE) source is likely the continuation of the source of Episode A since both are at the same section of the shock (i.e. the EUV wave) and close to each other. The northwestern (NW) source is coincident with (thus, possibly originates from) the interaction of the shock with a nearby mini-streamer-like structure. Comparing the simultaneously observed sources of the F and H branches of Episode A, we find that their centroids are separated by less than 200″. The centroids of the split bands of Episode B are cospatial within the observational uncertainties. This study shows the source evolution of a multi-lane type II burst and the source locations of different lanes relative to each other and to the EUV wave generated by a CME. The study indicates the intrinsic complexity underlying a type II dynamic spectrum.

Cold Solar Flares. I. Microwave Domain

Alexandra L. **Lysenko**1, Stephen M. White2, Dmitry A. Zhdanov3, Nataliia S. Meshalkina3, Aleksander T. Altyntsev3, Galina G. Motorina1,4,5, and Gregory D. Fleishman6,7
2023 ApJ 954 122
https://iopscience.iop.org/article/10.3847/1538-4357/acea20/pdf
We identify a set of ∼100 "cold" solar flares and perform a statistical analysis of them in the microwave range. Cold flares are characterized by a weak thermal response relative to nonthermal emission. This work is a follow-up of a previous statistical study of cold flares, which focused on hard X-ray emission to quantify the flare nonthermal component. Here, we focus on the microwave emission. The thermal response is evaluated by the soft X-ray emission

measured by the GOES X-ray sensors. We obtain spectral parameters of the flare gyrosynchrotron emission and reveal patterns of their temporal evolution. The main results of the previous statistical study are confirmed: as compared to a "mean" flare, the cold flares have shorter durations, higher spectral peak frequencies, and harder spectral indices above the spectral peak. Nonetheless, there are some cold flares with moderate and low peak frequencies. In the majority of cold flares, we find evidence of the Razin effect in the microwave spectra, indicative of rather dense flaring loops. We discuss the results in the context of the electron acceleration efficiency. **2010-06-12, 2012-07-10, 2012-07-06, 2012-07-14, 2012-08-15, 2013-04-24, 2014-01-08, 2014-06-29, 2014-11-21, 2015 May 8**

Statistics of "Cold" Early Impulsive Solar Flares in X-ray and Microwave domains

Alexandra L. **Lysenko**, Alexander T. Altyntsev, Natalia S. Meshalkina, Dmitriy Zhdanov, Gregory D. Fleishman

2018 ApJ 856 111

https://arxiv.org/pdf/1802.09288.pdf

http://sci-hub.tw/http://iopscience.iop.org/0004-637X/856/2/111/

Solar flares often happen after a preflare / preheating phase, which is almost or entirely thermal. In contrast, there are the so-called early impulsive flares that do not show a (significant) preflare heating but instead often show the Neupert effect--a relationship where the impulsive phase is followed by a gradual, cumulative-like, thermal response. This has been interpreted as a dominance of nonthermal energy release at the impulsive phase, even though a similar phenomenology is expected if the thermal and nonthermal energies are released in comparable amounts at the impulsive phase. Nevertheless, some flares do show a good quantitative correspondence between the nonthermal electron energy input and plasma heating, in such cases the thermal response was weak, which results in calling them "cold" flares. We undertook a systematic search of such events among early impulsive flares registered by Konus-Wind instrument in the triggered mode from 11/1994 to 04/2017 and selected 27 cold flares based on relationships between HXR (Konus-Wind) and SXR (GOES) emission. For these events we put together all available microwave data from different instruments. We obtained temporal and spectral parameters of HXR and microwave emissions of the events and examined correlations between them. We found that, compared with a `mean' flare, the cold flares: (i) are weaker, shorter, and harder in the X-ray domain, (ii) are harder and shorter, but not weaker in the microwaves, (iii) have a significantly higher spectral peak frequencies in the microwaves. We discuss the possible physical reasons for these distinctions and implication of the finding. **1998-05-07, 1999-06-19, 1999-07-30, 1999-11-09, 1999-11-14, 1999-12-02, 2000-03-10, 2000-03-18, 2000-05-18, 2001-10-12, 2001-11-01, 2002-05-29, 2002-08-10, 2002-08-18, 2002-08-20, 2003-10-23, 2005-09-08, 2011-09-19, 2012-07-08, 2013-11-05, 2014-01-02, 2014-01-31, 2014-02-08, 2014-10-18, 2014-10-27, 2015-05-07**

TABLE 1 Konus-Wind cold solar flare list

Search and statistical analysis of ”cold” solar flares using X-ray and microwave data

Alexandra **Lysenko**∗†1 , Alexander Altyntsev2 , Valentin Pal’shin , Natalia Meshalkina2 , Dmitriy Zhdanov2 , and Gregory Fleishman

CESRA **2016** p.62

http://cesra2016.sciencesconf.org/conference/cesra2016/pages/CESRA2016_prog_abs_book_v3.pdf

There is a subclass of solar flares that show noticeable nonthermal emission followed by only a modest or delayed heating. Such events are referred to as ”cold” solar flares here for brevity. Some examples of such flares were described earlier as case studies. Those studies show that the reasons of such a behavior may be quite different from each other in various cold flares and may involve either dense or tenuous plasma in flaring loop(s), suppressed chromospheric evaporation, and interaction between system of flare loops. We undertook a systematic search for cold solar flare candidates using Hard X-ray (HXR) data from KonusWind and Soft X-ray (SXR) data from GOES. The formal criterion of an event to be flagged as a cold flare candidate was the absence of reported GOES event at the time of Konus-Wind trigger. This way, we found 41 events-candidates from 05/1998 to 02/2014. For these events we put together all available microwave data from different instruments including OVSA, NoRP, RSTN, and BBMS. We obtained temporal and spectral parameters of HXR, SXR, and microwave emissions of the candidates along with their energetics in HXR and examined different relationships between these characteristics. In the X-ray domain, a comparison has been made between our flare subset and a reference set composed of C and M GOES class flares detected by Konus-Wind in the trigger mode. We present the statistical results and examine which of our cold flare candidates demonstrate suppressed or delayed heating and discuss the likely causes of the apparent lack or delay of the thermal response.

Solar plasma radio emission in the presence of imbalanced turbulence of kinetic-scale Alfvén waves

Olena **Lyubchyk**, Eduard Kontar, Yuriy Voitenko, Nicolas Bian, Donald Melrose

Solar Phys. 292:117 **2017**

https://arxiv.org/pdf/1707.02295.pdf

sci-hub.tw/10.1007/s11207-017-1140-1
We study the influence of kinetic-scale Alfv\'enic turbulence on the generation of plasma radio emission in the solar coronal regions where the plasma/magnetic pressure ratio is smaller than the electron/ion mass ratio. The present study is motivated by the phenomenon of solar type I radio storms associated with the strong magnetic field of active regions. The measured brightness temperature of the type I storms can be up to K for continuum emission, and can exceed K for type I bursts. At present, there is no generally accepted theory explaining such high brightness temperatures and some other properties of the type I storms. We propose the model with the imbalanced turbulence of kinetic-scale Alfv\'en waves producing an asymmetric quasilinear plateau on the upward half of the electron velocity distribution. The Landau damping of resonant Langmuir waves is suppressed and their amplitudes grow spontaneously above the thermal level. The estimated saturation level of Langmuir waves is high enough to generate observed type I radio emission at the fundamental plasma frequency. Harmonic emission does not appear in our model because the backward-propagating Langmuir waves undergo a strong Landau damping. Our model predicts polarization in the sense of the ordinary (o-) mode of type I emission.
CESRA Highlights #1525 Sept **2017** http://www.astro.gla.ac.uk/users/eduard/cesra/?p=1525

Type IV-like Solar Radio Burst Consisting of a Series of Spikes Observed by PSP

Bing **Ma**, Ling Chen, De-Jin Wu, Marc Pulupa, Stuart D. Bale
ApJ **2024**
https://arxiv.org/pdf/2403.07804.pdf
Solar and interplanetary radio bursts can reflect the existence and motion of energetic electrons and are therefore a kind of vital phenomenon in solar activities. The present study reported a solar radio burst (SRB) event observed by Parker Solar Probe (PSP) in its 8th orbital encounter phase, and it lasted about 20 hours in a frequency range of 0.5-15 MHz, called the type IV-like SRB. This type IV-like SRB consists of a series of numerous spikes with the center-frequency drifting slowly from ~5 MHz to ~1 MHz, and each individual spike appears a much faster frequency drifting and has a narrow frequency range of a few MHz and short duration of a few minutes. Based on the empirical models of the solar atmosphere adopted commonly, combining the in-situ measurement by PSP, we propose that these small-scale spikes were generated by a group of solitary kinetic Alfvén waves (SKAWs) in a magnetic loop accompanying coronal mass ejection (CME) and moving outwards, in which the frequency drifting of individual spike is caused by the SKAW's propagation and the center-frequency drifting may be attributed to the motion of the magnetic loop. **2021-04-26-27**

Solar Radio-Burst Forecast Based on a Convolutional Neural Network

Q. **Ma**, Q. F. Du, S. W. Feng, Y. C. Hou, W. Z. Ji & C. S. Han
Solar Physics volume 297, Article number: 130 (**2022**)
https://doi.org/10.1007/s11207-022-02069-3
A solar radio burst is the enhancement of radio emission during the release of solar magnetic energy. It is an important indicator of the level of solar activity. In this paper, we propose a solar radio-burst forecast model that takes the Solar and Heliospheric Observatory (SOHO)/Michelson Doppler Imager (MDI) full-disk solar magnetograms as inputs. The model takes advantage of a Convolutional Neural Network (CNN) to automatically extract the effective feature information from the input images. Through multiple trainings, the relationship between the magnetic-field characteristics of the full-disk solar magnetograms and the solar radio bursts is established, so it is possible to predict the presence or absence of a solar radio burst on that day. The experimental results demonstrate that the forecast Accuracy of the proposed model is 0.875 ± 0.007. The True Skill Statistic (TSS) is 0.723 ± 0.026, and the Heidke Skill Score (HSS) is 0.713 ± 0.019. These results indicate the strong reliability and wide applicability of the forecast model proposed in this paper. The proposed model is also used to predict solar type-II and type-III bursts, respectively. It is found that the prediction performance for type-III bursts is better than that of type-II bursts. The result is well explained from the differences of their formation mechanisms.

Discrepancy between the Low-frequency Cutoffs of Type III Radio Bursts Based on Simultaneous Observations by WIND and PSP

Bing **Ma** (马兵)1,2, Ling Chen (陈玲)1,3, Dejin Wu (吴德金)1,3, Marc Pulupa4, and Stuart D. Bale4
2022 ApJL 932 L26
https://iopscience.iop.org/article/10.3847/2041-8213/ac7525/pdf
The cutoff frequency is an important characteristic parameter of type III radio bursts. Employing the radio data of the Parker Solar Probe (PSP) in the encounter phases of its first five orbits, our previous work revealed that the maximum probability distribution of the cutoff frequency flo (~680 kHz) is remarkably higher than that based on Ulysses and WIND (~100 kHz) investigated by Leblanc et al. and Dulk et al. However, the main influencing factor of the discrepancy is still unknown though the possible reasons are discussed. In this study, we utilize the simultaneous observation by WIND and PSP to analyze statistically the distribution of the cutoff frequency of type III radio bursts, which had not been done before. Based on the automatic Canny edge detection and manual selection, we obtain the flo of 491 (WIND) and 1194 (PSP) type III bursts from their simultaneous observations in the same solar activity

period (from 2019 January 1 to 2020 July 31). The statistical results show that the dominant cutoff frequency measured by PSP (i.e., ∼700 kHz) is still significantly higher than that by WIND (i.e., ∼100 kHz). This implies that radiation attenuation is the main influencing factor for the difference in the statistical results of the cutoff frequency. **2019-03-23, 2019-04-05-06, 2020-07-21**

Statistics of Low Frequency Cutoffs for Type III Radio Bursts Observed by Parker Solar Probe during Its Encounters 1–5

Bing **Ma**1,2, Ling Chen1,3, Dejin Wu1, and Stuart D. Bale4,5,6,7
2021 ApJL 913 L1
https://doi.org/10.3847/2041-8213/abfb77
The low frequency cutoffs flo and the observed plasma frequency fp of 176 type III radio bursts are investigated in this paper. These events are observed by the Parker Solar Probe when it is in the encounter phase from the first to the fifth orbit. The result shows that the distribution of cutoffs flo is widely spread between 200 kHz and 1.6 MHz. While the plasma frequency fp at the spacecraft is between 50 and 250 kHz, which is almost all smaller than flo. The result also shows that the maximum probability distribution of flo (~680 kHz) is remarkably higher than that observed by Ulysses and Wind (~100 kHz) in previous research. Three possible reasons, i.e., solar activity intensity, event electing criteria, and radiation attenuation effect, are also preliminarily discussed.
CESRA # 2948 June **2021** http://www.astro.gla.ac.uk/users/eduard/cesra/?p=2948

Two Successive Type II Radio Bursts Associated with B-class Flares and Slow CMEs

Suli **Ma**, Huadong Chen
Front. Astron. Space Sci. 7:17. **2020**
https://arxiv.org/pdf/2004.14937.pdf
https://www.frontiersin.org/articles/10.3389/fspas.2020.00017/full
https://doi.org/10.3389/fspas.2020.00017
From **2018 Oct 12 to 13**, three successive solar eruptions (E1--E3) with B-class flares and poor white light coronal mass ejections (CMEs) occurred from the same active region NOAA AR 12724. Interestingly, the first two eruptions are associated with Type II radio bursts but the third is not. Using the soft X-ray flux data, radio dynamic spectra and dual perspective EUV intensity images, we comparatively investigate the three events. Our results show that their relevant flares are weak (B2.1, B7.9 and B2.3) and short-lived (13, 9 and 14 minutes). The main eruption directions of E1 and E2 are along ∼45◦ north of their radial directions, while E3 primarily propagated along the radial direction. In the EUV channels, the early speeds of the first two CMEs have apparent speeds of ∼320 km s−1 and ∼380 km s−1, which could exceed their respective local Alfve´n speeds of ∼300 km s−1 and ∼350 km s−1. However, the CME in the third eruption possesses a much lower speed of ∼160 km s−1. These results suggest that the observed Type II radio bursts in the eruptions E1 and E2 are likely triggered by their associated CMEs and the direction of eruption and the ambient plasma and magnetic environments may take an important place in producing Type II radio burst or shock as well.

Analysis of the event of 2004 November 10

Yuan **Ma** and LiYing Zhu
Solar and Stellar Variability: Impact on Earth and Planets, Proceedings IAU Symposium No. 264, **2009**, A.G. Kosovichev, A.H. Andrei & J.-P. Rozelot, eds., p. 273-275.
Y:\obridko\otchet09
The large burst of complex type which occurred at the metric, decimetric and microwave wavelengths from 0203 to 0304 UT on **2004 November 10** is analyzed in this present article, some prominent features of this event are obtained from the correlative analysis of this event with the H® flare and coronal mass ejection (CME) and the radiation process of this event is discussed based on these observational features.

Occurrence of bidirectional type III bursts in solar flares

Y. **Ma** · De YuWang · R.X. Xie · M. Wang · Y.H. Yan
Astrophys Space Sci (**2008**) 318: 87–92
The 13 pairs of type III bursts with the bidirectional drift structures recorded with the spectrograph in the frequency ranges of 230–300 MHz and 625–1500 MHz at the Yunnan Observatory and 2600–3800 MHz at the Beijing National Astronomical Observatories are analyzed in this present article and the outstanding characteristics of these events are obtained. These bursts respectively reveal that the separatrix frequency between the bursts with positive and negative drifts comes between 250 MHz and 3420 MHz, with a gap being between 0.6 MHz and 110 MHz; the duration is 53 ms–1880 ms and the frequency drift rate is between 45 MHz/s and 56000 MHz/s. The drift rate at metric wavelengths is relatively low, only a few decades of MHz while it is comparatively high at microwave wavelengths, reaching 56000 MHz/s. The qualitative explanation of these events is given in this paper.

Statistical Analysis of Decimetric Type III Bursts,
Y. **Ma**, R. X. Xie and M. Wang,
Solar Physics, Volume 238 Number 1, p. 105-115, **2006**.

Re-examining the correlation of complex solar type III radio bursts and solar energetic particles,

MacDowall, R. J., Richardson, I. G., Hess, R. A., and Thejappa, G.,
in Proceedings of IAU Symposium No. 257, *Universal Heliophysical Processes*, eds. N. Gopalswamy and D. F. Webb , 4, p. 335, **2009, File**

Interplanetary radio observations provide important information on particle acceleration processes at the Sun and propagation of the accelerated particles in the solar wind. Cane et al. (2002) have drawn attention to a class of prominent radio bursts that accompany >20 MeV solar proton events. They call these bursts 'type III-L' because: they are fast drifting (like normal type III bursts associated with electrons accelerated at impulsive solar flares); they are Long-lasting compared to normal type III bursts; they occur Late compared to the onset of the related solar event; and, they commence at Lower frequencies (~100 MHz) than normal type III bursts, suggesting that they originate higher in the corona at ~0.5 Rs above the Sun. We report on an analysis of the correlated radio and SEP events during 1996-2006 using the Wind Waves and near-Earth SEP data sets, and discuss whether the characteristics of the complex type III bursts (at less than 14 MHz) will permit them to serve as proxies for SEP event occurrence and intensity.

Fine Structure of a Solar Type II Radio Burst Observed by LOFAR

Jasmina **Magdalenić**1, Christophe Marqué1, Richard A. Fallows2, Gottfried Mann3, Christian Vocks3, Pietro Zucca2, Bartosz P. Dabrowski4, Andrzej Krankowski4, and Valentin Melnik5
2020 ApJL 897 L15

sci-hub.tw/10.3847/2041-8213/ab9abc
https://iopscience.iop.org/article/10.3847/2041-8213/ab9abc/pdf
https://doi.org/10.3847/2041-8213/ab9abc

Shock waves in the solar corona are closely associated with coronal mass ejections and flares. The longest-known and frequently studied signatures of coronal shock waves are metric type II radio bursts, which provide information on the shock driver and ambient plasma conditions. We report on outstanding high frequency/time resolution LOw Frequency ARray (LOFAR) observations of a metric type II radio burst. The LOFAR observations show a strong fragmentation of the type II emission, in both the frequency and time domains, during the whole duration of the event. A very unusual splitting of an already-split type II band, which we call the band-split of the band-split, was observed for the first time. The richness of fine structure, observed in both the fundamental and harmonic bands of the type II emission, is unprecedented. Fine structures, morphologically similar to those seen superposed on a type IV continuum, were observed for the first time within a type II burst. We classify the fine structures into three categories: simple narrowband, broadband, and complex fine structures, and discuss their properties. LOFAR observations of fragmented shock-associated radio emission have the potential of bringing new insight into the physics of coronal shock waves, and also new challenges for the theory of electron acceleration by shocks. **2014 August 25**

Triangulation of the continuum-like radio emission in a CME-CME interaction event

Jasmina **Magdalenic**∗1 , Manuela Temmer2 , Vratislav Krupar3,4, Christophe Marque5 , Astrid Veronig2 , and Bojan Vrsnak
CESRA **2016** p.69

http://cesra2016.sciencesconf.org/conference/cesra2016/pages/CESRA2016_prog_abs_book_v3.pdf

We present a study of the radio emission associated with the complex interaction of two coronal mass ejections (CMEs), successively launched from the same active region (NOAA AR 11158), on **February 14 and February 15, 2011**. Although this CME-CME interaction event was widely studied (e.g. Temmer et al., 2014, Maricic et al., 2014, Mishra & Srivastava, 2014) none of the analyses determined the origin of the associated continuum-like radio emission observed in the decameter-to-hectometer frequency range. The continuum-like emission patch has a particular morphology and might be considered either as a continuation of the decametric type II radio emission associated with the second CME, either as a continuation of the type III radio bursts associated with a flare from NOAA AR 11158. This ambiguity additionally complicates the question on the possible origin of the continuum-like emission. The association of this type of continuumlike radio emission and the CME-CME interaction was up to now established only by their temporal coincidence (Gopalswamy et al., 2001), which is not applicable in this event due to a complex and long-lasting interaction of the CMEs. The radio triangulation study (see also Magdalenic et al., 2014) provided us with the 3D source positions of the continuum-like emission and the associated type II burst, which were compared with the positions of the interacting CMEs. First results indicated that the continuum-like radio emission is not the continuation of the type III radio bursts, but it is also not the radio signature of the CME-CME interaction.

Fine structure of a type II radio burst observed by LOFAR

Jasmina **Magdalenic**∗1 , Christophe Marque2 , Richard Fallows3 , Gottfried Mann4 , Christian Vocks5 , and Lofar Solar Ksp Core Members

CESRA Abstract **2016**

http://cesra2016.sciencesconf.org/conference/cesra2016/pages/CESRA2016_prog_abs_book_v1.pdf

The M2.0 class flare peaking at 15:10 UT on **August 25, 2014** originated from the NOAA AR 2146, at that moment situated close to the west solar limb. The flare was associated with coronal dimmings, an EIT wave, a halo CME, and a type II radio burst observed in the meter to decameter wavelengths. A metric type II burst was observed by the LOFAR (LOw Frequency ARray) radio interferometer. The type II burst shows strong fragmentation of the radio emission, and although fine structure of type II burst was already reported, the richness of the fine structures observed in the August 25, 2014 event is unprecedented due to outstanding frequency and time resolutions, and exceptional sensitivity of LOFAR.

The fine structures within the type II burst are morphologically very similar to the ones usually seen superposed on type IV continuum emission. Together with herringbone structures, inverted J-bursts and U-bursts, we observed also narrowband bursts similar to simple narrowband super short structures (Magdalenic et al., 2006), i.e. spike-like, dot-like, sail-like and flag-like bursts, and a number of various unclassified bursts. The main characteristics of the fine structures observed within the type II burst are compared with the characteristics of type IV burst fine structures in the same wavelength range. We demonstrate how LOFAR observations bring new insight into the physics of coronal shock waves and their radio signatures, and therefore also new challenges for the theory of the electron acceleration at the shock waves in the solar corona.

Tracking the CME-driven Shock Wave on 2012 March 5 and Radio Triangulation of Associated Radio Emission

J. **Magdalenić**1, C. Marqué1, V. Krupar2, M. Mierla1,3, A. N. Zhukov1,4, L. Rodriguez1, M. Maksimović5, and B. Cecconi

2014 ApJ 791 115

We present a multiwavelength study of the **2012 March 5** solar eruptive event, with an emphasis on the radio triangulation of the associated radio bursts. The main points of the study are reconstruction of the propagation of shock waves driven by coronal mass ejections (CMEs) using radio observations and finding the relative positions of the CME, the CME-driven shock wave, and its radio signatures. For the first time, radio triangulation is applied to different types of radio bursts in the same event and performed in a detailed way using goniopolarimetric observations from STEREO/Waves and WIND/Waves spacecraft. The event on 2012 March 5 was associated with a X1.1 flare from the NOAA AR 1429 situated near the northeast limb, accompanied by a full halo CME and a radio event comprising long-lasting interplanetary type II radio bursts. The results of the three-dimensional reconstruction of the CME (using SOHO/LASCO, STEREO COR, and HI observations), and modeling with the ENLIL cone model suggest that the CME-driven shock wave arrived at 1 AU at about 12:00 UT on March 7 (as observed by SOHO/CELIAS). The results of radio triangulation show that the source of the type II radio burst was situated on the southern flank of the CME. We suggest that the interaction of the shock wave and a nearby coronal streamer resulted in the interplanetary type II radio emission.

FLARE-GENERATED TYPE II BURST WITHOUT ASSOCIATED CORONAL MASS EJECTION

J. **Magdalenić**1,2, C. Marqué1, A. N. Zhukov1,3, B. Vršnak2 and A. Veronig

2012 ApJ 746 152

We present a study of the solar coronal shock wave on **2005 November 14** associated with the GOES M3.9 flare that occurred close to the east limb (S06fl E60fl). The shock signature, a type II radio burst, had an unusually high starting frequency of about 800 MHz, indicating that the shock was formed at a rather low height. The position of the radio source, the direction of the shock wave propagation, and the coronal electron density were estimated using Nançay Radioheliograph observations and the dynamic spectrum of the Green Bank Solar Radio Burst Spectrometer. The soft X-ray, Hα, and Reuven Ramaty High Energy Solar Spectroscopic Imager observations show that the flare was compact, very impulsive, and of a rather high density and temperature, indicating a strong and impulsive increase of pressure in a small flare loop. The close association of the shock wave initiation with the impulsive energy release suggests that the impulsive increase of the pressure in the flare was the source of the shock wave. This is supported by the fact that, contrary to the majority of events studied previously, no coronal mass ejection was detected in association with the shock wave, although the corresponding flare occurred close to the limb.

ORIGIN OF CORONAL SHOCK WAVES ASSOCIATED WITH SLOW CORONAL MASS EJECTIONS

J. **Magdaleni´c**[1,2], C. Marqu´e[1], A. N. Zhukov[1,3], B. Vr˘snak[2], and T. ˘ Zic
Astrophysical Journal, 718:266–278, **2010** July; **File**

We present a multiwavelength study of five coronal mass ejection/flare events (CME/flare) and associated coronal shock waves manifested as type II radio bursts. The study is focused on the events in which the flare energy release, and not the associated CME, is themost probable source of the shock wave. Therefore, we selected events associated with rather slow CMEs (reported mean velocity below 500 km s−1). To ensure minimal projection effects, only events related to flares situated close to the solar limb were included in the study. We used radio dynamic spectra, positions of radio sources observed by the Nan¸cay Radioheliograph, *GOES* soft X-ray flux measurements, Large Angle Spectroscopic Coronagraph, and Extreme-ultraviolet Imaging Telescope observations. The kinematics of the shock wave signatures, type II radio bursts, were analyzed and compared with the flare evolution and the CME kinematics.We found that the velocities of the shock waves were significantly higher, up to one order of magnitude, than the contemporaneous CME velocities. On the other hand, shock waves were closely temporally associated with the flare energy release thatwas very impulsive in all events. This suggests that the impulsive increase of the pressure in the flare was the source of the shock wave. In four events the shock wave was most probably flare-generated, and in one event results were inconclusive due to a very close temporal synchronization of the CME, flare, and shock.

First multiple type II burst recorded at Humain associated with the CME/flare event on 18 March 2010

J. **Magdalenic**, C. Marque, A.N.Zhukov, D.Berghmans, B.Nicula, I. Dammasch
CEARA_**2010, Presentation File**

We present a multiwavelength study of large-scale coronal disturbances associated with the CME/flare event recorded on 18 March 2010. The evolution of the shock wave signatures, type II radio bursts, was analysed using dynamic spectra recorded by Humain (ROB) and the Nançay Decameter Array together with imaging by the Nançay Radioheliograph. Observations of the plasma dynamics in the low and high corona were provided by high time resolution PROBA 2 (SWAP and LYRA) and both STEREO spacecraft. This is the first multiple type II event with SIDC coordinated observations (Humain, SWAP and LYRA) available together with the STEREO data.
The first type II burst appeared at 11:19 UT in the frequency range of 200-30 MHz. The second, weaker type II burst appeared 6 minutes later and in the frequency range of 160-60 MHz. Applying the 3-fold Saito coronal density model we obtained shock speeds of about 1100 and 700 km/s, respectively.
Using the type II band-split from the 1st type II, we obtained the shock Alfven-Mach number of 1.3, and the Alfven speed of about 800 km/s. The shock waves were associated with the B5.3 flare in the NOAA AR 1056 (located at N17E47). The SWAP observations show few subsequent brightenings in the AR possibly associated with the event. The associated CME first appeared in the COR1 field of view at 11:25 UT at the height of about 1.5 solar radii. Both SECCHI COR1 and COR2 observed the CME as a limb event. We found that the CME speed was about 350 km/s that is significantly slower than the obtained shock speeds.

A Flare-Generated Shock during a Coronal Mass Ejection on 24 December 1996

J. **Magdalenic** · B. Vršnak · S. Pohjolainen · M. Temmer · H. Aurass · N.J. Lehtinen
Solar Phys, 253: 305–317, **2008**, DOI 10.1007/s11207-008-9220-x; **File**

We present a multiwavelength study of the large-scale coronal disturbances associated with the CME– flare event recorded on 24 December 1996. The kinematics of the shock wave signature, the type II radio burst, is analyzed and compared with the flare evolution and the CME kinematics. We employ radio dynamic spectra, position of the Nançay Radioheliograph sources, and LASCO-C1 observations, providing detailed study of this limb event. The obtained velocity of the shock wave is significantly higher than the contemporaneous CME velocity (1000 and 235 km s−1, respectively). Moreover, since the main acceleration phase of the CME took place 10 – 20 min after the shock wave was launched, we conclude that the shock wave on 24 December 1996 was probably not driven by the CME. However, the shock wave was closely associated with the flare impulsive phase, indicating that it was ignited by the energy release in the flare.

LOFAR observations of a jet-driven piston shock in the low solar corona

Ciara A. **Maguire**, Eoin P. Carley, Pietro Zucca, Nicole Vilmer, Peter T. Gallagher
ApJ **909** 2 **2021**

https://arxiv.org/pdf/2101.05569.pdf
https://doi.org/10.3847/1538-4357/abda51
The Sun produces highly dynamic and eruptive events that can drive shocks through the corona. These shocks can accelerate electrons, which result in plasma emission in the form of a type II radio burst. Despite the large number of type II radio bursts observations, the precise origin of coronal shocks is still subject to investigation. Here we present a well observed solar eruptive event that occurred on **16 October 2015**, focusing on a jet observed in the extreme ultraviolet (EUV) by the Atmospheric Imaging Assembly (SDO/AIA), a streamer observed in white-light by the Large Angle and Spectrometric Coronagraph (SOHO/LASCO), and a metric type II radio burst observed by the LOw Frequency Array (LOFAR). LOFAR interferometrically imaged the fundamental and harmonic sources of a type II radio burst and revealed that the sources did not appear to be co-spatial, as would be expected from the plasma emission mechanism. We correct for the separation between the fundamental and harmonic using a model which accounts for scattering of radio waves by electron density fluctuations in a turbulent plasma. This allows us to show the type II radio sources were located ∼0.5 R⊙ above the jet and propagated at a speed of ∼1000 kms−1, which was significantly faster than the jet speed of ∼200 kms−1. This suggests that the type II burst was generated by a piston shock driven by the jet in the low corona.

Evolution of the Alfvén Mach number associated with coronal mass ejection shock

Ciara A. **Maguire**, Eoin P. Carley, Joseph McCauley, Peter T. Gallagher
A&A 633, A56 (**2020**)
https://arxiv.org/pdf/1912.01863.pdf
https://doi.org/10.1051/0004-6361/201936449
The Sun regularly produces large-scale eruptive events, such as coronal mass ejections (CMEs) that can drive shock waves through the solar corona. Such shocks can result in electron acceleration and subsequent radio emission in the form of a type II radio burst. However, the early-phase evolution of shock properties and its relationship to type II burst evolution is still subject to investigation. Here we study the evolution of a CME-driven shock by comparing three commonly used methods of calculating the Alfvén Mach number (MA), namely: shock geometry, a comparison of CME speed to a model of the coronal Alfvén speed, and the type II band-splitting method. We applied the three methods to the **2017 September 2** event, focusing on the shock wave observed in extreme ultraviolet (EUV) by the Solar Ultraviolet Imager (SUVI) on board GOES-16, in white-light by the Large Angle and Spectrometric Coronagraph (LASCO) on board SOHO, and the type II radio burst observed by the Irish Low Frequency Array (I-**LOFAR**). We show that the three different methods of estimating shock MA yield consistent results and provide a means of relating shock property evolution to the type II emission duration. The type II radio emission emerged from near the nose of the CME when MA was in the range 1.4-2.4 at a heliocentric distance of ∼1.6 R⊙. The emission ceased when the CME nose reached ∼2.4 R⊙, despite an increasing Alfvén Mach number (up to 4). We suggest the radio emission cessation is due to the lack of quasi-perpendicular geometry at this altitude, which inhibits efficient electron acceleration and subsequent radio emission.
EGU2020 Presentation #11425 File

A Statistical Study of Low-Frequency Solar Radio Type III Bursts

Aroori **Mahender**, K. Sasikumar Raja, R. Ramesh, Vemareddy Panditi, Christian Monstein & Yellaiah Ganji
Solar Physics volume 295, Article number: 153 (**2020**)
https://link.springer.com/content/pdf/10.1007/s11207-020-01722-z.pdf
After inspecting 1531 type III bursts we found that 426 bursts were associated with flares, while the others might have been triggered by small scale features/weak energy events present in the solar corona. In this study, we have carried out a statistical analysis of various observational parameters like start time, lower- and upper-frequency cut-offs of type III bursts and their association with flares, variation of such parameters with flare parameters such as location, class, onset, and peak times. From this study, we found that most of the high frequency bursts (whose upper-frequency cut-off is >350 MHz>350 MHz) originate from western longitudes. We interpret that this could be due to the fact that Parker spirals from these longitudes are directed towards the Earth and high frequency bursts are more directive. Further we report that the number of bursts that reach Earth from western longitudes is higher than from eastern longitudes. **7 September 2017**

Type II solar radio burst band-splitting: Measure of coronal magnetic field strength

Ayman**Mahrous**, KhaledAlieldena, BojanVršnakb, MohamedYoussefa
Journal of Atmospheric and Solar-Terrestrial Physics Volume 172, July **2018**, Pages 75-82
http://sci-hub.tw/10.1016/j.jastp.2018.03.018
Studies of the relationship between solar radio bursts and CMEs are essential for understanding of the nature of type II bursts. In this study, we examine the type II solar radio burst recorded on **16 March 2016** by the Learmonth radio spectrograph and compare its characteristics with the kinematics of the associated CMEs observed by STEREO

and SOHO spacecraft. The burst showed a well-defined band-split, which was used to estimate the magnetic field strength in the solar corona. The magnetic field decreases from ≈ 4 G at R ≈ 2.6 R⊙to 0.62 G at R ≈ 3.77 R⊙ depending on the coronal electron density model employed. We found that two CMEs occurred successively in a 4-h interval. During this interval, a type II radio burst occurred, lasting for about 10 min. Tracking of the shock that produced type II burst and comparison with the CMEs heights as observed by STEREO and SOHO spacecraft help us to deduce the driver of the shock. According to the analysis, the type II burst occurrence was associated with the interaction of the shock driven by the second CME with a streamer located south of the first CME, since that the type II band-split significantly increased during the shock-streamer interaction. Our results show that the analysis of the type II burst band-split supplemented by the coronagraphic observations of the corona is an important tool for the understanding of the coronal eruptive processes.

THE RADIO–CORONAL MASS EJECTION EVENT ON 2001 APRIL 15

Dalmiro Jorge Filipe **Maia**, Ricardo Gama, Claude Mercier, Monique Pick, Alain Kerdraon, and Marian Karlicky

Astrophysical Journal, 660:874–881, **2007**

http://www.journals.uchicago.edu/doi/pdf/10.1086/508011

https://iopscience.iop.org/article/10.1086/508011/pdf

On **2001 April 15**, the Nanc¸ay radioheliograph observed fast-moving, expanding loops in images taken in the wavelength range between 164 and 432 MHz. We were able to follow the progression of the radio loops, starting from a few tenths to more than 1 R_ above the solar limb, with a time cadence of order seconds. The loops seen in radio agree very well with the features of the coronal mass ejection (CME) seen later, more than 2.5 R_ above the limb, in white-light images by the Large Angle Spectrometric Coronagraph (LASCO) experiment on board the Solar and Heliospheric Observatory (SOHO) spacecraft. The event is well associated with an energetic electron event seen by the Electron, Proton, and Alpha Monitor (EPAM) experiment on board the Advanced Composition Explorer (ACE) spacecraft. *A detailed transport model for the electrons shows that, not only the inferred onset at the Sun, but also the duration of the particle release, are similar for the radio loop and the in situ electron event detected near the Earth.*

Imaging and Spectral Observations of a Type-II Radio Burst Revealing the Section of the CME-Driven Shock that Accelerates Electrons

Satabdwa **Majumdar**, Srikar Paavan Tadepalli, Samriddhi Sankar Maity, Ketaki Deshpande, Anshu Kumari, Ritesh Patel, Nat Gopalswamy

Solar Phys. **296**, Article number: 62 **2021**

https://arxiv.org/pdf/2103.09536.pdf

https://link.springer.com/content/pdf/10.1007/s11207-021-01810-8.pdf

https://doi.org/10.1007/s11207-021-01810-8

We report on a multi-wavelength analysis of the **26 January 2014** solar eruption involving a coronal mass ejection (CME) and a Type-II radio burst, performed by combining data from various space-and ground-based instruments. An increasing standoff distance with height shows the presence of a strong shock, which further manifests itself in the continuation of the metric Type-II burst into the decameter-hectometric (DH) domain. A plot of speed versus position angle (PA) shows different points on the CME leading edge travelled with different speeds. From the starting frequency of the Type-II burst and white-light data, we find that the shock signature producing the Type-II burst might be coming from the flanks of the CME. Measuring the speeds of the CME flanks, we find the southern flank to be at a higher speed than the northern flank; further the radio contours from Type-II imaging data showed that the burst source was coming from the southern flank of the CME. From the standoff distance at the CME nose, we find that the local Alfven speed is close to the white-light shock speed, thus causing the Mach number to be small there. Also, the presence of a streamer near the southern flank appears to have provided additional favorable conditions for the generation of shock-associated radio emission. These results provide conclusive evidence that the Type-II emission could originate from the flanks of the CME, which in our study is from the the southern flank of the CME.

Speed and Acceleration of CMEs Associated with Sustained Gamma-Ray Emission Events Observed by Fermi/LAT

P. **Mäkelä**, N. Gopalswamy, S. Akiyama, H. Xie, S. Yashiro

ApJ **2023**

https://arxiv.org/pdf/2307.05585.pdf **File**

The sustained gamma-ray emission (SGRE) from the Sun is a prolonged enhancement of >100 MeV gamma-ray emission that extends beyond the flare impulsive phase.The origin of the >300 MeV protons resulting in SGRE is debated, both flares and shocks driven by coronal mass ejections (CMEs) being the suggested sites of proton acceleration. We compared the near-Sun acceleration and space speed of CMEs with 'Prompt' and 'Delayed' (SGRE) gamma-ray components (Ajello et al. 2021). We found that 'Delayed'-component-associated CMEs have higher initial

acceleration and space speed than 'Prompt-only'-component-associated CMEs. We selected halo CMEs (HCMEs) associated with type II radio bursts (shock-driving HCMEs) and compared the average acceleration and space speed between HCME populations with or without SGRE events, major solar energetic particle (SEP) events, metric, or decameter-hectometric (DH) type II radio bursts. **We found that the SGRE-producing HCMEs associated with a DH type II radio burs**t and/or a major SEP event have higher space speeds and especially initial accelerations than those without an SGRE event. We estimated the radial distance and speed of the CME-driven shocks at the end time of the 2012 January 23 and March 07 SGRE events using white-light images of STEREO Heliospheric Imagers and radio dynamic spectra of Wind WAVES. The shocks were at the radial distances of 0.6-0.8 au and their speeds were high enough (~975 km s−1 and ~750 km s−1, respectively) for high-energy particle acceleration. Therefore, we conclude that our findings support the CME-driven shock as the source of >300 MeV protons. **2012: January 23 and March 07**
Table A. CME and X-ray flare data for Fermi/LAT solar flares 2010-2017
Table B. **Cycle 24 HCMEs with type II radio bursts 2010-2017**

On the properties of solar energetic particle events associated with metric type II radio bursts

Pertti **Mäkelä**, Nat Gopalswamy, Hong Xie, Sachiko Akiyama, Seiji Yashiro, Neeharika Thakur
Sun and Geosphere, a special issue devoted to the ISWI Workshop, Trieste, Italy, 20 - 24 May, 2019
2020
https://arxiv.org/ftp/arxiv/papers/2001/2001.10506.pdf
Metric type II solar radio bursts and solar energetic particles (SEPs) are both associated with shock fronts driven by coronal mass ejections (CMEs) in the solar corona. Recent studies of ground level enhancements (GLEs), regular large solar energetic particle (SEP) events and filament eruption (FE) associated large SEP events have shown that SEP events are organized by spectral index of proton fluence spectra and by the average starting frequencies of the associated type II radio bursts. Both these results indicate a hierarchical relationship between CME kinematics and SEP event properties. In this study, we expand the investigations to fluence spectra and the longitudinal extent of metric type II associated SEP events including low-intensity SEP events. We utilize SEP measurements of particle instruments on the Solar and Heliospheric Observatory (SOHO) and Solar Terrestrial Relations Observatory (STEREO) spacecraft together with radio bursts observations by ground-based radio observatories during solar cycle 24. Our results show that low-intensity SEP events follow the hierarchy of spectral index or the hierarchy of the starting frequency of type II radio bursts. We also find indications of a trend between the onset frequency of metric type II bursts and the estimated longitudinal extent of the SEP events although the scatter of data points is quite large. These two results strongly support the idea of SEP acceleration by shocks. Stronger shocks develop closer to the Sun.
Table 1 Parameters of radio bursts, small SEP events, flares and CMEs. (2009-2017)

Direction-finding Analysis of the 2012 July 6 Type II Solar Radio Burst at Low Frequencies

Pertti **Mäkelä**1,2, Nat Gopalswamy2, and Sachiko Akiyama
2018 ApJ 867 40
sci-hub.tw/10.3847/1538-4357/aae2b6
The **2012 July 6** X1.1 flare at S13W59 and a halo coronal mass ejection (CME) with a space speed of ~1900 km s−1 were associated with type III and type II radio bursts. The metric-to-decametric type II radio burst extended down to ~5 MHz. Simultaneously, a slowly drifting feature with a harmonic structure was observed by Wind and Solar Terrestrial Relations Observatory radio receivers around and below 1 MHz, above the strong type III radio burst at lower frequencies. The radio direction-finding analysis of this lower-frequency interplanetary (IP) type II radio burst indicates that the radio source was located near the nose and possibly toward the southern flank of the CME-driven shock. These results provide an independent confirmation of the previous suggestions that when the metric and IP type II bursts are overlapping, the lower-frequency IP type II radio burst originates near the shock nose, whereas the source of the higher-frequency metric type II burst is closer to the Sun in the shock flank region. These results further support the idea that the coronal and IP type II bursts are produced by the same CME-driven shock.

Source Regions of the Type II Radio Burst Observed During a CME-CME Interaction on 2013 May 22

P. **Mäkelä**. N. Gopalswamy, M. J. Reiner, S. Akiyama, V. Krupar
ApJ **827** 141 **2016**
http://arxiv.org/pdf/1606.06989v1.pdf
We report on our study of radio source regions during the type II radio burst on **2013 May 22** based on direction finding (DF) analysis of the Wind/WAVES and STEREO/WAVES (SWAVES) radio observations at decameter-hectometric (DH) wavelengths. The type II emission showed an enhancement that coincided with interaction of two coronal mass ejections (CMEs) launched in sequence along closely spaced trajectories. The triangulation of the SWAVES source directions posited the ecliptic projections of the radio sources near the line connecting the Sun and the STEREO-A spacecraft. The WAVES and SWAVES source directions revealed shifts in the latitude of the radio source indicating that the spatial location of the dominant source of the type II emission varies during the CME-CME interaction. The WAVES source directions close to 1 MHz frequencies matched the location of the leading edge of the primary CME

seen in the images of the LASCO/C3 coronagraph. This correspondence of spatial locations at both wavelengths confirms that the CME-CME interaction region is the source of the type II enhancement. Comparison of radio and white-light observations also showed that at lower frequencies scattering significantly affects radio wave propagation.
See CESRA highlights #1042 Dec **2016** http://www.astro.gla.ac.uk/users/eduard/cesra/?p=1042

Estimating the Height of CMEs Associated with a Major SEP Event at the Onset of the Metric Type II Radio Burst during Solar Cycles 23 and 24

P. **Mäkelä**, N. Gopalswamy, S. Akiyama, H. Xie, and S. Yashiro
ApJ **2015**
http://cdaw.gsfc.nasa.gov/publications/makela/makela2015ApJ.pdf
We studied the coronal mass ejection (CME) height at the onset of 59 metric type II radio bursts associated with major solar energetic particle (SEP) events, excluding ground level enhancements (GLEs), during solar cycles 23 and 24. We calculated CME heights using a simple flare-onset method used by Gopalswamy et al. (2012b) to estimate CME heights at the metric type II onset for cycle-23 GLEs. We found the mean CME height for non-GLE events (1.72 R◎) to be ~12% greater than that (1.53 R◎) for cycle-23 GLEs. The difference could be caused by more impulsive acceleration of the GLE-associated CMEs. For cycle-24 non-GLE events, we compared the CME heights obtained using the flare-onset method and the 3-D spherical-shock fitting method and found the correlation to be good (CC=0.68). We found the mean CME height for cycle 23 non-GLE events (1.79 R◎) to be greater than for cycle 24 non-GLE events (1.58 R◎), but statistical tests do not definitely reject the possibility of coincidence. We suggest that the lower formation height of the shocks during cycle 24 indicates a change in the Alfvén speed profile because solar magnetic fields are weaker and e plasma density levels are closer to the surface than usual during cycle 24. We also found that complex type III bursts showing diminution of type III emission in the 7-14 MHz frequency range are more likely associated with events with the CME height at the type II onset above 2 R◎ , supporting suggestions that the CME/shock structure causes the feature. **Table. Event Data**

First observations and performance of the RPW instrument on board the Solar Orbiter mission

M. **Maksimovic**1, J. Souček2, T. Chust3, Y. Khotyaintsev4, M. Kretzschmar5,6, +++
A&A 656, A41 (**2021**)
The Radio and Plasma Waves (RPW) instrument on the ESA Solar Orbiter mission is designed to measure in situ magnetic and electric fields and waves from the continuum up to several hundred kHz. The RPW also observes solar and heliospheric radio emissions up to 16 MHz. It was switched on and its antennae were successfully deployed two days after the launch of Solar Orbiter on February 10, 2020. Since then, the instrument has acquired enough data to make it possible to assess its performance and the electromagnetic disturbances it experiences. In this article, we assess its scientific performance and present the first RPW observations. In particular, we focus on a statistical analysis of the first observations of interplanetary dust by the instrument's Thermal Noise Receiver. We also review the electro-magnetic disturbances that RPW suffers, especially those which potential users of the instrument data should be aware of before starting their research work.
CESRA #3215 **2022** https://www.astro.gla.ac.uk/users/eduard/cesra/?p=3215
11 Jul 2020

The Solar Orbiter Radio and Plasma Waves (RPW) instrument

M. **Maksimovic**1, S. D. Bale2,3,4, T. Chust5, Y. Khotyaintsev12, V. Krasnoselskikh6, ….
A&A 642, A12 (**2020**)
https://doi.org/10.1051/0004-6361/201936214
https://www.aanda.org/articles/aa/pdf/2020/10/aa36214-19.pdf
The Radio and Plasma Waves (RPW) instrument on the ESA Solar Orbiter mission is described in this paper. This instrument is designed to measure in-situ magnetic and electric fields and waves from the continuous to a few hundreds of kHz. RPW will also observe solar radio emissions up to 16 MHz. The RPW instrument is of primary importance to the Solar Orbiter mission and science requirements since it is essential to answer three of the four mission overarching science objectives. In addition RPW will exchange on-board data with the other in-situ instruments in order to process algorithms for interplanetary shocks and type III langmuir waves detections.

Interplanetary radio signatures and Solar Orbiter capabilities

Milan **Maksimovic**
CESRA Abstract **2016**
http://cesra2016.sciencesconf.org/conference/cesra2016/pages/CESRA2016_prog_abs_book_v1.pdf

I will review firstly the science objectives of the Radio & Plasmas Waves (RPW) instrument on the Solar Orbiter mission. Among those the study of the connectivity between the solar corona and the inner Heliosphere as close as from 0.3 AU is of prime importance. I will then present the RPW technical capabilities which will allow in-situ and remote sensing measurements related to the above objectives.

Langmuir wave harmonics due to driven nonlinear currents

David M. **Malaspina**1, Daniel B. Graham, 2, Robert E. Ergun1, Iver H. Cairns
JGR, Volume 118, Issue 11, pages 6880–6888, November **2013**
The conversion of Langmuir waves into electromagnetic radiation near the local plasma frequency (fpe) and twice the local plasma frequency (2fpe) occurs in diverse heliospheric environments including along the path of type III radio bursts, at interplanetary shocks, and in planetary foreshocks. This radiation has the potential to act as a probe of remote plasma conditions, provided that the conversion mechanism is well understood. One candidate conversion mechanism is the antenna radiation of localized Langmuir waves. Antenna radiation near 2fpe requires the presence of nonlinear currents at 2fpe. In this work, properties of these currents are predicted from theory and compared with observations of Langmuir wave electric fields made using the WAVES instrument on the STEREO spacecraft. It is found that the observed frequency structure, polarization, and wave number ratio are consistent with nonlinear current predictions, once electric fields near 2fpeconsistent with sheath effects are taken into account.

ANTENNA RADIATION NEAR THE LOCAL PLASMA FREQUENCY BY LANGMUIR WAVE EIGENMODES

David M. **Malaspina**1, Iver H. Cairns2, and Robert E. Ergun
2012 ApJ 755 45
Langmuir waves (LWs) in the solar wind are generated by electron beams associated with solar flares, interplanetary shock fronts, planetary bow shocks, and magnetic holes. In principle, LWs localized as eigenmodes of density fluctuations can emit electromagnetic (EM) radiation by an antenna mechanism near the local plasma frequency fp and twice the local plasma frequency. In this work, analytic expressions are derived for the radiated electric and magnetic fields and power generated near fp by LW eigenmodes. The EM wave power emitted near fp is predicted as a function of the eigenmode length scale L, maximum electric field, driving electron beam speed, and the ambient plasma density and temperature. The escape to a distant observer of fp radiation from a localized Langmuir eigenmode is also briefly explored as a function of the plasma conditions.

Three-dimensional reconstruction of type U radio bursts: a novel remote sensing approach for coronal loops

S. **Mancuso**, D. Barghini, A. Bemporad, D. Telloni, D. Gardiol, F. Frassati, I. Bizzarri, C. Taricco
A&A 669, A28 **2022**
https://arxiv.org/pdf/2212.02147.pdf
https://www.aanda.org/articles/aa/pdf/2023/01/aa43841-22.pdf
Type U radio bursts are impulsive coherent radio emissions produced by the Sun that indicate the presence of subrelativistic electron beams propagating along magnetic loops in the solar corona. In this work, we present the analysis of a type U radio burst that was exceptionally imaged on **2011 March 22** by the Nançay Radioheliograph (NRH) at three different frequencies (298.7, 327.0, and 360.8 MHz). Using a novel modelling approach, we show for the first time that the use of high-resolution radio heliograph images of type U radio bursts can be sufficient to both accurately reconstruct the 3D morphology of coronal loops (without recurring to triangulation techniques) and to fully constrain their physical parameters. At the same time, we can obtain unique information on the dynamics of the accelerated electron beams, which provides important clues as to the plasma mechanisms involved in their acceleration and as to why type U radio bursts are not observed as frequently as type III radio bursts. We finally present plausible explanations for a problematic aspect related to the apparent lack of association between the modeled loop as inferred from radio images and the extreme-ultraviolet (EUV) structures observed from space in the same coronal region

Radio evidence for a shock wave reflected by a coronal hole

S. **Mancuso**, A. Bemporad, F. Frassati, D. Barghini, S. Giordano, D. Telloni, C. Taricco
A&A 651, L14 **2021**
https://arxiv.org/pdf/2107.05931.pdf
https://www.aanda.org/articles/aa/pdf/2021/07/aa41387-21.pdf
https://doi.org/10.1051/0004-6361/202141387
We report the first unambiguous observational evidence in the radio range of the reflection of a coronal shock wave at the boundary of a coronal hole. The event occurred above an active region located at the northwest limb of the Sun and was characterized by an eruptive prominence and an extreme-ultraviolet (EUV) wave steepening into a shock. The EUV observations acquired by the Atmospheric Imaging Assembly (AIA) instrument on board the Solar Dynamics

Observatory(SDO) and the Extreme Ultraviolet Imager (EUVI) instrument on board the Solar TErrestrial RElations Observatory(STEREO-A) were used to track the development of the EUV front in the inner corona. Metric type II radio emission, a distinguishing feature of shock waves propagating in the inner corona, was simultaneously recorded by ground-based radio spectrometers. The radio dynamic spectra displayed an unusual reversal of the type II emission lanes, together with type III-like herringbone emission, indicating shock-accelerated electron beams. Combined analysis of imaging data from the two space-based EUV instruments and the Nancay Radioheliograph (NRH) evidences that the reverse-drifting typeiiemission was produced at the intersection of the shock front, reflected at a coronal hole boundary, with an intervening low-Alfvén-speed region characterized by an open field configuration. We also provide an outstanding data-driven reconstruction of the spatiotemporal evolution in the inner corona of the shock-accelerated electron beams produced by the reflected shock. **2011 August 11**

Three-dimensional reconstruction of CME-driven shock-streamer interaction from radio and EUV observations: a different take on the diagnostics of coronal magnetic fields

S. **Mancuso**, F. Frassati, A. Bemporad, D. Barghini
Astronomy & Astrophysics, Letters 624, L2 **2019**
https://arxiv.org/pdf/1903.06604.pdf
https://www.aanda.org/articles/aa/pdf/2019/04/aa35157-19.pdf
On **2014 October 30**, a band-splitted type II radio burst associated with a coronal mass ejection (CME) observed by the Atmospheric Imaging Assembly (AIA) on board the Solar Dynamic Observatory (SDO) occurred over the southeast limb of the Sun. The fast expansion in all directions of the plasma front acted as a piston and drove a spherical fast shock ahead of it, whose outward progression was traced by simultaneous images obtained with the Nançay Radioheliograph (NRH). The geometry of the CME/shock event was recovered through 3D modeling, given the absence of concomitant stereoscopic observations, and assuming that the band-splitted type II burst was emitted at the intersection of the shock surface with two adjacent low-Alfven speed coronal streamers. From the derived spatiotemporal evolution of the standoff distance between shock and CME leading edge, we were finally able to infer the magnetic field strength Bin the inner corona. A simple radial profile of the form $B(r)=(12.6\pm2.5)r^{-4}$ nicely fits our results, together with previous estimates, in the range $r=1.1-2.0$ solar radii.
CESRA #2212 June **2019** http://www.astro.gla.ac.uk/users/eduard/cesra/?p=2212

Combined Analysis of Ultraviolet and Radio Observations of the 7 May 2004 CME/Shock Event

Salvatore **Mancuso**
Solar Physics, Volume 273, Number 2, 511-523, **2011**
We report results from the combined analysis of UV and radio observations of a CME-driven shock observed on **7 May 2004** above the southeast limb of the Sun at 1.86 $R_\odot$ with the Ultraviolet Coronagraph Spectrometer (UVCS) on board the Solar and Heliospheric Observatory (SOHO). The coronal mass ejection (CME) was first detected in white-light by the SOHO's Large Angle and Spectrometric Coronagraph (LASCO) C2 telescope and shock-associated type II metric emission was recorded simultaneously by ground-based radio spectrographs. The shock speed (~ 690 km s^{-1}), as deduced from the analysis of the type II emission drift in the radio spectra and the pre-shock local electron density estimated with the diagnostics provided by UVCS observations of the O vi λλ 1031.9, 1037.6 doublet line intensities, is just a factor ~ 0.1 higher than the CME speed inferred by means of the white-light (and EUV) data in the middle corona. The local magnetosonic speed, computed from a standard magnetic field model, was estimated as high as ~ 600 km s^{-1}, implying that the CME speed was probably just sufficient to drive a weak fast-mode MHD shock ahead of the front. Simultaneously with the type II radio emission, significant changes in the O vi doublet line intensities and profiles were recorded in the UVCS spectra and found compatible with abrupt post-shock plasma acceleration and modest ion heating. This work provides further evidence for the CME-driven origin of the shocks observed in the middle corona.

Origin of the multiple metric type II radio burst structure associated with the 2002 July 23 CME

S. **Mancuso**, D. Avetta
Earth Moon Planets, 104 (**2009**), pp. 105–108

UV and Radio Observations of the Coronal Shock Associated with the 2002 July 23 Coronal Mass Ejection Event

S. **Mancuso** and D. Avetta

The Astrophysical Journal, Vol. 677, No. 1: 683-691, **2008**.
http://www.journals.uchicago.edu/doi/abs/10.1086/528839
We report on the analysis of a fast coronal mass ejection (CME)Ydriven shock observed on 2002 July 23 with the Ultraviolet Coronagraph Spectrometer (UVCS) on board the Solar and Heliospheric Observatory (SOHO). The CME was first detected in white light by the Large Angle and Spectrometric Coronagraph Experiment (LASCO), and shock-associated type II metric emission was recorded by several ground-based radio spectrographs. The evolution of the excess broadening of the O vi k1032 line profiles observed by UVCS at 1.63 R_ is consistent with the passage of a CME-driven shock surface enveloping a bubble-type, conically expanding CME, and its dynamics is found to be well associated with the complex, multiple type II radio emission detected in the metric band. Our results suggest that there might be a deficiency of ion heating in the present event with respect to what was observed in previous CME shocks detected by UVCS, and that this paucity might be attributed to different local plasma conditions, such as higher ambient coronal plasma _. We conclude that plasma _ could be an important parameter in determining the effect of ion heating at collisionless shock fronts in the solar corona.

Coronal transients and metric type II radio bursts - II. Accelerations at low coronal heights:

S. **Mancuso**
A&A 463 (**2007**) 1137-1141, **File**
In the companion Paper I, Mancuso & Raymond (2004A&A...413..363M) investigated the relationship between type ii and coronal mass ejection (CME) activity for a sample of twenty-nine CME/shock events that occurred between March and December 1999. Most of the events appeared to lead the type ii emission locations by several minutes and the two sets of speeds were not well-correlated, in apparent disagreement with a CME-driven origin interpretation of the coronal shocks. The above discrepancies were attributed to an artifact effect due to geometry, favoring emission at the flanks of the CME leading edges in correspondence with denser low-Alfven-speed coronal structures, where shock strengths are enhanced. An important caveat in the analysis carried out in Paper I is that the conclusions that supported the CME-driven shock front-flank scenario were based on sunward-extrapolated CME trajectories deduced from the analysis of Large Angle and Spectrometric Coronagraph (SOHO/LASCO) observations in the outer corona that might not be accurate at low coronal heights where significant accelerations should be present before the CMEs acquire the speeds inferred by coronagraphic images. In the present paper, we re-examine the above relationship for a subset of ten events by integrating the LASCO measurements with ancillary CME observations taken by other instruments (MLSO/Mk4, SOHO/EIT, and UVCS) at coronal heights comparable to the typical type ii radio emissions (1.2-2.5$R_{\odot}$). We investigate the bias introduced in the sunward extrapolation of LASCO data and discuss whether the presence of previously undetected CME accelerations at low coronal heights might have affected the conclusions put forth in the CME-driven shock front-flank scenario proposed in Paper I. We show that the new set of observations neither solve the problem of the timing between CMEs and shocks nor improve the correlation between CME and shock speeds, although acceleration effects are found to be important at the typical metric type ii heights and must be taken into account for a proper analysis of the CME/shock relationship.

Coronal transients and metric type II radio bursts. I. Effects of geometry

Mancuso, S., Raymond, J.C.:
2004, *Astron. Astrophys.* **413**, 363; **File**.
In this paper we investigate the relationship between type II and coronal transient activity in terms of emission originating from the top or the flanks of a bow/piston shock surface, extending just above the coronal mass ejection (CME) leading edge surface. For this purpose, we used ground-based metric type II radio burst observations of twenty-nine events in conjunction with Large Angle and Spectrometric Coronagraph (LASCO/SOHO) and UltraViolet Coronagraph Spectrometer (UVCS/SOHO) observations. With the refined density diagnostic offered by the UVCS instrument, we analyzed the type II dynamics in conjunction with the associated CME dynamics. Although we found some correlation, in all but a few cases the coronal transients appeared to lead the type II emission locations by several minutes, in apparent disagreement with a CME-driven origin interpretation. By applying a simple model, we found however that a piston-driven origin is certainly viable for all the events under study on the hypothesis that the radio emission originates in discrete locations above the top or the flanks of bow/piston shock surfaces extending just above the transient leading edges.

Bifurcation of the metric type II radio emission associated with the giant solar flare of April 2 2001

Mancuso, S.; Abbo, L.
Astronomy and Astrophysics, v.415, p.L17-L20 (**2004**); **File**
On **April 2 2001**, following one of the largest flares of the present solar cycle, intense and complex metric type II radio bursts were recorded by the Hiraiso Radio Spectrograph. Metric type II emission is a typical signature of the propagation of a coronal shock. The dynamic spectra of this event present a clear bifurcation of the radio emission lanes, which is very rare in the metric domain and requires a proper interpretation. We model this bifurcation as the

result of the interaction of a piston-driven spherical shock with a vertical current sheet located above the active region where the X20 flare occurred. The geometry of the expanding transient and the coronal electron density, necessary to derive the type II dynamics, are constrained through analysis of data obtained from the Solar and Heliospheric Observatory (SOHO) instruments. The model replicates successfully the observed bifurcation, supporting our interpretation. Furthermore, we propose that magnetic reconnection was triggered in the current sheet by the shock passage.

Parallel Evolution of Quasi-separatrix Layers and Active Region Upflows

C.H. **Mandrini**, D. Baker, P. Démoulin, G.D. Cristiani, L. van Driel-Gesztelyi, S. Vargas Domínguez, F.A. Nuevo, A.M. Vásquez, M. Pick

2015

http://arxiv.org/pdf/1507.01264v1.pdf

Persistent plasma upflows were observed with Hinode's EUV Imaging Spectrometer (EIS) at the edges of active region (AR) 10978 as it crossed the solar disk. We analyze the evolution of the photospheric magnetic and velocity fields of the AR, model its coronal magnetic field, and compute the location of magnetic null-points and quasi-sepratrix layers (QSLs) searching for the origin of EIS upflows. Magnetic reconnection at the computed null points cannot explain all of the observed EIS upflow regions. However, EIS upflows and QSLs are found to evolve in parallel, both temporarily and spatially. Sections of two sets of QSLs, called outer and inner, are found associated to EIS upflow streams having different characteristics. The reconnection process in the outer QSLs is forced by a large-scale photospheric flow pattern which is present in the AR for several days. We propose a scenario in which upflows are observed provided a large enough asymmetry in plasma pressure exists between the pre-reconnection loops and for as long as a photospheric forcing is at work. A similar mechanism operates in the inner QSLs, in this case, it is forced by the emergence and evolution of the bipoles between the two main AR polarities. Our findings provide strong support to the results from previous individual case studies investigating the role of magnetic reconnection at QSLs as the origin of the upflowing plasma. Furthermore, we propose that persistent reconnection along QSLs does not only drive the EIS upflows, but it is also responsible for a continuous metric radio noise-storm observed in AR 10978 along its disk transit by the Nan\c{c}ay Radio Heliograph. **9 to 14 December 2007**

How Can Active Region Plasma Escape into the Solar Wind from Below a Closed Helmet Streamerfl

C. H. **Mandrini**, F. A. Nuevo, A. M. Vásquez, P. Démoulin, L. van Driel-Gesztelyi, D. Baker, J. L. Culhane, G. D. Cristiani, M. Pick

E-print, Sept **2014**; Solar Phys., Volume 289, Issue 11, pp 4151-4171 **2014**

Recent studies show that active-region (AR) upflowing plasma, observed by the EUV-Imaging Spectrometer (EIS) onboard Hinode, can gain access to open-field lines and be released into the solar wind (SW) via magnetic-interchange reconnection at magnetic null-points in pseudo-streamer configurations. When only one bipolar AR is present on the Sun and is fully covered by the separatrix of a streamer, such as AR 10978 in **December 2007**, it seems unlikely that the upflowing AR plasma can find its way into the slow SW. However, signatures of plasma with AR composition have been found at 1 AU by Culhane et al. (Solar Phys. 289, 3799, 2014) that apparently originated west of AR 10978. We present a detailed topology analysis of AR 10978 and the surrounding large-scale corona based on a potential-field source-surface (PFSS) model. Our study shows that it is possible for the AR plasma to move around the streamer separatrix and be released into the SW via magnetic reconnection, which occurs in at least two main steps. We analyse data from the Nançay Radioheliograph (NRH) in a search for evidence of the chain of magnetic reconnections that we propose. We find a noise storm above the AR and several varying sources at 150.9 MHz. Their locations suggest that they might be associated with particles accelerated during the first-step reconnection process at a null point well outside of the AR. We find no evidence of the second reconnection step in the radio data, however. **Our results demonstrate that even when it appears highly improbable for the AR plasma to reach the SW, indirect channels involving a sequence of reconnections can make it possible.**

Kilometric type II radio emissions in Wind/WAVES TNR data and association with interplanetary structures near Earth

Franco **Manini**, Hebe Cremades, Fernando M. López, Teresa Nieves-Chinchilla

Solar Phys. **298**, 145 **2023**

https://arxiv.org/pdf/2311.08266.pdf

https://doi.org/10.1007/s11207-023-02235-1

Type II radio bursts arise as a consequence of shocks typically driven by coronal mass ejections (CMEs). When these shocks propagate outward from the Sun, their associated radio emissions drift down in frequency as excited particles emit at the local plasma frequency, creating the usual Type II patterns. In this work, we use dynamic spectra from the Wind/WAVES Thermal Noise Receiver (TNR) to identify Type II radio emissions in the kilometric wavelength range

(kmTIIs, f < 300 kHz) **between 1 January 2000 and 31 December 2012**, i.e. over a solar cycle. We identified 134 kmTII events and compiled various characteristics for each of them. Of particular importance is the finding of 45 kmTII events not reported by the official Wind/WAVES catalog (based on RAD1 and RAD2 data). We search for associations with interplanetary structures and analyze their main characteristics, in order to reveal distinctive attributes that may correlate with the occurrence of kmTII emission. We find that the fraction of interplanetary coronal mass ejections (ICMEs) classified as magnetic clouds (MCs) that are associated with kmTIIs is roughly similar to that of MCs not associated with kmTIIs. Conversely, the fraction of ICMEs with bidirectional electrons is significantly larger for those ICMEs associated with kmTIIs (74% vs. 48%). Likewise, ICMEs associated with kmTIIs are on average 23% faster. The disturbance storm time (DsT) mean value is almost twice as large for kmTII-associated ICMEs, indicating that they tend to produce intense geomagnetic storms. In addition, the proportion of ICMEs producing moderate to intense geomagnetic storms is twice as large for the kmTII-associated ICMEs. After this investigation, TNR data prove to be valuable not only as complementary data for the analysis of kmTII events but also for forecasting the arrival of shocks at Earth. **23-24 of January 2012**

Table 3.: List of the 134 identified kmTII events, their associations with shocks and ICMEs, and main characteristics

Type III radio bursts and excitation of Langmuir waves by energetic electrons

G. **Mann**, C. Vocks and A. Warmuth

A&A 660, A91 (**2022**)

https://doi.org/10.1051/0004-6361/202142804

https://www.aanda.org/articles/aa/pdf/2022/04/aa42804-21.pdf

Context. Solar activity occurs not only in terms of the well-known 11-year Sun spot cycle but also in terms of short-lived phenomena as radio bursts. For instance, type III radio bursts are the most common phenomenon of this activity in the Sun's radio radiation. In dynamic radio spectra, they appear as short-lived stripes of enhanced radio emission rapidly drifting from high to low frequencies. They are regarded as the radio signature of beams of energetic electrons travelling along magnetic field lines in the corona. The radio emission is thought to be plasma emission, that is to say the radio emission happens near the electron plasma frequency and/or its harmonics. Plasma emission means, that energetic electrons excite Langmuir waves, which convert into radio waves.

Aims. Initially, energetic electrons are injected in a small region in the corona. Due to their spatio-temporal evolution, they develop a beam-like velocity distribution function (VDF), which is able to excite Langmuir waves. The aim of the paper is to study the spatio-temporal behaviour of the generation of Langmuir waves under coronal cirumstances and its effect on type III radio bursts.

Methods. The generation of Langmuir waves is treated by means of the Maxwell-Vlasov equations. The results are discussed by employing plasma parameters usually found in the corona, for instance at the 150 MHz level.

Results. The Langmuir waves associated with the type III bursts are not generated by a monoenergetic electron beam, but by a population of energetic electrons with a broad velocity distribution. Hence, the Langmuir waves are produced by different parts of the energetic electron population at different times and positions.

Conclusions. In the case of type III bursts, the velocities derived from their drift rates in dynamic radio spectra are not the velocities of electrons, which generate the onset of the type III burst at a given frequency. That can lead to an apparent accelerated motion of the type III radio burst source.

Excitation of Langmuir waves at shocks and solar type II radio bursts

G. **Mann**1, C. Vocks1, A. Warmuth1, J. Magdalenic2,3, M. Bisi4, E. Carley5, B. Dabrowski6, P. Gallagher5, A. Krankowski6, B. Matyjasiak7, H. Rotkaehl7 and P. Zucca8

A&A 660, A71 (**2022**)

https://doi.org/10.1051/0004-6361/202142201

https://www.aanda.org/articles/aa/pdf/2022/04/aa42201-21.pdf

Context. In the solar corona, shocks can be generated due to the pressure pulse of a flare and/or driven by a rising coronal mass ejection (CME). Coronal shock waves can be observed as solar type II radio bursts in the Sun's radio radiation. In dynamic radio spectra, they appear as stripes of an enhanced radio emission slowly drifting from high to low frequencies. The radio emission is thought to be plasma emission, that is to say the emission happens near the electron plasma frequency and/or its harmonics. Plasma emission means that energetic electrons excite Langmuir waves, which convert into radio waves via non-linear plasma processes. Thus, energetic electrons are necessary for plasma emission. In the case of type II radio bursts, the energetic electrons are considered to be shock accelerated.

Aims. Shock drift acceleration (SDA) is regarded as the mechanism for producing energetic electrons in the foreshock region. SDA delivers a shifted loss-cone velocity distribution function (VDF) for the energetic electrons. The aim of the paper is to study in which way and under which conditions a shifted loss-cone VDF of electrons excites Langmuir waves in an efficient way in the corona.

Methods. By means of the results of SDA, the shape of the resulted VDF was derived. It is a shifted loss-cone VDF showing both a loss-cone and a beam-like component. The growth rates for exciting Langmuir waves were calculated in the framework of Maxwell-Vlasov equations. The results are discussed by employing plasma and shock parameters usually found in the corona at the 25 MHz level.

Results. We have found that moderate coronal shocks with an Alfven-Mach number in the range 1.59 < MA < 2.53 are able to accelerate electrons up to energies sufficient enough to excite Langmur waves, which convert into radio waves seen as solar type II radio bursts. **25 August 2014**

Tracking of an electron beam through the solar corona with LOFAR

G. **Mann**1, F. Breitling1, C. Vocks1, H. Aurass1, M. Steinmetz1, ……
A&A 611, A57 (**2018**)
https://www.aanda.org/articles/aa/pdf/2018/03/aa29017-16.pdf
http://sci-hub.tw/https://www.aanda.org/articles/aa/abs/2018/03/aa29017-16/aa29017-16.html
The Sun's activity leads to bursts of radio emission, among other phenomena. An example is type-III radio bursts. They occur frequently and appear as short-lived structures rapidly drifting from high to low frequencies in dynamic radio spectra. They are usually interpreted as signatures of beams of energetic electrons propagating along coronal magnetic field lines. Here we present novel interferometric LOFAR (LOw Frequency ARray) observations of three solar type-III radio bursts and their reverse bursts with high spectral, spatial, and temporal resolution. They are consistent with a propagation of the radio sources along the coronal magnetic field lines with nonuniform speed. Hence, the type-III radio bursts cannot be generated by a monoenergetic electron beam, but by an ensemble of energetic electrons with a spread distribution in velocity and energy. Additionally, the density profile along the propagation path is derived in the corona. It agrees well with three-fold coronal density model by (1961, ApJ, 133, 983). **June 23, 2012**

Radio signatures of shock-accelerated electron beams in the solar corona

G. **Mann**, V. N. Melnik, H. O. Rucker, A. A. Konovalenko and A. I. Brazhenko
A&A 609, A41 (**2018**)
https://www.aanda.org/articles/aa/pdf/2018/01/aa30546-17.pdf
Context. The Sun's activity can appear in terms of radio bursts. In the frequency range 8−33 MHz the radio telescope URAN-2 observed special fine structures appearing as a chain of stripes of enhanced radio emission in the dynamic radio spectrum. The chain drifts slowly from 26 to 23 MHz within 4 min. The individual structures consist of a "head" at the high-frequency edge and a "tail" rapidly drifting from the "head" to lower frequencies over an extent of ≈10 MHz within 8 s. Since they resemble the well-known "herring bones" in type II radio bursts, they are interpreted as shock accelerated electron beams.
Aims. The electron beams generating these fine structures are considered to be produced by shock drift acceleration (SDA). The beam electrons excite Langmuir waves which are converted into radio waves by nonlinear wave-plasma processes. That is called plasma emission. The aim of this paper is to link the radio spectral data of these fine structures to the theoretical results in order to gain a better understanding of the generation of energetic electrons by shocks in the solar corona.
Methods. Adopting SDA for generating energetic electrons, the accelerated electrons establish a beam-like velocity distribution. Plasma emission requires the excitation of Langmuir waves, which is efficient if the velocity of the beam electrons exceeds a few times thermal electron speed. That is the case if the angle between the shock normal and the upstream magnetic field is nearly perpendicular. Hence, the Rankine-Hugoniot relationships, which describe the shock transition in the framework of magnetohydrodynamics, are evaluated for the special case of nearly perpendicular shocks under coronal circumstances.
Results. The radio data deduced from the dynamic radio spectrum can be related in the best way to the theoretical results, if the electron beams, which generate these fine structures, are generated via SDA at an almost perpendicular shock, which is traveling nearly horizontally to the surface of the Sun. **April 7, 2011**

On a solar type III radio burst observed with LOFAR

Gottfried **Mann**∗1 , Richard Fallows2 , Frank Breitling3 , Christian Vocks3 , Mario Bisi4 , Peter Gallagher5 , Alain Kerdraon6 , Jasmina Magdalenic7 , Alec Mackinnon8 , Helmut Rucker9 , Alexandr Konovalenko10, Christophe Marque7 , Eduard Kontar8 , Bartosz Dabrowski11, Andrzej Krankowski12, Hamish Reid8 , and Bo Thide13
CESRA **2016** p.75
http://cesra2016.sciencesconf.org/conference/cesra2016/pages/CESRA2016_prog_abs_book_v3.pdf
A long lasting solar type III radio burst was observed in the frequency range 55-20 MHz in the spectrometer mode with LOFAR on **March 16, 2016**. The evaluation of the dynamic spectrum reveals that the type III burst is not generated by a monoenergetic electrons beam, but by an ensemble of electrons.

Interpretation of Tadpole Structures in the Solar Radio Radiation

Gottfried **Mann**∗1 , Viktor Melnik2 , Helmut H. O. Rucker3 , and Alexandr Konovalenko
CESRA **2016** p.74
http://cesra2016.sciencesconf.org/conference/cesra2016/pages/CESRA2016_prog_abs_book_v3.pdf
The new spectrometer on the Ukrainian radio telescope UTR-2 allows to observe the solar radio radiation at low frequencies (10-30 MHz) with a high spectral and temporal resolution. Tadpole structures were observed as special fine structures in the solar radio radiation. They show a fast drift (-2.13 MHz/s) in the dynamic radio spectrum. They appear as an ensemble of tadpoles drifting slowly (-8.3 kHz/s) from high to low frequencies. The tadpoles are interpreted as shock accelerated electron beams in the high corona. These electron beams are considered to be generated by shock drift acceleration. The comparison of the theoretical calculations and the observations leads to the conclusion that the shock associated with the tadpoles must be quasi-perpendicular.

Electron beams generated by shock waves in the solar corona.

Mann, G., Klassen, A.:
2005, *Astron. Astrophys.***441**, 319 – 326. doi:10.1051/0004-6361:20034396.

Formation and development of shock waves in the solar corona and the near-Sun interplanetary space

G. **Mann**, A. Klassen, H. Aurass, and H.-T. Classen
A&A 400, 329–336 (**2003**), **File**
At the Sun, shock waves are produced either by flares and/or by coronal mass ejections (CMEs) and are regarded as the source of solar energetic particle events. They can be able to generate solar type II radio bursts. The non-radial propagation of a disturbance is considered away from an active region through the corona into the interplanetary space by evaluating the spatial behaviour of the Alfv´en speed. The magnetic field of an active region is modelled by a magnetic dipole superimposed on that of the quiet Sun. Such a magnetic field structure leads to a local minimum of the Alfv´en speed in the range 1.2–1.8 solar radii in the corona as well as a maximum of 740 km s−1 at a distance of 3.8 solar radii. The occurrence of such local extrema has important consequences for the formation and development of shock waves in the corona and the near-Sun interplanetary space and their ability to accelerate particles. It leads to a temporal delay of the onset of solar energetic particle events with respect to both the initial energy release (flare) and the onset of the solar type II radio burst.

Coronal Transient Waves and Coronal Shock Waves

Mann, G.; Klassen, A.; Estel, C.; Thompson, B. J.
Proc. of 8th SOHO Workshop, ESA Special Publications 446, Edited by J.-C. Vial and B. Kaldeich-Schmann., p.477, **1999, File**
Coronal transient (or EIT) waves have been discovered by the EIT instrument aboard the SOHO spacecraft as a global wave phenomenon in the low corona. Most of them are associated with solar type II radio bursts appearing predominantly in the radio frequency range 40-100 MHz. Such type II radio bursts are signatures of shock waves travelling outwards in the upper corona. The mean EIT wave velocity of 290 km/s is well above the sound speed in the corona. Therefore, these waves are considered as fast magnetosonic waves propagating nearly perpendicular to the ambient magnetic field in the low corona. On the other hand, the type II burst related shock waves have mean velocities of 970 km/s, which must be well above the local Alfven speed. Considering both phenomena, i.e., coronal transient waves and type II burst related shock waves, to be caused by the same initial energy release (flare), these waves can be used as diagnostic tools for the magnetic field in the solar corona. Thus, a magnetic field strength of about 5 G is deduced from the EIT wave speeds at 0.08 solar radii above the photosphere. Such values are well expected above nonactive regions in the low corona. In the upper corona, i.e., at 0.5 solar radii above the photosphere, typical magnetic field strengths of about 2.5 G are deduced from the measurements. This value corresponds to a typical Alfven speed of 600-1000 km/s, which is well below the type II related shock speeds as expected.

Solar Radio Imaging at Arecibo: The Brightness Temperature and Magnetic Field of Active Regions

P. K. **Manoharan**, C. J. Salter, S. M. White, P. Perillat, F. Fernandez, B. Perera, A. Venkataraman, C. Brum
Solar Phys. 298, Article number: 124 **2023**
https://arxiv.org/pdf/2307.00328.pdf
https://doi.org/10.1007/s11207-023-02217-3
Strong solar magnetic fields are the energy source of intense flares and energetic coronal mass ejections of space weather importance. The key issue is the difficulty in predicting the occurrence time and location of strong solar eruptions, those leading to high impact space weather disturbances at the near-Earth environment. Here, we report

regular solar mapping made at X-band (8.1 -- 9.2 GHz) with the Arecibo 12-m radio telescope. This has demonstrated its potential for identifying active regions, about one half to a day in advance, when they rotate on to the central meridian of the Sun, and predicting the strongest flares and coronal mass ejections directed towards the Earth. Results show (i) a good correlation between the temporal evolution of brightness temperature of active regions and their magnetic configurations; (ii) the ability of the mapping data to provide a better picture of the formation sites of active regions and to accurately track their evolution across the solar disk, giving forewarning of intense solar eruptions leading to severe space weather consequences; (iii) the importance of long-term monitoring of the Sun at X-band for understanding the complex three-dimensional evolution of solar features as a function of solar activity. The key point in this study is the identification of the magnetic properties of active regions on the solar disk to aid in improving forecast strategies for extreme space-weather events. **29 March, 24 April, and 17 May 2022; 01-30 April 2022; 16 May 2022 and 03 January 2023**

Regular Solar Radio Imaging at Arecibo: Space Weather Perspective of Evolution of Active Regions

Periasamy K. **Manoharan**, Christopher J. Salter, Christiano M. Brum, Stephen M. White, Phil Perillat, Alfredo Santoni, Felix Fernandez, Tapasi Ghosh, Benetge Perera, Arun Venkataraman
White Paper Submitted to `Decadal Survey for Solar and Space Physics (Heliophysics) 2024-2033 **2022**
https://arxiv.org/pdf/2211.04472.pdf
The sudden release of magnetic energy on the Sun drives powerful solar flares and coronal mass ejections. The key issue is the difficulty in predicting the occurrence time and location of strong solar eruptions, i.e., those leading to the high impact space weather disturbances at the near-Earth environment. Solar radio imaging helps identify the magnetic field characteristics of active regions susceptible to intense flares and energetic coronal mass ejections. Mapping of the Sun at X-band (8.1 -- 9.3 GHz) with the 12-m radio telescope at the Arecibo Observatory allows monitoring of the evolution of the brightness temperature of active regions in association with the development of magnetic complexity, which can lead to strong eruptions. For a better forecasting strategy in the future, such ground-based radio observations of high-spatial and temporal resolution, along with a full polarization capability, would have tremendous potential not only to understand the magnetic activity of solar eruptions, but also for revealing the particle acceleration mechanism and additional exciting science.

Space Weather and Solar Wind Studies with OWFA **Review**

P. K. **Manoharan**, C. R. Subrahmanya, J. N. Chengalur
J. Astrophysics and Astronomy **2017**
https://arxiv.org/pdf/1703.00631.pdf
In this paper, we review the results of interplanetary scintillation (**IPS**) observations made with the legacy system of the Ooty Radio Telescope (ORT) and compare them with the possibilities opened by the upgraded ORT, the Ooty Wide Field Array (OWFA). The stability and the sensitivity of the legacy system of ORT allowed the regular monitoring of IPS on a grid of large number of radio sources and the results of these studies have been useful to understand the physical processes in the heliosphere and space weather events, such as coronal mass ejections, interaction regions and their propagation effects. In the case of OWFA, its wide bandwidth of 38 MHz, the large field of view of ∼27∘ and increased sensitivity provide a unique capability for the heliospheric science at 326.5 MHz. IPS observations with the OWFA would allow one to monitor more than 5000 sources per day. This, in turn, will lead to much improved studies of space weather events and solar wind plasma, overcoming the limitations faced with the legacy system. We also highlight some of the specific aspects of the OWFA, potentially relevant for the studies of coronal plasma and its turbulence characteristics.

Trieste CALLISTO station setup and observations of solar radio bursts

Marassi, Alessandro ; Monstein, Christian
Advances in Space Research, Volume 69, Issue 6, p. 2589-2600., **2022**
https://doi.org/10.1016/j.asr.2021.12.043
The Trieste CALLISTO station (http://radiosun.oats.inaf.it) was established in 2012 at the Basovizza Observing Station (45°38′37″ N, 13°52′34 E", 398 m above MSL) operated by the Italian National Institute for Astrophysics (INAF) - Astronomical Observatory of Trieste (Italy) to study solar radio bursts and the response of the Earth's ionosphere and geomagnetic field. To date, three 'Compound Astronomical Low-cost Low frequency Instrument for Spectroscopy and Transportable Observatory' (CALLISTO) spectrometers have been installed, with the capability of observing in the frequency ranges 45–80 MHz (from 30 December 2014), 220–420 MHz (from 1 June 2012 to 23 October 2012 and from 5 October 2013), 905–1730 MHz (from 30 December 2019). The three receivers are fed respectively by a dipole, log-periodic and cross-dipole antenna. Nominally, frequency spectra are obtained with 4 sweeps per second over in total 600 channels. Here, we describe the Trieste CALLISTO station setup, the local e-Callisto network digital archive, Trieste CALLISTO Radio Bursts Detection and Visualization System available via

web and present dynamic spectra of a sample of Type I, II, III, IV and V radio bursts. As an additional feature, we show also its capability to record lightning strikes.
CESRA #3339 Jun **2022** https://www.astro.gla.ac.uk/users/eduard/cesra/?p=3339 **2015-11-09**

Study of solar brightness profiles in the 18-26 GHz frequency range with INAF radio telescopes II. Evidence for coronal emission

M. **Marongiu**, A. Pellizzoni, S. Righini, S. Mulas, R. Nesti, A. Burtovoi, +++
A&A 684, A123 **2024**
https://arxiv.org/pdf/2402.07018.pdf
https://www.aanda.org/articles/aa/pdf/2024/04/aa48770-23.pdf

One of the most important objectives of solar physics is the physical understanding of the solar atmosphere, the structure of which is also described in terms of the density (N) and temperature (T) distributions of the atmospheric matter. Several multi-frequency analyses show that the characteristics of these distributions are still debated, especially for the outer coronal emission.
We aim to constrain the T and N distributions of the solar atmosphere through observations in the centimetric radio domain. We employ single-dish observations from two of the INAF radio telescopes at the K-band frequencies (18 - 26 GHz). We investigate the origin of the significant brightness temperature (TB) level that we detected up to the upper corona (∼800 Mm of altitude with respect to the photospheric solar surface).
To probe the physical origin of the atmospheric emission and to constrain instrumental biases, we reproduced the solar signal by convolving specific 2D antenna beam models. The analysis of the solar atmosphere is performed by adopting a physical model that assumes the thermal bremsstrahlung as the emission mechanism, with specific T and N distributions. The modelled TB profiles are compared with those observed by averaging solar maps obtained during the minimum of solar activity (2018 - 2020).
The T and N distributions are compatible (within 25% of uncertainty) with the model up to ∼60 Mm and ∼100 Mm of altitude, respectively. The analysis of the role of the antenna beam pattern on our solar maps proves the physical nature of the atmospheric emission in our images up to the coronal tails seen in our TB profiles. The challenging analysis of the coronal radio emission at higher altitudes, together with the data from satellite instruments will require further multi-frequency measurements. **2020-01-28, 2020-09-06**
Corrigendum **A&A, 686, C5 (2024)**

Study of solar brightness profiles in the 18-26 GHz frequency range with INAF radio telescopes I: solar radius

M. **Marongiu**, A. Pellizzoni, S. Mulas, S. Righini, R. Nesti, +++
A&A 684, A122 **2024**
https://arxiv.org/pdf/2401.13198.pdf
https://www.aanda.org/articles/aa/pdf/2024/04/aa48768-23.pdf

The Sun is an extraordinary workbench, from which several fundamental astronomical parameters can be measured with high precision. Among these parameters, the solar radius R⊙ plays an important role in several aspects, such as in evolutionary models. Despite the efforts in obtaining accurate measurements of R⊙, the subject is still debated and measurements are puzzling and/or lacking in many frequency ranges. We aimed to determine the mean, equatorial, and polar radii of the Sun (Rc, Req, and Rpol) in the frequency range 18.1 - 26.1 GHz. We employed single-dish observations from the newly-appointed Medicina "Gavril Grueff" Radio Telescope and the Sardinia Radio Telescope (SRT) throughout 5 years, from 2018 to mid-2023, in the framework of the SunDish project for solar monitoring. Two methods to calculate the radius at radio frequencies are considered and compared. To assess the quality of our radius determinations, we also analysed the possible degrading effects of the antenna beam pattern on our solar maps, using two 2D-models. We carried out a correlation analysis with the evolution of the solar cycle through the calculation of Pearson's correlation coefficient ρ. We obtained several values for the solar radius - ranging between 959 and 994 arcsec - and ρ, with typical errors of a few arcsec. Our R⊙ measurements, consistent with values reported in literature, suggest a weak prolatness of the solar limb (Req > Rpol), although Req and Rpol are statistically compatible within 3σ errors. The correlation analysis using the solar images from Grueff shows (1) a positive correlation between the solar activity and the temporal variation of Rc (and Req) at all observing frequencies, and (2) a weak anti-correlation between the temporal variation of Rpol and the solar activity at 25.8 GHz.

Solar radio emission as a disturbance of aeronautical radionavigation

C. **Marqué**, K.-L. Klein, C. Monstein, H. Opgenoorth, A. Pulkkinen, S. Buchert, S. Krucker, R. Van Hoof, P. Thulesen
Journal of Space Weather and Space Climate (JSWSC), 8, A42 **2018**
https://arxiv.org/pdf/1808.06878.pdf

On **November 4th 2015** secondary air traffic control radar was strongly disturbed in Sweden and some other European countries. The disturbances occurred when the radar antennas were pointing at the Sun. In this paper, we show that the

disturbances coincided with the time of peaks of an exceptionally strong (∼105 Solar Flux Units) solar radio burst in a relatively narrow frequency range around 1~GHz.
This indicates that this radio burst is the most probable space weather candidate for explaining the radar disturbances. The dynamic radio spectrum shows that the high flux densities are not due to synchrotron emission of energetic electrons, but to coherent emission processes, which produce a large variety of rapidly varying short bursts (such as pulsations, fiber bursts, and zebra patterns). The radio burst occurs outside the impulsive phase of the associated flare, about 30 minutes after the soft X-ray peak, and it is temporarily associated with fast evolving activity occurring in strong solar magnetic fields. While the relationship with strong magnetic fields and the coherent spectral nature of the radio burst provide hints towards the physical processes which generate such disturbances, we have so far no means to forecast them. Well-calibrated monitoring instruments of whole Sun radio fluxes covering the UHF band could at least provide a real-time identification of the origin of such disturbances, which reports in the literature show to also affect GPS signal reception.

The impact of the November 4th 2015 event on air traffic radars

Christophe **Marque**_y1, Karl Ludwig Klein2, Christian Monstein3, Hermann Opgenoorth4, Stephan Buchert4, Antti Pulkkinen5, and S□am Krucker6
CESRA **2016**, p.81
http://cesra2016.sciencesconf.org/conference/cesra2016/pages/CESRA2016_prog_abs_book_v3.pdf
On November 4th 2015, NOAA AR 12443 produced a relatively modest M3.7 are associated with one of the strongest L-band radio burst since 2011. This event had a severe impact on ATC radars operated in Sweden, triggering the closure of the swedish airspace for a couple of hours. We will present here the ongoing effort to analyse this event and to explain why these radars were so severely affected.

Solar observations at the Humain Radio Astronomy Station in Belgium

Christophe **Marque**∗1 , Jasmina Magdalenic1 , and Antonio Martinez Picar
CESRA **2016** p.55
http://cesra2016.sciencesconf.org/conference/cesra2016/pages/CESRA2016_prog_abs_book_v3.pdf
The Royal Observatory of Belgium performs daily solar radio observations for scientific and operational purposes at the Humain Radio Astronomy Station. Dynamic spectra that record non thermal emissions associated with solar eruptive events are produced in the range 45 - 1500 MHz. Two instruments are currently operated: an e-Callisto receiver covers the lower part of the band (45 - 440 MHz), and since the summer of 2015 a new digital receiver, named HSRS and based on a SDR device, monitors the upper part (275 - 1500 MHz). This poster presents these two instruments and gives examples of observations and instructions about accessing and processing the data. We briefly discuss the ongoing instrumental developments.

Multi wavelength investigation of the eruption of a sigmoidal quiescent filament*fl*

Ch. **Marque**, P. Lantos1, and J. P. Delaboudini_ere
A&A 387, 317{325 (**2002**), **File**
We report the _rst observation of a filament eruption in the metric and decimetric range, where the Behavior of the filament can be followed during the event via thermal radio emission diagnostics. The event, occurring on **February 28th 2001**, involved a quiescent filament in a sigmoid magnetic configuration, whose eruption is triggered by the birth of a small parasitic polarity. Faint radio bursts mark the beginning of the event, which shows the appearance of a brightness temperature depression associated with the filament seen in eit, and its propagation on the disk up to the limb. The event is associated with a halo CME observed with the coronagraphs lasco C2 and C3, which shows a significant spatial and temporal continuity with the radio observations. Finally, static dimmings, similar to what is currently observed in EUV or SXR domains, are also detected in the radio band, around the site of the eruption. Movies of the event are attached to this article.

An in-situ interplanetary U-burst: Observation and results

Juan Carlos **Martínez-Oliveros**, Saida Milena Diaz Castillo, Vratislav Krupar, Marc Pulupa, Stuart D. Bale, Benjamin Calvo Mozo
ApJ **2019**
https://arxiv.org/pdf/1910.04306.pdf
We report and examine the observation of an unusual and rare in-situ electron observation associated with a solar type III radio burst on **24 December 1996**. This radio event was accompanied by high energy electrons, measured by the Solid State Telescope (SST) on-board WIND spacecraft. The Type III radio emission started at ≈∼13:10~UT and was associated to a C2.1 GOES-class flare whose maximum was at 13:11~UT and hosted by the active region NOAA 8007/8004, located on the west limb at N05◦ W74◦/N06◦ W85◦. During this event, the observation of an electron

energy distribution likely to be associated with the radio emission was registered. The electrons arrive at the spacecraft predominantly from the anti-solar direction, suggesting that their general motion is Sunward along a closed magnetic field line. Leblanc et al. (1999) propose a model in which energetic electrons are injected into a coronal flux tube at one of its footpoints, releasing standard type-III emission. As the magnetic field then directs them back toward the magnetic-conjugate footpoint of the first, the electrons release subsequent emission whose radio profile is a quasi-time reversal of the standard. We have constructed a cylindrical flux-rope facsimile of this scenario that reproduces the U-burst profiles. We also report observational features indicating a secondary electron energy distribution and propose a scenario that explains this feature.

STEREO-Wind Radio Positioning of an Unusually Slow Drifting Event

J.C. **Martínez-Oliveros**, C. Raftery, H. Bain, Y. Liu, M. Pulupa, P. Saint-Hilaire, P. Higgins, V. Krupar, Säm Krucker, S.D. Bale

Solar Phys., Volume 290, Issue 3, pp 891-901 **2015**

http://arxiv.org/pdf/1410.3352v1.pdf

On **13 March 2010** an unusually long duration event was observed by radio spectrographs onboard the STEREO-B and Wind spacecraft. The event started at about 13:00 UT and ended at approximately 06:00 UT on 14 March. The event presents itself as slow drifting, quasi-continuous emission in a very narrow frequency interval, with an apparent frequency drift from about 625 kHz to approximately 425 kHz. Using the Leblanc, Dulk, and Bougeret (1998) interplanetary density model we determined that the drift velocities of the radio source are ≈33km s−1 and ≈52km s−1 for 0.2 and 0.5 times the densities of Leblanc model, respectively with a normalization density of 7.2cm−3 at 1AU and assuming harmonic emission. A joint analysis of the radio direction finding data, coronograph white-light observations and modeling revealed that the radio sources appear to be localized in regions of interaction with relatively high density and slow solar wind speed.

Determination of Electromagnetic Source Direction as an Eigenvalue Problem

Juan C. **Martínez-Oliveros**, Charles Lindsey, Stuart D. Bale and Säm Krucker

Solar Physics, Volume 279, Number 1 (**2012**), 153-171

Low-frequency solar and interplanetary radio bursts are generated at frequencies below the ionospheric plasma cutoff and must therefore be measured in space, with deployable antenna systems. The problem of measuring both the general direction and polarization of an electromagnetic source is commonly solved by iterative fitting methods such as linear regression that deal simultaneously with both directional and polarization parameters. We have developed a scheme that separates the problem of deriving the source direction from that of determining the polarization, avoiding iteration in a multi-dimensional manifold. The crux of the method is to first determine the source direction independently of concerns as to its polarization. Once the source direction is known, its direct characterization in terms of Stokes vectors, in a single iteration if desired, is relatively simple. This study applies the source-direction determination to radio signatures of flares received by STEREO. We studied two previously analyzed radio type III bursts and found that the results of the eigenvalue decomposition technique are consistent with those obtained previously by Reiner et al. (Solar Phys. 259, 255, 2009). For the type III burst observed on **7 December 2007**, the difference in travel times from the derived source location to STEREO A and B is the same as the difference in the onset times of the burst profiles measured by the two spacecraft. This is consistent with emission originating from a single, relatively compact source. For the second event of **29 January 2008**, the relative timing does not agree, suggesting emission from two sources separated by 0.1 AU, or perhaps from an elongated region encompassing the apparent source locations

The Formation Height of Millimetre-wavelength Emission in the Solar Chromosphere

Juan **Martinez-Sykora**, Bart De Pontieu, Jaime de la Cruz Rodriguez, Georgios Chintzoglou

ApJL **891** L8 **2020**

https://arxiv.org/pdf/2001.10645.pdf

https://doi.org/10.3847/2041-8213/ab75ac

In the past few years, the ALMA radio telescope has become available for solar observations. ALMA diagnostics of the solar atmosphere are of high interest because of the theoretically expected linear relationship between the brightness temperature at mm wavelengths and the local gas temperature in the solar atmosphere. Key for the interpretation of solar ALMA observations is understanding where in the solar atmosphere the ALMA emission originates. Recent theoretical studies have suggested that ALMA bands at 1.2 (band 6) and 3 mm (band 3) form in the middle and upper chromosphere at significantly different heights. We study the formation of ALMA diagnostics using a 2.5D radiative MHD model that includes the effects of ion-neutral interactions (ambipolar diffusion) and non-equilibrium ionization of hydrogen and helium. Our results suggest that in active regions and network regions, observations at both wavelengths most often originate from similar heights in the upper chromosphere, contrary to previous results. Non-equilibrium ionization increases the opacity in the chromosphere so that ALMA mostly observe spicules and fibrils along the

canopy fields. We combine these modeling results with observations from IRIS, SDO and ALMA to suggest a new interpretation for the recently reported "dark chromospheric holes", regions of very low temperatures in the chromosphere. **27 Apr 2017**

Extremely Microwave-Rich Solar Flare Observed with Nobeyama Radioheliograph

S. **Masuda**, M. Shimojo, T. Kawate, S. Ishikawa, and M. Ohno
Publ. Astron. Soc. Japan 65, 1 [6 pages] (**2013**)
http://pasj.asj.or.jp/v65/sp1/65S001/65S001.pdf
https://academic.oup.com/pasj/article/65/sp1/S1/2898369
A compact flare was observed with Nobeyama Radioheliograph (NoRH) slightly behind the west limb on **2011 March 10**. The microwave peak flux values at 17 and 34 GHz were about 210 and 133 sfu, respectively. From the correlation between the 17 GHz peak flux and the GOES 1–8 ˚A soft X-ray peak flux, M1.5-class is expected for this microwave flux. However, only the B1-level enhancement was detected in the GOES 1–8 ˚A soft X-ray light curve on the C1-level background during the flare period. In addition to microwaves, Suzaku detected hard X-ray emissions, even in the energy range above 100 keV. It is clear that high-energy electrons were effectively produced in this flare, while the thermal emission was very weak. Why did this flare have this unique feature? The following two cases are considered. One is the case that a magnetic trap for electrons works effectively, and that each electron continues to emit microwaves in its relatively long lifetime. The other is that the magnetic field around the looptop region is intense, and relatively a large number of lower-energy electrons emit microwaves. Considering the observational facts, such as the short duration and the small flare loop, the latter case is more plausible.

Microwave radio emissions as a proxy for coronal mass ejection speed in arrival predictions of interplanetary coronal mass ejections at 1 AU

Carolina Salas **Matamoros**1,2*, Karl Ludwig Klein1 and Gerard Trottet
J. Space Weather Space Clim., 7, A2 (**2017**)
http://www.swsc-journal.org/articles/swsc/pdf/2017/01/swsc160027.pdf
The propagation of a coronal mass ejection (CME) to the Earth takes between about 15 h and several days. We explore whether observations of non-thermal microwave bursts, produced by near-relativistic electons via the gyrosynchrotron process, can be used to predict travel times of interplanetary coronal mass ejections (ICMEs) from the Sun to the Earth. In a first step, a relationship is established between the CME speed measured by the Solar and Heliospheric Observatory/Large Angle and Spectrometric Coronagraph (SoHO/LASCO) near the solar limb and the fluence of the microwave burst. This relationship is then employed to estimate speeds in the corona of earthward-propagating CMEs. These speeds are fed into a simple empirical interplanetary acceleration model to predict the speed and arrival time of the ICMEs at Earth. The predictions are compared with observed arrival times and with the predictions based on other proxies, including soft X-rays (SXR) and coronographic measurements. We found that CME speeds estimated from microwaves and SXR predict the ICME arrival at the Earth with absolute errors of 11 ± 7 and 9 ± 7 h, respectively. A trend to underestimate the interplanetary travel times of ICMEs was noted for both techniques. This is consistent with the fact that in most cases of our test sample, ICMEs are detected on their flanks. Although this preliminary validation was carried out on a rather small sample of events (11), we conclude that microwave proxies can provide early estimates of ICME arrivals and ICME speeds in the interplanetary space. This method is limited by the fact that not all CMEs are accompanied by non-thermal microwave bursts. But its usefulness is enhanced by the relatively simple observational setup and the observation from ground, which makes the instrumentation less vulnerable to space weather hazards. **11 Apr 1997, 2002 Aug 23, 2003 Oct 24, 2004 Jun 16, 2008 Mar 25, 28 Oct 2011, 9 Mar 2012**
Table 1. Table of 41 events:
Table 3. Comparison between ICME arrival times measured at Wind spacecraft and predicted based on 9 GHz fluence:

Microwave emission as a proxy of CME speed in ICME arrival time predictions

Carolina Salas **Matamoros**_1,2, Karl-Ludwig Klein3,4, and G_erard Trottet3
CESRA **2016**, p.82
http://cesra2016.sciencesconf.org/conference/cesra2016/pages/CESRA2016_prog_abs_book_v3.pdf
The propagation of a coronal mass ejection (CME) to the Earth takes between about 13 hours and several days. Observations of early radiative signatures of CMEs therefore provide a possible means to predict the arrival time of the CME near Earth. The fundamental tool to measure CME speeds in the corona is coronography, but the Earthdirected speed of a CME cannot be measured by a coronagraph located on the Sun-Earth line. Various proxies have been devised, based on the coronographic measurement. As an alternative, we explore radiative proxies. In the present contribution we investigate if microwave observations can be employed as a proxy for CME propagation speed. Caroubalos (1964) had shown that the higher the uence of a solar radio burst near 3 GHz, the shorter is the time lapse between the solar event and the sudden commencement of a geomagnetic storm. We reconsider the relationship between CME speed and microwave uence for limb CMEs in cycle 23 and early

cycle 24. Then we use the microwave uence as a proxy of CME speed of Earth-directed CMEs, together with the empirical interplanetary acceleration model devised by Gopalswamy et al. (2001), to predict the CME arrival time at Earth. These predictions are compared with observed arrival times and with the predictions based on other proxies, including soft X-rays and coronographic measurements.

Calculated brightness temperatures of solar structures compared with ALMA and Metsähovi measurements

F. **Matković**, R. Brajša, M. Kuhar, A. O. Benz, H.-G. Ludwig, C. L. Selhorst, I. Skokić, D. Sudar, A. Hanslmeier

Astronomische Nachrichten/Astronomical Notes **2024**

https://arxiv.org/pdf/2402.18978.pdf

The Atacama Large Millimeter/submillimeter Array (ALMA) allows for solar observations in the wavelength range of 0.3−10 mm, giving us a new view of the chromosphere. The measured brightness temperature at various frequencies can be fitted with theoretical models of density and temperature versus height. We use the available ALMA and Metsähovi measurements of selected solar structures (quiet sun (QS), active regions (AR) devoid of sunspots, and coronal holes (CH)). The measured QS brightness temperature in the ALMA wavelength range agrees well with the predictions of the semiempirical Avrett−Tian−Landi−Curdt−Wülser (ATLCW) model, better than previous models such as the Avrett−Loeser (AL) or Fontenla−Avrett−Loeser model (FAL). We scaled the ATLCW model in density and temperature to fit the observations of the other structures. For ARs, the fitted models require 9%−13% higher electron densities and 9%−10% higher electron temperatures, consistent with expectations. The CH fitted models require electron densities 2%−40% lower than the QS level, while the predicted electron temperatures, although somewhat lower, do not deviate significantly from the QS model. Despite the limitations of the one-dimensional ATLCW model, we confirm that this model and its appropriate adaptations are sufficient for describing the basic physical properties of the solar structures.

Differences in physical properties of coronal bright points and their ALMA counterparts within and outside coronal holes

F. **Matković**, R. Brajša, M. Temmer, S. G. Heinemann, H.-G. Ludwig, S. H. Saar, C. L. Selhorst, I. Skokić, D. Sudar

A&A 670, A146 **2023**

https://arxiv.org/pdf/2212.09443.pdf

https://www.aanda.org/articles/aa/pdf/2023/02/aa44160-22.pdf

This study investigates and compares brightness and area of coronal bright points (CBPs) inside and outside of coronal holes (CHs) using the single-dish Band 6 observations by the Atacama Large Millimeter/submillimeter Array (ALMA), combined with extreme-ultraviolet (EUV) 193 A∘ filtergrams obtained by the Atmospheric Imaging Assembly (AIA) and magnetograms obtained by the Helioseismic and Magnetic Imager (HMI), both on board Solar Dynamics Observatory (SDO). The CH boundaries were extracted from the SDO/AIA images using the Collection of Analysis Tools for Coronal Holes (CATCH) and CBPs were identified in the SDO/AIA, SDO/HMI, and ALMA data. Measurements of brightness and areas in both ALMA and SDO/AIA images were conducted for CBPs within CHs and quiet Sun regions outside CHs. A statistical analysis of the measured physical properties resulted in a lower average CBP brightness in both ALMA and SDO/AIA data for CBPs within the CHs. Depending on the CBP sample size, the difference in intensity for the SDO/AIA data, and brightness temperature for the ALMA data, between the CBPs inside and outside CHs ranged from between 2σ and 4.5σ, showing a statistically significant difference between those two CBP groups. For CBP areas, CBPs within the CH boundaries showed smaller areas on average, with the observed difference between the two CBP groups between 1σ and 2σ for the SDO/AIA data, and up to 3.5σ for the ALMA data, indicating that CBP areas are also significantly different. Given the measured properties, we conclude that the CBPs inside CHs tend to be less bright on average, but also smaller in comparison to those outside of CHs. This conclusion might point to the specific physical conditions and properties of the local CH region around a CBP limiting the maximum achievable intensity (temperature) and size of a CBP. **2017-04-16, 2017-04-22**

Relationship of peak fluxes of solar radio bursts and X-ray class of solar flares: Application to early great solar flares

Keitarou **Matsumoto**, Satoshi Masuda, Masumi Shimojo, Hisashi Hayakawa

Publ. Astron. Soc. Jpn (**2023**)

https://arxiv.org/ftp/arxiv/papers/2310/2310.03135.pdf

Large solar flares occasionally trigger significant space-weather disturbances that affect the technological infrastructures of modern civilization, and therefore require further investigation. Although these solar flares have been monitored by satellite observations since the 1970s, large solar flares occur only infrequently and restrict systematic statistical research owing to data limitations. However, Toyokawa Observatory has operated solar radio observations at

low frequencies (at 3.75 and 9.4 GHz) since 1951 and captured the early great flares as solar radio bursts. To estimate the magnitudes of flares that occurred before the start of solar X-ray (SXR) observations with the Geostationary Operational Environmental Satellite (GOES) satellites, we show the relationship between microwave fluxes at 3.75 and 9.4 GHz and X-ray fluxes of flares that occurred after 1988. In total, we explored 341 solar flares observed with the Nobeyama Radio Polarimeters and Toyokawa Observatory from 1988-2014 and compared them with the SXR observations recorded by the GOES satellites. The correlation coefficient was approximately 0.7. Therefore, the GOES X-ray class can be estimated from the peak flux at 3.75 and 9.4 GHz with a large variance and an error of factor of 3 (1 sigma). Thus, for the first time, we quantitatively estimated the light curves of two early solar flares observed in 1956 February by the Toyokawa solar radio observations using the relationship between SXR thermal radiation and microwave nonthermal radiation (Neupert, 1968, ApJ, 153, 59). **1956 February 14 and 23**

Characteristics of the Accelerated Electrons Moving along the Loop Derived from Cyclical Microwave Brightenings at the Footpoints

Keitarou **Matsumoto**1, Satoshi Masuda1, and Takafumi Kaneko2
2023 ApJL 955 L39
https://iopscience.iop.org/article/10.3847/2041-8213/acf99c/pdf
https://arxiv.org/ftp/arxiv/papers/2310/2310.03090.pdf
Many particles are accelerated during solar flares. To understand the acceleration and propagation processes of electrons, we require the pitch-angle distributions of the particles. The pitch angle of accelerated electrons has been estimated from the propagation velocity of a nonthermal microwave source archived in Nobeyama Radioheliograph data. We analyzed a flare event (an M-class flare on **2014 October 22**) showing cyclical microwave brightenings at the two footpoint regions. Assuming that the brightenings were caused by the accelerated electrons, we approximated the velocity parallel to the magnetic field of the accelerated electrons as ∼7.7 × 104 and 9.0 × 104 km s −1. The estimated pitch angle of the accelerated electrons is 69°–80° and the size of the loss cone at the footpoint (estimated from the magnetic field strength in the nonlinear force-free field model) is approximately 43°. Most of the accelerated electrons could be reflected at the footpoint region. This feature can be interpreted as brightenings produced by bouncing motion of the accelerated electrons.
RHESSI Science Nuggets #459 2023
https://sprg.ssl.berkeley.edu/~tohban/wiki/index.php/Bouncing_motions_of_fast_electrons_using_Nobeyama_Radioheliograph

Radio Stars: from kHz to THz **Review**

Lynn D. **Matthews**
PASP **2018**
https://arxiv.org/pdf/1807.09798.pdf
Advances in technology and instrumentation have now opened up virtually the entire radio spectrum to the study of stars. An international workshop "Radio Stars: from kHz to THz" was held at the Massachusetts Institute of Technology Haystack Observatory on 2017 November 1-3 to enable the discussion of progress in solar and stellar astrophysics enabled by radio wavelength observations. Topics covered included the Sun as a radio star, radio emission from hot and cool stars (from the pre- to post-main-sequence), ultracool dwarfs, stellar activity, stellar winds and mass loss, planetary nebulae, cataclysmic variables, classical novae, and the role of radio stars in understanding the Milky Way. This article summarizes meeting highlights along with some contextual background information.

Radio Burst and Circular Polarization Studies of the Solar Corona at Low Frequencies

Patrick I. **McCauley**
Thesis **2019**
https://arxiv.org/pdf/1912.01747.pdf
Low-frequency (80-240 MHz) radio observations of the solar corona are presented using the Murchison Widefield Array (MWA), and several discoveries are reported. The corona is reviewed, followed by chapters on Type III bursts and circularly-polarized quiescent emission. The second chapter details new Type III burst dynamics. One source component at higher frequencies splits into two at lower frequencies, where the two components rapidly diverge. This is attributed to electron beams traversing a divergent magnetic field configuration, which is supported by extreme ultraviolet jet observations outlining a coronal null point. The third chapter uses Type III burst heights as density probes. Harmonic plasma emission implies ~4x enhancements over background models. This can be explained by electron beams traveling along dense fibers or by propagation effects that elevate apparent source heights. The quiescent corona is compared to model predictions to conclude that propagation effects can largely but not entirely explain the apparent density enhancements. The fourth chapter surveys over 100 spectropolarimetric observing runs. Around 700 compact sources are detected with polarization fractions from less than 0.5% to nearly 100%. They are interpreted as plasma emission noise storm sources down to levels not previously observable. A "bullseye" structure is reported for coronal holes, where an outer ring surrounds an oppositely-polarized central component that does not

match the sign expected of thermal bremsstrahlung. The large-scale polarization structure is shown to be well-correlated with that of a global magnetic field model. The last chapter summarizes results and outlines future work. A preliminary comparison of polarization images to model predictions is shared, along with coronal mass ejection observations revealing a radio arc that is morphologically similar to the white-light structure.

Chapter 2 Type III Solar Radio Burst Source Region Splitting due to a Quasi-separatrix Layer
Patrick I. McCauley, Iver H. Cairns, John Morgan, Sarah E. Gibson, James C. Harding, Colin Lonsdale, and Divya Oberoi Published in The Astrophysical Journal, 851:151 (**2017**)

Chapter 3 Densities Probed by Coronal Type III Radio Burst Imaging
Patrick I. McCauley, Iver H. Cairns, and John Morgan Published in Solar Physics, 293:132 (**2018**)

Chapter 4 The Low-Frequency Solar Corona in Circular Polarization
Patrick I. McCauley, Iver H. Cairns, Stephen M. White, Surajit Mondal, Emil Lenc, John Morgan, and Divya Oberoi Published in Solar Physics, 294:106 (**2019**)

The Low-Frequency Solar Corona in Circular Polarization

Patrick I. **McCauley**, Iver H. Cairns, Stephen M. White, Surajit Mondal, Emil Lenc, John Morgan, Divya Oberoi

Solar Phys. 294:106 **2019**

https://arxiv.org/pdf/1907.10878.pdf

sci-hub.se/10.1007/s11207-019-1502-y

We present spectropolarimetric imaging observations of the solar corona at low frequencies (80 - 240 MHz) using the Murchison Widefield Array (MWA). These images are the first of their kind, and we introduce an algorithm to mitigate an instrumental artefact by which the total intensity signal contaminates the polarimetric images due to calibration errors. We then survey the range of circular polarization (Stokes V) features detected in over 100 observing runs near solar maximum during quiescent periods. First, we detect around 700 compact polarized sources across our dataset with polarization fractions ranging from less than 0.5% to nearly 100%. These sources exhibit a positive correlation between polarization fraction and total intensity, and we interpret them as a continuum of plasma emission noise storm (Type I burst) continua sources associated with active regions. Second, we report a characteristic "bullseye" structure observed for many low-latitude coronal holes in which a central polarized component is surrounded by a ring of the opposite sense. The central component does not match the sign expected from thermal bremsstrahlung emission, and we speculate that propagation effects or an alternative emission mechanism may be responsible. Third, we show that the large-scale polarimetric structure at our lowest frequencies is reasonably well-correlated with the line-of-sight (LOS) magnetic field component inferred from a global potential field source surface (PFSS) model. The boundaries between opposite circular polarization signs are generally aligned with polarity inversion lines in the model at a height roughly corresponding to that of the radio limb. This is not true at our highest frequencies, however, where the LOS magnetic field direction and polarization sign are often not straightforwardly correlated.

2014-08-28-30, 2014-09-17, 2014-10-21, 2014-10-24, 2014-11-13-15, 2014-11-21, 2014-11-25, 2015-08-31, 2015-09-03, 2015-09-08, 2015-09-10, 2015-09-14, 2015-09-21-23, 2015-10-05, 2015-10-20, 2015-11-09, 2015-11-11, 2015-11-12, 2015-11-17, 2015-12-08-09

Densities Probed by Coronal Type III Radio Burst Imaging

Patrick I. **McCauley**, Iver H. Cairns, John Morgan

Solar Phys. 293:132 **2018**

https://arxiv.org/pdf/1808.04989.pdf

https://link.springer.com/content/pdf/10.1007%2Fs11207-018-1353-y.pdf

We present coronal density profiles derived from low-frequency (80-240 MHz) imaging of three type III solar radio bursts observed at the limb by the Murchison Widefield Array (MWA). Each event is associated with a white light streamer at larger heights and is plausibly associated with thin extreme ultraviolet rays at lower heights. Assuming harmonic plasma emission, we find average electron densities of 1.8 x10^8 cm^-3 down to 0.20 x10^8 cm^-3 at heights of 1.3 to 1.9 solar radii. These values represent roughly 2.4-5.4x enhancements over canonical background levels and are comparable to the highest streamer densities obtained from data at other wavelengths. Assuming fundamental emission instead would increase the densities by a factor of 4. High densities inferred from type III source heights can be explained by assuming that the exciting electron beams travel along overdense fibers or by radio propagation effects that may cause a source to appear at a larger height than the true emission site. We review the arguments for both scenarios in light of recent results. We compare the extent of the quiescent corona to model predictions to estimate the impact of propagation effects, which we conclude can only partially explain the apparent density enhancements. Finally, we use the time- and frequency-varying source positions to estimate electron beam speeds of between 0.24 and 0.60 c. **2014.10.14, 2015.09.23, 2015.10.27**

CESRA nugget #2032 Nov 2018 http://cesra.net/?p=2032

Type III Solar Radio Burst Source Region Splitting Due to a Quasi-Separatrix Layer

Patrick I. **McCauley**, Iver H. Cairns, John Morgan, Sarah E. Gibson, James C. Harding, Colin Lonsdale, Divya Oberoi
ApJ **851** 151 **2017**
https://arxiv.org/pdf/1711.04930.pdf
We present low-frequency (80-240 MHz) radio imaging of type III solar radio bursts observed by the Murchison Widefield Array (MWA) on **2015/09/21**. The source region for each burst splits from one dominant component at higher frequencies into two increasingly-separated components at lower frequencies. For channels below ~132 MHz, the two components repetitively diverge at high speeds (0.1-0.4 c) along directions tangent to the limb, with each episode lasting just ~2 s. We argue that both effects result from the strong magnetic field connectivity gradient that the burst-driving electron beams move into. Persistence mapping of extreme ultraviolet (EUV) jets observed by the Solar Dynamics Observatory reveals quasi-separatrix layers (QSLs) associated with coronal null points, including separatrix dome, spine, and curtain structures. Electrons are accelerated at the flare site toward an open QSL, where the beams follow diverging field lines to produce the source splitting, with larger separations at larger heights (lower frequencies). The splitting motion within individual frequency bands is interpreted as a projected time-of-flight effect, whereby electrons traveling along the outer field lines take slightly longer to excite emission at adjacent positions. Given this interpretation, we estimate an average beam speed of 0.2 c. We also qualitatively describe the quiescent corona, noting in particular that a disk-center coronal hole transitions from being dark at higher frequencies to bright at lower frequencies, turning over around 120 MHz. These observations are compared to synthetic images based on the Magnetohydrodynamic Algorithm outside a Sphere (MAS) model, which we use to flux-calibrate the burst data.
RHESSI Nuggets #311 November **2017**
http://sprg.ssl.berkeley.edu/~tohban/wiki/index.php/Unusual_Type_III_Burst_Dynamics_Produced_by_Diverging_Magnetic_Fields

GPU-based high-performance imaging for Mingantu spectral radioheliograph.

Mei Y, Wang F, Wang W, Chen L, Liu Y, Deng H, Dai W, Liu C, Yan Y.
Publications of the Astronomical Society of the Pacific (PASP). **2018**. 130(1): 014503.
https://iopscience.iop.org/article/10.1088/1538-3873/aa9608/pdf
https://doi.org/10.1088/1538-3873/aa9608
As a dedicated solar radio interferometer, the MingantU SpEctral RadioHeliograph (MUSER) generates massive observational data in the frequency range of 400 MHz–15 GHz. High-performance imaging forms a significantly important aspect of MUSER's massive data processing requirements. In this study, we implement a practical high-performance imaging pipeline for MUSER data processing. At first, the specifications of the MUSER are introduced and its imaging requirements are analyzed. Referring to the most commonly used radio astronomy software such as CASA and MIRIAD, we then implement a high-performance imaging pipeline based on the Graphics Processing Unit technology with respect to the current operational status of the MUSER. A series of critical algorithms and their pseudo codes, i.e., detection of the solar disk and sky brightness, automatic centering of the solar disk and estimation of the number of iterations for clean algorithms, are proposed in detail. The preliminary experimental results indicate that the proposed imaging approach significantly increases the processing performance of MUSER and generates images with high-quality, which can meet the requirements of the MUSER data processing.
The MUSER was built at Mingantu in Inner Mongolia, China.

Spectral features of a single Type III burst in the frequency range of 10-70 MHz

Valentin **Melnik**, Anatolii Brazhenko, Vladimir Dorovskyy, Anatolii Frantsuzenko, Mykola Shevchuk, Sergii Yerin, and Igor Bubnov
Front. Astron. Space Sci., Volume 11 : 1369003 **2024**
https://doi.org/10.3389/fspas.2024.1369003
https://www.frontiersin.org/journals/astronomy-and-space-sciences/articles/10.3389/fspas.2024.1369003/full
Spectral properties of a single type III burst in the wide frequency band from 10 to 70 MHz are studied in detail. It is shown that electrons corresponding to different levels of type III emission move with different velocities. Moreover, these electron velocities decrease from the maximum value, which corresponds to the 0.1 level of the maximum type III flux at its front, to the minimum value, corresponding to the 0.1 level of the maximum type III flux at its back. The velocity of electrons corresponding to the maximum type III flux was approximately 0.31 c. This value equals 0.6 of maximum velocity, and, namely, it was predicted by the gas dynamic theory of electron propagation through the coronal plasma. In addition, we adduce arguments that the type III radio emission is the harmonic emission. In supposition that type III electrons move through the Newkirk coronal plasma, we find electron velocities for every level of the type III burst. The duration dependence on frequency obtained from the observations is close to Elgaroy–Lingstad dependence. We discuss the contribution of electron velocity dispersion to the type III burst duration. In addition, we derived type III flux dependence on frequency in the frequency bands of 10–33 MHz and 33–62 MHz.

Properties of Type III and Type IIIb Bursts in the Frequency Band of 8-80 MHz during PSP Perihelion at the Beginning of April 2019

V.N.**Melnik**, A.I. Brazhenko, A.A. Konovalenko, A.V. Frantsuzenko, S.M. Yerin, V.V. Dorovskyy, I.M. Bubnov

Solar Physics **volume 296**, Article number: 9 **2021**

https://arxiv.org/ftp/arxiv/papers/2012/2012.08495.pdf

https://link.springer.com/content/pdf/10.1007/s11207-020-01754-5.pdf

Properties of type III and type IIIb bursts in the frequency band of 8-80 MHz observed by the radio telescopes Ukrainian Radio Interferometer of NASU-2 (URAN-2) (Poltava) and Giant Ukrainian Radio Telescope (GURT) (Kharkiv) during the Parker Solar Probe (PSP) perihelion in April 2019 are discussed. These correspond of those that were observed by PSP at frequencies <19 MHz. We analyze dependences of drift rates and durations on frequency for these bursts. We show that drift rate dependences on frequency agree well with those derived from the Newkirk corona if source velocities are between 0.17 and 0.2 c for both type IIIb bursts and type III bursts under the assumption that the first ones are fundamentals and the second ones are their harmonics. However, all observational dependences are flatter in comparison with the dependences for a Newkirk corona. We assume that this can be related with coronal temperature decreasing at heliocentric distances from 1.35 to 6.5 solar radii. Duration dependencies of type IIIb and type III bursts on frequency in the range of 10-70 MHz are also obtained. We note that the durations and drift rates of type III bursts as well as their dependences on frequency differ essentially from those for type IIIb bursts. **6-9 April 2019**

Radio Signature of a Distant behind-the-limb CME on 2017 September 6

V. N. **Melnik**1, H. O. Rucker2, A. I. Brazhenko3, M. Panchenko4, A. A. Konovalenko1, A. V. Frantsuzenko3, V. V. Dorovskyy1, and M. V. Shevchuk1

2020 *ApJ* **905** 10

https://arxiv.org/ftp/arxiv/papers/2012/2012.04706.pdf

https://doi.org/10.3847/1538-4357/abbfb3

We discuss properties of a Type IV burst, which was observed on **2017 September 6**, as a result of the powerful flare X 9.3. At decameter wavelengths this burst was observed by the radio telescopes STEREO A, URAN-2, and the Nancay Decameter Array at frequencies 5–35 MHz. This moving Type IV burst was associated with a coronal mass ejection (CME) propagating in the southwest direction with a speed of 1570 km s−1. The maximum radio flux of this burst was about 300 s.f.u. and the polarization was more than 40%. In the frequency range of 8–33 MHz it continued for more than 2 hr. For STEREO A the associated CME was behind the limb, and its longitudinal angle was about 160°. This moving Type IV burst was observed by STEREO A at frequencies of 5–15 MHz in spite of the low sensitivity of STEREO A. This means that the radio emission directivity of a Type IV burst is rather wide. Assuming the plasma mechanism of Type IV radio emission we derived the plasma density distribution in the CME core at distances of 5.6 Rs and 9.8 Rs (Rs is the solar radius), and its mass to be about 1016 g. It is planned that the minimum perihelion of the Parker Solar Probe (PSP) spacecraft will be at about 9 Rs . So we discuss in what conditions PSP will be in if it crosses a similar CME core.

First observation of the solar Type III burst decay and its interpretation

Valentin N. **Melnik**, Alexandr A. Konovalenko, Sergey M. Yerin, Igor M. Bubnov, Anatoliy I. Brazhenko, Anatoliy V. Frantsuzenko, Vladimir V. Dorovskyy, Mykola V. Shevchuk,

2019 *ApJ* **885** 78

https://arxiv.org/ftp/arxiv/papers/1909/1909.13073.pdf

https://doi.org/10.3847/1538-4357/ab46aa

A decay of Type III burst into two Type III bursts was registered during solar observations by GURT and URAN-2 radio telescopes on **April 18, 2017**. Such phenomenon was observed for the first time. Newborn Type III bursts have drift rates smaller than that of decaying Type III burst. Such decays of Type III bursts were predicted by a gas-dynamic theory of high-energy electron beams propagating through the thermal background plasma. In the frame of this theory Type III sources are beam-plasma structures moving with constant velocities. In our case the sum of velocities of newborn Type III sources equals the velocity of decaying Type III source. The last one is 0.33c in the case of fundamental radio emission and 0.2c at the harmonic radio emission of Type III burst. The density ratio of slow and fast newborn Type III sources is about 3.

CESRA #2451 Jan **2020** http://cesra.net/?p=2451

Interferometric Observations of the Quiet Sun at 20 and 25 MHz in May 2014

V.N. **Melnik**, V.A. Shepelev, S. Poedts, V.V. Dorovskyy, A.I. Brazhenko, H.O. Rucker

Solar Phys. 293:97 **2018**

https://arxiv.org/pdf/1806.08660.pdf

Results of solar observations at 20 and 25 MHz by the UTR-2 (\textit{Ukrainian T-shaped Radio telescope of the second modification}) radio telescope in the interferometric session from 27 May to 2 June 2014 are presented. In such

a case the different baselines 225, 450, and 675 m between sections of East--West and North--South arms of the radio telescope UTR-2 were used. On 29 May 2014, strong sporadic radio emission consisting of Type III, a Type II and a Type IV bursts was observed. On other days there was no solar radio activity in the decameter range. We discuss the results of observations of such the quiet Sun. Fluxes and sizes of the Sun in East--West and North--South directions were measured. The average fluxes were 1050--1100 Jy and 1480--1570 Jy at 20 and 25 MHz, respectively. Angular sizes of the quiet Sun in equatorial and polar directions were 55' and 49' at 20 MHz and 50' and 42' at 25 MHz. Brightness temperatures of radio emission were Tb = 5.1 10^5 K and Tb = 5.7 10^5 K at 20 and 25 MHz, respectively. **27-30 May 2014**

Decameter Type IV Burst Associated with a behind-the-limb CME Observed on 7 November 2013

V.N.**Melnik**, A.I.Brazhenko, A.A.Konovalenko, V.V.Dorovskyy, H.O.Rucker, M.Panchenko, A.V.Frantsuzenko, M.V. Shevchuk

Solar Phys. 293:53 **2018**

https://arxiv.org/ftp/arxiv/papers/1803/1803.01147.pdf

https://link.springer.com/content/pdf/10.1007%2Fs11207-018-1271-z.pdf

We report on the results of observations of a type IV burst by URAN-2 (Ukrainian Radio interferometer of Academy Scienses) in the frequency range 22 - 33 MHz, which is associated with the CME (coronal mass ejection) initiated by a behind-the-limb active region (N05E151). This burst was observed also by the radio telescope NDA (Nancay Decameter Array) in the frequency band 30 - 60 MHz. The purpose of the article is the determination of the source of this type IV burst. After analysis of the observational data obtained with the URAN-2, NDA, STEREO (Solar-Terrestrial Relations Observatory) A and B spacecraft, and SOHO (Solar and Heliospheric Observatory) spacecraft we come to the conclusion that it is a core of a behind-the-limb CME. We conclude that the radio emission can escape the center of the CME core at a frequency of 60 MHz and originates from the periphery of the core at frequency 30 MHz due to occultation by the solar corona at corresponding frequencies. We find plasma densities in these regions supposing the plasma mechanism of radio emission. We show that the frequency drift of the start of the type IV burst is governed by an expansion of the CME core. Type III bursts, which were observed against this type IV burst, are shown to be generated by fast electrons propagating through the CME core plasma. A type II burst registered at frequencies 44 - 64 MHz and 3 - 16 MHz was radiated by a shock with a velocity of about 1000 km s^{-1} and 800 km s^{-1}, respectively.

Decameter Type III Bursts with Changing Frequency Drift-Rate Signs

V.N.**Melnik**, A.I.Brazhenko, A.A.Konovalenko, C.Briand, V.V.Dorovskyy, P.Zarka, A.V.Frantsuzenko, H.O.Rucker, B.P.Rutkevych, M.Panchenko, L.Denis,T.Zaqarashvili, B.Shergelashvili

Solar phys. **2018**

https://arxiv.org/ftp/arxiv/papers/1802/1802.08336.pdf

We discuss properties of type III bursts which change sign of their drift rate from negative to positive and vice versa. Moreover such bursts may change sign of their drift rates more than once. These specific type III bursts were observed simultaneously by radio telescopes UTR-2, URAN-2 and NDA in frequency band 8-41 MHz. The negative drift rates of these bursts are close to those of usual decameter type III bursts and variate from -0.84 MHz/s to -5.56 MHz/s. The positive drift rates of specific type III bursts vary in the wider range from 0.44MHz/s to 12 MHz/s. Unlike inverted U-bursts these type III bursts still drift from the high frequencies to the low frequencies in spite of the change of the drift rates signs. Our basic explanation of the positive drift rate of these type III burst differs from the common assumption that positive drift rates of Type III bursts are connected with electron beam propagation towards the Sun. We propose that, even if electron beams move outward from the Sun, they can generate type III bursts with positive drift rates if in some regions of the solar corona the group velocities of type III radio emissions are lower than the velocities of the electron beams. **June 3, 2012, August 25, 2012, August 26, 2012**

Decameter Type III-Like Bursts

V.N.**Mel'Nik**, A.A.Konovalenko, H.O.Rucker, B.P.Rutkevych, V.V.Dorovskyy, E.P.Abranin, A.I.Brazhenko, A.A.Stanislavskii, A.Lecacheux

2018

https://arxiv.org/ftp/arxiv/papers/1802/1802.07311.pdf

We report the first observations of Type III-like bursts at frequencies 10-30 MHz. More than 1000 such bursts during 2002-2004 have been analyzed. The frequency drift of these bursts is several times that of decameter Type III bursts. A typical duration of the Type III-like bursts is 1-2 s. These bursts are mainly observed when the source active region is located within a few days from the central meridian. The drift rate of the Type III-like bursts can take a large value by considering the velocity of Type III electrons and the group velocity of generated electromagnetic waves. **13,26,28 July 2002, 18 Aug 2002**

Table 1. Number and occurrence rate of Type III-like bursts observed during five storm events of Type III bursts in 2002 – 2004.

Solar Type IV bursts at frequencies 10-30 MHz

V.N. **Melnik**, H. O. Rucker, A. A. Konovalenko, V.V. Dorovskyy, E.P. Abranin, A.I. Brazhenko, B.Thide, A. A. Stanislavskyy

2018

https://arxiv.org/ftp/arxiv/papers/1802/1802.06249.pdf

The results of the first observations of Type IV bursts at frequencies 10-30 MHz are presented. These observations were carried out at radio telescopes UTR-2 (Kharkov, Ukraine) and URAN-2 (Poltava, Ukraine) during the period 2003-2006. Detection of Type IV bursts in wide band from 10 to 30MHz with high sensitivity and time resolution allowed to study their properties in details. These bursts have fluxes 10-2000s.f.u. at maximum phase. Their durations are about 1-2 hours and even more. Some of Type IV bursts drift from high to low frequencies with drift rates about 10kHz/s. All observed Type IV bursts have fine structures in the form of sub-bursts with durations from 2s to 20s and frequency drift rates in a majority of 1-2MHz/s. In most cases, sub-bursts with negative drift rates were registered. Sometimes sub-bursts in absorption with durations 10-200s against Type IV burst background have been observed. The Type IV burst observed on **July 22, 2004** had zebra structure, in which single zebra stripes had positive, negative and infinite drift rates. **13 June 2003, July 22, 2003, August 3, 2003, August 19, 2003, June 4, 2004, July 13, 2004, July 21, 2004, July 22, 2004, July 23, 2005, July 27, 2005, July 28, 2005, July 31, 2005, 06 July 2006**

Properties of Decameter IIIb–III Pairs

V. N. **Melnik**, A. I. Brazhenko, A. V. Frantsuzenko, V. V. Dorovskyy, H. O. Rucker

Solar Physics February **2018**, 293:26

https://link.springer.com/content/pdf/10.1007%2Fs11207-017-1234-9.pdf

https://arxiv.org/ftp/arxiv/papers/1802/1802.06238.pdf

A large number of Type IIIb–III pairs, in which the first component is a Type IIIb burst and the second one is a Type III burst, are often recorded during decameter Type III burst storms. From the beginning of their observation, the question of whether the components of these pairs are the first and the second harmonics of radio emission or not has remained open. We discuss properties of decameter IIIb–III pairs in detail to answer this question. The components of these pairs, Type IIIb bursts and Type III bursts, have essentially different durations and polarizations. At the same time their frequency drift rates are rather close, provided that the drift rates of Type IIIb bursts are a little larger those of Type III bursts at the same frequency. Frequency ratios of the bursts at the same moment are close to two. This points at a harmonic connection of the components in IIIb–III pairs. At the same time there was a serious difficulty, namely why the first harmonic had fine frequency structure in the form of striae and the second harmonic did not have it. Recently Loi, Cairns, and Li (Astrophys. J.790, 67, 2014) succeeded in solving this problem. The physical aspects of observational properties of decameter IIIb–III pairs are discussed and pros and cons of harmonic character of Type IIIb bursts and Type III bursts in IIIb–III pairs are presented. We conclude that practically all properties of the IIIb–III pair components can be understood in the framework of the harmonic relation of the components of the IIIb–III pairs.

3 Apr 2011, 5 June 2011, 5 Sept 2011

CESRA nugget #1875 May **2018** http://cesra.net/?p=1875

Decameter type IV burst associated with behind-limb CME observed on November 7, 2013

Melnik V., Brazhenko A., Dorovskyy V., Rucker H., Panchenko M., Frantsuzenko A., Shevchuk M..

Proceedings of Ninth Workshop "Solar Influences on the Magnetosphere, Ionosphere and Atmosphere" Sunny Beach, Bulgaria, May 30 - June 3, **2017**, p. 13-18

http://ws-sozopol.stil.bas.bg/2017Sunny/Proceedings2017_V3.pdf

We report the results of observations of type IV burst by URAN-2 in the frequency range 22÷33 MHz, which is associated with the CME initiated by behind-limb active region (1500E). This burst was observed also by the radio telescope NDA in the frequency band 30÷60 MHz. CME's core was situated at the distance about 3Rs at the moment, when type IV burst registered at frequencies 22÷60 MHz. We conclude that the radio emission escape from the center of CME's core at frequency 60 MHz and comes from the periphery of the core at frequency 30 MHz due to occultation by the solar corona at corresponding frequencies. We find densities in these regions supposing plasma mechanism of radio emission. We show that the frequency drift of the leading edge of type IV burst is governed by expansion of CME's core. Type III bursts, which were observed against type IV burst, are shown to be generated by fast electrons propagating through the CME core plasma. Type II burst registered at frequencies 40÷50 MHz and 5÷16 MHz was radiated by a shock with velocity about 1000 km/s.

Interferometer Observations of Solar Type III Bursts by the Radio Telescope UTR-2

Valentin **Melnik** 1 , Valerii Shepelev 1 , Anatolii Brazhenko 2 , Vladimir Dorovskyy 1 , Helmut Rucker 3 , Stefaan Poedts

Sun and Geosphere, **2017**; 12/2: 105 -109

http://newserver.stil.bas.bg/SUNGEO//00SGArhiv/SG_v12_No2_2017-pp-105-109.pdf

Results of solar radio emission observations by radio telescopes UTR-2 and URAN-2 in **May-June 2014** are discussed. Observations by the radio telescope UTR-2 were carried out in the interferometer mode using West-East arm of the UTR-2 on 29 May and North-South arm on 2 June at frequencies 20 and 25 MHz. On 29 May some powerful simple type III bursts and groups of type III bursts were observed against type IV burst. There were only isolated weak type III bursts on 2 June. Analysis of visibility functions of radio emission sources at these frequencies was allowed to find spatial sizes of bursts sources, which changed mainly from 20` to 22` at 25 MHz and from 24` to 27` at 20 MHz. Also sources distances at these frequencies were obtained. In most cases radio emissions at frequencies 20 and 25 MHz escaped at distances 2.9Rs and 2.6 Rs, respectively. At these distances the radio emission at frequencies 10 and 12.5 MHz are generated in the Newkirk corona so we conclude that the observational radio emission occurred at the second harmonic. This fact is confirmed by the low polarizations of discussed type III bursts. Brightness temperatures of these bursts were in the range from 2.1 109 K to 4.5 1010 K for bursts on 29 May and only about 108 K for the burst observed on **2 June**. **29.05.2014**

Decameter Type III Bursts with Changing Frequency Drift-Rate Signs

V. N. **Melnik**, A. I. Brazhenko, A. A. Konovalenko, C. Briand, V. V. Dorovskyy, P. Zarka, A. V. Frantsuzenko, H. O. Rucker, B. P. Rutkevych, M. Panchenko, … show all 13

Solar Phys., **2015**, Volume 290, Issue 1, pp 193-203

We discuss properties of type III bursts that change the sign of their drift rate from negative to positive and vice versa. Moreover, these bursts may change the sign of their drift rates more than once. These particular type III bursts were observed simultaneously by the radio telescopes UTR-2 (Ukrainian T-shaped Radio telescope, Kharkov, Ukraine), URAN-2 (Ukrainian Radio telescope of the Academy of Sciences, Poltava, Ukraine), and by the NDA (Nançay Decametric Array, Nancay, France) in the frequency range 8 – 41 MHz. The negative drift rates of these bursts are similar to those of previously reported decameter type III bursts and vary from −0.7 MHz s−1 to −1.7 MHz s−1, but their positive drift rates vary in a wider range from 0.44 MHz s−1 to 6 MHz s−1. Unlike inverted U-bursts, the tracks of these type III bursts have C- or inverted C-shapes.

Our basic explanation of the positive drift rate of these type III bursts differs from the common assumption that positive drift rates of type III bursts are connected with electron beam propagation toward the Sun. We propose that, even if electron beams move outward from the Sun, they can generate type III bursts with positive drift rates if in some regions of the solar corona the group velocities of type III radio emissions are lower than the velocities of the electron beams.

See **CESRA highlight** #913 **2016** http://www.astro.gla.ac.uk/users/eduard/cesra/?p=913 **Aug 25, 2012**

Solar Decameter Spikes

V. N. **Melnik**, N. V. Shevchuk, A. A. Konovalenko, H. O. Rucker, V. V. Dorovskyy, S. Poedts, A. Lecacheux

Solar Physics, May **2014**, Volume 289, Issue 5, pp 1701-1714

We analyze and discuss the properties of decameter spikes observed in **July – August 2002** by the UTR-2 radio telescope. These bursts have a short duration (about one second) and occur in a narrow frequency bandwidth (50 – 70 kHz). They are chaotically located in the dynamic spectrum. Decameter spikes are weak bursts: their fluxes do not exceed 200 – 300 s.f.u. An interesting feature of these spikes is the observed linear increase of the frequency bandwidth with frequency. This dependence can be explained in the framework of the plasma mechanism that causes the radio emission, taking into account that Langmuir waves are generated by fast electrons within a narrow angle $\theta \approx 13^\circ - 18^\circ$ along the direction of the electron propagation. In the present article we consider the problem of the short lifetime of decameter spikes and discuss why electrons generate plasma waves in limited regions.

Unusual Solar Radio Burst Observed at Decameter Wavelengths

V. N. **Melnik**, A. I. Brazhenko, A. A. Konovalenko, H. O. Rucker, A. V. Frantsuzenko, V. V. Dorovskyy, M. Panchenko, A. A. Stanislavskyy

Solar Phys., 289, Issue 1, pp 263-278, **2014**

An unusual solar burst was observed simultaneously by two decameter radio telescopes UTR-2 (Kharkov, Ukraine) and URAN-2 (Poltava, Ukraine) on **3 June 2011** in the frequency range of 16 – 28 MHz. The observed radio burst had some unusual properties, which are not typical for the other types of solar radio bursts. Its frequency drift rate was positive (about 500 kHz s−1) at frequencies higher than 22 MHz and negative (100 kHz s−1) at lower frequencies. The full duration of this event varied from 50 s up to 80 s, depending on the frequency. The maximum radio flux of the unusual burst reached ≈103 s.f.u. and its polarization did not exceed 10 %. This burst had a fine frequency-time structure of unusual appearance. It consisted of stripes with the frequency bandwidth 300 – 400 kHz. We consider that several accompanied radio and optical events observed by SOHO and STEREO spacecraft were possibly associated with the reported radio burst. A model that may interpret the observed unusual solar radio burst is proposed.

Observations of Powerful Type III Bursts in the Frequency Range 10 – 30 MHz

V. N. **Melnik**, A. A. Konovalenko, H. O. Rucker, A. I. Boiko, V. V. Dorovskyy, E. P. Abranin & A. Lecacheux

Solar Physics, Volume 269, Number 2, 335-350, **2011**

The properties of powerful (flux >10−19 W m−2 Hz−1) type III bursts observed in July – August 2002 by the radio telescope UTR-2 at frequencies 10 – 30 MHz are analyzed. Most bursts have been registered when the active regions associated to these bursts were located near the central meridian or at 40fl – 60fl to the East or West from it. All powerful type III bursts drift from high to low frequencies with frequency drift rates 1 – 2.5 MHz s−1. It is important to emphasize that according to our observations the drift rate is linearly increasing with frequency. The duration of the bursts changes mainly from 6 s at frequency 30 MHz up to 12 s at 10 MHz. The instantaneous frequency bandwidth does not depend on the day of observations, i.e. on the disk location of the source active region, and is increasing with frequency.

The results of observational properties are discussed in the frame of the standard plasma model of type III bursts radio emission.

Solar S-bursts at Frequencies of 10 – 30 MHz

V.N. **Melnik** · A.A. Konovalenko · H.O. Rucker · V.V. Dorovskyy · E.P. Abranin · A. Lecacheux · A.S. Lonskaya

Solar Phys (**2010**) 264: 103–117

http://springerlink.com/content/g34l7m932g248u34/flp=56873041f573457c8b20fadfbf0814d1&pi=8

Solar S-bursts observed by the radio telescope UTR-2 in the period 2001 – 2002 are studied. The bursts chosen for a detailed analysis occurred in the periods 23 – 26 May 2001, 13 – 16 and 27 – 39 July 2002 during three solar radio storms. More than 800 S-bursts were registered in these days. Properties of S-bursts are studied in the frequency band 10 – 30 MHz. All bursts were always observed against a background of other solar radio activity such as type III and IIIb bursts, type III-like bursts, drift pairs and spikes. Moreover, Sbursts were observed during days when the active region was situated near the central meridian. Characteristic durations of S-bursts were about 0.35 and 0.4 – 0.6 s for the May and July storms, respectively. For the first time, we found that the instantaneous frequency width of S-bursts increased with frequency linearly. The dependence of drift rates on frequency followed the McConnell dependence derived for higher frequencies. We propose a model of S-bursts based on the assumption that these bursts are generated due to the confluence of Langmuir waves with fast magnetosonic waves, whose phase and group velocities are equal.

Decameter Type III-Like Bursts

V.N. **Mel'nik** · A.A. Konovalenko · H.O. Rucker · B.P. Rutkevych · V.V. Dorovskyy · E.P. Abranin · A.I. Brazhenko · A.A. Stanislavskii · A. Lecacheux

Solar Phys (**2008**) 250: 133–145

http://www.springerlink.com/content/x45670605023v415/fulltext.pdf

Observations of solar type II bursts at frequecies 10-30 MHz

Melnik, V. N., Konovalenko, A. A., Rucker, H. O., Stanislavsky, A. A., Abranin, E. P., Lecacheux, A., Mann, G., Warmuth, A., Zaitsev, V. V., Boudjada, M. Y., Dorovskii, V. V., Zaharenko, V. V., Lisachenko, V. N., & Rosolen, C.:

Solar Physics 222, 151, **2004**.

Expansion and Compression of a Flash Loop System during the Flare on January 15, 2022 According to Ultraviolet and Microwave Data

V. F. **Melnikov, *** and N. S. Meshalkina

Geomagnetism and Aeronomy, **2023**, Vol. 63, No. 7, 1054–1061

https://doi.org/10.1134/S0016793223070162

In this paper, we study the dynamics of a single loop structure in a C1.3 flare on **January 15, 2022**. A new type of behavior of flare loop was discovered. Unlike the previously known cases of visible contraction and expansion of flare loops in the phases of rise and decay of the flare radiation flux, respectively, the flare on **January 15, 2022** exhibited a directly opposite process: the loop increases in its height during the flare

intensity rise phase and contracts during the decay phase. Characteristic changes in the height, duration, and rate of the expansion and contraction of the loop structure were established. An increase of the electric current in the loop during the rise phase and its decrease during the contraction phase are proposed as an explanation of this behavior.

Properties of Gyrosynchrotron Emission in a Shrinking Flaring Loop

Victor **Melnikov**∗†1 and Leonid Filatov
CESRA Abstract **2016**
http://cesra2016.sciencesconf.org/conference/cesra2016/pages/CESRA2016_prog_abs_book_v1.pdf
Shrinking flaring loops recently became a popular topic in the solar flare physics. The flare loop shrinkage has not been predicted by so called the standard solar flare model. The standard model predicts just the opposite behavior, namely the expansion of a system of flaring loops during the flare development. The purpose of our work is modeling the microwave emission of such loops and comparing the obtained properties with the observed ones. First of all we model the dynamics of various parameters of nonthermal electrons injected into a non-stationary shrinking magnetic trap. The electron energy and pitch angle non-stationary spatial distributions in an extensive inhomogeneous magnetic trap have been obtained by numerically solving the non-stationary Fokker–Planck kinetic equation. It is shown that the high energy electrons are effectively accumulated and accelerated at the top of the shrinking trap due to the first order Fermi and betatron acceleration mechanisms. Spatial and temporal properties of gyrosynchrotron emission characteristics have been calculated for the obtained electron distributions. Specifically, the obtained solutions make it possible to explain the radio brightness peak that is frequently observed at the top of solar flare loops. Also, we found unexpectedly long time delays between emission light curves from the looptop and footpoint regions. The properties obtained are compared with the properties of the shrinking microwave loops for some flares observed with Nobeyama Radioheliograph.

Peak Frequency Dynamics in Solar Microwave Bursts

V.F. **Melnikov** · Dale E. Gary · Gelu M. Nita
Solar Phys (**2008**) 253: 43–73, DOI 10.1007/s11207-008-9275-8, **File (corrected)**
We analyze the dynamics of the broadband frequency spectrum of 338 microwave bursts observed in the years 2001 – 2002 with the Owens Valley Solar Array. A subset of 38 strong microwave bursts that show a single spectral maximum are studied in detail. Our main goal is to study changes in spectral peak frequency ν_{pk} with time. We show that, for a majority of these simple bursts, the peak frequency shows a high positive correlation with flux density – it increases on the rise phase in ≈83% of 24 bursts where it could be cleanly measured, and decreases immediately after the peak time in ≈62% of 34 bursts. This behavior is in qualitative agreement with theoretical expectations based on gyrosynchrotron self-absorption. However, for a significant number of events (≈30 – 36%) the peak frequency variation is much smaller than expected from self-absorption, or may be entirely absent. The observed temporal behavior of ν_{pk} is compared with a simple model of gyrosynchrotron radio emission. We show that the anomalous behavior is well accounted for by the effects of Razin suppression, and further show how an analysis of the temporal evolution of ν_{pk} can be used to uniquely determine the relative importance of self-absorption and Razin suppression in a given burst. The analysis technique provides a new, quantitative diagnostic for the gyrosynchrotron component of solar microwave bursts. Applying this analysis technique to our sample of bursts, we find that in most of the bursts (60%) the spectral dynamics of ν_{pk} around the time of peak flux density is caused by self-absorption. On the other hand, for a significant number of events (≈70%), the Razin effect may play the dominant role in defining the spectral peak and dynamics of ν_{pk}, especially on the early rise phase and late decay phase of the bursts.
See Melnikov**_Erratum.pdf**

Type-III Electron Beams: 3D Quasilinear Effects

Donald B. **Melrose**, James Harding & Iver H. Cairns
Solar Physics volume 296, Article number: 42 (**2021**)
https://doi.org/10.1007/s11207-021-01783-8
https://link.springer.com/content/pdf/10.1007/s11207-021-01783-8.pdf
A conventional model for the generation of Langmuir waves in Type-III radio bursts is based on a one-dimensional (1D) version of the quasilinear equations. In this model a wave with phase velocity vϕvϕ resonates with an electron with velocity v=vϕ, causing the waves to grow at a rate ∝dF(v)/dv>0, where F(v) is the 1D-distribution function. The backreaction on the electrons drives the electrons towards a plateau distribution: dF(v)/dv→0. In the 3D-generalization, none of these features apply: waves with phase speed vϕvϕ can resonate with electrons with speed v<vϕ, depending on the angle between the wave normal and the electron velocity, wave growth occurs only if the distribution function is both an increasing function of vv and also has an anisotropic pitch-angle distribution, and the backreaction involves diffusion in both speed vv and in pitch-angle αα. In this article we discuss implications of the generalization from 1D to 3D on models for Type-III bursts. An effect that is absent in 1D, but may be important in 3D, is scattering of Langmuir

waves by turbulence in the ambient plasma. Pitch-angle scattering by the scattered Langmuir waves may play an important role in the evolution of the Type-III beam.

Coherent emission mechanisms in astrophysical plasmas **Review**

D.B. **Melrose**

Reviews of Modern Plasma Physics December **2017**, 1:5

https://link.springer.com/content/pdf/10.1007%2Fs41614-017-0007-0.pdf

Three known examples of coherent emission in radio astronomical sources are reviewed: plasma emission, electron cyclotron maser emission (ECME) and pulsar radio emission. Plasma emission is a multi-stage mechanism with the first stage being generation of Langmuir waves through a streaming instability, and subsequent stages involving partial conversion of the Langmuir turbulence into escaping radiation at the fundamental (F) and second harmonic (H) of the plasma frequency. The early development and subsequent refinements of the theory, motivated by application to solar radio bursts, are reviewed. The driver of the instability is faster electrons outpacing slower electrons, resulting in a positive gradient ($df(v_\parallel)/dv_\parallel>0$ $df(v_\parallel)/dv_\parallel>0$) at the front of the beam. Despite many successes of the theory, there is no widely accepted explanation for type I bursts and various radio continua. The earliest models for ECME were purely theoretical, and the theory was later adapted and applied to Jupiter (DAM), the Earth (AKR), solar spike bursts and flare stars. ECME strongly favors the x mode, whereas plasma emission favors the o mode. Two drivers for ECME are a ring feature (implying $df(v)/dv>0$ $df(v)/dv>0$) and a loss-cone feature. Loss-cone-driven ECME was initially favored for all applications. The now favored driver for AKR is the ring-feature in a horseshoe distribution, which results from acceleration by a parallel electric on converging magnetic field lines. The driver in DAM and solar and stellar applications is uncertain. The pulsar radio emission mechanism remains an enigma. Ingredients needed in discussing possible mechanisms are reviewed: general properties of pulsars, pulsar electrodynamics, the properties of pulsar plasma and wave dispersion in such plasma. Four specific emission mechanisms (curvature emission, linear acceleration emission, relativistic plasma emission and anomalous Doppler emission) are discussed and it is argued that all encounter difficulties. Coherent radio emission from extensive air showers in the Earth's atmosphere is reviewed briefly. The difference in theoretical approach from astrophysical theories is pointed out and discussed. Fine structures in DAM and in pulsar radio emission are discussed, and it is suggested that trapping in a large-amplitude wave, as in a model for discrete VLF emission, provides a plausible explanation. A possible direct measure of coherence is pointed out.

Is Cyclotron Maser Emission in Solar Flares Driven by a Horseshoe Distribution?

D.B. **Melrose**, M.S. Wheatland

Solar Phys. Volume 291, Issue 12, pp 3637–3658 **2016**

https://arxiv.org/pdf/1610.04299v1.pdf

Since the early 1980s, decimetric spike bursts have been attributed to electron cyclotron maser emission (ECME) by the electrons that produce hard X-ray bursts as they precipitate into the chromosphere in the impulsive phase of a solar flare. Spike bursts are regarded as analogous to the auroral kilometric radiation (AKR), which is associated with the precipitation of auroral electrons in a geomagnetic substorm. Originally, a loss-cone-driven version of ECME, developed for AKR, was applied to spike bursts, but it is now widely accepted that a different, horseshoe-driven, version of EMCE applies to AKR. We explore the implications of the assumption that horseshoe-driven ECME also applies to spike bursts. We develop a 1D model for the acceleration of the electrons by a parallel electric field, and show that under plausible assumptions it leads to a horseshoe distribution of electrons in a solar flare. A second requirement for horseshoe-driven ECME is an extremely low plasma density, referred to as a density cavity. We argue that a coronal density cavity should develop in association with a hard X-ray burst, and that such a density cavity can overcome a long-standing problem with the escape of ECME through the second-harmonic absorption layer. Both the horseshoe distribution and the associated coronal density cavity are highly localized, and could not be resolved in the statistically large number of local precipitation regions needed to explain a hard X-ray burst. The model highlights the "number problem" in the supply of the electrons needed to explain a hard X-ray burst.

Plasma emission mechanisms.

Melrose, D. B.

Solar radiophysics: Studies of emission from the sun at metre wavelengths, McLean, D. J. and Labrum, N. R. eds., 177–210, **1985**.

Coherent emission

D. B. **Melrose**

Proceedings of the International Astronomical Union / Volume 4 / Symposium S257, pp 305 – 315, Published online: 16 Март **2009**

http://journals.cambridge.org/action/displayIssuefliid=4866212

The theory of plasma emission and of electron cyclotron maser emission, and their applications to solar radio bursts and to Jupiter's decametric radioation (DAM) and the Earth's auroral kilometric radiation (AKR) are reviewed, emphasizing the early literature and problems that remain unresolved. It is pointed out that there are quantitative measures of coherence in radio astronomy that have yet to be explored either observationally or theoretically.

The Use of Planar Feeds for Solar Radio Observations

J. E. **Mendoza-Torres**, E. Colín-Beltrán, A. Corona-Chávez, J. S. Palacios-Fonseca, B. Rodríguez-Pedroza, Y. E. Tlatelpa-Osorio, J. C. García-Santos, S. Sánchez-Urrieta
Solar Phys., **2015**, Volume 290, Issue 1, pp 295-299
We describe the results of test observations obtained with a 5-m single-dish radiotelescope (RT5) using novel planar feeds designed to detect circularly polarized emission in the 1.5 – 3.9 GHz band. The beam of such feeds is wide; nevertheless, solar scans have been successfully done using feeds at the focus of the primary mirror of the RT5. The sensitivity is about 1 sfu at each polarization and about 1.4 sfu at the I Stokes parameter. We estimate that it is possible to detect flares with fluxes above 5 sfu at the I Stokes parameter.

Subterahertz Radius and Limb Brightening of the Sun Derived from SST and ALMA

Fabian **Menezes**, Caius L. Selhorst, Carlos Guillermo Giménez de Castro, Adriana Valio
MNRAS Volume 511, Issue 1, March **2022**, Pages 877–885,
https://doi.org/10.1093/mnras/stab3501
https://arxiv.org/pdf/2111.15261.pdf
Measurements of the radius and limb brightening of the Sun provide important information about the solar atmosphere structure and temperature. The solar radius increases as the observation at radio frequency decreases, indicating that each emission originates higher in the atmosphere. Thus, different layers of the solar atmosphere can be probed by observing at multiple wavelengths. In this work, we determined the average radius and limb brightening at 100, 212, 230, and 405 GHz, using data from the Solar Submillimeter Telescope and ALMA's single-dish observations. For the first time, limb brightening values for frequencies of 212 and 405 GHz were estimated. At sub-THz frequencies, the observed limb brightening may affect the solar radius measurements. We use two different and well known approaches to determine the radius: the half-power method and the inflection-point method. We investigate how the antenna beam size and the limb brightening level, LB, can affect the radius measurements using both methods. Our results showed that the inflection-point method is the least affected by these parameters, and should thus be used for solar radius estimates at radio wavelengths. The measured average radii are 968"~±~3" (100 GHz), 963"~±~3" (212 GHz), 963"~±~2" (230 GHz), and 963"~±~5" (405 GHz). Finally, we used forward modeling to estimate the ranges of LB of the solar disk resulting in 5%-19% (100 GHz), 2%-12% (212 GHz), 6%-18% (230 GHz), and 3%-17% (405 GHz). Both radius and limb brightening estimates agree with previous measurements reported in the literature. **2015-12-17**

The subterahertz solar cycle: Polar and equatorial radii derived from SST and ALMA

Fabian **Menezes**, Caius L. Selhorst, Carlos Guillermo Giménez de Castro, Adriana Valio
ApJ **2021**
https://arxiv.org/pdf/2102.04570.pdf
At subterahertz frequencies -- \textit{i.e.}, millimeter and submillimeter wavelengths -- there is a gap of measurements of the solar radius as well as other parameters of the solar atmosphere. As the observational wavelength changes, the radius varies because the altitude of the dominant electromagnetic radiation is produced at different heights in the solar atmosphere. Moreover, radius variations throughout long time series are indicative of changes in the solar atmosphere that may be related to the solar cycle. Therefore, the solar radius is an important parameter for the calibration of solar atmospheric models enabling a better understanding of the atmospheric structure. In this work we use data from the Solar Submillimeter-wave Telescope (SST) and from the Atacama Large Millimeter/submillimeter Array (ALMA), at the frequencies of 100, 212, 230, and 405 GHz, to measure the equatorial and polar radii of the Sun. The radii measured with extensive data from the SST agree with the radius-vs-frequency trend present in the literature. The radii derived from ALMA maps at 230 GHz also agree with the radius-vs-frequency trend, whereas the 100-GHz radii are slightly above the values reported by other authors. In addition, we analyze the equatorial and polar radius behavior over the years, by determining the correlation coefficient between solar activity and subterahertz radii time series at 212 and 405 GHz (SST). The variation of the SST-derived radii over 13 years are correlated to the solar activity when considering equatorial regions of the solar atmosphere, and anticorrelated when considering polar regions. The ALMA derived radii time series for 100 and 230 GHz show very similar behaviors with those of SST.

Solar Radius at Subterahertz Frequencies and Its Relation to Solar Activity

Fabian **Menezes**, Adriana Valio
Solar Physics December **2017**, 292:195
https://link.springer.com/content/pdf/10.1007%2Fs11207-017-1216-y.pdf
https://arxiv.org/pdf/1712.06771.pdf

The Sun emits radiation at several wavelengths of the electromagnetic spectrum. In the optical band, the solar radius is 695 700 km, and this defines the photosphere, which is the visible surface of the Sun. However, as the altitude increases, the electromagnetic radiation is produced at other frequencies, causing the solar radius to change as a function of wavelength. These measurements enable a better understanding of the solar atmosphere, and the radius dependence on the solar cycle is a good indicator of the changes that occur in the atmospheric structure. We measure the solar radius at the subterahertz frequencies of 0.212 and 0.405 THz, which is the altitude at which these emissions are primarily generated, and also analyze the radius variation over the 11-year solar activity cycle. For this, we used radio maps of the solar disk for the period between 1999 and 2017, reconstructed from daily scans made by theSolar Submillimeter-wave Telescope (SST), installed at El Leoncito Astronomical Complex (CASLEO) in the Argentinean Andes. Our measurements yield radii of 966.5″±2.8″966.5″±2.8″ for 0.2 THz and 966.5″±2.7″966.5″±2.7″ for 0.4 THz. This implies a height of 5.0±2.0×1065.0±2.0×106 m above the photosphere. Furthermore, we also observed a strong anticorrelation between the radius variation and the solar activity at both frequencies.

Correction Solar Physics June **2018**, 293:89
https://link.springer.com/content/pdf/10.1007%2Fs11207-018-1308-3.pdf

Electron density and temperature in the solar corona from multifrequency radio imaging

C. **Mercier** and G. Chambe
A&A 583, A101 **(2015)**
http://www.aanda.org/articles/aa/pdf/2015/11/aa25540-14.pdf

Context. The 2D images obtained through rotational aperture synthesis with the Nançay Radioheliograph are suitable for quantitative exploitation. First results are presented.
Aims. We study the variations of the quiet corona in brightness and size during an 8-year period and derive electron density and temperature in the corona.
Methods. Images at 6 frequencies between 150 and 450 MHz for 183 quiet days between 2004 and 2011 were used. Measurements of the brightness temperature Tb beyond the limb allowed coronal density models to be derived in both EW and NS radial directions, with a weak dependence on the electron temperature. The total ranges in the heliocentric distance r are 1.15–1.60 R⊙ (EW) and 1.0–1.4 R⊙ (NS). The agreement between results from different frequencies, in the ranges of r where there is overlapping shows the robustness of the method. The electron temperature, in turn, can be derived from the comparison of the observed mean spectra on the disk with those predicted through transfer calculations from the density models derived from limb observations.
Results. The widths of the brightness profiles that were averaged yearly have minima at cycle minimum (2008–2009). These minima are more pronounced for EW profiles than for NS ones. The derived yearly-averaged density models along equatorial and polar diameters are consistent with isothermal and hydrostatic models. They are characterized by their density value n0 extrapolated down to the base of the corona and their scale-height temperature TH. Changes in n0 and TH with solar cycle are given for equatorial and polar regions. The kinetic temperature Te of electrons in the corona (~0.62 MK) is found to be significantly less than TH (~1.5 MK). This implies an ion temperature Ti ~ 2.2 MK.
Conclusions. The yearly-averaged variations of these models are less than the dispersion between models derived from other techniques, such as white light and EUV observations, partly because these two techniques are not time-averaged, and they refer to particular days. The radio models are generally less dense, which is compatible with isothermal hydrostatic equilibrium in their range of heliocentric distances, and they show different behaviors with the solar cycle in the equatorial or polar radial directions. The electron kinetic temperature Te is substantially less than TH.

Erratum A&A 585, C1 **(2016)**

The structure of solar radio noise storms

Claude **Mercier**, Prasad Subramanian, Gilbert Chambe, P. Janardhan
A&A, 576, A136 **2015**
http://arxiv.org/pdf/1412.8189v2.pdf

The Nan\c{c}ay Radioheliograph (NRH) routinely produces snapshot images of the full sun at frequencies between 150 and 450 MHz, with typical resolution 3 arcmin and time cadence 0.2 s. Combining visibilities from the NRH and from the Giant Meterwave Radio Telescope (GMRT) allows us to produce images of the sun at 236 or 327 MHz, with a large FOV, high resolution and time cadence. We seek to investigate the structure of noise storms (the most common non-thermal solar radio emission). We focus on the relation of position and altitude of noise storms with the observing frequency and on the lower limit of their sizes. We present results for noise storms on four days. The results consist of an extended halo and of one or several compact cores with relative intensity changing over a few seconds. We found that core sizes can be almost stable over one hour, with a minimum in the range 31-35 arcsec (less than previously reported) and can be stable over one hour. The heliocentric distances of noise storms are ∼1.20 and 1.35 R⊙ at 432 and 150 MHz, respectively. Regions where storms originate are thus much denser than the ambient corona and their vertical extent is found to be less than expected from hydrostatic equilibrium. The smallest observed sizes impose upper limits

on broadening effects due to scattering on density inhomogeneities in the low and medium corona and constrain the level of density turbulence in the solar corona. It is possible that scatter broadening has been overestimated in the past, and that the observed sizes cannot only be attributed to scattering. The vertical structure of the noise storms is difficult to reconcile with the classical columnar model. **2002 Aug 27, 2003 Jul 15, 2004 Aug 14, Apr. 06, 2006**
See **High resolution observations of radio noise storms in the solar corona**
Prasad **Subramanian** and Claude Mercier
CESRA Science Highlights #826 Sept **2016**
http://www.astro.gla.ac.uk/users/eduard/cesra/?p=826

Morphology of the quiet Sun between 150 and 450 MHz as observed with the Nançay radioheliograph

C. **Mercier** and G. Chambe
A&A 540, A18 (**2012**)
Context. Since its last upgrading in 2004, the Nançay radioheliograph (NRH) is able to produce reliable images of the quiet Sun in the 150–450 MHz range, which corresponds to the low and medium corona. These images are better than those previously obtained with the NRH or other instruments in this range and are suitable for quantitative and systematic exploitation.
Aims. We aim to study the radio aspects of the solar atmosphere. We aim to focuss on the description of the morphology and the comparisons with observations in EUV and X-ray ranges and with magnetic structures.
Methods. We used the rotational aperture synthesis technique (suitable for non time-varying objects) along with an original self-calibration procedure and a specific deconvolution algorithm (a variant of CLEAN that includes a scale analysis).
Results. We present results from radio imaging of the quiet Sun with the NRH. The analysis was carried over about 160 days during the summers (June-August) from 2004 to 2011. We confirms and extend our first results, which were published from a much smaller data sample. We emphasize new aspects of the corona observed in this frequency range, in particular the existence of coronal holes darker than previously reported and dark channels at high frequencies. We give examples that illustrate the complex morphology of coronal structures as revealed by radio imaging, the center-to-limb effects (radio occultation) and the variation with the phase of the solar cycle. We compare our images with large-scale coronal magnetic structures. We show that dark coronal holes and channels seen at high frequencies and bright ribbons seen at low frequencies seem to be associated with particular types of magnetic structures.
Conclusions. Detailed radio images in this frequency range are a new tool with high potential for investigating the low and middle corona, since these images can emphasize structures that are not (or much less) visible at other wavelengths. In the near future, there is much to learn from observations with NRH during the ascending part of the cycle (never observed at m/dcm wavelengths) and from composite images of combined NRH and GMRT data, which will have a much better resolution. In a second step, it will be interesting to obtain circularly polarized images (giving a diagnostic of the coronal magnetic field) and images with new-generation instruments, which will yield detailed images with shorter synthesis or even snapshot images, from which processes evolving on shorter time scales can be studied.

HIGH DYNAMIC RANGE IMAGES OF THE SOLAR CORONA BETWEEN 150 AND 450 MHz

Claude **Mercier** and Gilbert Chambe
Astrophysical Journal, 700:L137–L140, **2009** August
We present radio images of the quiet Sun obtained with the Nan¸cay Radioheliograph between 150 and 450 MHz, using the latest improvements in the instrument and in the data processing techniques. We emphasize new aspects of the corona observable in this frequency range, particularly the prominence of coronal holes, and discuss implications for future studies.

Combining visibilities from the giant meterwave radio telescope and the Nancay radio heliograph. High dynamic range snapshot images of the solar corona at 327 MHz

Mercier, C., Subramanian, P., Kerdraon, A., Pick, M., Ananthakrishnan, S., and Janardhan, P.
Astronomy and Astrophysics, Volume 447, Issue 3, March I **2006**, pp.1189-1201

See Highlights of Solar Radio Physics 5:
http://www.lesia.obspm.fr/cesra/highlights/highlight06-5.html

Heating manifestations at the onset of the 29 June 2012 flare

Meshalkina, Nataliya ; Altyntsev, Alexander
Solar-Terrestrial Physics, vol. 10, issue 3, pp. 11-17, **2024**
https://naukaru.ru/en/nauka/article/80893/view
https://naukaru.ru/en/storage/download/169703
Analysis of GOES data for the SOL**2012-06-29**T04:09 flare, class C4.6, shows a thermal character of the energy release for several minutes before the impulsive stage. Plasma heating to temperatures above 10 MK leads to the appearance of plasma jets along open field lines and in large loops. This work examines the relationship between the heated plasma and the flare structure and its dynamics, using observations in the X-ray, extreme ultraviolet (EUV), and radio-wave ranges. Particular attention is drawn to the detection of narrow-band fine temporal structures of radio emission before and after the impulsive stage of the flare in dynamic spectra. In the initial stage, broadband pulses in the decimeter range are observed which can be associated with the formation of thermal fronts in the jets. A series of super-bright drifting bursts in the centimeter range occurs after the end of the impulsive energy release in the flare kernel. Using data from the Siberian Solar Radio Telescope (5.7 GHz), we managed to localize the position of the source of the fine structure of drifting bursts at the remote footpoint of the large-scale flare loop.
CESRA #3884 **2024** https://www.astro.gla.ac.uk/users/eduard/cesra/?p=3884

THE 10 JULY 2012 EVENT: AN EXAMPLE OF NARROWBAND GYROSYNCHROTRON BURST?

Meshalkina1 N.S., Fleishman2,3 G.D., Altyntsev1 A.T.
Астрономия-**2018** Том 2 Солнечно-земная физика – современное состояние и перспективы С.141
http://www.izmiran.ru/library/eaas2018/eaas-2018-2.pdf
We have identified events with steep (narrowband) microwave spectra that do not show a prolonged trapping and imply some degree of source uniformity. We revealed event of **10 July 2012** with such narrow spectra, having low- and high-frequency spectral indices larger than 3 in absolute value during the flare. Based on an analysis of radio images dynamics we concluded that even narrowband burst had the complex structure, consisting of two sources - low and high frequency ones. The behavior of each was very differ that appeared in spectrum shape and spatial structure dynamics.

Study of flare energy release using events with numerous type III-like bursts in microwaves

N. S. **Meshalkina**, A. T. Altyntsev, D. A. Zhdanov, S. V. Lesovoi, A. A. Kochanov, Yan Yihua, Tan Chengming
E-print, June **2012**; Solar Phys. October **2012**, Volume 280, Issue 2, pp 537-549
The analysis of narrowband drifting of type III-like structures in radio bursts dynamic spectra allows to obtain unique information about primary energy release mechanisms in solar flares. The SSRT spatially resolved images and a high spectral and temporal resolution allow direct determination not only the positions of its sources but also the exciter velocities along the flare loop. Practically, such measurements are possible during some special time intervals when the SSRT (about 5.7 GHz) is observing the flare region in two high-order fringes; thus, two 1D scans are recorded simultaneously at two frequency bands. The analysis of type III-like bursts recorded during the flare **14 Apr 2002** is presented. Using-muliwavelength radio observations recorded by SSRT, SBRS, NoRP, RSTN we study an event with series of several tens of drifting microwave pulses with drift rates in the range from -7 to 13 GHz/s. The sources of the fast-drifting bursts were located near the top of the flare loop in a volume of a few Mm in size. The slow drift of the exciters along the flare loop suggests a high pitch-anisotropy of the emitting electrons.

On bandwidth of solar subsecond bursts in cm-range

Advances in Space Research, Volume 41, Issue 6, *Pages 936-942,* **2008**
N.S. **Meshalkina**, A.T. Altyntsev and Yan Yihua
The goal is to study parameters of drifting type III bursts, and find out the emission mechanism of these bursts and understand what factors affect instantaneous spectral bandwidth of these bursts.
We used simultaneous observations of microwave type III bursts with high temporal, spatial and spectral resolution from the Siberian Solar Radio Telescope (5.7 GHz, 14 ms resolution) and from the spectropolarimeters (5.2–7.6 GHz, 5 ms) of the National Astronomical Observatories.
Characteristic parameters such as starting frequency, total and instantaneous bandwidth, polarization degree, total duration, and rate of frequency drift were determined for the radio bursts. We analyzed and estimated parameters, which determine instantaneous bandwidth.

Broadband microwave sub-second pulsations in an expanding coronal loop of the 2011 August 10 flare

Hana **Meszarosova**, Jan Rybak, Larisa Kashapova, Peter Gomory, Susanna Tokhchukova, Ivan Myshyakov
A&A 593, A80 **2016**
http://arxiv.org/pdf/1609.04217v1.pdf

We studied the characteristic physical properties and behavior of broadband microwave sub-second pulsations observed in an expanding coronal loop during the GOES C2.4 solar flare on **2011 August 10**. We found sub-second pulsations and other different burst groups in the complex radio spectrum. The broadband (bandwidth about 1 GHz) sub-second pulsations (temporal period range 0.07-1.49 s, no characteristic dominant period) lasted 70 s in the frequency range 4-7 GHz. These pulsations were not correlated at their individual frequencies, had no measurable frequency drift, and zero polarization. In these pulsations, we found the signatures of fast sausage magnetoacoustic waves with the characteristic periods of 0.7 and 2 s. The other radio bursts showed their characteristic frequency drifts in the range of -262-520 MHz/s. They helped us to derive average values of 20-80 G for the coronal magnetic field strength in the place of radio emission. It was revealed that the microwave event belongs to an expanding coronal loop with twisted sub-structures observed in the 131, 94, and 193 A SDO/AIA channels. Their slit-time diagrams were compared with the location of the radio source at 5.7 GHz to realize that the EUV intensity of the expanding loop increased just before the radio source triggering. We reveal two EUV bidirectional flows that are linked with the start time of the loop expansion. Their positions were close to the radio source and propagated with velocities within a range of 30-117 km/s. We demonstrate that periodic regime of the electron acceleration in a model of the quasi-periodic magnetic reconnection might be able to explain physical properties and behavior of the sub-second pulsations. The depolarization process of the microwave emission might be caused by a plasma turbulence in the radio source. Finally, the observed EUV flows might be linked with reconnection outflows.

Broadband microwave sub-second pulsations and magnetoacoustic waves in an expanding coronal loop (2011 August 10 are)

Hana **Meszarosova**_1, Jan Rybak2, Larisa Kashapova3, Peter Gomory2, Susanna Tokhchukova4, and Ivan Myshyakov3
CESRA **2016**, p.99
http://cesra2016.sciencesconf.org/conference/cesra2016/pages/CESRA2016_prog_abs_book_v3.pdf

The complex microwave dynamic spectrum and the expanding loop images of the 2011 August 10 GOES C2.4 solar are are analyzed with a help of SDO/AIA/HMI, RHESSI and STEREO/SECCHI-EUVI imaging data. The complex radio spectrum shows broadband sub-second pulsations of temporal period range 0.1-1.5 s and is lasting about 70 s in frequency range 4-7 GHz. These pulsations have no polarization and no measurable frequency drift. In these pulsations are found signatures of fast sausage magnetoacoustic waves with the characteristic periods of 0.7 and 2.0 s. The location of the radio source at 5.7 GHz shows that this radio event belongs to the expanding coronal loop with twisted sub-structures observed in 131, 94, and 193 A SDO/AIA channels. The EUV intensity of the expanding loop increases just before the radio source triggering. Two EUV bi-directional ows are linked with the start time of the loop expansion close to the radio source and they are propagating with velocities in range of 30-117 km/s. The periodic regime of the electron acceleration in a model of the quasi-periodic magnetic reconnection might be convenient for an explanation of physical properties and behaviour of the sub-second pulsations under study.

Fast Magnetoacoustic Waves in a Fan Structure Above a Coronal Magnetic Null Point

H. **Mészárosová**, J. Dudík, M. Karlický, F. R. H. Madsen, H. S. Sawant
Solar Physics, April **2013**, Volume 283, Issue 2, pp 473-488

We analyze the **26 November 2005** solar radio event observed interferometrically at frequencies of 244 and 611 MHz by the Giant Metrewave Radio Telescope (GMRT) in Pune, India. These observations are used to make interferometric maps of the event at both frequencies with the time cadence of 1 s from 06:50 to 07:12 UT. These maps reveal several radio sources. The light curves of these sources show that only two sources at 244 MHz and 611 MHz are well correlated in time. The EUV flare is more localized with flare loops located rather away from the radio sources. Using SoHO/MDI observations and potential magnetic field extrapolation we demonstrate that both the correlated sources are located in the fan structure of magnetic field lines starting from a coronal magnetic null point. Wavelet analysis of the light curves of the radio sources detects tadpoles with periods in the range P=10 – 83 s. These wavelet tadpoles indicate the presence of fast magnetoacoustic waves that propagate in the fan structure of the coronal magnetic null point. We estimate the plasma parameters in the studied radio sources and find them consistent with the presented scenario involving the coronal magnetic null point.

Magnetoacoustic Wave Trains in the 11 July 2005 Radio Event with Fiber Bursts

H. **Mészárosová**, M. Karlický and J. Rybák
Solar Physics, Volume 273, Number 2, 393-402, **2011**
A dm-radio emission with fiber bursts observed on **11 July 2005** was analyzed using wavelet filtration and spectral methods. In filtered radio spectra we found structures with different characteristic period P and frequency drift FD: i) fiber substructures (composed of dot emissions) with P 1≈ 0.5 s, FD1=−87 MHz s−1 on average, ii) fiber structures with P 2≈1.9 s, and iii) drifting structures with P 3≈81.4 s, FD2=−8.7, +98.5, and −21.8 MHz s−1. In the wavelet spectra we recognized patterns having the form of tadpoles. They were detected with the same characteristic periods P as found for the filtered structures. The frequency drift of the tadpole heads is found to be equal to the frequency drift of some groups of fibers for the long-period wavelet tadpoles (P 3) and to the frequency drift of individual fibers for the short-period tadpoles (P 2). Considering these wavelet tadpoles as signatures of propagating magnetoacoustic wave trains, the results indicate the presence of several wave trains in the fibers' source. While the long-period wave trains trigger or modulate a whole group of fibers, the short-period ones look like being connected with individual fiber bursts. This result supports the model of fibers based on magnetoacoustic waves. Using a density model of the solar atmosphere we derived the velocities of the magnetoacoustic waves, 107 and 562 km s−1, and setting them equal to the Alfvén ones we estimated the magnetic field in the source of fiber bursts as 10.7 and 47.8 G.

Separation of drifting pulsating structures in a complex radio spectrum of the 2001 April 11 event

H. **Mészárosová**1, J. Rybák2 and M. Karlický1
A&A 525, A88 (**2011**)
Aims. We present new method of separating a complex radio spectrum into single radio bursts. The method is used in the analysis of the 0.8–2.0 GHz radio spectrum of the **2001 April 11** event, which was rich in drifting pulsating structures.
Methods. The method is based on the wavelet analysis technique, which separates different spatial-temporal components (radio bursts) that are difficult to recognize in the original radio spectrum.
Results. We show with this method that the complex radio spectrum observed during the 2001 April 11 event consists of at least four drifting pulsating structures (DPSs). These structures were separated with respect to their different frequency drifts. The DPSs indicate at least four plasmoids that are supposed to be formed in a flaring current sheet.

"Drifting tadpoles" in wavelet spectra of decimetric radio emission of fiber bursts

Meszarosova, H., Karlicky, M., Rybak, J., Jiricka, K.
E-print, Aug **2009**, A&A
For the first time, we have found drifting tadpoles in the wavelet spectra of the decimetric radio emission associated with the fiber bursts observed in **July 11, 2005**. These tadpoles were detected at all radio frequencies in the 1602−1780 MHz frequency range. The characteristic period of the wavelet tadpole patterns was found to be 81.4 s and the frequency drift of the tadpole heads is −6.8 MHz s−1 . These tadpoles are interpreted as a signature of the magnetoacoustic wave train moving along a dense flare waveguide and their frequency drift as a motion of the wave train modulating the radio emission produced by the plasma emission mechanism. Using the Aschwanden density model of the solar atmosphere, only low values of the Alfvfln speed and the magnetic field strength in the loop guiding this wave train were derived which indicates a neutral current sheet as the guiding structure. The present analysis supports the model of fiber bursts based on whistler waves.

TADPOLES IN WAVELET SPECTRA OF A SOLAR DECIMETRIC RADIO BURST

H. **Mészárosová**1, M. Karlick´y1, J. Ryb´ak2, and K. Ji˘ri˘cka
Astrophysical Journal, 697:L108–L110, **2009** June
http://solar.physics.montana.edu/cgi-bin/eprint/index.plflentry=10869
http://www.iop.org:80/EJ/toc/-alert=43192/1538-4357/697/2
In the solar decimetric type IV radio event observed on **2001 June 13**, we have found wavelet tadpole patterns for the first time. They were detected simultaneously at all radio frequencies in the 1.1–4.5 GHz frequency range. The characteristic period of the wavelet tadpole patterns was found to be 70.9 s. The parameters of the tadpoles on different frequencies are very similar and the correlations between individual radio fluxes are high. These tadpoles are interpreted as a signature of the magnetoacoustic wave train moving along the flare loop through the radio source and modulating its gyrosynchrotron emission.

Decimetric radio dot emissions

H. **Mészárosová**1, 2, M. Karlický2, H. S. Sawant1, F. C. R. Fernandes3, J. R. Cecatto1, and M. C. de Andrade

A&A 491, 555-560 (**2008**), DOI: 10.1051/0004-6361:20077762

Context. We study a rare type of solar radio bursts called decimetric dot emissions.
Aims. In the period 1999-2001, 20 events of decimetric dot emissions observed by the Brazilian Solar Spectroscope (BSS) in the frequency range 950-2640 MHz are investigated statistically and compared with radio fine structures of zebras and fibers.
Methods. For the study of the spectral characteristics of the dot emissions we use specially developed Interactive Data Language (IDL) software called BSSView and basic statistical methods.
Results. We have found that the dm dot emissions, contrary to the fine structures of the type IV bursts (i.e. zebras, fibers, lace bursts, spikes), are not superimposed on any background burst emission. In the radio spectrum, in most cases the dot emissions form chains that appear to be arranged in zebra patterns or fibers. Because some zebras and fibers, especially those observed with high time and high spectral resolutions, also show emission dots (but superimposed on the background burst emission), we compared the spectral parameters of the dot emissions with the dots being the fine structure of zebras and fibers. For both these dots, similar spectral characteristics were found. Some similarities of the dot emissions can be found also with the lace bursts and spikes. For some events the dot emissions show structural evolution from patterns resembling fibers to patterns resembling zebras and vice versa, or they evolve into fully chaotic patterns.
Conclusions. For the first time, we present decimetric dot emissions that appear to be arranged in zebra patterns or fibers. We propose that these emissions are generated by the plasma emission mechanism at the locations in the solar atmosphere where the double resonance condition is fulfilled.

Solar decimetric type III bursts in semi-closed magnetic field structures

H. **Mészárosová**[1, 2], M. Karlický[2], H. S. Sawant[1], F. C. R. Fernandes[3], J. R. Cecatto[1], and M. C. de Andrade[1]

A&A 484, 529-536 (**2008**)
http://www.aanda.org/10.1051/0004-6361:20077634

Aims. We investigate statistically seventeen groups of solar type III bursts, observed in the frequency range 950-2500 MHz using the Brazilian Solar Spectroscope (BSS) during the period 1999-2002.
Methods. Using specially-developed Interactive Data Language (IDL) software called BSSView, the spectral characteristic properties of the bursts were investigated. For illustration a semi-closed magnetic field structure with trapped electron beams was modelled using the particle-in-cell model.
Results. Most of the type III bursts studied in this paper have starting frequencies in the range 1100-1400 MHz and their average bandwidth, half-power duration, and interval between adjacent bursts are 116± 59 MHz, 108±41 ms, and 647± 643 ms, respectively. The number of bursts with negative frequency drift, which is on average -914±684 MHz s-1, is greater than the number with positive frequency drift, which is on average +807±675 MHz s-1. The type III bursts have power-law distribution function for their half-power duration $H(f_{start}) = 4.79 \times 10^{8} f_{start}^{-2.145 \pm 0.015}$, bandwidth $B_1(f_{start}) = 1.95 \times 10^{7} f_{start}^{-1.697 \pm 0.022}$ and $B_2(f_{start}) = 7.07 \times 10^{5} f_{start}^{-1.154 \pm 0.015}$, and frequency drift $D(f_{start}) = 0.43 f_{start}^{1.040 \pm 0.031}$. Most of the groups of type III bursts were also found to exhibit either positive or negative group frequency drifts of on average +53±38 MHz s-1 and -46±42 MHz s-1, respectively. The detailed statistical analysis suggests that in the frequency range studied there are two categories of type III bursts, the average parameters of which we provide in brackets for each type: a) numerous narrowband bursts (bandwidth ~100 MHz) with small frequency drift (~±500 MHz s-1) in groups with visible group drift (~±50 MHz s-1) and b) less numerous broader band bursts (bandwidth 171 MHz) with higher frequency drift (~±1800 MHz s-1) in groups without group drift. The statistics of the parameters of these drifting groups are presented for the first time. The drifting groups of type III bursts are interpreted as due to electron beams trapped in moving plasmoids, which are semi-closed magnetic field structures.

Long period variations of dm-radio and X-ray fluxes in three X-class flares:

H. **Meszarosova**, M. Karlicky, J. Rybak, F. Farnik and K. Jiricka

A&A 460 (2006) 865-874**, E-print, Dec 2006**

July 14, 2000, April 12, 2001, and April 15, 2001 flares by the Ondrejov radiospectrograph and Yohkoh spacecraft are studied by statistical methods. The characteristic period of about 300 s found in three X-class flares in their dm-radio and X-ray emissions is discussed.

Radio Emissions from Double RHESSI TGFs

Andrey **Mezentsev** and Thomas Gjesteland
RHESSI nuggets #295, March **2017**
http://sprg.ssl.berkeley.edu/~tohban/wiki/index.php/Radio_Emissions_from_Double_RHESSI_TGFs
The Earth's atmosphere is a rich source of high-energy radiations, including hard X-rays and gamma-rays, that RHESSI has been monitoring since launch. RHESSI's view is of course from space, looking down at the Earth. We introduced these surprisingly interesting terrestrial observations in earlier Nuggets. Here we describe interesting new features of RHESSI observations of **terrestrial gamma-ray flashes** and show how their feedback helps to understand the RHESSI data, specifically its clock data. These TGFs, associated with lightning, have extraordinary temporal precision. Reference [1] provides detailed information.
RHESSI detects gamma rays emerging from the atmosphere; these are the byproduct of the bremsstrahlung of relativistic runaway electrons produced deep in the thunderstorm cloud system. Here the electric fields can be high enough to produce the runaway, and the potential difference large enough (millions of volts) to produce gamma rays.

Statistical Analysis of Decimetric Radio Bursts, Flares, and Coronal Mass Ejections

G. **Michalek** · K. Puchowska · A. Rams
Solar Phys., **2009,** 275(1) Page: 113 – 124, DOI: 10.1007/s11207-009-9343-8
A statistical analysis of decimetric radio bursts (RBs), X-ray flares and coronal mass ejections (CMEs) is carried out. We consider all radio bursts recorded by the Cracow Solar Radio Telescope from the beginning of 1996 until the end of 2004. It is found that the decimetric radio bursts are associated and strongly correlated with X-ray flares. Correlation coefficients between RBs durations and the maximal fluxes of the radio bursts and flares are found to be 0.60 and 0.87, respectively. We also demonstrated that a significant population of the decimetric radio bursts are associated with CMEs. The correlation coefficient between the maximal radio flux density multiplied by the duration of the RBs versus velocity multiplied by width of CMEs is found to be 0.55.

Width of Radio-Loud and Radio-Quiet CMEs

G. **Michalek** · N. Gopalswamy · H. Xie
Solar Phys (**2007**) 246: 409–414
http://www.springerlink.com/content/l748x1p6538v6243/fulltext.pdf
In the present paper we report on the difference in angular sizes between radioloud and radio-quiet CMEs. For this purpose we compiled these two samples of events using *Wind*/WAVES and SOHO/LASCO observations obtained during 1996 – 2005.We show that the radio-loud CMEs are almost twice as wide as the radio-quiet CMEs (considering expanding parts of CMEs). Furthermore, we show that the radio-quiet CMEs have a narrow expanding bright part with a large extended diffusive structure. These results were obtained by measuring the CME widths in three different ways.

NUMERICAL STUDY OF A PROPAGATING NONTHERMAL MICROWAVE FEATURE IN A SOLAR FLARE LOOP

T. **Minoshim**a1,2 and T. Yokoyama
Astrophysical Journal, 686:701Y708, **2008**
http://www.journals.uchicago.edu/doi/pdf/10.1086/591268
We study the motion of electrons along a magnetic loop analytically and numerically, and compare the results with observations of the propagating feature of the nonthermal microwave source in the **1999 August 28** solar flare reported by Yokoyama et al. We model the electron motion with the Fokker-Planck equation and calculate the spatial distribution of the gyrosynchrotron radiation.We find that the microwave-propagating feature does not correspond to the motion of electrons with a specific initial pitch angle. This apparent propagating feature is a consequence of the motion of an ensemble of electrons with different initial pitch angles, which have different times and positions, producing strong radiation in the loop. We conclude that the nonthermal electrons in the 1999 August 28 flare were isotropically accelerated and then were injected into the loop.

Comparative Analysis of Non-Thermal Emissions and Study of Electron Transport in a Solar Flare

T. **Minoshima**, T. Yokoyama, and N. Mitani
E-print, Oct 2007. Ap. J., 673:598Y 610, **2008**
http://www.journals.uchicago.edu/doi/pdf/10.1086/523884
We study nonthermal emission in a solar flare occurring on 2003 May 29 using RHESSI hard X-ray (HXR) and Nobeyama microwave observations. This flare shows several typical behaviors of HXR and microwave emission: time delay of microwave peaks relative to HXR peaks, loop-top microwave and footpoint HXR sources, and a harder electron energy distribution from the microwave spectrum than from the HXR spectrum. In addition, we found that the

time profile of the spectral index of the higher energy (k100 keV) HXRs is similar to that of the microwaves, and is delayed relative to that of the lower energy (P100 keV) HXRs. We interpret these observations in terms of an electron transport model called trap-plus-precipitation. We numerically solved the spatially homogeneous Fokker-Planck equation to determine electron evolution in energy and pitch-angle space. By comparing observations with the behavior of HXR and microwave emission predicted by the model, we examine the pitch-angle distribution of the electrons injected into the flare site.We find that the observed spectral variations can be qualitatively explained if the injected electrons have a pitch-angle distribution concentrated perpendicular to the magnetic field lines rather than an isotropic distribution.

Solar radio bursts observations by Egypt- Alexandria CALLISTO spectrometer: First results

F. N. **Minta**, S. Nozawa, K. Kozarev, A. Elsaid, A. Mahrous
Adv Sp Res v. 72, # 3, p. 816-829 **2023**
https://arxiv.org/ftp/arxiv/papers/2302/2302.00289.pdf
The newly installed CALLISTO spectrometer, hosted by the Department of Space Environment, Institute of Basic and Applied Sciences- EJUST, commenced operation on August 14, 2021. The system contains a cross dipole long-wavelength array antenna with high sensitivity to monitor solar radio transients. Its antenna was strategically positioned and appeared to be in the center of the CALLISTO network of spectrometers. Moreover, in the northern section of Africa, the Egypt-Alexandria CALLISTO and ALGERIA-CRAAG stations are the only ones operating. There are no stations in the West African region, while stations in the eastern part of Africa are not working. Thus, Egypt-Alexandria station serves as a reference for other stations within the e-CALLISTO network. Despite the low solar activity, the instrument detected several solar radio bursts not limited to type II, type III, and type V. A vigorous case study was conducted on two selected radio burst events to validate the authenticity of the recorded events. Other solar radio stations at different geographical locations recorded all the radio bursts detected by the spectrometer. The case study included brief analyses that indicated a type II radio burst observed on October 09, 2021, between 06:30 and 07:00 UT, was associated with an M1.6 solar flare located at N18E08 within NOAA-AR 12882 and a CME with a shock front speed of ~978 km/s. However, the type III radio burst is neither CME nor solar flare associated. These analyses examine the instrument's capacity to provide real-time solar radio transient data 24 hours a day to mitigate the challenges of data gaps faced in the African continent. Hence, the instrument has become an integral part of space weather monitoring and forecasting over the region and other parts of the globe. **27 Aug 2021, 9 Oct 2021**

Assessing the spectral characteristics of band splitting type II radio bursts observed by CALLISTO spectrometers

F. N. **Minta**, S. Nozawa, K. Kamen, A. Elsaid, A. Ayman
Adv Sp Res. 1-14 (**2022**)
https://arxiv.org/ftp/arxiv/papers/2301/2301.13839.pdf
Metric type II radio bursts are usually early indicators of CME-driven shocks and other space weather phenomena in the solar corona. This paper presents a detailed investigation of the spectral properties of band-splitting type II radio bursts and their association with sunspot number. Using type II radio bursts in a frequency range 20 to 200MHz observed by CALLISTO from 2010 to 2017, it was discovered that the analyzed type II shock height, magnetic field strength, CME shock speed, and Alfven speed synchronize with the trajectory of the solar cycle 24. Also, the study revealed that the onset of the declining phase of solar cycle 24 has the highest electron density. The analysis ascertained that the frequency of type II bursts depicts a bimodal distribution during the study period, with peaks in 2012 and 2015. Further, a good correlation(with correlation factor R=0.87) was obtained between the estimated CME shock speeds from the dynamic spectra, and the associated CME speeds from SOHO-LASCO. Moreover, the study confirmed a significant correlation(R=0.8) between the absolute drift rates and the plasma frequency. Additionally, the study explored that 60% of the type II radio bursts considered in this study emanated from the western longitudes. Hence, these findings emphasize that the temporal dynamics of the physical conditions of band-splitting type II radio are essential parameters in space weather monitoring and forecasting. **June 13, 2010, May 02, 2013, Oct 25, 2013**
Table 1: Properties of band splitting type II radio bursts, CMEs, and solar flares. 2010-2017

Small Electron Events Observed by Parker Solar Probe/IS⊙IS during Encounter 2

J. G. **Mitchell1**,2, G. A. de Nolfo2, M. E. Hill3, E. R. Christian2, D. J. McComas4
2020 ApJ 902 20
https://doi.org/10.3847/1538-4357/abb2a4
https://iopscience.iop.org/article/10.3847/1538-4357/abb2a4/pdf
The current understanding of the characteristics of solar and inner heliospheric electron events is inferred almost entirely from observations made by spacecraft located at 1 astronomical unit (au). Previous observations within 1 au of the Sun, by the Helios spacecraft at ~0.3–1 au, indicate the presence of electron events that are not detected at 1 au or may have merged during transport from the Sun. Parker Solar Probe's close proximity to the Sun at perihelion provides an opportunity to make the closest measurements yet of energetic electron events. We present an overview of

measurements of electrons with energies between ~17 keV and ~1 MeV made by the Parker Solar Probe Integrated Science Investigation of the Sun (IS⊙IS) instrument suite during Encounter 2 (2019 March 31–April 10 with perihelion of ~0.17 au), including several small electron events. We examine these events in the context of the electromagnetic and solar wind environment measured by the FIELDS and SWEAP instruments on Parker Solar Probe. We find most of these electron enhancements to be associated with type III radio emissions that reach the local plasma frequency and one enhancement that appears to be primarily associated with abrupt changes in the local magnetic field. Together, these associations suggest that these are indeed the first measurements of energetic electron events within 0.2 au. **2019 April 2, 2019 April 5**

CME -Associated Energetic Ions at 0.23 AU -- Consideration of the Auroral Pressure Cooker Mechanism Operating in the Low Corona as a Possible Energization Process

D. G. **Mitchell**, J. Giacalone, R. C. Allen, M. E. Hill, R. L. McNutt, D. J. McComas, J. R. Szalay, N. A. Schwadron,
ApJ **2020**
https://arxiv.org/ftp/arxiv/papers/1912/1912.08891.pdf
We draw a comparison between a solar energetic particle event associated with the release of a slow coronal mass ejection close to the sun, and the energetic particle population produced in high current density field-aligned current structures associated with auroral phenomena in planetary magnetospheres. We suggest that this process is common in CME development and lift-off in the corona, and may account for the electron populations that generate **Type III radio bursts**, as well as for the prompt energetic ion and electron populations typically observed in interplanetary space. **Nov 2018**

Solar Radio Bursts Associated with In Situ Detected Energetic Electrons in Solar Cycles 23 and 24

Miteva, R., Samwel, S. W., Zabunov, S.:
2022, Universe, 8(5), 275, 20pp.
https://doi.org/10.3390/universe8050275
The first comprehensive analysis between the in situ detected solar energetic electrons (SEEs) from ACE/EPAM satellite and remotely observed radio signatures in solar cycles (SCs) 23 and 24 (1997–2019) is presented. The identified solar origin of the SEEs (in terms of solar flares, SFs, and coronal mass ejections, CMEs) is associated with solar radio emission of types II, III and IV, where possible. Occurrence rates are calculated as a function of the radio wavelength, from the low corona to the interplanetary space near Earth. The tendencies of the different burst appearances with respect to SC, helio-longitude, and SEE intensity are also demonstrated. The corresponding trends of the driver (in terms of median values of the SF class and CME projected speed) are also shown. A comparison with the respective results when using solar energetic protons is presented and discussed.
CESRA #3350 Jul **2022** https://www.astro.gla.ac.uk/users/eduard/cesra/?p=3350

Solar radio bursts: Implications to the origin of in situ particles

Rositsa **Miteva**
Sun and Geosphere, **2018**; 13/2: 145 -151
http://newserver.stil.bas.bg/SUNGEO//00SGArhiv/SG_v13_No2_2018-pp-145-151.pdf
The significance of the solar radio burst signatures for the solar energetic particle (SEP) classification is investigated in the current report. The solar radio bursts associated with the proton-producing solar flares and coronal mass ejections are usually of types II, III and IV. Based on the solar radio burst occurrences in different wavelength ranges, several categories for the SEP origin are adopted. This study evaluates the statistical differences in the flare and CME event samples related to each of these proton categories: flare-driven, CME-driven and mixed-contribution.

Solar energetic particles and radio burst emission

Rositsa **Miteva**, Susan W. Samwel, Vratislav Krupar
Journal of Space Weather and Space Climate 7, A37 **2017**
https://arxiv.org/pdf/1711.09348.pdf **File**
https://www.swsc-journal.org/articles/swsc/pdf/2017/01/swsc170028.pdf
We present a statistical study on the observed solar radio burst emission associated with the origin of in situ detected solar energetic particles. Several proton event catalogs in the period 1996−2016 are used. At the time of appearance of the particle origin (flare and coronal mass ejection) we identified radio burst signatures of types II, III and IV by inspecting dynamic radio spectral plots. The information from observatory reports is also accounted for during the analysis. The occurrence of solar radio burst signatures is evaluated within selected wavelength ranges during the solar cycle 23 and the ongoing 24. Finally, we present the burst occurrence trends with respect to the intensity of the proton events and the location of their solar origin.

Comparison of 30 THz impulsive burst time development to microwaves, H-alpha, EUV, and GOES soft X-rays

R. **Miteva**, P. Kaufmann, D. P. Cabezas, M. M. Cassiano, L. O. T. Fernandes, S. L. Freeland, M. Karlicky, A. Kerdraon, A. S. Kudaka, M. L. Luoni, R. Marcon, J.-P. Raulin, G. Trottet, S. M. White
A&A 586, A91 **2016**
http://arxiv.org/pdf/1512.01763v1.pdf
The recent discovery of impulsive solar burst emission in the 30 THz band is raising new interpretation challenges. One event associated with a GOES M2 class flare has been observed simultaneously in microwaves, H-alpha, EUV, and soft X-ray bands. Although these new observations confirm some features found in the two prior known events, they exhibit time profile structure discrepancies between 30 THz, microwaves, and hard X-rays (as inferred from the Neupert effect). These results suggest a more complex relationship between 30 THz emission and radiation produced at other wavelength ranges. The multiple frequency emissions in the impulsive phase are likely to be produced at a common flaring site lower in the chromosphere. The 30 THz burst emission may be either part of a nonthermal radiation mechanism or due to the rapid thermal response to a beam of high-energy particles bombarding the dense solar atmosphere. **1 August 2014**

The electron acceleration at shock waves in the solar corona:

R.**Miteva** and G.Mann
A&A 474 (**2007**) 617-625
we show that electrons can be accelerated by a resonant wave particle (i.e., whistler-electron) interaction. This mechanism acts in the case of quasi-perpendicular shock waves. After acceleration, the energetic electrons are reflected by the associated shock wave back into the upstream region. The theoretical results are compared with observations, e.g., solar type II radio bursts.

Coronal Magnetic Fields Derived from Simultaneous Microwave and EUV Observations and Comparison with the Potential Field Model

Shun **Miyawaki**, Kazumasa Iwai, Kiyoto Shibasaki, Daikou Shiota, Satoshi Nozawa
ApJ 818 8 **2016**
http://arxiv.org/pdf/1512.04198v1.pdf
We estimated the accuracy of coronal magnetic fields derived from radio observations by comparing them to potential field calculations and the DEM measurements using EUV observations. We derived line of sight component of the coronal magnetic field from polarization observations of the thermal bremsstrahlung in the NOAA active region 11150, observed around 3:00 UT on **February 3, 2011** using the Nobeyama Radioheliograph at 17 GHz. Because the thermal bremsstrahlung intensity at 17 GHz includes both chromospheric and coronal components, we extracted only the coronal component by measuring the coronal emission measure in EUV observations. In addition, we derived only the radio polarization component of the corona by selecting the region of coronal loops and weak magnetic field strength in the chromosphere along the line of sight. The upper limit of the coronal longitudinal magnetic fields were determined as 100 - 210 G. We also calculated the coronal longitudinal magnetic fields from the potential field extrapolation using the photospheric magnetic field obtained from the Helioseismic and Magnetic Imager (HMI). However, the calculated potential fields were certainly smaller than the observed coronal longitudinal magnetic field. This discrepancy between the potential and the observed magnetic field strengths can be explained consistently by two reasons; (a) the underestimation of the coronal emission measure resulting from the limitation of the temperature range of the EUV observations, (b) the underestimation of the coronal magnetic field resulting from the potential field assumption

Novel scaling laws to derive spatially resolved flare and CME parameters from sun-as-a-star observables

Atul **Mohan**1,2⋆, Natchimuthuk Gopalswamy1, Hemapriya Raju3,1 and Sachiko Akiyama1,2
A&A, 691, L8 (**2024**)
https://www.aanda.org/articles/aa/pdf/2024/11/aa51072-24.pdf
Coronal mass ejections (CMEs) are often associated with X-ray (SXR) flares powered by magnetic reconnection in the low corona, while the CME shocks in the upper corona and interplanetary (IP) space accelerate electrons often producing the type II radio bursts. The CME and the reconnection event are part of the same energy release process as highlighted by the correlation between reconnection flux (ϕrec) that quantifies the strength of the released magnetic free energy during the SXR flare, and the CME kinetic energy that drives the IP shocks leading to type II bursts. Unlike the Sun, these physical parameters cannot be directly inferred in stellar observations. Hence, scaling laws between unresolved sun-as-a-star observables, namely SXR luminosity (LX) and type II luminosity (LR), and the physical properties of the associated dynamical events are crucial. Such scaling laws also provide insights into the interconnections between the particle acceleration processes across low-corona to IP space during solar-stellar “flare-CME-type II” events. Using long-term solar data in the SXR to radio waveband, we derived a scaling law between two

novel power metrics for the flare and CME-associated processes. The metrics of "flare power" (Pflare = √(LXϕrec)) and "CME power" (PCME = √(LRVCME2)), where VCME is the CME speed, scale as Pflare ∝ PCME0.76 ± 0.04. In addition, LX and ϕrec show power-law trends with PCME with indices of 1.12 ± 0.05 and 0.61 ± 0.05, respectively. These power laws help infer the spatially resolved physical parameters, VCME and ϕrec, from disk-averaged observables, LX and LR during solar-stellar flare-CME-type II events.

CME-associated type-IV radio bursts: The solar paradigm and the unique case of AD Leo

Atul **Mohan**, Nat Gopalswamy, Surajit Mondal, Anshu Kumari, Sindhuja G
Proceedings of IAUS 388 **2024**
https://arxiv.org/abs/2410.00787
The type-IV bursts, associated with coronal mass ejections (CMEs), occasionally extend to the decameter-hectrometric (DH) range. We present a comprehensive catalog of simultaneous multi-vantage point observations of DH type-IV bursts by Wind and STEREO spacecraft since 2006. 73% of the bursts are associated with fast (>900kms−1) and wide (>600) CMEs, which are mostly geoeffective halo CMEs. Also, we find that the bursts are best observed by the spacecraft located within |600| line of sight (LOS), highlighting the importance of LOS towards active latitudes while choosing target stars for a type-IV search campaign. In young active M dwarfs, CME-associated bursts have remained elusive despite many monitoring campaigns. We present the first detection of long-duration type-III, type-IV, and type-V bursts during an active event in AD Leo (M3.5V; 0.4M⊙). The observed burst characteristics support a multipole model over a solar-like active region magnetic field profile on the star. 2004.11.09
The full catalog of /CME_list/radio/type4 1997-2023
https://cdaw.gsfc.nasa.gov/CME_list/radio/type4/

A catalog of multi-vantage point observations of type-II bursts: Statistics and correlations

Atul **Mohan**, Nat Gopalswamy, Hemapriya Raju, Sachiko Akiyama
Proceedings of IAUS 388 **2024**
https://arxiv.org/pdf/2410.00814
Coronal mass ejection (CME) often produces a soft X-ray (SXR) flare associated with the low-coronal reconnection and a type-II radio burst associated with an interplanetary (IP) CME-shock. SXR flares and type-II bursts outshine the background emission, making them sun-as-a-star observables. Though there exist SXR flare catalogs covering decades of observations, they do not provide the associated type-II luminosity. Besides, since radio burst emission could be beamed, the observed flux dynamic spectrum may vary with line of sight. Using long-term calibrated decameter-hectometric dynamic spectra from the Wind and STEREO spacecraft, we build a catalog of multi-vantage point observations of type-II bursts. Cross-matching with existing catalogs we compile the properties of the associated flare, reconnection, and the CME. Cross-correlation analysis was done between various parameters. Two novel metrics of flare and CME power show a strong correlation revealing a link between particle acceleration strengths in the low-corona and IP space. **2013.12.28**
Catalog of the multi-mission **DH type-II events and associated CMEs 2006-2023**
https://cdaw.gsfc.nasa.gov/CME_list/radio/multimission_type2/

Inter-planetary type-IV solar radio bursts: A comprehensive catalog and statistical results

Atul **Mohan**, Nat Gopalswamy, Anshu Kumari, Sachiko Akiyama, Sindhuja G
ApJ **971** 86 **2024**
https://arxiv.org/pdf/2406.00194
https://iopscience.iop.org/article/10.3847/1538-4357/ad5315/pdf
Decameter hectometric (DH; 1-14 MHz) type-IV radio bursts are produced by flare-accelerated electrons trapped in post-flare loops or the moving magnetic structures associated with the CMEs. From a space weather perspective, it is important to systematically compile these bursts, explore their spectro-temporal characteristics, and study the associated CMEs. We present a comprehensive catalog of DH type-IV bursts observed by the Radio and Plasma Wave Investigation (WAVES) instruments onboard Wind and STEREO spacecraft, covering the period of white-light CME observations by the Large Angle and Spectrometric Coronagraph (LASCO) onboard the SOHO mission between November 1996 and May 2023. The catalog has 139 bursts, of which 73% are associated with a fast (>900 km/s) and wide (>60o) CME, with a mean CME speed of 1301 km/s. All DH type-IV bursts are white-light CME-associated, with 78% of the events associated with halo CMEs. The CME source latitudes are within ±45o. 77 events had multi-vantage point observations from different spacecraft, letting us explore the impact of line of sight on the dynamic spectra. For 48 of the 77 events, there was good data from at least two spacecraft. We find that, unless occulted by nearby plasma structures, a type-IV burst is best viewed when observed within ±60o line of sight. Also, the bursts with a duration above 120 min, have source longitudes within ±60o. Our inferences confirm the inherent directivity in the type-IV emission. Additionally, the catalog forms a sun-as-a-star DH type-IV burst database. **2006-11-05, 2011-06-04, 2012-05-17, 2013-12-31, 2014-01-30, 2014-09-01, 2016-02-21, March 30, 2022, 2022-08-28, 2023-03-06**

The DH type-IV catalog
https://cdaw.gsfc.nasa.gov/CME_list/radio/type4/DHtypeIV_catalog.html

Solar-stellar atmospheric tomography with mm-radio snapshot spectroscopic imaging

Atul **Mohan**
PRE-IX conference proceedings **2023**
https://arxiv.org/pdf/2311.10294.pdf
Millimter (mm) frequencies are primarily sensitive to thermal emission from layers across the stellar chromosphere up to the transition region, while metrewave (radio) frequencies probe the coronal heights. Together the mm and radio band spectroscopic snapshot imaging enables the tomographic exploration of the active atmospheric layers of the cool main-sequence stars (spectral type: FGKM), including our Sun. Sensitive modern mm and radio interferometers let us explore solar/stellar activity covering a range of energy scales at sub-second and sub-MHz resolution over wide operational bandwidths. The superior uv-coverage of these instruments facilitate high dynamic range imaging, letting us explore the morphological evolution of even energetically weak events on the Sun at fine spectro-temporal cadence. This article will introduce the current advancements, the data analysis challenges and available tools. The impact of these tools and novel data in field of solar/stellar research will be summarised with future prospects.

Characterising coronal turbulence using snapshot imaging of radio bursts in 80-200 MHz

Atul **Mohan**
A&A 655, A77 **2021**
https://arxiv.org/pdf/2110.10073.pdf
https://www.aanda.org/articles/aa/pdf/2021/11/aa42029-21.pdf
https://doi.org/10.1051/0004-6361/202142029
Metrewave solar type-III radio bursts offer a unique means to study the properties of turbulence across the coronal heights.Theoretical models have shown that the apparent intensity and size of the burst sources evolve at sub-second scales under the influence of local turbulence. The properties of the evolution varies with frequency. However, observational studies remained difficult due to the lack of high fidelity imaging capabilities at these fine temporal scales simultaneously across wide spectral bands. I present a spectroscopic snapshot imaging (0.5 s, 160 kHz resolution) study of a type-III burst event across 80 - 200 MHz this http URL modelling the temporal variability of the source sizes and intensity at every observation frequency, the characteristics of coronal turbulence is studied across a heliocentric height range of ~1.54 - 1.75 R$\odot$. To understand the morphological evolution of the type-III source, a 2D Gaussian fitting procedure is used. The observed trends in the source area and integrated flux density are analysed in the framework of theoretical and data driven models.Results.The strength of density fluctuations ($\delta N/N$) in the corona is derived as a function of height (R). Combined with the archival low frequency data, $\delta N/N$ values across ~1.5 - 2.2 R$\odot$ agree within a few factors. The burst decay time (τdecay) and the FWHM of the source showed a power-law dependency with frequency, roughly consistent with the results from data driven models. However,the values of τdecay across frequency are higher than expected. The intrinsic sizes of the burst source were derived correcting for scatter broadening. This roughly matched the expected size of flux tubes at the coronal heights explored. I also report the observation of an intrinsic anti-phased pulsation in area and flux density of the source. **2015-11-11**
CESRA #3181 Jan **2022** https://www.astro.gla.ac.uk/users/eduard/cesra/?p=3181

Discovery of correlated evolution in solar noise storm source parameters: Insights on magnetic field dynamics during a microflare

Atul **Mohan**
ApJL **909** L1 **2021**
https://arxiv.org/pdf/2102.10153.pdf
https://iopscience.iop.org/article/10.3847/2041-8213/abe70a/pdf
A solar type-I noise storm is produced by accelerated particle beams generated at active regions undergoing magnetic field restructuring. Their intensity varies by orders of magnitude within sub-second and sub-MHz scales. But, the morphological evolution of these sources are not studied at these scales, due to the lack of required imaging cadence and fidelity in metrewave bands. Using data from the Murchison Widefield Array (MWA), this work explores the co-evolution of size, sky-orientation and intensity of a noise storm source associated with a weak microflare. The work presents the discovery of two correlated modes of evolution in the source parameters: a sausage like \s\ mode where the source intensity and size shows an anti-correlated evolution; and a torsional like \T\ mode where the source size and sky-orientation shows a correlated evolution. A flare mediated mode conversion is observed from \T\ to \s\ for the first time in these sources. These results support the idea of build up of magnetic stress energy in braided active region loops, which later go unstable causing flares and particle acceleration until they relax to a minimally braided state. The discovered mode conversion can be a future diagnostic to such active region phenomena. **3 Nov 2014**
CESRA #2846 Apr **2021** http://www.astro.gla.ac.uk/users/eduard/cesra/?p=2846

A weak coronal heating event associated with periodic particle acceleration episodes

Atul **Mohan**, Patrick I. McCauley, Alpha Mastrano, Divya Oberoi

2019 *ApJ* **883** 45

https://arxiv.org/pdf/1902.10426.pdf

https://doi.org/10.3847/1538-4357/ab3a94

Weak heating events are frequent and ubiquitous in the solar corona. They derive their energy from the local magnetic field and form a major source of local heating, signatures of which are seen in EUV and X-ray bands. Their radio emission arises from various plasma instabilities that lead to coherent radiation, making even a weak flare appear very bright. Hence, the radio observations probe nonequilibrium dynamics, providing complementary information on plasma evolution. However, a robust study of radio emission from a weak event among many simultaneous events requires high dynamic range imaging at subsecond and sub-MHz resolutions owing to its high spectrotemporal variability. Such observations were not possible until recently. This is among the first spatially resolved multiwaveband studies of active region loops hosting transient brightenings (ARTBs) and is dynamically linked to meter-wave type I noise storms. Observations at meter-wave, EUV, and X-ray bands are used, along with magnetogram data. We believe that this is the first spectroscopic radio imaging study of a type I source, the data for which were obtained using the Murchison Widefield Array. We report the discovery of 30 s quasi-periodic oscillations (QPOs) in the radio light curve riding on a coherent baseline flux. The strength of the QPOs and the baseline flux were enhanced during a microflare associated with the ARTB. Our observations suggest a scenario where magnetic stress builds up over an Alfvén timescale (30 s) across the typical magnetic field braiding scale and then dissipates via a cascade of weak reconnection events.

November 3, 2014

CESRA Highlights # 2385 Oct **2019** http://www.astro.gla.ac.uk/users/eduard/cesra/?p=2385

Evidence for Super-Alfvenic oscillations in sources of Solar type III radio bursts

Atul **Mohan**, Surajit Mondal, Divya Oberoi, Colin Lonsdale

2018 *ApJ* **875** 98

https://arxiv.org/pdf/1809.02588.pdf

sci-hub.se/10.3847/1538-4357/ab0ae5

At the site of their origin, solar meterwave radio bursts contain pristine information about the local coronal magnetic field and plasma parameters. On its way through the turbulent corona, this radiation gets substantially modified due to the propagation effects. Effectively disentangling the intrinsic variations in emission from propagation effects has remained a challenge. We demonstrate a way to achieve this, using snapshot spectroscopic imaging study of weak type III bursts using data from the Murchison Widefield Array (MWA). We use this study to present the first observational evidence for second-scale Quasi-Periodic Oscillations (QPOs) in burst source sizes and orientation with simultaneous QPOs in intensity. The observed oscillations in source sizes are so fast and so large that, they would require two orders of magnitude larger \alf speed than the typical 0.5 Mm/s, if interpreted within a MHD framework. These observations imply the presence of a quasi-periodic regulation mechanism operating at the particle injection site, modulating the geometry of energetic electron beams that generate type III bursts. In addition, we introduce a method to characterize plasma turbulence in mid coronal ranges, using such frequent weak bursts. We also detect evidence for a systematic drift in the location of the burst sources superposed on the random jitter induced by scattering. We interpret this as the motion of the open flux tube within which the energetic electron beams travel. **3 November 2014**

4D Data Cubes from Radio-Interferometric Spectroscopic Snapshot Imaging

Atul **Mohan**, Divya Oberoi

Solar Phys. 292:168 **2017**

https://arxiv.org/pdf/1710.10525.pdf

https://link.springer.com/content/pdf/10.1007%2Fs11207-017-1193-1.pdf

The new generation of low radio-frequency interferometric arrays have enabled the imaging of the solar corona at high spectro-temporal resolutions and sensitivity. In this article we introduce and implement a formalism to generate flux density and brightness temperature (TB) maps from such images, using independently obtained disc-integrated solar flux density dynamic spectra. These images collectively generate a 4D data cube, with axes spanning angular coordinates (θ,ϕ), frequency (ν) and time (t). This 4D data cube is the most informative data product which can be generated from interferometric radio data. It will allow us to track solar emission simultaneously in these four dimensions. We also introduce SPatially REsolved Dynamic Spectra (SPREDS), named in analogy to the usual dynamic spectra. For any arbitrary region, (θi,ϕj), in the maps, these 2D projections of the 4D data cube correspond to the dynamic spectrum of emission arising from there. We show examples of these data products using observations from the Murchison Widefield Array (MWA). These are also the first calibrated solar maps from the MWA.

3 November, 2014

Solar Chromospheric Temperature Diagnostics: a joint ALMA-Hα analysis

Momchil E. **Molnar**, Kevin P. Reardon, Yi Chai, Dale Gary, Han Uitenbroek, Gianna Cauzzi, Steven R. Cranmer

ApJ **2019**

https://arxiv.org/pdf/1906.08896.pdf

We present the first high-resolution, simultaneous observations of the solar chromosphere in the optical and millimeter wavelength ranges, obtained with ALMA and the IBIS instrument at the Dunn Solar Telescope. In this paper we concentrate on the comparison between the brightness temperature observed in ALMA Band 3 (3 mm; 100 GHz) and the core width of the Hα 656.3 nm line, previously identified as a possible diagnostic of the chromospheric temperature. We find that in the area of plage, network and fibrils covered by our FOV the two diagnostics are well correlated, with similar spatial structures observed in both. The strength of the correlation is remarkable, given that the source function of the mm-radiation obeys local thermodynamic equilibrium, while the Hα line has a source function that deviates significantly from the local Planck function. The observed range of ALMA brightness temperatures is sensibly smaller than the temperature range that was previously invoked to explain the observed width variations in Hα. We employ analysis from forward modeling with the RH code to argue that the strong correlation between Hα width and ALMA brightness temperature is caused by their shared dependence on the population number n2 of the first excited level of hydrogen. This population number drives millimeter opacity through hydrogen ionization via the Balmer continuum, and Hα width through a curve-of-growth-like opacity effect. Ultimately, the n2 population is regulated by the enhancement or lack of downward Lyα flux, which coherently shifts the formation height of both diagnostics to regions with different temperature, respectively. **April 23, 2017**

CESRA nugget #2348 Oct **2019** http://www.astro.gla.ac.uk/users/eduard/cesra/?p=2348

New Insights into Type-I Solar Noise Storms from High Angular Resolution Spectroscopic Imaging with the upgraded Giant Metrewave Radio Telescope

Surajit **Mondal**, Devojyoti Kansabanik, Divya Oberoi, Soham Dey

ApJ **975** 122 **2024**

https://arxiv.org/pdf/2408.13465

https://iopscience.iop.org/article/10.3847/1538-4357/ad77c2/pdf

Type-I solar noise storms are perhaps the most commonly observed active radio emissions from the Sun at meter-wavelengths. Noise storms have a long-lived and wideband continuum background with superposed islands of much brighter narrowband and short-lived emissions, known as type-I bursts. There is a serious paucity of studies focusing on the morphology of these two types of emissions, primarily because of the belief that coronal scattering will always wash out any features at small angular scales. However, it is important to { investigate} their spatial structures in detail to make a spatio-temporal connection with observations at extreme-ultraviolet/ X-ray bands to understand the detailed nature of these emissions. In this work, we use high angular resolution observations from the upgraded Giant Metrewave Radio Telescope to demonstrate that it is possible to detect structures with angular scales as small as $\sim 9\arcsec$, about three times smaller than the smallest structure reported to date from noise storms. Our observations also suggest while the individual type-I bursts are narrowband in nature, the bursts are probably caused by traveling disturbance(s) inducing magnetic reconnections at different coronal heights, and thus leading to correlated change in the morphology of the type-I bursts observed at a wide range of frequencies. **2022-06-25**

A Joint Microwave and Hard X-Ray Study Towards Understanding the Transport of Accelerated Electrons during an Eruptive Solar Flare

Surajit **Mondal**, Andrea F. Battaglia, Bin Chen, Sijie Yu

ApJ **966** 208 **2024**

https://arxiv.org/pdf/2404.14268.pdf

https://iopscience.iop.org/article/10.3847/1538-4357/ad3910/pdf

The standard flare model, despite its success, is limited in comprehensively explaining the various processes involving nonthermal particles. One such missing ingredient is a detailed understanding of the various processes involved during the transport of accelerated electrons from their site of acceleration to different parts of the flare region. Here we use simultaneous radio and X-ray observations from the Expanded Owens Valley Solar Array (EOVSA) and Spectrometer/Telescope for Imaging X-rays (STIX) onboard the Solar Orbiter (SolO), respectively, from two distinct viewing perspectives to study the electron transport processes. Through detailed spectral modeling of the coronal source using radio data and footpoint sources using X-ray spectra, we compare the nonthermal electron distribution at the coronal and footpoint sources. We find that the flux of nonthermal electrons precipitated at the footpoint is an order of magnitude greater than that trapped in the looptop, consistent with earlier works which primarily used X-ray for their studies. In addition, we find that the electron spectral indices obtained from X-ray footpoints is significantly softer than the spectral hardness of the nonthermal electron distribution in the corona. We interpret these differences based on transport effects and the difference in sensitivity of microwave and X-ray observations to different regimes of electron energies. Such an understanding is crucial for leveraging different diagnostic methods of nonthermal electrons simultaneously to achieve a more comprehensive understanding of the electron acceleration and transport processes of solar flares. 2021 May 7

Characterizing the Spectral Structure of Weak Impulsive Narrowband Quiet Sun Emissions

Surajit **Mondal**, Divya Oberoi, Ayan Biswas, Devojyoti Kansabanik

ApJ **2023**

https://arxiv.org/pdf/2306.16390.pdf

Weak Impulsive Narrowband Quiet Sun Emissions (WINQSEs) are a newly discovered class of radio emission from the solar corona. These emissions are characterized by their extremely impulsive, narrowband and ubiquitous nature. We have systematically been working on their detailed characterization, including their strengths, morphologies, temporal characteristics, energies, etc. This work is the next step in this series and focuses on the spectral nature of WINQSEs. Given that their strength is only a few percent of the background solar emission, we have adopted an extremely conservative approach to reliably identify WINQSES. Only a handful of WINQSEs meet all of our stringent criteria. Their flux densities lie in the $20 - 50$ Jy range and they have compact morphologies. For the first time, we estimate their bandwidths and find them to be less than 700 kHz, consistent with expectations based on earlier observations. Interestingly, we also find similarities between the spectral nature of WINQSEs and the solar radio spikes. This is consistent with our hypothesis that the WINQSEs are the weaker cousins of the type-III radio bursts and are likely to be the low-frequency radio counterparts of the nanoflares, originally hypothesized as a possible explanation for coronal heating. **2020 June 20**

Multifrequency microwave imaging of weak transients from the quiet solar corona

Surajit **Mondal**, Bin Chen, Sijie Yu

ApJ **949** 56 **2023**

https://arxiv.org/pdf/2301.07840.pdf

Understanding the dynamics of the quiet solar corona is important for answering key questions including the coronal heating problem. Multiple studies have suggested small-scale magnetic reconnection events may play a crucial role. These reconnection events are expected to involve accelerating electrons to suprathermal energies, which can then produce nonthermal observational signatures. However, due to the paucity of sensitive high-fidelity observations capable of probing these nonthermal signatures, most studies were unable to quantify their nonthermal nature. Here we use joint radio observations from the Very Large Array (VLA) and the Expanded Owens Valley Solar Array (EOVSA) to detect transient emissions from the quiet solar corona in the microwave (GHz) domain. While similar transients have been reported in the past, their nonthermal nature could not be adequately quantified due to the unavailability of broadband observations. Using a much larger bandwidth available now with the VLA and EOVSA, in this study, we are able to quantify the nonthermal energy associated with two of these transients. We find that the total nonthermal energy associated with some of these transients can be comparable to or even larger than the total thermal energy of a nanoflare, which underpins the importance of nonthermal energy in the total coronal energy budget. **February 1, 2020**

Study of radio transients from the quiet Sun during an extremely quiet time

Surajit **Mondal**, Divya Oberoi, Ayan Biswas

ApJ **943** 122 **2023**

https://arxiv.org/pdf/2212.00503.pdf

https://iopscience.iop.org/article/10.3847/1538-4357/aca899/pdf

In this work we study a class of recently discovered metrewave solar transients referred to as Weak Impulsive Narrowband Quiet Sun Emission \citep[WINQSEs,][]{mondal2020}. Their strength is a few percent of the quiet Sun background and are characterised by their very impulsive, narrow-band and ubiquitous presence in quiet Sun regions. \citet{mondal2020} hypothesised that these emissions might be the radio counterparts of the nanoflares and their potential significance warrants detailed studies. Here we present an analysis of data from an extremely quiet time and with an improved methodology over the previous work. As before, we detect numerous WINQSEs, which we have used for their further characterisation. Their key properties, namely, their impulsive nature and ubiquitous presence on the quiet Sun are observed in these data as well. Interestingly, we also find some of the observed properties to differ significantly from the earlier work. With this demonstration of routine detection of WINQSEs, we hope to engender interest in the larger community to build a deeper understanding of WINQSEs. **20 June, 2020**

A Search for the Counterparts of Quiet-Sun Radio Transients in Extreme Ultraviolet Data

Surajit **Mondal**

Solar Physics volume 296, Article number: 131 (**2021**)

https://arxiv.org/pdf/2107.04525.pdf

https://link.springer.com/content/pdf/10.1007/s11207-021-01877-3.pdf

https://doi.org/10.1007/s11207-021-01877-3

Nonthermal radio transients from the quiet Sun have been recently discovered and it has been hypothesized using rough calculations that they might be important for coronal heating. It is well realized that energy calculations using coherent emissions are often subject to poorly constrained parameters and hence have large uncertainties. However, energy

estimates using observations in the extreme ultraviolet (EUV) and soft X-ray bands are routinely done and the techniques are pretty well established. This work presents the first attempt to identify the EUV counterparts of these radio transients and then use them to estimate the energy deposited into the corona during the event. I show that the group of radio transients studied here is associated with a brightening observed in the EUV waveband and is produced by an energy release of ≈1025≈1025 ergs. The fact that the flux density of the radio transient is only ≈2≈2 mSFU suggests that it might be possible to do large statistical studies in the future for understanding the relationship between these radio transients and other EUV and X-ray counterparts, as well as for understanding their importance in coronal heating. **November 27, 2017**

Insights from snapshot spectroscopic radio observations of a weak Type I noise storm

Surajit **Mondal**, Divya Oberoi
ApJ **920** 11 **2021**
https://arxiv.org/pdf/2106.12779.pdf
https://doi.org/10.3847/1538-4357/ac1076
We present a high fidelity snapshot spectroscopic radio imaging study of a weak type I solar noise storm which took place during an otherwise exceptionally quiet time. Using high fidelity images from the Murchison Widefield Array, we track the observed morphology of the burst source for 70 minutes and identify multiple instances where its integrated flux density and area are strongly anti-correlated with each other. The type I radio emission is believed to arise due to electron beams energized during magnetic reconnection activity. The observed anti-correlation is interpreted as evidence for presence of MHD sausage wave modes in the magnetic loops and strands along which these electron beams are propagating. Our observations suggest that the sites of these small scale reconnections are distributed along the magnetic flux tube. We hypothesise that small scale reconnections produces electron beams which quickly get collisionally damped. Hence, the plasma emission produced by them span only a narrow bandwidth and the features seen even a few MHz apart must arise from independent electron beams. **27 November, 2017**

First radio evidence for impulsive heating contribution to the quiet solar corona

Surajit **Mondal**, Divya Oberoi, Atul Mohan
ApJL **895** L39 **2020**
https://arxiv.org/pdf/2004.04399.pdf
https://doi.org/10.3847/2041-8213/ab8817
This letter explores the relevance of nanoflare based models for heating the quiet sun corona. Using metrewave data from the Murchison Widefield Array, we present the first successful detection of impulsive emissions down to flux densities of ∼mSFU, about two orders of magnitude weaker than earlier attempts. These impulsive emissions have durations ≲1s and are present throughout the quiet solar corona. The fractional time occupancy of these impulsive emissions at a given region is ≲10%. The histograms of these impulsive emissions follow a powerlaw distribution and show signs of clustering at small timescales. Our estimate of the energy which must be dumped in the corona to generate these impulsive emissions is consistent with the coronal heating requirements. Additionally, the statistical properties of these impulsive emissions are very similar to those recently determined for magnetic switchbacks by the Parker Solar Probe (PSP). We hope that this work will lead to a renewed interest in relating these weak impulsive emissions to the energy deposited in the corona, the quantity of physical interesting from a coronal heating perspective, and explore their relationship with the magnetic switchbacks observed by the PSP. **November 27, 2017**
CESRA #2611 June **2020** http://www.astro.gla.ac.uk/users/eduard/cesra/?p=2611

Estimation of the physical parameters of a CME at high coronal heights using low frequency radio observations

Surajit **Mondal**, Divya Oberoi, Angelos Vourlidas
ApJ **893** 28 **2020**
https://arxiv.org/pdf/1909.12041.pdf
sci-hub.st/10.3847/1538-4357/ab7fab
Measuring the physical parameters of Coronal Mass Ejections (CMEs), particularly their entrained magnetic field, is crucial for understanding their physics and for assessing their geo-effectiveness. At the moment, only remote sensing techniques can probe these quantities in the corona, the region where CMEs form and acquire their defining characteristics. Radio observations offer the most direct means for estimating the magnetic field when gyrosynchontron emission is detected. In this work we measure various CME plasma parameters, including its magnetic field, by modelling the gyrosynchrotron emission from a CME. The dense spectral coverage over a wide frequency range provided by the Murchison Widefield Array (MWA) affords a much better spectral sampling than possible before. The MWA images also provide much higher imaging dynamic range, enabling us to image these weak emissions. Hence we are able to detect radio emission from a CME at larger distances (4.73R⊙) than have been reported before. The flux densities reported here are amongst the lowest measured in similar works. Our ability to make extensive measurements on a slow and otherwise unremarkable CME suggest that with the availability of data from the new generation

instruments like the MWA, it should now be possible to make routine direct detections of radio counterparts of CMEs.
November 4, 2015

Unsupervised generation of high dynamic range solar images: A novel algorithm for self-calibration of interferometry data

Surajit **Mondal**, Atul Mohan, Divya Oberoi, John S. Morgan, Leonid Benkevitch, Colin J. Lonsdale, Meagan Crowley, Iver H. Cairns
ApJ **875** 97 **2019**
https://arxiv.org/pdf/1902.08748.pdf
sci-hub.se/10.3847/1538-4357/ab0a01
Solar radio emission, especially at metre-wavelengths, is well known to vary over small spectral (≲100\,kHz) and temporal (<1\,s) spans. It is comparatively recently, with the advent of a new generation of instruments, that it has become possible to capture data with sufficient resolution (temporal, spectral and angular) that one can begin to characterize the solar morphology simultaneously along the axes of time and frequency. This ability is naturally accompanied by an enormous increase in data volumes and computational burden, a problem which will only become more acute with the next generation of instruments such as the Square Kilometre Array (SKA). The usual approach, which requires manual guidance of the calibration process, is impractical. Here we present the "Automated Imaging Routine for Compact Arrays for the Radio Sun (AIRCARS)", an end-to-end imaging pipeline optimized for solar imaging with arrays with a compact core. We have used AIRCARS so far on data from the Murchison Widefield Array (MWA) Phase-I. The dynamic range of the images is routinely from a few hundred to a few thousand. In the few cases, where we have pushed AIRCARS to its limits, the dynamic range can go as high as ∼75000. The images made represent a substantial improvement in the state-of-the-art in terms of imaging fidelity and dynamic range. This has the potential to transform the multi-petabyte MWA solar archive from raw visibilities into science-ready images. AIRCARS can also be tuned to upcoming telescopes like the SKA, making it a very useful tool for the heliophysics community.
CESRA nugget #2282 **2019** http://cesra.net/?p=2282

CALLISTO status report/newsletter #73, March 2018

Christian **Monstein**
Easter Solar Radio Burst Gallery from all over the world
http://files.mail-list.com/m/iswinewsletter/status-73-V0.pdf
March 30, 2018

Catalog of dynamic electromagnetic spectra

Christian **Monstein**
Physics, Astronomy and Electronics Work Bench **2016**
http://e-callisto.org/GeneralDocuments/BurstCatalog.pdf
This catalog demonstrates dynamic electromagnetic spectra observed by Callisto, Phoenix-3 and ARGOS radio spectrometers. In the first part natural spectra are presented while in the second part we concentrate on artificial (man-made) spectra. This catalog shall help the scientist to detect and identify weak solar radio bursts in highly interfered spectra as well as to separate natural dynamic time-frequency structures from man made rfi. In addition, Callisto spectrometers have proven to be a cheap and reliable instrument for radio frequency monitoring of terrestrial interference.

Predicted free–free emission at radio wavelengths from Coronal Mass Ejections: event on 2011 March 7

Daniela **Montes-Doria**, Ricardo F González, Jorge Cantó, Stanley Kurtz
MNRAS, Volume 509, Issue 2, January **2022**, Pages 1892–1898,
https://doi.org/10.1093/mnras/stab3085
We present an analytical model for the free–free emission at radio wavelengths produced by the interaction of a Coronal Mass Ejection (CME) with the ambient solar wind. Using our previous models, we show that a dense shell bounded by two shock fronts is formed from this interaction, whose dynamical evolution can be calculated based on considerations of the mass and momentum conservation for the shell. This structure undergoes two stages in its dynamical evolution: (1) A first one of constant velocity, when the shell is bounded by two shock fronts, and (2) a second one, in which a one-shock structure (the leading shock) is decelerated. Here, we compute the emission produced by these shocks, and present a comparison with synthetic observations of the **2011 March 7** CME. Our simplified model gives a physical insight into the free–free emission produced by shocks of CMEs.

Detection and Characterisation of a Coronal Mass Ejection using Interplanetary Scintillation measurements from the Murchison Widefield Array

J. **Morgan**, P. I. McCauley, A. Waszewski, R. Ekers, R. Chhetri
Space Weather **2023**
https://arxiv.org/pdf/2303.09134.pdf
We have shown previously that the Murchison Widefield Array (MWA), can detect hundreds of Interplanetary Scintillation (IPS) sources simultaneously across a field of view ∼30◦ in extent. To test if we can use this capability to track heliospheric structures, we undertook a search of 88 hours of MWA IPS data, and identified an observation likely to have a significant Coronal Mass Ejection (CME) in the field of view. We demonstrate that in a single 5-minute MWA observation we are able to localise and image a CME ∼33 hours after launch at an elongation of ∼37◦ from the Sun. We use IPS observables to constrain the kinematics of the CME, and describe how MWA IPS observations can be used in the future to make a unique contribution to heliospheric modelling efforts. **2016-05-15**

Solar Micro-Type III Burst Storms and Long Dipolar Magnetic Field in the Outer Corona

A. **Morioka**1, Y. Miyoshi2, K. Iwai3, Y. Kasaba4, S. Masuda2, H. Misawa1, and T. Obara
2015 ApJ 808 191
Solar micro-type III radio bursts are elements of the so-called type III storms and are characterized by short-lived, continuous, and weak emissions. Their frequency of occurrence with respect to radiation power is quite different from that of ordinary type III bursts, suggesting that the generation process is not flare-related, but due to some recurrent acceleration processes around the active region. We examine the relationship of micro-type III radio bursts with coronal streamers. We also explore the propagation channel of bursts in the outer corona, the acceleration process, and the escape route of electron beams. It is observationally confirmed that micro-type III bursts occur near the edge of coronal streamers. The magnetic field line of the escaping electron beams is tracked on the basis of the frequency drift rate of micro-type III bursts and the electron density distribution model. The results demonstrate that electron beams are trapped along closed dipolar field lines in the outer coronal region, which arise from the interface region between the active region and the coronal hole. A 22 year statistical study reveals that the apex altitude of the magnetic loop ranges from 15 to 50 RS. The distribution of the apex altitude has a sharp upper limit around 50 RS suggesting that an unknown but universal condition regulates the upper boundary of the streamer dipolar field.

Micro-Type III Radio Bursts

Akira **Morioka**, Yoshizumi Miyoshi, Satoshi Masuda, Fuminori Tsuchiya, Hiroaki Misawa, Hiroshi Matsumoto, Kozo Hashimoto, and Hiroshi Oya
Astrophysical Journal, Volume 657, Number 1, Page 567, **2007**.
http://www.journals.uchicago.edu/cgi-bin/resolveflApJ65712

Determining the acceleration regions of in situ electrons using remote radio and X-ray observations

D. E. **Morosan**, N. Dresing, C. Palmroos, J. Gieseler, I. C. Jebaraj, A. Warmuth, A. Fedeli, S. Normo, J. Pomoell, E. K. J. Kilpua, P. Zucca, B. Dabrowski, A. Krankowski, G. Mann, C. Vocks, R. Vainio
A&A **2024**
https://arxiv.org/pdf/2412.06477
Solar energetic particles in the heliosphere are produced by flaring processes on the Sun or shocks driven by coronal mass ejections. These particles are regularly detected remotely as electromagnetic radiation (X-rays or radio emission), which they generate through various processes, or in situ by spacecraft monitoring the Sun and the heliosphere. We aim to combine remote-sensing and in situ observations of energetic electrons to determine the origin and acceleration mechanism of these particles. Here, we investigate the acceleration location, escape, and propagation directions of electron beams producing radio bursts observed with the Low Frequency Array (LOFAR), hard X-ray (HXR) emission and, in situ electrons observed at Solar Orbiter (SolO) on **3 October 2023**. These observations are combined with a three-dimensional (3D) representation of the electron acceleration locations and results from a magneto-hydrodynamic (MHD) model of the solar corona in order to investigate the origin and connectivity of electrons observed remotely at the Sun to in situ electrons. We observed a type II radio burst with good connectivity to SolO, where a significant electron event was detected. However, type III radio bursts and Hard X-rays were also observed co-temporally with the elctron event but likely connected to SolO by different far-sided field lines. The injection times of the SolO electrons are simultaneous with both the onset of the type II radio burst, the group of type III bursts and the presence of a second HXR peak, however, the most direct connection to SolO is that of the type II burst location. The in situ electron spectra point to shock acceleration of electrons with a short-term connection to the source region.

Connecting remote and in situ observations of shock-accelerated electrons associated with a coronal mass ejection

D. E. **Morosan**, J. Pomoell, C. Palmroos, N. Dresing, E. Asvestari, R. Vainio, E. K. J. Kilpua, J. Gieseler, A. Kumari, I. C. Jebaraj
A&A 683, A31 **2023**
https://arxiv.org/pdf/2312.07166.pdf
https://www.aanda.org/articles/aa/pdf/2024/03/aa47873-23.pdf
One of the most prominent sources for energetic particles in our solar system are huge eruptions of magnetised plasma from the Sun called coronal mass ejections (CMEs), which usually drive shocks that accelerate charged particles up to relativistic energies. In particular, energetic electron beams can generate radio bursts through the plasma emission mechanism, for example, type II and accompanying herringbone bursts. Here, we investigate the acceleration location, escape, and propagation directions of various electron beams in the solar corona and compare them to the arrival of electrons at spacecraft. To track energetic electron beams, we use a synthesis of remote and direct observations combined with coronal modelling. Remote observations include ground-based radio observations from the Nancay Radioheliograph (NRH) combined with space-based extreme-ultraviolet and white-light observations from the Solar Dynamics Observatory (SDO), the Solar Terrestrial Relations Observatory (STEREO) and Solar Orbiter (SolO). We also use direct observations of energetic electrons from the STEREO and Wind spacecraft. These observations are then combined with a three-dimensional (3D) representation of the electron acceleration locations that combined with results from magneto-hydrodynamic models of the solar corona is used to investigate the origin and link of electrons observed remotely at the Sun to in situ electrons. We observed a type II radio burst followed by herringbone bursts that show single-frequency movement through time in NRH images. The movement of the type II burst and herringbone radio sources seems to be influenced by the regions in the corona where the CME is more capable of driving a shock. We also found similar inferred injection times of near-relativistic electrons at spacecraft to the emission time of the type II and herringbone bursts. **28 March 2022**

A type II solar radio burst without a coronal mass ejection

D. E. **Morosan**, J. Pomoell, A. Kumari, E. K. J. Kilpua, R. Vainio
A&A 675, A98 **2023**
https://arxiv.org/pdf/2305.11545.pdf
https://www.aanda.org/articles/aa/pdf/2023/07/aa45515-22.pdf
The Sun produces the most powerful explosions in the solar system, solar flares, that can also be accompanied by large eruptions of magnetised plasma, coronal mass ejections (CMEs). These processes can accelerate electron beams up to relativistic energies through magnetic reconnection processes during solar flares and CME-driven shocks. Energetic electron beams can in turn generate radio bursts through the plasma emission mechanism. CME shocks, in particular, are usually associated with type II solar radio bursts. However, on a few occasions, type II bursts have been reported to occur either in the absence of CMEs or shown to be more likely related with the flaring process. It is currently an open question how a shock generating type II bursts forms without the occurrence of a CME eruption. Here, we aim to determine the physical mechanism responsible for a type II burst which occurs in the absence a CME. By using radio imaging from the Nan{\c c}ay Radioheliograph, combined with observations from the Solar Dynamics Observatory and the Solar Terrestrial Relations Observatory spacecraft, we investigate the origin of a type II radio burst that appears to have no temporal association with a white-light CME. We identify a typical type II radio burst with band-split structure that is associated with a C-class solar flare. The type II burst source is located above the flaring active region and ahead of disturbed coronal loops observed in extreme ultraviolet images. The type II is also preceded by type III radio bursts, some of which are in fact J-bursts indicating that accelerated electron beams do not all escape along open field lines. The type II sources show single-frequency movement towards the flaring active region. The type II is located ahead of a faint extreme-ultraviolet (EUV) front propagating through the corona. **25 Oct 2013**

Shock-accelerated electrons during the fast expansion of a coronal mass ejection

D. E. **Morosan**, J. Pomoell, A. Kumari, R. Vainio, E. K. J. Kilpua
A&A 668, A15 **2022**
https://arxiv.org/pdf/2211.06049.pdf
https://www.aanda.org/articles/aa/pdf/2022/12/aa44432-22.pdf
Context. Some of of the most prominent sources for energetic particles in our Solar System are huge eruptions of magnetised plasma from the Sun called coronal mass ejections (CMEs), which usually drive shocks that accelerate charged particles up to relativistic energies. In particular, energetic electron beams can generate radio bursts through the plasma emission mechanism. The main types of bursts associated with CME shocks are type II and herringbone bursts. However, it is currently unknown where early accelerated electrons that produce metric type II bursts and herringbones propagate and when they escape the solar atmosphere. Aims. Here, we investigate the acceleration location, escape, and propagation directions of electron beams during the early evolution of a strongly expanding CME-driven shock wave associated with herrinbgone bursts. Methods. We used ground-based radio observations from the Nançay Radioheliograph combined with space-based extreme-ultraviolet and white-light observations from the Solar Dynamics Observatory and and the Solar Terrestrial Relations Observatory. We produced a three-dimensional (3D) representation of the electron acceleration locations which, combined with results from magneto-hydrodynamic (MHD) models of the

solar corona, was used to investigate the origin of the herringbone bursts observed. Results. Multiple herringbone bursts are found close to the CME flank in plane-of-sky images. Some of these herringbone bursts have unusual inverted J shapes and opposite drifting herringbones also show opposite senses of circular polarisation. By using a 3D approach combined with the radio properties of the observed bursts, we find evidence that the first radio emission in the CME eruption most likely originates from electrons that initially propagate in regions of low Alfvén speeds and along closed magnetic field lines forming a coronal streamer. **25 October 2013**

Exploring the circular polarisation of low-frequency solar radio bursts with LOFAR

Diana E. **Morosan**, Juska E. Räsänen, Anshu Kumari, Emilia K. J. Kilpua, Mario M. Bisi, Bartosz Dabrowski, Andrzej Krankowski, Jasmina Magdalenić, Gottfried Mann, Hanna Rothkaehl, Christian Vocks, Pietro Zucca

Solar Phys. **297**, Article number: 47 **2022**

https://arxiv.org/pdf/2203.14674.pdf

https://link.springer.com/content/pdf/10.1007/s11207-022-01976-9.pdf

The Sun is an active star that often produces numerous bursts of electromagnetic radiation at radio wavelengths. Low frequency radio bursts have recently been brought back to light with the advancement of novel radio interferometers. However, their polarisation properties have not yet been explored in detail, especially with the Low Frequency Array (LOFAR), due to difficulties in calibrating the data and accounting for instrumental leakage. Here, using a unique method to correct the polarisation observations, we explore the circular polarisation of different sub-types of solar type III radio bursts and a type I noise storm observed with LOFAR, which occurred during March-April 2019. We analysed six individual radio bursts from two different dates. We present the first Stokes V low frequency images of the Sun with LOFAR in tied-array mode observations. We find that the degree of circular polarisation for each of the selected bursts increases with frequency for fundamental emission, while this trend is either not clear or absent for harmonic emission. The type III bursts studied, that are part of a long--lasting type III storm, can have different senses of circular polarisation, occur at different locations and have different propagation directions. This indicates that the type III bursts forming a classical type III storm do not necessarily have a common origin but instead they indicate the existence of multiple, possibly unrelated, acceleration processes originating from solar minimum active regions. **2019-03-21, 2019-04-08**

Moving solar radio bursts and their association with coronal mass ejections

D. E. **Morosan**, A. Kumari, E. K. J. Kilpua, A. Hamini

A&A 647, L12 **2021**

https://arxiv.org/pdf/2103.05942.pdf

https://www.aanda.org/articles/aa/pdf/2021/03/aa40392-21.pdf

https://doi.org/10.1051/0004-6361/202140392

Context: Solar eruptions, such as coronal mass ejections (CMEs), are often accompanied by accelerated electrons that can in turn emit radiation at radio wavelengths. This radiation is observed as solar radio bursts. The main types of bursts associated with CMEs are type II and type IV bursts that can sometimes show movement in the direction of the CME expansion, either radially or laterally. However, the propagation of radio bursts with respect to CMEs has only been studied for individual events.

Aims: Here, we perform a statistical study of 64 moving bursts with the aim to determine how often CMEs are accompanied by moving radio bursts. This is done in order to ascertain the usefulness of using radio images in estimating the early CME expansion.

Methods: Using radio imaging from the Naçay Radioheliograph (NRH), we constructed a list of moving radio bursts, defined as bursts that move across the plane of sky at a single frequency. We define their association with CMEs and the properties of associated CMEs using white-light coronagraph observations. We also determine their connection to classical type II and type IV radio burst categorisation.

Results: We find that just over a quarter of type II and half of type IV bursts that occurred during the NRH observing windows in Solar Cycle 24 are accompanied by moving radio emission. All but one of the moving radio bursts are associated with white--light CMEs and the majority of moving bursts (90%) are associated with wide CMEs (>60 degrees in width). In particular, all but one of the moving bursts corresponding to type IIs are associated with wide CMEs; however, and unexpectedly, the majority of type II moving bursts are associated with slow white-light CMEs (<500 km/s). On the other hand, the majority of moving type IV bursts are associated with fast CMEs (>500 km/s). **14 June 2012**

Electron acceleration and radio emission following the early interaction of two coronal mass ejections

D. E. **Morosan**, E. Palmerio1 J. E. Räsänen, E. K. J. Kilpua, J. Magdalenić, B. J. Lynch, A. Kumari, J. Pomoell, M. Palmroth

A&A 642, A151 **2020**

https://arxiv.org/pdf/2008.10245.pdf
https://doi.org/10.1051/0004-6361/202038801
https://sci-hub.ru/10.1051/0004-6361/202038801
Context. Coronal mass ejections (CMEs) are large eruptions of magnetised plasma from the Sun that are often accompanied by solar radio bursts produced by accelerated electrons. Aims. A powerful source for accelerating electron beams are CME-driven shocks, however, there are other mechanisms capable of accelerating electrons during a CME eruption. So far, studies have relied on the traditional classification of solar radio bursts into five groups (Type I-V) based mainly on their shapes and characteristics in dynamic spectra. Here, we aim to determine the origin of moving radio bursts associated with a CME that do not fit into the present classification of the solar radio emission. Methods. By using radio imaging from the Nançay Radioheliograph, combined with observations from the Solar Dynamics Observatory, Solar and Heliospheric Observatory, and Solar Terrestrial Relations Observatory spacecraft, we investigate the moving radio bursts accompanying two subsequent CMEs on **22 May 2013**. We use three-dimensional reconstructions of the two associated CME eruptions to show the possible origin of the observed radio emission. Results. We identified three moving radio bursts at unusually high altitudes in the corona that are located at the northern CME flank and move outwards synchronously with the CME. The radio bursts correspond to fine-structured emission in dynamic spectra with durations of ~1 s, and they may show forward or reverse frequency drifts. Since the CME expands closely following an earlier CME, a low coronal CME-CME interaction is likely responsible for the observed radio emission.

The Nature and Origin of Moving Solar Radio Bursts Associated with Coronal Mass Ejections

Diana **Morosan**, Emilia Kilpua, Erika Palmerio, Benjamin Lynch, Jens Pomoell, Rami Vainio, Minna Palmroth, Juska Räsänen
EGU2020 Presentation #5379 **File**
22 Sep 2011, 14 June 2012, 2012.07.22, 22 May 2013, 26 Oct 2013, 2014.08.25,

Three-dimensional reconstruction of multiple particle acceleration regions during a coronal mass ejection⋆

D. E. **Morosan**1, E. Palmerio1,2, J. Pomoell1, R. Vainio3, M. Palmroth1,4 and E. K. J. Kilpua1
A&A 635, A62 (**2020**)
https://arxiv.org/pdf/2001.08473.pdf
https://doi.org/10.1051/0004-6361/201937133
Context. Some of the most prominent sources for particle acceleration in our Solar System are large eruptions of magnetised plasma from the Sun called coronal mass ejections (CMEs). These accelerated particles can generate radio emission through various mechanisms.
Aims. CMEs are often accompanied by a variety of solar radio bursts with different shapes and characteristics in dynamic spectra. Radio bursts directly associated with CMEs often show movement in the direction of CME expansion. Here, we aim to determine the emission mechanism of multiple moving radio bursts that accompanied a flare and CME that took place on **14 June 2012**.
Methods. We used radio imaging from the Nançay Radioheliograph, combined with observations from the Solar Dynamics Observatory and Solar Terrestrial Relations Observatory spacecraft, to analyse these moving radio bursts in order to determine their emission mechanism and three-dimensional (3D) location with respect to the expanding CME.
Results. In using a 3D representation of the particle acceleration locations in relation to the overlying coronal magnetic field and the CME propagation, for the first time, we provide evidence that these moving radio bursts originate near the CME flanks and that some are possible signatures of shock-accelerated electrons following the fast CME expansion in the low corona.
Conclusions. The moving radio bursts, as well as other stationary bursts observed during the eruption, occur simultaneously with a type IV continuum in dynamic spectra, which is not usually associated with emission at the CME flanks. Our results show that moving radio bursts that could traditionally be classified as moving type IVs can represent shock signatures associated with CME flanks or plasma emission inside the CME behind its flanks, which are closely related to the lateral expansion of the CME in the low corona**. *In addition, the acceleration of electrons generating this radio emission appears to be favoured at the CME flanks, where the CME encounters coronal streamers and open field regions.***
Movies associated to Fig. 1 are available at https://www.aanda.org

Three-dimensional reconstruction of multiple particle acceleration regions during a coronal mass ejection

D. E. **Morosan**, E. Palmerio, J. Pomoell, R. Vainio, M. Palmroth, E. K. J. Kilpua
A&A **2020**

https://arxiv.org/pdf/2001.08473.pdf

Context. Some of the most prominent sources for particle acceleration in our Solar System are large eruptions of magnetised plasma from the Sun called coronal mass ejections (CMEs). These accelerated particles can generate radio emission through various mechanisms. *Aims*. CMEs are often accompanied by a variety of solar radio bursts with different shapes and characteristics in dynamic spectra. Radio bursts directly associated with CMEs often show movement in the direction of CME expansion. Here, we aim to determine the emission mechanism of multiple moving radio bursts that accompanied a flare and CME that took place on **14 June 2012**. *Methods*. We used radio imaging from the Nancay Radioheliograph, combined with observations from the Solar Dynamics Observatory and Solar Terrestrial Relations Observatory spacecraft, to analyse these moving radio bursts in order to determine their emission mechanism and three-dimensional (3D) location with respect to the expanding CME. *Results*. In using a 3D representation of the particle acceleration locations in relation to the overlying coronal magnetic field and the CME propagation, for the first time, we provide evidence that these moving radio bursts originate near the CME flanks and some that are possible signatures of shock-accelerated electrons following the fast CME expansion in the low corona. *Conclusions.* The moving radio bursts, as well as other stationary bursts observed during the eruption, occur simultaneously with a type IV continuum in dynamic spectra, which is not usually associated with emission at the CME flanks. Our results show that moving radio bursts that could traditionally be classified as moving type IVs can represent shock signatures associated with CME flanks or plasma emission inside the CME behind its flanks, which are closely related to the lateral expansion of the CME in the low corona.

Extended radio emission associated with a breakout eruption from the back side of the Sun

D. E. **Morosan**, E. Palmerio, B. J. Lynch, E. K. J. Kilpua

A&A **2019**

https://arxiv.org/pdf/1912.05995.pdf

Context. Coronal mass ejections (CMEs) on the Sun are the largest explosions in the Solar System that can drive powerful plasma shocks. The eruptions, shocks, and other processes associated to CMEs are efficient particle accelerators and the accelerated electrons in particular can produce radio bursts through the plasma emission mechanism. Aims. Coronal mass ejections and associated radio bursts have been well studied in cases where the CME originates close to the solar limb or within the frontside disc. Here, we study the radio emission associated with a CME eruption on the back side of the Sun on **22 July 2012**. Methods. Using radio imaging from the Nançay Radioheliograph, spectroscopic data from the Nançay Decametric Array, and extreme-ultraviolet observations from the Solar Dynamics Observatory and Solar Terrestrial Relations Observatory spacecraft, we determine the nature of the observed radio emission as well as the location and propagation of the CME. Results. We show that the observed low-intensity radio emission corresponds to a type II radio burst or a short-duration type IV radio burst associated with a CME eruption due to breakout reconnection on the back side of the Sun, as suggested by the pre-eruptive magnetic field configuration. The radio emission consists of a large, extended structure, initially located ahead of the CME, that corresponds to various electron acceleration locations. Conclusions. The observations presented here are consistent with the breakout model of CME eruptions. The extended radio emission coincides with the location of the current sheet and quasi-separatrix boundary of the CME flux and the overlying helmet streamer and also with that of a large shock expected to form ahead of the CME in this configuration.

Multiple regions of shock-accelerated particles during a solar coronal mass ejection

Morosan, Diana E.; Carley, Eoin P.; Hayes, Laura A.; Murray, Sophie A.; Zucca, Pietro; Fallows, Richard A.; McCauley, Joe; Kilpua, Emilia K. J.; Mann, Gottfried; Vocks, Christian; Gallagher, Peter T.

Nature Astronomy VOL 3 | MAY **2019** | 452–461 |

sci-hub.se/10.1038/s41550-019-0689-z

https://arxiv.org/pdf/1908.11743.pdf

https://www.researchgate.net/publication/331183002_Multiple_regions_of_shock-accelerated_particles_during_a_solar_coronal_mass_ejection

The Sun is an active star that can launch large eruptions of magnetized plasma into the heliosphere, known as coronal mass ejections (CMEs). These can drive shocks that accelerate particles to high energies, often resulting in radio emission at low frequencies (<200 MHz). So far, the relationship between the expansion of CMEs, shocks and particle acceleration is not well understood, partly due to the lack of radio imaging at low frequencies during the onset of shock-producing CMEs. Here, we report multi-instrument radio, white-light and ultraviolet imaging of the second largest flare in solar cycle 24 (2008–present) and its associated fast CME (3,038± 288 km s−1). We identify the location of a multitude of radio shock signatures, called herringbones, and find evidence for shock-accelerated electron beams at multiple locations along the expanding CME. These observations support theories of non-uniform, rippled shock fronts driven by an expanding CME in the solar corona. **10 September 2017**

RHESSI Science Nuggets # 348 Apr **2019**
http://sprg.ssl.berkeley.edu/~tohban/wiki/index.php/Multiple_Regions_of_Shock-accelerated_Particles_during_a_Solar_Coronal_Mass_Ejection

Variable emission mechanism of a Type IV radio burst

D. E. **Morosan**, E. K. J. Kilpua, E. P. Carley, C. Monstein
https://arxiv.org/pdf/1902.01140.pdf

Context. The Sun is an active star and the source of the largest explosions in the solar system, such as flares and coronal mass ejections (CMEs). Flares and CMEs are powerful particle accelerators that can generate radio emission through various emission mechanisms. Aims. CMEs are often accompanied by Type IV radio bursts that are observed as continuum emission in dynamic spectra at decimetric and metric wavelengths, but their emission mechanism can vary from event to event. Here, we aim to determine the emission mechanism of a complex Type IV burst that accompanied the flare and CME on **22 September 2011**. Methods. We used radio imaging from the Nançay Radioheliograph, spectroscopic data from the e-Callisto network, ARTEMIS, Ondrejov, and Phoenix3 spectrometers combined with extreme-ultraviolet observations from NASA's Solar Dynamic Observatory to analyse the Type IV radio burst and determine its emission mechanism. Results. We show that the emission mechanism of the Type IV radio burst changes over time. We identified two components in the Type IV radio burst: an earlier stationary Type IV showing gyro-synchrotron behaviour, and a later moving Type IV burst covering the same frequency band. This second component has a coherent emission mechanism. Fundamental plasma emission and the electroncyclotron maser emission are further investigated as possible emission mechanisms for the generation of the moving Type IV burst. Conclusions. Type IV bursts are therefore complex radio bursts, where multiple emission mechanisms can contribute to the generation of the wide-band continuum observed in dynamic spectra. Imaging spectroscopy over a wide frequency band is necessary to determine the emission mechanisms of Type IV bursts that are observed in dynamic spectra.

Characteristics of type III radio bursts and solar S bursts

D. E. **Morosan**, P. T. Gallagher
Planetary Radio Emissions VIII, Austrian Academy of Sciences Press, Vienna, 357-368, **2017**
https://arxiv.org/pdf/1802.10460.pdf

The Sun is an active source of radio emission which is often associated with the acceleration of electrons arising from processes such as solar flares and coronal mass ejections (CMEs). At low radio frequencies (<100 MHz), numerous solar S bursts (where S stands for short) and storms of Type III radio bursts have been observed, that are not directly relates to flares and CMEs. Here, we expand our understanding on the spectral characteristic of these two different types of radio bursts based on observations from the Low Frequency Array (LOFAR). On **9 July 2013**, over 3000 solar S bursts accompanied by over 800 Type III radio bursts were observed over a time period of ~8 hours. The characteristics of Type III radio bursts are consistent to previous studies, while S bursts show narrow bandwidths, durations and drift rates of about 1/2 the drift rate of Type III bursts. Type III bursts and solar S bursts occur in a region in the corona where plasma emission is the dominant emission mechanism as determined by data constrained density and magnetic field models.

The Association of a J-burst with a Solar Jet

D. E. **Morosan**, P. T. Gallagher, R. A. Fallows, H. Reid, G. Mann, M. M. Bisi, J. Magdalenic, …….
A&A 606, A81 **2017**
https://arxiv.org/pdf/1707.03428.pdf
https://www.aanda.org/articles/aa/pdf/2017/10/aa29996-16.pdf

The Sun is an active star that produces large-scale energetic events such as solar flares and coronal mass ejections and numerous smaller-scale events such as solar jets. These events are often associated with accelerated particles that can cause emission at radio wavelengths. The reconfiguration of the solar magnetic field in the corona is believed to be the cause of the majority of solar energetic events and accelerated particles. Here, we investigate a bright J-burst that was associated with a solar jet and the possible emission mechanism causing these two phenomena.
Methods. We used data from the Solar Dynamics Observatory (SDO) to observed a solar jet, and radio data from the Low Frequency Array (LOFAR) and the Nancay Radioheliograph (NRH) to observe a J-burst over a broad frequency range (33-173 MHz) on **9 July 2013** at ~11:06 UT. The J-burst showed fundamental and harmonic components and it was associated with a solar jet observed at extreme ultraviolet wavelengths with SDO. The solar jet occurred at a time and location coincident with the radio burst with a velocity of 510 km s-1. The jet occurred in the northern hemisphere in the negative polarity region of an extended area of bipolar plage as opposed to a group of complex active regions in the southern hemisphere. Newly emerged positive flux in the negative magnetic polarity region of the bipolar plage appeared to be the trigger of the jet. Radio imaging showed that the J-burst emitting electrons originated in a region above the newly emerged magnetic field of positive polarity and then followed long, closed magnetic field lines.

The Propagation of Jet Related Type III Radio Bursts in the Solar Corona

Diana **Morosan**

CESRA **2016** p.76

http://cesra2016.sciencesconf.org/conference/cesra2016/pages/CESRA2016_prog_abs_book_v3.pdf

The Sun is an active star that produces large-scale energetic events such as solar flares and coronal mass ejections and numerous smaller scale events such as solar jets. The recon- figuration of the solar magnetic field in the corona is believed to be the cause of most solar energetic events. Here, we did a comprehensive study on a solar jet using data from the Solar Dynamics Observatory (SDO) and radio data from the Low Frequency Array (LOFAR) and the Nan ̧cay Radioheliograph (NRH). We observed a jet that occurred in the northern hemisphere which had a high velocity (514 km s-1) and it was associated with a radio source in the form of a Type III radio burst observed over a broad frequency range of 35–298 MHz by both LOFAR and NRH. There is evidence that the Type III radio burst travelled along a large closed magnetic field loop as opposed to open magnetic field lines. Newly emerged magnetic flux is also observed in the vicinity of the Type III and the jet. The first multifrequency image of a solar Type III burst imaged with both LOFAR tied-array imaging at low frequencies and NRH at higher frequencies is presented here, showing the importance of radio imaging in the analysis of solar eruptive events.

Conditions for electron-cyclotron maser emission in the solar corona

D. E. **Morosan**, P. Zucca, D. S. Bloomfield, P. T. Gallagher

A&A **2016**

http://arxiv.org/pdf/1604.04788v1.pdf

Context. The Sun is an active source of radio emission ranging from long duration radio bursts associated with solar flares and coronal mass ejections to more complex, short duration radio bursts such as solar S bursts, radio spikes and fibre bursts. While plasma emission is thought to be the dominant emission mechanism for most radio bursts, the electron-cyclotron maser (ECM) mechanism may be responsible for more complex, short-duration bursts as well as fine structures associated with long-duration bursts. Aims. We investigate the conditions for ECM in the solar corona by considering the ratio of the electron plasma frequency {\omega}p to the electron-cyclotron frequency {\Omega}e. The ECM is theoretically possible when {\omega}p/{\Omega}e < 1. Methods. Two-dimensional electron density, magnetic field, plasma frequency, and electron cyclotron frequency maps of the off- limb corona were created using observations from SDO/AIA and SOHO/LASCO, together with potential field extrapolations of the magnetic field. These maps were then used to calculate {\omega}p/{\Omega}e and Alfven velocity maps of the off-limb corona. Results. We found that the condition for ECM emission ({\omega}p/{\Omega}e < 1) is possible at heights < 1.07 R_sun in an active region near the limb; that is, where magnetic field strengths are > 40 G and electron densities are greater than 3x10^8 cm-3. In addition, we found comparatively high Alfv\'en velocities (> 0.02 c or > 6000 km s-1) at heights < 1.07 R_sun within the active region. Conclusions. This demonstrates that the condition for ECM emission is satisfied within areas of the corona containing large magnetic fields, such as the core of a large active region. Therefore, ECM could be a possible emission mechanism for high-frequency radio and microwave bursts. **2 July 2013**

LOFAR tied-array imaging and spectroscopy of solar S bursts

D. E. **Morosan**, P. T. Gallagher, P. Zucca, A. O'Flannagain, R. Fallows, H. Reid, J. Magdalenic, G. Mann,M. M. Bisi, A. Kerdraon, A. A. Konovalenko, A. L. MacKinnon, H. O. Rucker, B. Thide, C. Vocks, A. Alexov,J. Anderson, A. Asgekar, I. M. Avruch, M. J. Bentum, G. Bernardi, A. Bonafede, F. Breitling, J. W. Broderick, W. N. Brouw, H. R. Butcher, B. Ciardi, E. de Geus, J. Eisloffel, H. Falcke, W. Frieswijk, M. A. Garrett, J. Griessmeier, A. W. Gunst, J. W. T. Hessels, M. Hoeft, A. Karastergiou, V. I. Kondratiev, G. Kuper, J. van Leeuwen, D. McKay-Bukowski, J. P. McKean, H. Munk, E. Orru, H. Paas, R. Pizzo, A. G. Polatidis, A. M. M. Scaife, J. Sluman, C. Tasse, M. C. Toribio, R. Vermeulen, P. Zarka

A&A 580, A65 **2015**

http://arxiv.org/pdf/1507.07496v1.pdf

https://www.aanda.org/articles/aa/pdf/2015/08/aa26064-15.pdf

Context. The Sun is an active source of radio emission that is often associated with energetic phenomena ranging from nanoflares to coronal mass ejections (CMEs). At low radio frequencies (<100 MHz), numerous millisecond duration radio bursts have been reported, such as radio spikes or solar S bursts (where S stands for short). To date, these have neither been studied extensively nor imaged because of the instrumental limitations of previous radio telescopes.
Aims. Here, Low Frequency Array (LOFAR) observations were used to study the spectral and spatial characteristics of a multitude of S bursts, as well as their origin and possible emission mechanisms.
Methods. We used 170 simultaneous tied-array beams for spectroscopy and imaging of S bursts. Since S bursts have short timescales and fine frequency structures, high cadence (~50 ms) tied-array images were used instead of standard interferometric imaging, that is currently limited to one image per second.

Results. On **9 July 2013**, over 3000 S bursts were observed over a time period of ~8 hours. S bursts were found to appear as groups of short-lived (<1 s) and narrow-bandwidth (~2.5 MHz) features, the majority drifting at ~3.5 MHz/s and a wide range of circular polarisation degrees (2-8 times more polarised than the accompanying Type III bursts). Extrapolation of the photospheric magnetic field using the potential field source surface (PFSS) model suggests that S bursts are associated with a trans-equatorial loop system that connects an active region in the southern hemisphere to a bipolar region of plage in the northern hemisphere.
Conclusions. We have identified polarised, short-lived solar radio bursts that have never been imaged before. They are observed at a height and frequency range where plasma emission is the dominant emission mechanism, however they possess some of the characteristics of electron-cyclotron maser emission.

LOFAR tied-array imaging of Type III solar radio bursts

D. E. **Morosan**, P. T. Gallagher, P. Zucca, R. Fallows, E. P. Carley, G. Mann, et al.
2014, A&A 568, A67
http://arxiv.org/pdf/1407.4385v1.pdf
https://www.aanda.org/articles/aa/pdf/2014/08/aa23936-14.pdf
The Sun is an active source of radio emission which is often associated with energetic phenomena such as solar flares and coronal mass ejections (CMEs). At low radio frequencies (<100 MHz), the Sun has not been imaged extensively because of the instrumental limitations of previous radio telescopes. Here, the combined high spatial, spectral and temporal resolution of the Low Frequency Array (LOFAR) was used to study solar Type III radio bursts at 30-90 MHz and their association with CMEs. The Sun was imaged with 126 simultaneous tied-array beams within 5 solar radii of the solar centre. This method offers benefits over standard interferometric imaging since each beam produces high temporal (83 ms) and spectral resolution (12.5 kHz) dynamic spectra at an array of spatial locations centred on the Sun. LOFAR's standard interferometric output is currently limited to one image per second. Over a period of 30 minutes, multiple Type III radio bursts were observed, a number of which were found to be located at high altitudes (4 solar radii from the solar center at 30 MHz) and to have non-radial trajectories. These bursts occurred at altitudes in excess of values predicted by 1D radial electron density models. The non-radial high altitude Type III bursts were found to be associated with the expanding flank of a CME. The CME may have compressed neighbouring streamer plasma producing larger electron densities at high altitudes, while the non-radial burst trajectories can be explained by the deflection of radial magnetic fields as the CME expanded in the low corona. **2013 February 28**

Synthetic Radio Imaging for Quiescent and CME-flare Scenarios

Sofia-Paraskevi **Moschou** (1), Igor Sokolov (2), Ofer Cohen (3), Jeremy J. Drake (1), Dmitry Borovikov (4), Justin C. Kasper (2), Julian D. Alvarado-Gomez (1),Cecilia Garraffo
ApJ **867** 51 **2018**
https://arxiv.org/pdf/1809.09750.pdf
sci-hub.tw/10.3847/1538-4357/aae58c
Radio observations grant access to a wide range of physical processes through different emission mechanisms. These processes range from thermal and quiescent to eruptive phenomena, such as shock waves and particle beams. We present a new synthetic radio imaging tool that calculates and visualizes the Bremsstrahlung radio emission. This tool works concurrently with state-of-the-art Magnetohydrodynamic (MHD) simulations of the solar corona using the code BATS-R-US. Our model produces results that are in good agreement with both high and low frequency observations of the solar disk. In this study, a ray-tracing algorithm is used and the radio intensity is computed along the actual curved ray trajectories. We illustrate the importance of refraction in locating the radio emitting source by comparison of the radio imaging illustrations when the line-of-sight instead of the refracted paths are considered. We are planning to incorporate non-thermal radio emission mechanisms in a future version of the radio imaging tool. **March 7, 2011, October - November 2014 CR 2156**
CESRA # 2101 Jan **2019** http://www.astro.gla.ac.uk/users/eduard/cesra/?p=2101

MODELING OF GYROSYNCHROTRON RADIO EMISSION PULSATIONS PRODUCED BY MAGNETOHYDRODYNAMIC LOOP OSCILLATIONS IN SOLAR FLARES

George **Mossessian**1,2 and Gregory D. Fleishman
2012 ApJ 748 140
A quantitative study of the observable radio signatures of the sausage, kink, and torsional magnetohydrodynamic (MHD) oscillation modes in flaring coronal loops is performed. Considering first non-zero order effect of these various MHD oscillation modes on the radio source parameters such as magnetic field, line of sight, plasma density and temperature, electron distribution function, and the source dimensions, we compute time-dependent radio emission (spectra and light curves). The radio light curves (of both flux density and degree of polarization) at all considered radio

frequencies are then quantified in both time domain (via computation of the full modulation amplitude as a function of frequency) and in Fourier domain (oscillation spectra, phases, and partial modulation amplitude) to form the signatures specific to a particular oscillation mode and/or source parameter regime. We found that the parameter regime and the involved MHD mode can indeed be distinguished using the quantitative measures derived in the modeling. We apply the developed approach to analyze radio burst recorded by Owens Valley Solar Array and report possible detection of the sausage mode oscillation in one (partly occulted) flare and kink or torsional oscillations in another flare.

Pre-impulsive and Impulsive Phases of the Sub-Terahertz Flare of March 28, 2022

G.G. **Motorina**, Yu.T. Tsap, V.V. Smirnova, A.S. Morgachev, A.D. Shramko, A.S. Motorin
Geomagnetism and Aeronomy Volume 63, Issue 8, p.1218-1223 **2024**
https://arxiv.org/pdf/2311.02435.pdf

Properties of the solar radio spectrum, as well as the temporal profiles of flare emission, indicate the thermal nature of the sub-terahertz (sub-THz) component observed as the growth of radio emission in the frequency range of 100-1000 GHz. The sub-THz flare onset can be ahead of the impulsive phase for several minutes. However, the origin of the pre-impulsive and impulsive sub-THz emission remains unclear. The present work is devoted to a detailed analysis of the M4.0 X-class solar flare observed on **March 28, 2022** with the Bauman Moscow State Technical University Radio Telescope RT-7.5 at 93 GHz. We supply these data with multiwavelength solar observations in the X-ray (GOES, GBM/Fermi), extreme ultraviolet (AIA/SDO), and microwave ranges. The differential emission measure (DEM) responsible for EUV emission is determined by solving the inverse problem based on the AIA/SDO data. Using the DEM and assuming a thermal free-free emission mechanism in pre-impulsive and impulsive phases, we calculated the millimeter emission flux of coronal plasma of the flare source, which turned out to be much smaller than the observed values. We concluded that electrons accelerated in the corona and heat fluxes from the coronal loop top cannot be responsible for heating the sub-THz emission source located in the transition region and upper chromosphere. A possible origin of chromospheric heating in the pre-impulsive phase of the solar flare is discussed.
RHESSI Nuggets #463 Dec 2023 https://sprg.ssl.berkeley.edu/~tohban/wiki/index.php/Pre-impulsive_and_Impulsive_Phases_of_the_March_28,_2022_Sub-Terahertz_Flare

Joint radio, EUV, and X-ray analysis of the 2013 November 5 cold flare

Galina **Motorina**∗1 , Eduard Kontar2 , and Gregory Fleishman3
CESRA **2016** p.63
http://cesra2016.sciencesconf.org/conference/cesra2016/pages/CESRA2016_prog_abs_book_v3.pdf

Solar flares, transient brightenings in the solar atmosphere seen throughout electromagnetic spectrum, demonstrate remarkable variety of the energy partitions between the thermal and nonthermal components. There are flares with a dominating or purely thermal component, i.e., with little or no non-thermal electrons visible. These flares strongly contrast with the flares in which the nonthermal component clearly dominates over the thermal one. Therefore, there is a puzzle as what leads to such extreme phenomena as purely ‘thermal’ and purely ‘non-thermal’ flares. It has recently been recognized that some flares with dominating nonthermal component are in fact ‘cold flares’ (Bastian et al. 2007; Fleishman et al. 2011; Masuda et al. 2013) in which no or so modest thermal plasma response is detected that these events are not even listed as GOES flares. Here we analyze a 05-Nov-2013 cold flare with a combination of radio (NoRH, NoRP, SSRT, BBMS), X-ray (RHESSI), and EUV (SDO) data to understand the relationship between the thermal and nonthermal components in this flare in detail. Before, there were no analysis of cold flares employing both RHESSI and SDO/AIA data, where RHESSI provides information of non-thermal energetic particles, and SDO/AIA characterizes the thermal response at lower temperatures, approximately 0.6 MK – 16 MK. The microwave spectral and imaging data taken from Nobeyama and BBMS/SSRT instruments put significant additional constraints on the magnetic field and number density at the source of the flare. With these data we build a consistent detailed picture of particle acceleration and plasma heating in this cold flare and attempt a 3D modeling of the flaring volume. Based on this analysis, we arrive at important conclusions about the energy release, particle acceleration, and plasma heating in solar flares.

Quick Event During the Decay Phase of the Microwave Emission of a Flare on May 22, 2021.

Motyk, I.D., Kashapova, L.K., Setov, A.G. et al.
Geomagn. Aeron. 63, 1062–1071 (**2023**).
https://doi.org/10.1134/S0016793223070174

This paper presents the results of a study of a short event that occurred during the decay phase of a C6.0 circular flare (GOES). The event was simultaneously observed by the Irkutsk Incoherent Scatter Radar at 161 MHz and by the Siberian Radioheliograph (SRH) at 5.6 GHz. The SRH data were obtained at a single frequency, but with a high time resolution (0.2 s). This made it possible to localize the microwave source and carry out its temporal profile using

imaging photometry. The similarity of the time profiles at both frequencies and the close values of the periods of the quasi-periodic oscillations seen on both profiles indicate a close relationship between the emeission in the meter and microwave ranges. According to the images at 5.6 GHz, the burst source was located near the circular ribbon of the flare, but was not a part of it. The event was folowed by an eruption that manifested itself in the meter range as the Type II radio burst at frequencies above 200 MHz, while a burst at 161 MHz demonstrated the emission of the Type III radio burst. An analysis of the three-dimensional structure of the magnetic field, reconstructed on the basis of vector magnetograms, showed that the event source was located on relatively open field lines, which were above the dome structure of the circular flare. The active region topology near the microwave source of the event suggests the following scenario based on the expansion of the dome structure of the circular flare due to gas dynamic processes. This caused an impact on relatively open field lines, which resulted to eruption, acceleration of electrons, and their propagation along open field lines. It is shown that the event was triggered by a flare, despite the absence of a direct spatial connection between the burst and flare ribbons.

Estimating the coronal and chromospheric magnetic fields of solar active regions as observed with the Nobeyama Radioheliograph Compared with the Extrapolated Linear Force-Free Field

A. **Mouner**, Abdelrazek M. K. Shaltout, M. M. Beheary, K.A.K. Gadallah, K. A. Edris

2018

https://arxiv.org/ftp/arxiv/papers/1802/1802.04598.pdf

Adopting the thermal free-free emission mechanism, the coronal and chromospheric magnetic fields are derived from the polarization and spectral observations with the Nobeyama Radioheliograph at 1.76 cm. The solar active regions (AR) located near the disk center observed on **January 8, 2015** (AR 12257) and **December 4, 2016** (AR 12615) are used for the estimate of the chromospheric and coronal magnetic fields with the microwave radio observations. We compare solar radio maps of active regions for both intensity and circularly polarized component with the optical maps from observations with the Helioseismic and Magnetic Imager and the chromosphere and corona transition region images obtained with the Atmospheric Imaging Assembly instrument, on board the Solar Dynamic Observatory. We notice from the comparison between radio maps of both AR that the circular polarization degree in the AR 12257 is about 2 percent, but the AR 12615 has a higher existent value by 3 percent. Radio observations provide us for direct measurements of magnetic fields in the chromospheric and coronal layers. We estimate the coronal magnetic fields using the Atmospheric Imaging Assembly observations by adopting magnetic loops in the corona over some patches with weak photospheric magnetic fields. The coronal magnetic field derived from the Atmospheric Imaging Assembly data was from 90 to 240 Gauss. We also study the coronal magnetic fields based on the structure of the extrapolated field, where the result of the magnetic fields was in the range from 35 to 145 Gauss, showing that the difference in the coronal magnetic fields between both results is attributed to the assumption of the force-free approximation.

Origin of the type III radiation observed near the Sun

F. S. **Mozer**1,2, O. Agapitov1, S. D. Bale1,2, K. Goetz3, V. Krasnoselskikh4, M. Pulupa1, K. Sauer5 and A. Voshchepynets6

A&A, 690, L6 (**2024**)

https://www.aanda.org/articles/aa/pdf/2024/10/aa51134-24.pdf

Aims. We investigate processes associated with the generation of type III radiation using Parker Solar Probe measurements.

Methods. We measured the amplitudes and phase velocities of electric and magnetic fields and their associated plasma density fluctuations.

Results. 1. There are slow electrostatic waves near the Langmuir frequency and at as many as six harmonics, the number of which increases with the amplitude of the Langmuir wave. Their electrostatic nature is shown by measurements of the plasma density fluctuations. From these density fluctuations and the electric field magnitude, the k-value of the Langmuir wave is estimated to be 0.14 and $k\lambda d = 0.4$. Even with the large uncertainty in this quantity (more than a factor of two), the phase velocity of the Langmuir wave was < 10 000 km/s. 2. The electromagnetic wave near the Langmuir frequency has a phase velocity lower than 50 000 km/s. 3. We cannot determine whether there are electromagnetic waves at the harmonics of the Langmuir frequency. If they existed, their magnetic field components would be below the noise level of the measurement. 4. The rapid (less than one millisecond) amplitude variations typical of the Langmuir wave and its harmonics are artifacts resulting from the addition of two waves, one of which has small frequency variations that arise because the wave travels through density irregularities. None of these results are expected in or consistent with the conventional model of the three-wave interaction of two counter-streaming Langmuir waves that coalesce to produce the type III wave. They are consistent with a new model in which electrostatic antenna waves are produced at the harmonics by radiation of the Langmuir wave, after which at least the first harmonic wave evolved through density irregularities such that its wave number decreased and it became the type III radiation. **23 Mar 2023**

A New Mechanism For Generating Type-III Radiation From The Sun

Forrest **Mozer**, Oleksiy Agapitos, Stuart Bale, Keith Goetz, Vladimir Krasnoselskikh, Marc Pulupa, Konrad Sauer, Andrii Voshchepinets
2024
https://arxiv.org/ftp/arxiv/papers/2403/2403.05984.pdf
Because the conventional method of creating type-III radiation by coalescence of counter-propagating Langmuir waves has not been verified with in-situ data, Parker Solar Probe data was examined in search of such in-situ evidence, which was not found. Instead, a new mechanism for creating type-III radiation has been found as a result of observing slow Langmuir waves (~2200 km/sec) with electric fields as large as 300 mV/m during a developing type-III burst on **March 21, 2023**. Because of their slow phase velocities, these Langmuir waves had short wavelengths, several times the Debye length of 2.65 meters, and, as a result, k{\lambda}d~0.93. Such waves may be strongly damped to be replaced by new growing bursts of waves that create the characteristic Langmuir waveform that is composed of peaks and valleys of a few milliseconds duration. The average electron current that produced these Langmuir waves is estimated from the Generalized Ohms law to be ~15 microamps/m2 and, from the strahl, 8 microamps/m2. Peak currents were at least twice these averages. These Langmuir waves, acting as antennas, produced electrostatic harmonics having slow phase velocities (~2000 km/sec) at frequencies of n{\omega}p, where {\omega}p = 6.28*125 kHz is the Langmuir wave frequency and n = 2, 3, 4, 5, 6, and 7. Such waves are not the type-III emission. As at least the first harmonic wave evolved through the huge density irregularities, its wave number decreased and it became the electromagnetic wave that was the type-III radiation.

The First Low-frequency Radio Observations of the Solar Corona on ≈200 km Long Interferometer Baseline

V. **Mugundhan**1, R. Ramesh1, C. Kathiravan1, G. V. S. Gireesh2, Anshu Kumari1, K. Hariharan3, andIndrajit V. Barve2
2018 ApJL 855 L8
http://sci-hub.tw/http://iopscience.iop.org/2041-8205/855/1/L8/
The angular size of the smallest, compact radio source that can be observed in the solar atmosphere is one of the intriguing questions in low-frequency radio astronomy. This is important to understand density turbulence in the solar corona and the related angular broadening of the radio source sizes. We used a two-element interferometer with a baseline length of ≈200 km, operating at ≈53 MHz to infer the above limit. Our results indicate that radio sources of angular size ≤15" exist in the solar corona, where radio emission at the above frequency also originates. **2017 April 5**

Spectropolarimetric Observations of Solar Noise Storms at Low Frequencies

V. **Mugundhan**, R. Ramesh, C. Kathiravan, G. V. S. Gireesh, Aathira Hegde
Solar Physics March **2018**, 293:41
https://link.springer.com/content/pdf/10.1007%2Fs11207-018-1260-2.pdf
A new high-resolution radio spectropolarimeter instrument operating in the frequency range of 15 – 85 MHz has recently been commissioned at the Radio Astronomy Field Station of the Indian Institute of Astrophysics at Gauribidanur, 100 km north of Bangalore, India. We describe the design and construction of this instrument. We present observations of a solar radio noise storm associated with Active Region (AR) 12567 in the frequency range of ≈15--85 MHz≈15--85 MHz during **18 and 19 July 2016**, observed using this instrument in the meridian-transit mode. This is the first report that we are aware of in which both the burst and continuum properties are derived simultaneously. Spectral indices and degree of polarization of both the continuum radiation and bursts are estimated. It is found that
i) Type I storm bursts have a spectral index of ≈+3.5≈+3.5,
ii) the spectral index of the background continuum is ≈+2.9≈+2.9,
iii) the transition frequency between Type I and Type III storms occurs at ≈55 MHz≈55 MHz,
iv) Type III bursts have an average spectral index of ≈−2.7≈−2.7,
v) the spectral index of the Type III continuum is ≈−1.6≈−1.6, and
vi) the degree of circular polarization of all Type I (Type III) bursts is ≈90%≈90% (30%30%).
The results obtained here indicate that the continuum emission is due to bursts occurring in rapid succession. We find that the derived parameters for Type I bursts are consistent with suprathermal electron acceleration theory and those of Type III favor fundamental plasma emission.

Solar Type IIIb Radio Bursts as Tracers for Electron Density Fluctuations in the Corona

V. **Mugundhan**, K. Hariharan, R. Ramesh
Solar Physics November **2017**, 292:155
https://link.springer.com/content/pdf/10.1007%2Fs11207-017-1181-5.pdf
We present an estimation of the electron density modulation index (δNe Ne) for the first time using solar type IIIb radio burst observations. The mean value of δNe Ne is calculated to be ≈0.006 ± 0.002 over the heliocentric distance range r ≈ 1.6–2.2 R. The estimated δNe Ne shows a power law dependence on r with a power law index ≈0.31 ± 0.10.

The wavenumber (k) spectrum for the electron density fluctuation (δNe Ne)2 values shows a Kolmogorov-like behavior. Using δNe Ne and the Kolmogorov turbulence index, we estimated the amplitude of density turbulence [C2 n(r)] in the aforementioned range of r. **20 July 2016**
Table 1 List of type IIIb bursts recorded with FFTS. 2016
CESRA Highlights #1831 Apr **2018** http://cesra.net/?p=1831

LOW-FREQUENCY RADIO OBSERVATIONS OF THE SOLAR CORONA WITH ARCMINUTE ANGULAR RESOLUTION: IMPLICATIONS FOR CORONAL TURBULENCE AND WEAK ENERGY RELEASES

V. **Mugundhan**[1], R. Ramesh[1], Indrajit V. Barve[1], C. Kathiravan[1], G. V. S. Gireesh[1], P. Kharb[1], and Apurva Misra[2]
2016 *ApJ* **831** 154
We report on the first long baseline interferometer (length ≈8 km) observations of the solar corona at 37 MHz that were carried out recently with an angular resolution of ≈1′. The results indicate that, (1) discrete radio sources of the aforesaid angular size or even lesser are present in the solar corona from where radiation at the above frequency originates. This constrains the angular broadening of radio sources at low frequencies due to scattering by density turbulence in the solar corona; and (2) the observed sources in the present case correspond to the weakest energy releases in the solar atmosphere reported so far.

Performance assessment of GPS receivers during the September 24, 2011 solar radio burst event

Bilal **Muhammad**1*, Valentina Alberti2, Alessandro Marassi2, Ernestina Cianca1 and Mauro Messerotti2
J. Space Weather Space Clim., 5, A32 (**2015**)
http://www.swsc-journal.org/articles/swsc/pdf/2015/01/swsc150025.pdf
The sudden outburst of in-band solar radio noise from the Sun is recognized as one of the potential Radio Frequency Interference (RFI) sources that directly impact the performance of Global Navigation Satellite System (GNSS) receivers. On September 24, 2011, the solar active region 1302 unleashed a moderate M7.1 soft X-ray flare associated with a very powerful radio burst at 1415 MHz. The Solar Radio Burst (SRB) event spanned over three distinct episodes of solar radio noise emission that reached the maximum radio flux density of 114,144 Solar Flux Units (SFU) at 13:04:46 UTC. This paper analyzes the impact of September 24, 2011 SRB event on the performance of a significant subset of NAVSTAR Global Positioning System (GPS) receivers located in the sunlit hemisphere. The performance assessment is carried out in terms of Carrier-to-Noise power spectral density ratio (C/N0) degradation, dual-frequency pseudorange measurements availability, pseudorange residual errors, and dual-frequency positioning errors in the horizontal and vertical dimensions. We observed that during the SRB event the GPS C/N0 is reduced at most by 13 dB on L1 and 24 dB on L2. The C/N0degradation caused the loss of lock on GPS L1 and L2 signals and significant code-tracking errors. We noticed that many stations experienced less than four satellite measurements, which are the minimum required number of measurements for position estimation. The deteriorated satellite-receiver geometry due to loss of signal lock and significant code-tracking errors during the solar radio burst event introduced large positioning errors in both the horizontal and vertical dimensions. Rise in vertical positioning error of 303 m and rise in horizontal positioning of 55 m could be noticed during the solar radio burst event.

Study of the spatial association between an active region jet and a nonthermal type III radio burst⋆

Sargam M. **Mulay**1,2, Rohit Sharma3, Gherardo Valori4, Alberto M. Vásquez5, Giulio Del Zanna2, Helen Mason2 and Divya Oberoi6
A&A 632, A108 (**2019**)
https://doi.org/10.1051/0004-6361/201936369
https://arxiv.org/pdf/2009.14581.pdf
Aims. We aim to investigate the spatial location of the source of an active region (AR) jet and its relation with associated nonthermal type III radio emission.
Methods. An emission measure (EM) method was used to study the thermodynamic nature of the AR jet. The nonthermal type III radio burst observed at meterwavelength was studied using the Murchison Widefield Array (MWA) radio imaging and spectroscopic data. The local configuration of the magnetic field and the connectivity of the source region of the jet with open magnetic field structures was studied using a nonlinear force-free field (NLFFF) extrapolation and potential field source surface (PFSS) extrapolation respectively.
Results. The plane-of-sky velocity of the AR jet was found to be ∼136 km s−1. The EM analysis confirmed the presence of low temperature 2 MK plasma for the spire, whereas hot plasma, between 5 and 8 MK, was present at the footpoint region which also showed the presence of Fe XVIII emission. A lower limit on the electron number density was found to be 1.4 × 108 cm−3 for the spire and 2.2 × 108 cm−3 for the footpoint. A temporal and spatial correlation

between the AR jet and nonthermal type III burst confirmed the presence of open magnetic fields. An NLFFF extrapolation showed that the photospheric footpoints of the null point were anchored at the location of the source brightening of the jet. The spatial location of the radio sources suggests an association with the extrapolated closed and open magnetic fields although strong propagation effects are also present.
Conclusions. The multi-scale analysis of the field at local, AR, and solar scales confirms the interlink between different flux bundles involved in the generation of the type III radio signal with flux transferred from a small coronal hole to the periphery of the sunspot via null point reconnection with an emerging structure. **3 Sep 2013**

Multiwavelength study of 20 jets that emanate from the periphery of active regions

Sargam M. **Mulay,** Durgesh Tripathi, Giulio Del Zanna, and Helen Mason
CESRA highlights #959, Nov.**2016**
http://www.astro.gla.ac.uk/users/eduard/cesra/?p=959
We present a multiwavelength analysis of 20 EUV jets observed between August 2010 and June 2013. In this study, we included events which were observed on the solar disk within ±60◦ latitude and occurred at the periphery of active regions close to sunspots. We discuss the physical parameters of the jets and their relation with other phenomena such as nonthermal type-III radio bursts and magnetic activity in the photosphere. **2010 August 02**

Origin of Radio-quiet Coronal Mass Ejections in Flare Stars

D. J. **Mullan** and R. R. Paudel
2019 ApJ 873 1
https://doi.org/10.3847/1538-4357/ab041b
Type II radio bursts are observed in the Sun in association with many coronal mass ejections (CMEs). In view of this association, there has been an expectation that, by scaling from solar flares to the flares that are observed on M dwarfs, radio emission analogous to solar type II bursts should be detectable in association with M dwarf flares. However, several surveys have revealed that this expectation does not seem to be fulfilled. Here we hypothesize that the presence of larger global field strengths in low-mass stars, suggested by recent magnetoconvective modeling, gives rise to such large Alfvén speeds in the corona that it becomes difficult to satisfy the conditions for the generation of type II radio bursts. As a result, CMEs propagating in the corona/wind of flare stars are expected to be "radio-quiet" as regards type II bursts. In view of this, we suggest that, in the context of type II bursts, scaling from solar to stellar flares is of limited effectiveness.

Semantic Segmentation of Solar Radio Spikes at Low Frequencies

Pearse C. **Murphy**, Stéphane Aicardi, Baptiste Cecconi, Carine Briand, Thibault Peccoux
2024
https://arxiv.org/pdf/2403.08546.pdf
Solar radio spikes are short lived, narrow bandwidth features in low frequency solar radio observations. The timing of their occurrence and the number of spikes in a given observation is often unpredictable. The high temporal and frequency of resolution of modern radio telescopes such as NenuFAR mean that manually identifying radio spikes is an arduous task. Machine learning approaches to data exploration in solar radio data is on the rise. Here we describe a convolutional neural network to identify the per pixel location of radio spikes as well as determine some simple characteristics of duration, spectral width and drift rate. The model, which we call SpikeNet, was trained using an Nvidia Tesla T4 16GB GPU with ~100000 sample spikes in a total time of 2.2 hours. The segmentation performs well with an intersection over union in the test set of ~0.85. The root mean squared error for predicted spike properties is of the order of 23%. Applying the algorithm to unlabelled data successfully generates segmentation masks although the accuracy of the predicted properties is less reliable, particularly when more than one spike is present in the same 64 X 64 pixel time-frequency range. We have successfully demonstrated that our convolutional neural network can locate and characterise solar radio spikes in a number of seconds compared to the weeks it would take for manual identification.

Automatic detection of solar radio bursts in NenuFAR observations

Pearse C. **Murphy**, Baptiste Cecconi, Carine Briand, Stéphane Aicardi
PRE9 conference proceedings **2024**
https://arxiv.org/pdf/2401.04469.pdf
Solar radio bursts are some of the brightest emissions at radio frequencies in the solar system. The emission mechanisms that generate these bursts offer a remote insight into physical processes in solar coronal plasma, while fine spectral features hint at its underlying turbulent nature. During radio noise storms many hundreds of solar radio bursts can occur over the course of a few hours. Identifying and classifying solar radio bursts is often done manually although a number of automatic algorithms have been produced for this purpose. The use of machine learning algorithms for image segmentation and classification is well established and has shown promising results in the case of identifying Type II and Type III solar radio bursts. Here we present the results of a convolutional neural network applied to

dynamic spectra of NenuFAR solar observations. We highlight some initial success in segmenting radio bursts from the background spectra and outline the steps necessary for burst classification. **2022-05-19**

LOFAR observations of radio burst source sizes and scattering in the solar corona

Pearse C. **Murphy**, Eoin P. Carley, Aoife Maria Ryan, Pietro Zucca, Peter T. Gallagher
A&A 645, A11 **2021**
https://arxiv.org/pdf/2011.13735.pdf
Low frequency radio wave scattering and refraction can have a dramatic effect on the observed size and position of radio sources in the solar corona. The scattering and refraction is thought to be due to fluctuations in electron density caused by turbulence. Hence, determining the true radio source size can provide information on the turbulence in coronal plasma. However, the lack of high spatial resolution radio interferometric observations at low frequencies, such as with the LOw Frequency ARray (LOFAR), has made it difficult to determine the true radio source size and level of radio wave scattering. Here we directly fit the visibilities of a LOFAR observation of a Type IIIb radio burst with an elliptical Gaussian to determine its source size and position. This circumvents the need to image the source and then de-convolve LOFAR's point spread function, which can introduce spurious effects to the source size and shape. For a burst at 34.76 MHz, we find full width at half maximum (FWHM) heights along the major and minor axes to be $18.8' \pm 0.1'$ and $10.2' \pm 0.1'$, respectively, at a plane of sky heliocentric distance of 1.75 $R_\odot$. Our results suggest that the level of density fluctuations in the solar corona is the main cause of the scattering of radio waves, resulting in large source sizes. However, the magnitude of ε may be smaller than what has been previously derived in observations of radio wave scattering in tied-array images. **17 October 2015**

Simulations of radio-wave anisotropic scattering to interpret type III radio bursts measurements by Solar Orbiter, Parker Solar Probe, STEREO and Wind

S. **Musset**, M. Maksimovic, E. Kontar, V. Krupar, N. Chrisaphi, X. Bonnin, A. Vecchio, B. Cecconi, A. Zaslavsky, K. Issautier, S. D. Bale, M. Pulupa
A&A **2021**
https://arxiv.org/pdf/2109.13713.pdf
We use multi-spacecraft observations of invididual type III radio bursts in order to calculate the directivity of the radio emission, to be compared to the results of ray-tracing simulations of the radio-wave propagation and probe the plasma properties of the inner heliosphere. Ray-tracing simulations of radio-wave propagation with anisotropic scattering on density inhomogeneities are used to study the directivity of radio emissions. Simultaneous observations of type III radio bursts by four widely-separated spacecraft are used to calculate the directivity and position of the radio sources. The shape of the directivity pattern deduced for individual events is compared to the directivity pattern resulting from the ray-tracing simulations. We show that simultaneous observations of type radio III bursts by 4 different probes provide the opportunity to estimate the radio source positions and the directivity of the radio emission. The shape of the directivity varies from one event to another, and is consistent with anisotropic scattering of the radio-waves. **2020-07-11**

Constraints on the acceleration region of type III radio bursts from decimetric radio spikes and faint X-ray bursts

Sophie **Musset**, Eduard Kontar, Lindsay Glesener, Nicole Vilmer, Abdallah Hamini
A&A **2021**
https://arxiv.org/pdf/2101.07543.pdf
We study the release of energy during the gradual phase of a flare, characterized by faint bursts of non-thermal hard X-ray (HXR) emission associated with decimetric radio spikes and type III radio bursts starting at high frequencies and extending to the heliosphere. We characterize the site of electron acceleration in the corona and study the radial evolution of radio source sizes in the high corona. Imaging and spectroscopy of the HXR emission with Fermi and RHESSI provide a diagnostic of the accelerated electrons in the corona as well as a lower limit on the height of the acceleration region. Radio observations in the decimetric range with the ORFEES spectrograph provide radio diagnostics close to the acceleration region. Radio spectro-imaging with LOFAR in the meter range provide the evolution of the radio source sizes with their distance from the Sun, in the high corona. Non-thermal HXR bursts and radio spikes are well correlated on short timescales. The spectral index of non-thermal HXR emitting electrons is -4 and their number is about 2×1033 electrons/s. The density of the acceleration region is constrained between $1-5\times109$ cm-3. Electrons accelerated upward rapidly become unstable to Langmuir wave production, leading to high starting frequencies of the type III radio bursts, and the elongation of the radio beam at its source is between 0.5 and 11.4 Mm. The radio source sizes and their gradient observed with LOFAR are larger than the expected size and gradient of the size of the electron beam, assuming it follows the expansion of the magnetic flux tubes. These observations support the idea that the fragmentation of the radio emission into spikes is linked to the fragmentation of the acceleration process itself. The combination of HXR and radio diagnostics in the corona provides strong constrains on the site of electron acceleration. **9 Sep 2017**

Diffusive Transport of Energetic Electrons in the Solar Corona: X-ray and Radio Diagnostics

S. **Musset**, E. P. Kontar, N. Vilmer
A&A 610, A6 (**2018**)
https://arxiv.org/pdf/1710.00765.pdf
https://www.aanda.org/articles/aa/pdf/2018/02/aa31514-17.pdf
Imaging spectroscopy in X-rays with RHESSI provide the possibility to investigate the spatial evolution of the X-ray emitting electron distribution and therefore to study the transport effects on energetic electrons during solar flares. We study the energy dependence of the energetic electron scattering mean free path in the solar corona. We use the imaging spectroscopy technique with RHESSI to study the evolution of energetic electrons distribution in different part of the magnetic loop during the **2004 May 21** flare. These observations are compared with the radio observations of the gyrosynchrotron radiation of the same flare by Kuznetsov and Kontar (2015), and with the predictions of the diffusive transport model described by Kontar et al. (2014). The X-ray analysis shows a trapping of energetic electrons in the corona and a spectral hardening of the energetic electron distribution between the top of the loop and the footpoints. Coronal trapping of electrons is stronger for the radio-emitting electrons than for the X-ray-emitting electrons. These observations can be explained by the diffusive transport model derived by Kontar et al. (2014). We show that the combination of X-ray and radio diagnostics is a powerful tool to study electron transport in the solar corona in different energy domains. We show that the diffusive transport model can explain our observations; and in the range 25-500 keV, the electron scattering mean free path decreases with electron energy. We can estimate for the first time the scattering mean free path dependence on energy in the corona.
RHESSI Science Nuggets in October **2017** No. 309,
http://sprg.ssl.berkeley.edu/~tohban/wiki/index.php/Electron_Scattering_in_the_Flaring_Corona

Study of Time Evolution of Thermal and Non-Thermal Emission from an M-Class Solar Flare

Shunsaku **Nagasawa**, Tomoko Kawate, Noriyuki Narukage, Tadayuki Takahashi, Amir Caspi, Thomas N. Woods
ApJ **933** 173 **2022**
https://arxiv.org/pdf/2205.14369.pdf
https://iopscience.iop.org/article/10.3847/1538-4357/ac7532/pdf
We conduct a wide-band X-ray spectral analysis in the energy range of 1.5-100 keV to study the time evolution of the M7.6 class flare of **2016 July 23**, with the Miniature X-ray Solar Spectrometer (MinXSS) CubeSat and the Reuven Ramaty High Energy Solar Spectroscopic Imager (RHESSI) spacecraft. With the combination of MinXSS for soft X-rays and RHESSI for hard X-rays, a non-thermal component and three-temperature multi-thermal component -- "cool" (T≈ 3 MK), "hot" (T≈ 15 MK), and "super-hot" (T≈ 30 MK) -- were measured simultaneously. In addition, we successfully obtained the spectral evolution of the multi-thermal and non-thermal components with a 10 s cadence, which corresponds to the Alfvén time scale in the solar corona. We find that the emission measures of the cool and hot thermal components are drastically increasing more than hundreds of times and the super-hot thermal component is gradually appearing after the peak of the non-thermal emission. We also study the microwave spectra obtained by the Nobeyama Radio Polarimeters (NoRP), and we find that there is continuous gyro-synchrotron emission from mildly relativistic non-thermal electrons. In addition, we conducted a differential emission measure (DEM) analysis by using Atmospheric Imaging Assembly (AIA) onboard the Solar Dynamics Observatory (SDO) and determine that the DEM of cool plasma increases within the flaring loop. We find that the cool and hot plasma components are associated with chromospheric evaporation. The super-hot plasma component could be explained by the thermalization of the non-thermal electrons trapped in the flaring loop.
RHESSI Science Nuggets #431 Jun **2022**
https://sprg.ssl.berkeley.edu/~tohban/wiki/index.php/Thermal/Nonthermal_with_MinXSS_and_RHESSI

Quasi-periodic Pulsations in a Solar Microflare

V. M. **Nakariakov**1,2, S. Anfinogentov3, A. A. Storozhenko2, E. A. Kurochkin2, V. M. Bogod2,4, I. N. Sharykin3,5, and T. I. Kaltman2
2018 ApJ 859 154 DOI 10.3847/1538-4357/aabfb9
http://https//warwick.ac.uk/fac/sci/physics/research/cfsa/people/valery/research/eprints/Nakariakov_2018_ApJ_859_154.pdf
Irregular time evolution of the radio emission generated in a B2-class microflare (SOL**2017-01-25**T10:15), occurring on 2017 January 25 in active region 12,628, is studied. The microflare was apparently initiated by an appearance of an s-shaped loop, observed in the EUV band. The radio emission is associated with the nonthermal electrons detected with Ramaty High Energy Solar Spectroscopic Imager, and originates simultaneously from two opposite footpoints of a magnetic fan structure beginning at a sunspot. According to the active region geometry, the footpoints are situated in the meridional direction, and hence are observed by RATAN-600 simultaneously. The radio emission intensity signal, as well as the left-hand and right-hand circular polarization signals in the low-frequency band (3–4 GHz) show good correlation with each other, with the average characteristic time of the variation 1.4 ± 0.3 s. The polarization signal

shows a time variation with the characteristic time of about 0.7 ± 0.2 s. The irregular quasi-periodic pulsations of the radio emission are likely to be caused by the superposition of the signals generated at the local electron plasma frequencies by the interaction of nonthermal electrons with the plasma at the footpoints. In this scenario, the precipitation rate of the nonthermal electrons at the opposite footpoints could be modulated by the superposition of fundamental and second harmonic modes of sausage oscillations, resulting in the observed different characteristic times of the intensity and polarization signals. However, other mechanisms, e.g., the oscillatory regime of loop coalescence or magnetic null point oscillation could not be rigorously excluded.

Solar radiophysics — recent results on observations and theories Review

Valery M. **Nakariakov**, Larisa K. Kashapova and Yi-Hua Yan
Research in Astronomy and Astrophysics Volume 14 Number 7, E1, July **2014 File**
Solar radiophysics is a rapidly developing branch of solar physics and plasma astrophysics. Solar radiophysics has the goal of analyzing observations of radio emissions from the Sun and understanding basic physical processes operating in quiet and active regions of the solar corona. In the near future, the commissioning of a new generation of solar radio observational facilities, which include the Chinese Spectral Radio Heliograph (CSRH) and the upgrade of the Siberian Solar Radio Telescope (SSRT), and the beginning of solar observations with the Atacama Large Millimeter/submillimeter Array (ALMA), is expected to bring us new breakthrough results of a transformative nature. The Marie-Curie International Research Staff Exchange (MC IRSES) "RadioSun" international network aims to create a solid foundation for the successful exploitation of upcoming solar radio observational facilities, as well as intensive use of the existing observational tools, advanced theoretical modeling of relevant physical processes and observables, and training a new generation of solar radio physicists. The RadioSun network links research teams from China, Czech Republic, Poland, Russia and the UK. This mini-volume presents research papers based on invited reviews and contributed talks at the 1st RadioSun workshop in China. These papers cover a broad range of research topics and include recent observational and theoretical advances in solar radiophysics, MHD seismology of the solar corona, physics of solar flares, generation of radio emission, numerical modeling of MHD and plasma physics processes, charged-particle acceleration and novel instrumentation.

Solar and Heliospheric Physics with the Square Kilometre Array with Review

Valery M. **Nakariakov**, Mario M. Bisi, Philippa K. Browning, Dalmiro Maia, Eduard P. Kontar, Divya Oberoi, Peter T. Gallagher, Iver H. Cairns, Heather Ratcliffe
Proc. Of Science **2015**
E-print, Dec **2014**
http://arxiv.org/pdf/1507.00516v1.pdf
The fields of solar radiophysics and solar system radio physics, or radio heliophysics, will benefit immensely from an instrument with the capabilities projected for SKA. Potential applications include interplanetary scintillation (IPS), radio-burst tracking, and solar spectral radio imaging with a superior sensitivity. These will provide break through new insights and results in topics of fundamental importance, such as the physics of impulsive energy releases, magnetohydrodynamic oscillations and turbulence, the dynamics of post-eruptive processes, energetic particle acceleration, the structure of the solar wind and the development and evolution of solar wind transients at distances up to and beyond the orbit of the Earth. The combination of the high spectral, time and spatial resolution and the unprecedented sensitivity of the SKA will radically advance our understanding of basic physical processes operating in solar and heliospheric plasmas and provide a solid foundation for the forecasting of space weather events.
8th May 1998, 28 Feb 2013

Low-frequency solar radio type II bursts and their association with space weather events during the ascending phase of solar cycle 25

Theogene **Ndacyayisenga**, Jean Uwamahoro, Jean Claude Uwamahoro, Daniel Izuikedinachi Okoh, Kantepalli Sasikumar Raja, Akeem Babatunde Rabiu, Christian Kwisanga, and Christian Monstein.
Ann. Geophys., 42, 313–329, **2024**
https://doi.org/10.5194/angeo-42-313-2024
https://angeo.copernicus.org/articles/42/313/2024/angeo-42-313-2024.pdf
Type II solar radio bursts are signatures of the coronal shocks and, therefore, particle acceleration events in the solar atmosphere and interplanetary space. Type II bursts can serve as a proxy to provide early warnings of incoming solar storm disturbances, such as geomagnetic storms and radiation storms, which may further lead to ionospheric effects. In this article, we report the first observation of 32 type II bursts by measuring various plasma parameters that occurred between May 2021 and December 2022 in solar cycle 25. We further evaluated their accompanying space weather events in terms of ionospheric total electron content (TEC) enhancement using the rate of TEC index (ROTI). In this study, we find that at heliocentric distance ∼ 1–2 R , the shock and the Alfvén speeds are in the range 504–1282 and 368– 826 km−1 , respectively. The Alfvén Mach number is of the order of $1.2 \leq MA \leq 1.8$ at the above-mentioned heliocentric distance. In addition, the measured magnetic field strength is consistent with the earlier reports and follows a single power law $B(r) = 6.07r^{-3.96}$ G. Based on the current analysis, it is found that 19 out of 32 type II bursts are

associated with immediate space weather events in terms of radio blackouts and polar cap absorption events, making them strong indications of space weather disruption. The ROTI enhancements, which indicate ionospheric irregularities, strongly correlate with GOES X-ray flares, which are associated with the type II radio bursts recorded. The diurnal variability in ROTI is proportional to the strength of the associated flare class, and the corresponding longitudinal variation is attributed to the difference in longitude. This article demonstrates that since type II bursts are connected to space weather hazards, understanding various physical parameters of type II bursts helps to predict and forecast the space weather. **28 October 2021, 28 March 2022, 31 March 2022, 2 April 2022, 17 April 2022**
Table 1. e-CALLISTO Spectrometers, their geographical locations and their frequency ranges.
Table 2. Type II radio bursts observed by e-CALLISTO during the ascending phase of solar cycle 25 and their associated CMEs, GOES soft X-ray flares and estimated shock characteristics. 2021-2022

A Statistical Study of Solar Radio Type III Bursts and Space Weather Implication

Theogene **Ndacyayisenga**, Jean Uwamahoro, K. Sasikumar Raja, Christian Monstein
Advances in Space Research **2020**
https://arxiv.org/pdf/2012.01210.pdf
Solar radio bursts (SRBs) are the signatures of various phenomena that happen in the solar corona and interplanetary medium (IPM). In this article, we have studied the occurrence of Type III bursts and their association with the Sunspot number. This study confirms that the occurrence of Type III bursts correlates well with the Sunspot number. Further, using the data obtained using the e-CALLISTO network, we have investigated the drift rates of isolated Type III bursts and the duration of the group of Type III bursts. Since Type II, Type III, and Type IV bursts are signatures of solar flares and/or CMEs, we can use the radio observations to predict space weather hazards. In this article, we have discussed two events that have caused near-Earth radio blackouts. Since e-CALLISTO comprises more than 152 stations at different longitudes, we can use it to monitor the radio emissions from the solar corona 24 hours a day. Such observations play a crucial role in monitoring and predicting space weather hazards within a few minutes to hours of time. **7 Mar 2010, 2011-08-09, 2015-01-14, 6 Sep 2017,**

Coronal Diagnostics of Solar Type-III Radio Bursts Using LOFAR and PSP Observations

Mohamed **Nedal**, Kamen Kozarev, Peijin Zhang, Pietro Zucca
A&A **2023**
https://arxiv.org/pdf/2310.02677.pdf
This study aims to investigate the ambiguous source and the underlying physical processes of the solar type III radio bursts that occurred on **April 3, 2019**, through the utilization of multiwavelength observations from the LOFAR radio telescope and the PSP space mission, as well as incorporating results from a PFSS and MHD models. The primary goal is to identify the spatial and temporal characteristics of the radio sources, as well as the plasma conditions along their trajectory. Data preprocessing techniques are applied to combine high- and low-frequency observations from LOFAR and PSP between 2.6 kHz and 80 MHz. We then extract information on the frequency drift and speed of the accelerated electron beams from the dynamic spectra. Additionally, we use LOFAR interferometric observations to image the sources of the radio emission at multiple frequencies and determine their locations and kinematics in the corona. Lastly, we analyze the plasma parameters and magnetic field along the trajectories of the radio sources using PFSS and MHD model results. We present several notable findings related to type III radio bursts. Firstly, through our automated implementation, we were able to effectively identify and characterize 9 type III radio bursts in the LOFAR-PSP combined dynamic spectrum and 16 type III bursts in the LOFAR dynamic spectrum. Secondly, our imaging observations show that the electrons responsible for these bursts originate from the same source and within a short time frame of fewer than 30 minutes. Finally, our analysis provides informative insights into the physical conditions along the path of the electron beams. For instance, we found that the plasma density obtained from the MAS model is significantly lower than the expected theoretical density.

Investigating the Coronal Mass Ejections associated with DH type-II radio bursts and solar flares during the ascending phase of the solar cycle 24

Mohamed **Nedal** M.Youssef AymanMahrous RababHelal
Advances in Space Research Volume 63, Issue 5, 1 March **2019**, Pages 1824-1836
sci-hub.tw/10.1016/j.asr.2018.11.001
We studied a set of 74 CMEs, with shedding the light on the halo-CMEs (HCMEs), that are associated with decametric – hectometric (DH) type-II radio bursts (1–16 MHz) and solar flaresduring the period 2008–2014. The events were classified into 3 groups (disk, intermediate, and limb events) based on their longitudinal distribution.
We found that the events are mostly distributed around 15.32° and 15.97° at the northern and southern solar hemispheres, respectively. We found that there is a clear dependence between the longitude and the CME's width, speed, acceleration, mass, and kinetic energy. For the CMEs' widths, most of the events were HCMEs (~62%), while the partial HCMEs comprised ~35% and the rest of events were CMEs with widths less than 120°. For the CMEs' speeds, masses, and kinetic energies, the mean values showed a direct proportionality with the longitude, in which the limb events had the highest speeds, the largest masses, and the highest kinetic energies. The mean peak flux of the solar

flares for different longitudes was comparable, but the disk flares were more energetic. The intermediate flares were considered as gradual flares since they tended to last longer, while the limb flares were considered as impulsive flares since they tended to last shorter.
A weak correlation (R = 0.32) between the kinetic energy of the CMEs and the duration of the associated flares has been noticed, while there was a good correlation (R = 0.76) between the kinetic energy of the CMEs and the peak flux of the associated flares. We found a fair correlation (R = 0.58) between the kinetic energy of the CMEs and the duration of the associated DH type-II radio bursts.

Type II bursts,

Nelson, G.J., Melrose, D.B.,
1985. in: McLean, D. J. & Labrum, N. R. (Ed.), Solar Radiophysics: Studies of Emission from the Sun at Metre Wavelengths, pp. 333–359.

An alternative form of the fundamental plasma emission through the coalescence of Z-mode waves with whistlers

Sulan **Ni**, Yao Chen, Chuanyang Li, Jicheng Sun, Hao Ning, Zilong Zhang
2021
https://arxiv.org/pdf/2104.04267.pdf
Plasma emission (PE), i.e., electromagnetic radiation at the plasma frequency and its second harmonic, is a general process occurring in both astrophysical and laboratory plasmas. The prevailing theory presents a multi-stage process attributed to the resonant coupling of beam-excited Langmuir waves with ion-acoustic waves. Here we examine another possibility of the fundamental PE induced by the resonant coupling of Z-mode and whistler (W) waves. Earlier studies have been controversial in the plausibility and significance of such process in plasmas. In this study we show that the matching condition of three wave resonant interaction (Z+W ! O) can be satisfied over a wide regime of parameters based on the magnetoionic theory, demonstrate the occurrence of such process and further evaluate the rate of energy conversion from the pumped Z or W mode to the fundamental O mode with particle-in-cell (PIC) simulations of wave pumping. The study presents an alternative form of the fundamental PE, which could possibly play a role in various astrophysical and laboratory scenarios with both Z and W modes readily excited through the electron cyclotron maser instability.

Plasma Emission Induced by Electron Cyclotron Maser Instability in Solar Plasmas with a Large Ratio of Plasma Frequency to Gyrofrequency

Sulan **Ni**1, Yao Chen1, Chuanyang Li1, Zilong Zhang1, Hao Ning1, Xiangliang Kong1, Bing Wang1, and M. Hosseinpour2
2020 ApJL 891 L25
https://doi.org/10.3847/2041-8213/ab7750
In plasmas with a large ratio of plasma frequency to gyrofrequency (ω pe/Ωce), energetic electrons characterized by $\partial f/\partial v_{\perp} > 0$ can excite electron cyclotron maser instability (ECMI), generating waves of upper hybrid (UH), Z, and W modes. It has been presumed that these ECMI waves can somehow convert to escaping X–O modes as fundamental (F) or harmonic (H) plasma emission. Here we perform a fully kinetic, electromagnetic particle-in-cell simulation to investigate the proposed radiation process. ECMI is driven by energetic electrons with a Dory–Guest–Harris distribution representative of a double-sided loss cone, and ω pe/Ωce is set to be 10. We find that the electrostatic UH mode is the fastest-growing mode. Around the time when its energy starts to decline, the W mode grows to be dominant. During this stage, we observe significant F and H plasma emission. The F emission is in the O mode with a bandwidth around 0.1–0.2 Ωce, and the H emission is contributed by both X and O modes with a narrower bandwidth. We suggest that the O–F emission is caused by coalescence of almost counterpropagating Z and W modes, while the H emission arises from coalescence of an almost counterpropagating UH mode at relatively large wave number. Thus the plasma emission investigated here is induced by a combination of wave growth due to ECMI and further nonlinear wave-coupling processes. The result is relevant to understanding solar radio bursts as well as other astronomical radio sources that are excited by energetic electrons trapped within certain magnetic structures.

The Effect of Uniform and Non-uniform Electron Density Models for Determining Shock Speed of a Type II Solar Radio Burst

D P S **Nilagarathne**, J Adassuriya, H O Wijewardane
Proceedings of the Technical Sessions, 36 (**2020**)
https://arxiv.org/ftp/arxiv/papers/2308/2308.01570.pdf
Solar flare is one of the most important solar activities which emit all electromagnetic waves in gigantic burst. The radio emission can be used to determine the physical properties of the solar flares. The e-CALLISTO worldwide network is designed to detect the radio emission of the solar flares and this study used the spectroscopic data from the e-CALLISTO system. Among the five types of solar radio bursts, this study was focused on type II radio bursts. The

spectroscopic analysis estimated the shock speed of type II radio bursts using the uniform electron density model and the nonuniform electron density model of the sun. The shock speed is proportional to the electron density (Ne) and inversely proportional to the rate of change in electron density with altitude (dNe/dr). The determined shock speed at the altitude of one solar radius is 2131 km/s for uniform model and 766 km/s for non-uniform model. Although the uniform electron density model is widely used we attempted the non-uniform electron density since in the active region of the sun, the electron densities are non-uniform. The estimated shock speeds of uniform density model is relatively high so that it is reasonable to use non-uniform electron density model for shock speed estimation of type II radio bursts.

The dynamic chromosphere at millimeter wavelengths

Alexander **Nindos**, Spiros Patsourakos, Shahin Jafarzadeh, Masumi Shimojo
Front. Astron. Space Sci. 9: 981205. **2022**
doi 10.3389/fspas.2022.981205
https://www.frontiersin.org/articles/10.3389/fspas.2022.981205/pdf

The chromosphere is one of the most complex and dynamic layers of the solar atmosphere. The dynamic phenomena occur on different spatial and temporal scales, not only in active regions but also in the so-called quiet Sun. In this paper we review recent advances in our understanding of these phenomena that stem from the analysis of observations with the Atacama Large Millimeter/submillimeter Array (ALMA). The unprecedented sensitivity as well as spatial and temporal resolution of ALMA at millimeter wavelengths have advanced the study of diverse phenomena such as chromospheric p-mode-like and high-frequency oscillations, as well as small-scale, weak episodes of energy release, including shock waves. We review the most important results of these studies by highlighting the new aspects of the phenomena that have revealed as well as the new questions and challenges that have generated.

ALMA observations of the variability of the quiet Sun at millimeter wavelengths

A. **Nindos**, S. Patsourakos, C.E. Alissandrakis, T.S. Bastian
A&A 652, A92 **2021**
https://arxiv.org/pdf/2106.04220.pdf
https://www.aanda.org/articles/aa/pdf/2021/08/aa41241-21.pdf
https://doi.org/10.1051/0004-6361/202141241

Using Atacama Large Millimeter/submillimeter Array (ALMA) observations of the quiet Sun at 1.26 and 3 mm, we study spatially resolved oscillations and transient brightenings, i.e. small, weak events of energy release. Both phenomena may have a bearing on the heating of the chromosphere. At 1.26 mm, in addition to power spectra of the original data, we degraded the images to the spatial resolution of the 3 mm images and used fields of view of equal area for both data sets. The detection of transient brightenings was made after the oscillations were removed. At both frequencies we detected p-mode oscillations in the range 3.6-4.4 mHz. In the corrected data sets, the oscillations at 1.26 and 3 mm showed brightness temperature fluctuations of ~1.7-1.8% with respect to the average quiet Sun, corresponding to 137 and 107 K, respectively. They represented a fraction of 0.55-0.68 of the full power spectrum and their energy density at 1.26 mm was 0.03 erg cm−3. We detected 77 transient brightenings at 1.26 mm and 115 at 3 mm. Although the majority of the 1.26 mm events occurred in cell interior, their occurrence rate per unit area was higher than that of the 3 mm events. The computed low-end energy of the 1.26 mm transient brightenings (1.8×1023 erg) is among the smallest ever reported, irrespective of the wavelength of observation. However, their power per unit area is smaller than that of the 3 mm events, probably due to the detection of many weak 1.26 mm events. We also found that ALMA bright network structures corresponded to dark mottles/spicules seen in broadband Hα images from the GONG network. **12 April 2018**

Incoherent Solar Radio Emission **Review**

A. **Nindos**
Frontiers in Astronomy, Space Sciences **2020**,
https://arxiv.org/pdf/2007.14888.pdf
https://doi.org/10.3389/fspas.2020.00057
https://www.frontiersin.org/articles/10.3389/fspas.2020.00057/full

Incoherent solar radio radiation comes from the free-free, gyroresonance, and gyrosynchrotron emission mechanisms. Free-free is primarily produced from Coulomb collisions between thermal electrons and ions. Gyroresonance and gyrosynchrotron result from the acceleration of low-energy electrons and mildly relativistic electrons, respectively, in the presence of a magnetic field. In the non-flaring Sun, free-free is the dominant emission mechanism with the exception of regions of strong magnetic fields which emit gyroresonance at microwaves. Due to its ubiquitous presence, free-free emission can be used to probe the non-flaring solar atmosphere above temperature minimum. Gyroresonance opacity depends strongly on the magnetic field strength and orientation; hence it provides a unique tool for the estimation of coronal magnetic fields. Gyrosynchrotron is the primary emission mechanism in flares at frequencies higher than 1-2 GHz and depends on the properties of both the magnetic field and the accelerated electrons, as well as

the properties of the ambient plasma. In this paper we discuss in detail the above mechanisms and their diagnostic potential. **2 Aug 1985, 1992 July 1, 15 Oct 1994, 22 Oct 2000, 2004 June 27, 16 Mar 2017**

Transient brightenings in the quiet Sun detected by ALMA at 3 mm

A. **Nindos**, C. E. Alissandrakis, S. Patsourakos, T. S. Bastian
A&A 638, A62 **2020**
https://arxiv.org/pdf/2004.07591.pdf
https://www.aanda.org/articles/aa/pdf/2020/06/aa37810-20.pdf
Using ALMA observations, we performed the first systematic survey for transient brightenings (i.e. weak, small-scale episodes of energy release) in the quiet solar chromosphere at 3 mm. Our dataset included images of six 87" x 87" regions of the quiet Sun obtained with angular resolution of a few arcsec at a cadence of 2 s. The transient brightenings were detected as weak enhancements above the average intensity after we removed the effect of the p-mode oscillations. A similar analysis, over the same regions, was performed for simultaneous 304 and 1600 Å data obtained with the Atmospheric Imaging Assembly. We detected 184 3 mm transient brightening events with brightness temperatures from 70 K to more than 500 K above backgrounds of ∼7200−7450 K. Their mean duration and maximum area were 51.1 s and 12.3 Mm2, respectively, with a weak preference of appearing at network boundaries rather than in cell interiors. Both parameters exhibited power-law behavior with indices of 2.35 and 2.71, respectively. Only a small fraction of ALMA events had either 304 or 1600 Å counterparts but the properties of these events were not significantly different from those of the general population except that they lacked their low-end energy values. The total thermal energies of the ALMA transient brightenings were between 1.5×1024 and 9.9×1025 erg and their frequency distribution versus energy was a power law with an index of 1.67. We found that the power per unit area provided by the ALMA events could account for only 1\% of the chromospheric radiative losses (10\% of the coronal ones). Therefore, their energy budget falls short of meeting the requirements for the heating of the upper layers of the solar atmosphere and this conclusion does not change even if we use the least restrictive criteria possible for the detection of transient brightenings. **March 16, 2017**.

Solar physics with the Square Kilometre Array **Review**

Nindos, A. , Kontar, E. P. , Oberoi, D.
Advances in Space Research, Volume 63, Issue 4, p. 1404-1424. **2019**
https://arxiv.org/pdf/1810.04951.pdf
https://sci-hub.ru/10.1016/j.asr.2018.10.023
The Square Kilometre Array (SKA) will be the largest radio telescope ever built, aiming to provide collecting area larger than 1 km2. The SKA will have two independent instruments, SKA-LOW comprising of dipoles organized as aperture arrays in Australia and SKA-MID comprising of dishes in South Africa. Currently the phase-1 of SKA, referred to as SKA1, is in its late design stage and construction is expected to start in 2020. Both SKA1-LOW (frequency range of 50-350 MHz) and SKA1-MID Bands 1, 2, and 5 (frequency ranges of 350-1050, 950-1760, and 4600-15,300 MHz, respectively) are important for solar observations. In this paper we present SKA's unique capabilities in terms of spatial, spectral, and temporal resolution, as well as sensitivity and show that they have the potential to provide major new insights in solar physics topics of capital importance including (i) the structure and evolution of the solar corona, (ii) coronal heating, (iii) solar flare dynamics including particle acceleration and transport, (iv) the dynamics and structure of coronal mass ejections, and (v) the solar aspects of space weather. Observations of the Sun jointly with the new generation of ground-based and space-borne instruments promise unprecedented discoveries.

First high resolution look at the quiet Sun with ALMA at 3 mm

A. **Nindos**, C.E. Alissandrakis, T.S. Bastian, S. Patsourakos, B. De Pontieu, H. Warren, T. Ayres, H.S. Hudson, T. Shimizu, J.-C. Vial, S. Wedemeyer, V. Yurchyshyn
A&A 619, L6 **2018**
https://arxiv.org/pdf/1810.05223.pdf
We present an overview of high resolution quiet Sun observations, from disk center to the limb, obtained with the Atacama Large mm and sub-mm Array (ALMA) at 3 mm. Seven quiet Sun regions were observed with resolution of up to 2.5" by 4.5". We produced both average and snapshot images by self-calibrating the ALMA visibilities and combining the interferometric images with full disk solar images. The images show well the chromospheric network, which, based on the unique segregation method we used, is brighter than the average over the fields of view of the observed regions by ∼305 K while the intranetwork is less bright by ∼280 K, with a slight decrease of contrast toward the limb. At 3 mm the network is very similar to the 1600 \AA\ images, with somewhat larger size. We detected for the first time spicular structures, rising up to 15" above the limb with a width down to the image resolution and brightness temperature of ∼ 1800 K above the local background. No trace of spicules, either in emission or absorption, was found on the disk. Our results highlight ALMA's potential for the study of the quiet chromosphere. **March 16 2017**
CESRA #2044 Nov **2018** http://www.astro.gla.ac.uk/users/eduard/cesra/?p=2044

Solar Physics with the Square Kilometre Array **Review**

A. **Nindos**, E.P. Kontar, D. Oberoi

Advances in Space Research Volume 63, Issue 4, 15 February **2019**, Pages 1404-1424

https://arxiv.org/pdf/1810.04951.pdf

The Square Kilometre Array (SKA) will be the largest radio telescope ever built, aiming to provide collecting area larger than 1 km2. The SKA will have two independent instruments, SKA-LOW comprising of dipoles organized as aperture arrays in Australia and SKA-MID comprising of dishes in South Africa. Currently the phase-1 of SKA, referred to as SKA1, is in its late design stage and construction is expected to start in 2020. Both SKA1-LOW (frequency range of 50-350 MHz) and SKA1-MID Bands 1, 2, and 5 (frequency ranges of 350-1050, 950-1760, and 4600-15300 MHz, respectively) are important for solar observations. In this paper we present SKA's unique capabilities in terms of spatial, spectral, and temporal resolution, as well as sensitivity and show that they have the potential to provide major new insights in solar physics topics of capital importance including (i) the structure and evolution of the solar corona, (ii) coronal heating, (iii) solar flare dynamics including particle acceleration and transport, (iv) the dynamics and structure of coronal mass ejections, and (v) the solar aspects of space weather. Observations of the Sun jointly with the new generation of ground-based and space-borne instruments promise unprecedented discoveries.

Table 1: Instruments capable of performing solar radio spectroscopic imaging

CESRA #2295 Aug **2019** http://cesra.net/?p=2295

On the relationship of shock waves to flares and coronal mass ejections

A. **Nindos**[1], C. E. Alissandrakis[1] , A. Hillaris[2], and P. Preka-Papadema[2]

A&A 531, A31 (**2011**), **File**

http://arxiv.org/pdf/1105.1268v1.pdf

Context.Metric type II bursts are the most direct diagnostic of shock waves in the solar corona.

Aims.There are two main competing views about the origin of coronal shocks: that they originate in either blast waves ignited by the pressure pulse of a flare or piston-driven shocks due to coronal mass ejections (CMEs). We studied three well-observed type II bursts in an attempt to place tighter constraints on their origins.

Methods.The type II bursts were observed by the ARTEMIS radio spectrograph and imaged by the Nançay Radioheliograph (NRH) at least at two frequencies. To take advantage of projection effects, we selected events that occurred away from disk center.

Results. In all events, both flares and CMEs were observed. In the first event, the speed of the shock was about 4200 km s−1, while the speed of the CME was about 850 km s−1. This discrepancy ruled out the CME as the primary shock driver. The CME may have played a role in the ignition of another shock that occurred just after the high speed one. A CME driver was excluded from the second event as well because the CMEs that appeared in the coronagraph data were not synchronized with the type II burst. In the third event, the kinematics of the CME which was determined by combining EUV and white light data was broadly consistent with the kinematics of the type II burst, and, therefore, the shock was probably CME-driven.

Conclusions.Our study demonstrates the diversity of conditions that may lead to the generation of coronal shocks.

March 2, 2000, March 7, 2000, May 2, 2000

Radio Emission of Flares and Coronal Mass Ejections

Invited Review

A. Nindos · H. Aurass · K.-L. Klein · G. Trottet

Solar Phys, 253: 3–41, **2008**, DOI 10.1007/s11207-008-9258-9, **File**

We review recent progress on our understanding of radio emission from solar flares and coronal mass ejections (CMEs) with emphasis on those aspects of the subject that help us address questions about energy release and its properties, the configuration of flare –CME source regions, coronal shocks, particle acceleration and transport, and the origin of solar energetic particle (SEP) events. Radio emission from electron beams can provide information about the electron acceleration process, the location of injection of electrons in the corona, and the properties of the ambient coronal structures. Mildly relativistic electrons gyrating in the magnetic fields of flaring loops produce radio emission via the gyrosynchrotron mechanism, which provides constraints on the magnetic field and the properties of energetic electrons. CME detection at radio wavelengths tracks the eruption from its early phase and reveals the participation of a multitude of loops of widely differing scale. Both flares and CMEs can ignite shock waves and radio observations offer the most robust tool to study them. The incorporation of radio data into the study of SEP events reveals that a clear-cut distinction between flare-related and CME-related SEP events is difficult to establish.

Harmonic maser emissions from electrons with loss-cone distribution in solar active regions

Hao **Ning**, Yao Chen, Sulan Ni, Chuanyang Li, Zilong Zhang, Xiangliang Kong, Mehdi Yousefzadeh

ApJL 920, L40 **2021**

https://arxiv.org/pdf/2110.15514.pdf

https://doi.org/10.3847/2041-8213/ac2cc6

Electron cyclotron maser emission (ECME) is regarded as a plausible source for the coherent radio radiations from solar active regions (e.g., solar radio spikes). In this Letter, we present a 2D3V fully kinetic electromagnetic particle-in-cell (PIC) simulation to investigate the wave excitations and subsequent nonlinear processes induced by the energetic electrons in the loss-cone distribution. The ratio of the plasma frequency to the electron gyrofrequency ωpe/Ωce is set to 0.25, adequate for solar active region conditions. As a main result, we obtain strong emissions at the second-harmonic X mode (X2). While the fundamental X mode (X1) and the Z mode are amplified directly via the electron cyclotron maser instability, the X2 emissions can be produced by the nonlinear coalescence between two Z modes and between Z and X1 modes. This represents a novel generation mechanism for the harmonic emissions in plasmas with a low value of ωpe/Ωce, which may resolve the escaping difficulty of explaining solar radio emissions with the ECME mechanism.
CESRA # 3108 Nov **2021** https://www.astro.gla.ac.uk/users/eduard/cesra/?p=3108

Harmonic elctron-cyclotron maser emissions driven by energetic electrons of the horseshoe distribution with application to solar radio spikes

Hao **Ning**, Yao Chen, Sulan Ni, Chuanyang Li, Zilong Zhang, Xiangliang Kong, Mehdi Yousefzadeh
A&A 651, A118 **2021**
https://arxiv.org/pdf/2105.13631.pdf
https://www.aanda.org/articles/aa/pdf/2021/07/aa40427-21.pdf
https://doi.org/10.1051/0004-6361/202140427
Content. Electron-cyclotron maser emission (ECME) is the favored mechanism for solar radio spikes and has been investigated extensively since the 1980s. Most studies relevant to solar spikes employ a loss-cone-type distribution of energetic electrons, generating waves mainly in the fundamental X/O mode (X1/O1), with a ratio of plasma oscillation frequency to electron gyrofrequency (ωpe/Ωce) lower than 1. Despite the great progress made in this theory, one major problem is how the fundamental emissions pass through the second-harmonic absorption layer in the corona and escape. This is generally known as the escaping difficulty of the theory. Aims. We study the harmonic emissions generated by ECME driven by energetic electrons with the horseshoe distribution to solve the escaping difficulty of ECME for solar spikes. Methods. We performed a fully kinetic electromagnetic PIC simulation with ωpe/Ωce = 0.1, corresponding to the strongly magnetized plasma conditions in the flare region, with energetic electrons characterized by the horseshoe distribution. We also varied the density ratio of energetic electrons to total electrons (ne/n0) in the simulation. Results. We obtain efficient amplification of waves in Z and X2 modes, with a relatively weak growth of O1 and X3. With a higher-density ratio, the X2 emission becomes more intense, and the rate of energy conversion from energetic electrons into X2 modes can reach ∼0.06% and 0.17%, with ne/n0= 5% and 10%, respectively. Conclusions. We find that the horseshoe-driven ECME can lead to an efficient excitation of X2 and X3 with a low value of ωpe/Ωce, providing novel means for resolving the escaping difficulty of ECME when applied to solar radio spikes. The simultaneous growth of X2 and X3 can be used to explain some harmonic structures observed in solar spikes.

Two-stage energy release process of a confined flare with double HXR peaks

Hao **Ning**, Yao Chen, Zhao Wu, Yang Su, Hui Tian, Gang Li, Guohui Du, Hongqiang Song
ApJ **2018**
https://arxiv.org/pdf/1801.06641.pdf
A complete understanding of the onset and subsequent evolution of confined flares has not been achieved. Earlier studies mainly analyzed disk events so as to reveal their magnetic topology and cause of confinement. In this study, taking advantage of a tandem of instruments working at different wavelengths of X-rays, EUVs, and microwaves, we present dynamic details of a confined flare observed on the northwestern limb of the solar disk on **July 24th, 2016**. The entire dynamic evolutionary process starting from its onset is consistent with a loop-loop interaction scenario. The X-ray profiles manifest an intriguing double-peak feature. From spectral fitting, it is found that the first peak is non-thermally dominated while the second peak is mostly multi-thermal with a hot (~10 MK) and a super-hot (~30 MK) component. This double-peak feature is unique in that the two peaks are clearly separated by 4 minutes, and the second peak reaches up to 25-50 keV; in addition, at energy bands above 3 keV the X-ray fluxes decline significantly between the two peaks. This, together with other available imaging and spectral data, manifest a two-stage energy release process. A comprehensive analysis is carried out to investigate the nature of this two-stage process. We conclude that the second stage with the hot and super-hot sources mainly involves direct heating through loop-loop reconnection at a relatively high altitude in the corona. The uniqueness of the event characteristics and complete data set make the study a nice addition to present literature on solar flares.

Spatial and Spectral Behaviors of Solar Flares Observed in Microwaves

Zongjun **Ning,** Wenda Cao
Solar Phys. 257(2), Page: 335 – 350, **2009**
The spatial and spectral behaviors of two solar flares observed by the Nobeyama Radioheliograph (NoRH) on **24 August 2002 and 22 August 2005** are explored. They were observed with a single loop-top source and double footpoint sources at the beginning, then with looplike structures for the rest of the event. NoRH has high spatial and temporal resolution at the two frequencies of 17 and 34 GHz where a nonthermal radio source is often optically thin.

Such capabilities give us an opportunity to study the spatial and spectral behaviors of different microwave sources. The 24 August 2002 flare displayed a soft – hard – soft (SHS) spectral pattern in the rising – peak – decay phases at 34 GHz, which was also observed for the spectral behavior of both loop-top and footpoint sources. In contrast, the 22 August 2005 flare showed a soft – hard – harder (SHH) spectral pattern for its both loop-top and footpoint sources. It is interesting that this event showed a harder spectrum in the early rising phase. We found a positive correlation between the spectral index and microwave flux in both the loop-top source and the footpoint sources in both events. The conclusions drawn from the flux index could apply to the electron index as well, because of their simple linear relationship under the assumption of nonthermal gyrosynchrotron mechanism. Such a property of spatial and spectral behaviors of microwave sources gives an observational constraint on the electron acceleration mechanism and electron propagation.

EVIDENCE OF CHROMOSPHERIC EVAPORATION IN THE 2004 DECEMBER 1 SOLAR FLARE

Zongjun **Ning**1, Wenda Cao2, Jing Huang3, Guangli Huang1, Yihua Yan3, and Hengqiang Feng4
Astrophysical Journal, 699:15–22, **2009**
http://www.iop.org:80/EJ/toc/-alert=43190/0004-637X/699/1

In this paper, we present the radio and hard X-ray evidence of chromospheric evaporation during an M1.0 flare which occurred on 2004 December 1. The radio emission was observed by the Solar Broadband Radio Dynamic Spectrometer in China, which yielded dynamic spectra of decimetric emission. The hard X-ray emission was observed by *RHESSI*. In the radio spectra, the burst is characterized by two groups of parallel-drifting structures, some of which change their drifting rates from positive to negative. Based on the standard flare model, we may explain these decimetric bursts in terms of chromospheric evaporation. On the other hand, *RHESSI* observations show that the hard X-ray emission in the energy range of 10–15 keV tends to rise from two footpoints to the looptop and eventually merges into a single looptop source, which is accepted as evidence of hard X-ray chromospheric evaporation. Such processes happened twice in this event. The drifting radio structures occurred between them, at the same time as the third hard X-ray peak was observed at 25–50 keV.

RHESSI MICROFLARES WITH QUIET MICROWAVE EMISSION

Zongjun **Ning**
Astrophysical Journal, 686:674Y685, **2008**
http://www.journals.uchicago.edu/doi/pdf/10.1086/590652

We statistically study RHESSI microflares, or ‘‘weak events,’’ from the first month of 2003. In total, 94 events are selected from the RHESSI flare catalog in the 3Y6 and 12Y25 keV energy ranges. The sample differs from those of previous studies in that the events are characterized by having quiet microwave emission, based on observations from the Nobeyama Radio Polarimeters. These microflares cluster around GOES class C1.1 and are associated with active regions. Consistent with previous findings, the thermal plasma observed by RHESSI is found to be hot, 10MKPTP 15MK, with lowemission measure (1046 cm_3PEMP1047 cm_3) and density (1.0 ; 109 cm_3PneP12 ; 109 cm_3). The spectral fitting requires a steep nonthermal power-law component, with median index of 8.1. Further evidence for the presence of nonthermal electrons is that the estimated nonthermal energy is comparable to the thermal energy, having a median value of _4.0 ; 1028 ergs for the events studied here. Using the correlation between the time derivative of the light curve at 3Y6 keVand the 12Y25 keV hard X-ray flux, we investigate the Neupert effect in these microflares. Similar to findings for large flares, roughly half of these microflares (46 of 94) display the Neupert effect. RHESSI imaging shows that each event has a single source at 3Y12 keV. Such characteristics indicate that some in situ heating mechanism is at work in the local corona surrounding microflares, with the low microwave emission resulting from a lack of nonthermal electron propagation to the chromosphere.

High-Frequency Evolving Emission Lines for the 25 August 1999 Solar Flare

Zongjun **Ning** · H. Wu · F. Xu · X. Meng
Solar Phys (**2008**) 250: 107–113
http://www.springerlink.com/content/nn52v470m5527142/fulltext.pdf

We analyze a special kind of temporal fine structure in microwave radio emission for the **25 August 1999** solar flare observed by the PMO spectrometer over the range of 4.5 – 7.5 GHz. This flare displays continuum emission after a group of reverse-slope type III bursts around 6 GHz. High-resolution dynamic spectra reveal three evolving emission lines (EELs) following the type III group. They are characterized by isolated, narrow, and continuous emission strips, which display frequency fluctuations with time. Their frequency-drift rates are between −2 and 3 GHzs-1. Distinct from the EELs at lower frequencies, three EELs have a very short duration of a few seconds. They show an average bandwidth of $\Delta f \approx 330$ MHz and a relative bandwidth of $\Delta f/f \approx 0.057$. This is the first time that this kind of fine structure has been observed around 6 GHz.

Microwave and Hard X-Ray Spectral Evolution for the 13 December 2006 Solar Flare

Zongjun **Ning**
Solar Phys (**2008**) 247: 53–62
http://www.springerlink.com/content/ew0324n62152062u/fulltext.pdf
This paper explores the time evolution of microwave and hard X-ray spectral indexes in the solar flare observed by Nobeyama Radio Polarimeters (NoRP) and the Ramaty High Energy Solar Spectroscopy Imager (RHESSI) on 13 December 2006. The microwave spectral index, γ_{MW}, is derived from the emissions at two frequencies, 17 and 35 GHz, and hard X-ray spectral index, γ_{HXR}, is derived from RHESSI spectra. Fifteen subpeaks are detected at the microwave and hard X-ray emissions. The microwave spectral indexes tend to be harder than hard X-ray spectral indexes during the flare, which is consistent with previous findings. All detected subpeaks follow the soft-hard-soft spectral behaviours in the hard X-ray rise-peak-decay phases. However, the corresponding microwave subpeaks display different spectral behaviour, such as soft-hard-soft, soft-hard-harder, soft-hard-soft **+** hard or irregular patterns. These contradictions reveal the complicated acceleration mechanism for low- and high-energy electrons during this event. It is also interesting

MICROWAVE AND HARD X-RAY SPECTRAL EVOLUTION IN TWO SOLAR FLARES

Zongjun **Ning**
The Astrophysical Journal, 659: L69–L72, **2007**
2004 May 21 and November 3.
Although the microwave and hard X-ray emission are produced by electrons at very different energies, a correlation between their spectral indices is found, indicating a common acceleration mechanism.

DIFFERENT BEHAVIORS BETWEEN MICROWAVE AND HARD X-RAY SPECTRAL HARDNESS IN TWO SOLAR FLARES

Zongjun **Ning**
The Astrophysical Journal, 671: L197–L200, **2007**
http://www.journals.uchicago.edu/doi/pdf/10.1086/525249
We explore the spectral behaviors of microwave and hard X-ray emissions in two solar flares observed by the Nobeyama Radio Polarimeters (NoRP) and the *Reuven Ramaty High-Energy Solar Spectroscopic Imager* (*RHESSI*) on **2003 May 29 and 2004 January 6**. The microwave spectral index γ_{MW} is derived from the emissions at two frequency channels of 17 and 35 GHz, and the standard *RHESSI* data analysis is used to derive the hard X-ray spectral index γ_{HXR}. The 2003 May 29 flare displays a soft-hard-soft spectral behavior in the hard X-ray risepeak-decay phases, but a soft-hard-harder pattern in the microwave emission. The 2004 January 6 flare shows several soft-hard-soft spectral behaviors in its hard X-ray subpeaks, but only one soft-hard-soft pattern in the microwave emission from start to end. The imaging observations show that the thermal emission could be an important contribution to microwave spectral hardening with the time.

Frequency Distributions of Microwave Pulses for the 18 March 2003 Solar Flare

Zongjun **Ning**, H. Wu, F. Xu, X. Meng
Solar Phys., 242(1-2), Page: 101 – 109, 2007.

Positively Drifting Structures During the 18 March 2003 Solar Flare

Zongjun **Ning**, H. Wu, F. Xu, X. Meng
Solar Phys., 241 (1), Page: 77 – 84, **2007**.

Solar Partial N-burst_

Zong-Jun **Ning**1, Yu-Ying Liu1, Qi-Jun Fu1 and Fu-Ying Xu2
Chin. J. Astron. Astrophys. Vol. 3 (2003), No. 4, 381–390
(http://www.chjaa.org or http://chjaa.bao.ac.cn)
We present a new sub-class of type III solar radio burst at the high frequencies around 6.0 GHz. In addition to a descending and an ascending branch on the dynamic spectrum, it has an inverted morphology different from the simple type U-burst. We call it “partial N-burst” because it is interpreted as the known N-burst minus its first branch. The partial N-burst presented here was detected among a reverse slope type III (RS-III) burst group prior to the type V solar radio continuum and was simultaneously recorded by two spectrometers at the National Astronomical Observatories, Chinese Academy of Sciences (NAOC, 5.20–7.60 GHz) and at Purple Mountain Observatory (PMO, 4.50–7.50 GHz)

on 1999 August 25. After the N-burst and M-burst, the partial N-burst is a third piece of evidence for a magnetic mirror effect in solar radio observation, when the same electron is reflected at a pinched foot of a flare loop.

Narrowband frequency-drift structures in solar type IV bursts

Yukio **Nishimura**1, Takayuki Ono1, Fuminori Tsuchiya2, Hiroaki Misawa2, Atsushi Kumamoto1, Yuto Katoh1, Satoshi Masuda3, and Yoshizumi Miyoshi3

Earth Planets Space, **65**, 1555–1562, **2013, File**

We have established the Zao Solar Radiospectrograph (ZSR), a new solar radio observation system, at the Zao observatory of Tohoku University, Japan. We observed narrowband fine structures with type IV bursts with ZSR on **2 and 3 November 2008**. The observed fine structures are similar to fiber bursts in terms of the drift rates and the existence of emission and absorption stripes. Statistical analysis of the drift rates, however, shows that the observed fine structures are different from the ordinary fiber bursts as regards the sense and the magnitude of their drift rates. First, the observed drift rates include both positive and negative rates, whereas ordinary fiber bursts are usually characterized by negative drift rates. Second, the absolute values of the observed drift rates are tens of MHz s−1, whereas the typical drift rate of fiber bursts at 325 MHz is approximately −9 MHz s−1. In addition, all fine structures analyzed have narrow emission bands of less than 17 MHz. We also show that the observed narrowband emission features with drift rates of approximately 40 MHz s−1 can be interpreted as the propagation of whistler-mode waves, which is the same process as that underlying fiber bursts.

Particle Acceleration in Plasmoid Ejections Derived from Radio Drifting Pulsating Structures

N. **Nishizuka**1, M. Karlický2, M. Janvier3, and M. Bárta

2015 ApJ 799 126

http://arxiv.org/pdf/1412.7904v1.pdf

We report observations of slowly drifting pulsating structures (DPSs) in the 0.8-4.5 GHz frequency range of the RT4 and RT5 radio spectrographs at Ondřejov Observatory, **between 2002 and 2012. We found 106 events of DPSs**, which we classified into four cases: (I) single events with a constant frequency drift (12 events), (II) multiple events occurring in the same flare with constant frequency drifts (11 events), (III) single or multiple events with increasing or decreasing frequency drift rates (52 events), and (IV) complex events containing multiple events occurring at the same time in a different frequency range (31 events). Many DPSs are associated with hard X-ray (HXR) bursts (15-25 keV) and soft X-ray (SXR) gradient peaks, as they typically occurred at the beginning of HXR peaks. This indicates that DPS events are related to the processes of fast energy release and particle acceleration. Furthermore, interpreting DPSs as signatures of plasmoids, we measured their ejection velocity, their width, and their height from the DPS spectra, from which we also estimated the reconnection rate and the plasma beta. In this interpretation, constant frequency drift indicates a constant velocity of a plasmoid, and an increasing/decreasing frequency drift indicates a deceleration/acceleration of a plasmoid ejection. The reconnection rate shows a good positive correlation with the plasmoid velocity. Finally we confirmed that some DPS events show plasmoid counterparts in Solar Dynamics Observatory/Atmospheric Imaging Assembly images. **2002 Jan 23, 10 Apr 2002, 2002 May 21, 30 Aug 2002, 31 Aug 2002, 29 Sept 2002, 21 Nov 2002, 18 May 2003, 2 Jun 2003, 20 Oct 2003, 29 Oct 2003, 18 Nov 2003, 14 July 2005, 6 March 2011, 21 Dec 2011, 8 May 2012,** 2012 July 6, **13 June 2013,**

Table 1. Event list of the 106 DPS events during 2002-2012.

Data-Constrained Solar Modeling with GX Simulator

Gelu M. **Nita**, Gregory D. Fleishman, Alexey A. Kuznetsov, Sergey A. Anfinogentov, Alexey G. Stupishin, Eduard P. Kontar, Samuel J. Schonfeld, James A. Klimchuk, Dale E. Gary

ApJS **267** 6 **2023**

https://arxiv.org/pdf/2301.00795.pdf

https://iopscience.iop.org/article/10.3847/1538-4365/acd343/pdf

To facilitate the study of solar active regions and flaring loops, we have created a modeling framework, the freely distributed GX Simulator IDL package, that combines 3D magnetic and plasma structures with thermal and non-thermal models of the chromosphere, transition region, and corona. The package has integrated tools to visualize the model data cubes, compute multi-wavelength emission maps from them, and quantitatively compare the resulting maps with observations. Its object-based modular architecture, which runs on Windows, Mac, and Unix/Linux platforms, offers capabilities that include the ability to either import 3D density and temperature distribution models, or to assign numerically defined coronal or chromospheric temperatures and densities, or their distributions to each individual voxel. The application integrates FORTRAN and C++ libraries for fast calculation of radio emission (free-free, gyroresonance, and gyrosynchrotron emission) along with soft and hard X-ray and EUV codes developed in IDL. To facilitate the creation of models, we have developed a fully automatic model production pipeline that downloads the required SDO/HMI vector magnetic field data and (optionally) the contextual SDO/AIA images, performs potential or nonlinear force free field extrapolations, populates the magnetic field skeleton with parameterized heated plasma coronal models that assume either steady-state or impulsive plasma heating, and generates non-LTE density and temperature distribution models of the chromosphere that are constrained by photospheric measurements. The

standardized models produced by this pipeline may be further customized through a set of interactive tools provided by the graphical user interface. Here we describe the GX Simulator framework and its applications.

Dressing the Coronal Magnetic Extrapolations of Active Regions with a Parameterized Thermal Structure

Gelu M. **Nita**1, Nicholeen M. Viall2, James A. Klimchuk2, Maria A. Loukitcheva1,3,Dale E. Gary1, Alexey A. Kuznetsov4, and Gregory D. Fleishman
2018 ApJ 853 66
http://sci-hub.tw/10.3847/1538-4357/aaa4bf
The study of time-dependent solar active region (AR) morphology and its relation to eruptive events requires analysis of imaging data obtained in multiple wavelength domains with differing spatial and time resolution, ideally in combination with 3D physical models. To facilitate this goal, we have undertaken a major enhancement of our IDL-based simulation tool, GX_Simulator, previously developed for modeling microwave and X-ray emission from flaring loops, to allow it to simulate quiescent emission from solar ARs. The framework includes new tools for building the atmospheric model and enhanced routines for calculating emission that include new wavelengths. In this paper, we use our upgraded tool to model and analyze an AR and compare the synthetic emission maps with observations. We conclude that the modeled magneto-thermal structure is a reasonably good approximation of the real one. **23-May-2010**
CESRA Highlight #1798 **2018** http://cesra.net/?p=1798

EOVSA Implementation of a Spectral Kurtosis Correlator for Transient Detection and Classification

Nita, Gelu M.; Hickish, Jack; MacMahon, David; Gary, Dale E.
Journal of Astronomical Instrumentation Vol. 5, No. 4 (**2016**) id. 1641009-7366
https://arxiv.org/pdf/1702.05391.pdf
https://www.worldscientific.com/doi/pdf/10.1142/S2251171716410099
We describe in general terms the practical use in astronomy of a higher-order statistical quantity called spectral kurtosis (SK), and describe the first implementation of SK-enabled firmware in the Fourier transform-engine (F-engine) of a digital FX correlator for the Expanded Owens Valley Solar Array (EOVSA). The development of the theory for SK is summarized, leading to an expression for generalized SK that is applicable to both SK spectrometers and those not specifically designed for SK. We also give the means for computing both the $\hat{SK}$ estimator and thresholds for its application as a discriminator of RFI contamination. Tests of the performance of EOVSA as an SK spectrometer are shown to agree precisely with theoretical expectations, and the methods for configuring the correlator for correct SK operation are described. **2016 July, 10**

Automatic Detection and Measurement of Spectral Fine Structures Using Higher Order Statistical Estimators

Gelu **Nita**∗1 and Dale Gary
CESRA **2016** p.77
http://cesra2016.sciencesconf.org/conference/cesra2016/pages/CESRA2016_prog_abs_book_v3.pdf
Efficient automatic detection of spectral fine structures and accurate estimation of their characteristics is a key ingredient of any systematic study involving spectrally rich solar events. Many algorithms employed for the purpose of automatic detection of such transient features often rely on arbitrarily defined thresholds relative to an averaged background level. As an alternative to using such rather empirical methods, we demonstrate the feasibility of employing higher order statistical estimators such as the Sample to Model Ratio [Nita et al. 2014, ApJ, 789 (2), 152] and the Generalized Spectral Kurtosis [Nita and Gary 2010, MNRAS, 406(1), L60-L64], for which detection thresholds having user-defined probabilities of false alarm can be analytically defined. The ability of these statistical tools to provide accurate estimates of the spectral and temporal characteristics of the detected transients is illustrated using data obtained during the prototyping phase of Expanded Owens Valley Solar Array.

3D Radio and X-Ray Modeling and Data Analysis Software: Revealing Flare Complexity

Gelu M. **Nita**, Gregory D. Fleishman, Alexey A. Kuznetsov, Eduard P. Kontar, Dale E. Gary
ApJ, 799:236 **2015**
http://arxiv.org/pdf/1409.0896v1.pdf
http://sci-hub.tw/10.1088/0004-637X/799/2/236
We have undertaken a major enhancement of our IDL-based simulation tools developed earlier for modeling microwave and X-ray emission. The object-based architecture provides an interactive graphical user interface that allows the user to import photospheric magnetic field maps and perform magnetic field extrapolations to almost instantly generate 3D magnetic field models, to investigate the magnetic topology of these models by interactively creating magnetic field lines and associated magnetic flux tubes, to populate the flux tubes with user-defined nonuniform thermal plasma and anisotropic, nonuniform, nonthermal electron distributions; to investigate the spatial and spectral properties of radio and

X-ray emission calculated from the model, and to compare the model-derived images and spectra with observational data. The application integrates shared-object libraries containing fast gyrosynchrotron emission codes developed in FORTRAN and C++, soft and hard X-ray codes developed in IDL, a FORTRAN-based potential-field extrapolation routine and an IDL-based linear force free field extrapolation routine. The interactive interface allows users to add any user-defined radiation code that adheres to our interface standards, as well as user-defined magnetic field extrapolation routines. Here we use this tool to analyze a simple single-loop flare and use the model to constrain the 3D structure of the magnetic flaring loop and 3D spatial distribution of the fast electrons inside this loop. We iteratively compute multi-frequency microwave and multi-energy X-ray images from realistic magnetic fluxtubes obtained from an extrapolation of a magnetogram taken prior to the flare, and compare them with imaging data obtained by SDO, NoRH, and RHESSI instruments. We use this event to illustrate use of the tool for general interpretation of solar flares to address disparate problems in solar physics. 4-Aug-2011

Fitting FFT-derived Spectra: Theory, Tool, and Application to Solar Radio Spike Decomposition

Gelu M. **Nita**, Gregory D. Fleishman, Dale E. Gary, William Marin, Kristine Boone
ApJ, **2014**
http://arxiv.org/pdf/1406.2280v1.pdf
Spectra derived from fast Fourier transform (FFT) analysis of time-domain data intrinsically contain statistical fluctuations whose distribution depends on the number of accumulated spectra contributing to a measurement. The tail of this distribution, which is essential for separation of the true signal from the statistical fluctuations, deviates noticeably from the normal distribution for a finite number of the accumulations. In this paper we develop a theory to properly account for the statistical fluctuations when fitting a model to a given accumulated spectrum. The method is implemented in software for the purpose of automatically fitting a large body of such FFT-derived spectra. We apply this tool to analyze a portion of a dense cluster of spikes recorded by our FST instrument during a record-breaking event that occurred on **06 Dec 2006**. The outcome of this analysis is briefly discussed.

THREE-DIMENSIONAL STRUCTURE OF MICROWAVE SOURCES FROM SOLAR ROTATION STEREOSCOPY VERSUS MAGNETIC EXTRAPOLATIONS

Gelu M. **Nita**1, Gregory D. Fleishman1,2, Ju Jing3, Sergey V. Lesovoi4, Vladimir M. Bogod5, Leonid V. Yasnov6, Haimin Wang3 and Dale E. Gary
BBSO Preprint #1482, **2011** ApJ 737 82
We use rotation stereoscopy to estimate the height of a steady-state solar feature relative to the photosphere, based on its apparent motion in the image plane recorded over several days of observation. The stereoscopy algorithm is adapted to work with either one- or two-dimensional data (i.e., from images or from observations that record the projected position of the source along an arbitrary axis). The accuracy of the algorithm is tested on simulated data, and then the algorithm is used to estimate the coronal radio source heights associated with the active region NOAA 10956, based on multifrequency imaging data over seven days from the Siberian Solar Radio Telescope near 5.7 GHz, the Nobeyama Radio Heliograph at 17 GHz, as well as one-dimensional scans at multiple frequencies spanning the 5.98-15.95 GHz frequency range from the RATAN-600 instrument. The gyroresonance emission mechanism, which is sensitive to the coronal magnetic field strength, is applied to convert the estimated radio source heights at various frequencies, h(f), to information about magnetic field versus height B(h), and the results are compared to a magnetic field extrapolation derived from photospheric magnetic field observations obtained by Hinode and Michelson Doppler Imager. We found that the gyroresonant emission comes from heights exceeding the location of the third gyrolayer irrespective of the magnetic extrapolation method; implications of this finding for coronal magnetography and coronal plasma physics are discussed.

Statistics of the Spectral Kurtosis Estimator

Gelu M. **Nita**1 and Dale E. Gary1
BBSO Preprint # 1428, **2010**
Spectral Kurtosis (SK; defined by Nita et al. 2007) is a statistical approach for detecting and removing radio frequency interference (RFI) in radio astronomy data. In this paper, the statistical properties of the SK estimator are investigated and all moments of its probability density function are analytically determined. These moments provide a means to determine the tail probabilities of the estimator that are essential to defining the thresholds for RFI discrimination. It is shown that, for a number of accumulated spectra $M \geq 24$, the first SK standard moments satisfy the conditions required by a Pearson Type IV (Pearson 1985) probability distribution function (PDF), which is shown to accurately reproduce the observed distributions. The cumulative function (CF) of the Pearson Type IV is then found, in both analytical and

numerical forms, suitable for accurate estimation of the tail probabilities of the SK estimator. This same framework is also shown to be applicable to the related Time Domain Kurtosis (TDK) estimator (Ruf, Gross, & Misra 2006), whose PDF corresponds to Pearson Type IV when the number of time-domain samples is $M \geq 46$. The PDF and CF are determined for this case also.

The Generalized Spectral Kurtosis Estimator

Gelu M. **Nita**1 and Dale E. Gary1

BBSO Preprint # 1421, **2010**

Due to its conceptual simplicity and its proven effectiveness in real-time detection and removal of radio frequency interference (RFI) from radio astronomy data, the Spectral Kurtosis (SK) estimator is likely to become a standard tool of a new generation of radio telescopes. However, the SK estimator in its original form must be developed from instantaneous power spectral density (PSD) estimates, and hence cannot be employed as an RFI excision tool downstream of the data pipeline in existing instruments where any time averaging is performed. In this letter, we develop a generalized estimator with wider applicability for both instantaneous and averaged spectral data, which extends its practical use to a much larger pool of radio instruments.

Spike decomposition technique: modeling and performance tests

Gelu M. **Nita**1, Gregory D. Fleishman1;2, Dale E. Gary1

BBSO Preprint # **1369, 2008**

http://solar.njit.edu/preprints/nita1369.pdf

We develop an automated technique for ¯tting the spectral components of solar microwave spike bursts, which are characterized by narrow-band spectral features. The algorithm is especially useful for periods when the spikes occur in densely packed clusters, where the algorithm is capable of decomposing overlapping spike structures into individual spectral components. To test the performance and applicability limits of this data reduction tool, we perform comprehensive modeling of spike clusters characterized by various typical bandwidths, spike densities, and amplitude distributions. We ¯nd that, for a wide range of favorable combinations of input parameters, the algorithm is able to recover the characteristic features of the modeled distributions within reasonable con¯dence intervals. Having model-tested the algorithm against spike overlap, broadband spectral background, noise contamination, and possible malfunction of some spectral channels, we apply the technique to a spike cluster recorded by the Chinese Purple Mountain Observatory (PMO) spectrometer, operating above 4.5 GHz. We study variation of the spike distribution parameters, such as amplitude, band-width, and related derived physical parameters as a function of time. The method can be further applied to observations from other instruments and to other types of ¯ne structures.

The Relation Between Large-Scale Coronal Propagating Fronts and Type II Radio Bursts

Nariaki V. **Nitta**, Wei Liu, Nat Gopalswamy, Seiji Yashiro

Solar Phys., **2014**

http://www.lmsal.com/nitta/publ/SP_typeII_20140904.pdf

http://arxiv.org/pdf/1409.4754v1.pdf **File**

Large-scale, wave-like disturbances in extreme-ultraviolet (EUV) and type II radio bursts are often associated with coronal mass ejections (CMEs). Both phenomena may signify shock waves driven by CMEs. Taking EUV full-disk images at an unprecedented cadence, the Atmospheric Imaging Assembly (AIA) onboard the Solar Dynamics Observatory has observed the so-called EIT waves or large-scale coronal propagating fronts (LCPFs) from their early evolution, which coincides with the period when most metric type II bursts occur. This article discusses the relation of LCPFs as captured by AIA with metric type II bursts. We show examples of type II bursts without a clear LCPF and fast LCPFs without a type II burst. Part of the disconnect between the two phenomena may be due to the difficulty in identifying them objectively. Furthermore, it is possible that the individual LCPFs and type II bursts may reflect different physical processes and external factors. In particular, the type II bursts that start at low frequencies and high altitudes tend to accompany an extended arc- shaped feature, which probably represents the 3D structure of the CME and the shock wave around it, rather than its near-surface track, which has usually been identified with EIT waves. This feature expands and propagates toward and beyond the limb. These events may be characterized by stretching of field lines in the radial direction, and be distinct from other LCPFs, which may be explained in terms of sudden lateral expansion of the coronal volume. Neither LCPFs nor type II bursts by themselves serve as necessary conditions for coronal shock waves, but these phenomena may provide useful information on the early evolution of the shock waves in 3D when both are clearly identified in eruptive events. 2010-11-12, 2011-03-07, 2 Aug 2011, 10 Oct 2011, 2011-11-23, 26 Dec 2011. 5 Apr 2012, 4 Mar 2012, 2 july 2012, 12 Jul 2012, 27 Sep 2012, 2012-10-23

Solar Cycle Variations of the Radio Brightness of the Solar Polar Regions as Observed by the Nobeyama Radioheliograph

Nariaki V. **Nitta**, Xudong Sun, J. Todd Hoeksema, Marc L. DeRosa
E-print, Dec **2013**; **2014**, ApJL, 780, L23

We have analyzed daily microwave images of the Sun at 17 GHz obtained with the Nobeyama Radioheliograph (NoRH) in order to study the solar cycle variations of the enhanced brightness in the polar regions. Unlike in previous works, the averaged brightness of the polar regions is obtained from individual images rather than from synoptic maps. We confirm that the brightness is anti-correlated with the solar cycle and that it has generally declined since solar cycle 22. Including images up to 2013 October, we find that the 17 GHz brightness temperature of the south polar region has decreased noticeably since 2012. This coincides with a significant decrease in the average magnetic field strength around the south pole, signaling the arrival of solar maximum conditions in the southern hemisphere more than a year after the northern hemisphere. We do not attribute the enhanced brightness of the polar regions at 17 GHz to the bright compact sources that occasionally appear in synthesized NoRH images. This is because they have no correspondence with small-scale bright regions in images from the Atmospheric Imaging Assembly on board the Solar Dynamics Observatory with a broad temperature coverage. Higher-quality radio images are needed to understand the relationship between microwave brightness and magnetic field strength in the polar regions.

Statistical Study of Two Years of Solar Flare Radio Spectra Obtained with the Owens Valley Solar Array

Gelu M. **Nita**1, Dale E. Gary1, and Jeongwoo Lee1
2004 ApJ 605 528
https://iopscience.iop.org/article/10.1086/382219/pdf

We present results of analysis of 412 flares during 2001-2002 as detected by the Owens Valley Solar Array (OVSA). This is an in-depth study to investigate some results suggested by a previous study of solar bursts (Nita et al. 2002), which was limited to the peak time of the bursts at a few frequency bands. The new study includes the temporal dependence, at 4 s time resolution, of parameters measured at 40 frequencies in the range 1-18 GHz. We investigate distributions of burst parameters such as maximum flux density in the spectra, peak frequency, spectral slopes below and above the peak frequency (optically thick and thin slopes, respectively), and burst durations. We classify the microwave bursts according to their spectral properties and provide tables of averaged spectral parameters for each spectral type and for different frequency and intensity ranges.

Estimating the lateral speed of a fast shock driven by a coronal mass ejection at the location of solar radio emissions

S. **Normo**1,2, D. E. Morosan1,2, E. K. J. Kilpua1 and J. Pomoell1
A&A, 686, A159 (**2024**)
https://doi.org/10.1051/0004-6361/202449277
https://www.aanda.org/articles/aa/pdf/2024/06/aa49277-24.pdf

Context. Fast coronal mass ejections (CMEs) can drive shock waves capable of accelerating electrons to high energies. These shock-accelerated electrons act as sources of electromagnetic radiation, often in the form of solar radio bursts. Recent findings suggest that radio imaging of solar radio bursts can provide a means to estimate the lateral expansion of CMEs and associated shocks in the low corona.

Aims. Our aim is to estimate the expansion speed of a CME-driven shock at the locations of radio emission using 3D reconstructions of the shock wave from multiple viewpoints.

Methods. In this study, we estimated the 3D location of radio emission using radio imaging from the Nançay Radioheliograph and the 3D location of a CME-driven shock. The 3D shock was reconstructed using white-light and extreme ultraviolet images of the CME from the Solar Terrestrial Relations Observatory, Solar Dynamics Observatory, and the Solar and Heliospheric Observatory. The lateral expansion speed of the CME-driven shock at the electron acceleration locations was then estimated using the approximate 3D locations of the radio emission on the surface of the shock.

Results. The radio bursts associated with the CME were found to reside at the flank of the expanding CME-driven shock. We identified two prominent radio sources at two different locations and found that the lateral speed of the shock was between 800 and 1000 km s−1 at these locations. Such a high speed during the early stages of the eruption already indicates the presence of a fast shock in the low corona. We also found a larger ratio between the radial and lateral expansion speed compared to values obtained higher up in the corona.

Conclusions. We estimated for the first time the 3D expansion speed of a CME-driven shock at the location of the accompanying radio emission. The high shock speed obtained is indicative of a fast acceleration during the initial stage of the eruption. This acceleration leading to lateral speeds in the range of 800−1000 km s−1 is most likely one of the key parameters contributing to the presence of metric radio emissions, such as type II radio bursts. **1 September 2014**

Field distributions and shapes of Langmuir wave packets observed by Ulysses in an interplanetary type III burst source region

Nulsen, A. L.; Cairns, Iver H.; Robinson, P. A.
J. Geophys. Res., Vol. 112, No. A5, A05107, **2007**
There is no consensus on the mechanisms producing the intense bursty Langmuir wave packets routinely observed in source regions of interplanetary type III radio bursts. Using data from the Ulysses Fast Envelope Sampler (FES) near 4 AU, new analyses of the distributions of wavefields clearly separate the Langmuir waves into ``intense localized structures'' (ILSs) and ``other waves''. The wave amplitude distributions also show that the observed ILSs, but not the other waves, are inconsistent with pure stochastic growth theory (SGT). Furthermore, it is shown that the ILSs are unlikely to be driven thermal waves or generated by pure exponential growth and damping. The wave distributions, structure, and spacing of the ILSs are compared to predictions for collapsing Langmuir wave packets described by the Zakharov equations, in isolated density depressions and in fully developed strong turbulence, either beam driven or driven at long wavelengths. The results show that the observed ILSs are very unlikely to be collapsing wave packets in any of the cases considered. The observed ILSs are inconsistent with the predictions of self-organized criticality, electron holes, and refractive focusing of waves. Most are also inconsistent with the predictions of kinetic localization, but this mechanism cannot be eliminated for all ILSs. Other mechanisms not eliminated include trapping of Langmuir waves in density depressions at levels below the collapse threshold, superposition of such trapped waves and ``free'' Langmuir waves, and superposition of trapped waves with a wave packet formed by beam-driven Langmuir waves beating with products of electrostatic decay.

Preparing for Solar and Heliospheric Science with the SKAO: An Indian Perspective

Divya **Oberoi**, Susanta Kumar Bisoi, K. Sasikumar Raja, Devojyoti Kansabanik, Atul Mohan, Surajit Mondal, Rohit Sharma
J. Astrophys. Astr. **2022**
https://arxiv.org/pdf/2211.03791.pdf
The Square Kilometre Array Observatory (SKAO) is perhaps the most ambitious radio telescope envisaged yet. It will enable unprecedented studies of the Sun, the corona and the heliosphere and help to answer many of the outstanding questions in these areas. Its ability to make a vast previously unexplored phase space accessible, also promises a large discovery potential. The Indian solar and heliospheric physics community have been preparing for this science opportunity. A significant part of this effort has been towards playing a leading role in pursuing science with SKAO precursor instruments. This article briefly summarises the current status of the various aspects of work done as a part of this enterprise and our future goals.

Estimating solar flux density at low radio frequencies using a sky brightness model

Divya **Oberoi**, Rohit Sharma, Alan E. E. Rogers
Solar Phys. 292: 75 **2017**
https://arxiv.org/pdf/1701.07798v1.pdf
Sky models have been used in the past to calibrate individual low radio frequency telescopes. Here we generalize this approach from a single antenna to a two element interferometer and formulate the problem in a manner to allow us to estimate the flux density of the Sun using the normalized cross-correlations (visibilities) measured on a low resolution interferometric baseline. For wide field-of-view instruments, typically the case at low radio frequencies, this approach can provide robust absolute solar flux calibration for well characterized antennas and receiver systems. It can provide a reliable and computationally lean method for extracting parameters of physical interest using a small fraction of the voluminous interferometric data, which can be prohibitingly compute intensive to calibrate and image using conventional approaches. We demonstrate this technique by applying it to data from the Murchison Widefield Array and assess its reliability.

Solar observations with the Murchison Widefield Array

Divya **Oberoi**
CESRA Abstract **2016** p.47
http://cesra2016.sciencesconf.org/conference/cesra2016/pages/CESRA2016_prog_abs_book_v1.pdf
The Murchison Widefield Array (MWA), the low frequency SKA precursor located in the exquisitely radio quiet Western Australia, has been operational since mid-2013 and includes solar science among its key science objectives. Its large number of elements distributed over a small footprint make it exceptionally well suited for high fidelity imaging over small time and frequency integrations. In addition, its architecture allows distributing its 31 MHz of bandwidth over 80 to 300 MHz in 24 discreet chunks. These features allow MWA to trace the evolution of solar emission in morphology, time and also over a large frequency range with good time and frequency resolution. This talk will show

examples of imaging and nonimaging analysis of MWA data to highlight the variety of interesting solar science which can be pursued with them.

Observing the Sun with the Murchison Widefield Array

D. **Oberoi** (1), R. Sharma (1), S. Bhatnagar (2), C. J. Lonsdale (3), L. D. Matthews (3), I. H. Cairns and many others

31st URSI General Assembly and Scientific Symposium, **2014**

http://arxiv.org/pdf/1403.6250v1.pdf

The Sun has remained a difficult source to image for radio telescopes, especially at the low radio frequencies. Its morphologically complex emission features span a large range of angular scales, emission mechanisms involved and brightness temperatures. In addition, time and frequency synthesis, the key tool used by most radio interferometers to build up information about the source being imaged is not effective for solar imaging, because many of the features of interest are short lived and change dramatically over small fractional bandwidths.

Building on the advances in radio frequency technology, digital signal processing and computing, the kind of instruments needed to simultaneously capture the evolution of solar emission in time, frequency, morphology and polarization over a large spectral span with the requisite imaging fidelity, and time and frequency resolution have only recently begun to appear. Of this class of instruments, the Murchison Widefield Array (MWA) is best suited for solar observations. The MWA has now entered a routine observing phase and here we present some early examples from MWA observations.

FIRST SPECTROSCOPIC IMAGING OBSERVATIONS OF THE SUN AT LOW RADIO FREQUENCIES WITH THE MURCHISON WIDEFIELD ARRAY PROTOTYPE

Divya **Oberoi**1, Lynn D. Matthews1, Iver H. Cairns2, David Emrich3, Vasili Lobzin2, Colin J. Lonsdale1, et al.

Astrophysical Journal Letters, 728:L27 (7pp), **2011** February; **File**

We present the first spectroscopic images of solar radio transients from the prototype for the **Murchison Widefield Array**, observed on **2010 March 27**. Our observations span the instantaneous frequency band **170.9–201.6 MHz**. Though our observing period is characterized as a period of "low" to "medium" activity, one broadband emission feature and numerous short-lived, narrowband, non-thermal emission features are evident. Our data represent a significant advance in low radio frequency solar imaging, enabling us to follow the spatial, spectral, and temporal evolution of events simultaneously and in unprecedented detail. The rich variety of features seen here reaffirms the coronal diagnostic capability of low radio frequency emission and provides an early glimpse of the nature of radio observations that will become available as the next generation of low-frequency radio interferometers come online over the next few years.

High Temporal and Spectral Resolution Interferometric Observations of Unusual Solar Radio Bursts

D. **Oberoi** · E.R. Evarts · A.E.E. Rogers

Solar Phys (**2009**) 260: 389–400

We report very high temporal and spectral resolution interferometric observations of some unusual solar radio bursts near 1420 MHz. These bursts were observed on **13 September 2005**, 22 minutes after the peak of a GOES class X flare from the NOAA region 10808. Our observations show 11 episodes of narrow-band intermittent emission within a span of ≈8 s. Each episode shows a heavily frequency-modulated band of emission with a spectral slope of about −245.5 MHz s−1, comprising up to 8 individual blobs of emission and lasts for 10 – 15 ms. The blobs themselves have a spectral slope of ≈0 MHzs−1, are ≈200 – 250 kHz wide, appear every ≈400 kHz and last for ≈4 – 5 ms. These bursts show brightness temperatures in the range 1012 K, which suggests a coherent emission mechanism. We believe these are the first high temporal and spectral resolution interferometric observations of such rapid and narrow-bandwidth solar bursts close to 1420 MHz and present an analysis of their temporal and spectral characteristics.

Three-dimensional magnetic reconnection in a collapsing coronal loop system

Aidan M. **O'Flannagain**, Shane A. Maloney, Peter T. Gallagher, Philippa Browning, Jose Refojo

A&A 617, A9 **2018**

https://arxiv.org/pdf/1806.09365.pdf

Magnetic reconnection is believed to be the primary mechanism by which non-potential energy stored in coronal magnetic fields is rapidly released during solar eruptive events. Unfortunately, owing to the small spatial scales on which reconnection is thought to occur, it is not directly observable in the solar corona. However, larger scale processes, such as associated inflow and outflow, and signatures of accelerated particles have been put forward as evidence of reconnection. We explore the origin of a persistent Type I radio source that accompanies a coronal X--

shaped structure during its passage across the disk. Of particular interest is the time range around a partial collapse of the structure that is associated with inflow, outflow, and signatures of particle acceleration. Imaging radio observations from the NRH were used to localise the radio source. SDO AIA EUV observations from the same time period were analysed, looking for evidence of inflows and outflows. Further \texttt{mpole} magnetic reconstructions using SDO HMI observations allowed the magnetic connectivity associated with the radio source to be determined. The Type I radio source was well aligned with a magnetic separator identified in the extrapolations. During the partial collapse, gradual (1 km/s) and fast (5 km/s) inflow phases and fast (30 km/s) and rapid (80-100 km/s) outflow phases were observed, resulting in an estimated reconnection rate of ~ 0.06. The radio source brightening and dimming was found to be co-temporal with increased soft x-ray emission in both RHESSI and GOES. We interpret the brightening and dimming of the radio emission as evidence for accelerated electrons in the reconnection region responding to a gradual fall and rapid rise in electric drift velocity, in response to the inflowing and outflowing field lines. These results present a comprehensive example of 3D null-point reconnection**. 2 – 12 July 2013**
RHESSI Science Nuggets # 329 **2018**
http://sprg.ssl.berkeley.edu/~tohban/wiki/index.php/3D_Magnetic_Reconnection_at_a_Coronal_Null_Point
Large-scale reconnection involved in Type I radio noise storm.

The LOFAR radio environment

Offringa, A. R.; □ de Bruyn, A. G.; □ Zaroubi, S. □ and 93 more
Astronomy & Astrophysics, Volume 549, id.A11, 2013
https://www.aanda.org/articles/aa/pdf/2013/01/aa20293-12.pdf
Aims: This paper discusses the spectral occupancy for performing radio astronomy with the Low-Frequency Array (LOFAR), with a focus on imaging observations.
Methods: We have analysed the radio-frequency interference (RFI) situation in two 24-h surveys with Dutch LOFAR stations, covering 30-78 MHz with low-band antennas and 115-163 MHz with high-band antennas. This is a subset of the full frequency range of LOFAR. The surveys have been observed with a 0.76 kHz/1 s resolution.
Results: We measured the RFI occupancy in the low and high frequency sets to be 1.8% and 3.2% respectively. These values are found to be representative values for the LOFAR radio environment. Between day and night, there is no significant difference in the radio environment. We find that lowering the current observational time and frequency resolutions of LOFAR results in a slight loss of flagging accuracy. At LOFAR's nominal resolution of 0.76 kHz and 1 s, the false-positives rate is about 0.5%. This rate increases approximately linearly when decreasing the data frequency resolution.
Conclusions: Currently, by using an automated RFI detection strategy, the LOFAR radio environment poses no perceivable problems for sensitive observing. It remains to be seen if this is still true for very deep observations that integrate over tens of nights, but the situation looks promising. Reasons for the low impact of RFI are the high spectral and time resolution of LOFAR; accurate detection methods; strong filters and high receiver linearity; and the proximity of the antennas to the ground. We discuss some strategies that can be used once low-level RFI starts to become apparent. It is important that the frequency range of LOFAR remains free of broadband interference, such as DAB stations and windmills.

An In Situ Interplanetary "U-burst": Observation and Results

Juan Carlos Martínez **Oliveros**1, Saida Milena Díaz Castillo1,2, Vratislav Krupar3,4,5, Marc Pulupa1, Stuart D. Bale1,6, and Benjamín Calvo-Mozo2
2020 ApJ 897 170
https://doi.org/10.3847/1538-4357/ab96c3
https://arxiv.org/pdf/1910.04306.pdf
We report and examine the observation of an unusual and rare in situ electron observation associated with a solar type III radio burst on **1996 December 24**. This radio event was accompanied by high-energy electrons, measured by the Solid State Telescope on board the Wind spacecraft. The type III radio emission started at ≈13:10 UTC and was associated with a C2.1 GOES-class flare whose maximum was at 13:11 UTC and hosted by the active region NOAA 8007/8004, located on the west limb at N05° W74°/N06° W85°. During this event, the observation of an electron energy distribution likely to be associated with the radio emission was registered. The electrons arrive at the spacecraft predominantly from the antisolar direction, suggesting that their general motion is sunward along a closed magnetic field line. Leblanc et al. propose a model in which energetic electrons are injected into a coronal flux tube at one of its footpoints, releasing standard type-III emission. As the magnetic field then directs them back toward the magnetic-conjugate footpoint of the first, the electrons release subsequent emission whose radio profile is a quasi-time reversal of the standard. We have constructed a cylindrical flux rope facsimile of this scenario that reproduces the U-burst profiles. We also report observational features indicating a secondary electron energy distribution and propose a scenario that explains this feature.

THE 2010 AUGUST 1 TYPE II BURST: A CME-CME INTERACTION AND ITS RADIO AND WHITE-LIGHT MANIFESTATIONS

Juan Carlos Martínez **Oliveros**1, Claire L. Raftery1, Hazel M. Bain1, Ying Liu1, Vratislav Krupar2,3, Stuart Bale1,4 and Säm Krucker
2012 ApJ 748 66, **File**
We present observational results of a type II burst associated with a CME-CME interaction observed in the radio and white-light (WL) wavelength range. We applied radio direction-finding techniques to observations from the STEREO and Wind spacecraft, the results of which were interpreted using WL coronagraphic measurements for context. The results of the multiple radio direction-finding techniques applied were found to be consistent both with each other and with those derived from the WL observations of coronal mass ejections (CMEs). The results suggest that the type II burst radio emission is causally related to the CMEs interaction.

The Magnetic Field of the Solar Corona from Pulsar Observations
S.M. **Ord** · S. Johnston · J. Sarkissian
Solar Phys (2007) 245: 109–120

A New Component from the Quiet Sun from Radio to Gamma Rays: Synchrotron Radiation by Galactic Cosmic-Ray Electrons
Elena **Orlando**1,2, Vahe' Petrosian2, and Andrew Strong3
2023 ApJ 943 173
https://iopscience.iop.org/article/10.3847/1538-4357/acad75/pdf
The quiet Sun, i.e., in its nonflaring state or nonflaring regions, emits thermal radiation from radio to ultraviolet. The quiet Sun also produces nonthermal radiation observed in gamma rays due to interactions of Galactic cosmic rays (GCRs) with the solar atmosphere and photons. We report on a new component: the synchrotron emission by GCR electrons in the solar magnetic field. To the best of our knowledge this is the first time this emission has been theoretically claimed and modeled. We find that the measured GCR electrons with energies from tens of GeV to a few TeV produce synchrotron emission in X-rays, which is a few orders of magnitude lower than current upper limits of the quiet Sun set by RHESSI and FOXSI, with no energy losses included. For a radially decreasing solar magnetic field we find the expected synchrotron intensity to be almost constant in the solar disk, to peak in the close proximity of the Sun, and to quickly drop away from the Sun. We also estimate the synchrotron emission from radio to gamma rays, and we compare it with current observations, especially with LOFAR. While it is negligible from radio to UV compared to the solar thermal radiation, this emission can potentially be observed at high energies with NuSTAR and more promising future FOXSI observations. This could potentially allow for constraining GCR densities and magnetic-field intensities at the Sun. This study provides a more complete description and a possible new way for understanding the quiet Sun and its environment.

Thyr: A Volumetric Ray-Marching Tool for Simulating Microwave Emission
Christopher M. J. **Osborne**, Paulo J. A. Simões
MNRAS **2019**
https://arxiv.org/pdf/1903.04219.pdf
Gyrosynchrotron radiation is produced by solar flares, and can be used to infer properties of the accelerated electrons and magnetic field of the flaring region. This microwave emission is highly dependent on many local plasma parameters, and the viewing angle. To correctly interpret observations, detailed simulations of the emission are required. Additionally, gyrosynchrotron emission from the chromosphere has been largely ignored in modelling efforts, and recent studies have shown the importance of thermal emission at millimetric wavelengths. Thyr is a new tool for modelling microwave emission from three-dimensional flaring loops with spatially varying atmosphere and increased resolution in the lower corona and chromosphere. Thyr is modular and open-source, consisting of separate components to compute the thermal and non-thermal microwave emission coefficients and perform three-dimensional radiative transfer (in local thermodynamic equilibrium). The radiative transfer integral is computed by a novel ray-marching technique to efficiently compute the contribution of many volume elements. This technique can also be employed on a variety of astrophysics problems. Herein we present a review of the theory of gyrosynchrotron radiation, and two simulations of identical flare loops in low- and high-resolution performed with Thyr, with a spectral imaging analysis of differing regions. The high-resolution simulation presents a spectral hardening at higher frequencies. This hardening originates around the top of the chromosphere due to the strong convergence of the magnetic field, and is not present in previous models due to insufficient resolution. This hardening could be observed with a coordinated flare observation from active radio observatories.

Numerical simulations of reception properties of Solar Orbiter/RPW electric antennas.
Mykhaylo **Panchenko**∗1 , Georg Fischer1 , and Wolfgang Macher
CESRA **2016** p.56
http://cesra2016.sciencesconf.org/conference/cesra2016/pages/CESRA2016_prog_abs_book_v3.pdf

Solar Orbiter is an ESA mission that is planned to be launched in October 2018. The mission will enter an elliptical orbit around the Sun with a perihelion as low as 0.28 AU. The Radio and Plasma Waves (RPW) experiment is dedicated to measure magnetic and electric fields using a number of sensors and antennas, and it will determine the characteristics of electromagnetic and electrostatic waves in the solar wind up to 16 MHz. The overall performance of radio instruments aboard spacecraft depends crucially on the knowledge of the true antenna properties. We report the results of analysis of the reception properties of RPW E-field antennas. Studies were performed using numerical solutions of the underlying field equations by means of electromagnetic simulation software tools. Additionally, due to the attitude of the spacecraft it is expected uneven antenna solar illumination, which, in turn will result in a thermal bending effect. Using the computer simulations we have defined the influence of the thermal bending of the antennas on resulting effective antenna length vector. Corresponding calculations have been performed for various possible thermal bending which corresponds to different distances to the Sun.

Comparison of chromospheric diagnostics in a 3D model atmosphere
Hα linewidth and millimetre continua

Sneha **Pandit**1,2, Sven Wedemeyer1,2, Mats Carlsson1,2 and Mikołaj Szydlarski1,2
A&A 673, A137 (**2023**)
https://www.aanda.org/articles/aa/pdf/2023/05/aa45412-22.pdf
Context. The Hα line, one of the most studied chromospheric diagnostics, is a tracer of magnetic field structures, while the intensity of its line core provides an estimate of the mass density. The interpretation of Hα observations is complicated by deviations from local thermodynamic equilibrium (LTE) or instantaneous statistical equilibrium conditions. Meanwhile, millimetre (mm) continuum radiation is formed in LTE, and therefore the brightness temperatures from Atacama Large Millimetre-submillimetre Array (ALMA) observations provide a complementary view of the activity and the thermal structure of stellar atmospheres. These two diagnostics together can provide insights into the physical properties of stellar atmospheres, such as their temperature stratification, magnetic structures, and mass density distribution.
Aims. In this paper, we present a comparative study between synthetic continuum brightness temperature maps at mm wavelengths (0.3 mm to 8.5 mm) and the width of the Hα 6565 Å line.
Methods. We used the 3D radiative-transfer codes Multi3D and Advanced Radiative Transfer (ART) to calculate synthetic spectra for the Hα line and the mm continua, respectively, from an enhanced network atmosphere model with non-equilibrium hydrogen ionisation generated with the state-of-the-art 3D radiation magnetohydrodynamics (rMHD) code Bifrost. We use a Gaussian point spread function (PSF) to simulate the effect of ALMA's limited spatial resolution and calculate the Hα versus mm continuum correlations and slopes of scatter plots for the original and degraded resolution of the whole box, quiet sun, and enhanced network patches separately.
Results. The Hα linewidth and mm brightness temperatures are highly correlated and the correlation is highest at a wavelength of 0.8 mm, that is, in ALMA Band 7. The correlation systematically increases with decreasing resolution. On the other hand, the slopes decrease with increasing wavelength. The degradation of resolution does not have a significant impact on the calculated slopes.
Conclusions. With decreasing spatial resolution, the standard deviations of the observables, Hα linewidth, and brightness temperatures decrease and the correlations between them increase, but the slopes do not change significantly. These relations may therefore prove useful in calibrating the mm continuum maps observed with ALMA.

POLARIZED SYNCHROTRON EMISSIVITIES AND ABSORPTIVITIES FOR RELATIVISTIC THERMAL, POWER-LAW, AND KAPPA DISTRIBUTION FUNCTIONS

Alex **Pandya**1, Zhaowei Zhang1, Mani Chandra2, and Charles F. Gammie
2016 ApJ 822 34
Synchrotron emission and absorption determine the observational appearances of many astronomical systems. In this paper, we describe a numerical scheme for calculating synchrotron emissivities and absorptivities in all four Stokes parameters for arbitrary gyrotropic electron distribution functions, building on earlier work by Leung, Gammie, and Noble. We use this technique to evaluate the emissivities and the absorptivities for a thermal (Maxwell–Jüttner), isotropic power-law, and an isotropic kappa distribution function. The latter contains a power-law tail at high particle energies that smoothly merges with a thermal core at low energies, as is characteristic of observed particle spectra in collisionless plasmas. We provide fitting formulae and error bounds on the fitting formulae for use in codes that solve the radiative transfer equation. The numerical method and the fitting formulae are implemented in a compact C library called symphony. We find that the kappa distribution has a source function that is indistinguishable from a thermal spectrum at low frequency and transitions to the characteristic self-absorbed synchrotron spectrum, $\propto \nu^{5/2}$, at high frequency; the linear polarization fraction for a thermal spectrum is near unity at high frequency; and all distributions produce O(10%) circular polarization at low frequency for lines of sight sufficiently close to the magnetic field vector.

On Solar Recurrent Coronal Jets: Coronal Geysers as Sources of Electron Beams and Interplanetary Type-III Radio Bursts

Alin Razvan **Paraschiv** and Alina Donea

2019 ApJ 873 110
https://doi.org/10.3847/1538-4357/ab04a6
https://arxiv.org/pdf/1903.04682.pdf
Coronal jets are transitory small-scale eruptions that are omnipresent in solar observations. Active regions jets produce significant perturbations on the ambient solar atmosphere and are believed to be generated by microflare reconnection. Multiple sets of recurrent jets are identified in extreme-ultraviolet filter imaging. In this work we analyze the long timescale recurrence of coronal jets originating from a unique footpoint structure observed in the lower corona. We report the detection of penumbral magnetic structures in the lower corona. These structures, which we call "coronal geysers," persist through multiple reconnection events that trigger recurrent jets in a quasi-periodical trend. Recurrent jet eruptions have been associated with Type-III radio bursts that are manifestations of traveling non-thermal electron beams. We examine the assumed link, as the coronal sources of interplanetary Type-III bursts are still open for debate. We scrutinized the hypothesized association by temporally correlating a statistically significant sample of six Geyser structures that released at least 50 recurrent jets, with correspondent Type-III radio bursts detected in the interplanetary medium. Data analysis of these phenomena provides new information on small-scale reconnection, non-thermal electron beam acceleration, and energy release. We find that the penumbral Geyser-like flaring structures produce recurring jets. They can be long-lived, quasi-stable, and act as coronal sources for Type-III bursts, and, implicitly, upward accelerated electron beams. **25 Sep. 2011, 2012-06-30,2012-07-02, 2013-12-25, 2014-10-22, 2015-07-09**

Radio Emission from Masuda Sources

S.-H. **Park** and G.D. Fleishman
BBSO preprint #1440, **2010,** Solar Phys (2010) 266: 323–335
We note that different models, providing comparably good interpretation of the hard X-ray properties of so-called Masuda sources, can make distinctly different predictions for the radio emission produced at the Masuda source by the same population of accelerated electrons. Accordingly, we calculate the radio emission within a few competing models, *i.e.*, those involving magnetic, turbulent, and collisional trapping of the fast electrons in the coronal source. We show that even available incomplete radio observations of the classical Masuda event and a Masuda-like event on **31 December 2007**, recently reported by Krucker *et al*. (*Astrophys. J.* 714, 1108, 2010) are highly valuable in restricting the physical model of the source. Furthermore, our study proposes that combination of more complete high resolution X-ray and radio observations can allow unambiguous distinction between the competing Masuda source models.

Dispersive Evolution of Nonlinear Fast Magnetoacoustic Wave Trains

D. J. **Pascoe**, C. R. Goddard, and V. M. Nakariakov
2017 ApJL 847 L21
https://www2.warwick.ac.uk/fac/sci/physics/staff/research/davidpascoe/nonlinear_wavetrains.pdf
Quasi-periodic rapidly propagating wave trains are frequently observed in extreme ultraviolet observations of the solar corona, or are inferred by the quasi-periodic modulation of radio emission. The dispersive nature of fast magnetohydrodynamic waves in coronal structures provides a robust mechanism to explain the detected quasi-periodic patterns. We perform 2D numerical simulations of impulsively generated wave trains in coronal plasma slabs and investigate how the behavior of the trapped and leaky components depend on the properties of the initial perturbation. For large amplitude compressive perturbations, the geometrical dispersion associated with the waveguide suppresses the nonlinear steepening for the trapped wave train. The wave train formed by the leaky components does not experience dispersion once it leaves the waveguide and so can steepen and form shocks. The mechanism we consider can lead to the formation of multiple shock fronts by a single, large amplitude, impulsive event and so can account for quasi-periodic features observed in radio spectra.

Near-Earth Interplanetary Coronal Mass Ejections and Their Association with DH Type II Radio Bursts During Solar Cycles 23 and 24

Binal D. **Patel**, Bhuwan Joshi, Kyung-Suk Cho, Rok-Soon Kim & Yong-Jae Moon
Solar Physics volume 297, Article number: 139 (**2022**)
https://doi.org/10.1007/s11207-022-02073-7
https://arxiv.org/pdf/2210.14535.pdf
We analyse the characteristics of interplanetary coronal mass ejections (ICMEs) during Solar Cycles 23 and 24. The present analysis is primarily based on the near-Earth ICME catalogue (Richardson and Cane, 2010). An important aspect of this study is to understand the near-Earth and geoeffective aspects of ICMEs in terms of their association (type II ICMEs) versus absence (non-type II ICMEs) of decameter-hectometer (DH) type II radio bursts, detected by Wind/WAVES and STEREOS/WAVES. Notably, DH type II radio bursts driven by a CME indicate powerful MHD shocks leaving the inner corona and entering the interplanetary medium. We find a drastic reduction in the occurrence of ICMEs by 56% in Solar Cycle 24 compared to the previous cycle (64 versus 147 events). Interestingly, despite a significant decrease in ICME/CME counts, both cycles contain almost the same fraction of type II ICMEs (≈ 47%). Our analysis reveals that, even at a large distance of 1 AU, type II CMEs maintain significantly higher speeds compared to

non-type II events (523 km s−1 versus 440 km s−1). While there is an obvious trend of decrease in ICME transit times with increase in the CME initial speed, there also exists a noticeable wide range of transit times for a given CME speed. Contextually, Cycle 23 exhibits 10 events with shorter transit times ranging between 20 – 40 hours of predominantly type II categories while, interestingly, Cycle 24 almost completely lacks such "fast" events. We find a significant reduction in the parameter VICME×BzVICME×Bz, the dawn to dusk electric field, by 39% during Solar Cycle 24 in comparison with the previous cycle. Further, VICME×BzVICME×Bz shows a strong correlation with Dst index, which even surpasses the consideration of BzBz and VICMEVICME alone. The above results imply the crucial role of VICME×BzVICME×Bz toward effectively modulating the geoeffectiveness of ICMEs. **7 March, 2012.**

DH Type II Radio Bursts During Solar Cycles 23 and 24: Frequency-dependent Classification and their Flare-CME Associations

Binal D. **Patel** (USO/PRL), Bhuwan Joshi (USO/PRL), Kyung-Suk Cho (SSD/KASI), Rok-Soon Kim (DASS/UST)

Solar Phys. **296**, Article number: 142 **2021**

https://arxiv.org/pdf/2108.12990.pdf
https://link.springer.com/content/pdf/10.1007/s11207-021-01890-6.pdf
https://doi.org/10.1007/s11207-021-01890-6

We present the characteristics of DH type II bursts for the Solar Cycles 23 and 24. The bursts are classified according to their end frequencies into three categories, i.e. Low Frequency Group (LFG; 20 kHz ≤ f ≤ 200 kHz), Medium Frequency Group (MFG; 200 kHz < f ≤ 1 MHz), and High Frequency Group (HFG; 1 MHz < f ≤ 16 MHz). We find that the sources for LFG, MFG, and HFG events are homogeneously distributed over the active region belt. Our analysis shows a drastic reduction of the DH type II events during Solar Cycle 24 which includes only 35% of the total events (i.e. 179 out of 514). Despite having smaller number of DH type II events in the Solar Cycle 24, it contains a significantly higher fraction of LFG events compared to the previous cycle (32% versus 24%). However, within the LFG group the cycle 23 exhibits significant dominance of type II bursts that extend below 50 kHz, suggesting rich population of powerful CMEs travelling beyond half of the Sun-Earth distance. The events of LFG group display strongest association with faster and wider (more than 82% events are halo) CMEs while at the source location they predominantly trigger large M/X class flares (in more than 83% cases). Our analysis also indicates that CME initial speed or flare energetics are partly related with the duration of type II burst and that survival of CME associated shock is determined by multiple factors/parameters related to CMEs, flares, and state of coronal and interplanetary medium. The profiles relating CME heights with respect to the end frequencies of DH type II bursts suggest that for HFG and MFG categories, the location for majority of CMEs (≈65%-70%) is in well compliance with ten-fold Leblanc coronal density model, while for LFG events a lower value of density multiplier (≈3) seems to be compatible. **2011 November 26, 2013 May 22**

Investigation into CME Shock Speed Resulting from Type II Solar Radio Bursts
A Newly Designed Half-Wave Dipole Antenna (HWDA) Array System

F. A. M. **Pauzi**, Z. Z. Abidin, S. J. Guo, G. N. Gao, L. Dong & C. Monstein

Solar Physics volume 295, Article number: 42 (**2020**)

https://link.springer.com/content/pdf/10.1007/s11207-019-1404-z.pdf

An investigation into Type II solar radio bursts was carried out to understand the frequency gap between fundamental and harmonic emissions of the radio burst. This investigation focused on Type II solar radio bursts with flares and coronal mass ejections by relating the separation between fundamental and harmonic emissions. We used the Compound Astronomical Low-cost Low-frequency Instrument for Spectroscopy and Transportable Spectrometers (CALLISTO) and a newly designed low-frequency antenna array. This article describes the proposed new instrument in terms of its antenna design, the bandpass testing of the antenna, the new system significance in studying Type II solar radio bursts, and its comparison with other leading radio solar monitoring instruments. Upon setting up the new technology, the radio-frequency interference of the observation site at the University of Malaya was shown to emphasize the suitability of the selected site. This article also shows the preliminary results of the proposed new instrument by reporting the detection of a Type III solar radio burst that was confirmed by CALLISTO. Moreover, it also includes the optimal observation design and strategies for future detections. **3 November 2010, 17 April 2017**

Observations of solar chromospheric oscillations at 3 mm with ALMA

S. **Patsourakos**, C. E. Alissandrakis, A. Nindos, T. S. Bastian

A&A 634, A86 (**2020**)

https://arxiv.org/pdf/1912.03480.pdf
sci-hub.si/10.0000/www.aanda.org/articles/aa/ab

We studied chromospheric oscillations using Atacama Large millimeter and sub-millimeter Array (ALMA) time-series of interferometric observations of the quiet Sun obtained at 3 mm with a 2-s cadence and a spatial resolution of a few

arcsec. The same analysis, over the same fields of view and for the same intervals, was performed for simultaneous Atmospheric Imaging Assembly (AIA) image sequences in 1600 A. Spatially-resolved chromospheric oscillations at 3 mm, with frequencies of 4.2+−1.7 mHz are observed in the quiet Sun, in both cell and network. The coherence length-scale of the oscillations is commensurate with the spatial resolution of our ALMA observations. Brightness-temperature fluctuations in individual pixels could reach up to a few hundred K, while the spatially averaged power spectral densities yield rms in the range ~ 55-75 K, i.e., up to ~ 1 % of the averaged brightness temperatures and exhibit a moderate increase towards the limb. For AIA 1600 A, the oscillation frequency is 3.7 +- 1.7 mHz. The relative rms is up to 6 % of the background intensity, with a weak increase towards disk center (cell, average). ALMA 3 mm time-series lag AIA 1600 A by ~ 100 s, which corresponds to a formation-height difference of ~ 1200 km. The ALMA oscillations that we detected exhibit higher amplitudes than those derived from the lower (~ 10 arcsec) resolution observations at 3.5 mm by White et al. (2006). Chromospheric oscillations are, therefore, not fully resolved at the length-scale of the chromospheric network, and possibly not even at the spatial resolution of our ALMA observations. Any study of transient brightenings in the mm-domain should take into account the oscillations. **March 16, 2017**

pyCallisto: A Python Library To Process The CALLISTO Spectrometer Data

Ravindra **Pawase**, K. Sasikumar Raja

ApJ **2020**

https://arxiv.org/pdf/2006.16300.pdf

CALLISTO is a radio spectrometer designed to monitor the transient radio emissions/bursts originated from the solar corona in the frequency range 45−870 MHz. At present, there are ≳150 stations (together forms an e-CALLISTO network) around the globe continuously monitoring the Sun 24 hours a day. We have developed a pyCallisto, a python library to process the CALLISTO data observed by all stations of the e-CALLISTO network. In this article, we demonstrate various useful functions that are routinely used to process the CALLISTO data with suitable examples. This library is not only efficient in processing the data but plays a significant role in developing automatic classification algorithms of different types of solar radio bursts. **2015-11-04**

3D particle-in-cell simulation of electron acceleration by Langmuir waves in an inhomogeneous plasma

R. **Pechhacker**, D. Tsiklauri

E-print, May **2014**; Phys. Plasmas 21, 012903 (**2014**)

A possible solution to the unexplained high intensity hard x-ray (HXR) emission observable during solar flares was investigated via 3D fully relativistic, electromagnetic particle-in-cell (PIC) simulations with realistic ion to electron mass ratio. A beam of accelerated electrons was injected into a magnetised, Maxwellian, homogeneous and inhomogeneous background plasma. The electron distribution function was unstable to the beam-plasma instability and was shown to generate Langmuir waves, while relaxing to plateau formation. In order to estimate the role of the background density gradient on an unbound (infinite spatial extent) beam, three different scenarios were investigated: a) a uniform density background; b) a weak density gradient, n_R/n_L=3; c) a strong gradient case, n_R/n_L=10, where n_R and n_L denote background electron densities on the left and right edges of the simulation box respectively. The strong gradient case produced the largest fraction of electrons beyond 15 v_th. Further, two cases (uniform and strong gradient background) with spatially localized beam injections were performed aiming to show drifts of the generated Langmuir wave wavenumbers, as suggested in previous studies. For the strong gradient case, the Langmuir wave power is shown to drift to smaller wavenumbers, as found in previous quasi-linear simulations.

The effect of electron beam pitch angle and density gradient on solar type III radio bursts

Roman **Pechhacker** and David Tsiklauri

E-print, Jan **2013**

1.5D particle-in-cell simulations of a hot, low density electron beam injected into magnetized, maxwellian plasma were used to further explore the alternative non-gyrotropic beam driven electromagnetic (EM) emission mechanism, first studied in Tsiklauri, Phys. Plasmas 18, 052903 (2011). Variation of beam injection angle and background density gradient showed that the emission process is caused by the perpendicular component of the beam injection current, whereas the parallel component only produces Langmuir waves, which play no role in the generation of EM waves in our mechanism. Particular emphasis was put on the case, where the beam is injected perpendicularly to the background magnetic field, as this turned off any electrostatic wave generation along the field and left a purely electromagnetic signal in the perpendicular components. The simulations establish the following key findings: (i) Initially, waves at a few $\omega ce/\gamma$ are excited, mode converted and emitted at $\sim\omega pe$ (ii) The emission intensity along the beam axis is proportional to the respective component of the kinetic energy of the beam; (iii) The frequency of the escaping EM emission is independent of the injection angle; (iv) A stronger background density gradient causes earlier emission; (v) The beam electron distribution function in phase space shows harmonic oscillation in the perpendicular components at

the relativistic gyrofrequency; (vi) The requirement for cyclotron maser emission, ∂f∂v⊥>0, is fulfilled; (vii) The degree of linear polarization of the emission is strongly dependent on the beam injection angle; (viii) The generated electromagnetic emission is left-hand elliptically polarized as the pitch angle tends to 90fl and (ix) The generated electromagnetic energy is of the order of 0.1% of the initial beam kinetic energy.

Electron cyclotron maser emission mode coupling to the z-mode on a longitudinal density gradient in the context of solar type III bursts

Roman **Pechhacker** and David Tsiklauri
E-print, Jan **2013**
A beam of super-thermal, hot electrons was injected into maxwellian plasma with a density gradient along a magnetic field line. 1.5D particle-in-cell simulations were carried out which established that the EM emission is produced by the perpendicular component of the beam injection momentum. The beam has a positive slope in the distribution function in perpendicular momentum phase space, which is the characteristic feature of a cyclotron maser. The cyclotron maser in the overdense plasma generates emission at the electron cyclotron frequency. The frequencies of generated waves were too low to propagate away from the injection region, hence the wavelet transform shows a pulsating wave generation and decay process. The intensity pulsation frequency is twice the relativistic cyclotron frequency. Eventually, a stable wave packet formed and could mode couple on the density gradient to reach frequencies of the order of the plasma frequency that allowed for propagation. The emitted wave is likely to be a z-mode wave. The total electromagnetic energy generated is of the order of 0.1% of the initial beam kinetic energy. The proposed mechanism is of relevance to solar type III radio bursts, as well as other situations, when the injected electron beam has a non-zero perpendicular momentum, e.g., magnetron.

Solar observations with single-dish INAF radio telescopes: continuum imaging in the 18-26 GHz range

A. **Pellizzoni**, S. Righini, M. N. Iacolina, M. Marongiu, et al.
Solar Phys. **297**, Article number: 86 **2022**
https://arxiv.org/pdf/2205.00197.pdf
https://link.springer.com/content/pdf/10.1007/s11207-022-02013-5.pdf
We present a new solar radio imaging system implemented through the upgrade of the large single-dish telescopes of the Italian National Institute for Astrophysics (INAF), not originally conceived for solar observations.
During the development and early science phase of the project (2018-2020), we obtained about 170 maps of the entire solar disk in the 18-26 GHz band, filling the observational gap in the field of solar imaging at these frequencies. These solar images have typical resolutions in the 0.7-2 arcmin range and a brightness temperature sensitivity <10 K. Accurate calibration adopting the Supernova Remnant Cas A as a flux reference, provided typical errors <3% for the estimation of the quiet-Sun level components and for active regions flux measurements.
As a first early science result of the project, we present a catalog of radio continuum solar imaging observations with Medicina 32-m and SRT 64-m radio telescopes including the multi-wavelength identification of active regions, their brightness and spectral characterization. The interpretation of the observed emission as thermal bremsstrahlung components combined with gyro-magnetic variable emission pave the way to the use of our system for long-term monitoring of the Sun. We also discuss useful outcomes both for solar physics (e.g. study of the chromospheric network dynamics) and space weather applications (e.g. flare precursors studies). **23-Jun-2018, 17-Sep-2020, 23 Nov 2020, 3-Jan-2021**
Table 4.: Summary of Medicina and SRT observations. 2018-2020

THE EXPANDED VERY LARGE ARRAY: A NEW TELESCOPE FOR NEW SCIENCE

R. A. **Perley**, C. J. Chandler, B. J. Butler, and J. M. Wrobel
ApJL , 739:L1 (5pp), **2011**
http://sci-hub.tw/10.1088/2041-8205/739/1/L1
Since its commissioning in 1980, the Very Large Array (VLA) has consistently demonstrated its scientific productivity. However, its fundamental capabilities have changed little since 1980, particularly in the key areas of sensitivity, frequency coverage, and velocity resolution. These limitations have been addressed by a major upgrade of the array, which began in 2001 and will be completed at the end of 2012. When completed, the Expanded VLA—the EVLA—will provide complete frequency coverage from 1 to 50 GHz, a continuum sensitivity of typically 1 μJy beam−1 (in 9 hr with full bandwidth), and a modern correlator with vastly greater capabilities and flexibility than the VLA's. In this Letter, we describe the goals of the EVLA project, its current status, and the anticipated expansion of capabilities over the next few years. User access to the array through the Open Shared Risk Observing and Resident Shared Risk Observing programs is described. The following papers in this special issue, derived from observations in its early science period, demonstrate the astonishing breadth of this most flexible and powerful general-purpose telescope.

Solar 3.04 cm hydrogen line emission revealed in observations of the active region NOAA 10105

N. G. **Peterova**, N. A. Topchilo & T. P. Borisevich
Astronomy Reports, Volume 55, Number 9, 841-848, **2011**
Astronomicheskii Zhurnal, **2011**, Vol. 88, No. 9, pp. 912–919
RATAN-600 observations of a microwave source located above the active region NOAA 10105 obtained on September 7–20, 2002 with a frequency resolution of ∼10% have revealed a spectral feature near 3.04 cm that can be interpreted as a neutral hydrogen line. This feature was observed **September 11, 2002**, in both absorption and emission, and was detected in the spectra of various portions of the source (sunspot, flocculus, and background). The maximum line depth of (35 ± 5)% of the source brightness was observed at the start of the observations (9.2h UT) in the flocculus in absorption. The line intensity decreased rapidly with time, becoming less than the measurement errors by 9.7h UT. It is most likely that the 3.04 cm emission is related to a 2B chromospheric flare (M2.2 X-ray burst) observed at ∼7.5h UT in the floccular field, near the main sunspot of NOAA 10105. In this case, the total duration of the event was about two hours. These observations are consistent with earlier statistical studies, and refines these based on data with higher spatial resolution. Recommendations for further observational studies of the solar 3.04-cm hydrogen line are presented; requirements for theories of the 3.04 cm line taking into account nonequilibrium states of the active-region plasma are indicated.

Medium-term predictions of F10.7 and F30 cm solar radio flux with the adaptive Kalman filter

Elena **Petrova**, Tatiana Podladchikova, Astrid M. Veronig, Stijn Lemmens, Benjamin Bastida Virgili, Tim Flohrer
Astrophysical Journal Supplement Series **254** 9 **2021**
https://arxiv.org/pdf/2103.08059.pdf
https://doi.org/10.3847/1538-4365/abef6d
The solar radio flux at F10.7 cm and F30 cm is required by most models characterizing the state of the Earth's upper atmosphere, such as the thermosphere and ionosphere to specify satellite orbits, re-entry services, collision avoidance maneuvers and modeling of space debris evolution. We develop a method called RESONANCE ("Radio Emissions from the Sun: ONline ANalytical Computer-aided Estimator") for the prediction of the 13-month smoothed monthly mean F10.7 and F30 indices 1-24 months ahead. The prediction algorithm includes three steps. First, we apply a 13-month optimized running mean technique to effectively reduce the noise in the radio flux data. Second, we provide initial predictions of the F10.7 and F30 indices using the McNish-Lincoln method. Finally, we improve these initial predictions by developing an adaptive Kalman filter with the error statistics identification. The root-mean-square-error of predictions with lead times from 1 to 24 months is 5-27 sfu for the F10.7 and 3-16 sfu for F30 index, which statistically outperforms current algorithms in use. The proposed approach based on Kalman filter is universal and can be applied to improve the initial predictions of a process under study provided by any other forecasting method. Furthermore, we present a systematic evaluation of re-entry forecast as an application to test the performance of F10.7 predictions on past ESA re-entry campaigns for payloads, rocket bodies, and space debris that re-entered from June 2006 to June 2019. The test results demonstrate that the predictions obtained by RESONANCE in general also lead to improvements in the forecasts of re-entry epochs.

Fast single-dish scans of the Sun using ALMA

Neil **Phillips**, Richard Hills, Tim Bastian, Hugh Hudson, Ralph Marson, Sven Wedemeyer
"Revolution in Astronomy with ALMA - the third year -", Tokyo, December 2014, **2015**
http://arxiv.org/pdf/1502.06122v1.pdf
We have implemented control and data-taking software that makes it possible to scan the beams of individual ALMA antennas to perform quite complex patterns while recording the signals at high rates. We conducted test observations of the Sun in September and December, 2014. The data returned have excellent quality; in particular they allow us to characterize the noise and signal fluctuations present in this kind of observation. The fast-scan experiments included both Lissajous patterns covering rectangular areas, and double-circle patterns of the whole disk of the Sun and smaller repeated maps of specific disk-shaped targets. With the latter we find that we can achieve roughly Nyquist sampling of the Band~6 (230~GHz) beam in 60~s over a region 300" in diameter. These maps show a peak-to-peak brightness-temperature range of up to 1000~K, while the time-series variability at any given point appears to be of order 0.5 percent RMS over times of a few minutes. We thus expect to be able to separate the noise contributions due to transparency fluctuations from variations in the Sun itself. Such timeseries have many advantages, in spite of the non-interferometric observations. In particular such data should make it possible to observe microflares in active regions and nanoflares in any part of the solar disk and low corona.

SPADE: Small Phase Array Demonstrator for Solar Radio Astronomy Observations

Antonio Mart´ınez **Picar**∗†1 , Christophe Marque1 , and Jasmina Magdalenic
CESRA **2016** p.57
http://cesra2016.sciencesconf.org/conference/cesra2016/pages/CESRA2016_prog_abs_book_v3.pdf
The Royal Observatory of Belgium manages a radio astronomy facility in Humain, 120 km southeast of Brussels. Since 2008 the station is monitoring the Sun's activity in the frequency range of 45 – 1493 MHz. However, the evolving RFI situation in Europe, the prospect that digital signal processing can improve the quality of the collected scientific data, and that an array of simple antennas reduces the inherent risk of mechanical failures motivated us to design and build SPADE: a prototype of a phased array which includes eight low-frequency antennas and that will use Software Defined Radio receivers. SPADE will use digital techniques for RFI management and controlling the beam-forming operation, and produce dynamic spectrum observations of the Sun in the range of 20 – 80 MHz.

Homologous solar events on 2011 January 27: Build-up and propagation in a complex coronal environment

M. **Pick**, G. Stenborg, P. Demoulin, P. Zucca, A. Lecacheux
ApJ **2016**
http://www.lesia.obspm.fr/perso/pascal-demoulin/16/pick16_homologous_CMEs.pdf **File**
In spite of the wealth of imaging observations at extreme--ultraviolet, X--ray, and radio wavelengths, there are still a relatively small number of cases where the whole imagery becomes available to study the full development of a coronal mass ejection (CME) event and its associated shock. The aim of this study is to contribute to the understanding of the role of the coronal environment in the development of CMEs and formation of shocks, and on their propagation. We have analyzed the interactions of a couple of homologous CME events with the ambient coronal structures. Both events were launched in a direction far from the local vertical, and exhibited a radical change of their direction of propagation during their progression from the low corona into higher altitudes. Observations at extreme ultraviolet wavelengths from the Atmospheric Imaging Assembly instrument onboard the Solar Dynamic Observatory were used to track the events in the low corona. The development of the events at higher altitudes was followed with the white light coronagraphs onboard the Solar and Heliospheric Observatory. Radio emissions produced during the development of the events were well recorded by the Nancay solar instruments. By detecting accelerated electrons, the radio observations are an important complement to the extreme ultraviolet imaging. They allowed us to characterize the development of the associated shocks, and helped unveil the physical processes behind the complex interactions between the CMEs and ambient medium (e.g., compression, reconnection).

Coronal and Interplanetary Structures Associated with Type III Bursts

M. **Pick** · A. Kerdraon · F. Auchère · G. Stenborg · A. Bouteille · E. Soubrié
Solar Phys (2009) 256: 101–110, DOI 10.1007/s11207-009-9359-0, **2009, File**
STEREO SCIENCE RESULTS AT SOLAR MINIMUM
This paper pursues former studies of the coronal structures that are associated with radio type III bursts by taking advantage of the new capabilities of STEREO/SECCHI. The data analysis has been performed for 02 and 03 June 2007. During these two days several type III bursts, which were detected in the corona and in the interplanetary medium, occurred during the observing time of the Nançay radioheliograph. Electron beams accelerated in the same active region and producing type III emissions almost at the same time, can propagate in different well defined coronal structures below 15 R_. Then, these structures become imbedded in the same plasma sheet which can be tracked up to 0.25 AU. Inhomogeneities travel along these structures; their velocities measured between 15 and 35 R_ are typical of those of a slow solar wind. Comparison with PFSS magnetic field extrapolation shows that its connection with the IP magnetic field is different from what is suggested by the present observations.
These results are consistent with those obtained in the IP medium formerly by Buttighoffer (*Astron. Astrophys.* **335**, 295, 1998) who identified by *in situ* measurements at 1 AU and beyond, the sites where Langmuir waves, associated with local type III emissions, are excited.

Sixty-five years of solar radioastronomy: flares, coronal mass ejections and Sun–Earth connection **Review**

Monique **Pick** · Nicole Vilmer
Astron Astrophys Rev (**2008**) 16, 1–153, DOI 10.1007/s00159-008-0013-x, **File**
http://springer.r.delivery.net/r/rfl2.1.Ee.2Tp.1gRU2L.BxCVE%5f..T.GCuy.33ig.BHOEcK00
https://doi.org/10.1007/s00159-008-0013-x
https://sci-hub.ru/10.1007/s00159-008-0013-x
This paper will review the input of 65 years of radio observations to our understanding of solar and solar–terrestrial physics. It is focussed on the radio observations of phenomena linked to solar activity in the period going from the first discovery of the radio emissions to present days. We shall present first an overview of solar radio physics focussed on

the active Sun and on the premices of solar–terrestrial relationships from the discovery to the 1980s. We shall then discuss the input of radioastronomy both at metric/decimetric wavelengths and at centimetric/millimetric and submillimetric wavelengths to our understanding of flares.We shall also review some of the radio, X-ray and white-light signatures bringing new evidence for reconnection and current sheets in eruptive events. The input of radio images (obtained with a high temporal cadence) to the understanding of the initiation and fast development in the low corona of coronal mass ejections (CMEs) as well as the radio observations of shocks in the corona and in the interplanetary medium will be reviewed. The input of radio observations to our knowledge of the interplanetary magnetic structures (ICMEs) will be summarized; we shall show how radio observations linked to the propagation of electron beams allow to identify small scale structures in the heliosphere and to trace the connection between the Sun and interplanetary structures as far as 4AU.We shall also describe how the radio observations bring useful information on the relationship and connections between the energetic electrons in the corona and the electrons measured in-situ. The input of radio observations on the forecasting of the arrival time of shocks at the Earth as well as on Space Weather studies will be described. In the last section, we shall summarize the key results that have contributed to transform our knowledge of solar activity and its link with the interplanetary medium. In conclusion, we shall indicate the instrumental radio developments at Earth and in space, which are from our point of view, necessary for the future of solar and interplanetary physics.

Solar Source Regions for 3He-rich Solar Energetic Particle Events Identified Using Imaging Radio, Optical, and Energetic Particle Observations –

M. **Pick**, G. M. Mason, Y.-M. Wang, C. Tan , and L. Wang
E-print, Sep **2006**
We have identified the sources of six impulsive 3He-rich solar energetic particle events using imaging radio, optical, and energetic ion and electron data, together with calculated coronal fields obtained from extrapolating photospheric magnetograms using a potential field source surface (PFSS) model.

On the disk H⟨ and radio observations of the 28 October 2003 flare and coronal mass ejection event.
Pick, M., Malherbe, J.M., Kerdraon, A., Maia, D.J.F.:
2005, *Astrophys. J.* **631**, L97 – L100. doi:10.1086/497137.

Radio and X-Ray Signatures of Magnetic Reconnection behind an Ejected Flux Rope

Pick, M.; Démoulin, P.; Krucker, S.; Malandraki, O.; Maia, D.
The Astrophysical Journal, Volume 625, Issue 2, pp. 1019-1026. **2005**
https://iopscience.iop.org/article/10.1086/429530/pdf
We present a detailed study of a complex solar event observed on **2002 June 2**. Joint imaging EUV, X-ray, and multiwavelength radio observations allow us to trace the development of the magnetic structure involved in this solar event up to a radial distance of the order of 2 Rsolar. The event involves type II, III, and IV bursts. The type IV burst is formed by two sources: a fast-moving one (M) and a ``quasi-stationary'' one (S). The time coincidence in the flux peaks of these radio sources and the underlying hard X-ray sources implies a causal link. In the first part of our paper we provide a summary of the observations without reference to any coronal mass ejection (CME) model. The experimental results impose strong constraints on the physical processes. In the second part of our paper, we find that **a model with an erupting twisted flux rope, with the formation of a current sheet behind, best relates the different observations in a coherent physical evolution** (even if there is no direct evidence of the twisted flux rope). Our results show that multiwavelength radio imaging represents a powerful tool to trace the dynamical evolution of the reconnecting current sheet behind ejected flux ropes (in between sources M and S) and over an altitude range not accessible by X-ray observations.

Overview of Solar Radio Physics and Interplanetary Disturbances. Review

Pick, M.
(**2004**). Solar and Space Weather Radiophysics. Springer, Dordrecht: Astrophysics and Space Science Library. 314, 17–45.
https://link.springer.com/chapter/10.1007%2F1-4020-2814-8_2
Solar radio emission has been observed from a few hundred GHz down to a few kHz and has revealed a large variety of phenomena. Thanks to this broad frequency window, solar phenomena can be probed from a fraction of a solar radius out to 1 AU and beyond. This chapter reviews some topics of current interest in which radio astronomy has significantly contributed to transform our knowledge of the physics of the corona and of the interplanetary medium. Special emphasis is placed on the results which have emerged from coordinated studies of radio observations and data obtained in other spectral ranges. The few results presented in this chapter illustrate how major advances can be expected in the future from the Frequency Agile Solar Radiotelescope (FASR) instrument which will provide radio imaging observations covering simultaneously a broad radio spectrum.

Two-Part Interplanetary Type II Solar Radio Bursts

Silja **Pohjolainen**
Solar Phys. **2024**
https://arxiv.org/pdf/2412.15961
Two similar-looking, two-part interplanetary type II burst events from 2003 and 2012 are reported and analysed. The 2012 event was observed from three different viewing angles, enabling comparisons between the spacecraft data. In these two events, a diffuse wide-band type II radio burst was followed by a type II burst that showed emission at the fundamental and harmonic (F-H) plasma frequencies, and these emission bands were also slightly curved in their frequency-time evolution. Both events were associated with high-speed, halo-type coronal mass ejections (CMEs). In both events, the diffuse type II burst was most probably created by a bow shock at the leading front of the CME. However, for the later-appearing F-H type II burst there are at least two possible explanations. In the 2003 event there is evidence of CME interaction with a streamer, with a possible shift from a bow shock to a CME flank shock. In the 2012 event a separate white-light shock front was observed at lower heights, and it could have acted as the driver of the F-H type II burst. There is also some speculation on the existence of two separate CMEs, launched from the same active region, close in time. The reason for the diffuse type II burst being visible only from one viewing direction (STEREO-A), and the ending of the diffuse emission before the F-H type II burst appears, still need explanations. **17-18 June 2003, 17 May 2012**

Repeated Type III Burst Groups Associated with a B-Class Flare and a Narrow-Width CME

Silja **Pohjolainen**, Derek McKay, Nasrin Talebpour Sheshvan, Christian Monstein
Solar Phys. 298, Article number: 118 **2023**
http://sp.dy.fi/type3-27sep-final.pdf
We have analysed a solar event from **27 September 2021**, which included a small GOES B-class flare, a compact and narrow-width CME, and radio type III bursts that appeared in groups. The long-duration, repeated metric type III burst emission indicates continuous electron acceleration at high altitudes. The flaring active region was surrounded by strong magnetic fields and large-scale loops, that guided the outflow of the CME plasmoid and hence the narrow, bullet-like appearance of the CME. Radio imaging and EUV observations confirmed the direction of particle propagation and the depletion of matter from the solar disc. We observed V-shaped type III burst emission lanes, which also explain the field configuration and suggest a possible location for repeated reconnection that occurred at a constant altitude.

Separating the effects of earthside and far side solar events. A case study

Silja **Pohjolainen**, Nasrin Talebpour Sheshvan, Christian Monstein
Advances in Space Research Vol. **72**, Issue 9, Pages 4074-4081 **2023**
https://pdf.sciencedirectassets.com/271642/AIP/1-s2.0-S0273117723007317/main.pdf
https://arxiv.org/pdf/2310.04765.pdf
On **8 November 2013** a halo-type coronal mass ejection (CME) was observed, together with flares and type II radio bursts, but the association between the flares, radio bursts, and the CME was not clear. Our aim is to identify the origin of the CME and its direction of propagation, and to exclude features that were not connected to it. On the Earth-facing side, a GOES C5.7 class flare occurred close to the estimated CME launch time, followed by an X1.1 class flare. The latter flare was associated with an EUV wave and metric type II bursts. On the far side of the Sun, a filament eruption, EUV dimmings, and ejected CME loops were observed by imaging instruments onboard the Solar TErrestrial RElations Observatory (STEREO) spacecraft that were viewing the backside of the Sun. The STEREO radio instruments observed an interplanetary (IP) type II radio burst at decameter-hectometric wavelengths, which was not observed by the radio instrument onboard the Wind spacecraft located at L1 near Earth. We show that the halo CME originated from the eruption on the far side of the Sun, and that the IP type II burst was created by a shock wave ahead of the halo CME. The radio burst remained unobserved from the earthside, even at heliocentric source heights larger than 9 solar radii. During the CME propagation, the X-class flare eruption caused a small plasmoid ejection earthward, the material of which was superposed on the earlier CME structures observed in projection. The estimated heights of the metric type II burst match well with the EUV wave launched by the X-class flare. As this radio emission did not continue to lower frequencies, we conclude that the shock wave did not propagate any further. Either the shock driver died out, as a blast wave, or the driver speed no longer exceeded the local Alfvén speed.
CESRA #3681 **2023** https://www.astro.gla.ac.uk/users/eduard/cesra/?p=3681

Formation of Isolated Radio Type II Bursts at Low Frequencies

Silja **Pohjolainen**, Nasrin Talebpour Sheshvan
Solar Phys. **296**, Article number: 81 **2021**
https://arxiv.org/pdf/2104.09891.pdf
https://link.springer.com/content/pdf/10.1007/s11207-021-01828-y.pdf
https://doi.org/10.1007/s11207-021-01828-y

The first appearance of radio type II burst emission at decameter-hectometer (DH) waves typically occurs in connection, and often simultaneously, with other types of radio emissions. As type II bursts are signatures of propagating shock waves that are associated with flares and coronal mass ejections (CMEs), a rich variety of radio emissions can be expected. However, sometimes DH type II bursts appear in the dynamic spectra without other or earlier radio signatures. One explanation for them could be that the flare-CME launch happens on the far side of the Sun, and the emission is observed only when the source gets high enough in the solar atmosphere. In this study we have analysed 26 radio type II bursts that started at DH waves and were well-separated ('isolated') from other radio emission features. These bursts were identified from all DH type II bursts observed in 1998-2016, and for 12 events we had observations from at least two different viewing angles with the instruments onboard Wind and STEREO satellites. We found that only 30% of the type II bursts had their source origin on the far side of the Sun, but also that no bursts originated from the central region of the Sun (longitudes E30 - W40). Almost all of the isolated DH type II bursts could be associated with a shock near the CME leading front, and only few were determined to be shocks near the CME flank regions. In this respect our result differs from earlier findings. Our analysis, which included inspection of various CME and radio emission characteristics, suggests that the isolated DH type II bursts could be a special subgroup within DH type II bursts, where the radio emission requires particular coronal conditions to form and to die out. **20 April 1998, 25 October 2000 , 11 December 2001 , 22 December 2002, 31 December 2004, 1 February 2005, 27 March 2012 , 4 July 2013, 2 October 2013 , 2 April 2014 , 1 July 2015**

Cut-off features in interplanetary solar radio type IV emission

Silja **Pohjolainen**, Nasrin Talebpour Sheshvan
Advances in Space Research **2019**
https://arxiv.org/pdf/1906.07534.pdf
Solar radio type IV bursts can sometimes show directivity, so that no burst is observed when the source region in located far from the solar disk center. This has recently been verified also from space observations, at decameter wavelengths, using a 3D-view to the Sun with STEREO and Wind satellites. It is unclear whether the directivity is caused by the emission mechanism, by reduced radio wave formation toward certain directions, or by absorption/blocking of radio waves along the line of sight. We present here observations of three type IV burst events that occurred on 23, 25, and 29 July 2004, and originated from the same active region. The source location of the first event was near the solar disk center and in the third event near the west limb. Our analysis shows that in the last two events the type IV bursts experienced partial cut-offs in their emission, that coincided with the appearance of shock-related type II bursts. The type II bursts were formed at the flanks and leading fronts of propagating coronal mass ejections (CMEs). These events support the suggestion of absorption toward directions where the type II shock regions are located **2004-07-23, 2004-07-25, 2004-07-29**

Interplanetary radio type II and type IV bursts as indicators of propagating solar transients

Silja **Pohjolainen**, Nasrin Talebpour Sheshvan
Proceedings of 2nd URSI AT-RASC Meeting in Gran Canaria, 28 May - 1 June 2018 **2018**
https://arxiv.org/ftp/arxiv/papers/1806/1806.05065.pdf
Recent studies of interplanetary radio type II bursts and their source locations are reviewed. As these bursts are due to propagating shock waves, driven by coronal mass ejections, they can be followed to near-Earth distances and can be used to predict the arrival times of geo-effective disturbances. Radio type IV bursts, on the other hand, are usually due to moving magnetic structures in the low corona and trapped particles form at least part of the emission. The observed directivity of type IV emission may also be used for space weather purposes. **22 September 2011**

Propagation of Solar Energetic Particles during Multiple Coronal Mass Ejection Events

Silja **Pohjolainen**, Firas Al-Hamadani, Eino Valtonen
Solar Physics, **201**5
http://arxiv.org/pdf/1512.04881v1.pdf
We study solar energetic particle (SEP) events during multiple solar eruptions. The analysed sequences, on **24-26 November 2000, 9-13 April 2001, and 22-25 August 2005**, consisted of halo-type coronal mass ejections (CMEs) that originated from the same active region and were associated with intense flares, EUV waves, and interplanetary (IP) radio type II and type III bursts. The first two solar events in each of these sequences showed SEP enhancements near Earth, but the third in the row did not. We observed that in these latter events the type III radio bursts were stopped at much higher frequencies than in the earlier events, indicating that the bursts did not reach the typical plasma density levels near Earth. To explain the missing third SEP event in each sequence, we suggest that the earlier-launched CMEs and the CME-driven shocks either reduced the seed particle population and thus led to inefficient particle acceleration, or that the earlier-launched CMEs and shocks changed the propagation paths or prevented the propagation of both the electron beams and SEPs, so that they did not get detected near Earth even when the shock arrivals were recorded.
Table 5. Close-by events that show a are, a CME, and a decametric-hectometric (DH) type II burst, found from the list of Wind/WAVES type II bursts and CMEs at http://cdaw.gsfc.nasa.gov/CME list/radio/waves type2.html.

Origin of wide-band IP type II bursts⋆

S. **Pohjolainen**1, H. Allawi1,2 and E. Valtonen

E-print, Aug **2013**; A&A 558, A7 (**2013**)

Context. Different types of interplanetary (IP) type II bursts have been observed, where the more usual ones show narrow-band and patchy emissions, sometimes with harmonics, and which at intervals may disappear completely from the dynamic spectrum. The more unusual bursts are wide-band and diffuse, show no patches or breaks or harmonic emission, and often have long durations. Type II bursts are thought to be plasma emission, caused by propagating shock waves, but a synchrotron-emitting source has also been proposed as the origin for the wide-band type IIs.
Aims. Our aim is to find out where the wide-band IP type II bursts originate and what is their connection to particle acceleration.
Methods. We analyzed in detail 25 solar events that produced well-separated, wide-band IP type II bursts in 2001–2011. Their associations to flares, coronal mass ejections (CMEs), and solar energetic particle events (SEPs) were investigated.
Results. Of the 25 bursts, 18 were estimated to have heights corresponding to the CME leading fronts, suggesting that they were created by bow shocks ahead of the CMEs. However, seven events were found in which the burst heights were significantly lower and which showed a different type of height-time evolution. Almost all the analyzed wide-band type II bursts were associated with very high-speed CMEs, originating from different parts of the solar hemisphere. In terms of SEP associations, many of the SEP events were weak, had poor connectivity due to the eastern limb source location, or were masked by previous events. Some of the events had precursors in specific energy ranges. These properties and conditions affected the intensity-time profiles and made the injection-time-based associations with the type II bursts difficult to interpret. In several cases where the SEP injection times could be determined, the radio dynamic spectra showed other features (in addition to the wide-band type II bursts) that could be signatures of shock fronts.
Conclusions. We conclude that in most cases (in 18 out of 25 events) the wide-band IP type II bursts can be plasma emission, formed at or just above the CME leading edge. The results for the remaining seven events might suggest the possibility of a synchrotron source. These events, however, occurred during periods of high solar activity, and coronal conditions affecting the results of the burst height calculations cannot be ruled out. The observed wide and diffuse emission bands may also indicate specific CME leading edge structures and special shock conditions.

Table

Fragmented type II burst emission during CME liftoff

Silja **Pohjolainen**, Jens Pomoell and Rami Vainio

Proceedings of the International Astronomical Union / Volume 4 / Symposium S257, pp 357 – 359, Published online: 16 Март **2009**

http://journals.cambridge.org/action/displayIssuefliid=4866212

We have performed multiwavelength analysis on an event with a metric type II burst, which appeared first as fragmented emission lanes in the radio dynamic spectrum. The start frequency was unusually high. Since type II bursts are thought to be signatures of propagating shock waves, it is of interest to know how the shocks, and the type II bursts, are formed. This radio event was associated with a flare and a coronal mass ejection (CME), and we investigate their connection. Observations suggested that a propagating shock was formed due to the erupting structures, and the observed radio emission reflects the high densities in active region loops. We then utilised numerical MHD simulations, to study the shock structure induced by an erupting CME, in a model corona including dense loops. Our simulations show that the fragmented part of the type II burst can be formed when a coronal shock driven by a CME passes through a system of dense loops overlying an active region. To produce fragmented emission, the conditions for plasma emission have to be more favourable inside the loop than in the inter-loop area. The obvious hypothesis, consistent with our simulation model, is that the shock strength decreases significantly in the space between the denser loops. Outside the active region, the type II burst dies out when the changing geometry no longer favours the electron shock-acceleration.

Radio Bursts and Pulsations in Association with Flare, Ejecta, and Propagating Shock Waves

S. **Pohjolainen** · K. Hori · T. Sakurai

Solar Phys, 253: 291–303, **2008**, DOI 10.1007/s11207-008-9260-2; **File**

We investigate coronal transients associated with a GOES M6.7 class flare and a coronal mass ejection (CME) on **13 July 2004.** During the rising phase of the flare, a filament eruption, loop expansion, a Moreton wave, and an ejecta were observed. An EIT wave was detected later on. The main features in the radio dynamic spectrum were a frequency-drifting continuum and two type II bursts. Our analysis shows that if the first type II burst was formed in the low corona, the burst heights and speed are close to the projected distances, and speed of the Moreton wave (a chromospheric shock wave signature). The frequency drifting radio continuum, starting above 1 GHz, was formed almost two minutes prior to any shock features becoming visible, and a fast-expanding piston (visible as the continuum) could have launched another shock wave. A possible

scenario is that a flare blast overtook the earlier transient and ignited the first type II burst. The second type II burst may have been formed by the same shock, but only if the shock was propagating at a constant speed.
This interpretation also requires that the shock-producing regions were located at different parts of the propagating structure or that the shock was passing through regions with highly different atmospheric densities. This complex event, with a multitude of radio features and transients at other wavelengths, presents evidence for both blast-wave-related and CME related radio emissions.

CMEs, Shocks and their Radio Signatures

Silja **Pohjolainen**

ESPM Freiburg **2008, Presentation**

Coronal mass ejections (CMEs) are large-scale transients that can be observed at a multitude of wavelengths. The dynamics of CMEs are not known in detail. In the low corona, this is partly due to the lack of imaging data and partly because other processes can mask the CME initiation and liftoff phase. Flares, filament eruptions, waves, and wave-like features often occur simultaneously with CMEs. For example, a debate exists on coronal shock waves, whether they are CME-driven or due to flares, or both. With radio emission we can trace propagating shocks, electron beams, and rising structures, and the emission source locations can reveal their origin. With radio emission we can also follow CMEs to large distances in the interplanetary space and thus obtain their full kinematics.
This **overview** describes some of the most recent findings from the radio signatures during CME liftoff and propagation, and discusses how well the current models on CME and shock formation agree with the observations.

CME liftoff with high-frequency fragmented type II burst emission

S.**Pohjolainen**1, J. Pomoell2, and R. Vainio2

E-print, Sept 2008; A&A, 490, 357-363 (**2008**), DOI: 10.1051/0004-6361:200810049; **File**

http://solar.physics.montana.edu/cgi-bin/eprint/index.plflentry=7936

Aims: Solar radio type II bursts are rarely seen at frequencies higher than a few hundred MHz. Since metric type II bursts are thought to be signatures of propagating shock waves, it is of interest to know how these shocks, and the type II bursts, are formed. In particular, how are high-frequency, fragmented type II bursts createdfl Are there differences in shock acceleration or in the surrounding medium that could explain the differences to the ``typical" metric type IIsfl
Methods: We analyse one unusual metric type II event in detail, with comparison to white-light, EUV, and X-ray observations. As the radio event was associated with a flare and a coronal mass ejection (CME), we investigate their connection. We then utilize numerical MHD simulations to study the shock structure induced by an erupting CME in a model corona including dense loops.
Results: Our simulations show that the fragmented part of the type II burst can be formed when a coronal shock driven by a mass ejection passes through a system of dense loops overlying the active region. To produce fragmented emission, the conditions for plasma emission have to be more favourable inside the loop than in the interloop area. The obvious hypothesis, consistent with our simulation model, is that the shock strength decreases significantly in the space between the denser loops. The later, more typical type II burst appears when the shock exits the dense loop system and finally, outside the active region, the type II burst dies out when the changing geometry no longer favours the electron shock-acceleration.

Shock-related radio emission during coronal mass ejection lift-offfl (Research Note)

S. **Pohjolainen**

E-print, March **2008**, **File**; A&A, 483, 297-300 (**2008**)

Aims.We identify the source of fast-drifting decimetric–metric radio emission that is sometimes observed prior to the so-called flare continuum emission. Fast-drift structures and continuum bursts are also observed in association with coronal mass ejections (CMEs), not only flares.
Methods.We analyse radio spectral features and images acquired at radio, H_, EUV, and soft X-ray wavelengths, during an event close to the solar limb on **2 June 2003**.
Results.The fast-drifting decimetric–metric radio burst corresponds to a moving, wide emission front in the radio images, which is normally interpreted as a signature of a propagating shock wave. A decimetric–metric type II burst where only the second harmonic lane is visible could explain the observations. After long-lasting activity in the active region, the hot and dense loops could be absorbing or suppressing emission at the fundamental plasma frequency. The observed burst speed suggests a super-Alfv´enic velocity for the burst driver. The expanding and opening loops, associated with the flare and the early phase of CME lift-off, could be driving the shock. Alternatively, an instantaneous but fast loop expansion could initiate a freely propagating shock wave. The later, complex looking decametre–hectometre wave type III bursts indicate the existence of a propagating shock, although no interplanetary type II burst was observed during the event. The data does not support CME bow shock or a shock at the flanks of the CME as the origin of the fast-drift decimetric–metric radio source. Therefore super-Alfv´enic loop expansion is the best candidate for the initiation of the shock wave, and this result challenges the current view of metric/coronal shocks originating either in the flanks of CMEs or from flare blast waves.

Relation between coronal type II bursts, associated flares and CMEs

George **Pothitakis**[1], Panagiota Preka-Papadema[1], Xenophon Moussas[1], Constantine Caroubalos[2], Constantine Alissandrakis[4], Panagiotis Tsitsipis[3], Athanasios Kontogeorgos[3] and Alexander Hillaris[1]

Proceedings of the International Astronomical Union / Volume 4 / Symposium S257, pp 299 – 301,
Published online: 16 Μαρτ **2009**
http://journals.cambridge.org/action/displayIssuefliid=4866212

We study a sample of complex events; each includes a coronal type II burst, accompanied by a GOES SXR flare and LASCO CME. The radio bursts were recorded by the ARTEMIS-IV radio spectrograph (100-650 MHz range); the GOES SXR flares and SOHO/LASCO CMEs, were obtained from the Solar Geophysical Data (SGD) and the LASCO lists respectively. The radio burst-flare-CME characteristics were compared and two groups of events with similar behavior were isolated. In the first the type II shock exciter appears to be a flare blast wave propagating in the wake of a CME. In the second the type II burst appears CME initiated though it is not always clear if it is driven by the bow or the flanks of the CME or if it is a reconnection shock.

Characteristics of events with metric-to-decahectometric type II radio bursts associated with CMEs and flares in relation to SEP events

O. **Prakash**, Li Feng, G. Michalek, Weiqun Gan, Lei Lu, A. Shanmugaraju, S. Umapathy

ApSS March 2017, 362:56 **2017**

A gradual solar energetic particle (SEP) event is thought to happen when particles are accelerated at a shock due to a fast coronal mass ejection (CME). To quantify what kind of solar eruptions can result in such SEP events, we have conducted detailed investigations on the characteristics of CMEs, solar flares and m-to-DH wavelength type II radio bursts (herein after m-to-DH type II bursts) for SEP-associated and non-SEP-associated events, observed during the period of 1997-2012. Interestingly, 65% of m-to-DH type II bursts associated with CMEs and flares produced SEP events. The SEP-associated CMEs have higher sky-plane mean speed, projection corrected speed, and sky-plane peak speed than those of non-SEP-associated CMEs respectively by 30%, 39%, and 25%, even though the two sets of CMEs achieved their sky-plane peak speeds at nearly similar heights within LASCO field of view. We found Pearson's correlation coefficients between the speeds of CMEs speeds and logarithmic peak intensity of SEP events are cc = 0.62 and cc = 0.58, respectively. We also found that the SEP-associated CMEs are on average of three times more decelerated (-21.52 m/s2) than the non-SEP-associated CMEs (-5.63 m/s2). The SEP-associated m type II bursts have higher frequency drift rate and associated shock speed than those of the non-SEP-associated events by 70% and 25% respectively. The average formation heights of m and DH type II radio bursts for SEP-associated events are lower than for non-SEP-associated events. 93% of SEP-associated events originate from the western hemisphere and 65% of SEP-associated events are associated with interacting CMEs. The obtained results indicate that, at least for the set of CMEs associated with m-to-DH type II bursts, SEP-associated CMEs are more energetic than those not associated with SEPs, thus suggesting that they are effective particle accelerators. **2011-August-04**

Geoeffectiveness and flare properties of radio-loud CMEs

Prakash, O.; Shanmugaraju, A.; Michalek, G.; Umapathy, S.

Astrophysics and Space Science, Volume 350, Issue 1, pp.33-45, **2014**

A detailed investigation on geoeffective CMEs associated with meter to Deca-Hectometer (herein after m- and DH-type-II) wavelengths range type-II radio bursts observed during the period 1997-2005 is presented. The study consists of three steps: i) the characteristics of m-and DH-type-II bursts associated with flares and geoeffective CMEs; ii) characteristics of geo and non-geoeffective radio-loud and quiet CMEs, iii) the relationships between the geoeffective CMEs and flares properties. Interestingly, we found that 92 % of DH-type-II bursts are extension of m-type-II burst which are associated with faster and wider geoeffective DH-CMEs and also associated with longer/stronger flares. The geoeffective CME-associated m-type-II bursts have higher starting frequency, lower ending frequency and larger bandwidth compared to the general population of m-type-II bursts. The geoeffective CME-associated DH-type-II bursts have longer duration ($P \ll 1$ %), lower ending frequency (P=2 %) and lower drift rates (P=2 %) than that of DH-type-IIs associated with non-geoeffective CMEs. The differences in mean speed of geoeffective DH-CMEs and non-geoeffective DH-CMEs (1327 km s^{-1} and 1191 km s^{-1}, respectively) is statistically insignificant (P=20 %).However, the mean difference in width (339° and 251°, respectively) is high statistical significant (P=0.8 %). The geo-effective general populations of LASCO CMEs speeds (545 km s^{-1} and 450 km s^{-1}, respectively) and widths (252° and 60°, respectively) is higher than the non geo-effective general populations of LASCO CMEs (P=3 % and P=0.02 %, respectively). The geoeffective CMEs associated flares have longer duration, and strong flares than non-geoeffective DH-CMEs associated flares (P=0.8 % and P=1 %, respectively). We have found a good correlation between the geo-effective flare and DH-CMEs properties: i) CMEs speed—acceleration (R=-0.78, where R is a linear correlation coefficient), ii) acceleration—flare peak flux (R=-0.73) and, iii) acceleration— Dst index intensity (R=0.75). The radio-rich CMEs (DH-CMEs) produced more energetic storm than the radio-quiet CMEs (general populations of LASCO CMEs). The above results indicate that the DH-type-II bursts tend to be related with flares and geoeffective CMEs, although there is no physical explanation for the result. If the DH-type-II burst is a continuation of m-type-II burst, it could be a good indicator of geoeffective storms, which has important implications for space weather studies.

Kinematics and Flare Properties of Radio-Loud CMEs

O. **Prakash**, S. Umapathy, A. Shanmugaraju and V. Vasanth
Solar Physics, **2012**, , 281(2), 765-777.
https://link.springer.com/content/pdf/10.1007/s11207-012-0111-9.pdf

A detailed analysis of the characteristics of coronal mass ejections (CMEs) and flares associated with decameter-hectometer wavelength type-II radio bursts (hereafter DH-type-II radio bursts, DH-CMEs or radio-loud CMEs) observed in the period 1997 – 2008 is presented. A sample of 61 limb events is divided into two populations based on the residual acceleration: accelerating CMEs (a r>0) and decelerating CMEs (a r<0). We found that average speed (residual acceleration) of all limb DH-CMEs (called radio-loud CMEs) is nearly three (two) times greater than the average speed of the general population CMEs (radio-quiet CMEs). While the initial acceleration (a i) of the accelerating DH-CMEs is smaller than that of decelerating DH-CMEs (0.79 and 1.62 km s−2, respectively), the average speed and magnitude of residual acceleration of the accelerating and decelerating DH-CMEs are similar (⟨V CME⟩: 1254 km s−1 and 1303 km s−1; ⟨a r⟩: 0.026 km s−2 and 0.028 km s−2, respectively). The accelerating DH-CMEs attain their peak speed at larger heights than decelerating DH-CMEs. A good positive and negative linear correlation for accelerating and decelerating DH-CMEs (R a=0.74 and R d=−0.77, respectively) is found. The flares associated with accelerating DH-CME events have longer rise times and decay times than flares of decelerating DH-CME. The accelerating and decelerating DH-CMEs events associated with DH-type-II bursts have similar ending frequencies. The analysis of time lags between DH-type-II start and the flare onset shows that the delays are longer in accelerating DH-CMEs than decelerating DH-CMEs (P~7 %). However, the time lags between the DH-type-II start and the CMEs onset are similar.

Characteristics of DH type II bursts, CMEs and flares with respect to the acceleration of CMEs

O. **Prakash**, S. Umapathy, A. Shanmugaraju, P. Pappa kalaivani & Bojan Vršnak
Astrophysics and Space Science volume 337, pages47–64(**2012**)
https://link.springer.com/content/pdf/10.1007/s10509-011-0817-4.pdf

A detailed investigation on DH-type-II radio bursts recorded in Deca-Hectometer (hereinafter DH-type-II) wavelength range and their associated CMEs observed during the year 1997–2008 is presented. The sample of 212 DH-type-II associated with CMEs are classified into three populations: (i) Group I (43 events): DH-type-II associated CMEs are accelerating in the LASCO field view (a>15 m s−2); (ii) Group II (99 events): approximately constant velocity CMEs (−15<a<15 m s−2) and (iii) Group III (70 events): represents decelerating CMEs (a<−15 m s−2). Our study consists of three steps: (i) statistical properties of DH-type-II bursts of Group I, II and III events; (ii) analysis of time lags between onsets of flares and CMEs associated with DH-type-II bursts and (iii) statistical properties of flares and CMEs of Group I, II and III events. We found statistically significant differences between the properties of DH-type-II bursts of Group I, II and III events. The significance (P a) is found using the one-way ANOVA-test to examine the differences between means of groups. For example, there is significant difference in the duration (P a =5%), ending frequency (P a =4%) and bandwidth (P a =4%). The accelerating and decelerating CMEs have more kinetic energy than the constant speed CMEs. There is a significant difference between the nose height of CMEs at the end time of DH-type-IIs (P a ≪1%). From the time delay analysis, we found: (i) there is no significant difference in the delay (flare start—DH-type-II start and flare peak—DH-type-II start); (ii) small differences in the time delay between the CME onset and DH-type-II start, delay between the flare start and CME onset times. However, there are high significant differences in: flare duration (P a =1%), flare rise time (P a =0.5%), flare decay time (P a =5%) and CMEs speed (P a ≪1%) of Group I, II and III events. The general LASCO CMEs have lower width and speeds when compared to the DH CMEs. It seems there is a strong relation between the kinetic energy of CMEs and DH-type-II properties.

Type-II Bursts in Meter and Deca – Hectometer Wavelengths and Their Relation to Flares and CMEs: II

O. **Prakash** · S. Umapathy · A. Shanmugaraju · P. Pappa kalaivani · Bojan Vršnak
Solar Phys (**2010**) 266: 135–147

A study of the relationship between 38 type-II bursts recorded in meter and decahectometer (hereinafter m and DH) wavelength range and the associated flares and CMEs observed during the years 2000 – 2005 was carried out by Prakash *et al*. (2009). These events were divided into two classes: *i*) Class I, representing events where DH-type-II bursts are not a continuation of m-type-II bursts and *ii*) Class II, where DH-type-II bursts are a continuation of m-type-II bursts. In the present work, we extend the analysis of this sample of 38 events in three different steps: *i*) statistical properties of m- and DH-type-II bursts;

ii) analysis of time lags between onsets of flares and CMEs associated with type-II bursts; and *iii*) statistical properties and relation between flares and CMEs of Class I and Class II events. We found a significant difference between the properties of m- and DH-type-II bursts of Class I and Class II events. For example, there are significant differences in starting and ending frequencies, bandwidth and speed. From the time delay analysis, we found the following. *i*) In 64% of Class I events, flares start after the onset of CMEs and the remaining 36% of flares start before the onset of CMEs. On the other hand, in the case of Class II events, the values are 83% and 17%, respectively. *ii*) The difference between the mean values of delay between flare start and DH start has high statistical significance (probability *P* of null hypothesis < 1%). The time delays between the start of m-type-II burst and the CME onset are considerably larger for Class I events (*P* = 7%) than Class II events. *iii*) There are notable differences in: (a) delay between the flare and CME onset times (*P* <1%); (b) flare rise time of Class I and Class II events (*P* <5%). *iv*) While the flare rise time is well correlated with the lag between the flare start and the CME onset in Class I events, there is no such correlation for Class II events.

Type II bursts in Meter and Decameter – Hectometer Wavelength Ranges and Their Relation to Flares and CMEs

O. **Prakash** · S. Umapathy · A. Shanmugaraju · Bojan Vršnak
Solar Phys (**2009**) 258: 105–118
Statistical analysis of the relationship between type II radio bursts appearing in the metric (m) and decameter-to-hectometer (DH) wavelength ranges is presented. The associated X-ray flares and coronal mass ejections (CMEs) are also reported. The sample is divided into two classes using the frequency-drift plots: Class I, representing those events where DH-type-II bursts are not continuation of m-type-II bursts and Class II, where the DH-type-II bursts are extensions of m-type-II bursts. Our study consists of three steps: *i*) comparison of characteristics of the Class I and II events; *ii*) correlation of m-type-II and DH-type-II burst characteristics with X-ray flare properties and *iii*) correlation of m-type-II and DH-type-II burst characteristics with CME properties. We have found no clear correlation between properties of m-type-II bursts and DH-type-II bursts. For example, there is no correlation between drift rates of m-type-II bursts and DH-type-II bursts. Similarly there is no correlation between their starting frequencies. In Class I events we found correlations between X-ray flare characteristics and properties of m-type-II bursts and there is no correlation between flare parameters and DH-type-II bursts. On the other hand, the correlation between CME parameters and m-type-II bursts is very weak, but it is good for CME parameters and DH-type-II bursts. These results indicate that Class I m-type-II bursts are related to the energy releases in flares, whereas DH-type-II bursts tend to be related to CMEs. On the contrary, for Class II events in the case of m-type-II and DH-type-II bursts we have found no clear correlation between both flare and CMEs.

A new radio spectrograph at Culgoora.

Prestage, N.P., Luckhurst, R.G., Paterson, B.R., Bevins, C.S., Yuile, C.G.:
1994, Solar Phys. 150(1 – 2), 393. DOI. ADS.
https://link.springer.com/content/pdf/10.1007%2FBF00712901.pdf
IPS Radio and Space Services (IPS) commissioned a new radiospectrograph for solar observations in May 1992. The instrument operates over a frequency range from 18 MHz to 1.8 GHz and samples every three seconds. Digital data acquisition permits a variety of analysis procedures that were not previously possible. The operation of the new instrument is briefly described and some example radiospectrograms are presented. **4 June 1992. 23 October 1992, 30 March 1993**

Increase in Interference Levels in the 45 – 870 MHz Band at the Spanish e-CALLISTO Sites over the Years 2012 and 2019

Manuel **Prieto**, Javier Bussons Gordo, Javier Rodríguez-Pacheco…
Solar Physics volume 295, Article number: 11 (**2020**)
https://doi.org/10.1007/s11207-019-1577-5
https://link.springer.com/content/pdf/10.1007/s11207-019-1577-5.pdf
Two sets of radio-frequency interference (RFI) measurements in the 45 – 870 MHz band are compared. The first set was taken in 2012 at various sites in the province of Guadalajara (Spain) as part of a worldwide site-testing campaign for the deployment of an international network of solar radio-spectrometers, the Compound Astronomical Low-cost Low-frequency Instrument for Spectroscopy and Transportable Observatory (e-CALLISTO) array. Peralejos de las Truchas was found to be an ideal location, even for high-sensitivity non-solar observations, with the lowest interference levels ever measured in the framework of e-CALLISTO. The same set of measurements have been repeated seven years later using the same experimental setup at the same locations. The results presented in this article show that the RFI levels

after seven years have notably increased, at some places by a factor of two, thereby placing at risk broadband spectroscopic radio-astronomy studies from the ground.

The Connection of Solar Wind Parameters with Radio and UV Emission from Coronal Holes

D. V. **Prosovetsky** and I. N. Myagkova

Solar Physics, Volume 273, Number 2, 525-536, **2011, File**

This paper presents the results of a comparison between observations of coronal holes in UV (SOHO EIT) and radio emission (17, 5.7 GHz, 327 and 150.9 MHz, from NoRH, SSRT and Nançay radioheliographs), and solar wind parameters, from ACE spacecraft data over the period **12 March–31 May 2007**. The increase in the solar wind velocity up to ∼ 600 kms−1 was found to correlate with a decrease in the UV flux in the central parts of the solar disk. A connection between the parameters of the radio emission from three different layers of the solar atmosphere and the solar wind velocity near the Earth's orbit was discovered. Such a connection is suggestive of a common mechanism of solar wind acceleration from chromospheric heights to the upper corona.

A Model of Frequency Modulation of the 11-Year Cycle of Solar Activity.

Ptitsyna, N.G., Demina, I.M.

Geomagn. Aeron. 63, 1072–1078 (**2023**).

https://doi.org/10.1134/S0016793223070186

Using wavelet analysis, a study was made of variations in the length of the solar cycle and their characteristic features in 1700–2020. In addition to the stable 11-year component, in the spectrum of solar activity there are three components of the Gleissberg cycle: a ~115-year component is visible over the entire time interval and a ~60-year component occurs until 1875. The classical branch with a period of 88 years is separated in 1775–1910s. In the wavelet spectrum, the Dalton minimum is characterized by a sharp increase in the length of the 11-year component against the background of a decrease in amplitude in ~1800, and also by the fact that all three branches of the Gleissberg cycle are practically symphasic, and their amplitudes are close to the maximum. A model is constructed in which the period of the 11-year harmonic oscillation is modulated by three branches of the Gleissberg cycle. It is found that such a model of frequency modulation describes the general evolution of the spectrum and its main features well, in particular, the Dalton minimum.

Highly Polarized Type III Storm Observed with Parker Solar Probe

Marc **Pulupa**, Stuart D. Bale, Immanuel Christopher Jebaraj, Orlando Romeo, Säm Krucker

ApJ **2024**

https://arxiv.org/pdf/2412.05464

The Parker Solar Probe (PSP) spacecraft observed a large coronal mass ejection (CME) on **5 September 2022**, shortly before closest approach during the 13th PSP solar encounter. For several days following the CME, PSP detected a storm of Type III radio bursts. Stokes parameter analysis of the radio emission indicates that the Type III storm was highly circularly polarized. Left hand circularly polarized (LHC) emission dominated at the start of the storm, transitioning to right hand circularly polarized (RHC) emission at the crossing of the heliospheric current sheet on 6 September.
We analyze the properties of this Type III storm. The drift rate of the Type IIIs indicates a constant beam speed of ∼0.1c, typical for Type III-producing electron beams. The sense of polarization is consistent with fundamental emission generated primarily in the O-mode.
The stable and well organized post-CME magnetic field neatly separates the LHC- and RHC-dominated intervals of the storm, with minimal overlap between the senses of polarization. The proximity of PSP to the source region, both in radial distance and in heliographic longitude, makes this event an ideal case study to connect in situ plasma measurements with remote observations of radio emission. **5-6 Sep 2022**

Statistics and Polarization of Type III Radio Bursts Observed in the Inner Heliosphere

Marc **Pulupa**, Stuart D. Bale, Samuel T. Badman, John W. Bonnell, Anthony W. Case, Thierry Dudok de Wit, Keith Goetz, Peter R. Harvey, Alexander M. Hegedus, Justin C. Kasper, Kelly E. Korreck, Vladimir Krasnoselskikh, Davin Larson, Alain Lecacheux, Roberto Livi, Robert J. MacDowall, Milan Maksimovic, David M. Malaspina, Juan Carlos Martínez Oliveros, Nicole Meyer-Vernet, Michel Moncuquet, Michael Stevens, Phyllis Whittlesey

ApJS **246** 49 **2020**

https://arxiv.org/pdf/1912.03371.pdf

sci-hub.si/10.3847/1538-4365/ab5dc0

We present initial results from the Radio Frequency Spectrometer (RFS), the high frequency component of the FIELDS experiment on the Parker Solar Probe (PSP). During the first PSP solar encounter (2018 November), only a few small radio bursts were observed. During the second encounter (2019 April), copious Type III radio bursts occurred, including intervals of radio storms where bursts occurred continuously. In this paper, we present initial observations of

the characteristics of Type III radio bursts in the inner heliosphere, calculating occurrence rates, amplitude distributions, and spectral properties of the observed bursts. We also report observations of several bursts during the second encounter which display circular polarization in the right hand polarized sense, with a degree of polarization of 0.15-0.38 in the range from 8-12 MHz. The degree of polarization can be explained either by depolarization of initially 100% polarized o-mode emission, or by direct generation of emission in the o and x-mode simultaneously. Direct in situ observations in future PSP encounters could provide data which can distinguish these mechanisms. **30 March 2019, 1-4 Apr 2019, 17 Apr 2019**

Langmuir waves upstream of interplanetary shocks: Dependence on shock and plasma parameters,

Pulupa, M. P., S. D. Bale, and J. C. Kasper (**2010**),
J. Geophys. Res., 115, A04106, doi:10.1029/2009JA014680.
We have examined 178 interplanetary shocks observed by the Wind spacecraft to establish which shock and plasma parameters are favorable for the production of upstream Langmuir waves and therefore to determine which shocks are likely to generate interplanetary Type II radio bursts. Of the 178 shocks included in this study, 43 produced upstream Langmuir waves, as evinced by enhancements in wave power near the plasma frequency. The large number of observed shocks permits the use of statistical tests to determine which parameters control the upstream activity. The best predictor of activity is the de Hoffmann-Teller speed, a result consistent with the fast Fermi model of electron acceleration. Several other parameters, including the magnetic field strength and the level of solar activity (but not the Mach number), are also correlated with upstream activity. These additional parameters may be associated with an increased level of shock front curvature or upstream structure, leading to the formation of upstream foreshock regions, or with the generation of an upstream electron population favorable for shock reflection.

The Solar Probe Plus Radio Frequency Spectrometer: Measurement Requirements, Analog Design, and Digital Signal Processing†

M. **Pulupa**, S. D. Bale, J. W. Bonnell, T. A. Bowen, N. Carruth, K. Goetz, D. Gordon, P. R. Harvey, M. Maksimovic, J. C. Martínez-Oliveros, M. Moncuquet, P. Saint-Hilaire, D. Seitz, D. Sundkvist
JGR **2017** DOI: 10.1002/2016JA023345
http://sci-hub.cc/doi/10.1002/2016JA023345
The Radio Frequency Spectrometer (RFS) is a two channel digital receiver and spectrometer, which will make remote sensing observations of radio waves and *in situ* measurements of electrostatic and electromagnetic fluctuations in the solar wind. A part of the FIELDS suite for Solar Probe Plus (SPP), the RFS is optimized for measurements in the inner heliosphere, where solar radio bursts are more intense and the plasma frequency is higher compared to previous measurements at distances of 1 AU or greater. The inputs to the RFS receiver are the four electric antennas mounted near the front of the SPP spacecraft, and a single axis of the SPP search coil magnetometer (SCM). Each RFS channel selects a monopole or dipole antenna input, or the SCM input, via multiplexers. The primary data products from the RFS are auto and cross spectra from the selected inputs. The spectra are calculated using a polyphase filter bank (PFB), which enables the measurement of low amplitude signals of interest in the presence of high amplitude narrowband noise generated by spacecraft systems. We discuss the science signals of interest driving the RFS measurement objectives, describe the RFS analog design and digital signal processing, and show examples of current performance.

Structure on Interplanetary Shock Fronts: Type II Radio Burst Source Regions

M. **Pulupa** and S. D. Bale
http://www.journals.uchicago.edu/doi/pdf/10.1086/526405
The Astrophysical Journal, Vol. 676, No. 2: 1330-1337, **2008**.
We present in situ observations of the source regions of interplanetary (IP) type II radio bursts, using data from the Wind spacecraft during the period 1996–2002. We show the results of this survey, as well as in-depth analysis of several individual events. Each event analyzed in detail is associated with an interplanetary coronal mass ejection (ICME) and an IP shock driven by the ICME. Immediately prior to the arrival of each shock, electron beams along the interplanetary magnetic field (IMF) and associated Langmuir waves are detected, implying magnetic connection to a quasi-perpendicular shock front acceleration site. These observations are analogous to those made in the terrestrial foreshock region, indicating that a similar foreshock region exists on IP shock fronts. The analogy suggests that the electron acceleration process is a fast Fermi process, and this suggestion is borne out by loss cone features in the electron distribution functions. The presence of a foreshock region requires nonplanar structure on the shock front. Using Wind burst mode data, the foreshock electrons are analyzed to estimate the dimensions of the curved region.We present the first measurement of the lateral, shock-parallel scale size of IP foreshock regions. *The presence of these regions on IP shock fronts can explain the fine structure often seen in the spectra of type II bursts.*

Oscillation of solar radio emission at coronal acoustic cut-off frequency

O. S. **Pylaev**, T.V. Zaqarashvili, A. I. Brazhenko, V. N. Melnik, A. Hanslmeier, M. Panchenko
A&A 601, A42 **2017**
https://arxiv.org/pdf/1703.09929.pdf

Recent SECCHI COR2 observations on board STEREO-A spacecraft have detected density structures at a distance of 2.5--15~R propagating with periodicity of about 90~minutes. The observations show that the density structures probably formed in the lower corona. We used the large Ukrainian radio telescope URAN-2 to observe type IV radio bursts in the frequency range of 8--32~MHz during the time interval of 08:15--11:00~UT on **August 1, 2011**. Radio emission in this frequency range originated at the distance of 1.5--2.5 R according to the Baumbach-Allen density model of the solar corona. Morlet wavelet analysis showed the periodicity of 80~min in radio emission intensity at all frequencies, which demonstrates that there are quasi-periodic variations of coronal density at all heights. The observed periodicity corresponds to the acoustic cut-off frequency of stratified corona at a temperature of 1~MK. We suggest that continuous perturbations of the coronal base in the form of jets/explosive events generate acoustic pulses, which propagate upwards and leave the wake behind oscillating at the coronal cut-off frequency. This wake may transform into recurrent shocks due to the density decrease with height, which leads to the observed periodicity in the radio emission. The recurrent shocks may trigger quasi-periodic magnetic reconnection in helmet streamers, where the opposite field lines merge and consequently may generate periodic density structures observed in the solar wind.
CESRA highlight **#1450** **http://cesra.net/?p=1450**

On the second harmonic excitation in the electron beam-plasma instability

Maryamsadat **Rafiei**, Mostafa Sahrai, Mahboub Hosseinpour, and Abdolrasoul Esfandyari-Kalejahi
Front. Astron. Space Sci. 9:810751. **2022**
https://www.frontiersin.org/articles/10.3389/fspas.2022.810751/full
doi: 10.3389/fspas.2022.810751

The electron beam–plasma interaction is a fundamental nonlinear plasma process that is frequently taking place in space and laboratory plasmas. Such an interaction is found to generate electromagnetic waves observed in space plasmas. Using the two-dimensional electromagnetic particle in cell simulations, we investigated the second harmonic excitation in the electron beam–plasma instability. Results showed that, first, the Langmuir waves are excited in the system; then at longer time scales, following the excitation of ion acoustic waves, the second harmonic electromagnetic waves are excited. We found that in the case of background pair plasmas, where the masses are the same, there is no signature of waves in the second harmonic, which is a direct verification of the three-wave coupling mechanism for the generation of electromagnetic waves in the second harmonic.

Spectropolarimetric Imaging of Metric Type III Solar Radio Bursts

M. M. **Rahman**, Iver H. Cairns & Patrick I. McCauley
Solar Physics volume 295, Article number: 51 (**2020**)
https://link.springer.com/content/pdf/10.1007/s11207-020-01616-0.pdf

We present low-frequency (80 – 240 MHz) radio observations of circular polarization in 16 isolated type III solar radio bursts using the Murchison Widefield Array (MWA) between August 2014 and November 2015. For most of the bursts, near burst onset, we find on average 9%9% circular polarization at 80 MHz and 22%22% at 240 MHz whereas these percentages are 5%5% and 20%20% near burst maximum. The polarization fractions are neither constant in time nor uniform over the spatial extents of the bursts. We measure polarization fractions as a function of burst source's position. On average, near both burst onset and maximum, we find higher polarization near the disk center and lower polarization when the burst source is near the limb. We study total intensity (Stokes II), circularly polarized intensity (Stokes VV), and polarization fraction (|V|/I|V|/I) profiles for type III bursts with and without source motion as a function of position at times when the intensity of bursts is maximum. For the burst event with no source motion, we find symmetric profiles for Stokes II, VV, and |V|/I|V|/I. We find symmetric II and VV but asymmetric |V|/I|V|/I profiles for burst events which have source motion. We argue that this is due to the fundamental emission at the front of a type III electron beam and motion of the burst source. We then perform spectropolarimetric imaging studies of moving burst sources and analyze their motion. At burst onset, we obtain relatively higher polarization fractions, which is considered to be due to a large contribution from fundamental plasma emission at the front of the beam. At burst maximum, the polarization fraction is lower due to the combination of fundamental and harmonic components. After peak intensity, the emission is dominated again by the fundamental component that decays until the end of a burst with lesser polarization fraction than earlier. We argue that the fundamental radiation that decays over time after peak burst intensity is strongly scattered. This pattern of fundamental, fundamental and harmonic, and then fundamental emission with time at each frequency is consistent with the interpretations of Dulk, Suzuki, and Sheridan (Astron. Astrophys.130, 39, 1984), Robinson, Cairns, and Willes (Astrophys. J.422, 870, 1994), and Robinson and Cairns (Solar Phys.181, 363, 1998). We propose that scattering effects can be a viable reason for low polarization fractions in type III events. Finally, we investigate the variations of the decay time (tdtd) for three events with frequency (ff), finding that td∝f−2.0±0.1td∝f−2.0±0.1 and decreases more rapidly with increasing ff compared with previous lower-frequency

observations (td∝f−1.1±0.1td∝f−1.1±0.1). This is interpreted in terms of radial variations of the turbulence properties. **2015/08/25, 2015/09/18, 2015/11/11**
Table 1 Degree of circular polarization characteristics of type III bursts.

On the Relative Brightness of Coronal Holes at Low Frequencies

M. M. **Rahman**, Patrick I. McCauley, Iver H. Cairns
Solar Physics January **2019**, 294:7
https://link.springer.com/content/pdf/10.1007%2Fs11207-019-1396-8.pdf
We present low-frequency (80 – 240 MHz) radio observations of coronal holes (CHs) made with the Murchison Widefield Array (MWA). CHs are expected to be dark structures relative to the background corona across the MWA bandwidth due to their low densities. However, we observe that multiple CHs near disk center transition from being dark structures at higher frequencies to bright structures at lower frequencies (≲145 MHz≲145 MHz). We compare our observations to synthetic images obtained using the software suite FORWARD, in combination with the magnetohydrodynamic algorithm outside a sphere (MAS) model of the global coronal magnetic field, density, and temperature structure. The synthetic images do not exhibit this transition, and we quantify the discrepancy as a function of frequency. We propose that the dark-to-bright transition results from refraction of radio waves into the low-density CH regions, and we develop a qualitative model based on this idea and the relative optical depths inside and outside a CH as a function of frequency. We show that opacity estimates based on the MAS model are qualitatively consistent with our interpretation, and we conclude that propagation and relative absorption effects are a viable explanation for the dark-to-bright transition of CHs from high to low frequencies. **28 August 2014, 31 August 2015, 08 September 2015**

Solar and interplanetary parameters of CMEs with and without type II radio bursts

A. Mujiber **Rahman** a,⇑ , S. Umapathy a,1, A. Shanmugaraju b,2, Y.-J. Moon
Advances in Space Research 50 (**2012**) 516–525
We have analyzed 101 CMEs, and their associated ICMEs and interplanetary (IP) shocks observed during the period 1997–2005. The main aim of the present work is to study the interplanetary characteristics of metric and DH type II associated CMEs such as, shock strength, IP shock speed, ICME speed, stand off distance and transit time. Among these 101 CMEs, 38 events show both metric and DH type II bursts characteristics. There are no metric and DH type II association for 52 events. While DH type II alone is found in 7 cases, metric type II alone is found in 4 events. It is found that the mean speeds of CMEs increase progressively from CMEs without type II events to CMEs associated with metric and DH type IIs as suggested by Gopalswamy et al. (2005). In addition, we found that the speeds of ICMEs and IP shocks progressively increase in the following order: events without metric and DH type IIs, events with metric alone, events with DH alone and events with both metric and DH type IIs. Similarly the Mach number is found to increase in the same order. While there is not much change in the stand-off distance among these cases, it is minimum (_18 R_) for CMEs with speed greater than 2200 km/s. The above results confirm that more energetic CMEs can produce both metric and DH type IIs for which the interplanetary parameters such as mean values of ICME speed and IP shock speed and Mach number are found to be higher.

Spectral Analysis of Solar Radio Type III Bursts from 20 kHz to 410 MHz

K. Sasikumar **Raja**, Milan Maksimovic, Eduard P. Kontar, Xavier Bonnin, Philippe Zarka, Laurent Lamy, Hamish Reid, Nicole Vilmer, Alain Lecacheux, Vratislav Krupar, Baptiste Cecconi, Lahmiti Nora, Laurent Denis
ApJ **924** 58 **2022**
https://arxiv.org/pdf/2110.10935.pdf
https://iopscience.iop.org/article/10.3847/1538-4357/ac34ed/pdf
We present the statistical analysis of the spectral response of solar radio type III bursts over the wide frequency range between 20 kHz and 410 MHz. For this purpose, we have used observations that were carried out using both spaced-based (Wind/Waves) and ground-based (Nançay Decameter Array and Nançay Radioheliograph) facilities. In order to compare the flux densities observed by the different instruments, we have carefully calibrated the data and displayed them in Solar Flux Units. The main result of our study is that type III bursts, in the metric to hectometric wavelength range, statistically exhibit a clear maximum of their median radio flux density around 2 MHz. Although this result was already reported by inspecting the spectral profiles of type III bursts in the frequency range 20 kHz - 20 MHz, our study extends such analysis for the first time to metric radio frequencies (i.e., from 20 kHz to 410 MHz) and confirms the maximum spectral response around 2 MHz. In addition, using a simple empirical model we show that the median radio flux S of the studied dataset obeys the polynomial form Y=0.04X3−1.63X2+16.30X−41.24, with X=ln(FMHz) and with Y=ln(SSFU). Using the Sittler and Guhathakurtha model for coronal streamers \citep{Sit1999}, we have found that maximum of radio power falls therefore in the range 4 to 10 R⊙, depending on whether the type III emissions are assumed to be at the fundamental or the harmonic. **31 July 2014**
CESRA #3221 **2022** https://www.astro.gla.ac.uk/users/eduard/cesra/?p=3221

Erratum: **2024** ***ApJ*** 960 **93** https://iopscience.iop.org/article/10.3847/1538-4357/ad1111/pdf

Amplitude of solar wind density turbulence from 10--45 R⊙

K. Sasikumar **Raja**, Madhusudan Ingale, R. Ramesh, Prasad Subramanian, P. K. Manoharan, P. Janardhan
JGR **2016**
https://arxiv.org/pdf/1611.04282v1.pdf
We report on the amplitude of the density turbulence spectrum (C2N) and the density modulation index (δN/N) in the solar wind between 10 and 45R⊙. We derive these quantities using a structure function that is observationally constrained by occultation observations of the Crab nebula made in 2011 and 2013 and similar observations published earlier. We use the most general form of the structure function, together with currently used prescriptions for the inner/dissipation scale of the turbulence spectrum. Our work yields a comprehensive picture of a) the manner in which C2N and δN/N vary with heliocentric distance in the solar wind and b) of the solar cycle dependence of these quantities.

An Estimate of the Magnetic Field Strength Associated with a Solar Coronal Mass Ejection from Low Frequency Radio Observations

K. Sasikumar **Raja**1, R. Ramesh1, K. Hariharan1, C. Kathiravan1, and T. J. Wang
2014 ApJ 796 56
https://arxiv.org/pdf/1611.05249v1.pdf
We report ground based, low frequency heliograph (80 MHz), spectral (85-35 MHz), and polarimeter (80 and 40 MHz) observations of drifting, non-thermal radio continuum associated with the "halo" coronal mass ejection that occurred in the solar atmosphere on **2013 March 15**. The magnetic field strengths (B) near the radio source were estimated to be B 2.2 ± 0.4 G at 80 MHz and B 1.4 ± 0.2 G at 40 MHz. The corresponding radial distances (r) are r 1.9 R ⊙ (80 MHz) and r 2.2 R ⊙ (40 MHz). **2012 December 20, 2013 January 18, 2013 March 11**

LOW-FREQUENCY OBSERVATIONS OF TRANSIENT QUASI-PERIODIC RADIO EMISSION FROM THE SOLAR ATMOSPHERE

K. Sasikumar **Raja** and R. Ramesh
2013 ApJ 775 38
https://arxiv.org/pdf/1611.05227v1.pdf
We report low-frequency observations of quasi-periodic, circularly polarized, harmonic type III radio bursts whose associated sunspot active regions were located close to the solar limb. The measured periodicity of the bursts at 80 MHz was 5.2 s, and their average degree of circular polarization (dcp) was 0.12. We calculated the associated magnetic field B (1) using the empirical relationship between the dcp and B for the harmonic type III emission, and (2) from the observed quasi-periodicity of the bursts. Both the methods result in B 4.2 G at the location of the 80 MHz plasma level (radial distance r 1.3 R ⊙) in the active region corona.

Design and performance of a low frequency cross-polarized log-periodic dipole antenna

K. Sasikumar **Raja**, C. Kathiravan, R. Ramesh, M. Rajalingam, Indrajit V. Barve
ApJS 207, 2 **2013**
We report the design and performance of a cross-polarized log-periodic dipole (CLPD) antenna for observations of polarized radio emission from the solar corona at low frequencies. The measured isolation between the two mutually orthogonal log periodic dipole antennas was as low as ≈ -43 dBm in the 65-95 MHz range. We carried out observations of the solar corona at 80 MHz with the above CLPD and successfully recorded circularly polarized emission.

Solar Coronal Density Turbulence and Magnetic Field Strength at the Source Regions of Two Successive Metric Type II Radio Bursts

R. **Ramesh**1, C. Kathiravan1, and Anshu Kumari2
2023 ApJ 943 43
https://iopscience.iop.org/article/10.3847/1538-4357/acaea5/pdf
https://arxiv.org/pdf/2302.00071.pdf
We report spectral and polarimeter observations of two weak, low-frequency (≈85–60 MHz) solar coronal type II radio bursts that occurred on **2020 May 29** within a time interval ≈2 minutes. The bursts had fine structures, and were due to harmonic plasma emission. Our analysis indicates that the magnetohydrodynamic shocks responsible for the first and second type II bursts were generated by the leading edge (LE) of an extreme-ultraviolet flux rope/coronal mass ejection

(CME) and interaction of its flank with a neighboring coronal structure, respectively. The CME deflected from the radial direction by ≈25° during propagation in the near-Sun corona. The estimated power spectral density and magnetic field strength (B) near the location of the first burst at heliocentric distance r ≈ 1.35 R⊙ are ≈2 × 10−3 W2m and ≈1.8 G, respectively. The corresponding values for the second burst at the same r are ≈10−3 W2m and ≈0.9 G. The significant spatial scales of the coronal turbulence at the location of the two type II bursts are ≈62–1 Mm. Our conclusions from the present work are that the turbulence and magnetic field strength in the coronal region near the CME LE are higher compared to the corresponding values close to its flank. The derived estimates of the two parameters correspond to the same r for both the CME LE and its flank, with a delay of ≈2 minutes for the latter.
CESRA #3501 **2023** https://www.astro.gla.ac.uk/users/eduard/cesra/?p=3501

Polarization Observations of a Split-band Type II Radio Burst from the Solar Corona

R. **Ramesh**1 and C. Kathiravan1
2022 ApJ 940 80
https://iopscience.iop.org/article/10.3847/1538-4357/ac9c65/pdf
Using temporal observations of circular polarized harmonic plasma emission from a split-band type II solar radio burst at 80 MHz, we separately estimated the coronal magnetic field strengths (B) associated with the lower (L) and upper (U) frequency bands of the burst. The corresponding Stokes I and V data were obtained with the polarimeter operating at the above frequency in the Gauribidanur observatory. The burst was associated with a flare/coronal mass ejection on the solar disk. Simultaneous spectral observations with the spectrograph there in the frequency range 80–35 MHz helped to establish that the observed polarized emission was from the harmonic component of the burst. The B values corresponding to the polarized emission from the L and U bands at 80 MHz are BL ≈ 1.2 G and BU ≈ 2.4 G, respectively. The different values of B for the observed harmonic emission at the same frequency (80 MHz) from the two bands imply unambiguously that the corresponding fundamental emission at 40 MHz must have originated at different spatial locations. Two-dimensional radio imaging observations of the burst with the radioheliograph in the same observatory at 80 MHz indicate the same. As comparatively higher B is expected behind a propagating shock due to compression as well as the corresponding coronal regions being closer to the Sun, our results indicate that the sources of L- and U-band emission should be located ahead of and behind the associated coronal shock, respectively. These are useful to understand the pre- and postshock corona as well as locations of electron acceleration in a propagating shock.
2021 May 22

Circular Polarization Observations of Type II Solar Radio Bursts and the Coronal Magnetic Field

R. **Ramesh**1, C. Kathiravan1, and E. Ebenezer Chellasamy2
2022 ApJ 932 48
https://iopscience.iop.org/article/10.3847/1538-4357/ac6f05/pdf
It is well known that magnetic field strength (B) in the solar corona can be calculated using the Alfvén Mach number (MA) and Alfvén speed (vA) of the magnetohydrodynamic shock waves associated with coronal type II radio bursts. We show that observations of weak circularly polarized emission associated with the harmonic component of the type II bursts provide independent and consistent estimates of B. For the coronal type II burst observed on **2021 October 9**, we obtained B ≈1.5 G and ≈1.9 G at a heliocentric distance (r) of ≈1.8 R⊙, using the above two techniques, respectively.

New Results from the Spectral Observations of Solar Coronal Type II Radio Bursts

R. **Ramesh**1, C. Kathiravan1, and S. Surya Natarajan2
2022 ApJ 926 38
https://iopscience.iop.org/article/10.3847/1538-4357/ac4bd6/pdf
We carried out a statistical study of twenty-six type II radio bursts from the Sun observed with the Gauribidanur Low-frequency Solar Spectrograph in the frequency range 85–35 MHz during the period 2009–2019. Our results indicate that the average instantaneous bandwidth of the type II bursts in the above frequency range correlates with the angular width of the associated coronal mass ejections (CMEs). The correlation coefficient is ≈71%. This independently indicates that the coronal type II bursts reported in this work are mostly due to shocks driven by the CMEs. Moreover, it also suggests that the instantaneous bandwidth of the bursts could be due to electron acceleration (leading to type II bursts) occurring simultaneously at multiple locations of differing electron densities (i.e., plasma frequencies) along the shock surrounding the CME. **2014 December 5**
Table 1 Details Related to the Type II Bursts Observed with GLOSS during the Period 2009–2019 and the Associated SOHO/LASCO-C2 CMEs
CESRA #3231 **2022** **https://www.astro.gla.ac.uk/users/eduard/cesra/?p=3231**

Radio, X-Ray, and Extreme-ultraviolet Observations of Weak Energy Releases in the "Quiet" Sun

R. **Ramesh**1, C. Kathiravan1, N. P. S. Mithun2, and S. V. Vadawale2
2021 ApJL 918 L18
https://arxiv.org/pdf/2109.08455.pdf
https://doi.org/10.3847/2041-8213/ac1da3
We analyzed ground-based low frequency (<100 MHz) radio spectral and imaging data of the solar corona obtained with the facilities in the Gauribidanur observatory during the same time as the very weak soft X-ray flares (sub-A-class, flux <10−7Wm−2 in the 1–8 Å wavelength range) from the quiet Sun observed with the X-ray Solar Monitor (XSM) on board Chandrayaan-2 during the recent solar minimum. Nonthermal type I radio burst activity was noticed in close temporal association with the X-ray events. The estimated brightness temperature (Tb) of the bursts at a typical frequency like 80 MHz is ≈3 × 105 K. Extreme-ultraviolet (EUV) observations at 94 Å with the Atmospheric Imaging Assembly (AIA) on board the Solar Dynamics Observatory (SDO) revealed a brightening close to the same location and time as the type I radio bursts. As far as we know reports of simultaneous observations of X-ray and/or EUV counterpart to weak transient radio emission at low frequencies from the quiet Sun in particular are rare. Considering this and the fact that low frequency radio observations are sensitive to weak energy releases in the solar atmosphere, the results indicate that coordinated observations of similar events would be useful to understand transient activities in the quiet Sun. **2020 April 21**
RHESSI Nuggets #416 2021
https://sprg.ssl.berkeley.edu/~tohban/wiki/index.php/X-Rays_from_a_Type_I_Radio_Burst
CESRA #3090 Oct 2021 https://www.astro.gla.ac.uk/users/eduard/cesra/?p=3090

New results on the direct observations of thermal radio emission from a solar coronal mass ejection

R. **Ramesh**, A. Kumari, C. Kathiravan, D. Ketaki, T. J. Wang
Geophysical Research Letters v. 48, **Issue8**, e2020GL091048 **2021**
https://arxiv.org/pdf/2103.04148.pdf
https://doi.org/10.1029/2020GL091048
We report observations of thermal emission from the frontal structure of a coronal mass ejection (CME) using data obtained with the Gauribidanur RAdioheliograPH (GRAPH) simultaneously at 80 MHz and 53 MHz on **2016 May 1**. The CME was due to activity on the far-side of the Sun, but near its limb. No non-thermal radio burst activity were noticed. This provided an opportunity to observe the faint thermal radio emission from the CME, and hence directly estimate the electron density, mass, and magnetic field strength of the plasma entrained in the CME. Considering that CMEs are mostly observed only in whitelight and reports on their plasma characteristics are also limited, the rare direct radio observations of thermal emission from a CME and independent diagnosis of its plasma parameters are important measurements in the field of CME physics.
CESRA #3008 Aug **2021** **http://www.astro.gla.ac.uk/users/eduard/cesra/?p=3008**

Low frequency radio observations of the `quiet' corona during the descending phase of sunspot cycle 24

R. **Ramesh**, A. Kumari, C. Kathiravan, D. Ketaki, M. Rajesh, M. Vrunda
Geophysical Research Letters e2020GL090426 **2020**
https://arxiv.org/pdf/2009.02670.pdf
https://doi.org/10.1029/2020GL090426
We carried out a statistical study of the `quiet' solar corona during the descending phase of the sunspot cycle 24 (i.e. 2015 January - 2019 May) using data obtained with the Gauribidanur RAdioheliograPH (GRAPH) at 53 MHz and 80 MHz simultaneously. Our results show that the equatorial (east-west) diameters of the solar corona at the above two frequencies shrunk steadily. The decrease was found to be due to a gradual reduction in the coronal electron density (Ne). Independent estimates of Ne in the equatorial region of the `background' corona using white-light coronagraph observations indicate a decline consistent with our findings.
CESRA #2698 Oct **2020** http://www.astro.gla.ac.uk/users/eduard/cesra/?p=2698

New Evidence for Spatio-temporal Fragmentation in the Solar Flare Energy Release

R. **Ramesh**1, V. Mugundhan2, and K. Prabhu1
2020 ApJL 889 L25
ci-hub.si/10.3847/2041-8213/ab6a9c
We analyzed a group of type III radio bursts and a Hα flare from the Sun that were observed simultaneously on **2015 January 14**. The radio observations were in the spectral mode over the frequency range 85–35 MHz, and separately in the imaging mode at 80 MHz. The duration of the observations was ≈6 minutes. The centroids of the type III bursts and the Hα flare were independently scattered near the associated active region. But the displacements in the centroids of the two phenomenon are correlated with each other. This indicates that the individual bursts in a group of type III radio

bursts are most likely due to flaring activity at different locations in the active region at different times during the same flare interval.
CESRA # 2650 July **2020** http://www.astro.gla.ac.uk/users/eduard/cesra/?p=2650

Low-frequency Observations of Drifting, Non-thermal Continuum Radio Emission Associated with the Solar Coronal Mass Ejections

R. **Ramesh**1, P. Kishore1, Sargam M. Mulay2, Indrajit V. Barve1, C. Kathiravan1, and T. J. Wang
2013 ApJ 778 30
Low-frequency (80 MHz) imaging and spectral (85-20 MHz) observations of moving type IV radio bursts associated with coronal mass ejections (CMEs) from the Sun on three different days are reported. The estimated drift speed of the bursts is in the range 150-500 km s–1. We find that all three bursts are most likely due to second harmonic plasma emission from the enhanced electron density in the associated white-light CMEs. The derived maximum magnetic field strength of the latter is B 4 G at a radial distance of r 1.6 R ⊙.

LOW-FREQUENCY RADIO OBSERVATIONS OF PICOFLARE CATEGORY ENERGY RELEASES IN THE SOLAR ATMOSPHERE

R. **Ramesh**, K. Sasikumar Raja, C. Kathiravan, and A. Satya Narayanan
2013 ApJ 762 89
We report low-frequency (80 MHz) radio observations of circularly polarized non-thermal type I radio bursts ("noise storms") in the solar corona whose estimated energy is ~1021 erg. These are the weakest energy release events reported to date in the solar atmosphere. The plot of the distribution of the number of bursts (dN) versus their corresponding peak flux density in the range S to S+dS shows a power-law behavior, i.e., dN S γ dS. The power-law index γ is in the range –2.2 to –2.7 for the events reported in the present work. The present results provide independent observational evidence for the existence of picoflare category energy releases in the solar atmosphere which are yet to be explored.

THE LOCATION OF SOLAR METRIC TYPE II RADIO BURSTS WITH RESPECT TO THE ASSOCIATED CORONAL MASS EJECTIONS

R. **Ramesh**1, M. Anna Lakshmi2, C. Kathiravan1, N. Gopalswamy3, and S. Umapathy
2012 ApJ 752 107, **File**
Forty-one solar type II radio bursts located close to the solar limb (projected radial distance r 0.8 R ⊙) were observed at 109 MHz by the radioheliograph at the Gauribidanur observatory near Bangalore during the period 1997-2007. The positions of the bursts were compared with the estimated location of the leading edge (LE) of the associated coronal mass ejections (CMEs) close to the Sun. 38/41 of the type II bursts studied were located either at or above the LE of the associated CME. In the remaining 3/41 cases, the burst was located behind the LE of the associated CME at a distance of <0.5 R ⊙. Our results suggest that nearly all the metric type II bursts are driven by the CMEs
Table of type II bursts, 1997-2007

HIGH ANGULAR RESOLUTION RADIO OBSERVATIONS OF A CORONAL MASS EJECTION SOURCE REGION AT LOW FREQUENCIES DURING A SOLAR ECLIPSE

R. **Ramesh**, C. Kathiravan, Indrajit V. Barve and M. Rajalingam
2012 ApJ 744 165
We carried out radio observations of the solar corona in the frequency range 109-50 MHz during the annular eclipse of **2010 January 15** from the Gauribidanur Observatory, located about 100 km north of Bangalore in India. The radio emission in the above frequency range originates typically in the radial distance range 1.2-1.5 R ⊙in the "undisturbed" solar atmosphere. Our analysis indicates that (1) the angular size of the smallest observable radio source (associated with a coronal mass ejection in the present case) is 1' ± 03, (2) the source size does not vary with radial distance, (3) the peak brightness temperature of the source corresponding to the above size at a typical frequency like 77 MHz is 3 × 109 K, and (4) the coronal magnetic field near the source region is 70 mG.

LOW-FREQUENCY OBSERVATIONS OF POLARIZED EMISSION FROM LONG-LIVED NON-THERMAL RADIO SOURCES IN THE SOLAR CORONA

R. **Ramesh**, C. Kathiravan and A. Satya Narayanan
2011 ApJ 734 39

We report observations of circularly polarized emission from the solar corona at 77 MHz during the periods 2006 **August 11-18, 2006 August 23-29, and 2007 May 16-22** in the minimum phase between the sunspot cycles 23 and 24. The observations were carried out with the east-west one-dimensional radio polarimeter at the Gauribidanur observatory located about 100 km north of Bangalore. Two-dimensional imaging observations at 77 MHz during the same period with the radioheliograph at the same observatory revealed that the emission region co-rotated with the Sun during the three aforementioned periods. Their rotation rates, close to the central meridian on the Sun, are 46, 52, and 49 ± 05 per day, respectively. We derived the radial distance of the region from the above observed rotation rates and the corresponding values are 1.24 ± 0.03 R (2006 August 11-18), 1.40 ± 0.03 R (2006 August 23-29), and 1.32 ± 0.03 R (2007 May 16-22). The estimated lower limit for the magnetic field strength at the above radial distances and periods are 1.1, 0.6, and 0.9 G, respectively.

RADIO OBSERVATIONS OF WEAK ENERGY RELEASES IN THE SOLAR CORONA

R. **Ramesh** 1, C. Kathiravan 1, Indrajit V. Barve 1, G. K. Beeharry 2 and G. N. Rajasekara
2010 ApJL 719 L41

We report observations of weak, circularly polarized, structureless type III bursts from the solar corona in the absence of Hα/X-ray flares and other related activity, during the minimum between the sunspot cycles 23 and 24. The spectral information about the event obtained with the CALLISTO spectrograph at Mauritius revealed that the drift rate of the burst is –30 MHz s–1 is in the range 50-120 MHz. Two-dimensional imaging observations of the burst at 77 MHz obtained with the Gauribidanur radioheliograph indicate that the emission region was located at a radial distance of 1.5 R in the solar atmosphere. The estimated peak brightness temperature of the burst at 77 MHz is ~108 K. We derived the average magnetic field at the aforementioned location of the burst using the one-dimensional (east-west) Gauribidanur radio polarimeter at 77 MHz, and the value is 2.5 ± 0.2 G. We also estimated the total energy of the non-thermal electrons responsible for the observed burst as 1.1 × 1024 erg. This is low compared to the energy of the weakest hard X-ray microflares reported in the literature, which is about ~1026 erg. The present result shows that non-thermal energy releases that correspond to the nanoflare category (energy ~1024 erg) are taking place in the solar corona, and the nature of such small-scale energy releases has not yet been explored.

RADIOHELIOGRAPH OBSERVATIONS OF METRIC TYPE II BURSTS AND THE KINEMATICS OF CORONAL MASS EJECTIONS

R. **Ramesh**1, C. Kathiravan1, Sreeja S. Kartha1, and N. Gopalswamy2
Astrophysical Journal, 712:188–193, **2010** March, **File**

Assuming that metric type II radio bursts from the Sun are due to magnetohydrodynamic shocks driven by coronal mass ejections (CMEs), we estimate the average CME acceleration from its source region up to the position of the type II burst. The acceleration values are in the range ≈600–1240 m s−2, which are consistent with values obtained using non-radio methods. We also find that (1) CMEs with comparatively larger acceleration in the low corona are associated with soft X-ray flares of higher energy; the typical acceleration of a CME associated with X1.0 class soft X-ray flare being ≈1020 m s−2, and (2) CMEs with comparatively higher speed in the low corona slow down quickly at large distances from the Sun—the deceleration of a CME with a typical speed of 1000 km s−1 being ≈−15 m s−2 in the distance range of ≈3–32 *R*_.

ESTIMATION OF MAGNETIC FIELD IN THE SOLAR CORONAL STREAMERS THROUGH LOW FREQUENCY RADIO OBSERVATIONS

R. **Ramesh**, C. Kathiravan, and Ch. V. Sastry1
Astrophysical Journal, 711:1029–1032, **2010** March

The observations of circularly polarized thermal radio emission from solar coronal streamers at two low frequencies, viz., 77 and 109 MHz, are used to estimate the magnetic field strength (*B*) at their corresponding radial distances *r* ≈ 1.7 and 1.5 solar radii given by the electron density model of Newkirk. The estimated values of *B* at the above two distances are ≈ 5 ± 1 G and 6 ± 2 G, respectively.

A Low-Frequency (30 – 110 MHz) Antenna System for Observations of Polarized Radio Emission from the Solar Corona

R. **Ramesh** · C. Kathiravan · M.S. SundaraRajan · Indrajit V. Barve · C.V. Sastry
Solar Phys (**2008**) 253: 319–327

An interferometer antenna system to observe polarized radio emission from the solar corona at different frequencies in the range 30 – 110 MHz has been commissioned recently by the Indian Institute of Astrophysics at the Gauribidanur Radio Observatory (latitude 13fl36_12__N and longitude 77fl27_07__E), about 100 km north of Bangalore (http://www.iiap.res.in/centres_radio.htm). This paper describes the antenna system, associated analog/digital receiver setup, calibration scheme, and preliminary results.

The Gauribidanur Radioheliograph

R. **Ramesh**, K. R. Subramanian, M. S. SundaraRajan & Ch. V. Sastry
Solar Physics volume 181, pages439–453(**1998**)
https://link.springer.com/content/pdf/10.1023/A:1005075003370.pdf
A new radio heliograph for obtaining two-dimensional images of the solar corona sequentially at many frequencies in the range 40–150 MHz has been built by the Indian Institute of Astrophysics at the Gauribidanur Radio Observatory (lat. 13°36′12″ N and long. 77°27′07″ E) about 100 km north of Bangalore, India. This paper describes various aspects of the antenna system, receiver front end, digital hardware, the data acquisition and the calibration procedure. The performance of the instrument is illustrated with maps of the continuum emission from the undisturbed corona at different frequencies.

Center-to-Limb Variation of Solar Bursts Polarization at Millimeter Wavelengths

R. F. Hidalgo **Ramírez**, A. Morosi, D. Silva, P. J. A. Simoẽs, A. Valio
Solar Physics August **2019**, 294:108
sci-hub.se/10.1007/s11207-019-1503-x
Polarization of radio emission from solar flares provides essential information about plasma regimes confined to magnetic field in quiescent, pre-explosion, sudden energy release and decay phases. Observations of polarization are carried out continuously by the first time at two millimeter wavelengths of 6.67 and 3.34 mm (45 and 90 GHz, respectively) by two solar radio polarimeters named POEMAS operating at El Leoncito Observatory, Argentinian Andes. A total of 30 solar flares observed by the radio polarimeters, between 2012 and 2013, were analyzed. The degree of polarization was observed to increase and then decrease as the heliocentric angle increased. We found a weak correlation between the bursts' flux density and their heliocentric angle, i.e. solar bursts with higher flux density slightly tend to occur near the limb. **2012/07/10, 2013/11/05**
Table 1 List of solar bursts observed by POEMAS solar radio polarimeters between 2012 and 2013.

Large scale simulations of solar type III radio bursts: flux density, drift rate, duration and bandwidth

H. **Ratcliffe**, E. P. Kontar, H.A.S. Reid
2014 A&A 572, A111
http://arxiv.org/pdf/1410.2410v1.pdf
Non-thermal electrons accelerated in the solar corona can produce intense coherent radio emission, known as solar type III radio bursts. This intense radio emission is often observed from hundreds of MHz in the corona down to the tens of kHz range in interplanetary space. It involves a chain of physical processes from the generation of Langmuir waves to nonlinear processes of wave-wave interaction. We develop a self-consistent model to calculate radio emission from a non-thermal electron population over large frequency range, including the effects of electron transport, Langmuir wave-electron interaction, the evolution of Langmuir waves due to non-linear wave-wave interactions, Langmuir wave conversion into electromagnetic emission, and finally escape of the electromagnetic waves. For the first time we simulate escaping radio emission over a broad frequency range from 500~MHz down to a few MHz and infer key properties of the radio emission observed: the onset (starting) frequency, {identification as fundamental or harmonic emission}, peak flux density, instantaneous frequency bandwidth, and timescales for rise and decay. Comparing with the observations, these large scale simulations enable us to identify the processes governing the key type III solar radio burst characteristics.

Plasma radio emission from inhomogeneous collisional plasma of a flaring loop

Heather **Ratcliffe**, Eduard. P. Kontar
E-print, Dec **2013**, A&A, 562, A57 (**2014**)
The evolution of a solar flare accelerated non-thermal electron population and associated plasma emission is considered in collisional inhomogeneous plasma. Non-thermal electrons collisionally evolve to become unstable and generate Langmuir waves, which may lead to intense radio emission. We self-consistently simulated the collisional relaxation of electrons, wave-particle interactions, and non-linear Langmuir wave evolution in plasma with density fluctuations. Additionally, we simulated the scattering, decay, and coalescence of the Langmuir waves which produce radio emission at the fundamental or the harmonic of the plasma frequency, using an angle-averaged emission model. Long-wavelength density fluctuations, such as are observed in the corona, are seen to strongly suppress the levels of radio emission, meaning that a high level of Langmuir waves can be present without visible radio emission. Additionally, in

homogeneous plasma, the emission shows time and frequency variations that could be smoothed out by density inhomogeneities.

DENSITY FLUCTUATIONS AND THE ACCELERATION OF ELECTRONS BY BEAM-GENERATED LANGMUIR WAVES IN THE SOLAR CORONA
H. **Ratcliffe**, N. H. Bian, and E. P. Kontar
2012 ApJ 761 176
Non-thermal electron populations are observed throughout the heliosphere. The relaxation of an electron beam is known to produce Langmuir waves which, in turn, may substantially modify the electron distribution function. As the Langmuir waves are refracted by background density gradients and as the solar and heliospheric plasma density is naturally perturbed with various levels of inhomogeneity, the interaction of Langmuir waves with non-thermal electrons in inhomogeneous plasmas is an important topic. We investigate the role played by ambient density fluctuations on the beam-plasma relaxation, focusing on the effect of acceleration of beam electrons. The scattering of Langmuir waves off turbulent density fluctuations is modeled as a wavenumber diffusion process which is implemented in numerical simulations of the one-dimensional quasilinear kinetic equations describing the beam relaxation. The results show that a substantial number of beam electrons are accelerated when the diffusive timescale in wavenumber space τ D is of the order of the quasilinear timescale τql, while when τ D τql, the beam relaxation is suppressed. Plasma inhomogeneities are therefore an important means of energy redistribution for waves and hence electrons, and so must be taken into account when interpreting, for example, hard X-ray or Type III emission from flare-accelerated electrons.

Glasgow Callisto optimistic: first light comes in focus
Heather **Ratcliffe**, Eduard Kontar
RHESSI Science Nugget No. 187, Oct **2012**
A Callisto radio spectrometer was recently (October 2nd) installed at Glasgow's Acre Road Observatory, and began observing a few days later. Here we present the first-light observations and a second burst observed simultaneously by Callisto and RHESSI.

Joint Measurements of Flare Flux Densities at 210 – 212 GHz by Two Different Radio Telescopes
J.-P. **Raulin**, G. Trottet, G. Giménez de Castro, T. Lüthi, P. Kaufmann
Solar Physics, April **2014**, Volume 289, Issue 4, pp 1227-1237
Multiple-beam observations of solar flares at submillimeter wavelengths need detection with at least four beams to derive the flux density F of the emitting source, its size, and centroid position. When this condition is not fulfilled, the assumptions on the location and/or size of the emitting source have to be made in order to compute F . Otherwise, only a flux density range ΔF can be estimated. We report on simultaneous flare observations at 212 and 210 GHz obtained by the Solar Submillimeter Telescope (SST) and the Bernese Multibeam Radiometer for Kosma (BEMRAK), respectively, during two solar events on **28 October 2003**. For both events, BEMRAK utilized four beam information to calculate the source flux density F 210, its size and position. On the other hand, the SST observed the events with only one beam, at low solar elevation angles and during high atmospheric attenuation. Therefore, because of these poor observing conditions at 212 GHz, only a flux density range ΔF 212 could be estimated. The results show that ΔF 212 is within a factor of 2.5 of the flux density F 210. This factor can be significantly reduced (e.g. 1.4 for one of the studied events) by an appropriate choice of the 212 GHz source position using flare observations at other wavelengths. By adopting the position and size of the 210 GHz source measured by BEMRAK, the flux density at 212 GHz, F 212b, is comparable to F 210 within the uncertainties, as expected. Therefore our findings indicate that even during poor observing conditions, the SST can provide an acceptable estimate of the flux density at 212 GHz. This is a remarkable fact since the SST and BEMRAK use quite different procedures for calibration and flux density determination. We also show that the necessary assumptions made on the size of the emitting source at 212 GHz in order to estimate its flux density are not critical, and therefore do not affect the conclusions of previous studies at this frequency.

On Solar Intermediate Drift Radio Bursts at Decimeter and Meter Wavelength
G. **Rausche** · H. Aurass · G. Mann · M. Karlický · C. Vocks
Solar Phys (**2007**) 245: 327–343
http://www.springerlink.com/content/t16x724v7u903811/fulltext.pdf
Fiber – or intermediate drift – bursts are a continuum fine structure in some complex solar radio events. We present the analysis of such bursts in the X17 flare on **28 Oct. 2003**. Based on the whistler wave model of fiber bursts we derive the 3D magnetic field structures that carry the radio sources in different stages of the event and obtain insight into the energy release evolution in the main flare phase, the related paths of nonthermal particle propagation in the corona, and the involved magnetic field structures. Additionally, we test the whistler wave model of fiber bursts for the meter and the decimeter wave range.

It gives new insight into particle acceleration and propagation in the low flare and post-CME corona.

Analysis of a Type II Solar Radio Burst Observedon 20 October 2017

Whitham D. **Reeve**
ISWI Newsletter - Vol. 10 No. 006, **2018**
http://files.mail-list.com/m/iswinewsletter/Reeve-TypeII-Burst.pdf

Hot Plasma Flows and Oscillations in the Loop-top Region During the September 10 2017 X8.2 Solar Flare

Katharine K. **Reeves**, Vanessa Polito, Bin Chen, Giselle Galan, Sijie Yu, Wei Liu, Gang Li
ApJ **2020**
https://arxiv.org/pdf/2010.12049.pdf
In this study, we investigate motions in the hot plasma above the flare loops during the 2017 September 10 X8.2 flare event. We examine the region to the south of the main flare arcade, where there is data from the Interface Region Imaging Spectrograph (IRIS), and the Extreme ultraviolet Imaging Spectrometer (EIS) on Hinode. We find that there are initial blue shifts of 20--60 km/s observed in this region in the Fe XXI line in IRIS and the Fe XXIV line in EIS, and that the locations of these blue shifts move southward along the arcade over the course of about 10 min. The cadence of IRIS allows us to follow the evolution of these flows, and we find that at each location where there is an initial blue shift in the Fe XXIV line, there are damped oscillations in the Doppler velocity with periods of ~400 s. We conclude that these periods are independent of loop length, ruling out magnetoacoustic standing modes as a possible mechanism. Microwave observations from the Expanded Owens Valley Solar Array (EOVSA) indicate that there are non-thermal emissions in the region where the Doppler shifts are observed, indicating that accelerated particles are present. We suggest that the flows and oscillations are due to motions of the magnetic field that are caused by reconnection outflows disturbing the loop-top region.

A new approach to the maser emission in the solar corona

Stephane **Regnier**
A&A **2015**
http://arxiv.org/pdf/1507.07350v1.pdf
The electron plasma frequency ωpe and electron gyrofrequency Ωe are two parameters that allow us to describe the properties of a plasma and to constrain the physical phenomena at play, for instance, whether a maser instability develops. In this paper, we aim to show that the maser instability can exist in the solar corona. We perform an in-depth analysis of the ωpe/Ωe ratio for simple theoretical and complex solar magnetic field configurations. Using the combination of force-free models for the magnetic field and hydrostatic models for the plasma properties, we determine the ratio of the plasma frequency to the gyrofrequency for electrons. For the sake of comparison, we compute the ratio for bipolar magnetic fields containing a twisted flux bundle, and for four different observed active regions. We also study how ωpe/Ωe is affected by the potential and non-linear force-free field models. We demonstrate that the ratio of the plasma frequency to the gyrofrequency for electrons can be estimated by this novel method combining magnetic field extrapolation techniques and hydrodynamic models. Even if statistically not significant, values of $\omega pe/\Omega e \leq 1$ are present in all examples, and are located in the low corona near to photosphere below one pressure scale-height and/or in the vicinity of twisted flux bundles. The values of ωpe/Ωe are lower for non-linear force-free fields than potential fields, thus increasing the possibility of maser instability in the corona. From this new approach for estimating ωpe/Ωe, we conclude that the electron maser instability can exist in the solar corona above active regions. The importance of the maser instability in coronal active regions depends on the complexity and topology of the magnetic field configurations.
AR8151, AR8210, 2000 July 14, October-November 2003

Coronal Alfvén speeds in an isothermal atmosphere. I. Global properties

S. **Régnier**, E. R. Priest, and A. W. Hood
A&A 491, 297-309 (**2008)**, DOI: 10.1051/0004-6361:200810362
Aims. Estimating Alfvén speeds is of interest in modelling the solar corona, studying the coronal heating problem and understanding the initiation and propagation of coronal mass ejections (CMEs).
Methods. We assume here that the corona is in a magnetohydrostatic equilibrium and that, because of the low plasma β, one may decouple the magnetic forces from pressure and gravity. The magnetic field is then described by a force-free field for which we perform a statistical study of the magnetic field strength with height for four different active regions. The plasma along each field line is assumed to be in a hydrostatic equilibrium. As a first approximation, the coronal plasma is assumed to be isothermal with a constant or varying gravity with height. We study a bipolar magnetic field with a ring distribution of currents, and apply this method to four active regions associated with different eruptive events.
Results. By studying the global properties of the magnetic field strength above active regions, we conclude that (i) most

of the magnetic flux is localized within 50 Mm of the photosphere; (ii) most of the energy is stored in the corona below 150 Mm; (iii) most of the magnetic field strength decays with height for a nonlinear force-free field slower than for a potential field. The Alfvén speed values in an isothermal atmosphere can vary by two orders of magnitude (up to 100 000 km s^{-1}). The global properties of the Alfvén speed are sensitive to the nature of the magnetic configuration. For an active region with highly twisted flux tubes, the Alfvén speed is significantly increased at the typical height of the twisted flux bundles; in flaring regions, the average Alfvén speeds are above 5000 km s^{-1} and depart highly from potential field values.
Conclusions. We discuss the implications of this model for the reconnection rate and inflow speed, the coronal plasma β and the Alfvén transit time.

Numerical and Analytical Study of Electron Plasma Waves in Nonthermal Vasyliunas-Cairns Distributed Plasmas

Aman ur **Rehman**, Muhammad A. Shahzad, Shahzad Mahmood, Muhammad Bilal
JGR Volume126, Issue8 August **2021** e2021JA029626
https://agupubs.onlinelibrary.wiley.com/doi/epdf/10.1029/2021JA029626
https://doi.org/10.1029/2021JA029626
The Poison-Vlasov model in plasma kinetic theory is taken into account to study the propagation of electron plasma waves (or Langmuir waves) in hot, un-magnetized Vasyliunas-Cairns distributed plasmas (VCDPs). The longitudinal dielectric plasma response function is obtained for such nonthermal plasmas. The Landau damping rate of Langmuir waves (LWs) in nonthermal VCDP, which propagates with a phase speed greater than the effective thermal speed of the electrons, is also studied. The real and imaginary parts of the wave frequency are investigated analytically as well as numerically and a comparison between the numerical and analytical results is presented. The finding reveals that the dispersion curve and damping rate of the wave are significantly influenced by the simultaneous presence of two nonthermality parameters, that is, $'\alpha'$ and $'\kappa'$ (spectral index) in the hybrid (Vasyliunas-Cairns) distributed plasmas. It is discussed that results are quite distinctive from that obtained in nonthermal plasmas that have sole presence of either of the nonthermality parameters $'\alpha'$ or super-thermality spectral index $'\kappa'$ in Cairns or kappa distributed electron plasmas, respectively. The more realistic form of 3D and reduced 1D distribution function of VCDP has been used to analyze LWs in describing nonthermal plasmas with more energetic electron in VCDP case.

Fine structure of type III solar radio bursts from Langmuir wave motion in turbulent plasma

Hamish A. S. **Reid**, Eduard P. Kontar
2021 *Nature Astronomy*
https://doi.org/10.1038/s41550-021-01370-8
https://arxiv.org/pdf/2103.08424.pdf
The Sun frequently accelerates near-relativistic electron beams that travel out through the solar corona and interplanetary space. Interacting with their plasma environment, these beams produce type III radio bursts, the brightest astrophysical radio sources seen from the Earth. The formation and motion of type III fine frequency structures is a puzzle but is commonly believed to be related to plasma turbulence in the solar corona and solar wind. Combining a theoretical framework with kinetic simulations and high-resolution radio type III observations using the Low Frequency Array, we quantitatively show that the fine structures are caused by the moving intense clumps of Langmuir waves in a turbulent medium. Our results show how type III fine structure can be used to remotely analyse the intensity and spectrum of compressive density fluctuations, and can infer ambient temperatures in astrophysical plasma, both significantly expanding the current diagnostic potential of solar radio emission. **16th April 2015, 24th June 2015, 16th September 2015**
CESRA nuggets #3028 2021 https://www.astro.gla.ac.uk/users/eduard/cesra/?p=3028

A review of recent type III imaging spectroscopy **Review**

Hamish A. **Reid**
Front. Astron. Space Sci. 7: 56 **2020**
https://sci-hub.st/https://doi.org/10.3389/fspas.2020.00056
https://doi.org/10.3389/fspas.2020.00056
https://www.frontiersin.org/articles/10.3389/fspas.2020.00056/full
Solar type III radio bursts are the most common impulsive radio signatures from the Sun, stimulated by electron beams travelling through the solar corona and solar wind. Type III burst analysis provides us with a powerful remote sensing diagnostic tool for both the electron beams and the plasma they travel through. Advanced radio telescopes like the LOw Frequency ARray (LOFAR), the Murchison Widefield Array (MWA) and the Karl G. Jansky Very Large Array (VLA) are now giving us type III imaging spectroscopy with orders of magnitude better resolution than before. In this review, the recent observational progress provided by the new observations is discussed, including how this enhanced resolution has facilitated study of type III burst fine structure. The new results require more detailed theoretical understanding of how type III bursts are produced. Consequently, recent numerical work is discussed which improves our understanding of how electron beams, Langmuir waves and radio waves evolve through the turbulent solar system plasma. Looking

towards the future, some theoretical challenges are discussed that we need to overcome on our quest to understand type III bursts and the electron beams that drive them.

Spatial expansion and speeds of type III electron beam sources in the solar corona

Hamish A. S. **Reid**, Eduard P. Kontar
ApJ **867** 158 **2018**
https://arxiv.org/pdf/1809.00887.pdf
http://iopscience.iop.org/article/10.3847/1538-4357/aae5d4/pdf
A component of space weather, electron beams are routinely accelerated in the solar atmosphere and propagate through interplanetary space. Electron beams interact with Langmuir waves resulting in type III radio bursts. Electron beams expand along the trajectory, and using kinetic simulations, we explore the expansion as the electrons propagate away from the Sun. Specifically, we investigate the front, peak and back of the electron beam in space from derived radio brightness temperatures of fundamental type III emission. The front of the electron beams travelled at speeds from 0.2c--0.7c, significantly faster than the back of the beam that travelled between 0.12c--0.35c. The difference in speed between the front and the back elongates the electron beams in time. The rate of beam elongation has a 0.98 correlation coefficient with the peak velocity; in-line with predictions from type III observations. The inferred speeds of electron beams initially increase close to the acceleration region and then decrease through the solar corona. Larger starting densities and harder initial spectral indices result in longer and faster type III sources. Faster electron beams have higher beam energy densities, produce type IIIs with higher peak brightness temperatures and shorter FWHM durations. Higher background plasma temperatures also increase speeds, particularly at the back of the beam. We show how our predictions of electron beam evolution influences type III bandwidth and drift-rates. Our radial predictions of electron beam speed and expansion can be tested by the upcoming in situ electron beam measurements made by Solar Orbiter and Parker Solar Probe.

Solar type III radio burst time characteristics at LOFAR frequencies and the implications for electron beam transport

Hamish A. S. **Reid**, Eduard P. Kontar
A&A 614, A69 **2018**
https://arxiv.org/pdf/1802.01507.pdf
https://www.aanda.org/articles/aa/pdf/2018/06/aa32298-17.pdf
Solar type III radio bursts contain a wealth of information about the dynamics of electron beams in the solar corona and the inner heliosphere; currently unobtainable through other means. However, the motion of different regions of an electron beam (front, middle and back) have never been systematically analysed before. We characterise the type III burst frequency-time evolution using the enhanced resolution of LOFAR in the frequency range 30 to 70 MHz and use this to probe electron beam dynamics. Methods. The rise, peak and decay times with a 0.2 MHz spectral resolution were defined for a collection of 31 type III bursts. The frequency evolution is used to ascertain the apparent velocities of the front, middle and back of the type III sources and the trends are interpreted using theoretical and numerical treatments. The type III time profile was better approximated by an asymmetric Gaussian profile, not an exponential as previously used. Rise and decay times increased with decreasing frequency and showed a strong correlation. Durations were smaller than previously observed. Drift rates from the rise times were faster than from the decay times, corresponding to inferred mean electron beam speeds for the front, middle and back of 0.2, 0.17, 0, 15 c, respectively. Faster beam speeds correlate with smaller type III durations. We also find type III frequency bandwidth decreases as frequency decreases. The different speeds naturally explain the elongation of an electron beam in space as it propagates through the heliosphere. The rate of expansion is proportional to the mean speed of the exciter; faster beams expand faster. Beam speeds are attributed to varying ensembles of electron energies at the front, middle and back of the beam.
16-Sep-15

Imaging Spectroscopy of Type U and J Solar Radio Bursts with LOFAR

Hamish A. S. **Reid**, Eduard P. Kontar
A&A 606, A141 **2017**
https://arxiv.org/pdf/1706.07410.pdf
Context. Radio U-bursts and J-bursts are signatures of electron beams propagating along magnetic loops confined to the corona. The more commonly observed type III radio bursts are signatures of electron beams propagating along magnetic loops that extend into interplanetary space. Given the prevalence of solar magnetic flux to be closed in the corona, why type III bursts are more frequently observed than U-bursts or J-bursts is an outstanding question.
Aims. We use Low-Frequency Array (LOFAR) imaging spectroscopy between 30–80 MHz of low-frequency U-bursts and J-bursts, for the first time, to understand why electron beams travelling along coronal loops produce radio emission less often. Radio burst observations provide information not only about the exciting electron beams but also about the structure of large coronal loops with densities that are too low for standard extreme ultraviolet (EUV) or X-ray analysis.
Methods. We analysed LOFAR images of a sequence of two J-bursts and one U-burst. The different radio source positions were used to model the spatial structure of the guiding magnetic flux tube and then deduce the energy range of

the exciting electron beams without the assumption of a standard density model. We also estimated the electron density along the magnetic flux rope and compared it to coronal models.
Results. The radio sources infer a magnetic loop that is 1 solar radius in altitude with the highest frequency sources starting around 0.6 solar radii. Electron velocities were found between 0.13 c and 0.24 c with the front of the electron beam travelling faster than the back of the electron beam. The velocities correspond to energy ranges within the beam from 0.7–11 keV to 0.7–43 keV. The density along the loop is higher than typical coronal density models and the density gradient is smaller.
Conclusions. We found that a more restrictive range of accelerated beam and background plasma parameters can result in U-bursts or J-bursts, causing type III bursts to be more frequently observed. The large instability distances required before Langmuir waves are produced by some electron beams, and the small magnitude of the background density gradients makes closed loops less facilitative for radio emission than loops that extend into interplanetary space.
6th May 2015
UKSP Nugget: # 87 Feb 2018 http://www.uksolphys.org/uksp-nugget/87-giant-solar-loops-and-lofar-radio-observations/

Langmuir Wave Electric Fields Induced by Electron Beams in the Heliosphere

Hamish A. S. **Reid**, Eduard P. Kontar
A&A 598, A44 (**2017**)
https://arxiv.org/pdf/1611.07901v1.pdf
Solar electron beams responsible for type III radio emission generate Langmuir waves as they propagate out from the Sun. The Langmuir waves are observed via in-situ electric field measurements. These Langmuir waves are not smoothly distributed but occur in discrete clumps, commonly attributed to the turbulent nature of the solar wind electron density. Exactly how the density turbulence modulates the Langmuir wave electric fields is understood only qualitatively. Using weak turbulence simulations, we investigate how solar wind density turbulence changes the probability distribution functions, mean value and variance of the beam-driven electric field distributions. Simulations show rather complicated forms of the distribution that are dependent upon how the electric fields are sampled. Generally the higher magnitude of density fluctuations reduce the mean and increase the variance of the distribution in a consistent manor to the predictions from resonance broadening by density fluctuations. We also demonstrate how the properties of the electric field distribution should vary radially from the Sun to the Earth and provide a numerical prediction for the in-situ measurements of the upcoming Solar Orbiter and Solar Probe Plus spacecraft.
See CESRA Highlight #1209 Feb **2017** http://www.astro.gla.ac.uk/users/eduard/cesra/?p=1209

Coronal type III radio bursts and their X-ray flare and interplanetary type III counterparts

Hamish A. S. **Reid**, Nicole Vilmer
A&A 597, A77 **2017**
http://arxiv.org/pdf/1609.04743v1.pdf
Type III bursts and hard X-rays are both produced by flare energetic electron beams. The link between both emissions has been investigated in many previous studies, but no statistical studies have compared both coronal and interplanetary type III bursts with X-ray flares. Using coronal radio events above 100 MHz exclusively from type III bursts, we revisited long-standing questions: Do all coronal type III bursts have X-ray counterparts. What correlation, if any, occurs between radio and X-ray intensities. What X-ray and radio signatures above 100 MHz occur in connection with interplanetary type III bursts below 14 MHz. We analysed data from 2002 to 2011 starting with coronal type III bursts above 100 MHz. We used RHESSI X-ray data greater than 6 keV to make a list of 321 events that have associated type III bursts and X-ray flares, encompassing at least 28 percent of the initial sample of type III events. We examined the timings, intensities, associated GOES class, and any interplanetary radio signature. For our 321 events, the X-ray emission at 6 keV usually lasted longer than type III burst groups at frequencies greater than 100 MHz. A weak correlation was found between the type III radio flux at frequencies below 327 MHz and the X-ray intensity at 25-50 keV, with an absence of events at high X-ray intensity and low type III radio flux. Interplanetary type III bursts less than 14 MHz were observed for 54 percent of the events, increasing when events were observed with 25-50 keV X-rays. A stronger interplanetary association was present when 25-50 keV count rates were above 250 counts per second or 170 MHz fluxes were greater than 1000 SFU, relating to more energetic electrons above 25 keV and events where magnetic flux tubes extend into the high corona. On average type III bursts increase in flux with decreasing frequency, the rate varies from event to event. **20 Feb 2002, 02 Aug 2005, 12 Dec 2011**

Statistical Link Between Electrons Emitting X-rays and Type III Radio Bursts

Hamish A. S. **Reid**, Nicole Vilmer
RHESSI Science Nuggets #288 Dec **2016**
http://sprg.ssl.berkeley.edu/~tohban/wiki/index.php/Statistical_Link_Between_Electrons_Emitting_X-rays_and_Type_III_Radio_Bursts
Correlations across the radio and X-ray spectra imply related populations of source electrons. Click the title to read more.

Statistical studies on the link between X-rays and type III bursts have been performed over the years, but few have dealt with the correlation between type III bursts in the corona and interplanetary type III bursts - a comparison of meter waves and hectometer/kilometer waves (see Ref. [2]). We revisit here the hard X-ray-type III burst connection based on ten years of data obtained respectively with RHESSI, the Nançay Radioheliograph, the PHOENIX2 and 3 instruments, and the WAVES experiment on WIND
10 March 2003

Solar flare accelerated electrons from high and low radio frequencies

Hamish **Reid**∗†1 and Larisa Kashapova2
CESRA **2016** p.77
http://cesra2016.sciencesconf.org/conference/cesra2016/pages/CESRA2016_prog_abs_book_v3.pdf
Electrons accelerated during solar flares are known to produce microwaves at GHz frequencies through the gyrosynchrotron mechanism and type III radio bursts at MHz and kHz frequencies through plasma emission. Despite of their common origin, these frequency ranges are rarely analysed together. We examine the solar flare on the **29th June 2012** in radio frequencies over six orders of magnitude from 16 GHz to 20 kHz to understand better the spatial, temporal and spectral properties of the flare electron acceleration. Of particular interest in the flare is the fine structure observed in the gyrosynchrotron emission. We find this correlates with the type III emission above 100 MHz on scales of a few seconds indicating to a common accelerator. We found that peaks of the type III emission time profiles are delayed with respect to the peaks seen in the gyrosynchrotron. Using this delay and the radio image centroids we infer the location of an acceleration region in the low corona, close to the gyrosynchrotron emission.

Large coronal loops and solar radio J-bursts imaged using LOFAR

Hamish **Reid**∗†1 and Eduard Kontar
CESRA Abstract **2016**
http://cesra2016.sciencesconf.org/conference/cesra2016/pages/CESRA2016_prog_abs_book_v1.pdf
Solar radio U or J-bursts are believed to be signatures of electron beams propagating along closed magnetic loops. Although, like type III bursts they are generated by electron beams, J-bursts are rather rare events. J-bursts with a turnover around 40 MHz imply large magnetic loops on the scale of a solar radius. The density in such loops is normally too low for EUV or X-ray observations. Using LOFAR between 30-80 MHz we image a sequence of three J-bursts with a continuous frequency coverage, a huge improvement over the previous observations. From the centroids of the radio sources we obtain a fit to a magnetic loop of 1 solar radii in altitude and around 1.4 solar radii in length from base to apex. The density within the magnetic loop appears much higher and varying slower than the density models inferred from type III radio bursts. Such conditions could be the reason why we do not observe as many J-bursts or U-bursts as we would expect from the closed magnetic flux in the low corona.

Stopping frequency of type III solar radio bursts in expanding magnetic flux tubes

Hamish A. S. **Reid** & Eduard P. Kontar
A&A **577, A124 2015**
http://arxiv.org/pdf/1503.03395v1.pdf
Understanding the properties of type III radio bursts in the solar corona and interplanetary space is one of the best ways to remotely deduce the characteristics of solar accelerated electron beams and the solar wind plasma. One feature of all type III bursts is the lowest frequency they reach (or stopping frequency). This feature reflects the distance from the Sun that an electron beam can drive the observable plasma emission mechanism. The stopping frequency has never been systematically studied before from a theoretical perspective. Using numerical kinetic simulations, we explore the different parameters that dictate how far an electron beam can travel before it stops inducing a significant level of Langmuir waves, responsible for plasma radio emission. We use the quasilinear approach to model the resonant interaction between electrons and Langmuir waves self-consistently in inhomogeneous plasma, and take into consideration the expansion of the guiding magnetic flux tube and the turbulent density of the interplanetary medium. We find that the rate of radial expansion has a significant effect on the distance an electron beam travels before enhanced levels of Langmuir waves, hence radio waves, cease. Radial expansion of the guiding magnetic flux tube rarefies the electron stream to the extent that the density of non-thermal electrons is too low to drive Langmuir wave production. The initial conditions of the electron beam have a significant effect, where decreasing the beam density or increasing the spectral index of injected electrons would cause higher type III stopping frequencies. We also demonstrate how the intensity of large-scale density fluctuations increases the highest frequency to which Langmuir waves can be driven by the beam and how the magnetic field geometry can be the cause of type III bursts that are only observed at high coronal frequencies. **16 Feb 2014**

Solar Physics during the March 2015 Solar Eclipse

Hamish **Reid** and Hugh Hudson
RHESSI Science Nugget No. 247, March **2015**
http://sprg.ssl.berkeley.edu/~tohban/wiki/index.php/Solar_Physics_during_the_March_2015_Solar_Eclipse
A total solar eclipse is coming on 2015 March 20, presenting a good opportunity for many observatories - in particular, European radio observatories.

The low-high-low trend of type III radio burst starting frequencies and solar flare hard X-rays⋆

Hamish A. S. **Reid**1,2, Nicole Vilmer1 and Eduard P. Kontar
A&A 567, A85 (**2014**)
Aims. Using simultaneous X-ray and radio observations from solar flares, we investigate the link between the type III radio burst starting frequency and hard X-ray spectral index. For a proportion of events the relation derived between the starting height (frequency) of type III radio bursts and the electron beam velocity spectral index (deduced from X-rays) is used to infer the spatial properties (height and size) of the electron beam acceleration region. Both quantities can be related to the distance travelled before an electron beam becomes unstable to Langmuir waves.
Methods. To obtain a list of suitable events we considered the RHESSI catalogue of X-ray flares and the Phoenix 2 catalogue of type III radio bursts. From the 200 events that showed both type III and X-ray signatures, we selected **30 events which had simultaneous emission in both wavelengths**, good signal to noise in the X-ray domain and >20 s duration.
Results. We find that >50% of the selected events show a good correlation between the starting frequencies of the groups of type III bursts and the hard X-ray spectral indices. A low-high-low trend for the starting frequency of type III bursts is frequently observed. Assuming a background electron density model and the thick target approximation for X-ray observations, this leads to a correlation between starting heights of the type III emission and the beam electron spectral index. Using this correlation we infer the altitude and vertical extents of the flare acceleration regions. We find heights from 183 Mm down to 25 Mm while the sizes range from 13 Mm to 2 Mm. These values agree with previous work that places an extended flare acceleration region high in the corona. We also analyse the assumptions that are required to obtain our estimates and explore possible extensions to our assumed model. We discuss these results with respect to the acceleration heights and sizes derived from X-ray observations alone.

A Review of Solar Type III Radio Bursts

Hamish A. S. **Reid**, Heather Ratcliffe
Research in Astronomy and Astrophysics, Volume 14, Number 7, 773-804, **2014, File**
http://arxiv.org/pdf/1404.6117v1.pdf
Solar type III radio bursts are an important diagnostic tool in the understanding of solar accelerated electron beams. They are a signature of propagating beams of nonthermal electrons in the solar atmosphere and the solar system. Consequently, they provide information on electron acceleration and transport, and the conditions of the background ambient plasma they travel through. We review the observational properties of type III bursts with an emphasis on recent results and how each property can help identify attributes of electron beams and the ambient background plasma. We also review some of the theoretical aspects of type III radio bursts and cover a number of numerical efforts that simulate electron beam transport through the solar corona and the heliosphere.

The Low-High-Low Starting Frequency Trend in Groups of Type III Bursts," by Hamish Reid. The type III radio bursts echo the pattern of flare energy release.

Hamish **Reid**
RHESSI Science Nuggets, #242, December **2014**
The type III radio bursts echo the pattern of flare energy release. **10-Mar-2003, 18-Mar-2003**

The Low-High-Low Trend of Type III Radio Burst Starting Frequencies and Solar Flare Hard X-rays

Hamish A. S. **Reid**, Nicole Vilmer, Eduard P. Kontar
A&A, **2014**
http://arxiv.org/pdf/1403.1839v1.pdf
Using simultaneous X-ray and radio observations from solar flares, we investigate the link between the type III radio burst starting frequency and hard X-ray spectral index. For a proportion of events the relation derived between the starting height (frequency) of type III radio bursts and the electron beam velocity spectral index (deduced from X-rays) is used to infer the spatial properties (height and size) of the electron beam acceleration region. Both quantities can be related to the distance travelled before an electron beam becomes unstable to Langmuir waves. To obtain a list of suitable events we considered the RHESSI catalogue of X-ray flares and the Phoenix 2 catalogue of type III radio bursts. From the 200 events that showed both type III and X-ray signatures, we selected 30 events which had simultaneous emission in both wavelengths, good signal to noise in the X-ray domain and > 20 seconds duration. We

find that > 50 % of the selected events show a good correlation between the starting frequencies of the groups of type III bursts and the hard X-ray spectral indices. A low-high-low trend for the starting frequency of type III bursts is frequently observed. Assuming a background electron density model and the thick target approximation for X-ray observations, this leads to a correlation between starting heights of the type III emission and the beam electron spectral index. Using this correlation we infer the altitude and vertical extents of the flare acceleration regions. We find heights from 183 Mm down to 25 Mm while the sizes range from 13 Mm to 2 Mm. These values agree with previous work that places an extended flare acceleration region high in the corona. We analyse the assumptions required and explore possible extensions to our assumed model. We discuss these results with respect to the acceleration heights and sizes derived from X-ray observations alone**. Table**
14-Feb- 2002,20-Feb-2002, 19-Jul-2002, 10-Mar-2003, 18-Mar-2003, 26 Apr-2003, 9-Jun-2003, 9-Jul-2003, 22-Oct-2003, 28-May-2004, 25 Jul-2004

Evolution of the Solar Flare Energetic Electrons in the Inhomogeneous Inner Heliosphere

Hamish A. S. **Reid**, Eduard P. Kontar
Solar Physics, July **2013**, Volume 285, Issue 1-2, pp 217-232
E-print, Oct **2012**
Solar flare accelerated electrons escaping into the interplanetary space and seen as type III solar radio bursts are often detected near the Earth. Using numerical simulations we consider the evolution of energetic electron spectrum in the inner heliosphere and near the Earth. The role of Langmuir wave generation, heliospheric plasma density fluctuations, and expansion of magnetic field lines on the electron peak flux and fluence spectra is studied to predict the electron properties as could be observed by Solar Orbiter and Solar Probe Plus. Considering various energy loss mechanisms we show that the substantial part of the initial energetic electron energy is lost via wave–plasma processes due to plasma inhomogeneity. For the parameters adopted, the results show that the electron spectrum changes mostly at the distances before ~ 20 R ⊙. Further into the heliosphere, the electron flux spectrum of electrons forms a broken power law relatively similar to what is observed at 1 AU.

Characteristics of the flare acceleration region derived from simultaneous hard X-ray and radio observations

H. A. S. **Reid**1,2, N. Vilmer2 and E. P. Kontar1
A&A, Volume 529, A66, 8 p. May **2011**
We investigate the type III radio bursts and X-ray signatures of accelerated electrons in a well-observed solar flare in order to find the spatial properties of the acceleration region. Combining simultaneous RHESSI hard X-ray flare data and radio data from Phoenix-2 and the Nançay radioheliograph, the outward transport of flare accelerated electrons is analysed. The observations show that the starting frequencies of type III bursts are anti-correlated with the HXR spectral index of solar flare accelerated electrons. We demonstrate both analytically and numerically that the type III burst starting location is dependent upon the accelerated electron spectral index and the spatial acceleration region size, but weakly dependent on the density of energetic electrons for relatively intense electron beams. Using this relationship and the observed anti-correlation, we estimate the height and vertical extent of the acceleration region, giving values of around 50 Mm and 10 Mm, respectively. The inferred acceleration height and size suggest that electrons are accelerated well above the soft X-ray loop-top, which could be consistent with the electron acceleration between 40 Mm and 60 Mm above the flaring loop.

SOLAR WIND DENSITY TURBULENCE AND SOLAR FLARE ELECTRON TRANSPORT FROM THE SUN TO THE EARTH

Hamish A. S. **Reid** and Eduard P. Kontar
2010 ApJ 721 864
Solar flare accelerated electron beams propagating away from the Sun can interact with the turbulent interplanetary media, producing plasma waves and Type III radio emission. These electron beams are detected near the Earth with a double power-law energy spectrum. We simulate electron beam propagation from the Sun to the Earth in the weak turbulent regime taking into account the self-consistent generation of plasma waves and subsequent wave interaction with density fluctuations from low-frequency MHD turbulence. The rate at which plasma waves are induced by an unstable electron beam is reduced by background density fluctuations, most acutely when fluctuations have large amplitudes or small wavelengths. This suppression of plasma waves alters the wave distribution which changes the electron beam transport. Assuming a 5/3 Kolmogorov-type power-density spectrum of fluctuations often observed near the Earth, we investigate the corresponding energy spectrum of the electron beam after it has propagated 1 AU. We find a direct correlation between the spectrum of the double power-law below the break energy and the turbulent intensity of the background

plasma. For an initial spectral index of 3.5, we find a range of spectra below the break energy between 1.6 and 2.1, with higher levels of turbulence corresponding to higher spectral indices.

New Evidence for Third Harmonic Electromagnetic Radiation in Interplanetary Type III Solar Radio Bursts

M. J. **Reiner**, R. J. MacDowall
Solar Physics July **2019**, 294:91
sci-hub.se/10.1007/s11207-019-1476-9
This article provides new evidence for a third harmonic component in the electromagnetic radiation generated by interplanetary type III solar radio bursts observed locally near 1 AU. This evidence comes mainly from the analysis of the low-frequency radio emissions observed by the Wind spacecraft. The analysis examines, at high-time and high-frequency resolution, the local type III radiation that is occasionally observed at Wind. The associated Langmuir waves and energetic electron beams, as well as simultaneous observations from the Solar Terrestrial Relations Observatory (STEREO) and Ulysses spacecraft where possible, are used to confirm the local nature of the observed radiation and to help identify the solar origin. We find that the detection of a third harmonic component in the local type III radiation near 1 AU is exceedingly rare. However, our analyses indicate that, in addition to the more commonly observed second harmonic component, a third harmonic component is sometimes conspicuously evident in the local type III radiation. We find that the third harmonic component, when observed, is less intense than the second harmonic component, with the intensity ratio varying between 0.3 and 0.7. Sometimes the third harmonic component is expected to be detected, but it is not observed. **18 July 2001, 27 January 2002, 31 May 2003, 11 November 2011, 13 March 2012, 1 December 2013**
CESRA #2328 2019 http://www.astro.gla.ac.uk/users/eduard/cesra/?p=2328

Electron Exciter Speeds Associated with Interplanetary Type III Solar Radio Bursts

M. J. **Reiner**, R. J. MacDowall
Solar Phys. Volume 290, Issue 10, pp 2975-3004 **2015**
This article provides a comprehensive quantitative investigation of the kinematics of the electron exciters associated with interplanetary type III solar radio bursts. Detailed multispacecraft analyses of the radio and plasma wave data from the widely separated Wind and STEREO spacecraft are provided for five interplanetary type III bursts that illustrate different aspects of the problems involved in establishing the electron exciter speeds. The exciter kinematics are determined from the observed frequency drift and in-situ radiation characteristics for each type III burst. The analysis assumes propagation of the electron exciters along a Parker spiral, with origin at the associated solar active region, and curvature determined by the measured solar wind speed. The analyses take fully into account the appropriate light-propagation-time corrections from the radio source to the observing spacecraft as the exciters propagate along the Parker spiral path. For the five in-situ type III bursts analyzed in detail here, we found that their initial exciter speeds, near the Sun, ranged from 0.2c to 0.38c, where c is the speed of light. This is significantly higher than the exciter speeds derived from other recent analyses. The results presented here further suggest that the type III electron exciters normally decelerate as they propagate through the interplanetary medium. We argue based on the observations by the widely separated spacecraft that the initial part of the type III radiation usually occurs at the fundamental of the plasma frequency. Finally, we compare the results for the exciter speeds to all previous determinations and provide quantitative arguments to explain the differences.

Multipoint Observations of Solar Type III Radio Bursts from STEREO and *Wind*

M.J. **Reiner** · K. Goetz · J. Fainberg · M.L. Kaiser · M. Maksimovic · B. Cecconi · S. Hoang · S.D. Bale · J.-L. Bougeret
Solar Phys (**2009**) 259: 255–276
The twin STEREO and the *Wind* spacecraft make remote multipoint measurements of interplanetary radio sources of solar origin from widely separated vantage points. One year after launch, the angular separation between the STEREO spacecraft reached 45fl, which was ideal for locating solar type III radio sources in the heliosphere by three spacecraft triangulation measurements from STEREO and *Wind*. These triangulated source locations enable intrinsic properties of the radio source, such as its beaming characteristics, to be deduced. We present the first three-point measurements of the beaming characteristics for two solar type III radio bursts that were simultaneously observed by the three spacecraft in December of 2007 and in January of 2008. These analyses suggest that individual type III bursts exhibit a wide beaming pattern that is approximately beamed along the direction tangent to the Parker spiral magnetic field line at the source location.

Coronal mass ejection kinematics deduced from white light (Solar Mass Ejection Imager) and radio (Wind/WAVES) observations

M. J. **Reiner**, B. V. Jackson, D. F. Webb, D. R. Mizuno, M. L. Kaiser, J.-L. Bougeret
JGR Volume110, IssueA9 A09S14 **2005**
https://agupubs.onlinelibrary.wiley.com/doi/epdf/10.1029/2004JA010943
https://doi.org/10.1029/2004JA010943

White-light and radio observations are combined to deduce the coronal and interplanetary kinematics of a fast coronal mass ejection (CME) that was ejected from the Sun at about 1700 UT on **2 November 2003**. The CME, which was associated with an X8.3 solar flare from W56°, was observed by the Mauna Loa and Solar and Heliospheric Observatory (SOHO) Large-Angle Spectrometric Coronograph (LASCO) coronagraphs to 14 R⊙. The measured plane-of-sky speed of the LASCO CME was 2600 km s−1. To deduce the kinematics of this CME, we use the plane-of-sky white light observations from both the Solar Mass Ejection Imager (SMEI) all-sky camera on board the Coriolis spacecraft and the SOHO/LASCO coronagraph, as well as the frequency drift rate of the low-frequency radio data and the results of the radio direction-finding analysis from the WAVES experiment on the Wind spacecraft. In agreement with the in situ observations for this event, we find that both the white light and radio observations indicate that the CME must have decelerated significantly beginning near the Sun and continuing well into the interplanetary medium. More specifically, by requiring self-consistency of all the available remote and in situ data, together with a simple, but not unreasonable, assumption about the general characteristic of the CME deceleration, we were able to deduce the radial speed and distance time profiles for this CME as it propagated from the Sun to 1 AU. The technique presented here, which is applicable to mutual SMEI/WAVES CME events, is expected to provide a more complete description and better quantitative understanding of how CMEs propagate through interplanetary space, as well as how the radio emissions, generated by propagating CME/shocks, relate to the shock and CME. This understanding can potentially lead to more accurate predictions for the onset times of space weather events, such as those that were observed during this unique period of intense solar activity.

CONSTRAINTS ON CORONAL MASS EJECTION DYNAMICS FROM SIMULTANEOUS RADIO AND WHITE-LIGHT OBSERVATIONS

M. J. **Reiner**, A. Vourlidas, O. C. St. Cyr, J. T. Burkepile, R. A. Howard, M. L. Kaiser, N. P. Prestage, and J.-L. Bougeret
Astrophysical Journal, 590:533–546, **2003; File**

Simultaneous radio and white-light observations are used to deduce information on the dynamics of two coronal mass ejection (CME) events that occurred about 2 hr apart on **2001 January 20** and that were associated with eruptions from the same active region on the Sun. The analysis combines both space-based and ground-based data. The radio data were obtained from the WAVES experiment on the Wind spacecraft and from the Culgoora radiospectrograph in Australia. The white-light data were from the LASCO experiment on SOHO and from the Mk4 coronameter at the Mauna Loa Solar Observatory. For these CME events we demonstrate that the frequency drift rate of the type II radio emissions, generated by the shocks driven by the white-light CMEs, are consistent with the plane-of-sky height-time measurements, provided that the propagation direction of the CMEs and their associated radio sources was along a radial line from the Sun at a solar longitude of _E50_. These results imply that the ‘‘ true ’’ CME speeds were estimated to be _1.4 times higher than the measured plane-of-sky speeds and that the CMEs originated from solar eruptions centered near E50_. This CME origin is consistent with the known active region and flare site associated with these two CME events. Furthermore, we argue that the type II radio emissions generated by these CMEs must have originated in enhanced density regions of the corona. We investigate whether the type II radiation could have originated in one or more dense coronal streamers, whose densities were estimated from the polarization brightness measurements made by LASCO at that time. Finally, we use these radio and white-light observations to speculate about the dynamics and scales involved in the interaction between these two CMEs.

Solar Origin of the Radio Attributes of a Complex Type III Burst Observed on 11 April 2001

M.J. **Reiner** · K.-L. Klein · M. Karlický · K. Jiˇriˇcka · A. Klassen · M.L. Kaiser · J.-L. Bougeret
Solar Phys (2008) 249: 337–354
http://springerlink.com/content/yjp5074356767520/fulltext.pdf

We report here on the solar origin of distinctive radiation characteristics observed for a decametric type III solar radio burst that was associated with a major solar flare and CME on 11 April 2001. The associated decimeter (Ondˇrejov) and meter (Potsdam) wavelength emissions, as well as the GOES soft X-ray lightcurve, suggest that there were two successive events of energy release and electron acceleration associated with this solar eruption.
The Nançay radioheliograph images and additional evidence of plasmoid propagation suggest that the second event of electron acceleration resulted from coronal reconfigurations, likely caused by the erupting CME. These observational

analyses provide new insights into the physical origin of the distinguishing characteristics of complex type III-like radio emissions that are typically observed at decameter wavelengths during major solar eruptive events.

RADIO AND WHITE-LIGHT CORONAL SIGNATURES ASSOCIATED WITH THE RHESSI HARD X-RAY EVENT OF 2002 JULY 23

M. J. **Reiner**, S. Krucker, D. E. Gary, B. L. Dougherty, M. L. Kaiser, and J.-L. Bougeret
The Astrophysical Journal, 657, 1107-1116, **2007**, File
Simultaneous radio, white-light, and hard X-ray (HXR) observations for the 2002 July 23 _-ray flare event are used to establish the relationship of a complex type IIIYlike burst to the corresponding coronal mass ejection (CME) and the coronal electron acceleration signatures observed in the decimeter/microwave (dmYcm) emissions and X-rays.

Circular Polarization Observed in Interplanetary Type III Radio Storms

M. J. **Reiner**, J. Fainberg, M. L. Kaiser, J.-L. Bougeret
Solar Phys., 241(2), 351-370, 2007, File
We find that a small (usually less than 5%), but statistically significant, degree of circular polarization is present in all interplanetary type III radio storms below 1 MHz.
Based on the standard plasma emission theory of type III radiation, we discuss the implications of these observations for the magnitude and radial dependence of the solar magnetic field above active regions on the Sun.

CALLISTO Facilities in Peru: Spectrometers Commissioning and Observations of Type III Solar Radio Bursts

J.A. **Rengifo**, V.Loaiza-Tacuri, J.Bazo, W.R.Guevara Day
Solar Phys. **2020**
https://arxiv.org/pdf/2007.09203.pdf
The Astrophysics Directorate of CONIDA has installed two radio spectrometer stations belonging to the e-CALLISTO network in Lima, Peru. Given their strategic location near the Equator, it is possible to observe the Sun evenly throughout the whole year. To calibrated the antennas we analyzed the radio ambient background and measured their radiation pattern and beam-width. The stations took data from 2014 until 2016 in the metric and decimetric bands looking for radio burst. To understand the solar dynamics in these radio frequencies we have selected and analyzed type III Solar Radio Bursts candidates. The study of these bursts helps to understand the electron beams traversing the solar corona and the solar atmospheric density. We have obtained standard mean values for the associated plasma parameters with a starting negative frequency drift rate of -49.5 MHz/s and a later positive drift of 190.5 MHz/s, duration of 1.7 s and 114.3 MHz bandwidth.

Forward Modeling of Gyrosynchrotron Intensity Perturbations by Sausage Modes

V. E. **Reznikova**1,2, P. Antolin3, and T. Van Doorsselaere
2014 ApJ 785 86
To determine the observable radio signatures of the fast sausage standing wave, we examine gyrosynchrotron (GS) emission modulation using a linear three-dimensional magnetohydrodynamic model of a plasma cylinder. Effects of the line-of-sight angle and instrumental resolution on perturbations of the GS intensity are analyzed for two models: a base model with strong Razin suppression and a low-density model in which the Razin effect was unimportant. Our finding contradicts previous predictions made with simpler models: an in-phase variation of intensity between low (f < f peak) and high (f > f peak) frequencies is found for the low-density model and an anti-phase variation for the base model in the case of a viewing angle of 45fl. The spatially inhomogeneous character of the oscillating emission source and the spatial resolution of the model are found to have a significant effect on the resulting intensity.

Perturbations of gyrosynchrotron emission polarization from solar flares by sausage modes: forward modelling

Reznikova V.E., Van Doorsselaere T., and Kuznetsov A.A.
A&A 575, A47 **2015**
https://perswww.kuleuven.be/~u0041608/docs/2015reznikovapolarisation.pdf
We examined the polarization of the microwave flaring emission and its modulation by the fast sausage standing wave using a linear 3D magnetohydrodynamic model of a plasma cylinder. We analized the effects of the line-of-sight angle on the perturbations of the gyrosynchrotron intensity for two models: a base model with strong Razin suppression and a low-density model in which the Razin effect was negligible. The circular polarization (Stokes V) oscillation is in phase

with the intensity oscillation, and the polarization degree (Stokes V/I) oscillates in phase with the magnetic field at the examined frequencies in both models. The two quantities experience a periodical reversal of their signs with period equal to a half of the sausage wave period when seen at a 90 degree viewing angle, in this case, their modulation depth reaches 100%.

THREE-MINUTE OSCILLATIONS ABOVE SUNSPOT UMBRA OBSERVED WITH THE SOLAR DYNAMICS OBSERVATORY/ATMOSPHERIC IMAGING ASSEMBLY AND NOBEYAMA RADIOHELIOGRAPH

V. E. **Reznikova**1, K. Shibasaki1, R. A. Sych2,3 and V. M. Nakariakov
2012 ApJ 746 119
Three-minute oscillations over a sunspot's umbra in AR 11131 were observed simultaneously in UV/EUV emission by the Solar Dynamics Observatory (SDO)/Atmospheric Imaging Assembly (AIA) and in radio emission by the Nobeyama Radioheliograph (NoRH). We use 24 hr series of SDO and 8 hr series of NoRH observations to study spectral, spatial, and temporal variations of pulsations in the 5-9 mHz frequency range at different layers of the solar atmosphere. High spatial and temporal resolution of SDO/AIA in combination with long-duration observations allowed us to trace the variations of the cutoff frequency and spectrum of oscillations across the umbra. We found that higher frequency oscillations are more pronounced closer to the umbra's center, while the lower frequencies concentrate on the peripheral parts. We interpreted this discovery as a manifestation of variation of the magnetic field inclination across the umbra at the level of temperature minimum. Possible implications of this interpretation for the diagnostics of sunspot atmospheres are discussed.

Flare quasi-periodic pulsations with growing periodicity

V. E. **Reznikova**1,2 and K. Shibasaki1
A&A 525, A112 (**2011**), **File**
We conducted a wavelet analysis of the flare intensity variations for the long duration flare on **2005 August 22** observed with the Nobeyama Radioheliograph at frequencies 17 and 34 GHz and with the Ramaty High Energy Solar Spectroscopic Imager at 25–50 keV. We found that the signals contain a well-pronounced periodicity in which the oscillation period grows from 2.5 to 5 min. An analysis of the loop length and plasma temperature evolution during the flare allowed us to interpret the quasi-periodic pulsations in terms of the second standing harmonics of the slow magnetoacoustic mode. This mode can be generated by the initial impulsive energy release and work as a trigger for the repeated energy releases.

DYNAMICS OF THE FLARING LOOP SYSTEM OF 2005 AUGUST 22 OBSERVED IN MICROWAVES AND HARD X-RAYS

V. E. **Reznikova**1,2, V. F. Melnikov1,3, H. Ji4, and K. Shibasaki1
Astrophysical Journal, 724:171–181, **2010**
We studied the spatial dynamics of the flaring loop in the **2005 August 22** event using microwave (NoRH) and hard X-ray (*RHESSI*) observations together with complementary data from *SOHO*/MDI, SMART at Hida, *SOHO*/EIT, and *TRACE*.We have found that (1) the pre-flare morphology of the active region exhibits a strongly sheared arcade seen in Hα and the J-shape filament seen in EUV; (2) energy release and high-energy electron acceleration occur in a sequence along the extensive arcade; (3) the shear angle and the parallel (to the magnetic neutral line) component of the footpoint (FP) distance steadily decrease during the flare process; (4) the radio loop shrinks in length and height during the first emission peak, and later it grows; after the fourth peak the simultaneous descending of the brightest loop and formation of a new microwave loop at a higher altitude occur; (5) the hard X-ray coronal source is located higher than the microwave loop apex and shows faster upward motion; (6) the first peak on microwave time profiles is present in both the loop top and FP regions. However, the emission peaks that follow are present only in the FP regions.We conclude that after the first emission peak the acceleration site is located over the flaring arcade and particles are accelerated along magnetic field lines.We make use of the collapsing magnetic trap model to understand some observational effects.

2002 AUGUST 24 LIMB FLARE LOOP: DYNAMICS OF MICROWAVE BRIGHTNESS DISTRIBUTION

V. E. **Reznikova**1,2, V. F. Melnikov2,3, K. Shibasaki4, S. P. Gorbikov2, N. P. Pyatakov2, I. N. Myagkova5, and H. Ji1,6
The Astrophysical Journal, 697:735–746, **2009** May 20 doi:10.1088/0004-637X/697/1/735
http://www.iop.org:80/EJ/toc/-alert=43190/0004-637X/697/1
High-resolution radio observation of Nobeyama Radioheliograph at 17 and 34 GHz allowed studying the dynamics of microwave brightness distribution along the giant limb flaring loop in the event of **2002 August 24.** It is found that on the rising phase of the radio burst the brightness distribution was highly asymmetric, with a strong maximum

near the southern footpoint (SFP) and much weaker brightness enhancements near the loop top (LT) and northern footpoint. On the decay phase, the LT gradually becamemost bright. The similar dynamics of brightness distribution are shown to happen for all major temporal subpeaks of the burst. Results of our diagnostics show two important properties: (1) the number density of mildly relativistic electrons in the LT is much higher than near the footpoints (FPs) during rise, maximum and decay of each major peak; and (2) the ratio of the electron number densities in the LT and an FP increases from the maximum to decay phase. Model simulations with making use of the nonstationary Fokker–Planck equation have allowed us to find the model explaining the major properties of the microwave brightness distribution and dynamics. The model is characterized by a compact source of electrons located near the center of an asymmetric magnetic loop; the source is nonstationary, long lasting, and injecting high-energy electrons with the pitch-angle distribution mostly directed toward the SFP but also having a very weak isotropic component. This easily explains the observed brightness asymmetry. The observed dynamics comes due to two reasons: faster precipitation of electrons having their mirror points near the ends of the magnetic trap, and relatively faster decay of the lower energy electrons responsible for the gyrosynchrotron emission near the FPs with higher magnetic field.

MULTIPLE HARMONIC PLASMA EMISSION

Tongnyeol **Rhee**, Chang-Mo Ryu1, Minho Woo1, Helen H. Kaang1, Sumin Yi1, and Peter H. Yoon1,2,3
Astrophysical Journal, 694:618–625, **2009** March
http://www.iop.org/EJ/toc/-alert=43190/0004-637X/694/1
Electromagnetic radiation at the plasma frequency and/or its second harmonic, the so-called plasma emission, is widely accepted as the fundamental process responsible for solar type II and III radio bursts.
There have also been occasional observations of higher-harmonic plasma emissions in the solar-terrestrial environment. This paper presents the first demonstration of multiple harmonic emission by means of two-dimensional electromagnetic particle-in-cell simulation. This finding indicates that under certain circumstances the traditional mechanism of fundamental–harmonic pair emission might also be accompanied by higher-harmonic components. Consequently, the present findings are highly relevant to in situ observations of third- and/or higher-harmonic plasma emission in astrophysical and solar-terrestrial environments.

(From the detailed analysis, we conclude that, while the theory by Yi et al. (2007) adequately explains the excitation of ES multiple harmonic modes, as far as the EM multiple harmonic emissions are concerned, it is the Zlotnik–Cairns theory that better explains the simulation results. Specifically, we found that the Zlotnik–Cairns model provides qualitative explanations for the radiation-beam pattern and dynamical evolution.)

CME observations using LOFAR: Latest results from interplanetary scintillation and Faraday rotation

Fallows **Richard**∗1 , Mario Bisi2 , Elizabeth Jensen3 , Charlotte Sobey4 , Bernie Jackson5 , and Tarraneh Eftekhari6
CESRA Abstract **2016**
http://cesra2016.sciencesconf.org/conference/cesra2016/pages/CESRA2016_prog_abs_book_v1.pdf
Several observations using the Low Frequency Array (LOFAR - a radio telescope centred on the Netherlands with stations across Europe) have been undertaken to observe the passage of CMEs through interplanetary space. By measuring the interplanetary scintillation (IPS) of compact radio sources as a CME passes across the lines of sight, the velocity and relative density of the various components from nose to prominence material can be assessed. Observations of Faraday rotation (FR) in signals from polarised sources such as pulsars can be used as a remote-sensing method of determining magnetic fields: If the contributions from the interstellar medium and Earth's ionosphere can be accurately assessed and subtracted, this can act as a remote probe of the heliospheric magnetic field, representing one of the only methods by which global measurements of this parameter could be made. Here, we summarise the initial results of dedicated LOFAR observations designed to observe the full passage of several CMEs using measurements of IPS and present the first tentative results from attempts to determine heliosperic magnetic field parameters during the passage of a CME.

Tracking the motion of a shock along a channel in the low solar corona

J. **Rigney** (1 and 2 and 3), P. T. Gallagher (1), G. Ramsay (2), J. G. Doyle (2), D. M. Long (4 and3), O. Stepanyuk (5), K. Kozarev (5)
A&A 684, L7 **2024**
https://arxiv.org/pdf/2403.17659.pdf
https://www.aanda.org/articles/aa/pdf/2024/04/aa48452-23.pdf
Context. Shock waves are excited by coronal mass ejections (CMEs) and large-scale extreme-ultraviolet (EUV) wave fronts and can result in low-frequency radio emission under certain coronal conditions. Aims. In this work, we investigate a moving source of low-frequency radio emission as a CME and an associated EUV wave front move along a channel of a lower density, magnetic field, and Alfvén speed in the solar corona. Methods. Observations from the

Atmospheric Imaging Assembly on board the Solar Dynamics Observatory, the Nançay Radio Heliograph (NRH), and the Irish Low Frequency Array (I-LOFAR) were analysed. Differential emission measure maps were generated to determine densities and Alfvén maps, and the kinematics of the EUV wave front was tracked using CorPITA. The radio sources' positions and velocity were calculated from NRH images and I-LOFAR dynamic spectra. Results. The EUV wave expanded radially with a uniform velocity of ~ 500 km s−1 . However, the radio source was observed to be deflected and appeared to move along a channel of a lower Alfvén speed, abruptly slowing from 1700 km s−1 to 250 km s−1 as it entered a quiet-Sun region. A shock wave with an apparent radial velocity of > 420 km s−1 was determined from the drift rate of the associated Type II radio burst. Conclusions. The apparent motion of the radio source may have resulted from a wave front moving along a coronal wave guide or by different points along the wave front emitting at locations with favourable conditions for shock formation. **10 May 2022**

Scattering of energetic electrons by heat-flux-driven whistlers in flares

G. T. **Roberg-Clark**, O. V. Agapitov, J. F. Drake, M. M. Swisdak
2019 *ApJ* **887** 190
https://arxiv.org/pdf/1908.06481.pdf
https://doi.org/10.3847/1538-4357/ab5114
The scattering of electrons by heat-flux-driven whistler waves is explored with particle-in-cell (PIC) simulations relevant to the transport of energetic electrons in flares and the solar wind. The simulations are initiated with a large heat flux that is produced using a kappa distribution of electrons with positive velocity and a cold return current beam. This system represents energetic electrons escaping from a reconnection-driven energy release site. This heat flux system drives large amplitude oblique whistler waves propagating both along and against the heat flux, as well as electron acoustic waves. While the waves are dominantly driven by the low energy electrons, including the cold return current beam, the energetic electrons resonate with and are scattered by the whistlers on time scales of the order of a hundred electron cyclotron times. Electron perpendicular energy is increased while the field-aligned electron heat flux is suppressed. The resulting scattering mean-free-paths of energetic electrons are small compared with the typical scale size of energy release sites in flares, which might lead to the effective confinement of energetic electrons that is required for the production of very energetic particles.

First Spectral Analysis of a Solar Plasma Eruption Using ALMA

Andrew S. **Rodger**, Nicolas Labrosse, Sven Wedemeyer, Mikolaj Szydlarski, Paulo J.A. Simões, Lyndsay Fletcher
ApJ **2019**
https://arxiv.org/pdf/1902.01319.pdf
The aim of this study is to demonstrate how the logarithmic millimeter continuum gradient observed using the Atacama Large Millimeter/submillimeter Array (ALMA) may be used to estimate optical thickness in the solar atmosphere. We discuss how using multi-wavelength millimeter measurements can refine plasma analysis through knowledge of the absorption mechanisms. Here we use sub-band observations from the publicly available science verification (SV) data, whilst our methodology will also be applicable to regular ALMA data. The spectral resolving capacity of ALMA SV data is tested using the enhancement coincident with an X-ray Bright Point (XBP) and from a plasmoid ejection event near active region NOAA12470 observed in Band 3 (84-116 GHz) on **17/12/2015**. We compute the interferometric brightness temperature light-curve for both features at each of the four constituent sub-bands to find the logarithmic millimetre spectrum. We compared the observed logarithmic spectral gradient with the derived relationship with optical thickness for an isothermal plasma to estimate the structure's optical thicknesses. We conclude, within 90% confidence, that the stationary enhancement has an optical thickness between $0.02 \leq \tau \leq 2.78$, and that the moving enhancement has $0.11 \leq \tau \leq 2.78$, thus both lie near to the transition between optically thin and thick plasma at 100 GHz. From these estimates, isothermal plasmas with typical Band 3 background brightness temperatures would be expected to have electron temperatures of ~7370−15300 K for the stationary enhancement and between ~7440−9560 K for the moving enhancement, thus demonstrating the benefit of sub-band ALMA spectral analysis.

Spectral Gradient of the Thermal Millimetre Continuum as a Diagnostic for Optical Thickness in the Solar Atmosphere

Andrew S. **Rodger**, Nicolas Labrosse
A&A 617 L6 **2018**
https://arxiv.org/pdf/1808.07797.pdf
Aims. In this article we aim to show how the gradient of the thermal millimetre continuum spectrum, as emitted from the quiet solar atmosphere, may be used as a diagnostic for the optical thickness regime at the centre of the observing frequency band.
Methods. We show the theoretical derivation of the gradient of the millimetre continuum for both logarithmic- and linear-scale spectra. We compare this expression with the empirical relationship between the slope of the millimetre continuum spectrum and the plasma optical thickness computed from both isothermal and multi-thermal two-

dimensional cylindrical radiative transfer models.
Results. It is found that the logarithmic-scale spectral gradient provides a clear diagnostic for the optical thickness regime for both isothermal and multi-thermal plasmas, provided that a suitable correction is made for a non-constant gaunt factor over the frequency band. For the use of observers we present values for this correction at all ALMA bands and at a wide range of electron temperatures.
Conclusions. We find that the spectral gradient can be used to find (a) whether the source is fully optically thin, (b) the optical thickness of the source if it lies within the transitional regime between optically thin and thick plasma ({\tau} ≈ 10−1−101), or (c) whether the source is fully optically thick for an isothermal plasma. A multi-thermal plasma will act the same as an isothermal plasma for case (a), however, the transitional regime will only extend from {\tau} ≈ 10−1−100 . Above {\tau} = 1 the slope of the continuum will depend increasingly on the temperature gradient, as well as the optical thickness, reducing the reliability of the diagnostic.
Erratum A&A 623, C3 (2019) https://www.aanda.org/articles/aa/pdf/2019/03/aa33848e-18.pdf

Solar prominence modelling and plasma diagnostics at ALMA wavelengths

Andrew S **Rodger**, Nicolas Labrosse
Solar Phys. 292:130 **2017**
https://arxiv.org/pdf/1704.05385.pdf
Our aim is to test potential solar prominence plasma diagnostics as obtained with the new solar capability of the Atacama Large Millimeter / submillimeter Array (ALMA). We investigate the thermal and plasma diagnostic potential of ALMA for solar prominences through the computation of brightness temperatures at ALMA wavelengths. The brightness temperature, for a chosen line of sight, is calculated using densities of hydrogen and helium obtained from a radiative transfer code under non local thermodynamic equilibrium (NLTE) conditions, as well as the input internal parameters of the prominence model in consideration. Two distinct sets of prominence models were used: isothermal-isobaric fine-structure threads, and large-scale structures with radially increasing temperature distributions representing the prominence-to-corona transition region. We compute brightness temperatures over the range of wavelengths in which ALMA is capable of observing (0.32 - 9.6mm), however we particularly focus on the bands available to solar observers in ALMA cycles 4 and 5, namely 2.6 - 3.6mm (Band 3) and 1.1 - 1.4mm (Band 6). We show how the computed brightness temperatures and optical thicknesses in our models vary with the plasma parameters (temperature and pressure) and the wavelength of observation. We then study how ALMA observables such as the ratio of brightness temperatures at two frequencies can be used to estimate the optical thickness and the emission measure for isothermal and non-isothermal prominences. From this study we conclude that, for both sets of models, ALMA presents a strong thermal diagnostic capability, provided that the interpretation of observations is supported by the use of non-LTE simulation results.
CESRA highlight #1647 **2017** http://cesra.net/?p=1647

Ionospheric Disturbances and Their Impact on IPS Using MEXART Observations

M. **Rodríguez-Martínez**, H. R. Pérez-Enríquez, A. Carrillo-Vargas…
Solar Physics, July **2014**, Volume 289, Issue 7, pp 2677-2695
We study the impact of ionospheric disturbances on the Earth's environment caused by the solar events that occurred from **20 April to 31 May 2010**, using observations from the Mexican Array Radio Telescope (MEXART). During this period of time, several astronomical sources presented fluctuations in their radio signals. Wavelet analysis, together with complementary information such as the vertical total electron content (vTEC) and the Dst index, were used to identify and understand when the interplanetary scintillation (IPS) could be contaminated by ionospheric disturbances (IOND). We find that radio signal perturbations were sometimes associated with IOND and/or IPS fluctuations; however, in some cases, it was not possible to clearly identify their origin. Our Fourier and wavelet analyses showed that these fluctuations had frequencies in the range ≈ 0.01 Hz – ≈ 1.0 Hz (periodicities of 100 s to 1 s).

Detection of Solar Wind Disturbances: Mexican Array Radio Telescope IPS Observations at 140 MHz

E. **Romero-Hernandez**, J. A. Gonzalez-Esparza, E. Aguilar-Rodriguez, V. Ontiveros-Hernandez, P. Villanueva-Hernandez
Solar Phys. **2015**
The interplanetary scintillation (IPS) technique is a remote-sensing method for monitoring solar-wind perturbations. The Mexican Array Radio Telescope (MEXART) is a single-station instrument operating at 140 MHz, fully dedicated to performing solar-wind studies employing the IPS technique. We report MEXART solar-wind measurements (scintillation indices and solar-wind velocities) using data obtained during the 2013 and 2014 campaigns. These solar-wind measurements were calculated employing a new methodology based on the wavelet transform (WT) function. We report the variation of the scintillation indices versus the heliocentric distance for two IPS sources (3C48 and 3C147). We found different average conditions of the solar-wind density fluctuations in 2013 and 2014. We used the fittings of the radial dependence of the scintillation index to calculate g-indices. Based on the g-index value, we identified 17 events that could be associated with strong compression regions in the solar wind. We present the first ICME identifications in our data. We associated 14 IPS events with preceding CME counterparts by employing white-light

observations from the Large Angle and Spectrometric Coronagraph (LASCO) onboard the Solar and Heliospheric Observatory (SOHO) spacecraft. We found that most of the IPS events, detected during the solar maximum of Cycle 24 were associated with complex CME events. For the IPS events associated with single CME counterparts, we found a deceleration tendency of the CMEs as they propagate in the interplanetary medium. These results show that the instrument detects solar-wind disturbances, and the WT methodology provides solar-wind information with good accuracy. The MEXART observations will complement solar-wind IPS studies using other frequencies, and the tracking of solar-wind disturbances by other stations located at different longitudes.

Nonlinear analysis of decimetric solar bursts

Reinaldo R. **Rosa**1, Mauricio J. A. Bolzan2, Francisco C. R., Fernandes2, H. S. Sawant1 and Marian Karlick´y3

Solar and Stellar Variability: Impact on Earth and Planets, Proceedings IAU Symposium No. 264, **2009**, p. 279-281, A.G. Kosovichev, A.H. Andrei & J.-P. Rozelot, eds.

Y:\obridko\otchet09

The solar radio emissions in the decimetric frequency range (above 1 GHz) are very rich in temporal and spectral fine structures due to nonlinear processes occurring in the magnetic structures on the corresponding active regions. In this paper we characterize the singularity spectrum, f(®), for solar bursts observed at 1.6, 2.0 and 3 GHz. We interpret our findings as evidence of inhomogeneous plasma turbulence driving the underlying plasma emission process and discuss the nonlinear multifractal approach into the context of geoeffective solar active regions.

Gradient pattern analysis of short solar radio bursts

Adv. Space Res., V. 425, No. 5, *Pages 844-851, **2008***

R.R. **Rosa**, M. Karlický, T.B. Veronese, N.L. Vijaykumar, H.S. Sawant, A.I. Borgazzi, M.S. Dantas, E.B.M. Barbosa, R.A. Sych and O. Mendes

We analyze the weak component of the localized temporal pattern variability of 3 GHz solar burst observed by the *Ondrejov radiospectrograph*. A complex, short and weak impulsive sample from the time series was analyzed by applying a method based on the gradient pattern analysis and discrete wavelet decomposition. By analyzing canonical temporal variability patterns we show that the new method can reliably characterize the phenomenological dynamical process of short time series ($N \leqslant 10^3$ measurements) as the radio burst addressed here. In the narrowest sense, by estimating the mutual information distance in the gradient spectra, we show that the fluctuation pattern of the short and weak 3 GHz impulsive solar burst, with energetic amplitudes <350 SFU, is closer to the intermittent and strong MHD turbulent variability pattern.

Millisecond Microwave Spikes: Statistical Study and Application for Plasma Diagnostics

I.V. **Rozhansky**, G.D. Fleishman and G.-L. Huang

BBSO, #1358, **2008**

http://solar.njit.edu/preprints/rozhansky1358.pdf

Solar ALMA predictions: tutorial

Robert J. **Rutten**

Proceedings IAU Symposium 327, **2016**

https://arxiv.org/pdf/1611.05308v1.pdf

I have proposed that long Halpha fibrils are caused by heating events of which the tracks are afterwards outlined by contrails of cooling gas with extraordinary Halpha opacity and yet larger opacity at the ALMA wavelengths. Here I detail the radiative transfer background.

H-alpha features with hot onsets III. Fibrils in Lyman-alpha and with ALMA

Robert J. **Rutten**

A&A 2016

http://arxiv.org/pdf/1609.01122v1.pdf

In H-alpha most of the solar surface is covered by a dense canopy of long opaque fibrils, but predictions for quiet-Sun observations with ALMA have ignored this fact. Comparison with Ly-alpha suggests that the large opacity of H-alpha fibrils is caused by hot precursor events. Application of a recipe that assumes momentary Saha-Boltzmann extinction during their hot onset to millimeter wavelengths suggests that ALMA will observe the H-alpha fibril canopy, not acoustic shocks underneath, and will yield data more interesting than if this canopy were transparent.

Radio measurements of coronal magnetic fields in fan-spine configurations on the Sun

B. **Ryabov** and A. Vrublevskis
CESRA #3554 **2023** https://www.astro.gla.ac.uk/users/eduard/cesra/?p=3554
See https://doi.org/10.2478/lpts-2023-0011
1-3 Oct 2012

Depressed emission between magnetic arcades near a sunspot

B.I. **Ryabov**, K. Shibasaki
Baltic Astronomy Vol. 25, p. 225-235 **2016**
http://www.ltn.lv/~ryabov/paper5.pdf
The locations of the depressed emission in microwaves, EUV, and soft X-rays are compared with each other and with the location of the plasma outflow in the active region (AR) 8535. We found that two open-field regions overlap the regions of depressed emission near the ARs sunspot. These two open-field regions are simulated with the potential-field source-surface (PFSS) model under radial distances RSS = 1.8 R⊙ and RSS = 2.5 R⊙. Each open-field region locates between the arcades of the loops of the same magnetic polarity. The former open-field region covers the region of the plasma outflow, which is thus useful for the tests on connection to the heliosphere. The utmost microwave depression of the intensity in ordinary mode (the Very Large Array 15 GHz observations) overlaps the region of the plasma outflow as well and thus indicates this outflow. The lasting for 8 days depression in soft X-rays and the SOHO EIT 2.84x10-8m images is attributed to the evacuation of as hot coronal plasma as T≥ 2x106K from the extended in height ("open") magnetic structures. We conclude that the AR 8535 presents the sunspot atmosphere effected by the large-scale magnetic fields. **1999 May 9-13**

Reduced Coronal Emission above Large Isolated Sunspots

B. I. **Ryabov**, D. E. Gary, N. G. Peterova, K. Shibasaki, and N. A. Topchilo
Solar Phys., **2015**, Volume 290, Issue 1, pp 21-35
http://www.ltn.lv/~ryabov/paper_1.pdf
We analyse specific regions of reduced soft X-ray and microwave emission in five large isolated sunspots. The Nobeyama Radioheliograph 17 GHz observations reveal a local depression of microwave brightness in the peripheral area of the sunspots. The depression regions appear light (weak absorption) in the He 10830 fl line in areas with extended (flopenfl) field lines as indicated by potential field source surface model (PFSS) extrapolations up to 1.5 R□. The observed depressions of 3 fl 8% in ordinary mode at 17 GHz is interpreted as resulting from free-free emission under a decrease of 5 fl 10% in plasma density. Our model estimates show that it is the decrement of density in both coronal and lower layers above the depression region that accounts for the depression. We believe that such depression regions are good candidates for marking the location of outward plasma motions.

LOFAR imaging of the solar corona during the 2015 March 20 solar eclipse

A. M. **Ryan**, P. T. Gallagher, E. P. Carley, M. A. Brentjens, P. C. Murphy, C. Vocks, D. E. Morosan, H. Reid, J. Magdalenic, F. Breitling, P. Zucca, R. Fallows, G. Mann, A. Kerdraon, R. Halfwerk
A&A 648, A43 **2021**
https://arxiv.org/pdf/2102.05552.pdf
https://doi.org/10.1051/0004-6361/202039024
https://www.aanda.org/articles/aa/pdf/2021/04/aa39024-20.pdf
The solar corona is a highly-structured plasma which can reach temperatures of more than ~2 MK. At low frequencies (decimetric and metric wavelengths), scattering and refraction of electromagnetic waves are thought to considerably increase the imaged radio source sizes (up to a few arcminutes). However, exactly how source size relates to scattering due to turbulence is still subject to investigation. The theoretical predictions relating source broadening to propagation effects have not been fully confirmed by observations due to the rarity of high spatial resolution observations of the solar corona at low frequencies. Here, the LOw Frequency ARray (LOFAR) was used to observe the solar corona at 120-180 MHz using baselines of up to ~3.5 km (corresponding to a resolution of ~1-2') during the partial solar eclipse of **2015 March 20**. A lunar de-occultation technique was used to achieve higher spatial resolution (~0.6') than that attainable via standard interferometric imaging (~2.4'). This provides a means of studying the contribution of scattering to apparent source size broadening. It was found that the de-occultation technique reveals a more structured quiet corona that is not resolved from standard imaging, implying scattering may be overestimated in this region when using standard imaging techniques. However, an active region source was measured to be ~4' using both de-occultation and standard imaging. This may be explained by the increased scattering of radio waves by turbulent density fluctuations in active regions, which is more severe than in the quiet Sun.

The Sun at millimeter wavelengths V. Magnetohydrodynamic waves in a fibrillar structure

Maryam **Saberi**, Shahin Jafarzadeh, Sven Wedemeyer, Ricardo Gafeira, Mikolaj Szydlarski, David Jess, Marco Stangalini

A&A 693, A19 **2025**

https://arxiv.org/pdf/2411.14190

https://doi.org/10.1051/0004-6361/202451833

https://www.aanda.org/articles/aa/pdf/2025/01/aa51833-24.pdf

Magnetohydrodynamic (MHD) waves, playing a crucial role in transporting energy through the solar atmosphere, manifest in various chromospheric structures. Here, we investigated MHD waves in a long-lasting dark fibril using high-temporal-resolution (2~s cadence) Atacama Large Millimeter/submillimeter Array (ALMA) observations in Band 6 (centered at 1.25~mm). We detected oscillations in brightness temperature, horizontal displacement, and width at multiple locations along the fibril, with median periods and standard deviations of 240±114~s, 225±102~s, and 272±118~s, respectively. Wavelet analysis revealed a combination of standing and propagating waves, suggesting the presence of both MHD kink and sausage modes. Less dominant than standing waves, oppositely propagating waves exhibit phase speeds (median and standard deviation of distributions) of 74±204~km/s, 52±197~km/s, and 28±254~km/s for the three observables, respectively. This work demonstrates ALMA's capability to effectively sample dynamic fibrillar structures, despite previous doubts, and provides valuable insights into wave dynamics in the upper chromosphere. **22 April 2017**

A DECADE OF SOLAR TYPE III RADIO BURSTS OBSERVED BY THE NANÇAY RADIOHELIOGRAPH 1998-2008

P. **Saint-Hilaire**1, N. Vilmer2, and A. Kerdraon

2013 ApJ 762 60

We present a statistical survey of almost 10,000 radio type III bursts observed by the Nançay Radioheliograph from 1998 to 2008, covering nearly a full solar cycle. In particular, sources sizes, positions, and fluxes were examined. We find an east-west asymmetry in source positions that could be attributed to a 6fl ± 1fl eastward tilt of the magnetic field, that source FWHM sizes s roughly follow a solar-cycle-averaged distribution (dN/ds) 14 ν–3.3 s –4 arcmin–1 day–1, and that source fluxes closely follow a solar-cycle-averaged (dN/ds ν) 0.34 ν–2.9 S –1.7 ν sfu–1 day–1 distribution (when ν is in GHz, s in arcminutes, and S ν in sfu). Fitting a barometric density profile yields a temperature of 0.6 MK, while a solar wind-like (h –2) density profile yields a density of 1.2 × 106 cm–3 at an altitude of 1 RS , assuming harmonic emission. Finally, we found that the solar-cycle-averaged radiated type III energy could be similar in magnitude to that radiated by nanoflares via non-thermal bremsstrahlung processes, and we hint at the possibility that escaping electron beams might carry as much energy away from the corona as is introduced into it by accelerated nanoflare electrons.

Allen Telescope Array **Multi-frequency Observations of the Sun**

P. **Saint-Hilaire**, G. J. Hurford, G. Keating, G. C. Bower and C. Gutierrez-Kraybill

E-print, Nov 2011

Solar Physics, Volume 277, Number 2, 431-445, **2012, E-print File**

We present the first observations of the Sun with the Allen Telescope Array (ATA). We used up to six frequencies, from **1.43 to 6 GHz, and baselines from 6 to 300 m.** To our knowledge, these are the first simultaneous multi-frequency full-Sun maps obtained at microwave frequencies without mosaicing. The observations took place when the Sun was relatively quiet, although at least one active region was present each time. We present multi-frequency flux budgets for each of the sources on the Sun. Outside of active regions, assuming optically thin bremsstrahlung (free–free) coronal emission on top of an optically thick ≈ 10 000 K chromosphere, the multi-frequency information can be condensed into a single, frequency-independent, "coronal bremsstrahlung contribution function" [EMT] map. This technique allows the separation of the physics of emission as well as a measurement of the density structure of the corona. Deviations from this simple relationship usually indicate the presence of an additional gyroresonance-emission component, as is typical in active regions.

Simulating the emission of electromagnetic waves in the terahertz range by relativistic electron beams

J. I. **Sakai**[1]**,** Y. Nagasugi[1], S. Saito[1] and P. Kaufmann, A&A 457, 313-318 (**2006**)

Aims.We investigate the dynamics of relativistic electron beams propagating along a uniform magnetic field and the emission process of electromagnetic waves within the terahertz range from the solar photosphere. Our aim is to understand a new solar burst component emitting only in the terahertz range during the solar flare observed by Kaufmann et al. (2004).

Methods. We used a 2D3V fully relativistic electromagnetic particle-in-cell (PIC) simulation.

Results. We did three different kinds of simulations. The first simulation confirmed that the growth rate of relativistic electron beam instability agrees well with the theoretical estimation. From the second simulation of the electron beam with finite width, we found that the beams are confined along the magnetic field and the electromagnetic waves are generated forward of the electron beams. Some fraction of the electrons are accelerated more than the initial beam velocity. From the third simulation where the electron beams propagate into the high density region, we found that strong electromagnetic waves are generated backward to the electron beams. We also found that the higher frequency emission like 405 GHz, which originate in the strong magnetic field region, becomes stronger than the 212 GHz emission, as shown in the observation by Kaufmann et al. (2004). These simulation results could be applied to the electromagnetic wave emission from the solar photosphere during the solar flares.

Simulated enhancement of solar type II radio bursts during the collision of two shocks associated with coronal mass ejections

Sakai, J. I.; Mori, T.; Saito, S.; Tanaka, Y.; Aurass, H.
Astronomy and Astrophysics, Volume 454, Issue 3, August II **2006**, pp.983-988
Aims.We investigate how solar type II radio bursts can be enhanced when two fast magnetosonic shocks associated with coronal mass ejections (CMEs) collide. This work was motivated by recent observations showing that the radio signature is in the form of intense continuum-like radio emission following an interplanetary type II burst, when a fast CME overtakes a slow CME.
Methods: . We used a 2D3V fully relativistic, electromagnetic particle-in-cell (PIC) simulation.
Results: . We found that during the collision between a fast shock with Alfvén Mach M_A=3 and a slow wave with Alfvén Mach M_A=0.75, the radio emission with a broad band can be enhanced with an amplitude about ten times larger than for the undisturbed type II burst. We also found that when a fast shock with Alfvén Mach M_A=3 overtakes a slow shock with Alfvén Mach M_A=1.5, the enhancement of the radio emission is about five times greater than the undisturbed type II burst.

Emission of electromagnetic waves by proton beams propagating in nonuniform solar plasmas:

J. I. **Sakai** and Y. Nagasugi
A&A 470 (2007) 1117-1122
We investigate the dynamics of proton beams propagating along a uniform magnetic field, as well as across the magnetic field in nonuniform solar plasmas, paying attention to the emission process of electromagnetic waves. The aim is to understand a new solar-burst component emitting only in the terahertz range during the solar flare observed by Kaufmann et al. (2004, ApJ, 603, L121).

Polarisation and source structure of solar stationary type IV radio bursts⋆

Carolina **Salas-Matamoros**1 and Karl-Ludwig Klein
A&A 639, A102 (**2020**)
https://www.aanda.org/articles/aa/pdf/2020/07/aa37989-20.pdf
The reconfiguration of the magnetic field during and after a coronal mass ejection (CME) may be accompanied by radio emission from non-thermal electrons. In particular, stationary type IV bursts (also called storm continua) are emitted by electrons in closed magnetic configurations usually located in the wake of the outward-travelling CME. Although stationary type IV bursts, which stand out by their long duration (up to several hours) and strong circular polarisation, have been known for more than fifty years, there have been no systematic studies since the 1980s. In this work we use the data pool of the Nançay Radioheliograph together with white-light coronagraphy, EUV imaging and magnetography from the SoHO, Proba2, SDO and STEREO spacecraft to revisit the source structure and polarisation of a sample of seven well-defined stationary type IV bursts at decimetre-to-metre wavelengths. The radio sources are most often found in one leg, in one case both legs, of the magnetic flux rope erupting into the high corona during the CME. The cross-correlation of the brightness temperature time profiles in the event with sources in both legs implies that the radiating electrons have energies of a few tens of keV. Comparison with the magnetic field measured in the photosphere and its potential extrapolation into the corona shows that the radio emission is in the ordinary mode. This result was inferred historically by means of the hypothesis that the magnetic field orientation in the radio source was that of the dominant sunspot in the parent active region. This hypothesis is shown here to be in conflict with noise storms in the same active region. It is confirmed that the polarisation of stationary type IV continua may be strong, but is rarely total, and that it gradually increases in the early phase of the radio event. We find that the increase is related to the gradual disappearance of some weakly polarised or unpolarised substructure, which dominates the first minutes of the radio emission. **July 14, 2000, 2001 Oct 09, 2007 May 19, 2008 Apr 26, 2010 Apr 03, 2012 Mar 04, 2012 Jun 14 CESRA** #2677 **2020** http://www.astro.gla.ac.uk/users/eduard/cesra/?p=2677

Coronal mass ejection-related particle acceleration regions during a simple eruptive event

Carolina **Salas-Matamoros**1,5, Karl-Ludwig Klein1,2 and Alexis P. Rouillard3

A&A 590, A135 (**2016**) **File**
http://www.aanda.org/articles/aa/pdf/2016/06/aa28015-15.pdf
An intriguing feature of many solar energetic particle (SEP) events is the detection of particles over a very extended range of longitudes in the heliosphere. This may be due to peculiarities of the magnetic field in the corona, to a broad accelerator, to cross-field transport of the particles, or to a combination of these processes. The eruptive flare on **26 April 2008** provided an opportunity to study relevant processes under particularly favourable conditions since it occurred in a very quiet solar and interplanetary environment. This enabled us to investigate the physical link between a single well-identified coronal mass ejection (CME), electron acceleration as traced by radio emission, and the production of SEPs. We conduct a detailed analysis, which combines radio observations (Nançay Radio Heliograph and Nançay Decametre Array, Wind/Waves spectrograph) with remote-sensing observations of the corona in extreme ultraviolet (EUV) and white light, as well as in situ measurements of energetic particles near 1AU (SoHO and STEREO spacecraft). By combining images taken from multiple vantage points, we were able to derive the time-dependent evolution of the 3D pressure front that was developing around the erupting CME. Magnetic reconnection in the post-CME current sheet accelerated electrons, which remained confined in closed magnetic fields in the corona, while the acceleration of escaping particles can be attributed to the pressure front ahead of the expanding CME. The CME accelerated electrons remotely from the parent active region, owing to the interaction of its laterally expanding flank, which was traced by an EUV wave, with the ambient corona. SEPs detected at one STEREO spacecraft and SoHO were accelerated later, when the frontal shock of the CME intercepted the spacecraft-connected interplanetary magnetic field line. The injection regions into the heliosphere inferred from the radio and SEP observations are separated in longitude by about 140fl. The observations for this event show that it is misleading to interpret multi-spacecraft SEP measurements in terms of one acceleration region in the corona. The different acceleration regions are linked to different vantage points in the interplanetary space.

A method for the automated detection of solar radio bursts in dynamic spectra

Houssam **Salmane**1,2*, Rodolphe Weber1,3, Karim Abed-Meraim1, Karl-Ludwig Klein2 and Xavier Bonnin2
J. Space Weather Space Clim. **2018**, 8, A43
https://www.swsc-journal.org/articles/swsc/pdf/2018/01/swsc170092.pdf
The variability of the solar corona, including flares and coronal mass ejections, affects the space environment of the Earth (heating and ionization of the atmosphere, magnetic field disturbances, and bombardment by high-energy particles). Electromagnetic emissions are the first signatures of a solar eruptive event which by modifying the electron density in the ionosphere may affect airborne technology and radio communications systems. In this paper, we present a new method to detect automatically radio bursts using data from the Nançay Decametre Array (NDA) in the band 10 MHz–80 MHz. This method starts with eliminating unwanted signals (Radio-Frequency Interference, RFI and Calibration signals) by analyzing the dynamic spectrum of the signal recorded in time. Then, a gradient median filter is applied to smooth and to reduce the variability of the signal. After denoising the signal, an automated solar radio burst detection system is applied. This system is based on a sequential procedure with adaptive constant-false-alarm rate (CFAR like detector) aimed to extract the spectra of major solar bursts. To this end, a semi-automatic software package is also developed to create a data base of all possible events (type II, III, IV or other) that could be detected and used for our performance assessment.

An automated solar radio burst detection method to extract major bursts (type II, III and IV) from dynamic spectra

Houssam **Salmane**_y1, Karim Abed-Meraim1, Rodolphe Weber1, Xavier Bonnin2, and Karl-Ludwig Klein2,3
CESRA **2016**, p.83
http://cesra2016.sciencesconf.org/conference/cesra2016/pages/CESRA2016_prog_abs_book_v3.pdf
The Sun, and particularly its outer atmosphere, the corona, is a source of electromag-
netic emissions (EUV, X-rays, radio) and of energetic electrically charged particles. The
high-energy emissions may lead to major space weather events that affect space borne and
possibly airborne technology and radio communications depending on wave propagation in
the ionosphere.
This work aims at developing an automatic method for the detection of solar radio bursts in
dynamic spectra (Time-Frequency images) in the space environment of the Earth.
This method starts by eliminating unwanted signals (Radio-Frequency Interference RFI,
Calibration...). Then, a time-frequency median _lter followed by a magnitude-gradient me-
dian _lter is applied to improve the quality of the dynamical images to be interpreted and
to emphasis solar radio bursts. When the previous preprocessing phase is _nished, an auto-
mated solar radio burst detection system is applied. This system is based on a hierarchical
procedure with adaptive constant-false- alarm-rate (CFAR like) aimed to detect separately
the spectra of major solar bursts with or without insigni_cant events.

To evaluate the performance of our method, a semi-automatic software package is developed to create a data set of all possible events (type II, III or IV) that could be recognized. Finally, both our proposed system and the Automated Radio Solar Burst Identi_cation System (ARBIS) proposed by Lozbin are discussed and evaluated.
In this study we use the solar radio spectral data provided by the decametric spectrograph of the Nan_cay radio astronomy station.

High frequency waves in the corona due to null points

I. C. **Santamaria**, E. Khomenko, M. Collados, A. de Vicente
A&A **2017**
https://arxiv.org/pdf/1704.06551.pdf

This work aims to understand the behavior of non-linear waves in the vicinity of a coronal null point. In previous works we have showed that high frequency waves are generated in such magnetic configuration. This paper studies those waves in detail in order to provide a plausible explanation of their generation. We demonstrate that slow magneto-acoustic shock waves generated in the chromosphere propagate through the null point and produce a train of secondary shocks that escape along the field lines. A particular combination of the shock wave speeds generates waves at a frequency of 80 mHz. We speculate that this frequency may be sensitive to the atmospheric parameters in the corona and therefore can be used to probe the structure of this solar layer.

Subarcsecond imaging of a solar active region filament with ALMA and IRIS

João M. Da Silva **Santos**, Stephen White, Stephen White, Kevin Reardon, Gianna Cauzzi, Stanislav Gunár, Petr Heinzel, Jorrit Leenaarts, and Jorrit Leenaarts
Front. Astron. Space Sci. 9: 898115. **2022**
https://www.frontiersin.org/articles/10.3389/fspas.2022.898115/pdf
https://arxiv.org/pdf/2204.13178.pdf

Quiescent filaments appear as absorption features on the solar disk when observed in chromospheric lines and at continuum wavelengths in the millimeter (mm) range. Active region (AR) filaments are their small-scale, low-altitude analogues, but they could not be resolved in previous mm observations. This spectral diagnostic can provide insight into the details of the formation and physical properties of their fine threads, which are still not fully understood. Here, we shed light on the thermal structure of an AR filament using high-resolution brightness temperature (Tb) maps taken with ALMA Band 6 complemented by simultaneous IRIS near-UV spectra, Hinode/SOT photospheric magnetograms, and SDO/AIA extreme-UV images. Some of the dark threads visible in the AIA 304 Å passband and in the core of Mg ii resonance lines have dark (Tb << 5,000 K) counterparts in the 1.25 mm maps, but their visibility significantly varies across the filament spine and in time. These opacity changes are possibly related to variations in temperature and electron density in filament fine structures. The coolest Tb values (<< 5,000 K) coincide with regions of low integrated intensity in the Mg ii h and k lines. ALMA Band 3 maps taken after the Band 6 ones do not clearly show the filament structure, contrary to the expectation that the contrast should increase at longer wavelengths based on previous observations of quiescent filaments. The ALMA maps are not consistent with isothermal conditions, but the temporal evolution of the filament may partly account for this. **13 April 2019**
CESRA # 3325 Jun **2022** https://www.astro.gla.ac.uk/users/eduard/cesra/?p=3325

Heating of the solar chromosphere through current dissipation

J. M. da Silva **Santos**, S. Danilovic, J. Leenaarts, J. de la Cruz Rodríguez, X. Zhu, S. M. White, G. J. M. Vissers, M. Rempel
A&A **2022**
https://arxiv.org/pdf/2202.03955.pdf

The solar chromosphere is heated to temperatures higher than predicted by radiative equilibrium. This excess heating is larger in active regions where the magnetic field is stronger. We aim to investigate the magnetic topology associated to an area of enhanced millimeter (mm) brightness temperatures in a solar active region mapped by the Atacama Large Millimeter/submillimeter Array (ALMA) using spectropolarimetric coobservations with the 1-m Swedish Solar Telescope (SST). We use Milne-Eddington inversions, nonlocal thermodynamic equilibrium (non-LTE) inversions, and a magnetohydrostatic extrapolation to obtain constraints on the three-dimensional stratification of temperature, magnetic field, and radiative energy losses. We compare the observations to a snapshot of a magnetohydrodynamics simulation and investigate the formation of the thermal continuum at 3 mm using contribution functions. We find enhanced heating rates in the upper chromosphere of up to ∼5kWm−2 where small-scale emerging loops interact with the overlying magnetic canopy leading to current sheets as shown by the magnetic field extrapolation. Our estimates are about a factor of two higher than canonical values, but they are limited by the ALMA spatial resolution (∼1.2″). Band 3 brightness temperatures reach about ∼104K in the region, and the transverse magnetic field strength inferred from the non-LTE inversions is of the order of ∼500G in the chromosphere. We quantitatively reproduce many of the observed

features including the integrated radiative losses in our numerical simulation, and we conclude that the heating is caused by dissipation in current sheets. However, the simulation shows a complex stratification in the flux emergence region where distinct layers may contribute significantly to the emission in the mm continuum. **April 13, 2019**

ALMA observations of transient heating in a solar active region

J. M. da Silva **Santos**, J. de la Cruz Rodríguez, S. M. White, J. Leenaarts, G. J. M. Vissers, V. H. Hansteen
A&A 643, A41 **2020**
https://arxiv.org/pdf/2006.14564.pdf
https://doi.org/10.1051/0004-6361/202038755
https://www.aanda.org/articles/aa/pdf/2020/11/aa38755-20.pdf
We examined 3 mm signatures of heating events identified in Solar Dynamics Observatory (SDO) observations of an active region and compare the results with synthetic spectra from a 3D radiative magnetohydrodynamic simulation. We estimated the contribution from the corona to the mm brightness using differential emission measure analysis. We report the null detection of EBs in the 3 mm continuum at ∼1.2" spatial resolution, which is evidence that they are sub-canopy events that do not significantly contribute to heating the upper chromosphere. In contrast, we find the active region to be populated with multiple compact, bright, flickering mm bursts -- reminiscent of UVBs. The high brightness temperatures of up to ∼14200 K in some events may have a significant contribution (up to ∼7%) from the corona. We also detect FAF-like events in the 3 mm continuum that show rapid motions of >10000 K plasma launched with high plane-of-sky velocities (37−340kms−1) from nanoflare kernels. The mm FAFs are the brightest class of warm canopy fibrils that connect magnetic regions of opposite polarity. The simulation confirms that ALMA should be able to detect the mm counterparts of UVBs and small flares and thus provide a complementary diagnostic for impulsive heating in the solar chromosphere. **13 April 2019**
RHESSI Science Nugget, No. **427**, Feb **2022**
https://sprg.ssl.berkeley.edu/~tohban/wiki/index.php/Probing_chromospheric_current_sheets_using_SST_and_ALMA_co-observations

The multi-thermal chromosphere: inversions of ALMA and IRIS data

J. M. da Silva **Santos**, J. de la Cruz Rodríguez, J. Leenaarts, G. Chintzoglou, B. De Pontieu, S. Wedemeyer, M. Szydlarski
A&A 634, A56 **2020**
https://arxiv.org/pdf/1912.09886.pdf
https://doi.org/10.1051/0004-6361/201937117
Numerical simulations of the solar chromosphere predict a diverse thermal structure with both hot and cool regions. Observations of plage regions, in particular, feature broader and brighter chromospheric lines, which suggest that they are formed in hotter and denser conditions than in the quiet-Sun, but also imply a non-thermal component whose source is unclear. We revisit the problem of the stratification of temperature and microturbulence in plage now adding millimeter continuum observations provided by ALMA to inversions of near-ultraviolet IRIS spectra as a powerful new diagnostic to disentangle the two parameters. We fit cool chromospheric holes and track the fast evolution of compact mm brightnenings in the plage region. We use the STiC non-LTE inversion code to simultaneously fit real ultraviolet and millimeter spectra in order to infer the thermodynamic parameters of the plasma. We confirm the anticipated constraining potential of ALMA in non-LTE inversions of the solar chromosphere. We find significant differences between the inversion results of IRIS data alone compared to the results of a combination with the mm data: the IRIS+ALMA inversions have increased contrast and temperature range, and tend to prefer lower values of microturbulence in the chromosphere of plage. The average brightness temperature of the plage region at 1.25 mm is 8500 K, but the ALMA maps also show much cooler (∼3000 K) and hotter (∼11000 K) evolving features partially seen in other diagnostics. To explain the former, the inversions require the existence of localized, low temperature regions in the chromosphere where molecules such as CO could form. The hot features could sustain such high temperatures due to non-equilibrium hydrogen ionization effects in a shocked chromosphere - a scenario that is supported by low-frequency shock wave patterns found in the MgII lines probed by IRIS. **22 April 2017**
CESRA #2484 Feb **2020** http://www.astro.gla.ac.uk/users/eduard/cesra/?p=2484

Temperature constraints from inversions of synthetic solar optical, UV and radio spectra

João M. da Silva **Santos**, Jaime de la Cruz Rodríguez, Jorrit Leenaarts
A&A 620, A124 **2018**
https://arxiv.org/pdf/1806.06682.pdf
Context. High-resolution observations of the solar chromosphere at millimeter wavelengths are now possible with the Atacama Large Millimeter Array (ALMA), bringing with them the promise of tackling many open problems in solar physics. Observations from other ground and space-based telescopes will greatly benefit from coordinated endeavors with ALMA, yet the diagnostic potential of combined optical, ultraviolet and mm observations has remained mostly unassessed.

Aims. In this paper we investigate whether mm-wavelengths could aid current inversion schemes to retrieve a more accurate representation of the temperature structure of the solar atmosphere.
Methods. We performed several non-LTE inversion experiments of the emergent spectra from a snapshot of 3D radiation-MHD simulation. We included common line diagnostics such as Ca II H, K, 8542 Å and Mg II h and k, taking into account partial frequency redistribution effects, along with the continuum around 1.2 mm and 3 mm.
Results. We find that including the mm-continuum in inversions allows a more accurate inference of temperature as function of optical depth. The addition of ALMA bands to other diagnostics should improve the accuracy of the inferred chromospheric temperatures between log $\tau \sim [-6, -4.5]$ where the Ca II and Mg II lines are weakly coupled to the local conditions. However, we find that simultaneous multiatom, non-LTE inversions of optical and UV lines present equally strong constraints in the lower chromosphere and thus are not greatly improved by the 1.2 mm band. Nonetheless, the 3 mm band is still needed to better constrain the mid-upper chromosphere.
CESRA #2131 Feb **2019** http://cesra.net/?p=2131

POLARIZATION OF THE THERMAL RADIO EMISSION FROM OUTER SOLAR CORONA
Ch. V. **Sastry**
2009 ApJ 697 1934-1939 doi: 10.1088/0004-637X/697/2/1934
http://www.iop.org/EJ/toc/-alert=43190/0004-637X/697/2
The Haselgrove equations for radio-ray propagation in an anisotropic medium are used to determine the degree of circular polarization (dcp) of the low-frequency thermal radio emission from the outer solar corona with a magnetic field. The variation of dcp with frequency and magnetic field strength is investigated. It is found that weak magnetic fields can be detected by measuring the dcp at low frequencies.

Solar Radio Burst events on September 6, 2017 and its impact on GNSS signal frequencies
H. **Sato** , N. Jakowski , J. Berdermann, K. Jiricka , A. Heßelbarth , D. Banys, V. Wilken
Space Weather **2019**
sci-hub.se/10.1029/2019SW002198
During the intense solar radio bursts on **September 6, 2017**, GNSS signal interferences were observed at ground stations in the European longitude sector from 20°N to 70°N for all GNSS satellites in view including GPS, GLONASS and Galileo. The solar radio noise reduced the signal-to-noise ratio (SNR) with clear frequency dependence. The impact of the radio burst has been found at L2 and L5 frequencies, but not at L1 frequency. The ground observation of the solar radio spectrum between 1.0–2.0 GHz corresponds well to such frequency dependence. The maximum SNR reduction of -10 dB was found when the solar radio flux was pulsating around 2000 SFU level. Precise Point Positioning (PPP) results show that accuracy is reduced with stronger deviation for dual-frequency solutions than for single-frequency solutions based on L1 signal only. The positioning error refers rather to the solar EUV flare than to solar radio interferences. The results presented here are a clear indication of frequency-dependent GNSS performance degradation during strong space weather events.

Parametric Decay of Beam-Generated Langmuir Waves and Three-Wave Interaction in Plateau Plasmas: Implications for Type III Radiation
Konrad **Sauer** Klaus Baumgärtel Richard Sydora Daniel Winterhalter
JGR Volume124, Issue1 January **2019** Pages 68-89
sci-hub.tw/10.1029/2018JA025887
Inspired by the results of particle-in-cell simulations on beam-plasma interaction, we present a mechanism for the generation of radio waves in solar type III bursts which provides a closed chain of the conversion processes from beam-generated Langmuir waves into electromagnetic emission. The mechanism is characterized by two key steps. The first is a hitherto unknown parametric decay process in which the primary wave directly decays to low-k Langmuir waves (plasma oscillations) and ion acoustic waves. This decay becomes possible due to changes in the dispersion properties of longitudinal waves initiated by the presence of a beam or a plateau in the electron velocity distribution. A resonant three-wave interaction is established between the beam-induced Langmuir wave, the plasma oscillations, and the ion acoustic wave. Due to weak damping of the waves involved, this interaction persists after the beam has relaxed to a plateau and lasts as long as the latter exists. In the second step, low-k Langmuir waves in the range of “optical wavelengths” can linearly couple to obliquely propagating radio waves at the plasma frequency in a wave number region around the cross points where quasi-longitudinal and quasi-transverse modes approach each other. Our model does not need the persistence of the beam and the associated instability for radiation to be produced. Although the theory is local with respect to the plasma frequency, it may open a way to overcome Sturrock's (1964) dilemma of rapid beam relaxation on the one side and long-lived radiation on the other. The observed frequency variation is suggested to arise by “adiabatic” motion of the beam-created interaction region through the heliospheric plasma of decreasing electron density. Implications for the interpretation of in situ Langmuir waveforms and the diversity of their frequency spectra are discussed.

Parametric decay of current-driven Langmuir waves in plateau plasmas: Relevance to solar wind and foreshock events

Konrad **Sauer**, David M. Malaspina, Marc Pulupa, Chadi S. Salem
JGR Volume 122, Issue 7 July **2017** Pages 7005–7020

Langmuir amplitude modulation in association with type III radio bursts is a well-known phenomenon since the beginning of space observations. It is commonly attributed to the superposition of beam-excited Langmuir waves and their backscattered counterparts as a result of parametric decay. The dilemma, however, is the discrepancy between fast beam relaxation and long-lasting Langmuir wave activity. Instead of starting with an unstable electron beam, our focus in this paper is on the nonlinear response of Langmuir oscillations that are driven after beam stabilization by the still persisting current of the (stable) two-electron plasma. The velocity distribution function of the second population forms a plateau (index h) with a point at which associated with weak damping over a more or less extended wave number range k. As shown by particle-in-cell $\frac{\partial f_h}{\partial v} \sim 0$ simulations, this so-called plateau plasma drives primarily Langmuir oscillations at the plasma frequency (ωe) with k = 0 over long times without remarkable change of the distribution function. These Langmuir oscillations act as a pump wave for parametric decay by which an electron-acoustic wave slightly below ωe and a counterstreaming ion-acoustic wave are generated. Both high-frequency waves have nearly the same amplitude, which is given by the product of plateau density and velocity. Beating of these two wave types leads to pronounced Langmuir amplitude modulation, in reasonable agreement with solar wind and terrestrial foreshock observations made by the Wind spacecraft.

The Brazilian decimetric array and space weather

Hanumant S. **Sawant**a, , Natchimuthuk Gopalswamyb, Reinaldo R. Rosac, Robert A. Sychd, Sergey A. Anfinogentovd, Francisco C.R. Fernandese, , , José R. Cecattoa and Joaquim E.R. Costaa
Journal of Atmospheric and Solar-Terrestrial Physics, Volume 73, Issues 11-12, July **2011**, Pages 1300-1310

We report on the development and current status of the Brazilian Decimetric Array (BDA), which will play a vital role in filling the existing gaps in imaging the Sun at decimetric wavelengths. The BDA will operate in the following radio bands: 1.2–1.7, 2.8, and 5.6 GHz with high spatial and temporal resolutions. BDA can observe flares and coronal mass ejections (CMEs) in a spectral range poorly covered in the past, thus providing important information to space weather science. The smallest baseline of 9 m employed by the BDA combined with high sensitivity will readily identify large-scale structures such as coronal holes and provide information on wave flows from them. New methods are being developed to analyze the solar-disk data with high time resolution by using tomographic and spatial PWF techniques that can readily identify coronal holes in their initial stage. Efforts are also being made to analyze the BDA data in real time in conjunction with SOHO data for a better understanding of CMEs and coronal holes. This paper provides a brief description of the BDA, and the new techniques of data analysis.

Highlights of the Brazilian Solar Spectroscope

H.S. **Sawant**, J.R. Cecatto, H. Mészárosová, C. Faria, F.C.R. Fernandes, M. Karlický, M.C. de Andrade
Advances in Space Research, Volume 44, Issue 1, *Pages 54-57,* **2009**

The digital, decimetric (950–2500 MHz) Brazilian Solar Spectroscope (BSS, Sawant, H.S., Subramanian, K.R., Faria, C., et al. Brazilian Solar Spectroscope (BSS). Solar Phys. 200, 167–176, 2001) with high time (10–1000 ms) and frequency (1–10 MHz) resolution is in regular operation since April, 1998, at the National Space Research Institute (INPE) at São José dos Campos, Brazil. The BSS has now been upgraded with a new digital data acquisition and data processing system. The new version of the BSS has improved the observational possibilities with the capability to record up to 200 frequency channels available in the selectable frequency range 950–2500 MHz. The GPS receiver permits the acquisition of data with time accuracy in the order of 0.1 ms. The software system of the BSS is composed by two distinct modules: the first, data acquisition system provides a flexible Graphical User Interface (GUI) that allows one to choose the observational parameters. The second module is the real time visualization system that permits real time visualization of the observed dynamic spectrum and additionally allows procedures for visualization and preliminary analysis of the recorded solar spectra. Using the new visualization system, we have realized two new types of dm-radio fine structures: narrow band type III bursts with positive as well as negative group frequency drift and dots emissions arranged in zebra-like and fiber-like chains. Furthermore, we have found flare generated fast wave trains according to their tadpole signature in wavelet power spectra for a decimetric type IV radio event (June 6, 2000 flare).

Brazilian Decimetric Array (Phase-I)

H. S. **Sawant**, R. Ramesh, J. R. Cecatto, C. Faria, F. C. R. Fernandes, R. R. Rosa, M. C. Andrade, S. Stephany, L. B. T. Cividanes, C. A. I. Miranda, L. C. L. Botti, J. W. S. V. Boas, J. H. Saito, C. E. Moron, N. D. Mascarenhas, K. R. Subramanian, M. S. Sundararajan, E. Ebenezer, M. R. Sankararaman
Solar Phys., 242(1-2), Page: 213 – 220, 2007.

System Equivalent Flux Density of LWA1 Beams
Schinzel, F., and Polisensky, E.
2014, **Long Wavelength Array** Memo Series, No. 202
http://www.ece.vt.edu/swe/lwa/

Analysis of RHESSI Flares Using a Radio Astronomical Technique
E. J. **Schmah**l, R. L. Pernak, G. J. Hurford, J. Lee, S. Bong
Solar Phys. 240 (2), Page: 241 – 252, **2007**
The hard X-ray visibilities, which are mathematically identical to the visibilities of radio imaging, were input to software developed for mapping solar flares in the microwave domain using the Maximum Entropy Method (MEM).

Type II Radio Emission From Sun To Earth And In The Lower Corona
Joachim **Schmidt**∗1 and Iver Cairns
CESRA Abstract **2016**
http://cesra2016.sciencesconf.org/conference/cesra2016/pages/CESRA2016_prog_abs_book_v1.pdf
Type II radio emission is an important tracer of Coronal Mass Ejections (CMEs), shocks, and electron acceleration in the solar corona and the inner heliosphere. We focus first on the simulation of a CME event and the related radio emission on **29 November to 1 December 2013**, observed with STEREO and Wind, where the radio emission was observed intermittently from about 10 solar radii to 1 AU. The predictions agree very well with the observations: the frequencies are within 20 per cent of the observations, the intensities within a factor of 10 over the observed range of 6 orders of magnitude, and the time within 5%. We show that the intermittent bursts of radio emission occur predominantly when the magnetic field in a large enough volume is close to perpendicular to the normal of the CME-driven shock front. Additional causes are the growth of the radio-emitting volume upstream of the shock front and other variations of the local plasma parameters. We also simulated a CME event in the lower corona on **7 September 2014**, which led to a metric split-band type II burst observed by the Murchison Widefield Array (MWA). Again, we find excellent agreement between the observed and simulated radio emissions. We can show that the splitting of the bands is due to two spatially separated radio sources existing, one closer to the nose and one closer to a flank of the driven shock, which emit at different frequencies. The results suggest that we are close to quantitatively understanding type II solar radio bursts.

The solar type II radio bursts of 7 March 2012: detailed simulation analyses†
J. M. **Schmidt**, I. H. Cairns, and V. V. Lobzin
JGR, Volume 119, Issue 8, pages 6042–6061, **2014**
Type II solar radio bursts are often indicators for impending space weather events at Earth. They are consequences of shock waves driven by coronal mass ejections (CMEs) that move outwards from the Sun. We simulate such type II radio bursts by combining elaborate three-dimensional (3D) magnetohydrodynamic (MHD) predictions of realistic CMEs near the Sun with an analytic kinetic radiation theory developed recently. The simulation approach includes the reconstruction of initial solar magnetic fields, the dimensioning of the initial flux rope of the CME with STEREO spacecraft data, and the launch of the CME into an empirical data-driven corona and solar wind. In this paper we simulate a complicated double CME event (a very fast CME followed by a slower CME without interaction) and the related coronal and interplanetary type II radio bursts that occured on **7 March 2012**. We extend our previous work to show harmonic and interplanetary emission as well as the simulation's surprising ability (for these events at least) for predicting emission for two closely-spaced CMEs leaving the same active region. We demonstrate that the theory predicts well the observed fundamental and harmonic emission from ~20 MHz to 50 kHz, or from thehigh corona to near 1 AU. Specifically, the theory predicts flux, frequency, and time variations that are consistent with the presence or absence of observed type II emissions when interfering emissions are absent and are not inconsistent with observations when interfering type III bursts are present. The predicted and observed type II emission is predominantly fundamental for these 2 events. Harmonic emission occurs for the second CME only for a short time interval, when an extended shock has developed that can drive flank emission. The coronal and interplanetary emission follow closely hyperbolic lines in frequency-time space, consisting of a succession of islands of emission with varying intensity. The islands develop due to competition between the shock moving through varying coronal and solar wind magnetic field structures (e.g., loops and streamers), growth of the driven radio source due to the spherical expansion of the shock, and movement of the active radio sources from the shock's nose to its flanks.

Type II solar radio bursts predicted by 3D MHD CME and kinetic radio emission simulations†

J. M. **Schmidt***, Iver H. Cairns

JGR, Volume 119, Issue 1, pages 69–87, January **2014; File**

http://onlinelibrary.wiley.com/doi/10.1002/2013JA019349/pdf

Impending space weather events at Earth are often signalled by type II solar radio bursts. These bursts are generated upstream of shock waves driven by coronal mass ejections (CMEs) that move away from the Sun. We combine elaborate three-dimensional (3D) magnetohydrodynamic (MHD) predictions of realistic CMEs near the Sun with a recent analytic kinetic radiation theory in order to simulate two type II bursts. Magnetograms of the Sun are used to reconstruct initial solar magnetic and active region fields for the modeling. STEREO spacecraft data are used to dimension the flux rope of the initial CME, launched into an empirical data driven corona and solar wind. We demonstrate impressive accuracy in time, frequency, and intensity for the two type II bursts observed by the WIND spacecraft on **15 February 2011 and 7 March 2012**. Propagation of the simulated CME-driven shocks through coronal plasmas containing pre-existing density and magnetic field structures that stem from the coronal setup and CME initiation closely reproduce the isolated islands of type II emission observed. These islands form because of a competition between the growth of the radio source due to spherical expansion, and a fragmentation of the radio source due to increasingly radial fields in the nose region of the shock and interactions with streamers in the flank regions of the shock. Our study provides strong support for this theory for type II bursts and implies that the physical processes involved are understood. It also supports a near-term capability to predict and track these events for space weather predictions.

PREDICTION OF TYPE II SOLAR RADIO BURSTS BY THREE-DIMENSIONAL MHD CORONAL MASS EJECTION AND KINETIC RADIO EMISSION SIMULATIONS

J. M. **Schmidt**1, Iver H. Cairns1, and D. S. Hillan

2013 ApJ 773 L30; **File**

Type II solar radio bursts are the primary radio emissions generated by shocks and they are linked with impending space weather events at Earth. We simulate type II bursts by combining elaborate three-dimensional MHD simulations of realistic coronal mass ejections (CMEs) at the Sun with an analytic kinetic radiation theory developed recently. The modeling includes initialization with solar magnetic and active region fields reconstructed from magnetograms of the Sun, a flux rope of the initial CME dimensioned with STEREO spacecraft observations, and a solar wind driven with averaged empirical data. We demonstrate impressive accuracy in time, frequency, and intensity for the CME and type II burst observed on **2011 February 15**. This implies real understanding of the physical processes involved regarding the radio emission excitation by shocks and supports the near-term development of a capability to predict and track these events for space weather prediction.

Type II radio bursts: 2. Application of the new analytic formalism

Schmidt, J. M., and I. H. Cairns

J. Geophys. Res., 117, A11104, doi:10.1029/2012JA017932, **2012; File**

Type II radio bursts drift in frequency as shock waves and coronal mass ejections (CMEs) move through the Sun's corona and the solar wind. This paper applies an extended analytic theoretical model for type II radio bursts to an MHD simulation of the rippled shock front found upstream of the flanks of a CME. The theory treats the acceleration of electrons at the shock, formation of electron beams, growth of Langmuir waves, and conversion of Langmuir energy into radiation. The extended theory is entirely analytic and includes kappa electron velocity distribution functions for the ambient plasma electrons and the shock-reflected electrons. It also includes the plateauing of the electron beam, which releases energy for the Langmuir waves. This paper presents and discusses our numerical results for synthetic radio source regions and synthetic dynamic spectra, gained by applying our radiation model to an MHD simulation of a shock driven by a CME. The investigation reveals strong emission upstream of the flanks of the shock. A complicated rippled shock geometry develops with embedded “ripples” that stimulate short-lived “bright spot” radio sources, which lead to complicated substructures in the dynamic spectrum, and more extended sources that usually have a weaker and more diffuse radio emission. The natural development of ripples on the shock provides a natural link between the ripple theory of Knock, Cairns, and colleagues and the bolt-on model presented here.

Type II radio bursts: 1. New entirely analytic formalism for the electron beams, Langmuir waves, and radio emission

J. M. **Schmidt**1 and Iver H. Cairns1

JOURNAL OF GEOPHYSICAL RESEARCH, VOL. 117, A04106, **2012, File**

Type II radio bursts drift in frequency as shock waves and coronal mass ejections (CMEs) move through the Sun's corona and the solar wind. This paper extends the theoretical models for type II radio bursts of Knock et al. (2001, 2003), Knock and Cairns (2005), Cairns and Knock (2006) and Schmidt and Gopalswamy (2008). The theory treats the acceleration of electrons at the shock, formation of electron beams, growth of Langmuir waves, and conversion of Langmuir energy into radiation. An entirely analytical and more general formalism is developed, which includes kappa electron velocity distribution functions for the plasma electrons and the shock-reflected electron beam. The radiation model also includes the plateauing of the electron beam, which releases energy for the Langmuir waves. This paper has two parts. First, the new entirely analytical formalism is presented. Second, first numerical results for synthetic radio images and synthetic dynamic spectra are discussed, gained by applying our radiation model to MHD simulations of a shock driven by a CME. The results are compared with earlier analytic approaches. This work is also applicable to other shock-related emissions in space and astrophysical plasmas.

Synthetic radio maps of CME-driven shocks below 4 solar radii heliocentric distance,

Schmidt, J. M., and N. Gopalswamy
J. Geophys. Res., 113, A08104, **2008; File**
http://dx.doi.org/10.1029/2007JA013002
We present 2 1/2 D numerical MagnetoHydroDynamic (MHD) simulations of coronal mass ejections (CMEs) in conjunction with plasma simulations of radio emission from the CME-driven shocks. The CME-driven shock extends to an almost spherical shape during the temporal evolution of the CME. Our plasma simulations can reproduce the dynamic spectra of coronal type II radio bursts, with the frequency drift rates corresponding to the shock speeds. We find further, that the CME-driven shock is an effective radio emitter at metric wavelengths, when the CME has reached a heliocentric distance of about two solar radii ($R_\odot$). We apply our simulation results to explain the radio images of type II bursts obtained by radio heliographs, in particular to the banana-shaped images of radio sources associated with fast CMEs.

The effect of initial conditions on the electromagnetic radiation generation in type III solar radio bursts

H. **Schmitz**, D. Tsiklauri
E-print, May **2013**; Phys. Plasmas
Extensive particle-in-cell simulations of fast electron beams injected in a background magnetised plasma with a decreasing density profile were carried out. These simulations were intended to further shed light on a newly proposed mechanism for the generation of electromagnetic waves in type III solar radio bursts [D. Tsiklauri, Phys. Plasmas, 18, 052903 (2011)]. The numerical simulations were carried out using different density profiles and fast electron distribution functions. It is shown that electromagnetic L and R modes are excited by the transverse current, initially imposed on the system. In the course of the simulations no further interaction of the electron beam with the background plasma could be observed.

The Slowly Varying Corona. II. The Components of F 10.7 and Their Use in EUV Proxies

S. J. **Schonfeld**1,4, S. M. White2, C. J. Henney2, R. A. Hock-Mysliwiec2, and R. T. J. McAteer3
2019 ApJ 884 141
sci-hub.se/10.3847/1538-4357/ab3af9
https://arxiv.org/pdf/1910.12964.pdf
Using four years of full-disk-integrated coronal differential emission measures calculated in Schonfeld et al. (2017), we investigate the relative contribution of bremsstrahlung and gyroresonance emission in observations of F 10.7, the 10.7 cm (2.8 GHz) solar microwave spectral flux density and commonly used activity proxy. We determine that the majority of coronal F 10.7 is produced by the bremsstrahlung mechanism, but the variability observed over individual solar rotations is often driven by gyroresonance sources rotating across the disk. Our analysis suggests that the chromosphere may contribute significantly to F 10.7 variability and that coronal bremsstrahlung emission accounts for 14.2 ± 2.1 sfu (~20%) of the observed solar minimum level. The bremsstrahlung emission has a power-law relationship to the total F 10.7 at high activity levels, and this combined with the observed linearity during low activity yields a continuously differentiable piecewise fit for the bremsstrahlung component as a function of F 10.7. We find that the bremsstrahlung component fit, along with the Mg ii index, correlates better with the observed 5–37 nm spectrum than the common 81 day averaged F 10.7 proxy. The bremsstrahlung component of F 10.7 is also well approximated by the moderate-strength photospheric magnetic field parameterization from Henney et al. (2012), suggesting that it could be forecast for use in both atmospheric research and operational models.

Coronal Sources of the Solar F10.7 Radio Flux

S. J. **Schonfeld**1, S. M. White2, C. J. Henney2, C. N. Arge2, and R. T. J. McAteer

2015 ApJ 808 29
http://arxiv.org/pdf/1508.00599v1.pdf
We present results from the first solar full-disk $F_{10.7}$ (the radio flux at 10.7 cm, 2.8 GHz) image taken with the S-band receivers on the recently upgraded Karl G. Jansky Very Large Array in order to assess the relationship between the $F_{10.7}$ index and solar extreme ultraviolet (EUV) emission. To identify the sources of the observed 2.8 GHz emission, we calculate differential emission measures from EUV images collected by the Atmospheric Imaging Assembly and use them to predict the bremsstrahlung component of the radio emission. By comparing the bremsstrahlung prediction and radio observation we find that 8.1% ± 0.5% of the variable component of the $F_{10.7}$ flux is associated with the gyroresonance emission mechanism. Additionally, we identify optical depth effects on the radio limb which may complicate the use of $F_{10.7}$ time series as an EUV proxy. Our analysis is consistent with a coronal iron abundance that is four times the photospheric level. **2011 December 9**

Improved Type III solar radio burst detection using congruent deep learning models

Jeremiah **Scully**, Ronan Flynn, Peter Gallagher, Eoin Carley, Mark Daly
A&A 674, A218 **2023**
https://arxiv.org/pdf/2305.09327.pdf
Solar flares are energetic events in the solar atmosphere that are often linked with solar radio bursts (SRBs). SRBs are observed at metric to decametric wavelengths and are classified into five spectral classes (Type I--V) based on their signature in dynamic spectra. The automatic detection and classification of SRBs is a challenge due to their heterogeneous form. Near-realtime detection and classification of SRBs has become a necessity in recent years due to large data rates generated by advanced radio telescopes such as the LOw Frequency ARray (LOFAR). In this study, we implement congruent deep learning models to automatically detect and classify Type III SRBs. We generated simulated Type III SRBs, which were comparable to Type IIIs seen in real observations, using a deep learning method known as Generative Adversarial Network (GAN). This simulated data was combined with observations from LOFAR to produce a training set that was used to train an object detection model known as YOLOv2 (You Only Look Once). Using this congruent deep learning model system, we can accurately detect Type III SRBs at a mean Average Precision (mAP) value of 77.71%. **10 Sep 2017**

Simulating Solar Radio Bursts Using Generative Adversarial Networks

Jeremiah **Scully**, Ronan Flynn, Eoin Carley, Peter Gallagher & Mark Daly
Solar Physics volume 298, Article number: 6 (**2023**)
https://doi.org/10.1007/s11207-022-02099-x
https://www.aanda.org/articles/aa/pdf/2023/06/aa46404-23.pdf
Solar flares are one of the most extreme drivers of space weather in our solar system. The impulsive solar radio emission associated with a solar flare is known as a solar radio burst (SRB). They are generally studied in dynamic spectra and are classified into five major spectral classes, ranging from Type I to Type V, based on their form and frequency, and time duration. Due to their intricate characterisation, generating a training set for object-detection and classification models of such phenomena is a difficulty in machine learning. Current algorithms implement parametric modelling where the quantity, grouping, intensity, drift rate, heterogeneity, start–end frequency and start–end time of Type-III and Type-II radio bursts are all random. However, this model does not factor in the true shape or general features seen in real dynamic spectra observations of the Sun, which can be crucial when training classification or object-detection algorithms. In this research, we introduce a methodology named a Generative Adversarial Network (GAN) for generating realistic SRB simulations. By using real examples of Type-III and Type-II SRB data, we can train GANs to generate images almost comparable to real observed data. Furthermore, we evaluate the results of the generated model using human perception, then we compare and contrast the results using a metric known as the Fréchet Inception Distance.

Type III solar radio burst detection and classification: A deep learning approach

Jeremiah **Scully**, Ronan Flynn, Eoin Carley, Peter Gallagher, Mark Daly
Irish Signals & Systems Conference **2021**
https://arxiv.org/pdf/2105.13387.pdf
Solar Radio Bursts (SRBs) are generally observed in dynamic spectra and have five major spectral classes, labelled Type I to Type V depending on their shape and extent in frequency and time. Due to their complex characterisation, a challenge in solar radio physics is the automatic detection and classification of such radio bursts. Classification of SRBs has become fundamental in recent years due to large data rates generated by advanced radio telescopes such as the LOw-Frequency ARray, (LOFAR). Current state-of-the-art algorithms implement the Hough or Radon transform as a means of detecting predefined parametric shapes in images. These algorithms achieve up to 84% accuracy, depending on the Type of radio burst being classified. Other techniques include procedures that rely on Constant-FalseAlarm-Rate detection, which is essentially detection of radio bursts using a de-noising and adaptive threshold in dynamic spectra. It works well for a variety of different Types of radio bursts and achieves an accuracy of up to 70%. In this research, we

are introducing a methodology named You Only Look Once v2 (YOLOv2) for solar radio burst classification. By using Type III simulation methods we can train the algorithm to classify real Type III solar radio bursts in real-time at accuracy of 82.63% with a maximum 77 frames per second (fps).

The Solar Radius at 37 GHz through Cycles 22 to 24

Caius L. **Selhorst**, Juha Kallunki, C. G. Giménez de Castro, Adriana Valio, Joaquim E. R. Costa

Solar Phys. **294**, Article number: 175 **2019**

https://arxiv.org/pdf/1912.01671.pdf

https://link.springer.com/content/pdf/10.1007/s11207-019-1568-6.pdf

To better understand the influence of the activity cycle on the solar atmosphere, we report the time variation of the radius observed at 37 GHz (λ=8.1 mm) obtained by the Metsähovi Radio Observatory (MRO) through Solar Cycles 22 to 24 (1989-2015). Almost 5800 maps were analyzed, however, due to instrumental setups changes the data set showed four distinct behaviors, which requested a normalisation process to allow the whole interval analysis. When the whole period was considered, the results showed a positive correlation index of 0.17 between the monthly means of the solar radius at 37 GHz and solar flux obtained at 10.7 cm (F10.7). This correlation index increased to 0.44, when only the data obtained during the last period without instrumental changes were considered (1999-2015). The solar radius correlation with the solar cycle agrees with the previous results obtained at mm/cm wavelengths (17 and 48 GHz), nevertheless, this result is the opposite of that reported at submillimetre wavelengths (212 and 405 GHz).

Solar polar brightening and radius at 100 and 230 GHz observed by ALMA

Caius L. **Selhorst**, Paulo J. A. Simões, Roman Brajša, Adriana Valio, C. G. Giménez de Castro, Joaquim E. R. Costa, Fabian Menezes, Jean Pierre Rozelot, Antonio S. Hales, Kazumasa Iwai, Stephen White

ApJ **871** 45 **2019**

https://arxiv.org/pdf/1811.12158.pdf

sci-hub.tw/10.3847/1538-4357/aaf4f2

Polar brightening of the Sun at radio frequencies has been studied for almost fifty years and yet a disagreement persists between solar atmospheric models and observations. Some observations reported brightening values much smaller than the expected values obtained from the models, with discrepancies being particularly large at millimeter wavelengths. New clues to calibrate the atmospheric models can be obtained with the advent of the Atacama Large Millimeter/submillimeter Array (ALMA) radio interferometer. In this work, we analyzed the lower limit of the polar brightening observed at 100 and 230 GHz by ALMA, during its Science Verification period, **2015 December 16-20**. We find that the average polar intensity is higher than the disk intensity at 100 and 230 GHz, with larger brightness intensities at the South pole in eight of the nine maps analyzed. The observational results were compared with calculations of the millimetric limb brightnening emission for two semi-empirical atmospheric models, FAL- C (Fontenla et al. 1993) and SSC (Selhorst et al. 2005a). Both models presented larger limb intensities than the averaged observed values. The intensities obtained with the SSC model were closer to the observations, with polar brightenings of 10.5% and 17.8% at 100 and 230 GHz, respectively. This discrepancy may be due to the presence of chromospheric features (like spicules) at regions close to the limb.

Association of radio polar cap brightening with bright patches and coronal holes

Caius L. **Selhorst**, Paulo J. A. Simoes, Alexandre J. Oliveira e Silva, C. G. Gimenez de Castro, Joaquim E. R. Costa, Adriana Valio

ApJ **851** 146 **2017**

https://arxiv.org/pdf/1711.02163.pdf

http://iopscience.iop.org.sci-hub.tw/0004-637X/851/2/146/

Radio-bright regions near the solar poles are frequently observed in Nobeyama Radioheliograph (NoRH) maps at 17 GHz, and often in association with coronal holes. However, the origin of these polar brightening has not been established yet. We propose that small magnetic loops are the source of these bright patches, and present modeling results that reproduce the main observational characteristics of the polar brightening within coronal holes at 17 GHz. The simulations were carried out by calculating the radio emission of the small loops, with several temperature and density profiles, within a 2D coronal hole atmospheric model. If located at high latitudes, the size of the simulated bright patches are much smaller than the beam size and they present the instrument beam size when observed. The larger bright patches can be generated by a great number of small magnetic loops unresolved by the NoRH beam. Loop models that reproduce bright patches contain denser and hotter plasma near the upper chromosphere and lower corona. On the other hand, loops with increased plasma density and temperature only in the corona do not contribute to the emission at 17 GHz. This could explain the absence of a one-to-one association between the 17 GHz bright patches and those observed in extreme ultraviolet. Moreover, the emission arising from small magnetic loops located close to the limb may merge with the usual limb brightening profile, increasing its brightness temperature and width.

CESRA Highlight # 1807 March **2018** http://www.astro.gla.ac.uk/users/eduard/cesra/?p=1807

The 17 GHz active region number

C. L. **Selhorst**, J. E. R. Costa, C. G. Giménez de Castro, A. Valio, A. A. Pacini, K. Shibasaki
ApJ, 790 134, **2014**
http://arxiv.org/pdf/1406.2252v2.pdf

We report the statistics of the number of active regions (NAR) observed at 17 GHz with the Nobeyama Radioheliograph between 1992, near the maximum of cycle 22, and 2013, that also includes the maximum of cycle 24, and we compare with other activity indexes. We find that NAR minima are shorter than those of the sunspot number (SSN) and radio flux at 10.7 cm (F10.7). This shorter NAR minima could reflect the presence of active regions generated by faint magnetic fields or spotless regions, which were a considerable fraction of the counted active regions. The ratio between the solar radio indexes F10.7/NAR shows a similar reduction during the two minima analyzed, which contrasts with the increase of the ratio of both radio indexes in relation to the SSN during the minimum of cycle 23-24. These results indicate that the radio indexes are more sensitive to weaker magnetic fields than those necessary to form sunspots, of the order of 1500 G. The analysis of the monthly averages of the active region brightness temperatures shows that its long term variation mimics the solar cycle, although, due to the gyro-resonance emission, a great number of intense spikes are observed in the maximum temperature study. The decrease, in number, of these spikes is also evident during the current cycle 24, a consequence of the sunspot magnetic field weakening in the last years.

THE BEHAVIOR OF THE 17 GHz SOLAR RADIUS AND LIMB BRIGHTENING IN THE SPOTLESS MINIMUM XXIII/XXIV

C. L. **Selhorst**1, C. G. Giménez de Castro2, A. Válio2, J. E. R. Costa3 and K. Shibasaki
2011 ApJ 734 64

The current solar minimum has surprised the entire solar community because the spotless period is presently almost 2-3 years longer than the usual minima. To better understand this, we studied the variation of the solar radius and the polar limb brightening at 17 GHz, comparing the results from the minimum at the end of cycle XXIII with those of the previous one. Daily maps obtained by the Nobeyama Radioheliograph (NoRH) from 1992 through 2010 were analyzed. Whereas the variation of the solar radius at radio frequencies indicates the heating of the solar atmosphere due to solar activity, the limb brightening intensity depends on the organization of the polar magnetic field of the Sun, including the global dipole and the features formed around it. These features are more prominent during minima periods. As a common result, researchers have observed a decrease in both radius and limb brightness intensity at 17 GHz during the present minimum when compared with the previous one. The mean solar radius is 09 ± 06 smaller and the limb brightening reduced its intensity by around 20%. Both decrements are interpreted in terms of the weaker solar chromospheric activity of the present cycle. Measurement of the radius and limb brightening at 17 GHz can be used as an alternative solar activity index and should be included in the set of parameters used to predict future cycles.

The influence of spicules in the solar radius at multiple radio wavelengths

Caius L. **Selhorst**1,2, Adriana Silva-V´alio2, Priscila A. Martins2,
Daiane B. Seriacopi2, Pierre Kaufmann2 and Hugo Levato3
Solar and Stellar Variability: Impact on Earth and Planets, Proceedings IAU Symposium No. 264, **2009**, p. 285-287, A.G. Kosovichev, A.H. Andrei & J.-P. Rozelot, eds.
Y:\obridko\otchet09

In this work, we analyze observations of the solar radius at 22 and 43 GHz obtained with the 13.7 m antenna of the Itapetinga Radio Observatory (Atibaia, Brazil) and at submillimeter-wave frequencies, 212 and 405 GHz, obtained by the Solar Submillimeter-wave Telescope (SST) (El Leoncito, San Juan, Argentina). The radius is defined as the limb position where the intensity is equal to half of the quiet Sun value. These measured radii are then compared with those predicted by a model of the solar atmosphere proposed by Selhorst, Silva, and Costa (2005). The results show that at 22 and 43 GHz, the emission comes from regions high in the chromosphere. Furthermore, the Itapetinga observations yield radii of 985”±5” and 981”±6”, at 22 and 43 GHz respectively, consistent with the theoretical positions in the atmosphere. On other hand, the submillimeter observations resulted in a mean radius of 972”±3” and 975”±5” at 212 and 405 GHz, respectively, considered equal within the uncertainties. The latter results can be explained by the origin of the emission being very close to the region of minimum temperature, between the photosphere and chromosphere. This is a dynamic region largely affected by many solar features, like spicules and plages.

Multiwavelength Analysis of the Kinematics of a Long Duration Flare-CME Event on 27 January 2012

G. **Selvarani**, S. Prasanna Subramanian, A. Shanmugaraju & K. Suresh
Solar Physics volume 295, Article number: 121 (**2020**)
https://link.springer.com/content/pdf/10.1007/s11207-020-01693-1.pdf

We present a detailed analysis of a long-duration flare associated with a coronal mass ejection (CME) event that occurred on 27 January 2012 in the active region (AR) 11402. We analyze the kinematics of the CME and the close relationship between the flare, radio burst, and CME. We used STEREO (Solar Terrestrial Relations Observatory)/EUVI A (Extreme Ultraviolet Imager) and white light data from STEREO (COR1 A and COR2 A) and LASCO (Large Angle and Spectrometric COronagraph) (C2/C3) coronagraphs, and X-ray data from the GOES (Geostationary Operational Environmental Satellite) spacecraft. The height of the CME is measured using the Graduated Cylindrical Shell (GCS) model. Our results show that: i) the speed of the CME (1460 km/s at 2.54 R⊙) is comparable to the speed of the type II radio burst (1581 km/s), ii) the height of the type II radio burst is lower than that of the CME leading edge, iii) the CME acceleration phase is found to be related to the rise time of the flare and its propagation phase is related to the decay phase of the flare, iv) the type II radio burst origin is likely to be near the CME region where a CME-streamer interaction takes place around 1.6 R⊙, and v) the sequence of events and the CME kinematics show a close association between the CME and type II radio emissions.

Investigation on M-class Flare-Associated Coronal Mass Ejections with and Without DH Type II Radio Bursts

G. **Selvarani**, A. Shanmugaraju, Bojan Vrsnak, M. Bendict Lawrance
Sol Phys (**2017**) 292: 74. doi:10.1007/s11207-017-1097-0
http://link.springer.com/article/10.1007/s11207-017-1097-0

We perform a statistical analysis on 157 M-class soft X-ray flares observed during 1997 – 2014 with and without deca-hectometric (DH) type II radio bursts aiming at the reasons for the non-occurrence of DH type II bursts in certain events. All the selected events are associated with halo Coronal Mass Ejections (CMEs) detected by the Solar and Heliospheric Observatory (SOHO) / Large Angle Spectrometric and COronograph (LASCO). Out of 157 events, 96 (61%; “Group I”) events are associated with a DH type II burst observed by the Radio and Plasma Wave (WAVES) experiment onboard the Wind spacecraft and 61 (39%; “Group II”) events occur without a DH type II burst. The mean CME speed of Group I is \(1022~\mbox{km}/\mbox{s}\) and that of Group II is \(647~\mbox{km}/\mbox{s}\). It is also found that the properties of the selected M-class flares such as flare intensity, rise time, duration and decay time are greater for the DH associated flares than the non-DH flares. Group I has a slightly larger number (56%) of western events than eastern events (44%), whereas Group II has a larger number of eastern events (62%) than western events (38%). We also compare this analysis with the previous study by Lawrance, Shanmugaraju, and Vršnak (Solar Phys.290, 3365L, 2015) concerning X-class flares and confirm that high-intensity flares (X-class and M-class) have the same trend in the CME and flare properties. Additionally we consider aspects like acceleration and the possibility of CME-streamer interaction. The average deceleration of CMEs with DH type II bursts is weaker (\(a = - 4.39\mbox{ m}/\mbox{s}^{2}\)) than that of CMEs without a type II burst (\(a = -12.21\mbox{ m}/\mbox{s}^{2}\)). We analyze the CME-streamer interactions for Group I events using the model proposed by Mancuso and Raymond (Astron. Astrophys.413, 363, 2004) and find that the interaction regions are the most probable source regions for DH type II radio bursts. **2002 March 15**

Table 2 M-class flares and their associated CMEs and DH type IIs (eastern events).
Table 3 M-class flares and their associated CMEs and DH type IIs (western events).
Table 5 Comparison of LASCO C2 height with CME-streamer interaction height calculated using the Mancuso and Raymond (2004) model.

Energy distribution of solar flare events

S. **Sen**, A. Mangalam, R. Ramesh (Indian Institute of Astrophysics)
Proceedings of IAU Symposium 340 **2018**
https://arxiv.org/pdf/1805.08431.pdf

Observational evidence of the braiding of magnetic field lines has been reported. The magnetic reconnection within the loop (nanoflares) and with other loops (microflares) disentangle the field. The coronal field then reorganizes itself to attain a force-free field configuration. We have evaluated the power law index of the energy distribution f(E)=f0E−α by using a model of relaxation incorporating different profile functions of winding number distribution f(w) based on braided topologies. We study the radio signatures that occur in the solar corona using the radio data obtained from the Gauribidanur Radio Observatory (IIA) and extract the power law index by using the Statistic-sensitive nonlinear iterative peak clipping (SNIP) algorithm. We see that the power law index obtained from the model is in good agreement with the calculated value from the radio data observation.

Implications of Flat Optically Thick Microwave Spectra in Solar Flares for Source Size and Morphology

Shaheda Begum **Shaik**, Dale E. Gary
2021 *ApJ* **919** 44
https://doi.org/10.3847/1538-4357/ac0fdb
https://arxiv.org/pdf/2107.00192.pdf

The study aims to examine the spectral dynamics of the low-frequency, optically thick gyrosynchrotron microwave emission in solar flares to determine the characteristics of the emitting source. We present the high-resolution spectra of a set of microwave bursts observed by the Expanded Owens Valley Solar Array (EOVSA) during its commissioning phase in the 2.5−18 GHz frequency range with 1 second time resolution. Out of the 12 events analyzed in this study, nine bursts exhibit a direct decrease with time in the optically thick spectral index αl, an indicator of source morphology. Particularly, five bursts display "flat" spectrum (αl≤1.0) compared to that expected for a homogeneous/uniform source (αl≈2.9). These flat spectra at the low-frequencies (<10 GHz) can be defined as the emission from a spatially inhomogeneous source with a large area and/or with multiple emission components. In a subset of six events with partial cross-correlation data, both the events with flat spectra show a source size of ∼120 arcsec at 2.6−3 GHz. Modeling based on inhomogeneity supports the conclusion that multiple discrete sources can only reproduce a flat spectrum. We report that these flat spectra appear predominantly in the decay phase and typically grow flatter over the duration in most of the bursts, which indicates the increasing inhomogeneity and complexity of the emitting volume as the flare progresses. This large volume of flare emission filled with the trapped energetic particles is often invisible in other wavelengths, like hard X-rays, presumably due to the collisionless conditions in these regions of low ambient density and magnetic field strength. **2015: Mar 10, 12; Apr 21, May 5, Jun 21, Aug 22,24; Sep 24, 27**
Table 1. List of selected bursts observed by EOVSA (2015)

The growth of the longitudinal beam-plasma instability in the presence of an inhomogeneous background

Mohamad **Shalaby**, Avery E. Broderick, Philip Chang, Christoph Pfrommer, Ewald Puchwein, Astrid Lamberts
Journal of Plasma Physics **2020**
https://arxiv.org/pdf/2003.02849.pdf

We study the longitudinal stability of beam-plasma systems in the presence of a density inhomogeneity in the background plasma. Previous works have focused on the non-relativistic regime where hydrodynamical models are used to evolve pre-existing Langmuir waves within inhomogeneous background plasmas. Here, for the first time we study the problem with kinetic equations in a fully-relativistic way. We do not assume the existence of Langmuir waves, and we focus on the rate and the mechanism by which waves are excited in such systems from an initial perturbation. We derive the structure of the unstable modes and compute an analytical approximation for their growth rates. Our computation is limited to dilute and cold beams, and shows an excellent agreement with particle-in-cell simulations performed using the SHARP code. We show that, due to such an inhomogeneity, the virulent beam-plasma instabilities in the intergalactic medium are not suppressed but their counterparts in the solar wind can be suppressed as evidenced by propagating type-III solar radio bursts.

Relationship between microwave and metre ranges during an impulsive solar flare

J N **Shamsutdinova**, L K Kashapova, J Zhang, H Reid, D A Zhdanov
MNRAS, Volume 533, Issue 2, September **2024**, Pages 1453–1462,
https://doi.org/10.1093/mnras/stae1899
https://watermark.silverchair.com/stae1899.pdf

An analysis of solar flares with simple temporal structures can help us to understand the features and mechanisms of energy and particle propagation. A weak impulsive solar flare that occurred on **2021 June 3** provided such opportunity. For the purposes of the study, we used microwave observations with spatial resolution from the Siberian Radioheliograph (3–6 GHz) combined with various spectral radio and X-ray data. Flare topology analysis revealed a configuration consisting of a small loop or dome-like structure associated with a compact bright source, and a long high loop system associated with the diffuse source. This indicates a compact and relatively low-lying site of acceleration and initial energy release. The radio metre and the microwave emission demonstrated a peak-to-peak correlation in three of the four bursts. The delays obtained from comparing microwave and metre radio ranges are in good agreement with the delays from the metre dynamic spectrum analysis, but the different radio bursts had different delays. We found that the electron energies derived from metre dynamic spectrum analysis are lower than those shown by hard X-ray emissions. According to the results of theoretical simulations, this can be explained by the expansion of magnetic loops with altitude. The difference in drift velocities for various radio bursts can be the result of the different size of the loop where the electron beams are propagated. This can be a feature related to the configuration type of the studied flare.

Spatial and Spectral Evolution of Microwave and X-Ray Sources During the Solar Limb Flare on February 5, 2023.

Shamsutdinova, J.N., Kashapova, L.K., Li, Z. et al.
Sol Phys 299, 80 (**2024**).
https://doi.org/10.1007/s11207-024-02331-w

We present an empirical scenario of the energy release process during a solar limb flare on **February 5, 2023**. This event was observed by the Siberian Radioheliograph (SRH) within the 3 – 12 GHz range and the Advanced Space-based Solar Observatory / Hard X-ray Imager (ASO-S/HXI) within 10 – 300 keV range. The combination of these data allowed us to use information not only about the spectral features but also about the spatial evolution of the flare. The main source of the energy released was a small compact loop which was revealed in both the X-ray and microwave ranges. During the early phases of the flare evolution, a spectral analysis of microwave emission showed that thermal gyrosynchrotron emission turned to gyrosynchrotron emission of nonthermal electrons. This indicated the transition from the heating process to the acceleration processes. Spectral indices derived from hard X-ray and microwave data closely agree with each other and show the classical soft–hard–soft scenario of acceleration. The hardening of the average microwave spectrum at the end of the impulsive phase was caused by the contribution of jet emission to microwaves rather than by peculiarities of the acceleration processes.

SolarNuggets RHESSI Science Nugget, No. **482**, Dec **2024**
https://heliowiki.smce.nasa.gov/wiki/index.php/Spatial_and_Spectral_Evolution_of_Microwave_and_X-Ray_Sources_During_the_Limb_Flare_SOL2023-02-05

The Calibration of the 35–40 GHz Solar Radio Spectrometer with the New Moon and a Noise Source

ZiQian **Shang** (尚自乾)1, Zhao Wu (武昭)1, Yan Liu (刘岩)1, Yu Bai (白宇)1, Guang Lu (路光)1, YuanYuan Zhang (张园园)1, Lei Zhang (张磊)1, YanRui Su (苏艳蕊)2, Yao Chen (陈耀)1, and FaBao Yan (严发宝)1,2
2023 ApJS 268 45
https://iopscience.iop.org/article/10.3847/1538-4365/acee00/pdf

Calibrating solar radio flux has always been a concern in the solar community. Previously, fluxes were calibrated by matching load or the new Moon for relative calibration, and at times with the assistance of other stations' data. Moreover, the frequency coverage seldom exceeded 26 GHz. This paper reports the upgraded and calibrated Chashan Broadband Solar millimeter spectrometer (CBS) working from 35 to 40 GHz at the Chashan Solar Observatory (CSO). Initially, the calibration of the solar radiation brightness temperature is accomplished using the new Moon as the definitive source. Subsequently, the 35–40 GHz standard flux is achieved by establishing the correlation between the solar radio flux, brightness temperature, and frequency. Finally, the calibration of the solar radio flux is implemented by utilizing a constant temperature-controlled noise source as a reference. The calibration in 2023 February and March reveals that the solar brightness temperature is 11,636 K at 37.25 GHz with a standard deviation (STD) of 652 K. The solar radio flux's intensity is ∼3000–4000 solar flux units (SFU) in the range of 35–40 GHz with a consistency bias of ±5.3%. The system sensitivity is about ∼5–8 SFU by a rough evaluation, a noise factor of about 200 K, and the coefficient of variation of the system transmission slope of 6.5% @ 12 hr at 37.25 GHz. It is expected that the upgraded CBS will capture more activity during the upcoming solar cycle.

A Broadband Solar Radio Dynamic Spectrometer Working in the Millimeter-wave Band

ZiQian **Shang**1, Ke Xu1, Yang Liu2, Zhao Wu1, Guang Lu1, YuanYuan Zhang1, Lei Zhang1, YanRui Su2, Yao Chen1, and FaBao Yan1,2
2022 ApJS 258 25
https://iopscience.iop.org/article/10.3847/1538-4365/ac4257/pdf

Most solar radio telescopes operate below ∼18 GHz and cannot realize a complete frequency coverage of the microwave spectrum, especially in the optically thin regime during solar bursts, which can provide unique information about the magnetic field in the burst area in the solar corona. Therefore, the development of high-frequency microwave observation equipment is demanded by the solar radio community. In this paper, we present a microwave spectrum observation system operating at 35–40 GHz. In this system, the solar radio signal is acquired by an 80 cm Cassegrain circularly polarized antenna, which is then downconverted and channelized by a **35–40 GHz** analog front end. The processed signal is finally sent to the digital receiver to generate the microwave dynamic spectrum, which is transmitted by gigabit Ethernet transmission to a host computer. The system performance has been tested and obtained as follows: a noise figure of ∼300 K, system linearity of >0.9999, time resolution of about 134 ms (default), and frequency resolution of 153 kHz. We further conduct calibration for this system and find that the observed Sun–Moon ratio is about 43.1–53.3 @ 35.25 GHz during the new Moon, and is quite close to the theoretical value. The coefficient of variation of the

system is ~0.61% in a 9 hr test. The system has been designed, developed, and tested for over 1 yr in **Chashan Solar Observatory** and is expected to play an important role in the microwave burst study in the 25th solar cycle.

Temporal and Spatial Association Between a Solar Flare, CME, and Radio Burst on 19 November 2013

A. **Shanmugaraju**, M. Syed Ibrahim, K. Suresh, P. Vijayalakshmi & Sajal Kumar Dhara
Solar Physics volume 296, Article number: 77 (**2021**)
https://link.springer.com/content/pdf/10.1007/s11207-021-01823-3.pdf
https://doi.org/10.1007/s11207-021-01823-3

We present multi-wavelength and multi-instrument observations and analysis of a major X 1.0 class flare, radio burst, halo coronal mass ejection (CME), and loop eruption from the solar active region NOAA 11893 on **19 November 2013** (SOL2013-11-19T10:26). The aim of this work is twofold: The first aim to study the evolution of the loop eruption and the second is to find the link between this eruption and radio emissions. Initial signatures of eruption from the solar source region are confirmed using observations from the Atmospheric Imaging Assembly onboard the Solar Dynamics Observatory in the hot channel at 94 Å wavelength. These observations confirm that the source of the CME was associated with a magnetic-loop eruption, which was visible before the flare initiation. The photospheric magnetic configuration displayed a complex network of βδβδ sunspots. After the eruption, a CME was observed by the Solar and Heliospheric Observatory/Large Angle and Spectrometric Coronagraph with linear speed and acceleration of 740 kms−1 and −2 ms−2, respectively. Dynamic radio-spectrum observation from the Learmonth Observatory in the metric frequency range shows Type-III and Type-II radio emissions that reveal the field-line opening and coronal-shock formation closely associated with the CME. From the metric Type-II radio observation and assuming Newkirk's density model, we estimate the shock formation height range of 1.14--1.54 R⊙ with the corresponding shock speed (≈650 kms−1). With the heliographic observations from the Nançay heliograph at different frequencies we could disentangle Type-II bursts from Type-III bursts. Likely, the Type-III burst would correspond to the loop eruption while the Type-II comes from the northern flank of the CME.

Occurrence Rate of Radio-Loud and Halo CMEs in Solar Cycle 25: Prediction Using their Correlation with the Sunspot Number

A. **Shanmugaraju**, P. Pappa Kalaivani, Y.-J. Moon & O. Prakash
Solar Physics volume 296, Article number: 75 (**2021**)
https://arxiv.org/pdf/2103.13699.pdf
https://link.springer.com/content/pdf/10.1007/s11207-021-01818-0.pdf
https://doi.org/10.1007/s11207-021-01818-0

Solar coronal mass ejections (CMEs) are known for their space-weather and geomagnetic consequences. Among all CMEs, the so-called radio-loud (RL) and halo CMEs are considered the most energetic in the sense that they are usually faster and wider than the general population of CMEs. Hence the study of RL and halo CMEs has become important and the prediction of their occurrence rate in a future cycle will help their forecasting. In this article we predict the occurrence rates of RL and halo CMEs in Solar Cycle (SC) 25, obtaining good correlations between the numbers of RL and halo CMEs in each year and the yearly mean sunspot number in the previous two cycles. The values of the sunspot number predicted by NOAA/NASA for SC 25 are considered to be representative and the corresponding numbers of RL and halo CMEs are determined using linear relations. Our results show that the maximum number of RL and halo CMEs will be around 39±3 and 45±4, respectively. Removing backside events, a set of front-side events is also considered separately and front-side events in SC 25 are also predicted. The peak values of front-side RL and halo events have been estimated to be around 31±3 and 29±3, respectively. These results are discussed in comparison with the predicted sunspot number values by different authors.

Heights of Coronal Mass Ejections and Shocks Inferred from Metric and DH Type II Radio Bursts

A. **Shanmugaraju**, M. Bendict Lawrance, Y. J. Moon, Jae-Ok Lee, K. Suresh
Solar Physics September **2017**, 292:136

A set of 27 continuous events that showed extension of metric Type-II radio bursts (m-Type IIs) into the deca–hectometric (DH) domain is considered. The coronal mass ejections (CMEs) associated with this type of continuous event supply more energy to produce space-weather effects than the CMEs that produce Type-II bursts in any one region. Since the heights of shock formation at the start of m-Type IIs were not available from observations, they were estimated using kinematic modeling in previous studies. In the present study, the heights of shock formation during metric and DH Type-II bursts are determined using two methods: i) the CME leading-edge method and ii) a method employing known electron-density models and start/end frequencies. In the first method, assuming that the shocks are generated by the associated CMEs at the leading edge, the height of the CME leading edge (LE) is calculated at the onset and end of m-Type IIs using the kinematic equation with constant acceleration or constant speed. The LE heights of CMEs that are assumed to be the heights of shock formation/end of nearly 79% of m-Type IIs are found to be within

the acceptable range of 1--3 R⊙1--3 R⊙. For other events, the heights are beyond this range, for which the shocks might either have been generated at the CME flanks/flare-blast waves, or the initial CME height might have been different. The CME/shock height at the onset and end of 17 DH Type IIs are found to be in the range of 2--6 R⊙2--6 R⊙ and within 30 R⊙30 R⊙, respectively. In addition, the CME LE heights from observations at the onset and end of metric/DH Type IIs are compared with the heights corresponding to the observed frequency that is determined using the known electron-density models, and they are in agreement with the model results. The heights are also estimated using the space speed available for 15 halo CMEs, and it is found that the difference is smaller at the m-Type II start/end (0.02 to 0.66 R⊙0.66 R⊙) and slightly greater at the DH Type II end (0.19 to 1.94 R⊙1.94 R⊙). Finally, the possibility of CME–streamer interactions at the start of DH Type IIs is checked, and it is found that many of the events with streamers have lower start frequencies. In addition, these results are discussed in comparison with the values reported in the literature. This study will be useful to find the source region of metric and DH Type IIs and to understand the CME-shock propagation.
Table 1 27 continuous events and the estimated shock-formation heights (2001-2005)
Table 3 Halo events (height estimated using LASCO speed and space speed).
Table 4 Streamer associated (Group A*) and unassociated DH-Type-II events (Group B).

Halo Coronal Mass Ejections and Their Relation to DH Type-II Radio Bursts

A. **Shanmugaraju** , M. Bendict Lawrance
Solar Physics, Volume 290, Issue 10, pp 2963-2973 **2015**
A set of 88 halo CMEs observed by the Solar and Heliospheric Observatory/Large Angle Solar Coronagraph (SOHO/LASCO) during the period 2005 to 2010 is considered to study the relationship of these halo CMEs with Type-II radio bursts in the deca–hectametric (DH) wavelength range observed by Wind/(Plasma and Radio Waves: WAVES). Among the 88 events, 39 halo CMEs are found to be associated with DH Type-II radio bursts and their characteristics are analyzed with the following results: i) The heights of the CME leading edge at the time of the starting frequencies of many of the selected DH Type-II events (74 %) are in the range (2--10 R⊙) where the shocks are formed. ii) The mean speed of DH-associated halo CMEs (1610 km s−1) is nearly twice the mean speed (853 km s−1) of halo CMEs without DH Type-II radio bursts, implying that the peak of the Alfvén speed profile in the outer corona where DH Type-II radio bursts start might be around 800 km s−1. iii) The shock speed of DH Type-II radio bursts calculated using the heights of shock signatures of the corresponding CME events is found to be slightly higher than the CME speed. iv) The CME speed plays a major role in the determination of the ending frequency of DH Type-II radio bursts but not the starting frequency. v) The relationship between the characteristics of DH Type-II radio bursts and CMEs is explained in the context of the universal drift-rate spectrum.

Interaction Between Two CMEs During 14 – 15 February 2011 and Their Unusual Radio Signature

A. **Shanmugaraju**, S. Prasanna Subramanian, Bojan Vrsnak, M. Syed Ibrahim
Solar Physics, **2014**
We report a detailed analysis of an interaction between two coronal mass ejections (CMEs) that were observed on 14 – 15 February 2011 and the corresponding radio enhancement, which was similar to the “CME cannibalism” reported by Gopalswamy et al. (Astrophys. J. 548, L91, 2001). A primary CME, with a mean field-of-view velocity of 669 km s−1 in the Solar and Heliospheric Observatory (SOHO)/Large Angle Spectrometric Coronagraph (LASCO), was more than as twice as fast as the slow CME preceding it (326 km s−1), which indicates that the two CMEs interacted. A radio-enhancement signature (in the frequency range 1 MHz – 400 kHz) due to the CME interaction was analyzed and interpreted using the CME data from LASCO and from the Solar Terrestrial Relations Observatory (STEREO) HI-1, radio data from Wind/Radio and Plasma Wave Experiment (WAVES), and employing known electron-density models and kinematic modeling. The following results are obtained: i) The CME interaction occurred around 05:00 – 10:00 UT in a height range 20 – 25 R⊙. An unusual radio signature is observed during the time of interaction in the Wind/WAVES dynamic radio spectrum. ii) The enhancement duration shows that the interaction segment might be wider than 5 R⊙. iii) The shock height estimated using density models for the radio enhancement region is 10 – 30 R⊙. iv) Using kinematic modeling and assuming a completely inelastic collision, the decrease of kinetic energy based on speeds from LASCO data is determined to be 0.77×1023 J, and 3.67×1023 J if speeds from STEREO data are considered. vi) The acceleration, momentum, and force are found to be a=−168 m s−2, I=6.1×1018 kg m s−1, and F=1.7×1015 N, respectively, using STEREO data.

Interacting CMEs and their associated flare and SEP activities

A.**Shanmugaraju**, S.Prasanna Subramanian
2014 Astrophysics and Space Science, Volume 352, Issue 2, pp.385-393
http://arxiv.org/pdf/1405.6316v1.pdf
We have analyzed a set of 25 interacting events which are associated with the DH type II bursts. These events are selected from the Coronal Mass Ejections observed during the period 1997-2010 in SOHO/LASCO and DH type IIs in

Wind/WAVES. Their pre and primary CMEs from nearby active regions are identified using LASCO and EIT images and their height-time diagrams. Their interacting time and height are obtained, and their associated activities, such as, flares and solar energetic particles (>10pfu) are also investigated. Results from the analysis are: primary CMEs are much faster than the pre-CMEs, their X-ray flares are also stronger (X and M class) compared to the flares (C and M class) of pre-CMEs. Most of the events occurred during the period 2000-2006. From the observed width and speed of pre and primary CMEs, the pre-CMEs are found to be less energetic than the primary CMEs. While the primary CMEs are tracked up to the end of LASCO field of view, most of the pre-CMEs are tracked up to < 26Rs. The SEP intensity is found to be related with the integrated flux of the X-ray flares associated with the primary CMEs for nine events originating from the western region.

Table 1: Data corresponding to all the pre and primary CMEs observed during the period 1997 – 2010
1997 Nov 06, 2000 July 22, 2001 Jan 20, 2001 Apr 02, 2002 Apr 14, 2003 Mar 18, 2003 Nov 18, 2003 Dec 2, 2004 July 23, 2004 July 25, 2004 Nov 06, 2004 Nov 07, 2004 Dec 29, 2004 Dec 30, 2005 Jan 17, 2005 Jan 20, 2005 June 03, 2005 July 07, 2005 July 13, 2005 July 14, 2005 July 30, 2005 Sep 13, 2007 June 03, 2010 Aug 18

Correlation between CME and Flare Parameters (with and without Type II Bursts)

A. **Shanmugaraju**, Y.-J. Moon and Bojan Vršnak
Solar Physics, Volume 270, Number 1, 273-284, **2011, File**

CMEs and flares are the two energetic phenomena on the Sun responsible for generating shocks. Our main aim is to study the relation between the physical properties of CMEs and flares associated with and without type II radio bursts. We considered a set of 290 SOHO/LASCO CMEs associated with GOES X-ray flares observed during the period from January 1997 to December 2000. The relationship between the flares and CMEs is examined for the two sets i) with metric-type IIs and ii) without metric-type IIs. Physical properties such as rise time, duration, and strength of the flares and width, speed, and acceleration of CMEs are considered. We examined the energy relationship and temporal relationship between the CMEs and flares. First, all the events in each group were considered, and then the limb events in each group were considered separately. While there is a relationship between the temporal characteristics of flares and CME properties in the case of with-type IIs, it is absent in the case of all without-type IIs. Among all the relations studied, the correlation between flare duration and CME properties is found to be highly significant compared to the other relations. Also, the relationship between flare strength and CME speed found in the with-type II events is absent in the case of all without-type II events. However, when the limb without-type II events (with reduced time window between flare and CME) are studied separately, we found the energy relationship and the temporal relationship.

Type II Radio Bursts with High and Low Starting Frequencies

Annamalai **Shanmugaraju** · Y.-J. Moon · Bojan Vrsnak
Solar Phys (**2009**) 254: 297–310; **File**

We report on the detailed analysis of *i*) differences between the properties of type IIs with various starting frequencies (high: ≥100 MHz; low: ≤50 MHz; mid: 50 MHz ≤*f*≤ 100 MHz) and *ii*) the properties of CMEs and flares associated with them. For this study, we considered a sample of type II radio bursts observed by Culgoora radio spectrograph from January 1998 to December 2000. The X-ray flares and CMEs associated with these events are identified using GOES and SOHO/LASCO data. The secondary aim is to study the frequency dependence on other properties of type IIs, flares, and CMEs. We found that the type IIs with high starting frequencies have larger drift rate, relative drift rate, and shock speed than the type IIs with low starting frequencies. The flares associated with high frequency type IIs are of impulsive in nature with shorter rise time, duration and delay between the flare start and type II start times than the low frequency type IIs. There is a distinct power – law relationship between the flare parameters and the starting frequencies of type II bursts, whereas the trend in the CME parameters shows low correlation. While the mean speed of CMEs is larger for the mid-frequency group, it is nearly the same for the high and low frequency groups. On the other hand, the percentage of CME association (90%) is larger for low frequency type IIs than for the high frequency type IIs (75%).

X-ray plasma ejections associated with coronal type II shocks:

A. **Shanmugaraju**, Y.-J. Moon, Y.-H. Kim, K.-S. Cho, M. Dryer and S. Umapathy
A&A 458 (**2006**) 653-659 (Section 'The Sun')
http://publish.edpsciences.org/abstract/aa/v458/p653

Context: .Recent observations suggest that X-ray plasma ejections can drive coronal shocks and metric type IIs that are also generated in close association with the X-ray erupting features.
Aims: .The physical relationship between the plasma ejections and metric type II radio bursts are studied by analyzing the characteristics of ejecta and type IIs.
Methods: .We present the first comprehensive analysis of a set of 18 events of X-ray plasma ejections associated with coronal shocks inferred from metric type II radio bursts. For this study, we have utilized a list of 137 limb X-ray plasma ejection events and multi-wavelength observations from GOES X-ray, Yohkoh SXT, SOHO/LASCO, and SOHO/EIT.
Results: .(i) type IIs are reported only for about 15% of the 137 limb ejections; (ii) there exists a close temporal relationship among the starting time of type IIs, the hard X-ray flare peak, and the ejecta time; (iii) there exist negative

correlations between X-ray loop length and starting frequency, and between the ejecta height and starting frequency of type IIs; (iv) the type II formation height computed using the starting frequency and 1 × Newkirk electron density model is in close association with or above the height of X-ray ejecta; and (v) while there is no correlation between the speeds of type II and ejecta, there seems to be a weak correlation between the speeds of type II and CME.
Conclusions: . Though the results suggest that some type IIs are generated in close association with the X-ray erupting features, it is not likely that X-ray plasma ejections are the main drivers of all coronal shocks and metric type II radio bursts due to the absence of correlation between both speeds and mostly sub-Alfenic speeds of the ejections.

ORIGIN OF CORONAL SHOCKS WITHOUT MASS EJECTIONS

A. **SHANMUGARAJU** et al.

Solar Physics (**2006**) 233: 117–127, **File**

We present an analysis of all the events (around 400) of coronal shocks for which the shock-associated metric type IIs were observed by many spectrographs during the period April 1997–December 2000. The main objective of this analysis is to give evidence for the type IIs related to only flare-blast waves, and thus to find out whether there are any type II-associated coronal shocks without mass ejections. By carefully analyzing the data from multi-wavelength observations (Radio, GOES X-ray, Hα, SOHO/LASCO and SOHO/EIT-EUV data), we have identified only 30 events for which there were actually no reports of CMEs. Then from the analysis of the LASCO and EIT running difference images, we found that there are some shocks (nearly 40%, 12/30) which might be associated with weak and narrow mass ejections. These weak and narrow ejections were not reported earlier. For the remaining 60% events (18/30), there are no mass ejections seen in SOHO/LASCO. But all of them are associated with flares and EIT brightenings. Pre-assuming that these type IIs are related to the flares, and from those flare locations of these 18 cases, 16 events are found to occur within the central region of the solar disk (longitude $\leq 45^\circ$). In this case, the weak CMEs originating from this region are unlikely to be detected by SOHO/LASCO due to low scattering. The remaining two events occurred beyond this longitudinal limit for which any mass ejections would have been detected if they were present. For both these events, though there are weak eruption features (EIT dimming and loop displacement) in the EIT images, no mass ejection was seen in LASCO for one event, and a CME appeared very late for the other event. While these two cases may imply that the coronal shocks can be produced without any mass ejections, we cannot deny the strong relationship between type IIs and CMEs.

Multiple type II solar radio bursts.

Shanmugaraju, A., Moon, Y.J., Cho, K.S., Kim, Y.H., Dryer, M., Umapathy, S.: **2005**, *Solar Phys.* **232**, 87 – 103, **2005**. doi:10.1007/s11207-005-1586-4.

An investigation of solar maximum metric type II radio bursts: Do two kinds of coronal shock sources existfl

Shanmugaraju, A., Moon, Y.J., Dryer, M., Umapathy, S.: 2003, *Solar Phys.* **215**, 161 – 184, **2003**.

Study of Particle Acceleration using Fine Structures and Oscillations in Microwaves from Electron Cyclotron Maser

Rohit **Sharma**, Marina Battaglia, Sijie Yu, Bin Chen, Yingjie Luo, Sam Krucker

ApJ **970** 17 **2024**

https://arxiv.org/pdf/2405.04351

https://iopscience.iop.org/article/10.3847/1538-4357/ad4884/pdf

The accelerated electrons during solar flares produce radio bursts and nonthermal X-ray signatures. The quasi-periodic pulsations (QPPs) and fine structures in spatial-spectral-temporal space in radio bursts depend on the emission mechanism and the local conditions, such as magnetic fields, electron density, and pitch angle distribution. Radio burst observations with high frequency-time resolution imaging provide excellent diagnostics. In converging magnetic field geometries, the radio bursts can be produced via the electron-cyclotron maser (ECM). Recently, using observations made by the Karl G. Jansky Very Large Array (VLA) at 1--2 GHz, \cite{Yu2023} reported a discovery of long-lasting auroral-like radio bursts persistent over a sunspot and interpreted them as ECM-generated emission. Here, we investigate the detailed second and sub-second temporal variability of this continuous ECM source. We study the association of 5-second period QPPs with a concurrent GOES C1.5-class flare, utilizing VLA's imaging spectroscopy capability with an extremely high temporal resolution (50 ms). We use the density and magnetic field extrapolation model to constrain the ECM emission to the second harmonic o-mode. Using the delay of QPPs from X-ray emission

times, combined with X-ray spectroscopy and magnetic extrapolation, we constrain the energies and pitch angles of the ECM-emitting electrons to ≈4-8 keV and >26∘. Our analysis shows that the loss-cone diffusion continuously fuels the ECM via Coulomb collisions and magnetic turbulence between a 5 Mm--100 Mm length scale. We conclude that the QPP occurs via the Lotka-Volterra system, where the electron from solar flares saturates the continuously operating ECM and causes temporary oscillations. **2016-04-09**

Rotational properties of solar EUV corona using SDO/AIA-19.3-nm observations

Jaidev **Sharma**, Anil K Malik, Hari Om Vats, Shyamal Kumar Banerjee

Monthly Notices of the Royal Astronomical Society, Volume 521, Issue 1, May **2023**, Pages 1079–1085, https://doi.org/10.1093/mnras/stad544

In this article, we present the differential rotational profile of extreme ultraviolet (EUV) corona. For this purpose, we used observations with high resolution obtained from SDO/AIA at 19.3-nm wavelength from years 2011 to 2021. We found the higher rotation rate of the equatorial segment (14.8 deg d^{-1}) which drops about 13.5 deg d^{-1} on both sides of the poles. The average rotation rate (i.e. from 2011 to 2021) of the equatorial region of EUV corona is found to be higher than that of the photosphere, chromosphere, transition region, and corona. Furthermore, the average rotational gradient (as a function of latitude) of the EUV corona is lower than that of the photosphere and transition region. Interestingly, we found a significant correlation of the hemispheric rotational asymmetry with the solar activity indicator (SSNs) and EUV emission. The cross-correlation analysis indicates that the hemispheric rotational asymmetry leads the solar activity indicator (SSN) and EUV emission by about 1.5 months.

Detection of weak ubiquitous impulsive nonthermal emissions from the solar corona

Rohit **Sharma**, Divya Oberoi, Marina Battaglia, Sam Krucker

ApJ **937** 99 **2022**

https://arxiv.org/pdf/2208.07147.pdf

https://iopscience.iop.org/article/10.3847/1538-4357/ac87fc/pdf

A ubiquitous presence of weak energy releases is one of the most promising hypotheses to explain coronal heating, referred to as the nanoflare hypothesis. The accelerated electrons associated with such weak heating events are also expected to give rise to coherent impulsive emission via plasma instabilities in the meterwave radio band, making this a promising spectral window to look for their presence. Recently \citet{Mondal2020b} reported the presence of weak impulsive emissions from quiet Sun regions which seem to meet the requirements of being radio counterparts of the hypothesized nanoflares. Detection of such low-contrast weak emission from the quiet Sun is challenging and, given their implications, it is important to confirm their presence. In this work, using data from the Murchison Widefield Array, we explore the use of an independent robust approach for their detection by separating the dominant slowly varying component of emission from the weak impulsive one in the visibility domain. We detect milli-SFU level bursts taking place all over the Sun and characterize their brightness temperatures, distributions, morphologies, durations and association with features seen in EUV images. We also attempt to constraint the energies of the nonthermal particles using inputs from the FORWARD coronal model along with some reasonable assumptions and find them to lie in the sub-pico flare (∼1019−1021 ergs) range. In the process, we also discover perhaps the weakest type III radio burst and another one that shows clear signatures of weakest quasi-periodic pulsations. **3 Dec 2015**

Radio and X-ray Observations of Short-lived Episodes of Electron Acceleration in a Solar Microflare

Rohit **Sharma**, Marina Battaglia, Yingjie Luo, Bin Chen, Sijie Yu

ApJ **904** 94 **2020**

https://arxiv.org/pdf/2009.14497.pdf

https://doi.org/10.3847/1538-4357/abbd96

Solar flares are sudden energy release events in the solar corona, resulting from magnetic reconnection, that accelerates particles and heats the ambient plasma. During a flare, there are often multiple, temporally and spatially separated individual energy release episodes that can be difficult to resolve depending on the observing instrument. We present multi-wavelength imaging and spectroscopy observations of multiple electron acceleration episodes during a GOES B1.7-class two-ribbon flare on **2012 February 25**, observed simultaneously with the Karl G. Jansky Very Large Array (VLA) at 1--2 GHz, the Reuven Ramatay High Energy Solar Spectroscopic Imager (RHESSI) in X-rays, and the Solar Dynamics Observatory in extreme ultraviolet (EUV). During the initial phase of the flare, five radio bursts were observed. A nonthermal X-ray source was seen co-temporal, but not co-spatial, with the first three radio bursts. Their radio spectra are interpreted as optically thick gyrosynchrotron emission. By fitting the radio spectra with a gyrosynchrotron model, we derive the magnetic field strength and nonthermal electron spectral parameters in each acceleration episode. Notably, the nonthermal parameters derived from X-rays differ considerably from the nonthermal parameters inferred from the radio. The observations are indicative of multiple, co-temporal acceleration episodes during the impulsive phase of a solar microflare. The X-ray and radio burst sources likely originate from separate electron distributions in different magnetic loops.

CESRA #2832 March **2021** http://www.astro.gla.ac.uk/users/eduard/cesra/?p=2832

Propagation Effects in Quiet Sun Observations at Meter Wavelengths

Rohit **Sharma**, Divya Oberoi
ApJ **903** 126 **2020**
https://arxiv.org/pdf/2009.10604.pdf
https://doi.org/10.3847/1538-4357/abb949
Quiet sun meterwave emission arises from thermal bremsstrahlung in the MK corona, and can potentially be a rich source of coronal diagnostics. On its way to the observer, it gets modified substantially due to the propagation effects - primarily refraction and scattering - through the magnetized and turbulent coronal medium, leading to the redistribution of the intensity in the image plane. By comparing the full-disk meterwave solar maps during a quiet solar period and the modelled thermal bremsstrahlung emission, we characterise these propagation effects. The solar radio maps between 100 and 240 MHz come from the Murchison Widefield Array. FORWARD package is used to simulate thermal bremsstrahlung images using the self-consistent Magnetohydrodynamic Algorithm outside a Sphere coronal model. The FORWARD model does not include propagation effects. The differences between the observed and modelled maps are interpreted to arise due to scattering and refraction. There is a good general correspondence between the predicted and observed brightness distributions, though significant differences are also observed. We find clear evidence for the presence of significant propagation effects, including anisotropic scattering. The observed radio size of the Sun is 25--30\% larger in area. The emission peak corresponding to the only visible active region shifts by 8'--11' and its size increases by 35--40\%. Our simple models suggest that the fraction of scattered flux density is always larger than a few tens of percent, and varies significantly between different regions. We estimate density inhomogeneities to be in the range 1--10\%. **3 Dec 2015**
Erratum: 2021 *ApJ* **913** 153 https://iopscience.iop.org/article/10.3847/1538-4357/ac01df/pdf
CESRA # 2774 Feb **2021** http://www.astro.gla.ac.uk/users/eduard/cesra/?p=2774

Quantifying weak non-thermal solar radio emission at low radio frequencies

Rohit **Sharma**, Divya Oberoi, Mihir Arjunwadkar
2018 ApJ 852 69
https://arxiv.org/pdf/1709.00878.pdf
The recent availability of fine grained high sensitivity data from the new generation low radio frequency instruments such as the Murchison Widefield Array (MWA) have opened up opportunities for using novel techniques for characterizing the nature of solar emission at these frequencies. Here we use this opportunity to look for evidence for the presence of weak non-thermal emissions in the 100-240 MHz band, at levels weaker than have usually been probed. The presence of such features is believed to be a necessary consequence of nanoflare-based coronal and chromospheric heating theories. We separate the calibrated MWA solar dynamic spectra into a slowly varying and an impulsive, and hence non-thermal, component. We demonstrate that Gaussian mixtures modeling can be used to robustly model the latter and we estimate the flux density distribution as well as the prevalence of impulsive non-thermal emission in the frequency-time plane. Evidence for presence of non-thermal emission at levels down to ∼0.2 SFU (1 SFU = 104 Jy) is reported, making them the weakest reported emissions of this nature. Our work shows the fractional occupancy of the non-thermal impulsive emission to lie in the 17--45\% range during a period of medium solar activity. We also find that the flux density radiated in the impulsive non-thermal emission is very similar in strength to that of the slowly varying component, dominated by the thermal bremsstrahlung. Such significant prevalence and strength of the weak impulsive non-thermal emission has not been appreciated earlier. **August 26, 2014**

On properties of radio-rich coronal mass ejections

Joginder **Sharma** · Nishant Mittal · Vivek Tomar · Udit Narain
Astrophys Space Sci (**2008**) 317: 261–265, DOI 10.1007/s10509-008-9886-4
We have studied properties of the radio-rich coronal mass ejections (CMEs) (observed during 1997–2006) which produce type II (1–14 MHz) i.e. decametric–hectometric or DH radio burst. These DH CMEs are relatively faster and wider than the normal CMEs. The average speed and apparent width of these CMEs is 1048 km/s and 98fl, respectively. Majority (about 54%) of DH CMEs decelerate, but about 21% show positive acceleration. The remaining 25% move with little acceleration. These special characteristics of radio-rich CMEs could be used to identify the population of geoeffective CMEs, which are quite relevant to space weather.

LOFAR observations of fine spectral structure dynamics in type IIIb radio bursts

I.N. **Sharykin**, E.P. Kontar, A.A. Kuznetsov
Solar Phys. 293:115 **2018**
https://arxiv.org/pdf/1806.01046.pdf
http://sci-hub.tw/https://link.springer.com/article/10.1007/s11207-018-1333-2
Solar radio emission features a large number of fine structures demonstrating great variability in frequency and time. We present spatially resolved spectral radio observations of type IIIb bursts in the 30−80 MHz range made by the Low

Frequency Array (LOFAR). The bursts show well-defined fine frequency structuring called "stria" bursts. The spatial characteristics of the stria sources are determined by the propagation effects of radio waves; their movement and expansion speeds are in the range of 0.1-0.6c. Analysis of the dynamic spectra reveals that both the spectral bandwidth and the frequency drift rate of the striae increase with an increase of their central frequency; the striae bandwidths are in the range of ~20-100 kHz and the striae drift rates vary from zero to ~0.3 MHz s^-1. The observed spectral characteristics of the stria bursts are consistent with the model involving modulation of the type III burst emission mechanism by small-amplitude fluctuations of the plasma density along the electron beam path. We estimate that the relative amplitude of the density fluctuations is of dn/n~10^-3, their characteristic length scale is less than 1000 km, and the characteristic propagation speed is in the range of 400-800 km/s. These parameters indicate that the observed fine spectral structures could be produced by propagating magnetohydrodynamic waves. **16 April 2015**

Flare Energy Release in the Magnetic Field Polarity Inversion Line During M1.2 Solar Flare of March 15, 2015. Paper I. Onset of Plasma Heating and Electrons Acceleration

I.N. **Sharykin**, I.V. Zimovets, I.I. Myshyakov, N.S. Meshalkina

2018

https://arxiv.org/pdf/1805.05792.pdf

We present the study of SOL**2015-03-15** M1.2 flare, revealing acceleration of electrons and plasma heating in the sheared twisted magnetic structure in the polarity inversion line (PIL). The scope is to make the analysis of nonthermal electrons dynamics and plasma heating in the highly stressed magnetic loops interacting in the PIL by using X-ray, microwave, ultraviolet, and optical observations. It is found that the most probable scenario for the energy release in the PIL is the tether-cutting magnetic reconnection between the low-lying (3 Mm above the photosphere) magnetic loops within a twisted magnetic flux rope. Energetic electrons with the hardest spectrum were appeared at the onset of plasma heating up to the super-hot temperature of 40 MK. These electrons are localized in a thin magnetic channel with width of around 0.5 Mm with high average magnetic field of about 1200 G. The plasma beta in the super-hot region is less than 0.01. The estimated density of accelerated electrons is about 10^9 cm^-3 that is much less than the super-hot plasma density. The energy density flux of non-thermal electrons is estimated up to 3x10^12 ergs cm^-2s^-1 that is much higher than in the currently available radiative hydrodynamic models. These results revealed that one need to develop new self-consisting flare models reproducing 3D magnetic reconnection in the PIL with strong magnetic field, spatial filamentation of energy release, formation of high energy density populations of nonthermal electrons and appearance of the super-hot plasma.

Probing Twisted Magnetic Field Using Microwave Observations in an M Class Solar Flare on 11 February, 2014

I.N. **Sharykin**, A.A. Kuznetsov, I.I. Myshyakov

Solar Phys. 293:34 **2018**

https://arxiv.org/pdf/1801.04400.pdf

https://link.springer.com/content/pdf/10.1007%2Fs11207-017-1237-6.pdf

This work demonstrates the possibility of magnetic field topology investigations using microwave polarimetric observations. We study a solar flare of GOES M1.7 class that occurred on **11 February, 2014**. This flare revealed a clear signature of spatial inversion of the radio emission polarization sign. We show that the observed polarization pattern can be explained by nonthermal gyrosynchrotron emission from the twisted magnetic structure. Using observations of the Reuven Ramaty High Energy Solar Spectroscopic Imager, Nobeyama Radio Observatory, Radio Solar Telescope Network, and Solar Dynamics Observatory, we have determined the parameters of nonthermal electrons and thermal plasma and identified the magnetic structure where the flare energy release occurred. To reconstruct the coronal magnetic field, we use nonlinear force-free field (NLFFF) and potential magnetic field approaches. Radio emission of nonthermal electrons is simulated by the GX Simulator code using the extrapolated magnetic field and the parameters of nonthermal electrons and thermal plasma inferred from the observations; the model radio maps and spectra are compared with observations. We have found that the potential magnetic field approach fails to explain the observed circular polarization pattern; on the other hand, the Stokes V map is successfully explained by assuming nonthermal electrons to be distributed along the twisted magnetic structure determined by the NLFFF extrapolation approach. Thus, we show that the radio polarization maps can be used for diagnosing the topology of the flare magnetic structures where nonthermal electrons are injected.

Radio polarization signatures in twisted flare loops

I. N. **Sharykin**, A. A. Kuznetsov

RHESSI Science Nuggets #271 April **2016**

http://sprg.ssl.berkeley.edu/~tohban/wiki/index.php/Radio_polarization_signatures_in_twisted_flare_loops

Flux-rope geometry via radio polarization signs

Modelling of Nonthermal Microwave Emission From Twisted Magnetic Loops

I. N. **Sharykin**, A. A. Kuznetsov

Solar Phys. Volume 291, Issue 5, pp 1341-1355 **2016**

http://arxiv.org/pdf/1604.05618v1.pdf

Microwave gyrosynchrotron radio emission generated by nonthermal electrons in twisted magnetic loops is modelled using the recently developed simulation tool GX Simulator. We consider isotropic and anisotropic pitch-angle distributions. The main scope of the work is to understand impact of the magnetic field twisted topology on resulted radio emission maps. We have found that nonthermal electrons inside twisted magnetic loops produce gyrosynchrotron radio emission with peculiar polarization distribution. The polarization sign inversion line is inclined relatively to the axis of the loop. Radio emission source is more compact in the case of less twisted loop, considering anisotropic pitch-angle distribution of nonthermal electrons.

Onset of Electron Acceleration in a Flare Loop

I.N. **Sharykin**, S. Liu, L. Fletcher

2014

http://arxiv.org/pdf/1408.1413v1.pdf

We carried out detailed analysis of X-ray and radio observations of a simple flare loop that occurred on **12th August 2002**, with the impulsive hard X-ray (HXR) light curves dominated by a single pulse. The emission spectra of the early impulsive phase are consistent with an isothermal model in the coronal loop with a temperature reaching several keVs. A power-law high-energy spectral tail is evident near the HXR peak time, in accordance with the appearance of footpoints at high energies, and is well correlated with the radio emission. The energy content of the thermal component keeps increasing gradually after the disappearance of this nonthermal component. These results suggest that electron acceleration only covers a central period of a longer and more gradual energy dissipation process and that the electron transport within the loop plays a crucial role in the formation of the inferred power-law electron distribution. The spectral index of power-law photons shows a very gradual evolution indicating a quasi-steady state of the electron accelerator, which is confirmed by radio observations. These results are consistent with the theory of stochastic electron acceleration from a thermal background. Advanced modeling with coupled electron acceleration and spatial transport processes is needed to explain these observations more quantitatively, which may reveal the dependence of the electron acceleration on the spatial structure of the acceleration region.

Energy-releasing Process for the 2013 May 13 X1.7 Limb Flare: A Continued Study

Jinhua **Shen**1,2, Jianping Li3, Yu Huang3, Dong Li3, Yingna Su3, and Haisheng Ji3

2023 ApJ 950 71

https://iopscience.iop.org/article/10.3847/1538-4357/accc8c/pdf

In this paper, we reanalyze the X1.7 class limb flare that occurred on **2013 May 13** (SOL2013-05-13T01:56 UT), concentrating on the energy-releasing process using microwave observations mainly made by Nobeyama and X-ray observations made by RHESSI. The analysis was carried out in the context of EUV observations made by the Atmospheric Imaging Assembly on board Solar Dynamics Observatory. First, we complement the initiation process by showing that the initiation occurred together with material falling from a large-scale overlying prominence, a signature of drainage instability. The usual downward and upward motions of the microwave and X-ray sources are observed from their evolution. However, the microwave source's height shows a recurrent decrease and increase during its overall upward motion; it shows a kind of recurrent contraction and expansion. The time period of the recurrent contraction and expansion corresponds to the period of post-contraction oscillation of EUV loops, and the oscillatory motions are closely correlated with four microwave/hard X-ray peaks that unusually increased nonthermal emission levels by several times. X-ray spectra get hardened during the oscillation. In addition, the rapid contraction of magnetic loops located on the outside of the erupting flux rope occurs 5 minutes after the onset of the flare, showing that the contraction of the peripheral magnetic loops is more likely due to the vortex and sink flows generated by an upward erupting magnetic flux rope rather than a coronal implosion. The results can provide more insight into the physics of dynamic coronal magnetic field and particle acceleration during solar flares.

Coronal Quasi-periodic Fast-mode Propagating (QFP) Wave Trains **Review**

Yuandeng **Shen**, Xinping Zhou, Yadan Duan, Zehao Tang, Chengrui Zhou, Song Tan

Solar Phys. **2022**

https://arxiv.org/pdf/2112.14959.pdf **File**

QFP wave trains in the corona have been studied intensively in the past decade, thanks to the full-disk, high spatiotemporal resolution, and wide-temperature coverage observations taken by the SDO/AIA. In AIA observations, QFP wave trains are seen to consist of multiple coherent and concentric wavefronts emanating successively near the epicenter of the accompanying flares; they propagate outwardly either along or across coronal loops at fast-mode magnetosonic speeds from several hundred to more than 2000 km/s, and their periods are in the range of tens of seconds

to several minutes. Based on the distinct different properties of QFP wave trains, they might be divided into two distinct categories including narrow and broad ones. For most QFP wave trains, some of their periods are similar to those of quasi-periodic pulsations (QPPs) in the accompanying flares, indicating that they are probably different manifestations of the same physical process. Currently, candidate generation mechanisms for QFP wave trains include two main categories: pulsed energy excitation mechanism in association with magnetic reconnection and dispersion evolution mechanism related to the dispersive evolution of impulsively generated broadband perturbations. In addition, the generation of some QFP wave trains might be driven by the leakage of three and five minute oscillations from the lower atmosphere. As one of the new discoveries of SDO, QFP wave trains provide a new tool for coronal seismology to probe the corona parameters, and they are also useful for diagnosing the generation of QPPs, flare processes including energy release and particle accelerations. This review aims to summarize the main observational and theoretical results of the spatially-resolved QFP wave trains in extreme ultraviolet observations, and states briefly a number of questions that deserve further investigations. **2010 September 08, 2011 February 14, 2011 May 30, 2012 April 24, 2013 May 22, 2014 November 03, 2015 April 16**

2.10. Possible Manifestations of QFP Wave Trains in Radio

The occurrence of QFP wave trains is rather
*common and is frequently associated with **single pulsed global EUV waves**, ares and CMEs.*
***Table** 1. Physical parameters of the published QFP wave trains*

Source Region of the Decameter–Hectometric Type II Radio Burst: Shock–Streamer Interaction Region

Chenglong **Shen**1 , Chijian Liao1, Yuming Wang1, Pinzhong Ye1 and Shui Wang
Solar Physics, February **2013**, Volume 282, Issue 2, pp 543-552, **File**
D–H type II radio bursts are widely thought to be caused by coronal mass ejections (CMEs). However, it is still unclear where the exact source of the type IIs on the shock surface is. We identify the source regions of the decameter–hectometric (D–H) type IIs based on imaging observations from SOHO/LASCO and the radio dynamic spectrum from Wind/Waves. The analysis of two well-observed events suggests that the sources of these two events are located in the interaction regions between shocks and streamers, and that the shocks are enhanced significantly in these regions.
7 March 2011; 9 May 2011

STRENGTH OF CORONAL MASS EJECTION-DRIVEN SHOCKS NEAR THE SUN AND THEIR IMPORTANCE IN PREDICTING SOLAR ENERGETIC PARTICLE EVENTS

Chenglong **Shen**, Yuming Wang, Pinzhong Ye, X. P. Zhao, Bin Gui, and S. Wang
The Astrophysical Journal, 670:849–856, **2007** November 20, **file**
Coronal shocks are important structures, but there are no direct observations of them in solar and space physics. The strength of shocks plays a key role in shock-related phenomena, such as radio bursts and solar energetic particle (SEP) generation. This paper presents an improved method of calculating Alfve´n speed and shock strength near the Sun. This method is based on using as many observations as possible, rather than one-dimensional global models. Two events, a relatively slow CME on 2001 September 15 and a very fast CME on 2000 June 15, are selected to illustrate the calculation process. The calculation results suggest that the slow CME drove a strong shock, with Mach number of 3.43–4.18, while the fast CME drove a relatively weak shock, with Mach number of 1.90–3.21. This is consistent with the radio observations, which find a stronger and longer decameter-hectometric (DH) type II radio burst during the first event, and a short DH type II radio burst during the second event. In particular, the calculation results explain the observational fact that the slow CME produced a major solar energetic particle (SEP) event, while the fast CME did not. Through a comparison of the two events, the importance of shock strength in predicting SEP events is addressed.

Visibility and Origin of Compact Interplanetary Radio Type IV Bursts

Nasrin Talebpour **Sheshvan**, Silja Pohjolainen
Solar Phys. 293:148 **2018**
https://arxiv.org/pdf/1810.09208.pdf
https://link.springer.com/content/pdf/10.1007%2Fs11207-018-1371-9.pdf
We have analysed radio type IV bursts in the interplanetary (IP) space at decameter-hectometer (DH) wavelengths, to find out their source origin and a reason for the observed directivity. We used radio dynamic spectra from the instruments on three different spacecraft, STEREO-A, Wind, and STEREO-B, that were located approximately 90 degrees apart from each other in 2011-2012, and thus gave a 360 degree view to the Sun. The radio data was compared to white-light and extreme ultraviolet (EUV) observations of flares, EUV waves, and coronal mass ejections (CMEs) in five solar events. We find that the reason for observing compact and intense DH type IV burst emission from only one spacecraft at a time is due to the absorption of emission to one direction and that the emission is blocked by the solar disk and dense corona to the other direction. The geometry also makes it possible to observe metric type IV bursts in the low corona from a direction where the higher-located DH type IV emission is not detectable. In the absorbed direction

we found streamers present, and these were estimated to be the locations of type II bursts, caused by shocks at the CME flanks. The high-density plasma was therefore most probably formed by shock--streamer interaction. In some cases the type II-emitting region was also capable of stopping later-accelerated electron beams, visible as type III bursts that ended near the type II burst lanes. **2011-06-04, 2011-09-22, 2012-01-27, 2012-03-05**

Polarization properties of the decameter spikes

Mykola **Shevchuk**1* Valentin Melnik1 Anatolii Brazhenko2 Vladimir Dorovskyy1 Anatolii Frantsuzenko2 Stefaan Poedts3,4 Jasmina Magdalenic3,5
Front. Astron. Space Sci. 11: 1396326. **2024**
https://doi.org/10.3389/fspas.2024.1396326
https://www.frontiersin.org/articles/10.3389/fspas.2024.1396326/full
An analysis of the observational polarization properties of the decameter spikes is presented in the paper. It is shown that decameter spikes possess high degree of circular polarization with average value of about 60%. In the frames of "leading spot" theory we associated the spikes activity with a certain active region on the solar disk and determined the mode of the emission. Supposing plasma emission mechanism we link and determine coronal plasma and fast electron beam parameters. **14 June 2012**

The Storm of Decameter Spikes During the Event of 14 June 2012

N. V. **Shevchuk** , V. N. Melnik, S. Poedts, V. V. Dorovskyy, J. Magdalenic, A. A. Konovalenko,A. I. Brazh enk, C. Briand, A. V. Frantsuzenko and 2 more
Solar Phys. January **2016**, Volume 291, Issue 1, pp 211-228
An event on **14 June 2012**, observed with the radio telescopes UTR-2 (Kharkov, Ukraine), URAN-2 (Poltava, Ukraine), and NDA (Nançay, France) during a joint Summer campaign, is analyzed and discussed. The high solar activity resulted in a storm of spikes, and a storm of Type III bursts, Type IIIb bursts, and a Type IV burst observed in the decameter band. During the observed time interval, the average flux of radio emission changed twice. Using spikes as a tool for diagnostics of plasma parameters, we followed variations of the coronal temperature and the coronal magnetic field in the observed time interval. Thus, in frames of the model described in this article the observed decameter spikes' durations of 0.3 – 1 seconds correspond to the coronal plasma temperatures of ≈0.1--0.6×106 K. At the same time the spikes' frequency bandwidths of 25 – 80 kHz give us the magnetic-field value of about 2 G.

Influence of fine structures on gyrosynchrotron emission of flare loops modulated by sausage modes

Mijie **Shi**, Bo Li, Mingzhe Guo
ApJ Letter **2022**
https://arxiv.org/pdf/2209.07176.pdf
Sausage modes are one leading mechanism for interpreting short period quasi-periodic pulsations (QPPs) of solar flares. Forward modeling their radio emission is crucial for identifying sausage modes observationally and for understanding their connections with QPPs. Using the numerical output from three-dimensional magnetohydrodynamic (MHD) simulations, we forward model the gyrosynchrotron (GS) emission of flare loops modulated by sausage modes and examine the influence of loop fine structures. The temporal evolution of the emission intensity is analyzed for an oblique line of sight crossing the loop center. We find that the low- and high-frequency intensities oscillate in-phase at the period of sausage modes for models with or without fine structures. For low-frequency emissions where the optically thick regime arises, the modulation magnitude of the intensity is dramatically reduced by the fine structures at some viewing angles. On the contrary, for high-frequency emissions where the optically thin regime holds, the effect of fine structures or viewing angle is marginal. Our results show that the periodic intensity variations of sausage modes are not wiped out by the fine structures, and sausage modes remains a promising candidate mechanism for QPPs even when flare loops are fine-structured.

HIGH PERFORMANCE NEGATIVE DATABASE FOR MASSIVE DATA MANAGEMENT SYSTEM OF THE MINGANTU SPECTRAL RADIOHELIOGRAPH

Congming **Shi**, 1 Feng Wang,1, 2 Hui Deng,3 Yingbo Liu,4 Cuiyin Liu,3 and Shoulin Wei3
2018
https://arxiv.org/pdf/1705.06067.pdf
As a dedicated synthetic aperture radio interferometer, the MingantU SpEctral Radioheliograph (MUSER), initially known as the Chinese Spectral RadioHeliograph (CSRH), has entered the stage of routine observation. More than 23 million data records per day need to be effectively managed to provide high performance data query and retrieval for scientific data reduction. In light of these massive amounts of data generated by the MUSER, in this paper, a novel data management technique called the negative database (ND) is proposed and used to implement a data management system for the MUSER. Based on the key-value database, the ND technique makes complete utilization of the complement set of observational data to derive the requisite information. Experimental results showed that the proposed

ND can significantly reduce storage volume in comparison with a relational database management system (RDBMS). Even when considering the time needed to derive records that were absent, its overall performance, including querying and deriving the data of the ND, is comparable with that of an RDBMS. The ND technique effectively solves the problem of massive data storage for

Radio imaging of chromospheric magnetic field

Kiyoto **Shibasaki**_1
CESRA **2016**, p.85
http://cesra2016.sciencesconf.org/conference/cesra2016/pages/CESRA2016_prog_abs_book_v3.pdf
Free-free opacity of circularly polarized radio waves depends on magnetic _eld strength and its direction. By combining this fact and steep temperature gradient, optically thick radio emission coming from the upper chromosphere is polarized. Radio brightness temperature of right-handed-circularly-polarized emission is deviated from that of left-handed-circularly-polarized emission. Using this mechanism, we can measure magnetic _eld strength at the upper chromosphere. Inversion of polarization degree into magnetic _eld strength (line-of-sight component) is very simple and it is not inuenced by Doppler E_ect because of continuum emission. Radio images taken by the Nobeyama Radioheliograph at 17 GHz are used to get magnetic _eld images at the upper chromosphere. Measurement of very weak polarized signal is required to get chromospheric magnetic _eld outside strong active regions.

Long-Term Global Solar Activity Observed by the Nobeyama Radioheliograph

K. **Shibasaki**
Publ. Astron. Soc. Japan 65, No SP1, S17 [6 pages] (**2013**)
http://pasj.asj.or.jp/v65/sp1/65S017/65S017.pdf
The Nobeyama Radioheliograph has been observing the Sun at a frequency of 17 GHz regularly since 1992, providing synthesized full-disk images. This long period of continuous and consistent operation, providing wellcalibrated data of a uniform standard, makes possible long-term studies of solar activity, from full-disk down to the angular resolution of the instrument. By using about 7200 daily, full-disk images, it has been possible to generate a radio version of the butterfly diagram, which differs significantly from the sunspot butterfly diagram. The polar regions are bright at 17 GHz, with their brightness well-correlated with the polar magnetic field strengths. Both are anti-correlated with activity at low latitudes, such as active regions and solar flares. The 17 GHz butterfly diagram shows both high and low-latitude activity. The brightness of both these facets of solar activity shows a significant decline over the 20+ years observations that have been made. In the northern hemisphere, the radio brightnesses at low and high latitudes are strongly anti-correlated. However, this anti-correlation is weak in the southern hemisphere. We find a weakening of the synchronization of activity between the northern and southern hemispheres, and also between high and low latitude activity in the southern hemisphere. Possible causes of polar brightening and the meaning with respect to the general scenario of solar activity are discussed.

Radio Emission of the Quiet Sun and Active Regions (Invited Review)

K. **Shibasaki**, C. E. Alissandrakis and S. Pohjolainen
Solar Physics, Volume 273, Number 2, 309-337, **2011, File**
Solar radio emission provides valuable information on the structure and dynamics of the solar atmosphere above the temperature minimum. We review the background and most recent observational and theoretical results on the quiet Sun and active region studies, covering the entire radio range from millimeter to decameter wavelengths. We examine small- and large-scale structures, at short and long time scales, as well as synoptic aspects. Open questions and challenges for the future are also identified.

Simultaneous ALMA-Hinode-IRIS observations on footpoint signatures of a soft X-ray loop-like microflare

Toshifumi **Shimizu**, Masumi Shimojo, Masashi Abe
ApJ **922** 113 **2021**
https://arxiv.org/pdf/2109.11215.pdf
https://doi.org/10.3847/1538-4357/ac27a4
Microflares have been considered to be among the major energy input sources to form active solar corona. To investigate the response of the low atmosphere to events, we conducted an ALMA observation at 3 mm coordinated with IRIS and Hinode observations, on **March 19, 2017**. During the observations, a soft X-ray loop-type microflare (active-region transient brightening) was captured using Hinode X-ray telescope in high temporal cadence. A brightening loop footpoint is located within narrow field of views ALMA, IRIS slit-jaw imager, and Hinode spectro-

polarimeter. Counterparts of the microflare at the footpoint were detected in Si IV and ALMA images, while the counterparts were less apparent in C II and Mg II k images. Their impulsive time profiles exhibit the Neupert effect pertaining to soft X-ray intensity evolution. The magnitude of thermal energy measured using ALMA was approximately 100 times smaller than that measured in the corona. These results suggest that impulsive counterparts can be detected in the transition region and upper chromosphere where the plasma is thermally heated via impinging non-thermal particles. Our energy evaluation indicates a deficit of accelerated particles that impinge the footpoints for a small class of soft X-ray microflares. The footpoint counterparts consist of several brightening kernels, all of which are located in weak (void) magnetic areas formed in patchy distribution of strong magnetic flux at the photospheric level. The kernels provide a conceptual image in which the transient energy release occurs at multiple locations on the sheaths of magnetic flux bundles in the corona.

Comparison of solar multifrequency microwave data with other solar indices for understanding solar and stellar microwave data

Masumi **Shimojo**, Kosuke Namekata, Kazumasa Iwai, Ayumi Asai, Kyoko Watanabe
ApJ **965** 170 **2024**
https://arxiv.org/pdf/2402.11848.pdf
https://iopscience.iop.org/article/10.3847/1538-4357/ad2a7a/pdf
Thermal microwave emissions detected from stellar atmospheres contain information on stellar activity. However, even for the Sun, the relationship between multifrequency microwave data and other activity indices remains unclear. We investigated the relationships among the thermal microwave fluxes with 1, 2, 3.75 and 9.4 GHz, their circular polarizations, and several activity indices recorded during recent solar cycles and observed that these relationships can be categorized into two groups. In the first group, the relationship between the microwave fluxes and solar indices, which are strongly related to the active regions, can be well-fitted by using a linear function. In the second group, the fitting function is dependent on frequency. Specifically, the microwave fluxes at 1 and 2 GHz can be well-fitted to the total unsigned magnetic and extreme ultraviolet fluxes by employing a power-law function. The trend changes around 3.75 GHz, and of the trend for the 9.4 GHz fluxes can be fitted by using a linear function. For the first time, we present the relationship between circular polarization and solar indices. Moreover, we extrapolated these relationships of the solar microwave fluxes to higher values and compared them with the solar-type stars. We found that epsilon Eri, whose microwave emission originates from thermal plasma, follows the extrapolated relationship. However, to date, only one star's emission at 1--10 GHz has been confirmed as thermal emission. More solar-type stars should be observed with future radio interferometers to confirm that relationships based on solar data can be applied to stellar microwave data.
1 Jan 1996, 25 July 2000, 7 Jun 2007

Observing the Sun with the Atacama Large Millimeter/submillimeter Array (ALMA): Polarization Observations at 3 mm

Masumi **Shimojo**, Timothy S. Bastian, Seiji Kameno, Antonio S. Hales
Solar Phys. **299**, 20 **2024**
https://arxiv.org/pdf/2401.06343.pdf
https://doi.org/10.1007/s11207-024-02265-3
https://link.springer.com/content/pdf/10.1007/s11207-024-02265-3.pdf
The Atacama Large Millimeter-submillimeter Array (ALMA) is a general purpose telescope that performs a broad program of astrophysical observations. Beginning in late-2016, solar observations with ALMA became available, thereby opening a new window onto solar physics. Since then, the number of solar observing capabilities has increased substantially but polarimetric observations, a community priority, have not been available. Weakly circularly polarized emission is expected from the chromosphere where magnetic fields are strong. Hence, maps of Stokes V provide critical new constraints on the longitudinal component of the chromospheric magnetic field. Between 2019-2022, an ALMA solar development effort dedicated to making solar polarimetry at millimeter wavelengths a reality was carried out. Here, we discuss the development effort to enable solar polarimetry in the 3 mm band (ALMA Band 3) in detail and present a number of results that emerge from the development program. These include tests that validate polarization calibration, including evaluation of instrumental polarization: both antenna based "leakage" terms and off-axis effects (termed "beam squint" for Stokes V). We also present test polarimetric observations of a magnetized source on the Sun, the following sunspot in a solar active region, which shows a significant Stokes V signature in line with expectations. Finally, we provide some cautions and guidance to users contemplating the use of polarization observations with ALMA. **13 October 2022**
CESRA #3763 **2024** https://www.astro.gla.ac.uk/users/eduard/cesra/?p=3763

Over seven decades of solar microwave data obtained with Toyokawa and Nobeyama Radio Polarimeters

Masumi **Shimojo**, Kazumasa Iwai
Geoscience Data Journal **2022**

https://arxiv.org/ftp/arxiv/papers/2205/2205.07454.pdf
Monitoring observations of solar microwave fluxes and their polarization began in Japan during the 1950s at Toyokawa and Mitaka. At present (April 2022), monitoring observations continue with the Nobeyama Radio Polarimeters (NoRP) at the Nobeyama campus of the National Astronomical Observatory of Japan (NAOJ). In this paper, we present a brief history of the solar microwave monitoring observations preceding those now carried out by NoRP. We then review the solar microwave obtained at Toyokawa and Nobeyama and their metadata. The datasets are publicly provided by the Solar Data Archive System (SDAS) operated by the Astronomy Data Center of the NAOJ, via http (this https URL) and FTP (this ftp URL) protocols. **20 Jan 2005**

Estimating the Temperature and Density of a Spicule from 100 GHz Data Obtained with ALMA

Masumi **Shimojo**1,2, Tomoko Kawate3, Takenori J. Okamoto1, Takaaki Yokoyama4, Noriyuki Narukage1, Taro Sakao3,5, Kazumasa Iwai6, Gregory D. Fleishman7, and Kazunari Shibata
2020 ApJL 888 L28
sci-hub.si/10.3847/2041-8213/ab62a5
We succeeded in observing two large spicules simultaneously with the Atacama Large Millimeter/submillimeter Array (ALMA), the Interface Region Imaging Spectrograph (IRIS), and the Atmospheric Imaging Assembly (AIA) on board the Solar Dynamics Observatory. One is a spicule seen in the IRIS Mg ii slit-jaw images and AIA 304 Å images (Mg ii/304 Å spicule). The other one is a spicule seen in the 100 GHz images obtained with ALMA (100 GHz spicule). Although the 100 GHz spicule overlapped with the Mg ii/304 Å spicule in the early phase, it did not show any corresponding structures in the IRIS Mg ii and AIA 304 Å images after the early phase. It suggests that the spicules are individual events and do not have a physical relationship. To obtain the physical parameters of the 100 GHz spicule, we estimate the optical depths as a function of temperature and density using two different methods. One is using the observed brightness temperature by assuming a filling factor, and the other is using an emission model for the optical depth. As a result of comparing them, the kinetic temperature of the plasma and the number density of ionized hydrogen in the 100 GHz spicule are ~6800 K and 2.2 × 1010 cm−3. The estimated values can explain the absorbing structure in the 193 Å image, which appear as a counterpart of the 100 GHz spicule. These results suggest that the 100 GHz spicule presented in this Letter is classified to a macrospicule without a hot sheath in former terminology. **2017 April 26**

Estimating the temperature and density of a spicule from 100 GHz data obtained with ALMA

Masumi **Shimojo**, Tomoko Kawate, Takenori J. Okamoto, Takaaki Yokoyama, Noriyuki Narukage, Taro Sakao, Kazumasa Iwai, Gregory D. Fleishman, Kazunari Shibata
2020 *ApJL* **888** L28
https://arxiv.org/pdf/1912.05714.pdf
https://doi.org/10.3847/2041-8213/ab62a5
We succeeded in observing two large spicules simultaneously with the Atacama Large Millimeter/submillimeter Array (ALMA), the Interface Region Imaging Spectrograph (IRIS), and the Atmospheric Imaging Assembly (AIA) onboard the Solar Dynamics Observatory. One is a spicule seen in the IRIS Mg II slit-jaw images and AIA 304Å images (MgII/304A spicule). The other one is a spicule seen in the 100GHz images obtained with ALMA (100GHz spicule). Although the 100GHz spicule overlapped with the MgII/304A spicule in the early phase, it did not show any corresponding structures in the IRIS Mg II and AIA 304A images after the early phase. It suggests that the spicules are individual events and do not have a physical relationship. To obtain the physical parameters of the 100GHz spicule, we estimate the optical depths as a function of temperature and density using two different methods. One is using the observed brightness temperature by assuming a filling factor, and the other is using an emission model for the optical depth. As a result of comparing them, the kinetic temperature of the plasma and the number density of ionized hydrogens in the 100GHz spicule are ~6800 K and 2.2 x 10^10 cm^-3. The estimated values can explain the absorbing structure in the 193A image, which appear as a counterpart of the 100GHz spicule. These results suggest that the 100GHz spicule presented in this paper is classified to a macrospicule without a hot sheath in former terminology. **26 Apr 2017**

First ALMA Observation of a Plasmoid Ejection from an X-ray Bright Point

M. **Shimojo**, H. S. Hudson, S. M. White, T. S. Bastian, K. Iwai
ApJL 841 L5 **2017**
https://arxiv.org/pdf/1704.04881.pdf
Eruptive phenomena such as plasmoid ejections or jets are an important feature of solar activity with the potential for improving our understanding of the dynamics of the solar atmosphere. Such ejections are often thought to be signatures of the outflows expected in regions of fast magnetic reconnection. The 304 A EUV line of Helium, formed at around 10^5 K, is found to be a reliable tracer of such phenomena, but the determination of physical parameters from such observations is not straightforward. We have observed a plasmoid ejection from an X-ray bright point simultaneously at millimeter wavelengths with ALMA, at EUV wavelengths with AIA, in soft X-rays with Hinode/XRT. This paper

reports the physical parameters of the plasmoid obtained by combining the radio, EUV and X-ray data. As a result, we conclude that the plasmoid can consist either of (approximately) isothermal 10^5 K plasma that is optically thin at 100 GHz, or else a 10^4 K core with a hot envelope. The analysis demonstrates the value of the additional temperature and density constraints that ALMA provides, and future science observations with ALMA will be able to match the spatial resolution of space-borne and other high-resolution telescopes. **2015-12-17**

Variation of Solar Microwave Spectrum in the Last Half Century

M. **Shimojo**, K. Iwai, A. Asai, S. Nozawa, T. Minamidani, M. Saito

ApJ **848** 62 **2017**

https://arxiv.org/pdf/1709.03695.pdf

The total solar fluxes at 1, 2, 3.75, and 9.4 GHz were observed continuously from 1957 to 1994 at Toyokawa, and from 1994 until now at Nobeyama, Japan with the current Nobeyama Radio Polarimeters. We examined the multi-frequency and long-term datasets, and found that not only the microwave solar flux but also its monthly standard deviation well indicates the long-term variation of solar activity. Furthermore, we found that the microwave spectra at the solar minima of Cycle 20~24 agree with each other. These results show that the average atmospheric structure above the upper chromosphere in the quiet Sun has not varied for half a century, and suggest that the energy input for atmospheric heating from the sub-photosphere to the corona has not changed in the quiet Sun despite significantly differing strengths of magnetic activity in the last five solar cycles.

Observing the Sun with Atacama Large Millimeter/submillimeter Array (ALMA): High Resolution Interferometric Imaging

M. **Shimojo**, T.S. Bastian, A.S. Hales, S.M. White, K. Iwai, R.E. Hills, A. Hirota, N.M. Phillips, T. Sawada, P. Yagoubov, G. Siringo, S. Asayama, M. Sugimoto, R. Brajsa, I. Skokic, M. Barta, S. Kim, I. de Gregorio, S.A. Corder, H.S. Hudson, S. Wedemeyer, D.E. Gary, B. De Pontieu, M. Loukicheva, G.D. Fleishman, B. Chen, A. Kobelski, Y. Yan

Solar Phys. 292:87 **2017**

https://arxiv.org/pdf/1704.03236.pdf

Observations of the Sun at millimeter and submillimeter wavelengths offer a unique probe into the structure, dynamics, and heating of the chromosphere; the structure of sunspots; the formation and eruption of prominences and filaments; and energetic phenomena such as jets and flares. High-resolution observations of the Sun at millimeter and submillimeter wavelengths are challenging due to the intense, extended, low- contrast, and dynamic nature of emission from the quiet Sun, and the extremely intense and variable nature of emissions associated with energetic phenomena. The Atacama Large Millimeter/submillimeter Array (ALMA) was designed with solar observations in mind. The requirements for solar observations are significantly different from observations of sidereal sources and special measures are necessary to successfully carry out this type of observations. We describe the commissioning efforts that enable the use of two frequency bands, the 3 mm band (Band 3) and the 1.25 mm band (Band 6), for continuum interferometric-imaging observations of the Sun with ALMA. Examples of high-resolution synthesized images obtained using the newly commissioned modes during the solar commissioning campaign held in December 2015 are presented. Although only 30 of the eventual 66 ALMA antennas were used for the campaign, the solar images synthesized from the ALMA commissioning data reveal new features of the solar atmosphere that demonstrate the potential power of ALMA solar observations. The ongoing expansion of ALMA and solar-commissioning efforts will continue to enable new and unique solar observing capabilities. 16, 18, 20 Dec 2015

Unusual Migration of Prominence Activities in the Southern Hemisphere during Cycles 23–24

M. **Shimojo**

Publ. Astron. Soc. Japan 65, No SP1, S16 [6 pages] (**2013**)

http://pasj.asj.or.jp/v65/sp1/65S016/65S016.pdf

The solar activity in Cycles 23–24 shows differences from the previous cycles that were observed with modern instruments, e.g., long cycle duration and a small number of sunspots. To appreciate the anomalies further, we investigated the prominence eruptions and disappearances observed with the Nobeyama Radioheliograph for over 20 years. Consequently, we found that the occurrence of prominence activities in the northern hemisphere is normal because the period of the number variation is 11 years, and the migration of the producing region of the prominence activities traces the migration of 11 years ago. On the other hand, the migration in the southern hemisphere significantly differs from that in the northern hemisphere and the previous cycles. The prominence activities occurred over $\pm 50^{\circ}$ latitude in spite of the late decay phase of Cycle 23, and the number of prominence activities in the higher latitude region (over $\pm 65^{\circ}$) is very small, even near the solar maximum of Cycle 24. The results suggest that the anomalies of the global magnetic field distribution started at the solar maximum of Cycle 23. A comparison of the butterfly diagram of the prominence activities with the magnetic butterfly diagram indicates that the timing of "the rush to the pole" and the polar magnetic field closely relates to unusual migration. Considering that the rush to the

pole is made of the sunspots, the hemispheric asymmetry of the sunspots and the strength of the polar magnetic fields are essential for understanding the anomalies of the prominence activities.

Chromospheric and Coronal Radio Sources from Observations of the Partial Solar Eclipse of March 20, 2015, at the Mountain Astronomical Station of the Central Astronomical Observatory

A. D. **Shramko** and S. A. Guseva
Geomagn. and Aeronomy 58 4 464-468 **2018**
Geomagnetizm i Aeronomiya, **2018**, Vol. 58, No. 4, pp. 479–483.
http://sci-hub.tw/https://link.springer.com/article/10.1134/S0016793218040163
This paper presents the results of processing the data on the partial solar eclipse that occurred on **March 20, 2015**, and was observed with the RT-3 (λ = 4.9 cm) and RT-2 (λ = 3.2 cm) radio telescopes of the Kislovodsk Mountain Astronomical Station, Central Astronomical Observatory, Russian Academy of Sciences (MAS CAO RAS). They were compared with observations in the optical and X-ray ranges. The local radio sources at the limb and on the disc of the Sun were identified: an eruptive and a quiet prominence; filaments; a coronal hole; facular plages; and a sunspot group. The curves of the center-to-limb variations in the radio brightness of the undisturbed regions of the Sun were plotted for λ = 4.9 and λ = 3.2 cm. The solar radio maps were presented. The altitude of the radiating layer in the chromosphere above the sunspot and the facular sources for λ = 4.9 cm λ = 3.2 cm was compared.

A Genetic Algorithm to model Solar Radio Active Regions from 3D Magnetic Field Extrapolations

Alexandre José de Oliveira e **Silva**, Caius L. Selhorst, Joaquim E. R. Costa, Paulo J. A. Simões, C. Guillermo Giménez de Castro, Sven Wedemeyer, Stephen M. White, Roman Brajša, Adriana Valio
Frontiers in Astronomy and Space Sciences 9: 911118. **2022**
doi: 10.3389/fspas.2022.911118
https://arxiv.org/pdf/2205.03385.pdf
https://www.frontiersin.org/articles/10.3389/fspas.2022.911118/pdf
In recent decades our understanding of solar active regions (ARs) has improved substantially due to observations made with better angular resolution and wider spectral coverage. While prior AR observations have shown that these structures were always brighter than the quiet Sun at centimeter wavelengths, recent observations at millimeter and submillimeter wavelengths have shown ARs with well defined dark umbrae. Given this new information, it is now necessary to update our understanding and models of the solar atmosphere in active regions. In this work, we present a data-constrained model of the AR solar atmosphere, in which we use brightness temperature measurements of NOAA 12470 at three radio frequencies: 17 (NoRH), 100 and 230 GHz (ALMA). Based on our model, which assumes that the radio emission originates from thermal free-free and gyroresonance processes, we calculate radio brightness temperature maps that can be compared with the observations. The magnetic field at distinct atmospheric heights was determined in our modelling process by force-free field extrapolation using photospheric magnetograms taken by HMI/SDO. In order to determine the best plasma temperature and density height profiles necessary to match the observations, the model uses a genetic algorithm that modifies a standard quiet Sun atmospheric model. Our results show that the height of the transition region (TR) of the modelled atmosphere varies with the type of region being modelled: for umbrae the TR is located at 1080 +/- 20 km above the solar surface; for penumbrae, the TR is located at 1800 +/- 50 km; and for bright regions outside sunspots, the TR is located at 2000 +/- 100 km. With these results, we find good agreement with the observed AR brightness temperature maps. Our modelled AR can be used to estimate the emission at frequencies without observational coverage. **December 17, 2015**

Broken Power-law Energy Spectra of the Accelerated Electrons Detected in Radio and Hard X-Rays during the SOL2013-05-13 Event

Douglas Félix da **Silva**1,2 and Adriana Valio2
2021 ApJL 915 L1
https://doi.org/10.3847/2041-8213/ac0726
Solar flares, resulting from magnetic activity of the Sun, are among the most energetic events in the solar system and in extreme cases directly affect our highly technological society. In this work, we analyze a solar flare detected at millimeter and centimeter wavelengths, as well as X-rays above 1 MeV. Observations of solar flares at these energy bands provide diagnostics of the energetic accelerated electrons and the magnetic fields where the emission is produced. During the SOL**2013-05-13** solar flare, radio data were obtained by the telescope system POlarisation Emission of Millimeter Activity at the Sun, which observes the Sun at 45 and 90 GHz with polarization measurements, and at microwaves (1–15 GHz) by the Radio Solar Telescope Network. For the same event, X-ray emission was detected by the RHESSI and Fermi satellites. Spectra at both wavelengths were constructed and fit separately to yield the accelerated electron energy distribution that produced the emission. The optically thin radio spectral index was calculated by fitting the Ramaty model of gyrosynchrotron emission to the observed radio spectrum, whereas the hard

X-ray spectral index was obtained from the spectral fit assuming a thermal emission model plus a nonthermal broken power-law distribution. Finally, both spectral indexes were compared and confirmed that the index obtained from the radio spectrum agrees with the index of the X-ray spectrum for energies above the break energy of ~600 keV. Thus, the hard X-rays more energetic than 600 keV and high radio frequencies of solar flares are emitted by the same population of high-energy accelerated electrons. This result indicates that the accelerated electrons have an energy distribution best represented by a broken power law, with a breakup above energies around 1 MeV.

Spectral signature of solar active region in millimetre and submillimetre wavelengths

J F Valle **Silva**, C G Giménez de Castro, C L Selhorst, J-P Raulin, A Valio
Monthly Notices of the Royal Astronomical Society, Volume 500, Issue 2, January **2021**, Pages 1964–1969,
https://doi.org/10.1093/mnras/staa3354
Active regions were observed with different instruments covering the spectral band from 17 to 405 GHz. The observations were made with the Nobeyama Radioheliograph (17 GHz), the Atacama Large Millimetre Array (107 and 238 GHz), and the Solar Submillimeter Telescope (212 and 405 GHz). A procedure was developed that allows the comparison between observations taken with telescopes of different operational characteristics and mainly of different spatial resolution. The brightness temperature and density flux spectra of several active regions corresponding to a different phase of its lifetime were obtained. The flux density invariably increases in all cases from 107 to 405 GHz and the mean spectral index is ∼2 showing that the dominant emission mechanism at submillimeter frequencies is still thermal. We show that Solar Submillimeter Telescope (SST) and Atacama Large Millimeter/submillimeter Array (ALMA) observations are compatible within the uncertainties, a result of great interest for future joint observations.

Inferring the magnetic field asymmetry of solar flares from the degree of polarisation at millimetre wavelengths

Douglas F. da **Silva**, Paulo J. A. Simões, R. F. Hidalgo Ramírez, Adriana Válio
Solar Phys. 295:73 **2020**
https://arxiv.org/pdf/2005.01420.pdf
https://link.springer.com/content/pdf/10.1007%2Fs11207-020-01632-0.pdf
Polarisation measurements of solar flares at millimetre-waves were used to investigate the magnetic field configuration of the emitting sources. We analyse two solar flares (**SOL2013-02-17** and **SOL2013-11-05**) observed by the POlarisation Emission of Millimetre Activity at the Sun (POEMAS) at 45 and 90 GHz, at microwaves from 1 - 15 GHz by the Radio Solar Telescope Network (RSTN), and at high frequencies (212 GHz) by the Solar Submillimetre Telescope (SST). Also, hard X-rays from these flares were simultaneously detected by the Reuven Ramaty High-Energy Solar Spectroscopic Imager (RHESSI). The flux and polarisation radio spectra were fit using a model that simulates gyrosynchrotron emission in a spatially-varying 3D magnetic field loop structure. For the {modelling}, the magnetic loop geometry was fixed and the field strength was the only free parameter of the magnetic field. In addition, a uniform electron distribution was {assumed by} the model, with the number density of energetic electrons and the electron spectral index as free parameters. The fitted model reproduced reasonably well the observed degree of polarisation and radio flux spectra for each event yielding the physical parameters of the loop and flaring sources. Our results indicate that the high degree of polarisation during a solar flare can be explained by two sources located at the {footpoints} of highly asymmetric magnetic loops whereas low polarisation degrees arise from footpoint sources of symmetric magnetic loops.

Submillimeter radiation as the thermal component of the Neupert Effect

Jorge Fernando Valle **Silva**, C. Guillermo Giménez de Castro, Paulo José de Aguiar Simões, Jean-Pierre Raulin
Solar Phys. 294:150 **2019**
https://arxiv.org/pdf/1909.01435.pdf
https://link.springer.com/content/pdf/10.1007%2Fs11207-019-1542-3.pdf
The Neupert effect is the empirical observation that the time evolution of non-thermal emission (e.g. hard X-rays) is frequently proportional to the time derivative of the thermal emission flux (soft X-rays), or, vice versa, that time integrated non-thermal flux is proportional to thermal flux. We analyzed the GOES M2.2 event SOL**2011-02-14**T17:25, and found that the 212 GHz emission plays quite well the role of the thermal component of the Neupert effect. We show that the maximum of the hard X-ray flux for energies above 50 keV is coincident in time with the time-derivative of the 212 GHz flux, within the uncertainties. The microwave flux density at 15.4 GHz, produced by optically thin gyrosynchrotron mechanism, and hard-X rays above 25 keV mark the typical impulsive phase, and have similar time evolution. On the other hand, the 12 GHz emission is delayed by about 25 seconds with respect of the microwave and hard X-ray peak. We argue that this delay cannot be explained by magnetic trapping of non-thermal electrons. With all the observational evidence, we suggest that the 212 GHz emission is produced by thermal bremsstrahlung, initially in the chromosphere, and shifting to optically thin emission from thehot coronal loops at the end of the gradual phase.
RHESSI Science Nuggets #359 Oct **2019**

http://sprg.ssl.berkeley.edu/~tohban/wiki/index.php/Submillimeter_Radiation_as_the_Thermal_Component_of_the_Neupert_Effect
This Nugget has described a peculiar event (SOL2011-02-14T17:25) observed at the exceptionally high radio frequency of 212 GHz. The emission detected appears to be simple thermal bremsstrahlung during both the impulsive and gradual phases of the flare. During the impulsive phase the 212 GHz emission comes from a thermal source at chromospheric heights and its time derivative mimics the HXR flux conforming with the thermal counterpart of the Neupert effect. During the extended phase, the sub-THz emission might be characterized as optically thin thermal bremsstrahlung, from a coronal multi-thermal source as described in Ref. [5]. For full detail on these observations, please see Ref. [6].

The behavior of the spotless active regions during the solar minimum 23-24

Alexandre J. Oliveira e **Silva**, Caius L. Selhorst
Living Around Active Stars Proceedings IAU Symposium No. 328, 2016 **2017**
https://arxiv.org/pdf/1703.00926.pdf
In this work, we analysed the physical parameters of the spotless actives regions observed during solar minimum 23 - 24 (2007 - 2010). The study was based on radio maps at 17~GHz obtained by Imager (MDI) on board the Solar and Heliospheric Observatory (SOHO). The results shows that the spotless active regions presents the same radio characteristics of a ordinary one, they can live in the solar surface for long periods (>10 days), and also can present small flares.

Millimeter Observation of Solar Flares with Polarization

Silva, D. F.; Valio, A. B. M.
Ground-based Solar Observations in the Space Instrumentation Era
ASP Conference Series, Vol. 504, p. 55, **2016**
http://aspbooks.org/publications/504/055.pdf
We present the investigation of two solar flares on **February 17 and May 13, 2013**, studied in radio from 5 to 405 GHz (RSTN, POEMAS, SST), and in X-rays up to 300 keV (FERMI and RHESSI). The objective of this work is to study the evolution and energy distribution of the population of accelerated electrons and the magnetic field configuration. For this we constructed and fit the radio spectrum by a gyro synchrotron model. The optically thin spectral indices from radio observations were compared to that of the hard X-rays, showing that the radio spectral index is harder than the latter by 2. These flares also presented 10-15 % circular polarized emission at 45 and 90 GHz that suggests that the sources are located at different legs of an asymmetric loop.

Comparison of solar radio and EUV synoptic limb charts during the present solar maximum

A. J. Oliveira e **Silva**, C. L. Selhorst, P. J. A. Simões, C. G. Giménes de Castro
A&A **2016**
http://arxiv.org/pdf/1606.03406v1.pdf
The present solar cycle is particular in many aspects: it had a delayed rising phase, it is the weakest of the last 100 years, and it presents two peaks separated by more than one year. To understand the impact of these characteristics on the solar chromosphere and coronal dynamics, images from a wide wavelength range are needed. In this work we use the 17~GHz radio continuum, formed in the upper chromosphere and the EUV lines 304 and 171~{\AA}, that come from the transition region (He II) and the corona (Fe IX, X), respectively. We analyze daily images at 304 and 171~{\AA} obtained by the Atmospheric Imaging Assembly (AIA). The 17~GHz maps were obtained by the Nobeyama Radioheliograph (NoRH). To construct synoptic limb charts, we calculated the mean emission of delimited limb areas with 100" wide and angular separation of 5◦. At the equatorial region, the results show an hemispheric asymmetry of the solar activity. The northern hemisphere dominance is coincident with the first sunspot number peak, whereas the second peak occurs concurrently with the increase in the activity at the south. The polar emission reflects the presence of coronal holes at both EUV wavelengths, moreover, the 17~GHz polar brightenings can be associated with the coronal holes. Until 2013, both EUV coronal holes and radio polar brightenings were more predominant at the south pole. Since then they have not been apparent in the north, but thus appear in the beginning of 2015 in the south as observed in the synoptic charts. This work strengthens the association between coronal holes and the 17~GHz polar brightenings as it is evident in the synoptic limb charts, in agreement with previous case study papers. The enhancement of the radio brightness in coronal holes is explained by the presence of bright patches closely associated with the presence of intense unipolar magnetic fields.

Polarisation of solar flares at millimetre wavelengths

Douglas **Silva**1 , Paulo Simoes2 , and Adriana Valio∗
CESRA Abstract **2016**
http://cesra2016.sciencesconf.org/conference/cesra2016/pages/CESRA2016_prog_abs_book_v1.pdf

Solar flares are characterized by a sudden release of magnetic energy that accelerates particles producing emission throughout the entire electromagnetic spectrum and plasma heating. It is believed that a fraction of these accelerated particles are injected into bipolar magnetic fields. Measurements of right and left circularly polarized brightness temperature of flares at the frequencies of 45 and 90 GHz yield degrees of circular polarization that reached 5 to 40 % and were opposites at 45 and 90 GHz, always being reversed for the events. The interpretation of these results may be associated with the asymmetry of the field strength of magnetic loop legs. Here, we study the magnetic field configuration and energy distribution of accelerated particles in solar flares. For the study of these solar flares, we used the observations of the telescopes POEMAS (POlarization Emission of Millimeter Solar Activity), that monitor the Sun at 45 and 90 GHz with circular polarization. To study the interaction between the particles and magnetic field we applied a 3D model of a magnetic loop. Numerical simulations were performed and produced sources at 45 and 90 GHz in a three dimensional magnetic loop with maximum intensity in opposite polarities of a dipole loop. The simulations also reproduced the degree of polarization and radio spectra observed in each event. Thus, by means of the simulations, we obtained the location of 45 and 90 GHz sources with predominant intensities in opposite magnetic polarities and with reversed degree of polarization

Evidence that Synchrotron Emission from Nonthermal Electrons Produces the Increasing Submillimeter Spectral Component in Solar Flares

Adriana V.R. **Silva** · G.H. Share · R.J. Murphy · J.E.R. Costa · C.G. Giménez de Castro · J.-P. Raulin · P. Kaufmann

Solar Phys (**2007**) 245: 311–326

http://www.springerlink.com/content/c68077532823nh47/fulltext.pdf

We investigate the origin of the increasing spectra observed at submillimeter wavelengths detected in the flare on **2 November 2003** starting at 17:17 UT. This flare, classified as an X8.3 and 2B event, was simultaneously detected by **RHESSI** and the Solar Submillimeter Telescope (**SST**) at **212 and 405 GHz**. Comparison of the time profiles at various wavelengths shows that the submillimeter emission resembles that of the high-energy X rays observed by RHESSI whereas the microwaves observed by the Owens Valley Solar Array (OVSA) resemble that of ~50 keV X rays. Moreover, the centroid position of the submillimeter radiation is seen to originate within the same flaring loops of the ultraviolet and X-ray sources. Nevertheless, the submillimeter spectra are distinct from the usual microwave spectra, appearing to be a distinct spectral component with peak frequency in the THz range. Three possibilities to explain this increasing radio spectra are discussed: (1) gyrosynchrotron radiation from accelerated electrons, (2) bremsstrahlung from thermal electrons, and (3) gyrosynchrotron emission from the positrons produced by pion or radioactive decay after nuclear interactions. The latter possibility is ruled out on the grounds that to explain the submillimeter observations requires 3000 to 2 Ч 10_5 more positrons than what is inferred from X-ray and γ -ray observations. It is possible to model the emission as thermal; however, such sources would produce too much flux in the ultraviolet and soft X-ray wavelengths. Nevertheless we are able to explain both spectral components at microwave and submillimeter wavelengths by gyrosynchrotron emission from the same population of accelerated electrons that emit hard X rays and γ rays. We find that the same 5 Ч 10_{35} electrons inferred from RHESSI observations are responsible for the compact submillimeter source (0.5 arcsec in radius) in a region of 4500 G low in the atmosphere, and for the traditional microwave spectral component by a more extended source (50 arcsec) in a 480 G magnetic field located higher up in the loops. The extreme values in magnetic field and source size required to account for the submillimeter emission can be relaxed if anisotropy and transport of the electrons are taken into account.

Precise timing of flare footpoint sources from mid-infrared observations

Paulo **SIMÕES** et al.

RHESSI Science Nuggets #457 **2023**

https://sprg.ssl.berkeley.edu/~tohban/wiki/index.php/Precise_timing_of_flare_footpoint_sources_from_mid-infrared_observations

2014-09-24

Gyrosynchrotron Emission from Anisotropic Pitch-Angle Distribution of Electrons in 3-D Solar Flare Sources

P.J.A. **Simões** · J.E.R. Costa

Solar Phys (**2010**) 266: 109–121, DOI 10.1007/s11207-010-9596-2

We present calculations, made for the first time, of the gyrosynchrotron emission by mildly relativistic electrons with anisotropic pitch-angle distribution using a realistic magnetic loop model in three dimensions.We investigated the intensity, spectral index of the optically thin region of the spectrum, the spatial morphology and the dependency on the source position on the solar disk. The method to describe a three-dimensional source and the procedure to perform the calculations are presented.We have modified the Ramaty's gyrosynchrotron code to allow the evaluation of anisotropic pitch-angle electron distributions, as described in the complete formalism. We found that anisotropic electron distributions

affect the intensity of the radiation, spatial morphology and spectrum of spatially resolved sources. However, the spatially integrated spectrum of the emission seems to be insensitive to the electron pitch-angle distribution, as the magnetic field inhomogeneity smooths out the effects of the anisotropic distribution in the produced radiation, in contrast to homogeneous sources.

One-dimenssional electromagnetic simulation of multiple electron beams propagating in space plasmas

Simoes, F. J. R., Jr.; Alves, M. V.; Gaelzer, R.
J. Geophys. Res., Vol. 115, No. A6, A06105, **2010**
http://dx.doi.org/10.1029/2009JA014841
It is by now well known that electron beams play an important role in generating radio emissions such as type II and type III radio bursts, commonly observed by spacecraft in the interplanetary medium. Electron beams streaming back from Earth's bow shock into the solar wind have been proposed as a possible source for the electron plasma waves observed by spacecraft in the electron foreshock. Recent observations suggest that during the natural evolution of the foreshock plasma, multiple electron beams could be injected over a period of time, losing their individual identity to coalesce into a single beam. In this work, we use an electromagnetic particle-in-cell (PIC) code “KEMPO 1D, adapted” to simulate two electron beams that are injected into a plasma at different times. The first beam disturbs the background plasma and generates Langmuir waves by electron beam-plasma interaction. Subsequently, another beam is inserted into the system and interacts with the first one and with the driven Langmuir waves to produce electromagnetic radiation. The results of our simulation show that the first beam can produce electrostatic harmonics of the plasma frequency, while the second beam intensifies the emission at the harmonics that is produced by the first one. The behavior of the second beam is strongly determined by the preexisting Langmuir wave electric fields. The simulations also show, as a result of the interaction between both beams, a clear nonlinear frequency shift of the harmonic modes as well as an increase of electromagnetic and kinetic energies of the wave-particle system.

A long term multi-frequency study of solar rotation using solar radio flux and its relationship with solar cycles

Vivek Kumar **Singh**, Satish Chandra, Sanish Thomas, Som Kumar Sharma, Hari Om Vats
MNRAS **2021**
https://arxiv.org/pdf/2107.01448.pdf
This paper examines long-term temporal and spatial fluctuations in the solar rotation (more than four solar cycles) by investigating radio emission escapes from various layers of the solar atmosphere during the years 1967-2010. The flux modulation approach can also be used to investigate variations in solar rotation, which is a contentious topic in solar physics. The current study makes use of a time series of radio flux data at different frequencies (245-15400 MHz) obtained at Sagamore Hill Solar Radio Observatory in Massachusetts, USA, and other observatories from 1967 to 2010. The periodicity present in the temporal variation of time series is estimated through Lomb Scargle Periodogram (LSP). The rotation period estimated for five radio emissions (606, 1415, \& 2695 MHz; from corona, and 4995 \& 8800 MHz; from transition region) through statistical approach shows continuous temporal and spatial variation throughout the years. The smoothed rotation period shows the presence of ~ 22-yrs periodic and ~ 11-yrs components in it. The 22-year component could be linked to the reversal of the solar magnetic field (Hale's) cycle, while the 11-yrs component is most likely related to the sunspot (Schwabe's) cycle. Besides these two components, random components are also prominently present in the analyzed data. The cross-correlation between the sunspot number and the rotation period obtained shows a strong correlation with 11-yrs Schwabe's and 22-yr Hale cycle. The corona rotates faster or slower than transition region in different epoch. The swap of faster rotation speed between corona and transition region also follows the 22-yrs cycle.

Radial Differential Rotation of Solar Corona using Radio Emissions

Vivek Kumar **Singh**, Satish Chandra, Sanish Thomas, Som Kumar Sharma, Hari Om Vats
MNRAS **2021**
https://arxiv.org/pdf/2105.13169.pdf
The present work is an effort to investigate possible radial variations in the solar coronal rotation by analyzing the solar radio emission data at 15 different frequencies (275-1755 MHz) for the period starting from July 1994 to May 1999. We used a time series of disk-integrated radio flux recorded daily at these frequencies through radio telescopes situated at Astronomical Observatory of the Jagellonian University in Cracow. The different frequency radiation originates from different heights in the solar corona. Existing models, indicate its origin at the height range from nearly ~12,000 km (for emission at 275 MHz), below up to ~2,400 km (for emission at 1755 MHz). There are some data gaps in the time series used for the study, so we used statistical analysis using the Lomb-Scargle Periodogram (LSP). This method has successfully estimated the periodicity present in time series even with such data gaps. The rotation period estimated through LSP shows variation in rotation period, which is compared with the earlier reported estimate using auto

correlation technique. The present study indicates some similarity as well as contradiction with studies reported earlier. The radial and temporal variation in solar rotation period are presented and discussed for the whole period analyzed.

Automated Detection of Solar Radio Bursts using a Statistical Method

Dayal **Singh**, K. Sasikumar Raja, Prasad Subramanian, R. Ramesh, Christian Monstein
Solar Phys. 294:112 **2019**
https://arxiv.org/pdf/1906.11780.pdf
https://link.springer.com/content/pdf/10.1007%2Fs11207-019-1500-0.pdf
sci-hub.se/10.1007/s11207-019-1500-0
Radio bursts from the solar corona can provide clues to forecast space weather hazards. After recent technology advancements, regular monitoring of radio bursts has increased and large observational data sets are produced. Hence, manual identification and classification of them is a challenging task. In this paper, we describe an algorithm to automatically identify radio bursts from dynamic solar radio spectrograms using a novel statistical method. We used e-CALLISTO radio spectrometer data observed at Gauribidanur observatory near Bangalore in India during 2013 - 2014. We have studied the classifier performance using the receiver operating characteristics. Further, we studied type III bursts observed in the year 2014 and found that 75% of the observed bursts were below 200 MHz. Our analysis shows that the positions of the flare sites which are associated with the type III bursts with upper-frequency cut-off ≳200 MHz originate close to the solar disk center. **04 January 2013**

The Effect of the Parametric Decay Instability on the Morphology of Coronal Type III Radio Bursts

Chaitanya Prasad **Sishtla**, Immanuel Christopher Jebaraj, Jens Pomoell, Norbert Magyar, Marc Pulupa, Emilia Kilpua, Stuart D. Bale
ApJL **959** L33 **2023**
https://arxiv.org/pdf/2312.10398.pdf
https://iopscience.iop.org/article/10.3847/2041-8213/ad137e/pdf
The nonlinear evolution of Alfvén waves in the solar corona leads to the generation of Alfvénic turbulence. This description of the Alfvén waves involves parametric instabilities where the parent wave decays into slow mode waves giving rise to density fluctuations. These density fluctuations, in turn, play a crucial role in the modulation of the dynamic spectrum of type III radio bursts, which are observed at the fundamental of local plasma frequency and are sensitive to the local density. During observations of such radio bursts, fine structures are detected across different temporal ranges. In this study, we examine density fluctuations generated through the parametric decay instability (PDI) of Alfvén waves as a mechanism to generate striations in the dynamic spectrum of type III radio bursts using magnetohydrodynamic simulations of the solar corona. An Alfvén wave is injected into the quiet solar wind by perturbing the transverse magnetic field and velocity components which subsequently undergo the PDI instability. The type III burst is modelled as a fast-moving radiation source that samples the background solar wind as it propagates to emit radio waves. We find the simulated dynamic spectrum to contain striations directly affected by the multi-scale density fluctuations in the wind. **22/11/2021**

Whistler wave generation by non-gyrotropic, relativistic, electron beams

Marina **Skender**, David Tsiklauri
E-print, May **2014**; Phys. Plasmas 21, 042904 (**2014**)
Particle-in-cell code, EPOCH, is used for studying features of the wave component evident to propagate backwards from the front of the non-gyrotropic, relativistic beam of electrons injected in the Maxwellian, magnetised background plasma with decreasing density profile. According to recent findings presented in Tsiklauri (2011), Schmitz & Tsiklauri (2013) and Pechhacker & Tsiklauri (2012), in a 1.5-dimensional magnetised plasma system, the non-gyrotropic beam generates freely escaping electromagnetic radiation with properties similar to the Type-III solar radio bursts. In this study the backwards propagating wave component evident in the perpendicular components of the elecromagnetic field in such a system is presented for the first time. Background magnetic field strength in the system is varied in order to prove that the backwards propagating wave's frequency, prescribed by the whistler wave dispersion relation, is proportional to the specified magnetic field. Moreover, the identified whistlers are shown to be generated by the normal Doppler-shifted relativistic resonance. Large fraction of the energy of the perpendicular electromagnetic field components is found to be carried away by the whistler waves, while a small but sufficient fraction is going into L- and R- electromagnetic modes.

Flares detected in ALMA single-dish images of the Sun

I. **Skokić**, A. O. Benz, R. Brajša, D. Sudar, F. Matković, M. Bárta
A&A 669, A156 **2022**
https://arxiv.org/pdf/2211.16935.pdf
https://doi.org/10.1051/0004-6361/202244532

https://www.aanda.org/articles/aa/pdf/2023/01/aa44532-22.pdf
The (sub)millimeter radiation of solar flares is poorly understood. Without spatial resolution, it cannot be compared easily to flare emissions in other wavelengths. The Atacama Large Millimeter-submillimeter Array (ALMA) offers sufficient resolution for the first time. However, used as an interferometer, its field of view is smaller than an active region and ALMA cannot observe on demand when a flare occurs. We use readily available large scale single-dish ALMA observations of solar millimeter flares and compare them to well-known features observed in other wavelengths. The properties of these other flare emissions, correlating in space and time, may then be used to interpret the millimeter brightenings and vice versa. The aim is to obtain reliable associations, limited by the time and space resolution of single-dish observations. We collected ALMA observations at 3 mm and 1 mm and searched for millimeter brightenings during times given in a flare catalog. We found five events with 9 or more images that can be used for comparison in time and space. The millimeter brightenings are associated with a variety of flare features in cool (Hα, 30.4 nm), intermediate (17.1 nm), and hot (9.4 nm) lines. In several cases, the millimeter brightening peaked at the footpoint of a hot flare loop. In other cases the peak coincided with the top or footpoint of an active H{\alpha} filament. We found correlations also with post-flare loops and tops of a hot loop, and in some cases to no features at all. The wide field of view provided by the single-dish observations allowed for completely overviewing the flare activity in millimeter waves for the first time. The associated phenomena often changed during the flare in type and location, and may explain the sometimes bewildering behavior of millimeter flare emissions observed previously without spatial resolution. **2017-04-23, 2017-04-26, 2018-04-03, 2018-04-19, 2018-12-15**
CESRA #3417 Dec **2022** https://www.astro.gla.ac.uk/users/eduard/cesra/?p=3417

Correlation between the solar magnetic field strength and the millimeter brightness temperature

I. **Skokić**, D. Sudar, R. Brajša
Central European Astrophysical Bulletin, 44, (**2020**) 2, 1-11
https://arxiv.org/pdf/2203.11747
Images of the Sun at millimeter wavelengths obtained by ALMA show a significant correspondence with the magnetograms. In this paper, we investigate this correspondence by comparing ALMA full-disk solar image taken at 1.2 mm with a SDO/HMI magnetogram and analyze their correlation. It is found that chromospheric network and active regions show a positive correlation where brightness temperature is increasing with the line-of-sight magnetic field strength, while sunspots have a negative correlation. Quiet Sun regions do not show any dependence of the brightness temperature with the magnetic field. Thermal bremsstrahlung is given as the best explanation for the observed correlations.

ALMA solar observing modes

Ivica **Skokic**∗1 and Alma Solar Development Team2
CESRA Abstract **2016** p.44
http://cesra2016.sciencesconf.org/conference/cesra2016/pages/CESRA2016_prog_abs_book_v1.pdf
Atacama Large Millimeter/submillimeter Array (ALMA) is a new powerful interferometer built jointly by Europe, North America, East Asia and Chile. Designed for observations of a wide range of phenomena in a 84-950 GHz frequency range, ALMA is also capable of observing the Sun and opened recently for solar proposals. In this talk recent test and comissioning efforts will be covered and available solar observing modes, their capabilities, limitations and future plans will be described.

Time delay effect between long quasi-periodic oscillations of 37 GHz radio sources and the magnetic field of the nearest sunspots

V. V. **Smirnova**, A. Riehokainen, A. A. Solov'ev, J. Kallunki
Astrophysics and Space Science May **2015**, 357:149
Measurements and the interpretation of the time delay effect between long quasi-periodic oscillations of sunspot magnetic fields and nearby millimeter radio sources observed at 37 GHz were the main goals of this work. Ground-based radio telescope operated by Metsähovi Radio Observatory, Aalto University, Finland was used to obtain time series variations of radio intensity at 37 GHz frequency, as well as, the Helioseismic and Magnetic Imager instrument on-board the Solar Dynamics Observatory spacecraft was used to obtain the magnetic field time series variations. Lags (time delays) in the interval of 15–35 minutes were obtained by cross-correlation analysis of time series and by direct geometrical measurements of distances between the radio sources and nearby sunspots. These distances were in the interval of 11–24 Mm. Corresponding time delays were defined as the relation of these distances to the sound speed. Time delays obtained by two different independent methods turned to be very close. This fact confirms the interpretation of the phenomenon under the study as a process of propagation of disturbances from the slowly oscillating sunspot to the radio source with the sound speed.

Long-period oscillations of millimeter emission above sunspots

V. **Smirnova**1,2, A. Riehokainen1, V. Ryzhov3, A. Zhiltsov3 and J. Kallunki1

A&A 534, A137 (**2011**)
Aims. The investigation of long quasi-periodic oscillations in sunspots/active regions based on millimeter radio data was the main goal of this work.
Methods. Data from simultaneous monitoring observations of solar active regions at 37 GHz and 93 GHz at two different ground-based radio telescopes were obtained. We analyzed them with the methods of wavelet (Morlet) and global wavelet spectrum analysis.
Results. Two main ranges (10−60 and 80−130 min) of long quasi-periodic oscillations were found. We compared them with 17 GHz Nobeyama Radioheliograph (NoRH) data and obtained the same ranges for the long-period oscillations. The long-period oscillations found in this study are relatively stable and could be interpreted as a radial mode of sunspot oscillations.

Pulsations of microwave emission from a solar flare in a twisted loop caused by intrinsic MHD oscillations

C. **Smith**, M. Gordovskyy, P.K. Browning
MNRAS Volume 511, Issue 2, April **2022**, Pages 2880–2884,
https://doi.org/10.1093/mnras/stac250
https://arxiv.org/pdf/2201.08419.pdf
We present results revealing microwave pulsations produced in a model of a flaring twisted solar coronal loop, without any external oscillatory driver. Two types of oscillations are identified: slowly-decaying oscillations with a period of about 70-75s and amplitude of about 5-10% seen in loops both with and without energetic electrons, and oscillations with period of about 40s and amplitude of a few tens of percent observed only in loops with energetic electrons for about 100s after onset of fast energy release. We interpret the longer-period oscillations as the result of a standing kink mode modulating the average magnetic field strength in the loop, whilst the short-period intermittent oscillations associated with energetic electrons are likely to be produced by fast variations of the electric field which produces energetic electrons in this scenario. The slowly-decaying oscillations can explain the quasi-periodic pulsations often observed in the flaring corona.

Parameters of Type I Chains and Their Association with Flares in X-ray

Sodré, Z. A. L.; Fernandes, F. C. R.
Ground-based Solar Observations in the Space Instrumentation Era
ASP Conference Series, Vol. 504, p. 143, **2016**
http://aspbooks.org/publications/504/143.pdf
Chains of type I are associated with the Radio Noise Storms (RNS). We report the analysis of the parameters of the two RNS: one associated with the occurrence of solar flares in X-rays and one recorded on a day without the presence of a flare. The spectral information about the chains in these events were obtained from the e-CALLISTO (Compact Astronomical Low-cost Low-frequency Instrument for Spectroscopy and Transportable Observatory) network. On **07/May/2011** (day without flare) the bandwidth was in the range 5.7 - 91 MHz, the duration varied from 7 - 361 seconds, and the drift-rate frequency was in the range -5.2 - +2.5 MHz s-1. The day with flare (**01/August/2011**) had bandwidth in the range of 4.7 - 60 MHz, duration between 6 and 214 seconds, and frequency drift-rate varying from -6 to +1.8 MHz s-1.

Analysis of Chains of Metric Solar Type I Bursts

Z. A. L. **Sodré**, R. D. Cunha-Silva, F. C. R. Fernandes
Solar Phys., **2014**
Type I radio noise storms are believed to provide a diagnostic of electron acceleration in the corona. Most type I bursts appear in chains of five or more individual bursts. An analysis of the chain properties may indicate electron density, height of emission source, and magnetic-field intensity. We studied 255 chains of solar type I solar bursts recorded by the Compact Astronomical Low-cost Low-frequency Instrument for Spectroscopy and Transportable Observatory (CALLISTO-BLEN) spectrograph from **30 July to 9 August 2011** in the frequency range 170 – 870 MHz. Based on the morphological characteristics identified in the dynamic spectra, we determined the physical parameters for the events. The source electron density was found to be in the range 0.5 – 1.6×109 cm−3, the radial velocity of the emitting plasma varied from −1600 – 1500 km s−1, the magnetic-field strength was in the range 2.2 – 3.3 G, and the height of the source ranged from 0.95 to 1.15 solar radii. The results are consistent with previously reported values.

Turnover Frequency in Solar Microwave Bursts with an Extremely Flat Optically Thin Spectrum

Q. W. **Song**, H. Nakajima, G. L. Huang , B. L. Tan, Y. Huang, Z. Wu
Solar Phys. Volume 291, Issue 12, pp 3619–3635 **2016**
http://link.springer.com/article/10.1007/s11207-016-1004-0
Four microwave bursts have been selected from the Nobeyama Radio Polarimeter (NoRP) observations with an extremely flat spectrum in the optically thin part and a very hard spectral index between 0 and −1 in the maximum

phase of all bursts. It is found that the time evolution of the turnover frequency is inversely proportional to the time profiles of the radio flux in all bursts. Based on the nonthermal gyrosynchrotron theory of Ramaty (Astrophys. J.158, 753, 1969), the local magnetic field strength and the electron spectral index are calculated uniquely from the observed radio spectral index and the turnover frequency. We found that the electron energy spectrum is very hard (spectral index $1-2$), and the time variation of the magnetic field strength is also inversely proportional to the radio flux as a function of time in all bursts. Hence, the time evolution of the turnover frequency can be explained directly by its dependence on the local magnetic field strength. The high turnover frequency (several tens of GHz) is mainly caused by a strong magnetic field of up to several hundred gauss, and probably by the Razin effect under a high plasma density over \(10^{10}~\mbox{cm}^{-3}\) in the maximum phase of these bursts. Therefore, the extremely flat microwave spectrum can be well understood by the observed high turnover frequency and the calculated hard electron spectral index.
20040107, 20040716, 20131103, 20 131110

FREQUENCY DEPENDENCE OF THE POWER-LAW INDEX OF SOLAR RADIO BURSTS
Qiwu **Song**1,2, Guangli Huang1, and Baolin Tan
2012 ApJ 750 160
We process solar flare observations of Nobeyama Radio Polarimeters with an improved maximum likelihood method developed recently by Clauset et al. The method accurately extracts power-law behaviors of the peak fluxes in 486 radio bursts at six frequencies (1-35 GHz) and shows an excellent performance in this study. The power-law indices on 1-35 GHz given by this study vary around 1.74-1.87, which is consistent with earlier statistics in different solar cycles and very close to the simulations of the avalanche model by Lu.

CO-ANALYSIS OF SOLAR MICROWAVE AND HARD X-RAY SPECTRAL EVOLUTIONS. I. IN TWO FREQUENCY OR ENERGY RANGES
Qiwu **Song**1, Guangli Huang1 and Hiroshi Nakajima
2011 ApJ 734 113
Solar microwave and hard X-ray spectral evolutions are co-analyzed in the **2000 June 10 and 2002 April 10** flares, and are simultaneously observed by the Owens-Valley Solar Array in the microwave band and by Yohkoh/Hard X-ray Telescope or RHESSI in the hard X-ray band, with multiple subpeaks in their light curves. The microwave and hard X-ray spectra are fitted by a power law in two frequency ranges of the optical thin part and two photon energy ranges, respectively. Similar to an earlier event in Shao & Huang, the well-known soft-hard-soft pattern of the lower energy range changed to the hard-soft-hard (HSH) pattern of the higher energy range during the spectral evolution of each subpeak in both hard X-ray flares. This energy dependence is actually supported by a positive correlation between the overall light curves and spectral evolution in the lower energy range, while it becomes an anti-correlation in the higher energy range. Regarding microwave data, the HSH pattern appears in the spectral evolution of each subpeak in the lower frequency range, which is somewhat similar to Huang & Nakajima. However, it returns back to the well-known pattern of soft-hard-harder for the overall spectral evolution in the higher frequency range of both events. This frequency dependence is confirmed by an anti-correlation between the overall light curves and spectral evolution in the lower frequency range, but it becomes a positive correlation in the higher frequency range. The possible mechanisms are discussed, respectively, for reasons why hard X-ray and microwave spectral evolutions have different patterns in different energy and frequency intervals.

A tentative statistical analysis of flare events observed by NoRH and NoRP
Q.W. **Song** and G.L. Huang[a]
Advances in Space Research , Volume 41, Issue 8, Pages *1188-1190* (**2008**)
In this paper, we report the statistical analysis of flare events observed by NoRH during 1992–2005 and NoRP during 1994–2005. We give the power law indices for the frequency distribution of peak brightness temperature which is 1.87 ± 0.05 for 17 GHz observation and is 1.64 ± 0.04 for 34 GHz observation. We also present the frequency variation of power law indices for peak flux and total energy of flare for NoRP observation, which is mono-increasing from 1 to 17 GHz.

Radio Noise Storms and the Connection with the Reorganization of Photospheric Magnetic Fields
Z. A. L. **Sodré**, F. C. R. Fernandes, J. C. Santos, C. M. Wrasse
Solar Physics October **2019**, 294:140
https://link.springer.com/content/pdf/10.1007%2Fs11207-019-1534-3.pdf
This work presents the analysis of a Type-I radio noise storm (RNS) recorded by the CALLISTO spectrometers network. Considering that RNSs are associated with the reorganization of the photospheric magnetic field of active regions, we have analyzed the temporal evolution of the magnetic power spectra and the dissipation spectra of the photospheric magnetic field of two active regions (NOAA 11542 and NOAA 11543). This analysis was used to identify for which wave-numbers and time intervals this reorganization occurs. The Type-I emission is supposedly generated by

the fundamental emission of plasma, and the reorganization of the line-of-sight component of the photospheric magnetic field was investigated as a possible mechanism responsible for the maintenance process of the RNS. The analysis of the magnetic power spectra and the dissipation spectra showed that the RNS was probably generated and maintained by the reorganization of the magnetic field of NOAA 11542. The reorganization of the magnetic-energy spectra occurs mainly for wave-numbers smaller than 0.2 Mm−10.2 Mm−1 and the dissipation spectrum increases for wave-numbers around 1 Mm−11 Mm−1. **12 August 2012**

Direct Measurement of Low-Energy Electron Foreshock Beams

Jan **Soucek** , David Píša , Ondrej Santolík
JGR Volume124, Issue4 April **2019** Pages 2380-2392
sci-hub.se/10.1029/2019JA026470
Electrostatic plasma waves above and below the local electron plasma frequency represent a characteristic feature of the foreshock region. These waves are known to be generated by electron beams originating from the bow shock and their spectrum varies from narrowband intense waves close to foreshock edge to weaker broadband emissions further downstream. We present a statistical analysis of electron beams observed in the terrestrial foreshock by the Cluster spacecraft. We compared the energy of foreshock electron beams with the spectrum of electrostatic waves and established a clear correspondence between beam energy and spectrum of the waves. The broadband emissions are correlated with low-energy beams, while high-energy electron beams are associated with narrowband Langmuir waves. Next we solved the linear dispersion relation for a subset of observed electron plasma distributions. We discovered that while the observed electron distributions often exhibit a “bump on tail” feature necessary for an instability, the observed combination of beam energy, density, and temperature typically corresponds to a stable situation. This indicates that strongly unstable electron beams are quickly dissipated by the quasi-linear processes and only stable or marginally stable beams persist long enough to be observed by the instrument. **21 April 2011**

Comparison of Radioastronomical Estimates of the Coronal and Solar Wind Magnetic Field with Measurements from Parker Solar Probe

Steven R. **Spangler**
2020 Res. Notes AAS 4 147
https://iopscience.iop.org/article/10.3847/2515-5172/abb29a
https://doi.org/10.3847/2515-5172/abb29a
The Parker Solar Probe (PSP) spacecraft is measuring plasma properties of the solar wind to heliocentric distances as small as 0.125 au or 26.9 solar radii. One of the most important plasma parameters is the strength of the magnetic field. A variety of radioastronomical remote sensing measurements also provide information on the magnetic field, from the solar surface to heliocentric distances of about 10 solar radii. In this paper, we compare radioastronomical estimates from one technique, Faraday rotation of background radio sources, with the PSP measurements. The extrapolated radioastronomical values are in good agreement with the measurements at the first and second perihelion passages in 2018 and 2019. Future radio measurements could therefore complement PSP measurements as it approaches the ultimate perihelion of 9.8 solar radii.

Effect of the 24 September 2011 solar radio burst on precise point positioning service

V. **Sreeja**1,*, M. Aquino1, Kees de Jong2 and Hans Visse
Space Weather, Volume 12, Issue 3, pages 143–147, March **2014**
An intense solar radio burst occurred on 24 September 2011, which affected the tracking of Global Navigation Satellite Systems' (GNSS) signals by receivers located in the sunlit hemisphere of the Earth. This manuscript presents for the first time the impacts of this radio burst on the availability of Fugro's real-time precise point positioning service for GNSS receivers and on the quality of the L band data link used to broadcast this service. During the peak of the radio burst (12:50–13:20 UT), a reduction in the L band signal-to-noise ratio (SNR) is observed. For some receiver locations, a reset in the position filter is observed, which can be either due to the reduction in the L band SNR or the reduction in the number of tracked GNSS satellites. This reset in the position filter is accompanied by degradation in the positioning accuracy, which is also discussed herein.

Impact of the 24 September 2011 solar radio burst on the performance of GNSS receivers

V. **Sreeja**1,*, M. Aquino, 1, Kees de Jong
Space Weather, Volume 11, Issue 5, pages 306–312, May **2013**
https://agupubs.onlinelibrary.wiley.com/doi/epdf/10.1002/swe.20057
Intense solar radio bursts occurring at the L-band frequencies can significantly impact the performance of Global Navigation Satellite System (GNSS) receivers in the sunlit hemisphere of the Earth. An intense solar radio burst occurred on **24 September 2011**, with a maximum power of 110,000 solar flux units (10−22 W/m2/Hz) at 1.415 GHz. This manuscript aims to contribute insight on the impact of this solar radio burst on the performance of the GNSS receivers in the European and Latin American sectors. Maximum reductions of 11.0, 22.0, and 10.0 dB Hz in the carrier-to-noise density ratio (C/N0) of the GPS L1C/A, L2P, and L2C signals, respectively, were observed. The C/N0

reduction is modulated by the local solar incidence angle for the GPS L1C/A and L2P signals, whereas such modulation was not observed for the GPS L2C signal. The solar radio burst also had an adverse effect on the recorded GNSS pseudorange and carrier phase data, thereby causing positioning errors, which are also presented herein.

Parker Solar Probe detects solar radio bursts related with a behind-the-limb active region

Aleksander A. **Stanislavsky**, Igor N. Bubnov, Artem A. Koval, Serge N. Yerin
A&A 657, A21 **2022**
https://arxiv.org/pdf/2110.08644.pdf
https://www.aanda.org/articles/aa/pdf/2022/01/aa41984-21.pdf
https://doi.org/10.1051/0004-6361/202141984

Context. The interpretation of solar radio bursts observed by Parker Solar Probe (PSP) in the encounter phase plays a key role in understanding intrinsic properties of the emission mechanism in the solar corona. Lower time–frequency resolution of the PSP receiver can be overcome by simultaneous ground–based observations using more advanced antennas and receivers.
Aims. In this paper we present such observations for which the active active region 12 765, begetter of type III, J, and U solar bursts, was within sight of ground–based instruments and behind the solar limb of the PSP spacecraft.
Methods. We used a subarray of the Giant Ukrainian Radio Telescope to get the spectral properties of radio bursts at the frequency range of 8–80 MHz, as well as the PSP radio instruments with a bandwidth of 10.5 kHz–19.2 MHz, during solar observations on **June 5, 2020**.
Results. We directly detected the radio events initiated by the active region behind the solar limb of the PSP spacecraft, using special conditions in the solar corona, due to the absence of active regions from the PSP side. Following the generation mechanism of solar radio emission, we refined the density model for the solar corona above the active region 12765 responsible for the radio bursts. Based on the PSP spacecraft position near the Sun and delays of radio waves between space– and ground–based records, we found the corresponding radio responses on the PSP spectrogram.
Conclusions. The absence of sunspots from the PSP side contributes to the propagation of radio waves from a dense loop of the Sun to quiet regions with low densities, through which PSP instruments can detect the radiation.

The first detection of the solar U+III association with an antenna prototype for the future lunar observatory

Lev **Stanislavsky**, Igor Bubnov, Oleksandr Konovalenko, Petro Tokarsky, Serhiy Yerin
Research in Astronomy and Astrophysics **2021**
https://arxiv.org/pdf/2102.02533.pdf

We report about observations of the solar U+III bursts on **5 June of 2020** by means of a new active antenna designed to receive radiation in 4-70 MHz. This instrument can serve as a prototype of the ultra-long-wavelength radiotelescope for observations on the farside of the Moon. Our analysis of experimental data is based on simultaneous records obtained with the antenna arrays GURT and NDA in high frequency and time resolution, e-Callisto network as well as by using the space-based observatories STEREO and WIND. The results from this observational study confirm the model of Reid and Kontar (2017).

Solar bursts as can be observed from the lunar farside with a single antenna at very low frequencies

A.A. **Stanislavsky**, A.A. Konovalenko, S.N. Yerin, I.N. Bubnov, V.V. Zakharenko, Yu.G. Shkuratov, P.L. Tokarsky, Ya.S. Yatskiv, A.I. Brazhenko, A.V. Frantsuzenko, V.V. Dorovskyy, H.O. Rucker, Ph. Zarka
Astron. Nachr. / AN 339, No. 7-8, 559-570 (**2018**)
https://arxiv.org/pdf/1812.07973.pdf

Earth-based observations are complicated by the opacity of Earth's ionosphere at very low frequencies and strong man-made radio frequency interference. This explains long standing interest in building a low frequency radio telescope on the farside of the Moon. Experience from ground-based observations near the ionospheric cutoff in dealing with the interference, ionosphere, and wide-field imaging/dynamic range problems provides crucial information for future radioastronomic experiments on the Moon. In this purpose we observed non-intensive solar bursts on the example of solar drift pairs (DP) at decameter-meter wavelengths with large and small arrays as well as by a single crossed active dipole. We used the large Ukrainian radio telescope UTR-2, the URAN-2 array, a subarray of the Giant Ukrainian radio telescope (GURT) and a single crossed active dipole to get the spectral properties of radio bursts at the frequency range of 8-80 MHz during solar observations on **July 12, 2017**. Statistical analysis of upper and lower frequencies, at which DPs are recorded, shows that the occurrence of forward DPs is more preferable at lower frequencies of the decameter range of observations in comparison with reverse DPs generated more likely at meter wavelengths. We conclude that DPs can be detected not only by antenna arrays, but even by a single crossed active dipole. Thus the latter antenna has a good potential for future low-frequency radio telescopes on the Moon.

Revisiting the Frequency Drift Rates of Decameter Type III Solar Bursts Observed in July – August 2002

A. A. **Stanislavsky**, A. A. Konovalenko, E. P. Abranin, V. V. Dorovskyy, A. Lecacheux, H. O. Rucker, P. Zarka

Solar Physics November **2018**, 293:152

https://link.springer.com/content/pdf/10.1007%2Fs11207-018-1374-6.pdf

https://arxiv.org/pdf/1812.05875.pdf

Estimating for the frequency drift rates of type III solar bursts is crucial for characterizing their source development in the solar corona. According to Melnik et al. (Solar Phys.269, 335, 2011), the analysis of powerful decameter type III solar bursts, observed in July – August 2002, found a linear approximation for the drift rate versus frequency. The conclusion contradicts reliable results of many other well-known solar observations. In this paper we report on the reanalysis of the solar data with a more advanced method. Our study shows that the decameter type III solar bursts of July – August 2002, as standard type III bursts, follow a power law in frequency drift rates. We explain the possible reasons for this discrepancy.

An upgrade of the UTR-2 radio telescope to a multifrequency radio heliograph

Stanislavsky A., Konovalenko A., Koval A., Volvach Ya.

SUN and GEOSPHERE Vol.13, No.1 - **2018** p. 21-24

http://newserver.stil.bas.bg/SUNGEO//00SGArhiv/SG_v13_No1_2018-pp-21-24.pdf

http://ws-sozopol.stil.bas.bg/2017Sunny/Proceedings2017_V3.pdf

We present the broadband heliograph based on the UTR-2 radio telescope for obtaining the solar corona images in the frequency range 8-32 MHz with the frequency resolution 4 kHz, the time resolution up to 1 ms, and under the dynamic range about 90 dB. The instrument provides new possibilities to measure the non-thermal radiation in an unprecedented way for a better understanding of the radio emission processes in solar corona. We describe various aspects of the instrument including its antenna system, receiver front end, digital hardware and the data acquisition. This is the lowest-frequency heliograph operating in the world. It allows us to detect radio emission from solar radio sources in the upper solar corona near frequencies of ionosphere cut-off. The instrument performance is illustrated with source maps of solar radio bursts at low frequencies during the observational campaigns of 2013 and 2015. **9 April of 2013, July 10-12, 2015**

Solar Drift-Pair Bursts

Stanislavsky A. 1,2 , Volvach Ya. 1 , Konovalenko A. 1 , Koval A. 3

Sun and Geosphere, **2017**; 12/2: 99 -103

http://newserver.stil.bas.bg/SUNGEO//00SGArhiv/SG_v12_No2_2017-pp-99-103.pdf

In this paper a new sight on the study of solar bursts historically called drift pairs (DPs) is presented. Having a simple morphology on dynamic spectra of radio records (two short components separated in time, and often they are very similar) and discovered at the dawn of radio astronomy, their features remain unexplained totally up to now. Generally, the DPs are observed during the solar storms of type III bursts, but not every storm of type III bursts is linked with DPs. Detected by ground-based instruments at decameter and meter wavelengths, the DP bursts are limited in frequency bandwidth. They can drift from high frequencies to low ones and vice versa. Their frequency drift rate may be both lower and higher than typical rates of type III bursts at the same frequency range. The development of low-frequency radio telescopes and data processing provide additional possibilities in the research. In this context the fresh analysis of DPs, made from recent observations in the summer campaign of 2015, are just considered. Their study was implemented by updated tools of the UTR-2 radio telescope at 9-33 MHz. During **10-12 July of 2015**, DPs forming the longest patterns on dynamic spectra are about 7% of the total number of recorded DPs. Their marvelous resemblance in frequency drift rates with the solar S-bursts is discussed.

Solar type III bursts with high-frequency cut-off

A.A. **Stanislavsky**

Astronomische Nachrichten, vol. 338, issue 4, pp. 407-412, **2017**

https://arxiv.org/pdf/1812.07294.pdf

New results in the study of solar type III bursts observed with the UTR-2 radio telescope are presented. The main feature of these bursts is a high-frequency cut-off. The solar activity manifestation was connected with the emergency of a new group of solar spots behind the solar limb relative to an observer on the Earth. This burst type was identified by analyzing its frequency drift rate, duration and flux depending on frequency. The solar bursts were linked to a group of similar events. The cut-off frequency is different from burst to burst and lies within 30-55 MHz. The cut-off origin is considered in the context of propagation effects between the burst sources moving behind the solar limb and the ground-based radio instruments. **19 August 2012**

Coronal Magnetic Field Strength from Decameter Zebra-Pattern Observations: Complementarity with Band-Splitting Measurements of an Associated Type II Burst

A. A. **Stanislavsky**, A. A. Konovalenko, A. A. Koval, V. V. Dorovskyy, P. Zarka, H. O. Rucker
Solar Phys. **2015**, Volume 290, Issue 1, pp 205-218

A zebra pattern and a type II burst with band splitting were analyzed to study the coronal magnetic field in the height range of 1.9 – 2 solar radii. To this aim we used an extremely sensitive telescope (the Ukrainian decameter radio telescope, UTR-2) with a low-noise, high-dynamic-range spectrometer for the observations below 32 MHz. Based on the analysis of the spectral structures, the field strength obtained is 0.43 G. The value was found by fitting two different field indicators together under the assumptions that the shock wave front was perpendicular to the radial direction, and the radio emission of the type II burst was in the fundamental frequency. The result is compared to and agrees with coronal magnetic-field models.

Antenna Performance Analysis for Decameter Solar Radio Observations

Aleksander **Stanislavsky**, Aleksander Konovalenko, Eduard Abranin, Vladimir Dorovskyy, Valentin Mel'nik,Michael Kaiser, Alain Lecacheux, Helmut Rucker
Astronomische Nachrichten 330, 691(**2009**)
http://arxiv.org/pdf/1111.3226v1.pdf

Decameter wavelength radio emission is finely structured in solar bursts. For their research it is very important to use a sufficient sensitivity of antenna systems. In this paper we study an influence of the radiotelescope-antenna effective area on the results of decameter solar radio observations. For this purpose we compared the solar bursts received by the array of 720 ground-based dipoles and the single dipole of the radiotelescope UTR-2. It's shown that a larger effective area of the ground-based antenna allows us to measure a weaker solar emission and to distinguish a fine structure of strong solar events. This feature has been also verified by simultaneous ground- and space-based observations in the overlapping frequency range. **2006 July 6, 2007 August 17, 2007 August 21**

Turbulent propagation of high-energy electrons in a solar coronal loop

A. V. **Stepanov**1, T. Yokoyama2, K. Shibasaki3, and V. F. Melnikov4
A&A 465, 613-619 (**2007**)

The electrons undergo strong resonant scattering due to wave-particle interaction, and the emission front propagates with the wave phase velocity, which is much lower than the particle velocity.

Moving Type IV bursts.

Stewart, R. T.
Solar radiophysics: Studies of emission from the sun at metre wavelengths, McLean, D. J. and Labrum, N. R. eds., 361–383, **1985**.

Modeling of Solar Atmosphere Parameters Above Sunspots Using RATAN-600 Microwave Observations

A. G. **Stupishin**, T. I. Kaltman, V. M. Bogod, L. V. Yasnov
Solar Physics January **2018**, 293:13
https://link.springer.com/content/pdf/10.1007%2Fs11207-017-1228-7.pdf

Models of the upper transition region of sunspots have been derived based on the observed radio spectrum between 3 and 18 GHz from Radio Astronomical Telescope of the Academy of Sciences 600 (RATAN-600) observations. Our objective is to match the spectrum to show that, within the limits of the one-dimensional observations and modeling, we have obtained a reasonable description of the upper transition-region structure of sunspots. We have developed a diagnostic method, based on iterative correction of the temperature–height profile in the transition region and lower corona, and applied it to three selected active regions with unipolar gyroresonance sources. Good agreement is achieved between observed and modeled microwave spectra using one-dimensional, time-independent models in hydrostatic equilibrium characterized by a given temperature as a function of height. We found that above sunspots the upper height of a transition region is located at 2 – 2.3 Mm, and the temperature of the low corona is about 1.5 – 2.5 MK. **2011-09-13, 2011-10-10, 2013-11-18**

CESRA # 1853 May **2018** http://cesra.net/?p=1853

Modeling of solar atmosphere parameters above the active region using RATAN-600 radiotelescope observation

Alexey **Stupishin**_1, Vladimir Bogod2, Tatyana Kaltman2, and Leonid Yasnov1
CESRA **2016**, p.100
http://cesra2016.sciencesconf.org/conference/cesra2016/pages/CESRA2016_prog_abs_book_v3.pdf

This work is devoted to estimation of solar atmosphere parameters (electron density and temperature) above the active region based on the observation of polarized radioemission on RATAN-600 radiotelescope and on the 3-component photosphere magnetic _eld (SDO/HMI). We choose some number of active regions, including ones with high polarization degree on the high frequencies (which indicates the small contribution of free-free emission). Photosphere magnetic _eld 180-degrees ambiguity was resolved, then 3D model of the magnetic _eld was reconstructed in chromosphere and corona (_rst in potential approach, then in non-linear force-free approach).
To estimate electron density and temperature height pro_les we suggest an iterative _tting method, based on the calculation of free-free and cyclotron radioemission in the 2-18 GHz range, convolution of radiomaps with the telescope diagram and comparison with observed scans by several parameters (ux values, shape of the spectra, size of source). E_ective code for radioemission calculations was developed.
It was shown that the height of the transition region is 1-1.5 Mm lower, while electron density and temperature are 2 times greater than ones in the basic model of quiet Sun.
On the base of these estimations some future steps are discussed: possibility of the e_ective diagnostic of the solar atmosphere parameters, inuence of inhomogenity on the modeling results, possibility of 2D radiomaps using.

Quantifying the Magnetic Structure of a Coronal Shock Producing a Type II Radio Burst

W. **Su**, T.M. Li, X. Cheng, L. Feng, P.J. Zhang, P.F. Chen, M. D. Ding, L. J. Chen, Y. Guo, Y. Wang, D. Li, L. Y. Zhang

ApJ **929** 175 **2022**

https://arxiv.org/pdf/2203.11042.pdf

https://iopscience.iop.org/article/10.3847/1538-4357/ac5fac/pdf

Type II radio bursts are thought to be produced by shock waves in the solar atmosphere. However, what magnetic conditions are needed for the generation of type II radio bursts is still a puzzling issue. Here, we quantify the magnetic structure of a coronal shock associated with a type II radio burst. Based on the multi-perspective extreme-ultraviolet observations, we reconstruct the three-dimensional (3D) shock surface. By using a magnetic field extrapolation model, we then derive the orientation of the magnetic field relative to the normal of the shock front (θBn) and Alfvén Mach number (MA) on the shock front. Combining the radio observations from Nancay Radio Heliograph, we obtain the source region of the type II radio burst on the shock front. It is found that the radio burst is generated by a shock with MA≳1.5 and a bimodal distribution of θBn. We also use the Rankine-Hugoniot relations to quantify the properties of the shock downstream. Our results provide a quantitative 3D magnetic structure condition of a coronal shock that produces a type II radio burst. **6 Mar 2014**

Investigating the Conditions of the Formation of a Type II Radio Burst on 2014 January 8

W. **Su**, X. Cheng, M. D. Ding, P. F. Chen, Z. J. Ning, H. S. Ji

2016

http://arxiv.org/pdf/1609.05633v1.pdf

It is believed that type II radio bursts are generated by shock waves. In order to understand the generation conditions of type II radio bursts, in this paper, we analyze the physical parameters of a shock front. The type II radio burst we selected was observed by Siberian Solar Radio Telescope (SSRT) and Learmonth radio station and was associated with a limb CME occurring on **2014 January 8** observed by the Atmospheric Imaging Assembly (AIA) on board the Solar Dynamics Observatory (SDO). The evolution of the CME in the inner corona presents a double-layered structure that propagates outward. We fit the outer layer of the structure with a partial circle and divide it into 7 directions from -45◦ to 45◦ with an angular separation of 15◦. We measure the outer layer speed along the 7 directions, and find that the speed in the direction of -15◦ with respect to the central direction is the fastest. We use the differential emission measure (DEM) method to calculate the physical parameters at the outer layer at the moment when the type II radio burst was initiated, including the temperature (T), emission measure (EM), temperature ratio (Td/Tu), compression ratio (X), and Alfv\'en Mach number (MA). We compare the quantities X and MA to that obtained from band-splitting in the radio spectrum, and find that this type II radio burst is generated at a small region of the outer layer that is located at the sector in 45◦ direction. The results suggest that the generation of type II radio bursts (shock) requires larger values of X and MA rather than simply a higher speed of the disturbance.

A Type II Radio Burst without a Coronal Mass Ejection

W. **Su**, X. Cheng, M. D. Ding, P. F. Chen, J.Q. Sun

ApJ **804** 88 **2015**

http://arxiv.org/pdf/1503.00861v1.pdf

Type II radio bursts are thought to be a signature of coronal shocks. In this paper, we analyze a short-lived type II burst that started at 07:40 UT on **2011 February 28**. By carefully checking white-light images, we find that the type II radio burst is not accompanied by a coronal mass ejection, only with a C2.4 class flare and narrow jet. However, in the extreme-ultraviolet (EUV) images provided by the Atmospheric Imaging Assembly (AIA) on board the Solar Dynamics Observatory (SDO), we find a wave-like structure that propagated at a speed of ~ 600 km s−1 during the burst. The relationship between the type II radio burst and the wave-like structure is in particular explored. For this purpose, we first derive the density distribution under the wave by the differential emission measure (DEM) method, which is used to restrict the empirical density model. We then use the restricted density model to invert the speed of the shock that produces the observed frequency drift rate in the dynamic spectrum. The inverted shock speed is similar to the speed of the wave-like structure. This implies that the wave-like structure is most likely a coronal shock that produces the type II radio burst. We also examine the evolution of the magnetic field in the flare-associated active region and find continuous flux emergence and cancellation taking place near the flare site. Based on these facts, we propose a new mechanism for the formation of the type II radio burst, i.e., the expansion of the strongly-inclined magnetic loops after reconnected with nearby emerging flux acts as a piston to generate the shock wave.

High resolution observations of radio noise storms in the solar corona

Prasad **Subramanian** and Claude Mercier
CESRA Science Highlights #826 Sept **2016**
http://www.astro.gla.ac.uk/users/eduard/cesra/?p=826

Constraints on coronal turbulence models from source sizes of noise storms at 327 MHz

Subramanian, Prasad; Cairns, Iver
J. Geophys. Res., Vol. 116, No. A3, A03104, **2011**
We seek to reconcile observations of small source sizes in the solar corona at 327 MHz with predictions of scattering models that incorporate refractive index effects, inner scale effects, and a spherically diverging wavefront. We use an empirical prescription for the turbulence amplitude CN2(R) based on very long baseline interferometry observations by Spangler et al. of compact radio sources against the solar wind for heliocentric distances R ≈ 10–50 R . We use the Coles and Harmon model for the inner scale li(R), which is presumed to arise from cyclotron damping. In view of the prevalent uncertainty in the power law index that characterizes solar wind turbulence at various heliocentric distances, we retain this index as a free parameter. We find that the inclusion of spherical divergence effects suppresses the predicted source size substantially. We also find that inner scale effects significantly reduce the predicted source size. An important general finding for solar sources is that the calculations substantially underpredict the observed source size. Three possible, nonexclusive, interpretations of this general result are proposed. First and simplest, future observations with better angular resolution will detect much smaller sources. Consistent with this, previous observations of small sources in the corona at metric wavelengths are limited by the instrument resolution. Second, the spatially varying level of turbulence CN2(R) is much larger in the inner corona than predicted by straightforward extrapolation sunward of the empirical prescription, which was based on observations between 10 and 50 R . Either the functional form or the constant of proportionality could be different. Third, perhaps the inner scale is smaller than the model, leading to increased scattering. These results and interpretations are discussed and compared with earlier work.

Radio Emission Processes: Part I

K.R. **Subramanian**
2010, In: Gopalswamy, N., Hasan, S.S., Ambastha, A. (eds.)
Heliophysical Processes, Astrophysics and Space Science Proceedings, Springer, Berlin, p. 137-151,
File
This chapter provides an overview of the radio emission mechanisms
in the Solar atmosphere. Incoherent (free - free emission and gyro - emission)

and coherent (plasma emission and electron cyclotron maser emission) emission mechanisms are discussed.

A statistical study of the characteristics of type II doublet radio bursts

Subramanian, K.R., Ebenezer, E.
Astron. Astrophys., 451, Issue 2, 683-690, **2006**
We study the characteristics of doublet type II radio bursts in which two type II bursts occur in sequence and investigate their drivers.
The second type II burst starts at a lower frequency than to the first one. The normalized drift rate of the the first II burst is found to be nearly twice that of the second type II burst. For both the first and second type II bursts, their start frequencies and the drift rates are found to be correlated. The mean time difference between the start of the first and second type II burst is 8.1 min. There were no reports of two flares or CMEs except one case each. The first and second type II bursts start 5 and 15 min after the start of the GOES X-ray flares. The time difference between the CME onset and start of the first and second type II burst is close to the above values.

Electron acceleration in a post-flare decimetric continuum source:

P. **Subramanian**, S. M. White, M. KarlickIIJ, R. Sych, H. S. Sawant and S. Ananthakrishnan
A&A 468 (**2007**) 1099-1102 (Section 'The Sun')
http://www.aanda.org/10.1051/0004-6361:20077341
We have imaged a high brightness temperature ($\sim 10^{9}$K) post-flare source at 1060 MHz with the Giant Metrewave Radio Telescope (GMRT). We use information from these images and the dynamic spectrum from the Hiraiso spectrograph together with the theoretical method described in Subramanian & Becker (2006) to calculate the power input to the electron acceleration process.

Centre to limb brightness variations from ALMA full disk solar images

Davor **Sudar**, Roman Brajša, Ivica Skokić, Arnold O. Benz
Solar Phys. 294:163 **2019**
https://arxiv.org/pdf/1909.08952.pdf
https://doi.org/10.1007/s11207-019-1556-x
Science Verification (SV) data of solar observations with Atacama Large Millimeter-submillimeter Array (ALMA) telescope were released to the scientific community. Understanding the centre to limb brightness function is necessary to compare features in full disk images. Our goals are to find the empirical centre to limb brightness functions in two available spectral bands and create flattened images with centre to limb brightness variations removed. We used second-order polynomial fit of the cosine of incidence angle to data points as a function of radial distance to the centre of the solar disk. The method also includes iterative removal of outliers based on the interquartile range. Fitting functions for all available images proved to adequately describe the data with comparatively small errors in the fitting coefficients. In both bands we found brightening towards the limb which is a consequence of increase in electron temperatures with radial distance in this region of the solar atmosphere. This study found that the Tb of an active region has about 180 K difference between with and without the limb brightening at radial distance ≈0.75R⊙ in Band 6. We also made flattened images with limb brightening removed. The limb brightening effect in ALMA images is significant enough (of the order of 10% for Band 3 and about 15% in Band 6) that it can not be neglected in further analyses. Since the effect of the side lobes was not included in this study, these values probably represent the lower limit of the limb brightening. The shape of the limb brightening function can also be used to constrain electron densities and temperatures in various layers of the solar atmosphere. **2015/12/16-20**

Expansion of Solar Coronal Hot Electrons in an Inhomogeneous Magnetic Field: 1-D PIC Simulation

Jicheng **Sun**, Xinliang Gao, Yangguang Ke, Quanming Lu, Xueyi Wang, Shui Wang
ApJ **887** 96 **2019**
https://arxiv.org/ftp/arxiv/papers/1911/1911.07207.pdf
https://doi.org/10.3847/1538-4357/ab5060

The expansion of hot electrons in flaring magnetic loops is crucial to understanding the dynamics of solar flares. In this paper we investigate, for the first time, the transport of hot electrons in a magnetic mirror field based on a 1-D particle-in-cell (PIC) simulation. The hot electrons with small pitch angle transport into the cold plasma, which leads to the generation of Langmuir waves in the cold plasma and ion acoustic waves in the hot plasma. The large pitch angle electrons can be confined by the magnetic mirror, resulting in the different evolution time scale between electron parallel and perpendicular temperature. This will cause the formation of electron temperature anisotropy, which can generate the whistler waves near the interface between hot electrons and cold electrons. The whistler waves can scatter the large pitch angle electrons to smaller value through the cyclotron resonance, leading to electrons escaping from the hot region. These results indicate that the whistler waves may play an important role in the transport of electrons in flaring magnetic loops. The findings from this study provide some new insights to understand the electron dynamics of solar flares.

Wavelet-Based Characterization of Small-Scale Solar Emission Features at Low Radio Frequencies

Akshay **Suresh**, Rohit Sharma, Divya Oberoi, Srijan B. Das, Victor Pankratius, Brian Timar, Colin J. Lonsdale, Judd D. Bowman, Frank Briggs, Roger J. Cappallo, Brian E. Corey, …

ApJ **843** 19 **2017**

https://arxiv.org/pdf/1612.01016v1.pdf

http://sci-hub.cc/10.3847/1538-4357/aa774a

Low radio frequency solar observations using the Murchison Widefield Array have recently revealed the presence of numerous weak, short-lived and narrow-band emission features, even during moderately quiet solar conditions. These non-thermal features occur at rates of many thousands per hour in the 30.72 MHz observing bandwidth, and hence, necessarily require an automated approach for their detection and characterization. Here, we employ continuous wavelet transform using a mother Ricker wavelet for feature detection from the dynamic spectrum. We present the first statistical analysis of the properties of these features. In particular, we examine distributions of their peak flux densities, spectral spans, temporal spans and peak frequencies. We find these small-scale features to be amongst the weakest bursts reported in literature. The distribution of their peak flux densities follows a power law with an index of -2.23 in the 101.10−102.19 SFU range, implying that they can provide an energetically significant contribution to coronal and chromospheric heating. These features typically last for 1-2 seconds and possess bandwidths of about 4-5 MHz. Their occurrence rate remains fairly flat in the 140-210 MHz frequency range. At the time resolution of the data, they appear as stationary bursts, exhibiting no perceptible frequency drift. We observe a strong tendency for these features to cluster together in the dynamic spectrum. These features also appear to ride on a broadband background continuum, hinting at the likelihood of them being weak type-I bursts. **2014 August 31**

CESRA highlight #1473, Aug 2017 http://www.astro.gla.ac.uk/users/eduard/cesra/?p=1473

Investigation on Radio-Quiet and Radio-Loud Fast CMEs and Their Associated Flares During Solar Cycles 23 and 24

K. **Suresh**, A. Shanmugaraju

Solar Phys. Volume 290, Issue 3, pp 875-889 **2015**

We present the results of a detailed analysis on the differences between radio-loud (RL) and radio-quiet (RQ) fast coronal mass ejections (CMEs) (V≥900 km s−1) observed during the period 1996 – 2012. The analysis consists of three different steps in which we examined the properties of (i) RL and RQ CMEs, (ii) accelerating (class-A) and decelerating (class-D) CMEs among RL and RQ CMEs, and (iii) associated flares. The last two steps and events from a longer period are the extensions of the earlier work on RL and RQ CMEs that mainly aimed to determine the reason for the radio-quietness of some fast CMEs. During this period, we found that 38 % of fast CMEs are RL and 62 % of fast CMEs are RQ. Moreover, fewer RQ CMEs occur around the disc centre. The average speeds of RL and RQ CMEs are 1358 km s−1 and 1092 km s−1. Around 10 % of the RQ events are halo CMEs, but ≈ 66 % of RL events are halo CMEs. The mean acceleration or deceleration value of RL-CMEs is slightly greater than that of RQ-CMEs. When we divide these events based on their acceleration behaviour into class A and class D, there are no considerable differences between classes A and D of RL-CMEs or between classes A and D of RQ CMEs, except for their initial acceleration values. But there are significant differences among their associated flare properties. According to our study here, the RQ CMEs are less energetic than RL CMEs, and they are not associated with flares as strong as those associated with RL CMEs. This confirms the previous results that RQ CMEs do not often exceed the critical Alfvén speed of 1000 km s−1 in the outer corona that is needed to produce type II radio bursts.

Coronal Shocks Associated with Impulsive and Decaying Phases of Solar Flares

K. **Suresh** · S. Umapathy · A. Shanmugaraju · B. Vršnak

Solar Phys (**2010**) 264: 353–364; **File**
We have analyzed a set of 147 metric Type II radio bursts observed by Culgoora radio spectrograph from November 1997 to December 2006. These events were divided into two sets: The first subset contains Type II events that started during the impulsive phase of the associated solar flares and the second subset contains those starting during the decaying phase of flares. Our main aim is to differentiate the metric Type IIs, flares and coronal mass ejections (CMEs) of these two subsets. It is found that while Type II burst characteristics of both subsets are very similar, there are significant differences between flare and CME properties for these two subsets. Considering all analyzed relationships between the characteristics of Type IIs, flares and CMEs in these two Type II subsets, we conclude that most of the coronal shocks causing metric Type II bursts are driven by CMEs, but that a fraction of events are probably ignited by solar flares.

PHYSICAL CONDITIONS OF CORONAL PLASMA AT THE TRANSIT OF A SHOCK DRIVEN BY A CORONAL MASS EJECTION
R. **Susino**, A. Bemporad, and S. Mancuso
2015 ApJ 812 119
We report here on the determination of plasma physical parameters across a shock driven by a coronal mass ejection using white light (WL) coronagraphic images and radio dynamic spectra (RDS). The event analyzed here is the spectacular eruption that occurred on **2011 June 7**, a fast CME followed by the ejection of columns of chromospheric plasma, part of them falling back to the solar surface, associated with a M2.5 flare and a type-II radio burst. Images acquired by the Solar and Heliospheric Observatory/LASCO coronagraphs (C2 and C3) were employed to track the CME-driven shock in the corona between 2–12 R⊙ in an angular interval of about 110fl. In this interval we derived two-dimensional (2D) maps of electron density, shock velocity, and shock compression ratio, and we measured the shock inclination angle with respect to the radial direction. Under plausible assumptions, these quantities were used to infer 2D maps of shock Mach number MA and strength of coronal magnetic fields at the shock's heights. We found that in the early phases (2–4 R⊙) the whole shock surface is super-Alfvénic, while later on (i.e., higher up) it becomes super-Alfvénic only at the nose. This is in agreement with the location for the source of the observed type-II burst, as inferred from RDS combined with the shock kinematic and coronal densities derived from WL. For the first time, a coronal shock is used to derive a 2D map of the coronal magnetic field strength over intervals of 10 R⊙ altitude and ~110fl latitude.

Bursts of Type III and Type V.
Suzuki, S., and G. A. Dulk.
Solar radiophysics: Studies of emission from the sun at metre wavelengths, McLean, D. J. and Labrum, N. R. eds., 289–332, **1985**.

Siberian Radioheliograph: sunspot oscillations in 3–6 GHz band [Microwave response to sunspot oscillations]
Robert **Sych**, Alexander Altyntsev
MNRAS Volume 519, Issue 3, March **2023**, Pages 4397–4407,
https://doi.org/10.1093/mnras/stac3817
https://arxiv.org/pdf/2210.02044.pdf
We present the first observations of spatially resolved oscillation sources obtained with the Siberian Radioheliograph (SRH) at 3-6 GHz. We have found significant flux oscillations with periods of about 3, 5 and 13 minutes emitted from AR12833. The 3-minute periodicity dominates at higher frequencies. It was found that the apparent level of oscillations depends on the active region location on the disc, and scales down towards the limbs. The oscillations were studied in detail during one hour interval on **June 19, 2021**. We found that sources of 3-min oscillations were located above the umbra and their emission is extraordinary polarized. The 5 and 13-min periods were manifested in emission at lower frequencies, down to 2.8 GHz. Sources with 5-min periodicity were located near the umbra-penumbra boundary and in the pore region. Positions of sources with 13-min oscillations were different at 3.1 GHz and 4.7 GHz. We found consistency between spatial location of the oscillation sources in radio and UV in 171A and 304A. There is significant correlation of signals in two ranges. Time delays between microwave oscillations increase as the frequency decreases, which can be explained by upward propagation of periodic disturbances. The localization of oscillation sources is probably related to magnetic structures with different wave cutoff frequencies at different heights. The obtained results show that SRH can provide the spatial resolved observation of the oscillations in the intensity and polarization channels in 3-6 GHz band.

MHD waves in sunspots **Review**
Robert **Sych**

Chapter in AGU Monograph **2015**
http://arxiv.org/pdf/1509.06466v1.pdf
The review addresses the spatial frequency morphology of sources of sunspot oscillations and waves, including their localization, size, oscillation periods, height localization with the mechanism of cut-off frequency that forms the observed emission variability. Dynamic of sunspot wave processes, provides the information about the structure of wave fronts and their time variations, investigates the oscillation frequency transformation depending on the wave energy is shown. The initializing solar flares caused by trigger agents like magnetoacoustic waves, accelerated particle beams, and shocks are discussed. Special attention is paid to the relation between the flare reconnection periodic initialization and the dynamics of sunspot slow magnetoacoustic waves. A short review of theoretical models of sunspot oscillations is provided.

Sunspot waves and flare energy release

R. **Sych**, M. Karlický, A. Altyntsev, J. Dudík, L. Kashapova
A&A, 577, A43 **2014**
http://arxiv.org/pdf/1409.2947v1.pdf
We address a possibility of the flare process initiation and further maintenance of its energy release due to a transformation of sunspot longitudinal waves into transverse magnetic loop oscillations with initiation of reconnection. This leads to heating maintaining after the energy release peak and formation of a flat stage on the X-ray profile. We applied the time-distance plots and pixel wavelet filtration (PWF) methods to obtain spatio-temporal distribution of wave power variations in SDO/AIA data. To find magnetic waveguides, we used magnetic field extrapolation of SDO/HMI magnetograms. The propagation velocity of wave fronts was measured from their spatial locations at specific times. In correlation curves of the 17 GHz (NoRH) radio emission we found a monotonous energy amplification of 3-min waves in the sunspot umbra before the **2012 June 7** flare. This dynamics agrees with an increase in the wave-train length in coronal loops (SDO/AIA, 171 {\AA}) reaching the maximum 30 minutes prior to the flare onset. A peculiarity of this flare time profile in soft X-rays (RHESSI, 3-25 keV) is maintaining the constant level of the flare emission for 10 minutes after the short impulse phase, which indicates at the energy release continuation. Throughout this time, we found 30-sec period transverse oscillations of the flare loop in the radio-frequency range (NoRH, 17 GHz). This periodicity is apparently related to the transformation of propagating longitudinal 3-min waves from the sunspot into the loop transverse oscillations. The magnetic field extrapolation showed the existence of the magnetic waveguide (loop) connecting the sunspot with the energy release region. A flare loop heating can be caused by the interaction (reconnections) of this transversally oscillating waveguide with the underlying twisted loops.

Frequency drifts of 3-min oscillations in microwave and EUV emission above sunspots

R. **Sych**1,2, T. V. Zaqarashvili3,4, V. M. Nakariakov5,6, S. A. Anfinogentov2, K. Shibasaki7 and Y. Yan1
A&A 539, A23 (**2012**)
Aims. We analysed 3-min oscillations of microwave and extreme ultraviolet (EUV) emission generated at different heights of a sunspot atmosphere, studied the amplitude and frequency modulation of the oscillations, and its relationship with the variation of the spatial structure of the oscillations.
Methods. High-resolution data obtained with the Nobeyama Radioheliograph, TRACE and SDO/AIA were analysed with pixelised wavelet filtering (PWF) and wavelet skeleton techniques.
Results. Three-minute oscillations in sunspots appear in the form of recurring trains of 8–20 min duration (13 min in average). The typical interval between the trains is 30–50 min. The oscillation trains are transient in frequency and power. The relative amplitude of 3-min oscillations was about 3–8% and sometimes reached 17%. Recurring frequency drifts of 3-min oscillations were detected during the development of individual trains, with the period varying in the range 90–240 s. A wavelet analysis showed that there are three types of oscillation trains: with positive drifts (to high frequencies), negative drifts, and without a drift. Negative drifts, i.e., when the 3-min oscillation period gradually increases, were found to occur more often. The start and end of the drifts coincides with the start time and end of the train. Sometimes two drifts co-exist, i.e. during the end of the previous drift, a new drift appears near 160 s, when the frequency is in the low-frequency part of the 3-min spectrum, near 200 s. This behaviour is seen at all levels of the sunspot atmosphere. The speed of the drift is 4–5 mHz/h in the photosphere, 5–8 mHz/h in the chromosphere, and 11–13 mHz/h in the corona. There were also low-frequency peaks in the spectrum, corresponding to the periods of 10–20 min, and 30–60 min. The comparative study of the spatial structure of 3-min oscillations in microwave and EUV shows the appearance of new sources of the sunspot oscillations during the development of the trains.
Conclusions. These structures can be interpreted as waveguides that channel upward propagating waves, which in turn are responsible for the 3-min oscillations. A possible explanation of the observed properties are two simultaneously operating factors: dispersive evolution of the upward propagating wave pulses and the non-uniformity of the oscillation power distribution over the sunspot umbra with different wave sources that correspond to different magnetic flux tubes with different physical conditions and line-of-sight angles.

Relationship between wave processes in sunspots and quasi-periodic pulsations in active region flares

R. **Sych**, V.M. Nakariakov, M. Karlicky, and S. Anfinogentov
E-print, Aug **2009**, A&A
A phenomenological relationship between oscillations in a sunspot and quasi-periodic pulsations in flaring energy releases at an active region above the sunspot, is established. The analysis of the microwave emission recorded by the Nobeyama Radioheliograph at 17 GHz shows a gradual increase in the power of the 3-min oscillation train in the sunspot associated with AR 10756 before flares in this active region. The flaring light curves are found to be bursty with a period of 3 min. Our analysis of the spatial distribution of the 3-min oscillation power implies that the oscillations follow from sunspots along coronal loops towards the flaring site. It is proposed that quasi-periodic pulsations in the flaring energy releases can be triggered by 3-min slow magnetoacoustic waves leaking from sunspots. **28 Apr, 1 May 2005**

OBSERVATIONAL EVIDENCE OF PARTICLE ACCELERATION ASSOCIATED WITH PLASMOID MOTIONS

Shinsuke **Takasao**1, Ayumi Asai2,3, Hiroaki Isobe3,4, and Kazunari Shibata
2016 ApJ 828 103
https://arxiv.org/pdf/1611.00108v1.pdf
We report a strong association between the particle acceleration and plasma motions found in the **2010 August 18** solar flare. The plasma motions are tracked in the extreme ultraviolet (EUV) images taken by the Atmospheric Imaging Assembly (AIA) on board the Solar Dynamics Observatory and the Extreme UltraViolet Imager (EUVI) on the Solar Terrestrial Relations Observatory spacecraft Ahead, and the signature of particle acceleration was investigated by using Nobeyama Radioheliograph data. In our previous paper, we reported that in EUV images many plasma blobs appeared in the current sheet above the flare arcade. They were ejected bidirectionally along the current sheet, and the blobs that were ejected sunward collided with the flare arcade. Some of them collided or merged with each other before they were ejected from the current sheet. We discovered impulsive radio bursts associated with such plasma motions (ejection, coalescence, and collision with the post flare loops). The radio bursts are considered to be the gyrosynchrotron radiation by nonthermal high energy electrons. In addition, the stereoscopic observation by AIA and EUVI suggests that plasma blobs had a three-dimensionally elongated structure. We consider that the plasma blobs were three-dimensional plasmoids (i.e., flux ropes) moving in a current sheet. We believe that our observation provides clear evidence of particle acceleration associated with the plasmoid motions. We discuss possible acceleration mechanisms on the basis of our results.

The physics of solar spectral imaging observations in dm-cm wavelengths and the application on space weather **Review**

Baolin **Tan**, Yihua Yan, Jing Huang, Yin Zhang, Chengming Tan, Xiaoshuai Zhu
Advance in Space Research, 72:5563-5576 **2023**
https://arxiv.org/ftp/arxiv/papers/2311/2311.14360.pdf
Recently, several new solar radio telescopes have been put into operation and provided spectral-imaging observations with much higher resolutions in decimeter (dm) and centimeter (cm) wavelengths. These telescopes include the Mingantu Spectral Radioheliograph (MUSER, at frequencies of 0.4 - 15 GHz), the Expanded Owens Valley Solar Array (EOVSA, at frequencies of 1 - 18 GHz), and the Siberian Radio Heliograph (SRH, at frequencies of 3 - 24 GHz). These observations offer unprecedented opportunities to study solar physics and space weather, especially to diagnose the coronal magnetic fields, reveal the basic nature of solar eruptions and the related non-thermal energy release, particle accelerations and propagation, and the related emission mechanisms. These results might be the important input to the space weather modeling for predicting the occurrence of disastrous powerful space weather events. In order to provide meaningful reference for other solar physicists and space weather researchers, this paper mainly focus on discussing the potential scientific problems of solar radio spectral-imaging observations in dm-cm wavelengths and its possible applications in the field of space weather. These results will provide a helpful reference for colleagues to make full use of the latest and future observation data obtained from the above solar radio telescopes. **2004 December 1. 2005–1-15, 2006 December 13., 2011 February 24, 5 Nov 2011, 2015 December 17., 5 May 2017, 10 September 2017**
CESRA #3715 **2024** **https://www.astro.gla.ac.uk/users/eduard/cesra/?p=3715**

Diagnostic functions of solar coronal magnetic fields from radio observations **Review**

Baolin **Tan**
Research in Astronomy and Astrophysics **2022**

https://arxiv.org/pdf/2205.00136.pdf
In solar physics, it is a big challenge to measure the magnetic fields directly from observations in the upper solar atmosphere, including the chromosphere and corona. Radio observations are regarded as the most feasible approach to diagnose the magnetic field in solar chromosphere and corona. However, because of the complexity and diversity of the emission mechanisms, the previous studies have only presented the implicit diagnostic functions of the magnetic field for specific mechanism from solar radio observations. This work collected and sorted out all methods for diagnosing coronal magnetic field from solar radio observations, which are expressed as a set of explicit diagnostic functions. In particular, this work supplemented some important diagnostic methods missed in other reviews. This set of diagnostic functions can completely cover all regions of the solar chromosphere and corona, including the quiet region, active region and flaring source regions. At the same time, it also includes incoherent radiation such as bremsstrahlung emission of thermal plasma above the quiet region, cyclotron and gyro-synchrotron emissions of magnetized hot plasma and mildly relativistic nonthermal electrons above the active regions, as well as coherently plasma emission around flaring source regions. Using this set of diagnostic functions and the related broadband spectral solar radio imaging observations, we can derive the magnetic fields of almost all regions in the solar atmosphere,which may help us to make full use of the spectral imaging observations of the new generation solar radio telescopes (such as MUSER, EVOSA and the future FASR, etc.) to study the solar activities, and provide a reliable basis for the prediction of disastrous space weather events.

Energy and spectral analysis of confined solar flares from radio and X-ray observations

Chengming **Tan**, Karl-Ludwig Klein, Yihua Yan, Satoshi Masuda, Baolin Tan, Jing Huang, Guowu Yuan
Research in Astronomy and Astrophysics **2021**
https://arxiv.org/pdf/2108.02601.pdf
The energy and spectral shape of radio bursts may help us understand the generation mechanism of solar eruptions, including solar flares, CMEs, eruptive filaments, and various scales of jets. The different kinds of flares may have different characteristics of energy and spectral distribution. In this work, we selected 10 mostly confined flare events during **October 2014** to investigate their overall spectral behavior and the energy emitted in microwaves by using radio observations from microwaves to interplanetary radio waves, and X-ray observations of GOES, RHESSI, and Fermi/GBM. We found that: All the confined flare events were associated with a microwave continuum burst extending to frequencies of 9.4 - 15.4 GHz, and the peak frequencies of all confined flare events are higher than 4.995 GHz and lower than or equal to 17 GHz. The median value is around 9 GHz. The microwave burst energy (or fluence) as well as the peak frequency are found to provide useful criteria to estimate the power of solar flares. The observations imply that the magnetic field in confined flares tends to be stronger than that in 412 flares studied by Nita et al. 2004. All 10 events studied did not produce detectable hard X-rays with energies above 300 keV indicating the lack of efficient acceleration of electrons to high energies in the confined flares. **18, 22, 24, 27, 28, 29 Oct 2014**

Solar Fast Drifting Radio Bursts in an X1.3 Flare on 2014 April 25

Baolin **Tan**, Nai-hwa Chen, Ya-hui Yang, Chengming Tan, Satoshi Masuda, Xingyao Chen, H. Misawa
ApJ **885** 90 **2019**
https://arxiv.org/pdf/1909.13209.pdf
https://iopscience.iop.org/article/10.3847/1538-4357/ab4718/pdf
One of the most important products of solar flares are nonthermal energetic particles which may carry up to 50\% energy releasing in the flaring processes. In radio observations, nonthermal particles generally manifest as spectral fine structures with fast frequency drifting rates, named as solar fast drifting radio bursts (FDRBs). This work demonstrated three types of FDRBs, including type III pair bursts, narrow band stochastic spike bursts following the type III bursts and spike-like bursts superimposed on type II burst in an X1.3 flare on **2014 April 25**. We find that although all of them have fast frequency drifting rates, but they are intrinsically different from each other in frequency bandwidth, drifting rate and the statistical distributions. We suggest that they are possibly generated from different accelerating mechanisms. The type III pair bursts may be triggered by high-energy electron beams accelerated by the flaring magnetic reconnection, spike bursts are produced by the energetic electrons accelerated by a termination shock wave triggered by the fast reconnecting plasma outflows impacting on the flaring looptop, and spike-like bursts are possibly generated by the nonthermal electrons accelerated by moving magnetic reconnection triggered by the interaction between CME and the background magnetized plasma. These results may help us to understand the generation mechanism of nonthermal particles and energy release in solar flares.

Influence of Magnetic Reconnection-accelerated Electrons in Solar Wind on Onset Time Analysis of Impulsive Electron Events

Lun C. **Tan**
2019 ApJ 882 143
https://doi.org/10.3847/1538-4357/ab3580
Observations have shown that type III radio bursts (RBs) are generated by 1–10 keV flare electrons ejected from the exhaust of a magnetic reconnection site in a coronal (loop-top) source region. Surprisingly, it is generally accepted

without question that the injection of low-energy electrons occurs significantly earlier than the onset of the type III RBs. Therefore, it is necessary to re-examine the timing of flare electrons. For this, we observed a "normal" event in which the injection of low-energy electrons coincided with the injection of high-energy electrons, and "abnormal" events in which the low-energy electrons seemed to arrive earlier. A high background of low-energy particles lacking any evidence of velocity dispersion characterizes an abnormal event. Due to the existence of a reconnection acceleration that results in similar enhancements at magnetic islands confined by the heliospheric current sheet (HCS), HCS observations are used to establish the empirical criteria for the reconnection acceleration in impulsive electron events. Observations show that 2–8 keV electrons accelerated by magnetic reconnection can change the pitch-angle distribution of background electrons for a time interval of approximately 0.5 hr before or after the time of current-sheet crossing. Therefore, this reconnection acceleration in the solar wind can influence the onset time analysis of electrons by emulating the effect of the earlier arrival of flare electrons. In addition, a technique is developed for estimating the phase velocity of whistler waves in the ion dissipation range, which may significantly affect the pitch-angle scattering analysis of low-energy electrons.

FINE STRUCTURE EVENTS IN MICROWAVE EMISSION DURING SOLAR MINIMUM
Chengming **Tan**, Baolin Tan, Yihua Yan, Wei Wang, Linjie Chen, Fei Liu, Yujiang Dou
Solar-Terrestrial Physics. **2019**. Vol. 5. Iss. 2. P. 3–8.
Solnechno-zemnaya fizika, 2019. Vol. 5. Iss. 2. P. 4–10
https://naukaru.ru/en/storage/view/36892
The solar minimum is a period with a relatively smaller number of sunspots and solar eruptions, and has been less studied before. Since the radio signal rapidly responds to the change of solar plasma and magnetic field, we perform a comprehensive analysis of high resolution spectrum data from SBRS and MUSER: 1) a search for solar radio bursts of different kinds in recent solar minima (2007–2009 and 2016–2018); 2) an analysis of several typical radio burst events, negative and positive drifting bursts, for example the **November 22, 2015** and **August 29, 2016** events; superfine spectral structure events with mini-flares and even without sunspots, for example the **March 28, 2008** and **July 04, 2017** events. These results show that there were many radio bursts with a fine structure during solar minima. These events occurred not only in powerful flares, but also in faint flares (class C and B by GOES) or even without flares, but in regions related to weak brightenings or ejecta. We assume that the weak solar radio bursts observed by telescopes with high sensitivity and low interference will help us to understand the basic physical characteristics of small-scale solar eruptions.

Scaling-laws of Radio Spike Bursts and Their Constraints on New Solar Radio Telescopes
Tan, Bao-lin, Cheng, Jun, Tan Cheng-ming, Kou, Hong-xiang,
Chinese Astronomy and Astrophysics (ChA&A) , **2019**, 43, 59-74, **File**
sci-hub.se/10.1016/j.chinastron.2019.02.005
Radio observation is one of important methods in solar physics and space science. Sometimes, it is almost the sole approach to observe the physical processes such as the acceleration, emission, and propagation of non-thermal energetic particles, etc. So far, more than 100 solar radio telescopes have been built in the world, including solar radiometers, dynamic spectrometers, and radioheliographs. Some of them have been closed after the fulfillment of their primary scientific objectives, or for their malfunctions, and thus replaced by other advanced instruments. At the same time, based on some new technologies and scientific ideas, various kinds of new and much more complicated solar radio telescopes are being constructed by solar radio astronomers and space scientists, such as the American E-OVSA and the solar radio observing system under the framework of Chinese Meridian Project II, etc. When we plan to develop a new solar radio telescope, it is crucial to design the most suitable technical parameters, e.g., the observing frequency range and bandwidth, temporal resolution, frequency resolution, spatial resolution, polarization degree, and dynamic range. Then, how do we select a rational set of these parameters? The long-term observation and study revealed that a large strong solar radio burst is frequently composed of a series of small bursts with different time scales. Among them, the radio spike burst is the smallest one with the shortest lifetime, the narrowest bandwidth, and the smallest source region. Solar radio spikes are considered to be related to a single magnetic energy release process, and can be regarded as an elementary burst in solar flares. It is a basic requirement for the new solar radio telescope to observe and discriminate these solar radio spike bursts, even though the temporal and spatial scales of radio spike bursts actually vary with the observing frequency. This paper presents the scaling laws of the lifetime and bandwidth of solar radio spike bursts with respect to the observing frequency, which provide some constraints for the new solar radio telescopes, and help us to select the rational telescope parameters. Besides, we propose a spectrum-image combination mode as the best observation mode for the next-generation solar radio telescopes with high temporal, spectral, and spatial resolutions, which may have an important significance for revealing the physical essence of the various non-thermal processes in violent solar eruptions. **2011-08-09**
Table 1 The parameters of the main existing solar broadband dynamic spectrometers
Table 2 The parameters of the main existing solar radioheliographs

Diagnosing the Source Region of a Solar Burst on 26 September 2011 by Microwave Type III Pairs

Baolin **Tan**, Marian Karlicky, Hana Meszarosova, Larisa Kashapova, Jing Huang, Yan Yan, Eduard P. Kontar

Solar Phys. Volume 291, Issue 8, pp 2407–2418 **2016**

http://arxiv.org/pdf/1606.05410v1.pdf

This work reports a peculiar and interesting train of microwave type III pair bursts in the impulsive rising phase of a solar flare on **2011 September 26**. The observations include radio spectrometers at frequency of 0.80 - 2.00 GHz, hard X-ray (RHESSI and FERMI), EUV images of SWAP/PROBA-2 and magnetogram of HMI/SDO. By using a recently developed method (Tan et al. 2016a), we diagnosed the plasma density, temperature, plasma beta, magnetic field near the source region, the energy of energetic electrons and the distance between the acceleration region and the emission start sites of type III bursts. From the diagnostics, we find that: (1) The plasma density, temperature, magnetic field, and the distance between the acceleration region and the emission start sites almost have no obvious variations during the period of type III pair trains, while the energy of electrons has an obvious peak value which is consistent to the hard X-ray emission. (2) The plasma beta is much higher than an unity showing a highly dynamic process near the emission start site of type III bursts. (3) Although the reversed-slope type III branches drift slower at one order of magnitude than that of the normal type III branches, the related downgoing and upgoing electrons still could have same order of magnitude of energy. These facts indicate that both of the upgoing and downgoing electrons are possibly accelerated by similar mechanism and in a small source region. This diagnostics can help us to understand the microphysics in the source region of solar bursts.

CESRA highlights #1138 **2016** http://www.astro.gla.ac.uk/users/eduard/cesra/?p=1138

Microwave Type III Pair Bursts in Solar Flares

Baolin **Tan**, Hana Meszarosova, Marian Karlicky, Guangli Huang, Chengming Tan

ApJ 819 42 **2016**

http://arxiv.org/pdf/1601.05312v1.pdf

Solar microwave type III pair burst is composed of normal and reverse-sloped (RS) burst branches with oppositely fast frequency drifts. It is the most sensitive signature of the primary energy release and electron accelerations in flares. This work reported 11 microwave type III pair events in 9 flares observed by radio spectrometers in China and the Czech Republic at frequency of 0.80 - 7.60 GHz during 1994 - 2014. These type III pairs occurred in flare impulsive and postflare phases with separate frequency in range of 1.08 - 3.42 GHz and frequency gap 10 - 1700 MHz. The frequency drift increases with the separate frequency (f_{x}), the lifetime of each burst is anti-correlated to f_{x}, while the frequency gap is independent to f_{x}. In most events, the normal branches are drifting obviously faster than the RS branches. The type III pairs occurring in flare impulsive phase have lower separate frequency, longer lifetime, wider frequency gap, and slower frequency drift than that occurring in postflare phase. And the latter always has strong circular polarization. Further analysis indicates that near the flare energy-release sites the plasma density is about 10^{10} - 10^{11},cm^{-3} and temperature higher than 10^{7} K . These results provide new constraints to the acceleration mechanism in solar flares. **1994-01-05, 1998-04-15, 2006 December 13, 2011 September 26, 2012-02-12, 2012-07-02, 2013-04-11, 2014 April 04. 2014-08-01**

Diagnose Physical Conditions Near the Flare Energy-release Sites from Observations of Solar Microwave Type III Bursts

Baolin **Tan**, Marian Karlicky, Hana Meszarosova, Guangli Huang

Research in Astron. & Astrophys. (RAA), **201**5

http://arxiv.org/pdf/1511.08863v1.pdf

In the physics of solar flares, it is crucial to diagnose the physical conditions near the flare energy-release sites. However, so far it is unclear how do diagnose these physical conditions. Solar microwave type III burst is believed to be a sensitive signature of the primary energy release and electron accelerations in solar flares. This work takes into account the effect of magnetic field on the plasma density and developed s set of formulas which can be used to estimate the plasma density, temperature, magnetic field near the magnetic reconnection site and particle acceleration region, and the velocity and energy of electron beams. We applied these formulas to three groups of microwave type III pairs in a X-class flare, and obtained some reasonable and interesting results. This method can be applied to other microwave type III bursts to diagnose the physical conditions of source regions, and provide some basic information to understand the intrinsic nature and fundamental processes occurring near the flare energy-release sites. **13 Dec 2006**

Study of Calibration of Solar Radio Spectrometers and the Quiet-Sun Radio Emission

Chengming **Tan**1, Yihua Yan1, Baolin Tan1, Qijun Fu1, Yuying Liu1, and Guirong Xu

2015 ApJ 808 61
http://arxiv.org/pdf/1507.04866v1.pdf
https://www.researchgate.net/publication/280221076_Study_of_Calibration_of_Solar_Radio_Spectrometers_and_the_quiet-Sun_Radio_Emission
This work presents a systematic investigation of the influence of weather conditions on the calibration errors by using Gaussian fitness, least chi-square linear fitness, and wavelet transform to analyze the calibration coefficients from observations of the Chinese Solar Broadband Radio Spectrometers (at frequency bands of 1.0–2.0 GHz, 2.6–3.8 GHz, and 5.2–7.6 GHz) during 1997–2007. We found that calibration coefficients are influenced by the local air temperature. Considering the temperature correction, the calibration error will reduce by about 10%–20% at 2800 MHz. Based on the above investigation and the calibration corrections, we further study the radio emission of the quiet Sun by using an appropriate hybrid model of the quiet-Sun atmosphere. The results indicate that the numerical flux of the hybrid model is much closer to the observation flux than that of other ones.

Correlation of Electron Path Lengths Observed in the Highly Wound Outer Region of Magnetic Clouds with the Slab Fraction of Magnetic Turbulence in the Dissipation Range

Lun C. **Tan**1,2, Donald V. Reames3, Chee K. Ng4, Xi Shao1,2, and Linghua Wang
2014 ApJ 786 122.
Three magnetic cloud events, in which solar impulsive electron events occurred in their outer region, are employed to investigate the difference of path lengths L 0eIII traveled by non-relativistic electrons from their release site near the Sun to the observer at 1 AU, where L 0eIII = v l × (t l – t III), v l and t l being the velocity and arrival time of electrons in the lowest energy channel (~27 keV) of the Wind/3DP/SST sensor, respectively, and t III being the onset time of type III radio bursts. The deduced L 0eIII value ranges from 1.3 to 3.3 AU. Since a negligible interplanetary scattering level can be seen in both L 0eIII > 3 AU and ~1.2 AU events, the difference in L 0eIII could be linked to the turbulence geometry (slab or two-dimensional) in the solar wind. By using the Wind/MFI magnetic field data with a time resolution of 92 ms, we examine the turbulence geometry in the dissipation range. In our examination, ~6 minutes of sampled subintervals are used in order to improve time resolution. We have found that, in the transverse turbulence, the observed slab fraction is increased with an increasing L 0eIII value, reaching ~100% in the L 0eIII > 3 AU event. Our observation implies that when only the slab spectral component exists, magnetic flux tubes (magnetic surfaces) are closed and regular for a very long distance along the transport route of particles.

A Very Small and Super Strong Zebra Pattern Burst at the Beginning of a Solar Flare

Baolin **Tan**, Chengming Tan, Yin Zhang, Jing Huang, Hana Meszarosova, Marian Karlicky, Yihua Yan
ApJ, 790 151, **2014**
http://arxiv.org/pdf/1406.5209v1.pdf
Microwave emission with spectral zebra pattern structures (ZPs) is observed frequently in solar flares and the Crab pulsar. The previous observations show that ZP is only a structure overlapped on the underlying broadband continuum with slight increments and decrements. This work reports an extremely unusual strong ZP burst occurring just at the beginning of a solar flare observed simultaneously by two radio telescopes located in China and Czech Republic and by the extreme ultraviolet (EUV) telescope on board NASA's satellite Solar Dynamics Observatory on **2013 April 11**. It is a very short and super strong explosion whose intensity exceeds several times that of the underlying flaring broadband continuum emission, lasting for just 18 s. EUV images show that the flare starts from several small flare bursting points (FBPs). There is a sudden EUV flash with extra enhancement in one of these FBPs during the ZP burst. Analysis indicates that the ZP burst accompanying EUV flash is an unusual explosion revealing a strong coherent process with rapid particle acceleration, violent energy release, and fast plasma heating simultaneously in a small region with short duration just at the beginning of the flare.

Statistics and Classification of the Microwave Zebra Patterns Associated with Solar Flares

Baolin **Tan**1, Chengming Tan1, Yin Zhang1, H. Mészárosová2, and M. Karlický
2014 ApJ 780 129.
http://arxiv.org/pdf/1311.5305v1.pdf
The microwave zebra pattern (ZP) is the most interesting, intriguing, and complex spectral structure frequently observed in solar flares. A comprehensive statistical study will certainly help us to understand the formation mechanism, which is not exactly clear now. This work presents a comprehensive statistical analysis of a big sample with 202 ZP events collected from observations at the Chinese Solar Broadband Radio Spectrometer at Huairou and the Ondřejov Radiospectrograph in the Czech Republic at frequencies of 1.00-7.60 GHz from 2000 to 2013. After investigating the parameter properties of ZPs, such as the occurrence in flare phase, frequency range, polarization degree, duration, etc., we find that the variation of zebra stripe frequency separation with respect to frequency is the best indicator for a physical classification of ZPs. Microwave ZPs can be classified into three types: equidistant ZPs, variable-distant ZPs, and growing-distant ZPs, possibly corresponding to mechanisms of the Bernstein wave model,

whistler wave model, and double plasma resonance model, respectively. This statistical classification may help us to clarify the controversies between the existing various theoretical models and understand the physical processes in the source regions.

Table 1. List of solar flares with microwave ZPs during 2000 - 2013

SMALL-SCALE MICROWAVE BURSTS IN LONG-DURATION SOLAR FLARES

Baolin **Tan**

2013 ApJ 773 165

Solar small-scale microwave bursts (SMBs), including microwave dot, spike, and narrow-band type III bursts, are characterized by very short timescales, narrow frequency bandwidth, and very high brightness temperatures. Based on observations of the Chinese Solar Broadband Radio Spectrometer at Huairou with superhigh cadence and frequency resolution, this work presents an intensive investigation of SMBs in several flares that occurred in active region NOAA 10720 during **2005 January 14-21**. Especially for long-duration flares, the SMBs occurred not only in the early rising and impulsive phase, but also in the flare decay phase and even after the end of the flare. These SMBs are strong bursts with inferred brightness temperatures of at least 8.18 × 1011-1.92 × 1013 K, very short lifetimes of 5-18 ms, relative frequency bandwidths of 0.7%-3.5%, and superhigh frequency drifting rates. Together with their obviously different polarizations from background emission (the quiet Sun, and the underlying flaring broadband continuum), such SMBs should be individual, independent strong coherent bursts related to some non-thermal energy release and the production of energetic particles in a small-scale source region. These facts show the existence of small-scale strong non-thermal energy releasing activities after the flare maxima, which is meaningful for predicting space weather. Physical analysis indicates that a plasma mechanism may be the most favorable candidate for the formation of SMBs. From the plasma mechanism, the velocities and kinetic energy of fast electrons can be deduced and the region of electron acceleration can also be tracked.

MICROWAVE QUASI-PERIODIC PULSATION WITH MILLISECOND BURSTS IN A SOLAR FLARE ON 2011 AUGUST 9

Baolin **Tan** and Chengming Tan

2012 ApJ 749 28

A peculiar microwave quasi-periodic pulsation (QPP) accompanying a hard X-ray (HXR) QPP of about 20 s duration occurred just before the maximum of an X6.9 solar flare on **2011 August 9**. The most interesting aspect is that the microwave QPP consists of millisecond timescale superfine structures. Each microwave QPP pulse is made up of clusters of millisecond spike bursts or narrowband type III bursts. There are three different frequency drift rates: the global frequency drift rate of the microwave QPP pulse group, the frequency drift rate of the microwave QPP pulse, and the frequency drift rate of individual millisecond spikes or type III bursts. The physical analysis indicates that the energetic electrons accelerating from a large-scale highly dynamic magnetic reconnecting current sheet above the flaring loop propagate downward, impact the flaring plasma loop, and produce HXR bursts. The tearing-mode (TM) oscillations in the current sheet modulate HXR emission and generate HXR QPP; the energetic electrons propagating downward produce Langmuir turbulence and plasma waves, resulting in plasma emission. The modulation of TM oscillation on the plasma emission in the current-carrying plasma loop may generate microwave QPP. The TM instability produces magnetic islands in the loop. Each X-point will be a small reconnection site and will accelerate the ambient electrons. These accelerated electrons impact the ambient plasma and trigger the millisecond spike clusters or the group of type III bursts. Possibly, each millisecond spike burst or type III burst is one of the elementary bursts (EBs). A large number of such EB clusters form an intense flaring microwave burst.

MICROWAVE ZEBRA PATTERN STRUCTURES IN THE X2.2 SOLAR FLARE ON 2011 FEBRUARY 15

Baolin **Tan**1, Yihua Yan1, Chengming Tan1, Robert Sych1,2 and Guannan Gao

2012 ApJ 744 166

A zebra pattern (ZP) structure is the most intriguing fine structure on the dynamic spectrograph of a solar microwave burst. On **2011 February 15**, an X2.2 flare event erupted on the solar disk, which is the first X-class flare since the solar Schwabe cycle 24. It is interesting that there are several microwave ZPs observed by the Chinese Solar Broadband Radio Spectrometer (SBRS/Huairou) at a frequency of 6.40-7.00 GHz (ZP1) and at a frequency of 2.60-2.75 GHz (ZP2) and by the Yunnan Solar Broadband Radio Spectrometer (SBRS/Yunnan) at a frequency of 1.04-1.13 GHz (ZP3). The most important phenomenon is the unusual high-frequency ZP structure (ZP1, up to 7.00 GHz) that occurred in the early rising phase of the flare and the two ZP structures (ZP2, ZP3) with relatively low frequencies that occurred in the

decay phase of the flare. By scrutinizing the current prevalent theoretical models of ZP structure generations and comparing their estimated magnetic field strengths in the corresponding source regions, we suggest that the double plasma resonance model is the most probable one for explaining the formation of microwave ZPs, which may derive the magnetic field strengths at about 230-345 G, 126-147 G, and 23-26 G in the source regions of ZP1, ZP2, and ZP3, respectively.

MICROWAVE QUASI-PERIODIC PULSATIONS IN MULTI-TIMESCALES ASSOCIATED WITH A SOLAR FLARE/CME EVENT

Baolin **Tan**1, Yin Zhang, Chengming Tan, and Yuying Liu

Astrophysical Journal, 723:25–39, **2010**

Microwave observations of quasi-periodic pulsations (QPPs) in multi-timescales at the Solar Broadband Radio Spectrometer in Huairou (SBRS/Huairou) on **2006 December 13** are confirmed to be associated with an X3.4 flare/coronal mass ejection (CME) event. It is most remarkable that the timescales of QPPs are distributed in a broad range from hectoseconds (very long period pulsation, VLP,P >100 s), decaseconds (long period pulsation, LPP, 10 < P < 100 s), a few seconds (short period pulsation, SPP, 1 < P < 10 s), deciseconds (slow very short period pulsation, slow-VSP, 0.1 < P < 1.0 s), to centiseconds (fast very short period pulsation, fast-VSP, P < 0.1 s), and form a broad hierarchy. The statistical distribution of QPPs in logarithmic period–duration space indicates that all the QPPs can be classified into two groups: group I includes VLP, LPP, SPP, and some slow-VSPs distributed approximately around a line; group II includes fast-VSP and most of the slow-VSPs dispersively distributed away from the above line. This feature implies that the generation mechanism of group I is different from group II. Group I is possibly related to some MHD oscillations in magnetized plasma loops in the active region; e.g., VLPs may be generated by standing slow sausage mode coupling, resonating with the underlying photospheric 5 minute oscillation, with the modulation amplified and forming the main framework of the whole flare/CME process; LPPs, SPPs, and some slow-VSPs are most likely to be caused by standing fast modes or LRC-circuit resonance in current-carrying plasma loops. Group II is possibly generated by modulations of resistive tearing-mode oscillations in electric current-carrying flaring loops.

Observable Parameters of Solar Microwave Pulsating Structure and Their Implications for Solar Flare

Baolin **Tan**

E-print, June **2008**; Solar Phys (**2008**) 253: 117–131

From the observations with the Chinese Solar Broadband Radiospectrometer (SBRS/Huairou) in the frequency range of 1.10 - 2.06 GHz and 2.60 - 3.80 GHz during 2004 - 2006, we select 14 flare events which were associated with numerous fast microwave sub-second pulsating structures (period: P<0.5 s). In order to describe these sub-second pulsating structures comprehensively, we defined a set of observable parameters including emission frequency (f_{0}), bandwidth (b_{w}), polarization degree (r), period (P), duration (D), modulation depth (M), quality factor (Q), single pulse frequency drifting rate (R_{spfd}), global frequency drifting rate (R_{gfd}), and symmetrical factor of the pulse profile (S). Then based on a detailed analysis of the spectrograms of the fast pulsations which occurred in one of these flares (an X3.4 flare/CME event occurred on **13 Dec. 2006**), we discuss the possible relations among these observable parameters and their physical implications for the dynamical processes of solar eruptive events, and applied them to interpret the nature of the pulsations in the flare/CME event. Such study of microwave periodic pulsations provide us a useful tool to probe the details of the flare kernels, and understand the physical mechanism of solar eruptive processes.

Statistical study of radio drifting pulsation structures with associated CMEs and other observations

Tan, C.; Yan, Y. H.; Liu, Y. Y.; Fu, Q. J.; Wang, S. J.; Ji, H. R.; Chen, Z. J., Jing, H.R.

E-print, Sept 2007

Advances in Space Research**,** **Volume 41, Issue 6****, 2008**, Pages 969-975

In this work, 52 radio events were found accompanying with DPSs. They were all observed with the Solar Radio Spectrometers (0.625-7.6 GHz) of China during 1998-2004. Combining the radio observations with LASCO-C2, Goes-8 SXR, Ha, EUV and Trace observations, we analyzed all these events.

The Microwave Pulsations and the Tearing modes in the Current-Carrying Flare Loops
Baolin **Tan**, Yihua Yan, Chengming Tan, and Yuying Liu
E-print, August 2007; The Astrophysical Journal, 671:964Y972, **2007** December 10
X3.4 Flare/CME event on **December 13, 2006**

Effect of temperature anisotropy formed by fast electron beams moving in the flare loop on its excited electron-cyclotron maser instability
J. F. **Tang**1,2,⋆, D. J. Wu3, L. Chen3, C. M. Tan2 and J. B. Wang1
A&A, 690, A96 (**2024**)
https://doi.org/10.1051/0004-6361/202348081
https://www.aanda.org/articles/aa/pdf/2024/10/aa48081-23.pdf
Context. The electron-cyclotron maser instability (ECMI) is a significant coherent radio emission mechanism widely utilized in various astrophysical radio phenomena. It is well known that the velocity anisotropic distribution of energetic electrons, which leads to an inverted perpendicular population in the vertical direction with $\partial fb/\partial v\perp > 0$, can provide the free energy necessary for the ECMI.
Aims. The initial velocity distribution of energetic electrons leaving the acceleration region is typically isotropic or beam-like. However, as these energetic electrons travel along the magnetic field as fast electron beams (FEBs) in magnetic plasma, various velocity anisotropic distributions can emerge. In this paper, we examine the impact of temperature anisotropy formed by beam electrons traveling along a flare loop on the ECMI.
Methods. By neglecting the energy loss of energetic electrons as they traverse the corona and invoking the conservation of energy and magnetic moments, we established the relationship between momentum dispersion and the magnetic field. Utilizing the magnetic field model of the flare loop, we calculated the evolution of momentum dispersion and the growth rates of the ECMI as FEBs precipitate along the flare loop.
Results. The results demonstrate that the temperature anisotropy arising as FEBs descend along the flare loop significantly impacts the ECMI. The maximum growth rates of the excited modes exhibit a gradual increase initially and then decline rapidly after reaching a critical height for $\beta 0 = 0.2c$ and $0.15c$. The results also show that the growth rates of the O2 mode are one order of magnitude smaller than those of the O1 and X2 modes. This indicates that the harmonic radiation is X-mode polarized. Notably, the temperature anisotropy of FEBs as they precipitate along the flare loop with different magnetic field models or at different heights has similar effects on the ECMI.

Electron Cyclotron Maser Instability by Evolving Fast Electron Beams in the Flare Loops
Jianfei **Tang**, D Wu, L Chen, L Chen, C Tan, and J Wang
Front. Astron. Space Sci., 11:1404145 **2024**
https://www.frontiersin.org/articles/10.3389/fspas.2024.1404145/ful
https://www.frontiersin.org/articles/10.3389/fspas.2024.1404145/pdf
https://doi.org/10.3389/fspas.2024.1404145
The electron cyclotron maser instability (ECMI) stands as a pivotal coherent radio emission mechanism widely implicated in various astrophysical phenomena. In the context of solar activity, ECMI is primarily instigated by energetic electrons generated during solar eruptions, notably flares. These electrons, upon leaving the acceleration region, traverse the solar atmosphere, forming fast electron beams (FEBs) along magnetic field lines. It is widely accepted that as these FEBs interact with the ambient plasma and magnetic fields, they give rise to radio and hard X-ray emission. Throughout their journey in the plasma, FEBs undergo modifications in their energy spectrum and velocity spatial distribution due to diverse energy loss mechanisms and changes in ambient plasma parameters. In this study, we delve into the impact of the evolving energy spectrum and velocity anisotropic distribution of FEBs on ECMI during their propagation in flare loops. Our findings indicate that if we solely consider the progressively flattened lower energy cutoff behavior as FEBs descend along flare loops, the growth rates of ECMI decrease accordingly. However, when accounting for the evolution of ambient magnetic plasma parameters, the growth rates of ECMI increase as FEBs delve into denser atmosphere. This underscores the significant influence of the energy spectrum and velocity anisotropy distribution evolution of FEBs on ECMI. Our study sheds light on a more comprehensive understanding of the dynamic spectra of solar radio emissions.

Suprathermal Electron Transport and Electron Beam Formation in the Solar Corona

Bofeng **Tang**1,2, Haihong Che1,2, Gary P. Zank1,2, and Vladimir I. Kolobov2,3
2023 ApJ 954 43
https://iopscience.iop.org/article/10.3847/1538-4357/ace7be/pdf
Electron beams that are commonly observed in the corona were discovered to be associated with solar flares. These "coronal" electron beams are found ≥300 Mm above the acceleration region and have velocities ranging from 0.1c up to 0.6c. However, the mechanism for producing these beams remains unclear. In this paper, we use kinetic transport theory to investigate how isotropic suprathermal energetic electrons escaping from the acceleration region of flares are transported upwardly along the magnetic field lines of flares to develop coronal electron beams. We find that magnetic focusing can suppress the diffusion of Coulomb collisions and background turbulence and sharply collimate the suprathermal electron distribution into beams with the observed velocity within the observed distance. A higher bulk velocity is produced if energetic electrons have harder energy spectra or travel along a more rapidly expanding coronal magnetic field. By modeling the observed velocity and location distributions of coronal electron beams, we predict that the temperature of acceleration regions ranges from 5 × 106 to 2 × 107 K. Our model also indicates that the acceleration region may have a boundary where the temperature abruptly decreases so that the electron beam velocity can become more than triple (even up to 10 times) the background thermal velocity and produce the coronal type III radio bursts.

Electron Cyclotron Maser Emissions from Evolving Fast Electron Beams

J. F. **Tang**, D. J. Wu, L. Chen, G. Q. Zhao, C. M. Tan
ApJ **2016**
http://arxiv.org/pdf/1603.04496v1.pdf
Fast electron beams (FEBs) are common products of solar active phenomena. Solar radio bursts are an important diagnostic tool in the understanding of FEBs as well as the solar plasma environment in which they are propagating along solar magnetic fields. In particular, the evolutions of the energy spectrum and velocity distribution of FEBs due to the interaction with the ambient plasma and field when propagating can significantly influence the efficiency and property of their emissions. In this paper, we discuss some possible evolutions of the energy spectrum and velocity distribution of FEBs due to the energy loss processes and the pitch-angle effect caused by the magnetic field inhomogeneity, and analyze the effects of these evolutions on electron cyclotron maser (ECM) emission, which is one of the most important mechanisms of producing solar radio bursts by FEBs. The results show that the growth rates all decrease with the energy loss factor Q, but increase with the magnetic mirror ratio σ as well as with the steepness index δ. Moreover, the evolution of FEBs also can significantly influence the fastest growing mode and the fastest growing phase angle. This leads to the change of the polarization sense of ECM emission. In particular, our results also reveal that FEB that undergoes different evolution processes will generate different types of ECM emission. We believe the present results to be very helpful on more comprehensive understanding of dynamic spectra of solar radio bursts.

Excitation of Langmuir waves by the lower energy cutoff behavior of power-law electrons

Jianfei **Tang**, Dejin Wu, Guoqing Zhao, Ling Chen, Chengming Tan
Astrophysics and Space Science, **2014**
http://arxiv.org/pdf/1406.1380v1.pdf
Langmuir waves (LWs), which are believed to play a crucial role in the plasma emission of solar radio bursts, can be excited by streaming instability of energetic electron beams. However, solar hard X-ray observations imply that the energetic flare electrons usually have a power-law energy distribution with a lower energy cutoff. In this paper, we investigate LWs driven by the power-law electrons. The results show that power-law electrons with the steepness cutoff behavior can excite LWs effectively because of the population inversion distribution below the cutoff energy (Ec). The growth rate of LWs increases with the steepness index (δ) and decreases with the power-law index (α). The wave number of the fastest growing LWs (kλD), decreases with the characteristic velocity of the power-law electrons (vc=2Ec/me√) and increases with the thermal velocity of ambient electrons (vT). This can be helpful for us to understand better the physics of LWs and the dynamics of energetic electron beams in space and astrophysical plasmas.

Electron Cyclotron Maser Emission in Coronal Arches and Solar Radio Type V Bursts

J. F. **Tang**1,2, D. J. Wu3, and C. M. Tan
2013 ApJ 779 83
Solar radio type V bursts were classified as a special spectral class based on their moderately long duration, wide bandwidth, and sense of polarization opposite of associated type III bursts. However, type V bursts are also closely related to the preceding type III bursts. They have an approximately equal source height and the same dispersion of position with frequency. Electron cyclotron maser (ECM) instability driven by beam electrons has been used to explain type III bursts in recent years. We propose ECM emission as the physical process of type V solar radio bursts. According to the observed properties of type V and III bursts, we propose that energetic electrons in excited type V continuum are trapped in coronal loops, which are adjacent to the open field lines traced by type III electrons. With the proposed magnetic field configuration and the ECM emission mechanism, the observed properties of type V bursts, such as long duration, wide bandwidth, and opposite sense of polarization can be reasonably explained by our model.

Electron-cyclotron maser emission by power-law electrons in=coronal loops:

J. F. **Tang** and D. J. Wu
A&A 493 (**2009**) 623-628

Context. The electron-cyclotron maser (ECM) instability is an important mechanism that amplifies electromagnetic radiation directly by nonthermal electrons trapped in magnetic fields. The nonthermal electrons frequently have a negative power-law distribution with a lower energy cutoff (E_c), which will depress the instability.
Aims. In this paper, it is shown that the lower energy cutoff behavior of power-law electrons trapped in coronal loops can drive the ECM instability efficiently.
Methods. Based on the dispersive relation for high-frequency waves and distribution function for power-law electrons with a lower energy cutoff in a coronal loop, the growth rates of the O and X mode waves at fundamental and harmonic frequencies are calculated.
Results. The results show that the instability is driven when $\delta > \alpha$ because of a population inversion below the cutoff energy E_c, where δ is the steepness index describing the cutoff behavior and α the power-law spectrum index. The growth rates increase with δ and E_c, but decrease with α, σ, and Ω, where σ is the magnetic mirror ratio of the loop and Ω the ratio frequency in the loop.
Conclusions. This novel driving mechanism for the ECM emission can be expected to have a potential importance for understanding the microphysics of radio bursts from the Sun and others.

The 10.7 cm solar radio flux (F10.7)

K. F. **Tapping**
Space Weather, Volume 11, Issue 7, pages 394–406, July **2013**
http://onlinelibrary.wiley.com/doi/10.1002/swe.20064/pdf
The 10.7 cm solar radio flux, or F10.7 is, along with sunspot number, one of the most widely used indices of solar activity. This paper describes the equipment and procedures used to make the measurements and to calibrate them, and discusses some of the “most-asked” questions about the data.

The Next Generation of Canadian Solar Flux Monitoring

Tapping, Kenneth F.; Morton, Donald C.
Journal of Physics: Conference Series, Volume 440, Issue 1, article id. 012039 (**2013**).
The 10.7 cm solar radio flux (F10.7), provided by the National Research Council of Canada since 1947, is widely used as an index of solar activity and as a proxy for other solar quantities that are harder to measure. Over recent years needs have arisen that are difficult to meet with solar flux measurements at a single wavelength. F10.7 comprises contributions from multiple emission mechanisms. To separate these, multi-wavelength measurements are needed. A new instrument is under construction that will measure fluxes precisely in six bands at 2.8, 3.6, 6.0, 10.7, 18 and 21 cm.

Did the Sun Change Its Behaviour During the Decline of Cycle 23 and Into Cycle 24fl

K. F. **Tapping** and J. J. Valdés
Solar Physics, Volume 272, Number 2, 337-350, **2011**
The activity minimum between the end of cycle 23 and the beginning of cycle 24 was the longest and deepest since at least the beginning of the 20th century. This has led to speculation that the Sun is changing its behaviour. The sunspot number and 10.7-cm solar radio flux indices have traditionally been highly correlated, so a change in the relationship between them might flag at such a change. An examination of this relationship suggests a significant change in the relationship between activity in the photosphere and in the chromosphere/corona happened soon after the maximum of cycle 23 and has continued into cycle 24. However, there are indications of change as early as 1980.

Density Turbulence and the Angular Broadening of Outer Heliospheric Radio Sources at High Latitudes and in the Ecliptic Plane,

S. **Tasnim**, Gary. P. Zank, Iver H. Cairns, and L. Adhikari
The Astrophysical Journal, 928, id.125, **2022**
https://iopscience.iop.org/article/10.3847/1538-4357/ac5031/pdf
Density irregularities are responsible for the scattering of radio waves in the solar wind and astrophysical plasmas. These irregularities significantly affect the inferred physical properties of radio sources, such as size, direction, and intensity. We present here a theory of angular broadening due to the scattering of radio waves by density irregularities that improves the existing formalism used to investigate radio wave scattering in the outer heliosphere and the very

local interstellar medium. The model includes an inner scale and both latitudinal and radial dependencies for the density fluctuation spectra and propagation paths for the radiation both near and out of the ecliptic plane. Based on the pickup-ion-mediated solar wind model (PUI model) of Zank et al., we estimate the turbulence and solar wind quantities for the high-latitude fast solar wind. The predictions include the density variance, inner/dissipation scale, velocity correlation length, mean magnetic field, and proton temperature. The density turbulence amplitude is estimated in two ways. First, a simple scaling technique is used to extend the theoretical predictions of the PUI model for the high-latitude wind beyond the heliospheric termination shock. Second, the solar wind and turbulence quantities are calculated near the ecliptic plane using plasma and magnetometer data from the Voyager 2 spacecraft over the period 1977–2018. Based on the turbulence models and observations, we calculate the scattering angle of the radio sources in the high-latitude and near-ecliptic wind. Finally, we compare the numerical results with the analytic predictions from Cairns and Armstrong et al. and the observed source sizes.
CESRA #3278 May **2022** https://www.astro.gla.ac.uk/users/eduard/cesra/?p=3278

A Study of the 2012 January 19 Complex Type II Radio Burst Using Wind, SOHO, and STEREO Observations

T.B. **Teklu**, A.V. Gholap, N. Gopalswamy, S. Yashiro, P. Mäkelä, S. Akiyama, N. Thakur, H. Xie
URSI Asia-Pacific Radio Science Conference in Seoul, August 21-25, **2016**
http://arxiv.org/pdf/1605.09644v1.pdf
We report on a case study of the complex type II radio burst of **2012 January 19** and its association with a white light coronal mass ejection (CME). The complexity can be described as the appearance of an additional type II burst component and strong intensity variation. The dynamic spectrum shows a pair of type II bursts with fundamental harmonic structures, one confined to decameter-hectometric (DH) wavelengths and the other extending to kilometric (km) wavelengths. By comparing the speeds obtained from white-light images with that speed of the shock inferred from the drift rate, we show that the source of the short-lived DH component is near the nose.

Coronal mass ejections and radio related aspects (Review)

M. **Temmer**
CESRA_**2010, Presentation File**
Coronal mass ejections (CMEs) are the most violent activity signatures from our Sun. Discovered in the 70's, extensive studies were carried out particularly in the SOHO era, but still, our understanding of the physical characteristics of CMEs is limited. The present paper reviews recent results derived from studies of CMEs and associated flares, together with their radio related aspects. In particular we pay attention to recent STEREO results on the 3D propagation characteristics of CMEs in the interplanetary space which can be now tracked seamlessly from Sun to Earth. CME driven shocks indicated from interplanetary radio type II bursts are of special interest since, if Earth directed, are influencing the near Earth space environment and disturb our so called space weather.

A study on the relationship of type III radio bursts CME and solar flares during the active period October-November 2003

Michaella **Thanassa,** Eleftheria Mitsakou, Panagiota Preka-Papadema, Xenophon Moussas, Panagiotis Tsitsipis and Athanasios Kontogeorgos
Proceedings of the International Astronomical Union / Volume 4 / Symposium S257, pp 361 – 363, Published online: 16 Март **2009**
http://journals.cambridge.org/action/displayIssuefliid=4866212
Within a period of intense activity (20 October to 5 November 2003), the injection and propagation of near relativistic electrons, resulted in hundreds of type III bursts recorded by the ARTEMISIV radio spectrograph (20–650 MHz). For a number of these type III events association with GOES SXR/Hα flare and/or SOHO/LASCO CME was established. We study the variation of characteristic type III parameters and their relationship with features of the associated flares and/or CMEs.

Time Profile Study of Type III Solar Radio Bursts Using Parker Solar Probe

Tulsi **Thapa**1,2 and Yihua Yan1,2,3
2024 ApJ 972 2
https://iopscience.iop.org/article/10.3847/1538-4357/ad5e77/pdf
Solar type III radio bursts are crucial indicators of energetic electron activity in the solar corona and interplanetary space. Our assessment of 43 interplanetary type III bursts, recorded by the FIELDS instrument on board the Parker Solar Probe during Encounters 05 to 11, has led to significant and complex findings. We have analyzed time profile

features across a frequency range of 19–0.5 MHz, revealing dependencies on frequency and providing insights into duration, burst speeds, bandwidths, and drift rates. This novel analysis has unveiled a spectral index of −0.63 ± 0.04 for rise, −0.69 ± 0.03 for decay time, and −0.68 ± 0.03 for the total duration. We have determined the average electron beam velocities for front, middle, and back as 0.15c, 0.13c, and 0.08c, respectively. Our findings show that faster electron beams generate emissions with shorter duration. The average ratio of the front-to-back velocity is 1.87, and the ratio of front-to-middle velocity is 1.23. We have also discovered a strong relationship between burst duration with rise, peak, and decay times, particularly pronounced with decay time (correlation coefficient = 0.95). This indicates that the entire temporal profile, including rise, peak, and decay phases, collectively contributes to event duration and is not solely influenced by external factors like plasma conditions or electron beam dynamics but also by internal burst processes. These complex findings shed light on the physical mechanisms governing burst dynamics, revealing intricate interactions between electron beam characteristics and observed temporal and spectral traits of type III solar radio bursts.

CESRA Highlights #3848 **2024** https://www.astro.gla.ac.uk/users/eduard/cesra/?p=3848

Evidence for the Three Wave Interactions in the Vicinity of an Interplanetary Shock

G. **Thejappa**1

2022 ApJ 937 28

https://iopscience.iop.org/article/10.3847/1538-4357/ac8b07/pdf

We present the high time resolution in situ observations of coherent one-dimensional magnetic-field-aligned Langmuir wave packets with well-defined low frequency modulations (beats) in the upstream region of a coronal mass ejection driven supercritical quasi-perpendicular interplanetary (IP) shock. We show that these beat-type waveforms provide what is believed to be the first observational evidence for one of the most important three wave interactions, called the electrostatic decay instability (ESD) $L \rightarrow L' + S$ (L is the pump Langmuir wave excited by the shock accelerated electron beam, and L' and S are the daughter Langmuir and ion sound waves, respectively). We also show that (1) the spectra of these wave packets contain the signatures of L, L', and S, which satisfy the resonance conditions required for excitation of ESD, (2) the peak intensities of these wave packets well exceed the ESD threshold values, and (3) the speed of the electron beam estimated using the resonance conditions is very close to the typical observed speeds of the IP shock accelerated electron beams. The implication of these findings is that (1) the shock accelerated electron beams probably are stabilized by the three wave interaction $L \rightarrow L' + S$, and (2) the second harmonic radio emission $T_{2f_{pe}}$ of solar type II radio bursts probably is excited by the three wave merging $L + L' \rightarrow T_{2f_{pe}}$. 18 Feb 2011

Observational Evidence for Beat Phenomenon in Complex Solar Type III Radio Bursts

G. **Thejappa**[1] and R. J. MacDowall[2]

2021 *ApJ* **912** 61

https://doi.org/10.3847/1538-4357/abee74

We present new observational evidence for one of the most important three wave interactions, called the electrostatic decay instability (ESD) $L \rightarrow L' + S$ in the source regions of complex solar type III radio bursts (L is the electron beam-excited Langmuir wave, and L' and S are the ESD excited daughter Langmuir and ion sound waves, respectively). The STEREO in situ wave observations in the source regions of complex type III bursts show that Langmuir waves often occur as one-dimensional magnetic field aligned beat-type wave packets, with peak intensities well in excess of the threshold for excitation of ESD, and with spectra containing (a) two closely spaced narrow peaks (L and L') corresponding probably to the beating modes responsible for the beat patterns at frequencies very close to the local electron plasma frequency, fpe, and (b) narrow peaks at ion sound frequencies, fS, which are very close to beat frequencies. Using the FFT and higher order spectral techniques, we show that the frequency, wavevector and phase resonance conditions required for excitation of ESD are well satisfied for these wave packets, and the speeds of electron beams derived from the resonance conditions agree reasonably well with those derived from the drift rates of the associated type III events. We also show that the merging of (L) and (L') most probably is the excitation mechanism of the second harmonic radio emission $T_{2f_{pe}}$ of these type III bursts.

Detection of Extreme and Exceptional Langmuir Wave Packets in Solar Type III Radio Bursts

G. **Thejappa**, R. J. MacDowall

JGR Volume125, Issue6 June **2020** e2019JA027714

sci-hub.tw/10.1029/2019JA027714

We report the STEREO observations of two extreme and exceptional Langmuir wave packets, which are the most intense wave packets ever detected in solar type III bursts; their peak intensities E t ~ 215 and ~ 161 mVm−1 beat out the previous 107 mVm−1 record, reported by Thejappa and MacDowall (2018a; https://doi.org/10.3847/1538-

4357/aaca3b). These observations provide new evidence for (1) the four-wave interaction called the oscillating two-stream instability (OTSI), which is the coupling of two beam-excited Langmuir waves with an ion sound wave yielding downshifted and upshifted side bands, and (2) Langmuir solitons formed as a result of OTSI, and (3) density cavities created by their ponderomotive forces. The fast Fourier transform spectra of these wave packets provide what is believed to be the first evidence for harmonics of the electron plasma frequency, f p e up to the order of 5 with peak intensities falling off with increasing harmonic number. The higher order spectral analysis indicates that these harmonics probably correspond to the electromagnetic waves excited as a result of various three-wave interactions. We argue that although the observed characteristics also indicate that these wave packets could be collapsing wave packets formed as a result of nucleation instability, the observed evidence for OTSI and Langmuir solitons trapped inside the self-generated density cavities strongly favor the OTSI as the route for the spatial collapse of Langmuir waves in the present case. The implication of these findings for theories of solar type III radio bursts is discussed. **12 March 2014, 2016-02-18**

Evidence for Oscillating Two-stream Instability and Spatial Collapse of Langmuir Waves in a Solar Type II Radio Burst

G. **Thejappa**1 and R. J. MacDowall2
2019 ApJ 883 199
https://doi.org/10.3847/1538-4357/ab3bcf
We present the high time resolution in situ observations of Langmuir waves, likely excited by an electron beam accelerated by a coronal-mass ejection-driven super-critical quasi-perpendicular interplanetary shock into its upstream solar wind, which happens to be the source region of a solar type II radio burst. We show that (1) these waves occur as coherent localized magnetic-field-aligned, one-dimensional wave packets with durations of a few milliseconds and with peak intensities well in excess of the threshold for strong turbulence processes, (2) they provide what is believed to be the first evidence for: (a) the oscillating two-stream instability (OTSI) , where L 1 and L 2, U and D, and S are the pump Langmuir waves, up- and down-shifted side bands, and ion sound waves, respectively, (b) a three-wave interaction , where is the second-harmonic electromagnetic wave, (3) they satisfy the threshold condition for formation of collapsing solitons, and (4) they are accompanied by their ponderomotive force induced density cavities with , where is the level of ponderomotive force induced density fluctuations and is that of the ambient fluctuations. These findings strongly suggest that the observed wave packets provide evidence for the collapsing solitons formed as a result of OTSI. The implication is that the strong turbulence processes probably play very important roles in excitation of type II radio emissions as well as in stabilization of shock-accelerated electron beams.

Langmuir Solitons in Solar Type III Radio Bursts: STEREOObservations

G. **Thejappa**1 and R. J. MacDowall2
2018 *ApJ* **864** 122
http://iopscience.iop.org/article/10.3847/1538-4357/aad5e4/pdf
The source regions of solar type III radio bursts are regions of very intense Langmuir wave packets excited by the bump-on-tail distributions of energetic electrons accelerated during solar flares. We report the high time resolution observations of some of these wave packets, which provide unambiguous evidence for Langmuir solitons formed as a result of oscillating two-stream instability (OTSI), since (1) they occur as intense localized one-dimensional magnetic field aligned wave packets, (2) their measured half-widths and peak amplitudes are inversely correlated with each other, so that the narrower the wave packet is, the greater its amplitude; this inverse correlation is the characteristic feature of Langmuir solitons formed as a result of balance between the nonlinearity related self-compression and dispersion related broadening of the wave packets, (3) their FFT spectra contain peaks corresponding to sidebands and low frequency enhancements in addition to pump Langmuir waves, whose frequencies and wave numbers satisfy the resonance conditions of the four-wave interaction known as the OTSI, and (4) they are accompanied by their ponderomotive force induced density cavities. The implication of these observations for theories of solar radio bursts is discussed.

Observational Evidence for Langmuir Wave Collapse in the Source Region of a Solar Type III Radio Burst

G. **Thejappa**1 and R. J. MacDowall2
2018 ApJ 862 75
http://iopscience.iop.org/article/10.3847/1538-4357/aaca3b/pdf
High-time-resolution in situ wave observations show that Langmuir waves associated with solar type III radio bursts often occur as coherent localized one-dimensional magnetic-field-aligned wave packets with short durations of a few milliseconds and peak intensities well above the strong turbulence thresholds. In this paper, we report observations of a wave packet obtained by the time domain sampler of the STEREO WAVES experiment, which is unique in the sense that it is the most intense wave packet ever detected in association with a solar type III radio burst, with a peak intensity E t ~ 107 mVm−1. We show that this wave packet provides evidence for (1) oscillating two-stream instability

(OTSI), (2) a collapsing soliton formed as a result of OTSI, (3) the formation of a soliton–caviton pair, and (4) excitation of second and third harmonic electromagnetic waves. We also show that the peak intensity and spatial width satisfy the threshold condition for this wave packet to be the collapsing Langmuir wave packet formed as a result of nucleation processes even when $\delta n_b > \delta n_p$, where δn_b and δn_p are the levels of background and ponderomotive-force-induced density fluctuations, respectively. Thus, these observations provide unambiguous evidence for the spatial collapse of Langmuir waves in the source region of a type III radio burst, and the observed spectral evidence for OTSI and the ponderomotive-force-induced density cavity strongly suggest that OTSI is mostly likely responsible for the collapse of the observed wave packet. **2008-05-19**

Critical Fluctuations in Beam-plasma Systems and solar type III radio bursts, 2017, 16th AIAC: "Turbulence, Structures, and Particle Acceleration",

Thejappa, G., and MacDowall, R. J.,
J. Phys.: Conf. Conf. Series 900 (**2017**) 012019,
http://iopscience.iop.org/article/10.1088/1742-6596/900/1/012019/pdf
It is shown that the Langmuir waves are excited similar to critical fluctuations during phase transitions when the negative absorption due to electron beam traveling radially outward in the solar atmosphere is balanced by the positive absorption due to collisions in the corona and due to scattering on electron density inhomogeneities in the interplanetary medium. The effective temperature of the Langmuir fluctuations range from 1011 to 1013 K, explaining the majority of the type III bursts. The Rayleigh scattering and direct coupling due to density gradient as well as due to density inhomogeneities are discussed in the context of fundamental radiation and the combination scattering for second harmonic. The number density of electrons in type III beams is estimated and compared with observations. It is also shown that the stabilization of type III beams is achieved automatically since the instability does not develop in the case of critical fluctuations.
CESRA Highlight #1628 Dec **2017** http://cesra.net/?p=1628

Solar Type III Radio Bursts: Directivity Characteristics

G. **Thejappa** and R. J. MacDowall
Journal of Physics: Conference Series, Volume 642, Issue 1, article id. 012028 (**2015**)
Type III radio bursts are a group of fast drifting radio emissions associated with solar flares. These radio emissions are believed to be excited at the fundamental and second harmonic of the electron plasma frequency, fpe by the electron beam excited Langmuir waves through a mechanism called the plasma mechanism. This mechanism attributes the dipole and quadrupole beam patterns for the fundamental and harmonic emissions. To verify these predictions, we analyze the simultaneous observations of type III radio bursts by the STEREO A, B and Wind spacecraft located at different vantage points in the ecliptic plane, and determine their normalized peak intensities (directivity factors) at each spacecraft using their time profiles. Assuming that the sources of these bursts are located on the Parker spiral magnetic field lines emerging from the associated active regions, we estimate the angles between the magnetic field directions and the lines connecting the sources to the spacecraft (viewing angles). Based on the plots of the directivity factors versus the viewing angles, one can divide these bursts into (1) intense bursts emitted into a narrow cone centered around the tangent to the magnetic field, and (2) relatively weaker bursts emitting into a wider cone centered around the tangent to the magnetic field. We compute the distributions of ray trajectories emitted by an isotropic point source and show that the refraction focuses the fundamental and harmonic emissions into narrow and wider cones, respectively. The comparison of these distributions with observations indicates that the intense bursts visible to a narrow range of angles around the tangent to the magnetic field probably correspond to the fundamental, and the relatively weaker bursts visible to a wide range of angles probably are the harmonic emissions.
See CESRA highlight #968 Nov **2016**
http://cesra.net/?p=968

Comments of Sang **Hoang** **What is wrong ?**

Dear SWAVES community colleagues,
The recent CESRA new highlight (of 15 November 2016, http://cesra.net/?p=968) on "Solar Type III Radio Bursts: Directivity Characteristics" by G. Thejappa and R. J. MacDowall, gives us a new opportunity to present to the SWAVES community the history about the highlighted results (as illustrated by Figure 1 therein). These results were published in APJ (Vol. 745, No. 2, article id. 187, 9, 2012).
The history. Shortly after their publication in APJ, we emailed to the authors, particularly to Golla Thejappa, a series of comments pointing to serious problems raised by their results. However without any success. (In fact, we thought a comment paper would have been more efficient at doing that, unfortunately I was answered that this category of paper was not considered by APJ.) A second attempt to discuss with Golla Thejappa was given by the STEREO and Wind Waves Workshop on Solar Radio Emissions in October 2013, Santorini, Greece. At this workshop, we have presented a poster paper reviewing and discussing different measurements of the type III radiation diagram from meter and decameter to hecto and kilometer wavelenghts, including the G. Thejappa et al.'s paper. (A PDF file of the poster paper is attached herewith.) Around the poster, we had again a long and hard discussion with G. Thejappa, and once again

with no more progress.
The problem. To get the emission pattern of Type III Radio bursts, Thejappa et al. selected 65 Type III bursts that are simultaneously observed by the 3 spacecraft, STEREO A/B and Wind. For each burst observed at each s/c, w (Wind), a (STEREO A) and b (STEREO B), they calculate 3 "normalized peak intensities" (the peak intensities I in dB units (!) are extracted from the observed intensity time profiles) as :
Ra = Ia / (Ia+Ib+Iw), Rb = Ib / (Ia+Ib+Iw), and Rw = Iw / (Ia+Ib+Iw) (Note : these quantities are not given in the text of the highlight),
together with the "viewing angles" between the magnetic field directions passing the sources and the lines connecting them to the s/c.
These "normalized peak intensities" are then plotted (at 625 kHz) in Figure 1 of the highlight as a function of viewing angles (left panel).
Figure 1 suggests an "emission pattern" strongly concentrated on the direction of local magnetic field lines (within a cone of a few degrees)
and steadily falling at increasing viewing angles to ~100°, contrary to observations and previous diagram measurements which all point to a widespread visibility of Type III bursts as broad as -180° to 180° at lower frequencies (See the attached poster paper and references therein).
What is wrong ? (1) The use of "normalized peak intensities (in dB)" is at least inadequate and cannot, in any way, properly measure the shape of the diagram. To do this, each receiver has to be correctly calibrated in flux density as measured at the antenna terminals and corrected for the squarred distance of the s/c to the source (See the poster paper and references therein). (2) As a consequence of not using units of flux density, the pattern result depends strongly on the intensities measured by the Wind receiver which is the most sensitive, thanks to its much longer antenna as compared to STEREO. This explains the concentration of the data points, especially from Wind, with large scatter around the viewing angles near 0°. (3) The restricted range of viewing angles within ~100° results simply from a selection artefact : the method used requires that a selected burst must be simultaneously observed by the 3 s/c. Hence, because of their low sensitivity, the STEREO receivers can only detect bursts within viewing angles of ~100°, as justly seen in Figure 1, excluding other bursts that can be seen by Wind at viewing angles beyond 100°.
Hope this helps for Science.
Best regards,
Sang Hoang

Evidence for four- and three-wave interactions in solar type III radio emissions

G. **Thejappa**, R. J. MacDowall, and M. Bergamo
Ann. Geophys., 31, 1417-1428, **2013**
The high time resolution observations obtained by the STEREO/WAVES experiment show that in the source regions of solar type III radio bursts, Langmuir waves often occur as intense localized wave packets with short durations of only few ms. One of these wave packets shows that it is a three-dimensional field structure with WLneTe ~ 10−3, where WL is the peak energy density, and ne and Te are the electron density and temperature, respectively. For this wave packet, the conditions of the oscillating two-stream instability (OTSI) and supersonic collapse are satisfied within the error range of determination of main parameters. The density cavity, observed during this wave packet indicates that its depth, width and temporal coincidence are consistent with those of a caviton, generated by the ponderomotive force of the collapsing wave packet. The spectrum of each of the parallel and perpendicular components of the wave packet contains a primary peak at fpe, two secondary peaks at fpe ± fS and a low-frequency enhancement below fS, which, as indicated by the frequency and wave number resonance conditions, and the fast Fourier transform (FFT)-based tricoherence spectral peak at (fpe, fpe, fpe + fS, fpe − fS), are coupled to each other by the OTSI type of four-wave interaction (fpe is the local electron plasma frequency and fS is the frequency of ion sound waves). In addition to the primary peak at fpe, each of these spectra also contains a peak at 2fpe, which as indicated by the frequency and wave number resonance conditions, and the wavelet-based bicoherence spectral peak at (fpe, fpe), appears to correspond to the second harmonic electromagnetic waves generated as a result of coalescence of oppositely propagating sidebands excited by the OTSI. Thus, these observations for the first time provide combined evidence that (1) the OTSI and related strong turbulence processes play a significant role in the stabilization of the electron beam, (2) the coalescence of the oppositely propagating up- and down-shifted daughter Langmuir waves excited by the OTSI probably is the emission mechanism of the second harmonic radiation, and (3) the Langmuir collapse follows the route of OTSI in some of the type III radio bursts.

Observational evidence for the collapsing langmuir wave packet in a solar type III radio burst

G. **Thejappa**, R. J. MacDowall and M. Bergamo
JGR, **2013**, Volume 118, Issue 7, pages 4039–4052,
High time resolution observations from the STEREO spacecraft show that in solar type III radio bursts, Langmuir waves often occur as very intense one-dimensional magnetic field aligned field structures. One of these events

represents the most intense Langmuir wave packet with $\frac{W_L}{n_e T_e} \sim 7.2\times10^{-3}$ ever detected in a type III radio burst until now (*WL* is the peak energy density, and *ne* and *Te* are the electron density and temperature, respectively). The detailed analysis of this wave packet indicates that (1) its peak intensity is well above the threshold for the oscillating two stream instability (OTSI) and supersonic collapse, (2) its peak intensity and spatial scale satisfy the criterion for it to be a collapsing envelope soliton, (3) its low frequency components provide evidence for a density cavity, whose depth, width and temporal coincidence indicate that probably it is the ponderomotive force generated density cavity, and (4) its spectrum contains harmonic peaks at 2*fpe* and 3*fpe* (in addition to the main Langmuir wave peak at the electron plasma frequency, *fpe*), which as indicated by the bispectral analysis, probably are of the electromagnetic waves generated as a result of coalescence of two oppositely propagating Langmuir waves, and a Langmuir wave and a second harmonic electromagnetic wave, respectively. These characteristics strongly suggest that this wave packet and its associated density cavity represent the collapsing envelope soliton-caviton pair formed as a result of OTSI, and in the present case, the strong turbulence processes probably play key roles in the beam stabilization as well as conversion of Langmuir waves into escaping radiation at 2*fpe* and 3*fpe*.

In situ detection of strong Langmuir turbulence processes in solar type III radio bursts

Thejappa, G.; MacDowall, R. J.; Bergamo, M.
J. Geophys. Res., Vol. 117, No. A8, A08111, **2012**
http://dx.doi.org/10.1029/2012JA017695

The high time resolution observations obtained by the WAVES experiment of the STEREO spacecraft in solar type III radio bursts show that Langmuir waves often occur as intense localized wave packets. These wave packets are characterized by short durations of only a few ms and peak intensities, which well exceed the supersonic modulational instability (MI) thresholds. These timescales and peak intensities satisfy the criterion of the solitons collapsed to spatial scales of a few hundred Debye lengths. The spectra of these wave packets consist of primary spectral peaks corresponding to beam-resonant Langmuir waves, two or more sidebands corresponding to down-shifted and up-shifted daughter Langmuir waves, and low frequency enhancements below a few hundred Hz corresponding to daughter ion sound waves. The frequencies and wave numbers of these spectral components satisfy the resonance conditions of the modulational instability (MI). Moreover, the tricoherences, computed using trispectral analysis techniques show that these spectral components are coupled to each other with a high degree of coherency as expected of the MI type of four wave interactions. The high intensities, short scale lengths, sideband spectral structures and low frequency spectral enhancements and, high levels of tricoherences amongst the spectral components of these wave packets provide unambiguous evidence for the supersonic MI and related strong turbulence processes in type III radio bursts. The implication of these observations include: (1) the MI and related strong turbulence processes often occur in type III source regions, (2) the strong turbulence processes probably play very important roles in beam stabilization as well as conversion of Langmuir waves into escaping radiation at the fundamental and second harmonic of the electron plasma frequency, fpe, and (3) the Langmuir collapse probably follows the route of MI in type III radio bursts.

EVIDENCE FOR THE OSCILLATING TWO STREAM INSTABILITY AND SPATIAL COLLAPSE OF LANGMUIR WAVES IN A SOLAR TYPE III RADIO BURST

G. **Thejappa**1, R. J. MacDowall2, M. Bergamo1 and K. Papadopoulos
2012 ApJ 747 L1

We present observational evidence for the oscillating two stream instability (OTSI) and spatial collapse of Langmuir waves in the source region of a solar type III radio burst. High time resolution observations from the STEREO A spacecraft show that Langmuir waves excited by the electron beam occur as isolated field structures with short durations ~3.2 ms and with high intensities exceeding the strong turbulence thresholds. These short duration events are identified as the envelope solitons which have collapsed to spatial scales of a few hundred Debye lengths. The spectra of these wave packets contain an intense peak and two sidebands, corresponding to beam-resonant Langmuir waves, and down-shifted and up-shifted daughter Langmuir waves, respectively, and low-frequency enhancements below a few hundred Hz. The frequencies and wave numbers of these spectral components satisfy the resonance conditions of the OTSI. The observed high intensities, short scale lengths, sideband spectral structures, and low-frequency enhancements strongly suggest that the OTSI and spatial collapse of Langmuir waves probably control the nonlinear beam-plasma interactions in type III radio bursts.

EMISSION PATTERNS OF SOLAR TYPE III RADIO BURSTS: STEREOSCOPIC OBSERVATIONS

G. **Thejappa**1, R. J. MacDowall2 and M. Bergamo
2012 ApJ 745 187

Simultaneous observations of solar type III radio bursts obtained by the STEREO A, B, and WIND spacecraft at low frequencies from different vantage points in the ecliptic plane are used to determine their directivity. The

heliolongitudes of the sources of these bursts, estimated at different frequencies by assuming that they are located on the Parker spiral magnetic field lines emerging from the associated active regions into the spherically symmetric solar atmosphere, and the heliolongitudes of the spacecraft are used to estimate the viewing angle, which is the angle between the direction of the magnetic field at the source and the line connecting the source to the spacecraft. The normalized peak intensities at each spacecraft Rj = Ij /ΣIj (the subscript j corresponds to the spacecraft STEREO A, B, and WIND), which are defined as the directivity factors are determined using the time profiles of the type III bursts. It is shown that the distribution of the viewing angles divides the type III bursts into: (1) bursts emitting into a very narrow cone centered around the tangent to the magnetic field with angular width of ~2fl and (2) bursts emitting into a wider cone with angular width spanning from ~ – 100fl to ~100fl. The plots of the directivity factors versus the viewing angles of the sources from all three spacecraft indicate that the type III emissions are very intense along the tangent to the spiral magnetic field lines at the source, and steadily fall as the viewing angles increase to higher values. The comparison of these emission patterns with the computed distributions of the ray trajectories indicate that the intense bursts visible in a narrow range of angles around the magnetic field directions probably are emitted in the fundamental mode, whereas the relatively weaker bursts visible to a wide range of angles are probably emitted in the harmonic mode.

EFFECTS OF REFRACTION ON ANGLES AND TIMES OF ARRIVAL OF SOLAR RADIO BURSTS

G. **Thejappa**1, R. J. MacDowall2 and N. Gopalswamy

2011 ApJ 734 16

Solar type III and type II radio bursts suffer severe bending and group delay due to refraction while escaping from the source where the refractive index μ can be as low as ~0 to the observer where μ ~ 1. These propagation effects can manifest themselves as errors in the observed directions and times of arrival at the telescope. We describe a ray-tracing technique that can be used to estimate these errors. By applying this technique to the spherically symmetric density model derived using the data from the WIND/Waves experiment, we show that (1) the fundamental and harmonic emissions escape the solar atmosphere in narrow cones (at 625 kHz the widths of these escape cones are ~11 and ~8fl, respectively), (2) the errors in the angles as well as the times of arrival increase monotonically with the angle of arrival (at 625 kHz these errors are 026 and ~17.2 s for the fundamental and ~052 and ~7.6 s for the harmonic at the maximum possible angles of arrival of ~055 and ~4fl, respectively), and (3) the lower the frequencies are, the higher the errors in both the angles and times of arrival are. This implies that at 625 kHz the measured arrival angles and arrival times of the fundamental and harmonic are off by ~50% and ~13%, and ~3.4% and ~1.5%, respectively.

LOCALIZATION OF A TYPE III RADIO BURST OBSERVED BY THE *STEREO* SPACECRAFT

G. **Thejappa**1 and R. J. MacDowall2

Astrophysical Journal, 720:1395–1404, **2010**

Ray tracing calculations show that (1) emissions from a localized source escape as direct and reflected waves along different paths, (2) the reflected waves experience higher attenuation and group delay because they travel longer path lengths in regions of reduced refractive index, and (3) widely separated spacecraft “A” and “B” can detect the direct as well as reflected emissions escaping along different directions. It is proposed that the source of a radio burst observed by twin spacecraft “A” and “B” can be localized if at a given frequency the emission at one of them is identified as the direct emission and is identified at the other as the reflected emission by comparing the observed time delays ΔT, as well as intensity ratios *IB/IA* with the corresponding values of the direct and reflected emissions obtained for a given coronal model. A type III event observed by the *STEREO* spacecraft “A” and “B” shows that its characteristics are consistent with direct and reflected emissions by being less intense and delayed at “A” in comparison to that at “B.” By applying the proposed technique to this event, the location of its source is found to lie between the turning point of the ray and the harmonic layer corresponding to $f_{pe} = f/2$, where f and f_{pe} are the frequency of the emission and the electron plasma frequency, respectively. The comparisons of the widths of the fundamental and harmonic emission cones with the angular separation of spacecraft “A” and “B” indicate that the mode of the observed emission is probably the harmonic.

Localization of type II and type III radio burst sources using multi-spacecraft observations

G. **Thejappa**1 and R. J. MacDowall

Proceedings of the International Astronomical Union / Volume 4 / Symposium S257, pp 329 – 334, Published online: 16 Март **2009**

http://journals.cambridge.org/action/displayIssuefliid=4866212

A method for the localization of the radio burst sources associated with the flare accelerated electron beams and coronal mass ejection (CME) shocks is presented. This method involves the computations of the ray trajectories, time delays, and optical depths in the refracting solar atmosphere. The coordinates of the radiating source can be obtained by comparing the time delays and intensity ratios of the bursts observed by widely separated spacecraft with the computed group delays and intensity ratios at exit points of the rays from the solar atmosphere. This method is applied to a type III radio burst observed by the STEREO spacecraft.

Effects of Scattering on Radio Emission from the Quiet Sun at Low Frequencies

G. **Thejappa** and R. J. MacDowall
The Astrophysical Journal, Vol. 676, No. 2: 1338-1345, **2008**.
http://www.journals.uchicago.edu/doi/pdf/10.1086/528835
The observations of the quiet Sun atmeter and decameter wavelengths show that its brightness temperatures can be_1 order of magnitude lower than the expected values of 106 K and the apparent diameters can be very large. We examine whether this unusual behavior is due to refraction in the smoothly varying coronal plasma and scattering by random density fluctuations using an improved Monte Carlo simulation technique.

MONTE CARLO SIMULATION OF DIRECTIVITY OF INTERPLANETARY RADIO BURSTS

G. **Thejappa**, R. J. MacDowall and M. L. Kaiser
The Astrophysical Journal, 671:894Y 906, **2007** December 10
http://www.journals.uchicago.edu/doi/pdf/10.1086/522664
We have developed aMonte Carlo simulation code to study the effects of refraction due to spatial variation of the solar wind density and scattering due to random density fluctuations on directivities, time profiles, and sizes and positions of the apparent sources of the interplanetary type II and type III radio bursts excited at the fundamental (F) and second harmonic (H) of the electron plasma frequency, fpe.We have focused on the 120 kHz fundamental and harmonic emissions with sources at the heliocentric distances of 0.2097AU(_115 kHz plasma level), and 0.3875AU (_60 kHz plasma level), respectively, and computed the distributions of trajectories of traced rays in a refracting, as well as a refracting and scattering, medium. These distributions show that (1) the scattering by random density fluctuations extends the visibilities of F and H components from _18_ to _90_, and from _80_ to _150_, respectively; (2) the time profiles constructed using the dispersion of the arrival times of the scattered rays at any given frequency may contain two peaks corresponding to F and H emissions, or a single peak consisting of both F and H components (fundamental followed by the harmonic), or a single H peak depending on the speed of the electron beam and the observer's location; and (3) the scattering broadens the sizes of the fundamental and harmonic point sources to _25_ and _37_, and by elevating their apparent radial distances to f /3 and f /2 levels, respectively.We also present simultaneous observations of a type II and a couple of type III radio bursts by Ulysses and Wind spacecraft separated by more than 100_ and show that the widely visible radio bursts correspond either to a scattered fundamental, to a refracted or scattered harmonic, or to a mixture of scattered fundamental and harmonic emissions.

Particle-in-cell simulations of the relaxation of electron beams in inhomogeneous solar wind plasmas

J.O. **Thurgood**, D. Tsiklauri
J. Plasma Phys. **2016**
http://astro.qmul.ac.uk/~tsiklauri/jtdt2.pdf
https://arxiv.org/pdf/1612.01780v1.pdfPrevious theoretical considerations of electron beam relaxation in inhomogeneous plasmas have indicated that the effects of the irregular solar wind may account for the poor agreement of homogeneous modelling with the observations. Quasi-linear theory and Hamiltonian models based on Zakharov?s equations have indicated that when the level of density fluctuations is above a given threshold, density irregularities act to de-resonate the beam?plasma interaction, restricting Langmuir wave growth on the expense of beam energy. This work presents the first fully kinetic particle-in-cell (PIC) simulations of beam relaxation under the influence of density irregularities. We aim to independently determine the influence of background inhomogeneity on the beam?plasma system, and to test theoretical predictions and alternative models using a fully kinetic treatment. We carry out one-

dimensional (1-D) PIC simulations of a bump-on-tail unstable electron beam in the presence of increasing levels of background inhomogeneity using the fully electromagnetic, relativistic EPOCH PIC code. We find that in the case of homogeneous background plasma density, Langmuir wave packets are generated at the resonant condition and then quasi-linear relaxation leads to a dynamic increase of wavenumbers generated. No electron acceleration is seen ? unlike in the inhomogeneous experiments, all of which produce high-energy electrons. For the inhomogeneous experiments we also observe the generation of backwards-propagating Langmuir waves, which is shown directly to be due to the refraction of the packets off the density gradients. In the case of higher-amplitude density fluctuations, similar features to the weaker cases are found, but also packets can also deviate from the expected dispersion curve in (omega,k)-space due to nonlinearity. Our fully kinetic PIC simulations broadly confirm the findings of quasi-linear theory and the Hamiltonian model based on Zakharov?s equations. Strong density fluctuations modify properties of excited Langmuir waves altering their dispersion properties.

Self-consistent particle-in-cell simulations of fundamental and harmonic plasma radio emission mechanisms

J.O. **Thurgood**, D. Tsiklauri
A&A 584, A83 **2015**
http://arxiv.org/pdf/1509.07004v1.pdf
Aims. The simulation of three-wave interaction based plasma emission, thought to be the underlying mechanism for Type III solar radio bursts, is a challenging task requiring fully-kinetic, multi-dimensional models. This paper aims to resolve a contradiction in past attempts, whereby some studies indicate that no such processes occur. Methods. We self-consistently simulate three-waved based plasma emission through all stages by using 2D, fully kinetic, electromagnetic particle-in-cell simulations of relaxing electron beams using the EPOCH2D code. Results. Here we present the results of two simulations; Run 1 (nb/n0 = 0.0057, vb/{\Delta}vb = vb/Ve = 16) and Run 2 (nb/n0 = 0.05, vb/{\Delta}vb = vb/Ve = 8), which we find to permit and prohibit plasma emission respectively. We show that the possibility of plasma emission is contingent upon the frequency of the initial electrostatic waves generated by the bump-in-tail instability, and that these waves may be prohibited from participating in the necessary three-wave interactions due to frequency conservation requirements. In resolving this apparent contradiction through a comprehensive analysis, in this paper we present the first self-consistent demonstration of fundamental and harmonic plasma emission from a single-beam system via fully kinetic numerical simulation. We caution against simulating astrophysical radio bursts using unrealistically dense beams (a common approach which reduces run time), as the resulting non-Langmiur characteristics of the initial wave modes significantly suppresses emission. Comparison of our results also indicates that, contrary to the suggestions of previous authors, an alternative plasma emission mechanism based on two counter-propagating beams is unnecessary in an astrophysical context.

Two-dimensional time evolution of beam-plasma instability in the presence of binary collisions

S. F. **Tigik**1, L. F. Ziebell1, P. H. Yoon2,3 and E. P. Kontar
A&A 586, A19 (**2016**) **Open Access**
http://www.aanda.org/articles/aa/pdf/2016/02/aa27271-15.pdf
Energetic electrons produced during solar flares are known to be responsible for generating solar type III radio bursts. The radio emission is a byproduct of Langmuir wave generation via beam-plasma interaction and nonlinear wave-wave and wave-particle interaction processes. In addition to type III radio bursts, electrons traveling downwards toward the chromosphere lead to the hard X-ray emission via electron-ion collisions. Recently, the role of Langmuir waves on the X-ray-producing electrons has been identified as important, because Langmuir waves may alter the electron distribution, thereby affecting the X-ray profile. Both Coulomb collisions and wave-particle interactions lead electrons to scattering and energy exchange that necessitates considering the two-dimensional (2D) problem in velocity space. The present paper investigates the influence of binary collisions on the beam-plasma instability development in 2D in order to elucidate the nonlinear dynamics of Langmuir waves and binary collisions. The significance of the present findings in the context of solar physics is discussed.

The Murchison Widefield Array: The Square Kilometre Array Precursor at Low Radio Frequencies

Tingay, S. J.; Goeke, R.; Bowman, J. D.; Emrich, D.; Ord, S. M.; …
Publications of the Astronomical Society of Australia, **2013**, Volume 30, id.e007 21 pp.
https://www.cambridge.org/core/services/aop-cambridge-core/content/view/S1323358012000070
https://arxiv.org/pdf/1206.6945.pdf
The Murchison Widefield Array (MWA) is one of three Square Kilometre Array Precursor telescopes and is located at the Murchison Radio-astronomy Observatory in the Murchison Shire of the mid-west of Western Australia, a location chosen for its extremely low levels of radio frequency interference. The MWA operates at low radio frequencies, 80-300 MHz, with a processed bandwidth of 30.72 MHz for both linear polarisations, and consists of 128 aperture arrays (known as tiles) distributed over a ~3-km diameter area. Novel hybrid hardware/software correlation and a real-time

imaging and calibration systems comprise the MWA signal processing backend. In this paper, the as-built MWA is described both at a system and sub-system level, the expected performance of the array is presented, and the science goals of the instrument are summarised.

The Murchison Widefield Array: solar science with the low frequency SKA Precursor

Tingay, S. J.; Oberoi, D.; Cairns, I.; Donea, A.; Duffin, R.; Arcus, W. ….
Journal of Physics: Conference Series, Volume 440, Issue 1, article id. 012033 (**2013**).
https://arxiv.org/pdf/1301.6414.pdf
https://iopscience.iop.org/article/10.1088/1742-6596/440/1/012033/pdf
The Murchison Widefield Array is a low frequency (80 - 300 MHz) SKA Precursor, comprising 128 aperture array elements (known as tiles) distributed over an area of 3 km diameter. The MWA is located at the extraordinarily radio quiet Murchison Radioastronomy Observatory in the mid-west of Western Australia, the selected home for the Phase 1 and Phase 2 SKA low frequency arrays. The MWA science goals include: 1) detection of fluctuations in the brightness temperature of the diffuse redshifted 21 cm line of neutral hydrogen from the epoch of reionisation; 2) studies of Galactic and extragalactic processes based on deep, confusion-limited surveys of the full sky visible to the array; 3) time domain astrophysics through exploration of the variable radio sky; and 4) solar imaging and characterisation of the heliosphere and ionosphere via propagation effects on background radio source emission. This paper concentrates on the capabilities of the MWA for solar science and summarises some of the solar science results to date, in advance of the initial operation of the final instrument in 2013.

Comments on “Effects of Strong Regular Refraction in the Solar Radio Pulse Structure in Spike Events” by Afanasiev and Altyntsev and “Mathematical Modeling of the Formation of Type IIId Solar Decameter Radio Bursts with Echo Components” by Afanasiev

M.V. **Tinin**
Solar Phys (**2008**) 247: 429–433
Presented are some comments on the papers by Afanasiev and Altyntsev (*Solar Phys.* **234**, 151, 2006) and by Afanasiev (*Solar Phys.* **238**, 87, 2006) devoted to the study of the influence of solar corona inhomogeneities on the form of radio bursts. It is pointed out that in these papers incorrect use is made of methods used previously in investigations into radio wave propagation through a randomly inhomogeneous ionosphere.

Harmonic radio emission in randomly inhomogeneous plasma

Anna **Tkachenko**, Vladimir Krasnoselskikh, Andrii Voshchepynets
ApJ **908** 126 **2021**
https://arxiv.org/pdf/2012.12773.pdf
https://doi.org/10.3847/1538-4357/abd2bd
In present paper, we describe a theoretical model of generation of harmonic emissions of type III solar radio bursts. The goal of our study is to fully take into account the most efficient physical processes participating in generation of harmonic electromagnetic emission via nonlinear coupling of Langmuir waves in randomly inhomogeneous plasma of solar wind ($l+l' \rightarrow t$). We revisit the conventional mechanism of coalescence of primarily generated and back-scattered Langmuir waves in quasihomogeneous plasma. Additionally, we propose and investigate another mechanism that generates the harmonic emission only in a strongly inhomogeneous plasma: the nonlinear coupling of incident and reflected Langmuir waves inside localized regions with enhanced plasma density (clumps), in the close vicinity of the reflection point. Both mechanisms imply the presence of strong density fluctuations in plasma. We use the results of a probabilistic model of beam-plasma interaction and evaluate the efficiency of energy transfer from Langmuir waves to harmonic emission. We infer that harmonic emissions from a quasihomogeneous plasma are significantly more intense than found in previous studies. The efficiency of Langmuir waves conversion into electromagnetic harmonic emission is expected to be higher at large heliospheric distances for the mechanism operating in quasihomogeneous plasma, and at small heliocentric distances - for the one operating in inhomogeneous. The evaluation of emission intensity in quasihomogeneous plasma may also be applied for type II solar radio bursts. The radiation pattern in both cases is quadrupolar, and we show that emission from density clumps may efficiently contribute to the visibility of harmonic radio emission.

Understanding the Relationship between Solar Coronal Abundances and F10.7 cm Radio Emission

Andy S.H. **To**, Alexander W. James, T. S. Bastian, Lidia van Driel-Gesztelyi, David M. Long, Deborah Baker, David H. Brooks, Samantha Lomuscio, David Stansby, Gherardo Valori
ApJ **2023**
https://arxiv.org/pdf/2304.02552.pdf
Sun-as-a-star coronal plasma composition, derived from full-Sun spectra, and the F10.7 radio flux (2.8 GHz) have been shown to be highly correlated (r = 0.88) during solar cycle 24. However, this correlation becomes nonlinear during increased solar magnetic activity. Here, we use co-temporal, high spatial resolution, multi-wavelength images of the

Sun to investigate the underlying causes of the non-linearity between coronal composition (FIP bias) and F10.7 solar index correlation. Using the Karl G. Jansky Very Large Array (JVLA), Hinode/EIS (EUV Imaging Spectrometer), and the Solar Dynamic Observatory (SDO), we observed a small active region, AR 12759, throughout the solar atmosphere from the photosphere to the corona. Results of this study show that the magnetic field strength (flux density) in active regions plays an important role in the variability of coronal abundances, and it is likely the main contributing factor to this non-linearity during increased solar activity. Coronal abundances above cool sunspots are lower than in dispersed magnetic plage regions. Strong magnetic concentrations are associated with stronger F10.7 cm gyroresonance emission. Considering that as the solar cycle moves from minimum to maximum, the size of sunspots and their field strength increase with gyroresonance component, the distinctly different tendencies of radio emission and coronal abundances in the vicinity of sunspots is the likely cause of saturation of Sun-as-a-star coronal abundances during solar maximum, while the F10.7 index remains well correlated with the sunspot number and other magnetic field proxies. **2020 April 3 and 7**

Optimization of Solar-Wind Speed Models Using Interplanetary Scintillation Observations.

Tokumaru, M., Fujiki, K. & Watanabe, H.
Sol Phys 299, 110 (**2024**).
https://doi.org/10.1007/s11207-024-02356-1
Improvement of the model providing the boundary condition of the solar-wind speed near the Sun is essential for gaining a better forecast of space weather. We optimized the parameters of the distance from the coronal hole boundary (DCHB) model and the Wang–Sheeley (WS) model, which enabled the determination of solar-wind speed from observations of the Sun's magnetic field. In this study, we used solar-wind speed data derived from interplanetary scintillation (IPS) observations at the Institute for Space-Earth Environmental Research (ISEE) for six Carrington rotations in Solar Cycle 23 as reference data. A comparison of IPS observations and optimized DCHB models demonstrated strong-to-moderate positive correlations and small deviations, except for solar maximum data. The degraded correlation at the solar maximum is ascribed to the effect of the rapid structural evolution of the solar wind and coronal magnetic field. The performance of the optimized DCHB model was better than that of the optimized WS model. To solve a limitation of the DCHB model in reproducing slow-wind speeds, we propose a modified version of the DCHB model and optimize it for IPS observations. The optimized solutions for the modified DCHB model demonstrate performance comparable to that of the original model. The results obtained in this study suggest that the DCHB acts better as a controlling parameter for the solar-wind speed than the expansion factor and that both the optimized DCHB model and its modified version are useful for improving the estimation of the solar-wind speed at the source surface from magnetograph observations.

Interplanetary Scintillation Observations of Solar-Wind Disturbances During Cycles 23 and 24

Munetoshi **Tokumaru**, Ken'ichi Fujiki & Kazumasa Iwai
Solar Physics volume 298, Article number: 22 (**2023**)
https://doi.org/10.1007/s11207-023-02116-7
Interplanetary scintillation (IPS) analysis is an effective technique for remotely sensing solar-wind disturbances, such as stream-interaction regions (SIRs) and coronal mass ejections (CMEs), which are the main drivers of space weather. Here, we employed 327-MHz IPS observations conducted at the Institute of Space–Earth Environmental Research, Nagoya University for the period of 1997 – 2019 to determine IPS indices that represent the density-fluctuation level of the inner heliosphere. We then compared these indices with the solar-wind density and speed measured near the Earth. Consequently, we found weak but significant positive correlations between the IPS indices and both the solar-wind density and speed gradient at a time lag of 0 days. This suggests that an increase in IPS indices corresponds to the arrival of the compression region associated with SIR or CME at the Earth, which is consistent with model calculations. Significant negative correlations were observed between the IPS and disturbance storm time (Dst) indices at a time lag of a few days; however, the correlations were too weak to enable reliable predictions of space weather. Possible reasons for these weak correlations are also discussed. Using the IPS indices, we determined the solar-cycle variation in the occurrence rate of solar-wind disturbances for the analysis period. The occurrence rates exhibited two maxima corresponding to the solar maximum and minimum, which are generally consistent with the combined effects of CME and SIR. The lower occurrence rates in Cycle 24 than in Cycle 23 reflect a weaker solar activity. These results suggest that the proposed IPS indices are useful for studying the long-term characteristics of solar-wind disturbances.

Coronal Density Measurements Using Giant Radio Pulses of the Crab Pulsar at the Cycle 24/25 Minimum

Munetoshi **Tokumaru**, Ryuya Maeda, Kaito Tawara, Kazuhiro Takefuji & Toshio Terasawa
Solar Physics volume 297, Article number: 10 (**2022**)
https://link.springer.com/content/pdf/10.1007/s11207-021-01939-6.pdf
Accurate measurements of the coronal plasma density profile, which varies with the solar cycle (SC), are necessary to elucidate the solar wind acceleration. In this study, the Crab pulsar is observed using the 327 MHz radio telescope at the

Toyokawa Observatory of the Institute for Space-Earth Environmental Research of Nagoya University to investigate the coronal plasma density profile for radial distances between 5 and 60 solar radii at the SC24/25 minimum. We derive the dispersion measures (DMs) that represent the integration of plasma density along the line of sight (LOS) for giant radio pulses of the Crab pulsar. We find that the observed DMs increased above the interstellar background level when the LOS for the Crab pulsar approached the Sun in mid-June 2018 and 2019. This increase in DM is attributed to the effect of the coronal plasma. We determine the plasma density distribution by fitting a spherically symmetric model to the observed DM data. The flat radial slopes of the best-fit model are consistent with pulsar observations in the low-activity periods of past SCs, and they are attributed to the effect of the coronal hole over the south pole of the Sun. Our results show that the density level near the Sun is similar to those observed in the low activity periods of past SCs, implying recovery of the coronal plasma density from a significant reduction at the SC23/24 minimum.

Radio Sounding Measurements of the Solar Corona Using Giant Pulses of the Crab Pulsar in 2018

Munetoshi **Tokumaru**, Kaito Tawara, Kazuhiro Takefuji, Mamoru Sekido & Toshio Terasawa
Solar Physics volume 295, Article number: 80 (**2020**)
https://link.springer.com/content/pdf/10.1007/s11207-020-01644-w.pdf
Observations of the Crab pulsar at 327 MHz were made at the Toyokawa Observatory of the Institute for Space-Earth Environmental Research, during the solar occultation in mid-June 2018 to investigate the coronal plasma density in the weak sunspot cycle, Cycle 24. The dispersion measurements (DMs) were determined using giant pulses detected from observations of the Crab pulsar. The systematic increase in DM over the background level, observed during the period of the closest approach of the Crab pulsar's line-of-sight to the Sun, was ascribed to the effect of the coronal plasma. A coronal density model assuming spherical symmetry was determined by fitting it to the DM data, and was compared with those determined in past solar cycles. The best-fit model had large errors, and indicated a systematically higher value than those derived from past observations. The results obtained here are likely to be significantly affected by latitude/longitude variation in coronal plasma density, the time variation of the interstellar medium, mainly the Crab nebula, and increased measurement errors due to the reduced occurrence of giant pulses. Hence, further observations are needed to derive conclusions about a change of coronal density in the current cycle. **15 – 16 June 2018**

Auroral Kilometric Radiation and Electron Pairing

Rudolf A. **Treumann**1,2 and Wolfgang Baumjohann3*
Front. Phys., September **2020**
https://doi.org/10.3389/fphy.2020.00386
https://www.frontiersin.org/articles/10.3389/fphy.2020.00386/full
We suggest that pairing of bouncing medium-energy electrons in the auroral upward current region close to the mirror points may play a role in driving the electron cyclotron maser instability to generate an escaping narrow band fine structure in the auroral kilometric radiation. We treat this mechanism in the gyrotron approximation, for simplicity using the extreme case of a weakly relativistic Dirac distribution instead the more realistic anisotropic Jüttner distribution. Promising estimates of bandwidth, frequency drift and spatial location are given.

Electron cyclotron maser instability (ECMI) in strong magnetic guide field reconnection

R. A. **Treumann**, W. Baumjohann
2017 Annales Geophysicae, Volume 35, Issue 4, pp.999-1013
https://arxiv.org/pdf/1701.06961v1.pdf
https://angeo.copernicus.org/articles/35/999/2017/angeo-35-999-2017.pdf
Reconnection in strong current-aligned magnetic guide fields allows for the excitation of the electron-cyclotron-maser instability and emission of electromagnetic radiationfrom the electron exhaust at the {\sf X} point. The electrons in the guide field remain magnetized, with reconnection barely affected. The guide field is responsible for the asymmetric properties of the {\sf X} point and exhaust. Asymmetry in the electron population results in conditions favorable for ECMI. Fundamental mission beneath the guide field cyclotron is similar to electron hole emission discussed elsewhere. It can be treated in the proper exhaust frame, and maps the local magnetic field when moving together with the exhaust along the guide field. Many applications of this mechanism can be imagined. We propose an outline of the mechanism and discuss some of its advantages and prospects. Among potential applications are AKR in auroral physics, various types of solar radio emissions during flares, planetary emissions and several astrophysical scenarios involving the presence of strong fields and field-aligned currents. Escape of radiation from {\sf X} is no problem. However, observation from remote requires traversing the stop-band of X modes and implies source displacements to weaker fields.

Fundamentals of collisionless shocks for astrophysical application,

1. Non-relativistic shocks

R. A. **Treumann**

Astronomy and Astrophysics Review, Volume 17, Number 4, p. 409-535, **2009**

A comprehensive review is given of the theory and properties of nonrelativistic shocks in hot collisionless plasmas—in view of their possible application in astrophysics. Understanding non-relativistic collisionless shocks is an indispensable step towards a general account of collisionless astrophysical shocks of high Mach number and of their effects in dissipating flow-energy, in heating matter, in accelerating particles to high—presumably cosmic-ray—energies, and in generating detectable radiation from radio to X-rays. Non-relativistic shocks have Alfvénic Mach numbers $M_A \ll \sqrt{m_i/m_e}(\omega_{pe}/\omega_{ce})$, where m_i/m_e is the ion-to-electron mass ratio, and ω_{pe}, ω_{ce} are the electron plasma and cyclotron frequencies, respectively. Though high, the temperatures of such shocks are limited (in energy units) to $T < m_e c^2$. This means that particle creation is inhibited, classical theory is applicable, and reaction of radiation on the dynamics of the shock can be neglected. The majority of such shocks are supercritical, meaning that non-relativistic shocks are unable to self-consistently produce sufficient dissipation and, thus, to sustain a stationary shock transition. As a consequence, supercritical shocks act as efficient particle reflectors. All these shocks are microscopically thin, with shock-transition width of the order of the ion inertial length $\lambda_i = c/\omega_{pi}$ (with ω_{pi} the ion plasma frequency). The full theory of such shocks is developed, and the different possible types of shocks are defined. Since all collisionless shocks are magnetised, the most important distinction is between quasi-perpendicular and quasi-parallel shocks. The former propagate about perpendicularly, the latter roughly parallel to the upstream magnetic field. Their manifestly different behaviours are described in detail. In particular, although both types of shocks are non-stationary, they have completely different reformation cycles. From numerical full-particle simulations it becomes evident that, on ion-inertial scales close to the shock transition, all quasi-parallel collisionless supercritical shocks are locally quasi-perpendicular. This property is of vital importance for the particle dynamics near the quasi-parallel shock front. Considerable interest focusses on particle acceleration and the generation of radiation. Radiation from non-relativistic shocks results mainly in wave–wave interactions among various plasma waves. Non-thermal charged particles can be further accelerated to high energies by a Fermi-like mechanism. The important question is whether the shock can pre-accelerate shock-reflected particles to sufficiently high energies in order to create the seed-population of the non-thermal particles required by the Fermi mechanism. Based on preliminary full-particle numerical simulations, this question is answered affirmatively. Such simulations provide ample evidence that collisionless shocks with high-Mach numbers—even when non-relativistic—could probably by themselves produce the energetic seed-particle population for the Fermi-process.

Origin of the 30 THz emission detected during the 2012 March 13 solar flare at 17:20 UT

G. **Trottet**, J.-P. Raulin, A. MacKinnon, G. Giménez de Castro, P.J.A. Simões, D. Cabezas, V. de La Luz, M. Luoni, P. Kaufmann

Solar Phys. Volume 290, Issue 10, pp 2809-2826 **2015**

http://arxiv.org/pdf/1509.06336v1.pdf

Solar observations in the infrared domain can bring important clues on the response of the low solar atmosphere to primary energy released during flares. At present the infrared continuum has been detected at 30 THz (10 μm) in only a few flares. In this work we present a detailed multi-frequency analysis of SOL2012-03-13, including observations at radio millimeter and sub-millimeter wavelengths, in hard X-rays (HXR), gamma-rays (GR), H-alpha, and white-light. HXR/GR spectral analysis shows that the event is a GR line flare and allows estimating the numbers of and energy contents in electrons, protons and alpha particles produced during the flare. The energy spectrum of the electrons producing the HXR/GR continuum is consistent with a broken power-law with an energy break at ~800 keV. It is shown that the high-energy part (above ~800 keV) of this distribution is responsible for the high-frequency radio emission (> 20 GHz) detected during the flare. By comparing the 30 THz emission expected from semi-empirical and time-independent models of the quiet and flare atmospheres, we find that most (~80%) of the observed 30 THz radiation can be attributed to thermal free-free emission of an optically-thin source. Using the F2 flare atmospheric model this thin source is found to be at temperatures T~8000 K and is located well above the minimum temperature region. We argue that the chromospheric heating, which results in 80% of the 30 THz excess radiation, can be due to energy deposition by non-thermal flare accelerated electrons, protons and alpha particles. The remaining 20% of the 30 THz excess emission is found to be radiated from an optically-thick atmospheric layer at T~5000 K, below the temperature minimum region, where direct heating by non-thermal particles is insufficient to account for the observed infrared radiation.

Far infrared solar physics **Review**

G. **Trottet** and K.-L. Klein

Memorie della Societa Astronomica Italiana, v.84, p.405 (**2013**)

http://sait.oat.ts.astro.it/MmSAI/84/PDF/405.pdf

Measurements of the far infrared (FIR) continuum from stratospheric balloons or aircraft have addressed the temperature structure of the solar chromosphere in both the quiet Sun and non-flaring active regions. Although submillimeter observations of flares have been obtained over the past ten years, the infrared spectrum of solar flares is still unknown over a wavelength range of more than two orders of magnitude. We outline that spectral and imaging measurements in the FIR continuum, which extend those obtained at submillimeter wavelengths, constitute new key diagnostics of processes relating to the acceleration of relativistic electrons and ions and to the energy transport and deposition in flares. We briefly describe pioneer instrumental concepts studied to open the FIR domain to flare observations. Finally we emphasize the need of a future solar-dedicated mission, performing joint spectral and imaging observations from the FIR domain to high energy gamma-rays, in order to get a complete picture of particle acceleration and energy transport during flares.

Origin of the Submillimeter Radio Emission During the Time-Extended Phase of a Solar Flare

G. **Trottet**, J.-P. Raulin, G. Giménez de Castro, T. Lüthi, A. Caspi, C. H. Mandrini, M. L. Luoni and P. Kaufmann

Solar Physics, Volume 273, Number 2, 339-361, **2011**

sci-hub.se/10.1007/s11207-011-9875-6

Solar flares observed in the 200 – 400 GHz radio domain may exhibit a slowly varying and time-extended component which follows a short (few minutes) impulsive phase and can last for a few tens of minutes to more than one hour. The few examples discussed in the literature indicate that such long-lasting submillimeter emission is most likely thermal bremsstrahlung. We present a detailed analysis of the time-extended phase of the **27 October 2003 (M6.7)** flare, combining 1 – 345 GHz total-flux radio measurements with X-ray, EUV, and Hα observations. We find that the time-extended radio emission is, as expected, radiated by thermal bremsstrahlung. Up to 230 GHz, it is entirely produced in the corona by hot and cool materials at 7 – 16 MK and 1 – 3 MK, respectively. At 345 GHz, there is an additional contribution from chromospheric material at a few 104 K. These results, which may also apply to other millimeter–submillimeter radio events, are not consistent with the expectations from standard semiempirical models of the chromosphere and transition region during flares, which predict observable radio emission from the chromosphere at all frequencies where the corona is transparent.

Radio Submillimeter and Gamma-ray Observations of the 2003 October 28 Solar Flare

G. **Trottet**, S. Krucker, T. Luthi, A. Magun

E-print, Dec 2007; Ap.J. 678:509-514, **2008**

http://www.journals.uchicago.edu/doi/pdf/10.1086/528787

Radio observations at 210~GHz taken by the BErnese Multibeam RAdiometer for KOSMA (BEMRAK) are combined with hard X-ray and gamma-ray observations from the SONG instrument onboard CORONA-F and the Reuven Ramaty High Energy Solar Spectroscopic Imager (RHESSI) to investigate high energy particle acceleration during the energetic solar flare of 2003 October 28. Two distinct components at submillimeter wavelengths are found. The first is a gradual, long-lasting (>30 min) component with large apparent source sizes (~60 arcsec). Its spectrum below ~200 GHz is consistent with synchrotron emission from flare-accelerated electrons producing hard X-ray and $gamma$-ray bremsstrahlung assuming a magnetic field strength of >200 G in the radio source and a confinement time of the radio-emitting electrons in the source of less than 30 s. At even higher frequencies, the spectrum deviates from synchrotron emission and is increasing with frequency, as also seen in other large flares, but the interpretation is unclear. The other component is impulsive and starts simultaneously with high energy (>200 MeV/nucleon) proton acceleration and the production of pions. The derived radio source size is compact (<10 arcsec) and, within the uncertainties, the emission is co-spatial with the location of precipitating flare-accelerated >30 MeV protons as seen in Gamma-ray imaging of the 2.2 MeV line emission. The close correlation in time and space of radio emission with the production of pions suggests that synchrotron emission of positrons produced in charged-pion decay might be responsible for the observed compact radio source. However, order-of-magnitude approximations rather suggest that the derived numbers of positrons from charged-pion decay are probably too small compared to what is needed to produce the observed radio emission. Synchrotron emission from energetic electrons therefore appears as the most likely emission mechanism for the compact radio source seen in the impulsive phase although it does not account for its close correlation, in time and space, with pion production.

Sub-Terahertz Radiation Features from the Flare of Proxima Cen.

Tsap, Y.T., Stepanov, A.V. & Kopylova, Y.G.

Geomagn. Aeron. 63, 937–941 (**2023**).

https://doi.org/10.1134/S001679322307023X

A comparative analysis of stellar and solar flares at millimeter wavelength range has been carried out using the red dwarf Proxima Centauri as an example. The main attention is paid to the results of ALMA observations, which show that the flux of sub-THz radiation from stellar flares is an order of magnitude greater than that for solar flares, decreases with radiation frequency, and has a degree of linear polarization reaching tens of percent. We showed that the

synchrotron mechanism is responsible for the sub-THz radiation, which assumes the acceleration of electrons to ultrarelativistic energies. The observed relationship between sub-THz, radio, and X-ray emission from stellar flares is discussed. The hypothesis about the important role of flare energy release in the dense layers of the stellar atmosphere is substantiated.

Millimeter and X-Ray Emission from the 5 July 2012 Solar Flare

Y. T. **Tsap**, V. V. Smirnova, G. G. Motorina, A. S. Morgachev, S. A. Kuznetsov, V. G. Nagnibeda, V. S. Ryzhov

Solar Physics March **2018**, 293:50

http://sci-hub.tw/http://link.springer.com/10.1007/s11207-018-1269-6

The **5 July 2012** solar flare SOL2012-07-05T11:44 (11:39 – 11:49 UT) with an increasing millimeter spectrum between 93 and 140 GHz is considered. We use space and ground-based observations in X-ray, extreme ultraviolet, microwave, and millimeter wave ranges obtained with the Reuven Ramaty High-Energy Solar Spectroscopic Imager, Solar Dynamics Observatory(SDO), Geostationary Operational Environmental Satellite, Radio Solar Telescope Network, and Bauman Moscow State Technical University millimeter radio telescope RT-7.5. The main parameters of thermal and accelerated electrons were determined through X-ray spectral fitting assuming the homogeneous thermal source and thick-target model. From the data of the Atmospheric Imaging Assembly/SDO and differential-emission-measure calculations it is shown that the thermal coronal plasma gives a negligible contribution to the millimeter flare emission. Model calculations suggest that the observed increase of millimeter spectral flux with frequency is determined by gyrosynchrotron emission of high-energy (≳300≳300 keV) electrons in the chromosphere. The consequences of the results are discussed in the light of the flare-energy-release mechanisms.

Thermal plasma diagnostics and the origin of sub-THz solar bursts

Yuriy **Tsap**_y1,2, Galina Motorina_z2, Viktoria Smirnovax2,3, Alexander Morgachev{2,4, Valeriy Nagnibedak5, Sergey Kuznetsov__2,4, and Vladimir Ryzhovyy6

CESRA **2016**, p.101

http://cesra2016.sciencesconf.org/conference/cesra2016/pages/CESRA2016_prog_abs_book_v3.pdf

Solar ares on the **4 and 5 July 2012** observed with GOES, SDO, RHESSI, and the Bauman Moscow State Technical University Radio RT-7.5 are considered. Sub-THz uxes increases with frequency between 93 and 140 GHz for both events. Diagnostics of low energy (20-100 keV) accelerated electrons using RHESSI X-ray observations and collisional thick target model was carried out. As it follows from AIA/SDO regularization technique for recovering the di_erential emission measure thermal plasma with the temperature > 0.5 MK can not be responsible for the observed millimeter free-free emission due to the low spectral uxes. This contradicts calculations of millimeter emission for the isothermal model based on GOES observations. Both di_erent sensitivity of instruments onboard these satellites with respect to the temperature and the multi-thermal nature of are plasma could explain the obtained discrepancy. Numerical calculations have shown that a positive spectral slope of millimeter emission from the 4 and 5 July 2012 solar ares can be caused by the free-free emission of plasma with the temperature about 0.1 MK and the generation of gyrosynchrotron emission of high energy (> 100 keV) electrons in the solar chromosphere, respectively. The detailed analysis of spatial and temporal evolution of hard X-ray emission has shown that non-thermal pulsations from the 5 July 2012 solar are are connected with the displacement of the sources during the are energy release. The probable mechanisms of electron acceleration in solar ares in the light of the planning of solar ALMA observations are discussed.

On the origin of 140 GHz emission from the 4 July 2012 solar flare

Yuriy T. **Tsap**, Victoria V. Smirnova, Alexander S. Morgachev, Galina G. Motorina, Eduard P. Kontar, Valery G. Nagnibeda, Polina V. Strekalova

Advances in Space Research, V. 57, I. 7, p. 1449-1455 **2016**; DOI: 10.1016/j.asr.2015.12.037

http://arxiv.org/pdf/1604.01530v1.pdf

The sub-THz event observed on the **4 July 2012** with the Bauman Moscow State Technical University Radio Telescope RT-7.5 at 93 and 140~GHz as well as Kislovodsk and Metsahovi radio telescopes, Radio Solar Telescope Network (RSTN), GOES, RHESSI, and SDO orbital stations is analyzed. The spectral flux between 93 and 140 GHz has been observed increasing with frequency. On the basis of the SDO/AIA data the differential emission measure has been calculated. It is shown that the thermal coronal plasma with the temperature above 0.5~MK cannot be responsible for the observed sub-THz flare emission. The non-thermal gyrosynchrotron mechanism can be responsible for the microwave emission near 10~GHz but the observed millimeter spectral characteristics are likely to be produced by the thermal bremsstrahlung emission from plasma with a temperature of about 0.1~MK.

See CESRA Highlight #767 2016 http://cesra.net/?p=767

Chromospheric evaporation and pitch angle diffusion of trapped electrons in solar flare coronal loops

Yuriy T. **Tsap**, Yulia G. Kopylov, , Alexander V. Stepanov
Advances in Space Research, **2014**
The peculiarities of time delays between the peaks of hard X-ray and microwave emissions within the framework of the trap-plus-precipitation model are studied. Using the continuity equation it has been shown that time delays strongly depend on the chromospheric evaporation in the case of the Coulomb pitch angle diffusion of trapped electrons into the loss–cone. Based on the obtained results the origin of time delays as well as the role of Coulomb collisions in flare coronal loops are discussed.

Acceleration of solar cosmic rays and the fine spectral structure of type II radio bursts

Yu. T. **Tsap**, E. A. Isaeva
Cosmic Research, March **2013**, Volume 51, Issue 2, pp 108-113, **File**
Kosmicheskie Issledovaniya, **2013**, Vol. 51, No. 2, pp. 119–124.
On the basis of data, obtained by means of the ground-based solar service RSTN (Radio Solar Telescope Network) and the geostationary satellite system GOES, the relationship between the solar cosmic rays (SCR) intensity I p with the proton energy **E p > 1 MeV** and parameters of meter-decameter type II radio bursts in the frequency range of 25–180 MHz is studied. The process of proton acceleration by shock waves was characterized by the frequency drift velocity of radio bursts V mII and the relative difference between radio emission frequencies at the first two harmonics b. It is shown that the coefficient of correlation between I p and b increases with E p growing from 0.40 to 0.70, while a similar coefficient between I p and V mII does not exceed 0.30. Indications in favor of the two-stage SCR acceleration model are obtained. **Table:2000-2006**

Oscillating Magnetic Trap and Non-Thermal Emission from Solar Flares

Y. **Tsap**, Y. Kopylova, T. Goldvarg, and A. Stepanov
Publ. Astron. Soc. Japan 65, No. SP1, S6 [6 pages] (**2013**)
http://pasj.asj.or.jp/v65/sp1/65S006/65S006.pdf
A comparative analysis of the fine time structure of microwave and hard X-ray emissions from the flare event on **1992 November 5** is given. Based on wavelet analysis, quasi-periodic pulsations with a fundamental period of 6 s in both wave bands have been revealed. The anticorrelation of time profiles of microwave and hard X-ray emissions as well as time delays between the emission peaks in different wave bands are explained by the excitation of sausage oscillations of a flare loop modelling by a magnetic trap. It has been shown that the intermediate pitch angle diffusion regime of trapped electrons into the loss-cone should be realized in flare loops. The relation between time delays of emission peaks at different wave bands and the pulse duration has been investigated.

Microwave observations of compact radio sources during solar eclipses on RT-22

Yu. T. **Tsap**, L. I. Tsvetkov & S. A. Samis'ko
Astronomy Letters, Vol. 37, Issue 1, **2011**

Self-consistent particle-in-cell simulations of fundamental and harmonic radio plasma emission mechanisms

David **Tsiklauri**∗1 and Jonathan Thurgood2
CESRA Abstract **2016**
http://cesra2016.sciencesconf.org/conference/cesra2016/pages/CESRA2016_prog_abs_book_v1.pdf
Aims. The simulation of three-wave interaction based plasma emission, thought to be the underlying mechanism for Type III solar radio bursts, is a challenging task requiring fully-kinetic, multi-dimensional models. This paper aims to resolve a contradiction in past attempts, whereby some studies indicate that no such processes occur. Methods. We self-consistently simulate three-wave based plasma emission through all stages by using 2D, fully kinetic, electromagnetic particle-in-cell simulations of relaxing electron beams using the EPOCH2D code. Results. Here we present the results of two simulations; Run 1 (nb/n0 = 0.0057, vb/ Δvb = vb/V e = 16) and Run 2 (nb/n0 = 0.05, vb/ Δvb = vb/V e = 8), which we find to permit and prohibit plasma emission respectively. We show that the possibility of plasma emission is contingent upon the frequency of the initial electrostatic waves generated by the bump-in-tail instability, and that these waves may be prohibited from participating in the necessary three-wave interactions due to frequency conservation requirements. In resolving this apparent contradiction through a comprehensive analysis, in this paper we present the first self-consistent demonstration of fundamental and harmonic plasma emission from a single-beam system via fully kinetic numerical simulation. We caution against simulating astrophysical radio bursts using unrealistically dense beams (a common approach which reduces run time), as the resulting non-Langmuir characteristics of the initial wave

modes significantly suppresses emission. Comparison of our results also indicates that, contrary to the suggestions of previous authors, an alternative plasma emission mechanism based on two counter-propagating beams is unnecessary in an astrophysical context. Finally, we also consider the action of the Weibel instability which generates an electromagnetic beam mode. As this provides a stronger contribution to electromagnetic energy than the emission, we stress that evidence of plasma emission in simulations must disentangle the two contributions and not simply interpret changes in total electromagnetic energy as evidence of plasma emission.
J.O. **Thurgood**, D. Tsiklauri, "**Self-consistent particle-in-cell simulations of fundamental and harmonic radio plasma emission mechanisms**", Astron. Astrophys. 584, A83 (**2015**)

An alternative to the plasma emission model: Particle-in-cell, self-consistent electromagnetic wave emission simulations of solar type III radio bursts

David **Tsiklauri**

Physics of Plasmas, Volume 18, Issue 5, pp. 052903-052903-15 (**2011**).

http://arxiv.org/abs/1011.5832

High-resolution (sub-Debye length grid size and 10 000 particle species per cell), 1.5D particle-in-cell, relativistic, fully electromagnetic simulations are used to model electromagnetic wave emission generation in the context of solar type III radio bursts. The model studies generation of electromagnetic waves by a super-thermal, hot beam of electrons injected into a plasma thread that contains uniform longitudinal magnetic field and a parabolic density gradient. In effect, a single magnetic line connecting Sun to Earth is considered, for which five cases are studied. (i) We find that the physical system without a beam is stable and only low amplitude level electromagnetic drift waves (noise) are excited. (ii) The beam injection direction is controlled by setting either longitudinal or oblique electron initial drift speed, i.e., by setting the beam pitch angle (the angle between the beam velocity vector and the direction of background magnetic field). In the case of zero pitch angle, i.e., when vvec b.Evec $\perp$=0, the beam excites only electrostatic, standing waves, oscillating at local plasma frequency, in the beam injection spatial location, and only low level electromagnetic drift wave noise is also generated. (iii) In the case of oblique beam pitch angles, i.e., when vvec b.Evec $\perp$=0, again electrostatic waves with same properties are excited. However, now the beam also generates the electromagnetic waves with the properties commensurate to type III radio bursts. The latter is evidenced by the wavelet analysis of transverse electric field component, which shows that as the beam moves to the regions of lower density and hence lower plasma frequency, frequency of the electromagnetic waves drops accordingly. (iv) When the density gradient is removed, an electron beam with an oblique pitch angle still generates the electromagnetic radiation. However, in the latter case no frequency decrease is seen. (v) Since in most of the presented results, the ratio of electron plasma and cyclotron frequencies is close to unity near the beam injection location, in order to prove that the electromagnetic emission, generated by the non-zero pitch angle beam, oscillates at the plasma frequency, we also consider a case when the magnetic field (and the cyclotron frequency) is ten times smaller. Within the limitations of the model, the study presents the first attempt to produce synthetic (simulated) dynamical spectrum of the type III radio bursts in the fully kinetic plasma model. The latter is based on 1.5D non-zero pitch angle (non-gyrotropic) electron beam that is an alternative to the plasma emission classical mechanism for which two spatial dimensions are needed.

Vlasov-Maxwell, self-consistent electromagnetic wave emission simulations of type III solar radio bursts

David **Tsiklauri**

E-print, Aug **2010**, Solar Phys.

1.5D Vlasov-Maxwell simulations are employed to model electromagnetic emission generation in a fully self-consistent plasma kinetic model for the first time in the solar physics context. The simulations mimic the plasma emission mechanism and Larmor drift instability in a plasma thread that connects the Sun to Earth with the spatial scales compressed appropriately. The effects of spatial density gradients on the generation of electromagnetic radiation are investigated. It is shown that 1.5D inhomogeneous plasma with a uniform background magnetic field directed transverse to the density gradient is aperiodically unstable to Larmor-drift instability. The latter results in a novel effect of generation of electromagnetic emission at plasma frequency. When density gradient is removed (i.e. when plasma becomes stable to Larmor-drift instability) and a *low* density, super-thermal, hot beam is injected along the domain, in the direction perpendicular to the magnetic field, plasma emission mechanism generates non-escaping Langmuir type oscillations which in turn generate escaping electromagnetic radiation. It is found that in the spatial location where the beam is injected, the standing waves, oscillating at the plasma frequency, are excited. These can be used to interpret the horizontal strips observed in some dynamical spectra. Quasilinear theory predictions: (i) the electron free streaming and (ii) the beam long relaxation time, in accord with the analytic expressions, are corroborated via direct, fully-kinetic simulation. Finally, the interplay of Larmor-drift instability and plasma emission mechanism is studied by considering *dense* electron beam in the Larmor-drift unstable (inhomogeneous) plasma. The latter case enables one to study the deviations from the quasilinear theory. Supplementary material: * http://www.maths.qmul.ac.uk/~tsiklauri/movie1.mpg * http://www.maths.qmul.ac.uk/~tsiklauri/movie2.mpg * http://www.maths.qmul.ac.uk/~tsiklauri/movie3.mpg

Observation of Solar Radio Waves by CALLISTO Radio Spectrometer in Ibaraki University

Natsuki **Tsuda**, Satoshi
2017 ISWI Newsletter - Vol. 9 No. 010
ISWI Newsletter - Vol. 10 No. 006**, 2018**
http://files.mail-list.com/m/iswinewsletter/Observation-of-Solar-Radio-Waves-by-CALLISTO-Radio-Spectrometer-final-final.pdf
http://files.mail-list.com/m/iswinewsletter/ibaraki-CALLISTO.pdf
In the Sun, sudden explosion phenomena called solar flare occur and characteristic electromagnetic waves are emitted, but details of radiation mechanisms are not known. There are 5 types of solar radio bursts cause of solar flare, classified from time change of radio waves.
Solar radio type-III bursts appear in several kilo hertz to several giga hertz frequencies and they are characterized by a rapid frequency drift from high to low frequencies. These radio waves are emitted by high energy electron streams accelerated by solar flare. In Ibaraki University, we observe solar radio waves by CALLISTO radio spectrometer and meter wave band log-periodic antenna to understand generating progress of high energy electrons from solar flare.
C8 class flare occurred in **April 2nd, 2017** and we succeeded in the observation of solar radio type-III burst from this flare. This successful observation is the first observation using CALLISTO in Japan. Now we will analyze the data and compare with the data acquired at other observatories.

A New Look at Type III Bursts and their Use as Coronal Diagnostics

Samuel **Tun** Beltran, Sean Cutchin, Stephen White
2015 Solar Physics, Volume 290, Issue 9, pp 2423-2437
http://arxiv.org/ftp/arxiv/papers/1508/1508.00206.pdf
We present meter wave solar radio spectra of the highest spectrotemporal resolution achieved to date. The observations, obtained with the first station of the Long Wavelength Array (LWA1), show unprecedented detail of solar emissions across a wide bandwidth during a Type III/IIIb storm. Our flux calibration demonstrates that the LWA1 can detect Type III bursts much weaker than 1 SFU, much lower than previous observations, and that the distribution of fluxes in these bursts varies with frequency. The high sensitivity and low noise in the data provide strong constraints to models of this type of plasma emission. The continuous generation of electron beams in the corona revealed by the high density Type III storm is evidence for ubiquitous magnetic reconnection in the lower corona. Such an abundance of reconnection events not only contributes to the total coronal energy budget, but also provides an engine by which to form the populations of seed particles responsible for proton-rich solar energetic particle events. An active region with such levels of reconnection and the accompanying type III/IIIb storms is here proposed to be associated with an increase of SEP production if a CME erupts. The data's constraints on existing theories of type IIIIb production are used to make an association of the observed type IIIb storm to specific electron beam paths with increased inhomogeneities in density, temperature, and or turbulence. This scenario ties in the observed timing of III and IIIb storms, constrained theories of type III and IIIb emission, and the ability of the emitting AR to produce a strong SEP event. The result requires but a single observable to cement these ideas, the statistical correlation of type III/IIIb activity with SEP-productive AR.
12 – 15 April 2013

DERIVATION OF THE MAGNETIC FIELD IN A CORONAL MASS EJECTION CORE VIA MULTI-FREQUENCY RADIO IMAGING

Samuel D. **Tun**1,3 and A. Vourlidas2
2013 *ApJ* **766** 130
sci-hub.se/10.1088/0004-637x/766/2/130
The magnetic field within the core of a coronal mass ejection (CME) on **2010 August 14** is derived from analysis of multi-wavelength radio imaging data. This CME's core was found to be the source of a moving type IV radio burst, whose emission is here determined to arise from the gyrosynchrotron process. The CME core's true trajectory, electron density, and line-of-sight depth are derived from stereoscopic observations, constraining these parameters in the radio emission models. We find that the CME carries a substantial amount of mildly relativistic electrons (E < 100 keV) in a strong magnetic field (B < 15 G), and that the spectra at lower heights are preferentially suppressed at lower frequencies through absorption from thermal electrons. We discuss the results in light of previous moving type IV burst studies, and outline a plan for the eventual use of radio methods for CME magnetic field diagnostics.

THREE-DIMENSIONAL STRUCTURE OF A SOLAR ACTIVE REGION FROM SPATIALLY AND SPECTRALLY RESOLVED MICROWAVE OBSERVATIONS

Samuel D. **Tun**1, Dale E. Gary1, and Manolis K. Georgoulis2
Astrophysical Journal, 728:1 (16pp), **2011** February
We report on the structure of the solar atmosphere above active region (AR) 10923, observed on **2006 November 10**, as deduced from multi-wavelength studies including combined microwave observations from the Very Large Array

(VLA) and the Owens Valley Solar Array (OVSA). The VLA observations provide excellent image quality at a few widely spaced frequencies, while the OVSA data provide information at many intermediate frequencies to fill in the spectral coverage. Images at 25 distinct frequencies are used to provide spatially resolved spectra along many lines of sight in the AR, from which microwave spectral diagnostics are obtained for deducing maps of temperature, magnetic field, and column density. The derived quantities are compared with multiwavelength observations from the *Solar and Heliospheric Observatory* and *Hinode* spacecraft, and with a current-free magnetic field extrapolation. We find that a two-component temperature model is required to fit the data, in which a hot (>2MK) lower corona above the strong-field plage and sunspot regions (emitting via the gyroresonance process) is overlaid with somewhat cooler (~1MK) coronal loops that partially absorb the gyroresonance emission through the free–free (Bremsstrahlung) process. We also find that the extrapolated potential magnetic fields can quantitatively account for the observed gyroresonance emission over most of the AR, but in a few areas a higher field strength is required. The results are used to explore the coronal configuration needed to explain the observations. These results show that the bulk of free–free emission in both radio and X-rays emanates from two loop systems, distinguished by the location of their loop footpoints.We discuss the implications of such comparisons for studies of AR structure when better microwave spectral imaging becomes available in the future.

A Statistical Study of Microwave Flare Morphologies

V. **Tzatzakis** · A. Nindos · C.E. Alissandrakis
Solar Phys (**2008**) 253: 79–94, DOI 10.1007/s11207-008-9263-z
This study has been motivated by the detection of a small number of optically thin microwave bursts with maximum emission near the loop top, which is contrary to the prediction of isotropic gyrosynchrotron models. Using Nobeyama Radioheliograph (NoRH) high-spatial-resolution images at 17 and 34 GHz, we study the morphology at the radio peak of 104 flares that occurred relatively close to the limb. Using data from the Nobeyama Polarimeter we were able to determine whether the 17- and 34-GHz emissions came from optically thin or thick sources. We identified single-loop events, taking into account supplementary information from EUV and soft X-ray (SXR) images. We found optically thin emission from the top of the loop in 36% of single-loop events. In agreement with standard models, in this sample 46% and 18% of the events showed optically thin emission from the footpoints and optically thick emission from the entire loop, respectively. The derived percentage of events with gyrosynchrotron emission from isotropic populations of energetic electrons is possibly an upper limit. This point is illustrated by the analysis of an optically thin event that shows footpoint emission during the rise phase and loop-top emission during the decay phase. A model that takes into account both anisotropies in the distribution function of nonthermal electrons and time evolution can reproduce the observed transition from footpoint to loop-top morphology, if electrons with pitch-angle anisotropy are injected near one of the footpoints.

Behavior of the flare produced coronal MHD wavefront and the occurrence of type II radio bursts.

Uchida, Y.,
1974. Solar Phys. 39, 431–449.

Trends and Characteristics of High-Frequency Type II Bursts Detected by CALLISTO Spectrometers

A.C.**Umuhire** (1), J.Uwamahoro (2), K. Sasikumar Raja (3), A.Kumar (4), C.Monstein (5)
Advances In Space Research **2021**
https://arxiv.org/pdf/2106.09310.pdf
Solar radio type II bursts serve as early indicators of incoming geo-effective space weather events such as coronal mass ejections (CMEs). In order to investigate the origin of high-frequency type II bursts (HF type II bursts), we have identified 51 of them (among 180 type II bursts from SWPC reports) that are observed by ground-based Compound Astronomical Low-cost Low-frequency Instrument for Spectroscopy and Transportable Observatory (CALLISTO) spectrometers and whose upper-frequency cutoff (of either fundamental or harmonic emission) lies in between 150 MHz-450 MHz during 2010-2019. We found that 60% of HF type II bursts, whose upper-frequency cutoff ≥ 300 MHz originate from the western longitudes. Further, our study finds a good correlation ~ 0.73 between the average shock speed derived from the radio dynamic spectra and the corresponding speed from CME data. Also, we found that analyzed HF type II bursts are associated with wide and fast CMEs located near the solar disk. In addition, we have analyzed the spatio-temporal characteristics of two of these high-frequency type II bursts and compared the derived

from radio observations with those derived from multi-spacecraft CME observations from SOHO/LASCO and STEREO coronagraphs.

4.2. SEPs and the analyzed high starting frequency type II bursts

13 June 2010, August 22, 2015, November 04, 2015

Table 1: Details of the events: Type II bursts, CMEs and Flares (2010-2019)

Table 2: Type II bursts associated with SEP events (2011-2014)

CESRA #3067 **2021** https://www.astro.gla.ac.uk/users/eduard/cesra/?p=3067 **2011.02.13**

Properties of High-Frequency Type II Radio Bursts and Their Relation to the Associated Coronal Mass Ejections

A. C. **Umuhire**, N. Gopalswamy, J. Uwamahoro, S. Akiyama, S. Yashiro & P. Mäkelä

Solar Physics volume 296, Article number: 27 (**2021**) **File**

https://link.springer.com/content/pdf/10.1007/s11207-020-01743-8.pdf

Solar radio bursts are often early indicators of space weather events such as coronal mass ejections (CMEs). In this study, we determined the properties of a sample of 40 high-starting-frequency (≥ 150 MHz) type II radio bursts and the characteristics of the associated CMEs such as width, location and speed during 2010–2016. The high starting frequency implies shock formation closer to the solar surface, which has important ramifications for the analysis of particle acceleration near the Sun. We found the CME heliocentric distances at the onset time of metric type II bursts range from 1.16 to 1.90 solar radii (Rs). The study was also extended to 128 metric type II bursts to include lower-starting-frequency events for further analysis. The projected CME heights range from 1.15 to 2.85 Rs. The lower starting frequency correspond to shocks forming at larger heights. A weak correlation was found between the type-II starting frequency and CME heights, which is consistent with the density decline in the inner corona. The analysis confirmed a good correlation between the drift rate and the starting frequency of type II bursts (correlation coefficient ~ 0.8). Taking into account the radial variation of CMEs speeds from the inner corona to the interplanetary medium, we observed the deviations from the universal drift-rate spectrum of type II bursts and confirmed the previous results relating type II bursts to CMEs. **13 Feb 2011**

Table 128 type II bursts 2010-2015

CESRA #3067 Oct 2021 https://www.astro.gla.ac.uk/users/eduard/cesra/?p=3067

Solar Radio Observation Using CALLISTO at the USO/PRL, Udaipur

Kushagra **Upadhyay**, Bhuwan Joshi, Prabir K. Mitra, Ramit Bhattacharyya, Divya Oberoi, Christian Monstein

IEEE, 2019 IEEE MTT-S International Microwave and RF Conference (IMARC) **2020**

https://arxiv.org/pdf/2007.01655.pdf

This paper presents a detailed description of various subsystems of CALLISTO solar radio spectrograph installed at the USO/PRL. In the front-end system, a log periodic dipole antenna (LPDA) is designed for the frequency range of 40-900 MHz. In this paper LPDA design, its modifications, and simulation results are presented. We also present some initial observations taken by CALLISTO at Udaipur. **March 8, 2019, May 6, 2019**

Plasma Heating in an Erupting Prominence Detected from Microwave Observations with the Siberian Radioheliograph

A. M. **Uralov**, V. V. Grechnev, S. V. Lesovoi & M. V. Globa

Solar Physics volume 298, Article number: 117 (**2023**)

https://doi.org/10.1007/s11207-023-02210-w

A major eruptive flare occurred on **12 January 2022** in the northeast not far behind the solar limb (N32 E116). The eruption produced a fast coronal mass ejection (CME). The rising ejecta was observed by the telescopes in the extreme ultraviolet and by the multi-frequency Siberian Radioheliograph (SRH) in the 5.8 – 11.8 GHz range. We show how the slope of the decrease in the brightness temperature of the rising ejecta, measured from the microwave SRH images, is related to the heat inflow or outflow in its body during rapid expansion with high acceleration and under the assumption that the plasma ionization state changes insignificantly within the measurement interval. We found that the low-temperature plasma component in the erupting prominence underwent heating. Most likely, this was due to the predominance of ohmic heating because i) the polytropic index of expanding plasma expected in this case was closest to the experimentally measured one, and ii) the ohmic dissipation due to electron-proton collisions loses its efficiency during expansion much slower than the other mechanisms of heating or cooling.

Microwave Neutral Line Associated Source and a Current Sheet

A.M. **Uralov**, V.V. Grechnev, G.V. Rudenko, I.G. Rudenko, H. Nakajima

E-print, March 2008; Solar Phys. (**2008**) 249: 315–335

http://springerlink.com/content/hx055r63w8454618/fulltext.pdf

Neutral Line associated Sources (NLS) are quasi-stationary microwave sources projected onto vicinities of the neutral line of the photospheric magnetic field. NLS are often precursors of powerful flares, but their nature is unclear. We endeavor to reveal the structure of an NLS and to analyze a physical connection between such a source with a site of energy release in the corona above NOAA 10488 (October/November 2003; **3 Nov 2003**).

Reliability of 1.8-meter solar radio telescope at Metsähovi Radio Observatory for long-term solar monitoring

Minttu **Uunila** , Juha Kallunki

Astrophysics and Space Science September **2015**, 359:33

Our aim is to prove that long time series of solar observations measured with Metsähovi Radio Observatory's 1.8-meter solar radio telescope, RT-1.8, at 11.2 GHz are reliable, and that the data can be used for solar cyclicity studies. We give a detailed description of RT-1.8 and its calibration. We compare 14 years of Metsähovi Radio Observatory's solar data from solar cycles 23 and 24 to both Dominion Radio Astrophysical Observatory (DRAO 2015), Penticton, Canada 2.8 GHz and Nobeyama Solar Radio Observatory (NSRO 2015), Nobeyama, Japan 9.4 and 17.0 GHz data. Our results show high correlation between all data sets.

POlarization Emission of Millimeter Activity at the Sun (POEMAS): New Circular Polarization Solar Telescopes at Two Millimeter Wavelength Ranges

Adriana **Valio**, P. Kaufmann, C. G. Giménez de Castro, J.-P. Raulin, L. O. T. Fernandes, A. Marun

Solar Physics, April **2013**, Volume 283, Issue 2, pp 651-665

We present a new system of two circular polarization solar radio telescopes, POEMAS, for observations of the Sun at **45 and 90 GHz**. The novel characteristic of these instruments is the capability to measure circular right- and left-hand polarizations at these high frequencies. The two frequencies were chosen so as to bridge the gap at radio frequencies between 20 and 200 GHz of solar flare spectra. The telescopes, installed at CASLEO Observatory (Argentina), observe the full disk of the Sun with a half power beam width of 1.4∘, a time resolution of 10 ms at both frequencies, a sensitivity of 2 – 4 K that corresponds to 4 and 20 solar flux unit (=104 Jy), considering aperture efficiencies of 50±5 % and 75±8 % at 45 and 90 GHz, respectively. The telescope system saw first light in November 2011 and is satisfactorily operating daily since then. A few flares were observed and are presented here. The millimeter spectra of some flares are seen to rise toward higher frequencies, indicating the presence of a new spectral component distinct from the microwave one.

LOFAR: The LOw-Frequency ARray

M. P. **van Haarlem**1, M. W. Wise1,2⋆, A. W. Gunst1 et al.

A&A 556, A2 (**2013**)

http://www.aanda.org/articles/aa/pdf/2013/08/aa20873-12.pdf

LOFAR, the LOw-Frequency ARray, is **a new-generation radio interferometer** constructed in the north of the Netherlands and across europe. Utilizing a novel phased-array design, LOFAR covers the largely unexplored low-frequency range from 10–240 MHz and provides a number of unique observing capabilities. Spreading out from a core located near the village of Exloo in the northeast of the Netherlands, a total of 40 LOFAR stations are nearing completion. A further five stations have been deployed throughout Germany, and one station has been built in each of France, Sweden, and the UK. Digital beam-forming techniques make the LOFAR system agile and allow for rapid repointing of the telescope as well as the potential for multiple simultaneous observations. With its dense core array and long interferometric baselines, LOFAR achieves unparalleled sensitivity and angular resolution in the low-frequency radio regime. The LOFAR facilities are jointly operated by the International LOFAR Telescope (ILT) foundation, as an observatory open to the global astronomical community. LOFAR is one of the first radio observatories to feature automated processing pipelines to deliver fully calibrated science products to its user community. LOFAR's new capabilities, techniques and modus operandi make it an important pathfinder for the Square Kilometre Array (SKA). We give an overview of the LOFAR instrument, its major hardware and software components, and the core science objectives that have driven its design. In addition, we present a selection of new results from the commissioning phase of this new radio observatory.

Coronal Signatures of Flare Generated Fast Mode Wave at EUV and Radio wavelengths

V. **Vasanth**

Solar Phys. **299**, 63 **2024**

https://arxiv.org/pdf/2404.00135.pdf

https://link.springer.com/content/pdf/10.1007/s11207-024-02293-z.pdf

This paper presents a detailed study of the type II solar radio burst that occurred on **06 March 2014** using combined data analysis. It is a classical radio event consisting of type III radio burst and a following type II radio burst in the dynamic spectrum. The type II radio burst is observed between 235 - 130 MHz (120 - 60 MHz) in harmonic (fundamental) bands with the life time of 5 minutes between 09:26 UT - 09:31 UT. The estimated speed of type II burst by applying twofold Saito model is 650 km/s. An extreme ultraviolet (EUV) wave is observed with Atmospheric Imaging Assembly (AIA) onboard the Solar Dynamics Observatory (SDO) pass bands. The very close temporal onset association of EUV wave and flare energy release indicates that the EUV wave is likely produced by a flare pressure pulse. The eruption is also accompanied by a weak coronal mass ejection (CME) observed with the coronagraphs onboard Solar and Heliospheric Observatory (SOHO) and the twin Solar Terrestrial Relations Observatory (STEREO). The plane of sky speed of the CME was 252 km/s at SOHO/LASCO-C2 and 280 km/s at STEREO-B/SECCHI-COR1 FOV. The EUV wave has two wave fronts, one expanding radially outward, and the other one moving along the arcade. The source position of the type II burst imaged by the Nancay Radio Heliograph (NRH) shows that it was associated with the outward moving EUV wave. The CME is independent of the shock wave as confirmed by the location of NRH radio sources below the CME's leading edge. Therefore the type II radio burst is probably ignited by the flare. This study shows the possibility of EUV wave and coronal shock triggered by flare pressure pulse, generating the observed type II radio burst.

Source Imaging of a Moving Type-IV Solar Radio Burst and its Role in Tracking Coronal Mass Ejection From the Inner to the Outer Corona

V. **Vasanth**, Yao Chen, Maoshui Lv, Hao Ning, Chuangyang Li, Shiwei Feng, Zhao Wu, Guohui Du
2019 ApJ 870 30
https://arxiv.org/pdf/1810.11815.pdf
Source imaging of solar radio bursts can be used to track energetic electrons and associated magnetic structures. Here we present a combined analysis of data at different wavelengths for an eruption associated with a moving type-IV (t-IVm) radio burst. In the inner corona, the sources are correlated with a hot and twisted eruptive EUV structure, while in the outer corona the sources are associated with the top front of the bright core of a white light coronal mass ejection (CME). This reveals the potential of using t-IVm imaging data to continuously track the CME by lighting up the specific component containing radio-emitting electrons. It is found that the t-IVm burst presents a clear spatial dispersion with observing frequencies. The burst manifests broken power-law like spectra in brightness temperature, which is as high as 107-109 K while the polarization level is in-general weak. In addition, the t-IVm burst starts during the declining phase of the flare with a duration as long as 2.5 hours. From the differential emission measure analysis of AIA data, the density of the T-IVm source is found to be at the level of a few to several 108 cm−3 at the start of the burst, and the temperature reaches up to 5-8 MK. These observations do not favor gyro-synchrotron to be the radiation mechanism, yet in line with a coherent plasma emission excited by energetic electrons trapped within the source. Further studies are demanded to elucidate the emission mechanism and explore the full diagnostic potential of t-IVm bursts. **2014 June 15**
CESRA # 2143 Feb **2019** http://www.astro.gla.ac.uk/users/eduard/cesra/?p=2143

An Eruptive Hot-Channel Structure Observed at Metric Wavelength as a Moving Type-IV Solar Radio Burst

V. **Vasanth**, Yao Chen, Shiwei Feng, Suli Ma, Guohui Du, Hongqiang Song, Xiangliang Kong, Bing Wang
ApJL 830 L2 **2016**
http://arxiv.org/pdf/1609.06546v1.pdf
Hot channel (HC) structure, observed in the high-temperature passbands of the AIA/SDO, is regarded as one candidate of coronal flux rope which is an essential element of solar eruptions. Here we present the first radio imaging study of an HC structure in the metric wavelength. The associated radio emission manifests as a moving type-IV (t-IVm) burst. We show that the radio sources co-move outwards with the HC, indicating that the t-IV emitting energetic electrons are efficiently trapped within the structure. The t-IV sources at different frequencies present no considerable spatial dispersion during the early stage of the event, while the sources spread gradually along the eruptive HC structure at later stage with significant spatial dispersion. The t-IV bursts are characterized by a relatively-high brightness temperature ($\sim 107 - 109$ K), a moderate polarization, and a spectral shape that evolves considerably with time. This study demonstrates the possibility of imaging the eruptive HC structure at the metric wavelength and provides strong constraints on the t-IV emision mechanism, which, if understood, can be used to diagnose the essential parameters of the eruptive structure**. 2012 March 4.**

Investigation of the Geoeffectiveness of CMEs Associated with IP Type II Radio Bursts

V. **Vasanth**, Y. Chen, X. L. Kong, B. Wang
Solar Phys. Volume 290, Issue 6, pp 1815-1826 **2015**
We perform a statistical analysis of the geoeffectiveness of coronal mass ejections (CMEs) that are associated with interplanetary (IP) type II bursts in Solar Cycle 23 during the period 1997 – 2008. About 47 % (109 out of 232) of IP type II bursts are found to be associated with geomagnetic storms. Of these 47 %, 27 % are associated with moderate,

14 % with intense, and 6 % with severe geomagnetic storms. We find that the IP type II bursts and their corresponding end frequencies can be used as indicators of CME geoeffectiveness: the lower the type II burst end frequency, the higher the possibility of having a stronger storm. In addition, we show that various combinations of CME remote-sensing and IP type II parameters can be used to improve geomagnetic storm forecasting.

Studies on Longer Wavelength Type II Radio Bursts Associated with Flares and CMEs during the Rise and Decay Phase of 23rd Solar Cycle

V. **Vasanth** and S. Umapathy

Journal of Astrophysics Volume 2014 (**2014**), Article ID 168718, 13 pages

http://dx.doi.org/10.1155/2014/168718

A statistical study on the properties of CMEs and flares associated with DH-type II bursts in the 23rd solar cycle during the period 1997–2008 is carried out. A sample of 229 events from our recent work is used for the present study (Vasanth and Umapathy, 2013). The collected events are divided into two groups as (i) solar cycle rise phase events and (ii) solar cycle decay phase events. The properties of CMEs in the two groups were compared and the results are presented. It is noted that there is no difference in the properties of type II burst like start frequency and end frequency between the solar cycle rise phase events and decay phase events. The mean CME speed of solar cycle decay phase events (1373 km s−1) is slightly higher than the solar cycle rise phase events (1058 km s−1). The mean CME acceleration of solar cycle decay phase events (−15.18 m s−2) is found to be higher than that of the solar cycle rise phase events (−1.32 m s−2). There exists good correlation between (i) CME speed and width and (ii) CME speed and acceleration for solar cycle decay phase events (,) compared to solar cycle rise phase events (,). These results indicate that the type II bursts parameters do not depend upon the time of appearance in the solar cycle.

Investigation of the Coronal Magnetic Field Using a Type II Solar Radio Burst

V. **Vasanth**, S. Umapathy, Bojan Vršnak, Tomislav Žic, O. Prakash

Solar Phys., **2013**

http://arxiv.org/pdf/1305.1760v1.pdf

The type II solar radio burst recorded on **13 June 2010** by the Hiraiso Solar Observatory Radio Spectrograph was employed to estimate the magnetic-field strength in the solar corona. The burst was characterized by a well-pronounced band splitting, which we used to estimate the density jump at the shock and Alfvén Mach number using the Rankine–Hugoniot relation. We convert the plasma frequency of the type II burst into height [R] in solar radii using an appropriate density model, and then we estimated the shock speed [V s], coronal Alfvén velocity [V A], and the magnetic-field strength at different heights. The relative bandwidth of the band splitting was found to be in the range 0.2 – 0.25, corresponding to a density jump of X=1.44 – 1.56, and an Alfvén Mach number of M A=1.35 – 1.45. The inferred mean shock speed was on the order of V≈667 km s−1. From the dependencies V(R) and M A(R) we found that the Alfvén speed slightly decreases at R≈1.3 – 1.5 R⊙. The magnetic-field strength decreases from a value between 2.7 and 1.7 G at R≈1.3 – 1.5 R⊙, depending on the coronal-density model employed. Our results are in good agreement with the empirical scaling by Dulk and McLean (Solar Phys. 57, 279, 1978) and Gopalswamy et al. (Astrophys. J. 744, 72, 2012). Our results show that the type II band-splitting method is an important tool for inferring the coronal magnetic field, especially when independent measurements are made from white-light observations.

A Statistical Study on CMEs Associated with DH-Type-II Radio Bursts Based on Their Source Location (Limb and Disk Events)

V. **Vasanth**, S. Umapathy

Solar Physics, January **2013**, Volume 282, Issue 1, pp 239-247

We have statistically studied the 344 Coronal Mass Ejections (CMEs) associated with flares and DH-type-II radio bursts (1 – 14 MHz) during 1997 – 2008. We found that only 3 % of the total CMEs (344) compared to the general population CMEs (13208) drives DH-type-II radio bursts (Gopalswamy in Solar Eruptions and Energetic Particles, AGU Geophys. Monogr. 165, 207, 2006). Out of 344 events we have selected 236 events for further analysis. We divided the events into two groups: i) disk events (within 45fl from the disk center) and ii) limb events (beyond 45fl but within 90fl from the disk center). We find that the average CME speed of the limb events (1370 km s−1) is three times, while for the disk events (1055 km s−1) it is two times the average speed of the general population CMEs (433 km s−1). The average widths of the limb events (129fl) and disk events (116fl) are two times greater than the average width of the general population CMEs (58fl). We found a better correlation between the CME speed and width (correlation coefficient R=0.56) for the limb events than that of the disk events (R=0.47). The shock speed of the CMEs associated with DH-type-II radio bursts is found by applying Leblanc, Dulk, and Bougeret's (Solar Phys. 183, 165, 1998) electron density model; the disk events are found to have an average speed of 1190 km s−1 and that of the limb events is 1275 km s−1. From this study we compare the CME properties between limb and disk events. The properties like CME speed, width, shock speed, and correlation between CME speed and width are found to be higher for limb events than disk events. The results in disk events are subject to projection effects, and this study stresses the importance of these effects.

Characteristics of Type-II Radio Bursts Associated with Flares and CMEs

V. **Vasanth**, S. Umapathy, Bojan Vršnak and M. Anna Lakshmi

Solar Physics, Volume 273, Number 1, 143-162, **2011**

We present a statistical study of the characteristics of type-II radio bursts observed in the metric (m) and deca-hectometer (DH) wavelength range during 1997–2008. The collected events are divided into two groups: Group I contains the events of m-type-II bursts with starting frequency ≥ 100 MHz, and group II contains the events with starting frequency of m-type-II radio bursts < 100 MHz. We have analyzed both samples considering three different aspects: i) statistical properties of type-II bursts, ii) statistical properties of flares and CMEs associated with type-II bursts, and iii) time delays between type-II bursts, flares, and CMEs. We find significant differences in the properties of m-type-II bursts in duration, bandwidth, drift rate, shock speed and delay between m- and DH-type-II bursts. From the timing analysis we found that the majority of m-type-II bursts in both groups occur during the flare impulsive phase. On the other hand, the DH-type-II bursts in both groups occur during the decaying phase of the associated flares. Almost all m-DH-type-II bursts are found to be associated with CMEs. Our results indicate that there are two kinds of shock in which group I (high frequency) m-type-II bursts seem to be ignited by flares whereas group II (low frequency) m-type-II bursts are CME-driven.

Temporally resolved Type III solar radio bursts in the frequency range 3-13 MHz

Antonio **Vecchio**, Milan Maksimovic, Nicolina Chrysaphi, Eduard P. Kontar, Vratislav Krupar

ApJLetter 974:L18 **2024**

https://arxiv.org/pdf/2410.18765

Radio observations from space allow to characterize solar radio bursts below the ionospheric cutoff, which are otherwise inaccessible, but suffer from low, insufficient temporal resolution. In this Letter we present novel, high-temporal resolution observations of type III solar radio bursts in the range 3−13 MHz. A dedicated configuration of the Radio and Plasma Waves (RPW) High Frequency Receiver (HFR) on the Solar Orbiter mission, allowing for a temporal resolution as high as ∼0.07s (up to 2 orders of magnitude better than any other spacecraft measurements), provides for the very first time resolved measurements of the typical decay time values in this frequency range. The comparison of data with different time resolutions and acquired at different radial distances indicates that discrepancies with decay time values provided in previous studies are only due to the insufficient time resolution not allowing to accurately characterize decay times in this frequency range. The statistical analysis on a large sample of ∼500 type III radio bursts shows a power low decay time trend with a spectral index of −0.75±0.03 when the median values for each frequency are considered. When these results are combined with previous observations, referring to frequencies outside the considered range, a spectral index of −1.00±0.01 is found in the range ∼0.05−300 MHz, compatible with the presence of radio-wave scattering between 1 and 100 RSun. **2023 November 26**

SO Nugget #41 Oct 2024 https://www.cosmos.esa.int/web/solar-orbiter/-/science-nugget-temporally-resolved-type-iii-solar-radio-bursts-in-the-frequency-range-3-13-mhz

CESRA nugget #3896 2024 https://www.astro.gla.ac.uk/users/eduard/cesra/?p=3896

Solar Orbiter/RPW antenna calibration in the radio domain and its application to type III burst observations

A. **Vecchio**, M.Maksimovic, V. Krupar, X. Bonnin, A. Zaslavsky, P. L. Astier, M. Dekkali, B. Cecconi, S.D. Bale, T. Chust, E. Guilhem, Yu. V. Khotyaintsev, V. Krasnoselskikh, M. Kretzschmar, E. Lorfèvre, D. Plettemeier, J. Souček, M. Steller, Š. Štverák, P. Trávníček, A. Vaivads

A&A **2021**

https://arxiv.org/pdf/2109.07947.pdf

In order to allow for a comparison with the measurements from other antenna systems, the voltage power spectral density measured by the Radio and Plasma waves receiver (RPW) on board Solar Orbiter needs to be converted into physical quantities that depend on the intrinsic properties of the radiation itself.The main goal of this study is to perform a calibration of the RPW dipole antenna system that allows for the conversion of the voltage power spectral density measured at the receiver's input into the incoming flux density. We used space observations from the Thermal Noise Receiver (TNR) and the High Frequency Receiver (HFR) to perform the calibration of the RPW dipole antenna system. Observations of type III bursts by the Wind spacecraft are used to obtain a reference radio flux density for cross-calibrating the RPW dipole antennas. The analysis of a large sample of HFR observations (over about ten months), carried out jointly with an analysis of TNR-HFR data and prior to the antennas' deployment, allowed us to estimate the reference system noise of the TNR-HFR receivers. We obtained the effective length of the RPW dipoles and the reference system noise of TNR-HFR in space, where the antennas and pre-amplifiers are embedded in the solar wind

plasma. The obtained leff values are in agreement with the simulation and measurements performed on the ground. By investigating the radio flux intensities of 35 type III bursts simultaneously observed by Solar Orbiter and Wind, we found that while the scaling of the decay time as a function of the frequency is the same for the Waves and RPW instruments, their median values are higher for the former. This provides the first observational evidence that Type III radio waves still undergo density scattering, even when they propagate from the source, in a medium with a plasma frequency that is well below their own emission frequency.

Observations of the 2024 May 14 X8.7 Solar Flare with the Goldstone-Apple Valley Radio Telescope (GAVRT)

Thangasamy **Velusamy**1, Ryan Dorcey2, Nancy Kreuser-Jenkins2, Lisa Nichole Lamb2, Erica Pagano2, Marin M. Anderson1, Joseph Lazio1, and Steven Levin1
2024 Res. Notes AAS 8 163
https://iopscience.iop.org/article/10.3847/2515-5172/ad5a0d
The Goldstone-Apple Valley Radio Telescope (GAVRT) project conducts a regular monitoring program of the Sun. The GAVRT Solar Patrol project uses a 34 m diameter antenna to produce raster-scan maps of the Sun simultaneously at 4 frequencies ranging from approximately 3 to 14 GHz. On 2024 May 14, as part of regular GAVRT Solar Patrol observations, raster maps were produced when an X8.7 solar flare occurred in active region AR13664. Here we present the GAVRT maps of the May 14 flare along with microwave flux density spectra showing the non-thermal microwave burst emission from mildly relativistic electrons produced in this largest flare of Solar Cycle 25 to date. AR13664 reappeared as AR13697 and continued to be very active, producing X flares while GAVRT monitored its activity. GAVRT microwave data provide a powerful complement to the energetic electrons tracked by X-ray, millimeter-wave and γ-ray emissions.

Goldstone Apple Valley Radio Telescope Observations of 2012 Solar Eclipse: A Multi-wavelength study of cm-wavelength Gyroresonance Emission from Active Regions

T. **Velusamy**, T. B. H Kuiper, S. M. Levin R. Dorcey, N. Kreuser-Jenkins, J. Leflang
PASP **2020**
https://arxiv.org/ftp/arxiv/papers/2007/2007.05058.pdf
Goldstone Apple Valley Radio Telescope (GAVRT) is a science education partnership among NASA, the Jet Propulsion Laboratory (JPL), and the Lewis Center for Educational Research (LCER), offering unique opportunities for K -12 students and their teachers. The GAVRT program operates a 34-m radio telescope with a wide-band, low noise receiver, which is tunable in four independent dual-polarization bands from 3 to 14 GHz. The annular eclipse of the Sun on **2012 May 20** was observed by GAVRT as part of education outreach. In this paper we present the results of this eclipse data and discuss the multi-wavelength strip scan brightness distribution across three active regions. We derive the source brightness temperatures and angular sizes as a function of frequency and interpret the results in terms of the gyroresonance mechanism. We show examples of the increasing brightness and widening of source size (isogauss surface) with wavelength as evidence for gyroresonance emission layers of broader (diverging) isogauss surfaces of the magnetic field geometry in the corona above solar surface. We present an example how the derived frequency - brightness temperature relationship is translated to a magnetic field - brightness temperature relationship under the frame-work of gyroresonance emission. Our results demonstrate the usefulness of GAVRT bands as excellent probes to study the layers of the corona above the active regions (sun spots), in particular the prevalence of the gyroresonance mechanism. Our results provide a frame-work for multiwavelength cm-wavelength eclipse observations and illustrate how the GAVRT program and K- 12 student/teacher participation can produce science data useful to the scientific community and science missions.

Eruption of EUV Hot-Channel near Solar Limb and Associated Moving Type-IV Radio Burst

P. **Vemareddy**, P. Démoulin, K. Sasikumar Raja, J. Zhang, N. Gopalswamy, N. Vasantharaju
ApJ **927** 108 **2022**
https://arxiv.org/pdf/2201.06899.pdf
https://iopscience.iop.org/article/10.3847/1538-4357/ac4dfe/pdf
Using the observations from Solar Dynamics Observatory, we study an eruption of a hot-channel flux rope (FR) near the solar-limb on **February 9, 2015**. The pre-eruptive structure is visible mainly in EUV 131 A˚ images with two highly-sheared loop structures. They undergo slow rise motion and then reconnect to form an eruptive hot-channel as in the tether-cutting reconnection model. The J-shaped flare-ribbons trace the footpoint of the FR which is identified as the hot-channel. Initially, the hot channel is observed to rise slowly at 40 km s−1, followed by an exponential rise from 22:55 UT at a coronal height of 87±2 Mm. Following the onset of the eruption at 23:00 UT, the flare-reconnection adds to the acceleration process of the CME within 3 R⊙. Later on, the CME continues to accelerate at 8 m s−2 during its propagation period. Further, the eruption launched type-II followed by III, IVm radio bursts. The start and end times of type-IVm correspond to the CME core height of 1.5 and 6.1 R⊙, respectively. Also the spectral index is negative suggesting the non-thermal electrons trapped in the closed loop structure. Accompanied with type-IVm, this event is

unique in the sense that the flare ribbons are very clearly observed along with the erupting hot channel, which strongly supports that the hooked-part of J-shaped flare ribbons outlines the boundary of the erupting FR.

Fluctuation analysis of solar radio bursts associated with geoeffective X-class flares

T.B. **Veronese**a, , , R.R. Rosaa, M.J.A. Bolzanb, F.C. Rocha Fernandesc, H.S. Sawantd and M. Karlicky
Journal of Atmospheric and Solar-Terrestrial Physics, Volume 73, Issues 11-12, **2011**, Pages 1311-1316

High temporal resolution solar observations in the decimetric range (1–3 GHz) can provide additional information on solar active regions dynamics and thus contribute to better understanding of solar geoeffective events as flares and coronal mass ejections. The **June 6, 2000** flares are a set of remarkable geoeffective eruptive phenomena observed as solar radio bursts (SRB) by means of the 3 GHz Ondrejov Observatory radiometer. We have selected and analyzed, applying detrended fluctuation analysis (DFA), three decimetric bursts associated to X1.1, X1.2 and X2.3 flare-classes, respectively. The association with geomagnetic activity is also reported. DFA method is performed in the framework of a radio burst automatic monitoring system. Our results may characterize the SRB evolution, computing the DFA scaling exponent, scanning the SRB time series by a short windowing before the extreme event. For the first time, the importance of DFA in the context of SRB monitoring analysis is presented.

Magnetic Properties of Source Regions of CMEs and DH Type II Radio Bursts

P. **Vijayalakshmi**, A. Shanmugaraju & S. Aswin Amirtha Raj
Solar Phys. volume 298, Article number: 144 (**2023**)
https://doi.org/10.1007/s11207-023-02234-2

The Sun is a dynamic star that exhibits various phenomena, including solar flares, coronal mass ejections (CMEs), and Type II radio bursts. CMEs are large-scale eruptions of plasma and magnetic field from the Sun that can disrupt the interplanetary medium and the Earth's magnetic field. Type II radio bursts are radio emissions associated with shocks generated by the CMEs. Only a few CMEs are associated with Type II radio bursts and the reasons for the absence of these bursts are still under debate. The magnetic properties of source active regions (ARs) from where CMEs with and without decameter-hectometer (DH) Type II radio bursts originate are investigated. Relations between the speed of CMEs and the source region properties are also obtained for these two groups of events (with and without radio bursts). The data from the Solar Dynamics Observatory (SDO) and the Radio and Plasma Wave (WAVES) Experiment on board the Wind spacecraft and the CMEs observed by the Solar and Heliospheric Observatory (SOHO) mission for the period of 2010 – 2014 in Solar Cycle 24 are utilized for this study. The statistical properties (like range, mean, median, and standard deviation) of source AR magnetic properties and the speed of the CMEs associated with DH Type II radio bursts (first group called radio loud) are found to be higher than those of CMEs without DH Type II radio bursts (second group called radio quiet). In addition, we found a positive correlation between the magnetic properties of the source AR and the speed of the CMEs with DH Type II radio bursts, but it is absent for events without DH Type II bursts. We also found that the probability of CME-streamer interaction is higher for the first group than for the second group, which shows a strong relation between the CME-streamer interaction and Type II bursts. These results reveal distinct magnetic characteristics in the source region for radio loud and radio quiet CMEs.

Energetic electrons in the solar atmosphere as diagnosed from their radio and Hard X-ray signatures.

Nicole **Vilmer**∗1 and Hamish Reid
CESRA **2016** p.66
http://cesra2016.sciencesconf.org/conference/cesra2016/pages/CESRA2016_prog_abs_book_v3.pdf

Efficient particle acceleration is observed in association with solar flares. X-ray and radio emissions provide valuable information on the properties of electron acceleration, interaction and propagation in the solar atmosphere. In particular, radio emission from electron beams produced in association with solar flares provides crucial information on the relationship and connections between energetic electrons in the corona and electrons measured in situ. In this talk, we will address the question of the relation between escaping electrons that generate type III emissions in the corona and in the interplanetary medium and electrons confined to the lower atmosphere of the Sun that produce HXRs. We will present here the results of a study based on ten years of data (2002-2011) starting with a selection of 'coronal' type III bursts above 100 MHz. We use X-ray flare information from RHESSI (flares above 6 keV) to produce a list of more than 300 coronal type III bursts associated with X-ray emissions (see Reid and Vilmer, 2016). For these associated events, we will characterize the relative timings, the X-ray and radio intensities and the associated GOES class. We will also examine the percentage of the 'coronal' type III bursts associated with an interplanetary signature (i.e. an interplanetary type III burst detected below 12 MHz by the Wind/Waves experiment) and whether the association between coronal types III and interplanetary types III depends on the characteristics of the propagating electron beams. We will further describe how these studies can be continued in the future using the combination of ground-based measurements with Solar Orbiter and Solar Probe + observations.

LOFAR observations of the quiet solar corona

C. **Vocks**, G. Mann, F. Breitling, M. M. Bisi, B. Dabrowski, R. Fallows, P. T. Gallagher, A. Krankowski, J. Magdalenic, C. Marque, D. Morosan, H. Rucker
A&A 614, A54 **2018**
https://arxiv.org/pdf/1803.00453.pdf
https://www.aanda.org/articles/aa/pdf/2018/06/aa30067-16.pdf
Context. The quiet solar corona emits meter-wave thermal bremsstrahlung. Coronal radio emission can only propagate above that radius, Rω, where the local plasma frequency equals the observing frequency. The radio interferometer LOw Frequency ARray (LOFAR) observes in its low band (10 – 90 MHz) solar radio emission originating from the middle and upper corona. Aims. We present the first solar aperture synthesis imaging observations in the low band of LOFAR in 12 frequencies each separated by 5 MHz. From each of these radio maps we infer Rω, and a scale height temperature, T. These results can be combined into coronal density and temperature profiles.
Methods. We derived radial intensity profiles from the radio images. We focus on polar directions with simpler, radial magnetic field structure. Intensity profiles were modeled by ray-tracing simulations, following wave paths through the refractive solar corona, and including free-free emission and absorption. We fitted model profiles to observations with Rω and T as fitting parameters.
Results. In the low corona, Rω < 1.5 solar radii, we find high scale height temperatures up to 2.2 × 106 K, much more than the brightness temperatures usually found there. But if all Rω values are combined into a density profile, this profile can be fitted by a hydrostatic model with the same temperature, thereby confirming this with two independent methods. The density profile deviates from the hydrostatic model above 1.5 solar radii, indicating the transition into the solar wind.
Conclusions. These results demonstrate what information can be gleaned from solar low-frequency radio images. The scale height temperatures we find are not only higher than brightness temperatures, but also than temperatures derived from coronograph or extreme ultraviolet (EUV) data. Future observations will provide continuous frequency coverage. This continuous coverage eliminates the need for local hydrostatic density models in the data analysis and enables the analysis of more complex coronal structures such as those with closed magnetic fields. **8 August 2013.**

LOFAR observations of the quiet solar corona

Christian **Vocks**∗†1 , Gottfried Mann1 , Frank Breitling1 , Richard Fallows2 , Mario Bisi3 , Peter Gallagher4 , Alain Kerdraon5 , Jasmina Magdalenic6 , Alec Mackinnon7 , Helmut Rucker8 , Alexander Konovalenko9 , Christophe Marque6 , Eduard Kontar7 , Bartosz Dabrowski10, Andrzej Krankowski10, Hamish Reid7 , and Bo Thide1
CESRA **2016** p.40
http://cesra2016.sciencesconf.org/conference/cesra2016/pages/CESRA2016_prog_abs_book_v3.pdf
LOFAR is a novel radio interferometer consisting of a central core near Exloo in the Netherlands, remote stations in the Netherlands, and international stations. It observes in two frequency bands, the low band of 10 – 90 MHz, and the high band of 110 – 250 MHz. The Key Science Project ”Solar Physics and Space Weather with LOFAR” aims at observing the Sun with LOFAR. Solar radio radiation in the low and high band emanates from the upper and middle corona, respectively. The solar corona is not a simple layer with barometric density profile, but highly structured due to coronal magnetic fields. The density of the coronal plasma can be estimated by several means, e.g. coronograph data or radio occultation measurements of spacecraft signals. But they leave a gap in the high corona, at a solar distance of a few solar radii. This region is of special interest, since it is where the transition from a hydrostatic corona to the supersonic solar wind is located. If the Sun is observed at a given radio frequency, then the corona becomes opaque below the density level where that frequency corresponds to the local plasma frequency. Since the refractive index of the coronal plasma approaches zero there, diffraction effects also need to be considered. We will present LOFAR observations of the quiet Sun at different low-band frequencies. The diameter of the radio Sun increases with decreasing frequency, as expected. But the quiet Sun does not appear as a disk with constant brightness temperature. A derivation of the coronal height, where the observed frequency equals the local plasma frequency, requires fitting raytracing simulations, which include wave refraction and free-free emission and absorption, to intensity profiles from the images. We’ll present first results for a polar coronal density and temperature profile derived from LOFAR low band images.

Efficiency of Electromagnetic Emission by Electrostatic Turbulence in Solar Wind and Coronal Plasmas with Density Inhomogeneities

A. S. **Volokitin**1 and C. Krafft2,3
2020 ApJL 893 L47
https://doi.org/10.3847/2041-8213/ab74de
We present a new method to semianalytically calculate the radiation efficiency of electromagnetic waves emitted at specific frequencies by electrostatic wave turbulence in solar wind and coronal plasmas with random density fluctuations. This method is applied to the case of electromagnetic emission radiated at the fundamental plasma frequency ω p by beam-driven Langmuir wave turbulence during Type III solar bursts. It is supposed that the main radiation mechanism is the linear conversion of electrostatic to electromagnetic waves on the background plasma density fluctuations, at constant frequency. The radiation efficiency (emissivity) of such a process is larger than that

obtained in the framework of models where the low frequency density fluctuations and the corresponding ion sound waves are not external but produced by the electrostatic wave turbulence itself through nonlinear wave–wave interactions. Results show that the radiation efficiency of Langmuir wave turbulence into electromagnetic emissions at ω p is nearly constant asymptotically, with the electromagnetic energy density growing linearly with time, and is proportional to the average level of density fluctuations. Comparisons with another analytical method developed by the authors and with space observations are satisfactory.

Electromagnetic Wave Emissions from a Turbulent Plasma with Density Fluctuations

A. S. **Volokitin**1,2 and C. Krafft

2018 ApJ 868 104

In the solar wind, Langmuir turbulence can generate electromagnetic waves at the fundamental plasma frequency ω p . This process can likely result from either linear wave transformations on the ambient random density inhomogeneities or resonant three-wave interactions involving Langmuir waves and ion acoustic oscillations. In the presence of sufficiently intense plasma density fluctuations of scales much larger than the Langmuir wavelengths, the first mechanism may be more efficient than the second one. A new approach to calculate the electromagnetic wave emissions by Langmuir wave turbulence in plasmas with background density fluctuations is developed. The evolution of the Langmuir turbulence is studied by numerically solving the Zakharov equations in such a two-dimensional plasma. The dynamics of the spatial distributions of the electric currents with frequencies close to ω p is calculated, as well as their emission into electromagnetic waves. The efficiency of this radiation is determined as a function of the level of the Langmuir turbulence, the characteristics of the density fluctuations, the background plasma temperature, the position of the satellite receiver, and the durations of the source's emissions and spacecraft's observations. The results obtained by the theoretical modeling and numerical simulations are successfully compared with space observations of electromagnetic waves radiated during Type III solar radio bursts.

Comparative analysis of decametre 'drift pair' bursts observed in 2002 and 2015

Volvach, Ya.S., Stanislavsky A.A., Konovalenko A.A., Koval A.A., and Dorovskyy V.V.:

2016, Advanced in Astronomy and Space Physics 6, 24. doi: 10.17721/2227-1481.6.24-27

http://aasp.kiev.ua/volume6/024-027-Volvach.pdf

We report about new observations of solar 'drift pair' (DP) bursts by means of the UTR-2 radio telescope at frequencies 10-30 MHz. Our experimental data include both 'forward' and 'reverse' bursts with high frequency and time resolution. The records of 301 bursts, observed in **10-12 July of 2015**, are investigated. The main properties of these bursts (frequency bandwidth, central frequency and others) have been analysed. In this report our main attention is paid to the comparison of our observations with the similar observations of decametre DPs performed earlier during **13-15 July of 2002** in the same frequency range. Common features of DPs in the two different pieces of data samples have been found. This may indicate the possible presence of stability in the frequency-time properties of decametre DPs from one cycle of solar activity to another.

Statistics of electric fields' amplitudes in Langmuir turbulence: A numerical simulation study

A. **Voshchepynets**, A. Volokitin, V. Krasnoselskikh, C. Krafft

JGR Volume 122, Issue 4 April **2017** Pages 3915–3934

A systematic study of the properties of Langmuir turbulence generated by electron beams via bump-on-tail instabilities in strongly nonhomogeneous plasmas is presented. A statistical analysis of the Langmuir waves' amplitudes using numerical simulations based on two theoretical models is performed: a dynamical one and a probabilistic one. The former describes the self-consistent dynamics of wave-particle and wave-wave interactions. The latter is a modified version of the quasi-linear theory. To analyze the simulation data provided by the probabilistic model, a Pearson technique is used to classify the calculated probability distribution functions (PDFs) of the logarithm of the waves' amplitudes. It is demonstrated that the core parts of the PDFs belong to the Pearson types I, IV, and VI distributions, while the high-amplitude parts of the PDFs follow power law or exponential decay. Analysis of the PDFs calculated using the numerical simulations based on the dynamical model leads to the following additional results. In the small-amplitude parts of the PDFs, a universal scaling parameter is found, with a value not depending on the average levels of the density fluctuations and of the Langmuir turbulence. Second, the PDFs are obtained in the presence of wave decay processes. When those are weak, the PDFs show at large fields' amplitudes an exponential asymptotic behavior; during time evolution, the corresponding scaling parameter decreases until a universal probability distribution is reached, indicating that the wave decay processes are sufficiently strong. Such exponential type of distribution is a specific signature of transition states in the Langmuir turbulence.

Probabilistic model of beam-plasma interaction in randomly inhomogeneous solar wind

A. **Voshchepynets**, V. Krasnoselskikh

JGR Volume 120, Issue 12 December **2015** Pages 10,139–10,158

This paper is dedicated to the effects of plasma density fluctuations in the solar wind on the relaxation of the electron beams ejected from the Sun. The density fluctuations are supposed to be responsible for the changes in the local phase velocity of the Langmuir waves generated by the beam instability. Changes in the wave phase velocity during the wave propagation can be described in terms of probability distribution function determined by distribution of the density fluctuations. Using these probability distributions, we describe resonant wave particle interactions by a system of equations, similar to a well-known quasi-linear approximation, where the conventional velocity diffusion coefficient and the wave growth rate are replaced by the averaged in the velocity space. It was shown that the process of relaxation of electron beam is accompanied by transformation of significant part of the beam kinetic energy to energy of the accelerated particles via generation and absorption of the Langmuir waves. We discovered that for the very rapid beams with beam velocity vb>15vt, where vt is a thermal velocity of background plasma, the relaxation process consists of two well-separated steps. On first step the major relaxation process occurs and the wave growth rate almost everywhere in the velocity space becomes close to zero or negative. At the second stage the system remains in the state close to state of marginal stability long enough to explain how the beam may be preserved traveling distances over 1 AU while still being able to generate the Langmuir waves.

Probabilistic Model of Beam–Plasma Interaction in Randomly Inhomogeneous Plasma

A. **Voshchepynets**1,3, V. Krasnoselskikh1,3, A. Artemyev2, and A. Volokitin
2015 ApJ 807 38

We propose a new model that describes beam–plasma interaction in the presence of random density fluctuations with a known probability distribution. We use the property that, for the given frequency, the probability distribution of the density fluctuations uniquely determines the probability distribution of the phase velocity of waves. We present the system as discrete and consisting of small, equal spatial intervals with a linear density profile. This approach allows one to estimate variations in wave energy density and particle velocity, depending on the density gradient on any small spatial interval. Because the characteristic time for the evolution of the electron distribution function and the wave energy is much longer than the time required for a single wave–particle resonant interaction over a small interval, we determine the description for the relaxation process in terms of averaged quantities. We derive a system of equations, similar to the quasi-linear approximation, with the conventional velocity diffusion coefficient D and the wave growth rate γ replaced by the average in phase space, by making use of the probability distribution for phase velocities and by assuming that the interaction in each interval is independent of previous interactions. Functions D and γ are completely determined by the distribution function for the amplitudes of the fluctuations. For the Gaussian distribution of the density fluctuations, we show that the relaxation process is determined by the ratio of beam velocity to plasma thermal velocity, the dispersion of the fluctuations, and the width of the beam in the velocity space.

Radio Observations of Coronal Mass Ejections: Space Weather Aspects **Review**

Angelos **Vourlidas** , Eoin P Carley and Nicole Vilmer
Front. Astron. Space Sci. **7**:43 **2020**
https://www.frontiersin.org/articles/10.3389/fspas.2020.00043/full
https://sci-hub.st/10.3389/fspas.2020.00043 **File**

We review the current state-of-affairs in radio observations of Coronal Mass Ejections (CMEs) from a Space Weather perspective. In particular, we examine the role of radio observations in predicting or presaging an eruption, in capturing the formation stages of the CME, and in following the CME evolution in the corona and heliosphere. We then look to the future and identify capabilities and research areas where radio observations---particularly, spectropolarimetric imaging---offer unique advantages for Space Weather research on CMEs. We close with a discussion of open issues and possible strategies for enhancing the relevance and importance of radio astronomy for Space Weather science. **2003 June 17, 2003 November 1, 2010 January 15, Aug. 2, 2012**

Identification of a Peculiar Radio Source in the Aftermath of Large Coronal Mass Ejection Events

Angelos **Vourlidas**, Monique Pick, Sang Hoang, and Pascal Demoulin
The Astrophysical Journal Letters, Volume 656, Number 2, Page L105, **2007, File** [http://www.journals.uchicago.edu/cgi-bin/resolveflApJL21380]

We report the discovery of a new radio feature associated with coronal mass ejection (CME) events. The feature is a low-frequency (<1 MHz), relatively wide (~300 kHz) continuum that appears just after the main phase of the eruptive event, lasts for several hours, and exhibits a slow negative frequency drift.
We interpret this radio continuum as the lateral interaction of the CME with magnetic structures. Another possibility is that this continuum traces the reconfiguration of large-scale loop systems, such as streamers. In other words, it could be the large-scale counterpart of the post-CME arcades seen over active region neutral lines after big CME events.

Radio Observations of Coronal Mass Ejection4 **Review**

Vourlidas, A.
(**2004**). " in Solar and Space Weather Radiophysics: Current Status and Future Developments. Editors D. E. Gary and C. U. Keller (Dordrecht: Springer), Vol. 314, 223–242.
https://sci-hub.st/10.1007/1-4020-2814-8_11
In this chapter we review the status of CME observations in radio wavelengths with an emphasis on imaging. It is an area of renewed interest since 1996 due to the upgrade of the Nanc¸ay Radioheliograph in conjunction with the continuous coverage of the solar corona from the EIT and LASCO instruments aboard SOHO. Also covered are analyses of Nobeyama Radioheliograph data and spectral data from a plethora of spectrographs around the world. We will point out the shortcomings of the current instrumentation and the ways that FASR could contribute. A summary of the current understanding of the physical processes that are involved in the radio emission from CMEs is be given. **4 Nov 1997, 1998 April 20, 1998 May 2, 2000 February 17**

Origin of Coronal Shock Waves

Invited Review
Bojan **Vršnak** · Edward W. Cliver
Solar Phys, 253: 215–235, **2008**, DOI 10.1007/s11207-008-9241-5; **File**
The basic idea of the paper is to present transparently and confront two different views on the origin of large-scale coronal shock waves, one favoring coronal mass ejections (CMEs), and the other one preferring flares. For this purpose, we first review the empirical aspects of the relationship between CMEs, flares, and shocks (as manifested by radio t**ype II bursts** and Moreton waves). Then, various physical mechanisms capable of launching MHD shocks are presented. In particular, we describe the shock wave formation caused by a three-dimensional piston, driven either by the CME expansion or by a flare-associated pressure pulse. Bearing in mind this theoretical framework, the observational characteristics of CMEs and flares are revisited to specify advantages and drawbacks of the two shock formation scenarios. Finally, we emphasize the need to document clear examples of flare-ignited large-scale waves to give insight on the relative importance of flare and CME generation mechanisms for type II bursts/Moreton waves.

Multi-wavelength study of coronal waves associated with the CME-flare event of 3 November 2003

Vrsnak, B., Warmuth, A., Temmer, Veronig, A., Magdaleni˘c, J., Hillaris, A., Karlicky, M.:
Astron. Astrophys. 448(2), 739-752 **2006**, (e-print, **2005**)
The large flare/CME event that occurred close to the west solar limb on 3 November 2003 launched a large-amplitude large-scale coronal wave that was observed in Hα and Fe xii 195 Å spectral lines, as well as in the soft X-ray and radio wavelength ranges. The wave also excited a complex decimeter-to-hectometer type II radio burst, revealing the formation of coronal shock(s). The back-extrapolation of the motion of coronal wave signatures and the type II burst sources distinctly marks the impulsive phase of the flare (the hard X-ray peak, drifting microwave burst, and the highest type III burst activity), favoring a flare-ignited wave scenario. On the other hand, comparison of the kinematics of the CME expansion with the propagation of the optical wave signatures and type II burst sources shows a severe discrepancy in the CME-driven scenario. However, the CME is quite likely associated with the formation of an upper-coronal shock revealed by the decameter-hectometer type II burst. Finally, some six minutes after the launch of the first coronal wave, another coronal disturbance was launched, exciting an independent (weak) decimeter-meter range type II burst. The back-extrapolation of this radio emission marks the revival of the hard X-ray burst, and since there was no CME counterpart, it was clearly ignited by the new energy release in the flare.

Band-splitting of coronal and interplanetary type II bursts
II. Coronal magnetic field and Alfv´en velocity

B. **Vr˘snak**1, J. Magdaleni´c1;2, H. Aurass3, and G. Mann3
A&A 396, 673–682 (**2002**), **File**
Abstract. Type II radio bursts recorded in the metric wavelength range are excited by MHD shocks traveling through the solar corona. They often expose the fundamental and harmonic emission band, both frequently being split in two parallel lanes that show a similar frequency drift and intensity behaviour. Our previous paper showed that band-splitting of such characteristics is a consequence of the plasma emission from the upstream and downstream shock regions. Consequently, the split can be used to evaluate the density jump at the shock front and to estimate the shock Mach number, which in combination with the shock speed inferred from the frequency drift provides an estimate of the Alfv´en velocity and the magnetic field in the ambient

plasma. In this paper such a procedure is applied to 18 metric type II bursts with the fundamental band starting frequencies up to 270 MHz. The obtained values show a minimum of the Alfv´en velocity at the heliocentric distance R _ 2 amounting to v_A _ 400–500 km s^{-1}. It then increases achieving a local maximum of v_A _ 450–700 km s^{-1} at R _ 2:5. The implications regarding the process of formation and decay of MHD shocks in the corona are discussed. The coronal magnetic field in the range 1:3 < R < 3 decreases as R^{-3} to R^{-4}, or $H^{-1:5}$ to H^{-2} if expressed as a function of the height. The results are compared with other estimates of the coronal magnetic field in the range 1 < R < 10. Combined data show that below H < 0:3 the magnetic field is dominated by active region fields, whereas above H = 1 it becomes radial, behaving roughly as $B = 2$ _ R^{-2} with a plausible value of B _ 5 nT at 1 a.u.

Band-splitting of coronal and interplanetary type II bursts I. Basic properties

B. **Vr_snak**1, H. Aurass2, J. Magdaleni_c3, and N. Gopalswamy
A&A 377, 321{329 **(2001), File**

Abstract. Patterns analogous to the band-splitting of metric type II bursts are found in a number of type II bursts observed in the dekameter-kilometer wavelength range. A similarity of morphological and frequency-time characteristics of two emission components are indicative of a common source. Relative frequency splits span in the range _f=f = 0:05−0:6. At radial distances between 2 and 4 R_ only small splits around 0.1 can be found. In the interplanetary space the relative split on average increases with the radial distance, whereas the inferred shock velocity decreases. In three events extrapolations of the split components point to the base and the peak of the jump in the local plasma frequency caused by the associated shock passage at 1 AU. This is suggestive of the plasma radiation from the regions upstream and downstream of the shock. Adopting this interpretation, one _nds that the drop of _f=f at 2{4 R_ is congruent with the Alfv_en velocity maximum expected there. The split increase and the velocity decrease at larger distances can be explained as a consequence of declining Alfv_en speed in the interplanetary space.

Reduced Microwave Brightness Temperature in a Sunspot Atmosphere due to Open Magnetic Fields

A. **Vrublevskis** (1), B. I. Ryabov (1), S. M. White (2) ((1)
Solar Phys. **296**, Article number: 144 **2021**
https://arxiv.org/ftp/arxiv/papers/2102/2102.05476.pdf
https://link.springer.com/content/pdf/10.1007/s11207-021-01891-5.pdf
https://doi.org/10.1007/s11207-021-01891-5

Motivated by dark coronal lanes in SOHO / EIT 284 Å EUV observations we construct and optimize an atmosphere model of the AR 8535 sunspot by adding a cool and dense component in the volume of plasma along open field lines determined using the Potential Field Source Surface (PFSS) extrapolation. Our model qualitatively reproduces the observed reduced microwave brightness temperature in the northern part of the sunspot in the VLA observations from **13 May 1999** and provides a physical explanation for the coronal dark lanes. We propose application of this method to other sunspots with such observed dark regions in EUV or soft X-rays and with concurrent microwave observations to determine the significance of open field regions. The connection between open fields and the resulting plasma temperature and density change is of relevance for slow solar wind source investigations.

Glasgow Callisto and CMEless type II bursts

Peter **Wakeford** and Hugh Hudson
RHESSI Science Nugget No. 246, Feb **2015**
http://sprg.ssl.berkeley.edu/~tohban/wiki/index.php/Glasgow_Callisto_and_CMEless_type_II_bursts

In an earlier Nugget we noted the development of NOAA active region 2192, in October 2014; this region produced a remarkable series of major flares but few CMEs and no SEPs. We were thus quite surprised to find that our Glasgow Callisto radio observatory had actually detected type II bursts from some of these flares. **21 Oct 2014**

Statistical analysis of solar radio fiber bursts and relations with flares

Junlin **Wan**1,2, Jianfei Tang1,3, Baolin Tan2,3, Jinhua Shen1,3 and Chengming Tan2,3
A&A 653, A38 (**2021**)
https://www.aanda.org/articles/aa/pdf/2021/09/aa40498-21.pdf
https://doi.org/10.1051/0004-6361/202140498

Fiber bursts are a type of fine structure that frequently occurs in solar flares. Although observations and theory of fiber bursts have been studied for decades, their microphysical process, emission mechanism, and especially the physical links with the flaring process still remain unclear. We performed a detailed statistical study of fiber bursts observed by the Chinese Solar Broadband Radio Spectrometers in Huairou with high spectral-temporal resolutions in the frequency ranges of 1.10−2.06 GHz and 2.60−3.80 GHz during 2000−2006. We identify more than 900 individual fiber bursts in 82 fiber events associated with 48 solar flares. From the soft X-ray observations of the Geostationary Operational

Environmental Satellite, we found that more than 40% of fiber events occurred in the preflare and rising phases of the associated solar flares. Most fiber events are temporally associated with hard X-ray bursts observed by RHESSI or microwave bursts observed by the Nobeyama Radio Polarimaters, which implies that they are closely related to the nonthermal energetic electrons. The results indicate that most fiber bursts have a close temporal relation with energetic electrons. Most fiber bursts are strongly polarized, and their average duration, relative bandwidth, and relative frequency-drift rate are about 1.22 s, 6.31%, and −0.069 s−1. The average duration and relative bandwidth of fiber bursts increase with solar flare class. The fiber bursts associated with X-class flares have a significantly lower mean relative frequency-drift rate. The average durations in the postflare phase are clearly longer than the duration in the preflare and rising phases. The relative drift rate in the rising phase is clearly higher than that in preflare and postflare phases. The hyperbola correlation of the average duration and the relative drift rate of the fiber bursts is very interesting. These characteristics are very important for understanding the formation of solar radio fiber bursts and for revealing the nonthermal processes of the related solar flares.

Solar Radio Burst Prediction Based on a Multimodal Model.

Wang, Y.H., Feng, S.W., Du, Q.F. et al.
Sol Phys 299, 49 (**2024**).
https://doi.org/10.1007/s11207-024-02296-w
The rotation of the solar corona is not a fully resolved issue. Coronal holes (CHs) reveal sometimes more rigid, but in other cases more differential rotation profiles. We used two datasets of coronal bright points (CBPs), one within CHs, and one outside of CHs. We analyzed rotation profiles in the two datasets of CBPs and compared them to check if there is any difference between rotation profiles for CBPs within CHs and those outside of CHs. The reported rigidity of the CHs rotational profiles implies that Reynolds stresses, which are considered to be the main drivers of the solar differential profile, should also be different between the two datasets. Therefore, we analyzed the horizontal Reynolds stress for the two datasets as well. We also compared the meridional motion of the two datasets. In all cases the results between the two datasets were the same within the observational error. In both datasets the solar rotation profile is significantly differential and similar to the photospheric profile.

The Solar Origin of an In Situ Type III Radio Burst Event

Meiqi **Wang** (1), Bin Chen (1), Sijie Yu (1), Dale E. Gary (1), Jeongwoo Lee (1, 2), Haimin Wang (1), Christina Cohen (3)
ApJ **954** 32 **2023**
https://arxiv.org/pdf/2306.01910.pdf
https://iopscience.iop.org/article/10.3847/1538-4357/ace904/pdf
Solar type III radio bursts are generated by beams of energetic electrons that travel along open magnetic field lines through the corona and into interplanetary space. However, understanding the source of these electrons and how they escape into interplanetary space remains an outstanding topic. Here we report multi-instrument, multi-perspective observations of an interplanetary type III radio burst event shortly after the second perihelion of the Parker Solar Probe (PSP). This event was associated with a solar jet that produced an impulsive microwave burst event recorded by the Expanded Owens Valley Solar Array (EOVSA). The type III burst event also coincided with the detection of enhanced in situ energetic electrons recorded by both PSP at 0.37 AU and WIND at 1 AU, which were located very closely on the Parker spiral longitudinally. The close timing association and magnetic connectivity suggest that the in situ energetic electrons originated from the jet's magnetic reconnection region. Intriguingly, microwave imaging spectroscopy results suggest that the escaping energetic electrons were injected into a large opening angle of about 90 degrees, which is at least nine times broader than the apparent width of the jet spire. Our findings provide an interpretation for the previously reported, longitudinally broad spatial distribution of flare locations associated with prompt energetic electron events and have important implications for understanding the origin and distribution of energetic electrons in interplanetary space. **2019 April 15**

Solar radio-frequency reflectivity and localization of FRB from solar reflection

S **Wang**, J I Katz
Monthly Notices of the Royal Astronomical Society, 518, Issue 2, January **2023**, Pages 2119–2122,
https://doi.org/10.1093/mnras/stac3291
The radiation of a fast radio burst (FRB) reflects from the Moon and Sun. If a reflection is detected, the time interval between the direct and reflected signals constrains the source to a narrow arc on the sky. If both Lunar and Solar reflections are detected these two arcs intersect, narrowly confining the location on the sky. A previous paper calculated reflection by the Moon. Here, we calculate the reflectivity of the Sun in the 'flat Sun' approximation as a function of angle of incidence and frequency. The reflectivity is high at low frequencies ($\lesssim$100 MHz) and grazing incidence (angles $\gtrsim$60°), but exceeds 0.1 for frequencies $\lesssim$80 MHz at all angles. However, the intense thermal emission of the Solar corona likely precludes detection of the Solar reflection of even MJy Galactic bursts like FRB 200428.

Overexpansion-dominated Coronal Mass Ejection Formation and Induced Radio Bursts

B. T. **Wang**, X. Cheng, H. Q. Song, M. D. Ding
A&A **2022**
https://arxiv.org/pdf/2209.06508.pdf
Aims. Coronal Mass Ejections (CMEs) are the most fascinating explosion in the solar system; however, their formation is still not fully understood. Methods. Here, we investigate a well-observed CME on **2021 May 07** that showed a typical three-component structure and was continuously observed from 0 to 3 Rsun by a combination of SDO/AIA (0--1.3 Rsun), PROBA2/SWAP (0--1.7 Rsun) and MLSO/K-Cor (1.05--3 Rsun). Furthermore, we compare the morphological discrepancy between the CME white-light bright core and EUV blob. In the end, we explore the origin of various radio bursts closely related to the interaction of the CME overexpansion with nearby streamer. Results. An interesting finding is that the height increases of both the CME leading front and bright core are dominated by the overexpansion during the CME formation. The aspect ratios of the CME bubble and bright core, quantifying the overexpansion, are found to decrease as the SO/STIX 4--10 keV and GOES 1--8 A soft X-ray flux of the associated flare increases near the peaks, indicating an important role of the flare reconnection in the first overexpansion. The CME bubble even takes place a second overexpansion although relatively weak, which is closely related to the compression with a nearby streamer and likely arises from an ideal MHD process. Moreover, the CME EUV blob is found to be relatively lower and wider than the CME white-light bright core, may correspond to the bottom part of the growing CME flux rope. The interaction between the CME and the streamer leads to two type II radio bursts, one normally drifting and one stationary, which are speculated to be induced at two different sources of the CME-driven shock front. The bidirectional electrons evidenced by series of "C-shaped" type III bursts suggest that the interchange reconnection be also involved during the interaction of the CME and streamer.

Statistical properties of radio flux densities of solar flares

Wang Lu, Liu Si-ming, Ning Zong-jun
Research in Astronomy and Astrophysics **2020**
https://arxiv.org/pdf/2006.02121.pdf
Short timescale flux variations are closely related to the energy release process of magnetic reconnection during solar flares. Radio light curves at 1, 2, 3.75, 9.4, and 17 GHz of 209 flares observed by the Nobeyama Radio Polarimeter from 2000 to 2010 are analyzed with a running smooth technique. We find that the impulsive component (with a variation timescale shorter than 1 second) of 1 GHz emission of most flares peaks at a few tens of solar flux unit and lasts for about 1 minute and the impulsive component of 2 GHz emission lasts a shorter period and peaks at a lower flux level, while at the three high frequency channels the occurrence frequency of flares increases with the decrease of the flux density up to the noise level of the corresponding background. The gradual components of these emissions, however, have similar duration and peak flux density distributions. We also derive the power spectrum on different timescales and a normalized wavelet analysis is used to confirm features on short timescales. At a time resolution of 0.1 second, more than ~ 60% of these radio light curves show significant flux variation on 1 second or shorter time scales. This fraction increases with the decrease of frequency and reaches ~ 100% at 1 GHz, implying that short timescale processes are universal in solar flares. We also study the correlation between the impulsive radio flux densities and soft X-ray fluxes obtained with the GOES satellites and find that more than 65% of the flares with an impulsive component have their impulsive radio emission reach a peak value ahead of the soft X-ray fluxes and this fraction increases with the radio frequency. **2000.07.25, 2001.03.25, 2001.05.20, 2001.11.30, 2002.04.09, 2003.10.24, 2004.01.07, 2004.07.24, 2004.11.10, 13 Dec 2006**

Dynamic Spectral Imaging of Decimetric Fiber Bursts in an Eruptive Solar Flare

Zhitao **Wang**, Bin Chen, Dale E. Gary
ApJ **848** 77 **2017**
https://arxiv.org/pdf/1709.08137.pdf
Fiber bursts are a type of fine structure that is often superposed on type IV radio continuum emission during solar flares. Although studied for many decades, its physical exciter, emission mechanism, and association with the flare energy release remain unclear, partly due to the lack of simultaneous imaging observations. We report the first dynamic spectroscopic imaging observations of decimetric fiber bursts, which occurred during the rise phase of a long-duration eruptive flare on **2012 March 3**, as obtained by the Karl G. Jansky Very Large Array in 1--2 GHz. Our results show that the fiber sources are located near and above one footpoint of the flare loops. The fiber source and the background continuum source are found to be cospatial and share the same morphology. It is likely that they are associated with nonthermal electrons trapped in the converging magnetic fields near the footpoint, as supported by a persistent coronal hard X-ray source present during the flare rise phase. We analyze three groups of fiber bursts in detail with dynamic imaging spectroscopy and obtain their mean frequency-dependent centroid trajectories in projection. By using a barometric density model and magnetic field based on a potential-field extrapolation, we further reconstruct the 3-D source trajectories of fiber bursts, for comparison with expectations from the whistler wave model and two MHD-based models. We conclude that the observed fiber burst properties are consistent with an exciter moving at the propagation velocity expected for whistler waves, or models that posit similar exciter velocities.

High-resolution observations of flare precursors in the low solar atmosphere

Haimin **Wang**, Chang Liu, Kwangsu Ahn, Yan Xu, Ju Jing, Na Deng, Nengyi Huang, Rui Liu, Kanya Kusano, Gregory D. Fleishman, Dale E. Gary, Wenda Cao

Nature Astronomy 1, 0085 **2017**

https://arxiv.org/pdf/1703.09866.pdf

http://www.nature.com/articles/s41550-017-0085

Solar flares are generally believed to be powered by free magnetic energy stored in the corona, but the build up of coronal energy alone may be insufficient for the imminent flare occurrence. The flare onset mechanism is a critical but less understood problem, insights into which could be gained from small-scale energy releases known as precursors, which are observed as small pre-flare brightenings in various wavelengths, and also from certain small-scale magnetic configurations such as the opposite polarity fluxes, where magnetic orientation of small bipoles is opposite to that of the ambient main polarities. However, high-resolution observations of flare precursors together with the associated photospheric magnetic field dynamics are lacking. Here we study precursors of a flare using unprecedented spatiotemporal resolution of the 1.6 m New Solar Telescope, complemented by novel microwave data. Two episodes of precursor brightenings are initiated at a small-scale magnetic channel (a form of opposite polarity fluxes) with multiple polarity inversions and enhanced magnetic fluxes and currents, lying near the footpoints of sheared magnetic loops. The low-atmospheric origin of these precursor emissions is corroborated by microwave spectra. We propose that the emerging magnetic channel field interacts with the sheared arcades to cause precursor brightenings at the main flare core region. These high-resolution results provide evidence of low-atmospheric small-scale energy release and possible relationship to the onset of the main flare. **22 June 2015**

A Scenario for the Fine Structures of Solar Type IIIb Radio Bursts Based on the Electron Cyclotron Maser Emission

C. B. **Wang**

ApJ **806** 34 **2015**

http://arxiv.org/pdf/1504.01126v1.pdf

A scenario based on the electron cyclotron maser emission is proposed for the fine structures of solar radio emission in the present discussion. It is suggested that under certain conditions modulation of the ratio between the plasma frequency and electron gyro-frequency by ultra low frequency waves, which is a key parameter for excitation of the electron cyclotron maser instability, may lead to the intermittent emission of radio waves. As an example, the explanation of the observed fine-structure components in the solar type IIIb burst is discussed in detail. Three primary issues of the type IIIb bursts are addressed: 1) what is the physical mechanism that results in the intermittent emission elements that form a chain in the dynamic spectrum of type IIIb bursts, 2) what causes the split pair (or double stria) and the triple stria, 3) why in the events of fundamental-harmonic pair emission there is only IIIb-III, but IIIb-IIIb or III-IIIb cases are very rarely observed.

Coronal Magnetography of a Simulated Solar Active Region from Microwave Imaging Spectropolarimetry

Zhitao **Wang**, Dale E. Gary, Gregory D. Fleishman, Stephen M. White

2015 *ApJ* **805** 93

http://arxiv.org/pdf/1503.05239v1.pdf

We have simulated the Expanded Owens Valley Solar Array (EOVSA) radio images generated at multiple frequencies from a model solar active region, embedded in a realistic solar disk model, and explored the resulting datacube for different spectral analysis schemes to evaluate the potential for realizing one of EOVSA's most important scientific goals--coronal magnetography. In this paper, we focus on modeling the gyroresonance and free-free emission from an on-disk solar active region model with realistic complexities in electron density, temperature and magnetic field distribution. We compare the magnetic field parameters extrapolated from the image datacube along each line of sight after folding through the EOVSA instrumental profile with the original (unfolded) parameters used in the model. We find that even the most easily automated, image-based analysis approach (Level 0) provides reasonable quantitative results, although they are affected by systematic effects due to finite sampling in the Fourier (uv) plane. Finally, we note the potential for errors due to misidentified harmonics of the gyrofrequency, and discuss the prospects for applying a more sophisticated spectrally-based analysis scheme (Level 1) to resolve the issue in cases where improved uv coverage and spatial resolution are available.

Calibration and Data Processing for a Chinese Spectral Radioheliograph in the Decimeter Wave Range

W. **Wang**, Y. Yan, D. Liu, Z. Chen, C. Su, F. Liu, L. Geng, L. Chen, and J. Du

Publ. Astron. Soc. Japan 65, SP1, S18 [5 pages] (**2013**)

http://pasj.asj.or.jp/v65/sp1/65S018/65S018.pdf
The Chinese Spectral Radioheliograph is a solar-dedicated interferometric array with a frequency range from 400MHz to 15 GHz. There are 40 4.5m antennas with 400MHz to 2 GHz, and 60 2m antennas with 2 GHz to 15 GHz in this telescope. CSRH is under construction at Mingantu station, which is about 400 km away from Beijing in China. Now, CSRH-I, which includes an antenna, a receiver, and a correlator in the decimetric wave range, has already been established. CSRH-II is under construction and will be completed by the end of this year. This paper introduces the whole system of CSRH-I briefly, and presents delay measurements, polarization calibration, and some other results of calibration and data processing for CSRH-I.
See http://www.arcetri.astro.it/IAUSpS6/Proceedings/Geng.IAU.pdf

Reversed Drifting Quasi-periodic Pulsating Structure in the X1.3 Solar Flare on 30 July 2005

Rui **Wang**, Baolin Tan, Chengming Tan and Yihua Yan
Solar Physics
Volume 278, Number 2 (**2012**), 411-419
Based on the analysis of the microwave observations at the frequency range of 2.60 – 3.80 GHz in the solar X1.3 flare event observed at the Solar Broadband RadioSpectrometer in Huairou (SBRS/Huairou) on **30 July 2005**, an interesting reversed drifting quasi-periodic pulsating structure (R-DPS) is confirmed. The R-DPS is mainly composed of two drifting pulsating components: one is a relatively slow very short-period pulsation (VSP) with a period of about 130 – 170 ms, the other is a relatively fast VSP with a period of about 70 – 80 ms. The R-DPS has a weak left-handed circular polarization. Based on the synthetic investigations of Reuven Ramaty High Energy Solar Spectroscopic Imaging (RHESSI) hard X-ray, Geostationary Operational Environmental Satellite (GOES) soft X-ray observations, and magnetic field extrapolation, we suggest that the R-DPS possibly reflects flaring dynamic processes of the emission source regions.

Flux-rms relation in solar radio bursts

Lin **Wang**, Cheng Fang and Yu Ying Liu
Astrophysics and Space Science, Volume 318 Number 1-2, 79 – 86, **2008, File**
One recent discovery that provides a strong constraint on the mechanisms of astrophysical activities is the correlation between the flux and the root-mean-squared (rms) variability of X-ray emission. In this work we study the flux-rms relation of solar radio bursts. Four flares observed by the *Solar Radio Broadband Spectrometer* (SRBS) of China are analyzed. In these flares, fine structures (FSs) emerge at least in one frequency band of SRBS. We find that the flux-rms relation consists of two components. One relates to the non-FS emission and the other to the FS emission. The flux-rms relationship for the non-FS part of the radio bursts is clearly different from that for the FS part. The former shows a curve-like behavior, while the latter shows a dramatic variation. We propose a model to describe the flux-rms relation of the non-FS part. Our results imply that the non-FS part emission could be triggered by some multiplicative processes. On the contrary, multiplicative mechanisms should be excluded from the explanations of FSs in the radio bursts.

Solar Radio Spikes in 2.6 – 3.8 GHz during the 13 December 2006 Event

S.J. **Wang** · Y.H. Yan · Y.Y. Liu · Q.J. Fu · B.L. Tan · Y. Zhang
Solar Phys (**2008**) 253: 133–141
On **13 December 2006**, some unusual radio bursts in the range 2.6 – 3.8 GHz were observed during an X3.4 flare/CME event from 02:30 to 04:30 UT in active region NOAA 10930 (S06W27) with the digital spectrometers of the National Astronomical Observatories of China (NAOC). During this event many spikes were detected with the high temporal resolution of 8 ms and high frequency resolution of 10 MHz. Many of them were found to have complex structures associated with other radio burst types. The new observational features may reflect certain emission signatures of the electron acceleration site. In this paper, we present the results of the analysis of the new observational features of the complex spikes. According to the observed properties of the spikes, we identify five classes. Their observational parameters, such as duration, bandwidth, and relative bandwidth, were determined. Most spikes had negative polarization, but spikes with positive polarization were observed during a short time interval and were identified as a separate class. Based on the analysis of observations with *Hinode*/SOT (Solar Optical Telescope) we suggest that the sources of the spikes with opposite polarizations were different. Combined observations of spikes and fiber bursts are used to estimate the magnetic field strength in the source.

Microwave observations of a large-scale coronal wave with the Nobeyama radioheliograph

A. **Warmuth**1, K. Shibasaki2, K. Iwai3 and G. Mann
A&A 593, A102 (**2016**)
Context. Large-scale globally propagating waves in the solar corona have been studied extensively, mainly using extreme ultraviolet (EUV) observations. In a few events, corresponding wave signatures have been detected in microwave radioheliograms provided by the Nobeyama radioheliograph (NoRH). Several aspects of these observations seem to contradict the conclusions drawn from EUV observations.
Aims. We investigate whether the microwave observations of global waves are consistent with previous findings.
Methods. We revisited the wave of **1997 Sep. 24**, which is still the best-defined event in microwaves. We obtained radioheliograms at 17 and 34 GHz from NoRH and studied the morphology, kinematics, perturbation profile evolution, and emission mechanism of the propagating microwave signatures.
Results. We find that the NoRH wave signatures are morphologically consistent with both the associated coronal wave as observed by SOHO/EIT and the Moreton wave seen in Hα. The NoRH wave is clearly decelerating, which is typically found for large-amplitude coronal waves associated with Moreton waves, and its kinematical curve is consistent with the EIT wavefronts. The perturbation profile shows a pronounced decrease in amplitude. Based on the derivation of the spectral index of the excess microwave emission, we conclude that the NoRH wave is due to optically thick free-free bremsstrahlung from the chromosphere.
Conclusions. The wavefronts seen in microwave radioheliograms are chromospheric signatures of coronal waves, and their characteristics support the interpretation of coronal waves as large-amplitude fast-mode MHD waves or shocks.

Coronal waves, shocks, and associated radio signatures **Review**

Alexander **Warmuth**∗
CESRA **2016** p.37
http://cesra2016.sciencesconf.org/conference/cesra2016/pages/CESRA2016_prog_abs_book_v3.pdf
For over half a century there has been indirect evidence for large-scale waves and shocks propagating through the solar corona. High-cadence space-based observations, available for nearly decade now, have indeed revealed globally propagating wave-like perturbations in the solar corona. These observations have revealed a wealth of information about these phenomena, but have also sparked major controversies about their physical nature and their cause. I will review how the different observational characteristics have both constrained existing models and have led to the development of new models. In the discussion, I will emphasize two issues: the currently growing consensus on the physical nature of coronal waves, and the question of how type II radio bursts fit into the picture.

RAPID CHANGES OF ELECTRON ACCELERATION CHARACTERISTICS AT THE END OF THE IMPULSIVE PHASE OF AN X-CLASS SOLAR FLARE

Alexander **Warmuth**1, Gordon D. Holman2, Brian R. Dennis2, Gottfried Mann1, Henry Aurass1, and Ryan O. Milligan2
Astrophysical Journal, 699:917–922, **2009**
http://www.iop.org/EJ/toc/-alert=43190/0004-637X/699/1
obtained with *RHESSI*. This flare exhibits HXR pulses during the impulsive phase, with a particularly pronounced peak at the end of the impulsive phase. This peak is associated with HXR emission up to high energies (>300 keV) but does not show any Neupert effect (i.e., no simultaneous rise in soft X-rays). Fitting the spatially integrated photon spectra with a Maxwellian plus a nonthermal thick-target component reveals that the data are consistent with a high low-energy cutoff (≈ 100 keV) of the energetic electrons during the late peak. The high lowenergy cutoff straightforwardly explains the lack of a Neupert effect—while highly energetic electrons are produced efficiently, there is a lack of low-energy electrons that usually contain the bulk of the total energy. Hence, the energy input into the chromosphere remains too small to trigger chromospheric evaporation. This observation shows that the characteristics of electron acceleration can change dramatically and rapidly at the end of the impulsive phase of solar flares. This could be evidence for physically distinct acceleration processes acting in the same event, or alternatively for a sudden shift in the characteristic parameters of the accelerator. Using radio observations and comparing HXR images with magnetograms, we conclude that changes in the strength and the topology of the magnetic field in which the accelerator is working are responsible for the profound changes in the injected electron spectrum.

Constraining Electron Acceleration at a Standing Shock with HXR and Radio Observations

Warmuth, A.; Mann, G.; Aurass, H.
Central European Astrophysical Bulletin (CEAB), **2007**CEAB...31..135W
The acceleration of electrons to non-thermal energies in solar flares is one of the main unsolved questions in solar physics. One possibility for the production of these energetic electrons is acceleration at the reconnection outflow termination shock (TS). We use radio observations to constrain the characteristics of the TS, and hard X-ray and γ-ray observations provided by RHESSI and INTEGRAL to obtain the characteristics of the injected differential electron flux. Invoking relativistic shock-drift acceleration at the TS, we calculate differential electron fluxes, which are then compared with the observations. This approach allows us to answer the question if, and under which conditions, the TS is a viable electron accelerator.

The application of radio diagnostics to the study of the solar drivers of space weather

Warmuth, A., & Mann, G.:
2005, Springer Lecture Notes in Physics, Vol. 656, 49; **File**

A model of the Alfven speed in the solar corona.

Warmuth, A., & Mann, G.
Astron. Astrophys., 435, 1123-1135 (**2005**); **File**
We present an analytic model of the Alfven speed vA in the solar corona. The coronal magnetic field is modeled by a radial component representing the global field and by a dipole representing an active region. The free parameters of the model are constrained by actual observations of solar magnetic fields and coronal electron densities. The coronal magnetic field strength in the quiet Sun is determined by coronal seismology, using EIT waves as proxies for the fast magnetosonic speed vms, and thus for the magnetic field strength. Depending on the orientation of the dipole, we find local minima of vA (and vms) at the coronal base at distances of 0.2-0.3 solar radii from the center of the modelled active region (AR), as well as above the AR at comparable heights. For all dipole orientations, a global maximum is found at 3.5 solar radii. We apply our model to the study of the formation and propagation of coronal shock waves which are observed as flare waves and as type II radio bursts, using a sample of eight solar events. We find that flare waves are initially highly supermagnetosonic (with magnetosonic Mach numbers of Mms=~2-3). During their propagation, they decelerate until Mms=1 is reached. This behavior can be explained by a strong shock or large-amplitude simple wave that decays to an ordinary fast magnetosonic wave. The observed starting frequencies and Mach numbers of the associated type II bursts are consistent with the predictions of the model.

Resolving moving heliospheric structures using interplanetary scintillation observations with the Murchison Widefield Array

A. **Waszewski**, J.S. Morgan, R. Chhetri, R. Ekers, M.C.M. Cheung, N.D.R Bhat, M. Johnston-Hollitt
Space Weather **Volume21, Issue10** e2023SW003570 **2023**
https://arxiv.org/pdf/2309.10349.pdf
https://agupubs.onlinelibrary.wiley.com/doi/epdf/10.1029/2023SW003570
We have conducted a blind search in 49 consecutive days of interplanetary scintillation observations made by the Murchison Widefield Array from mid-2019, with overlapping daily observations approximately East and South-East of the Sun at an elongation of ∼30 degrees and a field of view of 30 degrees. These observations detect an unprecedented density of sources. In spite of these observations being taken at sunspot minimum, this search has revealed several interesting transitory features characterised by elevated scintillation levels. One solar wind enhancement is captured in two observations several hours apart, allowing its radial movement away from the Sun to be measured. We present here a methodology for measuring the plane-of-sky velocity for the moving heliospheric structure. The plane-of-sky velocity was inferred as 0.66±0.147ohr−1, or 480±106kms−1 assuming a distance of 1AU. After cross-referencing our observed structure with multiple catalogues of heliospheric events, we propose that the likely source of our observed structure is a stream-interaction region originating from a low-latitude coronal hole. This work demonstrates the power of widefield interplanetary scintillation observations to capture detailed features in the heliosphere which are otherwise unresolvable and go undetected. **2019-AUG-04**

ALMA Memo 628 -- High-cadence observations of the Sun

Sven **Wedemeyer**, Mikolaj Szydlarski, M. Carmen Toribio, Tobia Carozzi, Daniel Jakobsson, Juan Camilo Guevara Gomez, Henrik Eklund, Vasco M. J. Henriques, Shahin Jafarzadeh, Jaime de la Cruz Rodriguez
ALMA Memo 628 summarising the results of the ESO-funded ALMA development study "High-cadence Imaging of the Sun", concluded in 2023 (74 pages, 53 figures) **2024**

https://arxiv.org/pdf/2408.14265
The Atacama Large Millimeter/submillimeter Array (ALMA) offers new diagnostic capabilities for studying the Sun, providing complementary insights through high spatial and temporal resolution at millimeter wavelengths. ALMA acts as a linear thermometer for atmospheric gas, aiding in understanding the solar atmosphere's structure, dynamics, and energy balance. Given the Sun's complex emission patterns and rapid evolution, high-cadence imaging is essential for solar observations. Snapshot imaging is required, though it limits available visibility data, making full exploitation of ALMA's capabilities non-trivial. Challenges in processing solar ALMA data highlight the need for revising and enhancing the solar observing mode. The ALMA development study High-Cadence Imaging of the Sun demonstrated the potential benefits of high cadence observations through a forward modelling approach. The resulting report provides initial recommendations for improved post-processing solar ALMA data and explores increasing the observing cadence to sub-second intervals to improve image reliability.

Science development study for the Atacama Large Aperture Submillimeter Telescope (AtLAST) - Solar and stellar observations

Sven **Wedemeyer**, Miroslav Barta, Roman Brajsa, Yi Chai, Joaquim Costa, Dale Gary, +++
https://arxiv.org/pdf/2403.00920.pdf
Open Research Europe as part of a collection on the Atacama Large Aperture Submillimeter Telescope (AtLAST) **2024**
https://arxiv.org/pdf/2403.00920.pdf
Observations at (sub-)millimeter wavelengths offer a complementary perspective on our Sun and other stars, offering significant insights into both the thermal and magnetic composition of their chromospheres. Despite the fundamental progress in (sub-)millimeter observations of the Sun, some important aspects require diagnostic capabilities that are not offered by existing observatories. In particular, simultaneously observations of the radiation continuum across an extended frequency range would facilitate the mapping of different layers and thus ultimately the 3D structure of the solar atmosphere. Mapping large regions on the Sun or even the whole solar disk at a very high temporal cadence would be crucial for systematically detecting and following the temporal evolution of flares, while synoptic observations, i.e., daily maps, over periods of years would provide an unprecedented view of the solar activity cycle in this wavelength regime. As our Sun is a fundamental reference for studying the atmospheres of active main sequence stars, observing the Sun and other stars with the same instrument would unlock the enormous diagnostic potential for understanding stellar activity and its impact on exoplanets. The Atacama Large Aperture Submillimeter Telescope (AtLAST), a single-dish telescope with 50\,m aperture proposed to be built in the Atacama desert in Chile, would be able to provide these observational capabilities. Equipped with a large number of detector elements for probing the radiation continuum across a wide frequency range, AtLAST would address a wide range of scientific topics including the thermal structure and heating of the solar chromosphere, flares and prominences, and the solar activity cycle. In this white paper, the key science cases and their technical requirements for AtLAST are discussed. **December 18, 2015**

Prospects and challenges of numerical modelling of the Sun at millimetre wavelengths Review

Sven **Wedemeyer**, Gregory Fleishman, Jaime de la Cruz Rodriguez, Stanislav Gunar, Joao M. da Silva Santos, Patrick Antolin, Juan Camilo Guevara Gomez, Mikolaj Szydlarski, Henrik Eklund
Frontiers in Astronomy and Space Sciences 9:967878 **2022**
https://arxiv.org/pdf/2210.13894.pdf
https://doi.org/10.3389/fspas.2022.967878
https://www.frontiersin.org/articles/10.3389/fspas.2022.967878/pdf
The Atacama Large Millimeter/submillimeter Array (ALMA) offers new diagnostic possibilities that complement other commonly used diagnostics for the study of our Sun. In particular, ALMA's ability to serve as an essentially linear thermometer of the chromospheric gas at unprecedented spatial resolution at millimetre wavelengths and future polarisation measurements have great diagnostic potential. Solar ALMA observations are therefore expected to contribute significantly to answering long-standing questions about the structure, dynamics and energy balance of the outer layers of the solar atmosphere. In this regard, current and future ALMA data are also important for constraining and further developing numerical models of the solar atmosphere, which in turn are often vital for the interpretation of observations. The latter is particularly important given the Sun's highly intermittent and dynamic nature that involves a plethora of processes occurring over extended ranges in spatial and temporal scales. Realistic forward modelling of the Sun therefore requires time-dependent three-dimensional radiation magnetohydrodynamics that account for non-equilibrium effects and, typically as a separate step, detailed radiative transfer calculations, resulting in synthetic observables that can be compared to observations. Such artificial observations sometimes also account for instrumental and seeing effects, which, in addition to aiding the interpretation of observations, provide instructive tools for designing and optimising ALMA's solar observing modes. In the other direction, ALMA data in combination with other simultaneous observations enables the reconstruction of the solar atmospheric structure via data inversion techniques. This article highlights central aspects of the impact of ALMA for numerical modelling for the Sun, their potential and challenges, together with selected examples.

The Sun at millimeter wavelengths I. Introduction to ALMA Band 3 observations

Sven **Wedemeyer**, Mikolaj Szydlarski, Shahin Jafarzadeh, Henrik Eklund, Juan Camilo Guevara Gomez, Tim Bastian, Bernhard Fleck, Jaime de la Cruz Rodriguez, Andrew Rodger, Mats Carlsson

A&A 635, A71 **2020**
https://arxiv.org/pdf/2001.02185.pdf
https://www.aanda.org/articles/aa/pdf/2020/03/aa37122-19.pdf
We present an initial study of one of the first ALMA Band 3 observations of the Sun with the aim to characterise the diagnostic potential of brightness temperatures measured with ALMA on the Sun. The observation covers 48min at a cadence of 2s targeting a Quiet Sun region at disk-centre. Corresponding time series of brightness temperature maps are constructed with the first version of the Solar ALMA Pipeline (SoAP) and compared to simultaneous SDO observations. The angular resolution of the observations is set by the synthesized beam (1.4x2.1as). The ALMA maps exhibit network patches, internetwork regions and also elongated thin features that are connected to large-scale magnetic loops as confirmed by a comparison with SDO maps. The ALMA Band 3 maps correlate best with the SDO/AIA 171, 131 and 304 channels in that they exhibit network features and, although very weak in the ALMA maps, imprints of large-scale loops. A group of compact magnetic loops is very clearly visible in ALMA Band 3. The brightness temperatures in the loop tops reach values of about 8000-9000K and in extreme moments up to 10 000K. ALMA Band 3 interferometric observations from early observing cycles already reveal temperature differences in the solar chromosphere. The weak imprint of magnetic loops and the correlation with the 171, 131, and 304 SDO channels suggests though that the radiation mapped in ALMA Band 3 might have contributions from a larger range of atmospheric heights than previously assumed but the exact formation height of Band 3 needs to be investigated in more detail. The absolute brightness temperature scale as set by Total Power measurements remains less certain and must be improved in the future. Despite these complications and the limited angular resolution, ALMA Band 3 observations have large potential for quantitative studies of the small-scale structure and dynamics of the solar chromosphere. **2016-12-22**

ALMA Observations of the Sun in Cycle 4 and Beyond

S. **Wedemeyer**, B. Fleck, M. Battaglia, N. Labrosse, G. Fleishman, H. Hudson…
SSALMON White Paper with focus on potential solar science with ALMA in Cycle 4; 54 pages. Version 1.1, January 6th, **2016**
http://arxiv.org/ftp/arxiv/papers/1601/1601.00587.pdf
This document was created by the Solar Simulations for the Atacama Large Millimeter Observatory Network (SSALMON) in preparation of the first regular observations of the Sun with the Atacama Large Millimeter/submillimeter Array (ALMA), which are anticipated to start in ALMA Cycle 4 in October 2016. The science cases presented here demonstrate that a large number of scientifically highly interesting observations could be made already with the still limited solar observing modes foreseen for Cycle 4 and that ALMA has the potential to make important contributions to answering long-standing scientific questions in solar physics. With the proposal deadline for ALMA Cycle 4 in April 2016 and the Commissioning and Science Verification campaign in December 2015 in sight, several of the SSALMON Expert Teams composed strategic documents in which they outlined potential solar observations that could be feasible given the anticipated technical capabilities in Cycle 4. These documents have been combined and supplemented with an analysis, resulting in recommendations for solar observing with ALMA in Cycle 4. In addition, the detailed science cases also demonstrate the scientific priorities of the solar physics community and which capabilities are wanted for the next observing cycles. The work on this White Paper effort was coordinated in close cooperation with the two international solar ALMA development studies led by T. Bastian (NRAO, USA) and R. Brajsa, (ESO). This document will be further updated until the beginning of Cycle 4 in October 2016. In particular, we plan to adjust the technical capabilities of the solar observing modes once finally decided and to further demonstrate the feasibility and scientific potential of the included science cases by means of numerical simulations of the solar atmosphere and corresponding simulated ALMA observations.

Solar science with the Atacama Large Millimeter/submillimeter Array - A revolutionizing new view of our Sun **Review**

S. **Wedemeyer**, T. Bastian, R. Brajsa, M. Barta, H. Hudson, G. Fleishman, M. Loukitcheva, B. Fleck, E. P. Kontar, B. De Pontieu, S. K. Tiwari, Y. Kato, R. Soler, P. Yagoubov, J. H. Black, P. Antolin, E. Scullion, S. Gun'ar, N. Labrosse, A. O. Benz, H.-G. Ludwig, P. Hauschildt, J. G. Doyle, V. M. Nakariakov, S. K. Solanki, S. M. White, T. Ayres, P. Heinzel, M. Karlicky, T. Van Doorsselaere, D. Gary,C. E. Alissandrakis, A. Nindos, L. Rouppe van der Voort, M. Shimojo, T. Zaqarashvili, E. Perez
Space Sci. Rev. Volume 200, Issue 1, pp 1-73 **2016**
http://arxiv.org/pdf/1504.06887v2.pdf
The Atacama Large Millimeter/submillimeter Array (ALMA) is a new powerful tool for observing the Sun at high spatial, temporal, and spectral resolution. These capabilities can address a broad range of fundamental scientific questions in solar physics. The radiation observed by ALMA originates mostly from the chromosphere - a complex and dynamic region between the photosphere and corona, which plays a crucial role in the transport of energy and matter

and, ultimately, the heating of the outer layers of the solar atmosphere. Based on first solar test observations, strategies for regular solar campaigns are currently being developed. State-of-the-art numerical simulations of the solar atmosphere and modeling of instrumental effects can help constrain and optimize future observing modes for ALMA. Here we present a short technical description of ALMA and an overview of past efforts and future possibilities for solar observations at submillimeter and millimeter wavelengths. In addition, selected numerical simulations and observations at other wavelengths demonstrate ALMA's scientific potential for studying the Sun for a large range of science cases.
2006 Dec 6, 11 Nov 2010, 11 July 2012, 2014 Jul 31, August 1, 2014, September 7th, 2014
See CESRA highlight #1221, March **2017** **Solar Science with the Atacama Large Millimeter/Submillimeter Array — A New View of Our Sun**
S. Wedemeyer
http://www.astro.gla.ac.uk/users/eduard/cesra/?p=1221

Solar ALMA Observations - A new view of our host star

Sven **Wedemeyer**, Tim Bastian, Roman Brajsa, Miroslav Barta, Masumi Shimojo, Antonio Hales, Pavel Yagoubov, Hugh Hudson
ASP Conference Series, proceedings of "Revolution in Astronomy with ALMA: The 3rd year" (Tokyo, Japan, December 2014), eds. D. Iono, A. Wootten, L. Testi, **2015**
http://arxiv.org/pdf/1502.06397v1.pdf
ALMA provides the necessary spatial, temporal and spectral resolution to explore central questions in contemporary solar physics with potentially far-reaching implications for stellar atmospheres and plasma physics. It can uniquely constraint the thermal and magnetic field structure in the solar chromosphere with measurements that are highly complementary to simultaneous observations with other ground-based and space-borne instruments. Here, we highlight selected science cases.

Solar Simulations for the Atacama Large Millimeter Observatory Network

Sven **Wedemeyer**, Tim Bastian, Roman Brajsa, Miroslav Barta, Masumi Shimojo
ASP Conference Series, proceedings of "Revolution in Astronomy with ALMA: The 3rd year" (Tokyo, Japan, December 2014), eds. D. Iono, A. Wootten, L. Testi, **2015**
http://arxiv.org/pdf/1502.06379v1.pdf
The Atacama Large Millimeter/submillimeter Array (ALMA) will be a valuable tool for observing the chromosphere of our Sun at (sub-)millimeter wavelengths at high spatial, temporal and spectral resolution and as such has great potential to address long-standing scientific questions in solar physics. In order to make the best use of this scientific opportunity, the Solar Simulations for the Atacama Large Millimeter Observatory Network has been initiated. A key goal of this international collaboration is to support the preparation and interpretation of future observations of the Sun with ALMA.

SSALMON - The Solar Simulations for the Atacama Large Millimeter Observatory Network

S. **Wedemeyera**, T. Bastian, R. Brajsa, M. Barta, H. Hudson, G. Fleishman, M. Loukitcheva, B. Fleck, E. Kontar, B. De Pontieu, S. Tiwari, Y. Kato, R. Soler, P. Yagoubov, J. H. Black, P. Antolin, S. Gunar, N. Labrosse, A. O. Benz, A. Nindos, M. Steffen, E. Scullion, J. G. Doyle, T. Zaqarashvili, A. Hanslmeier, V. M. Nakariakov, P. Heinzel, T. Ayres, M. Karlicky, the SSALMON Group
Advances in Solar Physics (special issue of Advances in Space Research, AdSR), proceedings of the 14th European Solar Physics Meeting (ESPM-14, Dublin, Ireland, September 2014), **2015**
Advances in Space Research Volume 56, Issue 12, 15 December **2015**, Pages 2679–2692
http://www.sciencedirect.com/science/article/pii/S0273117715003671
http://arxiv.org/pdf/1502.05601v1.pdf
The Solar Simulations for the Atacama Large Millimeter Observatory Network (SSALMON) was initiated in 2014 in connection with two ALMA development studies. The Atacama Large Millimeter/submillimeter Array (ALMA) is a powerful new tool, which can also observe the Sun at high spatial, temporal, and spectral resolution. The international SSALMONetwork aims at coordinating the further development of solar observing modes for ALMA and at promoting scientific opportunities for solar physics with particular focus on numerical simulations, which can provide important constraints for the observing modes and can aid the interpretation of future observations. The radiation detected by ALMA originates mostly in the solar chromosphere - a complex and dynamic layer between the photosphere and corona, which plays an important role in the transport of energy and matter and the heating of the outer layers of the solar atmosphere. Potential targets include active regions, prominences, quiet Sun regions, flares. Here, we give a brief overview over the network and potential science cases for future solar observations with ALMA.

ALMA's high-cadence imaging capabilities for solar observations

Sven **Wedemeyer**, Asbjorn Parmer

proceedings of the conference "Revolution in Astronomy with ALMA - The 3rd year" (Tokyo, Japan, December 2014, **2015**

http://arxiv.org/pdf/1502.03580v1.pdf

The Atacama Large Millimeter/submillimeter Array offers an unprecedented view of our Sun at sub-/millimeter wavelengths. The high spatial, temporal, and spectral resolution facilitates the measurement of gas temperatures and magnetic fields in the solar chromosphere with high precision. The anticipated results will revolutionize our understanding of the solar atmosphere and may in particular result in major steps towards solving the coronal heating problem. Based on state-of-the-art 3D radiation magnetohydrodynamic simulations, we calculate the emergent continuum intensity (and thus brightness temperature maps) in the wavelength range accessed by ALMA and simulate instrumental effects for different array configurations. First results show that the local gas temperature can be closely mapped with ALMA and that much of the complex small-scale chromospheric pattern can be resolved.

Coronal Magnetic Field Measurements along a Partially Erupting Filament in a Solar Flare

Yuqian **Wei**, Bin Chen, Sijie Yu, Haimin Wang, Ju Jing, Dale E.Gary

ApJ **923** 213 **2021**

https://arxiv.org/pdf/2110.06414.pdf

https://iopscience.iop.org/article/10.3847/1538-4357/ac2f99/pdf

https://doi.org/10.3847/1538-4357/ac2f99

Magnetic flux ropes are the centerpiece of solar eruptions. Direct measurements for the magnetic field of flux ropes are crucial for understanding the triggering and energy release processes, yet they remain heretofore elusive. Here we report microwave imaging spectroscopy

Owens Valley Solar Array. This flare event is associated with a partial eruption of a twisted filament observed in H{\alpha} by the Goode Solar Telescope at the Big Bear Solar Observatory. The extreme ultraviolet (EUV) and X-ray signatures of the event are generally consistent with the standard scenario of eruptive flares, with the presence of double flare ribbons connected by a bright flare arcade. Intriguingly, this partial eruption event features a microwave counterpart, whose spatial and temporal evolution closely follow the filament seen in H{\alpha} and EUV. The spectral properties of the microwave source are consistent with nonthermal gyrosynchrotron radiation. Using spatially resolved microwave spectral analysis, we derive the magnetic field strength along the filament spine, which ranges from 600-1400 Gauss from its apex to the legs. The results agree well with the non-linear force-free magnetic model extrapolated from the pre-flare photospheric magnetogram. We conclude that the microwave counterpart of the erupting filament is likely due to flare-accelerated electrons injected into the filament-hosting magnetic flux rope cavity following the newly reconnected magnetic field lines. **6 Sep 2017, M1.4,19:26**

The science behind SURROUND: a constellation of CubeSats around the Sun

D. M. **Weigt**, L. A. Cañizares, S. A. Maloney, S. A. Murray, E. P. Carley, P. T. Gallagher, A. Macario-Rojas, N. Crisp, C. McGrath

Planetary, Solar and Heliospheric Radio Emissions IX, held 26-28 September, 2022 **2023**

https://arxiv.org/pdf/2308.04194.pdf

One of the greatest challenge facing current space weather monitoring operations is forecasting the arrival of coronal mass ejections (CMEs) and Solar Energetic Particles (SEPs) within their Earth-Sun propagation timescales. Current campaigns mainly rely on extreme ultra-violet and white light observations to create forecasts, missing out many potential events that may be hazardous to Earth's infrastructure undetectable at these wavelengths. Here we introduce the SURROUND mission, a constellation of CubeSats each with identical radio spectrometers, and the results of the initial Phase-0 study for the concept. The main goal of SURROUND is to monitor and track solar radio bursts (SRBs), widely utilised as a useful diagnostic for space weather activity, and revolutionise current forecasting capabilities. The Phase-0 study concludes that SURROUND can achieve its mission objectives using 3 - 5 spacecraft using current technologies with feasible SEP and CME forecasting potential: a first for heliospheric monitors.

Magnetic Properties of Metric Noise Storms Associated with Coronal Mass Ejections *

Ya-Yuan **Wen**, Jing-Xiu Wang and Yu-Zong Zhang

Chin. J. Astron. Astrophys. Vol. 7 (**2007**), No. 2, 265–280, **File**

Using Nanc¸ay Radioheliograph (NRH) imaging observations, combined with SOHO/Michelson Doppler Imager (MDI) magnetogram observations and coronal magnetic field extrapolation, we studied the magnetic nature of metric noise storms that are associated with coronal mass ejections (CMEs). Four events are selected: the events of **2000 July 14, 2001 April 26, 2002 August 16 and 2001 March 28.** The identified noise storm sources cover or partially cover the active regions (ARs), but the centers of storm sources are offset from the

ARs. Using extrapolated magnetic field lines, we find that the noise storm sources trace the boundary between the open and closed field lines. We demonstrate that the disappearance of noise storm source is followed by the appearance of the burst source. The burst sources spread on the solar disk and their distributions correspond to the extent of the CME in LASCO C2 field of view. All the SOHO/Extreme Ultraviolet Imaging Telescope (EIT) dimmings associated with noise storm sources are located at the periphery of noise storms where the magnetic lines of force were previously closed and low-lying. When the closed field becomes partially or fully open, the basic configurations of noise storm sources are changed, then the noise storm sources are no longer observed. These observations provide the information that the variations of noise storms manifest the restructuring or reconfiguring of the coronal magnetic field.

Investigating a Solar Wind Stream Interaction Region using Interplanetary Spacecraft Radio Signals: A Magnetohydrodynamic Simulation Study

David B. **Wexler**1, Ward B. Manchester2, Lan K. Jian3, Lynn B. Wilson III3, Natchimuthuk Gopalswamy3, Paul Song1, Jason E. Kooi4, Bart van der Holst2, and Elizabeth A. Jensen5
2023 ApJ 955 90
https://iopscience.iop.org/article/10.3847/1538-4357/acedac/pdf
Stream interaction regions (SIRs) are spiral heliospheric structures that arise at the interface between fast and preceding slow solar wind regions. SIR enhancements of density and magnetic field intensity, often with magnetic polarity inversion, are potentially geoeffective and therefore important in the analysis of space weather. We studied an MHD heliospheric simulation containing a well-defined SIR using a new instrument concept based on trans-heliospheric radio sensing: Faraday Effect Tracker of Coronal and Heliospheric structures (FETCH). FETCH uses line-of-sight radio propagation techniques to measure Faraday rotation and electron column density. Analysis of the simulated FETCH observations clearly demonstrated density and magnetic field enhancements, and magnetic polarity reversal, all of which were confirmed in Wind spacecraft measurements at 1 au. FETCH provided 4.5–5.7 days lead times for predicting the arrival of SIR features at Earth. The SIR radial speed was estimated to be 350–390 km s−1. These initial results hold promise that FETCH will be valuable in detecting and characterizing the inner heliosphere SIR properties well ahead of their presentation in the local geospace environment.

Slow solar wind acceleration through the middle corona: Spacecraft radio studies.

Wexler DB, Kooi JE, Jensen EA and Song P
(**2022**) Front. Astron. Space Sci. 9: 1047875.
doi: 10.3389/fspas.2022.1047875
https://www.frontiersin.org/articles/10.3389/fspas.2022.1047875/pdf
The “Middle Corona”, defined by recent consensus as the region spanning 1.5–6 solar radii (R⊙, heliocentric), is an important zone through which several structural and dynamic changes occur in coronal streamer regions. Among these is a regime change from high density, closed magnetic field structures to open field structures of much lower electron concentration. Along with this complex restructuring, the forming slow solar wind is channeled and accelerated through the middle corona. Solar wind (SW) outflow speeds can be estimated from trans-coronal radio observations. The method of radio frequency fluctuation (FF) analysis considers the frequency variations arising from density inhomogeneities crossing the sensing line-of-sight (LOS). Below 2 R⊙, where the SW is beginning to form and outflow speed is expected to be below the acoustic wave speed, the radio FF can be attributed to the density oscillations of acoustic waves crossing the radio sensing path. With increasing helioaltitudes through the middle corona, the FF are dominated by density disturbances advected across the sensing LOS. This property enables estimation of solar wind outflow speed at various heliodistances. The coronal plasma is believed to enter the middle corona in a subsonic state, then accelerate to exit the zone generally with supersonic, but sub-Alfvénic flows. Trans-coronal radio sensing complements imaging and other remote coronal observations, and helps bridge the observational gap across the full distance range of the middle corona. Radio techniques enrich the study of solar wind, and should be utilized in next-generation, multiwavelength campaigns that tackle the challenging physics of coronal plasma acceleration.

Coronal Electron Density Fluctuations Inferred from Akatsuki Spacecraft Radio Observations

D. **Wexler**, T. Imamura, A. Efimov, P. Song, L. Lukanina, H. Ando, E. Jensen, J. Vierinen & A. Coster
Solar Physics volume 295, Article number: 111 (**2020**)
https://link.springer.com/content/pdf/10.1007/s11207-020-01677-1.pdf
Trans-coronal radio observations were taken during the 2011 observing campaign of the Akatsuki spacecraft through superior conjunction. The observed X-band (8.4 GHz) signals exhibit frequency fluctuations (FF) that are produced by temporal variations in electron density along the radio ray path. A two-component model for interpretation of the FF is proposed: FF scales largely with acoustic wave amplitude through the inner coronal regions where the sound speed dwarfs the solar wind outflow speed, while FF in the region of solar wind acceleration is dominated by the increased

density oscillation frequency on the sensing path that results from bulk advection of the plasma inhomogeneities. An estimate of fractional electron density fluctuation is obtained from the mid-corona. A radial profile of slow solar wind speed is determined in the extended corona using mass-flux continuity principles. The coronal sonic point for slow solar wind is estimated to range from 4 to 5 solar radii from the heliocenter. **2011-06-25**

Faraday rotation fluctuations of MESSENGER radio signals through the equatorial lower corona near solar minimum

D. B. **Wexler**, E. A. Jensen, J. V. Hollweg, C. Heiles, A. I. Efimov, J. Vierinen, A. J. Coster
Space Weather Volume 15, Issue 2 February **2017** Pages 310–324
Faraday rotation (FR) of transcoronal radio transmissions from spacecraft near superior conjunction enables study of the temporal variations in coronal plasma density, velocity, and magnetic field. The MESSENGER spacecraft 8.4 GHz radio, transmitting through the corona with closest line-of-sight approach 1.63–1.89 solar radii and near-equatorial heliolatitudes, was recorded soon after the deep solar minimum of solar cycle 23. During egress from superior conjunction, FR gradually decreased, and an overlay of wave-like FR fluctuations (FRFs) with periods of hundreds to thousands of seconds was found. The FRF power spectrum was characterized by a power law relation, with the baseline spectral index being −2.64. A transient power increase showed relative flattening of the spectrum and bands of enhanced spectral power at 3.3 mHz and 6.1 mHz. Our results confirm the presence of coronal FRF similar to those described previously at greater solar offset. Interpreted as Alfvén waves crossing the line of sight radially near the proximate point, low-frequency FRF convey an energy flux density higher than that of the background solar wind kinetic energy, but only a fraction of that required to accelerate the solar wind. Even so, this fraction is quite variable and potentially escalates to energetically significant values with relatively modest changes in estimated magnetic field strength and electron concentration. Given the uncertainties in these key parameters, as well as in solar wind properties close to the Sun at low heliolatitudes, we cannot yet confidently assign the quantitative role for Alfvén wave energy from this region in driving the slow solar wind. **8-10 Nov 2009**

Electron Cyclotron Maser Emission and the Brightest Solar Radio Bursts

Stephen M. **White**, Masumi Shimojo, Kazumasa Iwai, Timothy S. Bastian, Gregory D. Fleishman, Dale E. Gary, Jasmina Magdalenic, Angelos Vourlidas
ApJ **969** 3 **2024**
https://arxiv.org/pdf/2405.01755
https://iopscience.iop.org/article/10.3847/1538-4357/ad4640/pdf
This paper investigates the incidence of coherent emission in solar radio bursts, using a revised catalog of 3800 solar radio bursts observed by the Nobeyama Radio Polarimeters from 1988 to 2023. We focus on the 1.0 and 2.0 GHz data, where radio fluxes of order 10 billion Jansky have been observed. Previous work has suggested that these bursts are due to electron cyclotron maser (ECM) emission. In at least one well studied case, the bright emission at 1 GHz consists of narrowband spikes of millisecond duration. Coherent emission at 1 GHz can be distinguished from traditional incoherent gyrosynchrotron flare emission based on the radio spectrum: gyrosynchrotron emission at 1 GHz usually has a spectrum rising with frequency, so bursts in which 1 GHz is stronger than higher frequency measurements are unlikely to be incoherent gyrosynchrotron. Based on this criterion it is found that, for bursts exceeding 100 sfu, three-quarters of all bursts at 1 GHz and half of all 2 GHz bursts have a dominant coherent emission component, assumed to be ECM. The majority of the very bright bursts at 1 GHz are highly circularly polarized, consistent with a coherent emission mechanism, but not always 100% polarized. The frequency range from 1 to 2 GHz is heavily utilized for terrestrial applications, and these results are relevant for understanding the extreme flux levels that may impact such applications. Further, they provide a reference for comparison with the study of ECM emission from other stars and potentially exoplanets. **1989-06-04, 1989-08-15, 1989-11-26, 1990-04-15, 1990-07-30, 1991-03-23, 1991-05-16, 1991-06-09, 1991-06-15, 1998-08-25, 2001-04-09, 2001-10-19, 2001-11-22, 2002-03-18, 2002-04-21, 2003-05-28, 2006 DECEMBER 06, 2006-12-13, 2011-02-15, 2012-03-05, 2012-03-07, 2022-01-29, 2022-06-13**
Table 1. NoRP solar radio bursts exceeding 104 sfu at 1.0 GHz 1989-2022

Observing the Sun with the Atacama Large Millimeter-submillimeter Array (ALMA): Fast-Scan Single-Dish Mapping

S.M. **White**, K. Iwai, N.M.Phillips, R.E. Hills, A. Hirota, P. Yagoubov, G. Siringo, M. Shimojo, T.S. Bastian, A.S. Hales, T. Sawada, S. Asayama, M. Sugimoto, R.G. Marson, W. Kawasaki, E. Muller, T. Nakazato, K. Sugimoto, R. Brajsa, I. Skokic, M. Barta, S. Kim, A. Remijan, I. de Gregorio, S.A. Corder, H.S. Hudson, M. Loukitcheva, B. Chen, B. De Pontieu, G.D. Fleishmann, D.E. Gary, A. Kobelski, S. Wedemeyer, Y. Yan
Solar Phys. 292:88 **2017**
https://arxiv.org/pdf/1705.04766.pdf
The Atacama Large Millimeter-submillimeter Array (ALMA) radio telescope has commenced science observations of the Sun starting in late 2016. Since the Sun is much larger than the field of view of individual ALMA dishes, the

ALMA interferometer is unable to measure the background level of solar emission when observing the solar disk. The absolute temperature scale is a critical measurement for much of ALMA solar science, including the understanding of energy transfer through the solar atmosphere, the properties of prominences, and the study of shock heating in the chromosphere. In order to provide an absolute temperature scale, ALMA solar observing will take advantage of the remarkable fast-scanning capabilities of the ALMA 12m dishes to make single-dish maps of the full Sun. This article reports on the results of an extensive commissioning effort to optimize the mapping procedure, and it describes the nature of the resulting data. Amplitude calibration is discussed in detail: a path that utilizes the two loads in the ALMA calibration system as well as sky measurements is described and applied to commissioning data. Inspection of a large number of single-dish datasets shows significant variation in the resulting temperatures, and based on the temperature distributions we derive quiet-Sun values at disk center of 7300 K at lambda=3 mm and 5900 K at lambda=1.3 mm. These values have statistical uncertainties of order 100 K, but systematic uncertainties in the temperature scale that may be significantly larger. Example images are presented from two periods with very different levels of solar activity. At a resolution of order 25 arcsec, the 1.3 mm wavelength images show temperatures on the disk that vary over about a 2000 K range. 17 December 2015, 7 December 2016

The Relationship Between Solar Radio and Hard X-ray Emission A Review

S. M. **White**1,5, A. O. Benz2, S. Christe3, F. F´arn´ık4, M. R. Kundu5, G. Mann6, Z. Ning7, J.-P. Raulin8, A. V. R. Silva-V´alio8, P. Saint-Hilaire9, N. Vilmer10, and A.Warmuth6

Space Sci. Rev., 159:225–261, **2011, File**

This **review** discusses the complementary relationship between radio and hard X-ray observations of the Sun using primarily results from the era of the *Reuven Ramaty High Energy Solar Spectroscopic Imager* satellite. A primary focus of joint radio and hard X-ray studies of solar flares uses observations of nonthermal gyrosynchrotron emission at radio wavelengths and bremsstrahlung hard X-rays to study the properties of electrons accelerated in the main flare site, since it is well established that these two emissions show very similar temporal behavior. A quantitative prescription is given for comparing the electron energy distributions derived separately from the two wavelength ranges: this is an important application with the potential for measuring the magnetic field strength in the flaring region, and reveals significant differences between the electrons in different energy ranges. Examples of the use of simultaneous data from the two wavelength ranges to derive physical conditions are then discussed, including the case of microflares, and the comparison of images at radio and hard X-ray wavelengths is presented. There have been puzzling results obtained from observations of solar flares at millimeter and submillimeter wavelengths, and the comparison of these results with corresponding hard X-ray data is presented. Finally, the review discusses the association of hard X-ray releases with radio emission at decimeter and meter wavelengths, which is dominated by plasma emission (at lower frequencies) and electron cyclotron maser emission (at higher frequencies), both coherent emission mechanisms that require small numbers of energetic electrons. These comparisons show broad general associations but detailed correspondence remains more elusive.

Solar radio bursts and space weather

White, S.M.:,

Asian J. Phys. **16**, 189 – 207, **2007**. **File**

https://arxiv.org/pdf/2405.00959

a non-CME type II burst that occurred on 16 July 2004.

Space Weather is the study of the conditions in the solar wind that can affect life on the surface of the Earth, particularly the increasingly technologically sophisticated devices that are part of modern life. Solar radio observations are relevant to such phenomena because they generally originate as events in the solar atmosphere, including flares, coronal mass ejections and shocks, that produce electromagnetic and particle radiations that impact the Earth. Low–frequency solar radio emission arises in the solar atmosphere at the levels where these events occur: we can use frequency as a direct measure of density, and an indirect measure of height, in the atmosphere. The main radio burst types are described and illustrated using data from the **Green Bank Solar Radio Burst Spectrometer**, and their potential use as diagnostics of Space Weather is discussed.

Energetic electron populations in solar flares

White, Stephen M.

High energy solar phenomena-A new era of spacecraft measurements. AIP Conference Proceedings, Volume 294, pp. 199-204 (**1994**).

Millimeter-interferometer observations of flares are used to study the MeV-energy electrons accelerated in solar flares. The focus of this study is a remarkable similarity found in the time profiles of emission associated with the impulsive onset of a flare. In a large fraction of flares, the impulsive phase emission at millimeter wavelengths consists of a rapid

rise (~5 seconds) linear in time to a sharp peak, followed by an exponential decay with a decay constant of order 15 seconds. The onset of millimeter emission may be delayed by several seconds with respect to the onset of hard X-rays. The implications of this homologous property are discussed briefly.

Analysis of type II and type III solar radio bursts

Jude **Wijesekera**

Journal of Physics: Conf. Series 1005 012046 **2018**

https://www.academia.edu/38790936//Analysis_of_type_II_and_type_III_solar_radio_bursts

Analysis_of_type_II_and_type_III_solar_radio_burstsSolar radio burst is an arrangement of a frequency space that variation with time. Most of radio burst can be identified in low frequency range such as below 200 MHz and depending on frequencies. Solar radio bursts were the first phenomenon identified in the field of radio astronomy field. Solar radio frequency range is from 70 MHz to 2.2 GHz. Most of the radio burst can be identified in a low frequency range such as below 200 MHz. Properties of low-frequency radio were analyzed this research. There are two types of solar radio bursts were analyzed, named as type II and type III radio bursts. Exponential decay type could be seen in type II, and a linear could be indicated in type III solar radio bursts. The results of the drift rate graphs show the values of each chosen solar radio burst. High drift rate values can be seen in type III solar flares whereas low to medium drift rate values can be seen in type II solar flares. In the second part of the research the Newkirk model electron density model was used to estimate the drift velocities of the solar radio bursts. Although the special origin of the solar radio burst is not known clearly we assumed. The chosen solar radio bursts were originated within the solar radius of 0.9 - 1.3 range from the photosphere. We used power low in the form of (x) = A × 10−bx were that the electron density related to the height of the solar atmosphere. The calculation of the plasma velocity of each solar radio burst was done using the electron density model and drift rates. Therefore velocity of chosen type II solar radio bursts indicates low velocities. The values are 233.2499 Km s−1, 815.9522 Km s−1 and 369.5425 Km s−1. Velocity of chosen type III solar radio bursts were 1443.058 Km s−1and 1205.05 $Km\ s$−1.

Calculation the Properties of recorded on 06th September 2017 type II Solar Radio Burst with CME using Matlab.

Jude **Wijesekera**, K.A.C Nilmini, E.M.V.B Ekanayake

Journal of Physics Volume1|Issue19 **2018**

https://www.academia.edu/38791060/Calculation_the_Properties_of_recorded_on_06th_September_2017_type_II_Solar_Radio_Burst_with_CME_using_Matlab?email_work_card=view-paper

Solar radio burst is an arrangement of a frequency space that varies with time. Solar radio frequency is ranging from 70 MHz to 2.2 GHz and most of the radio burst can be identified in low-frequency range (<200 MHz) Type II solar radio bursts are the most common radio burst and are slow frequency drift bursts. Most of the time they are accompanied by a second harmonic as well. The Type-II solar radio burst recorded on 06th September 2017 at12.00 pm by the Austria-Unigraz solar observatory was engaged to investigate the properties of type II solar radio burst with CME(Coronal Mass Ejection). Math lab software and mathematical models were used to analysis type II solar radio burst. The frequency distribution of type II bursts was approximated as an exponential and low drift rate value could be seen. The correlation coefficient between model frequency vs frequency was 0.973803. Newkirk model was used to estimate the drift velocities and electron density of the solar radio bursts. Although the special origin of the solar radio burst is not known clearly we assumed. Most of solar radio bursts were originated within the solar radius of 0.9 - 1.3 range from the photosphere. Further analysis also showed that the flux density of the burst was varying between 1.32 × 10−22$Wm2Hz$−1 to 0.42 × 10−22$Wm2Hz$−1. The average plasma velocity of type II solar radio bursts was determined as 1168.16 km s−1. Therefore, we could say that in this case, CME was used to increase the plasma velocity of solar burst type II and flux density.

Analysis of type II and type III solar radio bursts

Wijesekera, J. V.; Jayaratne, K. P. S. C.; Adassuriya, J.

Journal of Physics: Conference Series, Volume 1005, Issue 1, article id. 012046 (**2018**).

sci-hub.se/10.1088/1742-6596/1005/1/012046

https://iopscience.iop.org/article/10.1088/1742-6596/1005/1/012046/pdf

Solar radio burst is an arrangement of a frequency space that variation with time. Most of radio burst can be identified in low frequency range such as below 200 MHz and depending on frequencies. Solar radio bursts were the first phenomenon identified in the field of radio astronomy field. Solar radio frequency range is from 70 MHz to 2.2 GHz. Most of the radio burst can be identified in a low frequency range such as below 200 MHz. Properties of low-frequency radio were analyzed this research. There are two types of solar radio bursts were analyzed, named as type II and type III radio bursts. Exponential decay type could be seen in type II, and a linear could be indicated in type III solar radio bursts. The results of the drift rate graphs show the values of each chosen solar radio burst. High drift rate values can be seen in type III solar flares whereas low to medium drift rate values can be seen in type II solar flares.

In the second part of the research the Newkirk model electron density model was used to estimate the drift velocities of the solar radio bursts. Although the special origin of the solar radio burst is not known clearly we assumed. The chosen

solar radio bursts were originated within the solar radius of 0.9 - 1.3 range from the photosphere. We used power low in the form of (x) = A × 10-bx were that the electron density related to the height of the solar atmosphere. The calculation of the plasma velocity of each solar radio burst was done using the electron density model and drift rates. Therefore velocity of chosen type II solar radio bursts indicates low velocities. The values are 233.2499 Km s-1, 815.9522 Km s-1 and 369.5425 Km s-1. Velocity of chosen type III solar radio bursts were 1443.058 Km s-1and 1205.05Km s -1. **07-12-2013, 16-04-2014, 04-11-2015, 09-11-2015**

Solar Bursts.

Wild, J. P., S. F. Smerd, and A. A. Weiss.
ARA&A, 1, 291, **1963**. 10.1146/annurev. aa.01.090163.001451.

Very Large Array, SOHO, and RHESSI Observations of Magnetic Interactions and Particle Propagation across Large-Scale Coronal Loops

Robert F. **Willson** · Tyler D. Groff
Solar Phys (**2008**) 250: 89–105
http://www.springerlink.com/content/n376024232363501/fulltext.pdf

Noise storm of 1-2 July 2005

Very Large Array (VLA) observations at wavelengths of 20 and 91 cm have been combined with data from the SOHO and RHESSI solar missions to study the evolution of transequatorial loops connecting active regions on the solar surface. The radio observations provide information about the acceleration and propagation of energetic electrons in these large-scale coronal magnetic structures where energy release and transport take place. On one day, a long-lasting Type I noise storm at 91 cm was seen to intensify and shift position above the northern hemisphere region following an impulsive hard X-ray burst in the southern hemisphere footpoint region. VLA 20-cm observations as well as SOHO EIT EUV images showed evolving coronal plasma that appeared to move across the solar equator during this time period. This suggests that the **transequatorial loop acted as a conduit for energetic particles or fields that may have triggered magnetic changes in the corona** where the northern noise storm region was seen. On another day, a hard X-ray burst detected at the limb was accompanied by impulsive 20- and 91-cm burst emission along a loop connecting to an active region in the same hemisphere but about 5_ away, again suggesting particle propagation and remote flare triggering across interconnecting loops.

Type II and Type III Radio Bursts and their Correlation with Solar Energetic Proton Events

L.M. **Winter**, K. Ledbetter
ApJ **809** 105 **2015**
http://arxiv.org/pdf/1507.01620v1.pdf

Using the Wind/WAVES radio observations from 2010-2013, we present an analysis of the 123 decametric-hectometric (DH) type II solar radio bursts during this period, the associated type III burst properties, and their correlation with solar energetic proton (SEP) properties determined from analysis of the Geostationary Operational Environmental Satellite (GOES) observations. We present a useful catalog of the type II burst, type III burst, Langmuir wave, and proton flux properties for these 123 events, which we employ to develop a statistical relationship between the radio properties and peak proton flux that can be used to forecast SEP events. We find that all SEP events with a peak > 10 MeV flux above 15 pfu are associated with a type II burst and virtually all SEP events, 92%, are also associated with a type III radio burst. Based on a principal component analysis, the radio burst properties that are most highly correlated with the occurrence of gradual SEP events and account for the most variance in the radio properties are the type III burst intensity and duration. Further, a logistic regression analysis with the radio-derived principal component (dominated by the type III and type II radio burst intensity and type III duration) obtains SEP predictions approaching the human forecaster rates, with a false alarm rate of 22%, a probability of detection of 62%, and with 85% of the classifications correct. Therefore, type III radio bursts that occur along with a DH type II burst are shown to be an important diagnostic that can be used to forecast SEP events. **15 Feb 2011, 21 March 2011, 4-5 Aug 2011, 22 Sept 2011, 22 Oct 2011, 24 Jan 2012, 7-8 March 2012, 10 March 2012, 6 June 2012, 9 June 2012, 2 July 2012, 11 Apr 2013, 22-23 May 2013**
The Wind/WAVES type II and Type IV solar radio burst list is found here:
http://www-lep.gsfc.nasa.gov/ waves/data_products.html.

Inferences About the Magnetic Field Structure of a CME with Both In Situ and Faraday Rotation Constraints

Brian E. **Wood**1, Samuel Tun-Beltran1, Jason E. Kooi2, Emil J. Polisensky2, and Teresa Nieves-Chinchilla3
2020 ApJ 896 99
https://sci-hub.tw/https://iopscience.iop.org/article/10.3847/1538-4357/ab93b8

On 2012 August 2, two coronal mass ejections (CMEs; CME-1 and CME-2) erupted from the west limb of the Sun as viewed from Earth, and were observed in images from the white-light coronagraphs on the SOlar and Heliospheric Observatory and Solar TErrestrial RElations Observatory (STEREO) spacecraft. These events were also observed by

the Very Large Array (VLA), which was monitoring the Sun at radio wavelengths, allowing time-dependent Faraday rotation observations to be made of both events. We use the white-light imaging and radio data to model the 3D field geometry of both CMEs, assuming a magnetic flux rope geometry. For CME-2, we also consider 1 au in situ field measurements in the analysis, as this CME hits STEREO-A on August 6, making this the first CME with observational constraints from stereoscopic coronal imaging, radio Faraday rotation, and in situ plasma measurements combined. The imaging and in situ observations of CME-2 provide two clear predictions for the radio data: VLA should observe positive rotation measures (RMs) when the radio line of sight first encounters the CME, and the sign should reverse to negative within two hours. The initial positive RMs are in fact observed. The expected sign reversal is not, but the VLA data unfortunately end too soon to be sure of the significance of this discrepancy. We interpret an RM increase prior to the expected occultation time of the CME as a signature of a sheath region of deflected field ahead of the CME itself.
2012 August 2-6

A Multi-Peak Solar Flare with a High Turnover Frequency of The Gyrosynchrotron Spectra from the Loop-Top Source

Zhao **Wu**, Alexey Kuznetsov, Sergey Anfinogentov, Victor Melnikov, Robert Sych, Bing Wang, Ruisheng Zheng, Xiangliang Kong, Baolin Tan, Zongjun Ning, Yao Chen

ApJ **968** 5 **2024**

https://arxiv.org/pdf/2405.03116

https://iopscience.iop.org/article/10.3847/1538-4357/ad46ff/pdf

The origin of multiple peaks in lightcurves of various wavelengths remains illusive during flares. Here we discuss the flare of SOL**2023-05-09**T03:54M6.5 with six flux peaks as recorded by a tandem of new microwave and Hard X-ray instruments. According to its microwave spectra, the flare represents a high-turnover frequency (>15 GHz) event. The rather-complete microwave and HXR spectral coverage provides a rare opportunity to uncover the origin of such event together with simultaneous EUV images. We concluded that (1) the microwave sources originates around the top section of the flaring loops with a trend of source spatial dispersion with frequency;(2) the visible movement of the microwave source from peak to peak originates from the process of new flaring loops appearing sequentially along the magnetic neutral line; 3) the optically-thin microwave spectra are hard with the indices varying from -1.2 to -0.4, and the turnover frequency always exceeds 15 GHz; 4) higher turnover/peak frequency corresponds to stronger peak intensity and harder optically-thin spectra. Using the Fokker-Planck and GX simulator codes we obtained a good fit to the observed microwave spectra and spatial distribution of the sources at all peaks, if assuming the radiating energetic electrons have the same spatial distribution and single-power-law spectra but with the number density varying in a range of 30%. We conclude that the particle acceleration in this flare happens in a compact region nearing the looptop. These results provide new constraints on the acceleration of energetic electrons and the underlying flare intermittent reconnection process.

Gyrosynchrotron emission generated by nonthermal electrons with energy spectra of a broken power law

Zhao **Wu**, Yao Chen, Hao Ning, Xiangliang Kong, Jeongwoo Lee

2019 *ApJ* **871** 22

https://arxiv.org/pdf/1811.10853.pdf

sci-hub.tw/10.3847/1538-4357/aaf474

Latest observational reports of solar flares reveal some uncommon features of microwave spectra, such as unusually hard (or even positive) spectra, and/or a super-high peak frequency. For a better understanding of these features, we conduct a parameter study to investigate the effect of broken-power-law spectra of energetic electrons on microwave emission on the basis of gyrosynchrotron mechanism. The electron broken-power-law energy distribution is characterized by three parameters, the break energy (EB), the power-law indices below (δ1) and above (δ2) the break energy. We find that with the addition of the δ2 component of the electron spectra, the total flux density can increase by several times in the optically-thick regime, and by orders of magnitude in the optically-thin regime; the peak frequency (νp) also increases and can reach up to tens of GHz; and the degree of polarization (rc) decreases in general. We also find that (1) the variation of the flux density is much larger in the optically-thin regime, and the microwave spectra around the peak frequency manifest various profiles with the softening or soft-hard pattern; (2) the parameters δ1 and EB affect the microwave spectral index (α) and the degree of polarization (rc) mainly in the optically-thick regime, while δ2 mainly affects the optically-thin regime. The results are helpful in understanding the lately-reported microwave bursts with unusual spectral features and point out the demands for a more-complete spectral coverage of microwave bursts, especially, in the high-frequency regime, say, >10−20 GHz.

Microwave imaging of a hot flux rope structure during the pre-impulsive stage of an eruptive M7.7 solar flare

Z. **Wu**, Y. Chen, G. Huang, H. Nakajima, H. Song, V. Melnikov, W. Liu, G. Li, K. Chandrashekhar, F. Jiao

ApJL **2016**

http://arxiv.org/pdf/1603.02777v1.pdf
Corona structures and processes during the pre-impulsive stage of solar eruption are crucial to understanding the physics leading to the subsequent explosive energy release. Here we present the first microwave imaging study of a hot flux rope structure during the pre-impulsive stage of an eruptive M7.7 solar flare, with the Nobeyama Radioheliograph (NoRH) at 17 GHz. The flux rope is also observed by the SDO/AIA in its hot passbands of 94 and 131 \AA\. In the microwave data, it is revealed as an overall arcade-like structure consisting of several intensity enhancements bridged by generally weak emissions, with brightness temperatures (TB) varying from ~10,000~K to ~20,000 K. Locations of microwave intensity enhancements along the structure remain relatively fixed at certain specific parts of the flux rope, indicating that the distribution of emitting electrons is affected by the large scale magnetic configuration of the twisted flux rope. Wavelet analysis shows a pronounced 2-min period of the microwave TB variation during the pre-impulsive stage of interest. The period agrees well with that reported for AIA sunward-contracting loops and upward ejective plasmoids (suggested to be reconnection outflows). This suggests that both periodicities are controlled by the same reconnection process that takes place intermittently at a 2-min time scale. We infer that at least a part of the emission is excited by non-thermal energetic electrons via the gyro-synchrotron mechanism. The study demonstrates the potential of microwave imaging in exploring the flux rope magnetic geometry and relevant reconnection process during the onset of solar eruption. **19 July 2012**

A novel mechanism for electron-cyclotron maser

D. J. **Wu**1, L. Chen1, G. Q. Zhao1,2 and J. F. Tang
A&A 566, A138 (**2014**)
Context. It has been a long-standing puzzle on how to produce natural radio bursts of various cosmic objects, ranging from remote active galactic nuclei and pulsars to the nearest solar radio bursts and terrestrial auroral kilometer radiations.
Aims. An electron-cyclotron maser (ECM) driven by fast electron beams trapped in magnetic fields has been suggested as a dominant mechanism of producing natural high-power radio radiation. However, there have been two serious difficulties: the magnetization condition of requiring the electron gyrofrequency over the plasma frequency and the inversion condition of the perpendicular velocity distribution of the fast electrons, which has held back the popularization of ECM in the astrophysical community.
Methods. By including effects of self-generated Alfvén waves (AW) excited by the beam current, this paper proposes a novel, self-consistent ECM model.
Results. The results show that the self-generated AW can effectively make a density-depleted duct, in which the magnetization condition is easily satisfied, and result in the inversion condition of perpendicular velocity distribution of the beam electrons.
Conclusions. This self-consistent ECM model can effectively overcome the two difficulties, make ECM very easily occur, and, hence, has greatly interesting implications and general significance in radio astrophysics because of its self-consistency, simplicity, and efficiency.

Imaging interplanetary CMEs at radio frequency from solar polar orbit

Ji **Wu**, Weiying Sun , Jianhua Zheng, Cheng Zhang, Hao Liu, Jingye Yan, Chi Wang, Chuanbing Wang and Shui Wang
Advances in Space Research, Volume 48, Issue 5, 1 September **2011**, Pages 943-954
Coronal mass ejections (CMEs) represent a great concentration of mass and energy input into the lower corona. They have come to be recognized as the major driver of physical conditions change in the Sun–Earth system. Consequently, observations of CMEs are important for understanding and ultimately predicting space weather conditions. This paper discusses a proposed mission, the Solar Polar Orbit Radio Telescope (**SPORT) mission**, which will observe the propagation of interplanetary CMEs to distances of near 0.35 AU from the Sun. The orbit of SPORT is an elliptical solar polar orbit. The inclination angle between the orbit and ecliptic plane should be about 90fl. The main payload on board SPORT will be an imaging radiometer working at the meter wavelength band (radio telescope), which can follow the propagation of interplanetary CMEs. The images that are obtained by the radio telescope embody the brightness temperature of the objectives. Due to the very large size required for the antenna aperture of the radio telescope, we adopt interferometric imaging technology to reduce it. Interferometric imaging technology is based on indirect spatial frequency domain measurements plus Fourier transformation. The SPORT spacecraft will also be equipped with a set of optical and in situ measurement instruments such as a EUV solar telescope, a solar wind ion instrument, an energetic particle detector, a magnetometer, a wave detector and a solar radio burst spectrometer.

Study on the Temporal Evolution of the Radial Differential Rotation of Solar Corona Using Radio Emissions

N. B. **Xiang**, X. H. Zhao, L. H. Deng, F. Y. Li, Y. J. Wang, X. W. Tan
ApJ **2024**
https://arxiv.org/pdf/2411.18105

The daily measurements of the disc-integrated solar radio flux, observed by the Radio Solar Telescope Network (RSTN), at 245, 410, 610, 1415, 2695, 4995, and 8800 MHz during the time interval of 1989 January 1 to 2019 December 17, are used to investigate the temporal evolution of radial differential rotation of solar corona using the methods of Ensemble Empirical Mode Decomposition and wavelet analysis. Overall, the results reveal that over the 30-year period, the rotation rates for the observed solar radio flux within the frequency range of 245\textendash8800 MHz show an increase with frequency. This verifies the existence of the radial differential rotation of the solar corona over long timescales of nearly 3 solar cycles. Based on the radio emission mechanism, to some extent, the results can also serve as an indicator of how the rotation of the solar upper atmosphere varies with altitude within a specific range. From the temporal variation of rotation cycle lengths of radio flux, the coronal rotation at different altitudes from the low corona to approximately 1.3 R⊙ exhibits complex temporal variations with the progression of the solar cycle. However, in this altitude range, over the past 30 years from 1989 to 2019, the coronal rotation consistently becomes gradually slower as the altitude increases. Finally, the EEMD method can extract rotation cycle signals from these highly randomized radio emissions, and so it can be used to investigate the rotation periods for the radio emissions at higher or lower frequencies.

Understanding shock dynamics in the inner heliosphere with modeling and type ii radio data: a statistical study†

H. **Xie**, O. C. St. Cyr, N. Gopalswamy, D. Odstrcil, H. Cremades
JGR, Volume 118, Issue 8, pages 4711–4723, **2013, File**

[1] We study two methods of predicting interplanetary (IP) shock location and strength in the inner heliosphere: 1) the ENLIL simulation and 2) the kilometric type II (kmTII) prediction. To evaluate differences in the performance of the first method, we apply two sets of CME parameters from the cone model fitting and flux-rope (FR) model fitting as input to the ENLIL model for 16 halo CMEs. The results show that the ENLIL model using the actual CME speeds from FR-fit provided an improved shock arrival time (SAT) prediction. The mean prediction errors for the FR and cone-model inputs are 4.90 ± 5.92 hr and 5.48 ± 6.11 hr, respectively. A deviation of 100 kms− 1 from the actual CME speed has resulted in a SAT error of 3.46 hr on average.

[2] The simulations show that the shock dynamics in the inner heliosphere agrees with the drag-based model. The shock acceleration can be divided as two phases: a faster deceleration phase within 50Rs and a slower deceleration phase at distances beyond 50Rs. The linear fit deceleration in phase 1 is about one order magnitude lager than that in phase 2. When applying the kmTII method to 14 DH-km CMEs, we found that combining the kmTII method with the ENLIL outputs improved the kmTII prediction. Due to a better modeling of plasma density upstream of shocks and the kmTII location, we are able to provide a more accurate shock time-distance and speed profiles.

[3] The mean kmTII prediction error using the ENLIL model density is 6.7 ± 6.4 hr; it is 8.4 ± 10.4 hr when the average solar wind plasma density is used. Applying the ENLIL density has reduced the mean kmTII prediction error by ∼ 2 hr and the standard deviation by 4.0 hr. Especially, when we applied the combined approach to two interacting events, the kmTII prediction error was drastically reduced from 29.6 hr to −4.9 hr in one case and 10.6 hr to 4.2 hr in the other. Furthermore, the results derived from the kmTII method and the ENLIL simulation, together with white-light data, provide a valuable validation of shock formation location and strength. Such information has important implications for SEP acceleration.

Understanding Shock Dynamics in the Inner Heliosphere with Modeling and Type II Radio Data: the 2010-04-03 event

H. **Xie**, D. Odstrcil, L. Mays, O. C. St. Cyr, N. Gopalswamy, and H. Cremades
Journal of Geophysical Research, **2012**, 117, A4, CiteID A04105, **File**

The **2010 April 03** solar event was studied 4 using observations from STEREO SECCHI, SOHO LASCO, and Wind kilometric Type II data (kmTII) combined with WSA-Cone-ENLIL model simulations performed at the Community Coordinated Modeling Center (CCMC). In particular, we identified the origin of the coronal mass ejection (CME) using STEREO EUVI and SOHO EIT images. A flux-rope model was fit to the SECCHI A and B, and LASCO images to determine the CME's direction, size, and actual speed. J-maps from STEREO COR2/HI-1/HI-2 and simulations from CCMC were used to study the formation and evolution of the shock in the inner heliosphere. In addition, we also studied the time-distance profile of the shock propagation from kmTII radio burst observations. The J-maps together with in-situ data from the Wind spacecraft provided an opportunity to validate the simulation results and the kmTII prediction. Here we report on a comparison of two methods of predicting interplanetary shock arrival time: the ENLIL model and the kmTII method; and investigate whether or not using the ENLIL model density improves the kmTII prediction. We found that the ENLIL model predicted the kinematics of shock evolution well. The shock arrival times (SAT) and linear-fit shock velocities in the ENLIL model agreed well with those measurements in the J-maps along both the CME leading edge and the Sun-Earth line. The ENLIL model also reproduced most of the large scale structures of the shock propagation and gave the SAT prediction at Earth with an er ror of ~1 ± 7 hours. The kmTII method

predicted the SAT at Earth with an error of ~15 hours when using n0 = 4.16 cm-3, the ENLIL model plasma density near Earth; but it improved to ~2 hours when using n0 = 6.64 cm-3, the model density near the CME leading edge at 1 AU.

The evolution of a complex solar radio burst corresponding to special configuration of microwave sources

R.X. **Xie**, D.B. Ren and Y.Y. Liu
Adv. Space Res. 39(9), Pages 1476-1484, **2007**
A complex radio burst associated with periodic (~1 and 6 min) pulsations and several kinds fine structures, e.g., normal- and reverse-drifting type III bursts, zebra patterns, and slowly drifting structure was observed with the radio spectrometers (1.0–2.0, 2.6–3.8, 5.2–7.6, and 0.65–1.5 GHz) at the National Astronomical Observatories of China (NAOC) in Beijing and Yunnan on **19 October 2001**. In combination with the images of 17 and 34 GHz from NoRH and the magnetograms from MDI we reveal the existence and evolution of preexisting and new emerging sources, and find the horseshoe-shaped structure of microwave sources intensity during the late phase of the burst.

Interplanetary Scintillation Observation and Space Weather Modelling **Review**

Ming **Xiong**, Xueshang Feng, Bo Li, Jiansen He, Wei Wang, +++
Front. Astron. Space Sci., 10: 1159166 **2023**
https://www.frontiersin.org/articles/10.3389/fspas.2023.1159166/pdf
Interplanetary scintillation (IPS) refers to random fluctuations in radio intensity of distant small-diameter celestial object, over time periods of the order of 1 s. The scattering and scintillation of emergent radio waves are ascribed to turbulent density irregularities transported by the ubiquitous solar wind streams. The spatial correlation length of density irregularities and the Fresnel radius of radio diffraction are two key parameters in determining the scintillation pattern. Such a scintillation pattern can be measured and correlated between multi-station radio telescopes on the Earth. Using the “phase-changing screen” scenario based on the Born approximation, the bulk-flow speed and turbulent spectrum of the solar wind streams can be extracted from the single-station power spectra fitting and the multi-station cross-correlation analysis. Moreover, a numerical computer-assisted tomography (CAT) model, iteratively fit to a large number of IPS measurements over one Carrington rotation, can be used to reconstruct the global velocity and density structures in the inner heliosphere for the purpose of space weather modelling and prediction. In this review, we interpret the underlying physics governing the IPS phenomenon caused by the solar wind turbulence, describe the power spectrum and cross correlation of IPS signals, highlight the space weather application of IPS-CAT models, and emphasize the significant benefits from international cooperation within the Worldwide IPS Stations (WIPSS) network.Stations (WIPSS) network.

The first flare observation with a new solar microwave spectrometer working in 35-40 GHz

F. **Yan**, Z. Wu, Z. Shang, B. Wang, L. Zhang, Y. Chen
ApJ **942** L11 **2023**
https://arxiv.org/pdf/2212.12314.pdf
https://iopscience.iop.org/article/10.3847/2041-8213/acad02/pdf
https://doi.org/10.3847/2041-8213/acad02
The microwave spectrum contains valuable information about solar flares. Yet, the present spectral coverage is far from complete and broad data gaps exist above 20 GHz. Here we report the first flare (the X2.2 flare on **2022 April 20**) observation of the newly-built Chashan Broadband Solar millimeter spectrometer (CBS) working from 35 to 40 GHz. We use the CBS data of the new Moon to calibrate,and the simultaneous NoRP data at 35 GHz to cross-calibrate. The impulsive stage has three local peaks with the middle one being the strongest and the maximum flux density reaches 9300 SFU at 35-40 GHz. The spectral index of the CBS data (alpha_C) for the major peak is mostly positive, indicating the gyrosynchrotron turnover frequency (nu_t) goes beyond 35-40 GHz. The frequency ν_t is smaller yet still larger than 20 GHz for most time of the other two peaks according to the spectral fittings with NoRP-CBS data. The CBS index manifests the general rapid-hardening-then-softening trend for each peak and gradual hardening during the decay stage, agreeing with the fitted optically-thin spectral index (alpha_tn) for nu_t < 35 GHz. In addition, the obtained turnover frequency during the whole impulsive stage correlates well with the corresponding intensity (I_t) according to a power-law dependence (It~nu_t^4.8) with a correlation coefficient of 0.82.This agrees with earlier studies on flares with low turnover frequency (<17 GHz), yet being reported for the first time for events with a high turnover frequency (>20 GHz).
CESRA #3468 **2023** https://www.astro.gla.ac.uk/users/eduard/cesra/?p=3468
RHESSI #441 **2023** https://sprg.ssl.berkeley.edu/~tohban/wiki/index.php/A_slow_HOPE_with_microwave_context

Auto Recognition of Solar Radio Bursts Using the C-DCGAN Method

Fabao **Yan**, Weidan Zhang, Ziqian Shang, Yonglin Yu, Fuyun Han, Ruopu He, Enze Li, Wu Zhao, and Yao Chen
Front. Phys., **2021** |
https://www.frontiersin.org/articles/10.3389/fphy.2021.646556/full
https://doi.org/10.3389/fphy.2021.646556
Solar radio bursts can be used to study the properties of solar activities and the underlying coronal conditions on the basis of the present understanding of their emission mechanisms. With the construction of observational instruments, around the world, a vast volume of solar radio observational data has been obtained. Manual classifications of these data require significant efforts and human labor in addition to necessary expertise in the field. Misclassifications are unavoidable due to subjective judgments of various types of radio bursts and strong radio interference in some events. It is therefore timely and demanding to develop techniques of auto-classification or recognition of solar radio bursts. The latest advances in deep learning technology provide an opportunity along this line of research. In this study, we develop a deep convolutional generative adversarial network model with conditional information (C-DCGAN) to auto-classify various types of solar radio bursts, using the solar radio spectral data from the Culgoora Observatory (1995, 2015) and the Learmonth Observatory (2001, 2019), in the metric decametric wavelengths. The technique generates pseudo images based on available data inputs, by modifying the layers of the generator and discriminator of the deep convolutional generative adversarial network. It is demonstrated that the C-DCGAN method can reach a high-level accuracy of auto-recognition of various types of solar radio bursts. And the issue caused by inadequate numbers of data samples and the consequent over-fitting issue has been partly resolved.

Mingantu Spectral Radioheliograph for Solar and Space Weather Studies

Yihua **Yan**, Zhijun Chen, Wei Wang, Fei Liu, Lihong Geng, Linjie Chen, Chengming Tan, Xingyao Chen, Cang Su, and Baolin Tan
Front. Astron. Space Sci., 8:584043. **2021** |
https://doi.org/10.3389/fspas.2021.584043
https://www.frontiersin.org/articles/10.3389/fspas.2021.584043/full
The Chinese Spectral Radioheliograph (CSRH) covering 400 MHz-15 GHz frequency range was constructed during 2009–2016 in Mingantu Observing Station, National Astronomical Observatories, Chinese Academy of Sciences at Zhengxiangbaiqi, Inner Mongolia of China. The CSRH is renamed as MingantU SpEctral Radioheliograph (MUSER) after its accomplishment. Currently, MUSER consists of two arrays spreading over three spiral-shaped arms. The maximum baseline length is ∼3 km in both east-west and north-south directions. The MUSER array configuration is optimized to meet the needs of observing the full-disk Sun over ultrawide wavebands with images of high temporal, spatial and spectral resolutions and high dynamic range. The low frequency array, called MUSER-I, covers 400 MHz-2.0 GHz with 40 antennas of 4.5-m-diameter each and the high frequency array, called MUSER-II, covers 2–15 GHz with 60 antennas of 2-m-diameter each. The MUSER-I can obtain full-disk solar radio images in 64 frequency channels with a time cadence of 25 ms and a spatial resolution of 51.6″ to 10.3″ (corresponding to the frequency range 400 MHz to 2 GHz), whereas the MUSER-II can obtain full-disk solar images in 520 channels with a time cadence of 206.25 ms and a spatial resolution of 10.3″ to 1.3 (corresponding to the frequency range 2 to 15 GHz). A dynamic range of 25 dB can be obtained with snapshot images produced with the MUSER. An extension of MUSER in the further lower frequency range covering 30–400 MHz with an array of 224 logarithm-periodic dipole antennas (LPDAs) has been approved and will be completed during the next 4 years. The MUSER, as a dedicated solar instrument, has the following advantages providing simultaneous images over a wide frequency range with a unique high temporal-spatial-spectral resolutions; high-performing ultrawide-band dual-polarization feeds for wide-band signal collection; advanced high data-rate, large-scale digital correlation receiver for multiple-frequency and faster snapshot observations; and applications of new technologies such as using optical fiber to obtain remote antenna and wide-band analog signal transmission. The MUSER thus provides a unique opportunity to measure solar magnetic fields and trace dynamic evolution of energetic electrons in several radio frequencies, which, in turn, will help to have better understandings of the origin of various solar activities and the basic drivers of space weather. **13 Aug 2012, 11 November 2014, 17 December 2014, 22 November 2015**

New Interplanetary Scintillation Array in China for Space Weather

Yihua **Yan** 1,2, Wei Wang 1 , Linjie Chen 1 , Fei Liu 1 , Lihong Geng 1 , Zhijun Chen 1
Sun and Geosphere, **2018**; 13/2: 153 -155
http://newserver.stil.bas.bg/SUNGEO//00SGArhiv/SG_v13_No2_2018-pp-153-155.pdf
Interplanetary Scintillation (IPS) is a useful ground-based method to investigate solar wind structure and its parameters through the scintillation of distant, compact radio sources at radio wavelengths. Current worldwide IPS facilities include both single-site systems (which are typically a large telescope or array), and multi-site systems (which are typically more varied telescope/array sizes). To combine the advantages of both of these system types, we propose a new design for the IPS telescope in China, implementing a large collecting area at one main site, with smaller collecting areas at the other sites. This new IPS telescope concept is a part of the Phase-II Meridian Space Weather Monitoring Project under

the 2016-2020 National Infrastructure Program in China to be constructed in near future. Some specifications and basic considerations of this telescope are described in this paper.

Observations with MUSER

Yihua **Yan**
CESRA Abstract **2016** p.46
http://cesra2016.sciencesconf.org/conference/cesra2016/pages/CESRA2016_prog_abs_book_v1.pdf
Radio imaging spectroscopy over wide range wavelength in dm/cm-bands will open new windows on solar flares and coronal mass ejections by tracing the radio emissions from accelerated electrons. The Chinese Spectral Radioheliograph (CSRH) with two arrays in 400MHz-2GHz /2-15GHz ranges with 64/532 frequency channels have been established in Mingantu Observing Station, Inner Mongolia of China, since 2013 and is in test observations now. CSRH is renamed as MUSER (MingantU SpEctral Radioheliograph) after it's accomplishment. In this talk we present the initial observations with MUSER. *CSRH Team includes: Yihua Yan (PI), Zhijun Chen, Wei Wang, Fei Liu, Lihong Geng, Jian Zhang*, Linjie Chen, Sijie Yu, Donghao Liu, Sha Li, Jing Du, Cang Su and Baolin Tan, Huang Jing, Chengming Tan etc., from NAOC (*Peking University, Beijing, China). CSRH was supported by National Major Scientific Research Facility R&D Program ZDYZ2009-3

First radio burst imaging observation from Mingantu Ultrawide Spectral Radioheliograph,".

Yan, Y., Chen, L., and Yu, S.
(**2016**). " In Solar and Stellar Flares and their Effects on Planets. Editors A. G. Kosovichev, S. L. Hawley, and P.Heinzel (Vienna, Austria: IAU Symposium), Vol. 320, 427–435.
https://sci-hub.st/10.1017/S174392131600051X
https://www.cambridge.org/core/journals/proceedings-of-the-international-astronomical-union/article/first-radio-burst-imaging-observation-from-mingantu-ultrawide-spectral-radioheliograph/AF9B6C10AF060C7F8478392132856AB5
The Chinese Spectral Radioheliograph (CSRH) with two arrays in 400MHz-2GHz /2-15GHz ranges with 64/520 frequency channels have been established in Mingantu Observing Station, Inner Mongolia of China, since 2013 and is in test observations now. CSRH is renamed as Mingantu Ultrawide SpEctral Radioheliograph (MUSER) after its accomplishment. We introduce the progress and current status of MUSER. The first burst imaging results of MUSER is presented. **11 November 2014**

Progress on Chinese Spectral Radioheliograph –CSRH Construction

Yihua **Yan**1, Jian Zhang2, Zhijun Chen1, Wei Wang1, Fei Liu1 and Lihong Geng1
2011, File
The Chinese Spectral Radioheliograph (CSRH) with 40 antennas of 4.5 m covering 400 MHz – 2 GHz (CSRH-I) and 60 antennas of 2 m covering 2-15 GHz (CSRH-II) has been supported and is under construction in a radio quiet region in Inner Mongolia of China. The array of CSRH-I has been assembled and is tested now. The array of CSRH-II will be established during 2011-2013. The progress about the project is introduced.

Radio fine structures in dm–cm wavelength range associated with magnetic reconnection processes

Y. **Yan**, J. Huang, B. Chen, Y. Liu and C. Tan
Advances in Space Research
Volume 46, Issue 4, 16 August **2010**, Pages 413-418
Radio bursts with fine structures in decimetric–centimetric wave range are generally believed to manifest the primary energy release process during flare/CME events. By spectropolarimeters in 1–2 GHz, 2.6–3.8 GHz, and 5.2–7.6 GHz at NAOC/Huairou with very high temporal (1.25–8 ms) and spectral (4–20 MHz) resolutions, the zebra patterns, spikes, and new types of radio fine structures with mixed frequency drift features are observed during several significant flare/CME events. In this paper we will discuss the occurrence of radio fine structures during the impulsive phase of flares and/or CME initiations, which may be connected to the magnetic reconnection processes.

Diagnostics of Radio Fine Structures around 3 GHz with Hinode Data in the Impulsive Phase of an X3.4/4B Flare Event on 2006 December 13

Yihua **Yan**, Jing huang1 Bin chen1 and Takashi sakurai2
E-print, Oct 2007, PASJ, http://srg.bao.ac.cn/staff/yan/PASJ_Hinode_Yan_etal07.pdf
*Publ. Astron. Soc. Japan 59, pp.S815-S821 **(2007)***
[Abstract], [HTML], [PDF(3030kb)], [PS.gz(16978kb)]
Fine structures were observed in the radio spectra, which include spikes, reverse slope type III bursts, type U burst, V-shaped burst, pulsations, zebra patterns and ¯rstly-discovered sub-second spiky zebra-like structures, superimposed in the 2.6 { 3.8 GHz type IV bursts. The radio ¯ne structures during the impulsive phase of the flare may be closely

associated with coronal structures during the magnetic reconnection process as revealed by Hinode soft X-ray images. Thus these microwave ¯ne structure observations may provide very useful diagnostics in the primary energy release sites when they occur in the impulsive flare phase. For this flare event, the estimated coronal magnetic ¯eld is about 50 { 170 G in the rising phase of the flare with a source density of about 1£1011cm¡3. The field strength and plasma density are about 90-200 G and 1.27£1011cm¡3 around the flare maximum.

On the Coronal Magnetic Field Configuration and Solar Flare/CME Process

Yihua **Yan**

Space Sci. Rev. **2006**, **File**

The coronal magnetic field configuration is important for understanding the energy storage and release processes that account for flares and/or CMEs. Here we present a model which is based on the work for potential magnetic field problems that only applies the condition at infinity with the boundary condition on the solar surface specified. We also discuss some recent progress on general force-free field models. For some event analyses, we have employed MDI/SOHO longitudinal magnetogram insected into the synoptic magnetogram to obtain whole boundary condition over the solar surface. Globally, the extrapolated global magnetic field structures effectively demonstrate the case for the disk signature of the radio CMEs and the evolution of the radio sources during the CME/flare processes.

A radio burst and its associated CME on 17 March 2002 –

Y. **Yan**, M. Pick, M. Wang, S. Krucker, A. Vourlidas

Solar Physics (**2006**) 239: 277–292

the type III electron beams propagate in the interface highly compressed region between the ascending CME and the neighboring open field lines.

A Study on Non-coplanar Baseline Effects for Mingantu Spectral Radioheliograph

Qiu-ping **Yang**, Feng Wang, Hui Deng, Ying Mei, Wei Wang

Research in Astron. Astrophys. **2022**

https://arxiv.org/pdf/2208.09598.pdf

As a dedicated solar radioheliograph, the MingantU SpEctral RadioHeliograph (MUSER) has a maximum baseline of more than 3000 meters and a frequency range of 400 MHz -- 15 GHz. According to the classical radio interferometry theory, the non-coplanar baseline effect (i.e., w-term effect) would be considered and calibrated for such a radio instrument. However, little previous literature made the qualitative or quantitative analyses on w-term effects of solar radioheliograph in-depth. This study proposes a complete quantitative analysis of w-term effects for the MUSER. After a brief introduction of the MUSER, we systematically investigate the baseline variations over a year and analyze the corresponding variations of w-term. We further studied the effects of the w-term in the imaging for the specified extended source, i.e., the Sun. We discussed the possible effects of the w-term, such as image distortion and so on. The simulated results show that the w-term is an essential and unavoidable issue for solar radio imaging with high spatial resolution. **2015-11-01**

Impact of Shock Front Rippling and Self-reformation on the Electron Dynamics at Low-Mach-number Shocks

Zhongwei **Yang**1,2, Quanming Lu2, Ying D. Liu1,3, and Rui Wang1

2018 ApJ 857 36

http://sci-hub.tw/http://iopscience.iop.org/0004-637X/857/1/36/

Electron dynamics at low-Mach-number collisionless shocks are investigated by using two-dimensional electromagnetic particle-in-cell simulations with various shock normal angles. We found: (1) The reflected ions and incident electrons at the shock front provide an effective mechanism for the quasi-electrostatic wave generation due to the charge-separation. A fraction of incident electrons can be effectively trapped and accelerated at the leading edge of the shock foot. (2) At quasi-perpendicular shocks, the electron trapping and reflection is nonuniform due to the shock rippling along the shock surface and is more likely to take place at some locations accompanied by intense reflected ion-beams. The electron trapping process has a periodical evolution over time due to the shock front self-reformation, which is controlled by ion dynamics. Thus, this is a cross-scale coupling phenomenon. (3) At quasi-parallel shocks, reflected ions can travel far back upstream. Consequently, quasi-electrostatic waves can be excited in the shock transition and the foreshock region. The electron trajectory analysis shows these waves can trap electrons at the foot region and reflect a fraction of them far back upstream. Simulation runs in this paper indicate that the micro-turbulence at the shock foot can provide a possible scenario for producing the reflected electron beam, which is a basic condition for the **type II radio burst** emission at low-Mach-number interplanetary shocks driven by Coronal Mass Ejections (CMEs).

Wave emission of non-thermal electron beams generated by magnetic reconnection

Xin **Yao**, Patricio Muñoz, Jörg Büchner, Jan Benácek, Siming Liu, Xiaowei Zhou

ApJ **933** 219 **2022**
https://arxiv.org/pdf/2107.13746.pdf
https://iopscience.iop.org/article/10.3847/1538-4357/ac7141/pdf
Magnetic reconnection in solar flares can efficiently generate non-thermal electron beams. The accelerated electrons can, in turn, cause radio waves through kinetic instabilities as they propagate through the ambient plasma. We aim at investigating the wave emission caused by fast electron beams (FEBs) with characteristic non-thermal electron velocity distribution functions (EVDFs) generated by kinetic magnetic reconnection: bump-on-tail EVDFs along the separatrices and in the diffusion region, and perpendicular crescent-shaped EVDFs close to the diffusion region. For this sake we utilized 2.5D fully kinetic Particle-In-Cell (PIC) code simulations in this study. We found that: (1) the bump-on-tail EVDFs are unstable to cause electrostatic Langmuir waves via bump-on-tail instabilities and then multiple harmonic transverse waves from the diffusion region and the separatrices of reconnection. (2) The perpendicular crescent-shaped EVDFs, on the other hand, can cause multi-harmonic electromagnetic electron cyclotron waves through electron cyclotron maser instabilities in diffusion region of reconnection. Our results are applicable to diagnose the plasma parameters which control reconnection in solar flares by means of radio waves observations.

The effects of density inhomogeneities on the radio wave emission in electron beam plasmas

Xin **Yao**, Patricio A. Muñoz, Jörg Büchner
J. Plasma Phys. **2020**
https://arxiv.org/pdf/2005.08876.pdf
Type III radio bursts are radio emissions associated with solar flares. They are considered to be caused by electron beams in the solar corona. Magnetic reconnection is a possible accelerator of electron beams in the course of solar flares which causes unstable distribution functions, and density inhomogeneities. The properties of radio emission by electron beams in such environment are, however, still poorly understood. We capture the non-linear kinetic plasma processes of radio emissions in such plasmas by utilizing fully-kinetic Particle-In-Cell (PIC) code numerical simulations. Our model takes into account initial velocity distribution functions as they are supposed to be created by magnetic reconnection. These velocity distribution functions allow two distinct mechanisms of radio wave emissions: plasma emissions due to plasma-wave interactions and so called electron cyclotron maser emissions (ECME) due to wave-particle interactions. Our most important finding is that the number of harmonics of Langmuir waves increases with the density inhomogeneities. The harmonics are generated by the interaction of beam-generated Langmuir waves and their harmonics. In addition, we also find evidence for transverse harmonic electromagnetic wave emissions due to a coalescence of beam-generated and fundamental Langmuir waves with a vanishing wavevector. We investigate the effects of density inhomogeneities on the conversion process of the free energy of the electron beams to electrostatic and electromagnetic waves and the frequency shift of electron resonances caused by perpendicular gradients in the beam velocity distribution function. Our findings explain the observation of Langmuir waves and their harmonics in solar radio bursts and of the observed frequency shifts in these emissions.

A Comparative Study of Confined and Eruptive Solar Flares using Microwave Observations

Yashiro, S.; Akiyama, S.; Masuda, S.; Shimojo, M.; Asai, A.; Imada, S.; Gopalswamy, N.
American Geophysical Union, Fall Meeting **2015**, **abstract** #SH43B-2447
It is well known that about 10% X-class solar flares are not associated with coronal mass ejections (CMEs). These flares are referred to as confined flares, which are not associated with mass or energetic particles leaving the Sun. However, electrons are accelerated to MeV energies as indicated by the presence of microwave emission with a turnover frequency of ~15 GHz (Gopalswamy et al. 2009, IAU Symposium 257, p. 283). In this paper, we extend the study of confined flares to lower soft X-ray flare sizes (M and above) that occurred in the time window of the Nobeyama Radioheliograph (NoRH). We also make use of the microwave spectral information from the Nobeyama Radio Polarimeters (NoRP). During 1996 - 2014, NoRH and NoRP observed 663 flares with size M1.0 or larger. Using the CME observations made by SOHO/LASCO and STEREO/SECCHI, we found 215 flares with definite CME association (eruptive flares) and 202 flares that definitely lacked CMEs (confined flares). The remaining 146 flares whose CME association is unclear are excluded from the analysis. We examined the peak brightness temperature and the spatial size obtained by NoRH. Although there is a large overlap between the two populations in these properties, we found that microwave sources with the largest spatial extent and highest brightness temperature are associated with eruptive flares. Spectral analysis using NoRP data showed a tendency that more confined flares had higher turnover frequency (≥17 GHz). We also compare the NoRH images with the photospheric magnetograms to understand the difference in the magnetic structure of the two types of flare sources.

Homologous flare–CME events and their metric type II radio burst association

S. **Yashiro**a, b, , , N. Gopalswamyb, P. Mäkeläa, b, S. Akiyamaa, b, W. Uddinc, A.K. Srivastavad, N.C. Joshij, R. Chandrae, P.K. Manoharanf, K. Mahalakshmif, V.C. Dwivedif, R. Jaink, A.K. Awasthic, g, N.V. Nittah, M.J. Aschwandenh, D.P. Choudharyi
Advances in Space Research, Volume 54, Issue 9, 1 November **2014**, Pages 1941–1948
http://www.sciencedirect.com/science/article/pii/S0273117714004268

Active region NOAA 11158 produced many flares during its disk passage. At least two of these flares can be considered as homologous: the C6.6 flare at 06:51 UT and C9.4 flare at 12:41 UT on **February 14, 2011**. Both flares occurred at the same location (eastern edge of the active region) and have a similar decay of the GOES soft X-ray light curve. The associated coronal mass ejections (CMEs) were slow (334 and 337 km/s) and of similar apparent widths (43fl and 44fl), but they had different radio signatures. The second event was associated with a metric type II burst while the first one was not. The COR1 coronagraphs on board the STEREO spacecraft clearly show that the second CME propagated into the preceding CME that occurred 50 min before. These observations suggest that CME–CME interaction might be a key process in exciting the type II radio emission by slow CMEs.

Magnetic Field and Density Models in the Zebra Source Region

L. V. **Yasnov** & M. Karlický
Solar Physics volume 297, Article number: 133 (**2022**)
https://doi.org/10.1007/s11207-022-02067-5
Using the double-plasma resonance model of solar radio zebras, we analyze five models of the magnetic field and density in the zebra source region. We present analytical relations of zebra-stripe frequencies depending on the gyro-harmonic number. By fitting of observed zebra-stripe frequencies using model frequencies, we find that the determined gyro-harmonic number and corresponding magnetic field depend on the model used. We show that all previously analyzed zebras, where the absolute value of the difference between neighboring zebra-stripe frequencies increases with respect to increasing frequency, can be well fitted by the model with exponential dependencies of the magnetic field and density or by the model with smaller gradients of both of these variables. Although these models give different results, their more sophisticated versions give more similar results. We also present the models that can fit the zebras, if observed, where the absolute value of the difference between neighboring zebra-stripe frequencies decreases with respect to increasing frequency. We check all these models by a fitting of the zebra-stripe frequencies observed in the **21 June 2011** zebra event. In one model, although it reasonably describes the conditions in the atmosphere above the active region, the fit of the observed zebra-stripe frequencies could not be made.

Dynamics and Characteristics of Waves in the Zebra Radio Source

L. V. **Yasnov** & M. Karlický
Solar Physics volume 297, Article number: 35 (**2022**)
https://link.springer.com/content/pdf/10.1007/s11207-022-01950-5.pdf
We analyzed the **17 August 1998** zebra event and showed that some quasi-periodic oscillations modulate the zebra-stripe frequencies. We determined the period of these oscillations as Pn=2.01±0.03Pn=2.01±0.03 (in numbers of zebra stripes) and as Pf=11.8±0.17Pf=11.8±0.17 MHz. In the first part of the analyzed zebra, we found a stable density wave that slowly propagated with the frequency drift less than 0.4 MHz s−1. Then, a stationary density wave appeared followed by a transformation of the waves to ones with longer periods. These long-period waves were recorded before and after the time interval when no zebra stripes were observed. We interpreted these density waves as magnetosonic waves. We calculated their wavelength and propagating velocity, considering two types of density models of the solar atmosphere. We also estimated the characteristic density and magnetic-field strength as N≈9.2×108N≈9.2×108 cm−1 and B≈0.73 GB≈0.73 G, respectively. We found similar velocities derived from drifts of the density wave and velocities calculated from the density and magnetic-field strength considering gyro-harmonic numbers of zebra stripes.

On the Magnetoacoustic Waves and Physical Conditions in Zebra Radio Sources

L. V. **Yasnov**
Solar Physics volume 296, Article number: 139 (**2021**)
https://link.springer.com/content/pdf/10.1007/s11207-021-01886-2.pdf
https://doi.org/10.1007/s11207-021-01886-2
Analysis of the solar radio zebra-pattern (ZP) spectrum for the burst on **21 June 2011** has shown that the frequencies corresponding to the stripes of this ZP experience quasiperiodic oscillations relative to some average values. The period of such oscillations, expressed in the number of the ZP stripes, is 2.41±0.212.41±0.21, and expressed in frequencies, it is (5.00±0.685.00±0.68) MHz. The change in the period of oscillations with time anticorrelates with the amplitude of the oscillations. The values of the harmonic numbers for the corresponding bands are given, and thus the magnetic-field strength is also estimated on the basis of the theory of double plasma resonance (DPR). In addition, a possible change in the Lbh/LnhLbh/Lnh parameter in the ZP-generation region is taken into account (LbhLbh and LnhLnh respectively are the magnetic-field and density scales). Calculations of the frequency-drift rate, carried out using an improved method for its determination, have shown that the drift values (3--8 MHzs−13--8 MHzs−1) are in accordance with Kaneda et al. (Astrophys. J. Lett. 855, L29, 2018). By using two density models of the solar atmosphere, the wavelength of these oscillations has also been determined. For the model presented by Aschwanden (Space Sci. Rev. 101, 1, 2002), the wavelength is about 1370 km while for the barometric density model, the wavelength is about 4650 km. The wavelength increases with time; for example, in the first model, the wavelength increases with time from 1200 to

1490 km. The calculated kink and sausage wave velocities turned out to be significantly lower than the observed ones. The reason for this discrepancy requires additional analysis.

Magnetic Field, Electron Density and Their Spatial Scales in Zebra Pattern Radio Sources

L. V. **Yasnov** & M. Karlický
Solar Physics volume 295, Article number: 96 (**2020**)
https://link.springer.com/content/pdf/10.1007/s11207-020-01652-w.pdf
Zebra patterns (zebras) play an important role in the plasma diagnostics during solar flares. Considering their double plasma resonance (DPR) model, we present an improved method for the determination of the gyro-harmonic numbers of the zebra stripes that are essential in determining the electron density and magnetic field strength in zebra sources. Furthermore, we present the magnetic field and density spatial scales in zebra sources. Compared to the previous method, we change the basic assumption of the method. Namely, the assumption that the ratio R=Lbh/LnhR=Lbh/Lnh (LbhLbh and LnhLnh are the magnetic field and density scales) is constant in the whole zebra source is changed to its more generalized form, where the ratio RR is a linear function. Using this improved method, first, we determine the gyro-harmonic numbers of several observed zebras and variations of the spatial scales. Then, knowing the gyro-harmonic numbers of zebra stripes, we compute the electron plasma density and magnetic field strength in zebra sources. It is shown that in all cases the gyro-harmonic numbers of zebra stripes are quite high (> ≈50). This significantly reduces the magnetic field strength and thus increases the plasma beta parameter in zebra sources. The change in the ratio of the magnetic field and density scales along the axis of the radiating tube for the studied zebras is within ± 5 percent. For zebras at high frequencies, this ratio increases with the height, and for zebras at lower frequencies it decreases. The ratio of the magnetic field and density scales across the radiating tube is close to 1 and varies in the range 0.87–1.20. **25 October 1994, 17 August1998, 14 February 1999, 21 April 2002, 1 August 2010, 24 February 2011, 21 June 2011**

Alternative Models of Zebra Patterns in the Event on June 21, 2011

L. V. **Yasnov** & G. P. Chernov
Solar Physics volume 295, Article number: 13 (**2020**)
https://link.springer.com/content/pdf/10.1007/s11207-020-1585-5.pdf
https://arxiv.org/ftp/arxiv/papers/2001/2001.09893.pdf
The analysis of the spectral characteristics of the burst radio emission on **June 21, 2011** was carried out on the basis of an improved methodology for determining harmonic numbers for the corresponding stripes of the zebra structure. By using the parameters of the zebra structure in the time-frequency spectrum and basing on the double-plasma resonance model, the magnetic field and its dynamics, electron density, and the time variation of the distance between the stripes with harmonics s=55 and 56 and adjacent stripes near the frequency ≈183 MHz have been determined in the burst generation region. The relationships between the scale characteristics of the field and the density along and across the axis of the power tube and their dependence on time have been also determined. The field obtained (1.5 G for the first harmonic and 0.75 G for the second harmonic of the plasma frequency) turned out to be so small that, firstly, it fails to explain the dynamic features of the spectrum based on MHD waves, and secondly, it results in large values for plasma beta (>1). Other possible difficulties of the generation mechanism of bursts with zebra pattern based on the double-plasma resonance are also noted. Another possible mechanism, with whistlers, explains qualitatively the main observational characteristics of this zebra. The magnetic field required in this case is about 4.5 G, and the plasma beta is 0.14, which fully corresponds to the coronal conditions.

Growth Rates of the Upper-Hybrid Waves for Power-Law and Kappa Distributions with a Loss-Cone Anisotropy

Leonid V. **Yasnov**, Jan Benáček, Marian Karlický
Solar Phys. 294, 29 **2019**
https://link.springer.com/content/pdf/10.1007%2Fs11207-019-1415-9.pdf
https://arxiv.org/pdf/1904.05110.pdf
Fine structures of radio bursts play an important role in the diagnostics of the solar flare plasma. Among them the zebras, which are prevalently assumed to be generated by the double-plasma resonance instability, belong to the most important ones. In this paper we compute the growth rate of this instability for two types of the electron distribution: a) for the power-law distribution and b) for the kappa distribution, in both cases with the loss-cone type anisotropy. We find that the growth rate of the upper-hybrid waves for the power-law momentum distribution strongly depends on the pitch-angle boundary. The maximum growth rate is found for the pitch angle θc≈50∘θc≈50∘. For small angles the growth rate profile is very flat and for high pitch angles the wave absorption occurs. Furthermore, analyzing the growth rate of the upper-hybrid waves for the kappa momentum distribution we find that a decrease of the characteristic momentum pκpκ shifts the maximum of the growth rate to lower values of the ratio of the electron-plasma and electron-cyclotron frequencies, and the frequency widths of the growth rate peaks are very broad. But if we consider the kappa distribution which is isotropic up to some large momentum pmpm and anisotropic with loss-cone above this momentum then distinct peaks of the growth rate appear and thus distinct zebra stripes can be generated. It means that the

restriction of small momenta for the anisotropic part of distributions is of principal importance for the zebra stripe generation. Finally, for the zebra stripes observed on **1 August 2010**, the growth rates in dependence on the radio frequency are computed. It is shown that in this case the growth rate peaks are more distinct than in usually presented dependencies of growth rates on the ratio of the plasma and cyclotron frequencies. **1 August 2010**

Brightness temperature of radio zebras and wave energy densities in their sources

Leonid V. **Yasnov**, Jan Benáček, Marian Karlický
Solar Phys. 292:163 **2017**
https://arxiv.org/pdf/1702.01278.pdf
https://link.springer.com/content/pdf/10.1007%2Fs11207-017-1174-4.pdf
We estimated the brightness temperature of radio zebras (zebra pattern - ZP), considering that ZPs are generated in the loops having in their cross-section the exponential density profile. We took into account that when in plasma there is the source emitting in all directions then in an escape process from the plasma the emission obtains directional character nearly perpendicular to the constant density profile. Owing to a high directivity of the plasma emission the region from which the emission escapes can be very small. We estimated the brightness temperature of three observed ZPs for two values of the density height scale (1 and 0.21 Mm) and two values of the loop width (1 and 2 arcsec). In all cases high brightness temperatures were obtained. For the higher value of the the density height scale the brightness temperature was estimated as 1.1×1015 - 1.3×1017, and for the lower value as 4.7×1013 - 5.6×1015. These temperatures show that the observation probability of the burst with ZP, that is generated in the transition region with a steep gradient of the plasma density, is significantly higher than for the burst generated in the region with smoother changes of the plasma density. We also computed the saturation energy density of the upper-hybrid waves using a 3-D particle-in-cell model with the loss-cone type of distribution of hot electrons. We found that this saturated energy is proportional to the ratio of hot electron and background plasma densities. Thus, comparing the growth rate and collisional damping of the upper-hybrid waves we estimated minimal densities of hot electrons as well as minimal value of the saturation energy density of the upper-hybrid waves. Finally, we compared the computed energy density of the upper-hybrid waves with the energy density of the electromagnetic waves in the zebra. 2 May 1998, 14 February 1999, 6 June 2000

Physical Conditions in the Source Region of a Zebra Structure

L. V. **Yasnov**, M. Karlický, A. G. Stupishin
Solar Phys. Volume 291, Issue 7, pp 2037–2047 **2016**
We analyze the physical conditions in the source region of a zebra structure, observed with the Ondřejov radiospectrograph during the 1 August 2010 solar flare. To determine the gyro-frequency harmonic numbers of the observed zebra lines, we compute the magnetic field strength, the electron density, and their spatial scales in the source region of the zebra structure. The region where the flare occurred is analyzed using EUV (171 Å and 335 Å) observations. To determine the conditions in the zebra source region, the magnetic field structure is reconstructed using observed photospheric magnetic field data. By computing the dependence of the magnetic field vs. height in this reconstruction and by comparing the magnetic field strength derived from the zebra structure, we determine the dependence of the electron density vs. height in the zebra source-region. We identify the loops where the zebra structure was generated at heights of about 2.5 – 3.3 Mm. Assuming the barometric law for the electron density, we determine the temperature in the zebra source-region to be T≈2.0×104 KT≈2.0×104 K. Comparing the obtained values of the temperature and electron density in the zebra source-region with a model of the solar atmosphere, we find that the zebra structure was generated in the transition region, in agreement with our previous results.

On the Spectrum and Generation Regions of Solar Microbursts in the Decimeter Wave Band

L. V. **Yasnov**, A. A. Gofman, A. G. Stupishin
Solar Physics Volume 291, Issue 6, pp 1819-1828 **2016**
We analyze the nature and physical conditions in the generation regions of decimeter microbursts (MBs), which were discovered with the radiotelescope of the Russian Academy of Sciences (RATAN-600). One of the main peculiarities of MBs is an almost constant upper-frequency limit of about 1.1 GHz, which has not been explained in previously studied generation models. Here it is shown that this spectral peculiarity can be explained by the generation of the upper-hybrid waves at the double plasma resonance (DPR) and a subsequent transformation into low-frequency plasma waves considering free–free and cyclotron absorption. Model calculations show that MBs occur in the active regions where the magnetic-field strength is close to 100 G. MBs are most probably generated in the transition region of the solar atmosphere between main magnetic fields with opposite polarities.

Regions of Generation and Optical Thicknesses of dm-Zebra Lines

L. V. **Yasnov**, M. Karlický
Solar Physics Volume 290, Issue 7, pp 2001-2012 **2015**
Using a new model based on the double plasma resonance (DPR), we show that the zebra structure seen in solar radio bursts is generated in the transition region and at the tops of the magnetic arcade. The magnetic field in zebra sources is probably weaker than 150 gauss. According to this model, a generation of zebras in stronger magnetic fields is

improbable. The high-frequency boundary of decimetric zebras depends on the background electron plasma density, but not on the magnetic field strength in the generation regions. The bremsstrahlung absorption in atmospheric layers above the DPR zebra generation region and the cyclotron absorption in the DPR region and in the gyroresonance layers at higher altitudes limit the spectrum of zebras from both high-frequency and low-frequency sides. While the bremsstrahlung reduces the emission from the high-frequency side, the cyclotron absorption limits the low-frequency side. The observed frequency range and the number of observed zebra lines are determined not only by these absorptions, but also by appropriate distribution functions of superthermal electrons and plasma conditions in this region. Low-frequency (metric) zebra emissions can be generated at high altitudes. Computations show that such emissions can escape from the DPR generation region only at high gyro-harmonics (s>10) and with many zebra lines.

On the Nature of Neutral-Line-Associated Radio Sources

Leonid V. **Yasnov**

Solar Physics, April **2014**, Volume 289, Issue 4, pp 1215-1225

A number of authors claimed that radio sources above the neutral line of the magnetic field in solar active regions are due to non-thermal emission. This study shows that the thermal mechanism explains the radio emission from such sources. Models similar to those used for interpreting cyclotron lines were used in this study. Such models account for a steep decline in the spectrum at high frequencies and a low degree of polarization. The magnetic field between the two sunspots with an anti-parallel magnetic field has a lower gradient than the field above the sunspots. This, combined with the possibly high temperature in coronal loops connecting the sunspots, leads to the following conclusions. The optical thickness of the gyroresonance layers is increased and leads to more effective radiation at a harmonic number of 4 or 5. The lower gradient of the field between the sunspots also results in more rapid growth of emission intensity with increasing wavelength in this region than in the regions immediately above the sunspots. Additionally, the spatial averaging of the source structure due to the antenna beam pattern leads to a decrease in the degree of polarization in the region between the sunspots.

Peculiarities of polarized radio emission of solar active regions

L. V. **Yasnov**, T. I. Kal'tman & V. M. Bogod

Astronomy Reports, Vol. 55, Issue 1, **2011**

Relation between the Spatial Distribution and Spectral Index of Superthermal Electron Distribution in Solar cm-Radio Sources

L.V. **Yasnov** · M. Karlický

Solar Phys (**2010**) 264: 93–101

http://springerlink.com/content/g1112718g6545n07/flp=56873041f573457c8b20fadfbf0814d1&pi=7

A series of solar cm-radio bursts are analyzed by a new inverse method estimating spatial changes of the superthermal electron distribution in solar cm-radio burst sources. It is found that the measure of the spatial change of superthermal electrons in the radio source vn is always greater than that for the magnetic field vB and it is linearly dependent on the spectral index of the electrons δ as $vn \approx 0.5\delta$. This relation is explained in the simplified flare-loop model integrating the analytical solutions of the Fokker – Planck equation. The mean value of vB is found to be 0.36 ± 0.04, which is very close to the value of $vB = 0.38 \pm 0.02$ derived from the dependence of the magnetic field strength on the height in the active region measured by RATAN-600.

the new inversion method

Yasnov, L.V., Karlický, M.: 2009, *Solar Phys.* **260**, 363.

An Estimation of Spatial Variations of Magnetic Field and Superthermal Electron Distribution in cm-Radio Burst Sources

L.V. **Yasnov** · M. Karlický

Solar Phys (**2009**) 260: 363–373

The paper presents a new method of the estimation of spatial variations of the agnetic field and superthermal electron distribution in solar cm-radio burst sources. The method is based on minimization of the difference between the theoretical and observed radio fluxes and on the analysis of several burst spectra recorded in different moments of time. Several solar cm-radio bursts are analyzed by this method. It is found that the measure of the spatial variations of the superthermal electron distribution in the radio source is always larger than that for the magnetic field.

Long-Lived Microbursts in the Decimetric Wavelength Range and Their Connection with Noise Storms

L.V. **Yasnov** · V.M. Bogod · A.G. Stupishin
Solar Phys (**2008**) 249: 37–51
http://www.springerlink.com/content/8265gg4069573358/fulltext.pdf
In the present work a statistical analysis of long-lived microbursts (MBs) in the decimetric wavelength range was performed for the first time. Long-lived microbursts at decimetric wavelengths were observed with one-dimensional scans on the RATAN-600 radio telescope in intensity and circular polarization with a sensitivity of about 5 – 10 Jy. MBs have fluxes in the range of 0.001 – 0.1 s.f.u. and polarization degrees of 10 – 100%, and the duration of individual bursts is about 1 – 2 s. Microbursts and background sources exist for several days and appear at the sites of prolonged energy release. In this work MBs were compared with noise storms (NSs) in the metric wavelength range. Our analysis shows with high confidence that MBs are manifestation of NSs in the decimetric wavelength range. The reason for the significant difference in flux between MBs and NSs could be because MBs (unlike NSs) are related to incoherent generation of Langmuir waves. The nature of the MB emission is similar to the smoothly varying (background) emission of the NSs, but the MB emission is impulsive because of the high rate of pitch-angle diffusion.

Resonant Transition Radiation and Solar Radio Bursts

L.V. **Yasnov** · M. Karlický · E.V. Modin
Solar Phys (**2008**) 247: 351–378
This paper presents general relations for the intensity of the resonant transition radiation (RTR) and their detailed analysis. As an example of the use of the derived formulas for the RTR, the 24 December 1991 event is studied. It is shown that the observed decimetric burst can be generated by the RTR in the plasma with the density inhomogeneities at the level $\Delta N_2/N_2 = 2.5 \cdot 10^{-5}$.

Small-sized radio telescopes for monitoring and studies of solar radio emission at meter and decameter wavelengths

S. **Yerin** 1,2, A. Stanislavsky 1,2, I. Bubnov 1, A. Konovalenko 1 , P. Tokarsky 1, V. Zakharenko 1
Sun and Geosphere, **2019**; 14/1: 21 -24
http://newserver.stil.bas.bg/SUNGEO//00SGArhiv/SG_v14_No1_2019-pp-21-24.pdf
The paper shows development prospects of solar studies with small-sized sensitive radio telescopes such as the GURT active antenna which is an element of the phased array of the GURT radio telescope. Starting with GURT active antenna sensitivity calculations for solar observations, we compare our solar radio emission observations with the records of other radio telescopes. We discuss the potential of using this single antenna as an instrument for studying the active Sun manifestations from the lunar surface and suggest its possible adjustment to observe poor studied solar bursts under the terrestrial ionosphere cutoff. **2017-07-12, 2018-03-30**

ALMA Observations of the Solar Chromosphere on the Polar Limb

Takaaki **Yokoyama**, Masumi Shimojo, Takenori J. Okamoto, Haruhisa Iijima
ApJ **863** 96 **2018**
https://arxiv.org/pdf/1807.01411.pdf
http://sci-hub.tw/http://iopscience.iop.org/article/10.3847/1538-4357/aad27e/meta
We report the results of the Atacama Large Millimeter/sub-millimeter Array (ALMA) observations of the solar chromosphere on the southern polar limb. Coordinated observations with the Interface Region Imaging Spectrograph (IRIS) are also conducted. ALMA provided unprecedented high spatial resolution in the millimeter band (≈ 2.0 arcsec) at 100 GHz frequency with a moderate cadence (20 s). The results are as follows: (1) The ALMA 100 GHz images show saw-tooth patterns on the limb, and a comparison with SDO/AIA 171\AA\ images shows a good correspondence of the limbs with each other. (2) The ALMA 100 GHz movie shows a dynamic thorn-like structure elongating from the saw-tooth patterns on the limb, with lengths reaching at least 8 arcsec, thus suggesting jet-like activity in the ALMA microwave range. These **ALMA jets** are in good correspondence with IRIS jet clusters. (3) A blob ejection event is observed. By comparing with the IRIS Mg II slit-jaw images, the trajectory of the blob is located along the spicular patterns. **2017 April 29**

Constraining solar emission radius at 42 MHz during the 2024 total solar eclipse using a student-commissioned radio telescope

Olivia R. **Young**, Timothy E. Dolch, Joseph F. Helmboldt, Christopher Mentrek, +

ApJ **2025**
https://arxiv.org/pdf/2412.07034
Low-frequency solar radio emission is sourced in the solar corona, with sub-100 MHz radio emission largely originating from the ~105\,K plasma around 2 optical radii. However, the region of emission has yet to be constrained at 35--45\,MHz due to both instrumentation limitations and the rarity of astronomical events, such as total solar eclipses, which allow for direct observational approaches. In this work, we present the results from a student-led project to commission a low-frequency radio telescope array situated in the path of totality of the 2024 total solar eclipse in an effort to probe the middle corona. The Deployable Low-Band Ionosphere and Transient Experiment (DLITE) is a low-frequency radio array comprised of four dipole antennas, optimized to observe at 35--45\,MHz, and capable of resolving the brightest radio sources in the sky. We constructed a DLITE station in Observatory Park, a dark sky park in Montville, Ohio. Results of observations during the total solar eclipse demonstrate that DLITE stations can be quickly deployed for observations and provide constraints on the radius of solar emission at our center observing frequency of 42\,MHz. In this work, we outline the construction of DLITE Ohio and the solar observation results from the total solar eclipse that transversed North America in April 2024. **April 8, 2024**

Harmonic Electron Cyclotron Maser Emission along the Coronal Loop

Mehdi **Yousefzadeh**1, Yao Chen1, Hao Ning1, and Mahboub Hosseinpour2
2022 ApJ 932 35
https://arxiv.org/pdf/2209.06288
https://iopscience.iop.org/article/10.3847/1538-4357/ac6de3/pdf
Efficient radiation at second and/or higher harmonics of Ωce has been suggested to circumvent the escaping difficulty of the electron cyclotron maser emission mechanism when it is applied to solar radio bursts, such as spikes. In our earlier study, we developed a three-step numerical scheme to connect the dynamics of energetic electrons within a large-scale coronal loop structure with the microscale kinetic instability energized by the obtained nonthermal velocity distribution and found that direct and efficient harmonic X-mode (X2 for short) emission can be achieved due to the strip-like features of the distribution. That study only considered the radiation from the loop top at a specific time. Here we present the emission properties along the loop at different locations and timings. We found that, in accordance with our earlier results, few to several strip-like features can appear in all cases, and the first two strips play the major role in exciting X2 and Z (i.e., the slow extraordinary mode) that propagate quasi-perpendicularly. For the four sections along the loop, significant excitation of X2 is observed from the upper two sections, and the strongest emission is from the top section. In addition, significant excitation of Z is observed for all loop sections, while there is no significant emission of the fundamental X mode. The study provides new insight into coherent maser emission along the coronal loop structure during solar flares.

Harmonic ECME Excited by Energetic Electrons Travelling Inside A Coronal Loop

M. **Yousefzadeh**, H. Ning, Y. Chen
ApJ **909** 3 **2021**
https://arxiv.org/pdf/2101.01526.pdf
https://doi.org/10.3847/1538-4357/abd8d5
A complete understanding of solar radio bursts requires developing numerical techniques which can connect large-scale activities with kinetic plasma processes. As a starting point, this study presents a numerical scheme combining three different techniques: (1) extrapolation of magnetic field overlying a specific active region in order to derive the background field, (2) guiding-center simulation of dynamics of millions of particles within a selected loop to reveal the integral velocity distribution function (VDF) around certain sections of the loop, and (3) particle-in-cell (PIC) simulation of kinetic instabilities driven by energetic electrons initiated by the obtained distributions. Scattering effects at various levels (weak, moderate, and strong) due to wave/turbulence-particle interaction are considered using prescribed time scales of scattering. It was found that the obtained VDFs contain strip-like and loss-cone features with positive gradient, and both features are capable of driving electron cyclotron maser emission (ECME), which is a viable radiation mechanism for some solar radio bursts, in particular, solar radio spikes. The strip-like feature is important in driving the harmonic X mode, while the loss-cone feature can be important in driving the fundamental X mode. In the weak-scattering case, the rate of energy conversion from energetic electrons to X2 can reach up to ~2.9 * 10^-3 Ek0, where Ek0 is the initial kinetic energy of energetic electrons. The study demonstrates a novel way of exciting X2 mode in the corona during solar flares, and provides new sight into how escaping radiation can be generated within a coronal loop during solar flares. **September 6, 2011**
CESRA #2856 Apr **2021** http://www.astro.gla.ac.uk/users/eduard/cesra/?p=2856

Detection of long-lasting aurora-like radio emission above a sunspot

Yu, Sijie ; Chen, Bin , Sharma, Rohit ; Bastian, Timothy S. ; Mondal, Surajit ; Gary, Dale E. ; Luo, Yingjie ; Battaglia, Marina
Nature Astronomy, **2023**
https://arxiv.org/abs/2310.01240

Auroral radio emissions in planetary magnetospheres typically feature highly polarized, intense radio bursts, usually attributed to electron cyclotron maser (ECM) emission from energetic electrons in the planetary polar region that features a converging magnetic field. Similar bursts have been observed in magnetically active low-mass stars and brown dwarfs, often prompting analogous interpretations. Here we report observations of long-lasting solar radio bursts with high brightness temperature, wide bandwidth, and high circular polarization fraction akin to these auroral/exo-auroral radio emissions, albeit two to three orders of magnitude weaker than those on certain low-mass stars. Spatially, spectrally, and temporally resolved analysis suggests that the source is located above a sunspot where a strong, converging magnetic field is present. The source morphology and frequency dispersion are consistent with ECM emission due to precipitating energetic electrons produced by recurring flares nearby. Our findings offer new insights into the origin of such intense solar radio bursts and may provide an alternative explanation for auroral-like radio emissions on other flare stars with large starspots. **2016 April 9**

RHESSI Science Nuggets #461 **2023**

https://sprg.ssl.berkeley.edu/~tohban/wiki/index.php/Aurora-like_Radio_Emission_from_a_Sunspot

A Two-element Interferometer for Millimeter-wave Solar Flare Observations

YongLin **Yu** (于永林)1, Shuo Xu (许硕)1,2, Lei Zhang (张磊)1, ZiQian Shang (尚自乾)1 +++

2023 ApJS 267 14

https://iopscience.iop.org/article/10.3847/1538-4365/acd9af/pdf

In this paper, we present the design and implementation of a two-element interferometer operating in the millimeter-wave band (39.5–40 GHz) for observing solar radio emissions through nulling interference. The system is composed of two 50 cm aperture Cassegrain antennas installed on a common equatorial mount, with a separation of 230 wavelengths. The cross-correlation of the received signals effectively cancels out the quiet solar component of the high flux density (~3000 sfu) that reduces the detection limit due to atmospheric fluctuations. The system performance is as follows: the noise factor of the analog front end in the observation band is less than 2.1 dB, system sensitivity is approximately 12.4 K (~34 sfu) with an integration time constant of 0.1 ms (default), the frequency resolution is 153 kHz, and the dynamic range is ≥30 dB. Through actual testing, the nulling interferometer observes a quiet Sun with a low level of output fluctuations (up to 50 sfu) and has a significantly lower radiation flux variability (up to 190 sfu) than an equivalent single-antenna system, even under thick cloud cover. As a result, this new design can effectively improve observation sensitivity by reducing the impact of atmospheric and system fluctuations during observation.

CESRA # 3598 2023 https://www.astro.gla.ac.uk/users/eduard/cesra/?p=3598

Magnetic Reconnection During the Post-Impulsive Phase of a Long-Duration Solar Flare: Bi-Directional Outflows as a Cause of Microwave and X-ray Bursts

Sijie **Yu** (1), Bin Chen (1), Katharine K. Reeves (2), Dale E. Gary (1), Sophie Musset (3 and 4), Gregory D. Fleishman (1), Gelu M. Nita (1), Lindsay Glesener (4)

ApJ Volume 900, Issue 1, id.17 **2020**

https://arxiv.org/pdf/2007.10443.pdf **File**

https://iopscience.iop.org/article/10.3847/1538-4357/aba8a6/pdf

https://doi.org/10.3847/1538-4357/aba8a6

Magnetic reconnection plays a crucial role in powering solar flares, production of energetic particles, and plasma heating. However, where the magnetic reconnections occur, how and where the released magnetic energy is transported, and how it is converted to other forms remain unclear. Here we report recurring bi-directional plasma outflows located within a large-scale plasma sheet observed in extreme ultraviolet emission and scattered white light during the post-impulsive gradual phase of the X8.2 solar flare on **2017 September 10**. Each of the bi-directional outflows originates in the plasma sheet from a discrete site, identified as a magnetic reconnection site. These reconnection sites reside at very low altitudes (<180 Mm, or 0.26 R⊙) above the top of the flare arcade, a distance only <3% of the total length of a plasma sheet that extends to at least 10 R⊙. Each arrival of sunward outflows at the looptop region appears to coincide with an impulsive microwave and X-ray burst dominated by a hot source (10-20 MK) at the looptop, which is immediately followed by a nonthermal microwave burst located in the loopleg region. We propose that the reconnection outflows transport the magnetic energy released at localized magnetic reconnection sites outward in the form of kinetic energy flux and/or electromagnetic Poynting flux. The sunward-directed energy flux induces particle acceleration and plasma heating in the post-flare arcades, observed as the hot and nonthermal flare emissions.

CESRA Nuggets #2711 Oct **2020** http://www.astro.gla.ac.uk/users/eduard/cesra/?p=2711

Possible Detection of Subsecond-Period Propagating Magnetohydrodynamics Waves in Post-Reconnection Magnetic Loops during a Two-Ribbon Solar Flare

Sijie **Yu** (1), Bin Chen

ApJ **872** 71 **2019**

https://arxiv.org/pdf/1901.05379.pdf

sci-hub.tw/10.3847/1538-4357/aaff6d
Solar flares involve the sudden release of magnetic energy in the solar corona. Accelerated nonthermal electrons have been often invoked as the primary means for transporting the bulk of the released energy to the lower solar atmosphere. However, significant challenges remain for this scenario, especially in accounting for the large number of accelerated electrons inferred from observations. Propagating magnetohydrodynamics (MHD) waves, particularly those with subsecond/second-scale periods, have been proposed as an alternative means for transporting the released flare energy likely alongside the electron beams, while observational evidence remains elusive. Here we report a possible detection of such waves in the late impulsive phase of a two-ribbon flare. This is based on ultra-high cadence dynamic imaging spectroscopic observations of a peculiar type of decimetric radio bursts obtained by the Karl G. Jansky Very Large Array. Radio imaging at each time and frequency pixel allows us to trace the spatiotemporal motion of the source, which agrees with the implications of the frequency drift pattern in the dynamic spectrum. The radio source, propagating at 1000--2000 km s−1 in projection, shows close spatial and temporal association with transient brightenings on the flare ribbon. In addition, multitudes of subsecond-period oscillations are present in the radio emission. We interpret the observed radio bursts as \edit1{short-period} MHD wave packets propagating along newly reconnected magnetic flux tubes linking to the flare ribbon. The estimated energy flux carried by the waves is comparable to that needed for accounting for the plasma heating during the late impulsive phase of this flare. **2014 November 01**
RHESSI Science Nuggets #343 2019 http://sprg.ssl.berkeley.edu/~tohban/wiki/index.php/Short-Period_Waves
CESRA Nuggets #2166 March **2019** http://www.astro.gla.ac.uk/users/eduard/cesra/?p=2166

EFFECT OF A SAUSAGE OSCILLATION ON RADIO ZEBRA-PATTERN STRUCTURES IN A SOLAR FLARE

Sijie **Yu**1, V. M. Nakariakov2,3,4, and Yihua Yan
2016 ApJ 826 78
http://arxiv.org/pdf/1608.04289v1.pdf
Sausage modes that are axisymmetric fast magnetoacoustic oscillations of solar coronal loops are characterized by variation of the plasma density and magnetic field, and hence cause time variations of the electron plasma frequency and cyclotron frequency. The latter parameters determine the condition for the double plasma resonance (DPR), which is responsible for the appearance of zebra-pattern (ZP) structures in time spectra of solar type IV radio bursts. We perform numerical simulations of standing and propagating sausage oscillations in a coronal loop modeled as a straight, field-aligned plasma slab, and determine the time variation of the DPR layer locations. Instant values of the plasma density and magnetic field at the DPR layers allowed us to construct skeletons of the time variation of ZP stripes in radio spectra. In the presence of a sausage oscillation, the ZP structures are shown to have characteristic wiggles with the time period prescribed by the sausage oscillation. Standing and propagating sausage oscillations are found to have different signatures in ZP patterns. We conclude that ZP wiggles can be used for the detection of short-period sausage oscillations and the exploitation of their seismological potential.

Quasi-periodic Wiggles of Microwave Zebra Structures in a Solar Flare

Sijie **Yu**1, V. M. Nakariakov2,3,4, L. A. Selzer2, Baolin Tan1, and Yihua Yan
2013 ApJ 777 159
Quasi-periodic wiggles of microwave zebra pattern (ZP) structures with periods ranging from about 0.5 s to 1.5 s are found in an X-class solar flare on **2006 December 13** at the 2.6-3.8 GHz with the Chinese Solar Broadband Radio Spectrometer (SBRS/Huairou). Periodogram and correlation analysis show that the wiggles have two to three significant periodicities and are almost in phase between stripes at different frequencies. The Alfvén speed estimated from the ZP structures is about 700 km s–1. We find the spatial size of the wave-guiding plasma structure to be about 1 Mm with a detected period of about 1 s. This suggests that the ZP wiggles can be associated with the fast magnetoacoustic oscillations in the flaring active region. The lack of a significant phase shift between wiggles of different stripes suggests that the ZP wiggles are caused by a standing sausage oscillation.

RELAXATION OF MAGNETIC FIELD RELATIVE TO PLASMA DENSITY REVEALED FROM MICROWAVE ZEBRA PATTERNS ASSOCIATED WITH SOLAR FLARES

Sijie **Yu**, Yihua Yan, and Baolin Tan
2012 ApJ 761 136
It is generally considered that the emission of microwave zebra pattern (ZP) structures requires high density and high temperature, which is similar to the situation of the flaring region where primary energy is released. Therefore, a parameter analysis of ZPs may reveal the physical conditions of the flaring source region. This work investigates the variations of 74 microwave ZP structures observed by the Chinese Solar Broadband Radio Spectrometer (SBRS/Huairou) at 2.6-3.8 GHz in nine solar flares, and we find that the ratio between the plasma density scale height LN and the magnetic field scale height LB in emission sources displays a tendency to decrease during the flaring processes. The ratio LN /LB is about 3-5 before the maximum of flares. It decreases to about 2 after the maximum. The detailed analysis of three typical X-class flares implies that the variation of LN /LB during the flaring process is most

likely due to topological changes of the magnetic field in the flaring source region, and the stepwise decrease of LN /LB possibly reflects the magnetic field relaxation relative to the plasma density when the flaring energy is released. This result may also constrain solar flare modeling to some extent.

A Compact Source for Quasi-Periodic Pulsation in an M-class Solar Flare

Ding **Yuan**, Song Feng, Dong Li, Zhongjun Ning, Baolin Tan
ApJL **2019**
https://arxiv.org/pdf/1911.05217.pdf
Quasi-periodic pulsations (QPP) are usually found in the light curves of solar and stellar flares, they carry the features of time characteristics and plasma emission of the flaring core, and could be used to diagnose the coronas of the Sun and remote stars. In this study, we combined the Atmospheric Imaging Assembly (AIA) onboard the Solar Dynamics Observatory and the Nobeyama Radioheliograph (NoRH) to observe an M7.7 class flare occurred at active region 11520 on **19 July 2012**. A QPP was detected both in the AIA $131\unit{Å}$ bandpass and the NoRH $17\unit{GHz}$ channel, it had a period of about four minutes. In the spatial distribution of Fourier power, we found that this QPP originated from a compact source and that it overlapped with the X-ray source above the loop top. The plasma emission intensities in the AIA $131\unit{Å}$ bandpass were highly correlated within this region. The source region is further segmented into stripes that oscillated with distinctive phases. Evidence in this event suggests that this QPP was likely to be generated by intermittent energy injection into the reconnection region.

Distinct propagating fast wave trains associated with flaring energy releases

Ding **Yuan**1, Yuandeng Shen2, Yu Liu2, V.M. Nakariakov1, 3, Baolin Tan4, and Jing Huang4
E-print, March **2013**, A&A
Large-scale fast waves with perturbation of the EUV emission intensity are well resolved both in temporal and spatial scale by SDO/AIA. These waves are prone to propagate along the magnetic field line. We aim to probe the link between propagating fast wave trains and flaring energy releases. By measuring the wave parameters, we reveal their nature and investigate the potential to diagnose the energy source and wave guide. The spatial and temporal evolution of the wave amplitude and propagating speed is studied. The correlation of individual wave trains with flare-generated radio bursts is tested. Propagating wave pattern comprises distinct wave trains with varying periods. This characteristic signature is consistent with the patterns formed by waveguide dispersion, when different spectral components propagate at different phase and group speeds. The wave train releases are found to be highly correlated in start time with the radio bursts emitted by the non-thermal electrons that were accelerated in bursty energy releases. The wave amplitude is seen to reach the maximum in the midway of its course. This can be caused by a combined effect of the waveguide spread in the transverse direction and density stratification. The cross-sectional amplitude distribution perpendicular to the wave vector is found to follow well a Gaussian profile. The spatial structure is consistent with the kink mode polarised along the line-of-sight. The propagating speed is subject to deceleration, from ~735-845 km/s to ~600 km/s. This can be caused by the decrease in the local Alfvén speed and/or the projection effect. **30 May 2011**

Chapter 22 - The Effect of Solar Radio Bursts on GNSS Signals **Review**

Xinan **Yue**∗WeixingWan∗LimeiYan∗WenjieSun∗LianhuanHu∗William S.Schreiner†
In: Extreme Events in Geospace Origins, Predictability, and Consequences **2018**, Pages 541-554
http://sci-hub.tw/10.1016/B978-0-12-812700-1.00022-4
A solar radio burst (SRB) is the intense solar radio emission related to a solar flare and one of the extreme space weather events. If an SRB occurs with the enhancement in L band radio flux, it could influence the Global Navigation Satellite System (GNSS) signals through direct radio wave interferences. An SRB could result in reduction of signal-to-noise ratio (SNR) and instantaneous or long-period loss of lock (LOL) on GNSS signals. Therefore decreasing the observation quality, which subsequently will influence all the applications based on these observations such as radio occultation technique and precise GNSS positioning. An SRB will mainly affect stations located in the sunlit hemisphere during radio flux enhancement, while the strength of the influence depends on the solar incidence angle, the antenna pattern, the tracking algorithm, and some other factors. The threshold value of SRB flux value that could result in a significant effect on GNSS signals is believed to be between 1000–10,000 solar flux units (SFU; 1 SFU = 10− 22 W m− 2 Hz− 1) in L band. Significant SRBs can occur at solar minimum and maximum. During 2003–12, eight SRB events occurred that have shown degrading effects on GNSS signals in the literature, which is approximately 8.8 events per solar cycle. Although the occurrence ratio is not significantly high, we should pay sufficient attention to its side effects on modern society. **December 6, 2006**

The effect of solar radio bursts on the GNSS radio occultation signals.

Yue X, Schreiner WS, Kuo YH, Zhao B, Wan W, Ren Z, Liu L, Wei Y, Lei J, Solomon S, Rocken C. **2013**. J Geophys Res Space Phys 118: 5906–5918.
http://dx.doi.org/10.1002/ jgra.50525
https://agupubs.onlinelibrary.wiley.com/doi/epdf/10.1002/jgra.50525

Solar radio burst (SRB) is the radio wave emission after a solar flare, covering a broad frequency range, originated from the Sun's atmosphere. During the SRB occurrence, some specific frequency radio wave could interfere with the Global Navigation Satellite System (GNSS) signals and therefore disturb the received signals. In this study, the low Earth orbit-(LEO-) based high-resolution GNSS radio occultation (RO) signals from multiple satellites (COSMIC, CHAMP, GRACE, SAC-C, Metop-A, and TerraSAR-X) processed in University Corporation for Atmospheric Research (UCAR) were first used to evaluate the effect of SRB on the RO technique. The radio solar telescope network (RSTN) observed radio flux was used to represent SRB occurrence. An extreme case during **6 December 2006** and statistical analysis during April 2006 to September 2012 were studied. The LEO RO signals show frequent loss of lock (LOL), simultaneous decrease on L1 and L2 signal-to-noise ratio (SNR) globally during daytime, small-scale perturbations of SNR, and decreased successful retrieval percentage (SRP) for both ionospheric and atmospheric occultations during SRB occurrence. A potential harmonic band interference was identified. Either decreased data volume or data quality will influence weather prediction, climate study, and space weather monitoring by using RO data during SRB time. Statistically, the SRP of ionospheric and atmospheric occultation retrieval shows ~4% and ~13% decrease, respectively, while the SNR of L1 and L2 show ~5.7% and ~11.7% decrease, respectively. A threshold value of ~1807 SFU of 1415 MHz frequency, which can result in observable GNSS SNR decrease, was derived based on our statistical analysis.

Equipment and observational technique used to obtain dynamic spectra of the solar radio radiation at the KRIM station

Yu. F. **Yurovsky**

Kinematics and Physics of Celestial Bodies, November **2013**, Volume 29, Issue 6, pp 301–307

http://link.springer.com/article/10.3103/S0884591313060068

The equipment and observational technique used to obtain dynamic spectra of the solar radio radiation at the KRIM station (Crimean Astrophysical Observatory) that is a part of the e-CAL-LISTO worldwide network are described. The parameters of an antenna fabricated in the Radioastronomy Laboratory of the Crimean Astrophysical Observatory and a method for excluding the instrumental distortions that was developed at the KRIM station are outlined.

Original Russian Text © Yu.F. Yurovsky, 2013, published in Kinematika i Fizika Nebesnykh Tel, 2013, Vol. 29, No. 6, pp. 68–77.

Influence of Radio Wave Propagation on the Properties of Solar Microwave Bursts

Y.F. **Yurovsky**

Solar Phys (**2009)** 258: 267–275

Scintillation of radio signals passing through the solar corona is considered. An expression describing the dynamic spectrum of these scintillations on the basis of multibeam propagation of radio waves is derived. Properties of the analytically calculated spectrum are shown to coincide with zebra-structure properties of solar radio bursts. It is determined that the time profile of the scintillations caused by multibeam propagation may appear as impulses of emission or absorption or may have a sawtooth form. It is concluded that assuming specific emission source features is not the only way to explain the zebra structure, since the effect of multibeam propagation of radio waves through the solar corona and interplanetary space yields a simple explanation of the phenomenon discussed.

Spectrum of Fluctuations of Solar Noise Storms

Y.F. **Yurovsky**

Solar Phys (**2007**) 246: 415–418

http://www.springerlink.com/content/v752n03088095280/fulltext.pdf

The calculation of the Fourier transform of noise storm (NS) fluctuations showed that the power spectrum was adequately described by the expression $G(F) \sim 1/F$. Our results rule out the possibility that NS radiation is formed from random, short-term bursts (so-called type I bursts), since the spectrum of the sum of random short fluctuations is flat, but the real NS has a hyperbolic spectrum. This spectrum is monotonic and does not contain any components that exceed the level of the statistical fluctuations (*i.e.*, the results of observations do not reveal the presence of periodic or resonant properties of the emission source). The hyperbolic shape of the spectrum shows that the main energy of a NS is contained in the slower temporal fluctuations.

On the Efficiency of Radio Emissions at the Double Plasma Frequency in the Magnetosphere of Exoplanet HD189733b.

Zaitsev, V.V., Shaposhnikov, V.E., Khodachenko, M.L. et al.

Geomagn. Aeron. 63, 892–898 (**2023**).

https://doi.org/10.1134/S0016793223070307

On exoplanets with a weak magnetic field, the so-called plasma maser can be effectively implemented instead of an electron cyclotron maser. This maser involves the generation of plasma waves by energetic electrons and their conversion into radio emissions at the plasma frequency or at the double frequency. Under specific conditions, a maser effect occurs at the plasma frequency, which manifests itself in an exponential increase in radio emissions intensity with an increase in the energy of plasma waves. In this paper, we study the Raman scattering of excited plasma waves with the formation of an electromagnetic wave at the double plasma frequency in the plasmasphere of the exoplanet HD189733b, for which the three-dimensional structure of the plasma envelope has been studied. Although the maser effect is absent in the case of Raman scattering, the collisional absorption of radiation is significantly reduced at the second harmonic and the requirement for the brightness temperature in the source is reduced as well. It has been shown that the radio flux at the second harmonic increases sharply for this exoplanet from a few millijanskys at a frequency of 20 MHz to tens of janskys at a frequency of ≈4 MHz. This means that the decameter range near the cutoff frequency of the Earth's ionosphere is the most promising range for the detection of second harmonic radio emissions by modern radio telescopes. In this case, the radio emissions of the second harmonic can provide information about the properties of plasmaspheres around exoplanets at considerable distances that are inaccessible during observations at the main plasma frequencies.

Acceleration and Storage of Energetic Electrons in Magnetic Loops in the Course of Electric Current Oscillations

V. V. **Zaitsev**, A. V. Stepanov
Solar Physics October **2017**, 292:141
A mechanism of electron acceleration and storage of energetic particles in solar and stellar coronal magnetic loops, based on oscillations of the electric current, is considered. The magnetic loop is presented as an electric circuit with the electric current generated by convective motions in the photosphere. Eigenoscillations of the electric current in a loop induce an electric field directed along the loop axis. It is shown that the sudden reductions that occur in the course of type IV continuum and pulsating type III observed in various frequency bands (25 – 180 MHz, 110 – 600 MHz, 0.7 – 3.0 GHz) in solar flares provide evidence for acceleration and storage of the energetic electrons in coronal magnetic loops. We estimate the energization rate and the energy of accelerated electrons and present examples of the storage of energetic electrons in loops in the course of flares on the Sun or on ultracool stars. We also discuss the efficiency of the suggested mechanism as compared with the electron acceleration during the five-minute photospheric oscillations and with the acceleration driven by the magnetic Rayleigh–Taylor instability. **28 August 1990**
CESRA Highlights #1593 Oct **2017** http://www.astro.gla.ac.uk/users/eduard/cesra/?p=1593

On the Origin of Pulsations of Sub-THz Emission from Solar Flares

V. V. **Zaitsev**, A. V. Stepanov, P. Kaufmann
Solar Physics, Volume 289, Issue 8, pp 3017-3032 **2014**
We propose a model to explain fast pulsations in sub-THz emission from solar flares. The model is based on the approach of a flaring loop as an equivalent electric circuit and explains the pulse-repetition rate, the high-quality factor, Q≥103, low modulation depth, pulse synchronism at different frequencies, and the dependence of the pulse-repetition rate on the emission flux, observed by Kaufmann et al. (Astrophys. J. 697, 420, 2009). We solved the nonlinear equation for electric current oscillations using a Van der Pol method and found the steady-state value for the amplitude of the current oscillations. Using the pulse rate variation during the flare on **4 November 2003**, we found a decrease of the electric current from 1.7×1012 A in the flare maximum to 4×1010 A just after the burst. Our model is consistent with the plasma mechanism of sub-THz emission suggested recently by Zaitsev, Stepanov, and Melnikov (Astron. Lett. 39, 650, 2013).

Radio seismology of the outer solar corona

T. V. **Zaqarashvili**1,4, V. N. Melnik2, A. I. Brazhenko3, M. Panchenko1, A. A. Konovalenko2, A. V. Franzuzenko3, V. V. Dorovskyy2 and H. O. Rucker
E-print, Nov **2013**; A&A 555, A55 (**2013**)
http://arxiv.org/pdf/1305.2287v1.pdf
Context. Observed oscillations of coronal loops in extreme ultraviolet (EUV) lines have been successfully used to estimate plasma parameters in the inner corona (<0.2 R0, where R0 is the solar radius). However, coronal seismology in EUV lines fails for higher altitudes because of rapid decrease in line intensity.
Aims. We aim to use radio observations to estimate the plasma parameters of the outer solar corona (>0.2 R0).
Methods. We used the large Ukrainian radio telescope URAN-2 to observe type IV radio bursts at the frequency range of 8–32 MHz during the time interval of 09:50–12:30 UT on **April 14, 2011**. The burst was connected to C2.3 flare, which occurred in AR 11190 during 09:38–09:49 UT. The dynamic spectrum of radio emission shows clear quasi-periodic variations in the emission intensity at almost all frequencies.
Results. Wavelet analysis at four different frequencies (29 MHz, 25 MHz, 22 MHz, and 14 MHz) shows the quasi-periodic variation of emission intensity with periods of ~34 min and ~23 min. The periodic variations can be explained by the first and second harmonics of vertical kink oscillation of transequatorial coronal loops, which were excited by the

same flare. The apex of transequatorial loops may reach up to 1.2 R0 altitude. We derive and solve the dispersion relation of trapped magnetohydrodynamic oscillations in a longitudinally inhomogeneous magnetic slab. The analysis shows that a thin (with width to length ratio of 0.1), dense (with the ratio of internal and external densities of ≥20) magnetic slab with weak longitudinal inhomogeneity of the Alfvén speed may trap the observed oscillations. Seismologically estimated Alfvén speed inside the loop at the height of ~1 R0 is ~1000 km s-1. The magnetic field strength at this height is estimated as ~0.9 G. Extrapolation of magnetic field strength to the inner corona gives ~10 G at the height of 0.1 R0.
Conclusions. Radio observations can be successfully used for the sounding of the outer solar corona, where EUV observations of coronal loops fail. Therefore, radio seismology of the outer solar corona is complementary to EUV seismology of the inner corona.
CESRA highlight #1450 http://cesra.net/?p=1450 ***August 1, 2011***

Spatial localization of Langmuir waves generated from an electron beam propagating in an inhomogeneous plasma: Applications to the solar wind,

Zaslavsky, A., A. S. Volokitin, V. V. Krasnoselskikh, M. Maksimovic, and S. D. Bale (**2010**),
J. Geophys. Res., 115, A08103, doi:10.1029/2009JA014996.
It is known from in situ observations that large-amplitude spatially localized Langmuir waves are frequent in the solar wind, and usually correlated with the presence of suprathermal electron beams, during type III events or close to the electron foreshock. It seems that the influence of the solar wind density fluctuations on the propagation effects of the Langmuir waves play an important role in the formation of these wave packets. In this article, we focus on the mechanism of generation of localized wave packets by electron beams propagating in an inhomogeneous medium. To this purpose, we present a theoretical model based on the resolution of the high-frequency component of the Zakharov's equation in which a source term describing the electron beam has been introduced, and show that this model is able to reproduce classical results about beam plasma instability and wave trapping in density cavities. Then we present simulation results of the generation of Langmuir wave packets in typical solar wind conditions at 1 A.U., and discuss the origin and nature of their localization.

Slowly positively drifting bursts generated by large-scale magnetic reconnection

Alena **Zemanová**, Marian Karlický, Jana Kašparová, Jaroslav Dudík, Ján Rybák
A&A 690, A241 **2024**
https://arxiv.org/pdf/2408.12218
https://www.aanda.org/articles/aa/pdf/2024/10/aa50641-24.pdf
The slowly positively drifting bursts (SPDBs) are rarely observed in radio emission of solar flares. To understand how the SPDBs are generated, we studied the radio observations at 600--5000 MHz together with the imaging observations made in ultraviolet (UV) and extreme ultraviolet (EUV) during the SPDB-rich C8.7 flare of **2014 May 10** (SOL2014-05-10T0702). Because the SPDBs propagate towards locations of higher plasma density, we studied their associations with individual flare kernels, located either within the flare core itself, or distributed at longer distances, but connected to the flaring region by large-scale hot loops. For each kernel we constructed light curves using 1600 A and 304 A observations and compared these light curves with the temporal evolution of radio flux at 1190 MHz, representing all observed groups of SPDBs. We also analysed the UV/EUV observations to understand the evolution of magnetic connectivity during the flare. The flare starts with a growing hot sigmoid observed in 131 A. As the sigmoid evolves, it extends to and interacts with a half dome present within the active region. The evolving sigmoid reconnects at the respective hyperbolic flux tube, producing large-scale magnetic connections and an EUV swirl. Three groups of SPDBs are observed during this large-scale magnetic reconnection, along with a group of narrow-band type III bursts. The light curves of a kernel corresponding to the footpoint of spine line analogue show good agreement with the radio flux at 1190 MHz, indicating that the SPDBs are produced by the large-scale magnetic reconnection at the half dome. In addition, one of the kernels appeared in the neighbouring active region and also showed a similar evolution to the radio flux, implying that beams of accelerated particles can synchronize radio and UV/EUV light curves across relatively large distances.

Flare Expansion to a Magnetic Rope Accompanied by Rare Radio Bursts

Alena **Zemanová**, Marian Karlický, Jana Kašparová, and Jaroslav Dudík
2020 ApJ 905 111
https://doi.org/10.3847/1538-4357/abc424
https://arxiv.org/pdf/2101.08633.pdf
We present multispectral analysis (radio, Hα, ultraviolet (UV)/extreme ultraviolet (EUV), and hard X-ray) of a confined flare from **2015 March 12**. This flare started within the active region NOAA 12 297 and then it expanded into a large preexisting magnetic rope embedded with a cold filament. The expansion started with several brightenings located along the rope. This process was accompanied by a group of slowly positively drifting bursts in the 0.8–2 GHz range. The frequency drift of these bursts was 45–100 MHz s−1. One of the bursts had an S-like form. During the brightening of the rope we observed a unique bright EUV structure transverse to the rope axis. The structure was observed in a

broad range of temperatures and it moved along the rope with the velocity of about 240 km s−1. When the structure dissipated, we saw a plasma further following twisted threads in the rope. The observed slowly positively drifting bursts were interpreted considering particle beams and we show that one with the S-like form could be explained by the beam propagating through the helical structure of the magnetic rope. The bright structure transverse to the rope axis was interpreted considering line-of-sight effects and the dissipation-spreading process, which we found to be more likely.

A type II radio burst associated with solar filament–filament interaction

Liang **Zhang**1,2⋆, Ruisheng Zheng1,2 and Yao Chen1
A&A, 691, A4 (**2024**)
https://www.aanda.org/articles/aa/pdf/2024/11/aa49523-24.pdf

Aims. Solar radio type II bursts are often associated with coronal shocks driven by solar eruptions. In this study, we report a type II burst associated with filament–filament interaction.
Methods. Combining the high-quality multiwavelength observations from CHASE, SDO, STEREO, and CALLISTO, we conducted a detailed study of the type II burst associated with filament–filament interaction.
Results. On **2023 September 11**, an erupting filament (F1) likely disturbed a nearby long filament (F2), causing F2 to subsequently erupt. As a result of possible magnetic reconnection between ejective materials from the two filaments, loop-like structures formed perpendicular to them. Subsequently, the expansion of these loop-like structures triggered a strong coronal mass ejection (CME). Interestingly, a type II burst appeared on the solar spectrum around the time when the loop-like structures formed and the CME appeared above the occulting disk of STEREO/COR1. By converting the frequency of the type II burst to the coronal height using polarization brightness data recorded by the COR1 coronagraph and the spherically symmetric polynomial approximation technique, we determined the formation height of the type II burst to be around 1.45 R⊙, with a speed of approximately 440 km s−1. This is comparable to the observed height of the CME (∼1.43 R⊙), although slightly lower in speed (540 km s−1).
Conclusions. All these results indicate that the type II burst was closely associated with filament–filament interactions and was possibly excited by the accompanying CME at the flank. We suggest that the filament–filament interactions played an important role in producing the type II burst by acting as a piston to trigger a strong CME.

Forecasting Medium-Term F10.7 Using the Deep-Learning Informer Model.

Zhang, K., Zuo, P., Zou, Z. et al.
Sol Phys 299, 47 (**2024**).
https://doi.org/10.1007/s11207-024-02284-0

The daily 10.7-cm solar radio flux (F10.7) is one of the most important solar activity indices and has been widely applied in various space environment modeling as a crucial parameter. In this study, we adopt a deep-learning Informer model, based on the transformer architecture to predict the medium-term F10.7 index, which uses 48 historical daily F10.7 indices as input to directly forecast the following 1 – 27 days' F10.7 index. The model is demonstrated to be effective and to have superior performance compared with other widely-used forecasting techniques: two statistical methods provided by British Geological Survey (BGS), Space Weather Prediction Center (SWPC), and a multiflux neural network method provided by Collecte Localisation Satellites (CLS). In comparison, the Informer model significantly improves the forecast accuracy for the prediction horizon larger than 6 days, especially during the solar activity descending phase and at the solar activity minimum. For its effectiveness, accurate prediction capability and the advantage in F10.7 forecasting with longer horizon, the Informer could be potentially used as a candidate model for space weather operational forecasting.

Imaging spectroscopy of spectral bump in a type II radio burst

Peijin **Zhang**, Diana E. Morosan, Pietro Zucca, Sanna Normo, Bartosz Dabrowski, Andrzej Krankowski, Christian Vocks
A&A 684, L22 **2024**
https://arxiv.org/pdf/2403.19451.pdf
https://www.aanda.org/articles/aa/pdf/2024/04/aa49365-24.pdf

Context. Observations of solar type II radio bursts provide a unique opportunity to analyze the non-thermal electrons accelerated by coronal shocks and also to diagnose the plasma density distribution in the corona. However, there are very rare high-frequency resolution interferometric observations for type II radio bursts that are capable of tracking these electrons.
Aims. Recently, more spatially resolved high-resolution observations of type II radio bursts have been recorded with the Low-Frequency Array (LOFAR). Using these observations, we aim to track the location of a type II radio burst that experiences a sudden spectral bump.
Methods. Here, we present the first radio imaging observations for a type II burst with a spectral bump. We measure the variation in source location and frequency drift of the type II burst, and deduct the density distribution along its propagation direction.
Results. We identified a type II burst that experiences a sudden spectral bump in its frequency-time profile. The overall frequency drift rate is 0.06 MHz/s and it corresponds to an estimated speed of 295 km/s. The projected speed of the

radio source obtained from imaging is 380 km/s towards the east direction. At the spectral bump, a deviation in the source locations of the type II split bands is observed. The band separation increases significantly in the north-south direction.
Conclusions. The spectral bump shows an 8 MHz deviation at 60 MHz which corresponds to a 25% decrease in the plasma density. The estimated crossing distance during the spectrum bump in type II is 29 Mm suggesting that this density variation occurs in a confined area. This indicates that the shock most likely encounters the upper extent of a coronal hole. **23 May 2022**

Imaging a large coronal loop using type U solar radio burst interferometry

Jinge **Zhang**, Hamish A.S. Reid, Eoin Carley, Laurent Lamy, Pietro Zucca, Peijin Zhang, Baptiste Cecconi
ApJ **965** 107 **2024**
https://arxiv.org/pdf/2402.04822.pdf
https://iopscience.iop.org/article/10.3847/1538-4357/ad26fd/pdf
Solar radio U-bursts are generated by electron beams traveling along closed magnetic loops in the solar corona. Low-frequency (< 100 MHz) U-bursts serve as powerful diagnostic tools for studying large-sized coronal loops that extend into the middle corona. However, the positive frequency drift component (descending leg) of U-bursts has received less attention in previous studies, as the descending radio flux is weak. In this study, we utilized LOFAR interferometric solar imaging data from a U-burst that has a significant descending leg component, observed between 10 to 90 MHz on **June 5th, 2020**. By analyzing the radio source centroid positions, we determined the beam velocities and physical parameters of a large coronal magnetic loop that reached just about 1.3 R⊙ in altitude. At this altitude, we found the plasma temperature to be around 1.1 MK, the plasma pressure around 0.20 mdyn,cm−2, and the minimum magnetic field strength around 0.07 G. The similarity in physical properties determined from the image suggests a symmetric loop. The average electron beam velocity on the ascending leg was found to be 0.21 c, while it was 0.14 c on the descending leg. This apparent deceleration is attributed to a decrease in the range of electron energies that resonate with Langmuir waves, likely due to the positive background plasma density gradient along the downward loop leg.

Spatially resolved radio signatures of electron beams in a coronal shock

Peijin **Zhang**, Diana Morosan, Anshu Kumari, Emilia Kilpua
A&A 683, A123 (**2024**)
https://arxiv.org/pdf/2310.08155.pdf
https://www.aanda.org/articles/aa/pdf/2024/03/aa47799-23.pdf
Context. Type II radio bursts are solar radio burst associated with coronal shocks. Type II bursts usually exhibit fine structures in dynamic spectra that represent signatures of accelerated electron beams. So far, the sources of individual fine structures in type II bursts have not been spatially resolved in high-resolution low-frequency radio imaging.
Aims. The objective of this study is to resolve the radio sources of the herringbone bursts found in type II solar radio bursts and investigate the properties of the acceleration regions in coronal shocks
Methods. We use low-frequency interferometric imaging observations from the Low Frequency Array (LOFAR) to provide a spatially resolved analysis for three herringbone groups (marked as A, B, and C) in a type II radio burst that occurred on **2015 October 16th**.
Results. The herringbones in groups A and C have a undiversified frequency drift direction and propagation direction along frequency. They have similar value of frequency drift rates corresponding to that of type III bursts and previously studied herringbones. Group B has a more complex spatial distribution, with two distinct sources separated by 50 arcsec and no clear spatial propagation with frequency. One of the herringbones in group B was found to have an exceptionally large frequency drift rate. Conclusions. The characteristics deroved from imaging spectroscopy suggest that the studied herringbones originate from different processes. The herringbone groups A and C most likely originate from single-direction beam electrons, while group B may be explained by counterstreaming beam electrons

A New 6–15 GHz Solar Radio Observation System

Lei **Zhang**, Yanrui Su, Zhao Wu, Shuwang Chang, Yao Chen, and Fabao Yan
2023 ApJS 268 27
https://iopscience.iop.org/article/10.3847/1538-4365/ace7cc/pdf
In this study, we have developed a centimeter-band solar radio telescope covering the 6–15 GHz frequency band. The radio telescope has the outstanding advantages of a large instantaneous sampling bandwidth and wide frequency coverage. As a new solar radio telescope, its time resolution reaches a very high level of 0.26 ms at a frequency resolution of 3 MHz, which is very conducive to observing the fine structure of radio burst signals. In terms of the structure design, the system employs a 3 m diameter parabolic antenna to receive solar radio signals. The antenna has high gain and good directivity, and the pointing accuracy reaches 0.°02, which ensures the ability to accurately track the Sun in real time. In the analog signal processing module, the combination of radio frequency direct acquisition and down conversion is used to reduce the interference caused by multiple spectrum shifts. Regarding the digital receiver, a digital receiving module with high sampling rate and acquisition resolution is used for data acquisition and processing, which ensures that the observation system can obtain observation data with high time and frequency resolutions and

real-time data processing. During the trial operation of the system, solar radio bursts have been observed many times, and these observations have been supported by similar international observation equipment. According to a data comparison, the data obtained by our observation system are more precise. At present, equipment calibration methods are being improved and constructed to obtain more accurate observation data. **11 Jan 2023, 5 Feb 2023**
Table 1 Parameters of the Famous Observation Systems in the Centimeter Band
CESRA #3653 **2023** https://www.astro.gla.ac.uk/users/eduard/cesra/?p=3653

Fine structures of radio bursts from flare star AD Leo with FAST observations

Jiale **Zhang**, Hui Tian, Philippe Zarka, Corentin K. Louis, Hongpeng Lu, Dongyang Gao, Xiaohui Sun, Sijie Yu, Bin Chen, Xin Cheng, Ke Wang
ApJ **2023**
https://arxiv.org/pdf/2306.00895.pdf
Radio bursts from nearby active M-dwarfs have been frequently reported and extensively studied in solar or planetary paradigms. Whereas, their sub-structures or fine structures remain rarely explored despite their potential significance in diagnosing the plasma and magnetic field properties of the star. Such studies in the past have been limited by the sensitivity of radio telescopes. Here we report the inspiring results from the high time-resolution observations of a known flare star AD Leo with the Five-hundred-meter Aperture Spherical radio Telescope (FAST). We detected many radio bursts in the two days of observations with fine structures in the form of numerous millisecond-scale sub-bursts. Sub-bursts on the first day display stripe-like shapes with nearly uniform frequency drift rates, which are possibly stellar analogs to Jovian S-bursts. Sub-bursts on the second day, however, reveal a different blob-like shape with random occurrence patterns and are akin to solar radio spikes. The new observational results suggest that the intense emission from AD Leo is driven by electron cyclotron maser instability which may be related to stellar flares or interactions with a planetary companion.

RFI Flagging in Solar and Space Weather Low Frequency Radio Observations

Peijin **Zhang**, André R. Offringa, Pietro Zucca, Kamen Kozarev, Mattia Mancini
MNRAS Volume 521, Issue 1, May **2023**, Pages 630–637,
https://doi.org/10.1093/mnras/stad491
https://arxiv.org/pdf/2302.05523.pdf
https://academic.oup.com/mnras/article-pdf/521/1/630/49439708/stad491.pdf
Radio spectroscopy provides a unique inspection perspective for solar and space weather research, which can reveal the plasma and energetic electron information in the solar corona and inner heliosphere. However, Radio-Frequency Interference (RFI) from human activities affects sensitive radio telescopes, and significantly affects the quality of observation. Thus, RFI detection and mitigation for the observations is necessary to obtain high quality, science-ready data. The flagging of RFI is particularly challenging for the solar and space weather observations at low frequency, because the solar radio bursts can be brighter than the RFI, and may show similar temporal behavior. In this work, we investigate RFI flagging methods for solar and space weather observations, including a strategy for AOFlagger, and a novel method that makes use of a morphology convolution. These algorithms can effectively flag RFI while preserving solar radio bursts. **2022-05-19**

Deriving Large Coronal Magnetic Loop Parameters Using LOFAR J burst Observations

Jinge **Zhang**, Hamish A. S. Reid, Vratislav Krupar, Pietro Zucca, Bartosz Dabrowski, Andrzej Krankowski
Solar Phys. **298**, Article number: 7 **2023**
https://arxiv.org/pdf/2212.02161.pdf
https://link.springer.com/content/pdf/10.1007/s11207-022-02096-0.pdf
Large coronal loops around one solar radius in altitude are an important connection between the solar wind and the low solar corona. However, their plasma properties are ill-defined as standard X-ray and UV techniques are not suited to these low-density environments. Diagnostics from type J solar radio bursts at frequencies above 10 MHz are ideally suited to understand these coronal loops. Despite this, J-bursts are less frequently studied than their type III cousins, in part because the curvature of the coronal loop makes them unsuited for using standard coronal density models. We used LOw-Frequency-ARray (LOFAR) and Parker Solar Probe (PSP) solar radio dynamic spectrum to identify 27 type III bursts and 27 J-bursts during a solar radio noise storm observed on **10 April 2019**. We found that their exciter velocities were similar, implying a common acceleration region that injects electrons along open and closed magnetic structures. We describe a novel technique to estimate the density model in coronal loops from J-burst dynamic spectra, finding typical loop apex altitudes around 1.3 solar radius. At this altitude, the average scale heights were 0.36 solar radius, the average temperature was around 1 MK, the average pressure was 0.7 mdyn cm−2, and the average minimum magnetic field strength was 0.13 G. We discuss how these parameters compare with much smaller coronal loops.

Implications for additional plasma heating driving the extreme-ultraviolet late phase of a solar flare with microwave imaging spectroscopy

Jiale **Zhang**, Bin Chen, Sijie Yu, Hui Tian, Yuqian Wei, Hechao Chen, Guangyu Tan, Yingjie Luo, Xingyao Chen

ApJ **932** 53 **2022**

https://arxiv.org/pdf/2205.03518.pdf **File**

https://iopscience.iop.org/article/10.3847/1538-4357/ac6ce3/pdf

Extreme-ultraviolet late phase (ELP) refers to the second extreme-ultraviolet (EUV) radiation enhancement observed in certain solar flares, which usually occurs tens of minutes to several hours after the peak of soft X-ray emission. The coronal loop system that hosts the ELP emission is often different from the main flaring arcade, and the enhanced EUV emission therein may imply an additional heating process. However, the origin of the ELP remains rather unclear. Here we present the analysis of a C1.4 flare that features such an ELP, which is also observed in microwave wavelengths by the Expanded Owens Valley Solar Array (EOVSA). Similar to the case of the ELP, we find a gradual microwave enhancement that occurs about three minutes after the main impulsive phase microwave peaks. Radio sources coincide with both footpoints of the ELP loops and spectral fits on the time-varying microwave spectra demonstrate a clear deviation of the electron distribution from the Maxwellian case, which could result from injected nonthermal electrons or nonuniform heating to the footpoint plasma. We further point out that the delayed microwave enhancement suggests the presence of an additional heating process, which could be responsible for the evaporation of heated plasma that fills the ELP loops, producing the prolonged ELP emission. **July 14th, 2017**

Imaging of the Quiet Sun in the Frequency Range of 20-80 MHz

PeiJin **Zhang**, Pietro Zucca, Kamen Kozarev, Eoin Carley, ChuanBing Wang, Thomas Franzen, Bartosz Dabrowski, Andrzej Krankowski, Jasmina Magdalenic, Christian Vocks

ApJ **932** 17 **2022**

https://arxiv.org/pdf/2205.00065.pdf

https://iopscience.iop.org/article/10.3847/1538-4357/ac6b37/pdf

Radio emission of the quiet Sun is considered to be due to thermal bremsstrahlung emission of the hot solar atmosphere. The properties of the quiet Sun in the microwave band have been well studied, and they can be well described by the spectrum of bremsstrahlung emission. In the meter-wave and decameter-wave bands, properties of the quiet Sun have rarely been studied due to the instrumental limitations. In this work, we use the LOw Frequency ARray (LOFAR) telescope to perform high quality interferometric imaging spectroscopy observations of quiet Sun coronal emission at frequencies below 90~MHz. We present the brightness temperature spectrum, and size of the Sun in the frequency range of 20-80~MHz. We report on dark coronal regions with low brightness temperature that persist with frequency. The brightness temperature spectrum of the quiet Sun is discussed and compared with the bremsstrahlung emission of a coronal model and previous quiet Sun observations. **7, 14 Aug 2021**

Auto Recognition of Solar Radio Bursts Using the C-DCGAN Method.

Zhang W, Yan F, Han F, He R, Li E, Wu Z and Chen Y

(**2021**) Front. Phys. 9:646556.

https://www.frontiersin.org/articles/10.3389/fphy.2021.646556/full

https://doi.org/10.3389/fphy.2021.646556

Solar radio bursts can be used to study the properties of solar activities and the underlying coronal conditions on the basis of the present understanding of their emission mechanisms. With the construction of observational instruments, around the world, a vast volume of solar radio observational data has been obtained. Manual classifications of these data require significant efforts and human labor in addition to necessary expertise in the field. Misclassifications are unavoidable due to subjective judgments of various types of radio bursts and strong radio interference in some events. It is therefore timely and demanding to develop techniques of auto-classification or recognition of solar radio bursts. The latest advances in deep learning technology provide an opportunity along this line of research. In this study, we develop a deep convolutional generative adversarial network model with conditional information (C-DCGAN) to auto-classify various types of solar radio bursts, using the solar radio spectral data from the Culgoora Observatory (1995, 2015) and the Learmonth Observatory (2001, 2019), in the metric decametric wavelengths. The technique generates pseudo images based on available data inputs, by modifying the layers of the generator and discriminator of the deep convolutional generative adversarial network. It is demonstrated that the C-DCGAN method can reach a high-level accuracy of auto-recognition of various types of solar radio bursts. And the issue caused by inadequate numbers of data samples and the consequent over-fitting issue has been partly resolved. **2005 August 22**

Non-thermal electron energization during the impulsive phase of an X9.3 flare revealed by Insight-HXMT

P. **Zhang**, W. Wang, Y. Su, L.M. Song, C.K. Li, D.K. Zhou, S.N. Zhang, H. Tian, S.M. Liu, H.S. Zhao, S. Zhang

ApJ **918** 42 **2021**

https://arxiv.org/pdf/2106.09506.pdf

https://doi.org/10.3847/1538-4357/ac0cfb

The X9.3 flare SOL**20170906**T11:55 was observed by the CsI detector aboard the first Chinese X-ray observatory Hard X-ray Modulation telescope (Insight-HXMT). By using wavelets method, we report about 22 s quasiperiodic pulsations(QPPs) during the impulsive phase. And the spectra from 100 keV to 800 keV showed the evolution with the gamma-ray flux, of a power-law photon index from ∼1.8 before the peak, ∼2.0 around the flare peak, to ∼1.8 again. The gyrosynchrotron microwave spectral analysis reveals a $36.6 \pm 0.6 \arcsec$ radius gyrosynchrotron source with mean transverse magnetic field around 608.2 Gauss, and the penetrated ≥ 10 keV non-thermal electron density is about 106.7cm−3 at peak time. The magnetic field strength followed the evolution of high-frequency radio flux. Further gyrosynchrotron source modeling analysis implies that there exists a quite steady gyrosynchrotron source, the non-thermal electron density and transverse magnetic field evolution are similar to higher-frequency light curves. The temporally spectral analysis reveals that those non-thermal electrons are accelerated by repeated magnetic reconnection, likely from a lower corona source.

Parametric simulation studies on the wave propagation of solar radio emission: the source size, duration, and position

PeiJin **Zhang**, ChuanBing Wang, Eduard P. Kontar

ApJ **909** 195 **2021**

https://arxiv.org/pdf/2101.00911.pdf

https://doi.org/10.3847/1538-4357/abd8c5

The observed features of the radio sources indicate complex propagation effects embedded in the waves of solar radio bursts. In this work, we perform ray-tracing simulations on radio wave transport in the corona and interplanetary region with anisotropic electron density fluctuations. For the first time, the variation of the apparent source size, burst duration, and source position of both fundamental emission and harmonic emission at frequency 35 MHz are simulated as the function of the anisotropic parameter α and the angular scattering rate coefficient η=ϵ2/h0, where ϵ2=⟨δn2⟩/n2 is the density fluctuation level and h0 is its correlation length near the wave exciting site. It is found that isotropic fluctuations produce a much larger decay time than a highly anisotropic fluctuation for fundamental emission. By comparing the observed duration and source size with the simulation results in the parameter space, we can estimate the scattering coefficient and the anisotropy parameter η=8.9×10−5km−1 and α=0.719 with point pulse source assumption. Position offsets due to wave scattering and refraction can produce the co-spatial of fundamental and harmonic waves in observations of some type III radio bursts. The visual speed due to the wave propagation effect can reach 1.5\,c for η=2.4×10−4km−1 and α=0.2 for fundamental emission in the sky plane, accompanying with large expansion rate of the source size. The visual speed direction is mostly identical to the offset direction, thus, for the observation aiming at obtaining the source position, the source centroid at the starting point is closer to the wave excitation point.

CESRA #2860 May **2021** http://www.astro.gla.ac.uk/users/eduard/cesra/?p=2860

Generate Radioheliograph Image from SDO/AIA Data with Machine Learning Method

PeiJin **Zhang**, Chuanbing Wang, Guanshan Pu

Research in Astronomy and Astrophysics **2020**

https://arxiv.org/pdf/2006.13023.pdf

The radioheliograph image is essential for the study of solar short term activities and long term variations, while the continuity and granularity of radioheliograph data is not so ideal, due to the short visible time of the sun and the complex electron-magnetic environment near the ground-based radio telescope. In this work, we develop a multi-channel input single-channel output neural network, which can generate radioheliograph image in microwave band from the Extreme Ultra-violet (EUV) observation of the Atmospheric Imaging Assembly (AIA) on-board the Solar Dynamic Observatory (SDO). The neural network is trained with nearly 8 years of data of Nobeyama Radioheliograph (NoRH) at 17 GHz and SDO/AIA from January 2011 to September 2018. The generated radioheliograph image is in good consistency with the well-calibrated NoRH observation. SDO/AIA provides solar atmosphere images in multiple EUV wavelengths every 12 seconds from space, so the present model can fill the vacancy of limited observation time of microwave radioheliograph, and support further study of the relationship between the microwave and EUV emission.

2013-09-28, 2017-11-24, 2018-08-19

Interferometric Imaging with LOFAR Remote Baselines of the Fine Structures of a Solar Type IIIb Radio Burst

PeiJin **Zhang**, Pietro Zucca, Sarrvesh Seethapuram Sridhar, ChuanBing Wang, Diana E. Morosan, Bartosz Dabrowski, Andrzej Krankowski, Mario M. Bisi, Jasmina Magdalenic, Christian Vocks, Gottfried Mann

A&A **2020**

https://arxiv.org/pdf/2005.09419.pdf

https://www.aanda.org/articles/aa/pdf/2020/07/aa37733-20.pdf

Context. Solar radio bursts originate mainly from high energy electrons accelerated in solar eruptions like solar flares, jets, and coronal mass ejections. A subcategory of solar radio bursts with short time duration may be used as a proxy to understand the wave generation and propagation within the corona. Aims. Complete case studies of the source size, position and kinematics of short term bursts are very rare due to instrumental limitations. A comprehensive multi-

frequency spectroscopic and imaging study was carried out of a clear example of a solar type IIIb-III pair. Methods. In this work, the source of the radio burst was imaged with the interferometric mode, using the remote baselines of the LOw Frequency ARray (LOFAR). A detailed analysis of the fine structures in the spectrum and of the radio source motion with imaging was conducted. Results. The study shows how the fundamental and harmonic components have a significantly different source motion. The apparent source of the fundamental emission at 26.56MHz displaces away from the solar disk center at about 4 times the speed of light, while the apparent source of the harmonic emission at the same frequency shows a speed of < 0.02c. The source size of the harmonic emission, observed in this case, is smaller than that in previous studies, indicating the importance of the use of the remote baselines. **13 April 2019**
EGU2020 presentation #80 **File**

The Frequency Drift and Fine Structures of Solar S-bursts in the High Frequency Band of LOFAR

PeiJin **Zhang**1,2,3, Pietro Zucca3, ChuanBing Wang1,2,4, Mario M. Bisi5, Bartosz Dąbrowski6, Richard A. Fallows3, Andrzej Krankowski6, Jasmina Magdalenic7, Gottfried Mann8, Diana E. Morosan9Show full author list
2020 ApJ 891 89
sci-hub.si/10.3847/1538-4357/ab7005
Solar S-bursts are short duration (<1 s at decameter wavelengths) radio bursts that have been observed during periods of moderate solar activity, where S stands for short. The frequency drift of S-bursts can reflect the coronal density variation and the motion state of the electron beams. In this work, we investigate the frequency drift and the fine structure of the S-bursts with the Low Frequency Array (LOFAR). We find that the average frequency drift rate of the S-bursts within 20–180 MHz could be described by df/dt = −0.0077f 1.59, combined with previous results in low frequency. With the high time and frequency resolution of LOFAR, we can resolve the fine structures of the observed solar S-bursts. A fine drift variation pattern was found in the structure of S-bursts (referred to as solar Sb-bursts in this paper) during the type-III storm on **2019 April 13**, in the frequency band of 120–240 MHz. The Sb-bursts have a quasiperiodic segmented pattern, and the relative flux intensity tends to be large when the frequency drift rate is relatively large. This kind of structure exists in about 20% of the solar S-burst events within the observed frequency range. We propose that the fine structure is due to the density fluctuations of the background coronal density. We performed a simulation based on this theory that can reproduce the shape and relative flux intensity of the Sb-bursts. This work shows that the fine structure of solar radio bursts can be used to diagnose the coronal plasma.

On the Source Position and Duration of a Solar Type III Radio Burst Observed by LOFAR

PeiJin **Zhang**, SiJie Yu, Eduard Kontar, ChuanBing Wang
ApJ **885** 140 **2019**
https://arxiv.org/pdf/1909.08773.pdf
sci-hub.se/10.3847/1538-4357/ab458f
Solar type III radio bursts are excited by electron beams propagating outward from the Sun. The flux of type III radio burst has a time profile of rising and decay phase at a given frequency, which has been actively studied since 1970s. Several factors that may influence the duration of a type III radio burst has been proposed. However, the major cause of the duration is still an open question. In this work, to study the dominant cause of the duration, we investigate the source positions of the front edge, the peak, and the tail edge in the dynamic spectrum of a single and clear type III radio burst. The duration of this type III burst at a given frequency is about 3 second for decameter wave. The beam-formed observations by the LOw-Frequency ARray (LOFAR) are used, which can provide the radio source positions and the dynamic spectra at the same time. We find that, for this burst, the source positions of the front edge, the peak, and the tail edge split with each other spatially. The radial speed of the front edge, the peak, and the tail edge is 0.42 c, 0.25 c, and 0.16 c, respectively. We estimate the influences of the corona density fluctuation and the electron-velocity dispersion on the duration, and the scattering effect by comparison with a few short-duration bursts from the same region. The analysis yields that, in the frequency range of 30 - 41 MHz, the electron-velocity dispersion is the dominant factor that determines the time duration of type III radio bursts with long duration, while scattering may play important role in the duration of short bursts. **06 May 2015**
CESRA Highlights #**2497** Jan **2020** http://cesra.net/?p=2497

Forward Modeling of the Type III Radio Burst Exciter

Peijin **Zhang**, Chuanbing Wang, Lin Ye, Yuming Wang
Solar Physics May **2019**, 294:62
sci-hub.se/10.1007/s11207-019-1448-0
https://arxiv.org/pdf/1905.09510.pdf
In this work, we propose a forward-modeling method to study the trajectory and speed of the interplanetary (IP) Type-III radio burst exciter. The model assumes that the source of an IP Type-III radio burst moves outward from the Sun following the Parker spiral field line. Using the arrival time of the radio waves at multiple spacecraft, we are able to determine the trajectory of the radio source in the Ecliptic plane, and its outward speed, as well as the injection time and

longitude of the associated electron beam near the solar surface that triggers the Type-III radio burst. For the application of this method, we design a system to gather the arrival time of the radio wave from the radio dynamic spectra observed by Solar Terrestrial Relations Observatory(STEREO)/WAVES and Wind/WAVES. Then the system forward models the trajectory and speed of the radio burst exciter iteratively according to an evaluation function. Finally, we present a survey of four Type-III radio bursts that are well discussed in the literature. The modeled trajectories of the radio source are consistent with the previous radio-triangulation results, the longitude of the associated active region, or the location of Langmuir waves excited by the electron beam. **29 January 2008, 17 Jan 2010, 17 Nov 2010, 03 Nov 2011**

Similar behaviors between FRB 121102 and solar type III radio bursts

G. Q. **Zhang**, F. Y. Wang, Z. G. Dai

2019

https://arxiv.org/pdf/1903.11895.pdf

Fast radio bursts (FRBs) are bright milliseconds radio transients with large dispersion measures (DMs), and can be used as potential astrophysical and cosmological tools. Many models for FRB progenitors have been proposed. However, none of them can explain all the observational properties, meaning that FRBs remain one of the most intriguing mysteries in astronomy. The statistical properties of radio bursts can unveil the underlying physics. Here, we report statistical results of the repeating FRB 121102, and show that FRB 121102 and solar type III radio bursts share four statistical properties: power-law frequency distributions for energies, fluxes, durations and waiting times. All of the distributions can be explained by avalanche models of self-organized criticality (SOC) systems. It is well known that solar type III radio burst arises from the nonlinear conversion of Langmuir waves generated by two-stream instability of electron beams, which are accelerated by bursty magnetic reconnections. The similarities support that repeating FRBs are coherent emissions from magnetic-reconnection-driven beams in the magnetospheres of magnetars.

Imaging observations of chromospheric evaporation in a circular-ribbon flare

Q. M. **Zhang**, D. Li, Y. Huang

ApJ **2018**

https://arxiv.org/pdf/1811.11363.pdf

In this paper, we report our multiwavelength imaging observations of chromospheric evaporation in a C5.5 circular-ribbon flare (CRF) on **2014 August 24**. The flare was observed by the Atmospheric Imaging Assembly (AIA) on board the \textit{Solar Dynamics Observatory} (\textit{SDO}), X-ray Telescope (XRT) on board the \textit{Hinode} spacecraft, and ground-based Nobeyama Radioheliograph (NoRH). The CRF consisted of a discrete circular ribbon with a diameter of ∼1$\arcmin$ and a short inner ribbon observed in ultraviolet (UV), extreme-ultraviolet (EUV), soft X-ray (SXR), and especially in 17 GHz. The peak time (∼04:58 UT) of the flare in 17 GHz coincided with that in UV 1600 Å and SXR derivative as a hard X-ray proxy, implying the peak time of impulsive energy deposition in the lower atmosphere. Shortly after the peak time, converging motion and filling process in the flare loop were revealed in AIA 131 Å and two XRT filters (Be_thin and Be_med), which are clear evidence for chromospheric evaporation upflows. The chromospheric evaporation lasted for ∼6 minutes until ∼05:04 UT. The temperature, density, and apparent velocities of the upflows are ∼107 K, ∼1.8×1010 cm−3, and 50−630 km s−1 with a mean value of ∼170 km s−1. By comparison with previous models, we are able to estimate that energies above 5×1010 erg cm−2 s−1 are likely needed to explain the observational results. Since heating by thermal conduction does not seem to provide enough energy, alternative mechanisms such as nonthermal electrons or Alfvénic waves might need to be invoked.

A type III radio burst automatic analysis system and statistic results for a half solar-cycle with the Nançay Decameter Array data

Peijin **Zhang**, Chuan Bing Wang, Lin Ye

A&A 618, A165 **2018**

https://arxiv.org/pdf/1810.02921.pdf

We design an event recognition-analysis system that can automatically detect solar type III radio burst and can mine information of the burst from the dynamic spectra observed by Nancay Decameter Array (NDA). We investigate the frequency drift rate of type III bursts and the speed of electron beams responsible for the generation of the bursts. Several computer vision methods are used in this automatic analysis system. The Hough transform is performed to recognize the line segment associated with type III bursts in the dynamic spectra. A modified active contour model is used to track the backbone of the burst and estimate the frequency drift rate at different frequency channels. We run this system on the NDA data from 2012 to 2017, and give a statistical survey of the event number distribution, the starting and stopping frequencies of bursts, the frequency dependence of the drift rate, and the exciter speed using three corona density models. The median value of the average frequency drift rates is about 6.94MHz/s for 1389 simple well-isolated type III bursts detected in the frequency range 10--80 MHz of NDA observation. The frequency drift rate changes with frequency as df/dt=−0.0672f1.23 from a least-squares fitting. The average exciter speed is about 0.2c based the density models. We do not find any significant dependence of the drift rate and the exciter speed on the solar activity cycle.

CESRA #2050 **2018** http://www.astro.gla.ac.uk/users/eduard/cesra/?p=2050

Impulsive radio and hard X-ray emission from an M-class flare

Ping **Zhang**1,2,4, Yang Guo3, Lu Wang1,2 and Siming Liu
A&A 615, A48 (**2018**)
https://www.aanda.org/articles/aa/pdf/2018/07/aa31274-17.pdf

Context. Impulsive radio and hard X-ray emission from large solar flares are usually attributed to a hard distribution of high-energy electrons accelerated in the energy dissipation process of magnetic reconnection.
Aims. We report the detection of impulsive radio and hard X-ray emissions produced by a population of energetic electrons with a very soft distribution in an M-class flare: SOL**2015-08-27**T05:45 .
Methods. The absence of impulsive emission at 34 GHz and hard X-ray emission above 50 keV and the presence of distinct impulsive emission at 17 GHz and lower frequencies and in the 25–50 keV X-ray band imply a very soft distribution of energetic electrons producing the impulsive radio emission via the gyro-synchrotron process, and impulsive X-rays via bremsstrahlung.
Results. The spectrum of the impulsive hard X-ray emission can be fitted equally well with a power-law model with an index of ∼6.5 or a super-hot thermal model with a temperature as high as 100 MK. Imaging observations in the extreme-UV and X-ray bands and extrapolation of the magnetic field structure using a nonlinear force-free model show that energetic electrons trapped in coronal loops are responsible for these impulsive emissions.
Conclusions. Since the index of the power-law model is nearly constant during the impulsive phase, the power-law distribution or the super-hot component should be produced by a bulk energization process such as the Fermi and betatron acceleration of collapsing magnetic loops.

Solar EUV Flux Proxy Using Multifrequency Solar Radio Flux

Yongliang **Zhang**, Larry J. Paxton
Space Weather volume16, Issue5 May **2018** Pages 434-441
http://sci-hub.tw/https://onlinelibrary.wiley.com/doi/abs/10.1029/2017SW001763

We report a new solar extreme ultraviolet (EUV; 26–34 nm) proxy using solar radio fluxes at six different frequencies (410; 610; 1,415; 2,695; 4,995; and 8,800 MHz) from ground-based observations. The radio fluxes (2002–2008) are used to estimate the solar EUV flux under nonsolar flare conditions through an artificial neural network trained with coincidently observed solar EUV (26–34 nm) fluxes from the SOlar and Heliospheric Observatory/Solar EUV Monitor instrument. The radio fluxes at 610; 1,415; and 8,800 MHz are the three top contributors in the estimation of the solar EUV flux. The 1,415 MHz flux has the highest correlation coefficient (0.97) with the observed EUV flux. The estimated EUV flux retained the highest correlation coefficient (0.97) and had the lowest error in comparison with the observed EUV flux. The popular F10.7cm (2,800 MHz) is between 2,695 and 4,995 MHz, which have a minor contribution to the estimated EUV flux. On the other hand, F30cm (1,000 MHz) is between 610 and 1,415 MHz, the two major contributors to the estimated EUV flux. These features are consistent with a significantly better neutral density modeling using F30cm versus F10.7cm (Bruinsman, 2015, https://doi.org/10.1051/swsc/2015001). Similar results are obtained by applying the coefficients trained using a subset of the radio data (2002, 2004, and 2007) to a different subset of the data (2003, 2005, 2006, and 2008). These indicate that solar radio fluxes at multiple frequencies can be used to reliably retrieve solar EUV flux, one of the key parameters for space weather studies.

Solar Radio Bursts with Spectral Fine Structures in Preflares

Yin **Zhang**, Baolin Tan, Marian Karlický, Hana Mészárosová, Jing Huang, Chengming Tan, Paulo Simões
2015 *ApJ* **799** 30
http://arxiv.org/pdf/1411.4766v1.pdf

A good observation of preflare activities is important for us to understand the origin and triggering mechanism of solar flares, and to predict the occurrence of solar flares. This work presents the characteristics of microwave spectral fine structures as preflare activities of four solar flares observed by Ond\v{r}ejov radio spectrograph in the frequency range of 0.8--2.0 GHz. We found that these microwave bursts which occurred 1--4 minutes before the onset of flares have spectral fine structures with relatively weak intensities and very short timescales. They include microwave quasi-periodic pulsations (QPP) with very short period of 0.1-0.3 s and dot bursts with millisecond timescales and narrow frequency bandwidths. Accompanying these microwave bursts, there are filament motions, plasma ejection or loop brightening on the EUV imaging observations and non-thermal hard X-ray emission enhancements observed by RHESSI. These facts may reveal certain independent non-thermal energy releasing processes and particle acceleration before the onset of solar flares. They may be conducive to understand the nature of solar flares and predict their occurrence**. 2010-08-01, 2010-08-14, 2011-12-25, 2012-05-07**

Correlation Between Sharp Variation of the Transport Rate of Magnetic Helicity and Solar Eruptive Events

Yin **Zhang**1, Baolin Tan and Yihua Yan
E-print, June **2008**
In this letter we report a close relationship between the variations of the transport rate of the magnetic helicity (*dH/dt*) and the microwave burst. The latter may be regarded as a prompt signal of non-thermal energetic particles originated from the magnetic reconnection during solar flaring events. We analyze the observations of magnetograms of MDI/SOHO and SOT/Hinode, and the high-cadence microwave observation at 2.84 GHz obtained in Chinese Solar Broadband Radiospectrometer (SRBS/Huairou) of a flare/CME event which occurred in Active Region NOAA 10930 on **2006 December 13**. We ¯nd that there is a sharp jump of *dH/dt* around the onset and quench of the microwave burst at the frequency of **2.84 GHz**: the rate of *dH/dt* changes from negative to positive around the start of the eruption and recovers to negative when the eruption stopped. Furthermore the temporal pro¯le of *dH/dt* is consistent with that of the microwave burst. These results manifest that sharp variations of *dH/dt* are closely related to the solar eruption.

The effect of electron holes on cyclotron maser emission driven by horseshoe distributions

G. Q. **Zhao**, Y. H. Chu, H. Q. Feng, D. J. Wu
Physics of Plasmas **2016**
https://arxiv.org/pdf/1611.04451v1.pdf
https://arxiv.org/pdf/1611.04451v1.pdf This Brief Communication presents a quantitative investigation for the effect of electron holes on electron-cyclotron maser (ECM) driven by horseshoe distributions. The investigation is based on an integrated distribution function for the horseshoe distributions with electron holes. Results show that the presence of electron holes can significantly enhance the ECM growth rate by 2-3 times in a very narrow waveband. The present study suggests that these electron holes probably are responsible for some fine structures of radiations, such as narrowband events in auroral kilometric radiation and solar microwave spikes.

CYCLOTRON MASER EMISSION FROM POWER-LAW ELECTRONS WITH STRONG PITCH-ANGLE ANISOTROPY

G. Q. **Zhao**1, H. Q. Feng1, D. J. Wu2, L. Chen2, J. F. Tang3, and Q. Liu
2016 ApJ 822 58
Energetic electrons with power-law spectra are commonly observed in astrophysics. This paper investigates electron cyclotron maser emission (ECME) from the power-law electrons, in which strong pitch-angle anisotropy is emphasized. The electron distribution function proposed in this paper can describe various types of pitch-angle anisotropy. Results show that the emission properties of ECME, including radiation growth, propagation, and frequency properties, depend considerably on the types of electron pitch-angle anisotropy, and different wave modes show different dependences on the pitch angle of electrons. In particular, the maximum growth rate of the X2 mode rapidly decreases with respect to the electron pitch-angle cosine μ 0 at which the electron distribution peaks, while the growth rates for other modes (X1, O1, O2) initially increase before decreasing as μ 0 increases. Moreover, the O mode, as well as the X mode, can be the fastest growth mode, in terms of not only the plasma parameter but also the type of electron pitch-angle distribution. This result presents a significant extension of the recent researches on ECME driven by the lower energy cutoff of power-law electrons, in which the X mode is generally the fastest growth mode.

Influence of a CME's Initial Parameters on the Arrival of the Associated Inteplanetary Shock at Earth and the Shock Propagational Model Version 3

X. H. **Zhao** and X. S. Feng
2015 ApJ 809 44
Predicting the arrival times of coronal mass ejections (CMEs) and their related waves at Earth is an important aspect of space weather forecasting. The Shock Propagation Model (SPM) and its updated version (SPM2), which use the initial parameters of solar flare-Type II burst events as input, have been developed to predict the shock arrival time. This paper continues to investigate the influence of solar disturbances and their associated CMEs on the corresponding interplanetary (IP) shock's arrival at Earth. It has been found that IP shocks associated with wider CMEs have a greater probability of reaching the Earth, and the CME speed obtained from coronagraph observations can be supplementary to the initial shock speed computed from Type II radio bursts when predicting the shock's arrival time. Therefore, the third version of the model, i.e., SPM3, has been developed based on these findings. The new version combines the characteristics of solar flare-Type II events with the initial parameters of the accompanying CMEs to provide the prediction of the associated IP shock's arrival at Earth. The prediction test for 498 events of Solar Cycle 23 reveals that the prediction success rate of SPM3 is 70%–71%, which is apparently higher than that of the previous SPM2 model (61%–63%). The transit time prediction error of SPM3 for the Earth-encountered shocks is within 9 hr (mean-absolute). Comparisons between SPM3 and other similar models also demonstrate that SPM3 has the highest success rate and best prediction performance.

A Model for Radio Emission from Solar Coronal Shocks

G. Q. **Zhao**, L. Chen, D. J. Wu

2014, ApJ 786 47

http://arxiv.org/pdf/1403.5088v1.pdf

Solar coronal shocks are very common phenomena in the solar atmosphere and are believed to be the drivers of solar type II radio bursts. However, the microphysical nature of these emissions is still an open problem. This paper proposes that electron cyclotron maser (ECM) emission is responsible for the generation of radiations from the coronal shocks. In the present model, an energetic ion beam accelerated by the shock excites first Alfv\'en wave (AW) and then the excited AW leads to the formation of a density-depleted duct along the foreshock boundary of the shock. In this density-depleted duct, the energetic electron beam produced via the shock acceleration can effectively excite radio emission by the ECM instability. Our results show that this model may have potential application to solar type II radio bursts.

Solar Type III Radio Bursts Modulated by Homochromous Alfvén Waves

G. Q. **Zhao**1,2, L. Chen1, and D. J. Wu

2013 ApJ 779 31

Solar type III radio bursts and their production mechanisms have been intensively studied in both theory and observation and are believed to be the most important signatures of electron acceleration in active regions. Recently, Wu et al. proposed that the electron-cyclotron maser emission (ECME) driven by an energetic electron beam could be responsible for producing type III bursts and pointed out that turbulent Alfvén waves can greatly influence the basic process of ECME via the oscillation of these electrons in the wave fields. This paper investigates effects of homochromous Alfvén waves (HAWs) on ECME driven by electron beams. Our results show that the growth rate of the O-mode wave will be significantly modulated by HAWs. We also discuss possible application to the formation of fine structures in type III bursts, such as so-called solar type IIIb radio bursts.

EFFECTS OF ALFVÉN WAVES ON ELECTRON CYCLOTRON MASER EMISSION IN CORONAL LOOPS AND SOLAR TYPE I RADIO STORMS

G. Q. **Zhao**1,2,3, L. Chen1, Y. H. Yan3, and D. J. Wu

2013 ApJ 770 75

Solar type I radio storms are long-lived radio emissions from the solar atmosphere. It is believed that these type I storms are produced by energetic electrons trapped within a closed magnetic structure and are characterized by a high ordinary (O) mode polarization. However, the microphysical nature of these emissions is still an open problem. Recently, Wu et al. found that Alfvén waves (AWs) can significantly influence the basic physics of wave-particle interactions by modifying the resonant condition. Taking the effects of AWs into account, this work investigates electron cyclotron maser emission driven by power-law energetic electrons with a low-energy cutoff distribution, which are trapped in coronal loops by closed solar magnetic fields. The results show that the emission is dominated by the O mode. It is proposed that this O mode emission may possibly be responsible for solar type I radio storms.

Observations of Microwave Fine Structures by the Badary Broadband Microwave Spectropolarimeter and the Siberian Solar Radio Telescope

D. A. **Zhdanov**, V. G. Zandanov

Solar Phys., **2015**, Volume 290, Issue 1, pp 287-294

Observations of solar radio bursts with fine temporal and spectral structures may provide important information about the physical processes occurring in the solar corona. The Badary Broadband Microwave Spectropolarimeter instrument has been regularly observing solar radio emission in the 3.8 – 8.2 GHz range since August 2010. We present the statistical analysis of spectral and temporal fine structures of microwave emission during solar flares that occurred in 2011 – 2012. Fine structures were detected both during solar flares accompanied by microwave broadband emission and during weak solar flares when the microwave broadband emission was absent. A total of 235 events of solar origin were found and analyzed.

A New Position Calibration Method for MUSER Images

Zhichao **Zhou**, Yihua Yan, Linjie Chen, Wei Wang, Suli Ma

A&A **2022**

https://arxiv.org/abs/2208.10217

The Mingantu Spectral Radioheliograph (MUSER), a new generation of solar dedicated radio imaging-spectroscopic telescope, has realized high-time, high-angular, and high-frequency resolution imaging of the sun over an ultra-broadband frequency range. Each pair of MUSER antennas measures the complex visibility in the aperture plane for

each integration time and frequency channel. The corresponding radio image for each integration time and frequency channel is then obtained by inverse Fourier transformation of the visibility data. In general, the phase of the complex visibility is severely corrupted by instrumental and propagation effects. Therefore, robust calibration procedures are vital in order to obtain high-fidelity radio images. While there are many calibration techniques available -- e.g., using redundant baselines, observing standard cosmic sources, or fitting the solar disk -- to correct the visibility data for the above-mentioned phase errors, MUSER is configured with non-redundant baselines and the solar disk structure cannot always be exploited. Therefore it is desirable to develop alternative calibration methods in addition to these available techniques whenever appropriate for MUSER to obtain reliable radio images. In the case that a point-like calibration source containing an unknown position error, we have for the first time derived a mathematical model to describe the problem and proposed an optimization method to calibrate this unknown error by studying the offset of the positions of radio images over a certain period of the time interval. Simulation experiments and actual observational data analyses indicate that this method is valid and feasible. For MUSER's practical data the calibrated position errors are within the spatial angular resolution of the instrument. This calibration method can also be used in other situations for radio aperture synthesis observations.

Plasma Emission versus Electron Cyclotron Maser Emission due to Power-law Energetic Electrons in Differently Magnetized Coronal Plasmas

Xiaowei **Zhou**1, Dejin Wu1, and Ling Chen1
2022 ApJ 928 115
https://iopscience.iop.org/article/10.3847/1538-4357/ac5aae/pdf
By using self-consistent 2.5-dimensional particle-in-cell simulations, we study the excitation efficiency of electromagnetic waves by power-law energetic electrons with an anisotropic pitch-angle velocity distribution, which can simultaneously trigger the Langmuir and electron cyclotron maser instabilities, in differently magnetized coronal plasmas. It is found that the (transverse) electromagnetic waves can be excited much more efficiently in the case of strongly magnetized plasmas with $\omega ce > \omega pe$ than that of weakly magnetized plasmas with $\omega ce < \omega pe$, where ωce and ωpe are the electron cyclotron frequency and the electron plasma frequency, respectively. In particular, in a weakly magnetized plasma the electromagnetic wave is hardly excited effectively via the nonlinear coupling of Langmuir waves; although the Langmuir waves can be generated by the power-law energetic electrons, implying that the so-called plasma emission does not effectively work. These results can be helpful for us to better understand the physical mechanism of solar radio bursts.

Wave Excitation by Power-law-Distributed Energetic Electrons with Pitch-angle Anisotropy in the Solar Corona

Xiaowei **Zhou**1,2, Patricio A. Muñoz3, Jörg Büchner2,3, Siming Liu1,4, and Xin Yao2,3
2021 ApJ 920 147
https://doi.org/10.3847/1538-4357/ac18c1
Radio waves from the Sun are emitted, as a rule, due to energized electrons. Observations infer that the related energized electrons follow (negative) power-law velocity distributions above a break velocity Ub. They might also distribute anisotropically in the pitch-angle space. To understand radio wave generation better, we study the consequences of anisotropic power-law-distributed energetic electrons in current-free collisionless coronal plasmas utilizing 2.5-dimensional particle-in-cell simulations. We assume that the velocity distribution fu of the energized electrons follows a plateau ($\partial fu/\partial u = 0$) and a power-law distribution with spectral index α for velocities below and above Ub, respectively. In the pitch-angle space, these energized electrons are spread around a center $\mu c = 0.5$. We found that the energetic plateau-power-law electrons can more efficiently generate coherent waves if the anisotropy of their pitch-angle distribution is sufficiently strong, i.e., a small pitch-angle spread μs. The break velocity Ub affects the excitation dominance between the electrostatic and electromagnetic waves: for larger Ub electrostatic waves are mainly excited, while intermediate values of Ub are required for an excitation dominated by electromagnetic waves. The spectral index α controls the growth rate, efficiency, saturation, and anisotropy of the excited electromagnetic waves as well as the energy partition in different wave modes. These excited electromagnetic waves are predominantly right-handed polarized, in X- and Z-modes, as observed, e.g., in solar radio spikes. Additionally about 90% of the kinetic energy loss of the energetic electrons is dissipated, heating the ambient thermal electrons. This may contribute to the coronal heating.

Wave excitation by energetic ring-distributed electron beams in the solar corona

X. **Zhou**, P. A. Muñoz, J. Büchner, S. Liu
2020 *ApJ* **891** 92
https://arxiv.org/pdf/1907.12958.pdf
https://doi.org/10.3847/1538-4357/ab6a0d

We re-considered the properties of electromagnetic waves excited by ring-beam electron in the solar atmosphere as they are caused by magnetic reconnection. Due to the positive gradients in their velocity distribution along the both parallel and perpendicular directions to the ambient magnetic field, i.e., u∥·df/du∥>0 and df/du⊥>0, not only beam instability but also so called electron cyclotron maser (ECM) instability can be excited, respectively, which may generate escaping electromagnetic waves. In order to fully understand the properties of the waves generated in the course of the propagation of such beams, we investigated the intensity and polarization properties of these excited waves in dependence on the evolving beam density and coronal magnetic field strength. For this sake, we utilized 2.5-dimensional particle-in-cell (PIC) code numerical simulations. We found that predominantly electrostatic plasma waves are generated but also highly anisotropic and polarized electromagnetic whistler, Z, O and X-mode waves. Their intensity anisotropy strongly depends on the number density ratio between the ring-beam electrons and background electrons. Circular polarization degree (CPD) and spectrogram of the escaping electromagnetic waves with ω>ωpe and |ck/ω|<1 are also strongly anisotropic, but become more symmetric about the wave propagation direction θ=90∘ for denser ring-beam electron population. Meanwhile, with denser ring-beam electron population, escaping waves are predominantly left-handed polarized over a wide range of propagation directions. We discuss the consequences of our findings for using the solar radio burst observations to diagnose the beam and plasma conditions at the sites of their generation.

Diagnostics From Three Rising Submillimeter Bursts

Ai-Hua **Zhou**, Jian-Ping Li, Xin-Dong Wang
Research in Astronomy and Astrophysics **2015**
http://arxiv.org/pdf/1509.03929v1.pdf
In the paper we investigate three novel rising submillimeter (THz) bursts occurred sequentially in a super-Active Region NOAA 10486. The average rising rate of the flux density above 200 GHz is only 20 sfu/GHz (corresponding spectral index α of 1.6) for the THz spectral components of **2003 October 28 and November 4** bursts, while it can attain values of 235 sfu/GHz (α=4.8) for **2003 November 2** burst. The steeply rising THz spectrum can be produced by a population of high relativistic electrons with a low-energy cutoff of 1 MeV , while it only requires a low-energy cutoff of 30 keV for the two slowly rising THz bursts, via gyrosynchrotron (GS) radiation based on our numerical simulations of burst spectra in the magnetic dipole field case. The electron density variation is much larger in the THz source than that in microwave (MW) one. It is interesting that the THz source radius decreased by 20--50% during the decay phase for the three events, but the MW one increased by 28% for the 2003 November 2 event. In the paper we will present a calculation formula of energy released by ultrarelativistic electrons, accounting the relativistic correction for the first time. We find that the energy released by energetic electrons in the THz source exceeds that in microwave one due to the strong GS radiation loss at THz range, although the modeled THz source area is 3--4 orders smaller than the modeled MW one. The total energies released by energetic electrons via the GS radiation in radio sources are estimated, respectively, to be 5.2×1033, 3.9×1033 and 3.7×1032 erg for the October 28, November 2 and 4 bursts, which are 131, 76 and 4 times as large as the thermal energies of 2.9×1031, 2.1×1031 and 5.2×1031 erg estimated from the soft x-ray GOES observations.

A STUDY OF A NEW INCREASING SUBMILLIMETER SPECTRAL COMPONENT OF AN X28 SOLAR FLARE

A. H. **Zhou**1, J. P. Li1, and X. D. Wang2
Astrophysical Journal, 727:42 (5pp), **2011** January; **File**
In this paper, we study a novel spectral component that increases with frequency above 200 GHz in an X28 solar flare that occurred on **2003 November 4**. A maximum flux density of ~20,000 sfu was observed at 405 GHz at main phase. We model its spectra based on gyrosynchrotron (GS) radiation computations in the case of a magnetic dipole field. Our computations show that the new increasing submillimeter spectral component at the main peak P1 can be generated by energetic electrons with a harder spectral index (2.3), low-energy cutoff of 30 keV, and number density of 1010 cm−3 in a compact source (0.__5 radius) with a strong local magnetic field varying from 780 to 4590 G via GS emission. The associated microwave (MW) spectral component can be produced by energetic electrons via GS emission, but with a 10 keV low-energy cutoff and number density 1.2Ч106 cm−3 in an extended source (40__ radius) with mean magnetic field strengths from 100 to 576 G. The MW and submillimeter emission sources, inferred from the magnetic dipole field model, are located in the corona and ~1000 km low atmosphere levels above the photosphere, respectively. Energy flux, energy loss rate, and total energy released by energetic electrons are estimated for the first time. It is found that the energy flux can attain values of 7.2Ч1013 erg cm−2 s−1 in the submillimeter source. This value is four orders higher than that in the MW source. The energies released by electrons in the submillimeter and MW sources reach, respectively, 1.2Ч1032 and 1.9Ч1031 erg. The total energy released by energetic electrons is 1.4 Ч 1032 erg during the flare in the MW and submillimeter sources. The mean energy released by energetic electrons for a subsecond pulse, i.e., the fragment energy, is estimated to be about

5.2 Ч 1026 erg.

NEW EXPLANATIONS FOR SOME OBSERVATION PHENOMENA OF THE PEAK FREQUENCY OF SOLAR RADIO BURSTS

A. H. **Zhou**, G. L. Huang, and J. P. Li

Astrophysical Journal, 708:445–449, **2010** January

We present new explanations for some observation phenomena of the peak frequency of solar radio burst spectrum, based on spectrum calculations of gyrosynchrotron radiation in a model of magnetic dipole field. These observation phenomena are: (1) a remarkable constant peak frequency of microwave burst spectrum during their lifetime, (2) a composite CD-type burst with two distinct spectral components respectively peaking in centimeter (cm) and decimeter (dm) ranges, and (3) emission of solar flares in the submillimeter band above 100 GHz (THz) and a new increasing submillimeter spectral component. Our calculation results show that the peak frequency can maintain constant when the energy spectral index δ varies only in the range larger than 3, whereas other parameters hold constant. Two distinct spectral components of the dm and cm ranges of the CD-type burst can be produced simultaneously by the energetic electrons with softer energy spectral index (_6) and lower low-energy cutoff (_30 keV). The THz burst can be generated by energetic electrons with hard spectral index (~3) and high low-energy cutoff (~250 keV) in intense local magnetic fields (mean value Ï B = 2100 G) via gyrosynchrotron emission; while a harder spectral index, a higher low-energy cutoff, and higher magnetic field strength are required for the increasing submillimeter spectral component.

A Study of the Peak Frequency of the Geosynchronous Spectrum in a Nonuniform Source

A.H. **Zhou** · J.P. Li · X.D. Wang

Solar Phys (**2008**) 247: 63–75

http://www.springerlink.com/content/3080182532274x08/fulltext.pdf

This paper investigates in detail the peak frequency of gyrosynchrotron radiation spectrum with self and gyroresonance absorption for a model of nonuniform magnetic field. It is found that the peak frequency shifts from lower frequency to higher frequency with increases in the low-energy cutoff, number density, input depth of energetic electrons, magnetic field strength and viewing angle. When the number density and temperature of thermal electrons increase, the peak frequency also shifts to a slightly higher frequency. However, the peak frequency is independent of the energy spectral index, high-energy cutoff of energetic electrons and the height of the radio source's upper boundary. It is also found for the first time that there is a good linear correlation between the logarithms of the peak frequency and the low-energy cutoff, number density, input depth of energetic electrons, magnetic field strength, and viewing angle, respectively. Their correlation coefficients are higher than 0.95 and the standard errors are less than 0.06.

Microwave diagnostics of magnetic field strengths in solar flare loops

Rui **Zhu**, Baolin Tan, Yingna Su, Hui Tian, Yu Xu, Xingyao Chen, Yongliang Song, Guangyu Tan

SCIENCE CHINA Technological Sciences **2020** Vol. 60 No. 1

https://arxiv.org/pdf/2006.15014.pdf

We have performed microwave diagnostics of the magnetic field strengths in solar flare loops based on the theory of gyrosynchrotron emission. From Nobeyama Radioheliograph observations of three flare events at 17 and 34 GHz, we obtained the degree of circular polarization and the spectral index of microwave flux density, which were then used to map the magnetic field strengths in post-flare loops. Our results show that the magnetic field strength typically decreases from ~800 G near the loop footpoints to ~100 G at a height of 10--25 Mm. Comparison of our results with magnetic field modeling using a flux rope insertion method is also discussed. Our study demonstrates the potential of microwave imaging observations, even at only two frequencies, in diagnosing the coronal magnetic field of flaring regions. **September 16, 2005, July 10, 2012, March 10, 2015**

A Flare-Type IV Burst Event from Proxima Centauri and Implications for Space Weather

Andrew **Zic**, Tara Murphy, Christene Lynch, George Heald, Emil Lenc, David L. Kaplan, Iver H. Cairns, David Coward, Bruce Gendre, Helen Johnston, Meredith MacGregor, Danny C. Price, Michael S. Wheatland

ApJ **2020**

https://arxiv.org/pdf/2012.04642.pdf

Studies of solar radio bursts play an important role in understanding the dynamics and acceleration processes behind solar space weather events, and the influence of solar magnetic activity on solar system planets. Similar low-frequency bursts detected from active M-dwarfs are expected to probe their space weather environments and therefore the habitability of their planetary companions. Active M-dwarfs produce frequent, powerful flares which, along with radio emission, reveal conditions within their atmospheres. However, to date, only one candidate solar-like coherent radio burst has been identified from these stars, preventing robust observational constraints on their space weather environment. During simultaneous optical and radio monitoring of the nearby dM5.5e star Proxima Centauri, we detected a bright, long-duration optical flare, accompanied by a series of intense, coherent radio bursts. These detections include the first example of an interferometrically detected coherent stellar radio burst temporally coincident with a flare, strongly indicating a causal relationship between these transient events. The polarization and temporal structure of the trailing long-duration burst enable us to identify it as a type IV burst. This represents the most compelling detection of a solar-like radio burst from another star to date. Solar type IV bursts are strongly associated with space weather events such as coronal mass ejections and solar energetic particle events, suggesting that stellar type IV bursts may be used as a tracer of stellar coronal mass ejections. We discuss the implications of this event for the occurrence of coronal mass ejections from Proxima Cen and other active M-dwarfs.

Cylindrical and Spherical Pistons as Drivers of MHD Shocks

Tomislav **Žic** · Bojan Vršnak · Manuela Temmer · Carla Jacobs

Solar Phys (**2008**) 253: 237–247

We consider an expanding three-dimensional (3-D) piston as a driver of an MHD shock wave. It is assumed that the source-region surface accelerates over a certain time interval to achieve a particular maximum velocity. Such an expansion creates a large-amplitude wave in the ambient plasma. Owing to the nonlinear evolution of the wave front, its profile steepens and after a certain time and distance a discontinuity forms, marking the onset of the shock formation. We investigate how the formation time and distance depend on the acceleration phase duration, the maximum expansion velocity (defining also acceleration), the Alfvén velocity (defining also Mach number), and the initial size of the piston. The model differs from the 1-D case, since in the 3-D evolution, a decrease of the wave amplitude with distance must be taken into account. We present basic results, focusing on the timing of the shock formation in the low- and high-plasma-beta environment. We find that the shockformation time and the shock-formation distance are (1) approximately proportional to the acceleration phase duration; (2) shorter for a higher expansion velocity; (3) larger in a higher Alfvén speed environment; (4) only weakly dependent on the initial source size; (5) shorter for a stronger acceleration; and (6) shorter for a larger Alfvén Mach number of the source surface expansion. To create a shock causing a high-frequency type II burst and the Moreton wave, the source region expansion should, according to our results, achieve a velocity on the order of 1000 km s−1 within a few minutes, in a low Alfvén velocity environment.

PLASMA EMISSION BY COUNTER-STREAMING ELECTRON BEAMS

L. F. **Ziebell**1, L. T. Petruzzellis1, P. H. Yoon2,3, R. Gaelzer1, and J. Pavan

2016 ApJ 818 61

The radiation emission mechanism responsible for both type-II and type-III solar radio bursts is commonly accepted as plasma emission. Recently Ganse et al. suggested that type-II radio bursts may be enhanced when the electron foreshock geometry of a coronal mass ejection contains a double hump structure. They reasoned that the counter-streaming electron beams that exist between the double shocks may enhance the nonlinear coalescence interaction, thereby giving rise to more efficient generation of radiation. Ganse et al. employed a particle-in-cell simulation to study such a scenario. The present paper revisits the same problem with EM weak turbulence theory, and show that the fundamental (F) emission is not greatly affected by the presence of counter-streaming beams, but the harmonic (H) emission becomes somewhat more effective when the two beams are present. The present finding is thus complementary to the work by Ganse et al.

See CESRA highlight #1200 Feb **2017** http://cesra.net/?p=1200

Plasma Emission by Nonlinear Electromagnetic Processes

L. F. **Ziebell**1, P. H. Yoon2,3, L. T. Petruzzellis1, R. Gaelzer1, and J. Pavan

2015 ApJ 806 237

The plasma emission, or electromagnetic (EM) radiation at the plasma frequency and/or its harmonic(s), is generally accepted as the radiation mechanism responsible for solar type II and III radio bursts. Identification and characterization of these solar radio burst phenomena were done in the 1950s. Despite many decades of theoretical research since then, a rigorous demonstration of the plasma emission process based upon first principles was not available until recently, when, in a recent Letter, Ziebell et al. reported the first complete numerical solution of EM weak turbulence equations; thus, quantitatively analyzing the plasma emission process starting from the initial electron beam and the associated beam-plasma (or Langmuir wave) instability, as well as the subsequent nonlinear conversion of electrostatic Langmuir turbulence into EM radiation. In the present paper, the same problem is revisited in order to elucidate the detailed physical mechanisms that could not be reported in the brief Letter format. Findings from the present paper may be useful for interpreting observations and full-particle numerical simulations.

NONLINEAR EVOLUTION OF BEAM-PLASMA INSTABILITY IN INHOMOGENEOUS MEDIUM

L. F. **Ziebell**1, P. H. Yoon2,3,4, J. Pavan1 and R. Gaelzer5

2011 ApJ 727, 16

The problem of electron-beam propagation in inhomogeneous solar wind is intimately related to the solar type II and/or type III radio bursts. Many scientists have addressed this issue in the past by means of quasi-linear theory, but in order to fully characterize the nonlinear dynamics, one must employ weak-turbulence theory. Available numerical solutions of the weak-turbulence theory either rely on only one nonlinear process (either decay or scattering), or when both nonlinear terms are included, the inhomogeneity effect is generally ignored. The present paper reports the full solution of weak-turbulence theory that includes both decay and scattering processes, and also incorporating the effects of density gradient. It is found that the quasi-linear effect sufficiently accounts for the primary Langmuir waves, but to properly characterize the back-scattered Langmuir wave, which is important for eventual radiation generation, it is found that both nonlinear decay and scattering processes make comparable contributions. Such a finding may be important in the quantitative analysis of the plasma emission process with application to solar **type II and/or type III** radio bursts.

Spatially resolved observations of a coronal type II radio burst with multiple lanes

Zimovets I.V., Sadykov V.M.

Adv. Space Res. Volume 56, Issue 12, 15 December 2015, Pages 2811–2832 **2015**

http://www.sciencedirect.com/science/article/pii/S0273117715000939

http://dx.doi.org/10.1016/j.asr.2015.01.041

Relative dynamics of the radio sources of the metric type II burst with three emission lanes and coronal mass ejection (CME) occurred in the lower corona (r≲1.5R⊙) during the **SOL2011-02-16T14:19** event is studied. The observational data of the Nancay Radioheliograph (NRH) and the Atmospheric Imaging Assembly (AIA) onboard the Solar Dynamics Observatory (SDO) are used. These observations are also supplemented by the data sets obtained with the STEREO-A and -B, RHESSI, and GOES spacecraft, as well as with the ground-based solar radio spectrometers. It is found that the sources of the radio burst were located ahead of the expanding CME and had a complex spatial structure. The first and the second lanes were both emitted from the flmagnetic funnelfl fl a bundle of open magnetic field lines separated the south and north systems of magnetic loops of the active region. Due to the projection effect and limited angular resolution of the NRH it is not possible to determine, whether the spatial locations of the radio sources of the two first emission lanes differed or not. It is argued that the observations support the hypothesis that the radio sources of the first and second lanes could be emitted respectively ahead of and behind a front of the same weak (the Alfvén Mach number MA≈1.1fl1.2), fast mode, quasi-parallel piston MHD shock wave. However, the third lane of the burst was definitely emitted from a different place. Its radio sources were situated ahead of the north-west part of the CME propagated through the north system of magnetic loops. This indicates clearly that different emission lanes of the same type II burst can be a result of propagation of different parts of a single CME through regions with different physical conditions (geometries and plasma densities) in the lower corona.

Non-thermal “Burst-on-Tail” of Long-Duration Solar Event on 26 October 2003

I. **Zimovets**, A. Struminsky

Solar Physics, December **2012**, Volume 281, Issue 2, pp 749-763

Observations of a rare long-duration solar event of GOES class X1.2 from **26 October 2003** are presented. This event showed a pronounced burst of hard X-ray and microwave emission, which was extremely delayed (> 60 min) with respect to the main impulsive phase and did not have any significant response visible in soft X-ray emission. We refer to this phenomenon as a “burst-on-tail”. Based on TRACE observations of the growing flare arcade and some simplified estimation, we explain why a reaction of active region plasma to accelerated electrons may change drastically over time. We suggest that, during the “burst-on-tail”, non-thermal electrons were injected into magnetic loops of larger spatial scale than during the impulsive phase bursts, thus resulting in much smaller values of plasma temperature and emission measure in their coronal volume, and hence little soft X-ray flux. The nature of the long gap between the main impulsive phase and the “burst-on-tail” is, however, still an open question.

Spatially resolved observations of a split-band coronal type-II radio burst

I. **Zimovets**, N. Vilmer, A. C.-L. Chian, I. Sharykin, A. Struminsky

E-print, Aug **2012**; A&A, 547, A6 (**2012**)

Context. The origin of coronal type II radio bursts and the nature of their band splitting are still not fully understood, though a number of scenarios have been proposed to explain them. This is largely due to the lack of detailed spatially

resolved observations of type II burst sources and of their relations to magnetoplasma structure dynamics in parental active regions.
Aims. To make progress in solving this problem on the basis of one extremely well observed solar eruptive event.

Methods. The relative dynamics of multithermal eruptive plasmas, observed in detail by the Atmospheric Imaging Assembly onboard the Solar Dynamics Observatory, and of harmonic type II burst sources, observed by the Nançay Radioheliograph at ten frequencies from 445 to 151 MHz, was studied for the **3 November 2010** event arising from an active region behind the east solar limb. Special attention was given to the band splitting of the burst. Analysis was supplemented by investigation of coronal hard X-ray (HXR) sources observed by the Reuven Ramaty High-Energy Solar Spectroscopic Imager.
Results. We found that the flare impulsive phase was accompanied by the formation of a double coronal HXR source, whose upper part coincided with the hot ($T \approx 10$ MK) eruptive plasma blob. The leading edge (LE) of the eruptive plasmas ($T \approx 1-2$ MK) moved upward from the flare region with a speed of $v \approx 900-1400$ km s-1. The type II burst source initially appeared just above the LE apex and moved with the same speed and in the same direction. After ≈ 20 s, it started to move about twice as fast, but still in the same direction. At any given moment, the low-frequency component (LFC) source of the splitted type II burst was situated above the high-frequency component (HFC) source, which in turn was situated above the LE. We also found that at a given frequency the HFC source was located slightly closer to the photosphere than the LFC source.
Conclusions. Based on the set of established observational facts, we conclude that the shock wave, which could be responsible for the observed type II radio burst, was initially driven by the multi-temperature eruptive plasmas, but later transformed to a freely propagating blast shock wave. The preferable interpretation of the type II burst splitting is that its LFC was emitted from the upstream region of the shock, whereas the HFC was emitted from the downstream region. The shock wave in this case could be subcritical.

High-Resolution Time Profiles of Fiber Bursts at 1420 and 2695 MHz

P. **Zlobec**, M. Karlický
Solar Physics, May **2014**, Volume 289, Issue 5, pp 1683-1699
To obtain constraints for models of fiber bursts, high-resolution time (0.01 s) profiles of the fiber bursts recorded at 1420 and 2695 MHz by the Trieste radiometers are studied in detail. The fiber bursts were identified using Ondřejov radio spectra. During the years 2000 – 2005, 18 intervals with fiber bursts were selected; 26 groups were defined and about 700 fibers were analyzed in detail. More than 300 pulsations, present almost simultaneously with the fibers, were also selected and studied in order to find similarities or differences between these two types of fine structures. It was found that the polarization of the associated continuum, both for fiber bursts and pulsations, is practically the same. Evaluating the ratio between absorption over emission of many single fibers we found that this parameter is very different even for nearby bursts; however, we realized that this ratio shows a tendency to decrease with time. Finally, the time profile of one selected fiber burst was fitted using a recent model based on the modulation of the broadband radio emission by fast magnetoacoustic waves. The results are discussed.

Interpretation of the zebra pattern in the Jovian kilometric radiation

E. Ya. **Zlotnik**, V. E. Shaposhnikov, V. V. Zaitsev
JGR Volume 121, Issue 6 June **2016** Pages 5307–5318
The origin of a fine structure as quasi-harmonic parallel drifting stripes of enhanced brightness (zebra pattern) in the dynamic spectrum of Jovian kilometric radiation is discussed. A possible interpretation of the observed structure based on the effect of double plasma resonance (DPR) in the Jupiter magnetosphere is analyzed. It is shown that the observed features of the zebra pattern cannot be attributed to the DPR effect at electron cyclotron harmonics. The proposed scheme consists of excitation of ion cyclotron waves at the low hybrid frequency in the ion DPR regions and succeeding coalescence of these waves with a longitudinal wave at the upper hybrid frequency. The source parameters necessary for matching the expected and observed properties of the Jupiter zebra pattern are discussed.

"Fingerprint" fine structure in the solar decametric radio spectrum

E.Ya.**Zlotnik**, V.V.Zaitsev, V.N.Melnik, A.A.Konovalenko, V.V.Dorovsky
Solar Phys. Volume 290, Issue 7, pp 2013-2030 **2015, File**
http://www.iapras.ru/publication/preprint/fingerprint.pdf
A peculiar fine structure in the dynamic spectrum of the solar radio emission discovered by the Radio Telescope UTR-2 spectrograph (Kharkiv, Ukraine) in the frequency band 20-30 MHz is discussed. The structure is observed against the background of a broadband type IV radio burst and consists of the parallel drifting narrow bands of enhanced (versus the background) emission and absorption. The observed structure differs from the widely known zebra pattern at the meter and decimeter wavelengths by the opposite directions of the frequency drift within the limits of a single stripe at a given time. It is shown that the observed peculiarities can be understood in the framework of the plasma mechanism of

the radiation origin by virtue of the double plasma resonance effect in a nonuniform coronal magnetic trap. The source model providing the peculiar frequency drift of the zebra stripes is proposed. **22 July 2004**
We study a unique fine structure in the dynamic spectrum of the solar radio emission discovered by the UTR-2 radio telescope (Kharkiv, Ukraine) in the frequency band of 20 – 30 MHz. The structure was observed against the background of a broadband type IV radio burst and consisted of parallel drifting narrow bands of enhanced emission and absorption on the background emission. The observed structure differs from the widely known zebra pattern at meter and decimeter wavelengths by the opposite directions of the frequency drift within a single stripe at a given time. We show that the observed properties can be understood in the framework of the radiation mechanism by virtue of the double plasma resonance effect in a nonuniform coronal magnetic trap. We propose a source model providing the observed frequency drift of the stripes.

On Polarization of the Zebra Pattern in Solar Radio Emission

E. Y. **Zlotnik**, V. V. Zaitsev, A. T. Altyntsev
Solar Phys., **2013, File**
The problem of strong polarization of the zebra-type fine structure in solar radio emission is discussed. In the framework of the plasma mechanism of radiation at the levels of the double plasma resonance, the polarization of the observed radio emission may be due to a difference in rates of plasma wave conversion into ordinary and extraordinary waves or different conditions of escaping of these waves from the source. In a weakly anisotropic plasma which is a source of the zebra-pattern with rather large harmonic numbers, the degree of polarization of the radio emission at twice the plasma frequency originating from the coalescence of two plasma waves is proportional to the ratio of the electron gyrofrequency to the plasma frequency, which is a small number and is negligible. Noticeable polarization can therefore arise only if the observed radio emission is a result of plasma wave scattering by ions (including induced scattering) or their coalescence with low-frequency waves. In this case, the ordinary mode freely leaves the source, but the extraordinary mode gets into the decay zone and does not exit from the source. As a result, the outgoing radio emission can be strongly polarized as the ordinary mode. Possible reasons for the polarization of the zebra pattern in the microwave region are discussed.

Instability of Electrons Trapped by the Coronal Magnetic Field and Its Evidence in the Fine Structure (Zebra Pattern) of Solar Radio Spectra

E.Y. **Zlotnik**
Solar Phys, June **2013**, Volume 284, Issue 2, pp 579-588, **File**
Solar radio emission is a significant source of information regarding coronal plasma parameters and the processes occurring in the solar atmosphere. High resolution frequency, space, and time observations together with the developed theory make it possible to retrieve physical conditions in the radiation source and recognize the radiation mechanisms responsible for various kinds of solar radio emission. In particular, the high brightness temperature of many bursts testifies to coherent radiation mechanisms, that is, to plasma instabilities in the corona.
As an example, the fine structure of solar radio spectra looking like a set of quasiharmonic stripes of enhanced and lowered radiation, which is observed against the type IV continuum at the post-flare phase of activity, is considered. It is shown that such emission arises from a trap-like source filled with a weakly anisotropic equilibrium plasma and a small addition of electrons which have a shortage of small velocities perpendicular to the magnetic field. For many recorded events with the mentioned fine spectral structure the instability processes responsible for the observed features are recognized. Namely, the background type IV continuum is due to the loss-cone instability of hot non-equilibrium electrons, and the enhanced striped radiation results from the double-plasma-resonance effect in the regions where the plasma frequency fp coincides with the harmonics of electron gyrofrequency fB; fp = sfB. Estimations of the electron number density and magnetic field in the coronal magnetic traps, as well as the electron number density and velocities of hot electrons necessary to excite the radiation with the observed fine structure, are given. It is also shown that in some cases several ensembles of non-equilibrium electrons can coexist,in magnetic traps during solar flares and that its radio signature sensitively depends on the parameters of the distribution functions of the various ensembles.

A Special Radio Spectral Fine Structure Used for Plasma Diagnostics in Coronal Magnetic Traps

E.Y. **Zlotnik** · V.V. Zaitsev · H. Aurass · G. Mann
Solar Phys (**2009**) 255: 273–288
A specific combination of spectral fine structures in meter – decimeter dynamic spectra of solar radio burst emission is reported in observations carried out at the Astrophysical Institute Potsdam. We describe and interpret the occurrence of zebra patterns in fast drifting (type III burst-like) envelopes of absorbed continuum emission. A possible mechanism of the origin of such an involved spectral pattern is put forward, leading to a necessarily multinonequlibrium component coronal plasma. The suggested mechanism is based on the fact that during the passage of a fast electron beam through the corona the loss cone instability (which is caused by electrons captured in a magnetic trap generating the continuum) is quenched. As result, a fast drift burst appears in absorption, and the zebra pattern becomes visible on the low background emission. This zebra pattern is generated by a group of electrons with a nonequilibrium distribution over transverse velocities. In the absence of the beam the

pattern is invisible against the background of the stronger continuum. It is shown that the mechanism is sensitive to the distribution parameters of the different electron ensembles. Therefore the effect in dynamic radio spectra is comparatively rare but its proper existence underlines that the simultaneous presence of different ensembles of electrons in the flaring corona can be quite a frequent situation. This can explain some problems in deconvolving X-ray photon spectra to electron energy spectra.

ORIGIN OF ZEBRA PATTERN IN TYPE IV SOLAR RADIO EMISSION

E.Ya.**Zlotnik**

Cent.Eur.Astrophys.Bull. V.33 (**2009**), 1, 281-298. **File**

Abstract. Strong and weak aspects of different theories of fine structure on solar radio emission dynamic spectra observed as several or numerous quasi-equidistant bands of enhanced and reduced radiation (zebra pattern) are discussed. Most of the works which propose zebra pattern interpretation are based on the plasma mechanism of radio emission generation, which consists of excitation of plasma (electrostatic) waves and their subsequent transformation into electromagnetic emission. Plasma waves arise due to kinetic or hydrodynamic instability at the upper hybrid frequencies at the levels of double plasma resonance in a distributed source. Some works are devoted to considering whistlers as the main reason for stripes in emission and absorption occurring in the dynamic spectra. An alternative theory of zebra pattern origin suggests that of a compact source with trapped plasma waves is present in the corona. Another interpretation is based on special effects that may occur when radio waves propagate through some periodic structure in the corona.

All suggested mechanisms are analyzed with relation to their capability to give the best fit for the observed fine structure features in the framework of the source model with reasonable physical parameters. It is shown that the theory based on the effect of double plasma resonance in a nonhomogeneous coronal loop is the best-developed theory for the origin of zebra pattern at the meter-decimeter wavelengths at the present time.

Third harmonic plasma emission in solar type II radio bursts

E.Ya. **Zlotnik**1, A. Klassen2, K.-L. Klein3, H. Aurass2, and G. Mann2

Astron. Astrophys. 331, 1087{1098 (**1998**), **File**

We discuss consequences of the recently reported experimental evidence for third harmonic plasma emission during shock{excited solar radio bursts (type II bursts). Spectrographic and partly imaging observations of three type II bursts displaying three drifting bands with frequencies related as 1 : 2 : 3 have been studied. The radio data of these events were simultaneously recorded by the digital radiospectrograph of the Observatory of Solar Radioastronomy in Potsdam{Tremsdorf and the multifrequency radioheliograph of the Paris{Meudon Observatory in Nanc_ay. The data allow for determining the brightness temperature of radio emission in the three frequency bands. There are one to three orders of magnitude difference between the brightness temperature of the second and the third harmonic plasma emission in our burst sample.

Two non-linear processes { the coalescence of three plasma waves, and the coalescence of a plasma wave and an electromagnetic one at twice the plasma frequency { are considered to explain the occurrence of a third harmonic. The analysis shows that both processes can _t the observed brightness temperatures.The _rst process acts preferably at low phase velocities of plasmawaves and sharp electron density gradients in the source, the second in the case of high plasmawave phase velocities. This means regarding both processes, the occurrence of the third harmonic in type II burst emission due to non-linear coronal plasma processes demands for some additional speci_c conditions in the shock or foreshock region. Finally, we propose a method to distinguish between the two invoked non-linear processes by a statistical investigation of a larger type II burst sample.

Estimating the coronal supra-arcade downflows radio emission: from centimetre through submillimetre wavelengths

Ernesto **Zurbriggen**, C. Guillermo Giménez de Castro, Andrea Costa, Mariana Cécere, Caius L. Selhorst

Frontiers in Astronomy and Space Sciences 9:832607 **2022**

https://arxiv.org/pdf/2203.01366.pdf

https://doi.org/10.3389/fspas.2022.832607

https://www.frontiersin.org/articles/10.3389/fspas.2022.832607/full

Supra-arcade downflows (SADs) are infrequent, wiggly opaque structures observed to descend through the solar corona, mostly in EUV and soft X-ray frequencies. From their physical characteristics, SADs have been interpreted as voided (subdense) bubbles and are related to magnetic reconnection processes during long-term erupting flares. In this work we use numerical MHD simulations to compute flux density maps, which are convolved with telescope beams to synthesise images with the aim to assess the expected SADs emission at radio wavelengths and propose observing strategies, including the instruments that can be used. We assume that the emission is thermal bremsstrahlung from a fully ionised plasma without any appreciable gyroresonance contribution since magnetic fields are of the order of ~10 G. We find that SADs emission should be optically thin in the frequency [10-1000] GHz range, and the spatially integrated flux should be larger than 1 Jy. We conclude, therefore, that observing SADs in radio frequencies between [0.5-1000] GHz is feasible with present instrumentation. Moreover, since the emission is for the most part optically

thin, the flux density is proportional to temperature, density and line-of-sight depth, and when combined with EUV and soft X-ray images, may allow a better density and temperature determination of SADs.

Shock location and CME 3D reconstruction of a solar type II radio burst with LOFAR

P. **Zucca**, D. E. Morosan, A. P. Rouillard, R. Fallows, P. T. Gallagher, J. Magdalenic, K-L. Klein, G. Mann, …
A&A 615, A89 **2018**
https://arxiv.org/pdf/1804.01025.pdf
https://www.aanda.org/articles/aa/pdf/2018/07/aa32308-17.pdf
Type II radio bursts are evidence of shocks in the solar atmosphere and inner heliosphere that emit radio waves ranging from sub-meter to kilometer lengths. These shocks may be associated with CMEs and reach speeds higher than the local magnetosonic speed. Radio imaging of decameter wavelengths (20-90 MHz) is now possible with LOFAR, opening a new radio window in which to study coronal shocks that leave the inner solar corona and enter the interplanetary medium and to understand their association with CMEs. To this end, we study a coronal shock associated with a CME and type II radio burst to determine the locations at which the radio emission is generated, and we investigate the origin of the band-splitting phenomenon. **2013 October 26**
CESRA #2005 Oct **2018** http://cesra.net/?p=2005

Zucca P, Núñez M, Klein K. 2017. Exploring the potential of microwave diagnostics in SEP forecasting: The occurrence of SEP events. J Space Weather Space Clim 7(27): A13. https://doi.org/10.1051/swsc/2017011.

First observation of a solar type II radio burst below 50 MHz with the tied array beam mode of LOFAR

Pietro **Zucca**∗†1 , Diana Morosan2 , Peter Gallagher2 , Fallows Richard3 , Alexis Rouillard4 , Jasmina Magdalenic5 , and Karl Ludwig Klein
CESRA **2016** p.71
http://cesra2016.sciencesconf.org/conference/cesra2016/pages/CESRA2016_prog_abs_book_v3.pdf
Type II radio bursts are evidence of shocks in the solar atmosphere emitting radio waves ranging from metric to kilometric lengths. These shocks may be associated with coronal mass ejections (CMEs) reaching super-Alfvenic speeds. Radio imaging of the decameter wavelengths is now possible with the Low Frequency Array (LOFAR), opening a new radio window to study coronal radio shocks leaving the inner solar corona and entering the interplanetary medium and understand their association with CMEs. Here, we study a coronal shock associated with a CME and type II radio burst to determine the locations that shocks are excited in relation to the propagating CME and the ambient medium Alfven speed. The type II shock imaging and spectra were obtained using 91 simultaneous tied-array beams of LOFAR while the CME was observed by the Large Angle and Spectrometric Coronagraph (LASCO) on board the Solar and Heliospheric Observatory (SOHO). The radio emission associated with the type II shock was found to be located at the flank of the CME in a region where the Alfven speed reaches a local minimum. Using the tied array beam observing mode of LOFAR we were able to locate the type II radio shock position between 45 and 65 MHz and relate it to the expanding flank of a CME and a second CME leaving the inner corona

Understanding CME and associated shock in the solar corona by merging multi wavelengths observation

Pietro **Zucca**, Monique Pick, Pascal Demoulin, Alain Kerdraon, Alain Lecacheux, Peter T. Gallagher
2014 ApJ 795 68
http://arxiv.org/pdf/1409.3691v1.pdf; **File**
Using multi-wavelength imaging observations, in EUV, white light and radio, and radio spectral data over a large frequency range, we analyzed the triggering and development of a complex eruptive event. This one includes two components, an eruptive jet and a CME which interact during more than 30 min, and can be considered as physically linked. This was an unusual event. The jet is generated above a typical complex magnetic configuration which has been investigated in many former studies related to the build-up of eruptive jets; this configuration includes fan-field lines originating from a corona null point above a parasitic polarity, which is embedded in one polarity region of large Active Region (AR). The initiation and development of the CME, observed first in EUV, does not show usual signatures. In this case, the eruptive jet is the main actor of this event. The CME appears first as a simple loop system which becomes destabilized by magnetic reconnection between the outer part of the jet and the ambient medium. The progression of the CME is closely associated with the occurrence of two successive types II bursts from distinct origin. An important part of this study is the first radio type II burst for which the joint spectral and imaging observations allowed: i) to follow, step by step, the evolution of the spectrum and of the trajectory of the radio burst, in relationship with the CME evolution; ii) to obtain, without introducing an electronic density model, the B-field and the Alfvén speed.

2013 November 06

The formation heights of coronal shocks from 2D density and Alfvén speed maps

Pietro **Zucca**, Eoin P. Carley, D. Shaun Bloomfield, Peter T. Gallagher
E-print, March **2014**; A&A 564, A47 (**2014**)
http://arxiv.org/pdf/1402.4051v2.pdf

Super-Alfvénic shock waves associated with coronal mass ejections (CMEs) can produce radio emission known as Type II bursts. In the absence of direct imaging, accurate estimates of coronal electron densities, magnetic field strengths and Alfvén speeds are required in order to calculate the kinematics of shocks. To date, 1D radial models have been used, but these are not appropriate for shocks propagating in non-radial directions. Here, we study a coronal shock wave associated with a CME and Type II radio burst using 2D electron density and Alfvén speed maps to determine the locations that shocks are excited as the CME expands through the corona. Coronal density maps were obtained from emission measures derived from the Atmospheric Imaging Assembly (AIA) on board the Solar Dynamic Observatory (SDO) and polarized brightness measurements from the Large Angle and Spectrometric Coronagraph (LASCO) on board the Solar and Heliospheric Observatory (SOHO). Alfvén speed maps were calculated using these density maps and magnetic field extrapolations from the Helioseismic and Magnetic Imager (SDO/HMI). The computed density and Alfvén speed maps were then used to calculate the shock kinematics in non-radial directions. Using the kinematics of the Type II burst and associated shock, we find our observations to be consistent with the formation of a shock located at the CME flanks where the Alfvén speed has a local minimum. 1D density models are not appropriate for shocks that propagate non-radially along the flanks of a CME. Rather, the 2D density, magnetic field and Alfvén speed maps described here give a more accurate method for determining the fundamental properties of shocks and their relation to CMEs. **2011 Septemeber 22**

Observations of Low Frequency Solar Radio Bursts from the Rosse Solar-Terrestrial Observatory

P. **Zucca**, E. P. Carley, J. McCauley, P. T. Gallagher, C. Monstein, R. T. J. McAteer
E-print, 4 April **2012**, Solar Phys. October **2012**, Volume 280, Issue 2, pp 591-602
https://doi.org/10.1007/s11207-012-9992-x.

The Rosse Solar-Terrestrial Observatory (RSTO; www.rosseobservatory.ie) was established at Birr Castle, Co. Offaly, **Ireland** (53fl05'38.9", 7fl55'12.7") in 2010 to study solar radio bursts and the response of the Earthfls ionosphere and geomagnetic field. To date, three Compound Astronomical Low-cost Low- frequency Instrument for Spectroscopy and Transportable Observatory (**CALLISTO**) spectrometers have been installed, with the capability of observing in the frequency range 10fl870 MHz. The receivers are fed simultaneously by biconical and log-periodic antennas. Nominally, frequency spectra in the range 10fl400 MHz are obtained with 4 sweeps per second over 600 channels. Here, we describe the RSTO solar radio spectrometer set-up, and present dynamic spectra of a sample of Type II, III and IV radio bursts. In particular, we describe fine- scale structure observed in Type II bursts, including band splitting and rapidly varying herringbone features. **07June 2011, 22 September 2011, 21 October 2011**

Абрамов-Максимов В.Е., Бакунина И.А. Предвспышечные флуктуации микроволнового излучения активных областей

Сборник трудов XXVI Всероссийской ежегодной конференции по физике Солнца «Солнце и солнечно-земная физика – 2022» ГАО РАН. С. 9-12
http://www.gaoran.ru/russian/solphys/2022/book/conf2022.pdf

ПРЕДВЕСТНИКИ СОЛНЕЧНЫХ ВСПЫШЕК В МИКРОВОЛНОВОМ ДИАПАЗОНЕ
Абрамов-Максимов В.Е., Бакунина И.А.
Изв. КрАО Том: 117Номер: 1 Год: 2021 Страницы: 38-43

Представлено исследование пространственного распределения квазипериодических колебаний (КПК) микроволнового излучения в двух активных областях перед вспышками М-класса. Мы рассмотрели два случая: NOAA 11283 **6 сентября** и NOAA 11302 **25 сентября 2011** г. Использовались ежедневные наблюдения на радиогелиографе Nobeyama (NoRH) на частоте 17 ГГц. В обоих случаях были обнаружены предвспышечные цуги колебаний яркостной температуры микроволнового излучения активных областей. Длительность цугов составляет около 3-4 циклов колебаний. В обоих случаях источником обнаруженных колебаний являлась компактная зона в активной области, которая совпадает с областью максимальной яркости во время вспышки.

ПРЕДВСПЫШЕЧНАЯ ДИНАМИКА МИКРОВОЛНОВОГО ИЗЛУЧЕНИЯ И МАГНИТНОГО ПОЛЯ АКТИВНЫХ ОБЛАСТЕЙ СОЛНЦА

Абрамов-Максимов В.Е.1, Боровик В.Н.1, Опейкина Л.В.2, Тлатов А.Г.
*«Солнечная и солнечно-земная физика – **2015**» с. 7*

Preliminary study of three eruptive events with large M5-X class flares occurred in AR 11944 (January, 2014), AR 12192 (October, 2014), AR 12297 (March, 2015) using daily multiwavelength solar observations in the range of 1.65–6.0 cm made with the RATAN-600 radiotelescope and data obtained by the SDO/HMI is presented. We came to conclusion that the pre-flare dynamics of the microwave emission and magnetic field in these active regions with different sunspot areas, magnetic-field structures and flare-activity levels were quite different. We suppose that it would be necessary to create a catalogue of eruptive events with large flares and their precursors for developing methods of predicting large flares.

НАБЛЮДЕНИЯ КОРОНАЛЬНЫХ ДЫР НА СИБИРСКОМ РАДИОГЕЛИОГРАФЕ

АЛТЫНЦЕВ А.Т.[1], **ГЛОБА М.В.**[1], **МЕШАЛКИНА Н.С.**[1], **СЫЧ Р.А.**[1]

СОЛНЕЧНО-ЗЕМНАЯ ФИЗИКА Том: 10 Номер: 3 Год: 2024 Страницы: 5-12

Впервые выполнены многоволновые наблюдения корональной дыры (КД) с двумерным пространственным разрешением в диапазоне частот от 2.8 до 12 ГГц. На частотах ниже 6 ГГц средняя яркость по дыре в 1.5 раза меньше яркости спокойного Солнца. Распределение радиояркости по дыре неоднородно: отношение максимальных к минимальным яркостным температурам падает от нескольких раз на низких частотах до десятых долей на верхних принимаемым частотах. На частотах выше 6 ГГц контраст температур между КД и участками спокойного Солнца мал. Внутри КД наблюдаются яркие относительно спокойного Солнца компактные источники. В целом наблюдения КД с помощью СРГ перспективны как для исследования природы КД, так и как средство регулярного мониторинга в прикладных задачах прогнозирования характеристик солнечного ветра.

Спокойная корона Солнца: ежедневные изображения на длинах волн 8.8–10.7 см

Алтынцев А.Т., Глоба М.В., Мешалкина Н.С.

СОЛНЕЧНО-ЗЕМНАЯ ФИЗИКА Том 9 № 2 , **2023** С. 71–77.
https://naukaru.ru/ru/storage/viewWindow/123106

В работе обсуждаются результаты тестовых испытаний решетки диапазона 3–6 ГГц Сибирского радиогелиографа (СРГ). Проверен метод калибровки яркостных температур изображений с помощью известных в литературе измерений яркостной температуры спокойного Солнца в минимуме между 20 и 21 циклами солнечной активности. Полученные зависимости от времени интегрального потока Солнца на 2.8 ГГц подобны измеренным в обсерватории Dominion Radio Astrophysical Observatory (DRAO), однако абсолютные значения потоков СРГ занижены относительно потоков DRAO на 10–15 %. Спектральная плотность микроволнового потока Солнца на частоте 2.8 ГГц, так называемый индекс F10.7, является одним из основных индексов солнечной активности, используемых в качестве входных параметров в моделях ионосферы Земли. В работе рассмотрена связь величин полных потоков радиоизлучения с изменениями структуры источников на диске Солнца в течение интервала длительностью 50 дней. В период ежедневных наблюдений с 1 сентября по 20 октября 2021 г. количество активных областей на диске менялось в несколько раз, а величина интегральной плотности потока на частоте 2.8 ГГц — до 1.5 раз. В работе определены относительные вклады в интегральный поток тормозного излучения прилимбовых уярчений и факельных площадок, а также магнитотормозного излучения в магнитных полях активных областей. Проведено сравнение измеренных яркостных температур радиокарт СРГ с модельными, рассчитанными по данным наблюдений крайнего ультрафиолетового излучения (КУФ-излучения) на телескопе AIA/SDO. Результаты анализа могут быть использованы для организации на СРГ регулярных измерений скорректированного прокси-индекса солнечной активности F10.7, в котором исключен вклад гирорезонансного излучения. **1 сентября по 20 октября 2021 г.**

Когерентное микроволновое излучение как индикатор нетеплового энерговыделения в рентгеновской корональной точке.

Алтынцев А.Т., Мешалкина Н.С., Мышьяков И.И.

СОЛНЕЧНО-ЗЕМНАЯ ФИЗИКА Том 8. **2022**. № 2 С. 4–11.
https://naukaru.ru/ru/storage/viewWindow/94293
DOI: 10.12737/szf-82202201

Обнаружен отклик в узкой полосе 5–7 ГГц микроволнового излучения на появление корональной рентгеновской точки. Источник излучения в рентгеновском диапазоне представляет собой короткую петлю, расположенную в хвостовой части активной области и возникающую при пересоединении магнитных полей вблизи оснований высоких и низких петель, укорененных в близких порах противоположной полярности. Мощность энерговыделения мала, и в жестком рентгене генерации горячего компонента плазмы не наблюдалось. С помощью анализа изображений в мягком рентгеновском и крайнем ультрафиолетовом диапазонах показано, что микроволновое излучение имеет когерентную природу и генерируется на частоте около удвоенной плазменной частоты электронами с энергиями выше нескольких десятков килоэлектронвольт. Результат свидетельствует, что наблюдения микроволнового излучения обладают высоким диагностическим потенциалом обнаружения ускорительных процессов в слабых транзиентных событиях. Это следует учитывать

при планировании наблюдений на радиогелиографах нового поколения, создаваемых в настоящее время. **13 апреля 2019**

МНОГОВОЛНОВЫЙ СИБИРСКИЙ РАДИОГЕЛИОГРАФ

Алтынцев А.Т., С.В. Лесовой, М.В. Глоба, А.В. Губин, А.А. Кочанов, В.В. Гречнев и др.
Солнечно-земная физика. ***2020****. Т. 6. № 2, с. 37-50*
http://ru.iszf.irk.ru/images/9/98/%D0%96%D0%A1%D0%97%D0%A4_6_1_2020_37-50.pdf
DOI: 10.12737/szf-62202003

В статье обсуждаются характеристики, фундаментальные и прикладные задачи создаваемого на площадке Радиоастрофизической обсерватории ИСЗФ СО РАН Сибирского радиогелио-графа и комплекса спектрополяриметров интегрального потока излучения Солнца. Многоволновое картографирование Солнца в микроволновом диапазоне является мощным и относительно недорогим по сравнению с космическими технологиями средством слежения за процессами солнечной активности и средством диагностики параметров плазмы. Всепогодный мониторинг электромагнитного солнечного излучения в диапазоне от метровых до миллиметровых волн, включая измерения индекса солнечной активности на частоте 2.8 ГГц, причем, в месте расположения других разнообразных диагностических средств Гелиогеофизического комплекса, имеет особую ценность. Данные радиогелиографа необходимы для развития и реализации методов кратко-срочного прогноза солнечных вспышек, измерений кинематических характеристик и параметров плазмы корональных выбросов массы, прогноза характери-стик быстрых потоков солнечного ветра. **24 апреля 2017, 06.05.2019**

1. СИБИРСКИЙ РАДИОГЕЛИОГРАФ

1.1.Технические характеристики СРГ
1.2. Спектрополяриметры интегрального излучения Солнца
1.3. Технический задел и тестовые испы-тания систем радиогелиографа
1.4. Измерения спектров интегрального потока Солнца
1.5. Методики анализа данных https://badary.iszf.irk.ru/srhCorrPlot.php

Введение в радиоастрономию Солнца. **Review - книга**

Алтынцев А.Т., Кашапова Л.К.
Иркутск: Изд. ИГУ, 2014. 203 с.

Диагностика плазменных струй в короне Солнца

Анфиногентов С.А., Кальтман Т.И., Ступишин А.Г., Накаряков В.М., Лукичева М.А.
Солне чно-земная физика. **2021**. Т. 7, No 2. С. 3–11.
https://naukaru.ru/ru/storage/viewWindow/72935
DOI: 10.12737/szf-72202101

В статье рассматривается диагностика плазменных струй в короне Солнца по данным современных космических и наземных телескопов, наблюдающих Солнце в крайнем ультрафиолетовом (КУФ) и микроволновом диапазонах. Обсуждаются наблюдательные параметры КУФ- и радиоизлучения в событиях, связанных с плазменными струями, в зависимости от механизма образования, условий излучения и эволюции струй. Показаны возможности изучения солнечной короны, предоставляемые исследованием плазменных струй по наблюдениям одновременно в различных диапазонах. Для ряда струй измерены их первичные параметры и приведены предварительные результаты статистической обработки полученных данных. Подробно рассмотрены микроволновые наблюдения нескольких отдельных событий, выполненные с помощью наземных инструментов РАТАН-600, СРГ и радиогелиографа Нобеяма. Показаны диагностические возможности указанных инструментов при исследовании корональных струй. Для анализа трехмерной структуры коронального магнитного поля использованы данные SDO/HMI, по которым выполнена реконструкция поля в нижней короне. Полученная информация сопоставляется с результатами диагностики магнитного поля в основании короны по данным РАТАН-600. Целью разрабатываемых методов является определение физических механизмов, ответственных за генерацию, коллимацию и динамику плазменных струй в атмосфере Солнца.
2016-04-28, 2017-09-04, 2017-09-13, 2018-04-03, 2018-09-14, 2018-10-13

СТАТИСТИЧЕСКИЕ СВЯЗИ МЕЖДУ СОЛНЕЧНЫМИ КОСМИЧЕСКИМИ ЛУЧАМИ, РАДИОИЗЛУЧЕНИЕМ II ТИПА И КОРОНАЛЬНЫМИ ВЫБРОСАМИ МАССЫ

Базилевская Г.А., Логачёв Ю.И., Дайбог Е.И., Власова Н.А., Гинзбург Е.А., Ишков В.Н., Лазутин Л.Л., Нгуен М.Д., Сурова Г.М., Яковчук О.С.
Г и А Том: 61Номер: 5 Год: 2021 Страницы: 672-679
DOI: 10.31857/S0016794021050035

Радиоизлучение II типа часто сопровождает события в солнечных космических лучах и является индикатором распространения ударной волны в короне Солнца. С другой стороны, важную роль в ускорении солнечных протонов играет ударная волна, связанная с выбросами коронального вещества. Оба эти явления могут происходить без сопровождения солнечными космическими лучами, в то же время не все события солнечных космических лучей сопровождаются радиоизлучением II типа. Статистические связи между этими явлениями рассмотрены на базе Каталогов солнечных протонных событий 23 и 24-го циклов солнечной активности. Показано, что события солнечных космических лучей, сопровождаемые радиоизлучением II типа, относятся к наиболее мощным как по характеристикам частиц, так и по характеристикам источников.

ПРОСТРАНСТВЕННЫЕ И ВРЕМЕННЫЕ ОСОБЕННОСТИ ПОВЕДЕНИЯ МИКРОВОЛНОВОГО И УЛЬТРАФИОЛЕТОВОГО ИЗЛУЧЕНИЯ В ЭРУПТИВНЫХ СОБЫТИЯХ

БАКУНИНА И.А.[1], **МЕЛЬНИКОВ В.Ф.**[2], **ШАИН А.В.**[2], **АБРАМОВ-МАКСИМОВ В.Е.**[2], **ОРГАЧЕВ А.С.**[3]

Изв. Крао Том: 118Номер: 1 Год: 2022 Страницы: 65-74
https://www.elibrary.ru/download/elibrary_48073416_76156594.pdf

На сегодняшний день не вполне ясны наблюдательные признаки, определяющие способность активной области вызывать выброс вещества в высокие слои солнечной короны (coronal mass ejection – CME). Это затрудняет понимание физического механизма триггера CME. Данная работа посвящена поиску наблюдательных признаков, которые могут указывать на возникновение эруптивного процесса. Для этого мы провели сравнительный анализ условий до вспышки и во время вспышки для вспышечных событий, как сопровождаемых, так и не сопровождаемых CME. Мы изучили особенности пространственной и временной динамики микроволнового и ультрафиолетового излучений (данные радиогелиографа Нобеяма, SDO/AIA), а также магнитных полей (SDO/HMI) для 16 активных областей (АО). На этой выборке установлено, что вспышки, сопровождающиеся CME, чаще всего возникают в открытых магнитных конфигурациях, в областях со скрученными магнитными жгутами и со всплывающими потоками. CME также наблюдаются чаще всего во вспышках большей длительности и в тех АО, которые имеют более протяженные по площади источники в микроволновом излучении. **2012-03-09, 2013-11-03, 2014-09-28**

МАССЫ И РАДИОВСПЛЕСКИ II ТИПА В 23 И 24 ЦИКЛАХ

Биленко И.А.

АЖ Том: 99Номер: 7 Год: **2022** Страницы: 595-611

Рассмотрены события радиовсплесков II типа (РВII) в декаметровом и гектометровом диапазонах от 1 до 16 МГц и зависимости параметров сопутствующих корональных выбросов массы (КВМ) от фоновых характеристик плазмы и значений межпланетного магнитного поля (ММП) в областях начала регистрации каждого радиовсплеска в 23 и 24 циклах солнечной активности. ММП рассчитывалось по данным крупномасштабных фотосферных магнитных полей на расстояниях регистрации РВII. Результаты свидетельствуют, что число РВII, средние значения параметров плазмы и ММП изменяются в виде отдельных импульсов в обоих циклах и характер их изменения отличается в 23 и 24 циклах. Различия в параметрах плазмы, ММП и КВМ могли стать причиной снижения числа РВII в 24 цикле. Большинство РВII в 23 и 24 циклах, и основное снижение их числа в 24 цикле, наблюдаются для выбросов с альвеновскими числами Маха 1–2.9. Наибольшее число РВII в 23 цикле соответствует значениям ММП 0–30 μT, а в 24 – 30–50 μT. Основное снижение числа РВII в 24 цикле произошло за счет событий, наблюдавшихся при ММП 0–30 μT. Значительная часть регистрируемых, в основном, в периоды максимума солнечной активности КВМ с генерацией РВII, составляющая 61 (18.05%) в 23 цикле, и 31 (17.22%) в 24 цикле, имеют альвеновские числа Маха меньше единицы. Возможно, что в этих событиях реализуется иной, не плазменный, механизм генерации РВII.

О НОВОЙ КОНЦЕПЦИИ СПЕКТРАЛЬНОЙ РАДИОМЕТРИИ НА РАТАН-600

Богод В.М., Лебедев М.К., Овчинникова Н.Е., Рипак А.М., Стороженко А.А., Курочкин Е.А.

Изв. КрАО Том: 119Номер: 4 Год: 2023 Страницы: 17-26

Представлены результаты новых наблюдений радиоизлучения короны Солнца в диапазоне 1-3 ГГц на РАТАН-600. Сложность наблюдений в этом диапазоне обусловлена большим количеством помех искусственного происхождения (мобильная связь, спутниковая навигация, микроволновые печи, авиационные локаторы и др.). Задачи, связанные с проблемами преобразования магнитной энергии в энергию вспышек, нагрева короны, роли узкополосных явлений, квазипериодических пульсаций в солнечной короне, остаются актуальными. Стала насущной смена концепции приемной спектральной аппаратуры для радиотелескопа РАТАН-600. В САО РАН ведется работа по созданию серии спектральных комплексов нового поколения с перекрытием всего рабочего диапазона РАТАН-600. В данной статье мы представляем результаты первых серий наблюдений на панорамном спектральном радиометрическом комплексе в диапазоне 1-3 ГГц (ПСРК 1-3 ГГц) по исследованиям слабоконтрастных корональных структур. Становится доступной реализация режима наблюдений различных объектов: от мощных вспыхивающих радиоисточников до слабых структур, вплоть до радиограунляционного уровня. Разработаны и внедрены высокоскоростные средства приема и обработки информации с целью разделения полезных и помеховых сигналов в режиме реального времени. Эти параметры в совокупности с возможностями РАТАН-600 по эффективной площади и широкому частотному перекрытию позволили провести наблюдения слабых корональных структур в диапазоне 1-3 ГГц. Обсуждаются результаты первых серий наблюдений слабых корональных структур и их интерпретация по воздействию на тепловые процессы в короне.

СПЕКТРОРАДИОМЕТРИЯ СОЛНЕЧНОЙ КОРОНЫ НА РАТАН-600

БОГОД В. М.[*1], **ЛЕБЕДЕВ М. К.**[1], **ОВЧИННИКОВА Н. Е.**[1], **РИПАК А. М.**[1], **СТОРОЖЕНКО А. А.**[1]

КОСМИЧЕСКИЕ ИССЛЕДОВАНИЯ Том: 61Номер: 1 Год: 2023 Страницы: 31-38

Современные исследования радиоизлучения Солнца осложняются непрерывным усилением мощности и многочастотностью внешних помех, которые часто полностью перекрывают важные диапазоны частот. Многие актуальные задачи в солнечной радиоастрономии нуждаются в больших эффективных площадях радиотелескопов, высоких разрешениях по частоте и по времени, точных пространственных измерениях и большом динамическом диапазоне. Становится актуальным смена концепции приемной регистрирующей аппаратуры. В работе рассматриваются актуальные задачи физики солнечной короны в сочетании с оптимальными методами наблюдений на крупных инструментах. Рассмотрены особенности и трудности сочетания высоких параметров: динамического, пространственного, временного, частотного разрешений. Предложенные решения наблюдательного комплекса нового поколения реализуют возможности интеллектуального выбора условий регистрации в многооктавном режиме с многоканальностью более 8000 каналов/ГГц с временным разрешением до 8 мс/спектр. Становится доступным мультиобъектный режим наблюдений от мощных вспыхивающих объектов до слабых структур различной природы. Высокоскоростная обработка данных позволяет реализовать on-line режим устранения помех, который основан на быстром статистическом анализе спектра с выделением негауссовых (помеховых) структур. Предложены методы скоростного анализа данных большого объема (метод главных компонент) и их представления для пользователя. Приведены примеры работы комплекса в диапазоне 1–3 ГГц. Рассматриваются перспективы нового подхода для мультиобъектных радиоастрономических наблюдений при реализации режима слежения на РАТАН-600: от рекомбинационных линий до широкодиапазонных спектров, от слабоконтрастных флуктуаций до быстрых изменений во вспышках и др.

РАЗРАБОТКА ПРОЕКТА РЕКОНСТРУКЦИИ ГАВАНСКОЙ РАДИОАСТРОНОМИЧЕСКОЙ СТАНЦИИ В СОСТАВЕ РОССИЙСКИХ СЛУЖБ СОЛНЦА И КОСМИЧЕСКОЙ ПОГОДЫ

Богод В.М., Стороженко А.А., Тлатов А.Г., Кузанян К.М., Абунин А.А., Лесовой С.В., Pons O., Uratsuka M., Zaldívar R., Pablo S.

КОСМИЧЕСКИЕ ИССЛЕДОВАНИЯ Том: 59Номер: 2 Год: **2021** Страницы: 102-110

Необходимость воссоздания Гаванской наблюдательной солнечной станции сегодня диктуется важностью получения регулярного прогноза активности Солнца в широком диапазоне временных интервалов. Подробно описана концепция создаваемой наблюдательной сети, инфраструктура патрульной станции как элемента сети. Функции этой сети предоставят непрерывный наблюдательный материал для Российских служб Солнца и Космической Погоды и будут независимы от космических наблюдений, но способны использовать их для контроля качества. Рассмотрены физические основы комплексных наблюдений для широкого круга гелиогеофизических явлений.

МАГНИТОСФЕРА АКТИВНОЙ ОБЛАСТИ ПО РАДИОНАБЛЮДЕНИЯМ В ШИРОКОМ ДИАПАЗОНЕ ДЛИН ВОЛН

Богод В.М., Кальтман Т.И.

Астрономия-**2018** Том 2 Солнечно-земная физика – современное состояние и перспективы Стр. 35
http://www.izmiran.ru/library/eaas2018/eaas-2018-2.pdf

ИССЛЕДОВАНИЕ МАГНИТОСФЕР АКТИВНЫХ ОБЛАСТЕЙ НА СОЛНЦЕ МЕТОДАМИ РАДИОАСТРОНОМИИ

БОГОД В.М.✉1,2, КАЛЬТМАН Т. И✉1, ПЕТЕРОВА Н.Г.✉1, ЯСНОВ Л.В.

Космич. Исслед. Том: 55Номер: 1 Год: **2017** Страницы: 3-13 DOI: 10.7868/S0023420617010022

На основании детальных исследований структуры активных областей (АО) в 90-х годах была предложена концепция магнитосферы активной области. В нее входят практически все известные структуры, присутствующие в активной области – от радиогрануляции до шумовых бурь, излучение которых проявляется на радиоволнах. Концепция магнитосферы, рассматривающая с единых позиций проявления радиоизлучения активной области как единого активного комплекса, позволяет пролить свет на соотношение стабильных и активных процессов и их взаимосвязей. Особо важно определить основные пути переноса нетепловой энергии в тепловую. Доминирующую роль во всех процессах играет магнитное поле, измерение которого на корональных уровнях доступно радиоастрономическим методам. В связи с расширением диапазона волн и введением новых инструментов и современных возможностей моделирования становится возможным проведение анализа физических свойств плазменных структур магнитосферы АО и дать оценки корональных магнитных полей на уровнях переходной зоны хромосфера–корона и нижней короны. Оцениваются особенности и характеристики переходной области от S-компоненты к B-компоненте.

О РЕГИСТРАЦИИ ХОЛОДНОГО ВЕЩЕСТВА В ОБЛАСТИ СИЛЬНОГО МАГНИТНОГО ПОЛЯ СОЛНЕЧНЫХ ПЯТЕН И ИСТЕЧЕНИЕ ПЛАЗМЫ В КОРОНУ

В.М.**Богод**, Н.Г.Петерова, Б.И.Рябов, Н.А.Топчило

ИКИ-**2014** Сессия: Солнце

http://plasma2014.cosmos.ru/presentations
При наблюдении солнечных пятен в микроволновом диапазоне длин волн (2–10 см) обычно регистрируется источник излучения, яркость которого намного (1–2 порядка) превышает яркость спокойных участков Солнца. Однако при анализе поляризации излучения, достаточно часто на коротких волнах в обыкновенной моде выявляется источник, яркость которого на (2–4) КК даже ниже температуры спокойного Солнца. Благодаря высокому спектральному разрешению наблюдений на РАТАН-600 установлено, что это явление наблюдается в ограниченном диапазоне (1.7–3) см, соответствующем области сильного магнитного поля солнечного пятна, напряженностью ~ (2–3) КГс.
Помимо наблюдаемого пониженного значения радиояркости, эта область (SSRRB – SunSpot Region of Reduced radio Bridghtness), как показали модельные расчеты, также характеризуется «разреженностью» корональной плазмы, плотность которой существенно понижена (в 3-4 раза).
По своим параметрам SSRRB (низкая яркостная температура и пониженная плотность) напоминает корональную дыру. В пользу такой аналогии свидетельствуют и снимки групп пятен в линии He I 10830Å, указывающие на повышенное поглощение в этой линии, наблюдаемое в непосредственной близости к пятнам. Все это позволяет предполагать, что SSRRB образуется в результате истечения плазмы и может участвовать в формировании потоков солнечного ветра.

ПЕРВЫЕ РЕЗУЛЬТАТЫ РАДИОНАБЛЮДЕНИЙ СОЛНЦА И МОЩНЫХ ДИСКРЕТНЫХ ИСТОЧНИКОВ НА ИРКУТСКОМ РАДАРЕ

Р. В. **Васильев***, Д. С. Кушнарев, Л. К. Кашапова, В. П. Лебедев, А. В. Медведев, Н. И. Неведимов, К. Г. Ратовский

*АСТРОНОМИЧЕСКИЙЖУРНАЛ, **2013**, том 90,№11, с. 948–958*

С помощью Иркутского радара некогерентного рассеяния продемонстрировано, что такие радары, обычно используемые для исследования ионосферы Земли, благодаря своей высокой чувствительности позволяют при работе в пассивном режиме проводить также наблюдения астрономических радиоисточников. Выполнены наблюдения солнечных вспышек, сопровождавшихся корональными выбросами массы, и квазистационарных радиоисточников на Солнце. Кроме того, на протяжении нескольких месяцев исследовались мерцания наиболее ярких дискретных радиоисточников (Лебедь-А, Кассиопея-А и Крабовидная туманность); отмечается, что эти данные могут быть полезны для изучения ионосферы и межпланетного пространства.

Служба Солнца KRIM в радиодиапазоне

А.Е. Вольвач, К.В. Самисько, С.А. Самисько, И.В. Якубовская

Изв. КрАО, т.114, №2, 27-32, **2018**

https://jn.craocrimea.ru/index.php/izvcrao/article/view/548/589

Четыре робот-радиотелескопа КрАО, объединенные в Службу Солнца KRIM, ведут наблюдения Солнца в режиме мониторинга и алертов. Радиотелескоп РТ-22 оснащен поляриметрами на длины волн 0.8, 2.0, 2.3, 2.8 и 3.5 см, позволяющими регистрировать интенсивность и круговую поляризацию радиоизлучения. Диаграммы направленности на указанных волнах составляют 2.5–6.0′. Радиотелескоп РТ-2 принимает излучение сантиметрового диапазона длин волн для получения сведений о процессах, протекающих в нижней хромосфере. Радиотелескоп РТ-3 принимает излучение дециметрового диапазона длин волн с целью сбора сведений о процессах, происходящих в верхней хромосфере и нижней короне. Радиотелескоп РТ-М принимает излучение метрового диапазона длин волн для обнаружения корпускулярных потоков, направляющихся к Земле в результате солнечных вспышек. Одновременные наблюдения на четырех инструментах, которые перекрывают диапазон длин волн от 8 мм до 1.2 м, дают возможность получать информацию для анализа процессов энерговыделения в атмосфере Солнца и краткосрочного прогноза солнечной активности. Данные радиомониторинга солнечной активности сохраняются в реальном времени в цифровом виде и выставляются на сайты мировой службы Солнца, которая включает 14 наземных станций в кооперации с орбитальными обсерваториями.

Глоба М.В., Лесовой С.В. Калибровка амплитуд коэффициентов передачи антенн Сибирского радиогелиографа с использованием избыточности. С-З физика. Т. 7, №4,С. 104–110. Аннотация / Полный текст (PDF)

АНАЛИЗ ФИЗИЧЕСКИХ ХАРАКТЕРИСТИК ПОЛЯРНОЙ КОРОНАЛЬНОЙ ДЫРЫ НА СОЛНЦЕ В МИКРОВОЛНОВОМ ДИАПАЗОНЕ ДЛИН ВОЛН

Голубчина О.А.

ГиА Том: 62Номер: 1 Год: 2022 Страницы: 11-18

Приведен анализ результатов исследования полярной корональной дыры по данным наблюдений солнечного затмения **29.03.2006** г. на радиотелескопе РАТАН-600 в широком сантиметровом диапазоне длин волн λ = (1.03, 1.38, 2.7, 6.2, 13.0, 30.7) см. Кратко изложены обстоятельства затмения, методика обработки данных наблюдений. Обсуждены распределения яркостных температур в полярной корональной дыре Солнца от лимба оптического диска Солнца до расстояний, равных двум

его радиусам. Обнаружено резкое уменьшение интенсивности радиоизлучения полярной корональной дыры на длинах волн λ ≥ 6 см вблизи солнечного лимба. Исследован факт отсутствия регистрации полярной корональной дыры на длинах волн λ = (1.03, 1.38, 2.7) см с привлечением данных более ранних наблюдений спокойного Солнца на радиотелескопах БПР и РАТАН-600. Обсуждается обнаруженная в радиодиапазоне идентичность температурных свойств полярной и низкоширотных корональных дыр. В дискуссии представлен обзор некоторых результатов исследования полярной корональной дыры Солнца по наблюдениям на радиотелескопах БПР, РАТАН-600, РТ-22 (КРАО), NoRH и других радиотелескопах с использованием данных (EUV SOHO/EIT) и данных теоретических работ.

ХАРАКТЕРИСТИКИ ИЗЛУЧЕНИЯ ПОЛЯРНЫХ КОРОНАЛЬНЫХ ДЫР НА СОЛНЦЕ В ШИРОКОМ ДИАПАЗОНЕ РАДИОВОЛН

ГОЛУБЧИНА О.А.

Изв. КрАО Том: 118Номер: 1 Год: 2022 Страницы: 75-82

https://www.elibrary.ru/download/elibrary_48073417_10928017.pdf

В статье представлен краткий обзор основных результатов наблюдений радиоизлучения полярных корональных дыр на Солнце, полученных в широком диапазоне длин волн на различных радиотелескопах. Дан анализ результатов наблюдений на РАТАН-600 полярной корональной дыры (КД) в широком сантиметровом диапазоне длин волн (1.03–30.7) см. Полученные физические характеристики КД над северным полюсом Солнца сравниваются с характеристиками КД, расположенных в более низких широтах.

АНАЛИЗ РЕЗУЛЬТАТОВ ИССЛЕДОВАНИЯ НАБЛЮДЕНИЙ ПОЛЯРНОЙ КОРОНАЛЬНОЙ ДЫРЫ НА СОЛНЦЕ В МИКРОВОЛНОВОМ ДИАПАЗОНЕ ДЛИН ВОЛН

ГОЛУБЧИНА О. А.

АЖ Том: 98Номер: 4 Год: **2021** Страницы: 332-341

Представлен обзор основных результатов исследования полярной корональной дыры (КД) над Северным полюсом Солнца на основе наблюдений солнечного затмения **29 марта 2006** г. с помощью радиотелескопа РАТАН-600 в широком диапазоне сантиметровых длин волн: 1.03, 1.38, 2.7, 6.2, 13.0, 30.7 см – с привлечением наблюдательных и теоретических данных работ о свойствах корональных дыр на Солнце, опубликованных различными авторами. Обсуждаются полученные результаты: распределение яркостных температур полярной корональной дыры над Северным полюсом Солнца на расстояниях 1.005–2.0 радиуса оптического диска Солнца от центра солнечного диска; усиление микроволнового излучения полярной корональной дыры, зарегистрированное на коротких длинах волн; идентичность температурных свойств полярной КД и низкоширотных корональных дыр на Солнце в период минимальной солнечной активности. Сравнение полученных яркостных температур полярной корональной дыры с яркостными температурами крупных низкоширотных корональных дыр, наблюдавшихся ранее (1973–1976, 1984–1987 гг.) на близких длинах волн, свидетельствует об идентичности температурных свойств корональных дыр независимо от их расположения на Солнце и организации корональных дыр в период минимума солнечной активности.

ФИЗИЧЕСКИЕ ХАРАКТЕРИСТИКИ РАДИОИЗЛУЧЕНИЯ НАД ПОЛЯРНЫМИ ОБЛАСТЯМИ СОЛНЦА

Голубчина О.А.

Пулково *«Солнечная и солнечно-земная физика – **2015**», с.81*

In this paper the brief review of polar coronal holes observations in different wave lengths is given. Comparison of physical characteristics of coronal hole cm-radio emission above the North Pole of the Sun with characteristics of coronal holes, located outside of polar areas on a background of the quiet Sun which were received on RATAN-600 earlier is resulted. Results of comparisons have shown that properties of the polar coronal hole above the North Pole of the Sun are identical to properties of coronal holes located outside of polar areas on a background of the quiet Sun.

РАДИОИЗЛУЧЕНИЕ СОЛНЕЧНОЙ ВСПЫШКИ 12.02.2010 г. И РЕЖИМЫ УСКОРЕНИЯ ЭЛЕКТРОНОВ

Р. В. **Горгуца**1, В. А. Ковалев1, И. Г. Костюченко2, А. К. Маркеев1, Д. Е. Соболев1, В. В. Фомичев

ГЕОМАГНЕТИЗМ И АЭРОНОМИЯ, **2015**, том 55, № 3, с. 1–5

При анализе данных наблюдений радиовсплесков, полученных в ИЗМИРАН с помощью спектро_ графов метрового диапазона и радиометров на фиксированных частотах, использован дифферен_ циальный метод, с помощью которого обнаружено двухступенчатое (быстрое + медленное по срав_ нению с экспоненциальным законом) поведение потоков радиоизлучения на фазах возрастания и спада. Показано, что наблюдаемый быстрый режим возрастания потока на частоте 3013 МГц, со_ провождаемый уменьшением временно&го масштаба, может быть связан с быстрым режимом уско_ рения электронов, ответственных за магнитотормозное излучение вспышки в микроволновом диа_

пазоне.

СОЛНЕЧНЫЕ МИКРОВСПЛЕСКИ 18 ФЕВРАЛЯ 2011

Гофман А.А.1, Богод В.М.2, Яснов Л.В.1, Ступишина О.М.1, Ступишин А.Г.
Пулково *«Солнечная и солнечно-земная физика – **2015**», с.89*

The overall purpose of this paper is decimeter solar microbursts investigation. The phenomenon of the MB was proved by statistical analysis of the observation data. The highfrequency end of the spectrum and duration of a single burst were determined. Furthermore, the theoretical explanation of the nature and generation mechanism for the decimeter MB was proposed. With the assumption that the nature of the MB is the same for the solar noise storm (I type radiobursts in the meter wave band), the generation mechanism of decimeter microbursts as the incoherent Langmuir wave generation mechanism was proposed. Also, the estimation of upper-hybrid waves increments in the framework of known solar atmosphere model with considering the cyclotron and free-free absorption was made.

СОЛНЕЧНЫЕ ВСПЫШЕЧНЫЕ ЭРУПЦИИ С ДЛИТЕЛЬНОЙ ЭКРАНИРОВКОЙ ИЗЛУЧЕНИЯ В ЛИНИИ HeII 304 ˚A И В МИКРОВОЛНОВОМ ДИАПАЗОНЕ

В. В. **Гречнев**1, И.В.Кузьменко2, И.М.Черток3, А. М. Уралов1
*АСТРОНОМИЧЕСКИЙЖУРНАЛ, **2011**, том 88,№7, с. 692–703*

Извергнутая при солнечных эрупциях плазма с температурами, близкими к хромосферным, может экранировать часть излучения как компактных источников в активных областях, так и областей спокойного Солнца. Явления поглощения могут наблюдаться в микроволновом диапазоне в виде так называемых “отрицательных всплесков”, а также в линии HeII 304 ˚ A. Рассмотрены три эруптивных события, связанных с довольно мощными вспышками. По записям потока “отрицательного всплеска” на нескольких радиочастотах для одного из рассмотренных событий оценены параметры поглощав-шего излучение вещества выброса. В единичных событиях обнаружено “разрушение” эруптивного волокна и его распыление в виде облака по огромной поверхности, наблюдаемое в виде грандиозных депрессий излучения в линии HeII 304 ˚ A. Одно из трех известных нам таких событий рассматривается в данной статье, еще одно из рассмотренных — возможный кандидат.

МНОГОВОЛНОВЫЕ НАБЛЮДЕНИЯ ВСПЫШКИ 10 МАЯ 2012: УСКОРЕНИЕ ЧАСТИЦ И ВСПЛЫТИЕ МАГНИТНОГО ПОЛЯ

Григорьева И.Ю.1, Кузнецов А.А.2, Мешалкина Н.С.2, Мышьяков И.И.2
Пулково *«Солнечная и солнечно-земная физика – **2015**», с.99*

We present a study of the dynamics of a GOES M5.7 class flare, which occurred on 10 May 2012 in NOAA 11476, in a small group of spots near the neutral line of the local magnetic field. The properties of the hard X-ray (HXR) and microwave (MW) radiation associated with this flare are analyzed. The HXR spectra are constructed according to the Space Telescope Konus-WIND and RHESSI. Detailed analysis of one-dimensional SSRT observations (5.7 GHz) and NoRP polarimeters is made. Two-dimensional radio images (SSRT and NoRH) are reconstructed. The LOS-magnetogram (SDO / HMI) detected the emergence of a new magnetic flux in a small region adjacent to the north-west of one of the EUV flare activity centers (according to SDO / AIA). Comprehensive analysis shows that the increase in the MW radiation and in the HXR occurred almost simultaneously. Two polarized MW bursts with different properties are registered. The second burst was accompanied by appearance of a HXRsource (with energies up to 100 keV) in the loop top. We estimate the changes in the magnetic flux associated with the emergence of a new field with opposite polarity. These results directly suggest a link between the development of non-stationary processes (such as the current amplification and highly efficient particle acceleration) with the magnetic flux emergence. Such dramatic effects usually do not occur near the neutral line, but only in the events associated with large sunspots (like in powerful flares on 14 July 2000 and 20 May 2005).

РЕНТГЕНОВСКОЕ И МИКРОВОЛНОВОЕ ИЗЛУЧЕНИЕ СОЛНЕЧНОЙ ВСПЫШКИ 19 ИЮЛЯ 2012 ГОДА: ВЫСОКОТОЧНЫЕ НАБЛЮДЕНИЯ И КИНЕТИЧЕСКИЕ МОДЕЛИ

ГРИЦЫК П.А.1, СОМОВ Б.В.1

Том: 42Номер: 8 Год: **2016** Страницы: 586

Солнечная вспышка класса M7.7 **19 июля 2012** г. в 05:58 UT наблюдалась с высоким пространственным, временным и спектральным разрешением в жестком рентгеновском и оптическом диапазонах. Вспышка имела

место на краю солнечного диска, что позволило увидеть относительное расположение коронального и хромосферного источников рентгеновского излучения, определить их спектры. Для объяснения наблюдений коронального и незакрытого солнечным лимбом хромосферного источников мы применяем аккуратную аналитическую модель кинетического поведения ускоренных электронов во вспышке. Хромосферный источник жесткого рентгеновского излучения интерпретируется в приближении толстой мишени с обратным током, а корональный - в приближении тонкой мишени. Полученные оценки показателей наклона спектров жесткого рентгеновского излучения обоих источников согласуются с результатами наблюдений. Однако рассчитанная интенсивность излучения коронального источника в несколько раз ниже наблюдаемой. Учет эффекта ускорения быстрых электронов в коллапсирующей магнитной ловушке позволил нам устранить это противоречие. В результате моделирования получена оценка плотности потока энергии, переносимой электронами с энергиями выше 15 кэВ, которая составляет $\sim 5 \times 10^{10}$ erg cm^{-2} s^{-1}, что в ~5 раз превышает значения, характерные для модели толстой мишени без обратного тока. С целью независимой проверки модели рассчитан спектр микроволнового излучения в диапазоне 1-50 ГГц, который соответствует имеющимся данным радионаблюдений.

О ВОЗМОЖНОСТЯХ И ПРОБЛЕМАХ НАБЛЮДЕНИЙ МАГНИТНЫХ ПОЛЕЙ СОЛНЦА ДЛЯ ПРОГНОЗА КОСМИЧЕСКОЙ ПОГОДЫ

ДЕМИДОВ М.Л.

СОЛНЕЧНО-ЗЕМНАЯ ФИЗИКА Том: 3Номер: 1 Год: **2017** Страницы: 22-33

Важной составной частью актуальной в последние десятилетия проблемы космической погоды является прогноз параметров околоземного космического пространства, состояния ионосферы и геомагнитной активности на основе наблюдений различных явлений на Солнце. Особо значимы измерения магнитных полей, поскольку именно они определяют пространственную структуру внешних слоев солнечной атмосферы и в значительной степени параметры солнечного ветра. Ввиду отсутствия в настоящее время возможностей наблюдений магнитных полей непосредственно в короне практически единственным источником разнообразных моделей количественного расчета параметров гелиосферы являются измеряемые в фотосферных линиях ежедневные магнитограммы и получаемые на их основе синоптические карты. При этом оказывается, что результаты прогноза, в частности, скорости солнечного ветра на орбите Земли и положения гелиосферного токового слоя сильно зависят не только от выбранной модели расчетов, но и от исходного материала, поскольку магнитограммы различных инструментов (а зачастую и наблюдения в разных линиях на одном и том же телескопе) хотя и похожи морфологически, но могут значительно различаться при подробном количественном анализе. Детальному рассмотрению именно этого аспекта проблемы космической погоды посвящена значительная часть настоящей работы.

АДИАБАТНЫЙ СПЕКТР РАДИОИЗЛУЧЕНИЯ КОРОНАЛЬНЫХ ДЫР СОЛНЦА

ДРАВСКИХ А. Ф.[*1], **ДРАВСКИХ Ю. А.**[1]

АЖ Том: 100Номер: 5 Год: 2023 Страницы: 472-478

Корональные дыры на Солнце наблюдаются на отдельных частотах достаточно давно в диапазоне волн от радио до рентгена. Наблюдения в широком диапазоне радиочастот проводятся на радиотелескопе РАТАН-600. Анализ многолетних спектральных наблюдений радиотелескопа РАТАН-600 показал, что спектр излучения корональных дыр радикально отличается от спектра активных образований над пятнами, но, заметно отличаясь от спектра спокойного Солнца, имеет с ним и сходство. Установлено: радиоизлучение корональных дыр имеет адиабатный спектр и не содержит заметного когерентного излучения, т.е. рекомбинационных радиолиний и линий тонкой структуры водорода и других элементов.

РЕКОМБИНАЦИОННЫЕ РАДИОЛИНИИ НА СОЛНЦЕ

Дравских А.Ф., Дравских Ю.А.

АЖ Том: 99Номер: 6 Год: **2022** 496-505

Линии, наблюдаемые в астрономических объектах, позволяют получать уникальную информацию о них. В настоящее время в спектре Солнца обнаружена только одна радиолиния тонкой структуры водорода 22P3/2–22S1/2 на частоте 9845 МГц (3.05 см). Найдено также, что в спектре солнечных активных образований над пятнами с большой вероятностью наблюдаемы еще две линии тонкой структуры водорода: 32P3/2–32S1/2 и 32D3/2–32P1/2 на частотах 2917 и 3237 МГц (10.28 и 9.27 см). Анализ многолетних спектральных наблюдений Солнца на радиотелескопе РАТАН-600 показал, что в спектре солнечных активных образований над пятнами должны наблюдаться многочисленные рекомбинационные радиолинии водорода и других элементов.

ВОЗМОЖНОСТЬ ГЕНЕРАЦИИ УДАРНОЙ ВОЛНЫ В КОРОНЕ СОЛНЦА ПРИ ОТСУТСТВИИ КОРОНАЛЬНОГО ВЫБРОСА МАССЫ

ЕСЕЛЕВИЧ В.Г.✉1, ЕСЕЛЕВИЧ М.В.1, ЗИМОВЕЦ И.В.2,3,4, ШАРЫКИН И.Н.

АЖ Том: 94Номер: 9 Год: **2017** Страницы: 793-807

Исследовано солнечное событие SOL**2012-10-23**T03:13, связанное со вспышкой балла X1.8, в котором отсутствовал корональный выброс массы (КВМ), но наблюдался радиовсплеск II типа. Использовался метод построения профилей разностной яркости в УФ и ЭУФ каналах инструмента AIA/SDO в пространстве и во времени одновременно с анализом всплеска радиоизлучения II типа. Показано, что в данном событии происходят формирование и распространение области сжатия, впереди которой на расстояниях R< 1.3 R⊙ от центра Солнца (R⊙ - радиус Солнца) регистрируется столкновительная ударная волна. На основе сравнения с результатами анализа подобного типа события SOL**2011-02-28**T07:34, полученными в статье [1], был сделан следующий вывод. Предполагаемой причиной возбуждения области сжатия и ударной волны является кратковременное (импульсное) воздействие на окружающую плазму эруптивного высокотемпературного магнитного жгута. Его начальная неустойчивость и эрупция могут быть инициированы всплывающим магнитным потоком, а нагрев может быть следствием магнитного пересоединения. Остановка эрупции жгута может быть связана с его взаимодействием с окружающими магнитными структурами (корональными петлями).

О ВОЗМОЖНОЙ ПРИЧИНЕ ЧАСТОТНОГО РАСЩЕПЛЕНИЯ ГАРМОНИК СОЛНЕЧНОГО РАДИОВСПЛЕСКА ВТОРОГО ТИПА

В. Г. **Еселевич**, М. В. Еселевич, И. В. Зимовец

АЖ т92, №12, стр. 977-1008, **2015** **File**

На основе анализа данных инструмента AIA/SDO (канал 193 A˚) впереди коронального выброса массы в лимбовом событии на Солнце **13 июня 2010 г.** удалось одновременно зарегистрировать и измерить фронты двух различных ударных волн. Угловой размер каждого из этих фронтов относительно центра коронального выброса массы составил около 20◦, а их направления распространения отличались на ≈25◦ (по позиционному углу на ≈4◦). Более быстрый фронт, названный взрывной ударной волной, опережал фронт другой волны, названной поршневой, на $R \approx (0.02-0.03)$ ($R_$ — радиус Солнца) и имел максимальную начальную скорость $VB \approx 850$ км с−1 (у поршневой $VP \approx 700$ км с−1). Появление и движение этих ударных волн сопровождалось всплеском радиоизлучения II типа на фундаментальной частоте F и второй гармонике H. Каждая из частот была расщеплена на две близкие частоты $f1$ и $f2$, различающиеся на величину $\Delta f = f2 - f1$ _F,H. На основе проведенного анализа был сделан вывод о том, что наблюдаемое частотное расщепления Δf частот F и H радиоизлучения II типа может быть результатом одновременного распространения поршневой и взрывной ударных волн с различными скоростями в несколько разных направлениях, которые отличаются значениями концентрации корональной плазмы.

СТАТИСТИЧЕСКИЙ АНАЛИЗ МИКРОВСПЫШЕК ПО ДАННЫМ СПЕКТРОПОЛЯРИМЕТРА 4-8 ГГЦ

Жданов *Д.А., Алтынцев А.Т., Мешалкина Н.С., Анфиногентов С.А.*

СОЛНЕЧНО-ЗЕМНАЯ ФИЗИКА Том: 9Номер: 3 Год: **2023** Страницы: 111-121

https://elibrary.ru/download/elibrary_54625075_41027810.pdf

Радионаблюдения слабых событий являются одним из перспективных методов исследования энерговыделения и нетепловых процессов в солнечной короне. Развитие инструментальной базы позволяет вести радионаблюдения слабых транзиентных корональных явлений, таких как квазистационарные уярчания и слабые вспышки рентгеновского класса B и ниже, не доступные ранее для анализа. Используя наблюдения на спектрополяриметре Badary Broadband Microwave Spectropolarimeter (BBMS) мы измерили параметры спектров микроволнового излучения для трех десятков слабых солнечных вспышек рентгеновских классов от A до C1.5. Спектры свидетельствуют, что нагрев плазмы вызывается появлением потоков нетепловых электронов, которые можно обнаружить по формируемым ими всплескам микроволнового излучения, преимущественно с амплитудой ~5-6 с.е.п. (одна солнечная единица потока (с.е.п.) радиоизлучения равна 10^{-22} Вт/(м·Гц)) на частотах 4-5 ГГц. Диапазон индексов роста низкочастотной части спектра f^{α} меняется в широких пределах $\alpha=0.3\div15$. Распределение индексов спада высокочастотной части подобно распределениям обычных вспышек. Одно из объяснений появления больших значений f^{α} -эффект Разина, который может влиять на форму гиросинхротронного спектра, при генерации всплесков в плотной плазме при относительно слабых магнитных полях. Обнаружены два события, в которых появление нетепловых электронов приводит к генерации узкополосных всплесков на частотах около двойной плазменной частоты. Тестовые испытания Сибирского радиогелиографа (СРГ) показали возможности измерений структуры вспышечных источников с потоками ~1 с.е.п., что свидетельствует о высоком диагностическом потенциале создаваемого радиогелиографа для обнаружения процессов ускорения в слабых вспышечных событиях и их локализации в активных областях...

Таблица Сводная информация о событиях 2021

Микроволновые динамические спектры солнечных вспышек по данным спектрополяриметра 4–8 ГГц

ЖДАНОВ Д.А.

Автореферат **2018**

ИСТОЧНИКИ СОЛНЕЧНЫХ МИКРОВОЛНОВЫХ ВСПЛЕСКОВ III ТИПА

ЖДАНОВ Д.А.1, ЛЕСОВОЙ С.В.1, ТОХЧУКОВА С.Х.2
СОЛНЕЧНО-ЗЕМНАЯ ФИЗИКА Том: 2Номер: 2 Год: **2016** Страницы: 12-21
Микроволновые тонкие структуры позволяют изучать эволюцию плазмы в области энерговыделения. Сибирский солнечный радиотелескоп (ССРТ) является уникальным инструментом для исследования источников тонких структур на частоте 5.7 ГГц. Комплексный анализ радиоданных РАТАН-600, спектрополяриметра 4-8 ГГц и ССРТ совместно с данными в крайнем ультрафиолете позволил локализовать источники микроволновых дрейфующих всплесков III типа в событии **10 августа 2011** г. во всей полосе частот появления всплесков и определить наиболее вероятную область первичного энерговыделения. Для локализации источников всплесков III типа по данным РАТАН-600 была разработана оригинальная методика обработки данных. На частоте 5.7 ГГц источник всплесков был зафиксирован по двум координатам, а на частотах 4.5, 4.7, 4.9, 5.1, 5.3, 5.5 и 6.0 ГГц положения были зафиксированы по одной координате. Найдено, что размер источника всплесков на частоте 5.1 ГГц был максимальным относительно размеров источников на других частотах.

Эффект двойного плазменного резонанса и его роль в радиоастрономии **Review**

В.В. **Железняков**, Е.Я. Злотник, В.В. Зайцев, В.Е. Шапошников
УФН 186 (10) 1090–1116 (**2016**)
http://ufn.ru/ufn16/ufn16_10/Russian/r1610d.pdf
Эффект двойного плазменного резонанса состоит в резком усилении неустойчивости плазменных волн в магнитоактивной плазме при совпадении частоты верхнего гибридного резонанса с частотами циклотронных гармоник. Механизм радиоизлучения, основанный на этом эффекте, позволил решить проблему происхождения "зебра"-структуры в спектре радиоизлучения Солнца, Юпитера и пульсара в Крабе. Разнообразие этих астрономических объектов и успешная интерпретация таких спектров на основе эффекта двойного плазменного резонанса указывает на универсальный характер этого явления и допускает возможное действие общего механизма излучения в различных астрофизических условиях.

ОБ АНАЛОГИИ МЕЖДУ ЗЕБРА-СТРУКТУРАМИ В РАДИОИЗЛУЧЕНИИ СОЛНЦА И ПУЛЬСАРА В КРАБОВИДНОЙ ТУМАННОСТИ

Железняков В. В.1, Зайцев В. В.1, Злотник Е. Я.
Письма в АЖ, 38(9), 660-676, **2012**
Исследована тесная аналогия между солнечным радиоизлучением, обладающим квазигармонической структурой спектра, и одной из компонент микроволнового радиоизлучения пульсара в Крабовидной туманности в виде так называемой “зебра-структуры”. Механизм радиоизлучения этой компоненты может быть обеспечен неустойчивостью на двойном плазменном резонансе и реализован в экстраординарных для радиопульсара условиях, а именно, в нерелятивистской плазме с относительно слабым магнитным полем. Указано на возможные модели источника излучения в форме магнитной ловушки или нейтрального токового слоя с поперечным магнитным полем, локализованных в коротирующей области магнитосферы пульсара вдали от поверхности нейтронной звезды.

Природа суб-секундных высокодобротных пульсаций солнечных вспышек в терагерцовом диапазоне

В.В.**Зайцев**, А.В.Степанов, П.Кауфман
ИКИ-**2014**, Сессия: Солнце
http://plasma2014.cosmos.ru/presentations
LRC-модель пульсаций, связывающая модуляцию суб-ТГц излучения с собственными колебаниями электрического контура – вспышечной арки, объясняет следующие особенности пульсаций

Плазменный механизм суб-ТГц излучения хромосферы

ЗАЙЦЕВ В.В.1, СТЕПАНОВ А.В.2, МЕЛЬНИКОВ В.Ф.
ПАЖ 39, 726, **2013**
Рассмотрен плазменный механизм субтерагерцового излучения солнечных вспышек и определены условия его реализации в солнечной атмосфере. Предполагается, что источник локализован в хромосферных основаниях корональных магнитных петель, где электронная концентрация должна достигать значений см . Для этого необходим прогрев хромосферы на высотах км до корональных температур, что обеспечивает высокую степень ионизации, требуемую для ленгмюровских частот 400 ГГц, и уменьшает тормозное поглощение субтерагерцового излучения при выходе из источника. Порог возбуждения плазменных волн для электронно-ионных столкновений налагает ограничение на нижний предел концентрации энергичных электронов в источнике см . При этом предпочтительной оказывается генерация излучения на гармонике плазменной частоты , а не на основном тоне. Показано, что ускорение электронов и нагрев плазмы в источнике

субтерагерцового излучения могут реализоваться при развитии в хромосферных основаниях вспышечной петли баллонной моды желобковой неустойчивости. Желобковая неустойчивость приводит к проникновению внешней хромосферной плазмы внутрь петли и вызывает генерацию индукционного электрического поля, эффективно ускоряющего электроны и приводящего к нагреву хромосферы in situ. Показано, что возникающее при этом ультрафиолетовое излучение прогретой хромосферы не превышает уровня, наблюдаемого во время вспышек.

Sub-terahertz emission from solar flares: The plasma mechanism of chromospheric emission
Zaitsev V.V., Stepanov A.V., Melnikov V.F.
Astronomy Letters. 2013. Т. 39. № 9. С. 650-659.

- Генерация суб-ТГц излучения солнечных вспышек возникает в хромосферных основаниях вспышечных петель во время их сильного прогрева.
- Прогрев сопровождается высокой степенью ионизации нижней хромосферы, требующейся для ленгмюровских частот суб-ТГц диапазона,
$n \geq 10^{14}$ см$^{-3}$.
- Ключевая роль в суб-ТГц излучении хромосферы принадлежит неустойчивости Рэлея-Тейлора, которая приводит к проникновению внешней плазмы внутрь петли. Для этого необходим «предпрогрев» до 3×10^4 К при диссипации электрического тока (Каулинг!).
- Магнитное поле петли деформируется, что вызывает генерацию индукционного электрического поля, ускоряющего электроны.
- Ускоренные электроны дополнительно нагревают хромосферу *in situ* и возбуждают плазменные волны, рэлеевское и комбинационное рассеяние которых приводит к излучению на суб-мм .

О тонкой структуре спектра солнечного радиоизлучения на декаметровых волнах

Е.Я.**Злотник**, В.В.Зайцев, В.Н.Мельник, А.А.Коноваленко и В.В.Доровский
ИКИ-**2014**, Сессия: Солнце
http://plasma2014.cosmos.ru/presentations

- Тонкая структура спектра декаметрового излучения Солнца в виде “fingeprint” интерпретируется в рамках механизма ДПР в корональной ловушке со специфическим распределением электронной плотности по высоте и относительно быстрым уменьшением магнитного поля со временем. При этом автоматически объясняется быстрый частотный дрейф зебра-полос, существование на фиксированной гармонике в фиксированный момент времени двух частот, на которых наблюдается повышенное радиоизлучение, а также противоположное направление частотного дрейфа зебра-полос на этих частотах.
- Предложенная модель реализуется при разумных параметрах, определяющих физические условия в корональной ловушке (при небольших отклонениях распределения электронной концентрации от барометрического закона).
- Длительность всплеска и расположение гармоник в структуре “fingerprint” согласуются с предположением о том, что уменьшение магнитного поля вызвано прохождением альфвеновского импульса через область ловушки с захваченными электронами.

ТЕПЛОВОЕ ЦИКЛОТРОННОЕ ИЗЛУЧЕНИЕ ГОРЯЧИХ КОРОНАЛЬНЫХ ПЕТЕЛЬ И ОСОБЕННОСТИ ПОЛЯРИЗАЦИОННОЙ СТРУКТУРЫ ИСТОЧНИКОВ СОЛНЕЧНОГО МИКРОВОЛНОВОГО ИЗЛУЧЕНИЯ. I. ЯРКОСТНАЯ ТЕМПЕРАТУРА

Е. Я. **Злотник**1*, Т.И.Ка льтма н2, О. А. Шейнер
ПИСЬМА В АСТРОНОМИЧЕСКИЙЖУРНАЛ, **2007**, том 33,№3, с. 196–209, **File**

Обсуждается возможный вклад теплового циклотронного излучения горячих корональных магнитных петельв наблюдаемые характеристики микроволнового излучения, исходящего из активных областей на Солнце. В рамках простейшей трехмерной модели петли в виде горячего тора проведены расче-ты ожидаемых особенностей частотной и поляризационной структуры источников микроволнового излучения, связанных с солнечными пятнами и содержащих корональные петли. В первой части работы приведены результаты модельных расчетов двумерных распределений яркостных температур на разных длинах волн для обыкновенной и необыкновенной мод, а также зависимости яркостных температур от длины волны. Выяснено влияние на эти характеристики размера петли, электронной концентрации и положения источника на диске. Численные расчеты распределений и спектров яркостных температур подтвердили известное предположение о том, что при определенных условиях спектр излучения горячего волокна может содержатьцик лотронные линии, а знак поляризации излучения может меняться по диапазону. Полученные в данной статье результаты являются основой для расчетов интегральных характеристик излучения (потока от всего источника и поляризации), результаты которых вместе с обсуждением модели будут приведены во второй части работы.

ТЕПЛОВОЕ ЦИКЛОТРОННОЕ ИЗЛУЧЕНИЕ ГОРЯЧИХ КОРОНАЛЬНЫХ ПЕТЕЛЬ И ОСОБЕННОСТИ ПОЛЯРИЗАЦИОННОЙ СТРУКТУРЫ ИСТОЧНИКОВ СОЛНЕЧНОГО МИКРОВОЛНОВОГО ИЗЛУЧЕНИЯ. II. ИНТЕГРАЛЬНЫЕ ХАРАКТЕРИСТИКИ

Е. Я. **Злотник**1*, Т.И.Ка льтма н2, О. А. Шейнер

ПИСЬМА В АСТРОНОМИЧЕСКИЙЖУРНАЛ, **2007**, том 33,№5, с. 371–384, **File**

Приведены результаты расчетов ожидаемых характеристик интегрального спектра теплового циклотронного излучения активной области на Солнце, содержащей корональную магнитную петлю. В качестве трехмерной модели петли рассмотрен горячий тор. Показано, что излучение горячей петли может заметно изменить характеристики излучения активной области на сантиметровых и дециметровых волнах. При определенных параметрах петли частотный спектр излучения может иметь немонотонный и достаточно сложный характер с несколькими максимумами или содержать сравнительно узкополосные циклотронные линии. Поляризационная структура источника, содержащего горячую петлю, также оказывается достаточно сложной, и при определенных условиях имеет место неоднократная инверсия знака поляризации по диапазону наблюдаемых частот. Полученные спектрально-поляризационные особенности рассматриваются с точки зрения возможности объяснения некоторых нетипичных наблюдаемых свойств источников излучения, связанных с активными областями на Солнце.

Проект солнечного спектрополяриметра для прогноза космической погоды

Иванов Е.Ф., Губин А.В., Лесовой С.В., Рамзес Сальдивар Эстрада.

СОЛНЕЧНО-ЗЕМНАЯ ФИЗИКА Том 5 № 4 ,**2019** С. 26–33.
https://naukaru.ru/ru/storage/viewWindow/43577

Предлагается проект солнечного спектрополяриметра метрового диапазона, предназначенного для использования в сети наземных инструментов в рамках задачи прогноза космической погоды. Требования к такому инструменту — идентичность характеристик, относительная дешевизна, возможность удаленного управления и передачи данных через интернет — определили выбор SDR-решения (Software-Defined Radio) как основы предлагаемого проекта. Наряду с вышеперечисленными требованиями предложенное SDR-решение позволяет легко реализовать прием I- и V-параметров Стокса, что отличает данный проект от спектрополяриметров сети e-CALLISTO, принимающих преимущественно одну из линейных поляризаций. Размещение таких инструментов на различных долготах позволит круглосуточно регистрировать радиовсплески II типа, являющиеся признаками наиболее геоэффективных проявлений солнечной активности — коронального выбросов массы, существенно влияющих на космическую погоду.

ИССЛЕДОВАНИЕ ХАРАКТЕРИСТИК ДЕТЕКТОРА ТЕРАГЕРЦОВОГО ИЗЛУЧЕНИЯ ДЛЯ НАУЧНОЙ АППАРАТУРЫ “СОЛНЦЕ-ТЕРАГЕРЦ”

КАЛИНИН Е. В.[1], **ФИЛИППОВ М. В.***[1], **МАХМУТОВ В. С.**[1], **МАКСУМОВ О. С.**[1], **СТОЖКОВ Ю. И.**[1], **КВАШНИН А. А.**[1], **ИЗМАЙЛОВ Г. Н.**, **ОЗОЛИН В. В.**

КОСМИЧЕСКИЕ ИССЛЕДОВАНИЯ Том: 59 Номер: 1 Год: 2021 Страницы: 3-8

В данной работе приводится краткое описание отдельных элементов, которые могут быть включены в состав научной аппаратуры “Солнце-Терагерц”, предназначенной для проведения впервые внеатмосферного эксперимента на борту международной космической станции. Его целью является измерение терагерцового электромагнитного излучения как от спокойного Солнца, так и во время протекания активных процессов на Солнце (солнечные вспышки, выбросы корональной массы и т.д.), что необходимо для установления физической природы солнечной активности и солнечных вспышек. В качестве приемников терагерцового излучения рассмотрена возможность использования оптоакустических преобразователей (ячеек Голея), чувствительность, стабильность и время отклика которых определены в ходе предварительных лабораторных исследований в наземных условиях.

О РЕГИСТРАЦИИ 4-Й ГАРМОНИКИ ГИРОЧАСТОТЫ В МИКРОВОЛНОВЫХ СПЕКТРАХ ИЗЛУЧЕНИЯ НАД ПЯТНАМИ

КАЛЬТМАН Т.И.*1, БОГОД В.М.

Косич. исслед. Том: 57Номер: 1 Год: **2019** Страницы: 3-11
DOI: 10.1134/S0023420619010047

Спектральные поляризационные наблюдения радиоисточников над солнечными пятнами ведутся на радиотелескопе РАТАН-600 регулярно. При детальном анализе спектров обнаруживаются новые эффекты. В данной работе исследуется проявление радиоизлучения 4-й гармоники гирочастоты в микроволновых спектрах, получаемых с 1% частотным разрешением в диапазоне 3–18 ГГц. Регистрация необыкновенной моды в коротковолновой части спектра сопоставляется с модельными расчетами излучения 2–5 гармоник гирочастоты

на фоне теплового тормозного излучения флоккул, окружающих пятенную структуру активной области. Анализируются уярчение необыкновенной моды в коротковолновой части спектра и изломы в спектрах интенсивности излучения. Приводятся примеры интерпретации наблюдательного материала РАТАН-600 с возможным диагностированием излучения 4-й гармоники гирочастоты.

ИССЛЕДОВАНИЕ ХАРАКТЕРИСТИК И ОСОБЕННОСТЕЙ РАДИОИЗЛУЧЕНИЯ УСИЛЕННОЙ ХРОМОСФЕРНОЙ СЕТКИ СОЛНЦА НА ОСНОВЕ РЕАЛИСТИЧНОЙ МГД МОДЕЛИ

Кальтман Т.И.1, Кочанов А.А.

Пулково *«Солнечная и солнечно-земная физика – **2015**», с. 189*

We present calculations of polarized microwave emission of the quiet Sun area in the wavelength range of 1.7–30 cm. The calculations are performed with help of realistic MHD model of the solar atmosphere, obtained under Bifrost code [1, 2]. The model provides a detailed spatial distribution of the plasma parameters (density, temperature, magnetic field, and others.) At the granular boundaries a strong magnetic field (up to 2500 G) is present. The calculations show a non-trivial pattern of radio emission from chromospheric to coronal heights, allowing us to estimate the relative contributions of the free-free and gyro radiation mechanisms.

СТРУКТУРА БОЛЬШОЙ АКТИВНОЙ ОБЛАСТИ NOAA 12209 ПО МИКРОВОЛНОВЫМ НАБЛЮДЕНИЯМ НА РАТАН-600 И VLA

Кальтман Т.И.1, Бастиан Т.С.2, Богод В.М.1, Гэри Д.Е.3,
Тохчукова С.Х.1, Уайт С.М.4, Флейшман Г.Д.3,
Яснов Л.В.5, Ступишин А.Г.5, Чен Б.6

Пулково *«Солнечная и солнечно-земная физика – **2015**», с. 185*

The observational characteristics of an active region with a big spot are investigated with RATAN-600 scans 3–17.5 GHz and with VLA imaging data 1–8 GHz. The structure of AR 12209 (**November, 2014**) is analyzed and the flux, sizes and brightness temperature spectra of microwave emission are presented for both right and left polarization. On the base of the reconstructed magnetic field the microwave emission of AR 12209 is calculated and compared with observational data. The model calculations provide appropriate tools to estimate the effective heights of emission, optical depths of the different gyroresonance levels (1–5) and to draw a 2-D output fine structure of the brightness temperature distributions over the source region. The model calculations are compared with the observational data, and then a fitting of the model parameters is done by several iterations. This method allows to estimate the values of electron density and temperature of plasma at heights of gyroresonance levels and to receive an atmosphere model of transition region from microwave observations. Some problems associated with inhomogeneous distribution of the parameters of the observed solar plasma and the ability to come up with their realistic model is discussed

ОГРАНИЧЕНИЯ НА РЕЖИМЫ УСКОРЕНИЯ ЭЛЕКТРОНОВ В СОЛНЕЧНЫХ ВСПЫШКАХ

В. А. **Ковалев**1*, В. Ф. Мельников2

ПАЖ **2019**, том 45,№8, с. 586–590

DOI: 10.1134/S0320010819080059

На основе данных наблюдений микроволновых импульсных всплесков, зарегистрированных в обсерватории Нобеяма, получены ограничения на режимы ускорения электронов в солнечных вспышках. Из анализа эволюции инкремента нарастания радиопотока установлено, что ускорение электронов во время вспышки происходит в режиме, замедленном по сравнению с экспоненциальным. **07 марта 2012**

Статистические свойства аврорального километрового радиоизлучения по наблюдениям на спутнике ERG (ARASE).

Колпак В.И., Могилевский М.М., Чугунин Д.В., Чернышов А.А., Моисеенко И.Л., Кумамото А., Тсучия Ф., Касахара Е., Шойи М., Миеши Е., Шинохара И.

СЗФ Том 7. **2021**. № 1. С. 13–20.

https://naukaru.ru/ru/storage/viewWindow/67784

В данной работе впервые исследованы одновременно зарегистрированные одним спутником сигналы аврорального километрового радиоизлучения (АКР) от источников в авроральных областях Северного и Южного полушарий. В ходе выполнения настоящего исследования проведена подробная статистическая обработка непрерывных измерений АКР продолжительностью более двадцати месяцев на спутнике ERG

(Arase), которая позволила подтвердить ранее полученные результаты о расположении источников АКР и сезонных изменениях интенсивности излучения. Открытые вопросы о процессах в источнике АКР могут быть решены с использованием данных о диаграмме направленности излучения в различных геомагнитных условиях. Для ответа на эти вопросы сделана оценка угла раствора конуса диаграммы направленности АКР в вечернем и утреннем секторах магнитосферы Земли.

МОДЕЛИРОВАНИЕ СТРУКТУРЫ СПОКОЙНЫХ УЧАСТКОВ АТМОСФЕРЫ СОЛНЦА, СООТВЕТСТВУЮЩЕЙ ИЗЛУЧЕНИЮ В ДИАПАЗОНЕ ДЛИН ВОЛН 1–100 СМ

КРИССИНЕЛЬ Б.Б.

АЖ Том: 92Номер: 1 Год: **2015** Страницы: 66

Модель атмосферы спокойных участков Солнца, соответствующая излучению на волнах от 1 см до 1 м, представлена совокупностью ранжированных по размерам петель, спикул и свободного (межпетельного) вещества. Параметры свободного вещества находятся приближенным способом по исходным зависимостям от высоты температуры и плотности электронов атмосферы, составленным из известных моделей спокойных участков для центра диска. В модели 10 однотипных петель с радиусами R_{loop} от 3100 до 210 000 км, у которых частота появления и величина плотности электронов в вершине являются средними для петель определенного кластера размеров. Коэффициент разреженности петель, определяемый как число петель данного размера на площадке $2R_{loop} \times 2R_{loop}$, находится в пределах от 6 до 9. Высота начала корональной части петель h_0 равна 2275 км. Высотный профиль температуры корональной части петель определяется выражением $T_{lp}(h) = T_{\min} + (T_{\max\ loop} - T_{\min}) \left\{ \sin\left[\frac{\pi}{2} (h - h_0)/(R_{loop} - h_0) \right] \right\}^{0.25}$, где $T_{\min}$ - температура исходной модели на высоте h_0, $T_{\max\ loop}$ - температура вершины петли. В области ножек петель используются высотные профили исходной модели с учетом (для плотности) давления на высоте h_0. Спикулы ранжированы по высотам от 400 до 11 000 км. Расчет яркости заключается в суммировании по несложной логической схеме яркостей отдельных слоев компонентов атмосферы с учетом их вероятностей и общего коэффициента передачи. Вероятностные характеристики компонент атмосферы находятся итерационным способом по результатам сравнения расчетного экваториального распределения яркости с экспериментальными данными. Впервые получено хорошее согласие в широком диапазоне волн теоретического распределения яркости с наблюдательными данными, полученными на радиотелескопах РАТАН-600, NoRH, ССРТ.

Микроволновый индикатор потенциальной геоэффективности и жгутовая магнитная структура солнечной активной области.

Кудрявцева А.В., Мышьяков И.И., Уралов А.М., Гречнев В.В.

СЗФ Том 7. **2021**. № 1. С. 3–12.

https://naukaru.ru/ru/storage/viewWindow/66383

Выполнен анализ присутствия микроволнового источника над нейтральной линией (ИНЛ) в суперактивной области NOAA 12673, породившей ряд геоэффективных событий в сентябре 2017 г. Для оценки положения ИНЛ использовались данные Сибирского радиогелиографа в диапазоне 4–8 ГГц и Радиогелиографа Нобеяма на частоте 17 ГГц. Расчет коронального магнитного поля в нелинейном бессиловом приближении выявил протяженную структуру, состоящую из взаимосвязанных магнитных жгутов, расположенных практически по всей длине главной линии раздела полярностей фотосферного магнитного поля. ИНЛ проецируется в зону максимальных значений горизонтального магнитного поля — основной энергосо-держащей части этой структуры. В ходе каждой вспышки балла X активная область теряла магнитную спиральность и становилась источником КВМ. **6-7 Sep 2017**

Кузьменко И.В. Депрессия микроволнового излучения как отклик на возникновение джета

Сборник трудов XXVI Всероссийской ежегодной конференции по физике Солнца «Солнце и солнечно-земная физика – 2022» ГАО РАН.

http://www.gaoran.ru/russian/solphys/2022/book/conf2022.pdf 7-9 марта 2015

Ударная волна в солнечном событии, связанном с эрупцией крупного протуберанца

Кузьменко И.В.1 , Гречнев В.В.2

Тезисы XXV всероссийская ежегодная конференция «Солнечная и солнечно-земная физика-2021», Пулково, **2021**

http://www.gaoran.ru/russian/solphys/2021/gao2021.pdf

Эрупция крупного протуберанца, произошедшая **29 сентября 2013** г. вне активных областей, вызвала быстрый корональный выброс массы. Его высокая скорость предполагает наличие перед ним ударной волны, что подтверждается наблюдениями радиовсплеска II типа и окружающего выброс гало. Установлено, что ударная волна была импульсно возбуждена эруптивным протуберанцем и трансформировалась в головную позже на значительном расстоянии от Солнца. Расчётные положения фронта волны соответствуют её проявлениям на

изображениях. Радиоизлучение II типа от 30 МГц до 70 кГц было вызвано распространением одной и той же ударной волны. Характер возбуждения и эволюции ударной волны в этом событии оказался таким же, как и в исследованных ранее вспышечных событиях.

КОРОНАЛЬНЫЕ ДЖЕТЫ КАК ПРИЧИНА ВОЗНИКНОВЕНИЯ МИКРОВОЛНОВЫХ ОТРИЦАТЕЛЬНЫХ ВСПЛЕСКОВ

КУЗЬМЕНКО И.В.1

СОЛНЕЧНО-ЗЕМНАЯ ФИЗИКА Том: 6Номер: 3 Год: **2020** Страницы: 26-32

Исследована причина возникновения трех изолированных отрицательных радиовсплесков, зарегистрированных 10-11.04.2014 на ряде частот микроволнового диапазона по данным радиообсерватории Нобеяма, солнечной обсерватории Лермонт и Уссурийской астрофизической обсерватории. Такие всплески наблюдаются довольно редко и обычно связаны с поглощением радиоизлучения областей спокойного Солнца или радиоисточника веществом крупного эруптивного волокна. Анализ наблюдений солнечного события **10-11.04.2014** в различных спектральных диапазонах с использованием изображений, полученных по данным радиогелиографа в Нобеяме и космической обсерватории SDO/AIA, показал, что причиной всех трех депрессий радиоизлучения являлось затенение радиоисточника, расположенного на солнечном лимбе, веществом рекуррентных корональных джетов. Оценки параметров поглощающего вещества, выполненные с использованием разработанной ранее модели, подтвердили, что солнечное радиоизлучение поглощалось холодным веществом с температурой ~104 K, которое находилось в нижней части джетов.

Гирорезонансное излучение электронов с немаксвелловскими распределениями в солнечной короне

А.А. **Кузнецов**, Г.Д. Флейшман, В.П. Максимов, В.Э. Капустин

ИКИ, **2014**, Сессия: Солнце
http://plasma2014.cosmos.ru/presentations

СПЕКТРАЛЬНО-ПОЛЯРИЗАЦИОННЫЕ НАБЛЮДЕНИЯ СОЛНЕЧНОГО ЗАТМЕНИЯ **20.03.2015 г.** НА РАДИОТЕЛЕСКОПАХ РАТАН-600 И БПР (ДИНАМИКА И ХАРАКТЕРИСТИКИ АКТИВНЫХ ОБЛАСТЕЙ)

Курочкин Е.А.1, Богод В.М.1, Венгер А.П.1, Коржавин А.Н.1,
Петерова Н.Г.1, Стороженко А.А.1, Топчило Н.А.2, Шендрик А.В.1

Пулково *«Солнечная и солнечно-земная физика – **2015**», с.257*

The first results of solar eclipse observations at microwaves during March 20.2015 (phase ~ 0.4–0.8) are described. The observations during nearest days before and after eclipse in the period March 13-25, 2015 also were provided. The observations were made with the radiotelescopes RATAN -600 and LPR in the wavelength range (1.7–10 cm). The best spatial resolution of RATAN-600 is 17".12.5' (at 2 cm) and frequency resolution up to ~ 1%. All observations were carried out in solar tracking mode during time interval 4 hours at about the local noon (~ 9.5 h UT) with 8 min time cadence.

Тонкая структура короны по радионаблюдениям с высоким частотным разрешением

М. К. **Лебедев***, В. М. Богод, Н. Е. Овчинникова

Косм. Исследования **2024**

Наличие непрерывных процессов охлаждения и нагрева является важным условием, определяющим существование солнечной короны, для которой характерны температуры на уровне нескольких миллионов кельвинов. На эти процессы могут оказывать существенное влияние мелкомасштабные корональные образования, которые, в соответствии с идеями Паркера, в значительной мере определяют тепловой баланс короны и возмущения солнечного ветра. Наблюдения поляризованного излучения с высокой чувствительностью позволяют оценить сложную структуру магнитных полей, которые накапливают энергию, необходимую для возбуждения корональных эруптивных явлений, всплесков и вспышек. Однако на больших высотах корона становится оптически тонкой, и ее наблюдения представляют собой большую проблему, требующую использования инструментов с большой эффективной площадью. Многие исследователи отмечают, что область корональной магнитометрии является молодой и затратной для продвижения ввиду того, что экспериментальные наблюдения в оптических диапазонах ограничены низкой плотностью плазмы в короне, высокой температурой, а также недостаточной чувствительностью инструментария. В противоположность этому, в радиодиапазоне достижима более высокая чувствительность. В частности, диапазон 1–3 ГГц оптимален для регистрации весьма слабых корональных структур зарождающей активности, несмотря на ограничения по пространственному разрешению. Для организации радионаблюдений короны на крупном

радиотелескопе рефлекторного типа РАТАН-600 был создан широкодиапазонный спектрометр в диапазоне 1–3 ГГц. Он имеет сплошное перекрытие всего диапазона с предельными частотным и временным разрешениями при высокой чувствительности по потоку излучения. Проводятся результаты первых серий наблюдений слабых корональных структур, обсуждается их интерпретация по воздействию на тепловые процессы в короне.

Сибирский радиогелиограф - новые возможности исследования солнечной короны
Лесовой С.В., Губин А.В., Глоба М.В., Кочанов А.А., Алтынцев А.Т., Уралов А.М.
Plasma-**2022** Презентация
https://plasma2022.cosmos.ru/sites/default/files/presentations/lesovoi_SRH_plasma2022-pres.pdf
2022-01-07, 2022-01-12, 2022-01-20

Лесовой С.В., Глоба М.В. Измерение задержек в приемном тракте Сибирского радиогелиографа. С-З физика, т. 7, №4,С. 99–103. Аннотация / Полный текст (PDF)

СИБИРСКИЙ РАДИОГЕЛИОГРАФ: ПЕРВЫЕ РЕЗУЛЬТАТЫ
Лесовой С.В., Алтынцев А.Т., Кочанов А.А., Гречнев В.В., Губин А.В., Жданов Д.А., Иванов Е.Ф., Уралов А.М., Кашапова Л.К., Кузнецов А.А., Мешалкина Н.С., Сыч Р.А.
СОЛНЕЧНО-ЗЕМНАЯ ФИЗИКА Том: 3Номер: 1 Год: **2017** pp. 3-16
Начаты регулярные наблюдения активных процессов в атмосфере Солнца с помощью первой очереди многоволнового Сибирского радиогелиографа - Т-образной 48-антенной решетки с диапазоном рабочих частот 4-8 ГГц и мгновенной полосой приема 10 МГц. Антенны установлены на центральных антенных постах Сибирского солнечного радиотелескопа, максимальная база 107.4 м, угловое разрешение до 70″. Приведены примеры наблюдений диска Солнца на различных частотах, «отрицательных» всплесков и солнечных вспышек. Чувствительность по компактным источникам достигает 0.01 солнечных единиц потока (≈10-4 от полного потока Солнца) при времени накопления 0.3 с. Высокая чувствительность радиогелиографа обеспечивает мониторинг солнечной активности и позволяет исследовать активные процессы по характеристикам их микроволнового излучения, включая сверхслабые события, не регистрировавшиеся ранее 16 March 2016, **18 April 2016**, **9 June 2016, 23 July 2016, 9 August 2016**
See https://arxiv.org/pdf/1704.07100.pdf
CESRA highlight #1426 July **2017** http://www.astro.gla.ac.uk/users/eduard/cesra/?p=1426

КОРОТИРУЮЩИЕ ВОЗМУЩЕНИЯ СОЛНЕЧНОГО ВЕТРА В ДАННЫХ МОНИТОРИНГА МЕЖПЛАНЕТНЫХ МЕРЦАНИЙ: МОДЕЛИРОВАНИЕ И НАБЛЮДЕНИЯ
Лукманов *В.Р., Чашей И.В., Тюльбашев С.А., Субаев И.А.*
АЖ Том: 100Номер: 6 Год: **2023** Страницы: 546-556

Предложена простая модель ведущей части области взаимодействия разноскоростных потоков солнечного ветра, в которой повышенная концентрация плазмы задается в виде спиральной струи с прямоугольным сечением. В рамках модели рассчитаны двумерные динамические карты распределения уровня межпланетных мерцаний, адаптированные к конфигурации радиотелескопа БСА ФИАН. Для четырех магнитных бурь 2022 и 2023 г., вызванных коротирующими возмущениями, проведено сравнение модельных расчетов с данными серий наблюдений межпланетных мерцаний, содержащих период геомагнитного возмущения. В целом имеется качественное соответствие между расчетами и наблюдательными данными. Показано, что коротирующие возмущения проявляются в усилениях мерцаний за три дня до магнитной бури около 15–16 ч московского времени. В последующие двое суток усиление мерцаний смещается к более позднему времени. При этом усиления мерцаний в утреннем секторе отсутствуют. В период магнитной бури происходит усиление ночных мерцаний. Такая последовательность усилений мерцаний соответствует приближению возмущения к Земле с восточной стороны при вращении с Солнцем. Обсуждается качественное различие между данными наблюдений для коротирующих и распространяющихся крупномасштабных возмущений.

АНАЛИЗ ВОЗМОЖНОСТЕЙ КРАТКОСРОЧНОГО ПРОГНОЗА ГЕОМАГНИТНЫХ ВОЗМУЩЕНИЙ ПО НАБЛЮДЕНИЯМ КОРОНАЛЬНЫХ ВЫБРОСОВ МАССЫ НА РАДИОТЕЛЕСКОПЕ БСА ФИАН
Лукманов *В.Р., Чашей И.В., Тюльбашев С.А., Субаев И.А.*
АЖ Том: 100Номер: 6 Год: **2023** Страницы: 535-545
В мониторинговых данных, ежедневно получаемых на радиотелескопе Большая Синфазная Антенна (БСА), с апреля 2021 г. по октябрь 2022 г. выделено 11 событий, для которых после рентгеновских вспышек в солнечной

короне на Земле происходили магнитные бури. Данные мониторинга межпланетных мерцаний рассматривались совместно с данными о вспышечной активности Солнца и простой кинематической моделью распространения выброса. На основании найденных оценок скорости выброса между Солнцем и зондируемой областью в предположении постоянства скорости вычислялось время прихода выброса к Земле. Из 11 рассмотренных событий 7 связаны с уединенными вспышками, с последующим выбросом корональной массы (CME), а 4 имеют более сложный характер и, возможно, связаны с коротирующими возмущениями или наложением коротирующих и вспышечных возмущений. Для всей совокупности событий среднее время реального начала магнитной бури после времени, предсказанного моделью, составило 3.6 ч, а среднее время между началом усиления мерцаний и началом магнитной бури составило 20.1 ч. Для событий, связанных с уединенными вспышками, магнитная буря в среднем начиналась через 0.8 ч после предсказанного времени и через 15.6 ч после начала усиления мерцаний. Запаздывание магнитных бурь относительно предвычисленного времени, по-видимому, связано с торможением выброса между зондируемой областью солнечного ветра и орбитой Земли.

Особенности субтерагерцового излучения солнечных вспышек
В.С. **Махмутов**, Г.А. Базилевская, Ю.И. Стожков, А.А. Квашнин
ИКИ-2014, Сессия: Солнце
http://plasma2014.cosmos.ru/presentations

Яркие ультрафиолетовые узлы как возможные источники когерентного микроволнового излучения.
Мешалкина Н.С., Алтынцев А.Т.
СОЛНЕЧНО-ЗЕМНАЯ ФИЗИКА Том 9 № 4 , **2023**, С. 21–29.
https://naukaru.ru/ru/storage/viewWindow/138047
Особенностью события **6 сентября 2012** г. явилось то, что источники узкополосных (2–4 ГГц) субсекундных импульсов (ССИ) наблюдались в небольших областях вспышечных петель с так называемыми яркими ультрафиолетовыми узлами, которые характеризовались высокой плотностью плазмы до 10^{11} $см^{-3}$. Временные профили жесткого рентгеновского излучения вспышки хотя и подобны микроволновым кривым блеска, но не имеют структур, соответствующих ССИ. Анализ микроволновых, рентгеновских и ультрафиолетовых данных показал, что наблюдаемые импульсы микроволнового излучения с узкой спектральной полосой имеют когерентную природу и генерируются электронами с энергиями нескольких десятков килоэлектронвольт в ярких узлах на частоте около удвоенной плазменной. Результаты наблюдений свидетельствуют, что появление ярких узлов связано с локальными процессами энерговыделения при взаимодействии вспышечных петель.

ДИАГНОСТИКА АНИЗОТРОПИИ УСКОРЕННЫХ ЭЛЕКТРОНОВ ПО НАБЛЮДАЕМОЙ ПОЛЯРИЗАЦИИ МИКРОВОЛНОВОГО ИЗЛУЧЕНИЯ СОЛНЕЧНЫХ ВСПЫШЕЧНЫХ ПЕТЕЛЬ
Моргачев А.С.1,2, Кузнецов С.А.1,2, Мельников В.Ф.2
Пулково *«Солнечная и солнечно-земная физика – **2015**», с.285*
Purpose of our investigation is a verification of the hypothesis on longitudinal anisotropy of emitting electrons as a reason of the observed O-mode dominance of circular polarized microwave emission in solar flare loops. We used Nobeyama radio heliograph (NoRH) data on 17 & 34 GHz with high spatial resolution for polarization and brightness maps analysis, HMI/SDO magnetograms and AIA/SDO EUV maps for identification of magnetic field configuration. We have analyzed 33 events from NoRH data base and found signatures of electrons anisotropy for four of them. **28 о к т я б р я 2013**

Вклад теплового тормозного излучения в микроволновое излучение солнечных вспышечных петель
А. С. **Моргачев**, В. Е. Поляков, В. Ф. Мельников
Астрономический журнал, - **2014**, С. 399-408
Рассмотрен вклад теплового тормозного излучения в общий поток микроволнового излучения солнечной вспышечной петли. Данные об общем потоке принимаемого излучения получены с помощью радиогелиографа Нобеяма. Расчет потока теплового тормозного излучения в радиодиапазоне производился на основе определения интегральной температуры и концентрации горячей плазмы во вспышечной петле по потокам ее мягкого рентгеновского излучения. Для этого использовались данные спутников GOES-10 и GOES-12. Показано, что на фазе максимума всплеска влияние теплового тормозного излучения на общий поток и спектральный индекс микроволнового излучения незначительно (, , соответственно). На фазе спада всплеска вклад тормозного излучения может достигать высоких значений (до), что приводит к весомому уменьшению

наблюдаемого спектрального индекса (до). Поэтому при диагностике параметров ускоренных электронов по характеристикам их гиросинхротронного излучения наиболее точные результаты можно получить, исследуя характеристики излучения на фазе максимума всплеска.

Моторина Г.Г., Цап Ю.Т., Смирнова В.В., Моргачев А.С., Шрамко А.Д. **Предвестники солнечных вспышек и суб-терагерцовое излучение события 28.03.2022** …
Сборник трудов XXVI Всероссийской ежегодной конференции по физике Солнца «Солнце и солнечно-земная физика – 2022» ГАО РАН.
http://www.gaoran.ru/russian/solphys/2022/book/conf2022.pdf

ВРЕМЕННАЯ ЭВОЛЮЦИЯ ЭНЕРГЕТИЧЕСКОГО РАСПРЕДЕЛЕНИЯ ЭЛЕКТРОНОВ В СОЛНЕЧНЫХ ВСПЫШКАХ НА ОСНОВЕ RHESSI И SDO/AIA НАБЛЮДЕНИЙ
Моторина Г.Г.1,2, Контарь Э.П.
Пулково *«Солнечная и солнечно-земная физика – **2015**», с.289*
Diagnostics of flare plasma is typically carried out by means of studying of extreme ultraviolet radiation, while information about the nonthermal plasma component, the distribution of high-energy accelerated electrons can be obtained from X-ray data. Using simultaneous observations from SDO/AIA and RHESSI it became possible to study the energy distribution of hot/accelerated electrons in a wide energy range from 0.1 keV up to several tens of keV. Using a method of fitting with the differential emission measure both AIA and RHESSI data we can find the DEM and the energy distribution of electrons in the flare plasma. Using this method the temporal evolution of the DEM and the energy distribution of accelerated electrons was analyzed for one limb event. **8 мая 2015**

Результаты совместных наблюдений на Солнечном спектрополяриметре метрового диапазона и ряде других инструментов.
Муратова Н. О., Федотова А. Ю., Шамсутдинова Ю. Н.
СОЛНЕЧНО-ЗЕМНАЯ ФИЗИКА Том 8. **2022**. № 1 С. 24-33.
https://naukaru.ru/ru/storage/viewWindow/87260
Излучение Солнца регистрируется в широком диапазоне частот — от гамма- до радиоизлучения. Таким образом, совместные наблюдения на разных приборах и в различных частотных диапазонах позволяют представить комплексную картину развития событий на Солнце и подтвердить достоверность данных отдельных приборов. В статье приводится сравнительный анализ данных, полученных на Солнечном спектрополяриметре метрового диапазона (ССМД) и с помощью ряда других приборов. Для исследования были выбраны три события, зарегистрированные на ССМД в **2019** г.: радиовсплески III типа с 05:05 UT до 05:12 UT и II типа с 05:12 UT до 05:19 UT **6 мая** и III типа с 05:03 UT по 05:21 UT **14 апреля**. Для сравнения использовались данные следующих инструментов: ССМД, СРГ (Сибирский радиогелиограф), SDO/AIA (блок формирования изображений солнечной атмосферы Atmospheric Imaging Assembly на орбитальной обсерватории Solar Dynamics Observatory), Wind/WAVES (инструмент для исследования плазменных и радиоволновых явлений на космическом аппарате Wind), наземный радиоспектрополяриметр AMATERAS, космический аппарат GOES-14. Результаты проведенного анализа показали, что данные всех инструментов хорошо коррелируют друг с другом и соответствуют характерным особенностям каждого события. Данное исследование также помогло подтвердить достоверность данных, полученных на ССМД.

Результаты работы нового спектрополяриметра для наблюдения солнечного радиоизлучения в диапазоне 50–500 МГц.
***Муратова** Н.О., Муратов А.А., Кашапова Л.К.*
СОЛНЕЧНО-ЗЕМНАЯ ФИЗИКА Том 5. **2019**. № 3. С. 3–10.
https://naukaru.ru/ru/storage/view/39749
Наземные наблюдения в метровом радиодиапазоне представляют большой интерес для понимания процессов, происходящих в короне Солнца. Мы представляем основные принципы работы, схему и результаты первых наблюдений Солнечного спектрополяриметра метрового диапазона (ССМД), запущенного для наблюдения Солнца в диапазоне 50–500 МГц в апреле 2016 г. Основной задачей при конструировании прибора было создание современного цифрового спектрополяриметра, способного измерять полный вектор Стокса для спорадических явлений, наблюдаемых в диапазоне 50–500 МГц. Для приема радиоизлучения используется логопериодическая скрещенная антенна, принимающая горизонтальную и вертикальную поляризационные компоненты одновременно. Основой ССМД является цифровая часть, алгоритм работы которой построен на базе архитектуры FX-коррелятора. В основе получения динамических амплитудных спектров (зависимость

амплитуды от частоты и времени) лежит алгоритм быстрого преобразования Фурье (БПФ), реализованный по принципу поточной схемы и работающий в режиме реального времени. ССМД имеет 4608 частотных каналов, при ширине канала 97.66 кГц и шаге 97.66 кГц временное разрешение составляет 1 с. Спектрополяриметр покрывает широкий диапазон 50–500 МГц и позволяет получать полный вектор Стокса. На сегодняшний день с помощью ССМД проводятся регулярные наблюдения двух параметров вектора Стокса (I и V). Начиная с 2016 г. получены наблюдения ряда интересных явлений, произошедших во время солнечных вспышек, составляется каталог наблюдений. Мы планируем улучшение временных и частотных характеристик, запись полного вектора Стокса, а также калибровку инструмента. Идет работа над обеспечением доступа к данным в сети Интернет.**23.07.2016, 08.09.2017**

Долгопериодические колебания в активных областях Солнца по данным о магнитных полях и микроволновому излучению

Ю. А. **Наговицын**, Е. Ю. Наговицына, В. Е. Абрамов-Максимов
Астрономический журнал, 90(8) - **2013**, С. 692-696
На основе параллельных наблюдений SOHO MDI и радиогелиографа Nobeyama с 1-мин временнм разрешением проведено сравнительное исследование колебаний солнечных пятен и соответствующих им радиоисточников в активных областях AR 8949, AR 8951 и AR 8953 в диапазоне периодов от десятков до сотен минут. Показано, что для избранных активных областей радиоисточники удалены от соответствующих им пятен на расстояния км, и периоды долгопериодических колебаний для них больше на .

ПОВЫШЕННАЯ ЯРКОСТЬ МИКРОВОЛНОВОГО ИЗЛУЧЕНИЯ КАК ПРИЗНАК ВСПЫШЕЧНО-ПРОДУКТИВНЫХ АКТИВНЫХ ОБЛАСТЕЙ ПО НАБЛЮДЕНИЯМ АКТИВНОЙ ОБЛАСТИ NOAA 12 371

Петерова Н.Г., Топчило Н.А., Курочкин Е.А.
ГиА Том: 62Номер: 1 Год: 2022 Страницы: 28-39
Продолжена разработка методов прогнозирования солнечных вспышек с использованием наблюдений в микроволновом диапазоне волн на радиотелескопах с высоким угловым разрешением. Приведены результаты анализа наблюдений активной области NOAA 12 371, в квазиспокойном состоянии отличавшейся повышенной яркостью излучения в микроволновом диапазоне и породившей множественные эруптивные события. По наблюдениям на радиотелескопе РАТАН-600 в период события **21.06.2015** г. зафиксировано резкое изменение структуры изображения источника микроволнового излучения над NOAA 12 371, предположительно интерпретированное кратковременным нагревом плазмы над областью дельта-конфигурации магнитного поля в хвостовой части активной области. Благодаря высокой чувствительности РАТАН-600 при поляризационных измерениях удается в рамках известных моделей магнитного поля локализовать положение облака, в котором происходит высвечивание или ускорение быстрых частиц.

НАБЛЮДЕНИЯ СОЛНЕЧНОГО ЗАТМЕНИЯ 20.03.2015 г. НА ДВУХ РАДИОТЕЛЕСКОПАХ РТ-32 В ОБСЕРВАТОРИЯХ «СВЕТЛОЕ» И «ЗЕЛЕНЧУКСКАЯ» (предварительные результаты)

Рахимов И.А.1, Дьяков А.А.1, Ипатов А.В.1, Ильин Г.Н.1,
Коржавин А.Н.2, Петерова Н.Г.2, Топчило Н.А.
Пулково *«Солнечная и солнечно-земная физика – **2015**», с.313*
Results are given for observations of the active region NOAA 12303, executed during the partial solar eclipse in March 20, 2015 into two observatories – "Svetloe" near to St. Petersburg and "Zelenchuksky", in the North Caucasus. Use a completely steerable paraboloids of radio telescopes RT-32 with a field of view, limiting the contribution of the quiet Sun, has led to increase of sensitivity and the effective angular resolution of eclipse observations (about 1–3 arcsec at microwaves 3.5, 6.2 and 13 cm). The thin structure of radio images is revealed and explaned in the context of the cyclotron emission theory.

ИССЛЕДОВАНИЕ ПОЛЯРИЗАЦИИ МИЛЛИМЕТРОВОГО ИЗЛУЧЕНИЯ СОЛНЕЧНЫХ ВСПЫШЕК

Рыжов В.С., Шиврина П.И., Смирнова В.В.
Изв. КрАО Том: 119 Номер: 1 Год: 2023 Страницы: 11-18
В работе приведены оценки степени поляризации солнечных вспышек, зарегистрированных с помощью радиотелескопа РТ-7.5 МГТУ им. Н.Э. Баумана на частоте 93 ГГц. На основе данных картографирования полного солнечного диска определены временные профили интенсивности на правой и левой круговой поляризации для нескольких событий марта - июня 2022 г. Оценка верхнего предела степени круговой поляризации для максимальной фазы исследованных вспышек составила 5 %.

Корреляционный анализ абсолютных измерений солнечного потока на частотах 161 и 245 МГц.

Сетов А.Г., Кушнарев Д.С.
СОЛНЕЧНО-ЗЕМНАЯ ФИЗИКА Том 9 № 4 , 2023 С. 54–62.
https://naukaru.ru/ru/storage/viewWindow/138050

Излучение Солнца в метровом диапазоне длин волн происходит из верхних слоев солнечной короны. В статье представлены абсолютные измерения солнечного потока, проводимые на Иркутском радаре некогерентного рассеяния (частота 161 МГц) и в обсерватории Learmonth (частота 245 МГц). Проведен корреляционный анализ данных с целью выявления взаимосвязей между солнечными потоками на разных частотах. Фоновое излучение спокойного Солнца оказалось в ожидаемых рамках. Рассмотрено поведение фоновой и медленно меняющейся компонент излучения в солнечном цикле. Сопоставление коэффициента корреляции Пирсона и рангового коэффициента корреляции Спирмана показало нелинейный характер зависимости между потоком в метровом диапазоне и индексом F10.7. Корреляция между измерениями солнечного потока на частотах 161 и 245 МГц оказалась ниже, чем корреляции с индексом F10.7. Анализ внутрисуточной корреляции и автокорреляции показал наличие суточного хода, вносящего погрешность в измерения.

МИКРОВОЛНОВАЯ ДИАГНОСТИКА ВСПЫШЕЧНОЙ ПЛАЗМЫ МЕТОДОМ ФИТИРОВАНИЯ ПО ДАННЫМ СИБИРСКОГО РАДИОГЕЛИОГРАФА

СМИРНОВ Д.А.[1,2], **МЕЛЬНИКОВ В.Ф.**[2]

СОЛНЕЧНО-ЗЕМНАЯ ФИЗИКА Том: 10 Номер: 3 Год: 2024 Страницы: 27-39

В настоящей работе проведен анализ изображений и частотного спектра излучения в максимуме яркости радиоисточников во вспышках 20 января 2022 и 16 июля 2023 г., зарегистрированных Сибирским радиогелиографом в диапазонах 3-6 ГГц и 6-12 ГГц. Полученные данные о спектре использовались для радиодиагностики напряженности и ориентации магнитного поля, плотности плазмы и параметров ускоренных частиц в радиоисточнике. Радиодиагностика проводилась методом, основанным на минимизации функционала, содержащего интенсивности теоретически рассчитываемых и наблюдаемых частотных спектров левополяризованного и правополяризованного излучения. Поскольку форма такого многомерного функционала довольно сложна и минимизировать его стандартными подходами не представляется возможным, использовался генетический метод минимизации. В результате проведенной радиодиагностики определены особенности динамики напряженности и ориентации магнитного поля, а также концентрации и показателя энергетического спектра нетепловых электронов в области максимальной яркости радиоисточника. Установлено, что на фазе роста основных пиков излучения магнитное поле уменьшается, а на фазе спада, наоборот, увеличивается. Скорость этих изменений варьирует от нескольких единиц до 11 Гс/с для вспышки **20 января 2022** г. и составляет около 1 Гс/с для вспышки **16 июля 2023** г.

ПРЕДИМПУЛЬСНОЕ ВСПЫШЕЧНОЕ ЭНЕРГОВЫДЕЛЕНИЕ ПО ДАННЫМ СУБТЕРАГЕРЦОВОГО И РЕНТГЕНОВСКОГО ИЗЛУЧЕНИЯ СОЛНЦА

Смирнова В.В., Цап Ю.Т., Рыжов В.С.

Изв. КрАО Том: 119Номер: 1 Год: 2023 Страницы: 5-10

В работе изучены временные задержки между профилями рентгеновского и субтерагерцового (суб-ТГц) излучения в начальной фазе вспышек с целью выяснения природы нагрева переходной области и верхней хромосферы Солнца. Анализ ряда событий показывает, что для некоторых событий суб-ТГц излучение в начале вспышек опережает жесткое рентгеновское на 3-6 минут. Электронная теплопроводность корональной плазмы не может обеспечить эффективный нагрев переходной области и плазмы в области хромосферы, что предполагает тепловое вспышечное энерговыделение непосредственно на уровне хромосферы.

НАПРАВЛЕННАЯ ФИЛЬТРАЦИЯ ДЛЯ ОБРАБОТКИ ИЗОБРАЖЕНИЙ/ВИДЕОИЗОБРАЖЕНИЙ СОЛНЦА

ЛУН **СЮЙ**1, ЙИХУА ЯН1, ЦЗЮНЬ ЧЭН1

Солнечно-земная физика Том: 3Номер: 2 Год: **2017** Страницы: 10-17

В данной работе предлагается новый алгоритм повышения четкости изображений, использующий направленную фильтрацию для улучшения изображений и видеоизображений Солнца, который позволит легко выделять существенные мелкие структуры. Предлагаемый алгоритм может эффективно устранять шумы на изображениях, в том числе гауссовы и импульсные шумы. Кроме того, он может выделять волокнистые структуры на/за солнечным диском. Такие структуры наглядно демонстрируют развитие солнечной вспышки, протуберанца, выброса корональной массы, магнитного поля и т. д. Полученные экспериментальные результаты показывают, что предложенный алгоритм значительно повышает качество изображений Солнца по сравнению с первоначальными и несколькими классическими алгоритмами улучшения изображений, что облегчит определение **всплесков солнечного радиоизлучения по изображениям/ видеоизображениям Солнца**

О калибровке изображений Сибирского радиогелиографа

Федотова А.Ю., Алтынцев А.Т., Кочанов А.А., Лесовой С.В., Мешалкина Н.С.

Солнечно-земная физика. **2019**. Т. 5. No 4 С. 34–41.
https://naukaru.ru/ru/storage/viewWindow/43514

В статье обсуждается методика автоматической калибровки радиоизображений солнечного диска, получаемых по данным первой очереди многоволнового Сибирского радиогелиографа (СРГ). Т-образная антенная решетка

СРГ состоит из 48 антенн и работает на 32 частотах в диапазоне 4–8 ГГц. Методика реализована на языке программирования Python. Приведены примеры калибровок инструментальных значений СРГ по яркостным температурам спокойного и активного Солнца на нескольких частотах для четырех эруптивных событий: **19.06.2017, 25.07.2016, 24.04.2017 и 19.04.2017**. Приведены спектры для трех событий, а также оценки яркостной температуры по потоку, углового размера волокон и меры эмиссии.

ТОНКАЯ СТРУКТУРА СОЛНЕЧНЫХ РАДИОВСПЛЕСКОВ IV ТИПА, СВЯЗАННЫХ СО СТАЦИОНАРНЫМИ И ДВИЖУЩИМИСЯ ИСТОЧНИКАМИ

Фомичев В.В., Чернов Г.П.

Г и А Том: 63Номер: 2 Год: 2023 Страницы: 181-189

Рассмотрены различные виды тонкой структуры в континуальном излучении радиовсплесков IV типа применительно к разным типам источников излучения, стационарным и движущимся. В случае стационарных источников происхождение тонкой структуры связано как с процессами в отдельных магнитных петлях (квазипериодическое ускорение, магнитогидродинамические волны), так и с крупномасштабными процессами, связанными с распространением магнитогидродинамических возмущений, формированием петельных аркад и синхронными с ними процессами дискретного ускорения частиц, обуславливающих пульсирующий характер радиоизлучения. Для случая движущегося источника механизм генерации в значительной степени зависит от магнитной структуры источника (расширяющаяся магнитная арка или изолированное плазменное облако). В этом случае важна также связь с корональными выбросами массы и ударными волнами. Секундные пульсации объясняются магнитогидродинамическими колебаниями источника в виде магнитной петли или облака. Отсутствие прочей тонкой структуры в континууме движущихся всплесков IV типа может быть связано с критическим углом конуса потерь для возбуждения вистлеров.

ОЦЕНКИ МАГНИТНОГО ПОЛЯ В СОЛНЕЧНОЙ КОРОНЕ ПО РАДИОДАННЫМ

Фомичев В.В.

Астрономия-**2018** Том 2 Солнечно-земная физика – современное состояние и перспективы С.246

http://www.izmiran.ru/library/eaas2018/eaas-2018-2.pdf

On the basis of the analysis of types I, II and III solar radio bursts at meter radio waves a possibility of estimation of the magnetic field in the solar corona is discussed.

О ВОЗМОЖНОСТИ НАБЛЮДЕНИЙ СОЛНЕЧНЫХ СУБТЕРАГЕРЦОВЫХ ВСПЫШЕК НА РАДИОТЕЛЕСКОПЕ РАТАН-600

Хайкин В.Б., Макоев Г.А., Смирнова В.В.

Изв КРАО Том: 120Номер: 1 Год: 2024 траницы: 17-29

Предложен метод наблюдений солнечных субтерагерцовых вспышек (СТВ) на радиотелескопе РАТАН-600 в диапазоне 1-100 ГГц. Наблюдения СТВ предлагается проводить в процессе штатных многоазимутальных наблюдений Солнца с сокращенной апертурой на частоте 93 ГГц. Рассчитаны ожидаемые диаграммы направленности антенной системы на частотах 30, 93 и 140 ГГц (10, 3 и 2 мм) с учетом возможных ошибок поверхности элементов, ошибок их взаимной привязки, а также выноса первичного облучателя из фокуса. Получены их двумерные свертки с моделью Солнца, одномерные сканы которых соответствуют ожидаемым радиоизображениям Солнца на РАТАН-600 на указанных частотах. Оценены ожидаемые потоки СТВ в соответствии с моделью, согласно которой субтерагерцовое излучение генерируется за счет теплового тормозного механизма оптически толстой плазмы хромосферы и переходной области Солнца. Предложено проведение совместных наблюдений СТВ на РАТАН-600 в диапазоне 1-100 ГГц и на радиотелескопе РТ-7.5 МГТУ им. Н.Э. Баумана на частотах 93 и 140 ГГц. Это позволит уточнить W-образную форму спектра СТВ в дециметровом, сантиметровом и миллиметровом диапазонах длин волн, прояснить природу субтерагерцового излучения солнечных вспышек с положительным наклоном спектра.

ОБ ЭВОЛЮЦИИ ПОЛОС НА ДИНАМИЧЕСКИХ СПЕКТРАХ СОЛНЕЧНЫХ РАДИОВСПЛЕСКОВ II ТИПА

Цап Ю.Т., Исаева Е.А., Копылова Ю.Г.

ПАЖ Том: 46Номер: 2 Год: **2020** 147-152

DOI: 10.31857/S0320010820010064

Исходя из анализа динамических спектров излучения солнечных вспышек в метровом диапазоне длин волн, полученных с помощью наземной сети радиотелескопов Radio Solar Telescope Network, рассмотрена эволюция параметров гармоник солнечных радиовсплесков II типа. Установлено, что относительное расстояние между полосами ведет себя немонотонным образом и его значение может меняться в широких пределах от 0.1 до 3. Это можно объяснить генерацией электромагнитных волн на первой и второй гармонике плазменной частоты по разные стороны фронта ударной волны. Обсуждаются следствия полученных результатов.

АЛЬТЕРНАТИВНЫЕ МОДЕЛИ ЗЕБРА-СТРУКТУРЫ В СОЛНЕЧНОМ РАДИОИЗЛУЧЕНИИ

Чернов Г.П., Фомичев В.В.

Астрономия-**2018** Том 2 Солнечно-земная физика – современное состояние и перспективы С.266

http://www.izmiran.ru/library/eaas2018/eaas-2018-2.pdf

In the literature, discussion continues about the nature of the zebra–structure (ZS) in type IV radio bursts, and understanding even the most extended mechanism associated with double plasma resonance has been improved in series of works. Moreover, in the recent work [1] its

ineffectiveness was shown under the usually adopted conditions in the radio source. In this case in a number of works we demonstrated the possibility of modeling with whistlers to explain many thin components of ZS stripes, taking into account the effects of scattering whistlers on fast particles. This situation stimulates the search for new mechanisms. For example, earlier we showed the importance of explosive instability, at least for large flares with the ejections of protons. **1 августа 2010**

О СООТНОШЕНИИ СПЕКТРОВ МИКРОВОЛНОВЫХ ВСПЛЕСКОВ НА СОЛНЦЕ И ПОТОКОВ ПРОТОНОВ У ЗЕМЛИ

И. М. **Чертоk**1, В. В. Гречнев2, Н. С. Мешалкина2

АСТРОНОМИЧЕСКИЙЖУРНАЛ, ***2009****, том 86,№11, с. 1133–1144*

Анализ экстремального солнечного протонного события 20.01.2005 обострил дискуссию по давно обсуждаемой проблеме: ускоряются ли приходящие к Земле солнечные космические лучи во вспышке или в ударной волне перед быстро распространяющимся корональным выбросомfl При этом одним из важных является вопрос о связи между энергетическим спектром солнечных космических лучей и параметрами, характеризующими частотный спектр вспышечных микроволновых всплесков. В ряде работ по материалам предшествующих циклов солнечной активности было показано, что такая связь существует, в частности, для протонов с энергией десятки МэВ. В данной работе представлены результаты анализа этой связи по данным 1987–2008 гг. Установлено, что для событий, связанных со вспышками на западной половине диска, имеет место существенная корреляция между индексом δ, эквивалентным показателю степенного интегрального энергетического спектра протонов, зарегистрированных у орбиты Земли в диапазоне 10–100 МэВ, и такими параметрами радиовсплесков, как отношение пиковых потоков S на двух частотах (например, 9 и 15 ГГц) и частота спектрального максимума fm. Микроволновым всплескам с жестким частотным спектром (у которых $S9/S15 \leq 1$, $fm \geq 15$ ГГц) соответствуют потоки протонов с жестким (пологим) энергетическим спектром ($\delta \leq 1.5$). Вспышки же с мягким радиоспектром ($S9/S15 \geq 1.5$, $fm \leq 5$ ГГц) наоборот приводят к потокам протонов с мягким (крутым) энергетическим спектром ($\delta \geq 1.5-2$). Показано также, что мощные высокочастотные всплески с наиболее жестким радиоспектром ($fm \approx 30$ ГГц) могут служить информативным индикатором ускорения значительных потоков протонов во вспышках, происходящих в сильных магнитных полях. Эти результаты являются важным аргументом в пользу предположения, что частицы солнечных космических лучей (по крайней мере, их начального импульса) в основном ускоряются во вспышке в процессах импульсного и постэруптивного энерговыделения, а не в ударной волне на фронте коронального выброса.

НАБЛЮДЕНИЯ ЭРУПТИВНЫХ СОБЫТИЙ С ПОМОЩЬЮ СИБИРСКОГО РАДИОГЕЛИОГРАФА

ФЕДОТОВА А.Ю.1, АЛТЫНЦЕВ А.Т.1, КОЧАНОВ А.А.1, ЛЕСОВОЙ С.В.1, МЕШАЛКИНА Н.С.1

СОЛНЕЧНО-ЗЕМНАЯ ФИЗИКА Том: 4Номер: 3 Год: **2018** Страницы: 17-27

Описаны методы регистрации эруптивных событий с помощью первой очереди Сибирского солнечного радиогелиографа (СРГ-48). Приведены примеры зарегистрированных событий: 1) подъем протуберанца над лимбом, наблюдавшийся на последовательностях радиоизображений **24 апреля 2017** г.; 2) джет, зарегистрированный **2 августа 2017** г., холодное вещество которого экранировало излучение компактного микроволнового источника в течение нескольких десятков минут. Затенение джета проявилось на корреляционных кривых СРГ-48 в виде так называемого отрицательного всплеска. На примере такого всплеска на корреляционных кривых **9 февраля 2017** г. показано, что интервалы с депрессией микроволнового излучения локальных источников не всегда вызываются затенением их излучения. В данном событии радиояркость в течение десяти часов уменьшалась относительно повышенного квазистационарного излучения активной области АО 12635 во время развития ее магнитной структуры. Подобное поведение излучения активной области наблюдалось также в EUV, SXR и радиоизлучении на 17 ГГц.

ВЛИЯНИЕ РАДИАЛЬНЫХ БМЗ КОЛЕБАНИЙ НА ХАРАКТЕРИСТИКИ МИКРОВОЛНОВОГО И ЖЕСТКОГО РЕНТГЕНОВСКОГО ИЗЛУЧЕНИЯ ВСПЫШЕЧНОЙ ПЕТЛИ

Филатов Л.В.1, Мельников В.Ф.2, Кудрявцев И.В.2,3
Пулково *«Солнечная и солнечно-земная физика – **2015**», с.367*
In this article, a new effect important for the modulation of gyrosynchrotron and hard X-ray/gamma-ray emission is taken into account. The effect is associated with the modulation of nonthermal electrons number density produced by sausage mode oscillations in a flaring loop.

ТОНКАЯ СТРУКТУРА СОЛНЕЧНЫХ РАДИОВСПЛЕСКОВ IV ТИПА, СВЯЗАННЫХ СО СТАЦИОНАРНЫМИ И ДВИЖУЩИМИСЯ ИСТОЧНИКАМИ

DOI: 10.31857/S0016794022600466 **Г и А** Том: 63Номер: 2 Год: 2023 Страницы: 181-189

Рассмотрены различные виды тонкой структуры в континуальном излучении радиовсплесков IV типа применительно к разным типам источников излучения, стационарным и движущимся. В случае стационарных источников происхождение тонкой структуры связано как с процессами в отдельных магнитных петлях (квазипериодическое ускорение, магнитогидродинамические волны), так и с крупномасштабными процессами, связанными с распространением магнитогидродинамических возмущений, формированием петельных аркад и синхронными с ними процессами дискретного ускорения частиц, обуславливающих пульсирующий характер радиоизлучения. Для случая движущегося источника механизм генерации в значительной степени зависит от магнитной структуры источника (расширяющаяся магнитная арка или изолированное плазменное облако). В этом случае важна также связь с корональными выбросами массы и ударными волнами. Секундные пульсации объясняются магнитогидродинамическими колебаниями источника в виде магнитной петли или облака. Отсутствие прочей тонкой структуры в континууме движущихся всплесков IV типа может быть связано с критическим углом конуса потерь для возбуждения вистлеров.

СОЛНЕЧНЫЕ РАДИОВСПЛЕСКИ, СВЯЗАННЫЕ СО СТОЯЧИМИ УДАРНЫМИ ВОЛНАМИ

В. В. **Фомичев**, Г. П. Чернов
ГиА Том: 60Номер: 2 Год: **2020** Страницы: 139-152
Рассмотрен ряд явлений с радиовсплесками в дециметровом и сантиметровом диапазонах, похожих на всплески II типа в метровом диапазоне. Во всех явлениях радиовсплески обнаруживали остановку частотного дрейфа и его смену на обратный. Анализ всех имеющихся у нас данных о соответствующих вспышках свидетельствует о возникновении конечных ударных волн (termination shock), во фронтах которых происходило ускорение частиц. Это подтверждается рождением новых источников жесткого рентгеновского излучения и радиоизлучения быстрых всплесков (спайков), волокон и зебра-структуры. Источники дрейфующих полос с разворотом дрейфа располагались или между вспышечной петлей и нижней ударной волной, или между нижней и верхней ударными волнами. Оценки критического числа Маха для обычных параметров вспышечной плазмы показали, что значения (Мкр = 1.1–1.3) могут легко реализоваться в рассматриваемых явлениях, и излучение можно связать с бунемановской неустойчивостью. Реализация необходимых условий для генерации наблюдаемых всплесков электромагнитного излучения возможна в шлемовидных магнитных структурах в солнечной короне.

МОДЕЛЬ ЗЕБРА-СТРУКТУРЫ В СОЛНЕЧНОМ РАДИОИЗЛУЧЕНИИ

ЧЕРНОВ Г. П.1, ФОМИЧЕВ В. В.1, СЫЧ Р. А.2

Геомаг. и Аэрон. Том: 58Номер: 3 Год: **2018** Страницы: 411-422
Пронализирована сложная зебра-структура и радиоволокна (fiber bursts) в солнечном радиовсплеске IV типа **1 августа 2010** г. Показано, что все основные детали спорадической зебра-структуры в явлении удается объяснить в рамках модели зебра-структуры и радиоволокон при взаимодействии плазменных волн с вистлерами. Кроме того показано, что основные изменения полос зебра-структуры вызываются механизмом рассеяния быстрых частиц на вистлерах, приводящим к переключению неустойчивости вистлеров с нормального эффекта Доплера на аномальный.

РАЗВИТИЕ ВСПЫШЕЧНЫХ ПРОЦЕССОВ И ОСОБЕННОСТИ ТОНКОЙ СТРУКТУРЫ СОЛНЕЧНОГО РАДИОИЗЛУЧЕНИЯ

***Чернов** П., Фомичев В.В., Йан У., Тан Б., Тан Ч., Фу К.*
ГЕОМАГНЕТИЗМ И АЭРОНОМИЯ Том: 57Номер: 6 Год: **2017** Страницы: 794-807
С помощью всех доступных данных наземных и спутниковых наблюдений выяснена причина появления различных элементов тонкой структуры солнечных радиовсплесков в дециметровом и сантиметровом диапазонах волн. В некоторых явлениях быстрые пульсации, зебра-структура, волокна и спайки наблюдались практически одновременно. На примере двух явлений показано, что пульсации радиоизлучения вызываются частицами, ускоренными в области магнитного пересоединения, а зебра-структура возбуждается в источнике типа магнитной ловушки для быстрых частиц. Сложное сочетание странных волокон, зебра-структуры и спайков в явлении **1 декабря 2004** г. связывается с единым источником - магнитным островом, образующимся после коронального выброса массы. **January 21, 2013, 2013-06-21**
See https://arxiv.org/ftp/arxiv/papers/1711/1711.07531.pdf

ОСОБЕННОСТИ ТОНКОЙ СТРУКТУРЫ РАДИОИЗЛУЧЕНИЯ СОЛНЕЧНОЙ ВСПЫШКИ 12 ФЕВРАЛЯ 2010 Г.

ЧЕРНОВ Г.П.[1], **ФОМИЧЕВ В.В.**[1], **ГОРГУЦА Р.В.**[1], **МАРКЕЕВ А.К.**[1], **СОБОЛЕВ Д.Е.**[1], **ХИЛЛАРИС А.**[2], **АЛИССАНДРАКИС К.**[3]

Геомаг. и аэрономия Том: 54Номер: 4 Год: 2014 Страницы: 444
https://www.elibrary.ru/download/elibrary_21698913_72807137.pdf
DOI: 10.7868/S0016794014040038

Проанализированы записи радиоизлучения Солнца, полученные на спектрографе ИЗМИРАН (25□270 МГц) для события солнечной вспышки 12 февраля 2010 г. Отмечено, что в трех больших группах всплесков III типа наблюдалась разнообразная тонкая структура на фоне невысокого континуума. Согласно данным радиогелиографа Нансэ, источники всех трех групп всплесков располагались в одной активной области 11046 и их излучение сопровождалось всплесками в мягком рентгеновском диапазоне (космический аппарат GOES): в 07:21 UT C7.9, в 09:40 UT B9.6 и в 11:25 UT M8.3. После первой группы всплесков наблюдались классические волокна (fiber bursts) в сочетании с обратно дрейфующими волокнами с необычным дугообразным дрейфом. После третьей (самой мощной) группы наблюдались стабильные секундные пульсации и медленно дрейфующие волокна. Мгновенная полоса частот у них на порядок превышала полосу частот классических волокон, а частотный дрейф был в несколько раз меньше. Более сложные волокна наблюдались в самой слабой группе в интервале 09:40:30□09:42:00 UT. Они представляли собой узкополосные (0.5 МГц) волокна, периодически повторяющиеся в небольшой полосе частот (5□6 МГц) в течение нескольких секунд. Особенностью данного явления является также присутствие множества хаотически дрейфующих ансамблей волокон, пересекающихся и накладывающихся друг на друга. Предполагается, что появление таких структур может быть связано с существованием множества мелких ударных фронтов за передним краем коронального выброса массы.

О пространственных наблюдениях радиоисточников тонкой структуры солнечных радиовсплесков

Чернов Г.П., Фомичев В.В., Сыч Р.А., Yan Yihua, Fu Qijun, Жданов Д.А.
ИКИ-**2014**, Сессия: Солнце
http://plasma2014.cosmos.ru/presentations

РАДИОПРЕДВЕСТНИКИ КОРОНАЛЬНЫХ ВЫБРОСОВ МАССЫ, ЗАРЕГИСТРИРОВАННЫХ В ФЕВРАЛЕ - МАРТЕ 2023 ГОДА

ШЕЙНЕР О.А.✉[1], **ФРИДМАН В.М.**[1]
КОСМИЧЕСКИЕ ИССЛЕДОВАНИЯ Том: 62Номер: 2 Год: 2024 Страницы: 157-167
На основе анализа данных за февраль - март 2023 г. рассмотрены результаты исследований связи между возникновением спорадического микроволнового излучения, предшествующего явлениям корональных выбросов массы, и этими явлениями с целью разработки методов краткосрочного прогнозирования корональных выбросов массы по радиоданным.

ХРОМОСФЕРНЫЕ И КОРОНАЛЬНЫЕ ИСТОЧНИКИ В РАДИОДИАПАЗОНЕ ПО ЧАСТНОМУ СОЛНЕЧНОМУ ЗАТМЕНИЮ 20.03.2015 НА ГАС ГАО РАН

Шрамко А.Д., Гусева С.А.
Пулково *«Солнечная и солнечно-земная физика – **2015**», с.387*
The analysis of the observant data of a partial solar eclipse from 3/20/2015 on the data from radio telescopes RT-2 (λ3.2 cm) and RT-3 (λ4.9 cm).